

AD-A113 709

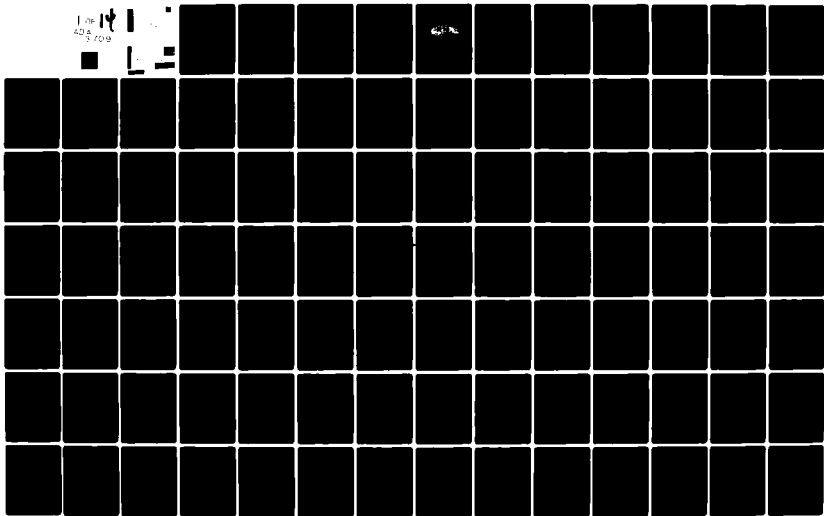
SOUTHEASTERN CENTER FOR ELECTRICAL ENGINEERING EDUCAT--ETC F/8 5/1
USAF SUMMER FACULTY RESEARCH PROGRAM. 1981 RESEARCH REPORTS. VO--ETC(U)
OCT 81 W D PEELE F49620-79-C-0038

UNCLASSIFIED

AFOSR-TR-82-0228

NL

1 of 1
425 709



AFOSR-TR- 82 - 0228

**AIR FORCE OFFICE OF SCIENTIFIC RESEARCH (AFSC)
NOTICE OF TRANSMITTAL TO DTIC
This technical report has been reviewed and is
approved for public release IAW AFR 190-12.
Distribution is unlimited.
MATTHEW J. KERPER
Chief, Technical Information Division**

**Approved for public release;
distribution unlimited.**

REPORT DOCUMENTATION PAGE		READ INSTRUCTIONS BEFORE COMPLETING FORM
1. REPORT NUMBER AFOSR-TR- 82-0228	2. GOVT ACCESSION NO.	3. RECIPIENT'S CATALOG NUMBER
4. TITLE (and Subtitle) USAF SUMMER FACULTY RESEARCH PROGRAM (VOL 2)	5. TYPE OF REPORT & PERIOD COVERED FINAL	
	6. PERFORMING ORG. REPORT NUMBER	
7. AUTHOR(s) PROF. WARREN D. PEELE	8. CONTRACT OR GRANT NUMBER(s) F49620-79-C-0038	
9. PERFORMING ORGANIZATION NAME AND ADDRESS SOUTHEASTERN CENTER FOR ELECTRICAL ENGINEERING EDUCATION 11th AND MASSACHUSETTS AVE. ST. CLOUD, FLORIDA 32769	10. PROGRAM ELEMENT, PROJECT, TASK AREA & WORK UNIT NUMBERS 61102F 2305/D5	
11. CONTROLLING OFFICE NAME AND ADDRESS AFOSR/XOT BOLLING AFB, DC 20332	12. REPORT DATE OCTOBER 1981	
	13. NUMBER OF PAGES 1300	
14. MONITORING AGENCY NAME & ADDRESS (if different from Controlling Office)	15. SECURITY CLASS. (of this report) UNCLASSIFIED	
	15a. DECLASSIFICATION DOWNGRADING SCHEDULE	
16. DISTRIBUTION STATEMENT (of this Report) APPROVED FOR PUBLIC RELEASE; DISTRIBUTION UNLIMITED		
17. DISTRIBUTION STATEMENT (of the abstract entered in Block 20, if different from Report)		
18. SUPPLEMENTARY NOTES		
19. KEY WORDS (Continue on reverse side if necessary and identify by block number)		
20. ABSTRACT (Continue on reverse side if necessary and identify by block number) The United States Air Force Summer Faculty Research Program (USAF-SFRP) is a program designed to introduce university, college, and technical institute faculty members to Air Force research. This is accomplished by the faculty members being selected on a nationally advertised competitive basis for a ten week assignment during the summer intersession to perform research at Air Force Laboratories/centers. Each assignment is in a subject area and at an Air Force facility mutually agreed upon by the faculty member and the Air Force. In addition to compensation and travel expenses, a cost of		

UNCLASSIFIED

SECURITY CLASSIFICATION OF THIS PAGE (When Data Entered)

20. Cont.

living allowance is also paid. The USAF-SFRP is sponsored by the Air Force Office of Scientific Research/Air Force Systems Command, United States Air Force, and is conducted by the Southeastern Center for Electrical Engineering Education, Inc.

RE: Classified References, Distribution Unlimited
No change in distribution statement per Ms. Christiani, AFOSR/XOPD

Accession For	
NTIS GRA&I	<input checked="" type="checkbox"/>
DTIC TAB	<input type="checkbox"/>
Unannounced	<input type="checkbox"/>
Justification	
PER CALL JC	
By	
Distribution/	
Availability Codes	
Avail and/or	
Dist Special	
A	

DTIC
COPY
INSPECTED
2

UNCLASSIFIED

SECURITY CLASSIFICATION OF THIS PAGE (When Data Entered)

1981 USAF/SCEEE SUMMER FACULTY
RESEARCH PROGRAM

Conducted by

Southeastern Center for

Electrical Engineering Education

under

USAF Contract Number F49620-79-C-0038

RESEARCH REPORTS

Volume II of II

Submitted to

Air Force Office of Scientific Research

Bolling Air Force Base

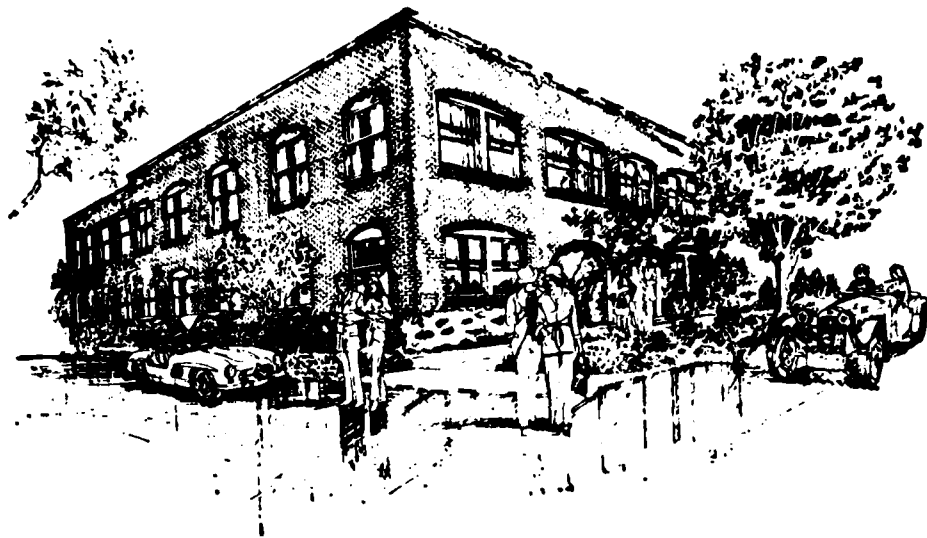
Washington D.C.

by

Southeastern Center for

Electrical Engineering Education

October 1981



SCEEE
©
1981

PREFACE

The United States Air Force Summer Faculty Research Program (USAF-SFRP) is a program designed to introduce university, college, and technical institute members faculty members to Air Force research. This is accomplished by the faculty members being selected on a nationally advertised competitive basis for a ten-week assignment during the summer intercession to perform research at Air Force laboratories/centers. Each assignment is in a subject area and at an Air Force facility mutually agreed upon by the faculty member and the Air Force. In addition to compensation and travel expenses, a cost of living allowance is also paid. The USAF-SFRP is sponsored by the Air Force Office of Scientific Research/Air Force Systems Command, United States Air Force, and is conducted by the Southeastern Center for Electrical Engineering, Inc.

The specific objectives of the 1981 USAF-SFRP are:

- (1) To develop the basis for continuing research of interest to the Air Force at the faculty member's institution.
- (2) To further the research objectives of the Air Force.
- (3) To stimulate continuing relations among faculty members and their professional peers in the Air Force.
- (4) To enhance the research interests and capabilities of scientific and engineering educators.

In the 1979 summer program, 70 faculty members participated, and in the 1980 and 1981 programs, 87 faculty members participated. These researchers were assigned to 25 USAF laboratories/centers across the country. This two volume document is a compilation of the final reports written by the assigned faculty members about their summer research efforts.

1981 USAF/SCEEE SUMMER FACULTY RESEARCH PROGRAM

LIST OF PARTICIPANTS

Page 2

NAME/ADDRESS	DEGREE, SPECIALTY, LABORATORY ASSIGNMENT
Dr. Jerome D. Braverman Professor & Chairman Rider College Dept. of Decision Science & Computers Lawrenceville, NJ 08648 (609) 896-5124	<u>Degree:</u> PhD, Statistics, 1966 <u>Specialty:</u> Statistical Inference, Statistical Decision Theory, Quality Control & Reliability <u>Assigned:</u> RADC (Griffiss)
Dr. Louis W. Buckalew Assistant Professor Alabama A & M University Dept. of Psychology Box 200 Normal, AL 35762 (205) 859-7451	<u>Degree:</u> MS, General Experimental Psychology, 1969 <u>Specialty:</u> Physiological Psychology <u>Assigned:</u> AMRL
Dr. Gale H. Buzzard Assistant Professor Duke University Dept. of Mechanical Engineering and Material Science Durham, NC 27706 (919) 684-2832	<u>Degree:</u> PhD, Mechanical Engineering, 1966 <u>Specialty:</u> Fluid Mechanics, Heat Transfer, System Dynamics <u>Assigned:</u> RPL
Dr. David A. Carlson Assistant Professor University of Massachusetts/Amherst Dept. of Electrical & Computer Engineering Amherst, MA 01003 (413) 545-0973	<u>Degree:</u> PhD, Computer Science, 1980 <u>Specialty:</u> Computer Science, Design & Analysis of Algorithms <u>Assigned:</u> HRL (Lowry)
Dr. Robert E. Carlson Assistant Professor Kent State University Dept. of Biological Science Kent, OH 44242 (216) 672-2266	<u>Degree:</u> PhD, Ecology & Limnology, 1975 <u>Specialty:</u> Ecology, Aquatic Biology <u>Assigned:</u> ESC
Dr. Junho Choi Assistant Professor Florida Institute of Technology Dept. of Electrical Engineering University Boulevard Melbourne, FL 32901 (305) 723-3701 X 430	<u>Degree:</u> PhD, Control Systems & Signal Processing, 1978 <u>Specialty:</u> Modern & Conventional Control Systems <u>Assigned:</u> ESMC

1981 USAF/SCEEE SUMMER FACULTY RESEARCH PROGRAM

LIST OF PARTICIPANTS

Page 3

NAME/ADDRESS	DEGREE, SPECIALTY, LABORATORY ASSIGNMENT
Dr. Hugh W. Coleman Associate Professor Mississippi State University Dept. of Mechanical Engineering P.O. Drawer ME Mississippi State, MS 39762 (601) 325-3260	<u>Degree:</u> PhD, Mechanical Engineering, 1976 <u>Specialty:</u> Turbulent boundary layers - Fluid Mechanics & Heat Transfer <u>Assigned:</u> AD
Dr. David L. Cozart Associate Professor The Citadel Dept. of Mathematics Charleston, SC 29409 (803) 792-7896	<u>Degree:</u> PhD, Mathematics, 1973 <u>Specialty:</u> Programming languages, Statistics <u>Assigned:</u> AL
Dr. Robert W. Cunningham Associate Professor Kent State University Dept. of Physics University Drive, NE New Philadelphia, OH 44663 (216) 339-3391	<u>Degree:</u> PhD, Physics, 1969 <u>Specialty:</u> Solid State Physics <u>Assigned:</u> ML
Dr. Larry R. Dalton Associate Professor SUNY/Stony Brook Dept. of Chemistry Long Island, NY 11794 (516) 246-8601/5068	<u>Degree:</u> PhD, Chemistry, 1972 <u>Specialty:</u> Physical Chemistry, Electronics & Instrumentation Microwaves <u>Assigned:</u> FJSRL
Dr. Charles B. Davis Assistant Professor University of Toledo Dept. of Mathematics Toledo, OH 43606 (419) 537-2297/2568	<u>Degree:</u> PhD, Statistics, 1976 <u>Specialty:</u> Mathematical & Applied Statistics <u>Assigned:</u> SAM
Dr. Carol A. Deakyne Assistant Professor College of the Holy Cross Chemistry Dept. Worcester, MA 01610 (617) 793-3367	<u>Degree:</u> PhD, Theoretical Chemistry, 1976 <u>Specialty:</u> Applications of Molecular Orbital Theory <u>Assigned:</u> GL
Dr. Donald W. Emerich Professor Mississippi State University Chemistry Dept. P.O. Box CH Mississippi State, MS 39762 (601) 325-3584	<u>Degree:</u> PhD, Chemistry, 1951 <u>Specialty:</u> Analytical Chemistry, Classical Electro-analytical Chemistry <u>Assigned:</u> RPL

1981 USAF/SCEEE SUMMER FACULTY RESEARCH PROGRAM

LIST OF PARTICIPANTS

Page 4

NAME/ADDRESS	DEGREE, SPECIALTY, LABORATORY ASSIGNMENT
Dr. Chris W. Eskridge Assistant Professor University of NB/Lincoln Dept. of Criminal Justice 103 Brace Laboratory Lincoln, NB 68588 (402) 472-3677	<u>Degree:</u> PhD, Public Administration, 1978 <u>Specialty:</u> Public Administration, Police Organization & Management <u>Assigned:</u> LMDC
Dr. Glenn E. Fanslow Associate Professor Iowa State University Electrical Engineering Dept. Coover Hall Ames, IA 50011 (515) 294-6576/2663	<u>Degree:</u> PhD, Electrical Engineering, 1962 <u>Specialty:</u> Applications of Microwave Power <u>Assigned:</u> APL
Dr. William A. Feld Assistant Professor Wright State University Dept. of Chemistry Dayton, OH 45433 (513) 873-2511	<u>Degree:</u> PhD, Chemistry, 1971 <u>Specialty:</u> Synthetic Organic & Polymer Chemistry <u>Assigned:</u> ML
Dr. John A. Fleming Assistant Professor Texas A & M University Dept. of Electrical Engineering College Station, TX 77843 (713) 845-7441 X 66	<u>Degree:</u> PhD, Electrical Engineering, 1977 <u>Specialty:</u> Electrical Systems <u>Assigned:</u> AL
Dr. Dennis R. Flentge Assistant Professor Cedarville College Dept. of Mathematics & Science Box 601 Cedarville, OH 45314 (513) 766-2211 X 311	<u>Degree:</u> PhD, Physical Chemistry, 1974 <u>Specialty:</u> Physical Chemistry, Catalysis, IR & EPR Spectroscopy <u>Assigned:</u> APL
Dr. Harold W. Fox Professor Ball State University Dept. of Business Muncie, IN 47306 (317) 285-5244	<u>Degree:</u> PhD, Economics, 1967 <u>Specialty:</u> Business Administration <u>Assigned:</u> BRMC
Dr. Peter Freymuth Associate Professor University of Colorado Aerospace Engineering Science Dept. Campus Box 429 Boulder, CO 80309 (303) 492-7611	<u>Degree:</u> PhD, Aerospace Engineering, 1965 <u>Specialty:</u> Turbulence, Thermal Anemometry, Stability <u>Assigned:</u> FJSRI.

1981 USAF/SCEEE SUMMER FACULTY RESEARCH PROGRAM

LIST OF PARTICIPANTS

Page 5

NAME/ADDRESS	DEGREE, SPECIALTY, LABORATORY ASSIGNMENT
Dr. Joel R. Fried Assistant Professor University of Cincinnati Chemistry Engineering Dept. Mail Location #171 Cincinnati, OH 45221 (513) 475-3500	<u>Degree:</u> PhD, Polymer Science & Engineering, 1976 <u>Specialty:</u> Mechanical Properties, Calorimetry & Rheology of Polymer Blends <u>Assigned:</u> ML
Dr. David E. Greene Assistant Professor Texas A & M University Industrial Engineering Dept. College Station, TX 77840 (713) 845-5531	<u>Degree:</u> PhD, Applied Mathematics, 1973 <u>Specialty:</u> Control Theory, Man Machine Systems, Biological Regulation, PDE, DE <u>Assigned:</u> SAM
Dr. Gurmohan S. Grewal Professor Southern University/Baton Rouge Dept. of Electrical Engineering P.O. Box 11060 Baton Rouge, LA 70813 (504) 771-2317	<u>Degree:</u> PhD, Electrical Engineering, 1969 <u>Specialty:</u> Control Systems, Simulation, State Estimation <u>Assigned:</u> AL
Dr. Paul B. Griesacker Associate Professor Gannon University Dept. of Physics Erie, PA 16508 (814) 871-7338	<u>Degree:</u> PhD, Physics, 1963 <u>Specialty:</u> Physical Optics, Coherent Radiation <u>Assigned:</u> RADC (Griffiss)
Dr. Vijay K. Gupta Assistant Professor Central State University Dept. of Chemistry Wilberforce, OH 45384 (513) 376-6423	<u>Degree:</u> PhD, Chemistry, 1968 <u>Specialty:</u> Physical Chemistry, Physical Organic Laboratory, Physical Science, General Chemistry <u>Assigned:</u> APL
Dr. Kenneth R. Hall Associate Professor Mississippi State University Aerospace Engineering Dept. P.O. Drawer A Mississippi State, MS 39762 (601) 325-3623	<u>Degree:</u> PhD, Aerospace Engineering, 1973 <u>Specialty:</u> Simulation, Flight Dynamics, Control, Optimization <u>Assigned:</u> AD
Dr. Robert M. Harnett Associate Professor & Director Clemson University System Engineering Dept. Clemson, SC 29631 (803) 656-3375	<u>Degree:</u> PhD, Industrial & Systems Engineering, 1974 <u>Specialty:</u> Operations Research, Optimi- zation <u>Assigned:</u> AD

1981 USAF/SCEEE SUMMER FACULTY RESEARCH PROGRAM

LIST OF PARTICIPANTS

Page 6

NAME/ADDRESS	DEGREE, SPECIALTY, LABORATORY ASSIGNMENT
Dr. Ronney D. Harris Professor Utah State University Dept. of Electrical Engineering UMC 41 Logan, UT 84321 (801) 750-2973	<u>Degree:</u> PhD, Electrical Engineering, 1964 <u>Specialty:</u> Aeronomy - Atmospheric Radiation Transfer <u>Assigned:</u> GL
Dr. Franklin D. Hill Professor Grambling State University Chemistry Dept. Grambling, LA 71245 (318) 247-8397	<u>Degree:</u> PhD, Biochemistry, 1960 <u>Specialty:</u> Lipid Metabolism <u>Assigned:</u> AMRL
Dr. Francis J. Jankowski Professor Wright State University Dept. of Engineering Dayton, OH 45434 (513) 873-2079/2403	<u>Degree:</u> ScD, Physics, 1949 <u>Specialty:</u> Systems Engineering, Nuclear Engineering, Mechanical Engin- eering, Human Factors Engineering <u>Assigned:</u> WL
Dr. Stanley E. Jones Associate Professor University of Kentucky Engineering Mechanics Lexington, KY 40506 (606) 258-2719	<u>Degree:</u> PhD <u>Specialty:</u> Applied Mathematics, Nonlinear Mechanics <u>Assigned:</u> AD
Dr. Paul R. Kalata Assistant Professor Drexel University Dept. of Electrical & Computer Engineering 32nd & Chestnut Street Philadelphia, PA 19104 (215) 895-2251	<u>Degree:</u> PhD, Electrical Engineering, 1974 <u>Specialty:</u> Control Theory, Estimation Theory <u>Assigned:</u> WL
Dr. Richard Y.C. Kwor Assistant Professor University of Notre Dame Dept. of Electrical Engineering Notre Dame, IN 46556 (219) 283-6269	<u>Degree:</u> PhD, Electrical Engineering, 1976 <u>Specialty:</u> Electrical Engineering <u>Assigned:</u> AL
Dr. Richard C. Liu Associate Professor Purdue University Dept. of Industrial Engineering Grissom Hall W. Lafayette, IN 47907 (317) 749-2948	<u>Degree:</u> PhD, IE (Manufacturing), 1973 <u>Specialty:</u> Manufacturing Engineering <u>Assigned:</u> MI.

1981 USAF/SCEEE SUMMER FACULTY RESEARCH PROGRAM

LIST OF PARTICIPANTS

Page 7

NAME/ADDRESS	DEGREE, SPECIALTY, LABORATORY ASSIGNMENT
Dr. William S. McCain Assistant Professor Tennessee State University Mechanical Engineering 3500 Centennial Blvd. Nashville, TN 37203 (615) 320-3555	<u>Degree:</u> PhD, Metallurgical Engineering, 1973 <u>Specialty:</u> Aluminum alloys, fabrication & heat treatments of aerospace alloys, rolling, forging, extrusion x-ray diffraction <u>Assigned:</u> ML
Dr. William S. McCormick Associate Professor Wright State University Engineering Dept. Dayton, OH 45435 (513) 873-2403	<u>Degree:</u> PhD, Electrical Engineering, 1967 <u>Specialty:</u> Electrical Engineering <u>Assigned:</u> AL
Dr. Donald F. McCoy Associate Professor University of Kentucky Dept. of Psychology Lexington, KY 40506 (606) 258-8589/5601	<u>Degree:</u> PhD, Experimental Psychology, 1966 <u>Specialty:</u> Learning, Operant Conditioning, Animal Performance <u>Assigned:</u> AMRL
Dr. Henry A. McGee, Jr. Professor & Dept. Head VPI & SU Chemistry Engineering Dept. Blacksburg, VA 24061 (703) 961-6631	<u>Degree:</u> PhD, Chemical Engineering, 1955 <u>Specialty:</u> Cryogenics, Molecular Phenomena & Processes <u>Assigned:</u> WL
Dr. Patrick J. McKenna Assistant Professor University of Florida Mathematics Dept. Gainesville, FL 32611 (904) 392-6721	<u>Degree:</u> PhD, Mathematics, 1976 <u>Specialty:</u> Partial Differential Equations <u>Assigned:</u> FDL
Dr. John R. McNeil Assistant Professor New Mexico State University Dept. of Electrical & Computer Engineering Las Cruces, NM 88003 (505) 646-3115	<u>Degree:</u> PhD, Electrical Engineering, 1977 <u>Specialty:</u> High Energy Laser Optics, Ion Beam Applications <u>Assigned:</u> WL
Dr. Louis A. Martin-Vega Associate Professor University of Florida Industrial & Systems Engineering Dept. Gainesville, FL 32611 (904) 392-1464 X 35	<u>Degree:</u> PhD, Industrial & Systems Engineering, 1975 <u>Specialty:</u> Scheduling, Applied IE & OR <u>Assigned:</u> LMC

1981 USAF/SCEEE SUMMER FACULTY RESEARCH PROGRAM

LIST OF PARTICIPANTS

Page 8

NAME/ADDRESS	DEGREE, SPECIALTY, LABORATORY ASSIGNMENT
Dr. Kishan G. Mehrotra Professor Syracuse University Dept. of Computer & Information Science 313 Link Hall Syracuse, NY 13210 (315) 423-2811	<u>Degree:</u> PhD, Statistics, 1971 <u>Specialty:</u> Discriminant Analysis, Non- parametric Reliability <u>Assigned:</u> SAM
Dr. David F. Miller Assistant Professor Wright State University Mathematics Dept. Dayton, OH 45435 (513) 873-2068/2785	<u>Degree:</u> PhD, Applied Mathematics, 1979 <u>Specialty:</u> Optimization Theory, Optimal Control <u>Assigned:</u> FDL
Dr. Levon Minnetyan Assistant Professor Clarkson College Dept. of Civil & Environmental Engineering Potsdam, NY 13676 (315) 268-4432	<u>Degree:</u> PhD, Structural Mechanics, 1974 <u>Specialty:</u> Nonlinear Structural Analysis, Structural Dynamics <u>Assigned:</u> FDL
Dr. Rex C. Moyer Director & Associate Professor Trinity University Thorman Cancer Laboratory Box 191, 715 Stadium Drive San Antonio, TX 78218 (512) 736-7231/7235	<u>Degree:</u> PhD, Microbiology, 1965 <u>Specialty:</u> Oncology, Microbiology, Virology, Tissue Culture <u>Assigned:</u> SAM
Dr. Steven B. Newman Assistant Professor Central Community State College Physics Dept. 1615 Stanley St. New Britain, CT 06050 (203) 827-7341	<u>Degree:</u> PhD, Atmospheric Sciences, 1978 <u>Specialty:</u> Cloud & Precipitation Physics, Analysis & Forecasting <u>Assigned:</u> GL
Dr. Eugene E. Niemi Jr. Associate Professor University of Lowell Mechanical Engineering Dept. One University Ave. Lowell, MA 01854 (617) 452-5000 X 2768/2312	<u>Degree:</u> PhD, Mechanical & Aerodynamic Engineering <u>Specialty:</u> Aerodynamics, Fluid Mechanics, Thermodynamics <u>Assigned:</u> AEDC
Dr. Samuel Noodleman Adjunct Professor University of Arizona Dept. of Electrical Engineering Tucson, AZ 85721 (602) 626-5210	<u>Degree:</u> B.S., Electrical Engineering, 1937 <u>Specialty:</u> Electric Machines, Rare Earth Magnet Materials <u>Assigned:</u> APL

1981 USAF/SCEEE SUMMER FACULTY RESEARCH PROGRAM

LIST OF PARTICIPANTS

Page 9

NAME/ADDRESS	DEGREE, SPECIALTY, LABORATORY ASSIGNMENT
Dr. William N. Norton Assistant Professor Southeastern LA University Biology Department Box 335 Hammond, LA 70402 (504) 549-2173	Degree: PhD, Entomology, 1975 Specialty: Electron Microscopy, Insect Physiology, Cell Biology, Histology Assigned: AMRL
Dr. Alan H. Nye Assistant Professor Rochester Institute of Technology Mechanical Engineering Dept. 1 Lomb Memorial Drive Rochester, NY 14623 (716) 475-6663	Degree: PhD, MEchanical & Aerospace Science, 1975 Specialty: Solar Magnetohydrodynamics Assigned: GL
Dr. Thomas E. Nygren Assistant Professor Ohio State University Dept. of Psychology 404C W. 17th Avenue Columbus, OH 43210 (614) 422-2935	Degree: PhD, Quantitative Psychology, 1975 Specialty: Measurement & Scaling; Mathe- matical Models of Decision Making Assigned: AMRL
Dr. William W. Payne Associate Professor Virginia Military Institute Civil Engineering Dept. Lexington, VA 24450 (703) 463-6331	Degree: PhD, Civil Engineering, 1976 Specialty: Structural Design & Analysis Assigned: ESC
Dr. John E. Powell Professor University of South Dakota School of Business Dept. of Mathematics Vermillion, SD 57069 (605) 677-5231	Degree: DBA, Quantitative Business Analysis, 1972 Specialty: Computer Applications to Business Assigned: LC
Dr. Robert H. Puckett Professor Indiana State University Dept. of Political Science Terre Haute, IN 47809 (812) 232-6311 X 2591	Degree: PhD, Political Science, 1961 Specialty: US Foreign Policy; American National Security Policy Assigned: AL
Dr. G. Frederic Reynolds Professor Michigan Technological University Dept. of Chemical & Chemical Engineering Houghton, MI 49931 (906) 487-2054	Degree: PhD, Chemistry, 1959 Specialty: Physical Chemistry (Spectroscopy) of Organic Molecules Assigned: EISRL

1981 USAF/SCEE SUMMER FACULTY RESEARCH PROGRAM

LIST OF PARTICIPANTS

Page 10

NAME/ADDRESS	DEGREE, SPECIALTY, LABORATORY ASSIGNMENT
Dr. Richard O. Richter Assistant Professor Washington University Civil & Environmental Engineering Pullman, WA 99164 (509) 335-2147/3175	<u>Degree:</u> PhD, Chemistry, 1959 <u>Specialty:</u> Physical Chemistry (Spectroscopy) of Organic Molecules <u>Assigned:</u> ESC
Dr. John J. Riggs Assistant Professor Tuskegee Institute Dept. of Pharmacology School of Veterinary Medicine Tuskegee Institute, AL 36088 (205) 727-8471	<u>Degree:</u> PhD, Pharmacology, 1976 <u>Specialty:</u> Cardiovascular Pharmacology <u>Assigned:</u> AMRL
Dr. Edward J. Rinalducci Professor GIT Dept. of Psychology Atlanta, GA 30332 (404) 894-4260/2680	<u>Degree:</u> PhD, Experimental Psychology, 1966 <u>Specialty:</u> Vision & Visual Perception, Engineering Psychology <u>Assigned:</u> HRL (Williams)
Dr. John M. Roberts Professor Rice University Dept. of Mechanical Engineering & Mathematical Science P.O. Box 1892 Houston, Texas 77001 (713) 527-8101 X3590	<u>Degree:</u> PhD, Metallurgical Engineering, 1960 <u>Specialty:</u> Elastic-Anelastic & Plastic Deformation of Materials <u>Assigned:</u> APL
Dr. Thomas A. Roth Associate Professor Kansas State University Dept. of Chemical Engineering Durland Hall Manhattan, KS 66506 (913) 532-5584	<u>Degree:</u> PhD, Metallurgical Engineering, 1967 <u>Specialty:</u> Metallurgical Engineering <u>Assigned:</u> ML
Dr. Charles D. Sanders Professor Coppin State College Dept. of Psychology 2500 W. North Ave. Baltimore, MD 21216 (301) 383-7410	<u>Degree:</u> PhD, Education & Counseling Psychology <u>Specialty:</u> Psychological Measurement & Evaluation <u>Assigned:</u> HRL (Williams)
Dr. Sarwan S. Sandhu Assistant Professor University of Dayton Chemical Engineering Dept. 300 College Park Ave. Dayton, OH 45469 (513) 229-2627	<u>Degree:</u> Chemical Engineering, Combustion, 1973 <u>Specialty:</u> Combustion, Heat Transfer, Effect Electrical Fields on Heat Transfer Kinetics, Thermodynamics & Laser Interferometry <u>Assigned:</u> APL

1981 USAF/SCEEE SUMMER FACULTY RESEARCH PROGRAM

LIST OF PARTICIPANTS

Page 11

NAME/ADDRESS	Degree, Specialty, Laboratory Assignment
Dr. Gerald W. Simila Assistant Professor California State University/Northridge Dept. of Geological Science 18111 Nordhoff St. Northridge, CA 91330 (213) 885-3541	<u>Degree:</u> PhD, Geophysics, 1980 <u>Specialty:</u> Seismology <u>Assigned:</u> WL
Dr. Vina Y. Sloan Professor Eastern Washington University Accounting & Decision Science Dept. 201 Kingston Hall Cheney, WA 99004 (509) 359-7972	<u>Degree:</u> MS, Industrial Engineering, 1981 <u>Specialty:</u> Operations Research Techniques; Corporate Planning <u>Assigned:</u> HRL (Williams)
Dr. Russell W. Smith Assistant Professor N. Texas State University Political Science Dept. Box 5338, NT Station Denton, Texas 76203 (817) 788-2321/2356	<u>Degree:</u> PhD, Political Science/Public Admin- istration, 1976 <u>Specialty:</u> Management <u>Assigned:</u> RPL
Dr. Stanley L. Spiegel Assistant Professor University of Lowell Mathematical Dept. One University Ave. Lowell, MA 01854 (617) 452-5000 X 2512	<u>Degree:</u> PhD, Physics, 1966 <u>Specialty:</u> Numerical Modeling & Computer Simulation <u>Assigned:</u> GL
Dr. Alan K. Stiffler Associate Professor Mississippi State University Dept. of Mechanical Engineering Drawer ME Mississippi State, MS 39762 (601) 325-3260	<u>Degree:</u> PhD, Mechanical Engineering, 1971 <u>Specialty:</u> Fluid Mechanics <u>Assigned:</u> AD
Dr. Lawrence Suchow Professor NJ Institute of Technology Dept. of Chemistry 323 High Street Newark, NJ 07102 (201) 645-5389	<u>Degree:</u> PhD, Chemistry, 1951 <u>Specialty:</u> Solid State Inorganic Chemistry <u>Assigned:</u> RADC (Hanscom)
Dr. Patrick J. Sweeney Associate Professor University of Dayton Engineering Management Dept. Kl. 361 300 College Park Dayton, OH 45469 (513) 229-2238	<u>Degree:</u> PhD, Mechanical Engineering, 1977 <u>Specialty:</u> OPS Research, Quality, Statistics <u>Assigned:</u> BRMC

1981 USAF/SCEEE SUMMER FACULTY RESEARCH PROGRAM

LIST OF PARTICIPANTS

Page 12

NAME/ADDRESS	DEGREE, SPECIALTY, LABORATORY ASSIGNED
Dr. Charles J. Teplitz Assistant Professor SUNY/ALBANY Dept. of Operations Management School of Business Albany, NY 12222 (518) 457-4951	<u>Degree:</u> DBA, Decision Science, 1980 <u>Specialty:</u> Operations Management & Physical Distribution <u>Assigned:</u> HRL (Wright-Patterson)
Dr. Albert N. Thompson Assistant Professor Fayetteville State University Dept. of Chemistry Fayetteville, NC 28301 (919) 486-1684	<u>Degree:</u> PhD, Inorganic Chemistry, 1978 <u>Specialty:</u> Porphyrins & Metalloporphyrins <u>Assigned:</u> SAM
Dr. Arthur R. Thorbjornsen Associate Professor University of Toledo Dept. of Electrical Engineering 2801 W. Bancroft Street Toledo, OH 43606 (419) 537-2406/2638	<u>Degree:</u> PhD, Electrical Engineering, 1972 <u>Specialty:</u> Computer aided design of integrated circuits, IC device modeling <u>Assigned:</u> AL
Dr. Richard M. Van Slyke Professor Stevens Institute of Technology Dept. of Electrical Engineering & Computer Science Hoboken, NJ 07030 (201) 420-5606	<u>Degree:</u> PhD, Operations Research, 1965 <u>Specialty:</u> Information Systems <u>Assigned:</u> ESD
Dr. Venugopal S. Veerasamy Assistant Professor Tennessee State University Dept. of Mechanical Engineering Downtown Campus Nashville, TN 37203 (615) 251-1513	<u>Degree:</u> PhD, Mechanical Engineering, 1980 <u>Specialty:</u> Propulsion Engineering, Thermal Sciences, Aeroacoustics <u>Assigned:</u> AEDC
Dr. M.C. Wang Associate Professor Pennsylvania State University Civil Engineering Dept. 212 Sackett Building University Park, PA 16802 (814) 863-0026	<u>Degree:</u> PhD, Geotechnical Engineering, 1968 <u>Specialty:</u> Geotechnical Engineering & Pavement Design <u>Assigned:</u> ESC
Dr. Alice Ward Assistant Professor Southern University/Baton Rouge Dept. of Biology P.O. Box 11068 Baton Rouge, LA 70813 (504) 771-5210	<u>Degree:</u> PhD, Cellular, Molecular, & Develop- mental Biology, 1975 <u>Specialty:</u> Cell Biology <u>Assigned:</u> SAM

LIST OF PARTICIPANTS

Page 13

NAME/ADDRESS

DEGREE, SPECIALTY, LABORATORY
ASSIGNED

Dr. Brenton J. Watkins
Assistant Professor
University of Alaska
Geophysical Institute
Fairbanks, AK 99701
(907) 479-7479

Degree: PhD, Geophysics, 1976
Specialty: Troposphere & Stratosphere
turbulence studies with high power
radar also incoherent scatter radar
ionospheric research
Assigned: GL

Dr. Hsi-Han Yeh
Associate Professor
University of Kentucky
Dept. of Electrical Engineering
Lexington, KY 40506
(606) 258-4649

Degree: PhD, Electrical Engineering, 1967
Specialty: Modern Control Theory
Assigned: FDL

Dr. Robert L. Yolton
Assistant Professor, Director
Pacific University
Dept. of Optometry
Forest Grove, OR 97116
(503) 357-6151 X 272

Degree: PhD, Psychology, 1975
Specialty: Visual System Function & Analysis
Assigned: SAM

Dr. Poh Shien Young
Associate Professor
Mississippi State University
Physics Dept.
Mississippi State, MS 39762
(601) 325-2806

Degree: PhD, Physics, 1966
Specialty: Space Physics, Cosmic Rays,
Mathematical Physics, Orbital
Determination, Optimal Control
Assigned: AD

PARTICIPANT LABORATORY ASSIGNMENT

1981 USAF/SCEEE SUMMER FACULTY RESEARCH PROGRAM

- APL AERO PROPULSION LABORATORY
(Wright-Patterson Air Force Base)
1. Dr. Glenn Fanslow - Iowa State University
 2. Dr. Dennis Flentge - Cedarville College
 3. Dr. Vijay Gupta - Central State University
 4. Dr. Samuel Noodleman - University of Arizona
 5. Dr. John Roberts - Rice University
 6. Dr. Sarwan Sandhu - University of Dayton
- AMRL AEROSPACE MEDICAL RESEARCH LABORATORY
(Wright-Patterson Air Force Base)
1. Dr. Louis Buckalew - Alabama A & M University
 2. Dr. Franklin Hill - Grambling State University
 3. Dr. Donald McCoy - University of Kentucky
 4. Dr. William Norton - Southern Louisiana University
 5. Dr. Thomas Nygren - Ohio State University
 6. Dr. John Riggs - Tuskegee Institute
- AD ARMAMENT DIVISION
(Eglin Air Force Base)
1. Dr. Hugh Coleman - Mississippi State University
 2. Dr. Kenneth Hall - Mississippi State University
 3. Dr. Robert Harnett - Clemson University
 4. Dr. Stanley Jones - University of Kentucky
 5. Dr. Alan Stiffler - Mississippi State University
 6. Dr. Poh Shien Young - Mississippi State University
- AEDC ARNOLD ENGINEERING DEVELOPMENT CENTER
(Arnold Air Force Station)
1. Dr. Eugene Niemi - University of Lowell
 2. Dr. Venugopal Veerasamy - Tennessee State University
- AL AVIONICS LABORATORY
(Wright-Patterson Air Force Base)
1. Dr. David Allender - Kent State University
 2. Dr. David Cozart - The Citadel
 3. Dr. John Fleming - Texas A & M University
 4. Dr. Gurmohan Grewal - Southern University/Baton Rouge
 5. Dr. Richard Kwor - University of Notre Dame
 6. Dr. William McCormick - Wright State University
 7. Dr. Robert Puckett - Indiana State University
 8. Dr. Arthur Thorbjornsen - University of Toledo
- BRMC BUSINESS RESEARCH MANAGEMENT CENTER
(Wright-Patterson Air Force Base)
1. Dr. Harold Fox - Ball State University
 2. Dr. Patrick Sweeney - University of Dayton
- ESMC EASTERN SPACE & MISSILE CENTER
(Patrick Air Force Base)
1. Dr. Junho Choi - Florida Institute of Technology

PARTICIPANT LABORATORY ASSIGNMENT (Continued)

ESD ELECTRONIC SYSTEMS DIVISION
(Hanscom Air Force Base)
 1. Dr. Richard Van Slyke - Stevens Institute of Technology

ESC ENGINEERING & SERVICES CENTER
(Tyndall Air Force Base)
 1. Dr. Robert Carlson - Kent State University
 2. Dr. William Payne - Virginia Military Institute
 3. Dr. Richard Richter - Washington State University
 4. Dr. M. C. Wang - Pennsylvania State University

FDL FLIGHT DYNAMICS LABORATORY
(Wright-Patterson Air Force Base)
 1. Dr. Patrick McKenna - University of Florida
 2. Dr. David Miller - Wright State University
 3. Dr. Levon Minnetyan - Clarkson College
 4. Dr. Hsi-Han Yeh - University of Kentucky

FJSRL FRANK J. SEILER RESEARCH LABORATORY
(USAF Academy)
 1. Dr. Larry Dalton - SUNY/Stony Brook
 2. Dr. Peter Freymuth - University of Colorado
 3. Dr. Frederic Reynolds - Michigan Technological University

GL GEOPHYSICS LABORATORY
(Hanscom Air Force Base)
 1. Dr. Carol Deakyne - College of the Holy Cross
 2. Dr. Ronney Harris - Utah State University
 3. Dr. Steven Newman - Central Community State College
 4. Dr. Alan Nye - Rochester Institute of Technology
 5. Dr. Stanley Spiegel - University of Lowell
 6. Dr. Brenton Watkins - University of Alaska

HRL/ASD HUMAN RESOURCES LABORATORY/ADVANCED SYSTEMS DIVISION
(Wright-Patterson Air Force Base)
 1. Dr. Charles Teplitz - SUNY/Albany

HRL/FTD HUMAN RESOURCES LABORATORY/FLYING TRAINING DIVISION
(Williams Air Force Base)
 1. Dr. Edward Rinalducci - Georgia Institute of Technology
 2. Dr. Charles Sanders - Coppin State College
 3. Dr. Vina Sloan - Eastern Washington University

HRL/PRD HUMAN RESOURCES LABORATORY/PERSONAL RESEARCH DIVISION
(Brooks Air Force Base)

HRL/TTD HUMAN RESOURCES LABORATORY/TECHNICAL TRAINING DIVISION
(Lowry Air Force Base)
 1. Dr. David Carlson - University of Massachusetts/Amherst

LMDC LEADERSHIP & MANAGEMENT DEVELOPMENT CENTER
(Maxwell Air Force Base)
 1. Dr. Chris Eskridge - University of Nebraska/Lincoln

PARTICIPANT LABORATORY ASSIGNMENT (Continued)

LC LOGISTICS COMMAND
(Wright-Patterson Air Force Base)
1. Dr. John Powell - University of South Dakota

LMC LOGISTICS MANAGEMENT CENTER
(Gunter Air Force Base)
1. Dr. Milton Alexander - Auburn University
2. Dr. Louis Martin-Vega - University of Florida

ML MATERIALS LABORATORY
(Wright-Patterson Air Force Base)
1. Dr. Robert Cunningham - Kent State University
2. Dr. William Feld - Wright State University
3. Dr. Joel Fried - University of Cincinnati
4. Dr. Richard Liu - Purdue University
5. Dr. William McCain - Tennessee State University
6. Dr. Thomas Roth - Kansas State University

RPL ROCKET PROPULSION LABORATORY
(Edwards Air Force Base)
1. Dr. Jay Benziger - Princeton University
2. Dr. Gale Buzzard - Duke University
3. Dr. Donald Emerich - Mississippi State University
4. Dr. Russell Smith - North Texas State University

RADC ROME AIR DEVELOPMENT CENTER
(Griffiss Air Force Base)
1. Dr. Aloysius Beex - Virginia Polytechnic Institute &
State University
2. Dr. Jerome Braverman - Rider College
3. Dr. Paul Griesacker - Cannon University

RADC/ET ROME AIR DEVELOPMENT CENTER/ELECTRONICS TECHNOLOGY
(Hanscom Air Force Base)
1. Dr. William Bradley - University of Alabama/Huntsville
2. Dr. Lawrence Suchow - New Jersey Institute of Technology

SAM SCHOOL OF AEROSPACE MEDICINE
(Brooks Air Force Base)
1. Dr. Martin Altschuler - SUNY/Buffalo
2. Dr. Charles Davis - University of Toledo
3. Dr. David Greene - Texas A & M University
4. Dr. Kishan Mehrotra - Syracuse University
5. Dr. Rex Moyer - Trinity University
6. Dr. Albert Thompson - Fayetteville State University
7. Dr. Alice Ward - Southern University/Baton Rouge
8. Dr. Robert Yolton - Pacific University

WL WEAPONS LABORATORY
(Kirtland Air Force Base)
1. Dr. Albert Biggs - University of Kansas
2. Dr. Francis Jankowski - Wright State University
3. Dr. Paul Kalata - Drexel University
4. Dr. Henry McGee - Virginia Polytechnic Institute &
State University

PARTICIPANT LABORATORY ASSIGNMENT (Continued)

WL

WEAPONS LABORATORY (Continued)
(Kirtland Air Force Base)

5. Dr. John McNeil - New Mexico State University
6. Dr. Gerald Simla - California State University/Northridge

RESEARCH REPORTS

1981 USAF-SCEEE SUMMER FACULTY RESEARCH PROGRAM

<u>Volume I</u> <u>Report No.</u>	<u>Title</u>	<u>Research Associate</u>
1	The Determination of Input Data Accuracy in the Maintenance Data Collection System	Dr. Milton J. Alexander
2	Superconducting Pair Binding Energy in Degenerate Fermi Systems	Dr. David W. Allender
3	Software for Rapid Remote 3-D Mapping of an Arbitrarily-Complex Object	Dr. Martin D. Altschuler
4	Enhanced Scene Resolution: 2-D Spectral Estimator Approaches	Dr. A.A. Beex
5	Decomposition of Nitromethane Over Metal Oxide Catalysts	Dr. Jay B. Benziger
6	Interaction Between an Electromagnetic Pulse and a Metal Cylinder Connected to a Parallel Plate Guide by a Wire	Dr. Albert W. Biggs
7	Electromagnetic Scattering From Dielectric and Composite Bodies	Dr. William G. Bradley
8	An Investigation of Nonparametric Maintainability and Reliability Test Procedures	Dr. Jerome D. Braverman
9	Environmental Effects on Affect and Psychomotor Performance	Dr. Louis W. Buckalew
10	Thermal Analysis of a Rocket Engine Altitude Test Facility Diffuser	Dr. Gale H. Buzzard
11	Rehosting the Advanced Instructional System	Dr. David A. Carlson
12	The Biological Degradation of Spilled Jet Fuels; A Literature Review	Dr. Robert E. Carlson
13	On-Axis Kalman Tracking Filter for U.S. Vandenberg Aris Systems	Dr. Junho Choi
14	Rough Surface Effects on Turbulent Boundary Layers	Dr. Hugh W. Coleman
15	Interpolation and Approximation Techniques for Gridded Terrain Data	Dr. David L. Cozart
16	Epitaxial Layer Evaluation of III-V Semiconductor Materials	Dr. Robert W. Cunningham

RESEARCH REPORTS (Continued)

<u>Report No.</u>	<u>Title</u>	<u>Research Associate</u>
17	(A) Spectroscopic Analysis and Optimization of the Oxygen/Iodine Chemical Laser and (B) Aluminum-27 NMR of Dialkylimidazolium Chloroaluminate Molten Salts	Dr. Larry R. Dalton
18	Some Aspects of Cardiac Risk Evaluation at the USAF School of Aerospace Medicine	Dr. Charles B. Davis
19	A Molecular Orbital Study of NO_3^- , H_2O , OH^- , HNO_3 , AND $\text{H}^+(\text{H}_2\text{O})_m(\text{CH}_3\text{CN})_k$ Cluster Ions	Dr. Carol A. Deakyne
20	Analysis of Several Solid Propellant Stabilizers by DC Polarographic Techniques	Dr. Donald W. Emerich
21	The Impact of Background Characteristics on OAP Test Scores: Developing Baseline Information	Dr. Chris W. Eskridge
22	Radiation Signatures From a Space Power System	Dr. Glenn E. Fanslow
23	Acetylene Terminated Systems: Quinoxalines and Isomeric Sulfones	Dr. William A. Feld
24	A Simulation Framework for the Evaluation of Terrain Following and Terrain Avoidance Techniques	Dr. John A. Fleming
25	Voltametric Studies of the Lithium/Vanadium Oxide Electrochemical Cell	Dr. Dennis R. Flentge
26	Project IMP: Institutionalization Methods and Policies at the Business Research Management Center	Dr. Harold Fox
27	Some Problems of Laser Velocimetry and Unsteady Aerodynamics of Current Interest to the Frank J. Seiler Research Laboratory	Dr. Peter Freymuth
28	Effects of Cloth Substrate and Finish on the Nitrogen Cure of Acetylene Terminated Sulfone (ATS) by Torsion Impregnated Cloth Analysis (TICA)	Dr. Joel R. Fried
29	Application of Conjoint Measurement Theory to the Quantification of Subjective Ratings	Dr. David E. Greene
30	Sensor Noise and Kalman Filter for Aided Inertial Navigation System	Dr. Gurmohan S. Grewal
31	Calibration of Wideband Optical Signal Processor	Dr. Paul B. Griesacker
32	Corrosion Studies of Calcium-Thionyl Chloride Electrolyte Systems	Dr. Vijay K. Gupta

RESEARCH REPORTS (Continued)

<u>Report No.</u>	<u>Title</u>	<u>Research Associate</u>
33	An Investigation Into State Estimation for Air-to-Air Missiles	Dr. Kenneth R. Hall
34	Optimal Recovery From Cratering Attacks on Airbase Prepared Surfaces	Dr. R. Michael Harnett
35	Infrared Clutter: Effects of Air Motion Produced by Auroral Zone Joule Heating	Dr. Ronney D. Harris
36	Catabolism of Toluene in the Bluegill Sunfish	Dr. Franklin D. Hill
37	Studies of the Engineering Design Process: Design of Explosively Driven Generators; Human Factors in Hazardous Activities	Dr. Francis Jankowski
38	Impact of Cylindrical Rods on Rigid Boundaries	Dr. Stanley E. Jones
39	An Information-Theoretic Approach to Target Estimation of a Conical Scan Controlled Laser Radar Tracking System	Dr. Paul Kalata
40	Electrical Characterization of Ion Implantation in GaAs	Dr. Richard Kwor
41	A Review of Current Data Base Systems for Flexible Manufacturing	Dr. Richard Liu
<u>Volume II</u>		
42	Homogeneous Compression of Rapidly Solidified Alumina, Powder Alloy Billets	Dr. William S. McCain
43	Imaging Radar Autofocus Update of an Inertial Navigation System by Means of a Kalman Filter	Dr. William S. McCormick
44	The Utility of the Animal Model Concept	Dr. Donald F. McCoy
45	Vibration-Rotation Relaxation in the HF Laser	Dr. Henry McGee
46	Appropriate Far-Field Boundary Conditions for the Numerical Solution of the Navier-Stokes Equations	Dr. Patrick J. McKenna
47	Constituent Monitoring of Evaporation Source Plumes	Dr. J. R. McNeil
48	Development of a Computer Assisted Aircraft Load Planning Model	Dr. Louis A. Martin-Vega
49	A Model for CATH Data and Some Results on the Arbitrary Right Censored Data	Dr. Kishan G. Mehrotra
50	A Direct State Space Approach to the Control of Sampled-Data Systems	Dr. David F. Miller

RESEARCH REPORTS (Continued)

<u>Report No.</u>	<u>Title</u>	<u>Research Associate</u>
51	Transient Analysis of Structures with Distinct Nonlinearities	Dr. Levon Minnetyan
52	Plasmid Fingerprints of Staphylococcus Aureus Strains Isolated From a Toxic Shock Syndrome Female Patient	Dr. Rex C. Moyer
53	An Investigation Into the Nature of the Melting Layer in Stratiform Clouds	Dr. Steven B. Newman
54	Jet Simulation Parameters for Wind Tunnel Model Thrust Reverser Testing	Dr. Eugene E. Niemi, Jr.
55	Analysis of the 60 KVA Permanent Magnet Alternator and a New Rotor Concept for these Type Machines	Dr. Samuel Noodleman
56	The Effects of JP-4 Aviation Fuel on Specific Internal Organs of the Fat-Head Minnow, Pimephale Promelus	Dr. William N. Norton
57	Observations of Sunspot Dynamics and Theoretical Effects of Inhomogeneities in the Solar Convection Zone	Dr. Alan H. Nye
58	Development of a Manual of use for Conjoint Scaling Techniques	Dr. Thomas E. Nygren
59	Evaluation of Nastran to Predict the Dynamic Response of Reinforced Concrete	Dr. William W. Payne, Jr.
60	An Analysis of the Availability, Accessibility and Timeliness of Cost Data Associated with the AFLC Aircraft Modification System with Emphasis on Class IV Modifications	Dr. John E. Powell
61	The Air Force Wright Aeronautical Laboratories Research and Development Planning Process	Dr. Robert H. Puckett
62	Coupling Reactions and Rearrangements of 1,3,5-Triazines	Dr. G. Frederic Reynolds
63	Adsorption of Trichloroethylene by Soils from Dilute Aqueous Systems	Dr. Richard O. Richter
64	The Effects of 2,3,7,8-Tetrachlorodibenzo-p-Dioxin (TCDD) Triiodothyronine (T ₃) Binding to Rat Isolated Hepatic Nuclei	Dr. John J. Riggs
65	Visual Cues in the Simulation of Low Level Flight	Dr. Edward J. Rinalducci

RESEARCH REPORTS (Continued)

<u>Report No.</u>	<u>Title</u>	<u>Research Associate</u>
66	A Metallurgical Investigation of the Internal Bronze Manufacturing Process of NB_3Sn Superconducting Wire	Dr. John M. Roberts
67	Investigation of the Mechanical Properties of Less Than 100% Dense Titanium Powder Metallurgy Compacts	Dr. Thomas Roth
68	Application of Task Analytic Techniques to the Design of a Flight Simulator Instructor/Operator Console	Dr. Charles D. Sanders
69	Study of Dynamic Behavior of a Bluff-Body Diffusion Flame in the APL Combustion Tunnel Facility	Dr. Sarwan S. Sandhu
70	Shear-Wave Velocity Structure Determined From Analysis Rayleigh-Wave Group-Velocity Dispersion	Dr. Gerald W. Simila
71	Operating Various Subsystems of the Total Simulation Systems for Flight Training	Dr. Vina Sloan
72	Enhancing Career Development at the Air Force Rocket Propulsion Laboratory	Dr. Russ Smith
73	Development of a Computer Algorithm for the Automatic Determination of Space Vehicle Potential Utilizing Electrostatic Analyzer Measurements	Dr. Stanley L. Spiegel
74	Plastic Rotating Band Loads and Sliding Resistance Forces	Dr. A. Kent Stiffler
75	Binary and Ternary Compositions and their Physical Properties	Dr. Lawrence Suchow
76	A System Dynamics Model of the Acquisition Process	Dr. Patrick J. Sweeney
77	Analysis of Maintenance Decisions at Lower Echelon Levels Involving Jet Aircraft Engines	Dr. Charles J. Teplitz
78	A Study of the Interaction of Hydrazine Methylhydrazine and Unsymdimethylhydrazine with Porphyrins, Metalloporphyrins, and some Metal Coordination Compounds	Dr. Albert N. Thompson
79	GaAs Mesfet Modeling	Dr. Arthur A. Thorbjornsen
80	Covering Problems in C^3I Systems	Dr. Richard Van Slyke
81	Effects of Acoustic Disturbances on the Boundary-Layer Transition in AEDC Wind Tunnels	Dr. Venugopal Veerasamy

RESEARCH REPORTS (Continued)

<u>Report No.</u>	<u>Title</u>	<u>Research Associate</u>
82	An Evaluation of Air Force Pavement Non-Destructive Testing Method	Dr. M.C. Wang
83	The Effect of One Hundred Percent Oxygen at One ATA and Increased Pressure on the Metabolism of an Organphosphate (Parathion) in the Rat	Dr. Alice Ward
84	Measurements of Turbulence in the Troposphere and Lower Stratosphere using the Millstone Hill 440 MHZ Radar	Dr. Brenton J. Watkins
85	Optimal Design of Digital Flight Control Systems Following an Analog Model	Dr. Hsi-Han Yeh
86	Amplitude Variability of the Steady State Visual Evoked Response	Dr. Robert L. Yolton
87	New Tests of Theories on Shaped Charge	Dr. Poh Shien Young

1981 USAF - SCEE SUMMER FACULTY RESEARCH PROGRAM

Sponsored by the

AIR FORCE OFFICE OF SCIENTIFIC RESEARCH

Conducted by the

SOUTHEASTERN CENTER FOR ELECTRICAL ENGINEERING EDUCATION

FINAL REPORT

HOMOGENEOUS COMPRESSION OF RAPIDLY SOLIDIFIED

ALUMINUM POWDER ALLOY BILLETS.

Prepared by:	Dr. William S. McCain
Academic Rank:	Assistant Professor
Department and University:	Mechanical Engineering Tennessee State University
Research Location:	Air Force Wright Aeronautical Laboratories, Materials Laboratory, Metals and Ceramics Division
USAF Research Colleague	Dr. H. L. Gegel
Date:	September 18, 1981
Contract No:	F49620 - 79 - C _ 0038

HOMOGENEOUS COMPRESSION OF RAPIDLY SOLIDIFIED

ALUMINUM POWDER ALLOY BILLETS

by

William S. McCain

ABSTRACT

A program to collect data required for developing constitutive equations for compressible solids was initiated. Billets of partially dense, rapidly solidified aluminum alloy CT-91(x7091) were warm and hot compressed under homogeneous strain conditions to develop flow curves and strain rate sensitivity data. These data are to form the basis for further work in materials behavior modeling, process modeling and process model validation.

ACKNOWLEDGEMENTS

The author wishes to express his appreciation to Air Force Systems Command, the Air Force Office of Scientific Research and the Materials Laboratory of AFWAL. In particular, he would like to express his appreciation to SCEE for making this Research Project possible. To Dr. Harold Gegel he would like to bestow his undying gratitude for being such an admirable Research Colleague. In addition, he wants to thank Jim Morgan and Jim Malas both of the Processing and High Temperature Materials Branch and Professor J.F. Thomas of Wright State University for the extra efforts they all made on his behalf.

Finally, a special debt of gratitude is due NRC Fellow Dr. S.M. Doravelu for his help in introducing the author to many new areas of interest.

1. INTRODUCTION:

The U.S. forging industry is comprised of approximately 300 companies with \$6 billion in annual sales and 75,000 employees. Productivity in this industry is vital for the nation's needs in transportation(automotive, aircraft), defense(ammunition, aerospace), and energy(drilling, turbines) areas. Research in aerospace technology has emphasized near net shape technology which includes such unit operations as powder metallurgy(P/M) produced preforms, hot die and isothermal forging and conventional forging.

In defining the goals of the Material Laboratory, the following observations were considered:

(a) Costs and availability of energy and materials are a problem for the entire industry.

(b) In conventional hot impression-die forging about 50% of the cost of forging is due to material utilization. On the average, nearly 30% of the incoming material, i.e., 15% of the forging costs, is lost into the flash as scrap. Thus, the trend is to forge flashless to near net dimensions. This requires innovation and improved engineering.

(c) Skilled die designers and die makers are key to a successful forge shop operation. However, according to the Forging Industry Association, there is and will continue to be a shortage of die makers. Therefore, CAD/CAM techniques must be developed and utilized to increase the productivity of die making.

(d) Often in the development of a forging process for a new part, extensive and expensive die trials and modifications are necessary.

A scientific understanding of metal flow and use mathematical methods for designing forging processes is not widely accepted in the industry. Most of current process development is by trial-and-error.

(e) The use of warm forging techniques, the temperature being dependent on the specific alloy, would benefit all of the aerospace forging companies. It would allow them to produce parts at lower total energy consumption, parts with more complex geometries and parts with controlled properties. Forging designed by metal flow analysis will also permit the design of preform shapes (blocker dies).

(f) The Metals and Ceramics Division has a major in-house and contractual program in powder metallurgy with emphasis on rapid solidification technology. Research on rapidly solidified powders has stressed alloy development with particular emphasis being given to the hardware end of the development. Very little attention has been given to processing P/M billets into precision shapes with desirable mechanical properties. This aspect of rapid solidification technology must receive increasing attention to realize the benefits of this new technology.

Based on the above observations, this work is concerned with the analytical modeling of deformation processes used to fabricate parts from P/M billet materials that may only be partially dense.

The objective of the research is to develop analytical models for metal flow analyses and microstructure/property control in compressible P/M materials. The task areas for this work are:

MATERIAL BEHAVIOR MODELING

PROCESS MODELING

PROCESS MODEL VALIDATION

The tasks on material behavior modeling and on process modeling will provide the science base and data necessary for predicting how a P/M

preform material that is not fully dense flows and compacts during shape making. The process model validation task will demonstrate the ability to predict by comparing analytical predictions with laboratory studies of metal flow and property/microstructure relationships.

11. OBJECTIVES

The objective of the project is to collect data required for developing constitutive equations and a workability model for X 7091 aluminum P/M alloy. These data will be subsequently used for developing materials behavior models for the above alloy.

111. TECHNICAL APPROACH

Previously⁽¹⁾ cold compaction, vacuum sintering and vacuum hot pressing studies had been performed to develop laboratory methods for preparing specimens or billets for subsequent mechanical property test as a function of temperature, strain rate and relative density. Procedures for producing controlled density preforms(billets) were developed, based on degassing and trial compaction experiments conducted at different combinations of pressure, temperatures and time

Using an Engstrom testing machine, continuous tests were used to generate data for constitutive equations. Specimens 15 mm by 10 mm diameter with relative densities 0.75, 0.85 and 1.0 and sintered for four hours at either 1050°F or 1100°F were used for the test. The test temperatures 200°C, 275°C, 350°C and 450°C. Strain rates covered a range from about 10^{-4} to 10^{-1} s^{-1} , a range sufficient to cover rates normally encountered during precision

forging of aluminum alloys.

To determine strain rate sensitivities, strain rates were doubled after 0.5 true plastic strain.

To insure homogeneous deformation, both ends of the billet were coated with a MoS₂ paste, and compression was carried out on smooth flat dies.

IV. RESULTS

Figures 1 and 2 are plots for true stress versus true strain. Fig. 1 at the various temperatures and Fig. 2 for different strain rates. For both figures relative densities are 0.75 and 0.85 and the sintering temperature was 1100°F. At all true strains, the flow stress for 0.85 relative density specimens is greater than that for 0.75 relative density specimens at corresponding strains. This indicates that initial relative densities influence the flow stresses. This fact must be taken into account in the development of the constitutive equations. Even in the hot working range, the flow curve still shows some hardening, which is apparently due to densification.

Figure 2 shows that at a given strain, as the flow stress increases, the strain rate sensitivity increases. This increase in flow is greater in the higher strain rate region. This behavior indicates greater rate sensitivities at the higher strain rates for compressible bodies. Fully dense or incompressible solids, on the other hand, show greater rate sensitivities at lower strain rates. The difference in this regard between compressible and incompressible bodies require further investigation to determine the deformation mechanism operative in compressible solids.

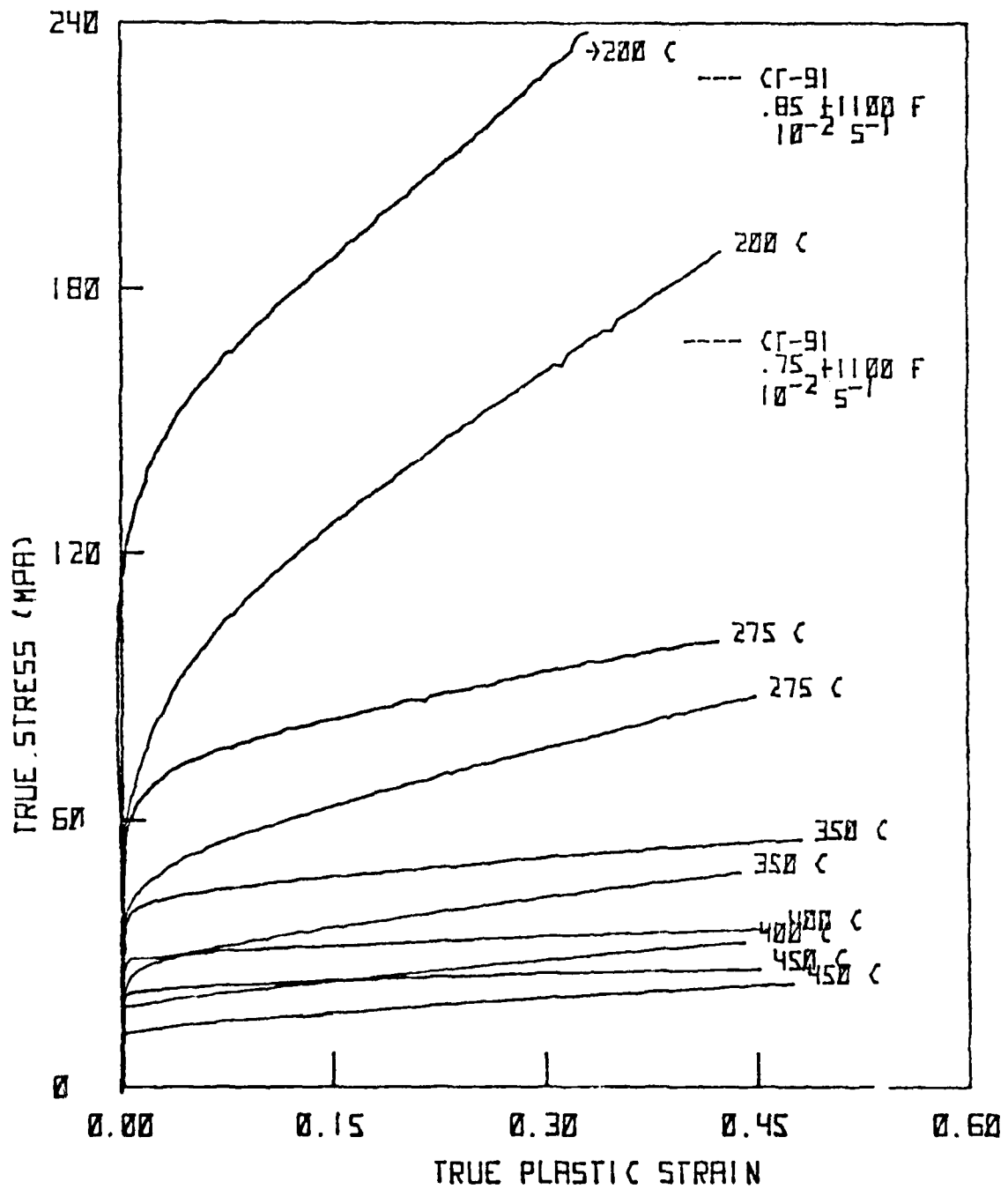


FIGURE 1. THE INFLUENCE OF COMPRESSION TEMPERATURE AND RELATIVE DENSITY ON FLOW STRESS. (1100°F SINTERING)

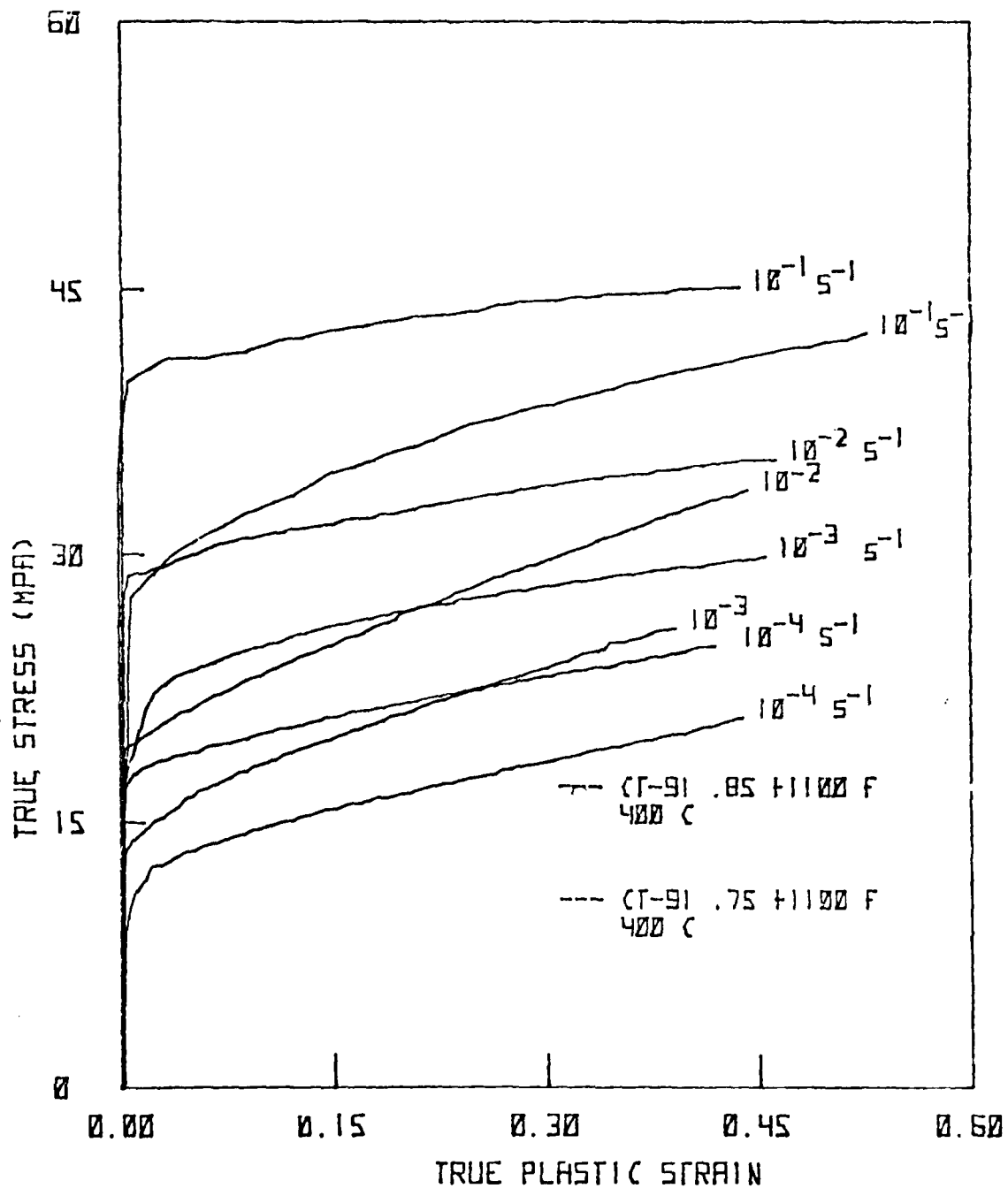


FIGURE 2. THE INFLUENCE OF STRAIN RATE AND RELATIVE DENSITY ON FLOW STRESS. (1100°F SINTERING)

Figures 3 and 4 show the flow curves for specimens sintered at 1050°F with relative densities of 0.75 and 0.85. In general, the behavior is the same as for 1100°F sintered specimens. This fact would indicate that the sintering temperatures have no appreciable influence on either flow stress or strain rate sensitivity.

V. RECOMMENDATIONS

The compression tests should be extended to samples with a relative density of 1.0 i.e., fully dense billets; after which the data can be used for developing constitutive relations among the process parameters.

Microstructure studies should be conducted to identify the deformation for the anomalous strain rate dependence of the strain rate sensitivity in CT-91 (X7071). In this regard parallel studies of the ingot metallurgy counterpart of CT-91 should also be conducted to help explain the difference in strain rate sensitivity.

The apparent lack of influence of the sintering temperature on either flow stress or rate sensitivity deserves further investigation. Sintering parameters (temperature and time) were too confined.

A broader investigation of sintering and its influence on flow stress and strain rate sensitivity would be useful in the pursuit of the optimum processing parameters for this alloy. These studies should include vacuum hot pressing at temperatures in the 975°F vicinity. The treatment times should be selected to develop several levels of relative densities.

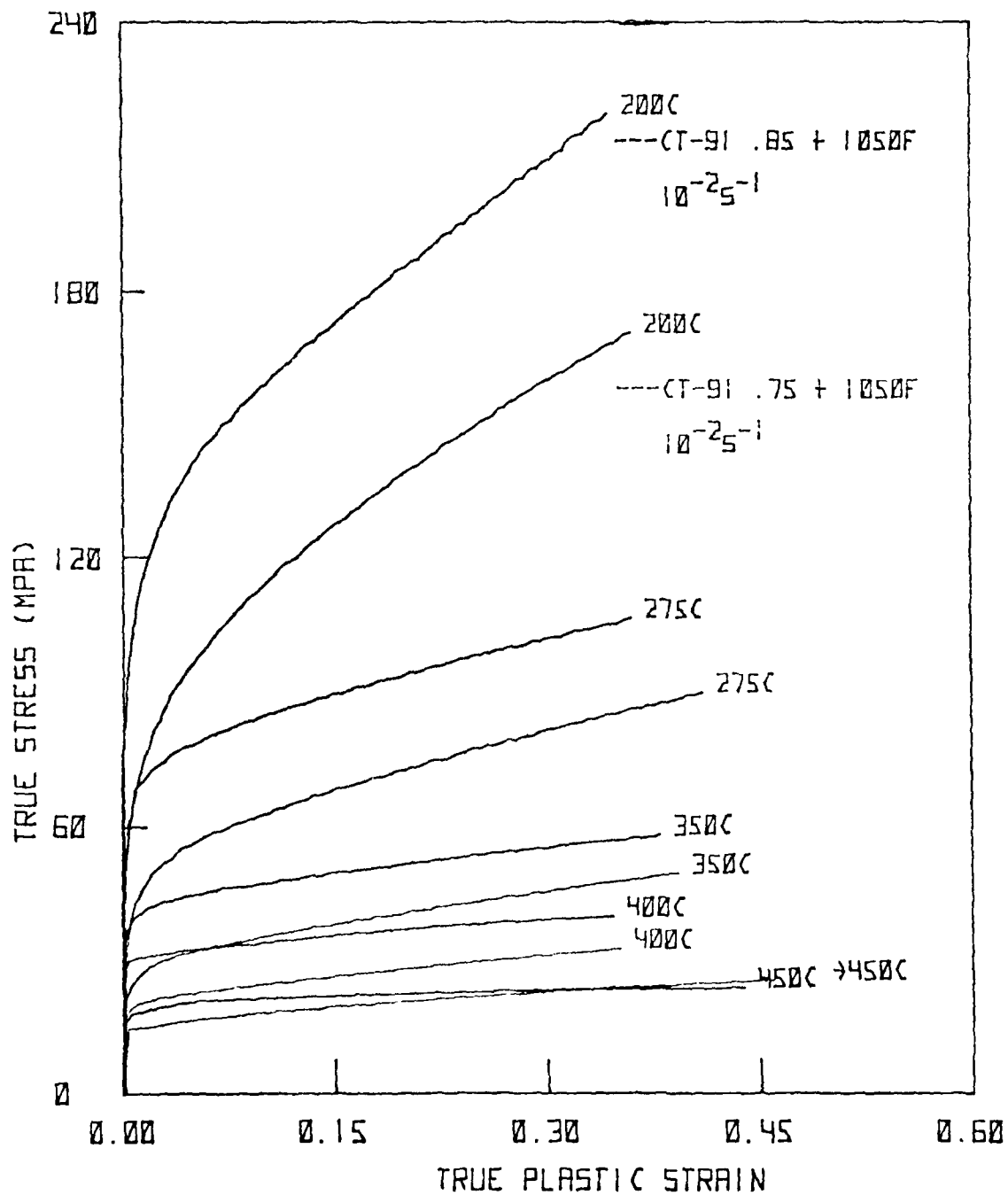


FIGURE 3. THE INFLUENCE OF COMPRESSION TEMPERATURE AND RELATIVE DENSITY ON FLOW STRESS, (1050 ° F SINTERING)

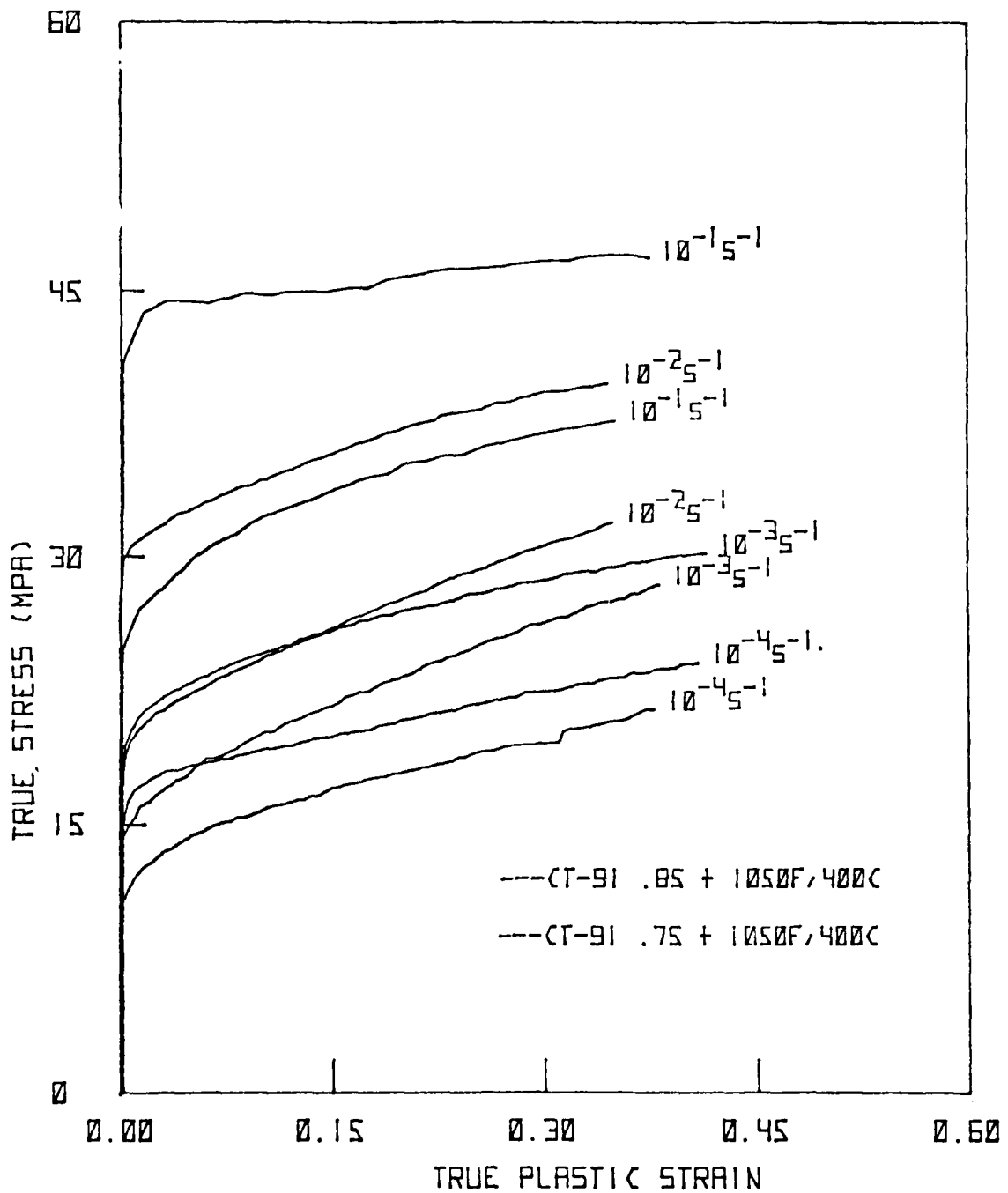


FIGURE 4. THE INFLUENCE OF STRAIN RATE AND RELATIVE DENSITY ON FLOW STRESS (1050°F SINTERING)

REFERENCES

1. J. T. Morgan, H. L. Gegel and J. C. Malas, "Consolidations of Metal Working Preforms", to be presented at The Powder Metallurgy Conference at Drexel University, September 1982.
2. Jim Morgan, "Optimization of Compact Parameters of Aluminum CT-91", Senior Design Project, Wright State University, Dayton, Ohio, June 1981.

1981 USAF - SCEEE SUMMER FACULTY RESEARCH PROGRAM

Sponsored by the

AIR FORCE OFFICE OF SCIENTIFIC RESEARCH

Conducted by the

SOUTHEASTERN CENTER FOR ELECTRICAL ENGINEERING EDUCATION

FINAL REPORT

IMAGING RADAR AUTOFOCUS UPDATE OF AN INERTIAL
NAVIGATION SYSTEM BY MEANS OF A KALMAN FILTER

Prepared by:	Dr. William S. McCormick
Academic Rank:	Associate Professor
Department and University:	Department of Engineering Wright State University
Research Location:	Air Force Avionics Laboratory, Radar RECCE Group
USAF Research Colleague:	Dr. Jack Bell
Date:	August 18, 1981
Contract No:	F49620-79-C-0038

IMAGING RADAR AUTOFOCUS UPDATE OF AN
INERTIAL NAVIGATION SYSTEM BY MEANS
OF A KALMAN FILTER

by

William S. McCormick

ABSTRACT

The value of an Autofocus update of an INS is investigated. Three cases are considered: (1) centripedal acceleration only; (2) centripedal and line-of-sight acceleration; and (3) centripedal and line-of-sight acceleration as well as attitude error effects. The extended Kalman filter configuration was employed using the versatile SOFE Monte Carlo simulation program. Measurement matrices were defined for each of the three cases. Simulation results indicated an observability problem for Case (1). Suggestion for further work was included.

ACKNOWLEDGEMENT

The author would like to thank the Air Force Systems Command, the Air Force Office of Scientific Research and the Southeastern Center for Electrical Engineering Education for providing an interesting and productive summer at the Avionics Lab of Wright Patterson Air Force Base, Dayton, Ohio.

In particular, he would like to extend special thanks to Stanton Musick, Dr. Jack Bell, and Mrs. Sandra Benning for their continued help throughout the summer.

I. INTRODUCTION

Imaging radar (SAR) has become an increasingly important all weather sensing technique for both reconnaissance and weapon delivery applications. Briefly stated, imaging radar provides high azimuth resolution by coherently processing the naturally occurring doppler return over the synthetic radar aperture. Because of the phase coherence requirement, any phase error accumulated over the aperture time will result in both a loss of resolution and a higher sidelobe level. Under normal circumstances, the radar processor will use the dynamic output of the inertial navigation system (INS) to compensate for aperture phase perturbations. Unfortunately, a typical unaided INS system will have an error state vector that increases with time until the imaging performance of the SAR radar becomes seriously degraded.

In order to correct for the uncompensated phase error, a number of iterative image restoration techniques have been developed under the generic name of "Auto-Focus" (AF) techniques. Although the details of the algorithms are proprietary, most autofocus techniques estimate various orders (e.g. quadratic, cubic, etc.) of phase error by measuring the relative displacement of a point target as processed in contiguous sub-arrays. Since the AF techniques must attempt a location estimate of a point target and since that target resolution is itself degraded by the phase error, it naturally follows that there will be a "lock-in" value for maximum accumulated phase error that must not be exceeded for successful autofocus operation. However, since the Auto-Focus algorithm is quite accurate and can essentially eliminate the phase error (provided it is operating within its "lock-in" range), it could also provide a potentially useful means of updating the INS system every aperture time. Assuming the AF scaler measurement contains adequate information on the INS error state vector, it would therefore appear possible to bound the growth of the error state vector by somehow integrating the AF measurement with the INS system. Performed optimally, such an AF update could well improve the INS-dependent SAR processor to such an extent that the AF mission time ("lock-in") is extended well beyond its present limit.

The optimal integration or augmentation of various sensors has traditionally been performed using the Kalman filter algorithm. Many

sensors¹ have been considered for INS augmentation including doppler radar, monopulse position fixing, star-trackers and loran/Omega type systems. No consideration has, however, been given to the potential value of AF algorithms as an INS update. With regard to the AF-INS Kalman filter update, a number of questions must be addressed. Some of these questions are as follows:

- (1) questions of observability or simply whether the scalar AF measurement contains enough information about the INS error state-vector to provide a useful filter update.
- (2) given the nonlinear nature of the AF measurement, the effects of trajectory dependent nonlinear noise must be considered.
- (3) since the Kalman filter will have a deleted state vector, the question of filter convergence must be investigated when the AF update is used.

II. OBJECTIVES

The principal objective of this study was to investigate the value of an "Auto-Focus" update of an INS using the Kalman filter algorithm. In particular, as discussed in Section I, the study will consider the value of the AF update as a means of extending the AF mission time or, equivalently, the time before the AF algorithm loses lock. A detailed consideration of observability, the effects of nonlinear noise and filter convergence will be considered for the following cases:

Case A: In the simplest case, only the centripetal acceleration term is considered as a contributor to quadratic phase error. This case implicitly assumes that the velocity vector is constant which is clearly an oversimplification. Since this measurement comprises only one scalar measurement and involves only 3 of the 13 state-variables, the question of observability is very important in this case.

Case B: For this case, the line of sight acceleration component is included as a source of quadratic phase error. Such a measurement is still scalar and nonlinear but now involves 9 of the 13 state-variables.

Case C: The attitude error states are included in their measurement which increases the total number of state-variables involved in the measurement to 12.

Case D: Using the complete measurement of the 12 state-variable dependent AF update of Case C, an investigation will be made into the performance degradation suffered by the Kalman filter when its measurement matrix is defined by the more computationally efficient assumptions of Cases A and B.

III. EVALUATION OF QUADRATIC PHASE ERROR

As developed in reference 2, the phase error, $\Psi(t)$, generated by aircraft motion over the aperture time can be represented in a Taylor series as,

$$\Psi(t) = \left(\frac{4\pi}{\lambda}\right) \left[R(o) + \left[\frac{\partial R(t)}{\partial t}\right]t + \left[\frac{\partial^2 R(t)}{\partial t^2}\right] \frac{t^2}{2} + \dots \right] \quad (1)$$

It is assumed in this study that the phase error is predominately low-frequency in origin and can be approximated well by neglecting the third order and higher terms of equation (1). Implicit in this statement is the assumption that both the line of sight and centripetal accelerations are constant over the aperture time. Referring to Figure 1, the centripetal acceleration component, $(V_T)^2/R$, will accumulate a quadratic phase error over an aperture time, τ , equal to

$$\Psi_{CENT}(t) = \left(\frac{4\pi}{\lambda}\right) \frac{(V_T)^2}{R} \frac{t^2}{2} \quad (2)$$

giving, with $V_T = V \sin \theta$, an accumulated phase error, of,

$$\Psi_{CENT}(t) \Big|_{t=T} = \left(\frac{2\pi}{\lambda}\right) \left[\frac{V^2 \sin^2 \theta}{\lambda R} \right] T^2 = \left(K_{CENT}\right) V^2 \quad (3)$$

where K_{CENT} is a system constant.

The line-of-sight (L.O.S.) acceleration component of $\left(\frac{4\pi}{\lambda}\right) \left(\frac{\partial^2 R}{\partial t^2}\right)$ is given by

$$\begin{aligned} \Psi_{L.O.S.}(t) &= \left(\frac{4\pi}{\lambda}\right) \left(\vec{A}_{L.O.S.} \cdot \overset{\rightarrow}{\mu}_{L.O.S.} \right) \frac{T^2}{2} \\ &= \left(K_{L.O.S.}\right) \left(\vec{A}_{L.O.S.} \cdot \overset{\rightarrow}{\mu}_{L.O.S.} \right) \end{aligned} \quad (4)$$

In the study, the assumption is also made that the antenna phase center is coincident with the body centroid of the aircraft. This assumption merely neglects the lever arm effects between phase center and body center and is quite reasonable physically; it also offers a considerable simplification since it essentially equates the aircraft (INS) and antenna reference systems.

IV. THE EXTENDED KALMAN FILTER

A voluminous literature exists on the Kalman filter. Basically, it is a minimum variance, recursive estimator that generates the optimum conditional mean estimate. In the usual continuous-discrete measurement form, the linear Kalman filter propagates the estimate, $\hat{\underline{x}}(t)$, and covariance, $P_f(t)$, according to the dynamic equations,

$$\dot{\hat{\underline{x}}}_f(t) = F(t) \hat{\underline{x}}_f(t) \quad (5)$$

and

$$\dot{P}_f(t) = F(t) P_f(t) + P_f(t) F^T(t) + Q_f(t) \quad (6)$$

where $F(t)$, $Q_f(t)$ are the filter dynamics and input noise levels respectively. At measurement time, the filter weights the new measurement according to its signal to noise properties and by the current state of knowledge of the state vector as expressed by the propagated covariance, $P_f(t)$. The measurement and update operations are defined by the gain matrix, \underline{K} , as follows:

$$\underline{K} = P_f^- H^T [H P_f^- H^T + R_f]^{-1} \quad (7)$$

$$\hat{\underline{x}}_f^+ = \hat{\underline{x}}_f^- + \underline{K} [Z_s - H \hat{\underline{x}}_f^-] \quad (8)$$

$$P_f^+ = P_f^- - \underline{K} H P_f^- \quad (9)$$

where H is the measurement sensitivity matrix, R_f is the measurement noise covariance, and Z_s is the measurement itself.

Since both the INS dynamics and the autofocus measurements are highly nonlinear, the above linear Kalman filter cannot be directly applied in the form of equation 5 through 9. Rather, the extended Kalman filter is used where the $F(t)$, $H(t)$ are now linearized about some estimated trajectory as,

$$F(t; \hat{\underline{x}}_f) = \left. \frac{\partial f(\underline{x}_f; t)}{\partial \underline{x}_f} \right|_{\underline{x}_f = \hat{\underline{x}}_f} \quad (10)$$

and

$$H(t_i; \hat{X}_f) = \frac{\partial h_f(X_f; t_i)}{\partial X_f} \Big|_{X_f = \hat{X}_f} \quad (11)$$

Figure 2 illustrates the extended Kalman filter configuration.

Although Figure 2 represents the usual or direct configuration, it is not an attractive configuration for INS applications because of the high computational requirements involved in propagating the full vector estimate, $\hat{X}_f(t)$. The indirect or error-state vector configuration is the approach normally used. This approach propagates the nonlinear, dynamic equation, $f(X_f; t)$, by linearizing about the trajectory as is already done with the covariance propagation. The time variation of the error state-vector is much slower than the full state vector which therefore permits real time operation.

V. THE KALMAN FILTER SIMULATION USING "SOFE" WITH THE LN-15 INS DYNAMICS

In order to study the effectiveness and sensitivity of the nonlinear Kalman filter, a Monte Carlo simulation is usually performed. In such a simulation, the actual measurement is generated by what is referred to as the "truth" model which is simply a higher order model of the particular INS under investigation. For the sake of the simulation, the "truth" error state-vector, $X_s(t)$, is considered as the actual error-vector which then allows the best Kalman estimate to be written directly as "true" + $X_s(t) - X_f(t)$ where the "true" trajectory is a tape input corresponding to some maneuver. The measurement is now written as

$$\text{Measurement} = (\text{TRUE} - \text{PREDICTED}) + \text{NOISE} \quad (12)$$

where the TRUE corresponds to the nonlinear measurement as given by the trajectory values and the PREDICTED is the nonlinear measurement as given by the best Kalman filter estimate, "True" + $X_s(t) - X_f(t)$. The noise is white, Gaussian measurement noise with a covariance of R_f .

During the study, the versatile Monte Carlo simulation program called SOFE was used exclusively. This program was written by Mr. Stanton Musick of the WPAFB Avionics Lab and features a variable -5- step integration subroutine and the Carlson sequential square root matrix inversion routine for Kalman filter gain, K , calculation.

The INS model chosen was the local-level Honeywell LN-15 system defined as a 1 n.m./hr. system. As listed in Appendix I, the "truth" model has 47 state variables and the filter model has 16 state variables.

VI. OBSERVABILITY TEST

Since the update on measurement constitutes an attempt to update a 13 state vector with a single scalar measurement, the question of observability becomes important. In the problem at hand, the question can be phrased as follows: "Is the implicit coupling of velocity, acceleration, and attitude components as contained in the LN-15 dynamics equations sufficient to allow the Kalman filter to update each vector component in the proper proportion."

As developed in reference 5, a measurement can be shown to be observable if the following observability matrix, ϕ , is invertible;

$$\phi = \begin{bmatrix} H^T & F^T H^T & (F^T)^2 H^T & \dots & (F^T)^{n-1} H^T \\ \vdots & \vdots & \vdots & \vdots & \vdots \end{bmatrix} \quad (13)$$

the matrix is a square nxn matrix. The degree of observability of the measurement can be quantified by the condition number, C, of ϕ defined as

$$C = \frac{\text{Determinant of } \phi}{\|\phi\|} \quad (14)$$

VII. THE MEASUREMENT AND H MATRICES FOR CASES A, B, AND C

Case A: Centripetal Acceleration Only

Referring to Section III, the measurement can be written directly as

$$K_{\text{CENT}} \left\{ (v_{T_e}^2 + v_{T_n}^2 + v_{T_z}^2) - (\hat{v}_e^2 + \hat{v}_n^2 + \hat{v}_z^2) \right\} \quad (15)$$

where $(v_{T_e}, v_{T_n}, v_{T_z})$ is the time velocity vector of the tape trajectory and

$(\hat{v}_e, \hat{v}_n, \hat{v}_z)$ is the best estimate of velocity given by

$$\begin{aligned} \hat{v}_e &= v_{T_e} + XS(4) - XF(4) \\ \hat{v}_n &= v_{T_n} + XS(5) - XF(5) \\ \hat{v}_z &= v_{T_z} + XS(6) - XF(6) \end{aligned} \quad (16)$$

where the first order perturbation of (13) yields the H matrix given as

$$\begin{aligned} H(4) &= -2 K_{CENT} (V_{T_E} + XS(4) - XF(4)) \\ H(5) &= -2 K_{CENT} (V_{T_E} + XS(5) - XF(5)) \\ H(6) &= -2 K_{CENT} (V_{T_E} + XS(6) - XF(6)) \end{aligned} \quad (17)$$

In this case, the nonlinear noise is only second order and has an explicit expression, R_A , given as

$$R_A = K_{CENT} \left\{ (XS(4) - XF(4))^2 + (XS(5) - XF(5))^2 + (XS(6) - XF(6))^2 \right\} \quad (18)$$

Case B: With Line of Sight But Without the Attitude Error

Referring again to Section III, the measurement term includes Case A plus the nonlinear term due to the line of sight acceleration given as follows

$$\begin{aligned} K_{L.O.S.} \left\{ A_{T_e} \cos \alpha_T + A_{T_n} \cos \beta_T + A_{T_z} \cos \gamma_T \right. \\ \left. - \hat{A}_e \cos \hat{\alpha} - \hat{A}_n \cos \hat{\beta} - \hat{A}_z \cos \hat{\gamma} \right\} \end{aligned} \quad (19)$$

where $(\cos \alpha_T, \cos \beta_T, \cos \gamma_T)$ and $(\cos \hat{\alpha}, \cos \hat{\beta}, \cos \hat{\gamma})$ are the true and estimated direction cosines of the unit vector between the target and the phase center and \vec{A}_T, \hat{A} are the true and estimated values of acceleration.

Since the LN-15 INS dynamic equations are basically second order (Newton's second law), the acceleration state vector is redundant and can be generated dynamically as follows

$$\vec{A} \approx (\vec{V}_t - \vec{V}_{(t-\tau)})/\tau \quad (20)$$

where $\vec{V}(t-\tau)$ is the velocity vector at the end of the previous integration interval and τ is the current size of the interval itself. The acceleration vector is augmented as XF(14), XF(15), XF(16) respectively. The true and estimated values of the direction cosines are calculated from the true and estimated coordinates of the aircraft position relative to the fixed point target being imaged. The equations are straightforward and are not included here.

The derivation of the new entries of the H matrix can be represented conveniently as the first order coefficients of the Taylor series expansion

of (17) or

$$\begin{aligned}
 & - (\hat{\delta} A_e) \cos(\hat{\alpha}) - (\hat{\delta} \hat{A}_n) \cos \hat{\beta} - (\hat{\delta} A_z) \cos \hat{\gamma} \\
 & + (\hat{A}_e) \sin(\hat{\alpha}) (\hat{\delta}\hat{\alpha}) + (\hat{A}_n) \sin(\hat{\beta}) (\hat{\delta}\hat{\beta}) \\
 & + (\hat{A}_z) \sin(\hat{\gamma}) (\hat{\delta}\hat{\gamma})
 \end{aligned} \tag{21}$$

where

$$\begin{aligned}
 \hat{A}_e &= A_{T_e} + XS(45) - XF(14) \\
 \hat{A}_n &= A_{T_n} + XS(46) - XF(15) \\
 \hat{A}_z &= A_{T_z} + XS(47) - XF(16) .
 \end{aligned} \tag{22}$$

In calculating the expressions of (17) and (19), the geographic frame is used which requires a position conversion from the earth frame (latitude, longitude) to (X_e, X_n) in the geographical frame; e.g. $(\hat{\delta}\hat{\alpha})$ geographical = $(R / RF) \hat{\delta}$ where $R = R_{EARTH} (1 - 2\epsilon + 3\epsilon \sin^2(L) + \hat{h})$ given that R_{EARTH} = radius of earth, ϵ = eccentricity, and \hat{h} equals estimated altitude and; the RF value equals the radius vector length from the imaged point target to the antenna phase center.

With regard to expression (19), the inclusion of position error in the form of $(\hat{\delta}\hat{\alpha}, \hat{\delta}\hat{\beta}, \hat{\delta}\hat{\gamma})$ is a direct result of the imaging radar application where the unit pointing vector has one end fixed at the imaged point throughout the entire aperture time while the other vector end fluctuates according to the uncertainty of the aircraft position. Such a position uncertainty term is not present in the H-matrix of the doppler-INS augmentation since the doppler measurement is not referenced to specific target points; i.e. the unit vector merely slides along the ground in a parallel fashion and is not fixed at one specific target.

For Case B, the nonlinear noise term is the sum of the nonlinear noise of Case A and a remainder term of the Taylor series expansion of expansion of (19) which can be handled as follows

$$\begin{aligned}
R(\text{remainder}) \leq \frac{1}{2} K_{\text{L.O.S.}} \left\{ \right. & \left. \begin{aligned}
& |\hat{A}_e|_M |\delta\hat{\alpha}|_M^2 + |\hat{A}_n|_M |\delta\hat{\beta}|_M^2 \\
& + |\hat{A}_z|_M |\delta\hat{\gamma}|_M^2 + |\delta\hat{A}_e|_M^2 + |\delta\hat{A}_n|_M^2 \\
& + |\delta\hat{A}_z|_M^2 + |\hat{A}_e|_M |\delta\hat{\alpha}|_M |\delta\hat{A}_e|_M \\
& + |\hat{A}_n|_M |\delta\hat{\beta}|_M |\delta\hat{A}_n|_M + |\hat{A}_z|_M |\delta\hat{\gamma}|_M |\delta\hat{A}_z|_M
\end{aligned} \right\} \quad (23)
\end{aligned}$$

where the subscript, M, refers to the maximum value expected over normal operation. Since this term is not known a priori, it is impossible to compensate for; however, under normal convergence, the nonlinear noise is expected to be masked by measurement noise.

Case C: Attitude Errors Included

The attitude error vector in geographical coordinates is given as $\vec{\epsilon} = (\epsilon_e, \epsilon_n, \epsilon_z)$ which leads directly to an additional nonlinear measurement component given as

$$\begin{aligned}
K_{\text{L.O.S.}} \left\{ \right. & \left. \begin{aligned}
& A_{T_e} \cos \alpha_T + A_{T_n} \cos \beta_T + A_{T_z} \cos \gamma_T \\
& - \hat{A}_e \cos (\hat{\alpha} + \hat{\epsilon}_e) - \hat{A}_n \cos (\hat{\beta} + \hat{\epsilon}_n) \\
& - \hat{A}_z \cos (\hat{\gamma} + \hat{\epsilon}_z)
\end{aligned} \right\} \quad (24)
\end{aligned}$$

The H matrix for $\underline{\epsilon}$ results from the perturbation term $\underline{A} \cdot \delta\underline{\mu}_A$, where \underline{A} is the acceleration and $\delta\underline{\mu}_A$ is the perturbation of the unit vector due to attitude error. As developed in Reference 6, the perturbation can be expressed as follows

$$(\underline{A})^T (\underline{\mu}_A)^* (\underline{\epsilon}^n) \quad (25)$$

where $(\underline{\mu}_A)^*$ is the shew-symmetric matrix given by

$$\underline{\mu}_A = \begin{bmatrix} 1 & \hat{\epsilon}_z & -\hat{\epsilon}_y \\ -\hat{\epsilon}_z & 1 & \hat{\epsilon}_x \\ \hat{\epsilon}_y & -\hat{\epsilon}_x & 1 \end{bmatrix} \begin{bmatrix} \\ \\ C_P^n \end{bmatrix} \begin{bmatrix} \cos \phi \\ 0 \\ \sin \phi \end{bmatrix} \quad (26)$$

where C_p^n is the platform to geographical transformation matrix for a wander azimuth mechanization given in terms of wander angle, α , as

$$C_p^n = \begin{bmatrix} \cos \alpha & \sin \alpha & 0 \\ \sin \alpha & \cos \alpha & 0 \\ 0 & 0 & 1 \end{bmatrix} \quad (27)$$

and where ϕ is the azimuth squint angle. Upon expanding, expression (26) becomes the column matrix

$$\hat{\mu}_A = \begin{bmatrix} \cos \alpha \cos \phi + \hat{\epsilon}_z (\sin \alpha \cos \phi) - \hat{\epsilon}_y \sin \phi \\ -\hat{\epsilon}_z (\cos \alpha \cos \phi) + (\sin \alpha \cos \phi) + \hat{\epsilon}_x \sin \phi \\ \hat{\epsilon}_y (\cos \alpha \cos \phi) - \hat{\epsilon}_x (\sin \alpha \cos \phi) + \sin \phi \end{bmatrix} \quad (28)$$

which from (25) leads to the expression for the new [H] components

$$[\hat{A}^n]^T (\hat{\mu}_A^n)^* = [H]^T \quad (29)$$

or

$$\begin{aligned} H(7) &= (\hat{A}_n) \{ \hat{\epsilon}_n (\cos \alpha \cos \phi) - \hat{\epsilon}_e (\sin \alpha \cos \phi) + \sin \phi \} \\ &\quad - (\hat{A}_z) \{ -\hat{\epsilon}_z (\cos \alpha \cos \phi) + (\sin \alpha \cos \phi) + \hat{\epsilon}_e \sin \phi \} \\ H(8) &= -(\hat{A}_e) \{ \hat{\epsilon}_n (\cos \alpha \cos \phi) - \hat{\epsilon}_e (\sin \alpha \cos \phi) + \sin \phi \} \\ &\quad + (\hat{A}_z) \{ \cos \alpha \cos \phi + \hat{\epsilon}_z (\sin \alpha \cos \phi) - \hat{\epsilon}_y \sin \phi \} \\ H(9) &= (\hat{A}_e) \{ -\hat{\epsilon}_z (\cos \alpha \cos \phi) + (\sin \alpha \cos \phi) \\ &\quad + \hat{\epsilon}_x (\sin \phi) \} - (\hat{A}_n) \{ \cos \alpha \cos \phi \\ &\quad + \hat{\epsilon}_z (\sin \alpha \cos \phi) - \hat{\epsilon}_n \sin \phi \} \end{aligned} \quad (30)$$

VIII. COMPUTER RESULTS

A. General Remarks

Major problems were encountered during the simulation with filter divergence and the "debugging" of computer execution errors. With regard to the "debugging" problem, it is indeed unfortunate that the WPAFB Cyber CDC possesses such a poor execution error diagnostic; many hours were spent in intriguing but unnecessary searches for yet another mode error. On the other hand, the problem of filter divergence was not unexpected and could in general be traced to one or all of the following three contributors:

1. The effect of higher order terms resulting from the nonlinear nature of the Autofocus measurement.
2. The lack of observability (or whether there is enough information in the update) in the measurement itself, which will allow $|XS-XF|$ to accumulate indefinitely.
3. The reduced state nature of the filter model.

The SOFE simulations were generally run over an 80 sec. trajectory with a 4 or 8 sec. Auto-Focus update interval. The available trajectory was a low-speed, low-altitude trajectory with some degree of maneuvering present.

B. Case A:

Using the complete nonlinear measurement of (15), the early runs were found to be divergent; that is, the difference; $|XS-XF|$ became increasingly large. Originally, it was thought that the nonlinear noise contribution to the update [which, from simple algebra, can be expressed as $\{(DS')^2/2(V_T DS')\}$ where $DS'=XS-XF$ and V_T is the true velocity] was the fundamental cause of the divergence. To counteract this effect, the measurement noise was increased but still the filter remained divergent. To resolve the role of the nonlinear noise effect, the nonlinear or higher-order terms were simply subtracted thereby linearizing the measurement. This was possible only in Case (A) where the higher order term (2nd order) was known in closed form; it is, of course, impossible to subtract this term in practice since XS is unknown. However, the filter continued to remain divergent even with this extreme fix which seem to suggest that the higher order terms were not the fundamental cause of the divergence.

The next factor considered was model divergence or the effect of the reduced order of the filter error state-vector. The deleted state problem

is especially serious in the high measurement accuracy case (e.g. Autofocus) since the filter, as expressed by its propagated covariance, becomes overconfident as to the accuracy of its estimate and ignores further measurement updates. In such a situation, the subtle differences between the truth and filter are accentuated and the filter eventually diverges. The standard technique for controlling this type of divergence is to artificially inject noise into the propagating covariance either by increasing the initial covariances or by introducing fictitious process noise (Q_F terms). Both methods were tried and eventually a Q_F level of 320 ft/sec² in the velocity states was found effective in controlling divergence. Even though this intellectually unsatisfying approach did control gross divergence, the updates themselves were not anymore effective; that is, the Kalman gain vectors were not receiving and processing the reassessment in an effective manner. By a process of elimination, the question of observability therefore became the center of attention. Initially, the observability matrix of (13) was programmed on the computer with a term added, $\frac{d\{(F^T)^{i-1} H^T\}}{dt}$, to the $(F^T)^i H^T$ column to account for the time varying nature of $F(t)$ as the operating point moved along the trajectory. Immediately, it became apparent that the 13 state observability matrix would be singular (zero determinant) because of the non-interactive longitude channel (first row of F) and the three {0} columns of the gyro-drift states. Accordingly, the 13 state matrix was reduced to 9 states and the program was rerun over the usual trajectory. The results indicated very marginal observability with the condition number of the Φ matrix lying between 0 and 10^{-20} ! These results, of course, apply to this particular trajectory only; other trajectories may possess better observability particularly violent maneuvers where all three velocity components are non-zero and rapidly changing. As an added support for the observability argument, Appendix II presents a 2nd order system with a similar nonlinear measurement; the observability criterion indicates regions of non-observability in the (X_1, X_2) state space.

Although the properties of the observability matrix are an analytically satisfying way of investigating observability, a more direct way is to simply look at the change in covariance at update. Referring to Figure 3(a,b,c),

for a high fictitious Q_f in the velocity states of 32, only the north velocity component receives a significant update while the other velocity components and the 10 other state variables are essentially unaffected. Figure 4(a,b,c) shows the update effect for a lower Q_f of 3.2; in this case, the effect is less dramatic due to the lower absolute value of the covariance. However, the large correction at the first update is interesting and was also reflected in an excellent initial filter update. For some reason, the quality of the update was not maintained. Figure 5(a,b,c) gives the covariance propagation for $Q_f = 0$ when the filter becomes divergent. The rapid monotonic decrease in $\sqrt{P_f}$ is an indication of the filter's absolute confidence in its erroneous state estimate which leads finally to the divergence. From the covariance plots, it would therefore appear that only the north component of velocity is observable for this particular trajectory given the LN-15 dynamics. The system observability should however improve in Case (B) and Case (C) since more state variables are included in the measurement matrix.

C. Case B:

While conceptually straightforward, the inclusion of the acceleration state vector in the SOFE simulation proved to be quite difficult. A fixed step integration mode was used for simplicity but problems were encountered trying to circumvent the 5 step numerical integration routine that is a permanent feature of SOFE. Many mode or execution errors were encountered. It was only on the last day of the ten week period that a "successful" run was completed. Early results indicate an improvement in observability based on the propagated covariance. The conditioning of the observability matrix was not checked however.

A follow-on grant proposal will propose completing Cases B,C, and D and resolving the observability question.

IX. RECOMMENDATIONS

In a follow on grant proposal, I will recommend the following tasks:

- (1) Cases B,C and D should be completed as outlined. Special attention should be given to the relative importance of observability and non-linear noise in all three cases. It should be emphasized that only an investigation of the complete case (Case C) can resolve the potential value of the Autofocus update.
- (2) If observability should continue to be a problem in Case C, the use of similarity transformations to isolate the observable and nonobservable states should be considered. The identification of the observable states could suggest additional state deletion or addition and also the type of additional sensor input necessary to augment the Autofocus update.
- (3) Because the Autofocus measurement is essentially a high signal to noise ratio measure, the presence of nonlinear noise could seriously degrade its potential usefulness. Accordingly, the use of the iterated, extended Kalman filter should be considered.
- (4) The use of the finite memory technique for controlling filter divergence should be investigated. This technique is intellectually more satisfying than merely adding a higher noise level to the covariance propagation.
- (5) If and when a satisfactory update is realized, the effects of different trajectories and update intervals should be investigated.
- (6) An adaptive Kalman filter configuration should also be considered. This suggestion is motivated by an observed improvement in attitude error observability when the appropriate H matrix entry was zeroed for velocity components below a certain threshold level.

REFERENCES

1. North Atlantic Treaty Organization, "Theory and Applications of Kalman Filtering," Published February, 1970.
2. R. Kitzerow, "Motion Compensation of Synthetic Aperture Radars (SAR)," Memorandum to AFSC/DLCAA, October, 1978.
3. S.H. Musick, "SOFE: A Generalized Digital Simulation For Optimal Filter Evaluation User's Manual," AFWAL-TR-80-1108.
4. W.S. Widnall and P.A. Grundy, "Inertia Navigation System Error Models," Intermetrics, TR-03-73, May 11, 1973.
5. A. Gelb, Applied Optimal Estimation, (MIT Press, Cambridge, Mass., 1974), p. 69.
6. S.H. Musick, "Radar Measurements and Measurement Matrices for EAR," AFAL-TM-76-48, May 12, 1976.

Figure 1: SAR Geometry

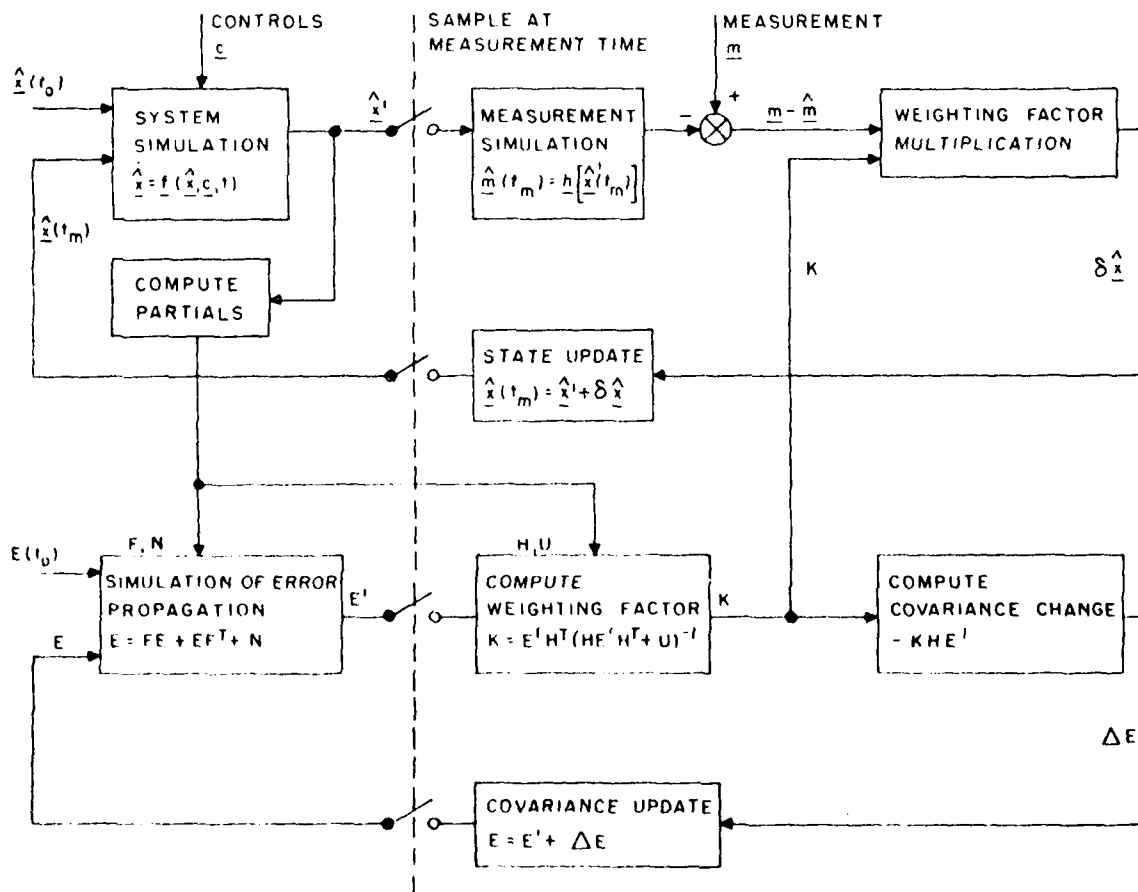
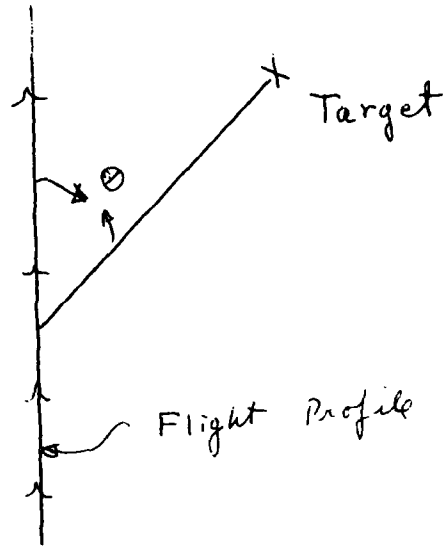


Figure 2: Extended Kalman Filter: Direct Configuration

R.M.S. OF EAST VELOCITY COMPONENT

$Q_f = 320.00$

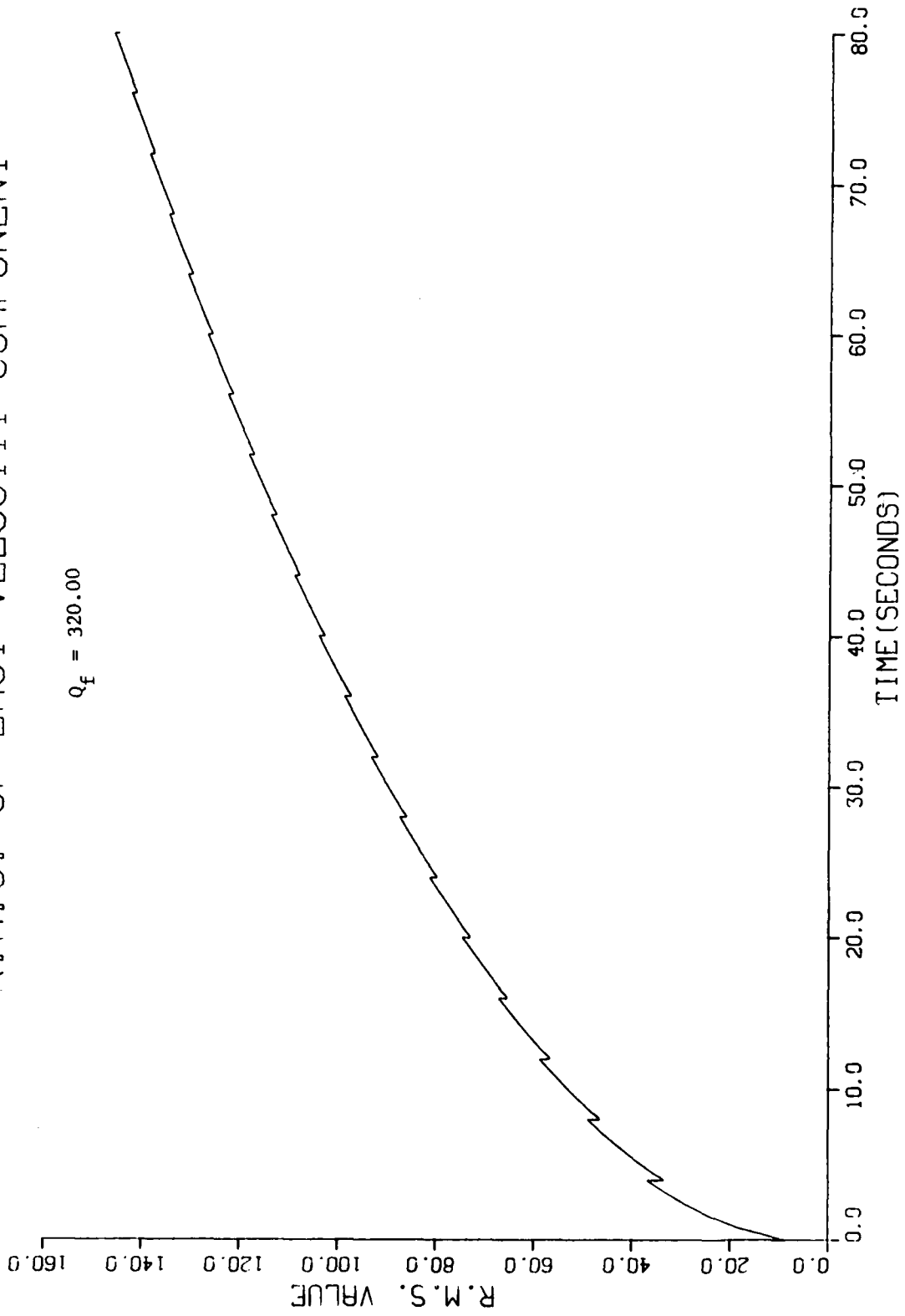


Figure 3-(a): R.M.S. OF EAST VELOCITY COMPONENT FOR $Q_f = 320.0$

R.M.S. OF NORTH VELOCITY COMPONENT

$Q_f = 320.00$

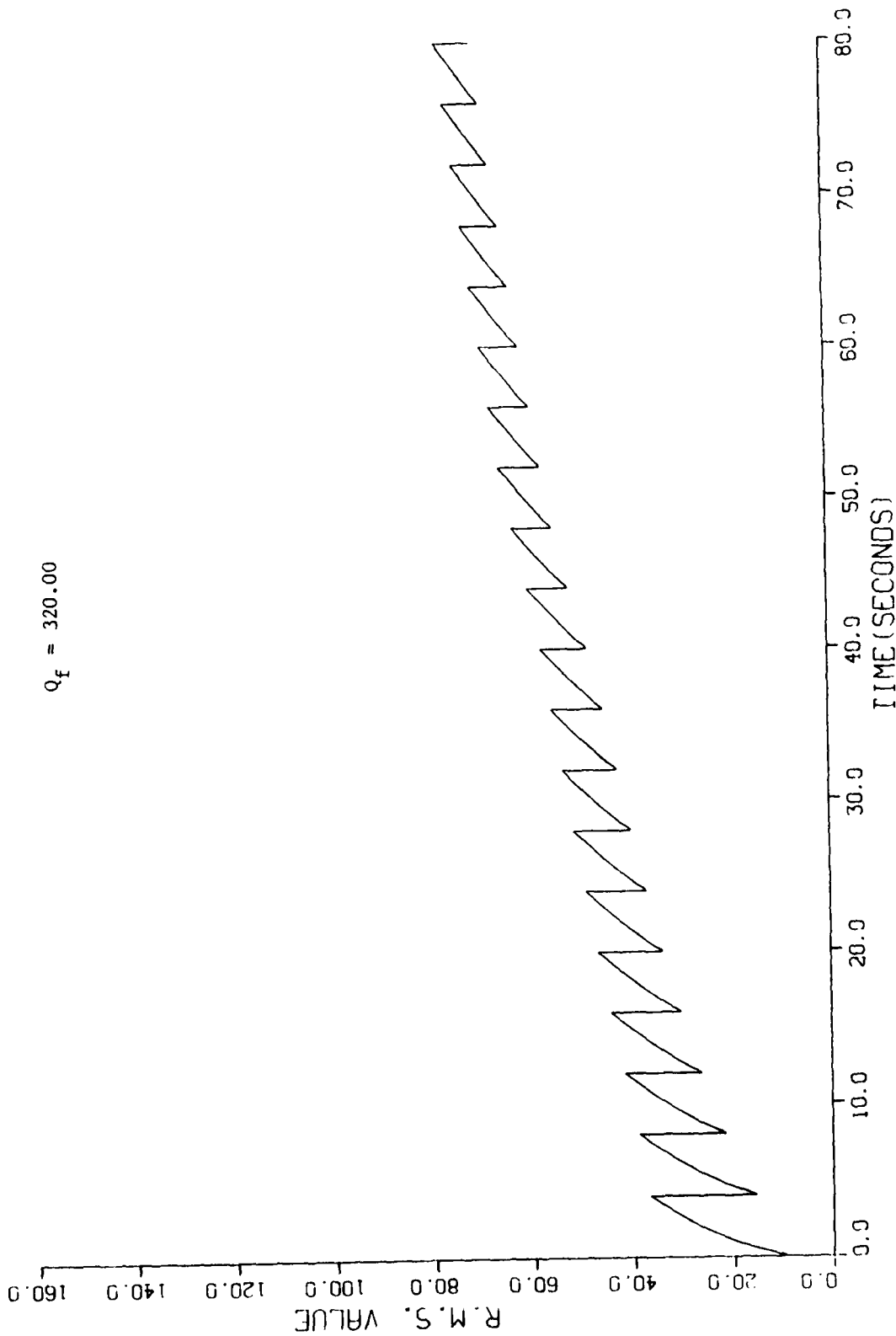


Figure 3-(b): R.M.S. OF NORTH VELOCITY COMPONENT FOR $Q_f = 320.0$

R.M.S. OF VERTICAL VELOCITY COMPONENT

$Q_f = 320.00$

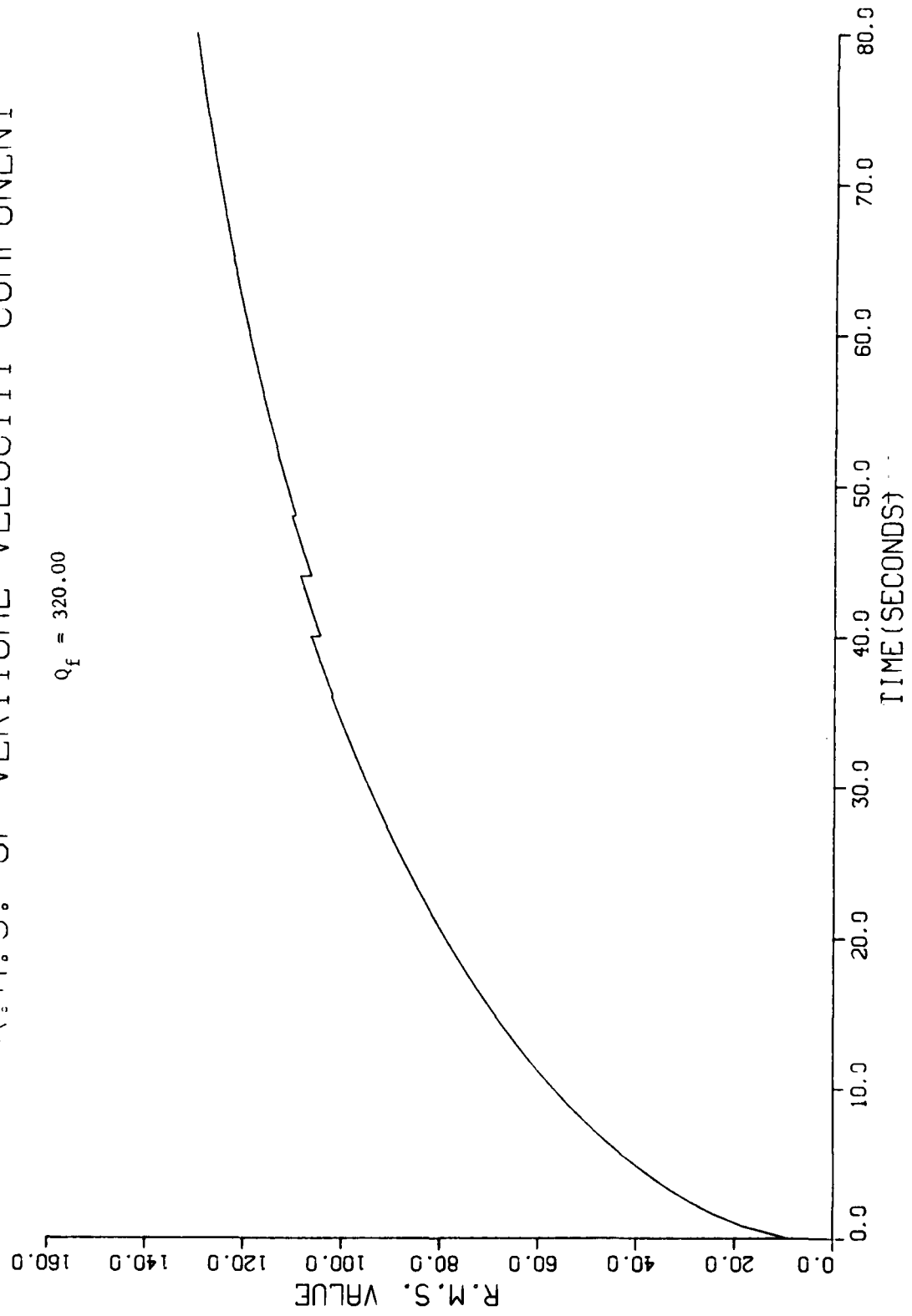


Figure 3-(c): R.M.S. OF VERTICAL VELOCITY COMPONENT FOR $Q_f = 320.0$

R.M.S. OF VERTICAL VELOCITY COMPONENT

$Q_f = 3.2$

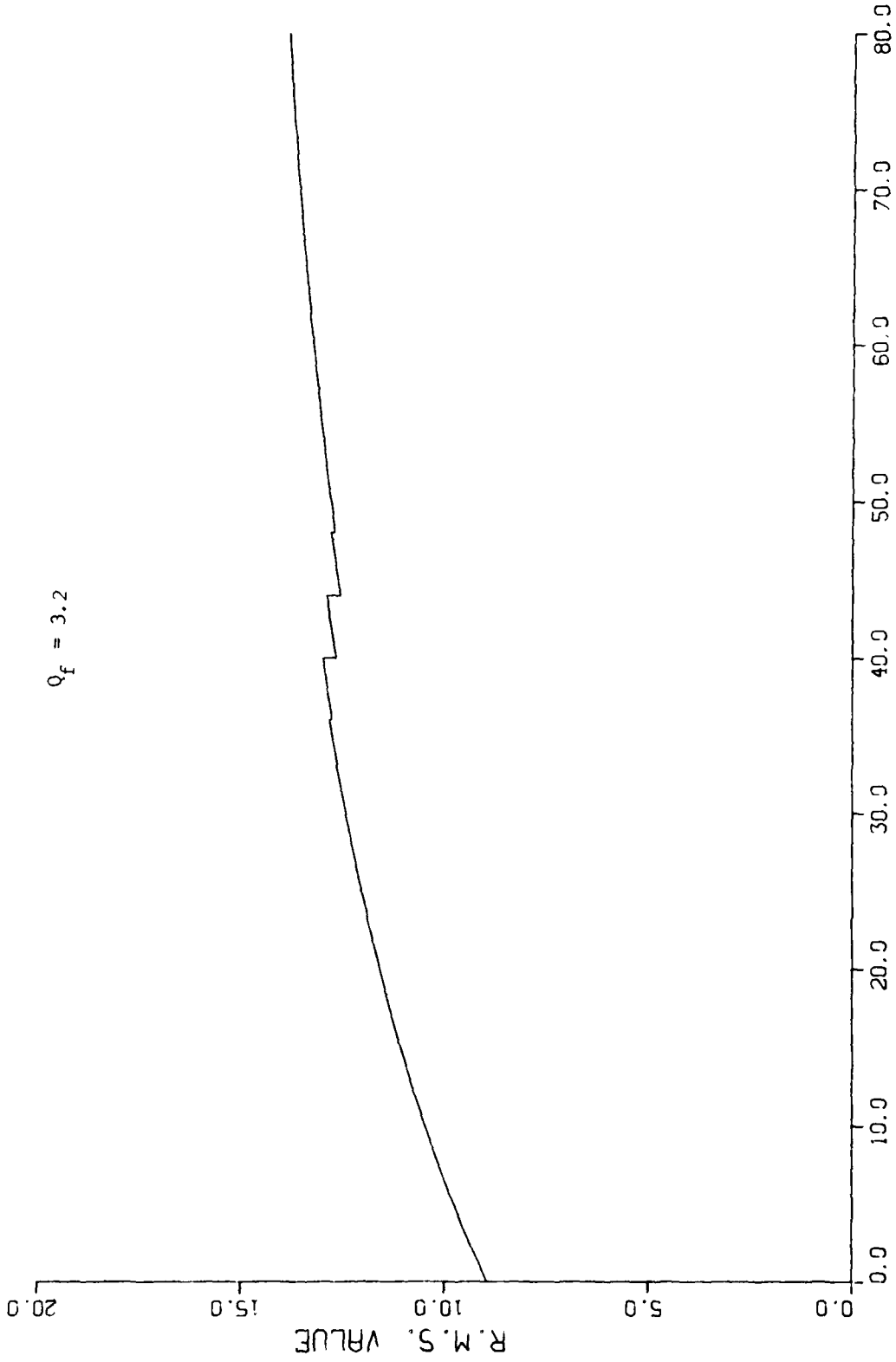


Figure 4-(c): R.M.S. OF VERTICAL VELOCITY COMPONENT OF $Q_f = 3.2$

R.M.S. OF NORTH VELOCITY COMPONENT

$Q_f = 3.2$

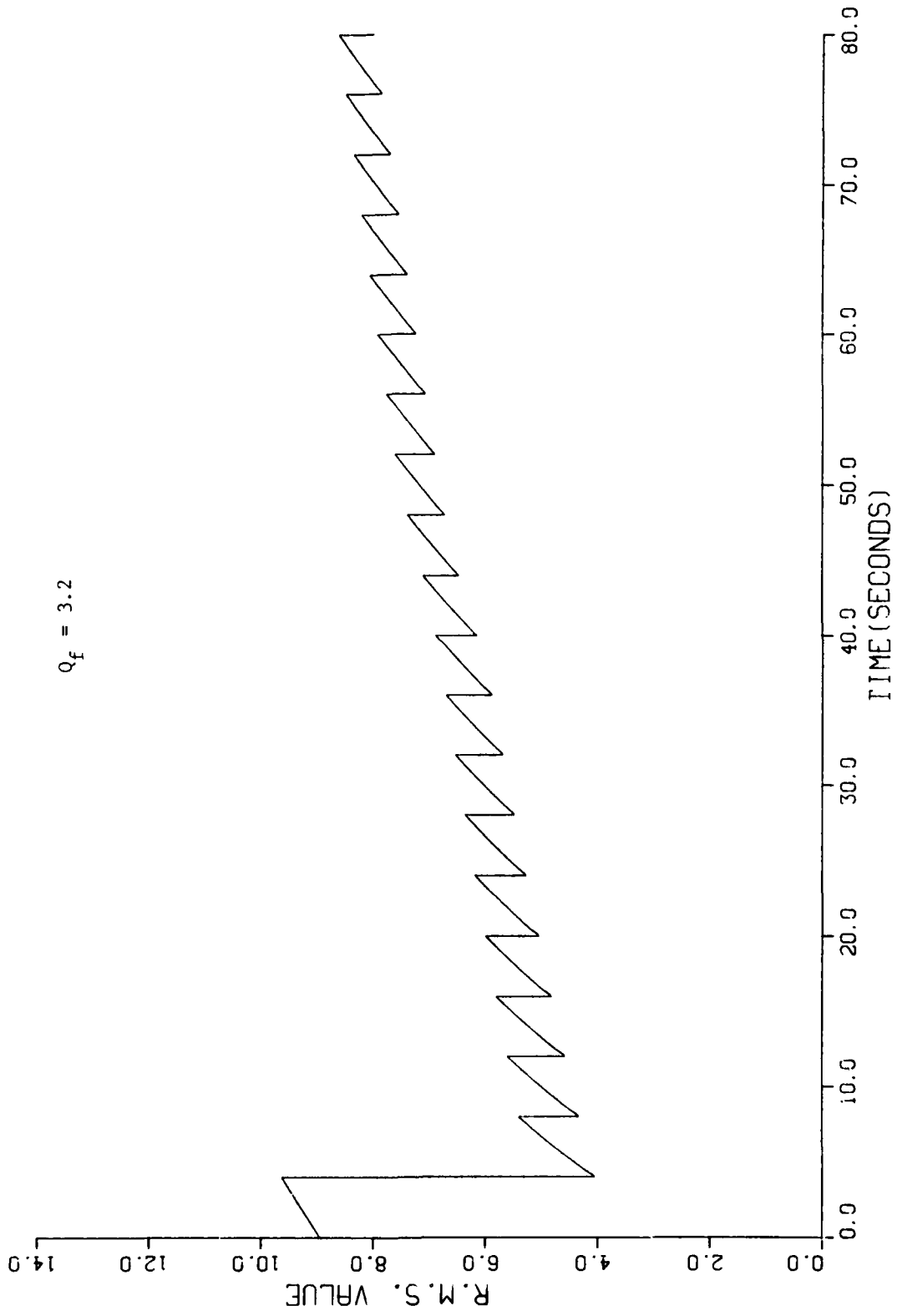


Figure 4-(b): R.M.S. OF NORTH VELOCITY COMPONENT FOR $Q_f = 3.2$

R.M.S. OF EAST VELOCITY COMPONENT

$Q_f = 3.2$

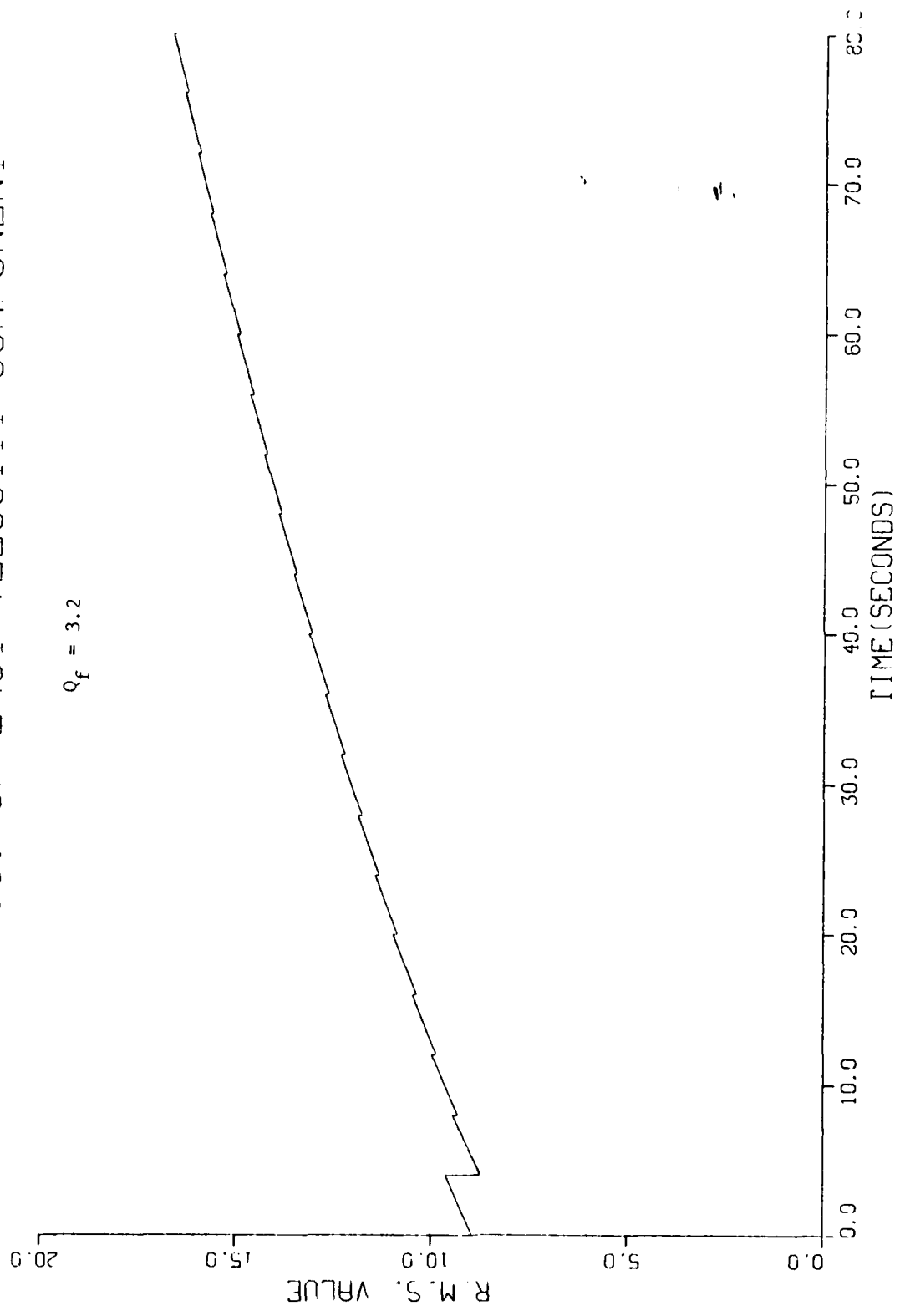


Figure 4-(a): R.M.S. OF EAST VELOCITY COMPONENT FOR $Q_f = 3.2$

R.M.S. OF EAST VELOCITY COMPONENT

$Q_f = 0.0$

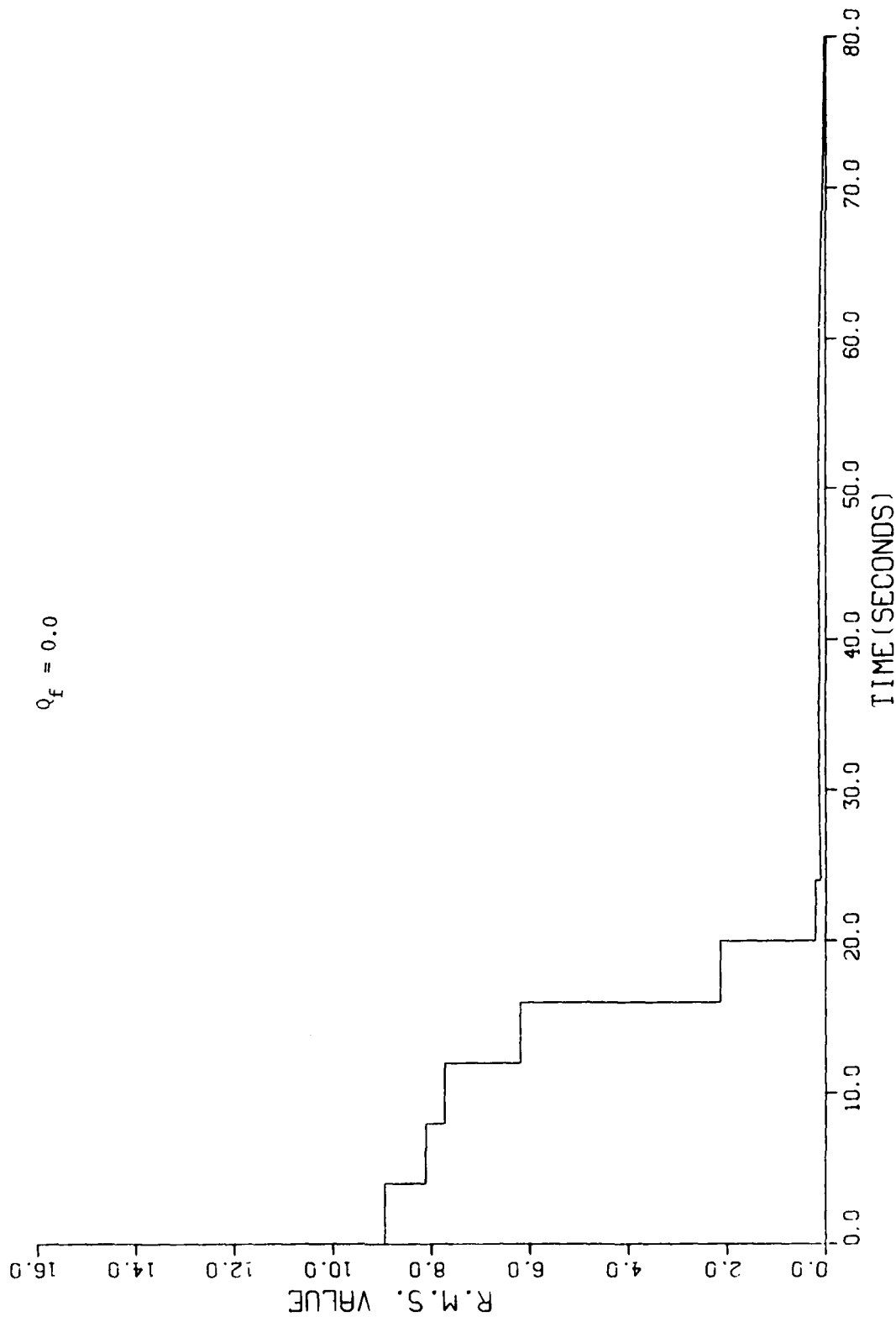


Figure 5-(a): R.M.S. OF EAST VELOCITY COMPONENT FOR $Q_f = 0.0$

R.M.S. OF NORTH VELOCITY COMPONENT

$Q_f = 0.0$

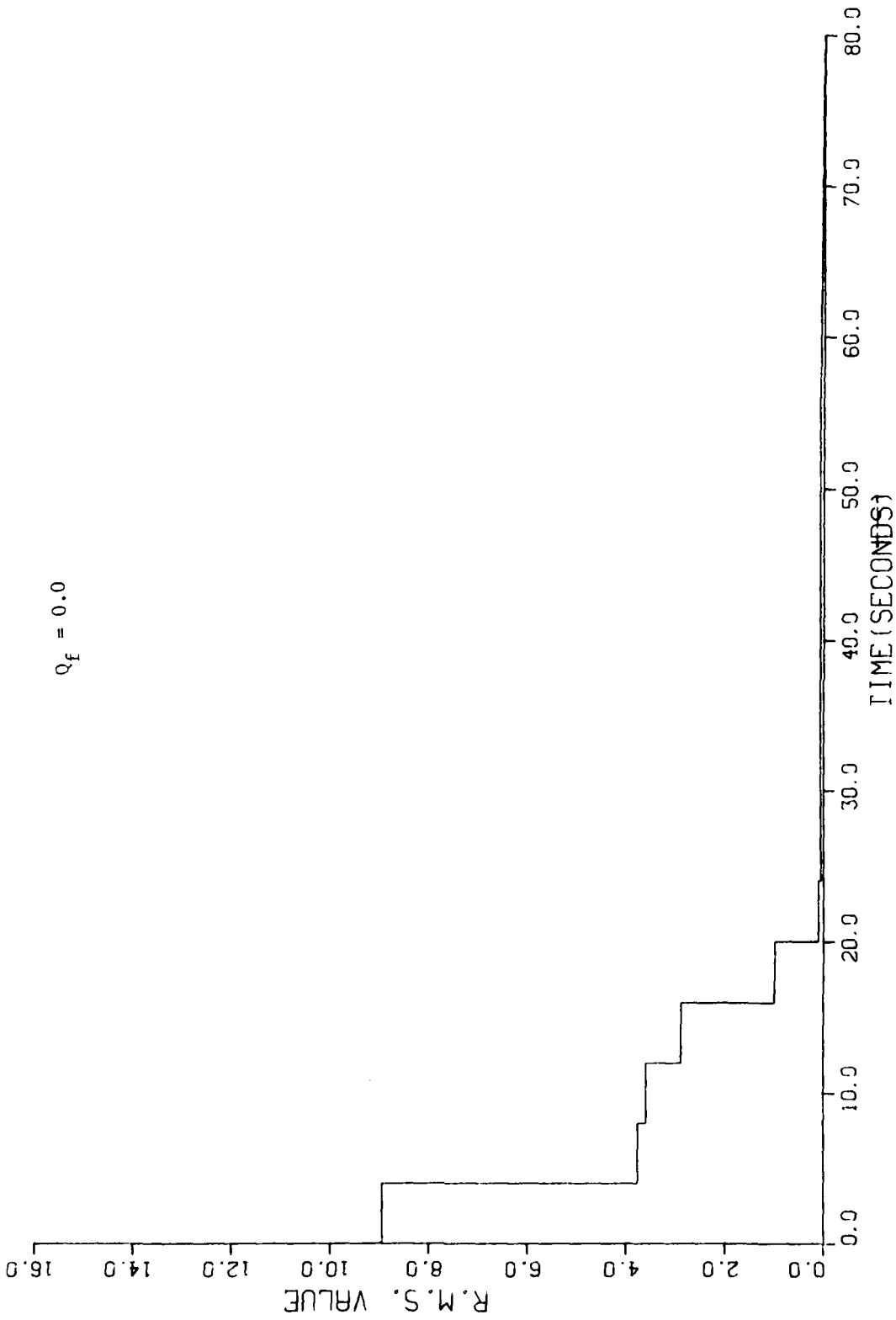


Figure 5-(b): R.M.S. OF NORTH VELOCITY COMPONENT FOR $Q_f = 0.0$

R.M.S. OF VERTICAL VELOCITY COMPONENT

$$Q_f = 0.0$$

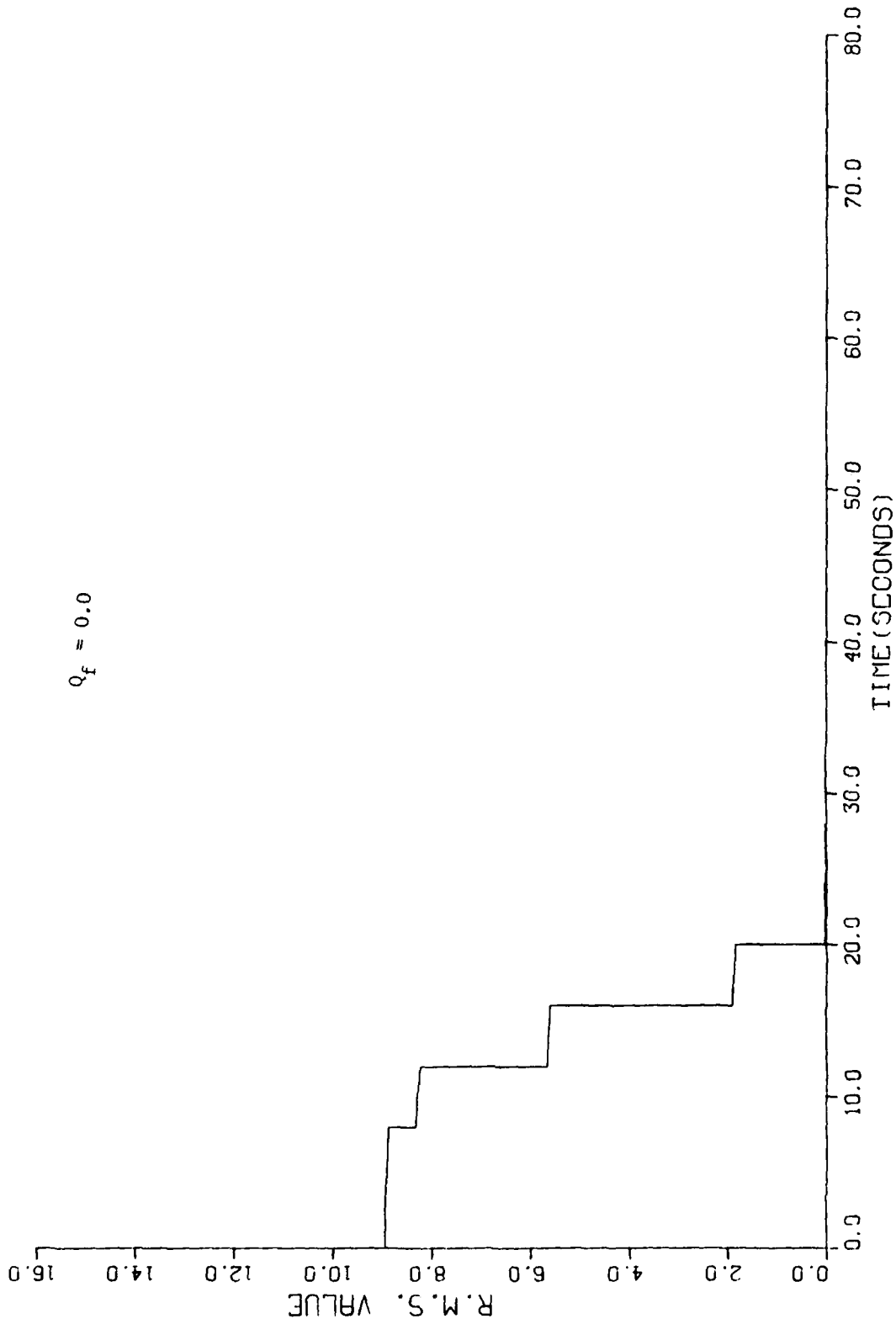


Figure 5-(c): R.M.S. OF VERTICAL VELOCITY COMPONENT FOR $Q_f = 0.0$

APPENDIX I

LN-15

TRUTH STATE INDEX	ERROR SOURCE	ERROR MODEL
1	EAST LONGITUDE	DYNAMIC
2	NORTH LATITUDE	DYNAMIC
3	ALTITUDE	DYNAMIC
4	EAST VELOCITY	DYNAMIC
5	NORTH VELOCITY	DYNAMIC
6	VERTICAL VELOCITY	DYNAMIC
7	EAST ATTITUDE	DYNAMIC
8	NORTH ATTITUDE	DYNAMIC
9	VERTICAL ATTITUDE	DYNAMIC
10	VERTICAL ACCELERATION	DYNAMIC
11	X GYRO DRIFT	RANDOM WALK
12	Y GYRO DRIFT	RANDOM WALK
13	Z GYRO DRIFT	RANDOM WALK
14	X GYRO G-SENS DRIFT, INPUT(X)	RANDOM CONSTANT
15	X GYRO G-SENS DRIFT, SPIN(Y)	RANDOM CONSTANT
16	Y GYRO G-SENS DRIFT, SPIN(X)	RANDOM CONSTANT
17	Y GYRO G-SENS DRIFT, INPUT(Y)	RANDOM CONSTANT
18	Z GYRO G-SENS DRIFT, SPIN(Y)	RANDOM CONSTANT
19	Z GYRO G-SENS DRIFT, INPUT(Z)	RANDOM CONSTANT
20	X GYRO G*G-SENS DRIFT	RANDOM CONSTANT
21	Y GYRO G*G-SENS DRIFT	RANDOM CONSTANT
22	Z GYRO G*G-SENS DRIFT	RANDOM CONSTANT
23	X GYRO SCALE FACTOR	RANDOM CONSTANT
24	Y GYRO SCALE FACTOR	RANDOM CONSTANT
25	Z GYRO SCALE FACTOR	RANDOM CONSTANT
26	X GYRO MISALIGNMENT ABT Y	RANDOM CONSTANT
27	X GYRO MISALIGNMENT ABT Z	RANDOM CONSTANT
28	Y GYRO MISALIGNMENT ABT X	RANDOM CONSTANT
29	Y GYRO MISALIGNMENT ABT Z	RANDOM CONSTANT
30	Z GYRO MISALIGNMENT ABT X	RANDOM CONSTANT
31	Z GYRO MISALIGNMENT ABT Y	RANDOM CONSTANT
32	X ACCELEROMETER BIAS	RANDOM WALK
33	Y ACCELEROMETER BIAS	RANDOM WALK
34	Z ACCELEROMETER BIAS	RANDOM WALK
35	X ACCELEROMETER SCALE FACTOR	RANDOM CONSTANT
36	Y ACCELEROMETER SCALE FACTOR	RANDOM CONSTANT
37	Z ACCELEROMETER SCALE FACTOR	RANDOM CONSTANT
38	X ACCEL MISALIGNMENT ABT Y	RANDOM CONSTANT
39	X ACCEL MISALIGNMENT ABT Z	RANDOM CONSTANT
40	Y ACCEL MISALIGNMENT ABT X	RANDOM CONSTANT
41	Y ACCEL MISALIGNMENT ABT Z	RANDOM CONSTANT
42	Z ACCEL MISALIGNMENT ABT X	RANDOM CONSTANT
43	Z ACCEL MISALIGNMENT ABT Y	RANDOM CONSTANT
44	BARD ALTIMETER BIAS	FIRST ORDER MARKOV
45	EAST ACCELERATION	
46	NORTH ACCELERATION	
47	VERTICAL ACCELERATION	

FILTER STATE INDEX	ERROR SOURCE	ERROR MODEL
1	EAST LONGITUDE	DYNAMIC
2	NORTH LATITUDE	DYNAMIC
3	ALTITUDE	DYNAMIC
4	EAST VELOCITY	DYNAMIC
5	NORTH VELOCITY	DYNAMIC
6	VERTICAL VELOCITY	DYNAMIC
7	EAST ATTITUDE	DYNAMIC
8	NORTH ATTITUDE	DYNAMIC
9	VERTICAL ATTITUDE	DYNAMIC
10	BARO ALTIMETER BIAS	FIRST ORDER MARKOV
11	X GYRO DRIFT	RANDOM WALK
12	Y GYRO DRIFT	RANDOM WALK
13	Z GYRO DRIFT	RANDOM WALK
14	AZIMUTH MEASUREMENT BIAS	FIRST ORDER MARKOV
15	ELEVATION MEASUREMENT BIAS	FIRST ORDER MARKOV

APPENDIX II

It is of interest to analytically investigate the observability of Case (A). Inasmuch as the F matrix of the LN-15 is far too complicated to be analytically tractable, a second-order system is instead analyzed using the nonlinear measurement, $x_1^2 + x_2^2$.

Consider the invariant, linear system given by

$$\ddot{x} + k_1 \dot{x} + k_2 x = f(t) \tag{A.2.1}$$

which, in state variable form, becomes

$$\begin{bmatrix} \dot{x}_1 \\ \dot{x}_2 \end{bmatrix} = \begin{bmatrix} 0 & F & 1 \\ -k_2 & & -k_1 \end{bmatrix} \begin{bmatrix} x_1 \\ x_2 \end{bmatrix} + \begin{bmatrix} 0 \\ f(t) \end{bmatrix} \tag{A.2.2}$$

where the measurement, z , is now

$$z = x_1^2 + x_2^2 \tag{A.2.3}$$

or

$$\underline{H}^T = \begin{bmatrix} 2x_1 \\ 2x_2 \end{bmatrix} \tag{A.2.4}$$

for the extended filter. Using expression (13), we have for the observability matrix, ϕ ,

$$\phi = \begin{bmatrix} 2x_1 & -2k_2 x_2 \\ 2x_2 & 2x_1 - 2k_1 x_2 \end{bmatrix} \tag{A.2.5}$$

with a determinant equal to

$$x_1^2 - k_1 x_1 x_2 + x_2^2 \tag{A.2.6}$$

which provides the following condition for nonobservability,

$$x_1^2 - k_1 x_1 x_2 + x_2^2 = (x_1 - c_1 x_2) (x_1 - c_2 x_2) = 0 \tag{A.2.7}$$

Nonobservable regions of (x_1, x_2) space (other than origin) are the straight lines, $x_1 - c_1 x_2$, if and only if c_1, c_2 are real numbers which correspond to the overdamped case which of course describe the F matrix of the highly overdamped LN-15 INS. Observability with the "Auto-Focus" update will be further complicated by the sparseness of the LN-15 F matrix and the fact that the measurement involves only a subset of state AF variables.

In summary, the above analogy does suggest that the AF update may well have serious observability problems.

1981 USAF-SCEEE SUMMER FACULTY RESEARCH PROGRAM

Sponsored by the

AIR FORCE OFFICE OF SCIENTIFIC RESEARCH

Conducted by the

SOUTHEASTERN CENTER FOR ELECTRICAL ENGINEERING EDUCATION

FINAL REPORT

THE UTILITY OF THE ANIMAL MODEL CONCEPT

Prepared by: Dr. Donald F. McCoy
Academic Rank: Associate Professor
Department and Department of Psychology
Univerisity: University of Kentucky
Research Location: Wright-Patterson Air Force Base
Aerospace Medical Research Laboratory
Acceleration Effects Branch
Biodynamics & Bioengineering Division
USAF Research Dr. Dana B. Rogers
Colleague:
DATE: August 6, 1981
CONTRACT NO.: F49620-79-C-0038

THE UTILITY OF THE ANIMAL MODEL CONCEPT

BY

DONALD F. MCCOY

ABSTRACT

The evaluation of aircrew performance can be accomplished in two separate but related ways. First, one can explore and describe the performance capabilities of the human operator under various simulated environments. Second, a researcher can use the behavior of an animal (preferably a primate) as a performance model for that of the human operator. Perhaps this simpler approach will lead to the discovery of fundamental behavioral mechanisms which support aircrew performance. Additionally, the animal preparation enables the use of various invasive procedures through which physiological substrates of performance can be elucidated. The viability of the animal model concept was delineated in two general ways during the reporting period. First, the utility of the animal preparation was described in a series of weekly seminars dealing with the logic, methods and application of animal learning concepts. Second, two animal behavior studies were initiated during the 10 week report period. These studies are currently in progress. It is believed that the results of these studies will demonstrate the viability of the animal model concept. Suggestions for future research along these lines are offered.

Acknowledgement

The author would like to thank the Air Force Systems Command, the Air Force Office of Scientific Research and the Southeastern Center for Electrical Engineering Education for providing him with the opportunity to spend a worthwhile and interesting summer at the Aerospace Medical Research Laboratory, Wright-Patterson Air Force Base, Ohio. He would like to acknowledge the laboratory, in particular the Acceleration Effects Branch, for its hospitality and excellent working conditions.

In addition, the author would like to thank Dr. Dana B. Rogers for his suggestions, cooperation and collaboration. Thanks are also due to Drs. James Veghte, Ralph Luciani, and Goerge Potor for their help and stimulating discussions. Finally, a special note of thanks is extended to A1C Debbie Keppel for her very capable and dedicated assistance.

I. INTRODUCTION

The performance of aircrew personnel is of critical importance in determining mission effectiveness. The predictability of mission effectiveness is, therefore, a direct function of the degree to which we can provide a through analysis of the individual behaviors which comprise performance.

In order to provide complete understanding of the behavioral concepts which determine performance, it is necessary to bring the behaviors into the laboratory situation and study them under carefully controlled conditions. It is only in this way that we can isolate, manipulate, and truly analyze the ways in which such factors determine performance. In this connection, the concept of simulation has relevance. A subject might, for example, be placed on a centrifuge and exposed to the acceleration forces which accompany the critical maneuvers of an aircraft. Under such conditions his ability to perform a visual tracking task might be analyzed. It is assumed that performance in the simulated gravity environment is similar to that which can be expected under actual flying conditions.

While the above paradigm may seem to be a direct way to assess and predict pilot performance, it is not without deficiencies, since it is likely that maximum control is not possible even under these conditions. The human is a notoriously poor subject for pure behavioral research. In the first place, the diversity and complexity of past experience makes it virtually impossible to equate subjects for degree of past learning. Further, their motivational systems are enormously complex and quite different across individuals. All of this makes for great degrees of individual differences in performance levels. Finally, with human subjects, the scientist is, for moral and/or ethical reasons, limited as to the degree and type of research he can conduct.

An alternative (but not necessarily incompatible) approach is to utilize the animal-model concept. Because of the relative simplicity of

the animal it is possible that fundamental behavioral mechanisms can be elucidated. In addition, it is possible with animals to employ invasive techniques which permit the identification of the physiological substrates of performance. Finally, the use of animals affords the scientist great degrees of experimental, behavioral, and statistical control in his research. In this sense, these animal data are "relatively pure". The degree to which the animal performance model is applicable to the human is an empirical question, the answer to which requires that both species be compared under identical conditions.

One popular measure of performance is the visual tracking task. Several years ago, we performed some experiments dealing with positive and negative support systems for tracking behavior in Rhesus monkeys ¹. This research was read with interest by various members of the Acceleration Branch of the Biodynamics & Bioengineering Division of AMRL. After visiting this laboratory on several occasions, it was agreed that the opportunity to apply my skills in this environment for a summer might be mutually beneficial. It was to this end that my involvement with the AMRL program in the Acceleration Branch was directed.

II. OBJECTIVES OF RESEARCH EFFORT

The overall objective of the research effort was quite general. It was to demonstrate the utility and viability of the animal model concept. Several approaches were taken in order to accomplish this objective. They were as follows:

- a. To assume directional responsibility for the animal performance portion of a previously designed tracking study.
- b. To propose and conduct an experiment which brings together to concept of the Feature-Positive Effect and the development of attention in primate tracking situations.
- c. To provide a series of weekly seminars on the logic,

techniques, and application of fundamental concepts of animal behavior.

III. TRACKING FOR POSITIVE REINFORCEMENT

The primary purpose of this endeavor is to develop a critical compensatory task which can be used by both human and non-human primates. This is necessary in order to compare the two species in terms of the phase plane analysis developed by Repperger et al.². Clearly, the first step in such a program is to establish reliable tracking performance in non-human primates.

Four Rhesus monkeys are receiving training on a visual compensatory tracking task requiring the subject to maintain a constant velocity drifting target on a CRT screen. The animals press translucent side panels on each side of the TV monitor to keep the picture on screen for a period of 20 seconds. The computer graphics presentation consists of a transparent container holding a simulated food pellet. The container moves left or right at a constant velocity. Pressing the side panel toward which the image is drifting reverses the direction of travel. At the twentieth second the container tilts completely allowing the "pellet" to drop out and fall the length of the screen. A pellet dispenser is located at the bottom of the screen where the actual pellet reward appears. If during the 20 second presentation the animal allows the container to drift behind either translucent side panel the container resumes an upright position and the 20 second timer is reset.

The most critical and laborious aspect of this study is the training of the animals to perform the above described task. This involves chair training, magazine training, response shaping and target familiarization. During chair training the animals are placed into restraint chairs daily. Magazine training consists of teaching the monkeys to accept the sucrose food pellets when they are delivered into the hopper. Response shaping involves teaching the animals to press the side panels in order to earn food pellets. Target familiarization requires that the animals respond appropriately on the panels in order to control the location of the target

on the CRT. The entire process requires different amounts of time for each subject. The "best" animals learn it in a minimum of five weeks.

Currently, two of the monkeys are in the target familiarization stage of training. The remaining two are undergoing response shaping. It is believed that all subjects will be completely trained within the next eight weeks. Manipulation to the various velocity-acceleration combinations required for the phase plane analysis will then be accomplished.

IV. FEATURE POSITIVE AND FEATURE NEGATIVE DISCRIMINATION LEARNING MAINTAINED BY NEGATIVE REINFORCEMENT

The ability to produce a reliable and efficient protocol for the development and maintenance of tracking behavior in subhuman primates has an important bearing on the utility of the animal model concept. From a behavioral standpoint, the production of tracking behavior in monkeys requires that the animal learn to (a) attend to specific aspects (features) of the environment, and (b) respond appropriately to various configurations of the features.

Unfortunately, it is presently difficult to characterize the essential criteria for producing tracking behavior in animals¹. In part, this is due to the variety of task parameters which have been used (e.g., pursuit vs. compensatory tracking, positive vs negative reinforcement, discrete vs continuous response). However, another equally important problem, and the one addressed in this research, deals with issue of the development of attention. Specifically, how can the researcher communicate to a nonverbal subject the behavioral rules which must be used in order to produce efficient tracking performance? Stated in a more analytic way, how can the researcher insure that his animal subjects attend to the critical stimuli in the tracking situation.

The concept of attention is currently popular in the area of animal learning. Although various theories of attention exist, all agree that a

primary element in the development of attention is that the relevant stimulus is highly correlated with a biologically significant event. Thus, stimuli which are correlated with (and therefore predictive of) biologically significant events (such as food or shock) are stimuli to which the subject will attend. The strength of attention is a direct function of the degree of correlation.

Related to the concept of attention is a body of literature known as the Feature Positive Effect (FPE)³. Basically, this phenomenon deals with the relationship between stimuli and reinforcers (biologically significant events). In one such arrangement, a compound stimulus consisting of a light and tone predicts food. The light alone, however, predicts no food. The critical element (i.e., feature) in this arrangement is the tone since this is the stimulus which distinguishes food trials from no-food trials. This procedure is called feature positive (FP) learning since the critical stimulus (tone) is correlated exclusively with positive, or food trials. FP learning is readily acquired by every organism studied, ranging from fish to humans.

Consider now the reverse arrangement, namely, that light alone predicts food and the tone and tone combination produces no food. The feature (tone) now predicts the absence of food since it is present only on negative (no food) trials. In other words, the feature-negative (FN) task is exceedingly difficult to learn. In fact, most subjects never learn it at all. The rate at which subjects learn the rate at which FP discriminations are learned is known as the Feature-Positive Effect, etc.

The feature-positive phenomenon is related to the feature-negative in an even more direct way. An example should be informative. Suppose an animal might be presented with an array of light panels, two of which are red, and the other green on S+ trials (i.e., trials on which the animal can earn food rewards by pressing any one of the panels). On S-trials (trials on which no food is available) the array consists of three red panels. Thus, this is a feature-positive task in which the feature is the green

light. Under these conditions, the animal will soon direct virtually all of its responses (panel presses) to the green feature; i.e., that stimulus element most predictive of food. Whenever and wherever the green light appears, the animal's response will follow. Thus, the monkey tracks the feature. In the FN case when the green light appears exclusively on S-trials, the subject will track negatively; i.e., it will actively avoid the feature. Thus, the feature-positive paradigm appears to be an interesting and efficient way to explore the development of attention (and subsequently tracking) in animals⁴.

Virtually all of the studies concerning the FPE have used positive reinforcement (i.e., food reward). The present proposal seeks to extend this body of data by exploring the FPE as supported by negative reinforcement, shock. This preparation has relevance to the typical tracking paradigm inasmuch as shock is the usual mode of behavioral control. Furthermore, it is of interest and importance regarding the present mission to establish clearly whether the tracking of a feature which predicts shock develops in the same manner and form as does that associated with food reinforcement. The degree to which we can specify the development of attention in the negative reinforcement setting is the degree to which we can delineate further the essential conditions necessary to establish tracking behavior in primates.

Experimental Design

I.	<u>Avoidance</u>	<u>S+</u>	<u>S-</u>
	FP	1 Red & 2 Green - Shock Avoidance	3 Green - No Avoid.
	FN	3 Green - Shock Avoidance	1 Red & 2 Green-No Avoid.
II.	<u>Escape: Feature Predicts Shock</u>		
		<u>S+</u>	<u>S-</u>
	FP	1 Red & 2 Green - Shock (Escape)	3 Green - No Shock
	FN	3 Green - Shock (Escape)	1 Red & 2 Green-No Shock

III. Escape: Feature Predicts Reinforcement (Shock Termination)

	S+	S-
FP	1 Red & Green - Shock (Escape)	3 Green - Shock (No (Escape)
FN	3 Green-Shock (Escape)	1 Red & 2 Green (Shock No Escape)

The response requirement for the animals in this experiment is to press the appropriate panels on S+ trials so as to escape or avoid shock. If the critical aspect of attention is determined by the predictability of shock by the feature, then the FPII group should learn more readily than the FPI or FPIII groups, since in the latter condition shock is not predictable from the feature alone. If, however, the critical attentional aspect in the negative reinforcement situation is reinforcement, (i.e., shock termination), then the FP I and FP III groups should also learn easily. The differences between groups FP I and FP III will point to the role of shock-reinforcement interaction. If the FPE is maintained, learning in the FN conditions should be universally attenuated.

The actual running of this experiment began late in the reporting period. Hardware development, computer acquisition and programming and protocol approval, caused the delay. Consequently, it is too early to report any definitive results aside from the fact that some learning is beginning to appear. This experiment will, however, continue beyond the ten week reporting period. The Acceleration Branch personnel are now qualified to carry out the remainder of this experiment.

V. RECOMMENDATIONS

At this point it is difficult to characterize in absolute terms the status of the above described experiments since they are not yet completed. Nevertheless, preliminary results appear favorable. Monkeys are learning the

food-supported tracking task, and escape and avoidance behaviors are beginning to emerge under the feature-positive paradigm. At this point then, the animal performance program appears viable.

Future tracking experiments should become increasingly complex. In addition, comparison of human and subhuman operators seems desirable and necessary. The relative utility of positive and negative reinforcement support systems should be explored also. Finally different types of response manipulanda should be evaluated. The proposed design to explore these relationships is a 2X2X2 factorial plan in which combinations of species (human vs subhuman primate), support source (positive vs negative reinforcement), and response manipulandum (stick vs panel) are present. This would be a repeated measures experiment in which various combinations of target acceleration and velocity are presented in each condition.

Follow-up research on the feature positive problem should examine conditions which determine the detectability of the feature itself. Various stimulus blocking and overshadowing paradigms should be studied. In addition, it seems prudent to empirically examine (and perhaps theoretically couch) the entire feature positive effect in terms of a signal detection model. These experiments would begin by exploring the relative saliency of the phenomenon under various signal (i.e. feature) noise ratios. Finally, in order to validate the animal model concept, these studies should be replicated using human subjects.

REFERENCES

1. D.F. McCoy, S.R. Aeschlemon, G. Nallan, & G.M. Pace, "A Comparison of Two Techniques For The Development And Maintenance Of Tracking Behavior In Monkeys". Aviation, Space and Environmental Medicine, Vol 44, pp 226-229, 1980.
2. Daniel W. Repperger, Sharon Ward, Earl Hartzell, Betty Glass, & Walt Summers. "An Algorithm to Ascertain Critical Regions of Human Tracking Ability", IEEE Trans. on Systems, Man & Cybernetics. Vol 9, pp 183-196, 1979.
3. E. Hearst, H.M. Jenkins, "Sign Tracking: The Stimuli-Reinforcer Relation and Directed Action". Psychonomic Society, 1974.
4. G.P. Pace, D.F. McCoy, G.B. Nallan, "Feature Positive and Feature Negative Learning in the Rhesus Monkey and Pigeon". American Journal of Psychology, Vol 93, pp 409-426, 1980.

1981 USAF - SCEEE SUMMER FACULTY RESEARCH PROGRAM

Sponsored by the

AIR FORCE OFFICE OF SCIENTIFIC RESEARCH

Conducted by the

SOUTHEASTERN CENTER FOR ELECTRICAL ENGINEERING EDUCATION

FINAL REPORT

VIBRATION-ROTATION RELAXATION IN THE HF LASER

Prepared by:	Henry A. McGee, Jr.
Academic Rank:	Professor and Head
Department and	Chemical Engineering Department
University:	Virginia Polytechnic Institute and State University
Research Location:	Air Force Weapons Laboratory (ARAC) Kirtland AFB, New Mexico 87117
USAF Research Colleagues:	Dr. Leroy E. Wilson and Maj Howard M. Brilliant
Date:	September 12, 1981
Contract No:	F49620-79-C-0038

VIBRATION-ROTATION RELAXATION IN THE HF LASER

by

Henry A. McGee, Jr.

ABSTRACT

The literature on rotational and vibrational relaxation in HF has been reviewed. The rates of these processes are critical to the design of large devices such as ALPHA, and yet our understanding is meagre. The areas of minimum understanding are identified and recommendations are made for further work.

ACKNOWLEDGEMENTS

I should like to thank the men and women of the Chemical Laser Branch, Advanced Laser Technology Division, Air Force Weapons Laboratory for the many kindnesses extended to me during my visit during the summer of 1981. They taught me much. I should particularly thank Dr. Leroy E. Wilson and Major Howard M. Brilliant for their scientific leadership as well as their great Western hospitality.

I. INTRODUCTION

The rates of vibrational/rotational relaxation processes are critical in both the design of a large laser such as ALPHA as well as in the final power efficiency, spectral distribution, and beam quality that one may expect from the device. The chemistry is



where product HF is produced in $v=1, 2,$ and $3.$ We are here not concerned with this pumping reaction which is both fast and also channels its exothermicity into vibration of the product. Rather we are concerned with the collisional rearrangement or relaxation of the nascent or primitive product distribution.

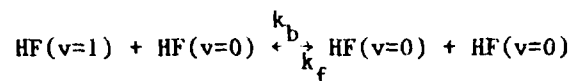
For example, in the laser we seek $v=3 \rightarrow v=2,$ but significant amounts of $v=3$ with a thermal rotational distribution (peaked at about $J=2$) undergoes a near resonant collision induced transformation into $v=2$ and $J=14.$ To the extent and rate that this occurs, we have lost the laser output at $v=3 \rightarrow v=2.$ Alternatively it is also possible that the energy may merely pool in $v=2, J=14$ and feed back into $v=3$ for subsequent lasing to $v=2.$ These sorts of rearrangements in v and J can occur in many forms as is clear from a consideration of the complexity of the v, J manifold for HF. And all of these collisional processes will depend upon the specific collision partner as well as upon the temperature, i.e., the translational energy of the impact.

So the relaxation dynamics that we seek are very complex.

II. OBJECTIVES OF THE RESEARCH EFFORT

A relaxation process is the name given to the attaining of an equilibrium distribution from some non-equilibrium distribution that might be produced by some fast energy input process. This input rate must clearly be fast relative to the relaxation rate or else relaxation would merely follow input, and a non-equilibrium distribution could never be produced. Suppose HF is all in its ground vibrational state ($v=0$) at $T,$ we may rapidly place some of these molecules in the $v=1$ state, and if

the gas temperature is held at T, the vibrational relaxation rate irrespective of J is



and

$$\frac{d(\text{HF})_1}{dt} = -k_f(\text{HF})_1(\text{HF})_0 + k_b(\text{HF})_0^2$$

The reverse reaction, k_b , is here so small as to be negligible, and

$$(\text{HF})_{v=1} = (\text{HF})_{v=1}^0 \exp(-k_f[\text{HF}]_{v=0}t)$$

We know k_b to be insignificant, for the equilibrium constant at T is large and negative.

The initial non-equilibrium distribution has been produced by chemical reaction or by laser pumping, and monitoring of the subsequent concentration as a function of time has been accomplished by observing the emission from $v=1 \rightarrow v=0$, or by some laser absorption process such as $v=1 \rightarrow v=2$. Several problems are immediately apparent.

a) We demand that $[\text{HF}]_{v=1} \ll [\text{HF}]_{v=0}$ so that collisions are only with $[\text{HF}]_{v=0}$ as the relaxer. This will yield the so-called self-relaxation rate.

b) We demand that the emission or absorption that is the probe or diagnostic procedure be directly proportional to the number density of $[\text{HF}]_v$ although an absolute measurement is unnecessary.

c) The efficiency of various collision partners is different. We must develop a kinetic analysis to allow a determination of the k of the added relaxer since $[\text{HF}]_{v=0}$ will always be present.

d) The rate of relaxation depends upon the specific v. We want to determine these different rates.

e) Within each v there is a rotational (J) manifold, and we expect the v-v rate to depend upon this underlying J structure. We may assume the J states to be at equilibrium, or we can experimentally determine the J states. We must know the rates of J relaxation to understand the v rates; the rates of the two modes are then inter-

related and to understand one, we must understand the other. Even if we are only interested in J-J rates, we expect that these rates will depend upon the v state.

f) In the relaxation of higher v states, we must know if transitions of $\Delta v > 1$ can occur. Just what is the role of multi-quantum transitions? Insofar as J-J relaxation plays a role in the v - v rates, we also must know the role of multi-quantum transitions in J-J relaxation.

g) Even the mechanism of v - v relaxation is uncertain. The excited species may go to $v=0$ and thermal J or it may more resonantly go to $v=0$ and high J. Either this process or the subsequent J-J rate could then be rate controlling in the overall relaxation of the HF(v ,J) state.

h) Overlaying all of these collision effects are changes in number density due both to spontaneous and to stimulated emission. These effects must be sorted from the collisional effects.

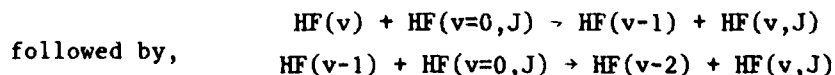
In the following pages we will examine each of these issues in detail and summarize our current best understanding.

III. KINETIC ANALYSIS

The analysis of much experimental kinetic data is similar, so it is appropriate to summarize this prior to reviewing the critical experiments themselves. We are interested in both vibrational and rotational relaxation in which the collision partner is the same chemical species as well as that for other collision partners. The language in the following development is in terms of vibration but the arguments are equally applicable to rotational relaxation. Let us look at these in turn.

(a) Self-Relaxation

If a relatively small fraction of HF is excited, the single quantum relaxation process could be,



and so forth. We here take the temperature to be so low that only $v=0$ relaxers are present, that is, the temperature is below about 600 K where

$v=1$ is present only to about 0.1%. Neglecting radiative process, the number densities of the several species can be written.

$$\frac{dn(v)}{dt} = -k_v n(v) n(v=0) \quad (1)$$

and

$$\frac{dn(v-1)}{dt} = -k_{v-1}^v n(v-1) n(v=0) = k_v n(v) n(v=0) \quad (2)$$

and so on. With $n(v=0)$ essentially unchanged with time, these differential equations can be integrated to yield

$$n(v) = n^0(v) \exp(-k_v nt) \quad (3)$$

and

$$n(v-1) = \frac{n^0(v)k_v}{k_v - k_{v-1}^v} [\exp(-k_{v-1}^v nt) - \exp(-k_v nt)] \quad (4)$$

and so on. Here n is the number density of HF at $v=0$, $n^0(v)$ is the initially produced number density of $n(v)$, and k_{v-1}^v is the rate coefficient of v into $v-1$. We recognize that species may leave v to enter any state, and thus $k_v = \sum_{n=1}^v k_{v-n}^v$. The actual experimental data will allow us to examine the probability of single vs. multi-quantum transitions, and we shall return

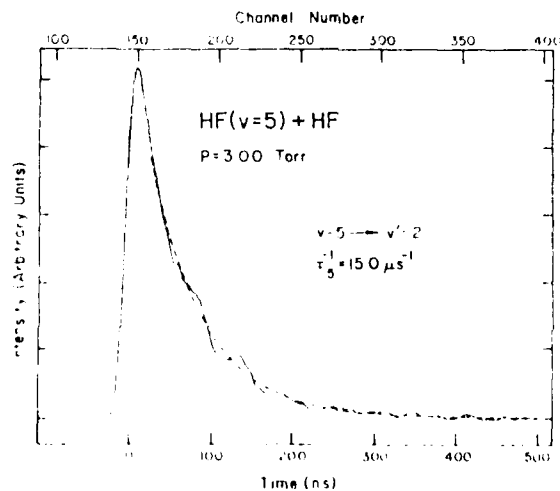


Fig. 1. Overtone vibration fluorescence ($\Delta v=3$) from HF ($v=5$). The solid curve is the difference signal obtained by averaging 500 laser pulses, and the broken curve is a single exponential fit to the data. From G. M. Jursich and F. F. Crim, *J. Chem. Phys.* 74, 4455(1981).

to this analysis later. To evaluate the fundamental constants, k_v , k_{v-1} , k_{v-1}^v etc. we require some analytical measurement of $n(v)$, $n(v-1)$, etc. as a function of time. Note that we do not need the absolute densities, but rather some measurement proportional to these densities will do.

Suppose we measure some radiative transition such as that in Fig. 1. Using the equation that we have derived for $n(v)$ vs. t , we find the time,

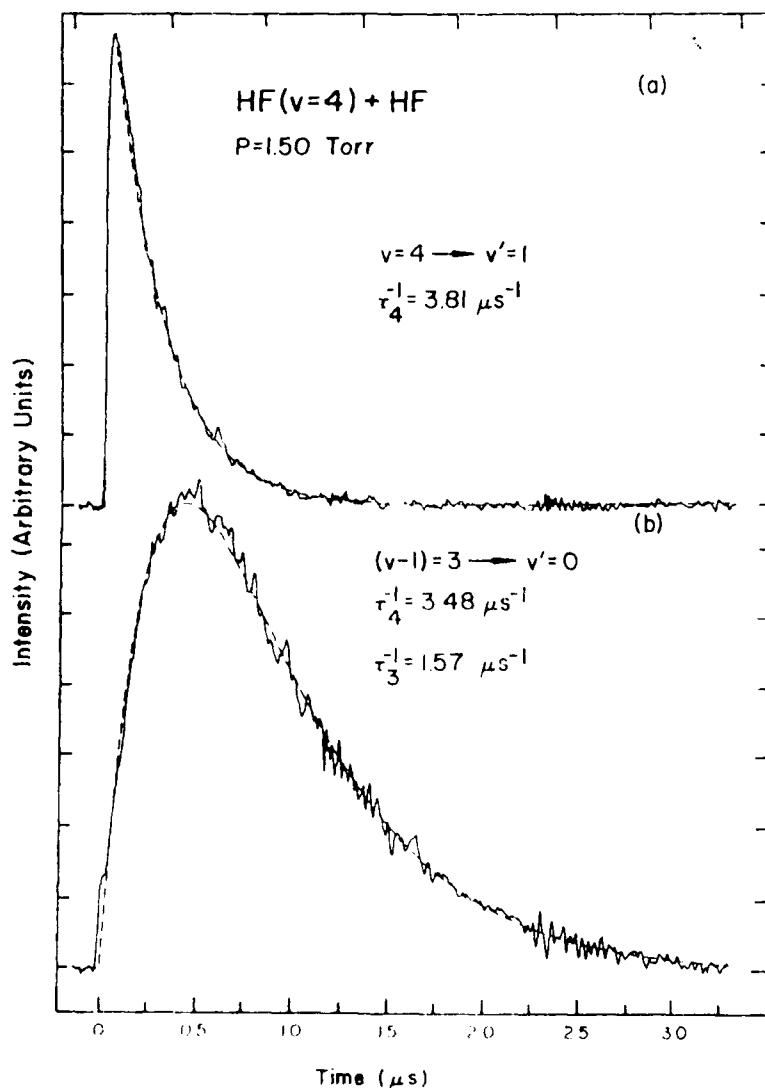


Fig. 2. Overtone vibration fluorescence ($\Delta v=3$). (a) Fluorescence from HF($v=4$). The solid curve is the difference signal obtained by averaging 2000 laser pulses, and the broken curve is a single exponential fit to the data. (b) Fluorescence from HF($v=3$) following excitation of HF($v=4$). The solid curve is the difference signal obtained by averaging 4000 laser pulses, and the broken curve is a fit of two exponentials Eq. 4 to the data which yields the indicated decay constants (τ_4^{-1} and τ_3^{-1}). From G. M. Jursich and F. F. Crim. *J. Chem. Phys.* 74, 4455(1981).

τ , at which $n(v)$ has fallen to $1/e$ of its initial value, $n^0(v)$, is $\tau^{-1} = k_v n^0(v)$. Since $n = p/RT$, at any experimental T and p , we can report the characteristic relaxation as either k_v , usually in the $\text{cm}^3/\text{molecule s}$ or as a time constant, τ , in s. Fig. 1. depicts $\tau = 15.0 \mu\text{s}$ for $k(v=5)$ at 300 K and 3.0 torr. Fig. 2(a) is the same sort of fit but for $(v=4)$.

The data of Fig. 2(b) are well represented by Eq. (4) with $\tau_4 = 3.48 \mu\text{s}$ and $\tau_3 = 1.57 \mu\text{s}$. The difference between $\tau_4 = 3.81 \mu\text{s}$ and $3.48 \mu\text{s}$ is an indication of the experimental error, and we will want to make sufficient measurements to obtain a sense of this overall uncertainty.

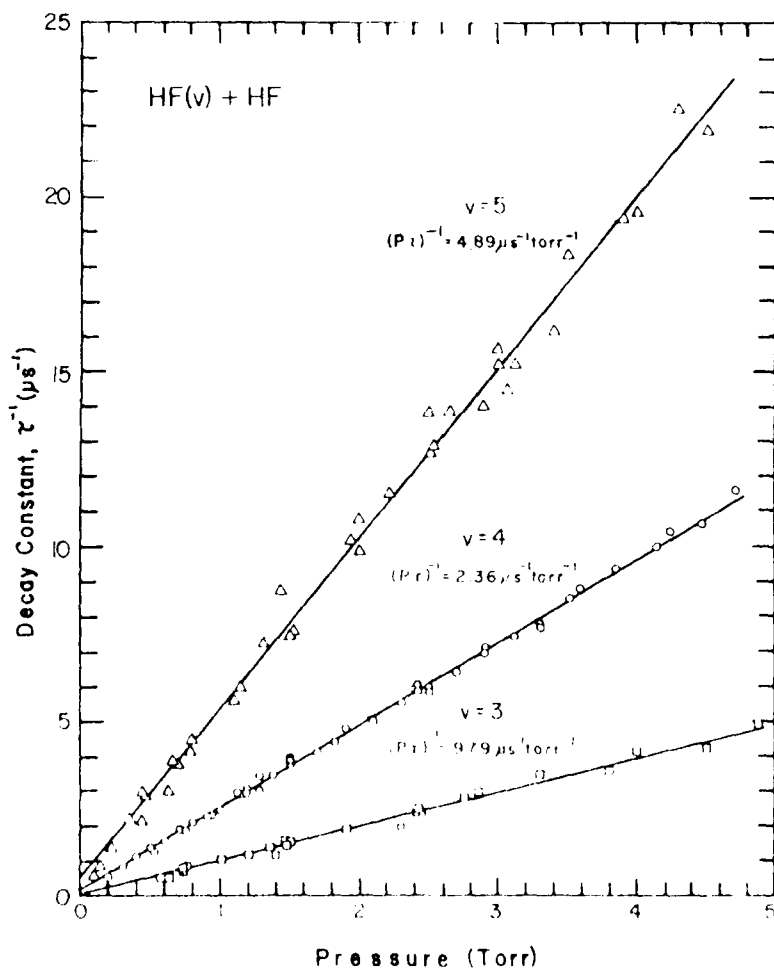


Fig. 3. Pressure dependence of observed decay constants for $\text{HF}(v = 3, 4, \text{ and } 5)$. From G. M. Jursich and F. F. Crim, *J. Chem. Phys.* 74, 4455(1981).

AD-A113 709

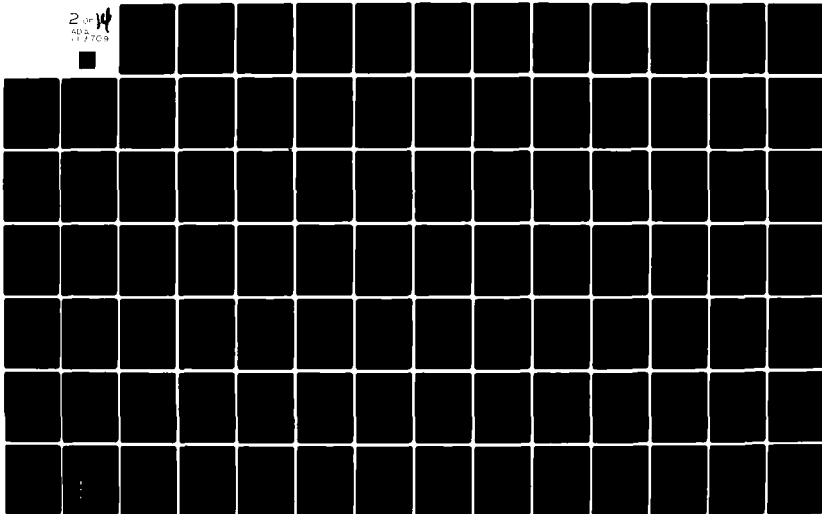
SOUTHEASTERN CENTER FOR ELECTRICAL ENGINEERING EDUCAT--ETC F/G 5/1
USAF SUMMER FACULTY RESEARCH PROGRAM. 1981 RESEARCH REPORTS, VO--ETC(U)
OCT 81 W D PEELE F49620-79-C-0038

UNCLASSIFIED

AFOSR-TR-82-0228

NL

2 of 4
AD 7709



The time constant, τ , will be a linear function of the pressure, for

$$\tau_v^{-1} = k_v n^o(v) = k_v p/RT \quad (5)$$

and the slope of such a curve will give k_v . Such a graph for $v=3, 4$ and 5 appears in Fig. 3 where the line is a least square fit to all the data.

At $v=4$ then, $(p\tau)^{-1} = 2.36 \mu\text{s}^{-1} \text{ torr}^{-1}$ which can be converted to k_v by Eq. (5), $k(v=4) = (p\tau)^{-1}RT = 7.23 \times 10^{-11} \text{ cm}^3/\text{molecule s}$.

(b) Alternate Collision Partners

Consider now a mixture of HF in, say argon, of mole fraction $x(\text{HF})$. The rate of loss of HF excited to level v is similar to Eq. (2) which integrates to

$$\tau^{-1} = [n(\text{A})+n(v=0)] [k_v^{\text{A}} + x_{\text{HF}} (k_v^{\text{HF}} - k_v^{\text{A}})] \quad (6)$$

The first bracket is p/RT , and a plot of $(p\tau)^{-1}$ is then linear in x_{HF} . Such data for HF($v=4$) appear in Fig. 4, and we see from Eq. (6) that the sum of the slope and intercept is k_v^{HF} , the self-relaxation coefficient, which can be compared with that determined for $v=4$ determined in pure HF. In this case, $(p\tau)^{-1} = (1.98 \pm 4.74)10^3 + (2.32 \pm 0.28)10^6 x_{\text{HF}}$ in units of $(\text{torr s})^{-1}$. And k_4^{HF} is $7.21 \times 10^{-11} \text{ cm}^3/\text{molecule s}$ which compares very well with the pure HF value. Argon with $k_4^{\text{A}} = 6.15 \times 10^{-14} \text{ cm}^3/\text{molecule s}$ is not nearly as efficient.

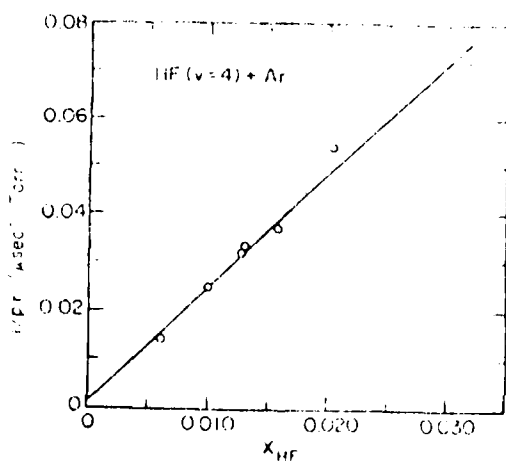


Fig. 4. $1/p\tau$ vs. $x_{\text{HF}}(v=4)$ in argon. From D. J. Douglas and C. B. Moore, J. Chem. Phys. 70, 1769(1979).

Probability Of Reaction

Rather than specific rate coefficients, some discussions are in terms rather of probabilities. At equilibrium the forward and reverse relaxation

rates are equal, and we can write

$$-k_f[\text{HF}(J-1)][\text{M}] + k_b[\text{HF}(J)][\text{M}] = 0$$

or

$$-ZP_J^{J-1}[\text{HF}(J-1)] + ZP_J^{J-1}[\text{HF}(J)] = 0$$

where Z is the rate of collision of an $\text{HF}(J-1)$ with M and P_J^{J-1} is the probability that $\text{HF}(J-1)$ will be changed to $\text{HF}(J)$ in that collision. Both $\text{HF}(J-1)$ and $\text{HF}(J)$ are similar in size and intermolecular force field, so taking Z to be equal for both,

$$k_f/k_b = P_J^{J-1}/P_{J-1}^J$$

At equilibrium the ratio of the number of species in adjoining levels is given by the appropriate Boltzmann factor, and the probabilities are then related as

$$P_J^{J-1} = P_{J-1}^J (g_J/g_{J-1}) \exp \{-(E_J - E_{J-1})/RT\}$$

Comparing characteristic rates as a specific rate coefficient vs. probability as written above, we see that an interconversion will require a collision frequency. This, in turn will require a collision diameter, and a calculated probability from a measured rate coefficient will implicitly reflect the choice made for this diameter.

IV. VIBRATION (EXPERIMENTAL)

There is good evidence that vibrational and rotational relaxation processes are closely interrelated. But for purposes of discussion, we will here make this somewhat artificial separation nonetheless.

Both the experimental data as well as theoretical predictions are in disagreement among themselves as to the extent of processes of $\Delta v > 1$.

Pro $\Delta v > 1$

Some of the most compelling data is from pure rotational lasing of HF from photoelimination experiments summarized in Fig 5. The earliest and the strongest lasing occurs at $15 \rightarrow 14$, $14 \rightarrow 13$, or $13 \rightarrow 12$ in each v , and it is striking that these rotational levels are opposite the thermal J levels

of the next higher v . At 300 K, the peak rotational population is at $J=2$, and 97% of the molecules are found within the $J=0$ to $J=5$ range. Even the very high J lines at $31 \rightarrow 30$ to $28 \rightarrow 27$ are at near resonant energy with thermal J in higher v states. Note that the $J=31$ state contains 53 kcal/mol of rotational energy which is about 35% of all available energy from CH_2CHF and CH_2CF_2 . One can well argue that the nascent HF in high v states is collisionally converted by Δv of as much as -5 and ΔJ of as much as +26. This conversion must be fast for these transitions have the highest gain,

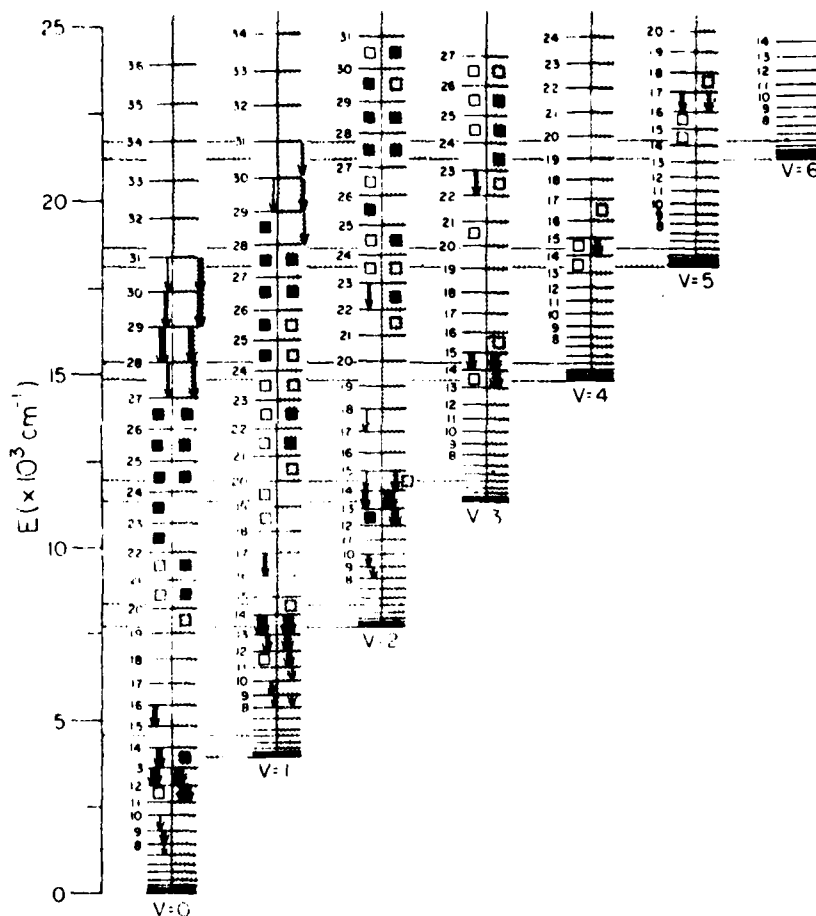


FIG. 5. Vibration-rotation energy level diagram for HF and observed rotational transitions. 50 torr samples, 1/100 mixtures are argon; left column CH_2CHF ; right column CH_2CF_2 ; arrow width and placement shows intensity and timing; parent absorption is indicated by rectangles: solid, absorption exceeding 5% per pass; open, exceeding 1%; horizontal crosshatching shows levels that are in near resonance with levels n , $J=0$ to $J=5$. From E.R. Sirkin and G.C. Pimentel, *J. Chem. Phys.* 75, 604(1981).

that is, they are earliest to threshold. They are also collision induced, for the addition of He, Ne, or A decreases time to threshold with effectiveness $A > Ne > He$. Such high J states could come from the nascent reaction as well, but it is interesting that a statistical analysis of the nascent J population, while not conclusive, nonetheless predicts negative gain at every J. Other transitions such as 0(16→15), 1(17→16), and 2(18→17) are insensitive to added buffer gas both as regards pressure and molecular weight. So these would appear to result from nascent production.

So although these data are not conclusive, they do provide a compelling argument for the production of high J states by nascent means but also with a large contribution from near resonant fast $v \rightarrow R$ collisionally induced transitions.

Although all calculations do not agree, some trajectory calculations suggest that transitions of $\Delta v > 1$ occur. These calculations are discussed in detail later in this report.

Case $\Delta v > 1$

From the earlier kinetic analysis, we can determine the ratio of the total molecules out of the level initially excited to the molecules that flow into and out of the next lower level. If this ratio is nearly one, we can safely argue that every molecule out of v has gone through v-1 and thus a Δv of unity is dominant. The areas under curves like those in Fig. 2 are an experimental measurement of this ratio provided the intensity from each of the two transitions is proportional in the same way to the number density of species in that level. The "corrected" experimental area is the actual area under the curve multiplied by a collection of efficiency and intensity factors such as the Einstein coefficient, the quantum efficiency of the photomultiplier tube detector, the number of laser pulses, etc. A similar correction could be written for all experiments in which observed intensity is to be related to an actual number density. These "corrected" areas may then be ratioed,

$$\frac{A_{v-1}}{A_v} = \frac{\int_0^{\infty} n_{v-1} dt}{\int_0^{\infty} n_v dt} = \frac{k_{v,v-1}}{k_{v-1}}$$

Now if we multiply both sides by k_{v-1}/k_v ,

$$k_{v,v-1}/k_v = (A_{v-1}/A_v)(k_{v-1}/k_v)$$

For excitation of $v=4$, Crim finds

$$k_{4,3}/k_4 = (A_3/A_4)(k_3/k_4) = 0.98 \pm 0.19$$

and we conclude that single quantum processes dominate. At least one other laboratory has reported similar results from a similar analysis.

Experiments to determine the rate of relaxation of vibrationally excited HF by several species other than HF($v=0$) have also reported only single quantum transitions.

Relaxation by Species Other Than HF($v=0$)

The efficiency of added species is

$$(p\tau)^{-1} = (1/RT) [k_M + x_{HF} (k_{HF} - k_M)] \quad (7)$$

Several possibilities are apparent. By knowing x_{HF} , we can measure τ and p , and deduce k_M since we know the self-relaxation rate, k_{HF} , from previous work. We could plot $p\tau$ vs. x_{HF} for a series of mixtures where we measure τ at whatever the convenient pressure. The plot should be straight with

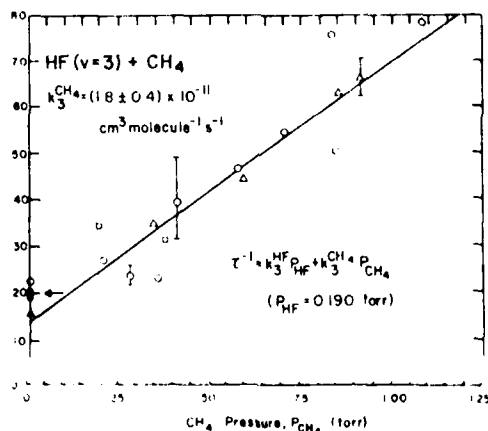


Fig. 6. Methane pressure dependence of the observed decay constant in a HF-CH₄ mixture. The arrows indicate the calculated intercept using the previously determined relaxation rate constant for HF(v) by HF(0). HF ($v=3$), $p_{HF}=0.190$ torr. From J. K. Lampert, G. M. Jursich and F. F. Crim, Chem. Phys. Lett. 71, 258(1980).

intercept k_M and slope $(k_{HF} - k_M)$ from which we could get another evaluation of k_M since k_{HF} is known. Such a plot appears in Fig. 4 for argon in HF, and such data are available for several relaxers with HF in several initial v states. Alternatively, one could plot τ^{-1} vs. the partial pressure of the relaxer while keeping the partial pressure of HF constant. From Eq. (7) above, it is clear that this plot will be a straight line of slope k_M/RT . Such a curve with CH_4 as the relaxer appears in Fig. 6, where the slope is 0.57 $(\text{torr } \mu\text{s})^{-1}$ and $k_{CH_4} = 1.8 \times 10^{-11} \text{ cm}^3/\text{molecule s}$. We may also determine k_{CH_4}

from each measurement of τ at a particular $\bar{p}(CH_4)$ since we know the total pressure and k_{HF} . The typical scatter in these individual measurements that is evident in Fig. 6 suggests that the averaging represented by the determination from the slope yields a more reliable value of $k(CH_4)$.

Interestingly, the deactivation of $HF(v=1)$ occurs over a wide range of rates from 1.1×10^5 $(\text{torr s})^{-1}$ for ClF_3 to 90 $(\text{torr s})^{-1}$ for SF_6 . There is no theory that successfully describes such data.

Relaxation as a Function of Temperature

The self-relaxation of HF at increased temperatures has been measured in the same way as depicted in Fig. 2 earlier by merely thermostating the HF cell at temperatures of interest. The experimental data together with several comparisons with theory appear in Fig. 7 where the inverse temperature dependence reflects the dominant influence of the van der Waals attraction. Note that the relaxation rate scales with v as $v^{2.7}$ at all temperatures.

An alternate, but less informative, way to present such data derives from the Landau-Teller analysis which predicts the experimental product, $p\tau$, to be linear in $T^{-1/3}$. The trajectory calculations of Wilkins do in fact yield such a linear plot, and these same data are also plotted in Fig. 7.

V. ROTATION (EXPERIMENTAL)

The coupling between vibration and rotation remains one of the crucial unanswered questions. Slow rotational relaxation will mean lower laser power

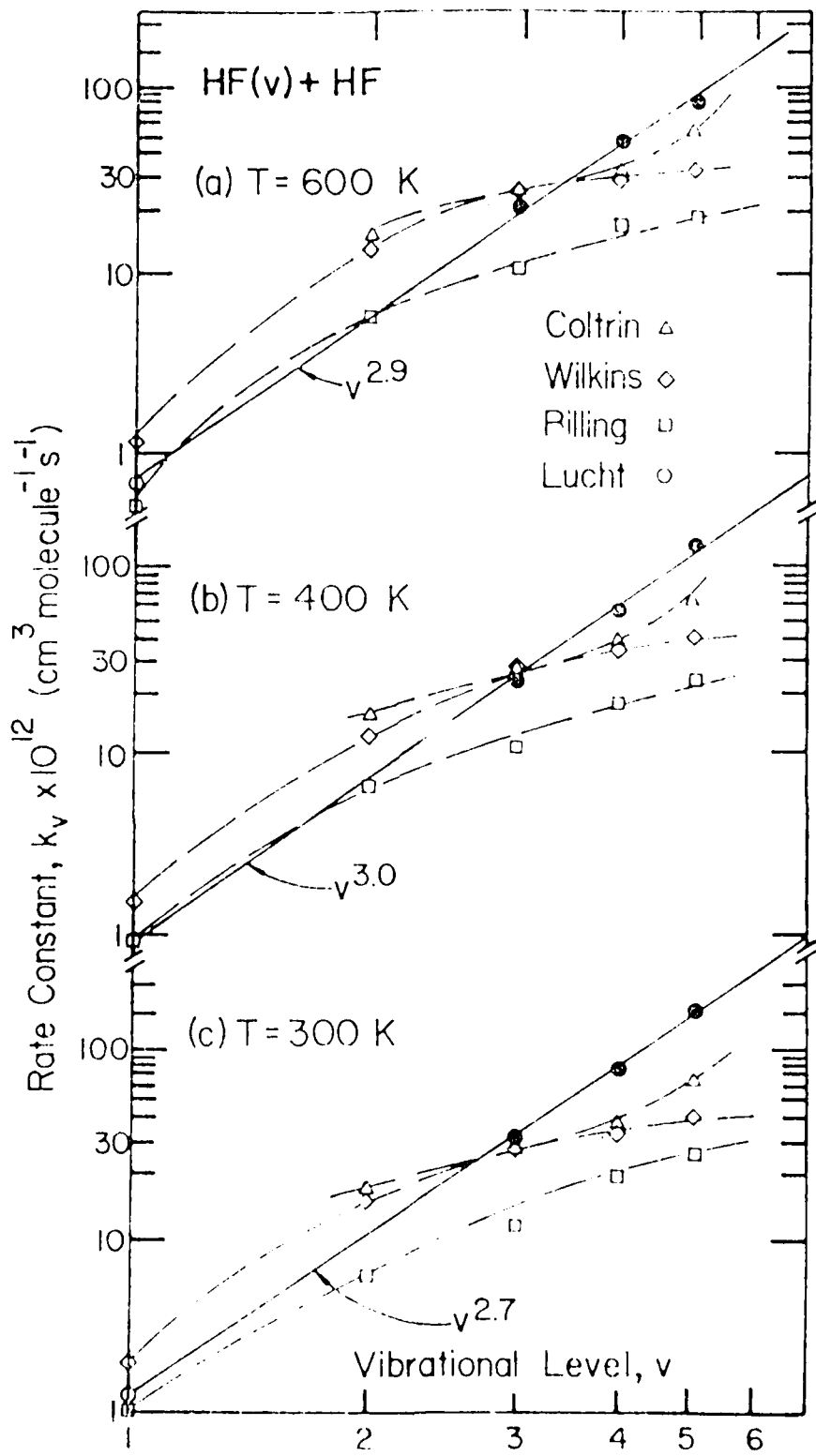


Fig. 7. Experimental and theoretical self-relaxation rates of HF at several temperatures. From T. J. Foster and F. F. Crim, *J. Chem. Phys.* 75, in press.

and a multiline output; whereas fast rotational relaxation allows single line emission from each vibrational level.

A qualitative, but nonetheless informative, insight into the rate of rotational equilibration is evident in Fig. 8. The emission when population is placed in $J' = 2$ follows the injection pulse as does that from nearby in $J' = 0$. Population placed progressively further away leaks very rapidly into the observed P(2) and P(3) lines with that placed furthest away in $J' = 5$ requiring $1.4 \mu\text{s}$ for the maximum to arrive in the levels from which the emission is being observed.

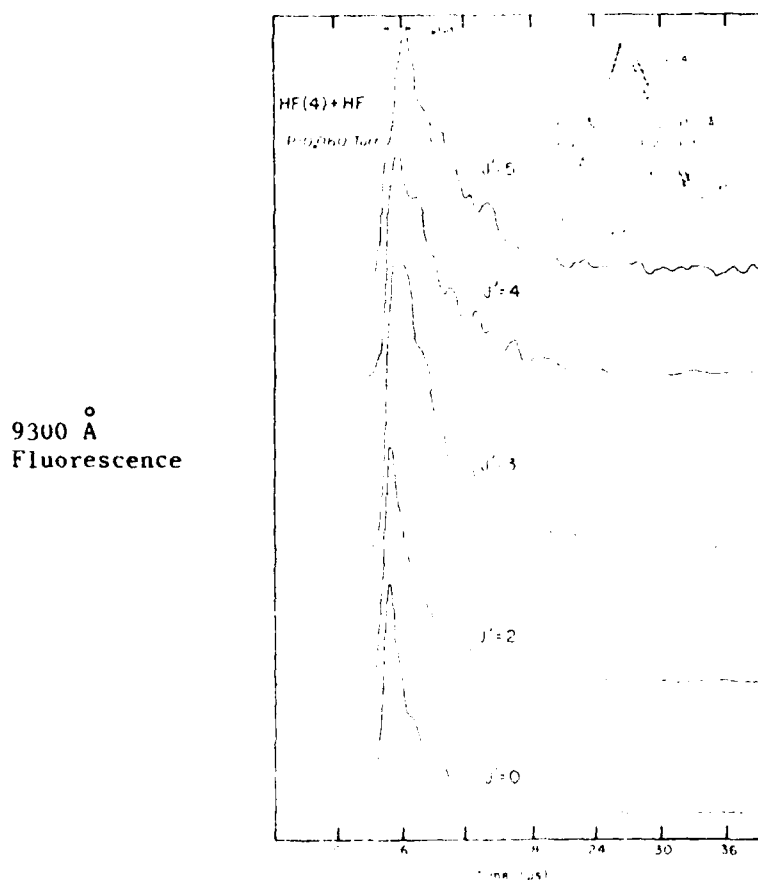


Fig 8. Temporal behavior of overtone vibration fluorescence upon excitation of different rotational states of $\text{HF}(v=4)$. The level diagram shows the excitation and detection scheme in which an initial rotational state (J') of $\text{HF}(v=4)$ is prepared and fluorescence coming primarily from $J' = 1$ and $J' = 2$ is observed. From J. K. Lampert, G. M. Jursich and F. F. Crim, *Chem. Phys. Lett.* 71, 258(1980).

The most direct method of observing the rate of rotational relaxation employs infrared double resonance, as portrayed in Fig. 9. Here population is placed in (in this case) $J=5$ of $v=1$ by a pulse of $P(6)$ from an HF driver laser or tunable laser. A second cw probe laser then monitors the arrival of population at $J \neq 5$ by absorption. The absorption of the probe laser is a measure of the difference in population between the affected J levels in $v=1$ and $v=2$. But since insufficient energy has been supplied in the pulse to populate $v=2$, the absorption measures the population in $v=1$.

Pure rotational lasing is a serious problem in understanding these sorts of data as we shall see. These laser transitions have a much more serious impact upon the populations below the J level that is pumped than for levels above the pumped level. Let us then consider first the higher levels and we will take the population there to be affected only by collision.

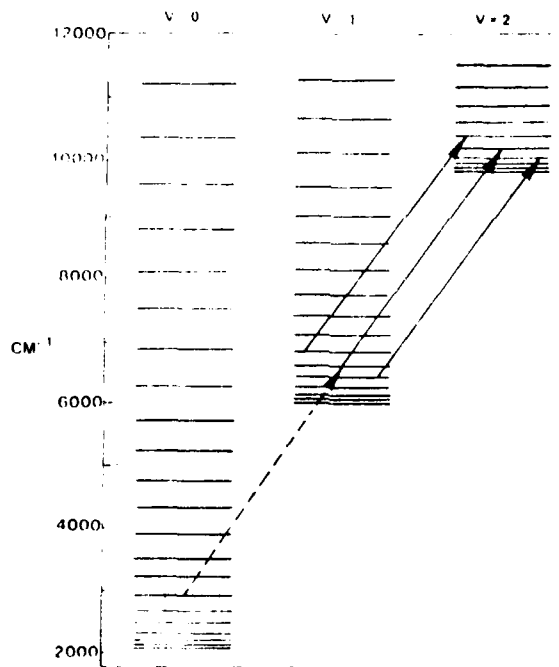


Fig. 9. Diagram of double-resonance experiment. The dashed line represents typical pumping pulses - solid lines represent cw probing of rotational levels. From J. J. Hinchey and R. H. Hobbs, J. Appl. Phys. 50, 628(1979).

"UP" Relaxation

Population placed in i leaks into the next higher level, j , as,

$$k_{ij} = (n\tau_{ij})^{-1} = RT (p\tau_{ij})^{-1}$$

Here τ_{ij} is the time for the population in i to fall to $1/e$ of its initial value which is taken to be the same as the time for the population in j to grow to $1/e$ of its maximum value, that is, for the absorption of the probe laser to grow to $1/e$ of its maximum value. Here again we ignore parallel paths and the simultaneous leakage from level j . Fitting the observed absorption vs. time data in this way, one determines τ whose values we expect to form a straight line vs. p (see Fig. 10). The slope of such a line is k and the rate of filling $J=6$ removed by $\Delta J=3$ from the fill point at $J=3$ is clearly slower than that for $\Delta J=1$ just as one intuitively knows must be the case. Deviations from linearity at increasing pressures must be due to omissions in our highly simplified kinetic model. Some transfer rate constants are summarized in Table I. Such data are rare, and several models that have achieved some currency are discussed in detail subsequently.

The population in a probed level at say $J=4$ (of $v=2$) after pumping to $J=0$ is influenced in a parallel way by $\Delta J = 1, 2, 3$ and 4 processes, each occurring at a different rate plus superradiance. Vibrational superradiance can confuse the data even when probing at J above the pumped J ($v=2$). But with pressure control, the weak dependence of lasing on pressure as compared to the collisional dependence, and the good fits to a single τ , all suggest

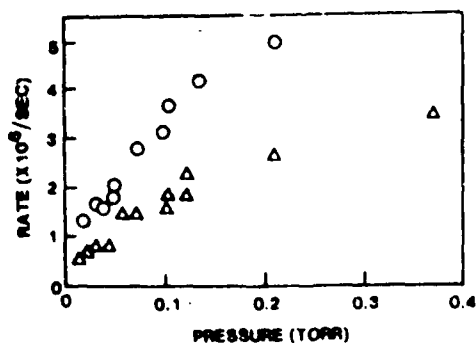


Fig. 10. Transfer rate, $1/\tau$, versus pressure for pumping the level $J=3$ and probing at $J=4$ (O) and $J=6$ (Δ). From J. J. Hinchey and R. H. Hobbs, *J. Chem. Phys.* 65, 2732(1976).

that radiative processes are not confusing the data. We determine a single phenomenological time constant while recognizing that the process is a composite thing.

The data at $v=1$ and $v=2$ appear in Fig. 11 and there appears to be a vibrational state effect causing a difference of as much as a factor of two in the rates. And yet the rotational constant changes by only 4% between $v=1$ and $v=2$. Uncertainties in the data however make any conclusions highly tentative.

"DOWN" Relaxation

Population placed in level i may also leak downwardly into lower levels, but here the measured time constants are confused by rotational lasing. This is evident from observation of the long wave emission as well as from the relative lack of pressure dependence of the characteristic time constant for absorption from the probe laser in infrared double resonance experiments. Lasing was always observed between the J level pumped and the next lower J , but cascading down the J ladder was not seen possibly due to detection sensitivity problems. The gains on these lines is such that we expect lasing even with no mirrors.

Using known optical characteristics of HF and an exponential correlation of collisional relaxation, one can readily make a computer simulation of the population in a level as a function of time with results as shown in Fig. 12.

TABLE I. Transfer rate constants.

Pump J	Probe J	$(1/P\tau_{ij})$ $\times (10^6 \text{ sec}^{-1} \text{ torr}^{-1})$	$K_{ij} (\times 10^6 \text{ sec}^{-1} \text{ torr}^{-1})$
2	3	104	22
2	4	50	6.3
2	5	27	1.6
2	6	19	0.42
2	7	12	0.083
3	4	48	6.0
3	5	24	1.4
3	6	19	0.42
3	7	17	0.12
3	8	11	0.02
4	5	58	3.4
4	6	34	0.76
4	7	30	0.21
4	8	10	0.017
5	6	68	1.5
5	7	33	0.23

Estimated statistical errors for values of $1/P\tau_{ij}$ and k_{ij} are $\pm 20\%$. From J. J. Hinchey and R. H. Hobbs, op. cit.

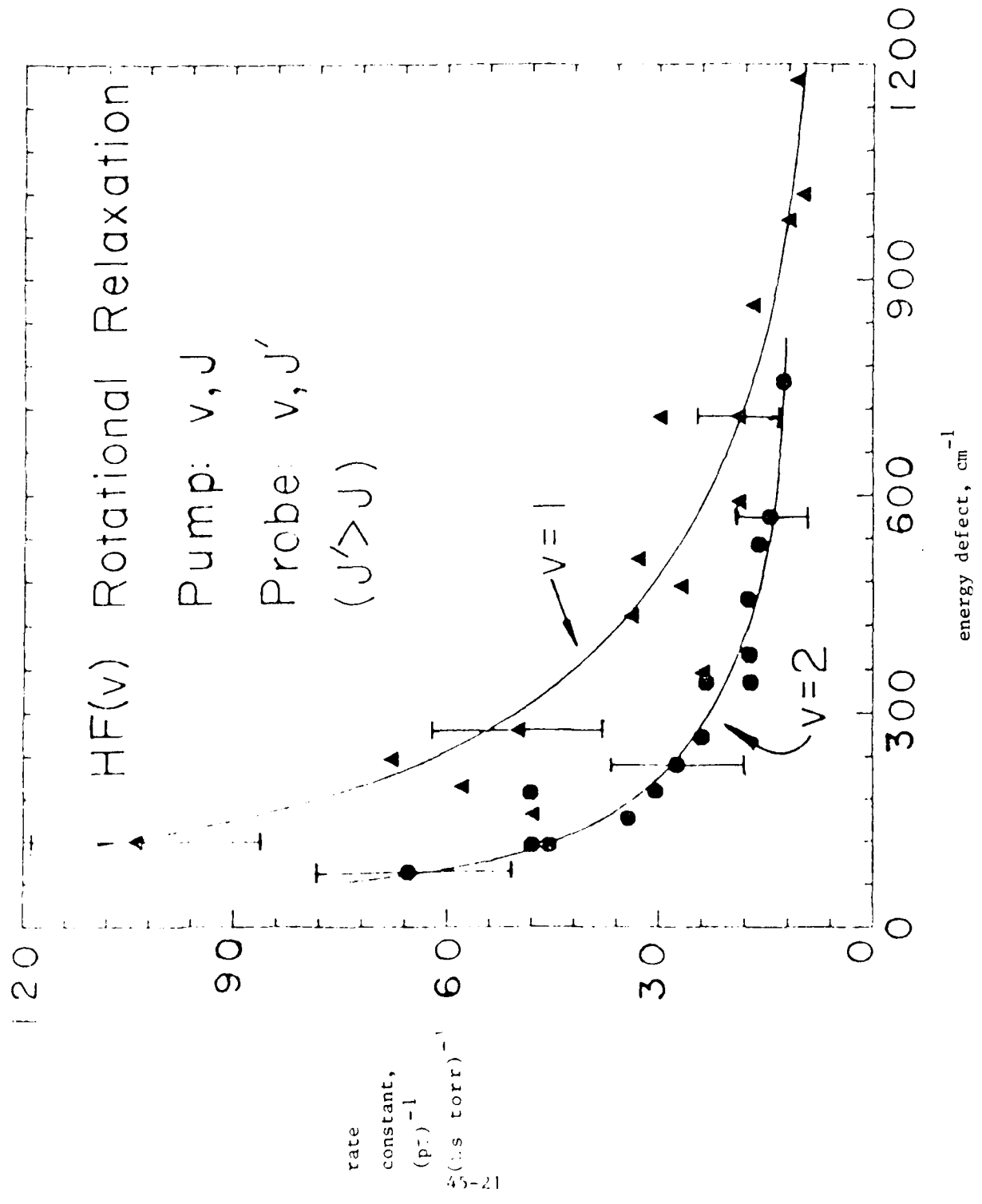


Fig. 11. Rotational relaxation rate constants as a function of energy defect; $v=1$ from Hitchen and Hobbs, *op. cit.*, and $v=2$ from R. A. Copeland, D. J. Pearson, and F. F. Crim. *Chem. Phys. Lett.* 81, 541 (1981).

Fig. 12b depicts population in the pumped level, and clearly with lasing from $5 \rightarrow 4$, the population never gets as high as would otherwise be the case. Fig. 12a depicts the arrival of this population in $J=4$ due to lasing. While in Fig. 12c, the population in $J=6$ is reduced somewhat due to the reduced population in $J=5$ due to lasing and the then corresponding slower rate by collision into the next higher level at $J=6$. Since lasing reduces the population in the "up" level only slightly, we conclude that "up" rates determined while ignoring rotational lasing are probably reasonably accurate.

It has been estimated that perhaps 10% of the power from a large laser device will be in the form of this unwanted long wave radiation.

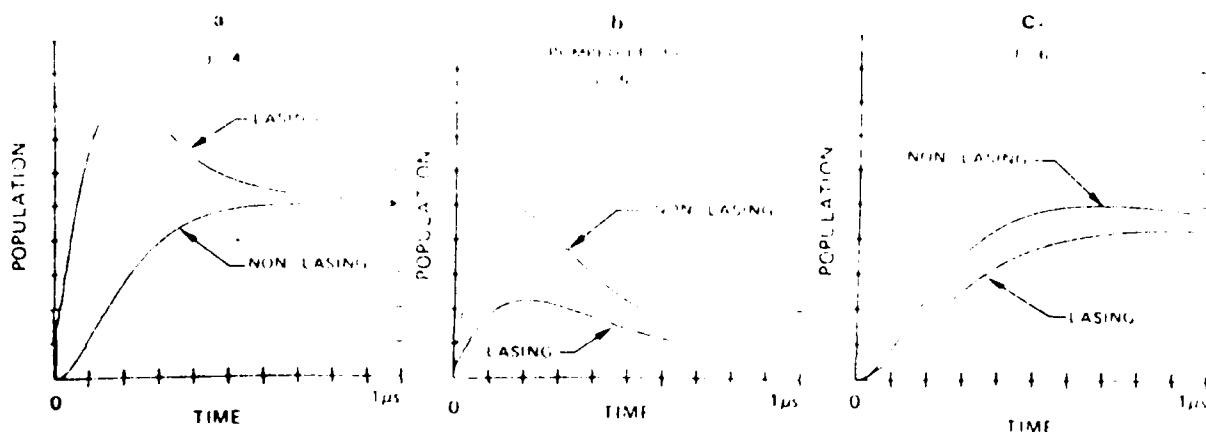


Fig. 12. Computer-generated comparisons of populations as a function of time under lasing and nonlasing conditions for the case of pumping $J=5$. From J. J. Hinchey and R. H. Hobbs, *J. Appl. Phys.* 50, 628(1979).

VI. THEORETICAL

Models for Rotational Relaxation

One model proposes that the specific rate coefficient exponentially depend upon the negative of the energy defect in the collision. That is, for



we write,

$$k = \alpha \bar{n}_i(v=1) \bar{n}_j(v=1) \exp\{-[(E_j - E_i) + (E_1 - E_k)]/kT\} \quad (8)$$

We could fit the measurements of k with this relationship with the pre-exponential factor as an adjustable parameter. It has been written as above with two Boltzmann factors to satisfy detailed balancing at equilibrium.

Here,

$$\bar{n}_i(v=1) = n_i(v=1)/n_0(v=1) = (2j+1) \exp(-\epsilon_j(v=1)/kT) / f_{\text{rot}}(v=1)$$

and

$$\bar{n}_j(v=1) = n_j(v=1)/n_0(v=1) = (2j+1) \exp(-\epsilon_j(v=1)/kT) / f_{\text{rot}}(v=1)$$

and from fitting Eq. (8) above to the data of Table I, we determine $\alpha = 2 \times 10^8 (\text{torr s})^{-1}$.

We had taken the growth of the probe laser absorption to be a simple exponential, but the real fill rate must depend upon many parallel processes.

$$\frac{dn_i(v=1)}{dt} = \sum_{i \neq j} \{k_{ij} n_i(v=1) - k_{ji} n_j(v=1)\} n(v=0)$$

where all of the $n(v=1)$ are much less than $n(v=0)$, and we replace $n(v=0)$ by p/RT . We can now use these k_{ij} 's (as correlated by Eq. 8) to predict the

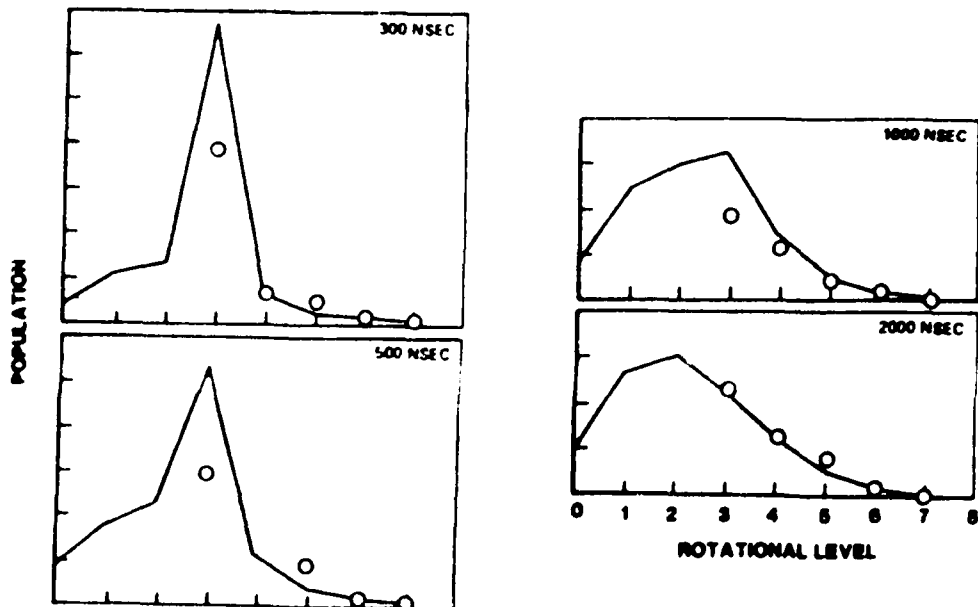


Fig. 13. Rotational population distributions at various times after pumping the level $J=3$ at 0.10 torr as compared to a computer simulation. From J. J. Hinchey and R. H. Hobbs, *J. Chem. Phys.* 65, 2732(1976).

population at each rotational level as a function of time. A comparison of the measured populations in several J states of $v=1$ with that predicted by Eq. 9 appears in Fig. 13. After 300 ns, the population is effectively all in $J=3$ where it was pumped, which evolves in 2 μ s to a Boltzmann distribution at the temperature of the experiment, 22°C. The fit is encouraging.

The mechanical or experimental problems of measuring such fast rates are certainly here evident. We expect the measured concentrations to err on the low side, for the relaxation is on a comparable time scale to the duration of the pump pulse and the response time of the particular detection system.

To the extent that the model is a realistic one, we can also gain insight into the extent of single vs. multi-quantum relaxation events. For all processes of $\Delta J = \pm 1$, we sum the values of k_{ij} and divide this by the sum of all k_{ij} 's regardless of ΔJ . And repeat this for $\Delta J = \pm 2$, $\Delta J = \pm 3$, etc. to determine then the percent of the total relaxation that is due to each type of event. For pumping into $J=3$, $v=1$ one finds

$\Delta J = \pm 1$	43%
$\Delta J = \pm 2$	32%
$\Delta J = \pm 3$	23%
all other	2%

where we have used the data of Table I and Eq. (8) to deduce the reverse rates from detailed balancing.

The slow rates of rotational relaxation at high J as given by Eq. (8) will pool energy and thus allow more time for superradiant long wave transitions to occur.

The effect of an added gas on these rates of rotational relaxation has been studied in a cursory way using the earlier kinetic analysis that takes the loss in population to arise from HF($v=0$) and added gas in direct proportion to their partial pressures. The transfer from $v=1$, $J=3$ to $J=4$ due to H_2 was 0.3×10^7 (torr s)⁻¹, due to He was 0.1×10^7 (torr s)⁻¹ and due to HF($v=0$) itself was 0.6×10^7 (torr s)⁻¹. H_2 is then less effective than HF, but more efficient than He suggesting that the rotation of H_2 may play a role in the rotational relaxation process.

Another exponential model has been suggested,⁹

$$P_J^J = N \exp(-CAE) \quad (10)$$

Where $P_{J'}^J$ is the probability of transition from J to J' , ΔE is the energy difference between the two states and N and C are adjustable constants. This model well correlates observations of the change in population in each J state as a function of time for HCl formed in the reaction $H+Cl_2$. The nascent HCl is in high J states ($J \approx 13$) which relax to a thermal distribution ($J \approx 3$) through a characteristic two-peak pattern. Eq. (10) well describes this pattern with no restriction on ΔJ , but the model does this, in a sense, automatically through its exponential dependence upon the energy change in the transition. This is in keeping with trajectory calculations¹³ where a transition from $J=15$ to $J=12$ occurred in about 1 in 1000 collisions. A transition from $J=3$ to $J=2$ occurred in about 1 in 3 collisions, while from $J=3$ to $J=0$ occurred in about 1 in 50 collisions. Even at low J , and much more so at higher J , a multi-quantum transition occurs with about an order of magnitude smaller probability than does a single quantum transition.

At $J=10$ the two exponential models predict relaxation rates different by an order of magnitude, and this difference grows rapidly as J increases.

These exponential models, however, do not fit all data, rather they underestimate the cross-section for large $J \rightarrow T$ transfers. A molecular beam of HF was pumped to several J states within $v=1$ and $v=2$ which then collided with Ar followed by observation of the infrared fluorescence. Here the data were well fit by,¹⁰

$$\sigma_{J \rightarrow J'} = (2J'+1) (T_f/T_i)^{\frac{1}{2}} (\Delta E_{JJ'})^{-\gamma} \quad (11)$$

where T_f and T_i are the final and initial relative translational energies respectively and ΔE is the energy transferred from translation to rotation of the HF. The collision was then typically, $HF(v=1, J=1) + Ar(T_i=4 \text{ kcal/mol})$ and the $J \rightarrow J'$ observed was $1 \rightarrow 2$ to $1 \rightarrow 9$. Eq. (11) well correlated these data, the cross-sections were unaffected either by varying T_i from 4 to 16 kcal/mol or by placing the HF in $v=1$ or $v=2$.

Trajectory Calculations

The most useful theoretical results on HF relaxation have come from trajectory calculations notwithstanding the mechanical difficulty that only one trajectory for a set of given initial conditions can be calculated at a time, and one must do many such calculations then to obtain averages that

may be related to reality. The quantum condition on the internal energy must be imposed at the end; there are several ways to this, and each involves approximations. A potential energy surface of some sort must be input to the trajectory calculations, and several choices have been explored. Trajectory calculations can however give us valuable insight into the relative contributions of parallel pathways and how each depends upon experimental parameters.

Specific computational details and assumptions are irrelevant to our purposes here, but it is proper to realize the nature of the results. Coltrin has obtained results for the relaxation of HF of $v=1$ to $v=7$ by HF($v=0$) as summarized in Table II, and the results suggest a preponderant probability of single quantum transitions.

TABLE II. Rate constants^a using quasiclassical cross-correlation method with Morse oscillator vibrational potentials.

System	k^{tot}	k^{V-V}	k^{V-RT}
1-0	0.2(0.1) ^{b,c}	...	0.2(0.1)
2-0	19(3)	17(3)	1.7(0.5)
3-0	28(4)	24(4)	4(1)
4-0	53(10)	31(7)	22(5)
5-0	69(10)	9(3)	60(10)
6-0	156(18)	14(3)	142(15)
7-0	455(49)	17(3)	438(48)

^aRate constants in units of 10^{-12} cc molecule⁻¹ sec⁻¹.

^bThe $v=1$ case only, the deactivation is completely V-RT.

^cValue in parentheses is one standard error.

From M. E. Coltrin and R. A. Marcus, J. Chem. Phys. 73, 4390(1980)

Experimentally one measures, of course, only the total relaxation rate. To obtain the results of Table II, at least 500 trajectories were used. These results compare well with experiment except at $v=1$, where relaxation must be v-T, where the trajectory calculation is low by an order of magnitude.

These workers have replaced the more realistic Morse potential in the surface with the same modified harmonic oscillator potential used by Billing and Poulsen,¹² and, although the other procedures and assumptions were somewhat different, the two results were equivalent.

Extensive trajectory calculations have also been made by Wilkins who has elected to use still another potential surface (a so-called London-Eyring-Polanyi-Sato surface). One of the most striking differences between the surface used by Coltrin and that of Wilkins is the depth of the potential well when two HF molecules approach head-to-tail, that is, on the most attractive colinear geometry. Coltrin obtains a depth of 6.9 kcal/mol vs. 2.7 kcal/mol obtained by Wilkins.¹³ Thus we expect more Coltrin trajectories to form van der Waals complexes with more time for interaction and then greater cross-sections for vibrational relaxation. And this is exactly what happens. Coltrin finds that such complexes occur in 30% of the trajectories, but these trajectories account for 60% of the v-v relaxation rate, and so the sticky collision is more efficient by a factor of 3.5.

The first comprehensive trajectory studies on HF were done by Wilkins¹³ using relative translational energies from 0.5 to 6 kcal/mol, and about 200 trajectories for each initial set of parameters. There was no evidence for collision complexes being formed which is surely an artifact of the potential energy surface that was chosen. Here one, two or even three quanta of vibrational energy may transfer into rotational energy of the same HF molecule. Table III lists the predicted total deactivation rates due to collision with HF(v=0). But, of course, much more detailed information may be obtained from these sorts of calculations, such as rates for particular v,J collisions and rates into specific v',J' states. This detailed information must be summed to obtain the total rates listed in Table III below. Multiquantum transitions (in both v and J) are common, and no van der Waals complexes are observed.

Table III

Deactivation of HF(v) by HF(v=0)

v	1	2	3	4	5	6
k	1.0	13.4	17.5	19.9	25.1	30.8

k is in units of 10^{12} cm³/mole s

Similar computations on the $H_2 + He$ system at a fixed relative translational energy of 0.5 eV is informative for its implications for the HF system. The results appear in Fig. 14. Here the cross-section of transfer out of J_i, v_i to all other J_f and v_f significantly increases as v_i is increased between 0 and 6. Also for a particular v_i , the cross-section as a function of J_i exhibits a minimum which occurs at about $J_i = 10, 8$ and 6 for $v=2, 4$ and 6, respectively. The trajectories reveal that the enhanced cross-section at high J is due to $J \rightarrow v$ transfer. Vibrational transitions of $\Delta v = \pm 1$ or 0 are dominant. Also resonant exchanges are, by far, the largest contributor to the cross-section, and hence multiquantum changes in J occur to match the change in v . Rotational energy transfer is here enhanced by vibration, and vibrational energy transfer increases with initial rotational energy.

The so-called "energy corrected sudden" scaling theory has been used to investigate the interaction of rotational and vibrational modes in relaxation processes of HF.¹⁵ Here $v-v$ processes are dominant only at low v , with $v-J,T$ processes of large ΔJ of about 10-12 probable at $n = 4$ to 5. These results are in keeping with the trajectory calculations.

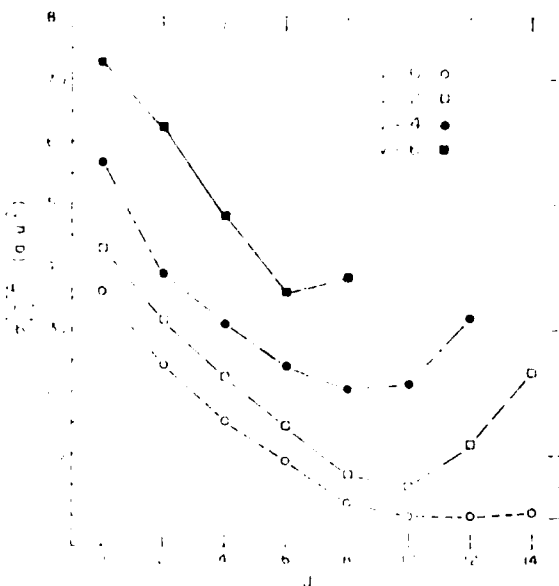


Fig. 14. Cross sections for transitions from J_i to all other states v_f, J_f as a function of J_i for initial vibrational states 0, 2, 4, and 6 at 0.5 eV collision energy. From D. L. Thompson, J. Chem. Phys. 75, 1829(1981).

Temperature Dependence

The trajectory calculations have been taken to the point of predicting the temperature scalability of the rates, and the results appear in Fig. 15.

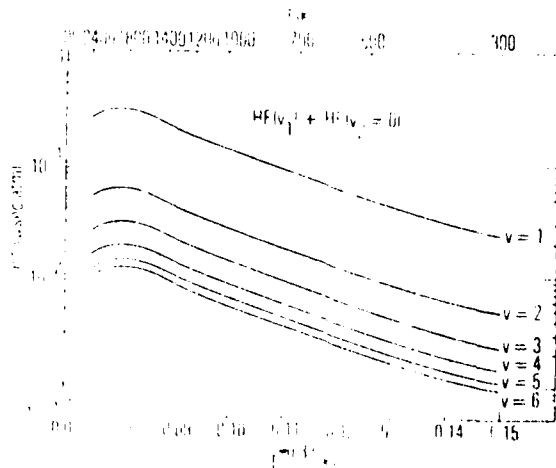
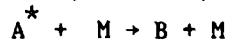


Fig. 15. Rate coefficients of vibrational relaxation of HF ($v=1$ through 6) by HF ($v=0$). pT ($\mu\text{sec atm}$) vs T and $T^{-1/3}$ with T in K. From R. L. Wilkins and M. A. Kwok, J. Chem. Phys. 73, 3198(1980).

As is evident from Fig. 15, the logarithm of the predicted rates vs. $T^{-0.33}$ are essentially linear over the temperature range of practical interest. This dependence is in keeping with so-called Landau-Teller theory.

Whether they be electronic, vibrational or whatever, collision induced changes in the state of a molecule, that is,



have been rather well correlated with temperature by¹⁷

$$\ln \sigma_M = \ln C + \epsilon_{A^*M}^*/kT$$

where C is a constant and $\epsilon_{A^*M}^*$ is the depth of the potential well between the colliding pair. This correlation imagines the interaction that produces the change of state to be predominantly attractive, and since this well depth is never really known, it is best to consider $\epsilon_{A^*M}^*/k$ as just an adjustable characteristic temperature. The data of Fig. 15 may be replotted to reveal that the correlation holds well for $v=1, 2, 3, 4,$ or 5 of HF where M is HF($v=0$) and $\epsilon/k = 520$ K. It is also well known that the potential well depth

correlates rather well with the critical temperature, so we are not surprised that the self-relaxation rates correlate rather well with this macroscopic property.¹⁸

VII. DISCUSSION AND RECOMMENDATIONS

We really do not know the mechanism of vibrational relaxation. Does a vibrational state having a thermal rotational distribution go to a lower vibrational state with the energy difference balanced by a concomitant ΔJ ? If the subsequent J-J relaxation is the rate determining step, to what relative extent do collisional and superradiant pathways occur? No critical experiment has been attempted to determine the mechanism of vibrational relaxation and this is needed. It would be desirable to pump, say the $J=1$ or 2 state (i.e., thermal at 298 K) of $v=1$ and probe for the arrival of population at $J=14$ of $v=0$. The transition of $v=1, J=2$ to $v=0, J=14$ is near resonant, that is, only small amounts of energy would need to transfer either to or from translation. Similar such probings at other resonant v to J transitions all along the manifold of energy levels would be informative. If multi-quantum transitions do in fact play a significant role, one could detect the arrival of population at $v=0, J=19$ from $v=2, J=2$.

We need more information on the extent of microwave superradiance. That is, to what extent is rotational relaxation a collisional or a radiant process, and what are the rates? The infrared double resonance experiments have given reasonable rate data on rotational relaxation where collision is the major mechanism, but those transitions where superradiance is a factor are poorly understood. The slow rates of collisional decay at high J 's prolong population in these levels and enhance the probability of superradiance.

The scaling of vibrational relaxation rates with v seems to go as $v^{2.7}$, but we have no theory to explain why this should be so. The scaling of this rate with temperature goes as $T^{-1/3}$ at each v , and we do have the Landau-Teller analysis to provide a rationalization. We see here a near linear decrease in rate with $T^{-1/3}$. The scaling of vibrational relaxation with temperature seems to fit rather

well with the idea that the dominant force in the transition is that of intermolecular attraction, i.e., the van der Waals forces between the excited species and the collision partner.

The paucity of data that exist suggest that the rate of rotational relaxation depends significantly upon the vibrational state within which the rotational states are relaxing. Again, we have no molecular model to rationalize this behavior.

A critical and as yet unanswered question is to what extent energy may merely pool in the upper rotational states and subsequently feed back into vibration. Alternatively, of course, this rotational energy could tumble down the J manifold by some combination of collision and superradiant processes.

The data are conflicting on the extent of multi-quantum transitions in both vibrational and in rotational transitions. This disagreement exists among the experimentalists as well as among the theorists, and it exists in our understanding of the rotational rates as well as the vibrational rates. We just do not understand the role of multi-quantum transitions.

Trajectory calculations provide heuristic insights that illuminate experimentation and hopefully ultimately lead to a theory of relaxation processes. The technique is too unwieldy for practical utilization. Further trajectory calculations at this time are relatively unimportant as compared with, for example, developing a reliable potential energy surface. Some insight into such surfaces that might be analogous to the van der Waals equation or the Redlich-Kwong equation of state of real gases is needed. As particular groups of species deviate from ideal gas behavior in some general way, so some potential energy surface should describe inelastic collisions of polar gases like HF. But we have no such insights as yet.

By some wise combination then of experiment and theory, we need molecular models of both rotational, and vibrational relaxation processes that would allow intelligent extrapolation and interpolation of the less than complete data that will always be available to the design engineer on a project like ALPHA.

Finally, and from a purely mechanical or instrumental point of view, the signal averaging technique of Crim would seem to be the

technique of choice in observing the low level signals that change over short time intervals that are characteristic of measurements of population density within the energy level manifold.

REFERENCES

1. G. M. Jursich and F. F. Crim, J. Chem. Phys. 74, 4455(1981).
2. D. J. Douglas and C. B. Moore, ibid. 70, 1769(1979).
3. E. R. Sirkin and G. C. Pimentel, ibid. 75, 604(1981).
4. J. K. Lampert, G. M. Jurisch and F. F. Crim, Chem. Phys. Letters 71, 258(1980).
5. T. J. Foster and F. F. Crim, J. Chem. Phys. 75, in press.
6. J. J. Hinchey and R. H. Hobbs, J. Appl. Phys. 50, 628(1979).
7. J. J. Hinchey and R. H. Hobbs, J. Chem. Phys. 65, 2732(1976).
8. R. A. Copeland, D. J. Pearson and F. F. Crim, Chem. Phys. Letters 81, 541(1981).
9. J. C. Polanyi and K. B. Woodall, J. Chem. Phys. 56, 1563(1972).
10. J. A. Barnes, M. Keil, R. E. Kutina and J. C. Polanyi, ibid. 72, 6306(1980).
11. M. E. Coltrin and R. A. Marcus, ibid. 73, 4390(1980).
12. G. D. Billing and L. L. Poulsen, ibid. 68, 5128(1978).
13. R. L. Wilkins, ibid. 67, 5838(1977).
14. D. L. Thompson, ibid. 75, 1829(1981).
15. A. E. DePristo, ibid. 74, 5037(1981).
16. R. L. Wilkins and M. A. Kwok, ibid. 73, 3198(1980).
17. C. S. Parmenter, et al., ibid. 70, 5442(1979).
18. R. J. London, ibid. 72, 779(1980).

1981 USAF - SCEEE SUMMER FACULTY RESEARCH PROGRAM

Sponsored by the

AIR FORCE OFFICE OF SCIENTIFIC RESEARCH

Conducted by the

SOUTHEASTERN CENTER FOR ELECTRICAL ENGINEERING EDUCATION

FINAL REPORT

THE ROLE OF FAR-FIELD BOUNDARY CONDITIONS IN NUMERICAL
SOLUTIONS OF THE NAVIER-STOKES EQUATIONS

Prepared by: Dr. Patrick J. McKenna
Academic Rank: Associate Professor
Department and University: Department of Mathematics
University of Florida
Research Location: Air Force Weapons Laboratory, Advanced Beam
Control Division, Advanced Laser Optics Branch
USAF Research Colleague: Dr. Wilbur Hankey
Date: September 7, 1981
Contract No: F49620-79-C-0038

APPROPRIATE FAR-FIELD BOUNDARY CONDITIONS FOR THE
NUMERICAL SOLUTION OF THE NAVIER-STOKES EQUATIONS

by

Patrick J. McKenna

ABSTRACT

The problem of prescribing fictitious far-field boundary conditions at an artificial boundary is discussed. Several boundary conditions which have been used in the literature are compared with two newly proposed sets. The proposed boundary conditions are shown to be non-reflecting and superior in both accuracy and time to convergence. Graphs showing the numerical results for the different types of boundary conditions are displayed and the wave motion is demonstrated. In particular, reflecting boundary conditions are shown give rise to fictitious variations of a periodic wavelike nature.

Acknowledgement

The author would like to thank the Air Force Systems Command, the Air Force Office of Scientific Research and the Southeastern Center for Electrical Engineering Education for providing him with the opportunity to spend a very worthwhile and interesting summer at the Flight Dynamics Laboratory, Wright Patterson, OH. He would like to acknowledge the laboratory, in particular the Computational Aerodynamics Group, for its hospitality and excellent working conditions.

Finally, he would like to thank Dr. Wilbur Hankey for suggesting this area of research and for his collaboration and guidance, and he would like to acknowledge many helpful discussions with Dr. Joseph Shang, Captains Gerry Hasen, Hardy Hegna, and Rick Newsome, Jeff Graham and Steve Scherr.

I. INTRODUCTION:

Attempting to determine fluid flow around an obstacle requires the solution of the Navier-Stokes equations;

$$\frac{\partial u}{\partial t} + \frac{\partial E}{\partial x} + \frac{\partial F}{\partial y} = 0 \quad (1)$$

where

$$u = \begin{bmatrix} \rho \\ \rho u \\ \rho v \\ \rho e \end{bmatrix} \quad E = \begin{bmatrix} \rho u^2 - \sigma_{xx} \\ \rho uv - \zeta_{xy} \\ \rho ve - u\sigma_{xx} - v\zeta_{xy} - \dot{q}_x \end{bmatrix}$$

$$F = \begin{bmatrix} \rho v \\ \rho uy - \zeta_{xy} \\ \rho v^2 - \sigma_{yy} \\ \rho ve - v\sigma_{yy} - u\zeta_{xy} - \dot{q}_y \end{bmatrix}$$

$$\begin{aligned} \sigma_{xx} &= -p - (2/3) \mu \vec{\nabla} \cdot \vec{u} + 2\mu u_x & \dot{q}_x &= k T_x \\ \zeta_{xy} &= \mu (u_y + v_x) & \dot{q}_y &= k T_y \\ \sigma_{yy} &= -p - (2/3) \mu \vec{\nabla} \cdot \vec{u} + 2\mu u_y & e &= cvT + \frac{u^2 + v^2}{2} \\ p &= \delta RT ; \mu = \mu(T) \end{aligned}$$

Here, the four dependent variables ρ , u , v , and e represent the physical quantities of density, x- and y- components of velocity, and internal energy.

Even a casual glance at this system of equations shows that it has many extremely difficult aspects. It is a system of four equations in the four basic unknowns, which is of mixed parabolic hyperbolic type. It is in two space dimensions and in addition is nonlinear. Any one of these problems would be sufficient to make obtaining an analytic solution difficult so it is fair to say that an analytic solution is out of the question. Thus these problems are "solved" by numerical methods.

What this means of course is subject to some interpretation. What usually happens is that a number of approximations are made to the original problem, in order to arrive at a discrete approximation which may then be solved by computer. Most obviously, "space" is interpreted, not as a continuum, but as a finite number of grid points. The value of pressure for example at a grid point is then used to calculate the value at nearby points, by means of a few terms in a Taylor series. Derivatives are approximated by finite differences. If the flow is around a body, then one assumes that velocity is zero on the surface of the cylinder, and the surface temperature is prescribed. The assumption is that if the grid is fine enough, and if time steps are sufficiently small, then this discrete model is a reasonable approximation of the original equations (1).

A method for solving supersonic flows that was found by experience to work well was MacCormack's alternating direction explicit scheme. Thus, this was a logical method to be experimented with for subsonic flow. However, the transition was not easy. The MacCormack method demands certain fictitious (or numerical) boundary conditions due to the difference algorithm which are not physically present, and which were arrived at by a process of computational experimentation. These methods did not work in the case of subsonic flow, although they did in the case of supersonic flow.

II. OBJECTIVES:

The purpose of this project was to explain this anomaly, and to arrive at improved far-field boundary conditions for the subsonic case. To do this, we will first review the theory for a single wave equation,

then for systems of linear hyperbolic partial differential equations, and finally, we shall discuss how numerical experiments with the Navier-Stokes equation confirm the predictions based on the elementary theory.

III. REVIEW OF NUMERICAL THEORY FOR ONE EQUATION:

Obviously the full system of equations (1) is too complicated to achieve a great deal with sophisticated mathematical analysis. Typically, mathematicians will work with simpler equations which in one way or another resemble the original system. One tries to use the mathematical insights of the simpler situation in the context of the more complicated one. This is obviously not one unbroken chain of reasoning, but more a process of educated guesswork.

Surprisingly, one equation which provides a great deal of insight is the simple wave equation

$$u_t + au_x = 0 \quad (2)$$

We consider this equation on the interval $[0,1]$. On the real line, the solutions to this equation would be waves running from left to right with velocity a , which are constant along the lines $x - at = d$, $d \in \mathbb{R}$.

Thus, if we consider this equation on the region $\{(x, t) \mid 0 \leq x \leq 1, t \geq 0\}$, then it will be analytically determined by the initial value $U(x, 0) = f(x)$, $0 \leq x \leq 1$ and the boundary value $u(0, t) = g(t)$. With these conditions, the initial boundary value problem is well posed. It is impossible to prescribe boundary conditions at $x = 1$ instead of $x = 0$ without either (a) limiting the initial values or (b) causing discontinuities. All of this makes perfect physical sense. In order to know what happens in a wave situation, we must give information on the initial conditions and also on the waves entering at the inflow point.

However, the MacCormack scheme which is equivalent to the Lax-Wendroff scheme requires some knowledge of $u(1, t)$. Indeed the value for u_{j-1}^{n+1} is given in terms of u_{j-2}^n , u_{j-1}^n and u_j^n . Therefore, the boundary point $x = 1$, ($j = J$) requires special treatment of some sort. This special treatment is called a "numerical boundary condition" or compatibility condition. The imposed can have an enormous impact on the successful numerical solutions of the problem.

Perhaps the best two recent summaries on this simple equation were accomplished by Kreiss [5] and Gottlieb and Turkel [2].

Kreiss is basically concerned with what can go wrong. He observes for example that if you overspecify, i.e. just make a guess at what $u(1, t)$ is going to be and then simply prescribe it, convergence to a steady state may or may not take place, depending on whether the number of grid points is even or odd. If this happens with this simple case obviously you don't want to try it in a more complicated case. (We shall have more to say on this later).

One method that works well is to use $u_x(1, t) = 0$, or in finite difference form $u_j^n = u_{j-1}^n$. A slight error in u at the outflow point is made, but since the flow is from left to right, this error does not propagate back into the x -domain. This is proved analytically in Parter [8] About the worst mistake that can be made is not to specify u at the incoming boundary. For example, one might confuse the inflow and outflow boundary and prescribe $u_1^n = u_2^n$, and $u_j = M$, all n . In this case as the space step and time step become small this conveys to a steady state on an interval $[0, T]$ where the steady state is determined by the initial conditions at the inflow point.

A moments reflection ought to convince us of how undesirable this is, since we do not know the correct steady state, our initial conditions are bound to be different from the correct solution. However, what we seem to converge to actually depends on the choice of the initial conditions. Again, we shall have more to say about this when we discuss computational solutions of the Navier-Stokes equations.

Another excellent paper on the same subject is by Gottlieb and Turkel [2]. In this paper, a comprehensive review of many different numerical boundary conditions is given. For example, in addition to the ones already mentioned at the outflow, one might consider $u_{xx} = 0$, which numerically is $u_{J-2} - 2u_{J-1} + u_J = 0$ or even $u_t + au_x = 0$ where $u_J^{n+1} = u_J^n + a(\Delta t/\Delta x)(u_{J-1}^n - u_J^n)$. This corresponds to a one-sided "upwind" difference approximation at the outflow boundary.

Their conclusion is that the upwind difference appears best, although the convergence of the scheme with $u_x = 0$ is just as fast (but less accurate).

IV. WELL POSED BOUNDARY CONDITIONS FOR LINEAR SYSTEMS:

The simplest systems of two linear wave equations to consider is

$$\begin{aligned} u_t + au_x &= 0 \\ v_t - bv_x &= 0 \end{aligned} \tag{3}$$

where $a_1 > 0$, $b > 0$, $0 \leq x \leq 1$, and $t \geq 0$. In this case the waves in u travel from left to right with velocity a , and the waves in v travel from right to left with velocity b . Clearly u must be given initially and at the left boundary, whereas the values of v must be given at the right boundary. This is analytically necessary in order to have enough information to solve the problem. However, there is a minor complication. The incoming

value of u may be given at $x = 0$ in terms of v (which, after all, is determined there), and the incoming value of v at 1 may be given in terms of u . Thus, the initial boundary value problem (3) is well posed if the initial conditions are

$$u(x, 0) = f(x) \quad v(x, 0) = g(x)$$

and the boundary conditions are

$$\begin{aligned} u(0, t) &= F_1(t) + c_1 v(0, t) \\ v(1, t) &= G_1(t) + c_2 u(1, t) \end{aligned} \quad (4)$$

Notice that if $c_1 = c_2 = 0$, then the problems are completely uncoupled, and each is a copy of the single equation in section IV.

For a moment, consider the case where $F_1(t) = G_1(t) = 0$, and $c_1 = c_2 = 1$. In this case, we get a different phenomenon. Let us assume that u is identically zero initially, and that v is identically 1. Then the square wave in v travels to the left, causing u to be non-zero at the in-flow boundary, and thereby propagating from left to right with velocity 1. When u reached $x = 1$ it would in turn influence v by the boundary condition (4) and a new disturbance would propagate in v from right to left. This is the reason that this boundary condition is called a "reflective boundary condition".

Notice that if both u and v travel from left to right, i.e. if

$$u_t + au_x = 0$$

$$v_t + bv_x = 0$$

where $a > 0$, $b > 0$, $0 \leq x \leq 1$ and $t \geq 0$, then this problem does not arise. The initial conditions of u and v must be specified as must the boundary conditions at $x = 0$. No reflections or coupling is allowed to take place.

For a general hyperbolic system of the form

$$\vec{u}_t + A\vec{u}_x = 0 \quad (4)$$

one must diagonalize the matrix A, i.e. one must find a matrix T so that

$$T A T^{-1} = D$$

where D is a diagonal matrix. One then makes the substitution $W = TU$ and the equation (5) transforms to

$$\vec{W}_t + D \vec{W}_x = 0$$

The number of positive eigenvalues of D identifies the right-running variables W_i and the negative ones identify left running variables at this point, we emphasize that the only way to be familiar with the wave nature of (5) is to look, not at the physical variables \vec{u} in which the problem was originally presented, but instead at the new variables W which are linear combinations of the old ones. Only then is the wave structure apparent.

If k is the number of positive eigenvalues, and if W_I represents the k-vector of these k coordinates of W_I and W_{II} is the n-k other coordinates, then unless W_I and W_{II} are independently prescribed at the left and right boundaries respectively then we may get reflective boundary conditions. For well-posedness, it is sufficient that at $x = 0$, W_I be given (possibly depending on W_{II}) and that at $x = 1$, W_{II} be given with possible dependence on W_I . Only then can acceptable boundary conditions be formulated in terms of the physical variables U.

V. THE NAVIER-STOKES EQUATIONS AND CHARACTERISTIC VARIABLES:

We now begin our discussion of the equations of gas dynamics. We will neglect viscosity for the purposes of this analysis. We will assume

For a general hyperbolic system of the form

$$\vec{u}_t + A \vec{u}_x = 0 \quad (4)$$

one must diagonalize the matrix A, i.e. one must find a matrix T so that

$$T A T^{-1} = D$$

where D is a diagonal matrix. One then makes the substitution $W = TU$ and the equation (5) transforms to

$$\vec{W}_t + D \vec{W}_x = 0$$

The number of positive eigenvalues of D identifies the right-running variables W_i and the negative ones identify left running variables at this point, we emphasize that the only way to be familiar with the wave nature of (5) is to look, not at the physical variables \vec{u} in which the problem was originally presented, but instead at the new variables W which are linear combinations of the old ones. Only then is the wave structure apparent.

If k is the number of positive eigenvalues, and if W_I represents the k-vector of these k coordinates of W_I and W_{II} is the n-k other coordinates, then unless W_I and W_{II} are independently prescribed at the left and right boundaries respectively then we may get reflective boundary conditions. For well-posedness, it is sufficient that at $x = 0$, W_I be given (possibly depending on W_{II}) and that at $x = 1$, W_{II} be given with possible dependence on W_I . Only then can acceptable boundary conditions be formulated in terms of the physical variables U.

V. THE NAVIER-STOKES EQUATIONS AND CHARACTERISTIC VARIABLES:

We now begin our discussion of the equations of gas dynamics. We will neglect viscosity for the purposes of this analysis. We will assume

that the flow is one-dimensional and subsonic and that the deviations from free-stream solutions are small. This will allow us to neglect second order terms.

There are many forms of this equation, but the one most suitable for the present discussion is

$$\frac{\partial u}{\partial t} + A \frac{\partial u}{\partial x} = 0 \quad (5)$$

where

$$A = \begin{pmatrix} 0 & 1 & 0 \\ (\gamma - 3)\frac{u^2}{2} & (3 - \gamma)u & \gamma - 1 \\ (\gamma - 1)4^3 - \frac{\gamma e u}{\rho} & \frac{\gamma e}{\rho} - \frac{3}{2}(\gamma - 1)u^2 & \gamma u \end{pmatrix}$$

and

$$U = \begin{pmatrix} \rho \\ \rho u \\ e \end{pmatrix}$$

or in terms of physical variables

$$\frac{\partial \tilde{U}}{\partial t} + \tilde{A} \frac{\partial \tilde{U}}{\partial x} = 0 \quad (6)$$

where

$$\tilde{A} = M^{-1} A M$$

and

$$M^{-1} = \begin{pmatrix} 1 & 0 & 0 \\ -u/p & 1/p & U \\ (\frac{\gamma-1}{2})u^2 & (1-\gamma)u & (\gamma-1) \end{pmatrix}$$

Here we make the key assumption that deviations from the free stream are going to be sufficiently small that we can treat the entries in the matrix \hat{A} as being approximately constant (at least locally). Denote these frozen variables by a 0-subscript. We then make the substitution

$$\begin{pmatrix} W_1 \\ W_2 \\ W_3 \end{pmatrix} = \begin{pmatrix} 1 & 0 & -1/c_o^2 \\ 0 & 1 & 1/\rho_o c_o \\ 0 & -1 & 1/\rho_o c_o \end{pmatrix} \begin{pmatrix} \rho \\ u \\ p \end{pmatrix} \quad (7)$$

and when this is substituted into (6) we obtain

$$\begin{aligned} \frac{\partial W_1}{\partial t} + u_o \frac{\partial W_1}{\partial x} &= 0 \\ \frac{\partial W_2}{\partial t} + (u_o + c_o) \frac{\partial W_2}{\partial x} &= 0 \\ \frac{\partial W_3}{\partial t} + (u_o - c_o) \frac{\partial W_3}{\partial x} &= 0 \end{aligned}$$

Notice now how this breaks down into two separate cases. On the one hand, if flow is supersonic then all wave motion is in the left to right direction. In this case all analytic boundary conditions ought be prescribed at the left hand side and only numerical boundary conditions prescribed at the right hand side.

Since the substitution (7) is equivalent to

$$\begin{aligned} \rho &= K_1 + (\rho_o/2c_o)(K_2 + K_3) \\ u &= 1/2 (K_2 - K_3) \\ p &= \rho_o c_o/2 (K_2 + K_3) \end{aligned}$$

it follows that prescribing all physical variables at the inflow and prescribing $\partial\rho/\partial x = \partial u/\partial x = \partial p/\partial x = 0$ at the outflow is sound in terms of analytical and numerical requirements.

However, we must now consider the case of subsonic flow. In this case the situation is completely different. Here, two of the variables W_1 and W_2 go left to right with velocities u and $u+c$ respectively, whereas one of the variables runs right to left with velocity $c_o - u_o$. While the

the variables W_2 and W_3 have no clear physical significance. Yet it is only by considering these variables that the full wave structure of the equations (5) or (6) can be understood. Thus, one would be led to predict, for small deviations from free stream conditions, that the best boundary conditions would be for an interval $(0, L)$

$$\begin{aligned}
 W_1(0,t) = K_1 & & \frac{dW_1}{dx}(L,t) = 0 \\
 W_2(0,t) = K_2 & & \frac{dW_2}{dx}(L,t) = 0 \\
 \frac{dW_3}{dx}(0,t) = 0 & & W_3(L,t) = K_3
 \end{aligned} \tag{8}$$

Note the curious aspect of these boundary conditions. In order to prescribe the numerical values K_1 and K_2 , we need to know accurately all three physical variables at some distance to the left. However, only the two combinations K_1 and K_2 are prescribed. This can be summarized by saying that while we have used all three pieces of information upstream, we have done so in such a way that one degree of freedom remains, thus allowing the waves in W_3 to exit without problems.

On the basis of the linearized model, various other combinations would be well-posed. For example, it is possible to prescribe K_3 in terms of either K_1 or K_2 at the outflow $x = L$. Thus at the outflow one may prescribe

$$W_2(L,t) = F_3(t) + c_1 W_1(L,t) + c_2 W_2(L,t)$$

For example if $c_1 = 0$, $c_2 = 1$, then this amounts to putting

$$u(L,t) = 1/2 F_3 \tag{9}$$

i.e., we prescribe velocity at the outflow.

Alternatively, we might take $c_1 = 0$, $c_2 = -1$ and we would get

$$p(L,t) = ((\rho_0 c_0)/2) F_3 \tag{10}$$

i.e. we prescribe velocity at the outflow. Many other combinations are possible, but as remarked in section IV, all these will cause errors in the initial data to be reflected back into the medium as waves running from right to left. For example, we would predict that an error in W_2 would be reflected back as an error in W_1 if we use boundary condition (10). As we shall see, this is exactly what happens.

At the inflow end, we may prescribe W_1 and W_2 in terms of W_3 . Thus the following boundary conditions are well posed;

$$W_1(o,t) = F_1 + c_1 W_3(o,t) \quad (11a)$$

$$W_2(o,t) = F_2 + c_2 W_3(o,t) \quad (11b)$$

For example, choosing $c_2 = +1$ in (11b) corresponds to

$$u(o,t) = (1/2) F_2$$

(i.e. prescribing u at the inflow) and $c_2 = -1$ corresponds to

$$p(o,t) = (\rho_o c_1 / 2) F_2$$

(i.e. prescribing p). One can prescribe the combination (u, ρ) by first choosing $c_2 = 1$ (thereby prescribing u) and then choosing $c_1 = \rho_o / c_o$, thereby prescribing ρ in terms of a given F , and a prescribed $u(o,t)$. Since (11a) and (11b) reduce to

$$u(1 + c_2) + \frac{p}{\rho_o c_o} (1 - c_2) = F_2$$

$$\rho - \frac{p}{\rho_o c_o} (\rho_o / c_o - c_1) + c_1 u = F_1$$

about the only condition we cannot prescribe is $u(o,t)$, $p(o,t)$, since there is no choice of c_1 , c_2 to eliminate ρ from these equations.

Again, we emphasize that each of these boundary conditions is reflecting, i.e. deviations from the free stream in the initial data get reflected

back as waves in W_1 and W_2 and then travel back downstream. About the worst thing that can be done is to prescribe reflecting boundary conditions at the inflow $x = 0$ and the outflow $x = L$. In this case errors can keep being reflected up and down the region, never being allowed to exit. This prevents convergence to a steady state and may even give rise to fictitious periodic oscillations.

We conclude this section with a review of the conclusions on boundary conditions. Based on the linear model, boundary conditions (8) seem optimal. Any other prescription of the physical variables, although well posed, causes reflections of the deviation from the true solution. If for example, only the physical variable p_∞ is known at the outflow then it is possible to prescribe p at the outflow, in such a manner that the problem remains well posed. We emphasize that this will cause errors to propagate upstream, thereby slowing the process of convergence to steady state. This may not be too bad, so long as the upstream boundary conditions are not also reflecting. On the other hand, if they are, then convergence to free stream may never occur.

VI. DISCUSSION OF NUMERICAL RESULTS - NONLINEAR COUPLING:

The one dimensional Navier-Stokes equations were solved with an alternative direction explicit MacCormack scheme, on a one-dimensional net with forty grid points. The code was an exact one-dimensional version of a three-dimensional code which had proved successful in many supersonic studies [6], [11]. There were two questions to answer. The first was, given that equation (7) is correct for infinitesimally small deviations from a constant free stream, how correct is it when deviations of an

intermediate (of the order of 10%) magnitude are there instead? It would be too much to hope that the variables W_1 , W_2 , and W_3 , remain uncoupled, but we should be able to get an idea of the order of magnitudes of the coupling involved. The second problem of course, is to assess the influence of the various types of boundary conditions commonly employed. We will deal with the latter problem in section VII.

To do this, we considered a uniform free stream situation, with pressure equal to 2000 lbs/ft², velocity equal to 548 ft/sec and density equal to 0.0023 slugs/ft³. We created a deviation from the steady state condition in a variety of ways as in [9], [10], and then watched the progress (or lack of it) to a steady state. A variety of different wrong initial conditions were used. One type was to impose a 10% deviation in one of the variables K_1 , K_2 , K_3 at the points $\{x_j, j=18,19,20,21,22\}$. We would then watch the disturbance, graphically as it propagated up or down stream. Another possibility was to put in uniformly wrong initial conditions where some or all of the characteristic variables W_1 , W_2 , W_3 are perturbed throughout by a percentage error of 10%. Each plot then showed the percentage error, with the different curves representing the progress of time as one ascends the plot. The curves are plotted every twenty five time steps when $\Delta t = (.9)(\Delta x)/(u+c)$. We also point out the percentage errors in W_1 , W_2 , and W_3 at the end of the run, so as to obtain information on relative accuracy and speed of convergence of the various methods.

Figure 1 gives the results of an experiment, which is ideal in terms of the linear theory. An initial disturbance in W_3 the left-running

of [10] could introduce more errors into the system, by increasing W_3 at the outflow point even more.

VIII. RECOMMENDATIONS:

We have completed an initial study of the one-dimensional Navier-Stokes equations and their far-field boundary conditions; and developed a one-dimensional code to provide numerical solutions. We have used this code to evaluate the impact of a variety of different boundary conditions upon the successful numerical solution of these problems. Several outstanding problems remain to be studied.

First one should examine the usefulness of the two recommended boundary condition sets in time dependent situations. It may well be that the difference between no-change characteristic boundary conditions and windward-difference characteristic boundary conditions will prove to be highly significant important in a time dependent problem. If so, this would be significant since a high proportion of work currently done at the Flight Dynamics Laboratory Computational Aerodynamics Group is of this type.

Recommendation for future efforts is to implement these characteristic boundary conditions in two and three-dimensional codes. This is presently in progress. As this is done, there is no doubt that further refinements will need to be considered.

In the discussion of our results, we noted, but did not stress, the following problem. Truly accurate time dependent solutions only exist if the C.F.L. number is close to 1. The time step is limited by a stability requirement that the C.F.L. number be less than 1. The problem with this is that the C.F.L. number is calculated on the basis of the fastest moving

wave, which is the fastest to leave the region. After a relatively short amount of time, only the slow-moving waves are left. This ought (at least for some cycle of iterations) allow us to use a larger time step. This has not yet been thoroughly explored and we recommend that a study be made of this problem. This could result in substantial savings of expenditure of computer time.

More work needs to be done to properly understand the nonlinear interactions between the characteristic waves. This problem is not understood at this time and a proper understanding might give a clue to correct posing of initial conditions in such a way as to minimize start-up shocks, as observed in figures 4 and 5.

Another problem to be investigated on the one-dimensional code is whether up-dating the coefficients ρ_0 , c_0 , u_0 to the $(n+1)^{st}$ time step values significantly accelerates convergence to steady state or improves accuracy. Either result would improve computational efficiency in the future.

Finally, we need to evaluate how appropriate these sets of boundary conditions are in the presence of stationary shock waves. This can be done first on a one-dimensional model problem.

characteristic variable is given (graphed as K_3) and we observe deflections in the variables W_1 W_2 W_3 . As one can readily see from the pictures, the disturbance propagates upstream rapidly until convergence is reached (.1% agreement with physical variables), which takes place within 130 time steps. This gives us six curves. Note that although a good deal of undershoot and overshoot in W_3 becomes apparent, there is no significant interaction with W_1 or W_2 . The same situation appears with initial disturbances in W_1 , the slow-moving right running wave. From this experiment it appears that deviations in either W_1 or W_3 will not effect either of the other two variables. However, as shown in Figures 2 and 3, when initial disturbances are in W_2 , an entirely different situation exists. Figure 2 shows a uniform initial disturbance in W_2 of minus ten percent, while W_1 and W_3 are left undisturbed. Initially the wave in W_2 , propagates rapidly out of the medium. Indeed, after fifty time steps, it is essentially gone from the picture. However, this does not happen without affecting the other two variables. Notice how, in the top graph, a large disturbance is left in W_1 after fifty time steps and in W_3 , we have that W_3 values one almost constant at minus eight percent. However, once the W_2 wave has made its exit, the other two variables uncouple and resume their normal wave motion, and the error can be seen propagating out of the solution in the usual way convergence is attained within three hundred iterations. These particular results illustrate what became increasingly clear throughout the series; perturbations in W_2 had a large effect on W_1 and W_3 whereas if W_2 was not perturbed, W_1 and W_3 behaved as if uncoupled. Perturbations in W_1 and W_3 had little effect on W_2 . No qualitative explanation of this phenomenon is known at this time.

Figure 3 shows the same phenomenon. Here an error of -10% is made in W_2 whereas errors of +10% are made in W_1 and W_3 . Again, we see that until the W_2 wave exists, there are massive disturbances in the wave structure of W_1 and W_2 . As soon as W_2 exists, (after 75 iterations) the regular wave structure reasserts itself and errors propagate out in a predictable wave-like manner. Again, convergence takes approximately three hundred and twenty five iterations. It seems clear that this is optimal given the limited wave velocity, so we can deduce that these effects are due to the nonlinear coupling. Thus, even after the W_2 wave exists it will take at least a minimum time of $\{L/(u-c), L/u\}$ seconds for the resulting errors to propagate out of the system.

VII. DISCUSSION OF NUMERICAL RESULTS - BOUNDARY CONDITIONS:

The linear "small deflection" theory predicts that the best boundary conditions would be the prescription of the characteristic variables at their point of entry with some form of (stable) numerical boundary condition for the point of exit. Here are two such schemes

INFLOW	OUTFLOW	
$W_1(0,t) = K_1$	$\frac{dW_1}{dx}(L,t) = 0$	
$W_2(0,t) = K_2$	$\frac{dW_2}{dx}(L,t) = 0$	(12)
$\frac{dW_3}{dx}(0,t) = 0$	$W_3(L,t) = K_3$	

Here K_1 and K_2 are numbers calculated from the known values of u, p, ρ at the inflow and K_3 is calculated from the known values of u and p at the outflow. Notice, however, the one "degree of freedom" is left at the inflow point. This allows the variables to adjust but in

compensating ways. The boundary conditions in the code are usually in terms of the physical variables so we translate (12) to physical variables.

INFLOW

$$\begin{aligned}
 p_1 &= \frac{\rho_o c_o}{2} [K_2 - u_2 - (1/\rho_o c_o) p_2] \\
 u_1 &= 1/2 [K_2 + u_2 - (1/\rho_o c_o) p_2] \\
 \rho_1 &= K_1 + (\rho_o/2c_o) [K_2 - u_2 + (1/\rho_o c_o) p_2]
 \end{aligned}$$

OUTFLOW

$$\begin{aligned}
 u_N &= 1/2 [u_{N-1} + (1/\rho_o c_o) p_{N-1} + K_3] \\
 p_N &= (\rho_o c_o/2) [K_3 + u_{N-1} + (1/\rho_o c_o) p_{N-1}] \\
 \rho_N &= (\rho_o/2c_o) [K_3 + u_{N-1}] - [1/(2 c_o^2)] p_{N-1} + \rho_{N-1}
 \end{aligned}$$

This set of boundary conditions is predicted to work well in the linear studies of one equation, occurring in [2] and [3]. We shall call these boundary conditions the "no-change characteristic boundary conditions". Another possibility, suggested by one-D analogues in [2], is the following:

INFLOW

$$\begin{aligned}
 w_1(o,t) &= K_1 \\
 w_2(o,t) &= K_2 \\
 \frac{\partial w_3}{\partial t} + (u-c)_1 \frac{\partial w_3}{\partial x} &= 0
 \end{aligned}$$

OUTFLOW

$$\begin{aligned}
 \frac{\partial w_1}{\partial t} + u_N \frac{\partial w_1}{\partial x} &= 0 \\
 \frac{\partial w_2}{\partial t} + (u+c)_N \frac{\partial w_2}{\partial x} &= 0 \\
 w_3(L,t) &= K_3
 \end{aligned} \tag{13}$$

where derivatives in the x-variable are downwind at the inflow and upwind at the outflow and forward in time. The numbers K_1, K_2, K_3 are prescribed as before. In terms of the physical variables these translate into

INFLOW

$$u_1^{n+1} = 1/2 [K_2 + u_1^n - (1/\rho_o c_o) p_1^n + (u_o - c_o) (\frac{\Delta t}{\Delta x}) [u_1^n - u_2^n + (1/\rho_o c_o) (p_2^n + p_1^n)]]$$

$$p_1^{n+1} = (\rho_o c_o / 2) [K_2 + (1/\rho_o c_o) p_1^n - u_1^n (u_o - c_o) (\Delta t / \Delta x) [u_2^n - u_1^n + (1/\rho_o c_o) (p_1^n + p_2^n)]]$$

$$\rho_1^{n+1} = K_1 + (\rho_o / 2 c_o) [K_2 + (1/\rho_o c_o) p_1^n - u_1^n + (u_o - c_o) (\Delta t / \Delta x) [u_2^n - u_1^n + (1/\rho_o c_o) (p_1^n - p_2^n)]]$$

OUTFLOW

$$u_N^{+1} = (1/2) [u_N^n + \frac{1}{\rho_o c_o} p_N^n - K_3 + (\Delta x / \Delta x) (u_o + c_o) [u_{N-1}^n - u_N^n + (1/\rho_o c_o) (p_{N-1}^n + p_N^n)]]$$

$$p_N^n = (\rho_o c_o / 2) [K_3 + u_N^n + (1/\rho_o c_o) p_N^n + (\Delta t / \Delta x) (u_o + c_o) [u_{N-1}^n - u_N^n + (1/\rho_o c_o) (p_{N-1}^n - p_N^n)]]$$

$$\rho_N^{n+1} = (\rho / 2 c_o) [K_3 + u_N^n + (1/\rho_o c_o) p_N^n + (\Delta t / \Delta x) (u_o + c_o) [u_{N-1}^n - u_N^n + (1/\rho_o c_o) (p_{N-1}^n - p_N^n)]]$$

$$+ \rho_N^n - (1/c_o^2) p_N^n + (\Delta t / \Delta x) u_o [\rho_{N-1}^n - \rho_N^n + (1/c_o^2) (p_N^n - p_{N-1}^n)]$$

We shall call these the "windward difference characteristic boundary conditions". Note: u_o , c_o can be different values at inflow and outflow.

The performance of the code with either of these was analyzed by posing initial conditions in which there was a disturbance in one or more of the characteristic variables either locally at the center of the grid or uniformly throughout the grid, of the order of 10%.

Thus figure 1 shows what happens if the disturbance is only in the third characteristics variable locally using the windward characteristic variables.

Figure 3 shows the effect of a plus +10% error in the initial conditions W_1 and W_3 and a -10% error in W_2 . (The first curve from the bottom is the initial state of the variable, and the others are the states at intervals of 25 iterations). In figure 2, we have an initial disturbance in W_2 of -10% with no initial disturbance in W_1 or W_3 . The pictures look essentially the same as figure 1. There is considerable nonlinear interaction until the

W_2 wave exists, and then uncoupled wave motion to the right in the first variable (W_1) and to the left in the third variable (W_3). There are no reflections when the W_1 and W_3 waves exit and convergence is reached in 300 iterations.

These computations were made using the windward differencing characteristic boundary conditions, although the same results were obtained with the no change characteristic boundary conditions.

In figure 4, we show the effect of a local disturbance at the center of the grid in the W_2 variable with the second set of B.C.'s and in figure 5 we show a speeded up version (every 50 iterations) of the same disturbance with the first set of B.C.'s. The third and fifth graphs on figure 4 are almost exactly the same as the second and fourth on figure 5. Figure 5 shows convergence being reached in 300 iterations.

We conclude that either of the first two sets of boundary conditions give optimal convergence since convergence cannot take place until the wave in W_2 exists (very quickly) and the residual (nonlinear) effects of W_2 on W_3 can exit upstream. If they can do this without any reflections, then the convergence is essentially optimal.

Sometimes, it is objected that in a wind tunnel experiment, the only variable known downstream is pressure and that we are requiring too much information in prescribing K_3 , which demands a knowledge of p and u at the outflow. Suppose, then we just prescribe p_∞ at the outflow using the otherwise successful conditions of $\frac{\partial W_1}{\partial x} = \frac{\partial W_2}{\partial x} = 0$ as complementary numerical boundary conditions. Then we could have, for example

INFLOW

$$W_1(o,t) = K_1$$

$$W_2(o,t) = K_2$$

$$\frac{dW_3}{dx} = (o,t) = 0$$

OUTFLOW

$$p = p_\infty$$

$$\frac{dW_1}{dx} (L,t) = 0 \quad (14)$$

$$\frac{dW_2}{dx} = (L,t) = 0$$

The inflow boundary conditions are precisely those of (12). The outflow boundary conditions (used by Steger [12]) are

$$p_N = p_\infty$$

$$\rho_N = (1/c_o^2)(p_\infty - p_{N-1}) + \rho_{N-1}$$

$$u_N = (1/\rho_o c_o)(p_{N-1} - p_\infty) + u_{N-1}$$

The predictions of section VI are clear. The fact that p is prescribed means that when a wave in W_2 comes downstream, it exits by adjusting the u values at $x = x_N$. This in turn causes disturbances in $W_3 = -u + (1/\rho_o c_o)p_\infty$ which cause a reflected wave upstream. This wave can be seen in figure 6. Since the upstream B.C. is non-reflecting, this means that the left running wave will exit without incidence. When composed with boundary conditions (12) or (13) it is obviously less desirable because of the magnitude of the reflection in W_3 . However it does converge in approximately 300 iterations, which is again almost optimal. The effect of these large oscillations in more complicated geometries may prove undesirable, however.

We briefly review our progress so far. Two sets of non-reflecting boundary conditions have been produced, both of which give optimal convergence but which rely on a great deal of information at both ends. The information, however, is used in such a way as to allow additional degrees of freedom for the waves to exit without repeated reflections. One reflecting

and one non-reflecting boundary condition can be combined to obtain almost optimal convergence at the cost of some large left running reflections, whose effect in more complicated geometries remains uncertain. While B.C. 12 was expected to be less accurate than B.C. 13, little evidence for this has been uncovered, except at the boundaries. Time dependent periodic flows (e.g. self excited oscillations) may prefer B.C. 13 however. We now consider some of the other boundary conditions which have been tried previously in the literature.

First we consider the case of reflecting boundary conditions. These occur in several places in the literature, for example in [10] and [12] and have been discussed in section VI. As we have seen, these arise from prescribing combinations of characteristic variables such as pressure downstream, and other combinations (perhaps to density and velocity upstream). In [10] Rudy and Strikwerda considered (among many others) the boundary conditions

<p>INFLOW</p> $u = u_{\infty}$ $T = T_{\infty}$ $\frac{dW_3}{dx} = 0$	<p>OUTFLOW</p> $\frac{du}{dx} = 0$ $\frac{dp}{dx} = 0$ $p = p_{\infty}$
---	---

and in [12] Steger uses

$u = u_{\infty}$ $\rho = \rho_{\infty}$ $\frac{dW_3}{dx} = 0$	$\frac{dW_1}{dx} = 0$ $\frac{dW_2}{dx} = 0$ $p = p_{\infty}$
---	--

Figure 7 shows the effects of an initial local disturbance in W_3 on both of these sets of boundary conditions, (13) on the left and (14) on the right. Note that first there is only a disturbance in the bottom picture. By iteration 75 (fourth curve up from the bottom) we can see reflections in both W_2 and W_1 although the W_2 deviation is a little harder to see. By iteration 125 it can be seen that the W_2 wave has travelled downstream and is reflected back upstream in W_3 . These reflections continued (somewhat smeared out) for at least 2000 iterations. Perhaps most startling is (at least at the beginning) how similar they are. A conclusion may be drawn from B.C.'s (14), (15), and (16). Prescribing physical values instead of characteristic values gives rise to reflection. If the reflections can occur only at one end, this does not impede convergence. However, reflecting conditions at both ends can be disastrous. This accounts for the "spurious pressure waves" mentioned by Moretti [7].

The case of prescription at the wrong end is now considered. In this case, the variables u , p , ρ are prescribed at the inflow and the conditions

$$\frac{du}{dx} = \frac{dp}{dx} = \frac{d\rho}{dx} = 0$$

are prescribed at the outflow. In this case, square wave disturbances which effected only the interiors of the domain exited as in figure 1, with some minor oscillations. However, when a uniformly wrong initial condition was imposed, convergence was very slow with large oscillations, and the solution converged to the wrong values, with errors of as much as 27%. The converged value was a function of the initial condition at the outflow end, as predicted in Gustafson and Kreiss [3]. The resulting graphs are given in figure 8.

Related to the above problem is the method of over prescription of boundaries. This method is mentioned in [9] as giving good results although the authors caution against it on the grounds of small oscillations being present. In fact the situation is much more serious. If initial waves in the interior of the domain are used with the initial conditions correct near the outflow, then the solution converges rapidly as the travelling waves exit without reflections and with minor oscillations. However, if the initial data is uniformly wrong with an error initially at the outflow point, then W_1 and W_2 converge rapidly but W_3 accumulates huge errors of the order of 70%. Eventually when W_1 and W_2 are converged, the correct value is propagated upwind in W_3 but taking large amounts of time to converge because of the large errors near the inflow point. Indeed, as W_2 becomes more accurate downstream the inaccuracies become much larger (140%) upstream. Particularly in a time dependent problem or in a problem with more complicated geometries, this could be truly disastrous. It points to another fact: if a new boundary condition is being tested, it is not sufficient to consider initial value perturbations from free stream which are non-zero in the interior only. In this case, we might have drawn totally wrong conclusions from the time taken for convergence.

In [10], a separate non-reflecting boundary condition is proposed. This boundary condition alters the value of K_3 , increasing it if the computed value of p is less than p_∞ , and decreasing it if the computed value of p is greater than p_∞ . Some thought shows that this cannot be optimal. Indeed, we can choose a variation from the initial conditions in which p is less than p_∞ , but because u is smaller than u_∞ , computed W_3 is actually larger than $W_{3,\infty}$. In this case, the proposed non-reflecting boundary condition

BIBLIOGRAPHY

- [1] Engquist, B., and Majda, A., "Absorbing Boundary Conditions for the Numerical Simulation of Waves", Math Comp. Vol. 31, pp 629-651, (1977).
- [2] Gottlieb, D., and Turkel, E., "Boundary Conditions for Multi-Step Finite Difference Methods for Time Dependent Equations", J. Comp. Phys. Vol. 26, pp 181-196 (1978).
- [3] Gustaffson, B., and Kreiss, H.O., "Boundary Conditions for Time Dependent Problems with an Artificial Boundary", Jour. Comp. Phys. Vol. 30, pp 333-351 (1979).
- [4] Gustaffson, B., Kreiss, H.O., and Sundstrom, A., "Stability Theory of Difference Approximations for Mixed Initial Boundary Value Problems II", Math. Comp., Vol. 26, pp 649-686 (1972).
- [5] Kreiss, H.O., "Stability Theory for Difference Approximations of Mixed Initial Boundary Value Problems I", Math. Comp., Vol. 22, pp 703-714 (1968).
- [6] MacCormack, R.W., "Numerical Solutions of the Interactions of a Shock Wave with Laminar Boundary Layer", Lecture Notes in Physics, Vol. 19, Springer Verlag (1976).
- [7] Moretti, G., Comment on "Stability Aspects of Divergent Subsonic Flow", AIAA Jour., Vol. 19, No. 5., p 669 (1981).
- [8] Parter, S.V., "Stability, Convergence and Pseudo-Stability of Finite Difference Equations for an Over-Determined Problem", Numer. Math., Vol. 4, pp 277-292 (1962).
- [9] Rudy, D. H., and Strikwerda, J.C., "Boundary Conditions for Subsonic Compressible Navier-Stokes Equations", Computers and Fluids, Vol. 9, pp 327-338 (1981).

- [10] Rudy, D.H., and Strikwerda, J.C., "A Non-reflecting Outflow Boundary Condition for Subsonic Navier-Stokes Calculations", Jour. Comp. Phys. Vol. 36, pp 55-70 (1980).
- [11] Shang, J.S., "Numerical Simulation of Wing Fuselage Interference", AIAA 19th Aerospace Sciences Meeting, AIAA-81-0048, Jan 12-15, 1981.
- [12] Steger, J.L., Pulliam, T.H., and Chima, R.V., "An Implicit Finite Difference Code for Inviscid and Viscous Cascade Flow", AIAA Preprint-80-1427, AIAA 13th Fluid and Plasma Dynamics Conference, July 14-16, 1980.
- [13] Yee, H.C., "Numerical Approximation of Boundary Conditions with Application to Inviscid Equations of Gas Dynamics", NASA Technical Memorandum 81265, March 1981.
- [14] Yee, H.C., Beam, R.M., and Warming, R.F., "Stable Boundary Approximations for a Class of Implicit Schemes for the One-Dimensional Inviscid Equations of Gas Dynamics", AIAA Paper 81-1009, presented at Palo Alto, CA, June 1981.

SQ IN IN K2

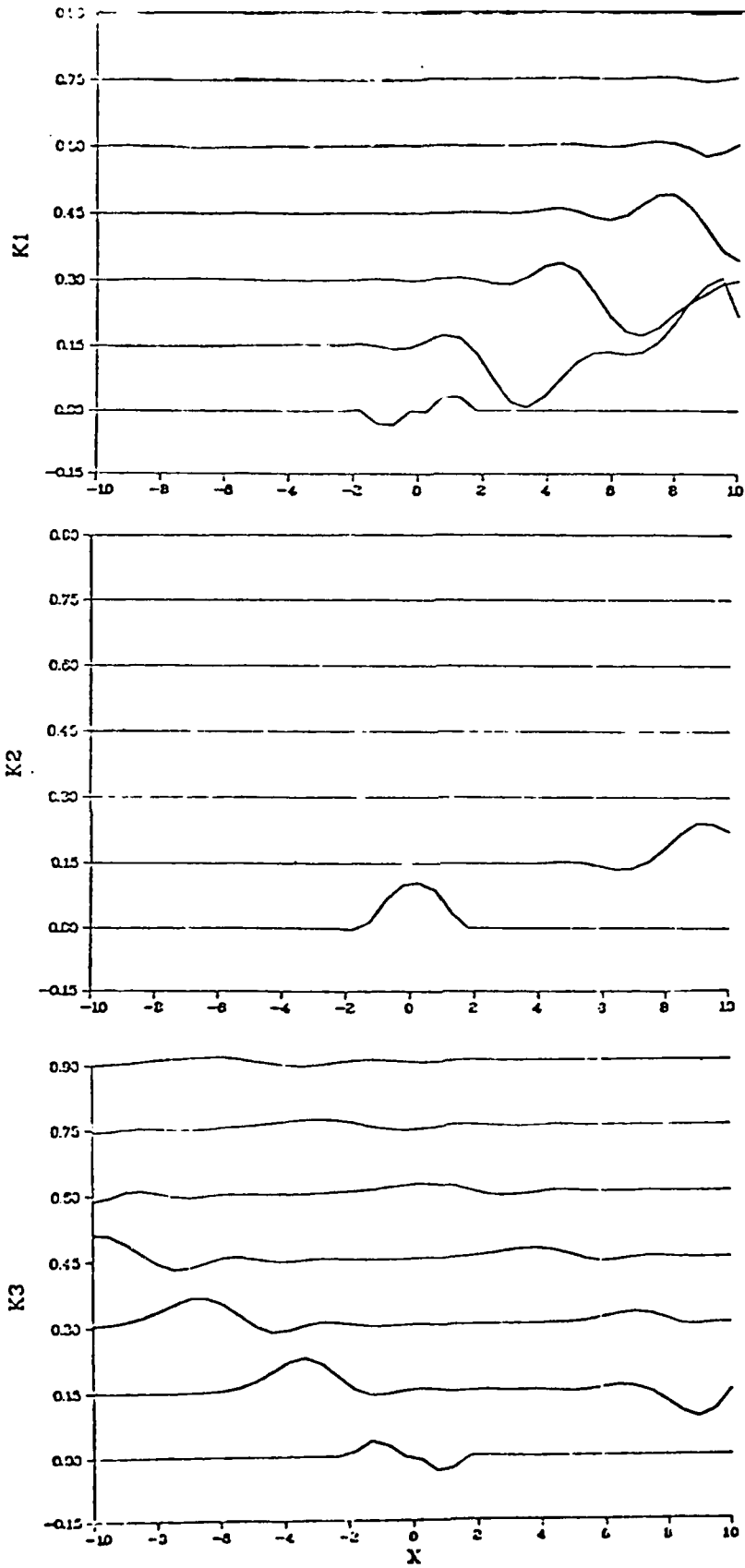


Figure 1
46-31

UNIF WRONG K2

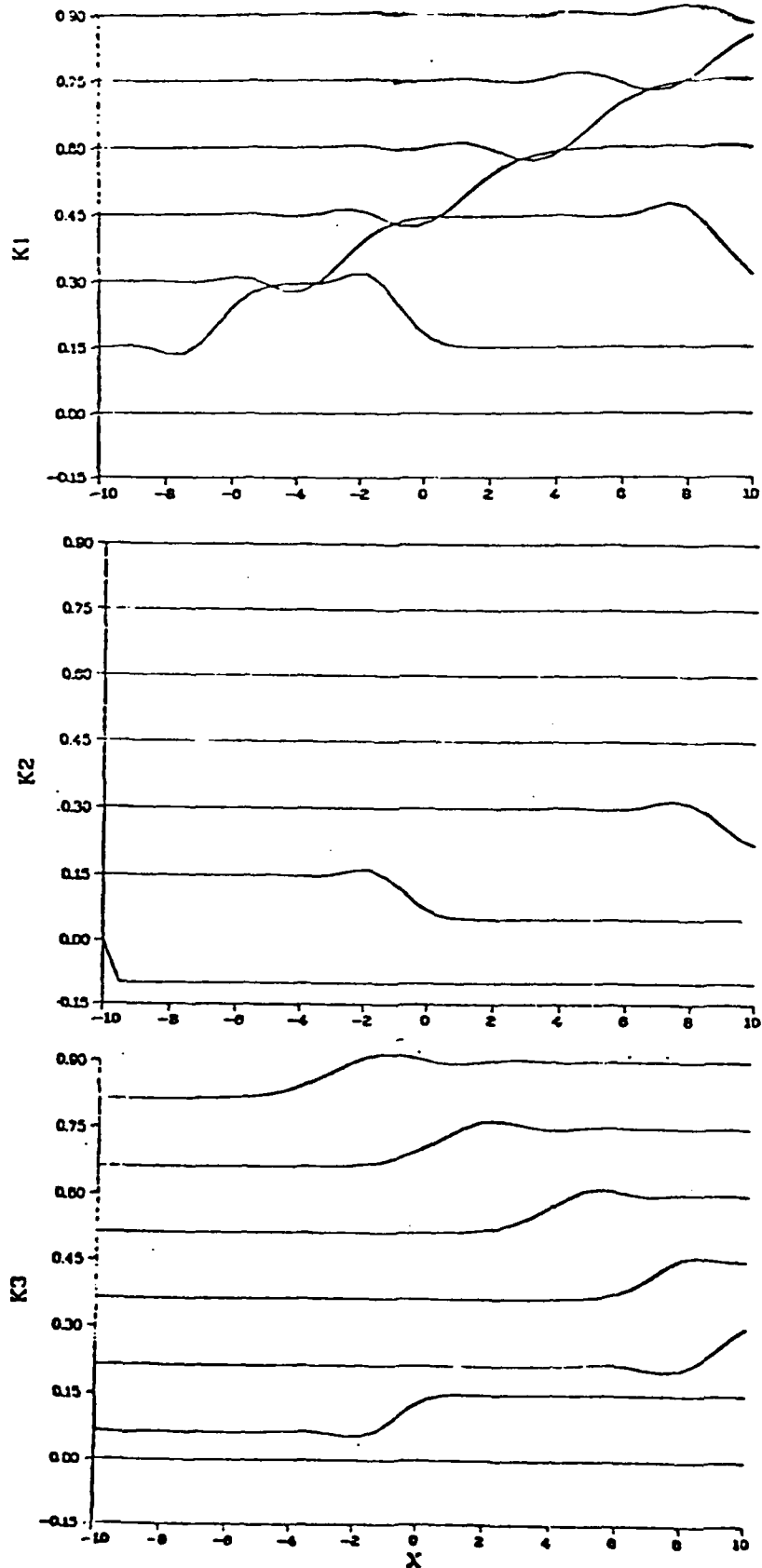


Figure 2
46-32

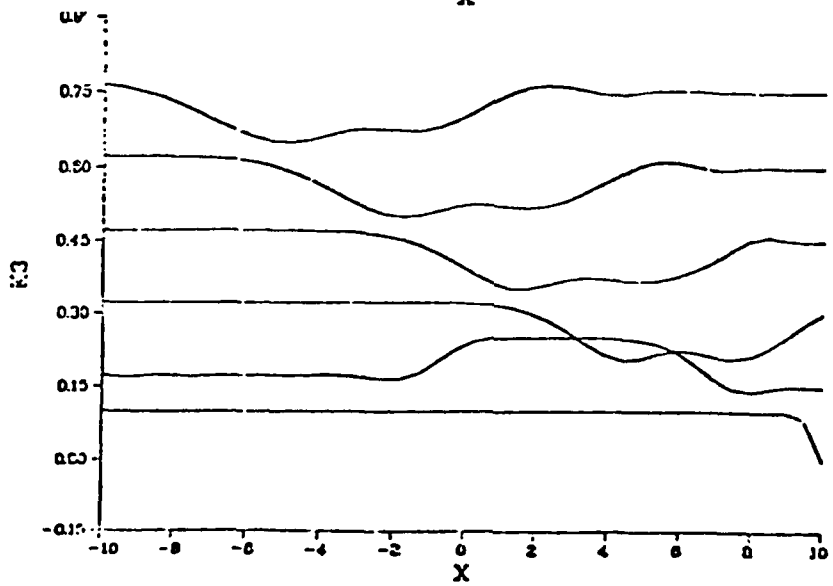
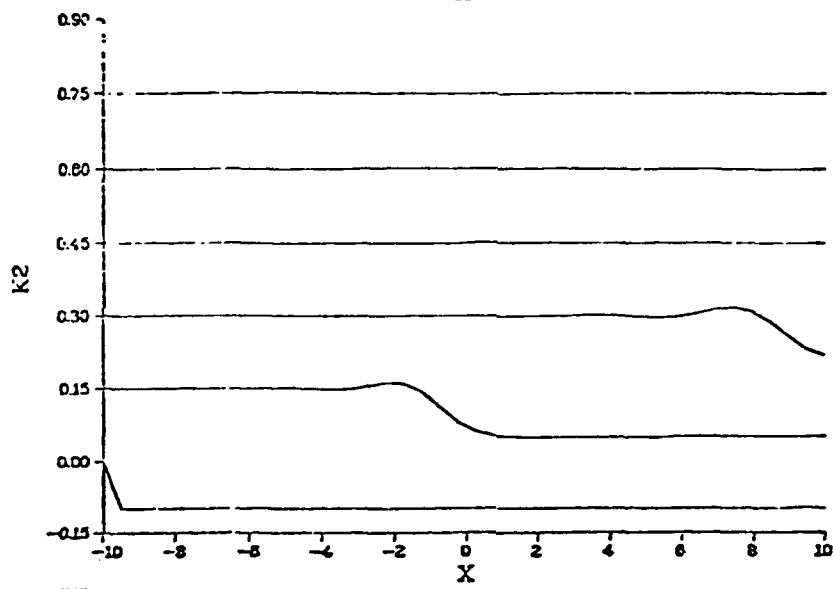
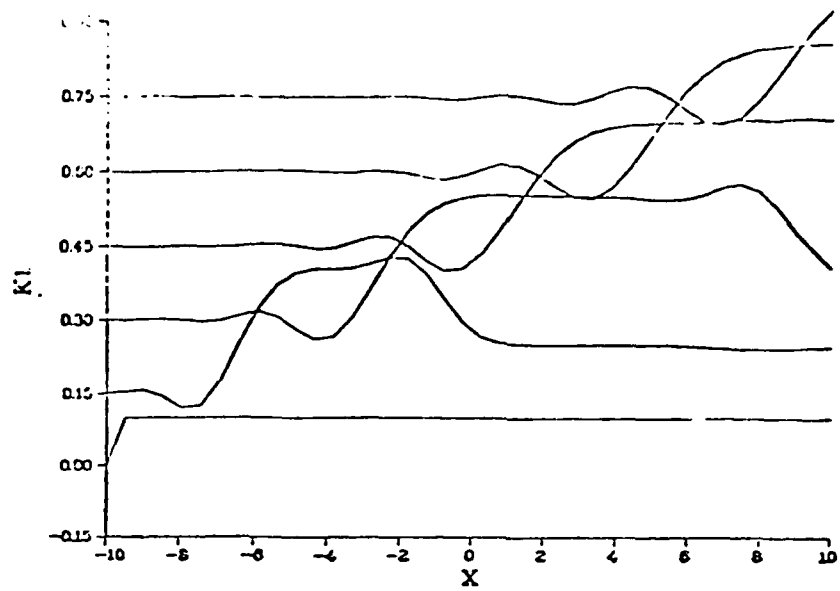


Figure 3
46-33

SQ WAV IN K3 G

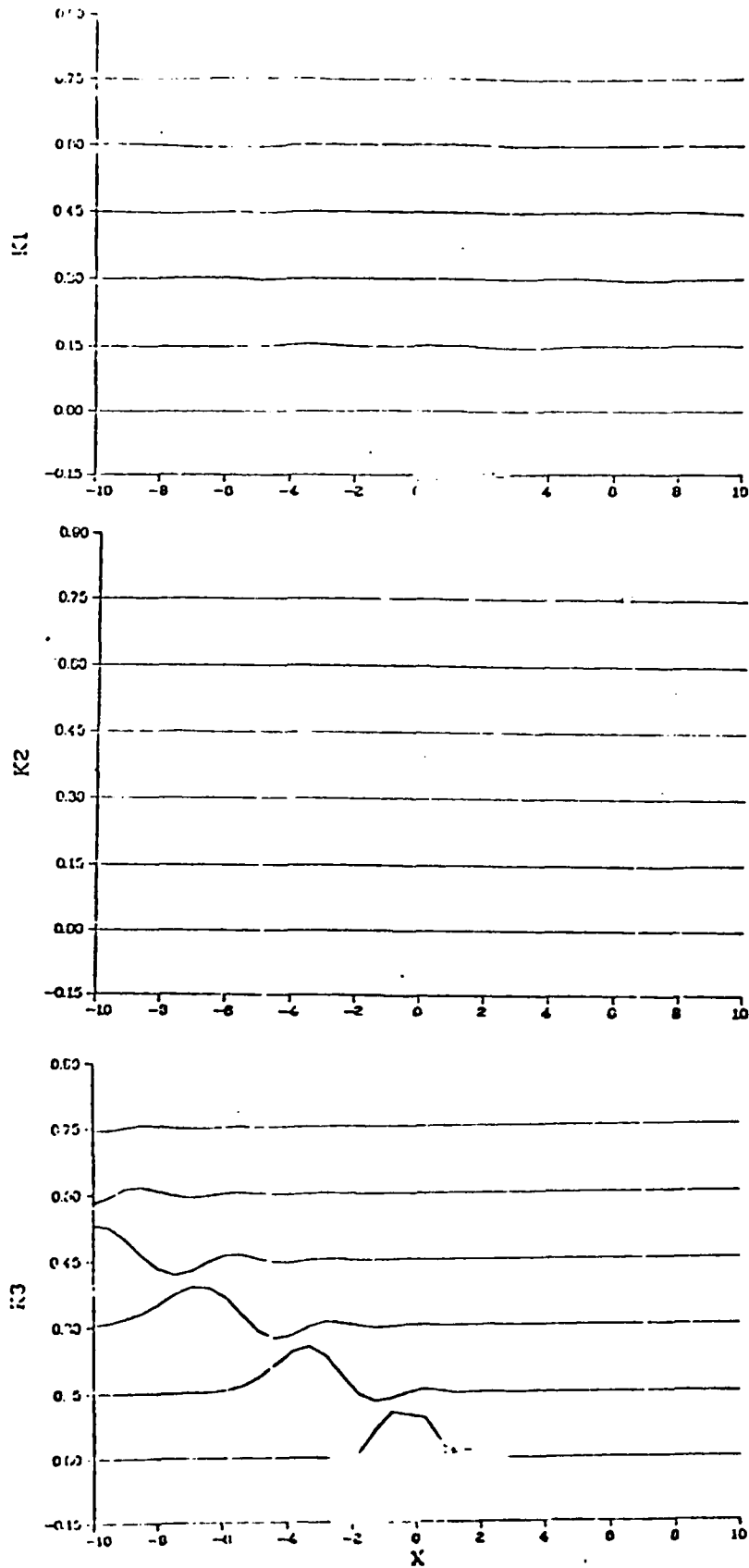


Figure 4
46-34

SQ WY IN 1.2 1

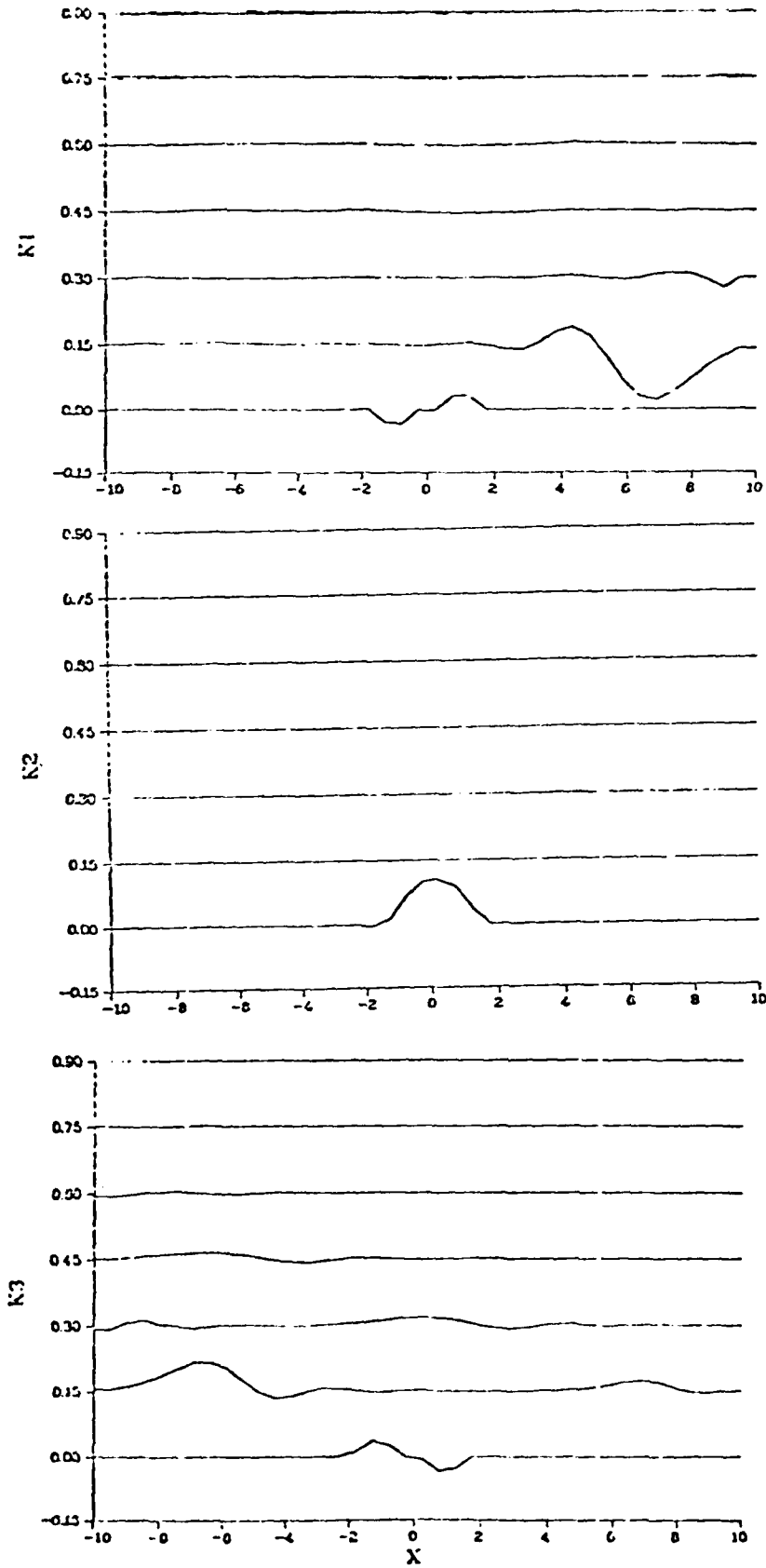


Figure 5
46-35

SQ WV IN KC (2)

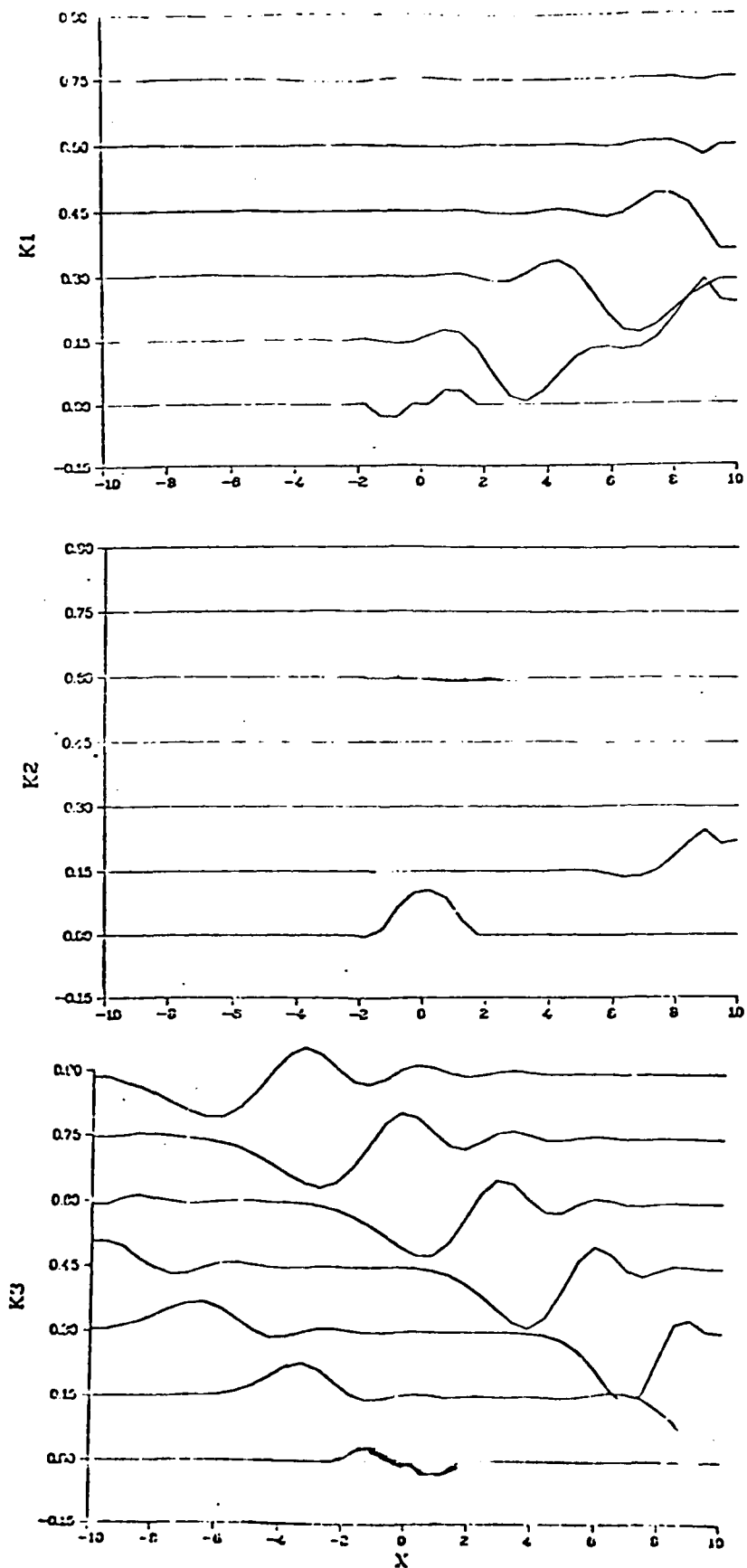
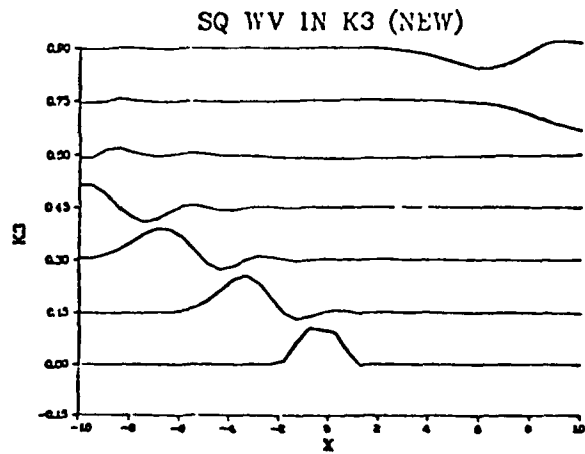
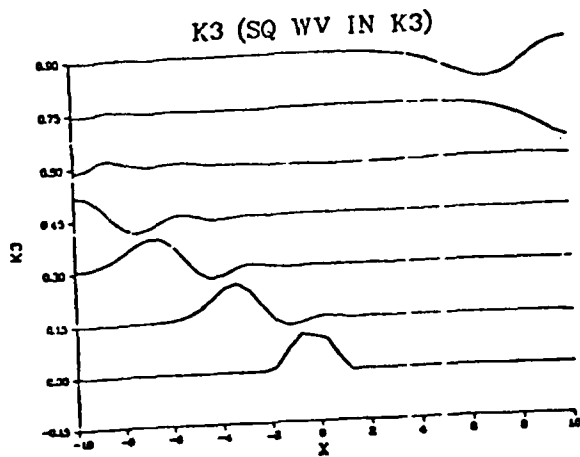
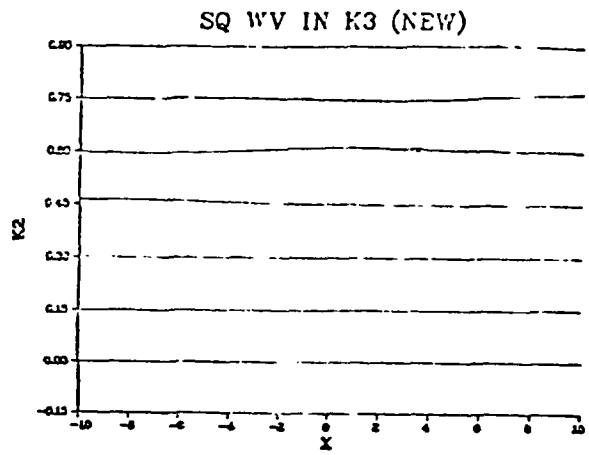
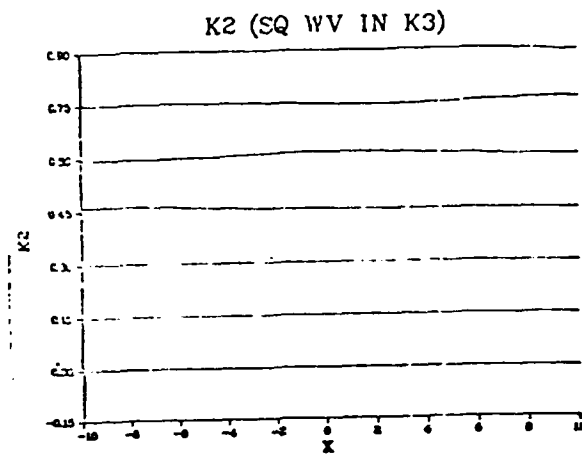
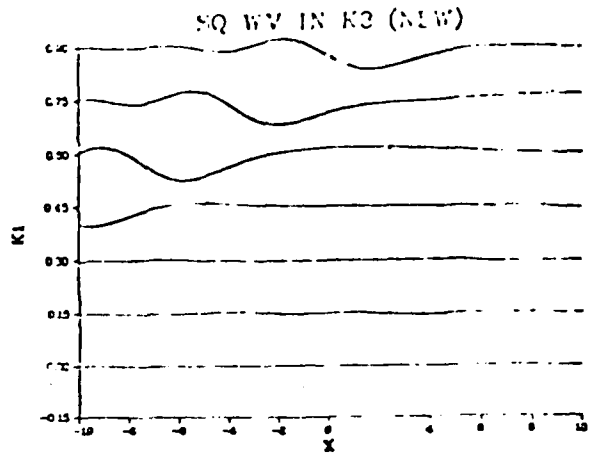
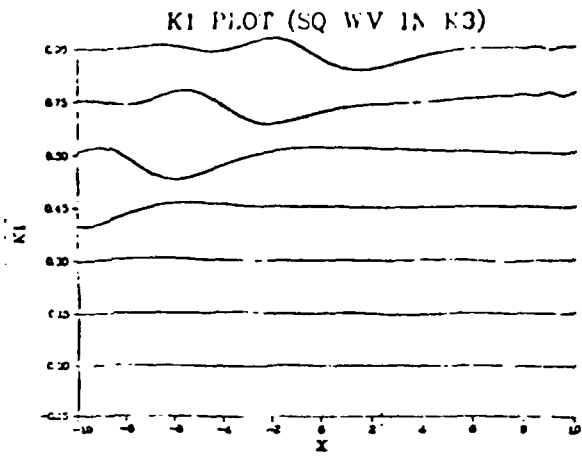


Figure 6
46-36

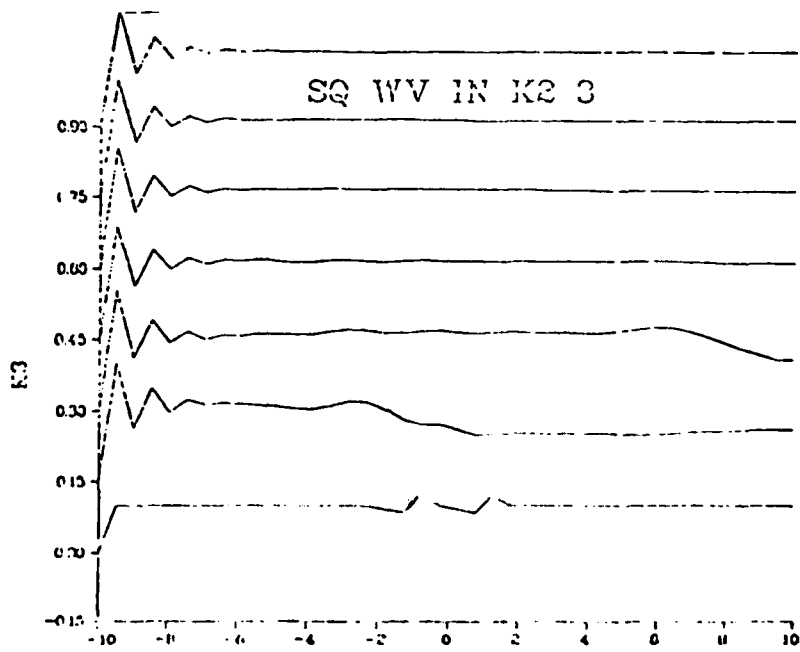
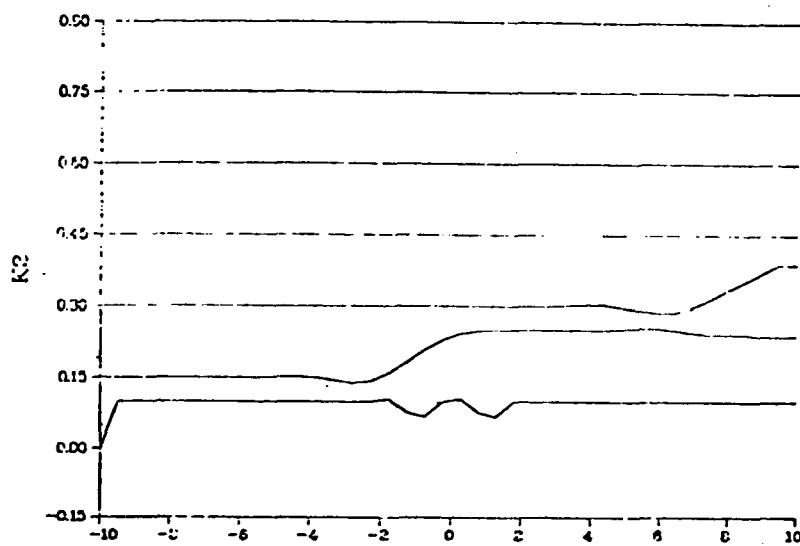
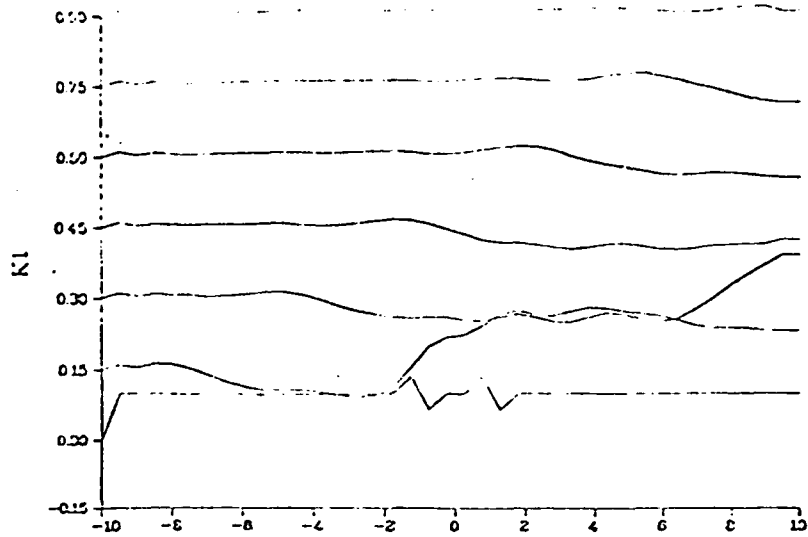


97
Labels

?

Figure 7

1 1 WV IN K2 3



X Figure 8
46-38

1981 USAF - SCEEE SUMMER FACULTY RESEARCH PROGRAM

Sponsored by the

AIR FORCE OFFICE OF SCIENTIFIC RESEARCH

Conducted by the

SOUTHEASTERN CENTER FOR ELECTRICAL ENGINEERING EDUCATION

FINAL REPORT

CONSTITUENT MONITORING OF EVAPORATION SOURCE PLUMES

Prepared by: Dr. J. R. McNeil
Academic Rank: Assistant Professor/Senior Scientist
Department and University: Department of Electrical Engineering/Institute for Modern Optics
Research Location: Air Force Weapons Laboratory, ARAO
USAF Research Colleague: Maj. Ron Lusk
Date: October 30, 1980
Contract No: F49620-79-0038

CONSTITUENT MONITORING OF EVAPORATION SOURCE PLUMES

by

Dr. J. R. McNeil

ABSTRACT

Thin film physical characteristics depend to a great extent upon the techniques used for deposition. In particular, films of ThF_4 have been deposited from different sources (boats, e-beam, etc.) and have displayed different absorption characteristics. A system of monitoring plume constituents has been implemented that employs mass spectroscopy. Drawbacks to this approach include low sensitivity for detecting plume constituents. Plans have been made to modify the deposition system in order to improve the sensitivity. Optical absorption and emission spectroscopy have been evaluated, but these techniques also appear to have low sensitivity to species in the plume, particularly molecular and impurity constituents.

ACKNOWLEDGMENTS

I am grateful for the sponsorship of the Air Force Systems Command, Air Force Office of Scientific Research, and the Air Force Weapons Laboratory. In particular, I wish to thank Lt. Col. Kenneth Jungling and Maj. Ron Lusk for suggesting this project and making proper arrangements for the work to occur.

I. INTRODUCTION

Characteristics of thin films depend to a great extent upon the techniques used for deposition. Films of ThF_4 , for example, have been observed to have absorption coefficients varying by nearly a factor of 10 when deposited under identical conditions except for the type of evaporation source used. Film cracking was observed in some cases and not in others; of those that cracked, the patterns observed were different for different sources employed.

Recently Hughes Research Laboratories has investigated impurities in ThF_4 material. They concluded that ThF_4 supplied by Cerac and believed to be of high purity actually contained as much as $\approx 5\%$ of $\text{ThL}(\text{OH})\text{F}_3$. This impurity is not detectable by Cerac's method of x-ray analysis. Hughes believes the OH content strongly influences the absorption of the film material at 3.8μ

It is not known what fraction of plume material coming from different sources (boats, e-beams, etc.) is ionized. The level of constituent ionization might be connected with the characteristics displayed by the resulting film. This is particularly the case for materials that disassociate during deposition, such as ZnS.

II. OBJECTIVES

The points above are the driving factors for establishing a system to monitor the constituents of plumes. The system would preferably have the sensitivity to detect impurities present on the order of 1%. This might provide a means of correlating physical characteristics displayed by the film with impurity content and thus remove some of the ambiguity of film deposition.

III. EXPERIMENTAL ARRANGEMENT

Mass spectroscopy was chosen as the technique for attempting to monitor plume constituents. The systems available at AFWL was the EAI Quad 250, with a range of 0 to 500 amu and a Varian unit with a range 0 to 100 amu. These systems were mounted on the ultrahigh vacuum system in the Developmental Optics Facility at AFWL. The deposition system had the capability of generating plumes using different resistively heated sources, e-beam and CO_2 laser heating. The deposition system was made operational, and a vacuum of 2×10^{-8} Torr was achieved, with several leaks located. Background mass spectra showed typical constituents of water, N_2 , etc.

IV. RESULTS

As a "warm up", sources of MgF_2 were examined. The first source was an e-beam generated plume. No spectra was observed using either of the mass spectrometers with the e-beam power supply set at maximum (10kV). Next several resistively heated boat sources were used. They were mounted in different positions inside the deposition chamber. After several boat-loads of MgF_2 were deposited, spectra of MgF_2 and Mg were observed using the Varian mass spectrometer. Deposition rate at the mass spec detector was approximately 10 Å/sec. The vapor source was an open, resistively heated boat. From what has been observed, the following problem areas can be identified:

1. The geometry of the source and mass spec must be changed to reduce their separation. At present, a boat loaded with material must be operated so hot in order to detect MgF_2 that it empties in 6 to 10 minutes of operation. Reducing the separation by at least a factor of 3 is required. However, this is complicated if source plumes other than those from directly heated boats are to be examined. Possibilities include recessing the mass spec head or obtaining a new bell jar, both of which would be expensive and time consuming.

2. There may be problems related to observing condensable vapor. This affects the sensitivity of the mass spec and is thus related to #1 above. Dielectric material can condense on the anode of the mass spec ionizer, reducing emission current and thus lowering sensitivity. During the 6 to 10 minutes of operation observing MgF_2 spectra with the Varian instrument, during which the density of MgF_2 in the ionizer was significant, the emission current dropped slightly from 4.1 to 4.0 mA. Was this reading real? This is something that can probably be lived with.

3. From what has been observed it is important to have the mass spec head in line of sight with the plume source. The EAI mass spec was mounted with a right angle valve above the source of MgF_2 , and operated with 1mA emission current, giving a sensitivity comparable to that of the Varian instrument. No MgF_2 spectrum was observed using the EAI instrument.

4. The e-beam source location is presently not within line of sight of the possible mass spec head positions. If any modifications of geometry are made, as mentioned in #1, this should be kept in mind (e.g. a port should be installed directly over the e-beam pockets). The present geometry probably explains why MgF_2 spectra has not been observed from the e-beam source.

5. The two mass spec instruments indicated different intensity ratios for the same two amu numbers. This might be due to a couple of things. The smaller Varian instrument could change in sensitivity with increasing amu, whereas the EAI, with a range of 500 amu, probably has less of a change over the same amu range. The result would be to indicate different ratios for materials of significantly different amu. Another possible explanation might be that the ionizer cathodes could be cracking molecules. With different geometries, different amounts of cracking might be expected.

V. RECOMMENDATIONS

Alternative approaches to monitoring the plume constituents might include emission and absorption spectroscopy. A small electron emission and accelerator arrangement could be constructed to straddle the plume to excite the constituents. However there would be problems associated with electrons dissociating molecular species in the plume and otherwise changing the plume. Also the spectra and Einstein A-coefficients of the molecular species are not all well known, and this would make it difficult to obtain quantitative measurements. This would also be the case in using absorption spectroscopy. However, an estimate of the optical path length, $k_0 \ell$, can be made following the techniques of Ladenburg and Reiche¹ using the expression

$$k_0 = \left(\frac{2}{\Delta \nu_0} \right) \left(\frac{\sqrt{\nu_{12}}}{\pi} \right) \left(\frac{\lambda_0^2 g_2}{8\pi g_1} \right) A_{21} N_1$$

Here λ_0 is the wavelength of the center of the transition, N_1 is the density of species in the upper level of the transition, and g_1 and g_2 are degeneracies of levels 1 and 2 (~ 1). Making reasonable assumptions for values of A_{21} ($\sim 10^8 \text{sec}^{-1}$) and $\Delta \nu_0$ ($\sim 10^9 \text{Hz}$) and calculating N_1 from knowledge of the deposition rate and species temperature ($\sim 10^{11} \text{cm}^{-3}$) yields a value of $k_0 \ell$ of .4 to 4. This is a reasonable range for performing absorption spectroscopy. However, this is applicable for atomic resonance transitions in the blue region of the spectrum, and this would not apply for molecular species. Also, impurity constituents would be at concentrations 10 to 100 times less than the major constituent, with N_1 and $k_0 \ell$ being correspondingly smaller. Thus the two optical spectroscopic techniques would be only partially applicable to monitoring plume constituents.

The decision was made to adapt the deposition chamber such that mass spectroscopic techniques could be used. Construction of the apparatus should begin within a month.

The final two weeks of this eight week effort were spent disassembling the uhv system and moving it. This was to prepare for clean-room modifications of the DOF.

REFERENCES

1. A. G. C. Mitchell and H. W. Zemansky, Resonance Radiation and Excited Atoms, (Cambridge University Press, London, 1971), Chapter III.

1981 USAF - SCEEE SUMMER FACULTY RESEARCH PROGRAM

Sponsored by the

AIR FORCE OFFICE OF SCIENTIFIC RESEARCH

Conducted by the

SOUTHEASTERN CENTER FOR ELECTRICAL ENGINEERING EDUCATION

FINAL REPORT

DEVELOPMENT OF A COMPUTER ASSISTED AIRCRAFT LOAD PLANNING MODEL

Prepared by : Dr. Louis A. Martin-Vega
Academic Rank : Visiting Associate Professor
Department and University : Department of Industrial and Systems Engineering,
University of Florida
Research Location: Air Force Logistics Management Center,
Gunter AFS, Alabama
USAF Research Colleague : Lt. Col Louis L. Osborne, Jr.
Date : September 10, 1981
Contract Number : F49620-79-C-0038

DEVELOPMENT OF A COMPUTER ASSISTED
AIRCRAFT LOAD PLANNING MODEL.

by

Louis A. Martin-Vega

ABSTRACT

The main objective of this applied research effort was to assist the Logistics Planning Office at Gunter AFS in their attempts to describe, model and develop computer assisted approaches to the aircraft load planning problem. Part of the research effort involved visits to locations where actual deployments were carried as well as meetings with experienced load planners throughout the course of the study. Information gathered from these visits and meetings was analyzed and documentation concerning the way the aircraft loading problem is approached by load planners was developed. A test data base was also developed and used to compare loading plans generated by manual load planners with existing computer assisted approaches. These comparisons resulted in a consensus that existing computer assisted approaches are still of limited practical value. Based on the insight obtained from the analysis, documentation and testing, a general methodology was developed which could serve as a foundation for the future development of computer assisted approaches. The feasibility of using microcomputer technology to assist in aircraft load planning was also explored yielding what appears to be a very promising area for future applied research in this area. Suggestions for basic research into the mathematical structure of the aircraft loading problem are also included.

ACKNOWLEDGEMENT

The author would like to express his sincere appreciation to the Air Force Systems Command, the Air Force Office of Scientific Research and the Southeastern Center for Electrical Engineering Education for providing him with the opportunity to spend a very worthwhile, interesting and rewarding summer at the Air Force Logistics Management Center, Gunter AFS, Alabama. The support and working conditions provided by the Logistics Management Center during my stay at Gunter were excellent.

A special note of appreciation is extended to Lt. Col. Lou Osborne for having suggested the area of study and for his collaboration and support throughout the ebbs and flows that I experienced during part of the summer. Lt. Col. Ed Baergen as well as the other members of the LGX were also instrumental in my feeling at home during my stay. Special thanks are also extended to Major John Mitchell, Sgt. Chin, Sgt Ernest Martin and the other members of the load planning group at Moody AFB, Georgia, for their assistance in the development of the test data base as well as their patience in the light of numerous questions regarding the load planning process. M/Sgt. William Clark played a special role in the development of this study and his contribution is gratefully acknowledged. The willing and able assistance and companionship I received from Lt. Karen Daniels, Lt. Kirk Yost, Lt. Barry Webb, Dr. Tom Payne and the group at the LMC Computer Center played a significant role in the development of the material contained in this report. An additional thank you is extended to the members of the Gunter MicroComputer Club for their interest in the problem and in particular to Airman Chip Hyde for his patience and willingness to provide me with orientation regarding the potential of microcomputer technology. A final note of appreciation is extended to the secretarial staff of the ISE Department at the University of Florida for their work in the preparation of this report.

I. INTRODUCTION:

A major priority effort of the Logistics Planning Office at Gunter Air Force Station is the development and use of computer technology for load planning Air Force mobility equipment/personnel on military cargo and Civil Reserve Air Fleet (CRAF) aircraft. Although the load planning process is currently carried out manually at the base level, it is felt by Air Force personnel that the adequacy of the manual process is limited to pre-planned peacetime deployment exercises exhibiting few, if any, changes in aircraft or equipment availability. Both the inadequacies of manual load planning and the frustrations encountered by load planners can best be appreciated when last minute changes occur in either the aircraft available for the deployment, the equipment to be deployed or the desires of the loadmasters. (For a more extensive description of these problems refer to (3, 7, 8)). Since last minute changes are considered the rule rather than the exception in any "real-time" deployment exercise, it is not hard to see why it is felt that any enhancement of mobility capability and effectiveness requires at least a partial automation of the load planning process.

The general load planning problem can be described as a situation where personnel and equipment are to be transported from one location to another subject to a set of restrictions. These restrictions include factors such as types and availability of aircraft as well as loading considerations such as maximum weight limits, type and size of equipment and many others. (Refer to (3) for a detailed listing of factors relevant to the loading problem). The objective is basically one of carrying out the move with the minimum number of aircraft which in some cases is akin to making the move in such a way that total fuel consumption is minimized. The support equipment to be transported is either packaged in pallets or consists of rolling equipment which are usually large enough to be transported as self-contained units. The related problem of creating pallet loads based on existing equipment requirements has been the subject of prior study (5,6). In so far as the loading problem is concerned it can be assumed that pallet loads have been previously designed and specified.

The peculiarities of any particular load planning problem are encased within the logistics of the deployment effort it is to serve. The basic objective of any deployment effort is to move one or more squadrons of fighter aircraft (say F-4's) from an origin to a destination in such a way that

combat readiness is attained at the destination. In order to achieve combat readiness a coordinated parallel move of support equipment and personnel must be carried out. It is at this point where the load planning phase comes into play. Insight into the logistics of a deployment effort can be obtained by referring to Figure 1. In this example it is assumed that the objective of the deployment is to move one or more squadrons of F-4's from origin (O) to destination (D), allowing for two enroute refueling or tanker positions, (A) and (B). The support squadrons fall into four general classifications:

ISE: Initial Support Equipment

Part of this squadron precedes the actual movement of the F-4's and has the responsibility of preparing the destination site for initial combat readiness. Since the characteristics of the destination may vary from that of a well equipped site to an extreme bare base condition, the size of this move will vary accordingly. Given the importance of this initial move, it is often the case that the first aircraft to be load planned are dedicated exclusively to this equipment.

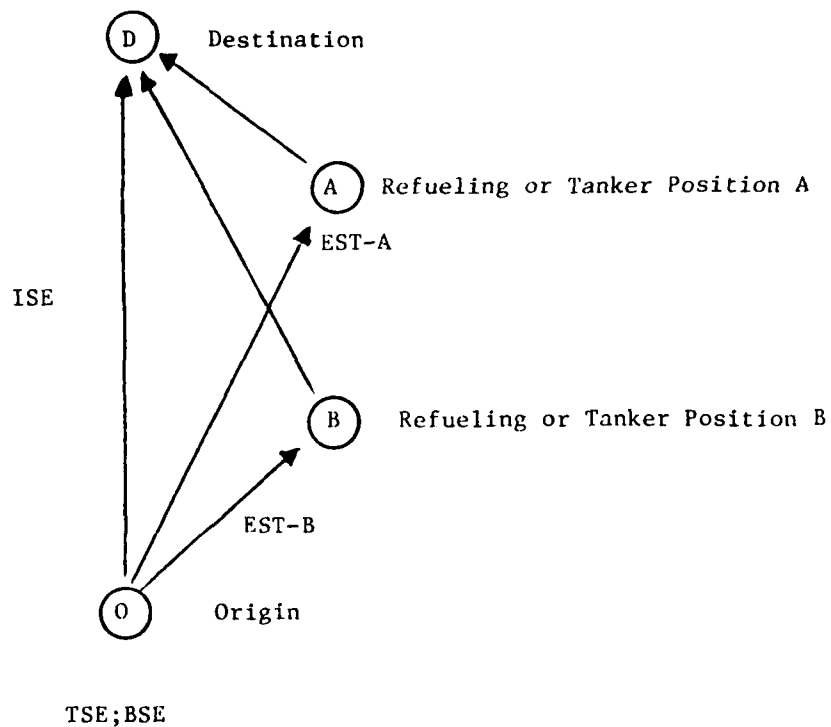
EST: Enroute Support Team

As the name suggests, this squadron provides support to the movement of the F-4's at the intermediate or refueling positions as may be required. The move will be divided among the refueling positions (i.e., EST-A and EST-B)

TSE: Tactical Support Equipment

BSE: Base Supply Equipment

These squadrons can either precede or follow the actual movement of the F-4's. Their arrival at the destination is tantamount to the completion of the deployment. As can be noted, the logistics of a deployment effort imply the movement of equipment and personnel with different time dependent priorities. It does not suffice "to move everything". It is also necessary to have particular items available at either the destination or refueling positions at certain strategic moments in order to carry out the move with the coordination required. It is this time dependent factor which becomes an additional crucial argument for the partial automation of the load planning process if one is to adequately serve a "real-time" deployment with "real-time" support.



- (i) The first group of equipment and passengers to be moved is part of ISE and is sent directly from the origin to the destination.
- (ii) The second group of equipment and passengers that go out is EST-A to the refueling point closest to the destination.
- (iii) EST-B goes to refueling point B, and then Both EST-A and EST-B advance to the destination as the F 4's pass points **(B)** and **(A)** respectively.
- (iv) TSE and BSE followup the movement of the F4's.

Figure 1
The Logistics of a Deployment Effort

Finally, it should be pointed out that research carried out on aircraft load planning, while acknowledging the theoretical aspects of the problem, consists basically of attempts to develop real-time interactive approaches to the problem. It is this approach which appears to be most amenable to incorporating the many practical details involved in an actual load planning situation. It suffices at this point to state that given the size and multiple constraints associated with practical loading problems, it is highly unlikely that any optimum real-time solution to the problem will be found. It was with this in mind that the objectives outlined in the following section were specified.

OBJECTIVES

The effort documented in this report is a study of the aircraft load planning process with the main objective of assisting the Logistics Planning Office in their attempts to describe, model and develop automated or partially automated approaches to the problem. Within this main objective the following specific steps were established as guidelines for this research:

(i) In order to develop a feel for the physical reality of the problem a location where a deployment is carried out would be visited. Part of the research effort would involve visits to the location to analyze and document the way the problem is approached at present by manual load planners. The objective here is to develop documentation that would provide insight into understanding the problem itself.

(ii) Using this location as a "test case", a data set corresponding to the loading problem faced by those doing manual load planning would be generated. This test data would then be used to compare the actual loading plans generated at the test site with plans developed by either load planners at other locations or existing automated approaches. A comparison of these results would then yield the basic structure of a load planning methodology as well as an evaluation of current manual and computerized load planning approaches.

(iii) Using the insight obtained from (i) and (ii), a methodology would then be developed based on this "test case" taking into consideration the eventual, at least partial, automation of the procedure itself.

(iv) Finally, it is expected that the work carried out would also assist in developing recommendations as to feasible directions for future work in load planning including the possibility of incorporating microcomputer technology in the load planning effort. These recommendations would then complete the contents of this report.

The following sections of the report follow the sequence established by the statement of objectives starting with a visit to Moody AFB, Georgia in early June.

III. ANALYSIS AND DOCUMENTATION OF MANUAL LOAD PLANNING PROCEDURES

Exercise Red Flag 81-4 was carried out at Moody AFB, Georgia between June 9 and June 12, 1981. The destination of this pre-planned deployment was Nellis AFB, Nevada. In addition to observing the various aspects of this deployment, conversations were held with personnel in charge of the load planning effort as well as with personnel previously in charge of load planning at this facility. Subsequently during the summer in the company of Lt. Yost of the AFLMC a series of meetings were held with M/Sgt. W. Clark, load planner for the Air Force Reserve at Dantley Field in Montgomery, Alabama. The following description is a summary of the insight obtained from these conversations and meeting. It is felt that this information is an accurate statement of the way load planning is presently approached by those who have responsibility for this task.

A. Pre-Load Plan Phase

One of the first insights obtained from the conversations at Moody and at Dantley was that the entire load planning operation can be divided into essentially two phases. The pre-load plan phase consists of all the steps to be carried out from the moment the origin deployment site (say Moody) receives its initial message from Headquarters announcing the exercise up to and including the moment the origin site replies with its estimate of the number of each type of aircraft it will need to carry out the deployment. These steps are documented in Figure 2, and can be summarized as follows:

Steps (1) and (2) consist of Headquarters advising the origin deployment site of an exercise and their submission of a description of the deployment (exercise package). Once information is acquired by the origin deployment site on the conditions of the destination site (3), the support groups are asked to submit a list of the equipment they would need to move ((4), (5)) in order to complete the exercise. This list is screened by the load planners (6) and after interacting again with the support groups a final list of equipment to be moved is agreed upon. This final list of equipment is then partitioned into various material handling units 7 and estimates of quantities to be moved are generated. Using these totals, estimates of the total weight of the support deployment are arrived at. In some instances, estimates of the total number of stations (i.e., aircraft cargo positions) and passenger positions are also generated (9B). This

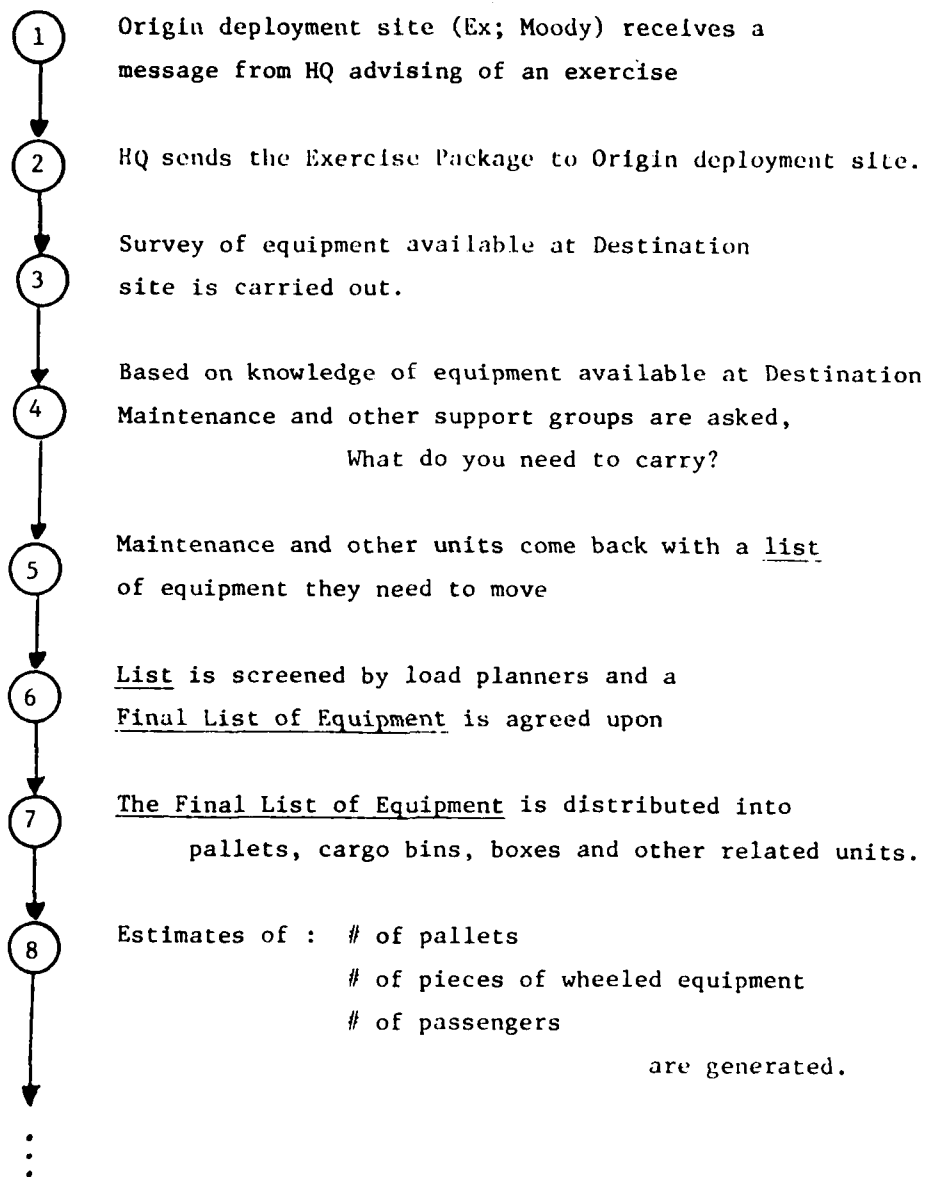


Figure 2
Pre-Load Plan Phase

Estimate of the Total Weight of the move is generated.

Estimate of the Total Number of Stations and People involved in the move is generated.

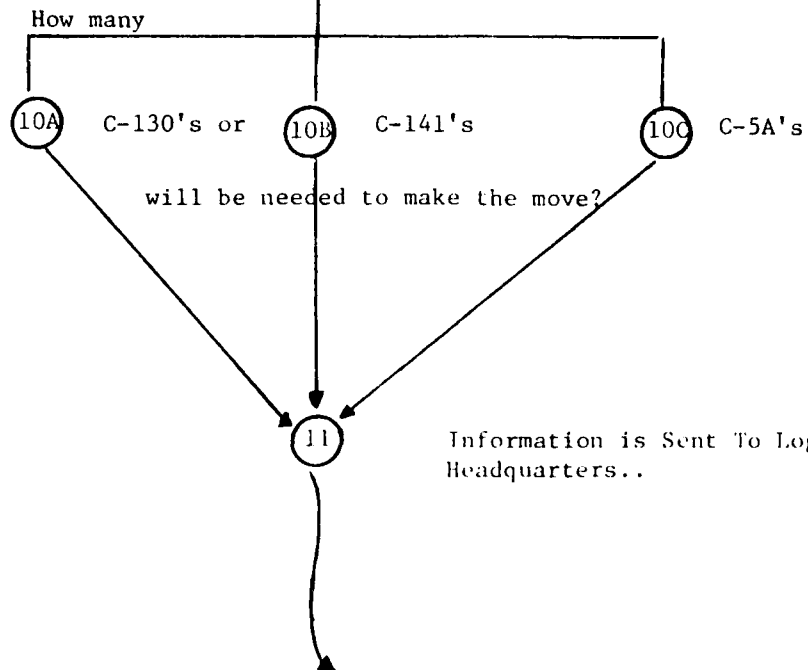


Figure 2 (cont.)

data is then used to determine the number of aircraft required for the move (10). Unless a prior expected aircraft mix has been provided by HQ, the usual assumption made by the load planners is that the move will be made on one type of aircraft and therefore estimates of the total number of either C-130's (10A), C-141's (10B), or C-5A's (10C) needed to individually carry out the whole move are generated. While this may appear to be rather complicated at first glance, most load planners will usually carry out their calculations for just one type of aircraft (say C-130's) and then use equivalency relationships (Ex: 2 C-130's carry approximately the same as 1 C-141) to generate estimates for the other type of aircraft. This information is then sent back to Logistics Headquarters (11) thus completing what we have called the pre-load plan phase.

B. The Actual Load Planning Phase:

The actual load planning phase is summarized in Figure 3. It commences with a reply from Logistics Headquarters informing the type and amount of aircraft assigned for the deployment (12). Up to this point most experienced load planners will have relied upon their knowledge of the characteristics of support equipment to generate the estimates of space and weight referred to in the pre-load plan phase. However, a formal check of the physical characteristics of the equipment (height, length, weight, cube) is usually conducted by referring to the BAMS 3 Mobility Equipment Listing maintained at most origin deployment sites (13). The aircraft mix information and the estimates of the physical characteristics of the equipment along with the number of people to be moved (9B) becomes the input data for the creation of the load plans (14). This information is summarized on standard MAC Passenger/Cargo Manifest forms consisting of schematics of the different aircraft which allow for manual positioning of equipment and passengers along with a listing of the equipment and its characteristics. (see Figure 4, for an example of a C-130 form).

While estimates of equipment weights have been used as data for the creation of load plans, it is not until the equipment packages are actually prepared that actual weight can be determined (15). An inspection of these equipment packages is carried out by the planners and differences between estimated weight and actual are noted (16). If the differences are not significant, then load plans are not altered. However, if the

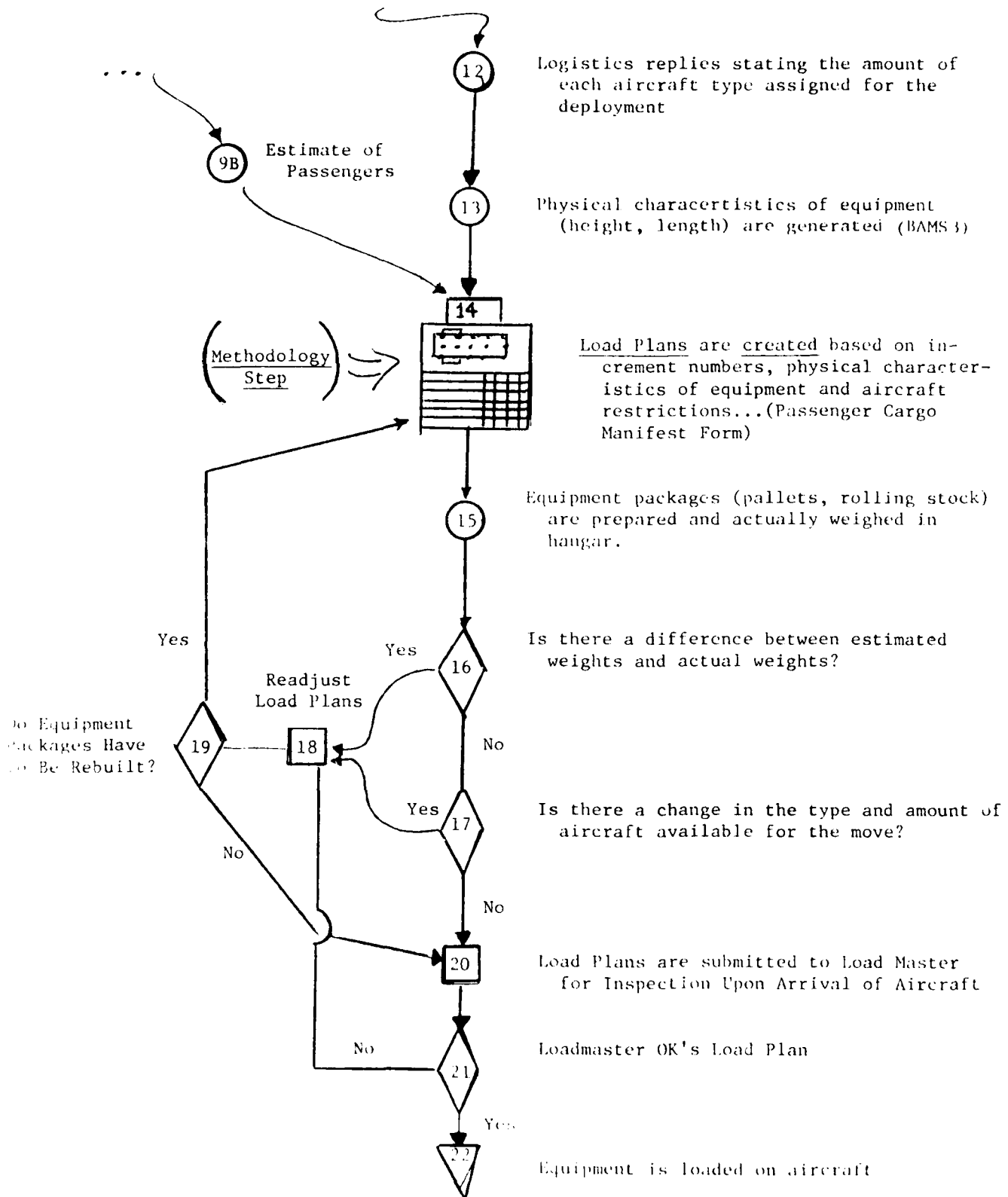


Figure 3
Actual Load Planning Phase
48-13

FORM 2-33
Sep 77

(1) To be completed by Air Force Pilot

C-130 PASSENGER/CARGO MANIFEST

ROW	1	2	3	4	5	6	7	8	9	10	11	12	13	14	15	16	17	18	19	20	21	22	23	24	25	26	27	28	29	30	31	32	33	34	35	36	37	38	39	40	41	42	43	44	45	46	47	48	49	50	51	52	53	54	55	56	57	58	59	60	61	62	63	64	65	66	67	68	69	70	71	72	73	74	75	76	77	78	79	80	81	82	83	84	85	86	87	88	89	90	91	92	93	94	95	96	97	98	99	100																																																							
245	246	247	248	249	250	251	252	253	254	255	256	257	258	259	260	261	262	263	264	265	266	267	268	269	270	271	272	273	274	275	276	277	278	279	280	281	282	283	284	285	286	287	288	289	290	291	292	293	294	295	296	297	298	299	300	301	302	303	304	305	306	307	308	309	310	311	312	313	314	315	316	317	318	319	320	321	322	323	324	325	326	327	328	329	330	331	332	333	334	335	336	337	338	339	340	341	342	343	344	345	346	347	348	349	350	351	352	353	354	355	356	357	358	359	360	361	362	363	364	365	366	367	368	369	370	371	372	373	374	375	376	377	378	379	380	381	382	383	384	385	386	387	388	389	390	391	392	393	394	395	396	397	398	399	400

1/8" = 1 FOOT

FORM 2-33
Sep 77

(1) To be completed by Air Force Pilot

C-130 PASSENGER/CARGO MANIFEST

Figure 4
C-130 Passenger/Cargo Manifest Form

differences cause any vital loading restrictions (essentially maximum weight at this point) to be violated, then a readjustment of load plans may be required [18]. If feasible plans cannot be created due to the differences, it may be the case that equipment packages would have to be torn down and rebuilt (19) causing essentially a second iteration of the whole process from step [14] onwards. This group of steps may also occur (and more frequently does occur) if a change is announced (usually on short notice) in the type and amount of aircraft available for the move (17). In this case it is very likely that some of the load plans will have to be scrapped rather than just readjusted leading one through steps [18] (19), and up to [14] again.

Given a set of "final" load plans, these plans are presented to the aircraft loadmasters upon their arrival with their aircraft. [20]. The loadmasters will then inspect the plans and recheck, height, weight, center of gravity and other restrictions before granting their approval for the actual loading to begin (21). Other considerations such as ease of loading and unloading of palletized and rolling stock equipment come into play in the inspection. If no changes are requested, then the actual loading is commenced (22). However, if changes are requested the load planner may find him/herself again in the readjusting, rebuilding and re-creation of load plans loop ([18], (19), [14]..) relying upon his/her experience to shorten the duration of this manual procedure.

It is in steps [14] and [18] where the experience of the load planner comes strongly into play. The amount of time required to create or adjust the load plans depends significantly upon his or her knowledge of both aircraft and equipment characteristics. Various loading restrictions such as maximum weight and height limits, center of gravity considerations, specific location of certain types of hazardous material and many others (refer to (3) for a detailed listing) must be taken into consideration in the creation of feasible load plans. However, as is to be expected, certain restrictions are in reality "more critical" than others and the experienced load planner is acutely aware of this. It was therefore not surprising to find that the methodology employed in the creation of load plans varies among load planners based on the amount of experience they have and the type of equipment they are accustomed to moving. Nonetheless it is felt that certain common elements can be exploited in an attempt to develop a load planning methodology. It is the development of this methodology which forms the basis for the next sections of this report.

Finally, it must be pointed out that the load planning procedure from step 14 onwards, is a manual procedure. While no computerized system can, nor should desire to replace, the insight of an experienced load planner, it is in these steps where the assistance of a computer based interactive system should be able to play a significant role. Reductions of the time required and the inherent tediousness and error proneness of having to manually go through iterations of the creation, readjustment, re-creation of load plans loop described by steps 18 , 19 , 14 etc .., while not critical for most pre-planned peacetime deployments, would be a very critical component of any real-time deployment effort.

IV THE MOODY TEST CASE

The documentation of the previous section presents the general procedure followed by load planners at the locations visited as part of this effort. The difference in the approaches followed are concentrated in the actual methodology used for the creation of load plans. In order to obtain additional insight into this part of the procedure the data used in the Moody deployment was compiled and used as a test case. The actual load plans generated at the test site will now be presented along with the load plans developed by M/Sgt. Clark when he was given the same data to analyze. In addition, the test data was fed into the New Mexico Air National Guard Computerized Aircraft Load Planning Model (10) allowing for an additional comparison between existing manual procedures and this first attempt in the Air Force to introduce automation into the load planning process.

A- The Test Data:

The list of equipment to be moved during Exercise Red Flag 81-4 is described in Table 1 along with their length, width, height and weight characteristics. The 31 items include both pallets and rolling stock as well as equipment which can occupy only specified positions in the aircrafts (Ex: Loxcart requires a position with Venting Equipment). The generations of this list is equivalent to having reached step 8 of the Pre-Load Plan Phase (see Figure 2). The total weight of the move was 89,987 lbs., well within the peacetime load limits of either one C-5A, two C-141A's or four C-130's (MAC Pamphlet 50-13, 10 Oct. 1980 page 2-1) and thus completing the equivalent of steps 9 , 10 , and 11 of the Pre-Load Plan Phase.

Table 1
List of Equipment To Be Moved
Operation Red Flag 81-4

<u>Description</u>	<u>Increment No</u>	<u>Length</u>	<u>Width</u>	<u>Height</u>	<u>Weight</u>
1. Compressor MC2A	T429	86	59	40	880
2. Compressor MC1A	T433	79	66	61	2150
3. Pallet 463L	I248	88	108	93	5200
4. Pallet 463L	I236	88	108	96	4000
5. Pallet 463L	I247	88	108	90	4000
6. Pallet 463L	I266	88	108	90	3717
7. Pallet 463L	I269	88	108	90	3880
8. Pallet 463L	I001	88	108	96	4500
9. Pallet 463L	I010	88	108	96	4200
10. Pallet 463L	T150	88	108	96	3600
11. Pallet 463L	I244	88	108	96	2000
12. Pallet 463L	I268	88	108	90	3520
13. Pallet 463L	I260	88	108	90	3120
14. Pallet 463L	I252	88	108	90	3420
15. Pallet 463L	I233	88	108	90	3350
16. Pallet 463L	I264	88	108	90	3380
17. Pallet 463L	I256	88	108	90	2000
18. Bomblift MJ1A	I113	148	53	42	3650
19. AM32A-60	I109	118	68	86	4290
20. Loxcart	I188	117	68	54	1100
21. AM32A-60	I145	118	68	68	3900
22. AM32A-60	I149	118	68	68	3900
23. NF2-lightall	I144	83	68	60	2150
24. NF2-lightall	I129	83	68	60	2150
25. Air Cond	I228	88	68	68	1120
26. Pallet 463L	I259	88	108	90	2415
27. Pallet 463L	I263	88	108	90	2335
28. Pallet 463L	I101	88	108	90	2150
29. Compressor M2A	I128	86	59	40	880
30. Compressor M1A	I125	79	66	61	2150
31. Compressor M2A	I141	86	59	40	880

89,987

B: Moody's Load Plan:

The day before the deployment word came in from HQ that instead of two C-141A's and two C-130's, a C-5A would be available to make the move. This greatly simplified the process since all items could be accommodated on this one aircraft. The load planning function became one of having only to locate the items on the C-5A, instead of first having to select which items would go on which aircraft and then locating them into positions as would have been the case had C-141A's and C-130's been used.

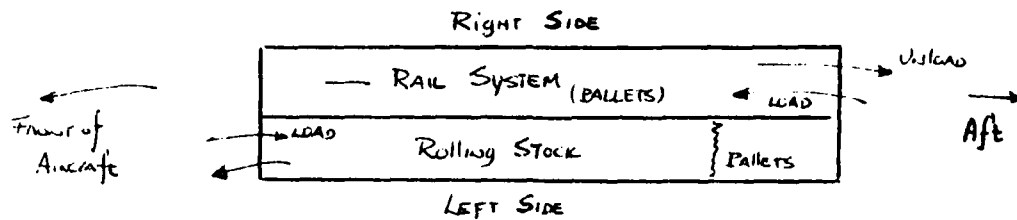
The load plan generated by the Moody planners is illustrated in Figure 5. The main considerations taken into account in the development of this load plan were the following:

(i) Identification of items that could be located on the ramps of the C-5A (stations 407-484 and 2007-2126). Possible choices for loading on the ramp are limited to items with a height of 76" or less. Twelve of the items on the list satisfied this constraint out of which two were chosen for loading on the front ramp (T429 and T433) and three were located on the back ramp (I128, I125 and I141). The rationale for choosing these particular five items is not clear although the fact that all are rolling stock items (compressors) would imply a material handling consideration.

(ii) The mainframe of the C-5A can be divided into two rectangles, each with the capacity to handle 16 items of standard pallet size (i.e., 88" long and 108" wide). Since all the remaining items satisfied the height constraint for the main frame (i.e., 96" or less) and weight was not really a factor in this move, the decision of where to locate the remaining items was based exclusively on handling considerations.

The main handling consideration is the difference that occurs between the loading of pallets versus the loading of rolling stock. Since rolling stock, by definition, has its own wheels, the floor is left flat and the items need only to be rolled on. The loading of pallets however (flat surface) requires preparing the floor with a rail system. In order to eliminate the inconvenience of loading and unloading that should occur if pallets and rolling were mixed arbitrarily (i.e., a section of the floor would be flat, another rail, etc.), the remaining 26 items were segregated into pallets and rolling stock. The right side of the aircraft (one rectangle) was then loaded completely with pallets (items I248 to I256). The rolling stock items (I113 to I228) were all

loaded on the left side, and the remaining three pallets (I259, I263 and I101) were located in the last three positions of the left side. This allowed for the following loading and unloading patterns:



i.e., Pallets & Rolling Stock could be loaded and unloaded simultaneously, thereby reducing the time the aircraft had to remain on the ground.

In synopsis, once the main restrictions were satisfied (height & weight constraints), attention was directed towards creating a load plan that would provide for ease of handling thereby speeding up the actual loading and unloading procedure. Considerations such as balancing the load on opposite sides of the aircraft, splitting the load into a 55-45 total weight distribution forward and aft of the center of gravity and individual floor stress factors were not critical in this deployment. In general, the C-5A is considered by the load planners at Moody to be the least critical aircraft with respect to weight which allowed them, in this case, to concentrate on other factors.

C: M/Sgt. Clark's Load Plan:

During the summer a series of meetings were held with M/Sgt. William Clark, a member of the Air Force Reserve Unit at Dantley Airfield in Montgomery, Alabama. M/Sgt. Clark is a load planner with over sixteen years experience. During the meeting he was provided with the Moody test data. In an attempt to gain additional insight into the load planning process, he was asked to develop load plans for the test data using both C-141A and C-130 aircraft.

One of the load plans developed by M/Sgt. Clark using C-141A aircraft is illustrated in Figure 6. The main characteristics of this aircraft that he considered relevant in the load planning process were:

- (i) The C-141A can be visualized as consisting of essentially 10 Cargo Pallet Positions.

531	621	711	801	891	981	1071	1161	1251	1352
I188 (1100)	I266 (3717)	I010 (4200)	I247 (4000)	I248 (5200)	I001 (4500)	I236 (4000)	I269 (3880)	T150 (3600)	T429 (880)

Total Weight: 35,077

I144 (2150)	I129 (2150)	I233 (3350)	I264 (3380)	I268 (3520)	I252 (3420)	I260 (3120)	I259 (2415)	I263 (2335)	T433 (2150)
----------------	----------------	----------------	----------------	----------------	----------------	----------------	----------------	----------------	----------------

Total Weight: 27,990

I109 (4290)	I113 (3650)	I149 (3900)	I101 (2150)	I141 (880)	I256 (2000)	I244 (2000)
I128 (880)	I228 (1120)	I145 (3900)	I125 (2150)	I141 (880)	I256 (2000)	I244 (2000)

Total Weight: 26,920

Figure 6
M/Sgt. Clark's Load Plan

C-141 A Cargo Pallet Positions

(ii) Position #10 is a ramp with a height limitation of 76". This same height limitation applies to position #1 (crew door).

(iii) Liquid oxygen or any other equipment requiring vents must be located in either position #1 or position #7 where venting equipment is available.

(iv) Hazardous material should be located either in position #1 or preferably in position #10 for possible jettisoning during flight if the need were ever to arise.

It is important to note that even though the MAC affiliation training manual for load planners has various other aircraft related restrictions, consideration of the above four along with general height and weight restrictions provided the basis for the load plan in Figure 6. The load plan itself was developed as follows:

(i) The equipment list was scanned and it was noted the individual weights of the equipment would not violate any of the weight restrictions of the individual cargo pallet positions. (i.e., pallet positions 1 through 9: Maximum weight 10,354 pounds; position #10: Maximum weight 7,500 pounds.) It was also quickly determined that total weight would not be a problem since the C-141A is capable of carrying up to 60,000 pounds.

(ii) Based on the total weight of the move (89,987 pounds), theoretically only two aircraft would be needed. However, the 31 pieces of equipment corresponded to more than 20 pallet positions, therefore requiring a total of three aircraft. (i.e., steps 9A and 9B of Figure 2).

(iii) Equipment with special characteristics were identified and assigned to either position #1 or position #10. A liquid oxygen cart (I188) was located in position #1 of the first aircraft (venting equipment) whereas a lightall (I144) and two compressors (T429 and T433) were assigned to position #1 of aircraft two and position #10 of aircrafts one and two respectively (i.e., height less than 76").

(iv) The remaining equipment on the list was segregated into pallets versus rolling stock. Aircraft one was completed with pallets where the heaviest pallets were located in the middle (I248, 5200 pounds in position 5 (station 891); I001, 4500 pounds in position 6 (station 981) and the assignments kept alternating in this same pattern in order of decreasing weight (known in load planning jargon as "pyramid loading"). Application of this technique becomes the load planners equivalent of approximating the "center of gravity" restriction without ever having to actually carry out the calculation.

(v) This same pattern is repeated in the second aircraft with the remaining pallets of standard size although a lightall (1129) was located in the second position. The two lightalls were apparently kept together for ease of handling.

(vi) After aircrafts one & two were loaded essentially with pallets, the remaining equipment (mostly rolling stock) was accommodated in aircraft three based upon the same idea of placing the heaviest total weight in the center and working outwards. The dimensions of the "rolling stock" as well as handling considerations were taken into account in accommodating the equipment on this aircraft.

The load plan for the C-130 followed the same steps outlined with the difference being that this aircraft has only six cargo pallet positions. A total of six C-130's were required to complete the move. Finally, it should be mentioned that it took M/Sgt Clark about 45 minutes to complete the load plan in Figure 6.

D: New Mexico Load Plans:

The New Mexico Air National Guard Aircraft Load Planning Model represents the first documented attempt within the Air Force to automate in some way the load planning process (refer to 7,8,10 for background information on the development of the program as well as a Users Guide developed by the AFLMC for those units that might be interested in trying out the model on an experimental basis). Use of the program is available at the AFLMC at Gunter through the ARPANET network. The Moody test data was fed into the program for both a C-5A deployment as well as for a move consisting of C-141A aircraft. The results obtained were the following:

(i) C-5A deployment:

Figure 7 illustrates the load plan obtained through the use of the program. The program does not output a schematic, but does provide coordinate locations of the loaded equipment allowing one to locate the equipment on a manifest form.

A comparison of this load plan with that developed by the Moody planners reveals first of all that the 31 pieces of equipment were all loaded, but crammed however towards the forward part of the aircraft. This is due to the underlying algorithm of the program which starts locating equipment in the lower left hand corner of the aircraft and continues loading from this point backwards.

Physical characteristics such as the left most stairwell are ignored (i.e., 1429 is partially loaded in the stairway) and two pieces of equipment (I113 and I248) overlap over a portion of the space. The program's determination in minimizing the use of space also allows items to be located in center aisle space (Ex: I248, I188, I44, I 228, I141). Of even greater importance is the fact that the main consideration of the Moody planners (ease of loading and unloading) never came into play and therefore pallets and rolling stock are interspersed throughout on both sides of the aircraft. Since the algorithm loads equipment in the order it is input, it would appear that the only way to achieve the rail system versus rolling stock effect so desired in the C-5A would be to prepare the list beforehand so that pallets and rolling stock would be alternated.

(ii) C-141A deployment:

Figure 8 illustrates one of eight load plans obtained by the New Mexico program when C-141A aircraft were specified. A comparison of this load plan with that developed by M/Sgt. Clark reveals first of all that even though the program was given three aircraft, it did not manage to load all of the equipment. (This was also true for the other seven plans generated by the program's switching routine). Since the program loads equipment in its input order, characteristics such as locating a liquid oxygen cart in position #1 will not be complied with unless the equipment list were scanned and prearranged prior to being input. (In this case, it was located on the ramp of aircraft one (I188) which is not feasible.)

The "pyramid effect" used by M/Sgt. Clark to alleviate center of gravity problems does not appear, nor will appear, unless the equipment list was pre-arranged to generate this effect. The segregation of pallets versus rolling stock does not occur, nor will occur, unless again the equipment list were pre-arranged. The objective of the program of pushing items forward could lead to center of gravity problems for aircraft that do not have a full load (like aircraft 3) or for cases where the equipment list is arbitrarily drawn up.

b: Summary:

This section has presented the results obtained when a "test case" set of data was submitted to experienced load planners for their use in the development of load plans. Although the number of details that have to be taken into account can vary greatly depending on the equipment and aircraft involved, in reality the load planners basically concentrate on satisfying a limited set of dominant characteristics and restrictions. This approach,

AD-A113 709

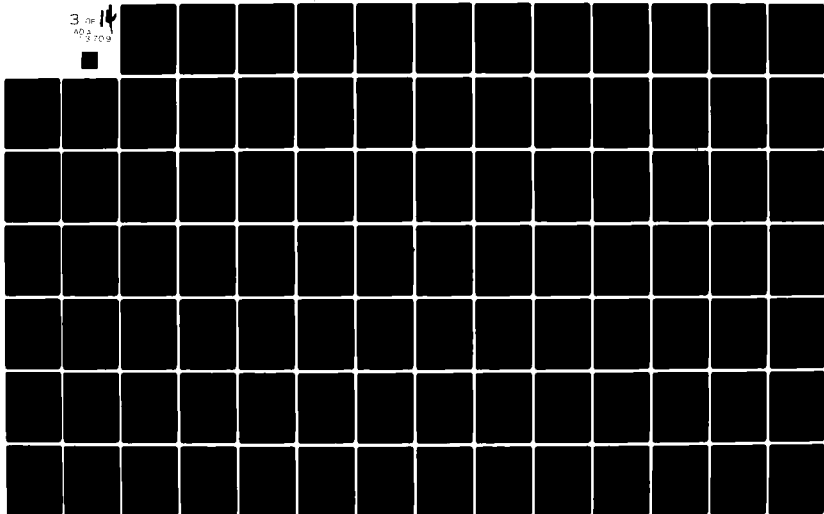
SOUTHEASTERN CENTER FOR ELECTRICAL ENGINEERING EDUCAT--ETC F/8 S/1
USAF SUMMER FACULTY RESEARCH PROGRAM. 1981 RESEARCH REPORTS, V0--ETC(U)
OCT 81 W D PEELE F49620-79-C-0038

UNCLASSIFIED

AFOSR-TR-82-0228

NL

3 of 4
AD-A113 709



arising, it appears more out of necessity than desire, has become the only rational way to deal manually with a problem that otherwise would be intractable if every detail in the MACS manuals and other sources were taken strictly into account. It will be these common elements which will serve as the basis for the load planning methodology described in the following section.

Finally, the test data also served as a means to compare one of the first automated approaches to load planning (the New Mexico program) with results generated by experienced load planners. Undoubtedly, the New Mexico program has its merits as a pioneering effort within the Air Force and has contributed in generating further interest in this kind of activity. However, based on comments provided by the load planners who had a chance to review the cases presented in this section as well as other runs of the program, the consensus was that in its present form, the program is of very limited practical value.

V A GENERAL AIRCRAFT LOAD PLANNING METHODOLOGY

Although it should be clear by now that the number of details that have to be taken into account in aircraft load planning will vary greatly depending on equipment and aircraft characteristics, it should be equally clear that any load planner or automated load planning procedure that strives to deal with all of these factors simultaneously will have followed a route paved with frustrations and ultimate failure. A common element in the approaches taken by the load planners that participated in this study involved viewing the process as a series of steps that concentrated on satisfying a small set of dominant characteristics and restrictions.

The load planning methodology outlined in this section is an attempt to lay a foundation for present and future attempts at partially automating this process based on those notions esteemed to be of greatest importance by the load planners themselves. The basis of the methodology is contained in Figures 9, 10 and 11 with Figures 11 through 14 illustrating the dominant considerations and restraints associated with the C-130, C-141A, C-141B and C-5A aircraft types respectively. The following is a summary of the information contained in the first three figures.

The first type of input to the load planning process is a list of the equipment to be moved along with its characteristics (height, weight, length, etc.) as well as symbols that identify hazardous equipment and/or equipment requiring aircraft venting equipment. The first objective of any automated procedure

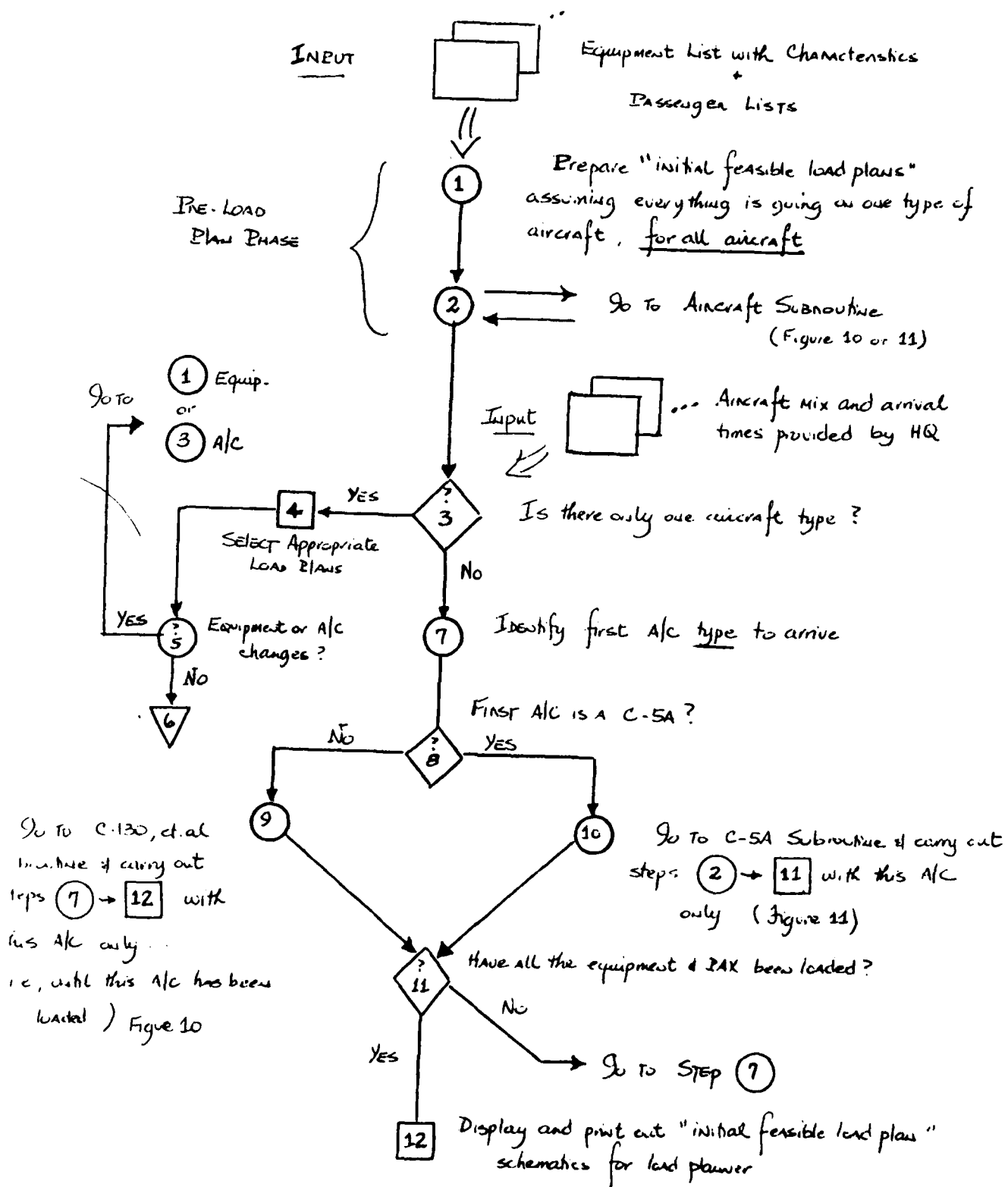


Figure 9
General Methodology
48-28

should be to assist in the Pre-Load Plan Phase by developing "initial feasible load plans" even before information is provided on the aircraft mix by Headquarters. (Figure 9 Step ①) One way to accomplish this is to assume that the complete deployment will be moved on one type of aircraft, generate "initial feasible load plans" for this type of aircraft and then repeat this step for the three remaining types of military aircraft used for deployments. (For example, say it is first assumed that the deployment will be carried out entirely on C-130's. Initial feasible load plans would be generated that would allocate all the equipment and passengers to C-130's only. This would then be repeated for C-141A's, C-141B's and C-5A's).

While this may appear at first glance to involve "unnecessary work", it should be emphasized that this part of the load planning process can be totally automated. Moreover, this same type of approach is taken by load planners when an aircraft mix has not been forthcoming despite the fact that they have to do it manually. Sub-routines would be developed for each aircraft type (actually only two sub-routines would be required due to the similarities between the loading procedure of C-130's and C-141A's and B's) such as those presented in Figures 10 and 11 which would terminate with a display and print out of schematics of the "initial feasible load plans". This output would not be final in any way since precisely one of the goals of any automated procedure should be to provide for interaction between the planner and the program. The generation of a graphical display and a printout of the schematic of the "initial load plans" is however critical in that it would allow for real-time enhancements or changes to the "initial load plans" by the planner with minimum effort. (This type of interaction is not possible with say the New Mexico program (10) nor the Army's AALPS package (3)).

The procedures presented in Figures 10 and 11 for generating the initial feasible load plans" incorporate these loading and aircraft characteristics that dominate the logic of the manual load planners that participated in this study. These characteristics have been discussed in Section IV and will not be repeated here except only to note that strategies such as:

- (i) Segregation of Pallets versus Rolling Stock
- (ii) "Pyramid Style" loading, or loading the heaviest pallet in the center position and working outwards
- (iii) Ease of loading and unloading on the C-5A and other manual "short cuts" used by the load planners play a crucial role in the development of the initial plans. The initial plans would be feasible in the sense that they satisfy the restraints found in Figures 12-15 for the aircraft types.

C-130; C-141A; C-141B; "Subroutine"

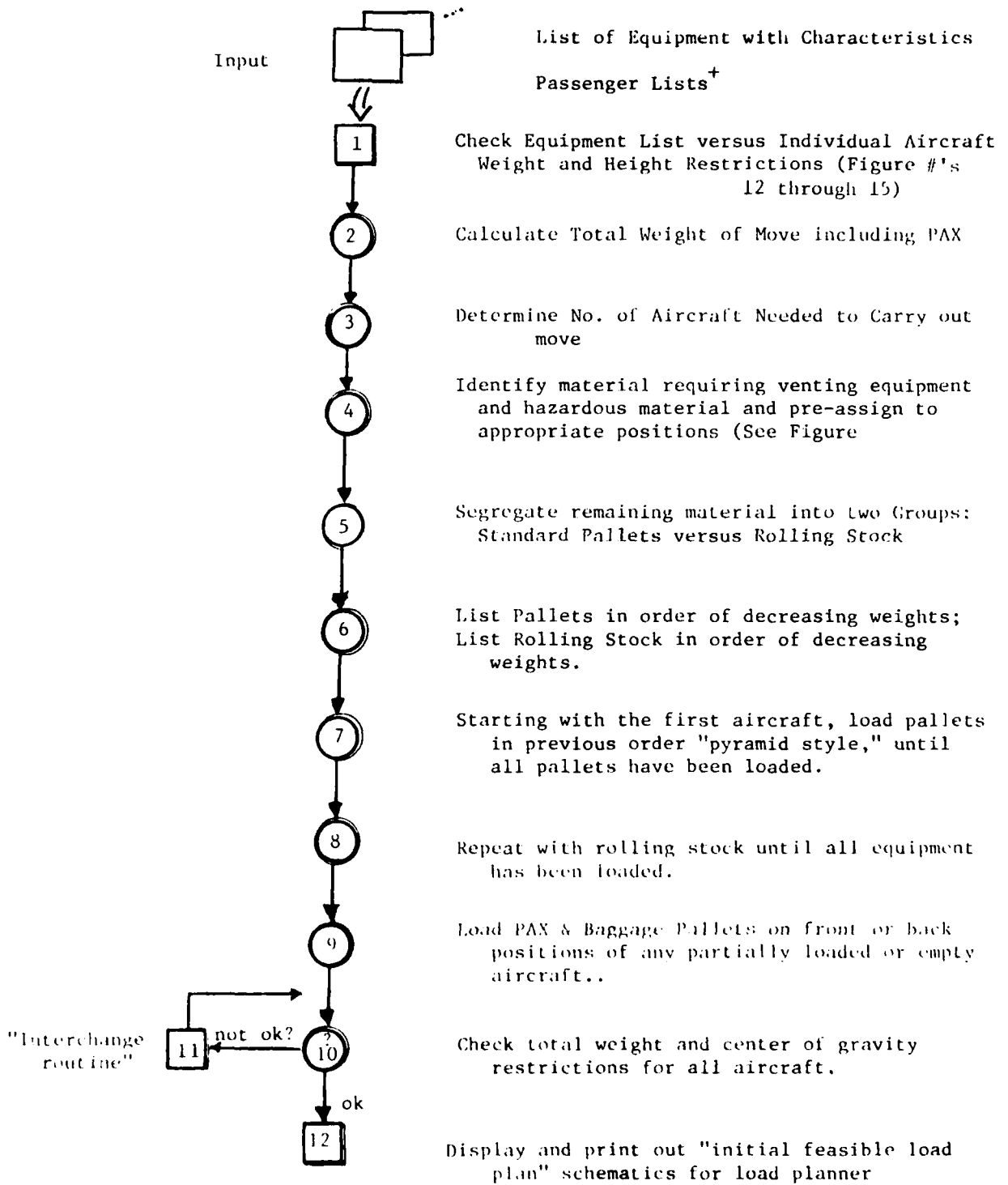
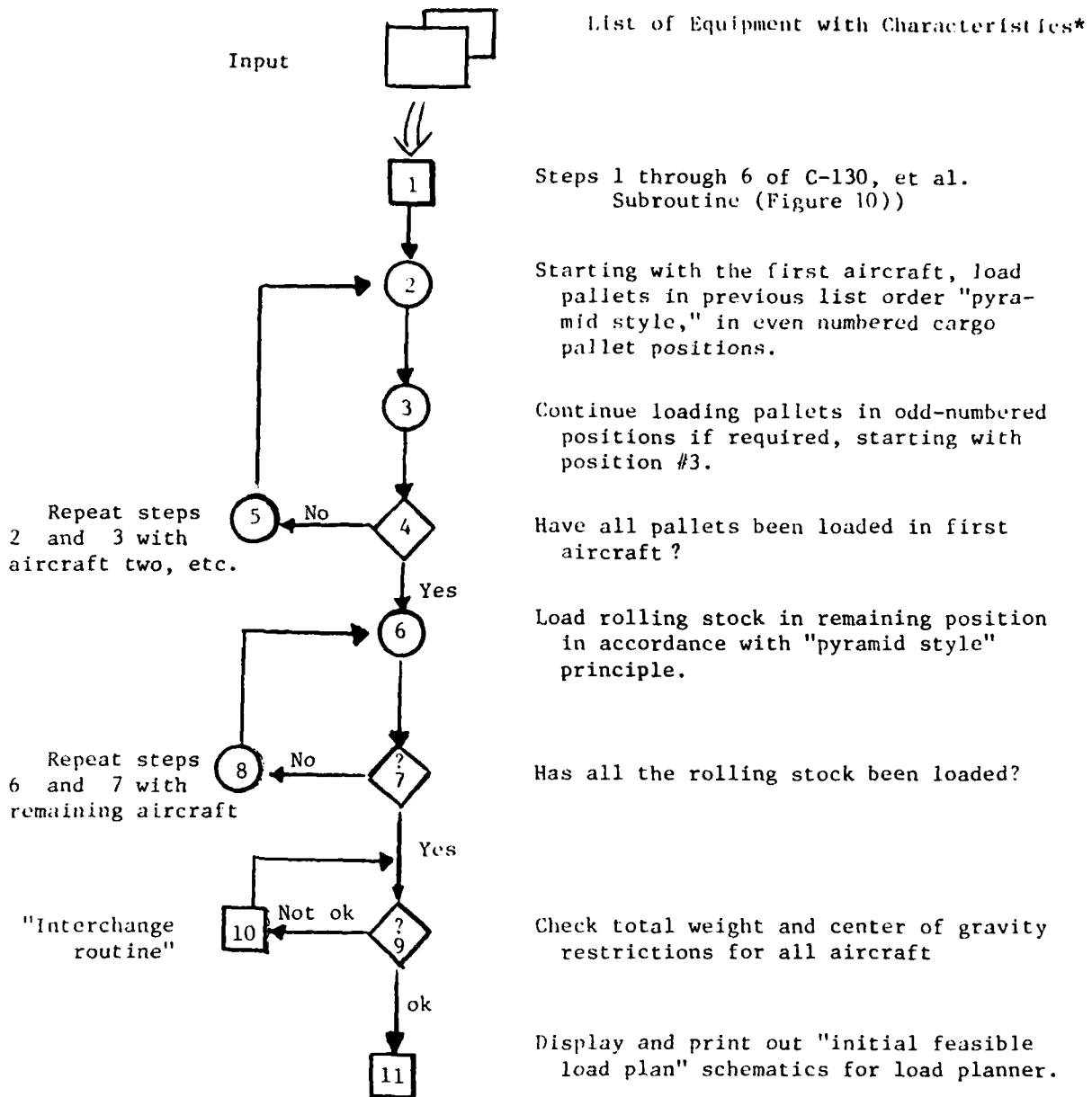


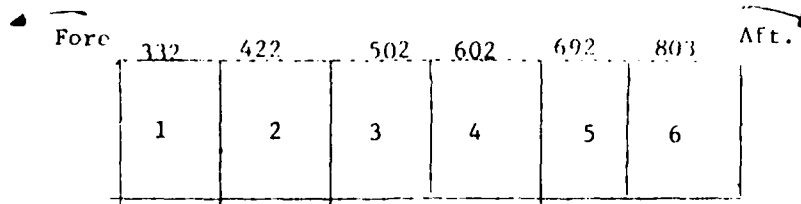
Figure 10

C-5A "Subroutine"



*Loading of Passengers can be done independently for C5A.

Figure 11
C-5A "Subroutine"



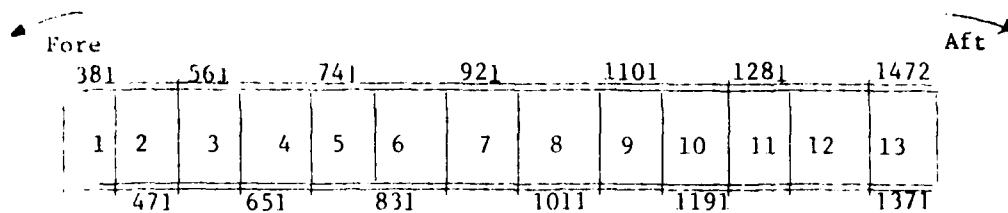
Basic Considerations and Restraints:

- 1) Consists of 6 cargo pallet positions
- 2) Weight Restrictions:
 - Maximum Total Weight (ACL): 25,000 pounds
 - Pallet Positions 1 through 4: Max Weight 10,354 pounds
 - Pallet Position 5: Max Weight 8,500 pounds
 - Pallet Position 6: Max Weight 4,664 pounds (Ramp)
- 3) Height Restrictions:
 - Maximum height of positions 1 through 5: 96 inches
 - Maximum height of position 6 : 76 inches
- 4) Other Considerations:
 - Hazardous material should be located in position #6
 - Material requiring venting equipment should be located in position #5
 - A six-inch aisle (walkway) must be provided on left hand side of pallets positioned in wheel well area (stations 577 to 597)
 - Unloaded center of gravity is at station 537. Load should be planned so that approximately 60% of the weight is forward of CG and 40% aft (i.e., aircraft is tail heavy).

Figure 12

C-130

48-33



Basic Considerations and Restraints:

- 1) Consists of 13 cargo pallet positions
- 2) Weight Restrictions:
 - Maximum Total Weight; (ACL): 72,900 pounds
 - Pallet positions 1 through 12: Max weight: 10,354 pounds
 - Pallet position 13 : Max weight: 7,500
- 3) Height Restrictions:
 - Positions 2 through 12: Max height: 96 inches
 - Positions 1 and 13 : Max height: 76 inches
- 4) Other Considerations:
 - Material requiring venting equipment should go in position 9.
 - Hazardous material should be located in positions 1 or 13.
 - Load should be planned so that approximately 40% of the weight is located forward of the unloaded center of gravity (Station position 877) and 60% is located aft of CG *

* This is the reverse of the C-141A & C-130.

Figure 14

C-141B (Stretch Model)

Fore ←

443	656	836	1016	1196	1376	1556	1736	1916									
2	4	6	8	10	12	14	16	18	20	22	24	26	28	30	32	34	36
1	3	5	7	9	11	13	15	17	19	21	23	25	27	29	31	33	35
566	746		926		1106		1286		1466		1646		1826		2065		

→ Aft

Basic Considerations and Restraints

- 1) Consists of 36 cargo pallet positions
- 2) Weight restrictions:
 - Maximum total weight (ACL) 205,000 pounds (Peacetime deployment Max ACL = 100,000 pounds)
 - Pallet positions 3 through 34: Max weight: 10,354 pounds
 - Pallet positions 1, 2 and 35, 36: Max weight: 7,500 pounds
- 3) Height restrictions:
 - Positions 3 through 34: Max height: 96 inches
 - Positions 1, 2 and 35, 36: Max height: 76 inches.
- 4) Handling Considerations:
 - When loading pallets, it is preferred that as many as possible be loaded on the RHS (even numbered positions) for ease of loading & unloading (K-loaders)
- 5) Other Considerations:
 - Material requiring venting equipment should go in positions 4 and 32
 - Hazardous material should be located in positions 35 or 36
 - Although it is the least critical aircraft with respect to weight, approximately 55% of the load should be located forward of the unloaded CC (station 1268) and 45% aft.
 - Pallet positions (ex: 1 and 2 or 13 and 14) should be "balanced" as well as possible.

Once Step (2) of Figure 9 has been completed and the "initial plans" have been approved and/or adjusted and approved by the load planner, it remains to wait and see what the actual aircraft mix will be. If the mix is not really a mix, but consists of only one type of aircraft then no further work would be required. If more than one type of aircraft is to be used, then a search of the existing "initial load plans" could lead to a feasible overall plan by taking subsets of the plans generated for each aircraft type. (Remember that schematics of these plans will have been printed out!) (Steps (3) through (6), Figure 9).

If not, then plans could be generated aircraft by aircraft in their order of arrival. This is accomplished by taking the first aircraft to arrive and assuming that the total move will be made solely on this aircraft. The appropriate aircraft sub-routine (either Figure 10 or Figure 11) is applied until this aircraft is completely loaded and its "initial load plan" is displayed and/or printed out. The equipment loaded on this aircraft is deleted from the input list and steps (7) through (12) are repeated with the next aircraft to arrive playing the role of the "first" aircraft. These steps are repeated until "initial feasible load plans" have been generated for all the aircraft to arrive, in their order of arrival.

Any changes or additional details related to peculiar equipment characteristics would, and should, be resolved through the interaction of the load planner and the program. The program would then play the role of an "auditor" in that it would check those changes made by the planner to the "initial load plans" to assure that they comply with feasibility restrictions. The decision on which plans to use would rest in the hands of the planner.

Finally, it must be mentioned that the methodology in this section, while general, does not pretend in any way to be all encompassing. On the contrary, it is presented as an example of the format that an effective computer-assisted load planning procedure could take since it would only pretend to automate those aspects of manual load planning that are "common denominators" without attempting to automate those details that are in fact more the exception rather than the rule. These must and should be left to the load planner, since the key to the success of any load planning methodology and resulting procedure will lie in the degree to which it strives to assist, rather than substitute, the load planner.

VI RECOMMENDATIONS

The purpose of this study was to assist the Logistics Planning Office of the AFLMC at Gunter, AFS in their efforts to describe and model the aircraft load planning process. The long range objectives of this effort by LGX is the development of automated or partially automated approaches to the aircraft load planning problem. The approach taken was of an applied nature in that information gathered through meetings with experienced load planners along with observations of actual deployments were used as the basis for the development of this report. Analysis and documentation of this information led to the identification of common characteristics within manual load planning procedures which were then used to develop the general methodology presented in the previous section. This methodology does not pretend to be an "all encompassing solution to load planning" but rather an example of the format that any effective computer assisted load planning procedure should take. Its basic strategy is one of using common elements of manual load planning procedures to satisfy a set of dominant aircraft characteristics thereby resulting in an automated process that develops initial feasible load plans. These initial plans would then be modified by the load planner in a real-time interactive mode to arrive at final load plan schematics.

One of the first efforts within the Air Force in applying computer technology to the aircraft load planning process is the work done by Hubner and Reid (7,8). The result of their effort was the development of a computer program written in Fortran for assisting load planners in their work. In this study a test data base was used to compare the effectiveness of Huebner and Reid's program versus manually generated load plans. While undoubtedly the New Mexico program has its merits as a pioneering effort within the Air Force, these comparisons revealed that in its present form, the program is of very limited practical value.

The important thing in this section is not so much to comment on the relative merits of the program but to note that when Huebner and Reid started their work, their stated objective was one of "optimally solving" (thereby potentially "totally automating") the aircraft load planning process. However, they soon realized that this approach was neither feasible (due mainly to the combinatorial complexity of the loading problem) nor practical. Their approach became one of developing a computer program that would assist load planners in the solution of their loading problems. In short, complete automation soon gave way to an interactive approach.

This reality was also perceived by two Danish researchers who developed an interactive computer system for the loading of cargo aircraft for Scandinavian Airlines (9). Given the standardization of containers and material handling equipment used by commercial airlines, the problem addressed by Larsen and Mikkelsen (9) is actually a simpler version of the problem faced by the Air Force. Yet even in this case, automation of the load planning process was not considered feasible, and an interactive system was employed.

The main argument for the use of an interactive approach for aircraft load planning is simply that it is the most effective way of combining the powers of the computer and the load planner. Anyone who has either observed or assisted in a load planning exercise can verify that the number of "little details" involved and "last minute changes" that occur cannot nor should not be left to a computer program to resolve. It is at this point in the load planning process where the practical experience of the load planner is irreplaceable. In an interactive system the load planner continues being the master at all stages, whereas the computer is the servant doing all the tedious work. While additional arguments may exist, it suffices at this point to recommend that the term "Computerized Load Planning" be scrapped and replaced by the notion of "Computer Assisted Interactive Load Planning".

Both the Huebner and Reid model (8) as well as the Danish model (9) demonstrate potential advantages of having a computer assist in the load planning process. Although various factors can be listed, the major advantages can be summarized as increased speed and accuracy of the load planning process including the rapid generation of alternate load plans for a given deployment. Both programs however, are written in Fortran, have large storage requirement and are resident at centralized locations. In the case of the New Mexico program, the results are stored in output files which must then be manually transcribed onto blank cargo manifest sheets in order to visualize or "see" the suggested load plan.

While it is possible that use can be made of an interactive model available on the ARPANET system, the argument here is that the culmination of any real-time base level Computer Assisted Interactive Load planning effort requires the addition of two more enhancements. These are:

- (i) The mobility associated with a small scale interactive system, and
- (ii) The visual interaction provided by a graphics capability.

It is felt that existing microcomputer technology can be used to incorporate these factors in what would eventually be a Mobile Computer Assisted Interactive Load Planning effort.

The potential use of microcomputer technology in load planning has already been illustrated during Operation Bright Star carried out by the New Mexico Air National Guard in Egypt during November, 1980 (8). During that exercise an Apple II with 48K, video monitor and disk drive was transported and used to assist in this deployment effort. Quoting from the report, "Even though the computer operated off of gas powered generators and in extremely sandy conditions, no hardware problems were encountered (thereby attesting to the durability of the equipment). A computer program was written in BASIC which graphically displayed the upper half of cargo manifests and was used to verify the validity of manually produced load plans".

As part of this summer's effort this researcher was able to confirm part of the results of Operation Bright Star by producing a small program on an Apple II system which duplicates the C-130 schematic that appears on aircraft cargo manifests. This program was written by Airman Chip Hyde of the Gunter Design Center on his in-house (dormitory) Apple system. Also during a meeting of the Gunter AFS Micro Computer Club on Thursday, July 8 the subject of using micro computers to assist in a load planning effort was discussed. The consensus of the members was that there should be very little difficulty in using microcomputers to assist the load planner in carrying out his current function. The question of developing a program that would in fact generate "good solutions" or "good initial load plans" on a microcomputer was felt to be a matter of greater complexity.

In synopsis, the use of microcomputer technology to assist the load planner in his function is a fertile area for future applied research. In light of the work being carried out on Interactive Computerized Load Planning at the AFLMC, a logical next step would be to explore the potential of using microcomputer technology to incorporate the features of mobility and visual interaction which are not provided by centrally located systems.

Finally, it should again be pointed out that research carried out on aircraft load planning has basically acknowledged but never actually explored the theoretical aspects of this problem. Given the size and multiple constraints associated with practical loading problems, it is highly unlikely that any "optimum" real-time solution to the problem will be found. Nonetheless a brief review of basic research related to the aircraft loading problem (1,2,4) allows one to state that an investigation into the particular structure of the aircraft loading problem has not been carried out. Basic research into special cases of the aircraft loading problem could yield insight into more clearly defining what the objective of the loading process should be as well as possibly

providing exact procedures for solving sub-problems that arise as part of the general load planning methodology presented in Section V (such as the C-130 sub-routine for example.) This theoretical effort would parallel and complement applied efforts in load planning as well as contributing to an expansion of knowledge in the general area of combinatorial scheduling.

References

1. Eilon, S. and Christofides, N., "The Loading Problem", Management Science, Vol. 17, No. 5, January, 1971, pp. 259-268.
2. Faaland, B. H., "The Multiperiod Knapsack Problem," Operations Research, Vol. 29, No. 3, May-June 1981., pp. 612-616.
3. Frankel, M. S., et.al., "Army Data Distribution System/Package," Quarterly Technical Report 2, July, 1980, Appendix A pp. 127-144, SRI International, Menlo Park, CA 94025.
4. Gilmore, P. C. and Gomory R. E., "The Theory and Computation of Knapsack Functions," Operations Research, Vol. 14, 1966, pp. 1045-1074.
5. Hodgson, T. J., "IPLS: Interactive Pallet Loading Systems", Research Report No. 81-9, ISE Department, University of Florida, Gainesville, Fl. 32611, June 1981.
6. _____, "On the Pallet Loading Problem", Research Report No. 81-11, ISE Department, University of Florida, Gainesville, Fl. 32611, August, 1981.
7. Huebner, W. F., Jr., and Reid, J. R., "Computerized Aircraft Loading" Paper presented at the Air National Guard A-7 conference, Des Moines, Iowa, November 13, 1978.
8. Huebner, W. F., Jr., "Strategic Airlift Computerized Loading", Paper presented at the Worldwide Logistics Planners Conference, Montgomery, Alabama, December 1, 1980.
9. Larsen, O., and Mikkelsen, G., "An Interactive System for the Loading of Cargo Aircraft", European Journal of Operational Research, April 1980, pp. 367-373.
10. Osborne, L., Jr., and Roncallo, C. A., "A Guide to the Use of the New Mexico Air National Guard Aircraft Load Planning Model", AFLMC Report No. 020711-2, July, 1981, Gunter A.F.S., Al. 36114.

1981 USAF - SCEEE SUMMER FACULTY RESEARCH PROGRAM

Sponsored by the
AIR FORCE OFFICE OF SCIENTIFIC RESEARCH

Conducted by the
SOUTHEASTERN CENTER FOR ELECTRICAL ENGINEERING EDUCATION

FINAL REPORT

A MODEL FOR CATH DATA AND SOME RESULTS ON THE ARBITRARY RIGHT
CENSORED DATA

Prepared by: Kishan G. Mehrotra

Academic Rank: Professor

Department and School of Computer and Information Science
University: Syracuse University

Research Location: Data Science Division, School of Aerospace
Medicine, Brooks Air Force Base, Texas

USAF Research
Colleague: Dr. Joel E. Michalek, Data Science Division

Date: August 31, 1981

Contract No: F49620 - 79 - C - 0038

A MODEL FOR CATH DATA AND SOME RESULTS ON THE
ARBITRARY RIGHT CENSORED DATA

by

Kishan G. Mehrotra

ABSTRACT

Two problems of interest in bio-statistics are considered in this paper. In the first part we discuss a model which can be used to predict the amount of blockage in arteries, given some important factors such as age, cholesterol and blood pressure. How well this model explains the data, collected at the School of Aerospace Medicine, Brooks AFB, Texas, is currently under investigation.

The problem of comparing two populations when the data is collected with arbitrary right censoring is also investigated. In past ten years several tests have been proposed to compare two populations under arbitrary right censoring schemes. First we prove that several, seemingly different, two sample tests are the same. Next, we perform a small sample study to compare the power and asymptotic level of significance of these tests.

Acknowledgement

The author would like to thank the Air Force Office of Scientific Research and the Southeastern Center for Electrical Engineering Education for providing him with the opportunity to spend a very worthwhile and interesting summer at the School of Aerospace Medicine, Brooks AFB, Texas. He would like to acknowledge Data Sciences division for its hospitality and excellent working conditions.

Finally, he would like to thank Drs. J. Michalek and D. Mihalko for their collaboration, and Dr. Richard Albanese for many helpful discussions.

OBJECTIVES OF THE RESEARCH EFFORT

The following objectives were discussed during the pre summer visit.

(i) Modelling of the Cath. data: This objective has been achieved to a reasonable degree of satisfaction.

(ii) Study and futher developments in the area of tests with arbitrary right censored data: This objective has also been achieved.

1. INTRODUCTION

Two problems of interest are studied in this report. In the first part we discuss a model to analyse data collected at the School of Aerospace Medicine on approximately seven hundred pilots. This data (called the cath. file) contains several measurements on each subject, such as their age, blood pressures, cholesterol high density lipid and of course a measure of amount of blockage of arteries in a small neighborhood of heart. It has been observed that one can arrive at a "reasonable" discriminant which will classify an individual as sick or non-sick, when an individual is defined as non-sick if score which measures the amount of blockage of arteries is less than two. The main objective of further research is to investigate a possibility of predicting the blockage score of a person given his cofactors such as age, cholesterol etc. A model with potential to handle this problem is studied in Section 2.1.

In Section 2.2 we describe the results of another investigation which arises in epidemiological studies. Prentice (1978) proposed a class of rank tests to compare two populations when the data is obtained in the context of arbitrary right censoring. Earlier Cox (1972) had also proposed a rank test for this problem which was later generalized by Morton (1979). It is shown that the rank tests of Prentice and Morton are the same. It is also proved that two alternative approaches to obtain exact, conditional variances of these rank test statistics give the same result. Finally, a small sample (empirical) study is performed to investigate which choice of variance produces best results.

2. RESULTS OF THE TWO STUDIES: In this section we describe our main results. First we consider a model for the cath. file and in Section 2.2 we describe results on the rank tests for equality of two populations.

2.1 A MODEL FOR THE CATH. FILE:

2.1.I The Background:

To analyse the data available in the Cath. file a first attempt was made by means of discriminant analysis. Persons in the Cath. file were divided into two groups. The first group consisted of persons who had a sum of some score less than 2. and the other group with a sum of some score greater or equal to 2. For simplicity of

presentation we would refer these two groups as non-sick and sick groups respectively. Logistic discrimination was applied to this data with two main covariates: age and cholesterol. The fit was good. Michalek (1980).

A problem of greater interest is prediction of the Cath. score given variables such as age, cholesterol, high density lipid etc. To get some preliminary information we first used the following approach. It was conjectured that the sum of sones random variable, S , is distributed as a poisson random variable whose intensity function $\lambda = \lambda(x)$ depends on the covariables x (age etc). That is

$$P(S = s | x) = [\exp - \lambda(x)] [\lambda(x)]^s / s! \quad s = 0, 1, \dots \quad (2.1)$$

However, an observation on the Cath. file immediately rules out the above model because the cell with $s=0$ has very - very large frequency, compared to other cells. It was decided to accomodate for this by way of considering the inflated poisson model. [See Johnson & Kolz (1969 page 205)]. In other words the following model was tried on the available data.

$$P[S=0 | x] = \alpha(x) + \{1 - \alpha(x)\} \exp(-\lambda(x))$$

$$P[S=s | x] = \{1 - \alpha(x)\} \exp(-\lambda(x)) (\lambda(x))^s / s!, \quad s = 1, 2, \dots$$

where $0 < \alpha(x) < 1$, $\lambda(x) > 0$ and $\alpha(x)$ is given by (2.2)

$$\alpha(x) = 1 - \{ (1 - \exp(-\lambda(x))) (1 + \lambda(x)) \}^{-1}$$

With $\alpha(x)$ given by (2.2), this model did not provide a very good fit.

A major objection is the lack of explanation of additional probability in the first cell. Lack of a good fit of (2.2) can be seen due to the choice of $\alpha(x)$ which depends on $\lambda(x)$ and thus lacks freedom of choice of a parameter.

We study these issues in the next section.

2.1.2. A MODEL FOR THE CATH DATA

To accomodate for some additional freedom in the choice of we consider $\alpha(x) = \{1 + \exp(\gamma'x)\}^{-1}$ and $\lambda(x)$ as before.

The reason for inflated poisson can be argued as follows. It is hypothesized that a blockage of arteries starts as follows. First a random event occurs which triggers the system so that the blockage

begins to grow.* This triggering occurs with probability,

$$P[\text{Trigger} = \text{Yes}] = 1 - \alpha(x) \quad , \quad 0 < \alpha(x) < 1$$

Given that the triggering mechanism has started

$$P[S = \delta | \text{Trigger} = \text{Yes}, x] = \frac{\exp(-\lambda(x)) \lambda(x)^\delta}{\delta!}, \delta = 0, 1, \dots$$

Thus, we naturally obtain an inflated poisson distribution for S. However, the Poisson distribution of S, given that the trigger has already started, still remains to be justified. In the remaining part of this section, we investigate this question. We conclude that the distribution of S is rather complicated and should not be approximated by the poisson distribution.

To obtain the sum of sonos a neighborhood of heart is divided in subsections. In each subsection blockage of arteries is measured and depending upon the percentage of blockage, a score is obtained, generally between zero and 5 (both inclusive). The sum of all these scores is what is known as sum of sonos.

As above, suppose the neighborhood of heart is divided in subsections. In the i th subsection we may have more than one place where blockage of arteries is obtained. We claim that this random variable Y_i the number of places where the blockage is starting to buildup, should behave like a poisson random variable with parameter $\lambda_i = \lambda_i(x)$. we justify this claim as follows.

Let us assume that each subsection is further subdivided in smaller regions called cells. Then two possible outcomes can be observed. Either in the cell the blockage has already triggered or not. Probability of a trigger in a cell, given by $\theta(x)$, is assumed to be very small. Thus, using the property that sum of Bernoulli random variables converges to a Poisson random variable, if the probability of success (trigger) is very small, we conclude that Y_i should behave like a poisson random variable with $\lambda_i(x) \propto \text{area}^\dagger$ of the subsection $\theta(x)$. Finally, if all subsections in the neighborhood are equal in size, then $\sum Y_i =$ total number of blockages should behave like a poisson random variable. Unfortunately, we do not have a record of

*Concept of triggering mechanism was first used by Dr. Charles Davis, visiting professor from the University of Toledo, Ohio. Some other discussions with him were also extremely useful.

†Area of a subsection is not necessarily the Euclidean area.

number of blockages. But due to this reason, it appears that distribution of sum of sones will not be a poisson random variable as used in our previous analysis.

Next, we wish to consider the distribution of blockage at a given point. It is assumed that triggering mechanism has already started. However, the trigger occurs at a random time T_0 in the individual's life and satisfies the distribution function $F_0(t)$. If the current age of this individual is A and the trigger occurred at age T_0 , then the amount of blockage will be proportional to $(A - T_0)$ and will also depend upon other variables i.e. cholesterol, smoking etc. We make a simple assumption that once the trigger has started, the blockage process builds up in a deterministic manner given by

$$\text{Blockage (Proportion)} = B = (\beta_0 + \beta^* x^*) (A - T_0) \quad (2.4)$$

where x^* is the collection of all other variables except age.

Thus one can obtain the distribution of B in terms of the distribution of T_0 . It remains to find a reasonable distribution for T_0 .

In actual practice, if there are γ_i (≥ 2) regions where blockage is observed then the sone score is obtained from the maximum blockage. It remains to find the distribution of maximum blockage in a subregion. In terms of our earlier development, the second problem can be handled as follows. Suppose γ_i is fixed.

Suppose $T_{01}, \dots, T_{0\gamma_i}$ denote the triggering time random variables. Let $T_i^* = \min_{0 \leq j \leq \gamma_i} (T_{0j})$. Then the maximum blockage corresponds to T_i^* . consequently, if we know the d.f. of T_i^* , using (2.4) we can find the d.f. of maximum blockage. On the other hand, if we only capture the essence of above discussion and ignore the details, it would appear that a reasonable distribution for percent blockage could be given by some extreme value distribution, whose parameters depend upon predictive variables x in some appropriate manner.

We further justify the above argument from slightly different argument.

Another model for Blockage random Variable.

Once again assume that a given subsection is divided in small cells. Assume that there is no triggering mechanism. Instead all small cells have a built-in potential for blockage and this blockage exists at each cell. However, we are only interested in the maxi-

imum blockage. Irrespective of the distribution of the blockage random variable, the distribution of maximum blockage must be an extreme value random variable.

2.1.3. ANALYSIS.

For simplicity we assume that the distribution of T_0 is given by the exponential random variable with density $\lambda^{-1} \exp(-t/\lambda)$ where the scale parameter is unknown. Assuming this, the distribution of

$\min_{1 \leq j \leq n} (T_{0j})$ is also exponential with parameter λ/γ . consequently using (2.4) we can find distribution of B.

Analysis of Cath analysis with the above assumptions will be investigated soon.

2.2 A COMPARATIVE STUDY OF SOME LINEAR RANK
TESTS FOR THE TWO-SAMPLE PROBLEM SUBJECT
TO RIGHT CENSORING*

2.2.1 Background: Gehan (1965) considered the problem of testing equality of two populations when the samples were obtained under arbitrary right censoring and proposed a generalization of the Wilcoxon rank test. Mantel (1966) also considered this problem and proposed a rank test which is popularly known as the Mantel-Haenszel or the log rank test. It can be seen that this is a generalization of the Savage score test. Since then several other rank tests have been proposed to test the equality of two populations. For example the two-sample specializations of Cox (1972), Peto and Peto (1972) and Prentice (1978). Some modifications of the Cox (1972) test have appeared recently; for example see Tarone and Ware (1977), Morton (1978).

In this paper, we study small sample properties of these rank tests when the two-samples are arbitrarily right censored. Only other simulation study of this nature, known to us, is by Lininger et al (1970) in which they have compared small sample power of the Mantel-Haenszel tests, with and without continuity correction, the Gehan test and a test of Cox based on scores.

In the first part of this paper we briefly review some rank tests. We present a general result which relates Prentice (1978) class of rank tests to Morton's generalization of the Cox statistic. We also demonstrate that although the two tests appear to be the same, they in fact are not identical. We also relate Prentice scores (defined in Section 2) to the "usual" score function (see Hajek and Sidak (1967)). Next three possible choices of variances are briefly reviewed.

In section 2.2.3, we present results of our simulation study.

2.2.2 Two classes of Rank tests and their interrelationship.

Let m and n denote the sizes of group 1 and 2 respectively and $N = m+n$. The combined sample of size N is subject to arbitrary right

*This research was jointly performed with Dr. Michalek, Brooks AFB, Texas and Dr. Mihalko, University of Nebraska, Lincoln, NE.

On the other hand Cox (1972), using the partial likelihood approach, obtained a test statistic which for the above two-sample problem reject the null hypothesis if $T_N > \text{constant}$, where

$$T_N = \sum_{j=1}^k \left(Z_{(j)} - \frac{r_{2j}}{r_j} \right) . \quad (2.2.3)$$

It is obvious that T_N depends only on the Z 's at actual failure times and their conditional expectations. The components $(Z_j - r_{2j}/r_j)$ are intuitively very appealing. These observations raise two questions: (i) Is it possible to write S_N in terms of $(Z_j - r_{2j}/r_j)$'s $j = 1, 2, \dots, k$? (ii) How do we choose weights w_j 's to improve T_N to T_N^* where

$$T_N^* = \sum_{j=1}^k \left(Z_{(j)} - \frac{r_{2j}}{r_j} \right) w_j \quad (2.2.4)$$

Prentice and Marek (1979) investigated the first question and proved that if scores c_i and C_i , given by (2.2.2) satisfy

$$(r_i - 1) C_i = r_i C_{i-1} - c_i \quad (2.2.5)$$

for $i=1, \dots, k$, then S_N can be written as T_N^* with $w_i = c_i - C_i$. They observed that (5) is satisfied for three scores in particular. We have proved that for c_i and C_i given by (2.2.2) equation (2.2.5) is always satisfied. Consequently, all statistics given by (2.2.1) have alternative representation in terms of T_N^* . From this it also follows that if the underlying error density is f , then the appropriate weights are given by

$$w_i = c_i - C_i . \quad (2.2.6)$$

conversely, we have shown that any T_N^* can be written as an S_N . To distinguish w_i 's from the Mortons weights described below. The weights given by (2.2.6) will be called the Prentice weights. To find appropriate weights in T_N^* Morton (1978) obtained the following result. Suppose that the most

appropriate nonparametric test would have given scores $a(j)$ to uncensored data. Then for the censoring situation, they be modified as

$$w_j^* = \begin{cases} a(j) + \frac{1}{R_{j+1}} \sum_{i \leq j} a(i) & \text{if a failure occurs at} \\ & \text{ordered observation,} \\ 0 & \text{if a censoring occurs,} \end{cases} \quad (2.2.7)$$

where R_j is number of persons at risk at the j th ordered observation.

It is natural to ask: Is it true that for the same error density f w_j and w_j^* are equivalent? By means of an example, we demonstrate that, in general, they are different.

Consider the logistic error density. In Kalbfleisch and Prentice (1980, page 147) it is shown that $C_i = 1 - 2 \prod_{j=1}^i r_j / (r_j + 1)$, $C_i = 1 - \prod_{j=1}^i r_j / (r_j + 1)$ consequently the Prentice weight is given by $w_i = - \prod_{j=1}^i r_j / (r_j + 1)$.

On the other hand, for this situation the $a(j)$'s are given by $\{2j / (N+1) - 1\}$ and therefore, since $R_j = N - j + 1$, $w_j^* = - (N+1-j)(N+1)^{-1}$

if a death occurs and 0 otherwise. In other words $w_j^* = - r_j / (N+1)$.

Thus, Morton's approach leads to the Grehan's Statistic and moreover the weights are different.

Remark 1: Observe that if the error distribution is logistic, then Prentice weight is given by the Kaplan-Meier estimator of the survival of function whereas the Morton's weight is the usual estimator of the survival function.

Remark 2: In the uncensored case whether we use scores $\hat{a}(j) = j$ or $a(j) = 2j / (N+1)$ we get the equivalent result. However, in general it appears that one should not use equivalent scores in (2.2.7). For example, if we use scores j in (2.2.7) we get $w_j^* = j(2N-j-1) / 2(N-j)$ which is obviously different than the weight obtained above.

2.2.3. Variances of test statistics: In the previous section we observed that the Prentice statistic can be written as weighted sum of $(U_j - r_{2j} / r_j)$ and conversely, any T_n^* can be written as S_n . From this observation it immediately follows that $E(S_n) = 0$.

In the following we use this observation to obtain four possible variances of S_n and three choices for the variance of T_N^* .

Variance (1): First choice of variance of S_n is obtained by the permutation argument, see Prentice (1978). In case of the two-sample problem under consideration, the variance is

$$\text{Var}^{(1)}(S_N) = \frac{r_{11} r_{12}}{r_1^2 (r_1 - 1)} \sum_{i=1}^k (C_i^2 + m_i C_i^2)$$

and is valid if the censoring is independent of group membership. Since every T_N^* can be written as S_N with appropriately defined C_i and C_i 's this variance applies to any T_N^* .

Variance (2): The variance is obtained using the Bernoulli distribution of Z_j and the fact that conditional covariance of Z_j and $Z_{j'}$ for $j \neq j'$ is zero, see Cox (1975). Thus, we obtain

$$\text{Var}^{(2)}(S_N) = \sum_{i=1}^k \omega_i^2 \frac{r_{11} r_{12}}{r_1^2}.$$

Note that in this case we have obtained a conditional variance given $\{k; r_{ij}, i=1, \dots, k, j=1, 2\}$

Variance (3): Morton (1978) has pointed out that if we replace $r_{11} r_{12} / [r_1 (r_1 - 1)]$ by its conditional expectation $r_{11} r_{12} / \{r_1 (r_1 - 1)\}$ we obtain a less conservative statistic. He makes this argument in the case when all ω_i 's are 1 (i.e. logrank test) and takes the conditional expectation given $\{r_i, i=1, \dots, k\}$. Using this argument, in general, we obtain

$$\text{Var}^{(3)}(S_N) = \{r_1 (r_1 - 1)\}^{-1} r_{11} r_{12} \sum_{i=1}^k \omega_i^2 (r_i - 1) r_i^{-1}.$$

We remark that this is also a conditional variance however conditioned on $\{r_{11}, r_{12}; r_i, i=1, \dots, k\}$ only.

Variance (4): This variance is obtained for Prentice Statistics only and is given by equation (6.20) of Kalbfleisch and Prentice (1980). $\text{Var}^{(4)}(S_N)$ is the "observed" Fisher information matrix based on the marginal likelihood. In general, this variance of T_N^* is not available. For instance, we do not know the density which generates the Gehan

weights, and therefore it is not possible to obtain this variance for the Gehan statistic.

However, we have also proved that the Variance (1) and Variance (3) are identical. Thus, in fact, there are only three possible choices of variances for S_N and two for T_N .

2.3 Relation between Prentice Score and scores obtained in the uncensored situation:

The Prentice (1978) scores given by (2) are given in terms of multiple integral. For logistic and exponential error model these scores are exactly known. We have shown that both of these can be written in terms of linear combinations of $a_N(j)$'s where

$$a_N(j) = \frac{n!}{(j-1)!(N-j)!} \int_0^1 \phi(u) u^{j-1} (1-u)^{N-j} du$$

is the ordinary score in the complete sample situation, see Hajek and Sidak (1967, page 64). Since $a_N(j)$'s are tabulated for some distributions, it is, therefore, possible to consider tests other than extensions of Wilcoxon and Savage score test.

All mathematical details of this section will be available soon in Technical Reports.

2.2.3 Small Sample Study and the Results:

We have studied Mortan's and Prentice's extension of the Wilcoxon statistic. Two possible variances corresponding to the Mortan statistic and three choices of the variance of the Prentice statistic give us five different statistics. These five statistics are compared when the underlying error distribution is logistic. These statistics are calculated one thousand times for samples of sizes 10, 20, 30 and 50 and with various proportion of censoring. They are compared in terms of their level of significance as well as powers.

Similarly Mortan and Prentice's extension of the Savage statistics are also compared. However, since the T_n and S_n are identical in this case, we compare only the test statistic which differ in terms of their variances.

Further details will be available in a Technical report.

REFERENCES

- Cox, D.R. (1972): Regression Models and life tables (with discussion)
J.R. Statist. Soc. B, 34, 187-220
- COX, D.R. (1975): Partial Likelihood. Biometrika, 62, 269-276
- Gehan, E.A. (1965): A generalized Wilcoxon test for comparing
arbitrarily singly - censored samples. Biometrika,
52, 203-223.
- Hajek, J. and Sidak, Z., (1967): Theory of Rank Tests, New York
Academic Press
- Kalbfleisch, J.D. and Prentice, R.L. (1980): The statistical
Analysis of Failure Time Data, New York, Wiley.
- Lininger, L., Gail, M.H., Green, S.B. and Byar, D.P. (1979):
Comparison of four tests for equality of survival courses
in the presence of stratification and censoring.
Biometrika, 66, 419-428.
- Mantel, N. (1966) Evaluation of survival data and two new rank order
statistics arising in its consideration.
Cancer Chemother. Rep, 50, 163-170.
- Michalck, Joel E. (1980): Personal communication.
- Morton, R. (1978): Regression analysis of life tables and related
nonparametric tests. Biometrika 65, 329-333.
- Peto, R. and Peto, J. (1972): Asymptotically efficient rank in
variant test procedures (with discussion) J.R. Statist.
Soc. A. 135, 182-206.
- Prentice, R.L. (1978): Linear rank tests with right censored data.
Biometrika, 65, 267-179.
- Prentice, R.L. and Marek, P. (1979). A qualitative discrepancy be-
tween censored data rank tests. Biometrics 35,
- Tarone, R.E. and Ware, James (1977): On distribution free tests
for equality of survival distribution. Biometrika 64,
156-160.

1981 USAF - SCEEE SUMMER FACULTY RESEARCH PROGRAM

Sponsored by the
AIR FORCE OFFICE OF SCIENTIFIC RESEARCH

Conducted by the
SOUTHEASTERN CENTER FOR ELECTRICAL ENGINEERING EDUCATION

FINAL REPORT

A DIRECT STATE SPACE APPROACH TO
THE CONTROL OF SAMPLED-DATA SYSTEMS

Prepared by: David F. Miller
Academic Rank: Assistant Professor
Department and University: Department of Mathematics and Statistics
Wright State University
Research Location: Air Force Wright Aeronautical Laboratories
Flight Dynamics Lab
Flight Control Division
USAF Research Colleague: David K. Bowser
Date: September 11, 1981
Contract: F49620-79-C-0038

A DIRECT STATE SPACE APPROACH TO
THE CONTROL OF SAMPLED-DATA SYSTEMS

by

David F. Miller

ABSTRACT

Simple and direct algorithms for the control of multivariable sampled-data systems are presented. Both the digital redesign and the direct digital design problems are considered. A "period optimal" digital control problem is formulated, and a general solution methodology is discussed. Emphasis is placed upon developing adaptive control design methods which are uncomplicated, responsive, and which avoid the computational complexities of many conventional state space techniques. Complete algorithmic solutions of the output matching and signal tracking problems for linear systems are given. In both cases, the solutions reduce to solving systems of linear equations. A unique feature of this work is the effective incorporation of conventional data holds into the digital controller for the purposes of smoothing and predicting sampled signals. A simple numerical example illustrates the effectiveness of the output matching algorithm.

ACKNOWLEDGEMENTS

The author would like to gratefully thank the Air Force Systems Command, Air Force Office of Scientific Research, for providing this exceptional research opportunity. Thanks also to the Air Force Wright Aeronautical Laboratories' Flight Dynamics Laboratory for its sincere interest in the SFRP program and for providing a stimulating and exciting research environment. Special thanks to David K. Bowser for his conscientious coordination of this research effort, making sure that the author felt welcome and was introduced to all available pertinent technical information. Thanks to Dr. Siva Banda and the entire Control Dynamics Branch, especially the Control Analysis Group, for the many helpful technical discussions and the warm hospitality. Thanks to Ronald O. Anderson and Vernon O. Hoehne for providing work space within their offices and for the comfortable and friendly working atmosphere. Special thanks also to Dr. William Wells for his introduction to the Control Analysis Group and to Dr. Edgar Rutter for his personal recommendation. Without their help, this valuable research experience would not have been made available. Finally, the author would very much like to express his appreciation to Ms. Linda Clere for her careful and professional typing of this report.

1. INTRODUCTION:

Recent advances in microcomputer technology have generated renewed interest in the design and implementation of sampled-data control systems, a subject area with an already mature and well-developed theory. ^{1,2,3,4} The Air Force ⁵ is actively investigating the feasibility of introducing digital flight control systems into its aircraft. The compactness, flexibility, reliability, and accuracy of microprocessors make them ideally suited for the responsive guidance and control requirements of the demanding high-speed flight environments of aircraft, missiles, and space vehicles. Since the motions of these and many other mechanical devices are, by nature, continuous, this study focuses upon the efficient utilization of digital (sampled) data to control dynamical systems (plants) that unfold smoothly in real-time.

In what follows, a digital controller (abbreviated DC) will be, very simply, a unit of computer software (subroutine, subprogram, etc.). It will generate, as is indicated in Figure 1, the (at least) peicewise continuous control signal $u^d(t)$, which will serve

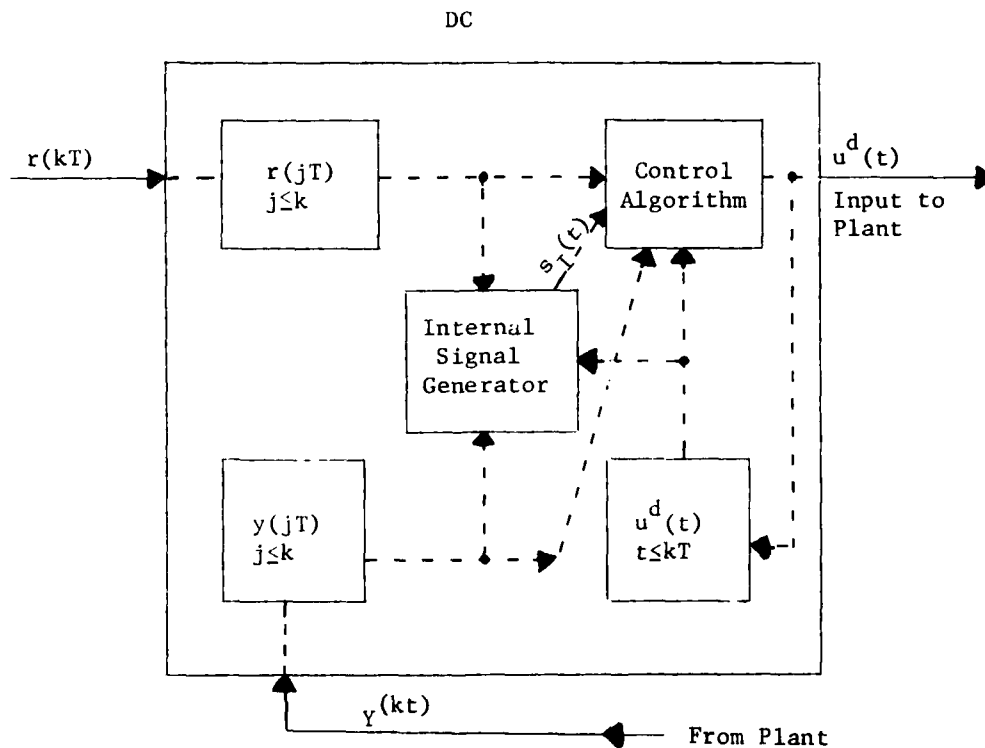


FIGURE 1. THE DIGITAL CONTROLLER DC

to drive a continuous plant. To generate $u^d(t)$ on the sampling interval $[kT, (k+1)T)$, DC processes received and stored samples $r(jT)$ and $y(jT)$, $j \leq k$, of input vectors $r(t)$ and plant output vectors $y(t)$. It may also use stored control action data for $t \leq kT$, and possibly other internally generated signals $s_1(t)$. (In practice, of course, only the most recent relevant information is retained, not all data.) The conventional z-domain (transfer function) controller $D(z)$, a ratio of polynomials in negative powers of z , defines a simple linear relation between input error samples $e(kT)$ and output pulses $u(kT)$. The digital controller DC by contrast, is essentially a non-linear control algorithm which constructs an entire control signal $u^d(t)$ of a pre-specified form. An important feature of the DC is that it is able to take better advantage of data samples by using relevant system models and the computational capabilities of the digital computer to smoothly predict the input and output signals $r(t)$ and $y(t)$ between sampling instants $t = kT$. This is accomplished by effectively implementing data holds (zero-order, higher-order, slewer, etc.) internally. Furthermore, other relevant signals $s_1(t)$ may be generated on-line. As an added unique feature, the controller output data hold may be effectively integrated into the control algorithm. Hence, full advantage of the character of this hold may be taken in the design process.

Digital redesign (emulation)^{6,7,8,9}, and direct digital design^{10,11,12,13} represent the two basic digital system design philosophies. In the former, an analog control system is designed using conventional s-plane techniques. One or more continuous elements (controllers) is then replaced with a digital element (preceeded and followed by sample and hold devices). The objective is to preserve as closely as possible, in the resulting digital system, the performance characteristics of the original continuous system. By contrast, direct digital designs are effected by designing the digital elements directly using z , w , or w' -plane techniques or other methods. The general approach discussed here is applied to both types of digital design problems. It is most closely related in flavor to the Model Algorithmic Control of Mehra, et al.^{10,11}, and

the Model Reference Adaptive techniques surveyed by Landau¹⁴. It employs, however, a general state space representation of the plant dynamics rather than Mehra's impulse response characterization.

In the sections which follow, it is shown that if the analog controller of a linear, multivariable, continuous feedback control system is replaced by an appropriately designed DC, then the outputs of the resulting digital system and the original continuous system can be matched exactly at all sampling instants. A simple numerical example illustrates the real-time applicability of this redesign technique. Importantly, the control algorithm defining DC is centered around, very simply, the solution of a system of linear equations. Furthermore, it is completely independent, in form, of the system input $r(t)$. This result significantly generalizes that of Kuo, et al.⁶, which is limited to state matching by the adjustment of forward and feedback gain matrices. It also generalizes Yeh and Yeh⁹, where it is proved that a conventional digital controller $D(z)$ can be designed that provides exact output matching, but only for that input with respect to which it is originally designed. It is shown further that a very general linear, multivariable digital control problem can be easily solved, one which includes for example Mehra's objective of tracking a desired reference trajectory. The solution once again depends simply on the solution of linear equations, an easy task for a high-speed digital computer. Time consuming numerical non-linear optimization problems and difficult Riccati equation solutions are thus completely avoided (a major objective of this study). Control algorithms are structured as straightforward algebraic manipulations of sampled data and pre-computed relevant system constants.

11. OBJECTIVES

The main objective of this project was to investigate state space design techniques for multivariable sample-data feedback control systems. Emphasis has been placed upon simple and direct control algorithms which are responsive and able to accommodate rapid sampling if system performance demands, while remaining free of excessive computational requirements. A simple numerical example is presented, leaving more extensive methods evaluation for later work. The specific objectives were:

- (1) To formulate an implementation oriented optimal digital control problem and suggest a general methodology for approaching its solution.
- (2) To develop direct adaptive control algorithms for linear systems which avoid the computational complexities that characterize many modern state space techniques.
- (3) To investigate the feasibility of incorporating data holds and signal predictors into the internal algorithmic structure of the digital controller, for added flexibility and improved system performance.
- (4) To provide data from a numerical example to support the validity of predictions of the theory developed.

III. THE OPTIMAL DIGITAL CONTROL PROBLEM

Many state space multivariable control problems assume the form (see Ref. 15) of the following optimal control problem (OCP):

$$\begin{aligned} \text{Min}_{u \in C} J(u) &= \int_0^{t_f} L(t, y(t), u(t)) dt + \sum_{k=1}^{t_f/T} \Phi(kT, y(kT), u(kT)) + \\ &+ \Psi(t_f, y(t_f), u(t_f)) \\ \text{(OCP)} \quad \dot{x}(t) &= f(t, x(t), u(t)), x(0) = x_0 \\ y(t) &= g(x(t)) \end{aligned} \tag{1}$$

where

u is a control function with values $u(t)$ in a control set $U \subset R^m$; C is a collection of controls u ; x , with values $x(t) \in R^n$ is the state trajectory corresponding to u ; y , with values $y(t) \in R^p$ is the vector of observable system outputs; $t_f > 0$ (possibly ∞), the final time has t_f/T an integer whenever $t_f < \infty$ for constant $T > 0$; and L, Φ , and Ψ are system performance measuring functions.

In words, (OCP) seeks, among all controls $u \in C$, one which drives x so as to minimize the performance criterion $J(u)$.

Let C^d be the class of controls u^d with values of a pre-specified form $u_k^d(t; \alpha_k^1, \alpha_k^2, \dots, \alpha_k^\ell)$ which is independent of k . That is, u^d is determined on $[kT, (k+1)T)$ by specifying particular values of the vector control variables $\alpha_k^1, \alpha_k^2, \dots, \alpha_k^\ell$ in the function $u_k^d(t; \alpha_k^1, \alpha_k^2, \dots, \alpha_k^\ell)$. Since u^d is determined by a discrete collection of control variables (to be chosen by the control algorithm), it is digital in nature. Hereafter, u^d will be referred to as a digital control.

Most commonly, if $\ell = 1$, $\alpha_k \equiv \alpha_k^1 \in R^m$, and C^d is defined to be all u^d of the form

$$u^d(t) = \alpha_k \text{ for } kT \leq t < (k+1)T, \quad k = 0, 1, \dots, \tag{2}$$

then the state equations (1) are excited by a piecewise constant signal. Such a signal may be identified with the output of the conventional zero-order hold. If all $u^d \in C$ have the form

$$u^d(t) = u^d(kT) + \alpha_k(t - kT) \quad kT \leq t < (k+1)T,$$

then each component $u_i^d(t)$ of $u^d(t)$ is continuous and piecewise linear (cf. the slower data hold⁴). If C is specified by

$$u_i^d(t) = u_i^d(kT) + \alpha_{k,i}^1 e^{\alpha_{k,i}^2} \sin \alpha_{k,i}^3 t, \quad kT \leq t < (k+1)T, \quad i=1,2,\dots,m,$$

where $\alpha_{k,i}^j$ is the i^{th} component of α_k^j , then the components of $u^d(t)$ are scaled products of exponentials and sine waves. When $C=C^d$, (OCP) will be referred to as the optimal digital control problem (ODC). It will be assumed in this work that $u \in R^m$, that is, that control signals are unconstrained. $u^d \in C^d$ should always be thought of as having been sequentially constructed on successive sampling intervals $[kT, (k+1)T)$, $k=0,1,2,\dots$, by a DC as in Figure 1. The DC will simply generate the control variables $\alpha_k^1, \alpha_k^2, \dots, \alpha_k^l$ using an appropriately designed programmable algorithm.

Kuo¹ discusses solutions of the (ODC) problem when equations (1) are linear, u^d assumes the form (2), and $J(u)$ may be rewritten in an equivalent form so that $L=0$. He describes in detail solution by the discrete maximum principle, a discrete version of the well-known Pontryagin maximum principle. The optimal linear digital regulator problem arises when L and Ψ are quadratic forms. It can be solved using either the discrete maximum principle or dynamic programming. Unfortunately, these classical solution techniques are not without problems. The maximum principle, for example, requires potentially prohibitively expensive solutions of systems of adjoint equations or of matrix Riccati equations. With dynamic programming, computationally unfeasible solutions of infinite dimensional (in the state variables) coupled systems of differential or difference equations are often necessary.

The general idea of the methodology presented here is to replace (ODC) with a related, simpler problem. This problem will not require, for its solution, the sophisticated and often cumbersome machinery of the classical theory. The problem will be called the period optimal digital control problem (PODC). It consists of the sequential construction of $u^d \in C^d$ solving, on each successive interval $[kT, (k+1)T)$, the control variable minimization problem

$$\text{Min}_{\alpha_k^1, \alpha_k^2, \dots, \alpha_k^l} \int_{kT}^{(k+1)T} L(t, y^d(t), u^d(t)) dt + \phi(kT, y^d(kT), u^d(kT)) \quad (3)$$

(PODC)

$$\dot{x}^d(t) = f(t, x^d(t), u^d(t)), \quad x^d(kT) = x_k^d, \quad y^d(t) = g(x^d(t)) \quad k=0,1,2,\dots \quad (4)$$

The d-superscripts emphasize that the system is digital in nature, being driven by a digital control. Given the initial state x^d , the solution of (PODC) with $k=0$ produces control variables $\alpha_0^1, \alpha_0^2, \dots, \alpha_0^v$ which determine u^d on $[0, T]$. The solution x^d of equations (4) on $[0, T]$ evaluated at $t=T$ determines the initial condition x_1^d for the $k=1$ minimization, and the process is repeated. The control u^d generated by these successive minimizations will be said to be optimal in (PODC).

For examples of performance criteria (3) for (PODC), let $s(t)$ be another R^n -valued trajectory. If $\phi=0$ and

$$L(t, y^d(t), u^d(t)) = \frac{1}{2} \sum_{i=1}^n w_i (s_i(t) - y_i^d(t))^2 \quad (5)$$

with weights w_i , then (PODC) will be referred to as the signal tracking problem. The objective of this problem is to follow $s(t)$ with the system output $y(t)$ so that the mean square tracking error is minimized. If $L=0$ and

$$\phi(kT, y(kT), u(kT)) = \frac{1}{2} \sum_{i=1}^n q_i (s_i(kT) - y_i^d(kT))^2 \quad (6)$$

with weights q_i , then (PODC) will be called the signal matching problem. The objective here is to force $s(t)$ and $y(t)$ to agree at the sampling instants $t=kT$. Both of these specific problems will be considered in more detail in the sections that follow. Obviously, many other performance objectives may be realized by the specification of an appropriate criterion (3). Indeed, the effectiveness and implementability of solution techniques for (PODC) will in large part depend upon the attention given to the choice of (3).

A control u^d which is optimal in (PODC) will not in general be optimal in (ODC). This is because the classical techniques which yield a solution to (ODC) enable the controller to effectively view, all at once, the entire evolution of the state variables from $t=0$ to $t=T_f$ with the help of the adjoint or Riccati equations. Potentially unacceptable performance at later times may be eliminated by appropriate control actions at earlier times thus producing a balanced, "over all" optimal system response. (PODC), by contrast, is narrowly focused on

successive sampling intervals $[kT, (k+1)T]$. However, since output updates $y(kT)$ will constantly be received by the DC, if the forms of the digital control u^d and the objective (3) are carefully chosen, the satisfactory realization of desired performance should be a realistic and achievable goal. Evidence supporting this prospect will be presented in the sections which follow. They will focus upon the solution of (PODC).

IV. OUTPUT MATCHING - THE DIGITAL REDESIGN PROBLEM

A new, easily implemented approach to digital redesign using DC's is presented in this section. Let $y(t)$ be the output of the closed-loop, multi-input multi-output control System I of Figure 2. System I may be thought of as the state space representation of the

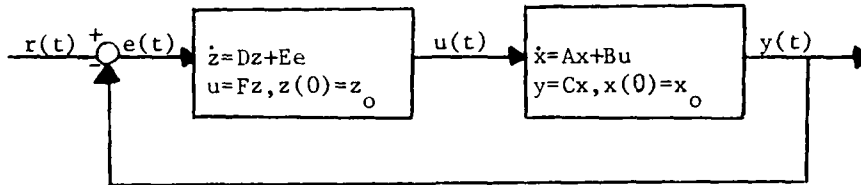


FIGURE 2. SYSTEM I

(previously designed) continuous linear feedback control system of Figure 3, for plant (plant-actuator) transfer function matrix

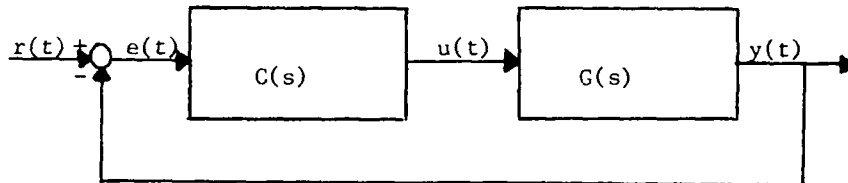


FIGURE 3. ELEMENTARY SERVO-MECHANISM

$G(s)$ and controller matrix $C(s)$ (see Ref. 16). $r(t)$, $e(t)$, and $y(t)$ are p -dimensional vectors (all vectors are column vectors unless otherwise indicated), $u(t)$, $x(t)$, and $z(t)$ are m , n , and q -dimensional respectively, and the matrices A , B , C , D , E , and F are of the corresponding appropriate dimensions. Digital redesign is accomplished by replacing $C(s)$ with a digital controller DC to give System II of Figure 4. The goal is to choose DC so that the output $y^d(t)$ (also p -dimensional) of the sampled-data System II matches $y(t)$ closely at $t = kT$, $k = 0, 1, 2, \dots$. Setting $s(t) = y(t)$, this is

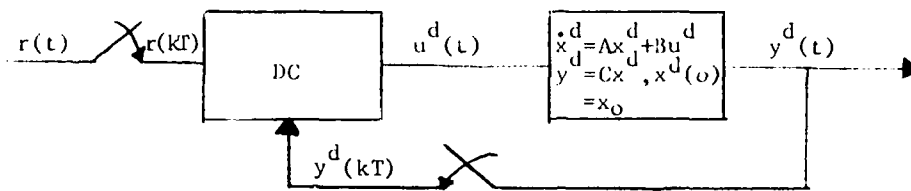


FIGURE 4. SYSTEM II

simply the output matching problem of Section III, the (PODC) problem with performance criterion (6) and state equations $\dot{x}^d(t) = Ax^d(t) + Bu^d(t)$, $x^d(0) = x_0^d$, $y^d(t) = Cx^d(t)$. Here $q_i = 1$ for each i .

For simplicity, let C^d be defined by (2). In this case, it will be shown that (6) can be driven to zero for each k . That is, perfect output matching can be achieved.

From linear systems theory, referring to System I, for each $k \geq 0$

$$x(t) = e^{A(t-kT)}x(kT) + \int_{kT}^t e^{A(t-\tau)}Bu(\tau)d\tau, \quad t \geq kT \quad (7)$$

so that

$$y((k+1)T) = Ce^{AT}x(kT) + C \int_0^T e^{A(T-\tau)}Bu(\tau)d\tau, \quad k=0,1,2,\dots \quad (8)$$

Similarly, since u^d in System II drives the same physical plant $G(s)$,

$$y^d((k+1)T) = Ce^{AT}x^d(kT) + C \int_0^T e^{A(T-\tau)}Bu^d(\tau)d\tau, \quad k=0,1,2,\dots \quad (9)$$

Thus, equating (8) and (9), a necessary and sufficient condition for perfect output matching (and hence minimization of (6)) is, in view of (2),

$$\left(C \int_0^T e^{A(T-\tau)}Bd\tau \right) \alpha_k = Ce^{AT}(x(kT) - x^d(kT)) + C \int_0^T e^{A(T-\tau)}Bu(\tau)d\tau, \quad k=0,1,2,\dots \quad (10)$$

In essence, the digital input α_k has the same net effect on $[kT, (k+1)T)$ as the continuous input $u(t)$, driving $y^d(t)$ to $y((k+1)T)$ as t approaches $(k+1)T$. Note that (10) is simply a system of p linear equations in m unknowns, the components of α_k . In practical situations, one expects that $p \leq m$ so that the equations most likely possess a solution.

The solution of equations (10) requires that the vector difference $x(kT) - x^d(kT)$ and the continuous control law $u(t)$ be known. Recognizing that $e(t) = r(t) - Cx(t)$ and $u(t) = Fz(t)$, it is easily verified that System I can be represented as a single linear system

$$\dot{\bar{x}}(t) = \bar{A}\bar{x} + \bar{B}r(t) \quad \bar{x}(0) = \bar{x}_0$$

where $\bar{x}(t) = \begin{bmatrix} x(t) \\ z(t) \end{bmatrix}$ is the closed-loop system state,

$$\bar{A} = \begin{bmatrix} A & BF \\ -EC & D \end{bmatrix}, \text{ and } \bar{B} = \begin{bmatrix} 0 \\ E \end{bmatrix}.$$

Thus,

$$\bar{x}(t) = e^{\bar{A}(t-kT)} \bar{x}(kT) + \int_0^{t-kT} e^{\bar{A}(t-kT-\tau)} \bar{B}r(\tau) d\tau, t \geq kT, k=0,1,2,\dots \quad (11)$$

and

$$u(t) = [0 \ F] \bar{x}(t) \text{ and } y(t) = [C \ 0] \bar{x}(t). \quad (12)$$

Again by standard theory,

$$x^d(kT) = e^{AT} x^d((k-1)T) + \left(\int_0^T e^{A(T-\tau)} B d\tau \right) \alpha_{k-1}, k=1,2,\dots \quad (13)$$

In theory, the right hand side of equations (10) can be computed using (11), (12), and (13). However, if the output matching technique is actually to be implemented as a sampled-data control system, at any sampling instant $t = kT$, only knowledge of observed inputs $r(jT)$ and $y(jT)$, $j \leq kT$, and previous control actions α_j , $j \leq k-1$, are available for the determination of α_k (refer to Figure 4). Therefore, estimates (predictions) of $r(t)$, $u(t)$, and $x(kT) - x^d(kT)$ are provided in the following manner.

If $s(t)$ is a continuous signal sampled at instants $t = kT$, let $\tilde{s}(t)$ represent a function which predicts the values of $s(t)$ on $(kT, (k+1)T)$ based only upon observations $s(jT)$ and possibly other fixed parameters. $\tilde{s}(t)$ may be thought of as the output of a conventional hold device (e.g., $s(t) = s(kT) + \frac{s(kT) - s(k-1)T}{T} (t - kT)$, $t \in (kT, (k+1)T)$ for a first-order hold), or simply as some other suitably generated signal. If $\tilde{r}(t)$ predicts $r(t)$, $\bar{x}(kT)$ may be approximated, using (11), by

$$\bar{x}(kT) \approx e^{AT} \bar{x}((k-1)T) + \int_0^T e^{\bar{A}(T-\tau)} \bar{B} r((k-1)T + \tau) d\tau. \quad (14)$$

(This approximation is a sample of an internally generated signal $s_1(t)$. Refer to Figure 1.) Replacing kT with $(k+1)T$ in (14), $u((k+1)T)$ may be approximated. The signal $u(t)$ may then be predicted on $(kT, (k+1)T)$ by a suitable function $\tilde{u}^+(t)$ of the estimates $u(jT), j \leq k+1$ (e.g., $\tilde{u}^+(t) = u(kT) + \frac{u((k+1)T) - u(kT)}{T} (t - kT)$). Loosely speaking, $\tilde{u}^+(t)$ is used to predict the control that $C(s)$ would exercise on $(kT, (k+1)T)$ if the closed-loop system state actually was $\bar{x}(kT)$ as estimated by (14).

Substituting $\tilde{u}^+(t)$ for $u(t)$ in (10), along with the estimate of the difference $x(kT) - x^d(kT)$ provided by (13) and (14), the vector control variable α_k may be determined (approximately). An attractive feature of the predictors $\tilde{r}(t)$ and $\tilde{u}^+(t)$ is that their specific forms may be chosen so that the integrals in (10) and (14) may be numerically pre-computed (as well as those in (13)) being essentially independent of k . Simple algebraic expressions in the $r(jT)$ and $u(jk)$ result. Furthermore, the coefficient matrix $C \int_0^T e^{A(T-\tau)} B d\tau$ of system (10) can also be pre-computed. Thus, the solution of (10) when $p=m$ may be effectively pre-programmed (e.g., using (pseudo-) inverses) thereby reducing the solution of the output matching problem to an algorithmic sequence of algebraic manipulations. It is interesting to note that if $p < m$, then $m-p$ control variables may be conveniently assigned arbitrarily, their values perhaps influenced by other design considerations.

Because of the approximations made, on-line output matching as outlined above will not be exact. Also, in actual operation the control system will be truly adaptive only if the information contained in the observations $y^d(kT)$ is utilized. Assume that $y(t)$ is a vector of observable states of the plant state vector $x(t)$, and hence observable states of $x(t)$. (That is, the component $y_i(t) = x_j(t)$ for some j , for each $i=1, 2, \dots, p$.) Then, only the unobservable components of $x(t)$ must be estimated using (14). For convenience, assume that $y_i(t) = x_i(t)$, $i=1, 2, \dots, p$, and hence $y_i^d(t) = x_i^d(t)$, $i=1, 2, \dots, p$ also. The approximations

$\bar{x}(kT), k=1,2,\dots$, should now be sequentially computed using (14) by first setting $\bar{x}_i((k-1)T) = y_i^d((k-1)T), i=1,2,\dots,p$. The remaining components $\bar{x}_i((k-1)T), i>p$, are those generated by (14) during the preceding iteration of the output matching algorithm. Similarly, the approximations $x^d(kT)$ in (13) should be generated by redefining the first p components of the previously computed estimate $x^d((k-1)T)$ to be $x_i^d((k-1)T) = y_i^d((k-1)T)$. This is perhaps the most important step in the implementation of the algorithm. It permits an estimate to be made of the response $\bar{x}(kT)$ (and hence $u(kT)$) that would be observed if the system found itself in state $\bar{x}((k-1)T)$ at $t=(k-1)T$. Thus, at time $t=kT$, given the prediction $\bar{x}((k+1)T)$ generated by (14), the algorithm is able to use $\tilde{u}^+(t)$ to estimate the character of the control $u(t)$ that would be issued by $C(s)$ on $[kT, (k+1)T)$ if $\bar{x}(kT)$ were the system state at $t=kT$. It then essentially uses $\tilde{u}^+(t)$ to estimate $y((k+1)T)$ through (8), and adjusts α_k in (10) so that $y^d((k+1)T)$ matches $y((k+1)T)$. (Perhaps a better predictor $u^+(t)$ could be generated by replacing $r(t)$ with $\tilde{r}(t)$ in (11) and then setting $\tilde{u}^+(t)$ equal to $u(t)$ as given by (12). This $\tilde{u}^+(t)$ could then be substituted into (10) to determine α_k . Now, however, troublesome multiple integrals arise which may produce computational difficulties as well as numerical inaccuracies.)

The on-line application of the output matching technique when the outputs are observable states may be out-lined as the following algorithm. A numerical simulation employing this algorithm is given in Section VI.

Output Matching Algorithm

- I. Set $k = 0, x^d(0) = x_o^d, \bar{x}(0) = \bar{x}_o = \begin{bmatrix} x_o^d \\ 0 \\ z_o \end{bmatrix}$. Go to III.
- II. Compute $x^d(kT)$ using (13). Set $x_i^d(kT) = y_i^d(kT), i = 1,2,\dots,p$, for on-line observations $y_i^d(kT)$.
- III. Set $\bar{x}_i(kT) = y_i(kT), i = 1,2,\dots,p$ ($y_i(kT)$ as in II). Compute $\bar{x}((k+1)T)$ using predictor $\tilde{r}(t)$ and (14).
- IV. Determine α_k using predictor $\tilde{u}^+(t)$ and (10). Set $k = k+1$. Go to II.

The sequential approximation of $\bar{x}((k+1)T)$ using (14) (as in III above) is subject to the accumulation of errors in the estimation of the unobserved states. Hence, the algorithm out-lined may be in general well-suited only for the case when all of the states $x(t)$ are observable. In this case, complete state matching is guaranteed by (10). To minimize the effects of errors one may introduce, in the usual fashion, a suitably designed asymptotic observer (assuming that (A,C) is observable) with state estimator $\hat{x}(t)$ satisfying

$$\begin{aligned}\dot{\hat{x}}(t) &= (\bar{A}-K\bar{C})\hat{x}(t) + \bar{B}r(t) + Ky(t) \\ \hat{x}(0) &= \bar{x}_0.\end{aligned}$$

Here $y(t)=Cx(t)$ is the output of the plant $G(s)$, $\bar{C}=[C;0]$ (see (12)), and K is an appropriately specified gain matrix. Thus, $x(kT)$ may be estimated by $\hat{x}(kT)$ (instead of by (14)), with $\hat{x}(kT)$ in turn being approximated by

$$\begin{aligned}\hat{x}(kT) &\approx e^{(\bar{A}-K\bar{C})T} \hat{x}((k-1)T) + \int_0^T e^{(\bar{A}-K\bar{C})(T-\tau)} \\ &\quad \cdot \left[\bar{B}\tilde{r}((k-1)T+\tau) + K\tilde{y}((k-1)T+\tau) \right] d\tau\end{aligned}\quad (15)$$

where $\tilde{y}(t)$ is an appropriate output predictor and $x_i((k-1)T) = y_i^d((k-1)T)$, $i=1,2,\dots,p$.

V. DIRECT DIGITAL DESIGN

In this section the general methodology of Section IV is extended to the direct design of sampled-data control systems. Referring to Figure 5, the design goal is to construct a digital controller DC that will generate a control signal u^d , which in turn will drive plant equations (1)

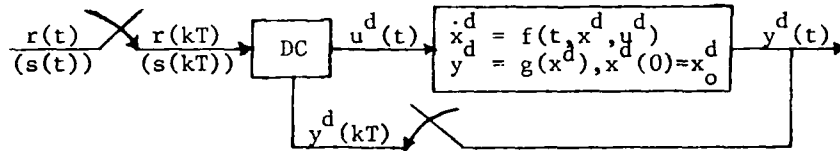


FIGURE 5 - THE DIGITAL CONTROL SYSTEM

so as to realize a given control objective. A popular, effective, and really quite general objective is embodied in the signal tracking problem of Section III, a (PODC) problem with $\phi = 0$ and L given by (5). The tracked signal $s(t)$ may appear as a portion of the input $r(t)$, or it may be generated internally by DC, or it may be a combination of both. For example, if $s(t)=r(t)$ is the reference input signal, the the signal tracking (PODC) becomes the classical design problem of forcing the system output to follow input command signals. If $s(t)=s_I(t)$ is internally generated then $y^d(t)$ is made to follow a desired or preferred trajectory. (cf. Mehra's^{10,11} MAC where preferred trajectories are exponentials leading to an ultimate set point c.).

The minimization of mean square tracking error does not necessarily ensure that $s(t)$ and $y^d(t)$ match closely at sampling instants, as is depicted in Figure 6. This is particularly true if T is large relative to the highest frequency component of $s(t)$, since the character of $y^d(t)$ is

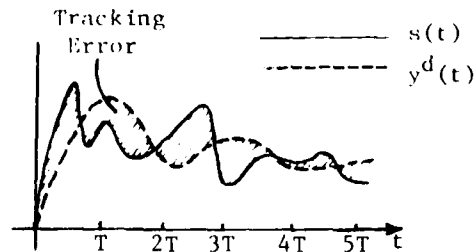


FIGURE 6 - MEAN SQUARE TRACKING ERROR

determined by the specific forms of $u^d(t)$ and the plant dynamics. Hence, the variability of possible outputs $y^d(t)$ is limited. Since DC makes control decisions based upon collected data samples, perhaps the signal matching criterion of Section IV would provide a more reliable measure of system performance. But here again, depending upon the magnitude of T , signal matching does not imply effective signal tracking. Since it is often desirable to keep T as large as possible, perhaps the sequential minimization of

$$\frac{1}{2} \sum_{i=1}^p \int_{kT}^{(k+1)T} w_i (s_i(t) - y_i^d(t))^2 dt + \frac{1}{2} \sum_{i=1}^p q_i (s_i(kT) - y_i^d(kT))^2 \quad (16)$$

offers an advantageous compromise.

The performance index (16) is a particular form of the (PODC) index (3), and obviously many other indices may be chosen by varying L and \mathbf{I} . One might even choose to add the Ψ term from (OCP) if, for example, it is desired to ensure that after a certain finite time t_f the output $y^d(t)$ is steered to a preferred state. As has been emphasized, the goal here is to find direct solution techniques for (PODC). Computationally tractable problems characteristically require the specification of an uncomplicated performance criterion. The quadratic nature of (16) makes it particularly attractive and it is this criterion that will be considered in the remainder of this section.

Let the plant dynamics in Figure 5 be

$$\begin{aligned} \dot{x}^d(t) &= Ax^d(t) + Bu^d(t), \quad x^d(0) = x_o^d \\ y^d(t) &= Cx^d(t). \end{aligned} \quad (17)$$

If $u^d(t) = \alpha_k$ is applied to (17) on $[kT, (k+1)T)$, (16) is given by

$$\begin{aligned} F(\alpha_k) &= \frac{1}{2} \sum_{i=1}^p \int_{kT}^{(k+1)T} w_i (s_i(t) - y_i^d(t))^2 dt + \frac{1}{2} \sum_{i=1}^p q_i (s_i(kT) - y_i^d(kT))^2 \\ &= \frac{1}{2} \sum_{i=1}^p \int_{kT}^{(k+1)T} w_i \left[s_i(t) - C_i \left[e^{A(t-kT)} x^d(kT) + \int_0^t e^{A(t-\tau)} B d\tau \right] \alpha_k \right]^2 dt \\ &\quad + \frac{1}{2} \sum_{i=1}^p q_i \left[s_i(kT) - C_i \left[e^{AT} x^d(kT) + \int_0^T e^{A(T-\tau)} B d\tau \right] \alpha_k \right]^2 \end{aligned}$$

where C_i is the i th row of C .

Since $F(\alpha_k)$ is strictly convex, a necessary and sufficient condition for its minimization is that the gradient of F with respect to the m components $\alpha_{k,i}$ of α_k be zero. Setting $\nabla F(\alpha_k) = 0$, the following system of linear equations results:

$$\sum_{i=1}^p \int_{kT}^{(k+1)T} w_i y_i(t) \phi_j^i(t) dt + \sum_{i=1}^p q_i y_i(kT) \phi_j^i(T) \quad (18)$$

$$= \sum_{i=1}^p \int_{kT}^{(k+1)T} w_i s_i(t) \phi_j^i(t) dt + \sum_{i=1}^p q_i s_i(kT) \phi_j^i(T) \quad j = 1, 2, \dots, m$$

where $\phi_j^i(t)$ is the j th component of the row vector

$$\phi^i(t) = C_i \int_0^t e^{\Lambda(t-\tau)} B d\tau \quad (19)$$

and of course

$$y_i^d(t) = C_i \left[e^{\Lambda(t-kT)} x^d(kT) + \left(\int_0^t e^{\Lambda(t-\tau)} B d\tau \right) \alpha_k \right]. \quad (20)$$

Equations (18) constitute a direct design algorithm for (PODC) with performance index (16) and class C^d defined by (2). As in Section IV, using suitable predictors $\tilde{x}^d(t)$ (or $\hat{x}^d(t)$) and $\tilde{s}(t)$ of $x^d(t)$ and $s(t)$ based upon samples $s(kT)$, observations $y^d(kT)$, and the plant model (17), the integrals in (18), (19), and (20) may be pre-computed. Thus, the design algorithm may again be implemented as simply a system of linear equations for the control vector α_k . Even though the coefficient matrix of system (18) involves the system states $x^d(kT)$, its (pseudo-) inverse can again be pre-computed (at least in theory), reducing the sample-data direct design control algorithm defining DC to a series of algebraic manipulations.

Note that equations (18) do not appear to explicitly involve the system input $r(t)$. This is because, quite simply, either $s(t)=r(t)$, or a portion of $s(t)$ is generated by DC internally making use of the input samples $r(kT)$. In particular, $s(t)$ may be the output $y(t)$ of a linear system as in system I of Figure 2. In this case, $s(t)$ may be predicted on $[kT, (k+1)T]$ from (closed-loop) system state equations (e.g., from equations (11)) and the integral of $s(t)$ in (18) may be computed in a straight forward fashion.

VI. AN OUTPUT MATCHING EXAMPLE

In this section the output matching algorithm is applied to the closed-loop feedback control system I of Figure 7, with plant transfer function

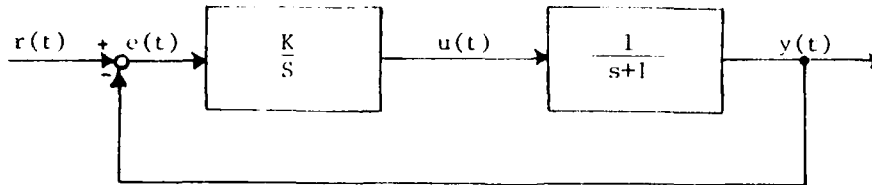


FIGURE 7 - SYSTEM I

$\frac{1}{s+1}$ and continuous compensator $\frac{K}{s}$. For all $K \neq 0$, this system is open-loop unstable (unit step response: $y(t) = K(t + e^{-t} - 1)$) and closed-loop stable. Setting the gain $K=2$ (resulting in damping ratio $\zeta = .351$) the closed-loop unit step response is easily seen to be

$$y(t) = 1 - \frac{\sqrt{7}}{7} e^{-1/2t} \sin \frac{\sqrt{7}}{2} t - e^{-1/2t} \cos \frac{\sqrt{7}}{2} t. \quad (21)$$

The object is to replace the continuous controller s with a DC (refer to Figure 4) so that $y^d(t)$ and $y(t)$ agree at $t=kT$, $k=0,1,2,\dots$. The plant state equation is simply $\dot{y} = -y + u$. It follows that if u^d has form (2),

$$y((k+1)T) = e^{-T} y(kT) + \int_0^T e^{-(T-\tau)} u(kT+\tau) d\tau$$

and

$$y^d((k+1)T) = e^{-T} y^d(kT) + \alpha_k \int_0^T e^{-\tau} d\tau \quad (22)$$

with α_k a scalar. The requirement $y^d(k+1)T = y((k+1)T)$ given that $y^d(jT) = y(jT)$, $j \geq k$, forces

$$\alpha_k \int_0^T e^{-\tau} d\tau = \int_0^T e^{-(T-\tau)} u(kT+\tau) d\tau$$

or

$$\alpha_k = \frac{\int_0^T e^{-(T-\tau)} u(kT+\tau) d\tau}{1 - e^{-T}} \quad (23)$$

This is simply equation (10).

The closed-loop system state $\bar{x} = \begin{bmatrix} y \\ u \end{bmatrix}$ satisfies

$$\begin{aligned} \dot{y} &= -y + u \\ \dot{u} &= -2y + 2r \end{aligned}$$

or, assuming zero initial conditions,

$$\begin{aligned} \dot{\bar{x}} &= A\bar{x} + br \\ \bar{x}(0) &= 0 \end{aligned}$$

where $A = \begin{bmatrix} -1 & 1 \\ -2 & 0 \end{bmatrix}$ and $b = \begin{bmatrix} 0 \\ 2 \end{bmatrix}$. (The bars over A and b have been dropped as a notional convenience.) It follows that

$$u((k+1)T) = e_2^{AT} \begin{bmatrix} y(kT) \\ u(kT) \end{bmatrix} + 2 \int_0^T e_2^{A(T-\tau)} r(\tau) d\tau \quad (24)$$

where e_i^{AT} is the i^{th} row of the matrix e^{AT} with j^{th} element e_{ij}^{AT} . An easy computation shows that

$$\begin{aligned} e_{21}^{AT} &= -\frac{4}{\sqrt{7}} e^{-\frac{1}{2}t} \sin \frac{\sqrt{7}}{2} t \\ e_{22}^{AT} &= \frac{\sqrt{7}}{7} e^{-\frac{1}{2}t} \sin \frac{\sqrt{7}}{2} t + e^{-\frac{1}{2}t} \cos \frac{\sqrt{7}}{2} t. \end{aligned} \quad (25)$$

Let the predictor $\tilde{u}^+(t)$ be given by

$$\tilde{u}^+(t) = u(kT) + \frac{u((k+1)T) - u(kT)}{T} (t - kT) \quad kT \leq t < (k+1)T. \quad (26)$$

Let $r(t) \equiv 1$, a unit step function. Note that $u(t)$ is the only component of $\bar{x}(t)$ that needs estimation. Letting $\tilde{r}(t) = r(t) \equiv 1$, (24) becomes the second component equation of (14) which here is an exact equality. Substituting $\tilde{u}^+(t)$ as given by (26) for $u(t)$ in (23) and integrating results in the approximation

$$\alpha_k \approx u(kT) + \frac{T-1+e^{-T}}{T(1-e^{-T})} \left[u((k+1)T) - u(kT) \right]. \quad (27)$$

Therefore, using (22), (24), and (27), the output matching algorithm of Section IV assumes the following simplified form:

Output Matching Algorithm

I. Set $k=0$, $y^d(0)=y(0)=u(0)=0$,

$$\theta_1 = e_{21}^{AT}, \theta_2 = e_{22}^{AT}, \theta_3 = \int_0^T e_{22}^{AT} d\tau,$$

$$\theta_4 = \frac{T-1+e^{-T}}{T(1-e^{-T})}, \theta_5 = e^{-T}, \theta_6 = 1 - \theta_5.$$

II. $y^d(kT) = \theta_5 y^d((k-1)T) + \theta_6 \alpha_{k-1}$.

III. Set $y(kT)=y^d(kT)$.

$$u((k+1)T) = \theta_1 y(kT) + \theta_2 u(kT) + \theta_3$$

IV. $\alpha_k = u(kT) + \theta_4 [u((k+1)T) - u(kT)]$.

Set $k=k+1$. Go to II.

Letting $T=1$, system I was redesigned using the output matching algorithm. The results of hand calculations on the interval $[0,5]$ are listed in Table 1. The (on-line) responses $y^d(kT)$ and $y(kT)$ were simulated by (22) and (21)

K	$u(kT)$	α_{k-1}	$y^d(kT)$	$y(kT)$	Absolute Error
1	1.517868	.8833690	.5583956	.6289264	.0705308
2	1.5847347	1.5567865	1.1894988	1.2574212	.0679224
3	1.0485244	1.2726728	1.2420747	1.2131373	.0289374
4	.8028136	.9055265	1.0293356	.9687450	.0659060
5	.9007514	.8598111	.8975960	.9122874	.0146914

TABLE 1 — OUTPUT MATCHING ALGORITHM DATA

respectively. As can be seen, $y^d(t)$ quite effectively matches $y(t)$ at $t=kT$, and certainly more accuracy could be achieved if T were reduced. Intersample simulations of $y^d(t)$ and $y(t)$ were run on the Air Force Institute of Technology program TOTAL and the results are graphed in Figure 7. Note that on each interval $[kT, (k+1)T)$, $y^d(t)$ is an exponential function as determined by $G(s) = \frac{1}{s+1}$. By way of comparison, the continuous controller

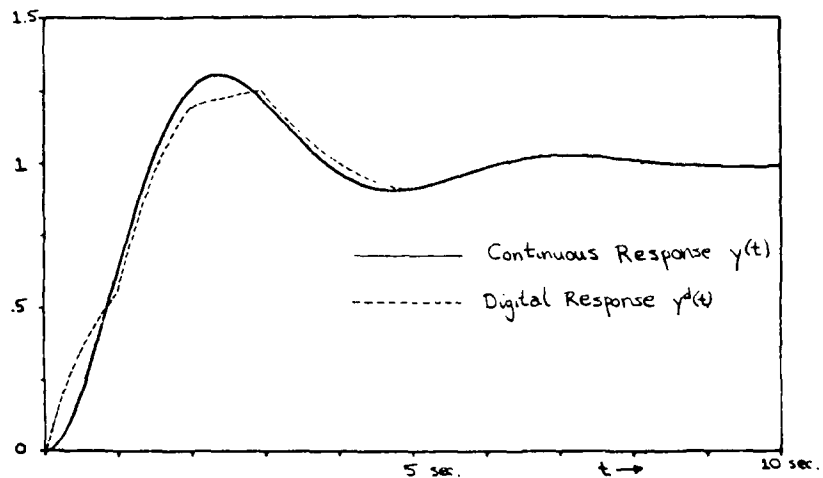


FIGURE 7 - UNIT STEP RESPONSES COMPARED

$C(s)$ was converted into the z - form $\frac{T(z+1)}{z-1}$ using the popular Tustin transform. This discrete transfer function was provided with ideal samplers and a zero-order output hold and was then inserted into system I in the place of $C(s)$. A TOTAL simulation of the unit step response of the resulting digitized system for various values of T is given in Figure 8.

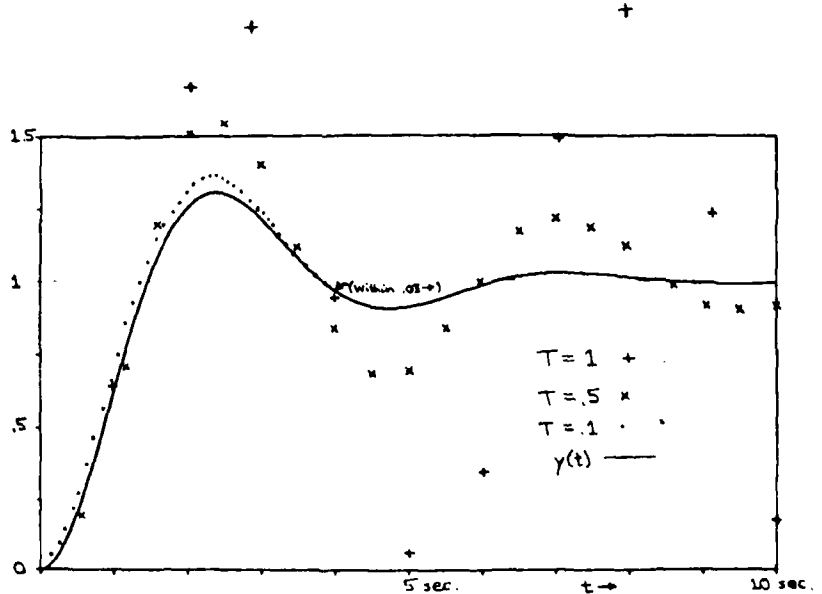


FIGURE 8 - TUSTIN TRANSFORMED UNIT STEP RESPONSE

Note that when $T=1$ (since the poles of the closed-loop z - transfer function of the digitized system lie approximately on the unit circle) the unit step response is a sustained oscillation with output values ranging between 0 and 2. Output matching comparable to that achieved in Figure 7 is possible only when $T=.1$, an increase of a full order of magnitude in the rate of sampling.

As a final note, consider the question of stability. System I of Figure 7 is stable for all $K \neq 0$. When $\frac{K}{s}$ is replaced by DC as is done here for $K=2$, must it necessarily follow that the resulting sampled-data system is stable? Intuitively, at least with respect to the unit step response of Figure 7, if $y^d(t)$ matches $y(t)$ at $t=kT$, $k=0,1,2,\dots$, then eventually close matching should result for all t . Thus, if $y(t)$ displays a stable response, so should $y^d(t)$. One can actually demonstrate this fact mathematically for the simple example discussed here though the proof is somewhat involved and hence will be omitted. The algorithm appears to function smoothly and efficiently, apparently without accumulation of errors in the estimated state component $u(t)$ (refer to Section IV). Its adaptive nature seems to guarantee a robustness and self-correcting character which promises to carry over into higher dimensional settings.

VI. RECOMMENDATIONS

This study has focused upon the digital control problem (PODC) formulated in Section III. If the control variables u_k^i enter the plant dynamics linearly, then (PODC) lends itself to a direct solution which is easily implemented. Complete theories for the linear multivariable output matching and signal tracking problems have been given. The simple numerical example of Section VI supports the feasibility of the direct methodology. The obvious next step in this research should be the numerical application of the general approach presented to larger scale and more realistic models.

If the redesign technique of Section IV is to be of value, it must be effective when applied to the multiloop, highly interconnected configurations (see ref. 7) characteristic of flight control systems. If such a system is represented as a whole in state space form, state dimensionality could become a serious problem. Perhaps a more satisfactory digital design would be achieved if each controller were replaced individually starting with the ones in the innermost loop and working outwards. With regard to Section V, direct multivariable designs should be undertaken. A convenient test example might be the missile control problem of reference 11. Particular attention should be given to the classification of those trajectories $s(t)$ which may be easily and accurately integrated in equations (18). The incorporation of stochastic disturbances into system models and observation processes should be investigated. Also, since the algorithms considered here are based upon plant models with relevant operational parameters held fixed, the pre-computed system constants (generalized gains) in (10) and (18) depend upon these specific parameter values. Since the parameter values depend upon system operating conditions (e.g., aircraft flight conditions), the (gain) scheduling of these constants should be studied to ensure that the control system can adapt to a changing environment.

The effects of the forms of digital controls upon system performance should be carefully evaluated. The incorporation of the output data hold into the control algorithm should increase design effectiveness. Perhaps u^d can be tailored to better meet the needs of each particular operational environment. Attention should also be given to the signal predictors $s(t)$. Is there an advantage to employing higher order predictors? What kinds of signals can best be predicted internally (as $s_I(t)$ signals)? Also in need of consideration are the introduction of the observer \hat{x} (see Section IV) to improve performance and importantly, the introduction of constraints through

the control set U since only limited (bounded) control action is possible in actual physical settings.

As mentioned, the specific problems considered here are easily solved because the control variables enter the plant dynamics, and after differentiation, the performance index linearly. For this reason, non-linear control problems with similar characteristics should yield to similar solution techniques. Specific non-linear examples need to be constructed to test this hypothesis. In fact, even problems with control variables entering in a non-linear fashion should be solvable provided that the equations that result from equating the gradient of the performance index to zero can be efficiently solved. This of course requires that the index itself be appropriately structured. The interplay between the forms of the dynamics and the performance indices needs investigation.

As always in problems of digital control, the effects of sampling rates upon performance need to be assessed. Although it is usually difficult to give precise mathematical analyses of these effects, they represent an important problem area which should receive serious consideration. The accommodation of multi-rate and variable rate sampling by the design algorithms given should also be examined. Because of the simplicity of the control designs, this accommodation should take place in a straightforward fashion.

Finally, the questions of stability and robustness of the sampled-data systems employing the DC controllers need serious consideration. As mentioned in Section VI, there is no immediate guarantee of system stability. Preliminary results however indicate that in a sense that can be made precise, both stability and robustness are present. These results provide encouragement that uncomplicated, direct control of sampled-data systems is a realistic objective.

REFERENCES

1. Kuo, B.C., Digital Control Systems (Holt, Rinehart and Winston, Inc., New York, 1980).
2. Franklin, G.F., and J.D. Powell, Digital Control of Dynamic Systems (Addison-Wesley, 1980).
3. Dorf, R.C., Modern Control Systems, Third Ed. (Addison-Wesley, 1980).
4. Whitbeck, R.F., and L.G. Hofman, "Analysis of Digital Flight Control Systems with Flying Qualities Applications," Vol. II, Technical Report AFFDL-TR-78-115, 1978.
5. Emrick, H.L., and G.K. Hellman, "Development of Digital Design Methods," Proc. JACC, Charlottesville, N.C., 1981.
6. Kuo, B.C., G. Singh and R.A. Yackel, "Digital Approximation of Continuous-Data Control Systems by Point-by-Point State Comparison," in Computers and Elec. Eng., Vol. 1, Pergamon Press, 1973, pp. 155-170.
7. Rattan, K.S., "Digitalization of Existing Continuous-Data Control Systems," Technical Manual AFWAL-TM-80-105-FIGC, 1980.
8. Tabak, D., "Digitalization of Control Systems," Computer Aided Design, Vol. 3, No. 2, 1971, pp. 13-18.
9. Yeh, H.H., and C.S. Yeh, "On the Digital Controller Design for Point-by-Point Output Matching," 10th Annual South-Eastern Symposium on System Theory, March 1978, Mississippi State University.
10. Mehra, R.K., et al., "Model Algorithmic Control Using IDCOM for the F100 Jet Engine Multivariable Control Design Problem," in Alternatives for Linear Multivariable Control, Ed. by Sain, et al. (NEC Inc., Oak Brook, Ill., 1978), pp. 71-87.

REFERENCES (Contd)

11. Mehra, R.K., et al., "Basic Research In Digital Stochastic Model Algorithmic Control," Technical Report AFWAL-TR-80-3125, 1980.
12. Richalet, J.R., et al., "Model Predictive Heuristic Control: Applications to Industrial Processes," Automatica, 1978, pp. 413-428.
13. Whitbeck, R.F., and D.G.J. Didalensky, "Multi-rate Control Systems with Simulation Applications," Vol. I, Technical Report AFWAL-TR-80, 1980.
14. Landau, I.D., "A Survey of Model Reference Adaptive Techniques (Theory and Applications)," Automatica, Vol. 10, 1974, pp. 353-379.
15. Fleming, W., and R. Rishel, Deterministic and Stochastic Optimal Control (Springer-Verlag, New York, 1975).
16. Peczkowski, J.L., and M.K. Sain, "Linear Multivariable Synthesis with Transfer Functions," in Alternatives for Linear Multivariable Control, Ed. by Sain, et al. (NEC Inc., Oak Brook, Ill., 1978), pp. 71-87.

1981 USAF - SCEEE SUMMER FACULTY RESEARCH PROGRAM

Sponsored by the

AIR FORCE OFFICE OF SCIENTIFIC RESEARCH

Conducted by the

SOUTHEASTERN CENTER FOR ELECTRICAL ENGINEERING EDUCATION

FINAL REPORT

TRANSIENT ANALYSIS OF STRUCTURES WITH DISTINCT NONLINEARITIES

Prepared by:	Levon Minnetyan
Academic Rank:	Assistant Professor
Department and University:	Department of Civil and Environmental Engineering Clarkson College of Technology
Research Location:	Air Force Wright Aeronautical Laboratories, Flight Dynamics Laboratory Structures and Dynamics Division
USAF Research Colleague:	Tony G. Gerardi
Contract No:	F49620-79-C-0038

TRANSIENT ANALYSIS OF STRUCTURES
WITH DISTINCT NONLINEARITIES

By

Levon Minnetyan

ABSTRACT

A new hybrid method is formulated for the transient response analysis of certain structural systems with isolated nonlinear components. The method is aimed to achieve an optimal solution path that will reliably predict the dynamic response of all structural components. Options on substructuring and requirements for orthogonality of rigid body and flexible modes are stated. The solution procedure incorporates a time-history analysis of the nonlinear response with a frequency domain analysis of the linear modes. The linear modes that affect the response of nonlinear structural components are also included in the time-history analysis. The resulting nonlinear response time-histories are used as external inputs for the analyses of linear substructures. The response of linear structural components is determined through the frequency domain. The frequency domain analysis uses a larger number of modal coordinates to realistically simulate the details of substructural response. The application of the method to the modeling of taxiing aircraft is studied.

ACKNOWLEDGEMENTS

The support of Air Force Systems Command, Air Force Office of Scientific Research in providing this excellent research opportunity is gratefully acknowledged. Thanks are also due to Air Force Wright Aeronautical Laboratories, Flight Dynamics Laboratory for their hospitality and particularly to the Structures and Dynamics Division for providing a productive research environment. Special thanks are due to Tony G. Gerardi for suggesting the research area and for his sincere and outspoken guidance and support during this research. Helpful technical discussions with Dr. James J. Olsen, Dr. Vippera B. Venkayya, and Captain Robert C. Knarr are also acknowledged. Finally, expert typing of this report by Ms Karen A. Brink is appreciated.

1. INTRODUCTION:

Nonlinear behavior often plays an important role in the transient structural response. Nonlinearities may be due to inelastic material behavior, specially designed nonlinear energy absorption and attitude control devices, or due to geometric nonlinearities that result from large structural deformations.

With the advent of high speed digital computers, the time-history analysis has become a standard method for the prediction of nonlinear dynamic response. Two numerical methods have emerged for the incorporation of nonlinear properties in structural analysis. The first method uses variable structural stiffness properties. The piecewise linear stiffness matrix depends on the state of deformation of the structure. In the second method, the initial linear elastic stiffness matrix is preserved intact. The nonlinear properties are taken into account by means of additional effective coordinate forces. Equilibrium iterations at consecutive time increments are carried out to balance the equations of dynamic equilibrium. Most nonlinear computer programs incorporate both methods and use step-iterative or mixed procedures. Detailed formulations of these methods are given in references ^{1,2}.

In theory, it is possible to simulate the total structural behavior by a direct dynamic analysis of a finite element model. However, the transient response analysis of the full finite element model is prohibitively expensive. Also, past experience has shown that such analyses of complex structures can be numerically unreliable.

The second method of nonlinear analysis that keeps the initial stiffness matrix unchanged is particularly convenient for the expression of the equations of motion in terms of an orthogonal modal basis. Nonlinear terms can be extracted from the total stiffness matrix by substructuring ³. The contributions of these nonlinear terms are treated as additional coordinate forces. The vibration eigenvalue problem need be formulated only once at the beginning of the time-history solution. The modal superposition method can be used for a change of basis from n nodal to p modal coordinates, $p \leq n$, prior to the time-history solution.

For most types of loadings, the contributions of low frequency modes are the most significant in predicting the dynamic response of major structural components. It is often satisfactory to truncate the modal superposition

series when the response is obtained to a desired degree of accuracy. Also, the mathematical idealization of a large and complex structure tends to be less reliable in predicting the higher modes of vibration. Nevertheless, some of the higher vibration modes may be significant in representing the behavior of critical structural components. In such cases, the original finite element model must be sufficiently refined to yield meaningful vibration information on the high frequency modes.

The necessity of including higher vibration modes is especially relevant when force-related quantities such as internal loads are being estimated. It can be shown that structural deformations are given by the product of the orthogonal mode shape matrix and the modal amplitude vector. On the other hand, the vector of elastic forces can be expressed as the product of the structural mass matrix, mode shape matrix, and a vector of modal amplitudes which are multiplied by corresponding modal frequencies. Because each mode contribution is multiplied by the square of the modal frequency to represent forces, it is evident that the higher modes are of greater significance in defining loads in the structure than they are in the displacements. Consequently, it is necessary to include more modal components to define the forces to any desired degree of accuracy than to define the displacements.

Many complex systems contain both linear and nonlinear structural components. The types of structures that are particularly addressed in this research are those with mostly linear characteristics. However, significant nonlinearities exist in some limited regions of the structure. The most immediate and relevant example of such a dynamic system is an aircraft taxiing over an irregular surface. The vehicle superstructure may be assumed linear but the suspension system is highly nonlinear⁴. It is necessary to perform a time-history integration of the equations of motion to estimate the nonlinear suspension response. To account for the vehicle flexibility during taxiing, the fundamental elastic vibration modes should also be included in the model. The modal superposition series can be truncated after a few modes since the higher frequency vibrations do not affect the suspension response. However, the time-history analysis is not practical to simulate the response of all critical aircraft components; especially those that are affected by the high frequency modes. It is not practical to include the higher vibration modes with numerical reliability within the constraints of time-domain discretization. It would be necessary to decrease the time increment by several

orders of magnitude to simulate the higher frequency modes consistently. Such refinement of the time step with the addition of a greater number of modal coordinates makes the time-history analysis approach prohibitively expensive for design calculations. A simple, efficient, and reliable method is needed to simulate aircraft total structural response for comparison with critical design limits to establish relevant runway repair criteria.

To accomplish this task, a hybrid analytical method is formulated; aimed at defining an optimal solution path that will reliably predict dynamic response. The method incorporates a time-history analysis for the nonlinear response with a frequency domain analysis of the linear modes. First the time-history analysis including the nonlinear components and a small number of linear modes is to be conducted. Partial decoupling of the nonlinearities from the rest of the structure constitutes the second step. The remaining linear dynamic subsystem can be analyzed through the frequency domain under external forces and interactions from the nonlinear components. Frequency domain analysis can also be used to compute the total structural response when the nonlinear dynamic forces are measured from actual tests.

The results of this research are applicable to the transient response analysis of all surface tracking vehicles. There is a need for the dynamic modeling of high speed sleds that are used to simulate the flight environment of supersonic vehicles. These sleds utilize a special high speed test track and rails to which they are connected by nonlinear slipper-springs⁵. Consecutive sleds may be connected to each other by nonlinear couplers.

Future applications of the results may include the modeling of large space structures that will consist of multiple linear substructures with some nonlinear components. It is envisioned that the linear substructures will be attached to each other by nonlinear energy absorbing couplers to prevent vibration propagation⁶. The nonlinear couplers will be needed to absorb energy input that is originated by attitude control adjustments or by docking space vehicles.

II. OBJECTIVES:

The main objective of this research is to investigate alternative modeling techniques to simulate the transient dynamic response of partially nonlinear structures. This report concentrates on the mathematical formulations of the results, leaving numerical demonstration of the viability

of these methods to the implementation stage. The specific objectives are:

(1) To study and expose new and useful methods that will be efficient and reliable in predicting the dynamic response of partially nonlinear structures; in particular the transient response of taxiing aircraft to runway roughness.

(2) To formulate a mathematical procedure that will evaluate the dynamic response of the linear elastic substructures when the nonlinear component responses are measured during tests. This objective is geared to address the specific problem of computing the response of an aircraft vehicle structure when the suspension forces are measured.

III. FORMULATION OF THE NONLINEAR PROBLEM:

In general, for time-history analysis, the equations of nodal coordinate dynamic equilibrium can be written as:

$$[m] \{\ddot{u}\} + [c] \{\dot{u}\} + [k] \{u\} = \{P\} - \{P_E\} \quad (1)$$

where

$[m]$ = structure nodal mass matrix

$\{u\}$ = list of nodal coordinate displacements

$[c]$ = structure damping matrix

$[k]$ = structure piecewise linear tangent stiffness matrix (includes both constant and variable stiffness coefficients)

$\{P\}$ = list of external loads

$\{P_E\}$ = list of effective loads equivalent to unbalanced coordinate forces. $\{P_E\}$ are usually calculated by equilibrium iterations within a piecewise linear solution interval.

The above formulation, Eq. (1), is not convenient for representation in terms of an orthogonal modal basis. When the structure stiffness matrix is re-assembled at each solution step, it becomes also necessary to redefine and reanalyze the vibration eigenvalue problem.

The transformation to modal coordinates becomes practical only if the nonlinearities are accounted for in terms of additional effective loads. To achieve this, the total stiffness matrix $[k]$ in Eq. (1) can be separated

into its linear and nonlinear components

$$[k] = [k^0] + [k^{NL}] \quad (2)$$

where

$[k^0]$ = constant linear elastic stiffness matrix

$[k^{NL}]$ = nonlinear stiffnesses which depend on the state of deformation

Substituting Eq. (2) into Eq. (1)

$$[m] \{\ddot{u}\} + [c] \{\dot{u}\} + [k^0] \{u\} + [k^{NL}] \{u\} = \{P\} - \{P_E\} \quad (3)$$

The nonlinear effects can be expressed as additional coordinate loads

$$\{P_{NL}\} = [k^{NL}] \{u\} \quad (4)$$

Combining the nonlinear effects with the unbalanced coordinate forces

$$\{P_{NL/E}\} = \{P_{NL}\} + \{P_E\} \quad (5)$$

the equations of dynamic equilibrium are written as

$$[m] \{\ddot{u}\} + [c] \{\dot{u}\} + [k^0] \{u\} = \{P\} - \{P_{NL/E}\} \quad (6)$$

The cumulative effective loads $\{P_{NL/E}\}$ are contributed due to nonlinear elemental forces. They also include corrections for the discretizing error. $\{P_{NL}\}$ loads are determined at each time step from nonlinear component properties. The balanced nonlinear forces $\{P_{NL/E}\}$ are obtained by equilibrium iterations of the equations of motion.

To change the solution basis from n nodal to p modal coordinates, $p \leq n$, an orthogonal transformation can be written

$$\begin{matrix} \{u\} & = & \{\phi\} & \{\eta\} \\ n \times 1 & & n \times p & p \times 1 \end{matrix} \quad (7)$$

where η are the generalized modal coordinates and $\{\phi\}$ is the modal shape matrix whose columns are the orthogonal eigenvectors $\{\phi\}$ of the vibration problem defined by

$$[k^0] \{\phi\} = \omega^2 [m] \{\phi\} \quad (8)$$

where ω is the natural frequency corresponding to $\{\phi\}$. The vibration problem need be formulated only once at the beginning of time-history analysis due to the exclusion of the variable components from the stiffness matrix $[k^0]$. The equations of motion can be written in modal coordinates

$$\begin{matrix} [M] & \{\ddot{\eta}\} & + & [C] & \{\dot{\eta}\} & + & [K] & \{\eta\} & = & \{\phi\}^T & \{F - P_{NL/E}\} \\ p \times p & p \times 1 & & p \times p & p \times 1 & & p \times p & p \times 1 & & p \times n & n \times 1 \end{matrix} \quad (9)$$

where

$$\begin{aligned} [M] &= \text{generalized mass matrix; } [M] = \{\phi\}^T [m] \{\phi\} \\ [C] &= \text{modal damping matrix; } C_{jj} = 2\zeta_j \omega_j M_j, C_{ij} = 0 \\ [K] &= \text{modal stiffness matrix; } K_{jj} = \omega_j^2 M_{jj}, K_{ij} = 0 \\ \zeta_j &= j\text{th modal damping ratio} \end{aligned}$$

The time-history integration of the equations of motion can now be accomplished more efficiently in terms of the modal coordinates. The conditions of orthogonality among the rigid body and flexible modes will be discussed in the next section. It should be noted that although time-history integration is performed using the modal coordinates, some nodal displacements must be calculated at each time step to evaluate the effective load vector $\{P_{NL/E}\}$ in Eq. (6). Generally this does not pose a problem since the effective loads usually act only at a small number of nodal coordinates.

The structures of interest in this research are composed of linear substructures which are joined together by nonlinear couplers. The total stiffness matrix $[k]$ consists of substructural stiffness matrices $[k^{ss^i}]$, plus a few nonlinear off diagonal coupling terms as shown schematically

by small shaded areas in Figure 1. When the nonlinear coupling terms are

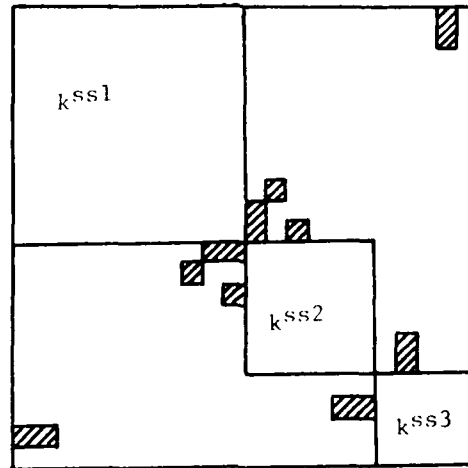


Figure 1. Stiffness Matrix Configuration

separated from the total stiffness matrix according to Eq. (2), the vibration problems are also automatically decoupled for individual substructures. Now Eq. (8) can be written as

$$[k^{ssi}] \{\phi^{ssi}\} = \omega^2 [m^{ssi}] \{\phi^{ssi}\} \quad (10)$$

where

$[k^{ssi}]$ = i th linear substructure stiffness matrix

$\{\phi^{ssi}\}$ = a vibration mode shape vector for the i th substructure

$[m^{ssi}]$ = mass matrix for the i th substructure

The off-diagonal terms shown in Figure 1 need not necessarily be nonlinear in order to formulate the problem in the above manner. Once substructures are decoupled according to their physical boundaries, it becomes possible to model the critical regions with more accurate finite element representations without numerical interference from other regions. For important substructures the vibration problem can be formulated to a higher degree of accuracy to determine significant local dynamic response.

IV. MODELING OF LINEAR SUBSTRUCTURES

In the previous section, the time-history analysis of the overall structural response is formulated. To complete the analysis, each linear substructure is considered separately from the surrounding nonlinear and linear components. The interactive forces between a particular substructure and its surroundings are now considered as external loads at the substructure boundaries. The dynamic response of critical substructure components can be computed on the basis of a greater number of modes through the frequency domain.

The substructure of interest may be represented by a finite element model. The finite element model of a structure consists of a number of nodes connected by idealized discrete elements. In general, each node may possess six degrees of freedom which completely define nodal translations and rotations. The required refinement of the finite element model depends upon structural geometry, boundary conditions and applied loading.

The dynamic equations for free vibration of a linear substructure can be written as

$$[m] \{\ddot{u}\} + [k] \{u\} = \{0\} \quad (11)$$

where

$\{u\}$ = list of substructure nodal displacements

$[k]$ = stiffness matrix of the unconstrained substructure

$[m]$ = substructure mass matrix

The solution of the harmonic equations, Eq. (11), constitutes a generalized eigenvalue problem of the form ⁷

$$[k] \{\phi\} = \omega^2 [m] \{\phi\} \quad (12)$$

where

ω = natural frequency of unconstrained substructure

$\{\phi\}$ = mode shape vector corresponding to ω

The stiffness and mass matrices in Eq. (12) are written for the unconstrained structure. The mass matrix is positive definite, the stiffness matrix is semi-definite. Common numerical procedures that require the inverse of the stiffness matrix to solve the eigenvalue problem cannot be used directly. However, a special method can be used to make the eigenproblem soluble. Introducing an eigenvalue shift, $\mu = \omega^2 - \delta$, in Eq. (12) yields

$$[k] \{\phi\} = (\mu + \delta) [m] \{\phi\} \quad (13)$$

or

$$\left[[k] - \mu [m] \right] \{\phi\} = \delta [m] \{\phi\} \quad (14)$$

the shifted matrix $[k^*] = [k] - \mu [m]$ will be nonsingular even if $[k]$ is singular. In this method, the mode shapes are not changed and the frequency change is accounted for exactly by the shift ⁸.

The definition of the free vibration problem with respect to the unconstrained substructure is necessary to render the rigid body modes orthogonal to the elastic vibration modes ⁹. Accordingly, the mode shape vectors $\{\phi\}$ are defined relative to the dynamic center of mass of the flexible substructure. The dynamic center of mass can be defined as the instantaneous center of structural mass during dynamic response. The behavior of the dynamic center of mass is described by the rigid body modes of motion. Thus, the dynamic center of mass will remain stationary during free vibrations of an unconstrained structure.

In general, any structure coordinate displacement can be expressed as the sum of rigid body displacement contributions plus the effect of elastic structural deformations. The elastic deformations can be expressed in terms of the amplitudes of flexible vibration modes. If we write the modal superposition equations for all structure coordinates in matrix form, then

$$\begin{matrix} \{u\} & = & \{\phi_R\} & \{u_R\} & + & \{\phi_F\} & \{q\} \\ nx1 & & nx6 & 6x1 & & nx(p-6) & (p-6)x1 \end{matrix} \quad (15)$$

where

$\{u_R\}$ = vector of rigid body displacements

$[\phi_R]$ = vector of rigid body modal influence coefficients. Each column of $[\phi_R]$ lists the displacements at structure coordinates due to a unit displacement of the corresponding rigid body coordinate.

$[\phi_F]$ = mode shape matrix of the flexible modes. Each column of $[\phi_F]$ represents a mode shape vector.

$\{q\}$ = flexible mode amplitudes

The superposition equations, Eq. (15) may be combined into a single matrix of rigid body plus flexible modal influence coefficients

$$\begin{matrix} \{u\} \\ nx1 \end{matrix} = \begin{bmatrix} \phi_R & \vdots & \phi_F \end{bmatrix} \begin{matrix} \{u_R\} \\ q \end{matrix} \quad (16)$$

defining new symbols for the combined matrices

$$\{u\} = [\phi] \{q\} \quad (17)$$

where $[\phi]$ is the total modal transformation matrix obtained from the solution of the unconstrained free vibration problem.

It can be observed that in Eq. (15) if u_j is in the same direction as the j^{th} rigid body mode u_{Rj} , then $\phi_{Rij} = 1$. If coordinate j corresponds to a rigid body rotation and u_j is a linear displacement, then ϕ_{Rij} is the moment arm of u_j from the j^{th} rigid body rotation axis.

For the unconstrained free vibration problem, the orthogonality of the rigid body and flexible modes can be ascertained by the use of conservation of momentum principle⁹. The list of system momenta, $\{m_0\}$, in terms of nodal coordinates can be written as

$$\{m_0\} = [m] \{\dot{u}\} \quad (18)$$

Substituting $\{\dot{u}\} = [\phi] \{\dot{q}\}$ in Eq. (18) and premultiplying each side of the equation by $[\phi]^T$:

$$[\phi]^T \{m_0\} = [\phi]^T [m] [\phi] \{\dot{q}\} \quad (19)$$

From the definition of the generalized mass matrix, $M = [\phi]^T [m] [\phi]$, thus

$$[\phi]^T \{m\dot{o}\} = [M] \{\dot{n}\} \quad (20)$$

Separating the rigid body and the flexible modes in Eq. (20)

$$\begin{bmatrix} [\phi_R]^T \\ [\phi_F]^T \end{bmatrix} \{m\dot{o}\} = \begin{bmatrix} M_{RR} & M_{RF} \\ M_{FR} & M_{FF} \end{bmatrix} \begin{bmatrix} \dot{u}_R \\ \dot{q} \end{bmatrix} \quad (21)$$

We now write the first row of Eq. (21)

$$[\phi_R]^T \{m\dot{o}\} = [M_{RR}] \{\dot{u}_R\} + [M_{RF}] \{\dot{q}\} \quad (22)$$

By definition, $[\phi_R]^T \{m\dot{o}\}$ represents the vector sum of system momenta about the dynamic center of mass ¹⁰. During the free vibrations of an unconstrained structure, the dynamic center of mass will remain stationary in an inertial frame of reference since there are no external impulses. Thus all mode shape vectors are required to have their zeros at the dynamic center of mass. The principle of impulse and momentum for a system of particles states that the vector sum of system momenta about the dynamic center of mass is equal to the momentum vector of the total system mass as if it was concentrated at the center of mass ¹⁰.

In our case

$$[\phi_R]^T \{m\dot{o}\} = [M_{RR}] \{\dot{u}_R\} \quad (23)$$

Substituting Eq. (23) in Eq. (22), the obvious result is $[M_{RF}] \{\dot{q}\} = \{0\}$. Since $\{\dot{q}\} \neq 0$, then $[M_{RF}] = \{0\}$, which indicates that the generalized mass matrix is a diagonal matrix and the rigid body modes are orthogonal to the flexible vibration modes.

Since the modal equations of motion are orthogonal, they can be written separately for each mode. For the rigid body modes, the generalized stiffness and damping are zero, thus

$$M_{jj} \ddot{u}_{Rj} = F_{Rj} \quad (j = 1, \dots, 6) \quad (24)$$

where

$$\begin{aligned} M_{jj} &= j^{\text{th}} \text{ rigid body inertia} \\ \ddot{u}_{Rj} &= j^{\text{th}} \text{ rigid body acceleration} \\ F_{Rj} &= j^{\text{th}} \text{ rigid body force; } F_{Rj} = \{\phi_{Rj}\}^T \{P_{SS}\} \\ \{P_{SS}\} &= \text{list of substructure nodal coordinate forces} \end{aligned}$$

Similarly, for each flexible mode

$$M_{jj} \ddot{q}_j + 2 \zeta_j \omega_j M_{jj} \dot{q}_j + \omega_j^2 M_{jj} q_j = F_j \quad (25)$$

where

$$\begin{aligned} M_{jj} &= j^{\text{th}} \text{ flexible mode generalized mass} \\ \omega_j &= j^{\text{th}} \text{ mode natural frequency} \\ \zeta_j &= j^{\text{th}} \text{ modal damping (ratio of critical)} \\ F_j &= j^{\text{th}} \text{ flexible mode generalized load } F_j = \{\phi_{Fj}\}^T \{P_{SS}\} \end{aligned}$$

The modal equations of motion, Eqs. (24) and (25), can be solved separately and the structural response can be evaluated by modal superposition.

The alternative to unconstrained formulation of the substructural vibration problem is a constrained formulation that fixes the modal shape vectors at chosen constraint coordinates. The most appropriate choice is to fix the substructure at the points of interaction with its surroundings. Because the most significant forces will act at the constraint points, this approach may be more favorable in representing the system with a smaller number of modes. The disadvantage is that the generalized mass matrix will now have off-diagonal terms which render the rigid-body modes non-orthogonal to the flexible modes.

The equations of motion for a substructure in terms of the generalized modal coordinates are now written as

$$\begin{bmatrix} M_{RR} & M_{RF} \\ M_{FR} & M_{FF} \end{bmatrix} \begin{Bmatrix} \ddot{\eta}_R \\ \ddot{\eta}_F \end{Bmatrix} + \begin{bmatrix} 0 & 0 \\ 0 & C_F \end{bmatrix} \begin{Bmatrix} \dot{\eta}_R \\ \dot{\eta}_F \end{Bmatrix} + \begin{bmatrix} 0 & 0 \\ 0 & K_F \end{bmatrix} \begin{Bmatrix} \eta_R \\ \eta_F \end{Bmatrix} = \begin{Bmatrix} F_R \\ F_F \end{Bmatrix} \quad (26)$$

The submatrices M_{RF} and M_{FR} are no longer zero. The interaction forces do not contribute to $\{F_F\}$ since the modal deformation shape vectors are zero at the attachment points.

From the second row of Eq. (26)

$$[M_{FR}] \{\ddot{\eta}_R\} + [M_{FF}] \{\ddot{\eta}_F\} + [C_F] \{\dot{\eta}_F\} + [K_F] \{\eta_F\} = \{F_F\} \quad (27)$$

rearranging

$$[M_{FF}] \{\ddot{\eta}_F\} + [C_F] \{\dot{\eta}_F\} + [K_F] \{\eta_F\} = \{F_F\} - [M_{FR}] \{\ddot{\eta}_R\} \quad (28)$$

Thus, if the generalized forces acting on the flexible modes and the rigid body accelerations are given, then the equations of motion can be uncoupled and solved for the response of the flexible modes. This is a possible alternative to the unconstrained formulation if the rigid body accelerations are computed during the time history analysis of the total nonlinear problem. At this stage, it is difficult to compare the constrained and unconstrained substructural formulations with respect to efficiency and reliability. However, if the input quantities are to be measured by direct testing rather than by time-history estimation, then the unconstrained formulation is the choice as it is not possible to measure the accelerations of the dynamic center of mass.

V. FREQUENCY DOMAIN ANALYSIS AND COMPUTATION OF TOTAL STRUCTURAL RESPONSE:

The basic assumptions which permit a frequency domain analysis are that the nonlinear substructure interaction forces are known and the linear systems are represented by orthogonal generalized coordinates. In Section III it was assumed that a few flexible modes were sufficient to estimate the nonlinear coupling forces. In this section, a greater number of modes is assumed to represent the substructures in detail. The frequency domain

analysis can be also used to compute the elastic forces when nonlinear response is measured by testing.

The time-history dynamic forces are first converted to the frequency domain by Discrete Fourier Transformation (DFT). The DFT coefficients are defined as ⁸

$$C_{n+1}(\bar{\omega}_n) = \Delta\tau \sum_{\tau=0}^{N-1} F(\tau) e^{-2\pi i n \tau / N}; \quad n=0, \dots, N-1 \quad (29)$$

where

$$i = \sqrt{-1}$$

$$\Delta\tau = T/N$$

T = total time period considered (includes an attached period of F(τ) = 0 to take into account the periodic nature of DFT)

N = number of discrete time intervals in T

$\bar{\omega}_n$ = forcing frequency of n cycles per second

C($\bar{\omega}_n$) = coefficients which define the discretized harmonic amplitude function

The complex-Frequency-Response-Function (CFRF), $H_j(\bar{\omega}_n)$, for each j^{th} generalized structural mode under the forcing frequency $\bar{\omega}_n$ is defined as ⁸

$$H_j(\bar{\omega}_n) = \frac{1}{-\bar{\omega}_n^2 M_{jj} + i \bar{\omega}_n C_{jj} + K_{jj}} \quad (30)$$

where

$$i = \sqrt{-1}$$

M_{jj} , C_{jj} , K_{jj} = j^{th} generalized modal mass, damping, and stiffness respectively

For the rigid body modes $C_{jj} = K_{jj} = 0$, and

$$H_j(\bar{\omega}_n) = \frac{1}{-\bar{\omega}_n^2 M_{jj}} \quad (31)$$

It can be shown that the total response of a system to any forcing input can be written by means of Inverse Fourier Transformations (IFT). The displacements of the j^{th} modal coordinate are given by ⁸

$$\eta_j(\tau) = \frac{\Delta\bar{\omega}}{2\pi} \sum_{n=0}^{N-1} H_j(\bar{\omega}_n) C_j(\bar{\omega}_n) e^{i\bar{\omega}_n\tau} \quad (32)$$

or since $\bar{\omega}_n = n\Delta\bar{\omega}$ and $\Delta\bar{\omega} = \bar{\omega}_n/N$; $\eta_j(\tau) = \frac{\Delta\bar{\omega}}{2\pi} \sum_{n=0}^{N-1} H_j(n+1)C_j(n+1)e^{2\pi i n\tau/N}$ (33)

Both the DFT harmonic amplitude coefficients of the generalized forces, Eq. (29), and the IFT to solve for generalized displacements, Eq. (33), can be rapidly generated by modern Fast Fourier Transform (FFT) algorithms ¹¹.

Modal accelerations can be evaluated from the second time derivative of Eq. (33)

$$\ddot{\eta}_j(\tau) = \frac{\Delta\bar{\omega}}{2\pi} \sum_{n=0}^{N-1} H_j(n+1)C_j(n+1) \left(\frac{-4\pi^2 n^2}{N^2}\right) e^{2\pi i n\tau/N} \quad (34)$$

The structure nodal coordinate displacements can be obtained from the modal superposition equations

$$\begin{matrix} \{u(\tau)\} \\ n \times 1 \end{matrix} = \begin{matrix} [\phi] \\ n \times p \end{matrix} \begin{matrix} \{n(\tau)\} \\ p \times 1 \end{matrix} \quad (35)$$

Other response parameters such as stresses or loads developed in various structural components can be evaluated directly from the displacements. For example, the elastic forces $\{f\}$ which resist the deformation of the structure are given directly by the displacements and the structure stiffness coefficients.

$$\{f(\tau)\} = [k] \{u(\tau)\} = [k] [\phi] \{n(\tau)\} \quad (36)$$

An alternative expression for the elastic forces can be written in terms of the structure mass matrix and natural frequencies. Expanding Eq. (36) in terms of the modal contributions

$$\{f(\tau)\} = [k] \{\phi_1\} \eta_1(\tau) + [k] \{\phi_2\} \eta_2(\tau) + \dots + [k] \{\phi_p\} \eta_p(\tau) \quad (37)$$

Substitute Eq. (12) in each term of Eq. (37)

$$\{f(\tau)\} = \omega_1^2 [m] \{\phi_1\} \eta_1(\tau) + \omega_2^2 [m] \{\phi_2\} \eta_2(\tau) + \dots + \omega_p^2 [m] \{\phi_p\} \eta_p(\tau) \quad (38)$$

Combining back into matrix form

$$\{f(\tau)\} = [m] [\phi] \left\{ \begin{array}{c} \omega_j^2 \eta_j \\ \uparrow \\ \downarrow \end{array} \right\} (\tau) \quad (39)$$

where $\{\omega_j^2 \eta_j(\tau)\}$ represents a vector of modal amplitudes, each multiplied by the square of its modal frequency.

In Eq. (36), if $[k]$ is the substructure stiffness matrix and $\{u(\tau)\}$ is the list of substructure coordinate displacements then $f(\tau)$ are the total elastic forces at the substructure nodal coordinates. To obtain the internal stresses at particular locations in the substructure, the elemental stiffness matrices and the corresponding element vertex displacements are used.

$$\{f'(\tau)\} = [k'] \{u'(\tau)\} \quad (40)$$

where prime indicates the quantities that are defined with respect to elemental vertex coordinates.

If elemental stiffness information is not available, the internal forces can also be obtained in a different manner. First the total elastic forces are determined at the structure coordinates according to Eq. (36). Then a section is passed through the structure including the nodal coordinates where the internal stresses are required. Eq. (36) is partitioned into three groups of coordinates and is written as

$$\left\{ \begin{array}{c} f_1 \\ \hline f_2^* \\ \hline f_3^* \end{array} \right\} = \left[\begin{array}{ccc|ccc} k_{11} & & & k_{12} & & & 0 \\ \hline & k_{21} & & & k_{22} & & k_{23} \\ \hline 0 & & & & & k_{32} & k_{33} \end{array} \right] \left\{ \begin{array}{c} u_1^* \\ \hline 0 \\ \hline 0 \end{array} \right\} \quad (41)$$

where $\{f_2\}$ correspond to the coordinates through which the section is passed. $\{f_1\}$ and $\{f_3\}$ are attached to nodes on either side of the section.

Fixing one side of the substructure separated by the section we write $\{u_2\} = \{u_3\} = \{0\}$. From the first row of Eq. (41)

$$\{u_1^*\} = [k_{11}]^{-1} \{f_1\} \quad (42)$$

where $\{u_1^*\}$ are the pseudo-displacements if the elastic forces $\{f_1\}$ were applied on the substructure with the assumed sectional fixity. The actual internal forces, $\{f_2^*\}$, at the sectioned coordinates can now be obtained from the pseudo-reactions or

$$\{f_2^*\} = [k_{21}] \{u_1^*\} \quad (43)$$

Eq. (43) is a rather indirect and inefficient method of evaluating internal loads. It should only be used as a last resort when elemental stiffness information is not available.

VI. APPLICATION OF METHOD TO TAXIING AIRCRAFT

The analysis of taxiing aircraft response over irregular runways is of immediate concern. Currently the Air Force is in the process of assessing the operability requirements for specific aircraft on Battle Damaged Repaired (BDR) runways. It is necessary to have an analysis capability that will determine the total aircraft response to possible runway repair profiles. With the use of an efficient and reliable mathematical model, parametric studies can be made to map out acceptable runway repair patterns and tolerances.

To determine the response of taxiing aircraft, the equations of dynamic equilibrium are written for the aircraft vehicle and the unsprung masses of the suspension systems. First, the nonlinear time-history analysis is carried out in terms of the rigid-body and flexible modal coordinates. Runway irregularly induced forces are transmitted through tires that are represented by linear or nonlinear springs. Landing gear unsprung masses transmit the tire loads to the nonlinear suspension struts. The suspension struts are multiple level energy absorption and dissipation systems. Strut forces are highly nonlinear functions of strut deformation and velocity of deformation. The strut forces are transmitted to the aircraft vehicle

at the gear attachment points.

In simulating taxiing aircraft over irregular runways, the vertical, longitudinal, and pitch rigid body modes are significant for the vehicle. The roll mode is also needed when runway irregularities are asymmetrical. Only the vertical modes are usually considered for the unsprung suspension masses. Vehicle flexibility is taken into account in terms of the elastic free vibration modes. Assuming that the flexible vibration modes are determined with respect to the unconstrained vehicle structure, the generalized mass matrix is diagonal including the rigid body modes. However, because the nonlinear forces depend upon all coordinate deformations, the equations of motion must be solved simultaneously. Presently the FDL-TAXI computer program is successfully being used to perform the time-history integrations in the above described manner. The FDL-TAXI program is relatively simple compared to other computer programs that serve the same purpose. Yet, TAXI has been validated by extensive tests and yields excellent simulations for the nonlinear strut forces. Details of the TAXI program are well documented in reference ¹². The remainder of this section is to delineate the computation of linear vehicle response from the results of the TAXI computer program.

Considering a symmetric irregularity profile, the modal transformation equations, Eq. (15), can be written as

$$\begin{matrix} \{u\} = [\phi_R] \{u_R\} + [\phi_F] & \{q\} \\ n \times 1 & n \times 3 & 3 \times 1 & n \times (p-3) & (p-3) \times 1 \end{matrix} \quad (44)$$

where

$\{u_R\}$ = the displacements of vertical, longitudinal, and pitch rigid body modes

$[\phi_R]$ = matrix of rigid body influence coefficients corresponding to vertical, longitudinal, and pitch modes

The other symbols are defined as in Eq. (15). However, the total number of modes considered, p , is now a larger number than that used in the time-history analysis. The aircraft vehicle is considered as a single linear

substructure including sprung masses of the suspension systems. The vehicle linear response under the time-history suspension strut forces, aerodynamic forces, and gravity can be obtained through the frequency domain. The orthogonal modal equations of motion Eq. (24) and Eq. (25), yield the CFRF given by Eq. (31) and Eq. (30) respectively.

The time-history forces are first transformed to generalized modal coordinates as indicated in Eq. (24) and Eq. (25). The generalized forces are converted to the frequency domain by the discretized harmonic-amplitude coefficients of Eq. (29). The harmonic-amplitude coefficients are combined with the modal CFRF in the frequency domain. Inverse transformation by Eq. (32) yields the real modal response. The vehicle nodal coordinate displacements, accelerations, elastic forces and internal loads are obtained by modal superposition as explained in the previous section.

VII. RECOMMENDATIONS

A new hybrid method has been formulated for the transient response analysis of partially nonlinear structures. At this stage, the results are vulnerable to testing. The viability of this method must be demonstrated by its implementation to systems which have been or can be physically tested. The comparison of the developed method to time-history analysis with parametric discretization refinements of the time domain can help evaluate the relative efficiency and reliability of the new method.

Other combinations of time-history and frequency domain analyses should also be studied. An interactive method that resorts to a frequency domain analysis at each time increment may be cost effective for a realistic representation of the higher modes. A step-iterative procedure can make time-history corrections from higher frequency modal response evaluations.

In Section IV, the unconstrained and constrained formulations for substructural free vibration problems were explained. It was shown that the accelerations of the dynamic center of mass must also be evaluated by time-history analysis if a constrained vibration problem is to define the modal basis. The acceleration vector of the dynamic center of mass is not expected to be sensitive to the higher vibration modes. However, the necessity of restraining the frequency domain analysis by force and acceleration information from only the lower modes may squeeze out the higher vibration modal response

from the simulation. The relative merits and deficiencies of the constrained and unconstrained free vibration formulations should be studied to assess the best choice for a particular application. The possibility of numerical improvements in the substructural vibration problems should also be explored. Tradeoff studies which assess the relation of substructure size to modal accuracy would help identify realistic vibration problem formulations.

The number of modes to be included to represent the response of a specific component to a given accuracy will usually be different for each case. The number of necessary modes can be assessed by consecutive sampling, comparison with test data or by engineering intuition and experience. The formulation outlined in this report assumes that the original finite element model is sufficiently accurate to extract the required modal information necessary to define the response of critical components. It would be helpful to study specific modeling requirements before the method is applied to a given system.

Finally, it is recommended that the proposed method be first implemented by its application to simulate taxiing aircraft. Test data on the component dynamic response of specific aircraft already exists. There are also a number of independent time-history simulation results that have tried to predict the dynamic response. Physical property data for specific tested aircraft is available at the FDL. The results of the present method can be immediately compared to existing test data and simulations when applied to those aircraft. Nevertheless, it is conceded that the best validation for a transient response model can be obtained by the use of a controlled loading environment. It is hoped that after implementation to taxiing aircraft, the new model can be evaluated by parallel testing on a ground induced loading facility such as AGILE (Aircraft Ground Induced Loading Environment) which is being planned by FDL.

REFERENCES

1. Przemieniecki, J. S., Theory of Matrix Structural Analysis, McGraw-Hill Book Company, 1968.
2. Mallett, R. H., and Marcal, P. V., "Finite Element Analysis of Non-linear Structures," Proceedings, American Society of Civil Engineers, Volume 94, No. ST9, Journal of the Structural Division, pp. 2081 - 2105, 1968.
3. Bathe, K. J., and Gracewski, S., "On Nonlinear Dynamic Analysis Using Substructuring and Mode Superposition," Computers and Structures, Volume 13, No. 5-6, pp. 699 - 707, October-December 1981.
4. Gerardi, T. G., and Riechers, J. T., Test and Evaluation of the High Pressure Strut Concept on the F-4 Main Landing Gear, Report No. AFWAL/FIBE-81-1, May 1981.
5. Tischler, V. A., Venkayya, V. B., and Palazotta, A. N., "Dynamic Analysis of High Speed Rocket Sleds," ASME Paper No. 81-DET-42, to be presented at the Design Engineering Technical Conference, September 20 - 23, 1981, Hartford, Connecticut
6. Card, M. F., and Boyer, W. J., "Large Space Structures - Fantasies and Facts," AIAA/ASME/ASCE/AHS, 21st Structures, Structural Dynamics and Materials Conference, Collection of Technical Papers, Part 1, pp. 101 - 123, Seattle, Washington, May 12 - 14, 1980.
7. Crandall, S. H., Engineering Analysis, McGraw-Hill Book Company, 1956.
8. Clough, R. W., and Penzien, J., Dynamics of Structures, McGraw-Hill Book Company, 1975.
9. Meirovitch, L., Elements of Vibration Analysis, McGraw-Hill Book Company, 1975.

10. Meriam, J. L., Engineering Mechanics, Volume 2: Dynamics, John Wiley and Sons, Inc., 1978.

11. International Mathematical and Statistical Libraries (IMSL), IMSL Reference Manual, Edition 7, IMSL, Inc., 1979.

12. Gerardi, A. G., Digital Simulation of Flexible Aircraft Response to Symmetrical and Asymmetrical Runway Roughness, AFFDL-TR-77-37, Air Force Flight Dynamics Laboratory, Wright-Patterson AFB OH 45433, August 1977.

1981 USAF-SCEEE SUMMER FACULTY RESEARCH PROGRAM

Sponsored by the

AIR FORCE OFFICE OF SCIENTIFIC RESEARCH

Conducted by the

SOUTHEASTERN CENTER FOR ELECTRICAL ENGINEERING EDUCATION

FINAL REPORT

PLASMID FINGERPRINTS OF STAPHYLOCOCCUS AUREUS STRAINS ISOLATED FROM

A TOXIC SHOCK SYNDROME FEMALE PATIENT

Prepared by:	Dr. Rex C. Moyer
Academic Rank:	Associate Professor
Department and University:	Department of Biology Trinity University
Research Location	Division of Epidemiology, School of Aerospace Medicine, Brooks Air Force Base, Texas
USAF Research Colleague:	Dr. Louis Blouse
Date:	August 24, 1981
Contract No:	F49620-79-C-0038

PLASMID FINGERPRINTS OF STAPHYLOCOCCUS AUREUS STRAINS
ISOLATED FROM A TOXIC SHOCK SYNDROME FEMALE PATIENT

by

Rex C. Moyer

ABSTRACT

The objective was to use plasmid fingerprinting as a means of identifying various strains of a bacterial pathogen isolated during disease outbreaks among Air Force personnel and to determine if it would help track nosocomial infections.

Four isolates of Staphylococcus aureus from the urine, cervix, and throat from a female patient with toxic shock syndrome which could not be differentiated by conventional techniques were used as models. Escherichia coli V517 and other strains with plasmids of known molecular weight were used as reference DNA. Plasmid DNAs were purified by several techniques (and modifications thereof). DNAs were electrophoresed on 0.8% agarose vertical slab gels. The electropherograms were stained with ethidium bromide and photographed with long wave UV light. Molecular weights of plasmid DNAs were estimated by comparison of their migration with plasmids of known molecular weight. The plasmid fingerprints of S. aureus isolates from the 3 different body sites were all unique but plasmid fingerprints from the two isolates from urine were identical. Different

DNA isolation techniques yielded different plasmid fingerprints, therefore, precise numbers of plasmids and their molecular weights were not obtained.

I conclude that plasmid fingerprinting can differentiate various S. aureus strains and probably will be useful for tracking nosocomial infections.

ACKNOWLEDGEMENT

I would like to thank the Air Force Systems Command, the Air Force Office of Scientific Research and the Southeastern Center for Electrical Engineering Education for providing me the opportunity to participate in a valuable research experience at the Division of Epidemiology, School of Aerospace Medicine, Brooks Air Force Base, Texas. My thanks are particularly directed to the members of the Microbiology Branch, for their help and for making my brief stay very pleasant.

My personal thanks to Dr. Louis Blouse and Captain Barbara Schramm for their collaboration and guidance and to Dr. Jerome Schmidt for many helpful discussions.

I. INTRODUCTION:

The design of procedures to halt nosocomial epidemics requires the identification of reservoirs of infection and the mode of pathogen transmission. Thus, the identification and differentiation of bacteria isolated during epidemiological studies is often required. Methods of bacterial species identification include biotyping, antimicrobial susceptibility patterns, serotyping, bacteriocin production, bacteriocin susceptibility, and phage typing. Unfortunately, no typing schemes have been developed for many bacterial pathogens and those that do exist for some pathogens such as Staphylococcus aureus, are insufficient for strain identification.

Recently, many clinical and epidemiological laboratories have been using agarose gel electrophoresis of the total plasmid contents (plasmid fingerprints) of nosocomial bacteria as excellent markers of individual strains and as tools for investigating the epidemiology of nosocomial infections.

Parisi and Hecht (1980)¹ have studied the plasmid fingerprints of Staphylococcus epidermidis nosocomial isolates and have confirmed the utility of the procedure.

Toxic shock syndrome is a disease predominantly of young women. The clinical features of this acute illness are fever, diarrhea, conjunctivitis, myalgia, marked hypotension and rash. The onset of the disease occurs during menses and the frequent recovery of S. aureus

from the vagina from women with the disease has prompted epidemiological studies on possible menses-related risk factors. Tampon usage was found to be a significant risk factor of the disease² and S. aureus infection appears to always be associated with the disease².

The pathogenesis of toxic shock syndrome by S. aureus infection is poorly understood but the serious, systemic manifestations of a local (vaginal) infection suggest that a toxin or toxins are involved.

Attempts have been made to identify the characteristics of S. aureus that are always or very commonly present in toxic shock syndrome - associated S. aureus strains to serve as markers in epidemiological studies³. Certain phenotypic traits of the bacteria were more commonly associated with isolates for toxic shock syndrome patients than isolates from non-toxic shock syndrome patients³. Since toxic shock syndrome - like strains were recovered from approximately 20% of healthy or only slightly symptomatic women from whom S. aureus was a vaginal inhabitant³, these traits are not adequate as markers for epidemiological studies.

The Epidemiology Division had earlier received four S. aureus strains isolated from the urine, cervix, and throat of a female patient with toxic shock syndrome. I have not had access to the results of the biotyping, antibiotic sensitivity, and phage typing tests performed on these four clinical isolates, but Dr. Louis Blouse, Chief, Microbiology Branch, Epidemiology Division informed me (personal communication)

that the four S. aureus isolates were indistinguishable by the tests performed. Thus, Dr. Blouse recommended that I investigate the use of plasmid fingerprints of the four clinical S. aureus isolates from a female patient with toxic shock syndrome to determine if these four isolates could be differentiated by this technique. I was selected to perform this study because of my experience both as a microbiologist and as a molecular biologist working with DNA.

II. OBJECTIVES:

Conventional tests for identification of various strains within a bacterial species are insufficient for many isolates of S. aureus. Plasmid fingerprinting is a technique which has great potential for strain identification within a species and thus for tracking the mode of transmission of hospital-acquired infections. Plasmid fingerprinting is a tool currently under investigation in many laboratories for bacterial pathogen study. Much research has been done on the genetics of S. aureus plasmids, especially as they relate to the host's toxin production and antibiotic resistance. However, plasmid fingerprinting of S. aureus has not been used as a tool for epidemiological investigations, to my knowledge.

My objective for this ten-week period was to investigate the possibility of using plasmid fingerprinting of bacterial pathogens as an additional tool in strain identification in various disease outbreaks occurring in Air Force personnel. The Epidemiology Division currently does not use plasmid fingerprinting for bacterial strain identification.

The toxic shock syndrome isolates provided a convenient test system since the four isolates could not be differentiated by conventional techniques. Ultimately, plasmid fingerprinting may be applied to strain identification of many different medically important bacteria.

III. MATERIALS AND METHODS

A. Bacterial Strains and source

1. Staphylococcus aureus strains (toxic shock syndrome isolates).

129	2011	UA	Y	(urine isolate)
130	2105	CX		(cervical isolate)
131	2011	UA	White	(urine isolate)
132	2066	T/C		(throat isolate)

2. Strain from Dr. Joseph Parisi, University of Missouri

Medical School

Escherichia coli

<u>Strain</u>	<u>Plasmid</u>	<u>Plasmid Mass (daltons)</u>
V517		1.36 x 10 ⁶
		1.79 x 10 ⁶
		2.03 x 10 ⁶
		2.63 x 10 ⁶
		3.39 x 10 ⁶
		3.67 x 10 ⁶
		4.82 x 10 ⁶
		35.84 x 10 ⁶

3. Eschirichia coli strains (from Dr. Al McManus, Surgical Research Unit, Fort Sam Houston)

<u>Strain</u>	<u>Plasmid</u>	<u>Plasmid Mass (daltons)</u>
J53-1	Sa-1	26 x 10 ⁶
J53	R6K	26 x 10 ⁶
J53	R46	33 x 10 ⁶
J53	RP4	36 x 10 ⁶
J53	R1	62 x 10 ⁶
J53-1	R621-A	65 x 10 ⁶
J53-1	R16	69 x 10 ⁶
Rc712	Col b	70 x 10 ⁶
J33-1	RA-1	86 x 10 ⁶
Foc 600		
J53-1	R4466	
J53	R124	
J53-1		
J53	R386	
J53	R387	
J53-1	R726	
J62-1		
J53-1	R401	
J53	A391	
*C601	138E	2 plasmids (?)
*C601	RP1	40 x 10 ⁶

between the procedures employed and, at this point, there is no way of knowing which if any, of these procedures yielded the "true" fingerprint. The protocols are all detailed in my research note book, a copy of which was placed in the hands of Dr. Louis Blouse.

Preparation #1 - Hansen and Olsen⁵ technique

Preparation #2 - Modified Elwell and Falkow⁶ and Hansen and Olsen⁵ techniques. Modification caused by lack of certain reagents.

Preparation #3 - Slightly modified Elwell and Falkow⁶ technique. Slight modification caused by lack of certain reagents.

Preparation #4 - Combination of certain components of the Elwell and Falkow⁶ and Hansen and Olsen⁵ techniques but including a deproteinization step using a neutralized phenol-chloroform mixture (1:1).

2. E. coli V517 contains eight different plasmids of known molecular weight for use in estimating the molecular weights of unknown plasmids (Macrina et al⁴). Three different preparations of E. coli V517 DNA have been made.

Preparation #1 - Hansen and Olsen⁵ technique

Preparation #2 - Hansen and Olsen⁵ technique

Preparation #3 - Modified and shortened procedure using portions of the following procedures: Hansen and Olsen⁵, Elwell and Falkow⁶, Macrina et al⁴, and Clewell and Helinski⁷.

3. The following E. coli strains from Dr. McManus have been grown, harvested and DNA extracted by the same procedure as preparation #3 of E. coli V517.

J53-1	Sa-1	26×10^6
J53	R46	33×10^6
J53	RP4	36×10^6
J53	R-1	62×10^6
Rc712	Col b	70×10^6

D. Agarose Gel Electrophoresis

Agarose gel electrophoresis to separate the plasmids of various sizes from each other and from chromosomal DNA was performed essentially as described by Hansen and Olsen⁵. Electrophoresis procedures have been performed in my laboratory at Trinity University using a vertical slab gel apparatus (Model 220) purchased from Bio Rad. All agarose gels made to date were 0.8% in E buffer as described by (Meyers et al⁸). A recent modification has been to produce a 3 ml of 1.2% agarose (in E buffer) at the bottom of the gel to slow the migration of low molecular weight plasmids. Electrophoresis was carried out at 100 volts, about 30 miliamps for 2-3 hours or until the tracking dye reached the bottom of the gel.

E. Photography of Plasmid DNA Electropherograms.

Gels after electrophoresis were removed from apparatus and stained with about 1 ug/ml of Ethidium bromide (in distilled water) for 15 - 30 minutes. Gloves were worn for all procedures using ethidium

bromide. The gels were rinsed briefly with deionized water and photographed essentially as described by Parisi' (personal communication from Dr. Joseph Parisi to Dr. Louis Blouse) except that the polaroid PN 55 film was exposed for 90 seconds rather than 50-60 seconds.

F. Estimation of Plasmid Molecular Weights.

Plasmid DNA molecular weights were estimated by the method of Meyers et al⁸ using plasmids of E. coli V517 (Macrina et al⁴) as known reference markers to establish the standard curve.

IV. RESULTS:

Plasmid DNA was extracted by five different procedures from S. aureus strains 129, 130, 131, and 132. Plasmid DNA was extracted from E. coli V517 by three different procedures. Plasmid DNA was also extracted from the five additional E. coli strains each bearing one plasmid -- Sa-1, R46, RP4, R-1, and Col b. All these DNAs were analyzed by electrophoresis on fifteen separate 0.8% agarose vertical slab gels. Each slab gel could fractionate 10 or 20 samples, depending upon the type of sample - well-forming comb used to insert into the molten agarose.

Figure 1 shows representative plasmid fingerprints of electropherogram gel No. 8 DNA from preparations 1, 2 and 3 of E. coli V517 and preparation No. 2 from S. aureus strains 129, 130, 131 and 132. Figure 1 shows quite clearly that E. coli V517 DNA preparation No. 3 yielded distinct plasmid bands. Each band migrated the appropriate distance through the agarose gel to yield a straight line when each band was assigned its molecular weight as published by Macrina et al⁴.

Tracts 6, 7, 8, and 9 (from the left) show relatively distinct (plasmid) DNA bands from S. aureus strains 129, 130, 131, and 132, respectively. Streaking in the low molecular weight region (bottom) of the gel is very likely due to RNA since extraction procedures utilizing an RNAase treatment shows lessened or no such streaking in their electropherograms.

Figure 2 shows a typical standard curve (from gel No. 14) generated from the plasmids from E. coli Col b strain. A standard curve was prepared for every gel and they were generally parallel but the absolute values varied slightly -- probably due to small differences in time of electrophoresis for each gel. Some standard curves differed slightly in slope which was probably due to small differences in agarose concentration or electrolyte concentration in the gels.

Tables 1 through 3 show the results of the analyses of the electropherograms of gels 5-15. These data include DNA preparations 1-5 of the four S. aureus strains.

Table 4 shows the molecular weights of E. coli V517 plasmids. DNA preparation No. 3 of E. coli V517 shows several DNA bands more than those described by Macrina et al⁴. Only preparation No. 3 produced the highest molecular weight plasmid (36 megadalton) described for E. coli V517. Procedures used in preparations 1 and 2 did not produce this 36 megad plasmid.

The numbers of (plasmid) DNA bands varied from preparation to preparation and from gel to gel even from the same preparations within a strain. Preparations 2 and 5 produced the greatest number of DNA bands in all four of the S. aureus strain DNAs. However, even these preparations stored poorly because a number of DNA bands disappeared upon subsequent electrophoretic analysis.

A great deal of similarity appeared in the plasmid fingerprints of strains 129 and 131 which one might expect since they were both urine isolates. However,...strain 131 as seen in track No. 8 (Fig. 1) shows three tight bands at the top of the smear region with estimated molecular weights of 1.45, 1.50, and 1.55 million, respectively; whereas strain 129 only shows one sharp band (on top of the RNA smear). It is possible that the other small molecular weight bands of strain 129 are obscured by the RNA smear.

The plasmid fingerprints of 129/131, 130, and 132, however, were all distinct and one can easily distinguish differences in the plasmid fingerprints and thus the strains merely by inspection of the photographs of the electropherograms (e.g., tracts 6, 7, 8, and 9 in Fig. 1).

V. DISCUSSION:

Different extraction procedures produced different plasmid fingerprints even within a single strain. This was true both for the number of bands produced on electropherograms and also the sharpness and clarity of the bands. In these experiments, the best plasmid profiles of the four S. aureus strains were produced by preparations 2 and 5.

I would define "best" by stating that these preparations gave the greatest number of and sharpest (plasmid) DNA bands. I think some caution must be made in this assumption till future experimentation confirms or denys this. Even these preparations appeared to deteriorate even though the DNAs were stored frozen and kept in an ice bath when thawed for sampling for electrophoresis. This can be interpreted in several - not necessarily mutually exclusive ways; (1) DNAse molecules survive the purification process and continue to degrade the DNA; (2) RNA or protein components of the plasmid DNA superhelix exist and these are degraded by RNAase or protease; (3) plasmid DNAs may be sticking to the sides of the glass tube or precipitating in the tube, as precipitates are sometimes observed upon thawing; (4) Larger plasmid DNA molecules may be subject to shear forces created by drawing the DNA up in capillary tubes. It is possible that all of these phenomena are occurring and thus steps must be taken in future studies to rule them out or eliminate them. The least likely possibility, to me, appears to be the first--surviving DNAase. This is because the DNAs are stored in the presence of EDTA which chelates divalent cations Ca^{++} and Mg^{++} which are required by known DNAases for activity. It cannot be ruled out, however, that nucleases not required divalent cations persist to degrade the plasmids. One observation does, to some extent, support the enzymatic degradation of plasmids hypotheses. That is, DNA prepared from E. coli V517 and the other E. coli

strains were prepared similarly - yet E. coli V517 DNA was much more stable than the other E. coli DNA. This suggests that V517 may possess fewer or less active nucleases than the other strains. Other interpretations of this observation are also possible.

It is quite clear from these experiments also that extraction procedures that yield good plasmid fingerprints from one species may be ineffective for another species. This observation was also made by Dr. Al McManus (personal communication).

The E. coli strains all possessed plasmids of known molecular weight to use as a reference for estimation of the molecular weights of the plasmids from S. aureus. Unfortunately, the E. coli strains carrying the high molecular weight plasmids to aid in estimating the molecular weights of the large S. aureus plasmids were obtained late in the project. Therefore, through much of the project, the plasmid fingerprints of the four S. aureus strains had to be analyzed without high molecular weight reference molecules. This resulted in a greater error in the estimated molecular weights of the large plasmids of S. aureus.

The best plasmid fingerprints were obtained from E. coli V517 (Fig 1). Preparation No. 3 of E. coli V517 DNA (Fig. 1) produced good plasmid fingerprints and also showed more DNA bands than described by Macrina et al⁴. The same procedure (No. 3) that yielded excellent plasmid fingerprints of E. coli V517 produced rather poor plasmid fingerprints from the E. coli strains carrying plasmids Sa-1, R46, RP4, R-1, and Col b (data not shown).

Plasmid fingerprints from these strains generally produced one or two DNA bands more than expected, and the bands were generally fuzzy and indistinct. The stability of the DNA from these strains was poor as repetitive tests of the same DNA preparation yielded different - often disappearing - DNA bands on the electropherograms. Even with these difficulties, the plasmid DNA from Sa-1, R46, RP4, and Col b did aid in the analysis of some gels and did help confirm the slope of the regression line used for estimation of plasmid molecular weights. DNA from strain R-1 did not yield a band which migrated an appropriate distance for its known molecular mass of 62 megadaltons (Dr. Al McManus, Fort Sam Houston, personal communication).

The experiments made to date cannot yet provide an optimal plasmid DNA extraction/purification procedure even though they do provide suggestions for future studies. Neither is it possible to yet assign the absolute number of plasmids to each S. aureus strain or to assign each plasmid a molecular weight. This study does, in my opinion obtain the goal of the project. That is, the data do support that plasmid fingerprinting of these S. aureus strains does differentiate the strains where conventional techniques do not. Thus, I conclude that plasmid fingerprinting could be developed to be used as a tool for identifying and tracking diseases of epidemiological significance.

VI. RECOMMENDATIONS

Any agency whose mission is to identify and trace the source of infectious disease must attempt to accomplish these tasks with the tools at hand. Unfortunately, the available protocols are insufficient for differentiating various strains within some pathogenic species. Thus with opportunistic pathogens such as S. aureus which colonize several sites of most people, it is impossible to determine which strain is responsible for a given disease. The problem has recently become more acute with the upsurge of antibiotic resistance among previously antibiotic sensitive bacteria.

Large organizations with many personnel scattered over the earth must constantly deal with infectious disease and occasionally epidemics. With the increased resistance of existing disease agents and the advent of new diseases such as Legionnaires Disease, it behooves the diagnostic and epidemiology laboratories to constantly update and upgrade their diagnostic procedures through research and education.

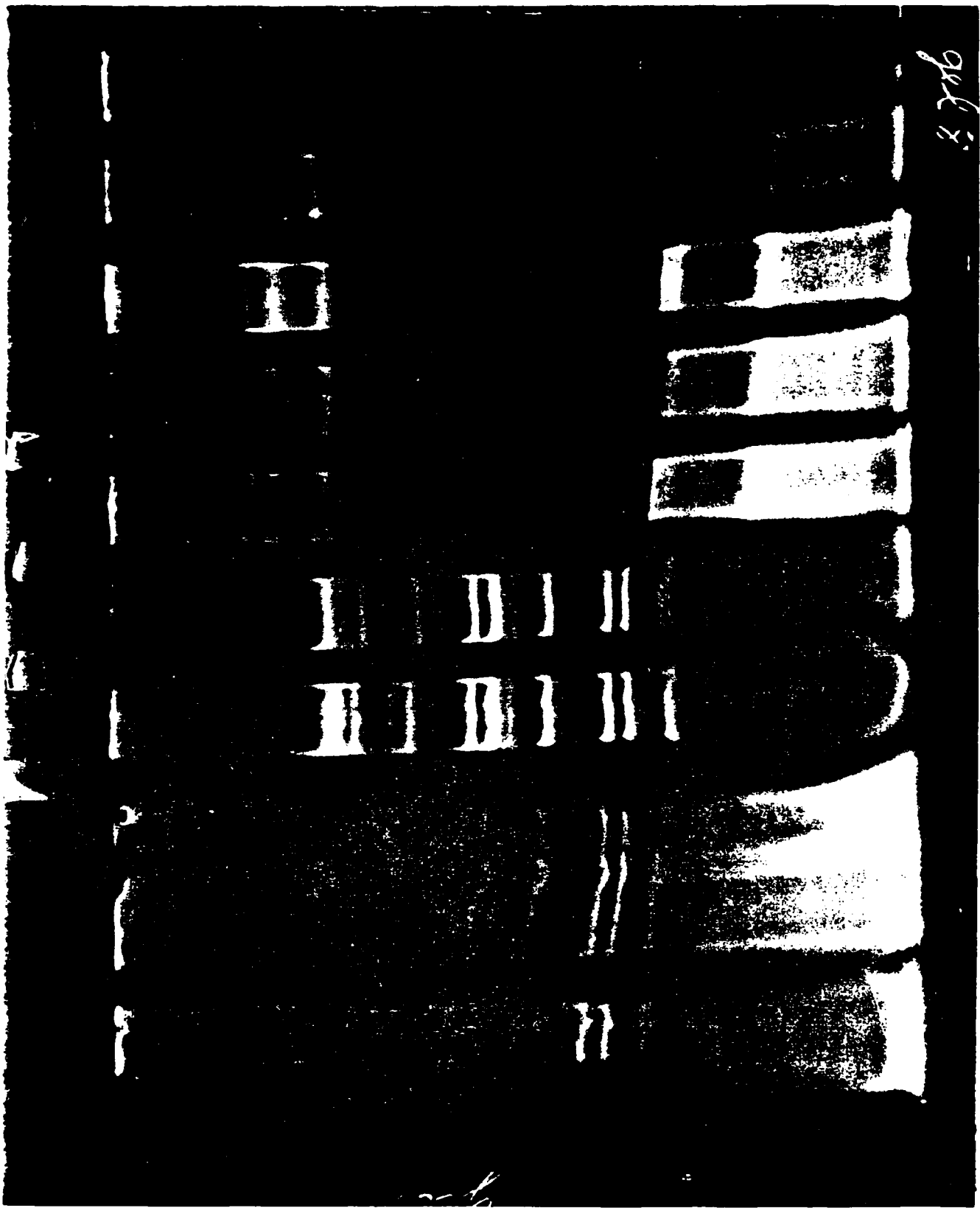
This research as well as personal communications with active medical/clinical microbiologists (i.e., Dr. Louis Blouse, Dr. Al McManus, Capt. Barbara Schramm) and literature sources, all indicate a gap in our technology for tracking nosocomial infections. This research and literature sources as well as personal communications supports the contention that plasmid fingerprints of various strains of a pathogenic species are sufficiently different and sufficiently stable to serve as means for differentiation between the strains.

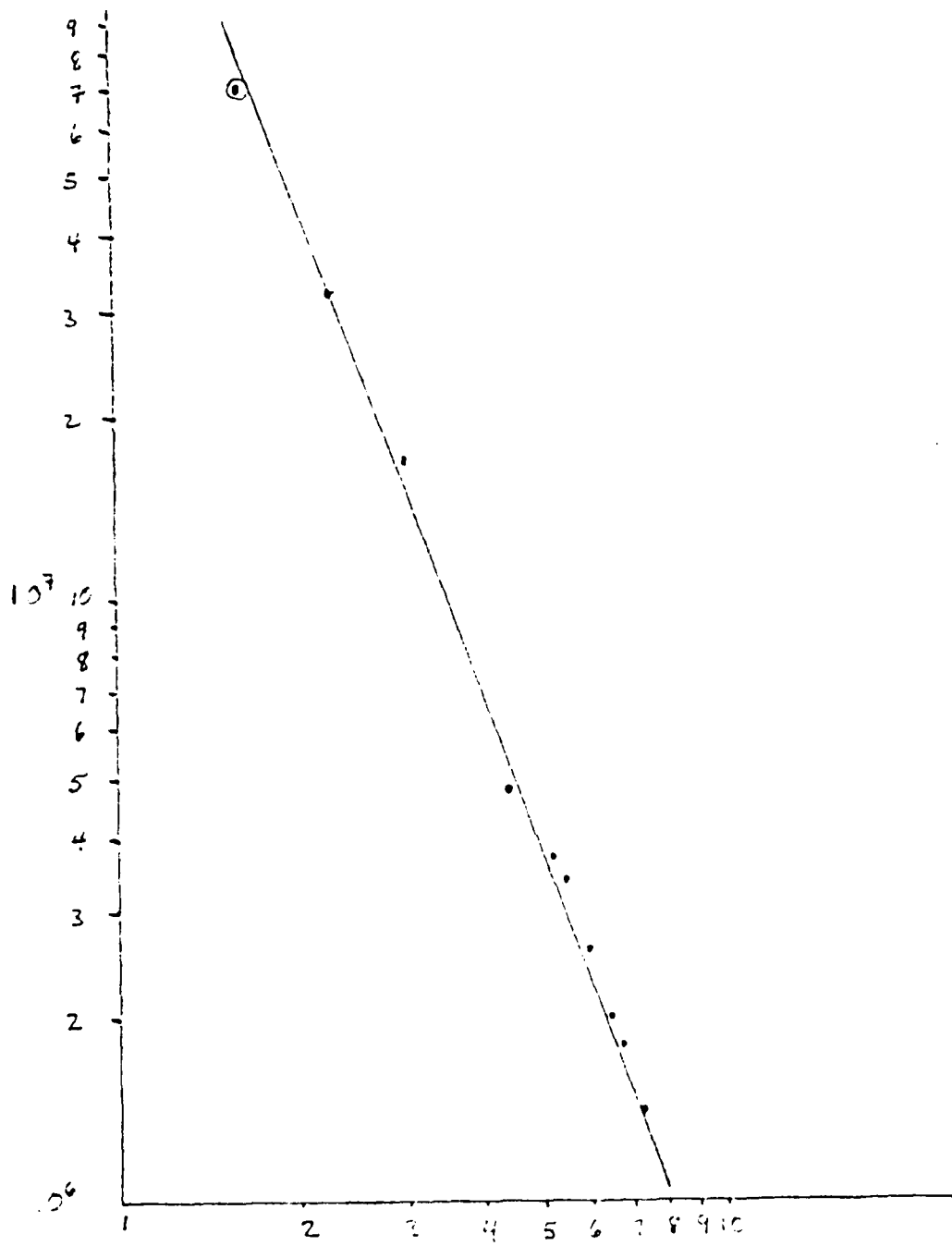
I would recommend that the Air Force put forth some degree of effort to utilize plasmid fingerprinting to supplement contemporary techniques in certain disease-producing bacterial species where the conventional techniques are inadequate. Exactly which pathogenic species these words apply to would have to be determined by Air Force epidemiologists and physicians. Air Force planners would also have to determine the level of funding in this endeavor. It might be more cost effective to determine which pathogenic organisms are of greatest concern to Air Force medicine and then fund contracts and grants to outside investigators to develop protocols for plasmid fingerprinting those organisms.

FIGURE 1. Photograph of gel No. 8 electropherogram.

A 20 ul sample composed of 15 ul DNA and 5 ul of tracking dye was applied to each well. Electrophoresis was at 100 volts, 27 milliamps for 3 hours. The gel was stained with 1 ug/ml ethidium promide, rinsed and illuminated with long wave length ultraviolet light for photography. The samples from left to right are:

<u>Tract No.</u>	<u>Source of DNA</u>
1	<u>E. coli</u> V517-1 (preparation no. 1)
2	<u>E. coli</u> V517-2 (preparation no. 2, PEG precipitate)
3	<u>E. coli</u> V517-3 (preparation no. 2, ethanol precipitate)
4	<u>E. coli</u> V517-3 (preparation no. 3, PEG precipitate)
5	<u>E. coli</u> V517-3 (preparation no. 3, ethanol precipitate)
6	<u>S. aureus</u> 129-2 (preparation no. 2)
7	<u>S. aureus</u> 130-2 (preparation no. 4)
8	<u>S. aureus</u> 131-2 (preparation no. 2)
9	<u>S. aureus</u> 131-2 (preparation no. 2)
10	<u>E. coli</u> V517-1 (preparation no. 1)





RELATIVE MIGRATION (CM)

FIGURE 2. Standard Curve for Estimating Weights of Plasmid DNA.
 The standard curve was plotted from the distances migrated by the plasmid DNA in gel No. 14 electropherogram and the published molecular weights assigned to each plasmid. The reference plasmids are from E. coli strains V517 (.-.) and Col b (-0-).

TABLE 1. ESTIMATED MOLECULAR WEIGHTS OF PLASMID DNA BANDS OF STAPHYLOCOCCUS AUREUS STRAINS 129, 130, 131, and 132 OBSERVED IN GELS NO. 5 & 6.

Strain No.	<u>129-1</u>	<u>129R01</u>	<u>129-2</u>	<u>129-2</u>	<u>129-3</u>	<u>129-3 (20 ul)</u>
Gel No.	<u>gel 5</u>	<u>gel 5</u>	<u>gel 5</u>	<u>gel 6</u>	<u>gel 6</u>	<u>gel 6</u>
Mw			0.9			
(millions)	24.5	26.5	1.35	1.25	1.25	1.3
			27.5	19.5	28.0	2.3
			45.0	25.0	41.0	23.0
			90.0	60.0		28.0
Strain No.	<u>130-1</u>	<u>130R-1</u>	<u>130-2</u>	<u>130-2</u>	<u>130-3</u>	<u>130-3 (20 ul)</u>
Gel No.	<u>gel 5</u>	<u>gel 5</u>	<u>gel 5</u>	<u>gel 6</u>	<u>gel 6</u>	<u>gel 6</u>
Mw			0.9			
(millions)	26.5	26.5	1.35			
			26.0	18.5	25.0	26.5
			58.0	43.0		
Strain No.	<u>131-1</u>	<u>131R-1</u>	<u>131-2</u>	<u>131-2</u>	<u>131-3</u>	--
Gel No.	<u>gel 5</u>	<u>gel 5</u>	<u>gel 5</u>	<u>gel 6</u>	<u>gel 6</u>	
Mw			0.90			
(millions)	26.5	26.5	1.37	1.3	1.20	
			25.3	21.0	2.1	
			37.5	25.5	23.0	
			66.0	47.0		
				60.0		
Strain No.	<u>132-1</u>	<u>132R-1</u>	<u>132-2</u>	<u>132-2</u>	<u>132-3</u>	
Gel No.	<u>gel 5</u>	<u>gel 5</u>	<u>gel 5</u>	<u>gel 6</u>	<u>gel 6</u>	
Mw			0.96			
(millions)	26.5	26.5	1.45			
			25.0	23.0	22.0	
			74.0	55.0	47.0	
			340.0			

I. Strain No. - 1, 2, or 3 indicates the DNA preparation No.

TABLE 2. ESTIMATED MOLECULAR WEIGHTS OF PLASMID DNA BANDS OF *S. AUREUS* STRAINS 129, 130, 131, and 132 OBSERVED IN GELS NO. 7, 8, 13, 15

	129-2 gel 7	129-2 gel 7	129-2 gel 8	129-2 gel 13	129-2 gel 15	129-3 gel 7	129-3 gel 7	129-3 gel 13
1	0.86	0.86	0.99	-	-	-	-	-
2	1.35	1.35	1.67	1.55	-	1.15	1.15	1.5
3	2.6	2.6	-	2.85-3.10	-	2.2	2.35	2.8
4	74	64	12	23.5-37	16	74	80	35-57
5	150	78	20.5	36-60	17.5	112	135	-
6	186	112	32	94-190	-	195	250	-
7	-	200	56	-	-	-	-	-
8	2.1x10 ⁹	-	1.75x10 ⁹	-	-	-	-	-
	130-2 gel 7	130-2 gel 7	130-2 gel 8	130-2 gel 13	130-2 gel 15	130-3 gel 7	130-3 gel 7	130-3 gel 13
	0.86	0.84	1.06	-	-	-	-	-
	1.15	1.30	1.5	-	-	-	-	-
	-	-	11.3	23.5-37	17.5	-	-	22-34
	74	74	18	-	-	78	94	-
	186	186	-	-	-	-	-	-
	131-2 gel 7	131-2 gel 7	131-2 gel 8	131-2 gel 12	131-3 gel 7	131-3 gel 12	131-4 gel 10	131-4 gel 11
	0.84	0.84	1.05	-	-	-	-	-
	1.15	1.25	1.45	-	1.15	-	-	-
	1.25	-	1.50	1.4	-	1.4	1.65	-
	2.35	-	1.55	2.5	2.35	2.5	-	2.0-2.3
	62	64	10.5	29	-	33	13.5	14.5-28.5
	74	80	19-26	42	-	-	-	16.5-34
	140	112	27	72	112	-	-	-
	200	200	68	115	195	-	-	-
	1.2x10 ⁹	1.2x10 ⁹	1/75x10 ⁹	-	310	-	-	-
	132-2 gel 7	132-2 gel 7	132-2 gel 8	132-2 gel 12	132-2 gel 7	132-2 gel 12	132-4 gel 10	132-4 +RNase gel 11
	0.80	0.84	0.98	-	-	-	-	-
	1.15	-	1.42	1.5	-	-	-	-
	2.35	-	11.3	-	-	-	-	-
	74	90	19	29	-	-	13.5	2.3-2.75
	185	222	45	62	110	30	29	14.5-29
	380	430	320	400	800	60	-	28-65
	1.75x10 ⁹	1.2x10 ⁹	-	-	6.0x10 ⁹	-	-	-

TABLE 3. ESTIMATED MOLECULAR WEIGHTS OF PLASMID DNA BANDS OF *S. AUREUS* STRAINS 129, 130, 131, AND 132 OBSERVED IN GELS NO. 10, 11, 13, 14, AND 15.

129-4 gel 10	129-4 gel 11	129-4 gel 13	129-4+RNase gel 11	129-5 gel 14	129-5 gel 15	129-5 gel 15	
-	-	-	-	1.53	-	-	1
1.25	-	1.55	-	2.42	-	-	2
13.5	2.0-2.3	2.8	1.95-2.1	68	-	-	3
22	13-25	22-35	2.7 -34	99	18	17.5	4
-	15.5-32	-	13-25	140	20.5	21	5
-	-	-	-	390	30	-	6
-	-	-	-	570	-	-	7
-	-	-	-	1.2x10 ⁹	-	-	8
130-4 gel 10	130-4 gel 11	RNase 130-4 gel 11	130-4 gel 13	130-5 gel 14	130-5 gel 15		
1.25	-	-	-	-	-		
1.8	-	-	-	-	-		
13.5	11.5-21.5	13.25	23.5-36	-	17.5		
-	-	-	-	115	20		
-	-	-	-	400	27.5		
-	-	-	-	720	-		
RNase 131-4 gel 11	131-4 gel 12	131-5 gel 14	131-5 gel 15				
-	-	-	-				
-	1.4	-	-				
-	1.63	1.6	-				
2.0-2.3	2.5	2.4	-				
14.5-28.5	-	38	16				
19-40	74	88	19				
-	-	115	27.5				
-	-	270	-				
-	-	300	-				
-	-	560	-				
-	-	980	-				
132-4 +RNase gel 11	132-4 gel 12	132-5 gel 14	132-5 gel 15				
-	-	-	-				
-	-	-	17.5				
2.35-2.85	-	-	22.5				
14.5-29	27.5	-	30				
32-76	53	112	42				
-	-	280	260				
-	-	1.7x10 ⁹	-				

REFERENCES

1. J.T. Parisi and D.W. Hecht, "Plasmid Profiles in Epidemiologic Studies of Infections by Staphylococcus epidermidis," J. Infect. Dis., Vol. 141, pp. 637-643, 1980.
2. K.N. Shands, G.P. Schmidt, B.B. Dan, D. Blum, R.J. Guidotti, N.T. Hargrett, R.L. Anderson, D.L. Hill, C.V. Broome, J.D. Band, and D.W. Fraser, "Toxic-shock Syndrome in Menstruating Women. Association with Tampon Use on Staphylococcus aureus and Clinical Features in 52 cases," N. Engl. J. Med., Vol. 303, pp. 1436-1442, 1980.
3. A.G. Barbour, "Vaginal Isolates of Staphylococcus aureus Associated with Toxic Shock Syndrome," Infect. Immun., Vol. 33, pp. 442-449, 1981.
4. F.L. Macrina, D.J. Kopecko, K.R. Jones, D.J. Ayers, and S.M. McCowen, "A Multiple Plasmid-Containing Escherichia coli Strain: Convenient Source of Size Reference Plasmid Molecules, Plasmid," Vol. I, 417-420, 1978.
5. J.B. Hanser and R.H. Olsen, "Isolation of Large Bacterial Plasmids and Characterization of the P2, "Incompatibility Group Plasmids PMG1 and PMG5," J. Bacteriol., Vol. 135, pp. 227-238, 1978.
6. L.P. Elwell and S. Falkow, "The Characterization of Plasmids That Carry Antibiotic Resistance Genes, Antibiotics in Laboratory Medicine," V. Lorian, ED., Williams and Wilkins, Baltimore, pp. 433-453, (1980).

7. D.B. Clewell and D.R. Helinski, "Properties of a Supercoiled Deoxyribonucleic Acid-Protein Relaxation Complex and Strand Specificity of the Relaxation Event," Biochemistry Vol. 9, pp. 4428-4440, 1970.
8. J.A. Meyers, D. Sanchez, L.P. Elwell, and S. Falkow, "Simple Agarose Gel Electrophoretic Method for the Identification and Characterization of Plasmid Deoxyribonucleic Acid," J. Bacteriol., Vol. 127, pp. 1529-1537, 1976.

1981 USAF - SCEE SUMMER FACULTY RESEARCH PROGRAM

Sponsored by the

AIR FORCE OFFICE OF SCIENTIFIC RESEARCH

Conducted by the

SOUTHEASTERN CENTER FOR ELECTRICAL ENGINEERING EDUCATION

FINAL REPORT

AN INVESTIGATION INTO THE NATURE OF THE MELTING LAYER

IN STRATIFORM CLOUDS

Prepared by: Dr. Steven B. Newman

Academic Rank: Assistant Professor

Department and University: Physics-Earth Sciences Department
Central Connecticut State College

Research Location: Air Force Geophysics Laboratory
Meteorology Division, Cloud Physics Branch

USAF Research Colleague: Dr. Arnold A. Barnes, Jr.

Date: 1 September 1981

Contract No: F49620-79-C-0038

AN INVESTIGATION INTO THE NATURE OF THE MELTING LAYER
IN STRATIFORM CLOUDS

by

Dr. Steven B. Newman

ABSTRACT

Research into the nature of the melting layer in mixed stratiform clouds has been conducted in the Cloud Physics Branch of the Air Force Geophysics Lab (AFGL). An extensive reference list has been compiled, covering some 35 years of published work concerning the melting layer and the radar bright band.

In addition, the problem of defining the boundaries of the melting layer have been examined. It is postulated that the 0°C dry bulb isotherm may not always be the best threshold level for the top of the melting layer. Instead, the 0°C wet bulb level is examined, and a relationship between air mass stability and the height difference between these two levels is developed. The lower boundary of the melting layer remains undefined, primarily due to lack of a concrete definition of the "end" of melting.

A simple model of snowflake aggregation and breakup has been developed. It is shown that at reasonable cloud ice contents, the aggregation and breakup of snowflakes just above the melting layer results in considerable ice multiplication, as well as growth. The increase in both size and number concentration of snowflakes entering the melting layer may play a considerable role in enhancing the radar echo intensity in the melting layer resulting in the radar bright band.

ACKNOWLEDGEMENTS

The author wishes to acknowledge the cooperation and assistance of the entire staff of the Cloud Physics Branch of AFGL. In particular, the author is grateful to Dr. Arnold A. Barnes, Jr., Cloud Physics Branch Chief, Lt. Col. Robert C. Schaller, and Mr. Morton Glass, who have all provided valuable guidance and insight into the research reported herein. Ms. Patricia Walsh and Capt. Lawrence Gibbons had compiled the major part of the reference list prior to my arrival at AFGL. Their contribution in searching the literature, reviewing and selecting the pertinent articles is greatly appreciated. The author also acknowledges the assistance of Mr. John Powers of Systems and Applied Sciences Corporation for providing upper air data for K-Index calculations.

This research has been sponsored by the Air Force Systems Command, Air Force Office of Scientific Research, and the Air Force Geophysics Laboratory, and the author hereby acknowledges their support.

I. INTRODUCTION

The Air Force Geophysics Laboratory (AFGL) is the Air Force center for research in the environmental sciences. AFGL interacts with a family of 12 other research and development laboratories in the Air Force Systems Command (AFSC) to identify emerging research and technology needs and integrate scientific advances into Air Force technology.

The Meteorology Division of AFGL satisfies several requirements of operational commands by bringing together pertinent technologies to solve specific problems. Within the division, the Cloud Physics Branch is heavily involved in research in the area of melting layer processes and also in an aircraft icing program for improving forecasting of atmospheric icing conditions for both design and operational use by the Air Force.

II. OBJECTIVES

The main objective of this research was to investigate some of the cloud microphysical processes associated with the melting layer in stratiform clouds.

We have attempted to extend previously derived models of snowflake aggregation and melting and to investigate the interaction with the ambient atmosphere.

This research has not attempted to completely model the melting layer, but rather to provide a "first look" at some of the processes occurring within it. As such, it is limited to static or simplified

dynamic models.

Compilation of an extensive melting layer reference list was also a major objective of this research, as was a first attempt to accurately define the upper and lower limits of the melting layer.

It should be noted that this research is only in its early stages, thus any conclusions which are drawn here must be regarded as purely preliminary in nature, and will doubtless need further study.

III. LITERATURE SEARCH

Using a list of over sixty references already compiled by Ms. Walsh and Capt. Gibbons of the Cloud Physics Branch, the author completed an exhaustive search of the existing literature on the radar bright band and the melting layer. The excellent facilities of the AFGL Research Library, and the cross-referencing from citations as they were found and abstracted were used to prepare a list of approximately 90 books, papers and monographs. This is probably the most extensive reference list pertaining to the bright band and the melting layer ever compiled. It represents the sum total of what is presently known about the nature of these phenomena. The entire reference list is reproduced here in Appendix A. The author would appreciate hearing from anyone who might know of other references which are not included in this list.

IV. DEFINING THE MELTING LAYER

The definition of the melting layer has presented one of the major problems encountered thus far; although on the surface, such a definition would appear to be quite straightforward.

Logically, one would choose, a priori, the 0°C dry bulb isotherm as the upper boundary of the melting layer. Indeed, all the previous research we have seen does define the top of the melting layer in just this way. However, a possibility exists that melting may not actually begin when frozen precipitation particles fall past the 0°C dry bulb level in clouds.

In most clouds, a relative humidity of 100% is not always maintained. In fact, many clouds have relative humidities which are less than 100%. In such cases, the wet bulb and dry bulb temperatures will not be equal at any given height, and the 0°C wet bulb isotherm will be located somewhat below (in terms of height) the 0°C dry bulb isotherm.

The Glossary of Meteorology defines the wet bulb temperature thus:

WET-BULB TEMPERATURE -- The temperature that an air parcel would have if cooled adiabatically to saturation at constant pressure by evaporation of water into it, all latent heat supplied by the parcel.

--Glossary of Meteorology

This is significant in that melting of snowflakes will not begin until the wet bulb temperature rises above 0°C. This is because the snowflake or ice crystal behaves as a wet bulb, thus the air

immediately surrounding the flake or crystal will be cooled, by evaporation, to the wet bulb temperature.

Previous research (Austin and Bemis, 1950; Hooper and Kippax, 1950; Browne, 1952; Mason, 1955; Gupta, et. al., 1961) indicates that the radar bright band is always found at some distance below the 0°C dry bulb isotherm (Fig. 1). The actual distance is found to be quite variable. Hooper and Kippax (1950) reported a gap of 330 ± 150 feet between the 0°C isotherm and the radar bright band; while Gupta, et. al. (1961) reported a gap of approximately 4700 feet.

Present research indicates that, for situations where the 0°C dry bulb isotherm is located above ground level, the distance between the 0°C dry bulb isotherm and the 0°C wet bulb isotherm is directly related to the stability of the air mass. Using the K-Index (George, 1960) as a measurement of stability, we have found a good relationship between this index and the distance between the 0°C dry bulb and 0°C wet bulb isotherms. These results are summarized in Fig. 2. Note that high values of K (greater than 30) are indicative of strong air mass instability with the likelihood of thunderstorms high. Values of K lower than approximately 15 indicate very stable air. The solid line on the figure is the best fit curve to the data, and would call for a 1300 meter difference for a K-Index of 0, and a 100 meter difference for a K-Index of 40.

In a cloud with relative humidity near 100%, the gap between the 0°C wet bulb isotherm and the 0°C dry bulb isotherm is on the order of 100 to 150 m. This is within the range of values reported in the above mentioned literature. It is possible, then, that the top of the radar bright band may correspond well with the 0°C wet bulb isotherm, where melting has progressed to the point of providing a liquid coating to the snowflakes. In fact, it is also possible that in the shallow layer between the 0°C dry bulb and the 0°C

wet bulb levels, any water droplets present in the cloud may remain supercooled, even if the ambient temperature is slightly higher than 0°C.

Defining the top of the melting layer also presents a problem because it is not a constant height surface. As snowflakes begin melting, they take up latent heat from the surrounding atmosphere. The resultant cooling will cause the top of the melting layer to lower, locally, in altitude (Fig. 3). This lowering will be non-uniform due to non-uniform melting rates and non-uniform precipitation areas in the cloud. In some cases, the effect can be expected to be highly localized, producing convective overturn in those areas where the local lapse rate becomes superadiabatic. Such overturn incidents could result in downbursts of cold air, or momentary occurrences of heavy precipitation at the ground.

Defining the bottom of the melting layer also presents some problems which, at the present time, have not been resolved. The radar bright band is rarely more than a few hundred meters thick, yet the melting layer is known to extend well below the lower boundary of the bright band.

If we define the bottom of the melting layer as the level at which there is no more frozen precipitation, then we may be setting a boundary which is too low in altitude. Snowflakes are rarely observed at temperatures above +4°C.¹ A more logical method would be to establish a threshold level below which a given percentage of snowflakes and ice crystals will have completely melted. Although this is probably somewhere between +3°C and +5°C for total melting of 90% of the snowflakes², the +5°C level has been the most widely used threshold temperature for the bottom of the melting layer. The reasons for this choice appear to be entirely arbitrary, without any supporting data.

¹ Morton Glass, AFGL, private conversation.

² Capt. Ian Cohen, AFGL, private conversation.

Unfortunately, we do not have sufficient flight data with which to attempt any such definition ourselves. Only one or two flights actually penetrated the melting layer, and these were specifically studying icing processes just above the melting layer. More flights specifically aimed at studying the melting layer need to be made in order to obtain enough reliable data to accurately define melting layer boundaries, both upper and lower.

V. A SNOWFLAKE AGGREGATION MODEL

Lhermitte and Atlas (1963), as well as Mason (1955) have suggested that a possible explanation for the enhancement of the radar echo intensity in the melting layer is aggregation of snowflakes with ice crystals just above the 0°C isotherm. Lo and Passarelli (1981) have found evidence of aggregation at temperatures much lower than had previously been thought possible. Observations by Hobbs (1973) indicate that, while very large aggregates may be found at ground level when temperatures are near 0°C , in clouds, aggregates of maximum dimension greater than 5 mm are uncommon. However, observations made during AFGL flights indicate that in the region between -3°C and 0°C , aggregates larger than 5 mm do exist. The model presented herein does not allow for such larger aggregates; however, further refinement will take these observations into account.

Using the aggregational growth equation given by Rogers (1979), a simple aggregation model has been developed. The equation for growth of a snowflake by aggregation is,

$$dm/dt = EM \pi R^2 \Delta u \quad (1)$$

where E is the mean collection efficiency of the snowflake, R the snowflake radius, Δu the difference in fallspeed between the snowflakes and the ice crystals, and M is the cloud ice content, which can be related to the ice crystal number density, N, by

$$M = Nv \rho \quad (2)$$

where v is the average ice crystal volume and ρ the average ice crystal density.

The cloud ice content differs from the cloud liquid water content in that no supercooled droplets are counted in deriving the value of M. Thus use of M in the model means that any growth by diffusion or accretion is effectively ignored. Only growth by aggregation is considered.

Mason (1971) relates the diameter, D, of a stellar dendritic snowflake to its mass, m, by

$$m = 0.027D^2 \quad (3)$$

And, substituting into Eq. (1) gives

$$1/R dR/dt = 4.63EM \pi \Delta u \quad (4)$$

Integration of Eq. (4) from $R=R_0$ to $R=R_f$, and from $t = 0$ to $t = t_f$ yields,

$$R_f = R_0 \exp(4.63EM \pi \Delta u t) \quad (5)$$

In obtaining solutions for this expression, a number of simplifying assumptions have been made.

- a. All snowflakes fall at a constant speed of 1 m/sec; while all ice crystals fall at a constant speed of 0.5 m/sec. These are valid assumptions, according to Magono (1953), and Rogers (1979), respectively; however, Passarelli (1978) has shown that the fallspeed of aggregating dendritic flakes is related to the diameter of the dendrite.
- b. The lapse rate of temperature is constant during the model run.
- c. Aggregates have a maximum dimension of 5 mm. Upon growing larger than this size they spontaneously break up into smaller particles. The model then resumes aggregational growth with a new 1 mm diameter snowflake, until it falls to the 0°C level. If the particle again reaches 5 mm before reaching the 0°C level, it breaks up once again, resulting in the same recycling process.
- d. The snowflakes aggregate in the layer from -10°C to 0°C. Layer thickness depends on the lapse rate.

We examine the case of a snowflake with initial maximum dimension of 1 mm falling through the layer with constant lapse rates of -4°C/km, -5°C/km and -6°C/km. Solution of Eq. (5) for 10 second intervals of growth are shown in Figs. 4 through 6. Cloud ice contents are 1.0 and 1.5 g/m³, respectively, for each lapse rate.

Note that the aggregation rate increases as the flakes approach the freezing level (curves become more vertical). This is to be expected as the growing flakes sweep out a greater area and collide more frequently with ice crystals.

At lapse rates of $-5^{\circ}\text{C}/\text{km}$ and $-6^{\circ}\text{C}/\text{km}$, breakup does not occur when the cloud ice content is $1.0 \text{ g}/\text{m}^3$ (Figs. 5a and 6a). However, breakup is seen to occur at all three lapse rates when the cloud ice content is $1.5 \text{ g}/\text{m}^3$. Fig. 4b illustrates how the growth then continues from 1 mm diameter until the freezing level is reached. The number of small particles which result each time a growing aggregate breaks up cannot be determined at the present time. However, if the flake were to splinter entirely into 1 mm diameter particles, there would be 25 for every 5 mm diameter snowflake undergoing breakup. It is reasonable to assume that some of the broken fragments will be larger, and some will be smaller than 1 mm, but in any case, aggregation and breakup appears to be a powerful mechanism for ice multiplication. Also note that the size of the ice particles entering the melting layer after resumption of growth is considerably larger than those that began the aggregation process, ranging from 1.75 to 3.25 mm in diameter for the case of $-4^{\circ}\text{C}/\text{km}$ lapse rate and $1.5 \text{ g}/\text{m}^3$ cloud ice content.

Thus aggregational growth and breakup will yield greater numbers of larger snowflakes than were present before aggregation began. This in itself may account for a large part of the radar echo enhancement (bright band) in the melting layer, especially when these flakes become water-coated.

VI. RECOMMENDATIONS

The research done here during the summer of 1981 represents only the initial phase of an extensive study of melting layer processes being conducted by AFGL.

Most of what is known about the melting layer comes from ground-based radar observations. In more recent years, Doppler

radar has been utilized to give profiles of particle fallspeeds.

However, there is a singular lack of in situ data concerning the microphysics of the melting layer. The 5 or 6 flights by the C-130 which we looked at provided very little data, as they were mostly confined to altitudes above the 0°C isotherm. In the 1 or 2 flights which did penetrate the melting layer, only limited data were obtained as the time in the melting layer was short.

At this time, AFGL does not have a research aircraft, either Air Force operated or under contract. Such an aircraft is necessary to continue the research and gather enough reliable data in the melting layer to allow reasonable conclusions regarding its nature to be drawn.

Among the important parameters which can be studied with new flight data are:

- a. Cloud ice content
- b. Liquid water content
- c. Droplet size distribution
- d. Ice crystal number density
- e. Snowflake aggregation and breakup

The last has been shown to be an important ice multiplication mechanism; however, the aggregation model developed herein is relatively simple and contains many assumptions. A larger data base would allow refinement of the model to a point where growth of snowflakes by other mechanisms (accretion, diffusion, etc.), as well as more realistic assumptions, could also be considered, and the growth of a snowflake could be more fully and accurately modeled.

Also, we need to understand more fully how a snowflake melts

when it falls past the 0°C level. Exactly what happens to it? Does it retain its shape until fully melted? How does its fallspeed change? What effect does collision with water droplets have when it is partially melted? Such studies can be done in the laboratory, possibly augmented by in-cloud observations. Some of these studies are currently being done for AFGL under contract.

In addition, I believe that more radar observations of the melting layer be made. There is some disagreement as to the effect of particles in the melting layer on the polarization of the returning radar pulse. This is an area that needs further study.

The first description of the radar bright band was published approximately 35 years ago (Ryde, 1946). The research being conducted at AFGL represents one of the first major attempts in those 35 years to describe the melting layer by studying it from the inside as well as the outside.

FIGURES

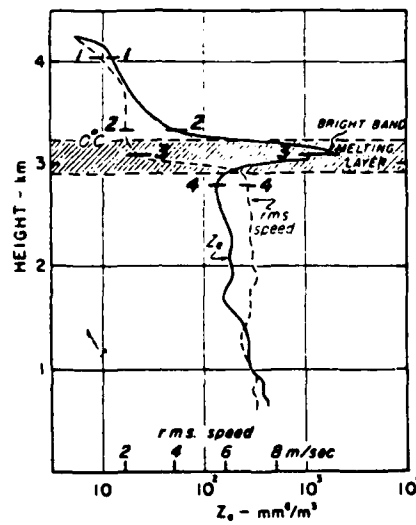


Fig. 1. Profile of radar reflectivity versus height. Note that maximum radar reflectivity is found below the 0°C isotherm (after Lhermitte and Atlas, 1963).

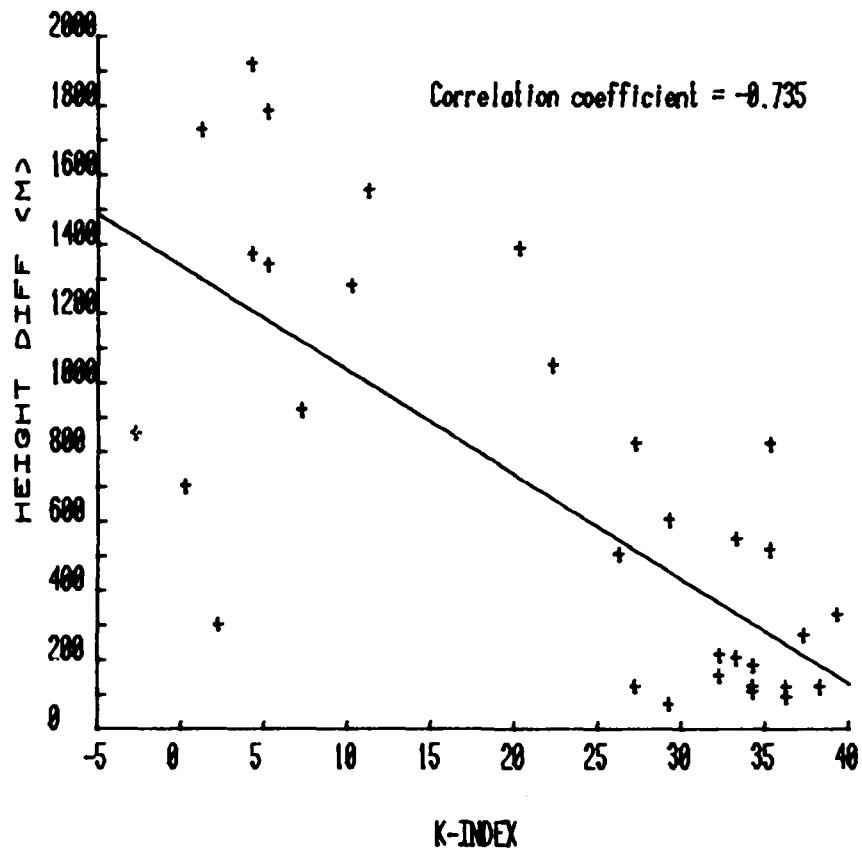


Fig. 2. K-Index vs. height difference between 0°C dry bulb isotherm and 0°C wet bulb isotherm. Solid line represents best fit to data.

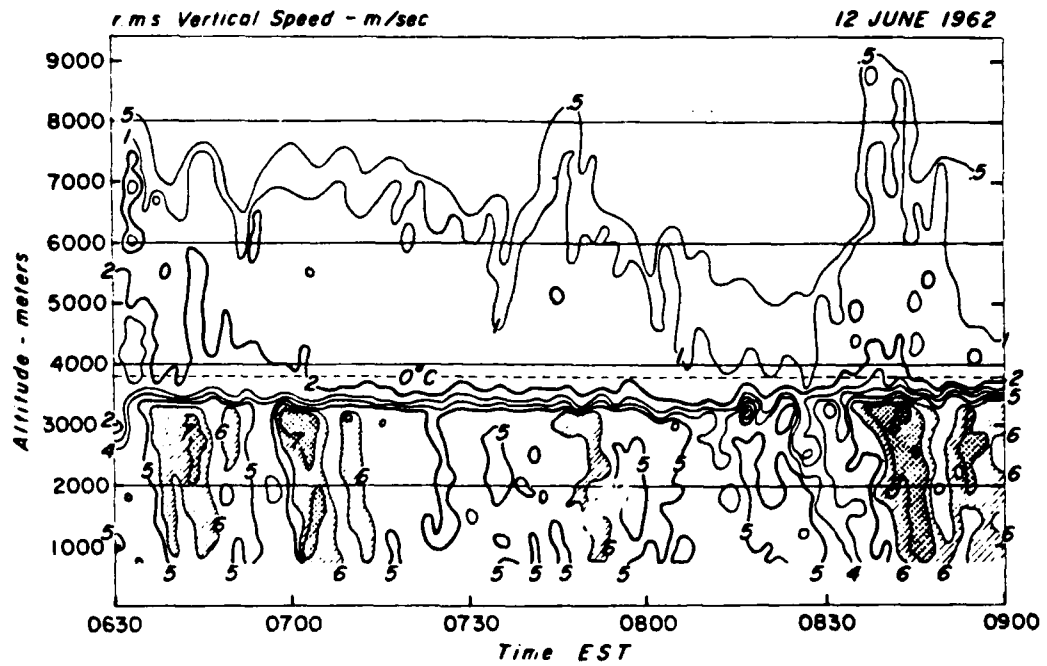


Fig. 2. Time versus height profile of radar reflectivity. The bright band is easily seen. Note changes in the level of the bright band with time (after Lhermitte and Atlas, 1963).

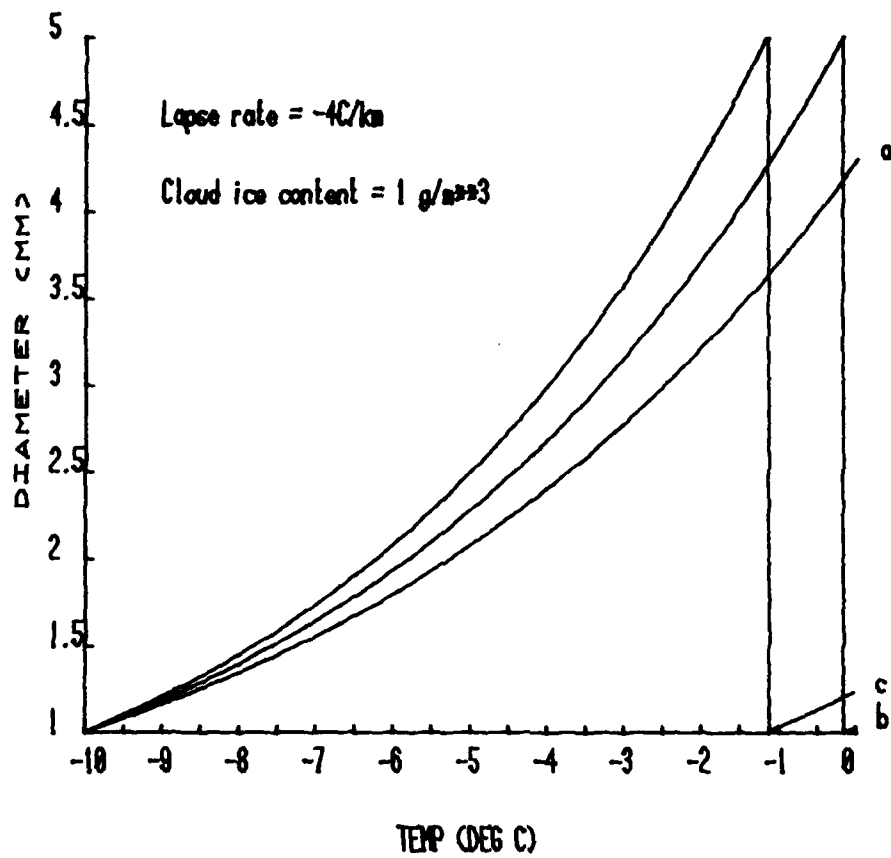


Fig. 4a. Aggregational growth and breakup of a 1 mm diameter snowflake falling through the layer from -10°C to 0°C . Lapse rate is constant at $-4^{\circ}\text{C}/\text{km}$. Cloud ice content is $1.0 \text{ g}/\text{m}^3$. Curves are for mean collection efficiencies of a) 0.8 b) 0.9 and c) 1.0 .

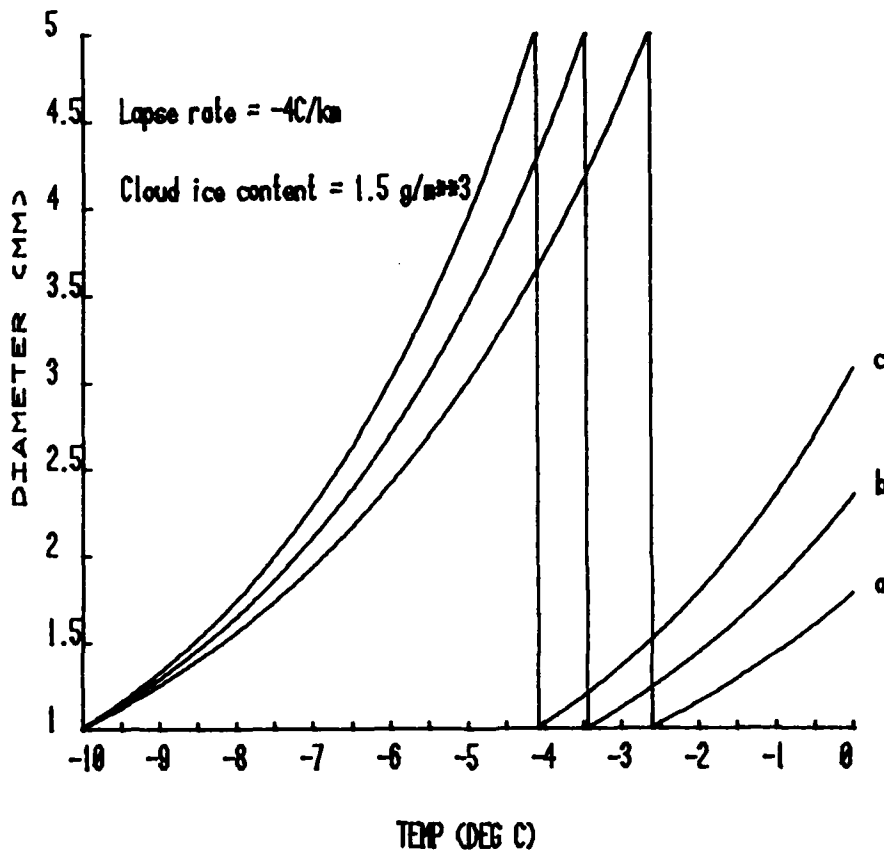


Fig. 4b. Aggregational growth and breakup of a 1 mm diameter snowflake falling through the layer from -10°C to 0°C . Lapse rate is constant at $-4^{\circ}\text{C}/\text{km}$. Cloud ice content is $1.5 \text{ g}/\text{m}^3$. Curves are for mean collection efficiencies of a) 0.8 b) 0.9 and c) 1.0 .

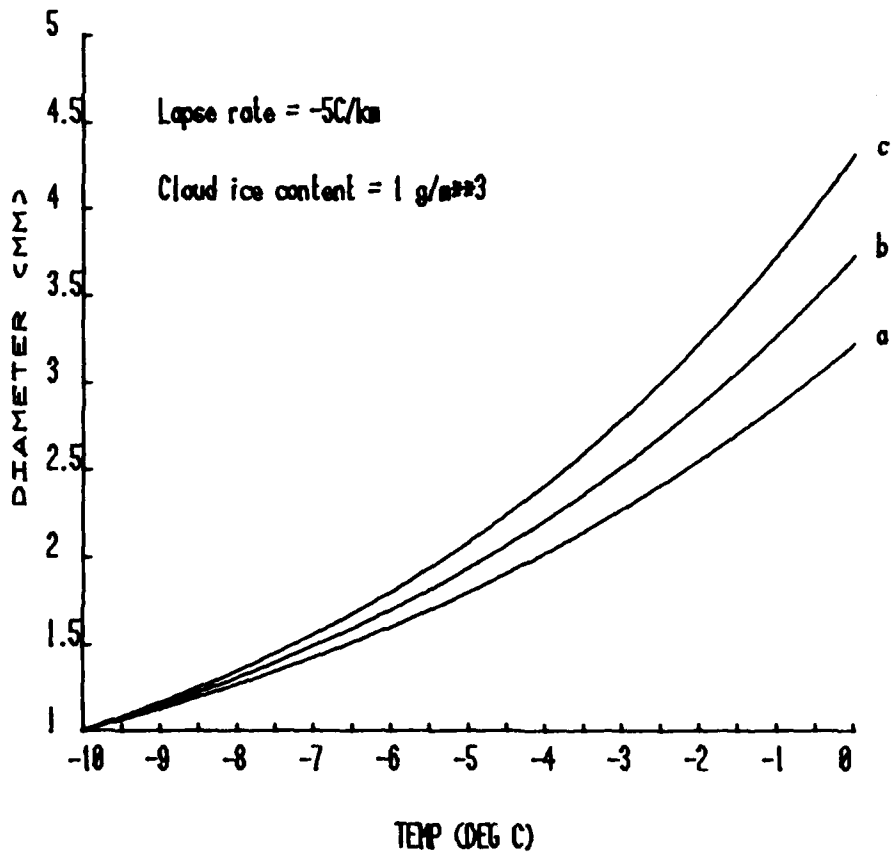


Fig. 5a. Aggregational growth and breakup of a 1 mm diameter snowflake falling through the layer from -10°C to 0°C . Lapse rate is constant at $-5^{\circ}\text{C}/\text{km}$. Cloud ice content is $1.0 \text{ g}/\text{m}^3$. Curves are for mean collection efficiencies of a) 0.8 b) 0.9 and c) 1.0 .

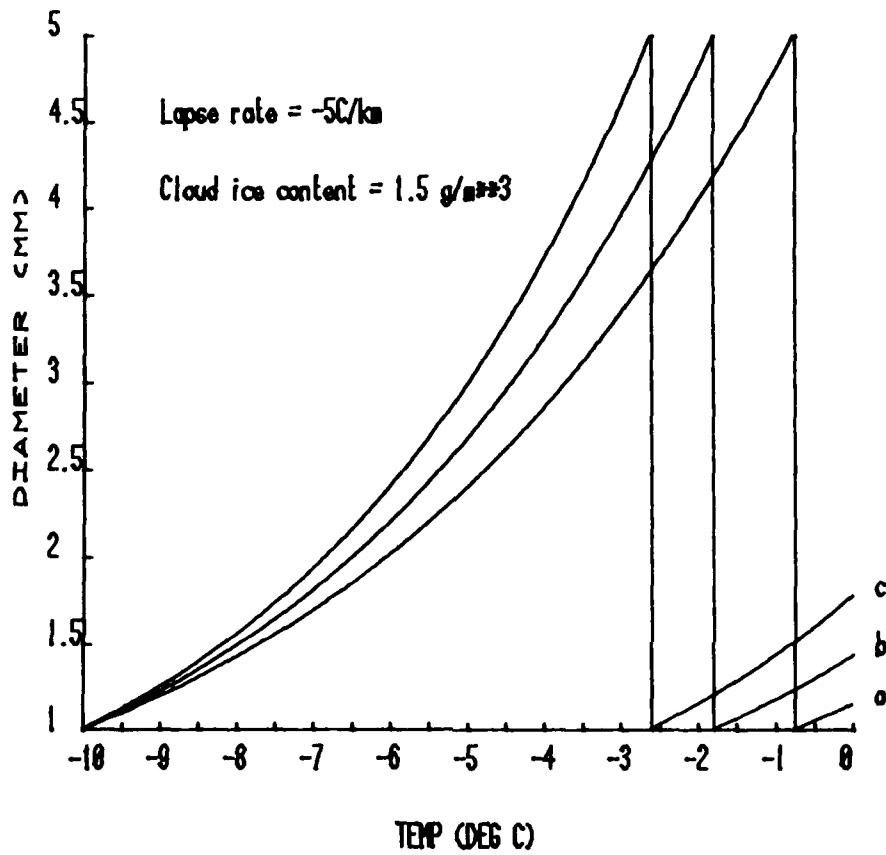


Fig. 5b. Aggregational growth and breakup of a 1 mm diameter snowflake falling through the layer from -10°C to 0°C . Lapse rate is constant at $-5^{\circ}\text{C}/\text{km}$. Cloud ice content is $1.5 \text{ g}/\text{m}^3$. Curves are for mean collection efficiencies of a) 0.8 b) 0.9 and c) 1.0 .

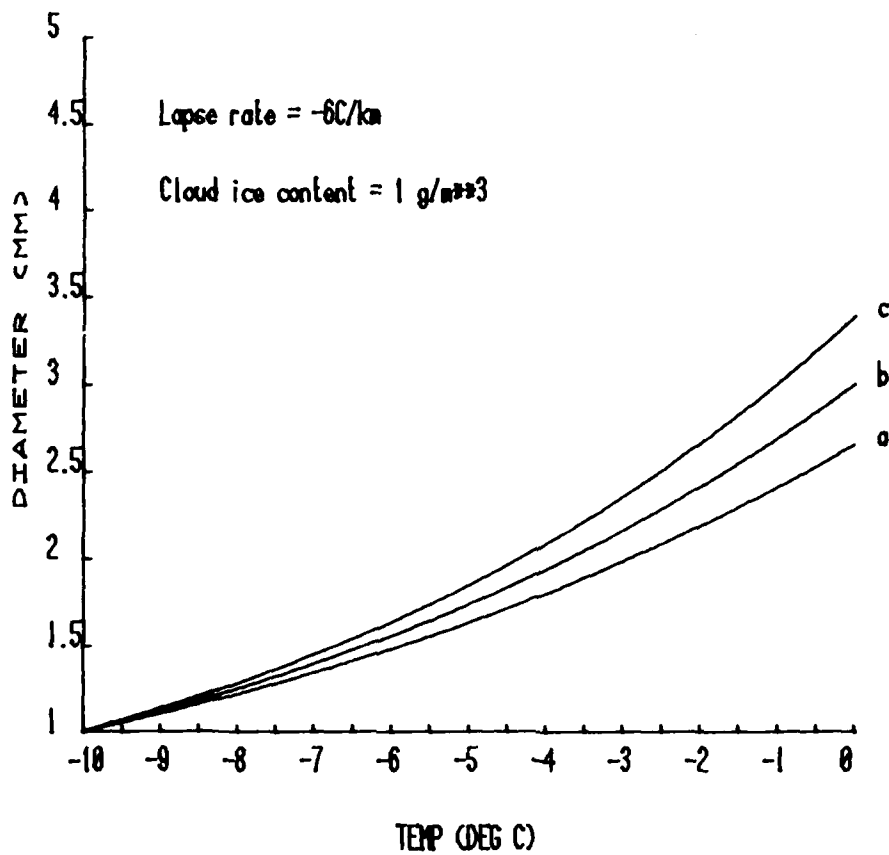


Fig. 6a. Aggregational growth and breakup of a 1 mm diameter snowflake falling through the layer from -10°C to 0°C . Lapse rate is constant at $-6^{\circ}\text{C}/\text{km}$. Cloud ice content is $1.0 \text{ g}/\text{m}^3$. Curves are for mean collection efficiencies of a) 0.8 b) 0.9 and c) 1.0 .

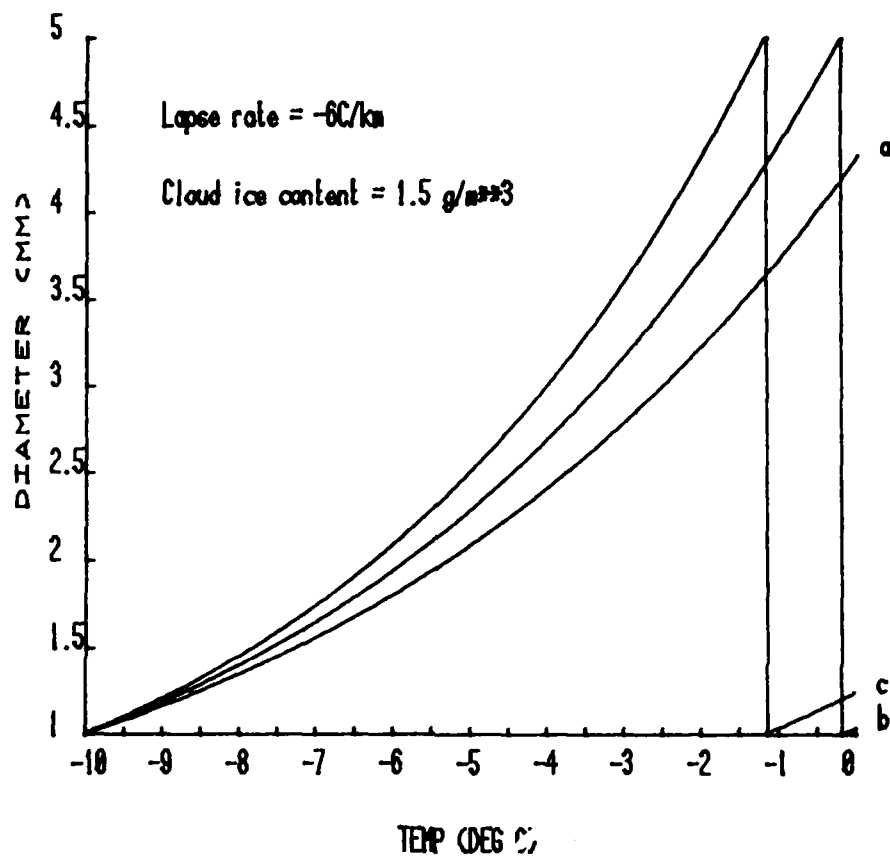


Fig. 6b. Aggregational growth and breakup of a 1 mm diameter snowflake falling through the layer from -10°C to 0°C . Lapse rate is constant at $-6^{\circ}\text{C}/\text{km}$. Cloud ice content is $1.5 \text{ g}/\text{m}^3$. Curves are for mean collection efficiencies of a) 0.8 b) 0.9 and c) 1.0 .

REFERENCES

1. Austin, P.M. and A. Bemis, 1950: A quantitative study of the bright band in radar precipitation echoes. J. Meteor., 7, 165-171.
2. Browne, I.C., 1952: Radar studies of clouds. Ph.D. Thesis, Cambridge University, England.
3. George, J.J., 1960: Weather Forecasting for Aeronautics. Academic Press, New York, 410-415.
4. Gupta, B., A. Mani and S. Ventikeshwaran, 1961: Some observations of melting band in radar echoes at Poona. Ind. J. Meteor. and Geophys., 12, 317-322.
5. Hobbs, P.V., 1973: Ice in the atmosphere: a review of the present position. In Physics and Chemistry of Ice (eds. Whalley, Jones and Gold), Royal Society of Canada, Ottawa, 308-319.
6. Hooper, J. and A. Kippax, 1950: The bright band: a phenomenon associated with radar echoes from falling rain. Quart. J. Roy. Meteor. Soc., 76, 125-131.
7. Lhermitte, R. and D. Atlas, 1963: Doppler fallspeed and particle growth in stratiform precipitation. Proc. Tenth Conf. on Radar Meteorology, Washington, D.C., 297-302.
8. Lo, K. and R. Passarelli, Jr., 1981: A new sampling technique for quantitative airborne studies of snow growth: theory and examples. J. Atmos. Sci., In press.

9. Magono, C., 1953: On the growth of snowflake and graupel. Science Reports of Yokohama National University, Sect. I, No. 3, 33-40.
10. Mason, B.J., 1955: Radar evidence for aggregation and orientation of melting snowflakes. Quart. J. Roy. Meteor. Soc., 81, 262.
11. _____, 1971: The Physics of Clouds. Clarendon Press, London, England.
12. Passarelli, R., Jr., 1978: Theoretical and observational study of snow-size spectra and snowflake aggregation efficiencies. J. Atmos. Sci., 35, 882-889.
13. Rogers, R.R., 1979: A Short Course in Cloud Physics. Pergamon Press, New York.
14. Ryde, J., 1946: The attenuation of radar echoes produced at centimetre wavelengths by various meteorological phenomena. Report of Conf. on Meteor. Factors in Radio Wave Propagation., London, England, 169-189.

APPENDIX A

MELTING LAYER REFERENCE LIST

1. Affronti, F. and L. Ciattaglia, 1970: Detection of the bright band layer with the Meteor-50 radar. Rivista di Meteorologia Aeronautica, Rome, 30 (4), 47-53.
2. Atlas, D., M. Kerker and W. Hitschfeld, 1953: Scattering and attenuation by non-spherical atmospheric particles. J. Atm. and Terr. Phys., 3, 108-119.
3. Atlas, D., R. Tatehira, R. Srivastava, W. Marker and R. Carbone, 1969: Precipitation-induced mesoscale wind perturbations in the melting layer. Quart. J. Royal Met. Soc., 95, 544.
4. Austin, P.M. and A. Bemis, 1950: A quantitative study of the bright band in radar precipitation echoes. J. Meteor., 7, 165-171.
5. Bailey, J. and W. Macklin, 1968: Heat transfer from artificial hailstones. Quart. J. Royal Met. Soc., 94, 93.
6. Battan, L., 1977: Rain resulting from melting ice particles. J. Appl. Met., 16, 595-604.
7. _____ and J. Theiss, 1976: Rain resulting from melting snow. Proc. Int. Conf. on Cloud Physics, Boulder, CO, 567-571.
8. _____, _____ and A. Kassander, Jr., 1964: Some Doppler radar observations of a decaying thunderstorm. Proc. Eleventh Weather Radar Conf., Boston, MA, 362-365.
9. Bigg, E.K., 1953: The formation of atmospheric ice crystals by the freezing of droplets. Quart. J. Royal Met. Soc., 79, 510-519.

10. Blanchard, D.C., 1957: The supercooling, freezing and melting of giant waterdrops at terminal velocity in air. Proc. Conf. on Physics of Cloud and Precip. Particles, Pergamon Press, 233-249.
11. Browne, I.C., 1952: Radar studies of clouds. Ph.D. Thesis, Cambridge University
12. _____ and N. Robinson, 1952: Cross-polarization of the radar melting band. Nature (London), 170, 1078-1079.
13. Byers, H. and R. Coons, 1947: The 'bright line' in radar cloud echoes and its probable explanation. J. Meteor., 4, 75.
14. Cheng, R., 1978: Ice pellet melting--ejection of microdroplets. Bull. of the Amer. Met. Soc., 59, 512.
15. Cunningham, R., 1947: A different explanation of the bright-line. J. Meteor., 4, 163.
16. Doviak, R. and C. Weil, 1972: Bistatic radar detection of the melting layer. J. Appl. Met., 11, 1012-1016.
17. Drake, J. and B.J. Mason, 1966: The melting of small ice spheres and cones. Quart. J. Royal Met. Soc., 92, 500.
18. DuToit, P., 1967: Doppler radar observations of drop sizes in continuous rain. J. Appl. Met., 6, 1082-1087.
19. Dyer, R., 1968: Doppler measurements in stratiform rain. Proc. Thirteenth Radar Met. Conf., Montreal, Que., 144.

20. Ekpenyong, B. and R. Srivastava, 1970: Radar characteristics of the melting layer--a theoretical study. Univ. of Chicago Dept. of Geophys. Sciences and Ill. Inst. of Tech. Dept. of Elec. Eng., Technical Report No. 16, Lab. for Atm. Probing, Chicago, Ill.
21. Fleagle, R.J. and J.A. Businger, 1963: An Introduction to Atmospheric Physics, Academic Press, New York.
22. Fletcher, N.H., 1962: The Physics of Rainclouds, Cambridge University Press, Cambridge, Great Britain.
23. Fukuta, N., 1969: Experimental studies on the growth of small ice crystals. J. Atm. Sci., 26, 522.
24. _____ and L. Walter, 1970: Kinetics of hydrometeor growth from a vapor-spherical model. J. Atm. Sci., 27, 1160.
25. Fukuta, N., 1973: Thermodynamics of cloud glaciation. J. Atm. Sci., 30, 1645.
26. _____, L. Neubauer, and D. Erickson, 1979: Final Report to NSF under Grant No. ENV 77-15346.
27. _____, W. Guo, and T. Guo, 1974: Kinetics of hydrometeor growth-spheroidal model. Conf. on Cloud Physics, Tucson AZ.
28. _____, Y. Paik, W. Saxena, J. Armstrong, A. Gorove, T. Guo and W. Guo, 1973: Final Report to NSF under Grant No. GA-29525.

29. Great Britain Meteorological Office, 1965: Ice Accretion on Aircraft.
30. Gunn, R. and G. Kinzer, 1949: The terminal velocity of fall for water droplets in stagnant air. J. Meteor., 6, 243-248.
31. Gunn, K. and J. Marshall, 1958: The distribution with size of aggregate snowflakes. J. Meteor., 15, 452-461.
32. Gupta, B., Mani, A. and S. Ventikeshwaran, 1961: Some observations of melting band in radar echoes at Poona. Ind. J. Met. and Geophys., 12, 317-322.
33. Gvelesviani, A. and A. Kartsivadze, 1968: On the melting of spherical hailstones. Proc. Int. Conf. on Cloud Physics, Toronto, Ont., 422-425.
34. Harrold, T. and K. Browning, 1967: Meso-scale wind fluctuations below 1500 metres. Meteorology Magazine, 96, 367-379.
35. Heysfield, G., 1979: Doppler radar study of a warm frontal region. J. Atm. Sci., 36, 2093-2107.
36. Hoffer, T. and S. Mallen, 1968: A vertical wind tunnel for small droplet studies. J. Appl. Met., 7, 290.
37. Hogg, D., F. Guiraud and E. Burton, 1980: Simultaneous observations of cool cloud liquid by ground-based microwave radiometry and icing of aircraft. J. Appl. Met., 19, 893-895.

38. Hooper, J. and A. Kippax, 1950: The bright band: a phenomenon associated with radar echoes from falling rain. Quart. J. Royal Met. Soc., 76, 125-131.
39. Houze, R., Jr., J. Locatelli, and P. Hobbs, 1976: Dynamics and cloud microphysics of the rainbands in an occluded frontal system. J. Atm. Sci., 33, 1921-1936.
40. Imai, I., M. Fujiwara, I. Ichimura and Y. Toyama, 1955: Radar reflectivity of falling snow. J. Met. Res., Tokyo, 7, 422.
41. Johnson, D., 1981: Analytical solution for cloud drop concentration. J. Atm. Sci., 38, 215-218.
42. Kerker, M., P. Langleben and K. Gunn, 1951: Scattering of microwaves by a melting spherical ice particle. J. Meteor., 8, 424.
43. Knight, C.A., 1979: Observations of the morphology of melting snow. J. Atm. Sci., 36, 1123-1130.
44. Kramers, H., 1946: Heat transfer from spheres to flowing media. Physica, 12, 61-80.
45. Lagourette, B., 1976: Study of dielectric properties of disperse micro-crystals of ice near melting temperature. J. De Physique., 37, 945-954.
46. Langleben, M., 1954: The terminal velocity of snowflakes. Quart. J. Royal Met. Soc., 80, 174-181.

47. Lhermitte, R., and D. Atlas, 1963: Doppler fallspeed and particle growth in stratiform precipitation. Proc. Tenth Conf. on Radar Met., Washington, D.C., 297-302.
48. List, R., 1963: General heat and mass exchange of spherical hailstones. J. Atm. Sci., 20, 189-197.
49. _____ and J. Dussault, 1967: Quasi-steady-state icing and melting conditions and heat and mass transfer of spherical and spheroidal hailstones. J. Atm. Sci., 24, 522-529.
50. List, R. and D. Parsons, 1968: Simulation of the total heat transfer of spherical hailstones. Helvetica Physica Acta, 41, 1016-1020.
51. List, R. and R. Schemenauer, 1971: Free fall behavior of planar snow crystals, conical graupel and small hail. J. Atm. Sci., 28, 110-115.
52. Locatelli, J. and P. Hobbs, 1974: Fall speeds and masses of solid precipitation particles. J. Geophys. Res., 19, 2185-2197.
53. Ludlam, F.H., 1958: The hail problem. Nubila, 1, 12-96.
54. Ludlam, F., 1980: Clouds and Storms, The Pennsylvania State University Press, University Park, PA.
55. Macklin, W., 1963: Heat transfer from hailstones. Quart. J. Royal Met. Soc., 89, 360.
56. _____, 1964: Factors affecting the heat transfer from hailstones. Quart. J. Royal Met. Soc., 90, 84-90.

57. Magono, C. and T. Nakamura, 1965: Aerodynamic studies of falling snowflakes. J. Met. Soc. (Japan), 43, 139-147.
58. Marier, D., 1967: The sleet bright band. Report No. WBTM-ER-26, Weather Bureau Eastern Region Headquarters, Garden City, NY
59. Mason, B.J., 1955: Radar evidence for aggregation and orientation of melting snowflakes. Quart. J. Royal Met. Soc., 81, 262.
60. _____, 1971: The Physics of Clouds, Clarendon Press, London, Great Britain
61. McCormick, K., 1970: Reflectivity and attenuation observations of hail and the radar bright band. Proc. 14th Radar Met. Conf., Tucson, AZ, 19-24.
62. Medzhitov, R., 1964: Cloud microstructure and icing of airplanes over Belcrussia. Moscow Tsentralnyi Institut Prognozov, Trudy, 136, 101-115.
63. Ohtake, T., 1965: Preliminary observations of size distribution of snowflakes at just above and below the melting layer. Proc.Int. Conf. on Cloud Physics, Tokyo, Japan, 271.
64. _____, 1969: Observations of the size distribution of hydrometeors through the melting layer. J. Atm. Sci., 26, 545-557.

65. Pace, J. and R. Stewart, 1980: The effect of melting particles on the thermodynamic and microphysical characteristics of Sierra Nevada winter storms. VIII Int. Conf. on Cloud Physics, Clermont-Ferrand, France, 563-564.
66. Passarelli, R., 1976: Coordinated Doppler radar and aircraft observations of riming growth and drop breakup in stratiform precipitation. Proc. Int. Conf. on Cloud Physics, Boulder, CO, 500-505.
67. _____, 1978: Theoretical and observational study of snow-size spectra and snowflake aggregation efficiencies. J. Atm. Sci., 35, 882.
68. Pruppacher, H. and J. Klett, 1980: Microphysics of Clouds and Precipitation, Reidel Publishing Co., Dordrecht, Holland.
69. Pruppacher, H. and M. Neiburger, 1968: Proc. Int. Conf. on Cloud Physics, Toronto, Ont., 389.
70. Ramana Murty, B., A. Roy and K. Biswas, 1965: Radar echo intensity below the bright band. J. Atm. Sci., 22, 91-94.
71. Richter, J. and H. Hitney, 1980: The effects of atmospheric refractivity on microwave propagation. Atmospheric Water Vapor, Academic Press, New York, NY.
72. Rogers, R.R., 1976: A Short Course in Cloud Physics, Pergamon Press, New York, NY.

73. Ryde, J., 1946: The attenuation of radar echoes produced at centimetre wavelengths by various meteorological phenomena. Report of Conf. on Met. Factors in Radio Wave Propagation, London, Great Britain, 169-189.
74. Sassen, K., 1975: Laser depolarization 'bright band' from melting snowflakes. Nature, 255, 316-318.
75. _____, 1976: Polarization diversity lidar returns from virga and precipitation: anomalies and the bright band analogy. J. Appl. Met., 15, 292-300.
76. Sekhon, R. and R. Srivastava, 1970: Snow size spectra and radar reflectivity. J. Atm. Sci., 27, 299-307.
77. Takeda, T., and Y. Fujiyoshi, 1978: Microphysical processes around melting layer in precipitating clouds as observed by vertical pointing radar. J. Met. Soc. Japan, 56, 293-303.
78. Vonnegut, B. and C. Moore, 1960: Visual analogue of radar bright band phenomenon. Weather, 15, 272-279.
79. Weiss, R., J. Locatelli and P. Hobbs, 1977: Deduction of ice particle types in the vicinity of the melting layer from Doppler radar measurements. J. Appl. Met., 16, 314-316.
80. Wexler, R., 1955a: An evaluation of the physical effects in the melting layer. Proc. Fifth Weather Radar Conf., 329-334.
81. _____, 1955b: The melting layer. Proc. First Conf. on Physics of Clouds and Precipitation Particles, 306-314.

82. Wexler, R. and D. Atlas, 1956: Factors influencing radar-echo intensities in the melting layer. Quart. J. Royal Met. Soc., 82, 349-351.
83. _____, 1958: Moisture supply and growth of stratiform precipitation. J. Meteor., 15, 531.
84. Wexler, R., J.R. Reed and J. Honig, 1954: Atmospheric cooling by melting snow. Bulletin of the Amer. Meteor. Soc., 35, 48-51.
85. Yokoyama, T. and H. Tanaka, 1980: Effects of coalescence in a melting layer in two-wavelength microwave backscattering. VIII Int. Conf. on Cloud Physics, Clermont-Ferrand, France
86. Zikmunda, J. and G. Vali, 1972: Fall patterns and fall velocities of rimed ice crystals. J. Atm. Sci., 29, 1334-1347.
87. Zwack, P. and C. Anderson, 1970: Showers and continuous precipitation. Proc. 14th Radar Meteorology Conf., 335-338.

1981 USAF - SCEEE SUMMER FACULTY RESEARCH PROGRAM

Sponsored by the

AIR FORCE OFFICE OF SCIENTIFIC RESEARCH

Conducted by the

SOUTHEASTERN CENTER FOR ELECTRICAL ENGINEERING EDUCATION

FINAL REPORT

JET SIMULATION PARAMETERS FOR WIND TUNNEL MODEL

THRUST REVERSER TESTING

Prepared by: Dr. Eugene E. Niemi, Jr.
Academic Rank: Associate Professor
Department and University: Mechanical Engineering Department
University of Lowell
Research Location: Arnold Engineering Development Center, Directorate
of Technology, Aeromechanics Branch
USAF Research Colleague: Dr. Keith L. Kushman
Date: September 4, 1981
Contract No: F49620-79-C-0038

JET SIMULATION PARAMETERS FOR WIND TUNNEL MODEL

THRUST REVERSER TESTING

by

Eugene E. Niemi, Jr.

ABSTRACT

An investigation is made of the simulation requirements necessary for wind tunnel tests of aircraft models using thrust reversers. Dimensional analyses are reviewed to determine the kinds of parameters that theoretically must be scaled to accurately represent a thrust reverser test. Previous test results are examined as a guide in deciding which of these parameters are most important in simulation.

It is found that the following parameters should be simulated to get reliable wind tunnel test data from thrust reversers: ratio of jet exit static pressure to free stream static pressure, p_e/p_∞ ; jet exit Mach number, M_e ; jet exit specific heat ratio, γ_e ; and product of gas constant and temperature of exiting jet, $(RT)_e$. Various gases are suggested for use in wind tunnel tests, based on these results.

The hysteresis effect in thrust reverser flow attachment to an aircraft fuselage is examined. Suggestions for future research in this area are made.

Recommendations for future wind tunnel tests to study thrust reverser behavior are made. Several types of tests are recommended.

ACKNOWLEDGMENTS

The author wishes to thank the Air Force Systems Command, the Air Force Office of Scientific Research, and the Southeastern Center for Electrical Engineering Education for providing him with the opportunity to spend his summer research assignment at the Arnold Engineering Development Center, Arnold AFS, Tennessee. He would like to thank the Arnold Center, in particular the Aeromechanics Branch, and the Directorate of Technology, for their hospitality.

The author would also like to thank Dr. Keith Kushman for suggesting this area of research, and Mr. Marshall Kingery for assistance with program details at the Arnold Center.

I. INTRODUCTION

The U. S. Air Force has developed a renewed interest in the use of thrust reversers for fighter aircraft. The concept of using thrust reversers on fighters is not new, however, having been investigated at least as early as 1959. Reference 1 describes full scale wind tunnel tests on a YF-86D aircraft using thrust reversers, and reference 2 describes flight tests on an F-94C aircraft using fully modulating target-type thrust reversers for in-flight thrust control.

The reason for this new interest is that the use of thrust reversers on current generation fighter aircraft in the landing mode may offer advantages worthy of investigation. Reverse thrust is also being considered as a tactical maneuvering technique in the transonic speed range.

The effect of thrust reverser deployment on an aircraft is a more specific application of the jet aircraft nozzle/afterbody topic. This topic has been of interest for several years, primarily for predicting the effect of a jet or rocket engine exhaust plume on the aerodynamics of a flight vehicle. Thrust reverser testing is a newer application of this topic, just now starting to be reexamined at the various Air Force Laboratories.

Wind tunnel tests on scale models are necessary to determine the effects of thrust reverser deployment on various aircraft configurations. This requires simulation of the wind tunnel model jet exhaust flow using either a cold gas exhaust or some type of hot jet exhaust.

The requirement for matching the representation of exhaust flow in wind tunnel tests is the subject of this paper.

II. OBJECTIVES

The general purpose of this project was to make a study of the simulation required in wind tunnel tests of thrust reversers (and nozzle/afterbodies) to be conducted in the future at various Air Force Laboratories, particularly the Arnold Engineering Development Center (AEDC). Simulation in this case refers to how accurately the exhaust plume must be modeled, whether by using cold gas or various hot gases. The specific objectives of this study can be summarized as follows:

- 1) To assess the total scope of simulation likely to be required in future thrust reverser and nozzle/afterbody testing to be conducted at AEDC.

- 2) To identify those simulation parameters considered most pertinent to testing, based on present knowledge.
- 3) To recommend, in general terms, future testing activities in the thrust reverser, nozzle/afterbody area that will improve the Air Force's ability to accurately predict the performance of fighter aircraft using thrust reversers.

III. PROBLEM AREAS WITH THRUST REVERSER DEPLOYMENT

A number of problems can arise due to deployment of thrust reversers, and these will be described in this section. The purpose of describing these possible problem areas is to point out the need for accurate simulation of thrust reverser flow field effects during wind tunnel testing.

In general terms, the types of problems that can arise are as follows: changes in aircraft stability and control, changes in aircraft drag, exhaust gas reattachment and/or reingestion into the engine inlet, heating of surfaces due to jet impingement, buffeting, and wind tunnel wall interference (tunnel testing only). The more important of these problems will be described in more detail below.

Changes in Aircraft Stability and Control

Aircraft stability changes can occur directly as a result of the exhaust gas impinging on various portions of the aircraft, or indirectly if the exhaust flow causes changes in the pressure distribution on parts of the aircraft. Direct exhaust gas impingement can also cause airframe buffeting or heating of surfaces. In these cases, the adequacy of simulating the far field of the jet exhaust becomes an important factor. This raises the question of whether or not a hot jet exhaust can be adequately simulated using a cold gas in the wind tunnel tests.

Changes in Aircraft Drag

Exhaust jet effects due either to normal thrust operation, or due to reversed flow can cause changes in aircraft drag and power required. Figure 1 on the next page shows a schematic of the flow field around a typical nozzle/afterbody configuration when the exhaust flow is in the conventional rearward direction. When the jet exhaust leaves the nozzle exit,

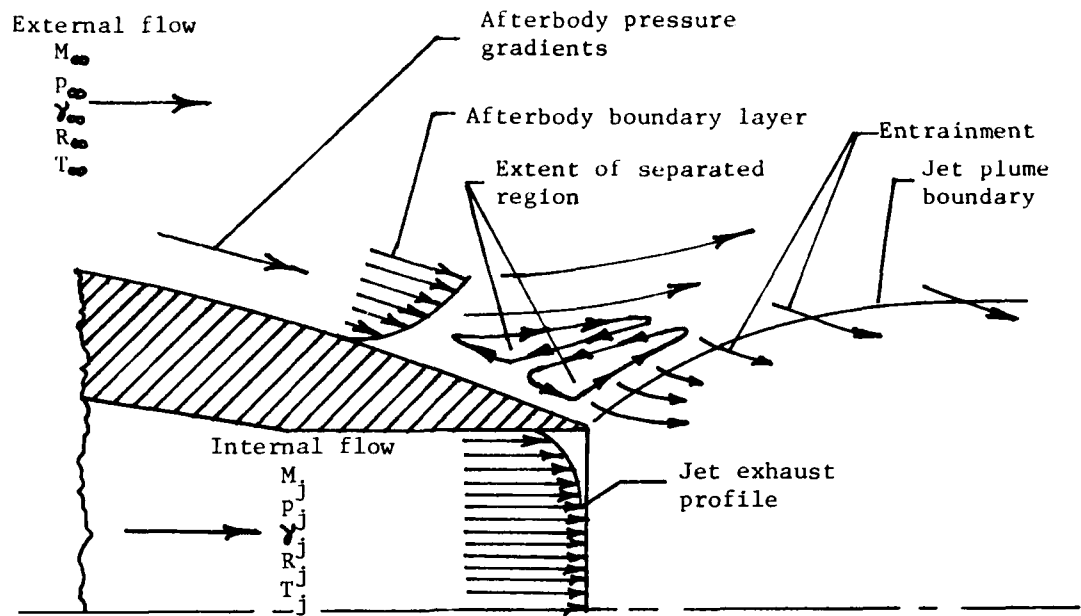


Figure 1. Factors influencing afterbody drag.

(Figure taken from ref.18 , see Section IV for nomenclature)

it influences the afterbody pressure distribution in two ways: by presenting a "body" which the external flow must negotiate, the so-called plume blockage; and by entraining fluid from the vicinity of the afterbody. These two effects tend to oppose each other, with plume blockage acting to raise the afterbody pressures, and the entrainment effect tending to lower them. Both effects are functions of the gas properties of the jet exhaust.

The net effect is a pressure change on the aircraft afterbody which causes a change in aircraft drag. The effect will vary depending on whether a hot gas or cold gas is used to simulate the jet exhaust.

Jet Reattachment to Fuselage

Another problem that can occur for certain thrust reverser operating conditions is reattachment of the reversed jet to the aircraft fuselage. This effect was reported in wind tunnel tests by Munniksmä³, and was also noted in wind tunnel tests⁴ conducted in July, 1981 at AEDC. The reattachment - detachment of the reversed jet exhibits a hysteresis effect that is different for a hot jet than for a cold jet, again raising the question of what type of jet simulation is necessary in wind tunnel tests.

Munniksma found abrupt changes occurring in aircraft pitching moment during jet attachment-detachment, and the effect was different for hot jets and cold jets.

Exhaust Gas Reingestion

An additional problem occurring as a result of the above described jet attachment effect is the possibility of reingesting the hot exhaust gases back into the engine inlet. This could result in drastic changes in engine performance, and would need to be thoroughly investigated before thrust reversers could be used in flight. This raises the possibility of having to simulate both engine inlet flow and exhaust flow simultaneously during wind tunnel testing.

Wind Tunnel Wall Effects

Finally, wind tunnel testing of configurations with simulated thrust reversers can cause considerable tunnel wall interference effects requiring tunnel blockage corrections that may more nearly approximate those encountered in V/STOL model testing, than in conventional aircraft testing.

Young⁵ summarizes the work of investigators in England who are studying the problem of reversed thrust blockage corrections.

Calculations done by Jacocks at AEDC in support of the thrust reverser tests planned in reference 4 showed considerable wall effects. To keep the computational mesh size down, calculations were done for reversed thrust testing in a simulated 8 foot tunnel, although the tests were actually conducted in the 16 foot transonic tunnel.

Summary of Various Investigations

A number of investigations have been made on the effect of deploying thrust reversers while in flight. Reference 6 is typical of tests conducted on wind tunnel models to determine stability and control changes occurring due to thrust reverser deployment on a single engine fighter model. The reader can consult the bibliography in this reference to identify additional work in this area.

Among the conclusions determined for the model fighter configuration tested were the following:

- 1) For certain blocker door positions, large nose-up or nose-down pitching moments could occur, presenting

potentially hazardous operation.

- 2) Reversed thrust decreased stabilizer effectiveness by 30 to 40 percent for most subsonic Mach numbers.
- 3) Reverse thrust mode produced a significant loss in directional stability and control at subsonic Mach numbers.

Hydrogen peroxide decomposition products were used to simulate the hot gas exhaust in these tests.

Extrapolation of these kinds of conclusions to the prototype flight vehicle makes it extremely important that one can place confidence in the validity of the jet exhaust simulation being used in the wind tunnel tests.

Typical wind tunnel data on a full scale airplane using thrust reversers is presented by Falarski and Mort.⁷ It was found that for some operating conditions, the lower exhaust plume from the thrust reverser would attach to the nacelle and fuselage lower surfaces. This attachment could be delayed by the addition of spoilers to the nacelle. For certain operating conditions, exhaust plume reingestion would occur when the aircraft was in the presence of a ground plane. Increasing reversed thrust also caused a reduction in longitudinal stability and control because the reverser exhaust plumes interfered with the horizontal tail.

In reference 1, various problems due to thrust reverser usage on the YF-86D were described. Among these were exhaust gas reingestion, elevation of skin temperatures, and buffeting of tail surfaces. The major aerodynamic effect of thrust reverser deployment was a change in aircraft stability due to a large nose-down pitching moment. No significant steady state effects occurred with the lateral characteristics, but there were some occasional directional oscillations due to random separation of reversed flow exhaust gases from the fuselage.

Additional wind tunnel studies and flight test data could be cited showing similar effects, but the references given should be sufficient to show the importance of using valid simulation or scaling laws in designing any wind tunnel tests for investigating thrust reverser phenomena. Additional test data can be located by consulting the bibliographies in references 6 and 7.

IV. OVERVIEW OF SIMULATION PARAMETERS

To conduct any jet effects testing in a wind tunnel, it is necessary to know what model scaling laws apply, which variables are of primary importance in scaling, and which ones are of lesser importance. This section of this report will cover jet scaling laws.

An extensive review of the literature was conducted to see what work has been done on the jet simulation problem in general, particularly with regard to modeling by use of dimensionless ratios. Bridgeman⁸ and Langhaar⁹ cover the topics of dimensional analysis and modeling in general terms, but one must turn to other references to get more specific information on modeling of jets.

Modeling of Jet Flows and Exhausts

Figure 2 is a schematic of a typical nozzle/afterbody and exhaust plume configuration, and shows many of the variables important in jet scaling studies (the meaning of the symbols can be found in the Nomenclature section at the end of this report).

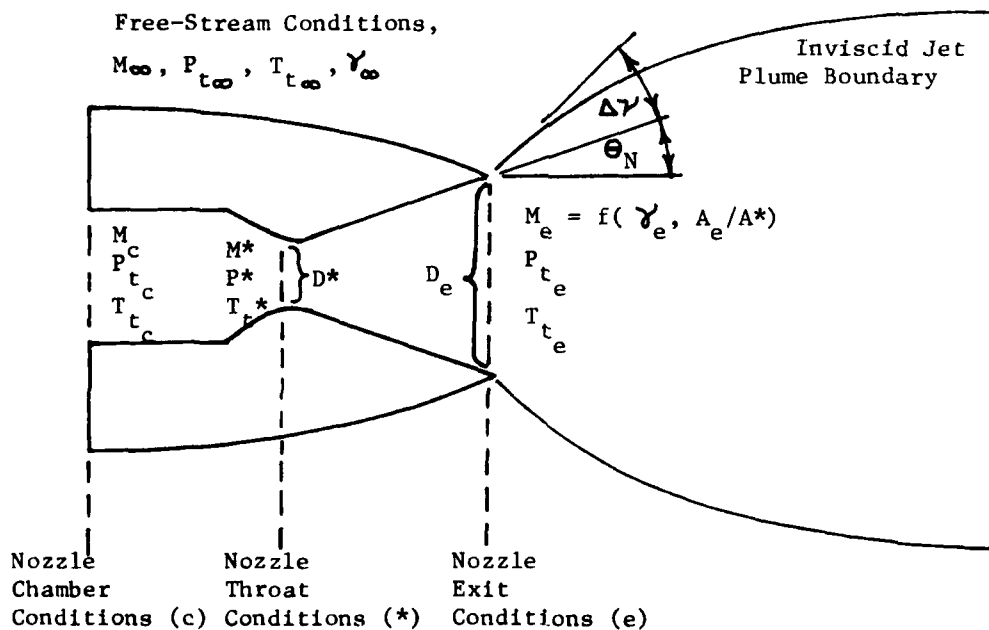


Figure 2. Schematic of nozzle and exhaust plume.
(Figure taken from ref. 20)

Pai¹⁰ does a brief dimensional analysis of jet flow and concludes that the following variables are of importance in the study of free jet flows:

$$\text{Jet Reynolds Number:} \quad R_e = U_e D_e / \nu_e \quad (1)$$

$$\text{Jet Mach Number:} \quad M_e = U_e / a_e \quad (2)$$

$$\text{Jet Prandtl Number:} \quad Pr_e = C_{p_e} \mu_e / k_e \quad (3)$$

$$\text{Jet Specific Heat Ratio:} \quad \gamma_e = C_{p_e} / C_{v_e} \quad (4)$$

$$\text{Jet Nusselt Number:} \quad N_e = h_e D_e / k_e \quad (5)$$

For jet mixing with gases of different kinds (i.e., engine exhaust and air), Pai states that the diffusion equation must be added to the fundamental equations.

One of the more complete evaluations of jet scaling factors, done by dimensional analysis, is presented by Li, Yoler, and Morgan.¹¹ After a considerable discussion of many of the physical variables, the authors conclude that ". . . a fairly accurate simulation of jet-on effects can be insured by matching the following important non-dimensional parameters:"

- R_∞ - free stream Reynolds number
- M_∞ - free stream Mach number
- γ_e / γ_∞ - ratio of specific heat ratios, jet to free stream
- M_e / M_∞ - ratio of jet exit to free stream Mach numbers
- U_e / U_∞ - ratio of jet to free stream velocities
- p_e / p_∞ - ratio of jet exit pressure to free stream static pressure
- ρ_e / ρ_∞ - ratio of jet exit to free stream density
- α - aircraft angle of attack
- D/L - aircraft "diameter" to length ratio (i.e., geometric scaling)
- D_e/L - ratio of nozzle exit diameter to aircraft length
- $(D_e - D^*)/L$ - nozzle exit minus throat diameter, to aircraft length

Matching these quantities also assures that the following additional ratios are automatically satisfied: ratio of jet kinetic energy to free stream kinetic energy, and ratio of jet mass flow to free stream mass flow. Factors judged to be of lesser importance in this study were diffusion

coefficients, molecular weights, temperature ratios, heat capacities, and viscosity ratios.

Note that many of the parameters are dependent on each other. It should be pointed out that although this study felt that temperature ratio, T_e/T_∞ , might be of lesser importance, other references (to be cited later) indicate that temperature is an important factor. Heat transfer coefficients were also neglected. The study was made for rearward facing jet exhausts, but its conclusions should also apply for the case of thrust reverser simulation. The report concluded by recommending the use of heated helium as one of the best gases to simulate hot gas exhausts. No experimental data were cited to prove or disprove the relative importance of many of the ratios examined.

Pindzola¹² also does a very complete study of jet simulation in ground test facilities, and breaks down the requirements for simulation into two regions: jet exit effects and downstream effects. He shows that the jet exit effects can be simulated by matching the initial inclination angle, $\Delta\gamma$, of the jet. This can be accomplished by duplicating the jet exit static pressure ratio, p_e/p_∞ , the nozzle exit angle, θ_N , and the similarity parameter, $\gamma_e M_e^2 / \sqrt{M_e^2 - 1}$. This will match the initial jet turning angle even if the γ_e values are different. These requirements are in addition to matching the free stream conditions.

To match downstream effects a short distance from the nozzle, in addition to the above required simulation, it is necessary to match the product of gas constant and temperature, $(RT)_e$, at the jet exit. Matching of $(RT)_e$ also appears to provide a means of simulating the mixing boundary, but no correlation parameters are available for use in predicting full scale results from data obtained from unmatched conditions of $(RT)_e$.

When wing or tail surfaces are immersed in or placed near to a jet exhaust, Pindzola states that duplication of jet momentum appears to be the most critical jet flow parameter for simulation.

Some references discuss scaling momentum ratio, others talk about scaling dynamic pressure. These are equivalent, since it can be shown that

$$\frac{q_e}{q_\infty} = \frac{\rho_e U_e^2}{\rho_\infty U_\infty^2} = \left(\frac{p_e}{p_\infty} \right) \left(\frac{\gamma_e M_e^2}{\gamma_\infty M_\infty^2} \right)$$

Therefore, the reference 11 requirement to scale the density ratio, ρ_e/ρ_∞ , and velocity ratio, U_e/U_∞ , individually; also automatically satisfies the requirement to scale the momentum ratio. Similarly, a requirement to scale the pressure ratio, p_e/p_∞ , and the ratio of $\gamma_e M_e^2 / \gamma_\infty M_\infty^2$ also automatically scales the momentum (or dynamic pressure) ratio. However, a requirement to scale only the momentum ratio is not as stringent, since scaling the momentum ratio does not automatically satisfy scaling ρ_e/ρ_∞ , U_e/U_∞ , or p_e/p_∞ .

Jet Mixing Simulation

Mixing along the jet boundary is governed by the viscosities, momentums, and heat transfer rates of the local elements of the flow at the jet boundary. As pointed out by Pindzola¹², very little work has been done in deriving simulation parameters for the mixing processes along the jet boundary. The best way to obtain information on these parameters then is to look at some of the principles involved in heat transfer simulation, in addition to general flow simulation.

Schlichting¹³ shows that the dimensionless ratios involved in convective heat transfer are the Reynolds number, Prandtl number, Grashof number, and Eckert number. The Reynolds number and Prandtl number were referred to earlier in Pai's analysis of jet scaling parameters. The Grashof number is important only where buoyancy forces predominate, such as in free convection, and would be unimportant for the types of flow of interest here. The temperature field and coefficients of heat transfer are functions of the Eckert number when temperature differences are large and simultaneously when velocities are large and on the order of the velocity of sound. This is the case in the study of jet mixing and heat transfer from jet exhausts, and therefore would apply to hot jets at transonic speeds.

The definition of the Eckert number and its relationship to the Mach number is as follows:

$$E = \frac{U_\infty^2}{C_p (\Delta T)_o} = (\gamma - 1) M^2 \frac{T_\infty}{(\Delta T)_o} \quad (6)$$

where: $(\Delta T)_o$ is a temperature difference governing heat transfer rate, such as between the jet exhaust and the free stream.

The effect of the Eckert number in jet mixing studies needs to be explored further.

The effect of turbulent mixing would also involve such things as eddy viscosity, and it appears that the freestream and jet turbulence intensity, T , may also be an important factor in determining jet mixing characteristics. It is apparent that more work needs to be done in this area to more clearly define the factors affecting jet mixing, and how they may be scaled.

In summary then, it appears that jet mixing may be simulated if the Reynolds numbers, Prandtl numbers, Eckert numbers, and turbulence intensities are simulated, in the free stream and in the jet exhaust.

At this point, if one did not have some experimental evidence to rely on for guidance, it would appear that the simulation requirements are very complex. Simulation of virtually every parameter would seem to be required, an almost impossible task. Heated gases or multi-component gas mixtures would be required to simulate all the actual hot gas properties. Fortunately, the simulation requirements can be relaxed somewhat, based on experimental data that are available to show the effect of the more important variables. Some of these test data will be reviewed in the next sections, and the effect of relaxing the simulation requirements somewhat will be discussed in a subsequent section.

Review of Experimental Data on Jet Simulation

Some additional facts relative to jet simulation have been gleaned from the literature and are summarized in the sections to follow.

Spring.¹⁴ Spring states that correlation studies of experimental data showed that the most consistent behavior for near field effects was obtained when they were plotted versus the jet momentum to free stream momentum ratio, $(\rho U_e^2)/(\rho U_\infty^2)$.

Chrans and Collins.¹⁵ These investigators studied the lateral injection of argon, helium, and nitrogen from a sonic nozzle into a supersonic stream, using various stagnation temperatures for the gases. It was found that stagnation temperature had no significant effect on jet penetration height, but did affect the bow shock radius somewhat. Molecular weight had a small effect on jet penetration height and a more important effect on bow shock radius. Jet momentum, not jet mass, was found to be the main

determinant of the observed jet effects.

Gilman.¹⁶ Gilman was able to obtain comparable near field effects for helium and air, and from two different jet configurations, when test data were compared on a momentum basis at the same chamber pressure. However, the tests were for a supersonic free stream, and he did not expect the correlation to work as well for a subsonic free stream.

Tolhurst, Kelly, and Greif.¹ In reference 1 discussed earlier, a full scale YF-86D aircraft was tested in the wind tunnel to determine the effects of thrust reverser use. The various problems that were found have already been described. The major aerodynamic effect of thrust reverser use was a change in aircraft stability due to a large nose-down pitching moment.

For the range of variables tested in these experiments, it was possible to correlate pitching moment changes and stabilizer buffeting with the ratio of reversed thrust to free stream momentum, $F_G/q_\infty S$, where

- F_G - gross thrust from engine
- q_∞ - free stream dynamic pressure
- S - wing area.

A simplified dimensional analysis of thrust reverser effects on horizontal tail forces was conducted. The ability to determine a non-dimensional ratio that served to correlate tail buffet data makes it appear that fluctuations in angle of attack and dynamic pressure, as well as the mean flow field near the tail, are determined by $F_G/q_\infty S$.

The test results indicated that it should not be necessary to duplicate the full scale engine tail-pipe pressures and temperatures to obtain similarity between the test flow field and the actual flow field as long as the quantity $F_G/q_\infty S$ is duplicated.

These results on the far field effects, although somewhat in conflict with those of other studies to be quoted later, are in agreement with the results of Spring, Chrans and Collins, and Gilman. They all expressed the result that the most important scaling parameter was the momentum ratio, which is closely related to $F_G/q_\infty S$. It may be that the horizontal tail in the F-86 tests had an integrating effect on the disturbed flow field at this distance from the jet, in such a manner that variations were averaged out across the span of the tail. For other configurations, or positions

of control surfaces in the thrust reverser flow field, the importance of the other effects might become apparent.

Squire.¹⁷ Some early data are presented by Squire, on jet characteristics in general, and on the effect of jet momentum and temperature on the downwash at the tailplane of an aircraft. It is shown that the jet momentum is the main contributor to downwash angle at the tailplane, and that jet temperature has a smaller, secondary effect. However, extrapolation of Squire's data from cold jet to hot jet conditions indicates that, although temperature is secondary to momentum, it may still be important enough to require consideration.

Compton.¹⁸ Compton reports experimental data obtained with nacelle models having afterbodies with two different boattail angles. Tests were conducted for subsonic speeds and transonic speeds using both air for a simulated exhaust, and hot exhaust gases formed from the decomposition of various concentrations of hydrogen peroxide. Afterbody pressure drag coefficients were obtained from integrations of experimental pressure distributions.

It was found that the use of cold air to represent the actual exhaust could cause afterbody drag to be overpredicted by as much as 17%, compared to the values obtained from hot gas decomposition which approximated a dry turbojet exhaust. It was also found that corrections for plume blockage did not eliminate very much of the drag difference. Thus, the effect of jet entrainment on afterbody drag was seen to be significant, and affected primarily by the temperature of the jet.

Corrections for plume shape differences could be made by relating the drag to the computed initial inclination angle of the jet plume. Entrainment differences were difficult to predict, but seemed to be approximately a straight line function of the product of the jet exhaust gas constant and local temperature, $(RT)_e$.

Compton's work and results appear to be a forerunner of the type of work conducted recently by the Air Force at AEDC.

Review of AEDC Work in Jet Simulation

Considerable work has been done at AEDC in the area of jet simulation for nozzle afterbody configurations. Both experimental and theoretical work have been done. In this section, coverage will be given primarily to recent

experimental work oriented toward jet simulation and comparison of hot and cold gas jet effects.

Galigher, Yaros, and Bauer.¹⁹ These investigators experimented with three boattail geometries over a Mach number range from 0.6 to 1.5, using cold air and burning ethylene-air mixtures to simulate the exhaust plume. Exhaust temperatures were varied from 540° R to 2900° R. Afterbody pressure distributions were measured and converted to afterbody pressure drag coefficient.

An attempt was made to adjust the cold air test data to predict hot gas effects by just increasing cold air nozzle pressure ratio to match the jet plume initial inclination angle of the hot jets. This procedure would not collapse all the data for different hot gas temperatures onto a single curve. In other words, jet entrainment effects due to temperature differences were found to be just as important as jet plume blockage effects due to jet turning angle.

Peters.²⁰ Peters studied various jet simulation parameters to characterize the shape of the inviscid jet plume boundary. Tests were conducted over transonic Mach numbers and at jet temperatures varying between 540° R and 3300° R, using cold air and burning ethylene-air mixtures. Exit area ratio of the boattails was also varied.

For underexpanded nozzle flow, Peters found that correlation parameters that characterize the inviscid jet plume boundary provided significantly better hot and cold jet simulation than nozzle total pressure ratio (NPR). Nozzle total pressure ratio is an older correlation parameter that does not work nearly as well as other parameters which characterize the inviscid plume shape. However, at nozzle design conditions, nozzle pressure ratio correlated drag data as good as any other variables.

It was found that the modified inviscid plume shape parameters, $(\Delta\gamma)(A/A^*)$, and $(p_e/\gamma p_\infty)(A/A^*)$ gave good drag correlation for many different test conditions.

Peters.²¹ To study the effect of independent variations in exhaust gas constant, R , and specific heat ratio, γ , on afterbody drag, Peters used cold gas mixtures of nitrogen and hydrogen, and nitrogen, hydrogen, and ethylene individually. Gas constants were varied between $55 < R < 767$ ft-lbf/lbm-°R, and specific heat ratios were varied between $1.2 < \gamma < 1.4$.

It was found that the gas constant affected afterbody drag solely through entrainment (jet mixing), while the specific heat ratio affected afterbody drag primarily by controlling inviscid jet plume shape. The specific heat ratio effects were predictable by duplicating an inviscid jet plume shape parameter such as nozzle static pressure ratio, NSPR. The entrainment effects varied linearly with \sqrt{R} and \sqrt{RT} .

Bauer.²² Bauer develops a theory for predicting entrainment effects. A brief numerical study indicated that entrainment was correlated by the parameter $(RT)_e$, which is in agreement with the experimental results found by Peters.²¹ Bauer showed that matching the jet initial turning angle, $\Delta\psi$, correlated hot and cold afterbody drag for supersonic flow, but entrainment correction was necessary for subsonic and transonic flow.

Peters.²³ This investigation by Peters develops an experimental method for correcting afterbody drag coefficient data for the effect of jet gas constant (and by inference, temperature). Tests were conducted using cold nitrogen, hydrogen, helium, and nitrogen-hydrogen mixtures to determine effects of changes in gas constant on afterbody drag coefficient. Three nozzle exit area ratios were tested over a wide range of pressure ratios at Mach numbers between 0.6 and 1.2.

No jet simulation parameter correlating jet mixing effects was isolated, but experimental corrections for mixing could be made if data were available at several values of gas constant. This is because it was found that afterbody incremental drag coefficient at a fixed inviscid jet plume shape decreased linearly with increasing jet gas constant, R_e . By inference, the same correction was expected to be valid for changes in the $(RT)_e$ product. Thus, experimental corrections for temperature should be valid if data are available for several gas constants.

These results and the results presented in reference 21 are in agreement with the results obtained by Compton.¹⁸

Summary. All the detailed work for correlating plume shape and jet entrainment effects conducted to date is for nozzle/afterbody tests only, and does not address the larger picture of thrust reverser testing and complete aircraft configurations. Thus, the validity of methods such as presented in reference 23 (especially with the wide data scatter) must be taken cautiously if they are to be extrapolated to more complex configurations.

Comparison of Experimental Results

Review of the literature available indicates an apparent conflict in the relative importance of certain variables required for jet simulation. This is especially true concerning the effect of jet temperature on the flow field induced by the jet. Some investigators have found jet temperature to be of negligible importance if jet momentum is scaled. However, recent nozzle/afterbody work has found the temperature to be an important effect.

It might be expected that a configuration as simple as a nozzle/afterbody would be affected only by near field jet effects. If this were the case, then the jet plume corrections outlined in reference 20 would enable one to adjust nozzle pressure ratio (or some other inviscid plume shape parameter) for a cold air jet to simulate the plume shape for a hot jet. As pointed out in reference 19, however, this procedure did not work when scaling cold air data to an ethylene-air hot jet.

Although other investigators (Squire, Gilman, Strike, etc.) found momentum scaling adequate for tail surface forces, the nozzle/afterbody tests in particular seem to show the importance of the entrainment $(RT)_e$ effect in jet testing. This is probably due to the fact that jet entrainment occurs directly along the geometric axis of a nozzle/afterbody, thus directly changing the entrainment drag of the object. In the case of other geometries such as tail surfaces, the entrainment effects are further removed from the geometry of the object.

For the aircraft configuration studied by Squire¹⁷, the downwash at the tailplane would be due to an entrainment effect far enough removed from the tailplane location to be of secondary importance. For tailplanes located closer to the jet exhaust, the temperature effect on downwash might be more significant.

Squire does make the interesting point that as a hot jet develops downstream of the exit, the mass flow, temperature, and velocity all vary, whereas the momentum remains constant. Thus, it is proposed that a cold jet should have the same momentum as the hot jet it represents.

Squire also refers to test data for jets impinging on wings, and states that the increase in wing drag is a function of the jet momentum only.

V. SIMULATION REQUIREMENTS

In this section, the significance of the information reviewed in the previous section will be used to determine requirements for jet simulation. First, the requirements for complete jet simulation will be examined, followed by a look at the effect of relaxing some of the simulation requirements. Finally, minimum simulation requirements will be examined, followed by recommendations for a practical compromise on simulation.

Optimum Jet Simulation

Examination of the total simulation picture using information from all the sources examined indicates that theoretically complete simulation would be obtained only if all the dimensionless ratios developed by Li, Yoler, and Morgan¹¹ were matched. These ratios were listed in the section entitled Modeling of Jet Flows and Exhausts, and will not be repeated here. In addition, the temperature ratio would have to be matched to simulate entrainment effects.

Representation of the interference effects of the downstream jet requires simulation of the mixing processes along the jet boundary, in addition to simulation of near field effects. The mixing along the jet boundary is governed by the viscosities, momentums, and heat transfer rates of the fluid particles of the mixing flows, so complete simulation involves essentially complete representation of the actual engine exhaust. This means duplication of jet Reynolds number, Prandtl number, diffusion coefficients, and turbulence level, and requires using gases other than cold air to simulate the exhaust.

Effect of Relaxing Simulation Requirements

It is desirable now to examine the effects of relaxing the above simulation requirements somewhat, in light of the experimental data reviewed in the last few sections

The interference effect consists primarily of two parts: the near field effect in the immediate vicinity of the jet exhaust, and the far field effect if the jet ultimately impinges on any part of the aircraft structure. Hensel²⁴ discusses the importance of the various parameters on these two parts of the jet interference. The near field interference effects can be simulated if the following three parameters are matched: ratio of jet exit

static pressure to free stream static pressure, p_e/p_∞ ; jet exit Mach number, M_e ; and jet exit specific heat ratio, γ_e . The exit static pressure ratio is considered of first order importance in defining the shape of the jet boundary immediately after exit from the nozzle. For an underexpanded jet, γ_e and M_e will determine the initial turning angle of the jet boundaries after exit from the nozzle (Prandtl-Meyer expansion), and this will obviously define the jet plume shape in the immediate vicinity of the jet exit.

If γ_e cannot be matched (which is the case when using air), then the initial jet inclination angle can be matched by using the simulation parameter $\gamma_e M_e^2 / \sqrt{M_e^2 - 1}$, when using a supersonic nozzle. However, the jet boundary variation will not be matched beyond the initial turning angle if M_e is not matched. For a sonic nozzle, the above simulation parameter does not apply, and both M_e and γ_e must be individually matched for correct jet simulation. Recall that the simultaneous matching of nozzle exit static pressure ratio, specific heat ratio, and Mach number also satisfies the scaling requirement for momentum ratio.

For simulating far field effects, or for where any significant jet impingement is involved, then it becomes necessary to simulate the jet internal properties as well. This requires matching of six additional jet internal properties, which are taken care of if the following three parameters are matched simultaneously: γ_e , M_e , and $(RT)_e$.

Minimum Jet Simulation

The minimum effort that must be expended to obtain some degree of simulation of jet effects occurs when only near field effects need be modeled. This can be accomplished with a cold air jet, which limits one to matching only p_e/p_∞ and $\gamma_e M_e^2 / \sqrt{M_e^2 - 1}$, if the model nozzle geometry is left as a variable. This will match initial jet expansion angle and jet momentum ratio. If the model nozzle geometry is preset, then a cold air jet allows one to match only the jet momentum ratio.

Of course, these requirements are in addition to the customary wind tunnel requirements which require matching M_∞ , R_∞ , γ_∞ , and satisfying model external geometric similarity.

Practical Jet Simulation

As in all aerodynamic modeling tests conducted over the years, experience has shown that the effect of certain parameters is less important than the effect of other parameters. In the case of wind tunnel tests on thrust reversers, jet impingement and far field effects are involved as well as near field effects. Experimental data examined to date indicates that minimum jet simulation will not be sufficient, since near field plume modeling is not adequate.

It is recommended that the following parameters be matched in thrust reverser testing and in future nozzle/afterbody testing:

- p_e/p_∞ - ratio of jet exit static pressure to free stream static pressure
- M_e - jet exit Mach number
- γ_e - jet exit specific heat ratio
- $(RT)_e$ - product of gas constant and temperature of exiting jet.

These are again in addition to the usual tunnel flow simulation requirements and geometric model scaling. To satisfy the γ_e and $(RT)_e$ scaling requirements, it is necessary to use a hot gas exhaust such as obtained from burning ethylene or decomposing hydrogen peroxide, or by using various gas mixture combinations at more nearly ambient temperatures. Recommended gases will be covered in the next section.

Selection of Candidate Gases

There are a number of gases or gas mixtures available that will approximate the required values of specific heat ratio and gas constant to simulate a turbojet exhaust. It would be ideal if cold air could be used, but analyses and tests have shown that cold air will provide only minimum simulation for near field effects, and is not suitable for more involved testing.

There are several arguments against using exhaust gases other than cold air, namely the additional complexity and cost of the required test equipment, and the cost of the gases involved. However, when one considers the high basic operating cost of the larger tunnels, the cost of the model, and the importance of the use to which the data will be put; it is "penny

wise and pound foolish" to conduct any tests that do not adequately simulate the desired prototype conditions. To quote from an earlier Air Force Summer Design Study,²⁵ ". . . the accuracy or precision of present instrumentation is probably at least an order of magnitude better than the accuracy of simulation of the test being conducted in the wind tunnel." Thus, it is very important that the tunnel model scaling laws have been properly assessed before a test is conducted or resulting data interpreted.

Simulation of a turbojet exhaust can be obtained in three basic possible ways:

- 1) Using mixtures of two or three component cold gases -- this avoids the need for combustion or heating the gas, but introduces some complexity due to the need to accurately mix the gases.
- 2) Burning a fuel-air mixture approximating the turbojet exhaust characteristics -- a mixture of ethylene and air is suitable for this.
- 3) Using compounds that decompose in such a way that the resulting products approximate the $(RT)_e$ product for a turbojet exhaust -- hydrogen peroxide is suitable in this regard.

A brief table of some possible turbojet exhaust gas simulations is given below, with data for air given as a comparison.

Gas	γ_e	R_e (ft/ $^{\circ}$ R)	T_e ($^{\circ}$ R)	$(RT)_e$ (ft)
Turbojet Exhaust ²⁷	1.34	53.4	1600	8.5×10^4
Cold Air	1.4	53.3	520	2.8×10^4
N_2 - H_2 Mixture ²¹ with molecular weight = 6.68	1.4	231	630	14.6×10^4
Ethylene-Air ²¹ (burned)	1.33	53.4	1550	8.3×10^4
H_2O_2 (90% conc.) ²⁷	1.27	69.9	1820	12.7×10^4

An extensive study of cold gas mixtures, including three component gas mixtures that also satisfy the simulation requirements can be found in Tempelmeyer's work.²⁶

Hydrogen peroxide decomposition products should be good for simulation purposes without requiring the use of an actual combustor. In addition to the match shown in the table for gas constant and specific heat ratio, the kinematic viscosities and thermal conductivities of a hydrogen peroxide jet and turbojet exhaust are close to each other. Therefore, jet interface mixing phenomena should be closely simulated if the thrust coefficients and ratios of jet temperature to stream temperature are close. Actual limits of applicability would have to be determined by experimental comparisons.

More data on the characteristics of hydrogen peroxide and the equipment required for its use can be found in reference 27.

VI. THRUST REVERSER FLOW FIELD ATTACHMENT

As mentioned previously, when a thrust reverser is used on an aircraft either during the landing roll or in flight, there is a possibility for the exhaust flow reattaching to the fuselage. This phenomenon is illustrated in Figure 3 below.

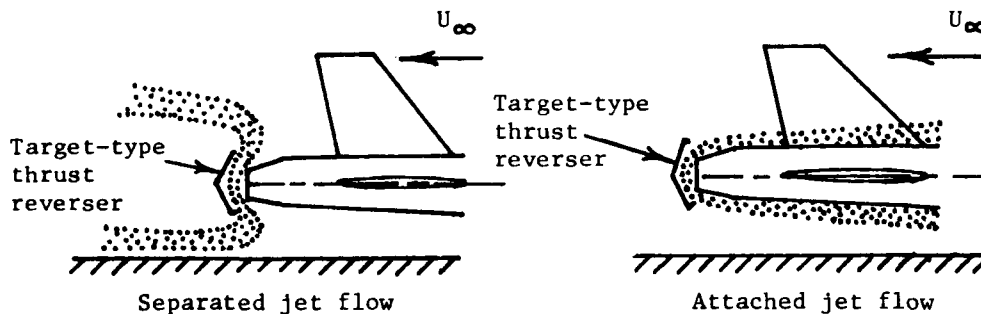


Figure 3. Possible modes for thrust reverser flow.

The reattachment phenomenon is a function of nozzle pressure ratio, jet characteristics, forward speed, and thrust reverser-boattail geometry. This attachment of the thrust reverser jet to the aircraft afterbody is a variation of the so-called "Coanda effect," but occurring under the somewhat different conditions of compressible flow and with a main stream flow approaching from the opposite direction. This same behavior was reported in the Dutch tests of reference 3.

In the tests conducted at AEDC⁴, a hysteresis effect in the jet behavior

during attachment-detachment was noted, although this type of hysteresis effect was not reported in the Dutch tests. Nevertheless, a hysteresis effect is also common to the more general Coanda effect. Obviously, any type of hysteresis would cause significant changes in aircraft drag and stability that would need thorough investigation.

In the work done by Bourque and Newman²⁸, the hysteresis effect was noted in terms of the range of angles over which an incompressible jet would attach to an adjacent sidewall.

The Coanda effect is a viscous phenomenon, as explained in reference 29, and is a function of flow entrainment along the edge of the jet. Perry²⁹ develops a theory for predicting jet reattachment location for an incompressible jet, and Olson³⁰ develops a theory for predicting reattachment conditions for a two-dimensional, compressible jet. Very recent work done in this area can be found described in reference 31.

In the thrust reverser tests conducted at AEDC, a similar Coanda type effect occurred with the reversed exhaust jet either attaching to the nozzle afterbody or staying detached, in a geometry similar to that shown in Figure 3. This is a three dimensional axisymmetric Coanda effect. Time did not permit searching for any references in the literature on three dimensional Coanda effects. Significant differences existed between the test conditions causing the cold jet to attach and the conditions causing a hot jet to attach.

Since attachment-detachment of the jet to the nozzle/afterbody can cause large changes in drag and stability, this area needs to be researched thoroughly. In addition, jet attachment can cause high afterbody skin temperatures and exhaust gas reingestion into the engine inlet. Thus, considerable work will have to be done to develop theories and experiments to study this phenomenon. Particularly needed is the development of a simplified theory for predicting Coanda effect in three dimensional, axisymmetric flow.

As mentioned earlier, Peters points out that jet entrainment effects are a function of the $(RT)_e$ product for the gas. Therefore, wind tunnel experiments simulating the jet attachment phenomenon will require matching the $(RT)_e$ product in the tunnel tests, as well as the exhaust gas specific heat ratio.

It will be recalled that certain investigations²¹ showed that the $(RT)_e$ product for an actual exhaust gas could be simulated by either matching the higher temperature, or by using a cooler gas having a higher gas constant,

as long as the product of gas temperature and gas constant matched the $(RT)_e$ product for the actual exhaust. Wind tunnel simulation of the thrust reverser hysteresis effect would provide an acid test of this concept, since the Coanda effect occurs because of entrainment and mixing along the jet boundary.

VII. RECOMMENDATIONS

Based on the data evaluated in this study, recommendations for future testing can now be made. Recommendations will be addressed toward five kinds of testing efforts and how they should be handled. These are as follows:

- 1) Complete aircraft configurations, without thrust reversers, with exhaust in conventional rearward direction.
- 2) Complete aircraft configurations with thrust reversers operating.
- 3) Future basic nozzle/afterbody testing.
- 4) Current AEDC thrust reverser tests.
- 5) Future basic thrust reverser testing.

Complete Aircraft Configurations Without Thrust Reversers

For this kind of test, where exhaust plume simulation is desired, testing with a simulated cold air jet will be adequate. The reason for this is because the afterbody drag is only a portion of the total aircraft drag. Testing with cold air to simulate the exhaust plume will result in some error, but it is a comparatively small error compared to the total configuration drag, and in light of the accuracy to which drag can be determined from a wind tunnel test.

The nozzle pressure ratio of the cold air jet should be adjusted to give an exhaust plume matching the calculated shape of the actual exhaust plume. In this manner, plume blockage effects on drag will be modeled, although the entrainment effect on drag will be in error by some amount. However, this error will be conservative.

This type of test is recommended for conventional configurations having no unusual characteristics that might be abnormally affected by the exhaust plume.

Complete Aircraft Configurations With Thrust Reversers

In this kind of test, with thrust reversers in operation, it is important that exhaust effects be simulated as accurately as possible. It is recommended that plume simulation be done with scaled engines (such as the ethylene air combustors), or decomposition products of hydrogen peroxide. The

wind tunnel tests reported in reference 6 provide a good example of how this should be done. The models should be build-up models with detachable wings and tail surfaces. In this manner, body-alone, body-wing, and body-wing-tail configurations can be tested if necessary to isolate any problem areas that may arise due to thrust reverser usage.

If hot plume duplication must be avoided because of model temperature considerations, then the three component gas mixtures of reference 26 could be used as a minimum. Use of cold air for thrust reverser tests will not provide adequate simulation and is discouraged.

If flow situations are discovered where extensive jet attachment to the fuselage occurs, then it will be necessary to avoid these conditions in flight, unless the model tests are conducted with inlet flow simulated also.

Movable control surfaces may be required on the model, to determine the effect of the hot plume on the control surfaces, and pressure measurements should be made on the afterbody, together with Schlieren photography and Thermovision studies of the flow field.

Basic Nozzle/Afterbody Testing

Considerable testing of basic nozzle/afterbodies has been done at Arnold Center. The correlation studies to date have shown that both plume blockage and jet entrainment must be simulated. Integrated afterbody pressure drag has been used extensively as the determining parameter for equal jet effects on boattails. This may not be a valid measure for more complicated geometries, since it is an averaging axial measurement only. The effects of skin friction drag may also need to be considered.

For the immediate future, basic nozzle/afterbody testing can be done in any of three ways: using ethylene-air combustion (or a similar arrangement), decomposing hydrogen peroxide, or using two or three component gas mixtures at ambient temperatures.

Further research, either analytical or experimental, is necessary to determine the importance of diffusion coefficients, jet Reynolds number, and jet Prandtl number on the jet mixing process. When these effects have been determined, it may be that one of the three methods outlined above will prove to be superior for modeling actual exhausts.

Conduct of the thrust reverser testing and analyses outlined in the next

sections will also shed more light on the best way to proceed with future basic nozzle/afterbody tests.

Current AEDC Thrust Reverser Testing

Prior to performing the more complicated tests suggested in the next section, it is recommended that the tests conducted at AEDC in conjunction with reference 4 be thoroughly analyzed, and the same types of correlation attempts be applied to them as for conventional hot gas vs. cold gas nozzle/afterbody tests conducted to date.

Since the reverse thrust jet attachment-detachment is a complicated flow phenomenon, any successful correlation studies conducted between hot and cold gases will shed much more light into the relative importance of various similarity parameters. In particular, since the attachment-detachment hysteresis effect was different for hot and cold gases, correlation parameters that will collapse the hot and cold gas hysteresis data onto one curve would be most useful.

Future Basic Thrust Reverser Testing

Earlier reported studies showed a conflict in the need to simulate temperature ratio in the jet -- several studies found that matching momentum ratio was adequate when control surfaces were immersed in a jet. To resolve this question, it is recommended that wind tunnel tests be conducted for a nozzle/afterbody thrust reverser configuration with a single stabilizer surface located in the reversed flow as shown in Figure 4.

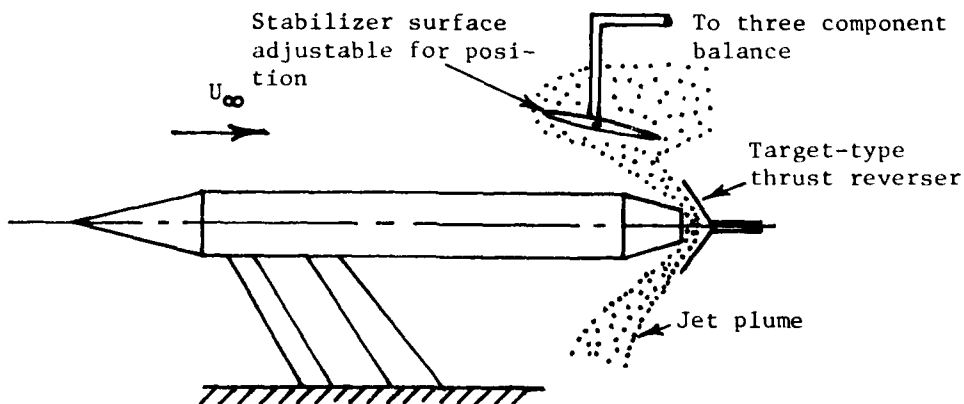


Figure 4. Thrust reverser test arrangement

Forces and moments acting on the stabilizer should be measured with a three component balance, and the stabilizer should be designed to be adjustable horizontally, vertically, and in angle of incidence. Tests should be conducted with the three exhaust gases recommended for complete configuration thrust reverser testing: burning ethylene-air mixtures, decomposing hydrogen peroxide, and three-component cold gas mixtures. Pressure distribution should also be measured over the afterbody as in conventional nozzle afterbody tests.

Schlieren, Thermovision, and flow field probing can all be used to determine changes in jet mixing patterns for different exhaust gases. Testing the stabilizer in various positions will show if the requirement for jet temperature modeling, as well as momentum modeling, arises only for certain positions of the surface relative to the exhaust.

Data analysis and correlation studies should be done in the same manner as previous testing has been handled.

Wind Tunnel Wall Effects

The testing of thrust reversers causes considerably more wall effects than conventional testing. Thus, additional effort will be required for determining wind tunnel boundary corrections during thrust reverser tests.

For the time being, it is recommended that tunnel blockage corrections be applied using a method like that of Hackett and Wilsden.³² This method has shown good drag correlation for models up to 10% of test section area.

Analytical Work

Analytical efforts should be concentrated on developing mathematical models for the three-dimensional, axisymmetric Coanda effect. The eventual goal of this theoretical development would be to predict conditions under which a cold or hot jet attach to a nozzle afterbody with thrust reverser.

Conclusions

A review of jet simulation parameters has been conducted, and those simulation parameters considered most pertinent to thrust reverser testing have been identified.

Recommendations for future testing efforts have been made. Considerable additional understanding of the jet attachment and scaling phenomena should be realized if these recommendations are followed.

REFERENCES

1. Tolhurst, W. H., Jr., M. W. Kelly, and R. K. Greif, "Full-Scale Wind Tunnel Investigation of the Effects of a Target-Type Thrust Reverser on the Low-Speed Aerodynamic Characteristics of a Single-Engine Jet Airplane," NASA TN D-72, Sept., 1959.
2. Anderson, S. B., G. E. Cooper, and A. E. Faye, Jr., "Flight Measurements of the Effect of a Controllable Thrust Reverser on the Flight Characteristics of a Single-Engine Jet Airplane," NASA Memo 4-26-59A, 1959.
3. Munniksma, R., "Some Experience with Jet Reverser Model Testing, using Hot and Cold Jets in Ground Proximity," Proc. of the 35th Semi-Annual Meeting of the Supersonic Tunnel Association, Vought Aeronautics Co., Dallas, Texas, March 8-9, 1971.
4. Price, E., and W. Peters, "AEDC/AFWAL Hot/Cold Jet Simulation," Test Project Criteria, Test No. TF-599, AEDC, May 14, 1981.
5. Young, A. D., "Wind Tunnel Corrections for High Angles of Attack, A Brief Review of Recent U. K. Work," Wind Tunnel Corrections for High Angle of Attack Models, AGARD Report No. 692, May 8, 1980.
6. Mercer, C. E., and D. L. Maiden, "Effects of an In-Flight Thrust Reverser on the Stability and Control Characteristics of a Single-Engine Fighter Airplane Model," NASA TN D-6886, Sept., 1972.
7. Falarski, M. D., and K. W. Mort, "Full-Scale Wind Tunnel Investigation of a Target-Type Thrust Reverser on the A-37B Airplane," NASA TM X-1985, Ames Research Center, April, 1970.
8. Bridgeman, P. W., Dimensional Analysis, Yale University Press, New Haven, Conn., 1931.
9. Langhaar, H. L., Dimensional Analysis and Theory of Models, John Wiley and Sons, 1951.
10. Pai, S. I., Fluid Dynamics of Jets, D. Van Nostrand Co., Inc., New York, 1954.
11. Li, T. Y., Y. A. Yoler, and A. J. A. Morgan, "The Design of Wind Tunnel

- Experiments for the Study of Jet-On Effects," NAVORD Report 3473, China Lake, California, April 12, 1955.
12. Pindzola, M., "Jet Simulation in Ground Test Facilities," AGARDograph 79, NATO, Nov., 1963.
 13. Schlichting, H., Boundary-Layer Theory, McGraw-Hill Book Co., New York, Sixth Ed., 1968.
 14. Spring, D. J., "An Experimental Investigation of the Interference Effects Due to a Lateral Jet, Issuing from a Body of Revolution over the Mach Number Range of 0.8 to 4.5," Report No. RD-TR-68-10, U. S. Army Missile Command, August, 1968.
 15. Chrans, L. J., and D. J. Collins, "Stagnation Temperature and Molecular Weight Effects in Jet Interaction," AIAA Journal, Vol. 8, No. 2, Feb., 1970, pp. 287-293.
 16. Gilman, B. G., "Control Jet Interaction Investigation," Journal of Spacecraft and Rockets, April, 1971.
 17. Squire, H. B., "Jet Flow and Its Effects on Aircraft," Aircraft Engineering, March, 1950, pp. 62-67.
 18. Compton, W. B., III, "Effects of Jet Exhaust Gas Properties on Exhaust Simulation and Afterbody Drag," NASA TR R-444, Oct., 1975.
 19. Galigher, L. L., S. F. Yaros, and R. C. Bauer, "Evaluation of Boattail Geometry and Exhaust Plume Temperature Effects on Nozzle Afterbody Drag at Transonic Mach Numbers," AEDC-TR-76-102, Oct., 1976.
 20. Peters, W. L., "An Evaluation of Jet Simulation Parameters for Nozzle Afterbody Testing at Transonic Mach Numbers," AEDC-TR-76-109, Oct., 1976.
 21. Peters, W. L., "Jet Simulation Techniques: Simulation of Temperature Effects by Altering Gas Composition," AEDC-TR-78-43, March, 1979.
 22. Bauer, R. C., "A Method for Estimating Jet Entrainment Effects on Nozzle-Afterbody Drag," AEDC-TR-79-85, Feb., 1980.
 23. Peters, W. L., "Experimental Method for Correcting Nozzle Afterbody Drag for the Effects of Jet Temperature," AEDC-TR-80-38, July, 1981.

24. Hensel, R. W., "A Survey of Recent Developments in Wind Tunnel Testing Techniques at Transonic and Supersonic Speeds," ARO, Inc., TN, 1964.
25. Collins, F. G., "Summary of the 1977 USAF/OSR/ASEE Summer Design Study Program on the Integration of Wind Tunnels and Computers," AIAA 10th Aerodynamic Testing Conference, San Diego, April 19-21, 1978.
26. Tempelmeyer, K. E., "An Analytical Study of Hot Jet Simulation with a Cold Gas Mixture," AEDC-TN-58-54, Sept., 1958.
27. Runckel, J. F., and J. M. Swihart, "A Hydrogen Peroxide Hot-Jet Simulator for Wind-Tunnel Tests of Turbojet-Exit Models," NASA Memo. 1-10-59L, Feb., 1959.
28. Bourque, C., and B. G. Newman, "Reattachment of a Two-Dimensional, Incompressible Jet to an Adjacent Flat Plate," The Aeronautical Quarterly, Vol. XI, Aug., 1960.
29. Perry, C. C., "Two-Dimensional Jet Attachment," Ph.D. Dissertation, Mechanical Engineering, Univ. of Michigan, 1967.
30. Olson, R. E., "Reattachment of a Two-Dimensional Compressible Jet to an Adjacent Plate," Presented at the Symposium on Fluid Jet Control Devices, Winter Annual Meeting of ASME, New York, Nov. 28, 1962.
31. Hoch, J., and L. M. Jiji, "Two-Dimensional Turbulent Offset Jet-Boundary Interaction," Journal of Fluids Engineering, Vol. 103, March, 1981.
32. Hackett, J. E., and D. J. Wilsden, "Estimation of Wind Tunnel Blockage from Wall Pressure Signatures: A Review of Recent Work at Lockheed-Georgia," AIAA 10th Aerodynamic Testing Conference, San Diego, April 19-21, 1978.

NOMENCLATURE

A	Nozzle cross-sectional area
a	Speed of sound
C_p	Constant pressure specific heat
C_v	Constant volume specific heat
D	Diameter (nozzle or body)
E	Eckert number
F_G	Gross thrust of engine
h	Convective heat transfer coefficient
k	Thermal conductivity
L	Length
M	Mach number
N	Nusselt number
NPR	Nozzle total-to-free-stream-static pressure ratio, P_t / P_∞
NSPR	Nozzle exit static-to-free-stream-static pressure ratio, P_e / P_∞
Pr	Prandtl number
p, P	Pressure
q	Dynamic pressure
R	Reynolds number or gas constant
S	Reference area (wing or stabilizer)
T	Temperature or turbulence intensity
$(\Delta T)_0$	Temperature difference
U	Velocity
α	Angle of attack
$\Delta \gamma$	Incremental Prandtl-Meyer angle
γ	Ratio of specific heats
θ_N	Nozzle divergence half-angle
ν	Kinematic viscosity
μ	Dynamic viscosity

SUBSCRIPTS

c	Chamber
e	Exit
j	Jet
t	Total
∞	Free-stream
*	Throat conditions

1981 USAF-SCEE SUMMER FACULTY RESEARCH PROGRAM
Sponsored by the
AIR FORCE OFFICE OF SCIENTIFIC RESEARCH
Conducted by the
SOUTHEASTERN CENTER FOR ELECTRICAL ENGINEERING EDUCATION
FINAL REPORT
ANALYSIS OF THE 60KVA PERMANENT MAGNET ALTERNATOR
AND A NEW ROTOR CONCEPT FOR THESE MACHINES

Prepared by: Samuel Noodleman
Academic Rank: Adjunct Professor
Department and Department of Electrical Engineering
University: University of Arizona
Research Location: Aero Propulsion Laboratory WPAFB, OH
Power Systems Branch, Generator and Distribution
Research Facility

USAF Research
Colleague: Dr. William U. Borger

Date: 31 July 1981
Contract No: F49620-79-C-0038

ANALYSIS OF THE 60 KVA PERMANENT MAGNET
ALTERNATOR AND A NEW ROTOR CONCEPT
FOR THESE TYPE MACHINES

by

Samuel Noodleman

ABSTRACT

The design of the 60 KVA alternator as used in the VSCF Power Generating System was reviewed and calculations made of the flux distribution in the machine.

The study concentrated on the permanent magnet rotor design. An analysis of the flux produced by the magnets in the rotor with the present tangential configuration shows that much of the flux is lost in leakage. Only about 50 percent of the magnetic field as generated in the permanent magnets reaches the stator windings and generates useful electrical energy.

A rotor design using the permanent magnets in a radial orientation is proposed. This concept requires less permanent magnet material and will provide more electrical output for the same size and weight. Because the fields generated by the currents in the stator windings do not link as much iron in the proposed rotor, the stator winding inductances are reduced and the inherent voltage regulation of the alternator is improved.

An analysis is also made of the new rotor concept with higher energy rare earth-cobalt magnet materials and some of the design changes required to better utilize this type permanent magnet material.

ACKNOWLEDGEMENTS

The author would like to thank the Air Force Systems Command, The Air Force Office of Scientific Research, and the Southeastern Center for Electrical Engineering Education for his appointment as a Summer Faculty Research Program Associate and SCEE Fellow.

He would like to thank the personnel of the Generator and Distribution Research Facility, Power Systems Branch for their assistance and hospitality during his stay in the Dayton area. The author would also like to thank Captain F. C. Brockhurst for his comments and the use of his library. Finally, he would like to express his special appreciation to Dr. W. U. Borger for suggesting this challenging investigation and for making available the many drawings, specifications and technical details required for this study.

I. INTRODUCTION

The 60 KVA VSCF system consists of a permanent magnet alternator generating electric power into a solid state converter. The converter takes the variable frequency, variable voltage as produced by the alternator and converts this energy into constant frequency three phase electric power. As low weight is a major requirement for the components in an aircraft system, the alternator is designed for as high a speed as practical to reduce both size and weight. Also the electrical output is required to be a constant 400 Hz. Consequently, for best conversion from variable frequency to the constant 400 Hz, the converter system requires that the minimum input frequency be about three times that value or 1200 Hz.

These are some of the basic factors of the VSCF system which determine the design parameters of the alternator. By selecting 15,000 R.P.M. as the practical minimum speed to generate the required 1200 Hz, the alternator poles can be calculated. ^{1, 14}

$$P = \frac{120 f}{\text{R.P.M.}} \quad (1)$$

Where: P is the number of poles

f is the frequency in hertz

and R.P.M. is the rotor speed in revolutions/minute

$$\text{or } P = \frac{120 \times 1200}{15,000} = 9.6 \text{ poles}$$

Thus, a 10 pole machine is required.

In order to hold the stresses within the rotor to safe values with present materials, it is necessary to limit the rotor tip speed at the highest rotor speed to about 650 ft/sec. The rotor diameter can then be calculated.

$$D = \frac{720 V_t}{\pi \text{ R.P.M. max}} \quad (2)$$

Where: D is the rotor diameter in inches

Vt is the rotor tip speed in feet/sec

and R.P.M. max is the maximum speed the rotor must withstand.

As the prime mover driving the alternator covers a 2:1 speed range,
R.P.M. max is 30,000 R.P.M.

Thus,

$$D = \frac{720 \times 650}{\pi \times 30,000} = 4.97 \text{ inches}$$

The rotor diameter is selected as 5.00 inches. Other requirements are determined by the capability of available solid state devices to be compatible with the voltage and current ratings selected for the alternator. This results in having the alternator develop an RMS voltage of about 180 Volts (L-N) with a nine phase winding.

The resulting dimensions and design parameters of the present 60 KVA machine are listed in Table I.

TABLE I

STATOR

Outside Diameter	6.050 inches
Inside (bore) Diameter	5.090 inches
Stator Stack Length	4.751 inches
No. of Stator Slots	90
Stator Skewed One Slot	
Stator Slot Details see Fig 1.	

STATOR WINDING

Two turns throw 1-10, one turn throw 2-11 etc. with 9 conductors in hand No. 22 QML magnet wire. Winding: 9 phases 10 poles no parallel circuit. Total turns/phases 15.

TABLE I (cont'd)

ROTOR ASSEMBLY

Outside Diameter	5.000 inches
Inside Diameter	2.287 inches
Stack Length	4.751 inches
Shrink Ring Thickness	0.300 inches

The Shrink Ring is made up with magnetic and non-magnetic sections. The non-magnetic sections are shrunk over the permanent magnet sections and are of a constant length of .661 inches. The magnetic sections are ground to fit and the ring is welded with alternate sections and shrunk over the ground Rotor O.D. of 4.400 inches. Machining the Shrink Ring to 5.000 inches provides a net Shrink Ring thickness of 0.300 inches. The Rotor is made up of four sections each section 1.188 inches wide, resulting in the 4.751 dimension. Rotor Details see Fig. 1.

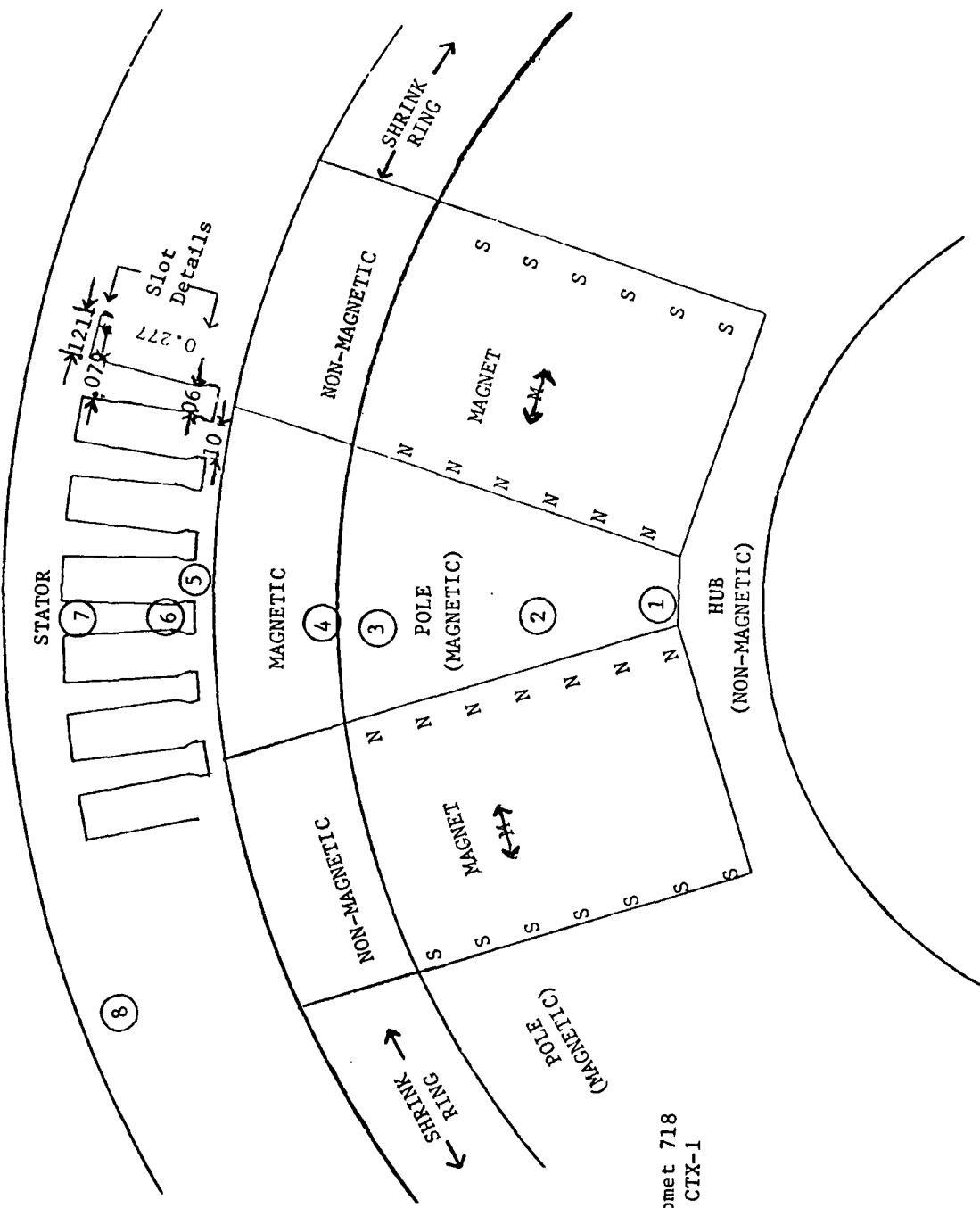
MAGNETS

Ten magnets per rotor section, four sections for forty magnets. Magnet material SmCo_5 . Magnets thermally stabilized at 250°C to remove irreversible effects.

Initial Magnet Dimensions	.930" x .6613" x 1.183"
Finished Magnet Dimensions	.904" x .6613" x 1.183"

MAGNET PROPERTIES 5, 6, 11

Residual Induction (Br) Gauss	9,200	min.
Coercive Force (Hc) Oersteds	8,800	min.
Intrinsic Coercive Force (Hci) Oersteds	15,000	min.
Max. Energy Product (B x H) G. - Oe.	21×10^6	min.
Recoil Permeability	1.05	max.
Reversible Temp. Coef. % per $^\circ\text{C}$	0.05	max.
Irreversible Temp. Coef. at 250°C %	2.5	max.



MATERIALS

- Stator Lam. Van. Permendur
- Pole Steel 1010
- Magnets Sm Co5
- Hub Inconel 750
- Shrink Ring Non-Magnetic Pyromet 718
- Shrink Ring Magnetic Pyromet CTX-1

Fig.1 - Present Alternator with Tangential Oriented Rotor

II. OBJECTIVES

The purpose of this study is to analyze the design of the present 60 KVA VSCF alternator particularly in regard to the magnet arrangement in the permanent magnet rotor. The design uses a rotor configuration in which the magnets are tangentially oriented in relation to the air gap. The construction details of this design are illustrated in Figure 1. An analysis of the flux distribution is made to determine the flux densities in the various sections and the flux leakage for this configuration.

A new rotor design with the magnets radially oriented is considered. This design uses the same material as in the present rotor, as these materials have been tested and proven suitable for this application. The radial design will attempt to use a shrink ring of the same dimensions as in the present machine if possible. The goal is to design a radially oriented rotor with improved performance and interchangeable with the present rotor so that comparable tests could be made by replacing the present rotor with one of the new design.

It is not the intent in this study to make up drawing details of the new rotor or manufacture a prototype rotor.

During this analysis, consideration will be given to the problems of magnetizing the magnets in a completed rotor assembly and a comparison made of the energy required to magnetize each type rotor.

A study will also be made of the possibilities of using higher energy magnet materials in a new design for higher output and better alternator performance.

III. THE CURRENT MACHINE

In every design there are many trade-offs and options^{2,3} which can result in different approaches to meet the specifications and requirements of an application. As this machine must operate at the highest speed practical, a prime requirement is a mechanical design which will insure mechanical integrity of the rotor structure. Similarly due to the requirement for light weight and high output the heat capacity of the copper and iron is inadequate to supply normal cooling, and special cooling methods are needed to keep the parts within their temperature ratings. Neither stress analyses of the rotating structures or the methods for dissipating the heat within the machine will be considered in this report.

Because of the high speed required of the rotor, a 0.3 inch thick containment band is necessary to adequately encase it and prevent its destruction at the temperatures and speed specified for this design, also, .045 inches of mechanical clearance is necessary. This total gap of about 0.35 inches is too great for a permanent magnet of reasonable proportions to provide the required flux in relation to the other dimensions of this design. Consequently the concept of a shrink ring of alternate magnetic and non-magnetic sections capable of withstanding the rotational forces within the rotor and providing a low reluctance path for the magnet flux is the unique concept of this design.^{2,3,4} This type of shrink ring allows a design of minimum size and weight meeting the desired performance specifications.

Figure 1 shows the configuration and construction of this machine and its materials. The dimension details are listed in Table I.

IV. DESIGN REVIEW CALCULATIONS

For the air gap and tooth opening dimensions as specified, a calculation of Carter's coefficient shows a value of 1.2.¹³ Consequently, the net air gap is $1.2 \times .045 = .054$ inches. For an initial calculation of the flux developed by the magnets, assume that the m.m.f.'s required by all of the magnetic sections to be about 10 percent of the air gap m.m.f. Thus, the operating slope of the magnets as a first approximation is:^{11,12}

$$\frac{B}{H} \cong \frac{.331}{.054 \times 1.1} = 5.6$$

Thus from fig. 4, the average induction of the magnet is about 7.7 KG.

Note that only half of the magnet thickness of 0.663 inches is used as magnet m.m.f. for this configuration as each magnet must drive flux through two poles. The magnetic circuit can be simulated by an electrical schematic as shown in fig. 2.

- M - Magnet M.M.F.
- Rm - Magnet Reluctance
- Rp - Pole Reluctance
- Rsh - Shrink Ring Reluctance
- Rt - Teeth Reluctance
- Ry - Yoke Reluctance
- Rg - Air Gap Reluctance

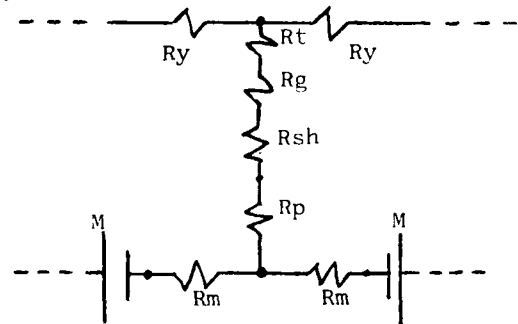


Fig. 2 Electric schematic of magnetic circuit of tangentially oriented rotor.

It must be realized that this electrical schematic does not accurately represent the actual magnetic circuit since there are no magnetic insulators that can prevent this flux leakage. Moreover, in this configuration the magnet flux is gradually fed into the pole from both magnet sides. Thus the flux within the pole is gradually increased from zero at its base to maximum where the pole arc interfaces with the magnetic portion of the shrink ring. Also the pole reluctance is not constant being highest at the base and minimum at the top of the pole. None of these factors are simulated in this circuit. However, the electric circuit equivalent helps to illustrate the distribution of current (flux) in the various sections and the voltage drops (m.m.f.) of this type circuit.

IV-1 FLUX CALCULATIONS

For the assumed induction of 7.7 kilogauss developed by the magnets, the total flux produced is $2 \times 7.7 \times 6450 \times .904 \times 4.751 = 426,600$ lines/pole.

The flux across the air gap can be determined from the no load voltage generated by the machine. At 15,000 R.P.M., the R.M.S. voltage (Line to Neutral) is about 180 volts. This value should agree with the requirement that the peak voltage which can occur between any two phases must not exceed 1200 volts, a peak limit of the solid state devices in the controller. In a nine phase system the maximum voltage between lines occurs between phase 1 and either phase 5 or phase 6 as indicated in fig. 3.

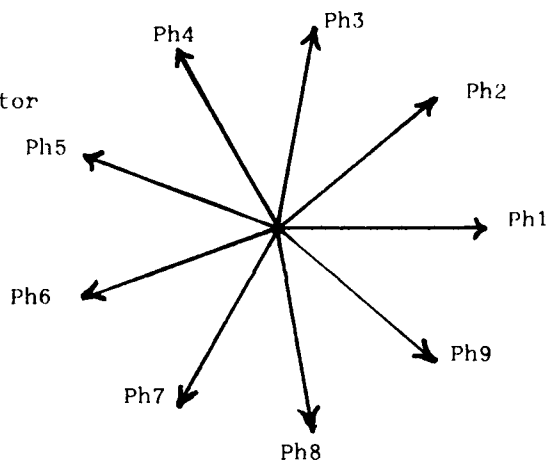
Fig. 3

Phase Voltages for Nine Phase Alternator

Angle between Phases 40°

$V_o =$ R.M.S. Phase Voltage

(Line to Neutral)



$$\text{Thus } V_{\max} \approx V_o + V_o \cos 20^\circ = 1.939 V_o$$

$$\text{or } V_{\max} \approx \frac{1200}{1.414} = 848.7 \text{ volts (R.M.S.)}$$

$$\text{Thus } V_o \approx \frac{848.7}{1.939} = 437.6 \text{ (L-N) at the maximum speed of the machine}$$

Allowing 10 percent for overspeed at the top speed of 30,000 R.P.M.

$$V_o \approx \frac{15,000}{33,000} \times 437.6 = 199 \text{ volts at 15,000 R.P.M.}$$

Accordingly, allowing for magnet tolerances and dimensional tolerances which could affect this maximum voltage, a value of 180 volts is an acceptable nominal value for the no load voltage at 15,000 R.P.M.

$$V_o = 4.4 N f K_p K_d \phi \times 10^{-8} \quad 1, 13, 14 \quad (3)$$

Where V_o is the developed R.M.S. voltage/phase

N is the number of turns/phase

f is the frequency of the fundamental voltage

K_p and K_d are pitch and distribution factors and

ϕ is the flux/pole in lines.

$$\phi = \frac{180 \times 10^8}{4.44 \times 15 \times 1250 \times .994} = 217,500 \text{ lines}$$

(since this is a full pitch winding $K_p = 1.0$ and for a nine phase machine $K_d = 0.994$) ^{13,14}

The difference between the 426,600 lines produced by the magnets as fed into the pole and the 217,500 lines in the airgap is the leakage flux of 209,100 lines. This leakage occurs all along the ends of the magnets and poles and at the bottom and top of the magnets.

IV-2 M.M.F. CALCULATIONS ^{11, 14, 12}

Using these flux calculations, the m.m.f. drops in the magnetic circuit can be determined and compared with the original assumptions that they are 10 percent of the airgap m.m.f.

$$(a) \text{ Air Gap M.M.F.} = \frac{7.7 \times 6450 \times .054}{3.19} = 341 \text{ A.T.}$$

(b) The M.M.F. in the Stator Teeth can be calculated as follows: The flux/pole through the teeth is approximately 217,000 lines.

$$\text{The Average Teeth/pole} = \frac{\text{No. of Teeth} \times \text{Pole Span}}{\text{No. of Poles}} \quad (4)$$

From the dimensions of the rotor, the pole span is .567. Thus,

$$T_p = \frac{90}{10} \times .567 = 5.1 \text{ teeth/pole}$$

The minimum tooth width as shown in fig. 1 occurs at the tooth tip and is 0.06 inches.

Thus, the Tooth Area carrying average flux = $5.1 \times .06 \times 4.751 \times .93 = 1.352 \text{ in}^2$ where 0.93 is an assumed stacking factor for the .006 Vanadium Permendur Stator Stack. Thus,

$$B_{t_{\max}} = 217,000/1.35 = 160,700 \text{ lines/in}^2 = 24.9 \text{ kg}$$

The maximum tooth width occurs at the base of the tooth and is .079 inches.

$$\text{The tooth area} = 1.78 \text{ in}^2. \text{ Thus,}$$

$$B_{t_{\min}} = 217,000/1.78 = 121,910 \text{ lines/in}^2 = 18.9 \text{ kg}$$

in the teeth. From fig. 5. M.M.F. in teeth = 51 A.T.

(c) M.M.F. In Yoke Section

The flux in the yoke section will vary from zero when that yoke section is in line with the center of the rotor poles to a maximum when that yoke section is in line with the center of the magnets. The yoke width is 0.163 inches and the yoke area is 0.72 in^2 . As the flux splits into two equal parts in the yoke, the maximum flux density in the yoke = $\frac{217,000}{2 \times .72} = 150,694 \text{ lines} = 23.4 \text{ kg}$.

Assuming the flux density varies sinusoidally from zero to 23.4 kg over the arc length of .924 inches from fig. 5 the m.m.f. yoke = 9 A.T.

(d) M.M.F. In Magnetic Section of Shrink Ring

The average shrink ring arc = 0.813 inches. Therefore, the ring area = 3.86 in^2 .

$$B_{\text{sh ring}} = \frac{218,000}{3.86} = 56,476 \text{ lines/in}^2 = 8.76 \text{ kg}$$

Thus, from fig. 6, M.M.F. shrink ring = $.3 \times 14 \times 2.02 = 8.5 \text{ A.T.}$

The total M.M.F.'s for all the magnetic sections = 51 (teeth) + 9 (yoke) + 8.5 (sh. ring) + 2 (remaining sections) $\approx 73 \text{ A.T.}$ The original assumption of the m.m.f. of the magnetic sections being 10 percent of the air gap.

M.M.F. $\approx .1 \times 841 = 84 \text{ A.T.}$ is acceptable.

(e) The Total M.M.F. Required for the Flux Densities Calculated

$$841 \text{ (air gap)} + 73 \text{ (total remaining magnetic sections)} = 914 \text{ A.T.}$$

This M.M.F. reflected to the magnet = $914/.331 = 2761 \text{ A.T./in} = 1367 \text{ Oe}$.

From fig. 4 at 1367 Oe, $B = 7.8 \text{ kg}$ compared to the 7.7 kg for the initial calculated operating point of the magnets.

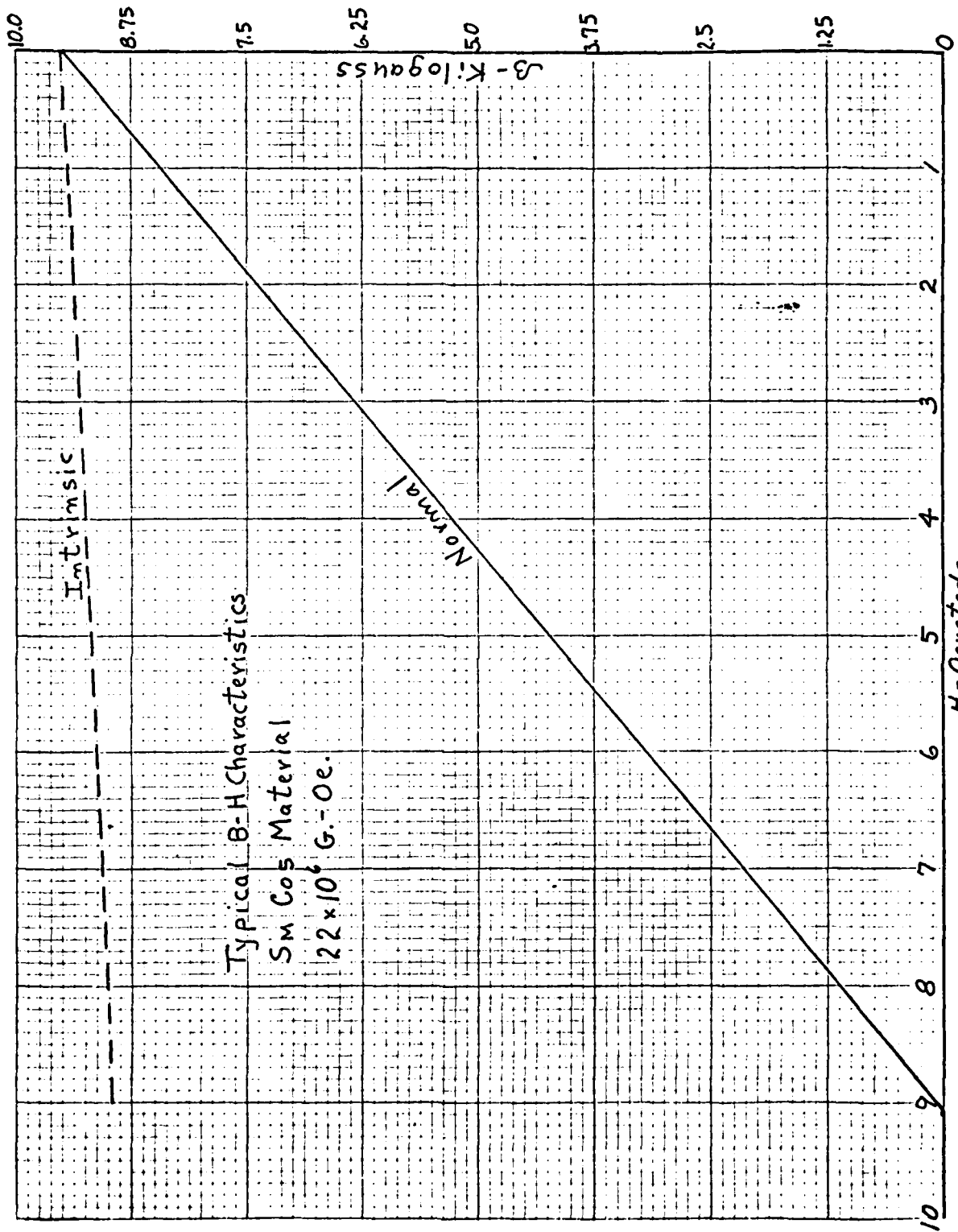


Figure 4 Typical demagnetization curve SmCo₅ material

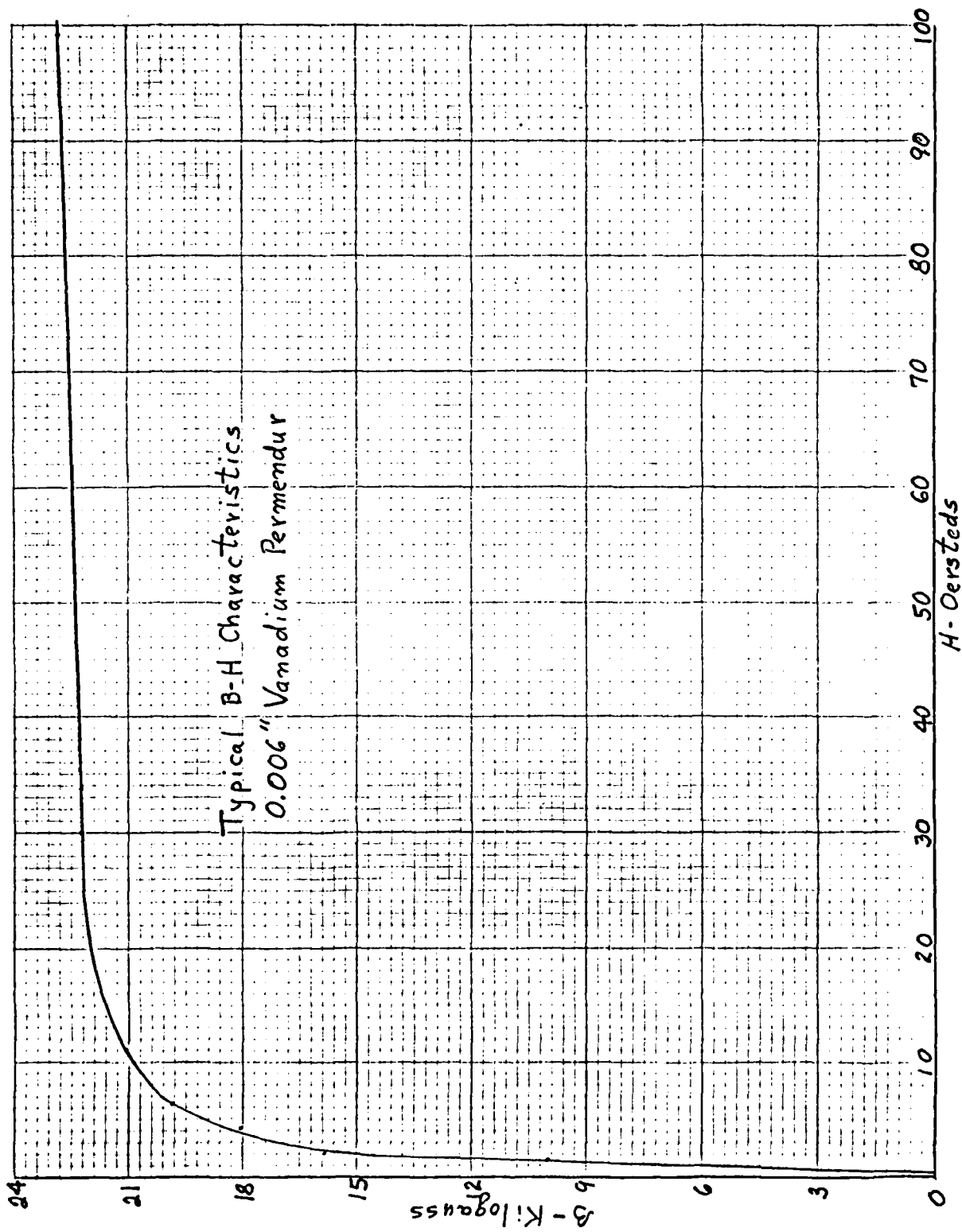


Figure 5 Typical magnetization curve Vanadium Permendur

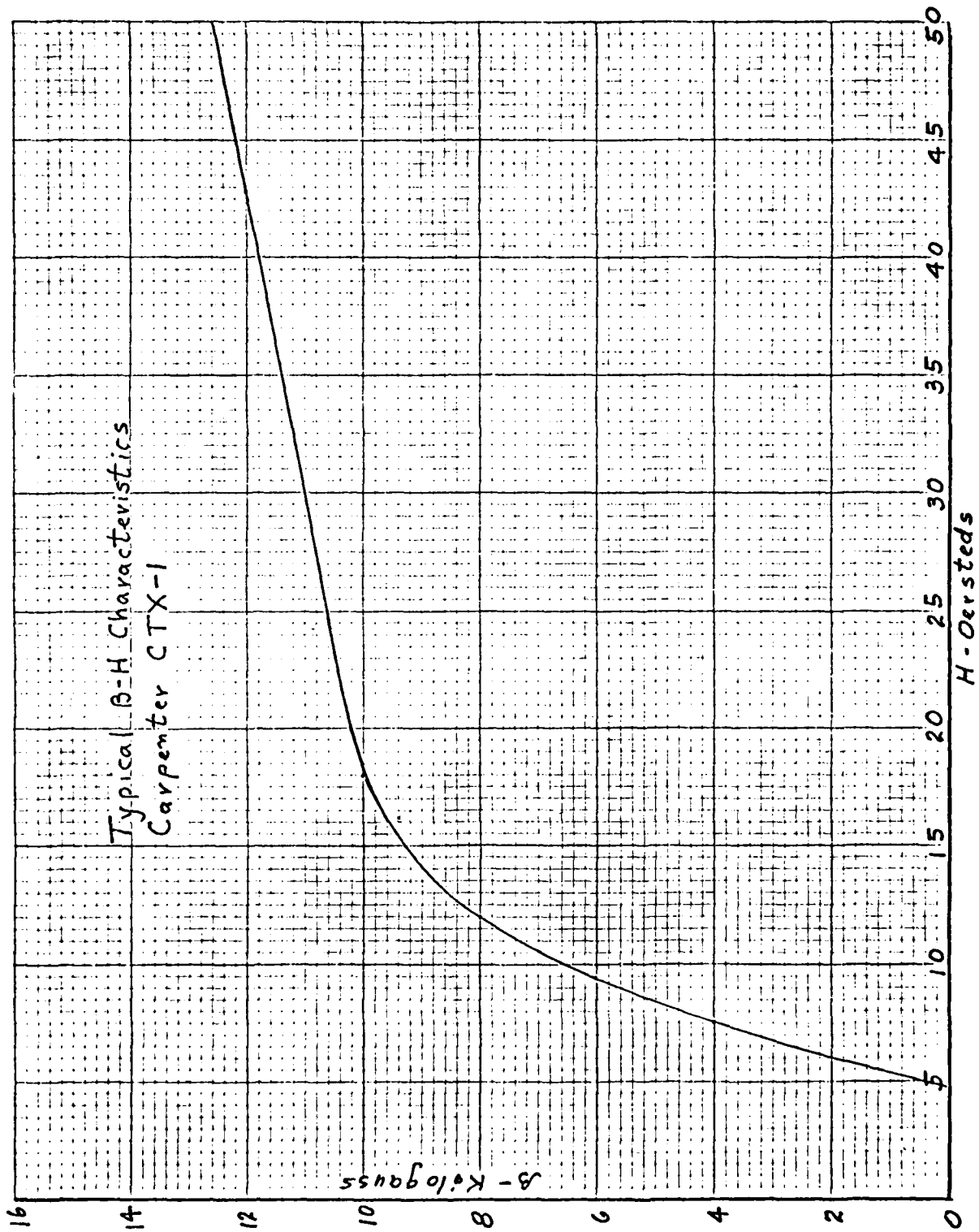


Figure 6 Typical magnetization curve Pyromet CTX-1

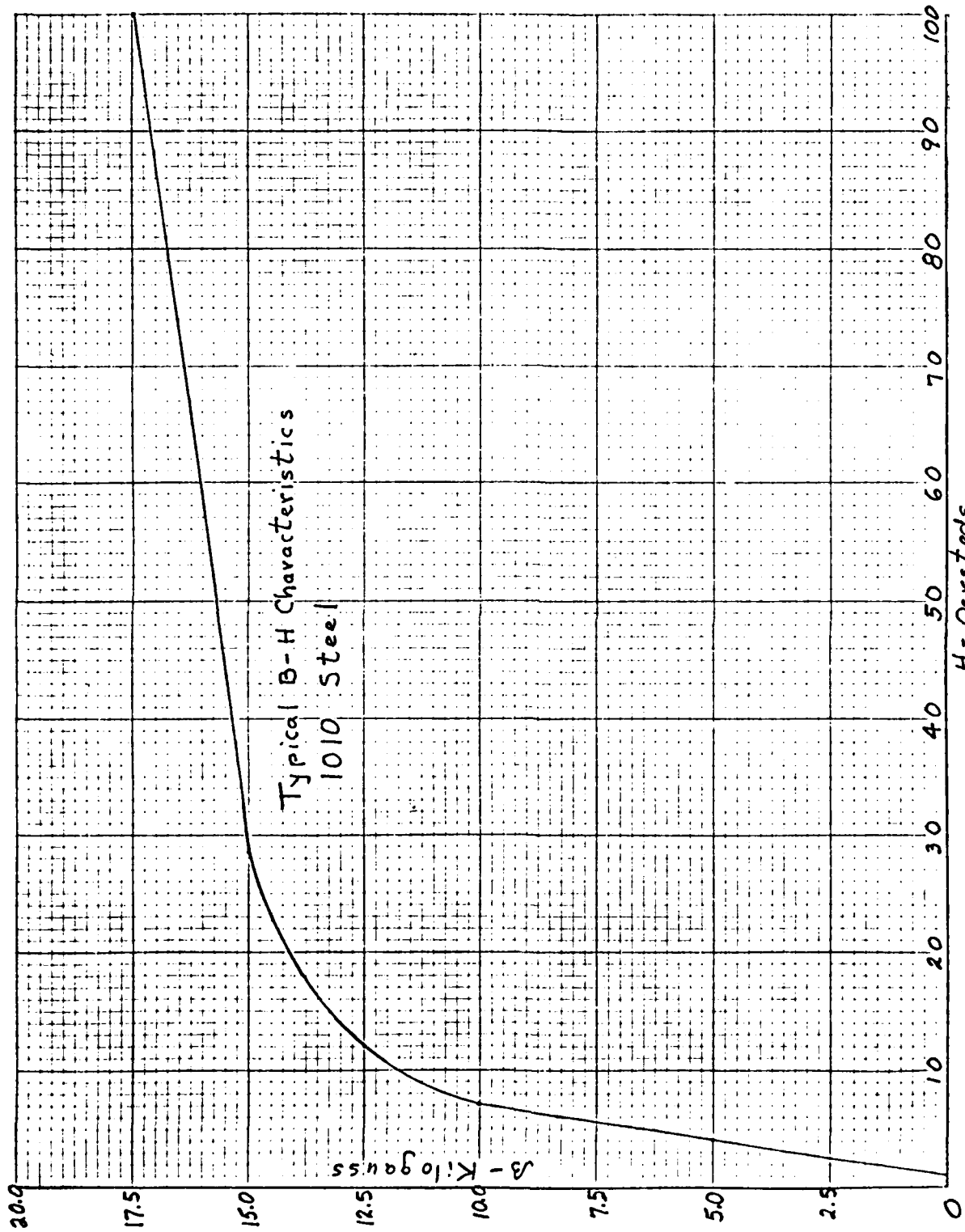


Figure 7 Typical magnetization curve 1010 steel

IV.3 The calculated flux distribution for the sections of figure 1 are summarized in Table II.

TABLE II

<u>Section No.</u>	<u>Flux/Pole(lines)</u>	<u>Area of Section(in²)</u>	<u>Flux Density (kg)</u>
1	40,000	1.6	3.9
2	135,000	2.6	8.0
3	230,000	3.4	10.5
4	218,000	3.86	8.8
5	217,000	4.38	7.7
6	217,000	1.35	24.9
7	216,000	1.78	18.8
8	108,000	.72	23.3

IV.4 WEIGHT CALCULATIONS ¹³

The weights of the various components can be determined as follows:

(a) Stator Core

Assume that the density of Vanadium Permendur is 0.300 lb/in³, and that the stacking factor for this material as processed in a stator core is 0.93.

Yoke volume = 13.3 in³, thus yoke wt. = 4.0 lbs

Tooth volume = 9.6 in³, thus tooth wt. = 2.9 lbs

Weight of Stator Core = 6.9 lbs

(b) Copper Windings

The mean length of the turns of the windings can be determined as follows: Assuming that the coil end extensions = 1.0 inches, then

$$\text{M.L.T.} = 2[\text{coil end ext.} + \text{stack length} + \pi \times \text{Mean Coil} \text{ Diameter} \times \text{teeth linked/teeth total}] \quad (5)$$

Diameter x teeth linked/teeth total]

$$= 2[1.0 + 4.76 + \pi \times 5.448 \times 9/90]$$

$$= 15 \text{ inches}$$

Total copper length of windings = 9 (cond. in hand) x
 15 (turns/ph) x 15/12 (m.l.t. in ft) x 9 (no. of phase)
 = 1519 ft.

For no. 22, the weight of conductor per 1,000 ft = 2.06 lbs. thus,
 1519 ft. x 2.06 lb/1,000 ft = 3.13 lbs net copper wt.

The winding resistances/ph = M.L.T x No. of turns x Resistance per cond. (6)
 No. of cond. in hand

For no. 22, resistance per ft = .0162 ohms. thus,
 R/ph = 15/12 x 15 x .0162/9 = .0338 ohms.

(c) Magnets

Assuming the density of the magnet material is 0.295 lbs/in³,
 Magnet Volume = .663 x .904 (finished magnet size) x 1.183 = .73 in³.
 Total Magnet Weight = 40 x .73 x .295 = 8.6 lbs.

(d) Shrink Ring

Volume of non-magnetic section = .663 x .309 x 10 x 4.751 = 9.73 in³.
 Weight of non-magnetic section = 9.73 x .297 = 2.9 lbs.
 Volume of magnetic section = $\pi/4[5.00^2 - 4.382^2] \times 4.751 - 9.73 = 11.9 \text{ in}^3$.
 Weight of magnetic section = 9.73 x .2937 = 3.5 lbs.
 Total Weight of Shrink = 6.4 lbs.

(e) Poles

Total pole volume $\approx 18 \text{ in}^3$.
 Assuming a density of 0.28 lb/in³ for 1010 steel.
 Pole Weight = 18 x .28 ≈ 5.0 lbs.

(f) Hub

Hub Volume $\approx 5.8 \text{ in}^3$ Inconel.
 Assuming a density of 0.28 lb/in³ for Inconel 750.
 Hub Weight = 5.8 x .28 ≈ 1.6 lbs.
 Total Rotor Weight = 6.4 + 5.0 + 8.0 + 1.6 = 21.6 lbs.

IV-5 DESIGN COMMENTS

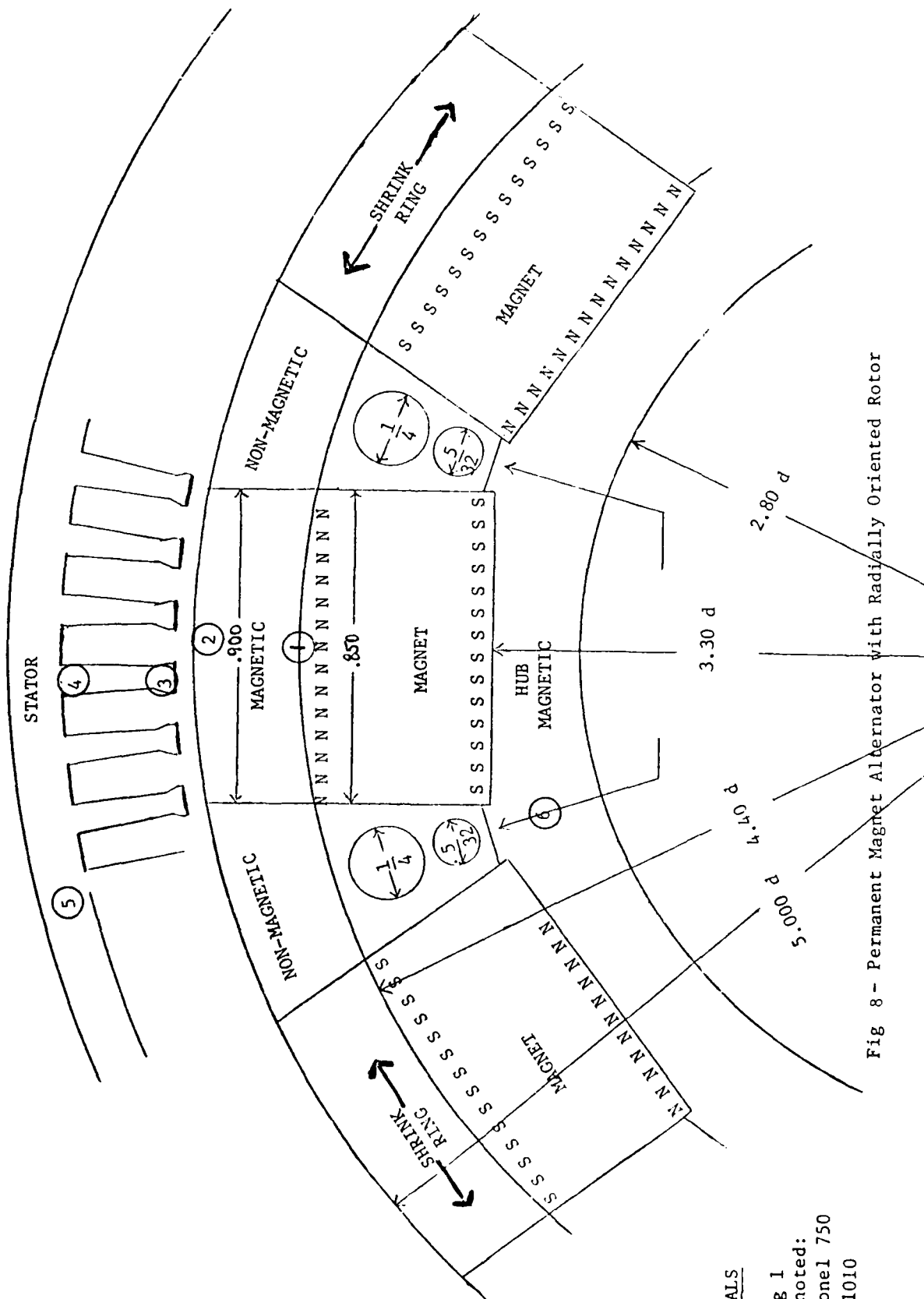
As discussed previously, there are many options in selecting a design which will not only meet all the performance requirements and yet be compatible with the tooling and processes of the manufacturer and cost effective in meeting company goals.

The following suggestions are respectfully submitted for consideration:

1. The present design shows that both the stator width and rotor width are 4.751 inches. This requires that during the assembly of each machine all dimensions and tolerances must combine exactly in order for the rotor pole iron to be in exact alignment with the stator iron. This is a difficult and costly assembly process. A better solution may be to provide some overhang so that the rotor is wider than the stator thus compensating for tolerance build up during assembly.

2. The present design skews the stator. Skewing is necessary to reduce the cogging during start up as a motor and the ripple voltage as a generator. However, even one slot skew will make it more difficult to insert the windings in the slot. A more satisfactory approach may be to skew the rotor the equivalent of one stator slot. The rotor is presently constructed in four sections. Thus, indexing each rotor section $1\frac{1}{3}^{\circ}$ with respect to the prior section could provide the necessary skew.

3. The reasoning behind the tangentially oriented rotor is usually that the flux from the two magnets combine in the pole to provide higher air gap flux densities than possible with the radial design. While higher air gap densities are possible with this type configuration, much of the flux is lost in leakage and the magnet material is not used as effectively as in a radial design. When higher gap densities are required than the B_r value of the magnet material, they can be obtained in a radial design by using pole shoes to concentrate the magnet flux.^{7,8} For this application, the operating B in the air gap is less than the B_r value of the magnet material, and a radial design should be considered.



MATERIALS

Same as Fig 1
 except as noted:
 Wedges Inconel 750
 Hub Steel 1010

Fig 8 - Permanent Magnet Alternator with Radially Oriented Rotor

V. DESIGN OF RADIALY ORIENTED ROTOR

The goals for this rotor design are to provide a rotor interchangeable mechanically with the rotor in the current machine and to use as many of the same materials as practical that are used in the present rotor. The stator remains the same. The initial design approach was to use the existing shrink ring for the containment ring of this new rotor. However, the chord dimension of the magnetic section of the shrink ring at the 4.4 inch diameter is only 0.719 inches long. For a 5.00 inch rotor length specified to allow for overhang in place of the present 4.751 length, the magnet area would be 3.595 in². For a desired air gap flux/pole of 217,500 lines the magnet must develop a flux density of

$$\frac{217,500}{3.595} = 60,500 \text{ lines/in}^2 = 9.38 \text{ KG}$$

This is too close to the B_r value of the present magnet material to be a satisfactory design.

Consequently, the design was changed to use a shrink ring of the same materials as the present ring but with the magnetic section of the shrink ring having sides parallel to the orientation of the magnets and of a width of 0.900 inches. The configuration and materials list of this design is shown in fig. 8. The dimensions and details are listed in Table III.

TABLE III
STATOR - SAME AS CURRENT MACHINE

ROTOR ASSEMBLY

Outside Diameter	5.000 inches
Inside Diameter	2.800 inches
Stack Length	5.000 inches
Shrink Ring Thickness	0.300 inches

The shrink ring is made up of magnetic and non-magnetic sections. The magnetic section is located over the permanent magnets and is of a constant length of 0.900 inches.

The rotor is made up of four sections, each section 1.250 inches wide resulting in the 5.000 width dimension. Rotor Details see fig. 8.

MAGNETS

Ten magnets per rotor section, four sections for forty magnets. Magnet material SmCo5. Magnets thermally stabilized at 250°C to remove irreversible effects.

Initial Magnet Dimension .56 x .850 x 1.250

Finished Magnet Dimension .55 max, .504 min x .850 x 1.25

Magnet properties, same as in current machine.

V.1 FLUX CALCULATIONS

Following the same procedures as in section IV, the approximate operating slope is now:

$$B/H = .527/.054 \times 1.1 = 8.9$$

Thus from fig. 4, the induction of the magnets is about 8.3 KG.

Note that the flux is practically constant through the magnet area and in the magnetic section of the shrink ring. The magnet width is 0.850 inches. The flux/pole from the magnet is:

$$8.3 \times 6450 \times .850 \times 5.00 = 227,523 \text{ lines}$$

There will be about 5 to 10 percent leakage as the magnet flux is forced through the air gap. Consequently, the air gap flux is about

$$.93 \times 227,523 = 211,596 \text{ lines}$$

which is comparable with the air gap flux calculated in Section IV.1. The flux and the flux densities in the teeth and yoke of the stator would be slightly less than those shown in Section IV.3. The flux in the iron section below the magnets, the rotor yoke, splits into two equal sections similar to the flux in the stator yoke. However, the flux in this area remains constant through each section of the iron.

The area of the yoke at the point of maximum flux is about $.33 \times 5 = 1.65 \text{ in}^2$.
 Thus, flux density at this section = $\frac{227,523}{2 \times 1.65} = 68,946 \text{ lines/in}^2 = 10.7 \text{ kg}$

V · 2 M.M.F. CALCULATIONS

The m.m.f. drops in the rotor yoke are negligible. Thus, the total m.m.f. is somewhat less than shown in IV·2. The calculated flux distribution for the sections in Figure 8 are summarized in Table IV.

TABLE IV

<u>Section No.</u>	<u>Flux/pole (lines)</u>	<u>Area of Section (in²)</u>	<u>Flux Density (KG)</u>
1	227,500	4.26	8.38
2	211,600	4.53	7.24
3	211,600	1.35	24.3
4	211,600	1.78	18.4
5	105,500	.72	22.7
6	113,750	1.65	10.7

V · 3 WEIGHT CALCULATIONS

(a) The stator core and copper weights are the same as listed in Section IV·4 (a and b)

(b) Magnets

$$\text{Magnet Volume} = .525 \times .85 \times 1.25 = .5578 \text{ in}^3.$$

$$\text{Magnet Weight} = 40 \times .5578 \times .295 = 6.6 \text{ lbs.}$$

(c) Shrink Ring

$$\text{Volume of Magnetic Section} = .90 \times .309 \times 1.25 \times 4 \times 10 = 13.9 \text{ in}^3.$$

$$\text{Weight of Magnetic Section} = 13.9 \times .2937 = 4.08 \text{ lbs.}$$

$$\text{Volume of Non-Magnetic Section} = \frac{\pi}{4} [5.00^2 - 4.382^2] \times 5 - 13.9 = 8.9 \text{ in}^3.$$

$$\text{Weight of Non-Magnetic Section} = 8.9 \times .297 = 2.64 \text{ lbs.}$$

$$\text{Total Weight of Shrink Ring} = 6.7 \text{ lbs.}$$

(d) Non-Magnetic Wedges

Volume of Non-Magnetic Sections $\approx 5.9 \text{ in}^3$.

Weight of Non-Magnetic Sections = $5.9 \text{ in}^3 \times .28 \approx 1.7 \text{ lbs.}$

(e) Rotor Hub

Volume of Rotor Hub = $\pi/4[3.3^2 - 2.8^2] \times 5 = 12 \text{ in}^3$.

Weight of Rotor Yoke = $12 \times .28 = 3.36 \text{ lbs.}$

Total Rotor Weight = $6.6 + 6.7 + 1.7 + 3.36 = 18.4 \text{ lbs.}$

V -4 Non-Magnetic Spacers Between Magnets

The non-magnetic wedges were proposed to be fabricated from Inconel 750 and even with the air holes of 1/4 and 9/64 diameters add about 1.7 lbs to the rotor. A more suitable approach may be to cast these sections in aluminum as discussed in Reference 11, page 274 and shown in fig 7.35 of this reference. This would result in the weight of the aluminum wedges and *^{end rings} of about 1.8 lbs. Of course, for this process the magnets in the rotor assembly would have to be magnetized after casting and finished machining as discussed in Section VIII. Since the pentagonal hub has flats which serve to locate the magnets it may be possible to eliminate the non-magnetic wedges completely. This would reduce this rotor weight about 1.8 lbs. The shrink ring could be designed with recesses to help support the magnets. A stress analysis of the new rotor should be made for this approach. The non-magnetic wedges as proposed for any of the three concepts would also help cool the magnets and keep magnet temperatures below the values occurring in the current machine. The Inconel 750 wedges have air holes to help cool these areas. The aluminum wedges with end rings would have good heat conductivity and help cool the magnets. The cast aluminum wedges and end rings would also serve as damper windings providing torque during starting and reducing hunting, and the air spaces only between the magnets would serve as fans to provide air circulation for cooling and minimum losses in these areas.

V.5 Figure 9 shows the electric schematic equivalent of the magnetic circuit of the radially oriented rotor.¹⁴

- M - Magnet M.M.F.
- Rm - Magnet Reluctance
- Rsh - Shrink Ring Reluctance
- Rg - Air Gap Reluctance
- Rt - Teeth Reluctance
- Ry - Yoke Reluctance
- Rh - Hub Reluctance

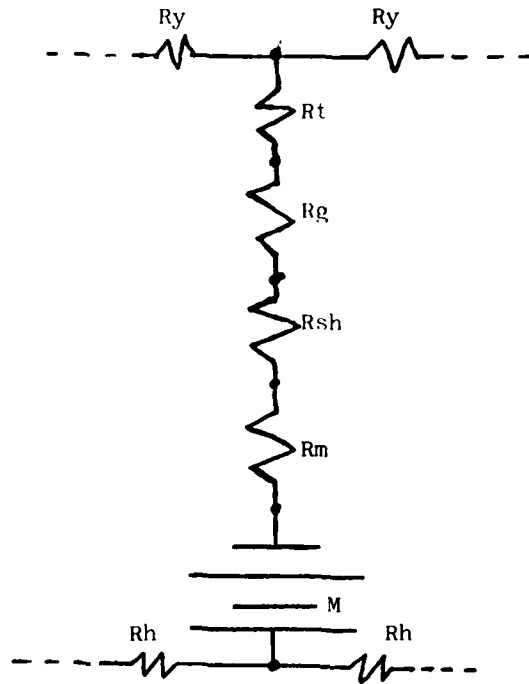


Fig. 9 Electric Schematic of magnetic circuit of Radially Oriented Rotor

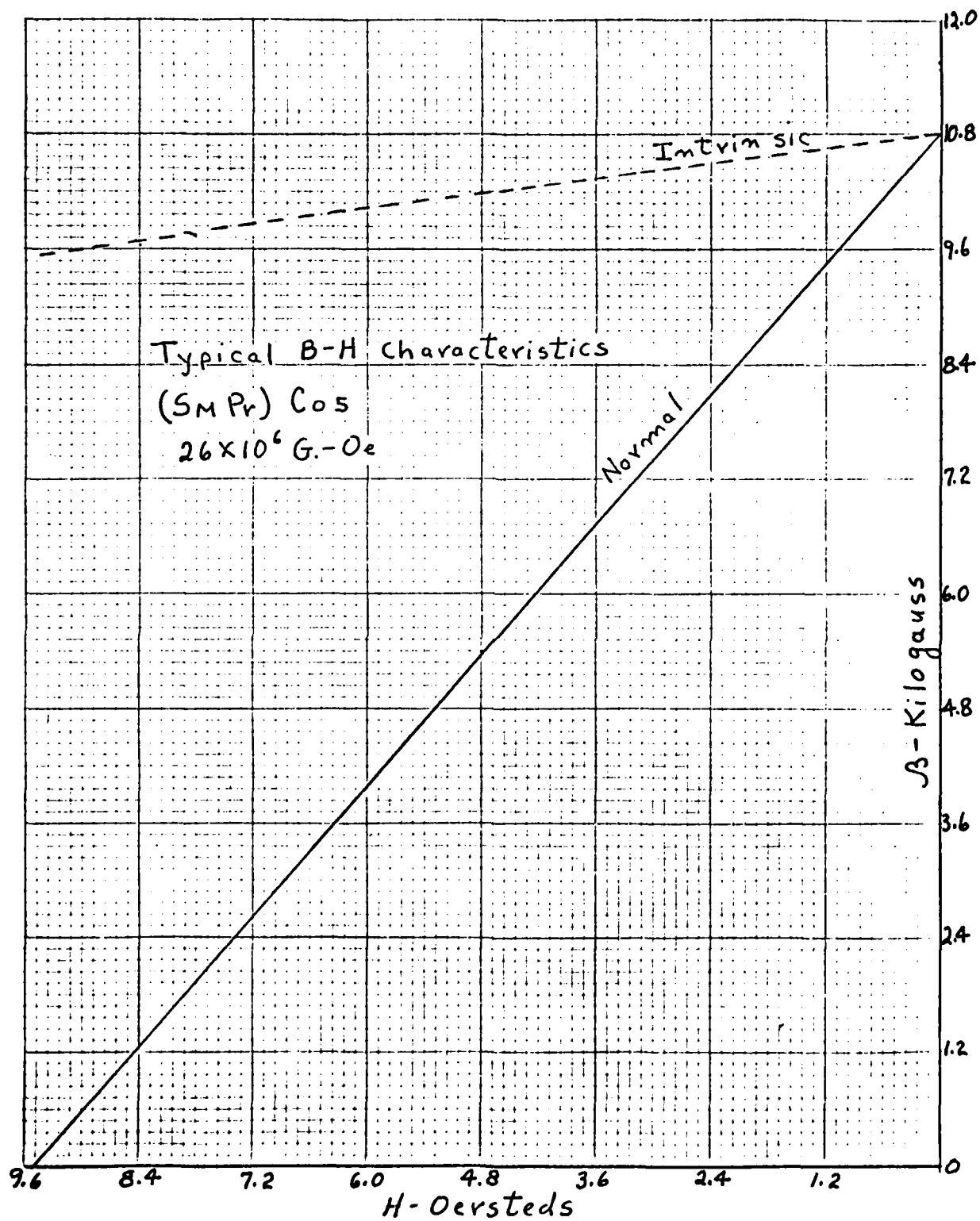


Figure 10 Typical demagnetization curves (SmPr)Co₅ material.

VI DESIGN WITH HIGHER ENERGY MAGNET MATERIALS

In the late 1970's when the VSCF system was first developed, SmCo₅ magnets with an energy product of 22×10^6 G-Oe were a "state of the art" material. At the present time most of the manufacturers of rare earth-cobalt magnets can supply materials with comparable properties to those listed in the magnet properties of Table I.

Magnet manufacturers are now developing new materials having higher energy products and improved characteristics. Within the next few years, there will be available materials having energy products of 26×10^6 G-Oe or higher, both in the ReCo₅ alloys and in the Re₂Co₁₇ alloys.^{5,6,9,10} Figure 10 shows the B-H characteristics of a (SmPr)Co₅ material having an energy product of 26×10^6 G-Oe and an H_{ci} value 15,000 Oe. A machine designed with this magnet material would have improved performance. In accordance with the requirements of maintaining an interchangeable rotor assembly and the same stator dimensions as the present machine, (not necessarily an optimum design approach) the following is suggested.

VI-1 Rotor Design with 26×10^6 G-Oe Material

The rotor to be constructed dimensionally the same as the rotor shown in figure 8, except that the magnet width is 1.000 instead of 0.850 inches. The magnet material would be (SmPr)Co₅ with properties as illustrated in figure 10. The non-magnetic wedges for this construction could be any of the methods suggested in section V-4.

Since the flux/pole for this rotor is so high as to cause the present stator to become highly saturated, a new stator core and winding is required. The lamination for this stator core is shown in figure 11. The dimensions and details are listed in Table V.

TABLE V

STATOR

Same dimensions as shown in Table I, except stator lamination as shown in figure 11.

STATOR WINDING

One turn, throw 1-10, one turn, throw 2-11 etc. with 4 conductors
No. 22 QML, 5 conductors No 23 QML magnet wire. Winding 9 phases,
10 poles no parallel circuits. Total turns/phase 10.

ROTOR

Same overall dimensions as shown in Table III, except inside diameter
2.700. Shrink Ring same as in Table III, except magnetic section 1.00
inches wide. Rotor Details are similar to fig. 8 and that the Rotor
Bore is 2.700 instead of 2.800.

MAGNETS

Ten magnets per rotor section, four sections for forty magnets. Magnet
material (SmPr)₅Co₅. Magnets thermally stabilized at 250°C to remove
irreversible effects.

Initial Magnet Size .56 x 1.000 x 1.250

Finished Magnet Size .55 max, .504 min x 1.000 x 1.250

Magnet Properties ^{9,10}

Residual Induction (Br) Gauss	10,400 min.
Coercive Force (Hc) Oersted	9,000 min.
Intrinsic Coercive Force (Hci) Oersteds	15,000 min.
Max. Energy Product (BxH) G-Oe.	23.4 x 10 ⁶ min.
Recoil Permeability	1.05 max.
Reversible Temp. Coef. % per °C	0.05 max.
Irreversible Temp Coef at 250°C %	2.5 max.

VI-2 FLUX CALCULATIONS

Following the same procedures as in Section V-1, the approximate
operating slope of the magnet is $B/H = .527/.054 \times 1.1 = 8.9$

Note: Carter's Coefficient for this formulation is 1.14 rather than 1.2
This would raise the slope somewhat from that shown.

Thus, from figure 10, the magnet induction is about 9.5 kg.

The flux/pole developed by the magnet is

$$9.5 \times 6450 \times 1.00 \times 5.00 = 306,375 \text{ lines}$$

and the air gap flux is about

$$.93 \times 306,375 = 284,928 \text{ lines}$$

From Equation (3), the no load R.M.S. voltage at 15,000 R.P.M. =
 $4.44 \times 10 \times 1250 \times .994 \times 284,928 \times 10^{-8} = 157 \text{ volts.}$

(while this voltage is lower than the no load voltage of the present machine for the same operating conditions, the IR drop and reactance drops will be much less for this design. Also the effects of armature reaction will be less providing better regulation and a stiffer machine)

The flux and flux densities for the same sections as shown in figure 8 are summarized in Table VI.

TABLE VI

<u>Section No.</u>	<u>Flux/pole (lines)</u>	<u>Area of Section (in²)</u>	<u>Flux Density (KG)</u>
1	306,380	5.00	9.5
2	284,900	5.00	8.8
3	284,900	2.00	22.1
4	284,000	2.37	18.6
5	142,000	1.10	20.0
6	153,150	1.50	15.8

The m.m.f. drops in the magnetic sections are comparable with those in the other designs.

VI -3 WEIGHT CALCULATIONS

(a) Stator Core

The yoke volume = 20.1 in^3

Thus yoke weight = 6.0 lbs.

Tooth volume = 7.84 in^3

Thus teeth weight = 2.35 lbs.

Weight of Stator Core = 8.35 lbs.

(b) Copper Windings

From equation (5) the M.L.T. of this winding is

$$2[1.0 + 4.751 + \pi \times 5.32 \times 9/90]$$
$$= 14.8 \text{ inches}$$

Total Copper Length of #22

$$= 4 \text{ (cond. in hand)} \times 10 \text{ (turns/ph)} \times 14.8/12 \text{ (M.L.T. in ft)}$$
$$\times 9 \text{ (No. of phases)} = 444 \text{ ft.}$$

For No. 22 weight of cond/1000 ft \approx 2.06 lbs. Thus,
weight of #22 portion of winding = .916 lbs.

Total Copper Length of #23 =

$$5 \times 10 \times 14.8/12 \times 9 = 555 \text{ ft.}$$

For No. 23 weight of cond/1,000 ft \approx 1.64 lbs. Thus,
weight of #23 portion of winding = 0.91 lbs.

Total Copper Weight = 1.83 lbs.

The winding resistance/phase can be calculated from equation (6)

For the No. 22 conductors, the resistance = .0162 ohm/ft

$$14.8/12 \times 10 \times .0162/4 = .0500$$

For the No. 23 conductors the resistance = .0203 ohm/ft

$$14.8/12 \times 10 \times .0203/5 = .0500$$

Thus Res/ph = .05 x .05/(.05 + .05) = .0250 ohms

Total Stator Weight = 8.35 + 1.83 = 10.20 lbs.

(c) Magnets

$$\text{Magnet volume} = .525 \times 1.0 \times 1.25 \times 40 = 26.25 \text{ in}^3$$

$$\text{Magnet weight} = 26.25 \times .295 = 7.74 \text{ lbs.}$$

(d) Shrink Ring

$$\text{Volume of Magnetic Section} = 1.00 \times .309 \times 5 \times 10 = 15.45 \text{ in}^3.$$

$$\text{Weight of Magnetic Section} = 15.45 \times .2937 = 4.54 \text{ lbs.}$$

$$\text{Volume of Non-Magnetic Section} = \pi/4[5.00^2 - 4.382^2] \times 5 - 15.45 = 7.35 \text{ in}^3.$$

$$\text{Weight of Non-Magnetic Section} = 7.35 \times .297 = 2.18 \text{ lbs.}$$

$$\text{Total Weight of Shrink Ring} = 6.7 \text{ lbs.}$$

(e) Non-Magnetic Wedges

$$\text{For the non-magnetic wedges shown in Figure 8 the volume} = 5.2 \text{ in}^3.$$

$$\text{Weight of Non-Magnetic Wedges} = 5.2 \times .28 = 1.5 \text{ lbs.}$$

(f) Rotor Hub

$$\text{Volume of Rotor Hub} = \pi/4[3.3^2 - 2.6^2] \times 5 = 16.2 \text{ in}^3.$$

$$\text{Weight of Rotor Hub} = 16.2 \times .28 = 4.5 \text{ lbs}$$

$$\text{Total Rotor Weight} = 7.7 + 6.7 + 1.5 + 4.5 = 20.4 \text{ lbs.}$$

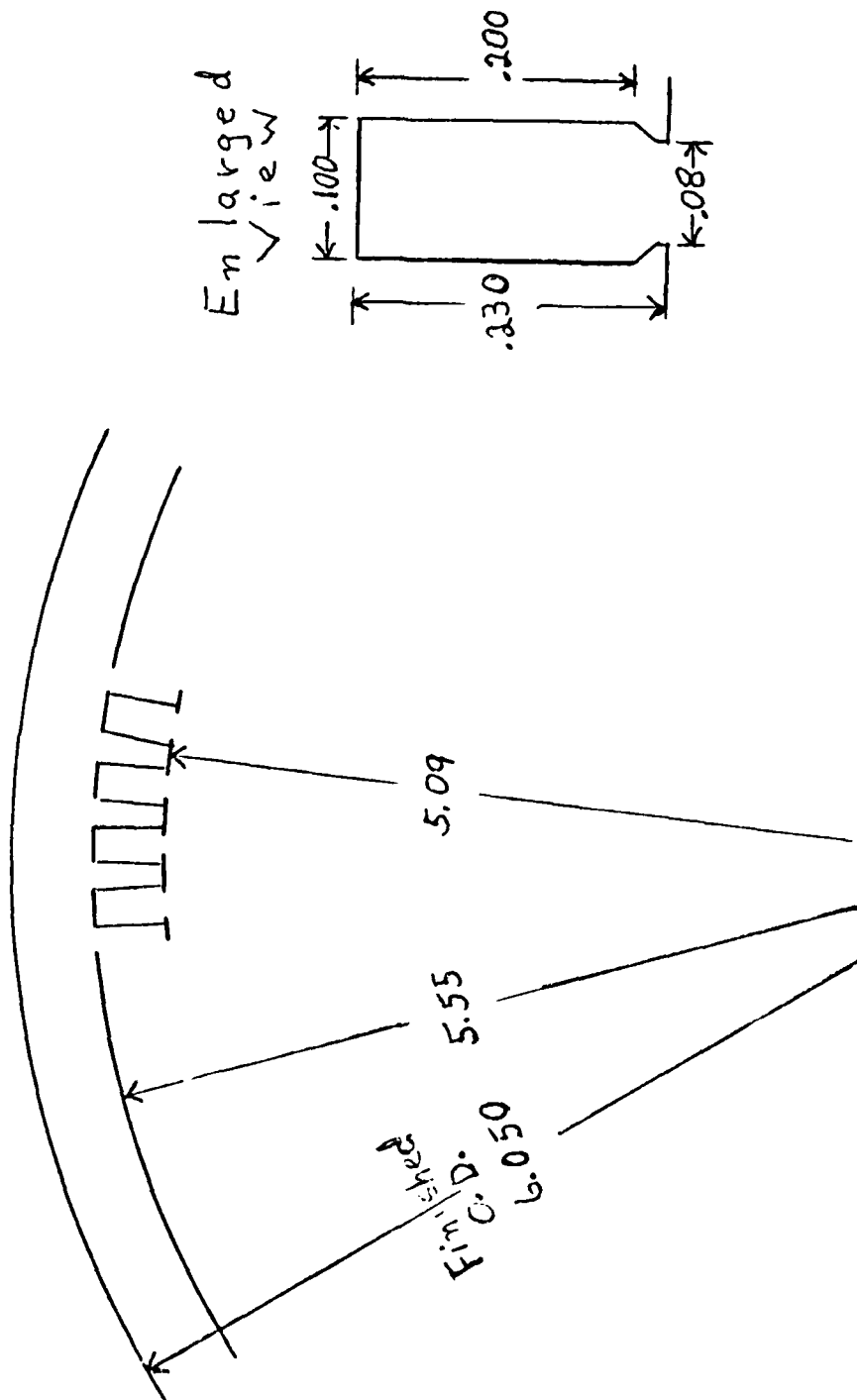


Figure 11 Lamination and Slot Details for Machine Using 26×10^6 G. Oe. Material

VII MAGNETIZATION IN SITU ^{7.8.11}

The process of magnetizing the magnets in the present rotor is to magnetize each of the forty magnets individually and install the magnetized pieces into the rotor sections. This method requires handling strongly magnetized material, processing and machining the magnetized parts which is difficult and time consuming. The ideal method is to assemble the ten magnets required for one rotor section, finish machine the assembly and then magnetize all ten magnets in place.

The amount of energy required for magnetizing a rotor section can be approximated as follows:

Magnets in a "virgin state" ^{5,6} can be magnetized by field intensities around 15,000 oersteds. The sketch shown in fig 12 illustrates the pole details and the fields from the magnetizing fixture required to achieve full magnetization.

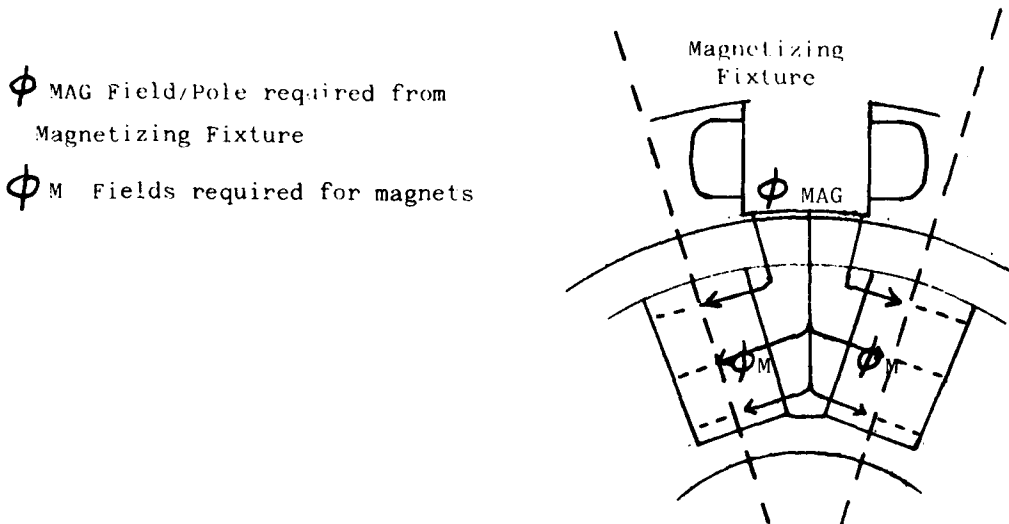


Figure 12 Magnetizing tangentially oriented rotor.

Each magnet requires a flux of about $15 \times 6450 \times .904 \times 1.187 = 103,817$ lines. Thus, the fixture must provide a minimum of $2 \times 103,817$ or 207,634 lines plus sufficient additional flux to allow for any leakage of flux during the magnetization process. The average arc length in the magnetic section of the Shrink Ring is $\pi \times 4.6/10 - .663 = .782$ inches.

Therefore, the average area for this section is

$$.782 \times 1.187 = .928 \text{ in}^2$$

The flux density in this section is

$$\frac{207,634}{.928} = 223,743 \text{ lines/in}^2 \text{ or } 34.7 \text{ KG}$$

This section is, therefore, fully saturated and has a permeability about the same as air. The m.m.f. to drive the flux through the shrink ring section is

$$AT_{sh} = .3 \times \frac{223,743}{3.19} = 21,042 \text{ Amp Turns}$$

Similarly about one-half of the pole can be considered fully saturated. The m.m.f. for the pole section can be approximated as follows: At the midsection of the pole the flux is approximately one-half of 207,634 or 103,800 lines.

The pole arc is $3.5\pi/10 - .663 = .437$ inches

Pole Area = $.437 \times 1.187 = .519 \text{ in}^2$. Therefore,

Av. Pole Flux Density = $103,800/.519 = 200,000 \text{ lines/in}^2 = 31 \text{ kg}$
 or this section of the pole is also fully saturated. Thus,

$$\text{At Pole} \cong .45 \times 200,000/3.19 \cong 28,213.$$

The m.m.f. required for the magnets is

$$AT_m = .663/2 \times 15 \times 6450/3.19 = 10,040 \text{ Amp Turns}$$

$$\text{Total M.M.F.} = 21,000 + 28,200 + 10,000$$

$$\cong 59,200 \text{ Ampere Turns/pole}$$

When leakage is considered the m.m.f./pole could require 100,000 Ampere Turns/pole to properly magnetize the magnets as an assembly.

Now let us consider the case of the radial rotor design.

See figure 13.

ϕ MAG Field/Pole required from Magnetizing Fixture

ϕ M Fields required for magnets

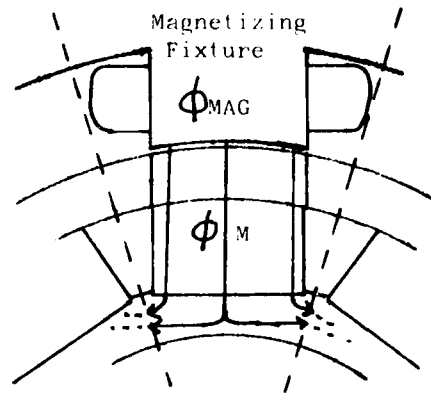


Figure 13 Magnetizing radially oriented rotor

Again assume 15,000 oersteds is required to fully magnetize the magnets.

Each magnet requires a field of $15 \times 6450 \times .850 \times 1.250 = 102,797$ lines.

Since all of these lines must pass through the magnetic section of the shrink ring, and the average area is about the same as the magnet area.

$$AT_{sh} = \frac{.3 \times 15 \times 6450}{3.19} \approx 9099$$

(As the shrink ring is not fully saturated, the actual m.m.f. is somewhat less than this value)

Similarly, the average m.m.f. for magnetizing the magnets is

$$AT_{magnet} = \frac{.55 \times 15 \times 6450}{3.19} = 16,681$$

As the densities in the iron yoke section are low, the m.m.f. for this section is negligible and the total m.m.f. = $9100 + 16,700 \approx 25,800$ AT/pole.

It would take less than one-half the energy to fully magnetize the radial design rotor. Also the leakages would be somewhat less as the paths through air (saturated sections plus magnet) are less.

VIII SUMMARY

This study is based on the drawings, specifications and information on the alternator developed for the first prototype 60KVA system. From preliminary tests of the system, the alternator is required to produce 76.7 KVA at 76% power factor to develop the rated system output of 60KVA 95% power factor. At this load, the alternator phase voltage is 155 volts. Thus, the alternator current is 55 amperes.

A major factor which limits the performance of the system is the commutating reactance of the alternator.⁴ High reactance causes the converter to dissipate more energy during its switching mode and also results in poorer voltage regulation. The alternator reactances are the result of the inductances of the stator windings and the mutual inductances developed between the stator windings and the rotor.^{13,14} Tests of the inductance of permanent magnet machines show that stators with rotors which have rare earth magnet poles only have about one half the inductance of these same stators with rotors using conventional iron poles.^{7,8} This data provides a basis for estimating the relative inductances expected for the radial design in comparison with the present tangential design. These factors and the other parameters previously developed in this report are summarized in Table VII. The data applicable to the current machine is listed in parenthesis after each item and the percent value of this parameter for the radial designs is shown in the appropriate column.

TABLE VII

Parameters	Radial Designs Using	
	22 x 10 ⁶ G. Oe. in percent	26 x 10 ⁶ G. Oe. in percent
Stator Weight (10.1 lbs.)	100	101
Rotor Weight (21.6 lbs.)	85	94
Resistance/phase (.034 ohms)	100	74
*Inductance/phase (50 microhenries)	70	40
No Load Voltage (180 volts/ph)	97	87
Full Load Voltage (155 volts/ph)	106	97

*Based on calculation of steady state synchronous reactance.

The better voltage regulation of the radial designs is due not only to the lower inductance of the stator windings but also due to the higher resistance to armature reaction. This characteristic results in an even better comparison of voltage regulation of these machines at higher transient overloads.

An important characteristic of rare earth magnets is that the fields generated are highly directional in the direction of orientation. Leakage is reduced when the magnetic configuration incorporates this characteristic. Also leakage is minimized by placing the source of the m.m.f. as close to the working gap as practical. The radial design utilizes both these principles within the practical limits of a construction which meets the requirements of the application. Another advantage of the radial design over the tangentially oriented concept is the greater ease of magnetization of the magnets in the assembled structure as discussed in Section VII.

IX RECOMMENDATIONS

One major objective of this study is to produce a design which allows for interchangeable rotors. It is suggested that future programs include the manufacture of one or more rotors of the radial design so that overall performance comparisons can be made. This is important as once a design is in production, with the major investment made for the tooling and manufacturing equipment required to efficiently produce these machines, the cost of changing to another concept is high. Moreover, once a design has been approved and in production additional alternator ratings are developed by changing stack length as required and utilizing the same manufacturing equipment and methods.

The radial concepts should be given full consideration before a major investment is made in the production drawings, tooling and special manufacturing equipment required to produce the tangentially oriented rotor for this type alternator.

REFERENCES

1. H. L. Southall and F.C. Brockhurst, Permanent Magnet and Superconducting Generators in Airborne, High Power Systems. Technical Report AFAPL-TR-79-2073. Interim Report for Period 1 February 1978 through 31 March 1979. pp. 8-10, 65-67.
2. E. Richter, T.W. Newman, Synchronous Machine Designs Using Different Types of Permanent Magnets, Proceedings of the Fifth International Workshop on Rare Earth-Cobalt Permanent Magnets and their Applications. Roanoke VA, June 1981, pp. 2-7, 14-16.
3. E. Richter, Power Density Considerations for Permanent Magnet Machines, Electric Machines and Electro Mechanics 4:21-32, 1979 pp. 21-23, 28-30.
4. M.M. Youn, High Speed PMG Containment Study for VSCF System 0547-3758/81 0000-0971 1981 IEEE pp. 971-973, 975-976.
5. D.L. Martin, Permanent Magnet Characterization Measurements General Electric Report No. 81 CRD 086 May 1981 pp. 8-10.
6. H.F. Mildrum, G.S. Graves and Z.A. Abelnour, Engineering Properties of High Energy Product Sintered Rare Earth-Cobalt Permanent Magnets Proceedings of the Fifth International Workshop on Rare Earth-Cobalt Permanent Magnets and Their Applications. Roanoke VA, June 1981.
7. S. Noodleman, Rare Earth Permanent Magnet Motors and Generators, Proceedings of the First AFAPL Generators and Motors Seminar, Technical Report AFAPL-TR-79-2090, Wright Patterson AFB, OH pp. 22-32.
8. S. Noodleman, Rare Earth-Cobalt Magnets and Their use in D.C. Machines International Conference on Electric Machines, Brussels Belgium September 1978.

9. K.S.V.L. Narasimham, Higher Energy Product Rare Earth-Cobalt Permanent Magnets, Proceedings of the Fifth International Workshop on Rare Earth-Cobalt Permanent Magnets and Their Applications, Roanoke VA, June 1981 pp. 636-642.
10. H.F. Mildrum, Hard Permanent Magnet Development Trends and Their Application to A.C. Machines, Paper to be presented at the IAS-IEEE Annual Conference, Philadelphia PA, October 1981 pp. 2-6

TEXT BOOKS

11. McCaig M. Permanent Magnets in Theory and Practice, John Wiley and Sons, Inc. New York NY 1962.
12. Parker R. J. and Studders R., Permanent Magnets and Their Applications John Wiley and Sons, Inc. New York NY 1962.
13. Jain G.C. Design Operation and Testing of Synchronous Machines Asia Publishing House, NY.
14. Del Toro V. Electromechanical Devices for Energy Conversion and Control Systems, Prentice Hall, Inc. Englewood Cliffs, NJ.

1981 USAF - SCEEE SUMMER FACULTY RESEARCH PROGRAM

Sponsored by the

AIR FORCE OFFICE OF SCIENTIFIC RESEARCH

Conducted by the

SOUTHEASTERN CENTER FOR ELECTRICAL ENGINEERING EDUCATION

FINAL REPORT

THE EFFECTS OF JP-4 AVIATION FUEL ON SPECIFIC INTERNAL ORGANS OF

THE FAT-HEAD MINNOW, PIMEPHALE PROMELUS

Prepared by: Dr. William N. Norton
Academic Rank: Assistant Professor
Department and University: Department of Biology
Southeastern Louisiana University
Research Location: Toxic Hazards Division, Aerospace Medical Research
Laboratory
USAF Research Colleague: Dr. James M. Livingston
Date: August 24, 1981
Contract No.: F49620-79-0038

THE EFFECTS OF JP-4 AVIATION FUEL ON SPECIFIC INTERNAL ORGANS

OF THE FAT-HEAD MINNOW, PIMEPHALE PROMELUS

by

William N. Norton

ABSTRACT

Water-soluble fractions of petroleum-derived JP-4 fuel induce ultrastructural alterations of the kidney, gill, pseudo-branch and nasal epithelium of the fat-head minnow, Pimephale promelus. There appears to be no common ultrastructural effect among the organs studied in regard to the degradation of a specific cellular organelle. The sole tissue which exhibits extensive cellular degradation is the nasal epithelium. The lesions are manifested in the form of myeloid bodies and electron-dense figures. A proliferation of vacuoles and a disruption of mitochondria-tubule complexes is evident in the pseudo-branch of experimental fish. Cellular membranes associated with the surface of gill filaments and secondary lamellae maintain their integrity throughout the investigation, however, focal sites of pillar cell degradation are evident. Within the kidney endothelial cells associated with convoluted tubules undergo degradation as characterized by the fragmentation of plasma membranes.

Acknowledgement

The author would like to extend his appreciation to the Air Force Systems Command, the Air Force Office of Scientific Research and the Southeastern Center for Electrical Engineering Education for providing him with the opportunity to spend a productive and enjoyable summer at the Aerospace Medical Research Laboratory, Wright-Patterson, AFB, Ohio. In particular, gratitude is extended to Mr. Dave Matte and Airman Russ Nieser for their cooperation, aid and helpful suggestions.

Finally, the author wishes to thank Major James M. Livingston for suggesting this area of research, and for his guidance throughout the duration of the project.

I. INTRODUCTION:

The US Air Force daily consumes large quantities of petroleum-derived JP-4 aviation fuel. The possibility exists of accidental spills and consequential seepage of fuel into the aquatic environment. In order to predict the biological consequences of such a phenomenon, basic information is required regarding the effects of acute and chronic exposures of fuel to various aquatic organisms. The fat-head minnow, Pimephales promelus, was chosen as the model system for the present investigation primarily because of its ubiquitous nature, and the substantial amount of biological information regarding the fish which has been accumulated.¹

Petroleum-derived aviation fuel consist of a variety of organic compounds including toluene, benexene, xylene and naphthalene. Investigators have determined that the rate of aromatic hydrocarbon accumulation in aquatic organisms is highly species specific.² Toluene, an aromatic hydrocarbon, is capable of accumulating in a variety of organs once uptake has occurred.³ However, no information pertaining to the histopathology of such a phenomenon has been published. Additional compounds such as benzene, xylene and naphthalene have been analyzed as to their relative toxicities to aquatic organisms.^{3,4,5}

There is a paucity of information regarding histopathological and physiological responses of aquatic vertebrates to the aromatic hydrocarbons mentioned above. Investigators report that juvenile striped bass exhibit increases in respiratory rates after exposure to sub-lethal concentrations of benzene. Histopathological investigations of mummichogs exposed to sub-lethal quantities of naphthalene indicate that the toxicity is due primarily to a generalized blood stasis.⁷ As indicated previously a void exists in regard to information concerning the cellular effects of exposure of fuel components to aquatic organisms. The present study attempts to provide some insight into the toxic effects of the water-soluble fractions of JP-4 on the ultrastructure of selected organs of a vertebrate, the fat-head minnow.

II. OBJECTIVES

The primary objective of the present investigation was to determine the ultrastructural effects, if any, of the water-soluble fractions of petroleum-derived JP-4 fuel on specific organs of the fat-head minnow. The initial protocol established exposures of fish to several concentrations of JP-4, (20, 40 and 60 percent); however, due to time limitation only fish exposed to the 40 percent solution were critically analyzed. The study is considered to be acute since the longest period of exposure is 48 hours. The investigators were hopeful of obtaining sufficient ultrastructural information regarding focal lesions to provide some insight as to biochemical or physiological alterations.

III. MATERIALS AND METHODS

Fat-head minnows of varying weights were distributed into 4 groups of 12 fish each. Three of the groups were released into separate 20 gallon tanks containing 20, 40, and 60 percent solutions, respectively, of water-soluble fractions of petroleum-derived JP-4. The remaining group was maintained in a 20 gallon tank of water and functioned as a control.

At the time period of 6, 12, 24, and 48 hours subsequent to the initial exposure 3 fish from each tank were removed and placed in a 3% glutaraldehyde-3% paraformaldehyde solution which was buffered with 0.1M sodium cacodylate (ph 7.4). To enhance fixation of the internal organs, a longitudinal slit was cut from the anus to the pectoral fins. Sections of gill, pseudo-branch, nasal epithelium and kidney were excised and placed in vials containing cold fixative.

After a fixation period of 3 hours the tissues were rinsed in cold buffer and post-fixed in 2% osmium tetroxide for 2 hours. Subsequent to a rinse in buffer the tissues were dehydrated in a graded series of ethanol and embedded in Epon 812. Thin sections were cut by an ultramicrotome and then stained with lead citrate and uranyl acetate. The tissues were examined by a JEOL 100B transmission electron microscope at 60 KV.

IV. RESULTS

Gill:

There was no evidence of a consistent or repetitive form of cellular degradation among the gills examined. Focal lesions were associated with a variety of organelles, but no distinct pattern developed regardless of the time points studied.

Granulocytes were present within the gill filaments and secondary lamellae, however, as compared to control tissue the concentration appeared to be within normal ranges. Chloride and mucoid cells located at the base of secondary lamellae displayed no irregularities. Epithelial cells forming the outer surface of lamellae exhibited occasional signs of degradation in all fish examined. However, there was no indication of fragmentation or dissociation of the plasma membrane directly contacting the fuel.

Pillar cells, whose lateral extensions form the inner surface of capillaries within the gill, displayed no evidence of irregularities among cytoplasmic organelles. There were, however, focal sites of degradation along the membrane bordering the lumen of several capillaries. There was no indication of a disruption of the basal lamina positioned between the pillar cells and the second layer of epithelial cells.

Pseudo-branch:

The adverse ultrastructural effects of JP-4 on pseudo-branch did not appear to be related temporally, since alterations were evident in fish examined from all time points. Control cells were characterized by an orderly arrangement of mitochondria positioned within an elaborate system of tubules. The tubules extend to that region of the cell which contacts the basal lamina positioned adjacent to the capillary systems of the pseudo-branch.

Vacuoles of various diameters were evident within a majority of the cells examined in experimental fish. Occasional mitochondrial degradation was manifested in the form of distensions of the outer membrane, and in some instances by the development of myeloid figures. Mitochondrial disruption and vacuole formation were observed in tissues analyzed from all experimental samples. Although morphometric analysis were not conducted, random scans of pseudo-branch

indicated that substantial numbers of cells were at least partially affected by the fuel. In addition to the actual destruction of mitochondria, cells frequently displayed a dissociation of the mitochondria-tubule complex. In essence, the latter organelles were unable to maintain the close association noted in control tissue.

Kidney:

Endothelial cells normally associated with the basal lamina of proximal and distal convoluted tubules were frequently observed in a state of disruption. Plasma membranes of the aforementioned cells appeared fragmented with a resulting exposure of the basal lamina to the peritubular vessels. At the sites of alteration some dissociation of the basal lamina was noted.

Multiple cells comprising the proximal convoluted tubules possessed large numbers of vesicles whose origins appeared to be the terminal regions of the agranular endoplasmic reticulum system. This phenomenon was evident in controls, however, not to the extent observed in experimental tissue. No ultrastructural alterations were detected among cells comprising the glomeruli.

Nasal Epithelium:

Cellular abasement, characterized by the formation of myeloid figures and electron-dense bodies, was pronounced throughout the nasal epithelial region. Little alteration was noted among the receptor cells. Cilia, projecting from sensory receptors into the nasal lumen, were unaffected by the water-soluble components of the fuel. The magnitude of epithelial disruption appeared to be correlated with the length of exposure to the fuel.

V. DISCUSSION

Information obtained from the present investigation indicates that the water-soluble fractions of petroleum-derived JP-4 fuel at the 40% exposure level induce ultrastructural alterations among the tissues examined. The solvent effect of aromatic hydrocarbons one might expect on cellular membranes is not observed. Within each tissue the ultrastructural effects appear to be repro-

lucible and predictable. As to the degree of physiological or biochemical disruption, determinations are less tenuous. Based strictly on ultrastructural observations the physiological capabilities of damaged cells are in many instances difficult to ascertain. With the latter statement in mind, although cellular degradation was evident in all the experimental tissues examined, the gills and kidneys displayed minimal toxic effects of the fuel and appeared to be functional organs.

Cellular disruptions was most pronounced in the nasal epithelial region. Although lesions in this area would not result in death, the degradation may explain the deviated behavioral patterns characteristic of fish when exposed to fuel.

The significance of the dissociation of mitochondria-tubule complexes present in cells of the pseudo-branch is difficult to determine since the latter organelles basically appear normal in structure. It is possible that the close association is required for a particular biochemical process, and that the disruptive nature of the fuel would adversely affect normal functions. There were relatively few observations of cells in the latter stages of degradation which is usually characterized by the presence of multiple myeloid figures and massive disruption of organelles.

The tissue least affected ultrastructurally by the fuel appears to be the gills. Occasionally granulocytes were noted in the secondary lamellae, but the same cellular arrangement was observed in control tissue. Plasma membranes forming the surface of gill filaments and lamellae apparently are unaffected structurally by direct contact with the fuel.

Acute exposures of JP-4 to the kidney appears to alter selectively the endothelial cells associated with the distal and proximal convoluted tubules. This phenomenon indicates a lack of uniformity in regard to the effects of JP-4 on endothelial cells as a whole. Comparable cells of the pseudo-branch and gills displayed very little, if any, susceptibility to the fuel.

In summary, the water-soluble components of JP-4 at the 40% concentration level are capable of inducing ultrastructural alterations in the organs selected for the present investigation. Whether the effects are of such magnitude to disrupt critical biochemical pathways has yet to be determined.

VI. RECOMMENDATIONS

The present investigation could represent the initial phase of a more comprehensive analysis of the effects of JP-4 on aquatic systems. Several related studies could complement the results obtained from the present project. The author recommends the following:

1. Utilize the scanning electron microscope to analyze on a 3 dimensional scale the cellular surfaces of tissues exposed to JP-4. The proposed investigation would supplement current transmission electron microscopy studies. The significant depth of field provided by the scanning electron microscope would enable the investigator to study structures which are difficult to visualize and interpret if sectioned and observed in a transmission mode.
2. Analyze the ultrastructural effects of a relatively high concentration of JP-4 on those organs investigated in the present study. Ideally several fish should be chemically fixed just prior to death to enable a monitoring for lesions which may indicate critical sites of action of the fuel. The investigation would provide some insight as to the question of whether identical effects are produced at high and low concentrations and if additional alterations are initiated. At the lower concentrations of fuel the toxic effects may be reversible, while exposures at the higher levels may induce the formation of irreversible lesions which possibly could cause death of the cell.
3. There should be an establishment of LC-50 values for the exposures of both whole fuel and water-soluble fractions to the fat-head minnow. The information would be valuable for future experiments, and on a practical basis for environmental projections.
4. By means of autoradiography or affinity labeling experiments, information could be assimilated to determine if fuel components are sequestered within specific sites of the cells. The data may enable the investigator to correlate ultrastructural observations with biochemical and physiological information.

REFERENCES

1. Bond, C.A., Biology of Fishes, (W.B. Saunders, Philadelphia, 1979).
2. Neff, J.M., D. Dixit, G.A. Cox, and J.W. Anderson, "Accumulation and Release of Petroleum Derived Aromatic Hydrocarbons by Four Species of Marine Animals," Marine Biology, Vol. 38, 1976, pp. 278-289.
3. Berry, W.O. and J.W. Fisher, "Transfer of ¹⁴C-Toluene From Mosquito Larvae to Bluegill Sunfish," Bull. Environm. Contam. Toxicol., Vol. 23, 1979, 733-736.
4. Meyerhoff, R.D., "Acute Toxicity of Benzene, a Component of Crude Oil, to Juvenile Striped Bass (Morone Saxatilis)," J. Fish. Res. Board Can., Vol. 32, 1975, pp. 1864-1866.
5. Benville, P.E., and S.D. Korn, "The Acute Toxicity of Six Monocyclic Aromatic Crude Oil Components to Striped Bass (Monrone Saxatilis) and Bay Shrimp (Crago Franciscorum)," Calif. Fish and Game, Vol. 4, 1977, pp. 204-209.
6. Brocksen, R.W., and H.C. Bailey, "The Respiratory Response of Juvenile Chinook Salmoon and Striped Bass Exposed to Benzene, a Water Soluble Component of Crude Oil," Conf. on Prev. and Control of Oil Spills, 1973, pp. 783-791.
7. DiMichele, L. and M.H. Taylor, "Histopathological and Physiological Responses of Fundulus Heteroclitus to Naphthalene Exposure," J. Fish Res. Board Can., Vol. 35, 1978, pp. 1060-1066.

1981 USAF - SCEEE SUMMER FACULTY RESEARCH PROGRAM

Sponsored by the

AIR FORCE OFFICE OF SCIENTIFIC RESEARCH

Conducted by the

SOUTHEASTERN CENTER FOR ELECTRICAL ENGINEERING EDUCATION

FINAL REPORT

OBSERVATIONS OF SUNSPOT DYNAMICS AND

THEORETICAL EFFECTS OF INHOMOGENEITIES

IN THE SOLAR CONVECTION ZONE

Prepared by: Dr. Alan E. Nye

Academic Rank: Assistant Professor

Department and University: Mechanical Engineering Department
Rochester Institute of Technology

Research Location: Air Force Geophysics Laboratory (AFSC)
Space Physics Division
Solar Physics Branch
Sacramento Peak Observatory, Sunspot, N.M.

USAF Research Colleague: None

Date: October 2, 1981

Contract No: F49620-79-C-0038

OBSERVATIONS OF SUNSPOT DYNAMICS AND
THEORETICAL EFFECTS OF INHOMOGENEITIES
IN THE SOLAR CONVECTION ZONE

By

Alan H. Nye

ABSTRACT

Observations giving high resolution in wavelength, time, and horizontal space were taken of sunspots to determine the characteristics of oscillations at different heights. There was a high correlation between velocity and magnetic field fluctuations in the umbral photosphere. These oscillations excite waves which move the penumbra vertically in phase. There was no correlation between velocities observed at chromospheric and photospheric levels. This implies that wave mode eigenfunctions are sharply peaked in height, which imposes useful constraints on any theoretical sunspot model.

Observations of the surface of the solar convection zone show the presence of trapped nonradial acoustic waves whose frequencies shift with time. A theoretical analysis of a simple model shows that inhomogeneities in the sound speed will lead to shifts in the eigenfrequencies of the trapped modes. An arbitrary two dimensional perturbation on a uniform sound speed is decomposed into its fourier components, each of which causes a shift of a single eigenfrequency. The eigenfunctions are all perturbed which leads to a spreading of the ridges in the (k, ω) plane similar to those observed.

ACKNOWLEDGEMENT

The author would like to thank the Air Force Systems Command, the Air Force Office of Scientific Research, and the Southeastern Center for Electrical Engineering Education for the opportunity to participate in this program and to be involved in this interesting and worthwhile research project. He would like to acknowledge the Air Force Geophysics Laboratory, in particular the Solar Physics Branch, for its hospitality at the Sacramento Peak Observatory.

Finally, he would like to thank Dr. Lawrence Cram and Dr. John H. Thomas for their collaboration and guidance.

I. INTRODUCTION:

The structure of the solar atmosphere and the transport of energy through it, particularly in the presence of intense magnetic fields are important areas of basic research in solar physics. The Air Force is interested in these topics because of the adverse effect of solar flares on communication. Solar flares occur in magnetic active regions and are probably the result of the explosive release of energy stored in the magnetic field structure.

The present project is concerned with two aspects of solar structure and energy transport. The first aspect is the transport of energy through a region of intense magnetic fields: a sunspot. A sunspot is a relatively dark region of the surface of the sun whose umbral temperature (3000 K) is considerably lower than the normal photospheric temperature (6000 K) and is the location of intense magnetic fields (~ 3000 gauss). The magnetic field is obviously affecting the normal energy transport through the solar surface, but the mechanism is not well understood. Velocity and intensity oscillations have been observed in sunspots for several years.^{1,2,3} The oscillations may indicate energy propagation along the magnetic field or they may be standing waves with no energy transport. There are many different types of time dependent behavior: umbral oscillations, umbral flashes, umbral dots, and penumbral waves. The objective of this phase of the project was to determine the individual properties of these phenomena and the relationships, if any, between them.

The second aspect of the project is concerned with the structure of the solar convection zone. Recent studies^{4,5,6,7} have shown that the five minute oscillations of the solar envelope are trapped high-order nonradial p-modes of (acoustic) waves. High-order modes, by virtue of their large horizontal wavenumber, offer the possibility of studying laterally localized inhomogeneities in the solar envelope. The sphericity of the sun is of secondary importance for the high-order p-modes. This has aroused interest in the possibility of probing the solar convection zone with techniques similar to those used in terrestrial seismology. Observations of the solar surface on a large spatial scale and with a long time series can be converted to a diagram which shows the power in oscillations as a function of frequency

and wavenumber. These diagrams can be used to determine global characteristics of the convection zone. The power lies along ridges in the k_n, ω diagram which have some width. Additionally, these ridges may shift position with time. The spreading and shifting of the ridges are related to inhomogeneities in the convection zone. These may be supergranules, giant cells or even intense magnetic flux tubes which have yet to emerge through the solar surface. A probe which could determine the scale of convective elements with depth would be extremely important in helping to understand the details of energy transport in the sun. This project involved a theoretical study of the effect of inhomogeneities on the eigenfunctions of a model acoustic cavity which lead to spreading of the original eigenfunctions of the unperturbed cavity.

II. OBJECTIVES:

As discussed above there were two basic features of this project. The first involved the structure of velocity oscillations in sunspots. The specific objectives were:

- 1.) To determine the individual properties of several types of observed sunspot oscillations. The observational program was designed to give high resolution in wavelength, time, and horizontal space.
- 2.) To use velocity observations taken simultaneously in several different spectral lines to obtain information at different heights in a sunspot. This could determine whether the oscillations are standing waves or propagating waves.
- 3.) To determine if there is any relationship between the various types of oscillations.

The second feature consisted of a theoretical study of the effect of inhomogeneities in the solar convection zone on observable properties at the solar surface. The specific objectives were:

- 1.) To develop a method of computing the eigenfunctions of an acoustic cavity in the presence of variations in the sound speed.
- 2.) To apply this technique to specific functional forms of the sound speed.

3.) To extend, if possible, the method to arbitrary forms of sound speed variation.

By studying a simplified model of the solar convection zone, it is possible to understand how the sound speed variation affects the eigenfunctions and eigenfrequencies. The solutions for a more realistic model are sufficiently complicated that physical insight would be lost in numerical techniques.

111. OBSERVATIONS AND DATA REDUCTION:

We have carried out a series of observations of dynamical phenomena in sunspots based upon photographic spectra obtained with the Sacramento Peak Observatory Vacuum Tower Telescope and Eschelle Spectrograph. The observational program was designed to give high resolution in wavelength, time, and horizontal space. In addition, several spectral lines formed at different heights were observed to give some resolution in the vertical dimension. Data of good to excellent quality has been obtained for sunspots on two days, and include several time series of one hour or longer.

Sunspots were observed simultaneously in five spectral lines: Calcium H and K, Fe 6303, Ti 5713, and Magnesium b. The selection provides information at different heights as well as magnetic and nonmagnetic data. In addition, white light and Ca K slit-jaw pictures were obtained.

The data reduction was begun with the 18 August 1980 observations. The spot was at radius vector $R = 0.55$ ($\mu = 0.84$). The slit crossed the center of the umbra, extending into the photosphere on both sides of the sunspot. A light bridge in the umbra intersected the slit. Exposures were made every 20 seconds for a total time series of 71 minutes. Visual inspection of the Ca K spectral line showed that there were frequent umbral flashes occurring throughout the observing period.

The Fe 6303 data was reduced, using the Sacramento Peak fast microphotometer. The film was digitized with a step size of 0.25 arc seconds in the spatial dimension and $10\text{m}\text{\AA}$ in wavelength. Each observation in Fe 6303 consists of two images: the left and right hand circular polarizations. After digitization, the measured densities were converted to intensities using calibrated standards. The polarization

images for each frame were registered in space using a hair line and in wavelength using an O_2 telluric line that lies close to Fe 6303. By adding and subtracting the two polarization images, Stokes intensity (I) profiles and circular polarization (V) profiles were obtained.

Several different parameters were calculated from the intensity and V profiles for each spatial point at each time. The continuum intensity was determined by averaging points outside the spectral lines in the I profile. The position of the center-of-gravity of the I profile was located to measure velocity. The residual intensity of Fe 6303 was calculated by dividing the central intensity of the I profile by the continuum intensity. From the V profile, the positions and values of the extrema, V_{\max} and V_{\min} , were determined together with the equivalent width of the profile $|V_{\lambda}|$.

These quantities were then used to derive several parameters, including the magnetic field intensity (from the separation of the extrema) and the Doppler shift. The line-of-sight projection magnetic field and a Doppler shift were also determined from the positions of the centroids of the $I \pm V$ profiles. Each frame was then registered spatially into a time series by cross-correlating it to the mean of the data. It is important to note that the velocities, as determined from the V profile, are not corrupted by photospheric scattered light. Since the velocities come from magnetic information, they clearly represent motions in the sunspot.

The Calcium K data from the 18 August 1980 observations was reduced next using the same spatial and wavelength step sizes as the Fe 6303 data. Calcium K is formed in the chromosphere several hundred kilometers above the height of formation of Fe 6303. Velocity and intensity time series were determined for calcium K. This data was compared to the simultaneous photospheric data to determine if there was any correlation between oscillations at the two heights.

The Fe 6303, Calcium H, and Ti 5713 photographic data for the 21 August 1980 sunspot were also reduced to digital form using the Sacramento Peak Observatory fast microphotometer. However, due to a combination of hardware and software problems, only the data from the 18 August 1980 observations has been analyzed thusfar. The problems encountered were beyond the control of the Air Force Geophysics

Laboratory as Sacramento Peak Observatory is operated by the Association of Universities for Research in Astronomy Inc., under contract with the National Science Foundation. The Air Force maintains a Solar Physics branch of the Space Physics division at Sacramento Peak, but is not responsible for the operation of the computer or data reduction facilities there.

IV. ANALYSIS OF SUNSPOT OBSERVATIONS:

Several important features have been found in the 18 August 1980 observations. The first of these is the ejection of a magnetic feature from the outer edge of the penumbra. This appears as a polarity reversal with an initial total field strength of about 1000 gauss, and it appears to decrease as the feature moves away from the sunspot. The proper motion of the feature is about 2 km/s. The velocity field measured in the V profile shows a downflow of 400m/s on the spotward side of the moving magnetic feature. A plot of residual intensity also shows the feature moving away from the sunspot as a "line gap." The variation of magnetic field across the sunspot shows the strongest field lies in the darkest portion of the umbra and this is just to the right of the light bridge where the field is relatively weak. There is also a feature in the right side penumbra that changes with time, but does not move.

The second important result is the observation of umbral oscillations at the photospheric level. These oscillations are visible everywhere in the umbra, but their amplitude is lower in the darkest part of the umbra where the magnetic field strength is the largest. The peak amplitude is approximately 200 m/s and these velocity peaks appear to propagate back and forth horizontally along the slit. This would imply some overtone mode of membrane oscillation of the entire umbra. Some waves propagate across the entire umbra while others seem to originate near the light bridge. Power spectra were calculated for the photospheric velocity time series at forty points within the sunspot umbra. The average of these shows a peak in power at a period of 270 seconds. As this period is close to the 300 second oscillation period of the surrounding solar photosphere, it is important to emphasize the

sunspot oscillations are measured from the magnetic V profile and are therefore not due to scattered photospheric light.

The photospheric umbral velocity oscillations are related to other photospheric features. The magnetic field, as measured by the separation of the maxima of the Stokes V profiles shows an oscillation which is strongly correlated to the velocity oscillations. This is not surprising as the magnetic field exerts a restoring force which will support oscillations, but this is the first time that this measurement has been made. Velocity oscillations are also observed in the penumbral photosphere where the entire penumbra appears to be oscillating vertically in phase. These penumbral oscillations are excited by the umbral oscillations.

The Calcium K data shows that at the chromospheric level there are oscillations everywhere within the umbra with periods in the range 140 to 190 seconds. There is a distinct boundary for the oscillations, however, and no oscillations are observed in the penumbra. This is a surprising result inasmuch as the magnetic field configuration at chromospheric levels has less horizontal variation than in the photosphere.

The umbral flashes which were obvious in the photographic images are much less distinct when the data is converted to intensities using the calibrated standards. Apparently the umbral flashes correspond to umbral oscillations of greater (by a factor of 2-3) than usual amplitude. The high contrast film used in the observations makes these oscillations appear as umbral flashes. In comparing the calcium K velocities to the Fe 6303 velocities it was found that there is no correlation between the velocities at the two heights in the sunspot atmosphere and therefore nothing definite can be said about the vertical propagation of the waves. Since both oscillations are presumably generated by overstable convection at a lower level the lack of correlation would imply that the velocity eigenfunctions are sharply peaked functions of height. This information will be extremely useful for calculating theoretical models of sunspot structure. A preliminary version of this work was presented⁸ at a conference on the physics of sunspots held at Sacramento Peak Observatory - July, 1981.

V. PERTURBATION ANALYSIS:

In the absence of rotation⁷ and other perturbations, each high-order p-mode is characterized by its frequency ω , its horizontal wavenumber (in the direction of propagation) k_H , and a radial quantum number, m , which counts the number of nodes in the eigenfunction in the radial direction. The dispersion equation for non-radial solar p-modes yields, for each value of $m \geq 0$, a relationship between ω and k_H , which can be plotted as a curve in the (k_H, ω) plane. It is observed that essentially all of the oscillatory power in the solar velocity field lies along ridges in the (k_H, ω) plane, close to the theoretical locii.

The present study focuses on the distortions of the (k_H, ω) diagram which result from horizontal and radial inhomogeneities, such as convective cells and submerged magnetic flux concentrations. The model is highly idealized, but because it provides an analytical solution, it illustrates many of the relevant effects without cumbersome numerical analysis.

Consider pure acoustic (pressure) modes in an isothermal rectangular box with rigid walls at $x = 0, X$; $z = 0, Z$ and of infinite extent in the y direction. X (horizontal) is taken to be much larger than Z (vertical) so that the rigid reflections at $z = 0$ and $z = Z$ are analogous to the trapping of solar p-modes between the atmospheric cut-off and the internal envelope reflection.⁹ The reflections at $x = 0$ and $x = X$ may be regarded as analogous to the fact that global solar p-modes must have an integral number of nodes around the solar circumference.

The wave equation, in the absence of inhomogeneities is:

$$\nabla^2 \psi - \frac{1}{c_0^2} \frac{\partial^2 \psi}{\partial t^2} = 0 \quad (1)$$

which after Fourier analyzing in the time domain becomes

$$\nabla^2 \psi + \frac{\omega^2}{c_0^2} \psi = 0 \quad (2)$$

where c_0 is the uniform sound speed and ω is the wave frequency of oscillation. The ratio ω/c_0 is defined as k which is the wavenumber of

the oscillation. There are an infinite set of solutions of the unperturbed wave equation of the general form:

$$\psi_{lm} = \sqrt{\frac{z}{X}} \sin \frac{l\pi x}{X} \sqrt{\frac{z}{Z}} \sin \frac{m\pi z}{Z} \quad (3)$$

where l and m are integers, as the boundary conditions require. The wavenumber is composed of a horizontal k_u and vertical k_v component and the dispersion equation provides a relation between ω , k_u , and k_v in the form

$$\omega^2 c_0^2 = k_{lm}^2 = \pi^2 \left[\frac{l^2}{X^2} + \frac{m^2}{Z^2} \right] \quad (4)$$

The solutions of this dispersion equation form curves in the (k_u, ω) plane which are direct analogs of the structure of the solar (k_u, ω) plane.

In the presence of inhomogeneities in the sound speed, the wave equation becomes¹⁰

$$\nabla^2 \psi + \left[\frac{\omega^2}{c_0^2} - \epsilon U(x, z) \right] \psi = 0 \quad (5)$$

where c_0 is the unperturbed sound speed, ϵ is the scale factor of the perturbation on the sound speed, and U is a function of the inhomogeneity and its spatial derivatives. The solutions of equation (5) are the solutions of the standard wave equation plus perturbation terms.

$$\phi_{lm}(x, z) = \psi_{lm}(x, z) + \epsilon \sum_{p \neq l} \sum_{q \neq m} \text{I.F.} \psi_{pq}(x, z) \quad (6)$$

where I.F. is an integrating factor given by

$$\text{I.F.} = \frac{\int_0^X \int_0^Z \psi_{pq}(x_0, z_0) U(x_0, z_0) \phi_{lm}(x_0, z_0) dx_0 dz_0}{K_{lm}^2 - k_{pq}^2} \quad (7)$$

The K_{lm} terms are the perturbed eigenvalues given by:

$$K_{lm}^2 = k_{lm}^2 + \epsilon \int_0^X \int_0^Z \psi_{lm}(x_0, z_0) U(x_0, z_0) \phi_{lm}(x_0, z_0) dx_0 dz_0 \quad (8)$$

The perturbed eigenvalues are determined by the perturbed eigenfunctions, ϕ_{lm} . However, since ϵ is taken to be a small term, $\epsilon^2 \rightarrow 0$ and ϕ_{lm} in equation (8) is replaced by ψ_{lm} . That is, the expansion is cut off after the first term. Likewise, the integrating factor (equation 7) contains the perturbed eigenfunction ϕ_{lm} which can be replaced by ψ_{lm} to first order. Once the sound speed perturbation is specified, U can be determined and then the perturbed eigenfunctions and eigenvalues are calculated.

VI. TWO DIMENSIONAL PERTURBATIONS:

The success of the perturbation technique depends on the form of the sound speed perturbation. This function and its derivatives determine the function $U(x, z)$ which in turn controls whether the integrals in the perturbed eigenfunctions and eigenvalues have an analytical solution or not.

At first a specific two dimensional form was chosen for the sound speed,

$$C^2(x, z) = C_0^2 + \epsilon f(x) F(z) \quad (9)$$

where the perturbation term was assumed to be separable into two one dimensional functions, $f(x)$ and $F(z)$. In this case the U function becomes:

$$U(x, z) = \frac{1}{C_0^2} \left[\frac{1}{2} \left(F \frac{d^2 f}{dx^2} + f \frac{d^2 F}{dz^2} \right) + \frac{\omega^2}{C_0^2} f F \right] \quad (10)$$

Then single cosine functions were taken for $f(x)$ and $F(z)$.

$$f(x) = \cos \frac{n\pi x}{X} \quad F(z) = \cos \frac{\Delta\pi z}{Z} \quad (11)$$

where n and Δ represent the integral number of waves in x and z of the sound speed perturbation which fit in the rigid box. For these functions, U becomes:

$$U(x, z) = \frac{1}{C_0^2} \left[\frac{\omega^2}{C_0^2} - \frac{\pi^2}{2} \left(\frac{n^2}{X^2} + \frac{\Delta^2}{Z^2} \right) \right] \cos \frac{n\pi x}{X} \cos \frac{\Delta\pi z}{Z} \quad (12)$$

Substituting the function U [equation(12)] into equation (8), we find the perturbed eigenvalues:

$$K_{lm}^2 = k_{lm}^2 \left(1 - \epsilon/4C_0^2 \right) \quad (13)$$

or in terms of the eigenfrequencies

$$\Omega_{lm}^2 = \omega_{lm}^2 \left(1 - \epsilon/4C_0^2 \right) \quad (14)$$

However, these equations are only for the special case where $n=2l$ and $\Delta=2m$ simultaneously. Otherwise there is no perturbation of the eigenfrequency. This means that of the infinite set of eigenfrequencies of the rigid acoustic cavity the only oscillation affected will be the particular one whose horizontal and vertical wavenumbers are exactly one half those of the sound speed perturbation.

The eigenfunctions become:

$$\phi_{lm}(x,z) = \psi_{lm}(x,z) + \frac{\epsilon}{2c_0^2 \sqrt{XZ}} \left[\frac{\omega^2}{c_0^2} - \frac{\pi^2}{2} \left(\frac{R^2}{X^2} + \frac{\Delta^2}{Z^2} \right) \right] \cdot \left\{ \frac{\sin(l \pm R) \frac{\pi x}{X} \sin(m \pm \Delta) \frac{\pi z}{Z}}{k_{lm}^2 - k_{(l \pm R)(m \pm \Delta)}^2} \right\} \quad (16)$$

where the term in { } represents the sum of four products obtained by taking all combinations of + and - terms. The subscripts of the k^2 term in the denominator are two integer values where the + and - terms agree with those in the numerator. Here, all the eigenfunctions are perturbed as opposed to the eigenvalues where only one is affected.

VII. ARBITRARY PERTURBATIONS:

When the sound speed perturbation was composed of a single cosine function in each direction, the value of one eigenfrequency was shifted downward in the (k_n, ω) plane. However, an arbitrary sound speed perturbation can be Fourier decomposed into a series of cosine terms in the x and z directions, each of which will shift one particular eigenfrequency.

Let the two dimensional sound speed be:

$$c^2(x,z) = c_0^2 + \epsilon G(x,z) \quad (17)$$

where the perturbation $G(x,z)$ is completely arbitrary, but can be represented by:

$$G(x,z) = \sum_i \sum_j \alpha_{ij} \cos \frac{i\pi x}{X} \cos \frac{j\pi z}{Z} \quad (18)$$

where the α_{ij} are the dimensionless coefficients of the fourier expansion. In this case the $U(x,z)$ term in equation (5) becomes:

$$U(x,z) = \frac{1}{c_0^2} \sum_i \sum_j \left[\frac{\omega^2}{c_0^2} - \frac{\pi^2}{2} \left(\frac{i^2}{X^2} + \frac{j^2}{Z^2} \right) \right] \alpha_{ij} \cos \frac{i\pi x}{X} \cos \frac{j\pi z}{Z} \quad (19)$$

This form of $U(x,z)$ is integrable in equations (6) and (8) and allow the eigenvalues and eigenfunctions to be written in analytical form. The perturbed eigenvalues are:

$$K_{lm}^2 = k_{lm}^2 \left(1 - \frac{\epsilon}{4C_0^2} \alpha_{ij} \right). \quad (20)$$

Thus, the eigenfrequencies are:

$$\Omega_{lm}^2 = \omega_{lm}^2 \left(1 - \frac{\epsilon}{4C_0^2} \alpha_{ij} \right), \quad (21)$$

only for $i=2l$ and $j=2m$. That means that for each coefficient of the Fourier expansion of the arbitrary sound speed perturbation, only one specific eigenfrequency is shifted. Typically there are far more wave modes l, m than components in the perturbation i, j . Therefore, only some of the eigenfrequencies are shifted. It should be possible, therefore to use observed shifts in the (k_n, ω) plane to determine the α_{ij} and then using equation (18) to calculate the form of the inhomogeneity in the sound speed below the visible surface of the sun.

All of the eigenfunctions are perturbed and are given by:

$$\begin{aligned} \phi_{lm}(x, z) = & \psi_{lm}(x, z) + \frac{\epsilon}{2C_0^2 \sqrt{xz}} \sum_i \sum_j \left[\frac{\omega^2}{C_0^2} - \frac{\pi^2}{2} \left(\frac{i^2}{x^2} + \frac{j^2}{z^2} \right) \right] \\ & \cdot \alpha_{ij} \left\{ \frac{\sin(l \pm i) \frac{\pi x}{x} \sin(m \pm j) \frac{\pi z}{z}}{K_{lm}^2 - k_{(l \pm i)(m \pm j)}^2} \right\} \end{aligned} \quad (22)$$

Again, the last term $\{ \}$ in equation (22) represents the sum of four products corresponding to all combinations of $(l \pm i)$ times $(m \pm j)$. The subscripts of k^2 agree with the $()$ in the sine terms.

The perturbations of the eigenfunctions occur at shifted values of the wavenumber. Therefore, when power spectra are taken in order to plot a (k_n, ω) diagram, the original curves are spread out due to the inhomogeneity in the sound speed.

The spreading and shifting of the curves in the observed solar (k_n, ω) diagram could be explained by the presence of inhomogeneities in the convection zone. The technique described above demonstrates the possible effects produced by sound speed variations caused by convective eddies or local magnetic flux concentrations.

The applicability of this tool for probing the depths of the sun is limited, however, by the assumptions made in the analysis. First the undisturbed sound speed was taken to be constant in contrast to a linear variation of c^2 with depth in the solar convection zone. This was done so that an analytical solution could be obtained which would allow the perturbation effects to be studied in detail. Second, the analysis gives perfect resolution of the individual eigenmodes whereas the temporal and spatial resolution of the observations are restricted, and comparisons at this point would be of limited value.

VIII. RECOMMENDATIONS:

The analysis of the sunspot observations has revealed many important results. The relationship between the photospheric umbral velocity and magnetic field oscillations was expected, but never before observed. The analysis of the Fe 6303 magnetic line has proved to be a very sensitive probe of the sunspot umbral photosphere. The fact that there was no correlation between oscillations in Fe 6303 and Ca K (formed in the chromosphere) leads to serious questions about the presumed connection between the driving functions of the two wave modes. These observations give important constraints on any theoretical sunspot model. Improved models must give wave mode eigenfunctions which vary sharply with height. Horizontal structure should be included with the goal of modeling the overtone mode of membrane oscillation observed in the photosphere.

In terms of follow on research, I propose the following:

First, the observations from 21 August, 1980 which were reduced to digital data must be analyzed. This will serve to confirm the results obtained from the 18 August 1980 data. Perhaps further relationships among the oscillations will be determined.

Second, more sunspot observations should be made. The analysis developed has proved to be a powerful technique with promise of new, useful results.

Third, theoretical sunspot models can be improved using these observations and much can be learned about energy transport mechanisms in the presence of intense magnetic fields.

The second aspect of this project was concerned with the effect of inhomogeneities in the sound speed on the trapped nonradial modes of acoustic waves in the solar convection zone. The perturbation technique used in this analysis shows that for a simplified model of the convection zone there is a direct correlation between the shifted eigenfrequencies and the coefficients of the Fourier decomposition of an arbitrary sound speed perturbation. Therefore, observed shifts of the ridges in the solar (k_n, ω) diagram should give an indication of the structure of the convection zone below the visible surface.

Future research should be in the following areas:

First, a good inversion technique needs to be developed to go from the observed shifts in eigenfrequency back to the Fourier coefficients. Theoretical models of the sound speed variation in convective cells or magnetic flux elements could be used to calculate perturbed eigenfrequencies. These could then be used with the inversion technique to return to the original model as a test of the method.

Second, the spreading of the ridges in the observed (k_n, ω) diagram is due in part to lack of observational resolution. Longer time series observations are required (either from space or a polar observing site) to improve the quality of the observed (k_n, ω) diagrams.

Third, the effect of velocities in the convection zone needs to be studied. Convective flows will Doppler shift the acoustic waves which will lead to shifts in the eigenfrequencies. A perturbation analysis similar to the one discussed above might be possible as long as the flow velocities are much smaller than the sound speed.

REFERENCES

1. J.M. Beckers and R.B. Schultz, "Oscillatory Motions in Sunspots," Solar Phys., Vol. 27, pp. 61-70, 1972.
2. A. Bhatnager, W.C. Livingston, and J.W. Harvey, "Observations of Sunspot Umbral Velocity Oscillations," Solar Phys., Vol 27, pp. 80-88, 1972.
3. R.G. Giovanelli, "Oscillations and Waves in a Sunspot," Solar Phys., Vol. 27, pp. 71-79, 1972.
4. R.K. Ulrich, "The Five-Minute Oscillations on the Solar Surface," Astrophys J., Vol 162, pp. 993-1002, 1970.
5. H. Ando and Y. Osaki, "Nonadiabatic Nonradial Oscillations: An Application to the Five-Minute Oscillation of the Sun," Publ. Astron. Soc. Japan, Vol. 27, pp. 581-603, 1975.
6. F.-L. Deubner, "Acoustic Waves and the Geometric Scale in the Solar Atmosphere," Solar Phys., Vol. 40, pp. 333-335, 1975.
7. F.-L. Deubner, R.K. Ulrich, and E.J. Rhodes, "Solar p-Mode Oscillations as a Tracer of Radial Differential Rotation," Astron. Astrophys, Vol. 72, pp. 177-185, 1979.
8. A.H. Nye, L.E. Cram, J.H. Thomas, and J.M. Beckers, "Observations of Dynamical Phenomena in Sunspots," to appear in the Proceedings of Sacramento Peak Observatory Summer Workshop on the Physics of Sunspots, July 14-17, 1981.
9. J. Leibacher and R.F. Stein, "A New Description of the Solar Five-Minute Oscillation," Astrophys. Letters, Vol 7, pp. 191-192, 1971.
10. P.M. Morse and H. Feshbach, "Methods of Theoretical Physics," (McGraw-Hill, New York, 1953) p. 1432.

1981 USAF - SCEEE SUMMER FACULTY RESEARCH PROGRAM

Sponsored by the

AIR FORCE OFFICE OF SCIENTIFIC RESEARCH

Conducted by the

SOUTHEASTERN CENTER FOR ELECTRICAL ENGINEERING EDUCATION

FINAL REPORT

DEVELOPMENT OF A MANUAL OF USE FOR CONJOINT SCALING TECHNIQUES

Prepared by:	Thomas E. Nygren
Academic Rank:	Associate Professor
Department and University:	Department of Psychology Ohio State University
Research Location:	Aerospace Medical Research Laboratory, Human Engineering Division
USAF Research Colleague:	Gary B. Reid
Date:	14 August 1981
Contract No.	F49620-79-C-0038

DEVELOPMENT OF A MANUAL OF USE FOR

CONJOINT SCALING TECHNIQUES

by

Thomas E. Nygren

ABSTRACT

Conjoint measurement methodology offers a new and potentially useful approach for obtaining psychological scale values for components of multi-dimensional attributes. An investigation of this methodology and its mathematical foundations was conducted. Six computer based algorithms that can be used to perform specific kinds of conjoint analyses were generalized and documented for wider application as subjective assessment techniques. Following a discussion of the mathematical foundations, the six programs (CONJOINT, PCJM2, NONMETRG, MONANOVA, DISTRIB, and DUALDIST) are each summarized with respect to their function as conjoint analysis techniques. Shortcomings of the current state of lack of systematic research efforts dealing with methodological and statistical issues in conjoint analysis are discussed. Suggestions for further research are then presented.

Acknowledgement

The author would like to thank the Air Force Office of Scientific Research for making it possible for him to spend a productive summer at the Human Engineering Branch of the Aerospace Medical Research Laboratory, Wright-Patterson AFB, Ohio. In particular, collaboration with Col. Robert O'Donnell, Dr. Gary Reid, and Dr. Clark Shingledecker on this project was essential to its success. I would like to thank each of them for their help throughout the planning and execution of the project.

I. INTRODUCTION

Subjective scaling techniques are an integral part of much of social science research. In many situations it is assumed that the variable of interest is a complex phenomenon that is multidimensional in nature. That is, it is recognized that the ordering of scores produced by an individual on this variable may be based on the joint effects of two or more independent variables. The multidimensionality of the phenomenon, of itself, poses no real problem to the research since, in many cases, standard statistical procedures like analysis of variance or multiple regression techniques may be used. These procedures, however, are primarily used to assess the predictive ability of the independent variables rather than to estimate psychological scale values.

Often the researcher may be interested in one or both of the following more basic issues. First, can the composition rule by which the independent variables combine to produce the joint effect on the dependent variable be established empirically? In addition, it may not be possible to obtain initial measurements for the independent variables themselves, but only for their resultant joint effects. Secondly, then, can the independent and dependent variables be scaled simultaneously according to some specified composition rule in a way that preserves the order of the joint effects in the data? This question, as Tversky¹ points out in his 1967 paper, is the conjoint measurement problem, and the composition rule is the conjoint measurement model.

There are, of course, many composition rules that might be hypothesized. The simplest such rule is an additive one which suggests that the independent variables combine in an independent additive fashion to produce the joint effect. For example, let a_1 be a level of factor A_1 , a_2 be a level of factor A_2 , and a_3 be a level of factor A_3 . We might hypothesize that the joint effects of these three factors could be described as

$$f(a_1, a_2, a_3) = f_1(a_1) + f_2(a_2) + f_3(a_3) \quad (1)$$

where f , f_1 , f_2 , and f_3 are separate and identifiable numerical functions. Additive models like the three-factor model illustrated in Equation 1 have been and continue to be an integral part of many important

psychological theories. Until recently, however, even for this simple model, there has not been a satisfactory means by which one could simultaneously estimate all four functions f , f_1 , f_2 , and f_3 . Conjoint measurement theory provides a means to do this and herein lies its power. Just as important, however, is the result of the theory (to be described below) which indicates that only ordinal relations are required among the data points in order to produce resultant scales unique up to an affine transformation. The implications of this result will become more apparent following the presentation of an illustrative application and the basic theory of conjoint measurement.

The present project grew out of two separate interests in conjoint measurement theory. The first is an interest in the basic mathematical foundations and extensions of the theory as it presently exists as a theory of measurement. The second area of interest is associated with using this new methodology in a substantive area of psychology where it might make a significant contribution to both psychological theory and research methodology. The modeling of mental workload is one such area. For example, obtaining subjective estimates of mental workload for Air Force pilots seems critical if we hope to obtain the best design of an aircraft system for optimal man-machine interaction. Workload is a variable that seems particularly well-suited for a conjoint measurement approach because of its multidimensional nature.

Previous research by Reid, Shingledecker, and Eggemeier² and others^{3,4} indicates that three factors appear to affect perceived workload. These are the time load, the mental effort load, and the psychological stress load associated with performing the task. All three of these factors are difficult to measure independently, yet their joint effects produce workload situations that can be reliably and meaningfully compared. One might, of course, use count variables or physical variables as measures of time, effort, and stress and then use standard statistical procedures to combine their effects. This is often a useful practice in psychological research. It may, however, as Krantz⁵ has suggested, be a pointless effort in some cases to rely solely on these count or physical variables as operational definitions of a psychological variable. All that one may have when he/she is done, is merely another measure of the physical or

count variable. One hopes that this measure is highly correlated with the psychological variable of interest, although there is no guarantee that it will be. In this case, little may have been accomplished, since new measurement has not actually been obtained for the variable. In the case of workload, for example, it might be much more productive in terms of enhancing the theory, to use a methodology like conjoint measurement which could lead to the establishment of the empirical laws and a new measurement structure for workload that more simply and accurately describes the concept. A conjoint measurement approach would not force one to operationally define the time, effort, and stress variables a priori. Rather, it may be possible to scale each of these variables along with their joint effects simultaneously.

II. OBJECTIVES

This project had three distinct objectives. The first of these was to extensively survey the conjoint measurement literature in an attempt to find the scaling procedures that appear most promising as subjective scaling techniques in substantive areas like the study of workload as described above. Due to time constraints for the project, the survey was limited to the most widely used conjoint techniques, those employing simple polynomial models like the additive model illustrated in Equation 1.

The second objective was to take the scaling techniques written in the form of complex computer programs and generalize them so that they may be used in a wider range of potential applications. In recent years, there have been a number of significant advancements in conjoint measurement methodology. Advancements in applied research using this methodology have not kept pace largely because the computer programs that do the conjoint scaling have not been compared or examined in sufficient detail to establish meaningful generalizations about their properties as scaling techniques. Meeting the second objective would make such comparisons possible.

The final objective was somewhat related to the second in that in addition to a lack of generalizations about the scaling techniques to aid applied researchers, there is also a lack of documentation for many of these programs. There is no single detailed reference that critically

analyzes and adequately describes conjoint measurement methodology, nor is there any adequate "users' guide" for researchers who desire to use these scaling techniques. The third objective was to begin to remedy the documentation problem by initiating the development of a "manual of use" for some of the currently available conjoint scaling and testing computer programs.

III. FOUNDATIONS OF CONJOINT MEASUREMENT

Prior to an introduction to the mathematical foundations of conjoint measurement it might be useful to review two terms that are generally differentiated in the literature. First, we define conjoint measurement as the procedure whereby we specify for a given combination rule, the conditions under which there exist measurement scales for the dependent and independent variables, such that the order of the joint effects of the independent variables in the data are preserved by the numerical composition rule. We then define conjoint analysis (sometimes referred to as numerical conjoint measurement) as the procedure whereby the actual numerical scale values for the joint effects and the levels of the independent variables are obtained. Thus, there are effectively two separate and independent processes in the conjoint measurement methodology. First, one attempts to find the appropriate combination rule and then, assuming the rule is valid, finds numerical functions that "best" fit the order of the joint effects in the data according to the specified rule.

Although the mathematical foundations of conjoint measurement theory have been established for some time, it was not until Luce and Tukey⁶, Krantz⁷, and Tversky¹ established the sufficient conditions for additive and polynomial conjoint measurement, that interest in the measurement technique began to increase. Luce and Tukey restricted their initial discussion to establishing the sufficient conditions for additive conjoint measurement in two factors. In their discussion of the foundations of additive conjoint measurement, Luce and Tukey showed that given:

- (1) the set $A = A_1 \times A_2$, where A_1 and A_2 are non-empty sets,
- (2) a binary relation λ on $A_1 \times A_2$ (where " λ " might be a relation like "is preferred to", "is larger than", "is greater in workload than", etc.), and

(3) if $\langle \Lambda_1, \Lambda_2, \succ \rangle$ is an empirical relational system that satisfies the axiom structure of a weak order (i.e., \succ is connected and transitive), solvability, cancellation, and the Archimidean property, then,

THEOREM: There exist real-valued functions ϕ on A , ϕ_1 on A_1 , and ϕ_2 on A_2 such that for all (a_1, a_2) and (b_1, b_2) in A

- (i) $(a_1, a_2) \succ (b_1, b_2)$ if $\phi(a_1, a_2) \succ \phi(b_1, b_2)$,
- (ii) $\phi(a_1, a_2) = \phi_1(a_1) + \phi_2(a_2)$,
- (iii) if ϕ' , ϕ'_1 , and ϕ'_2 are any other functions which satisfy (i) and (ii) above, then there exist real numbers $\alpha > 0$, β_1 , and β_2 such that $\phi'_1 = \alpha\phi_1 + \beta_1$, $\phi'_2 = \alpha\phi_2 + \beta_2$, and $\phi' = \alpha\phi + \beta_1 + \beta_2$.

It is important to recognize the power inherent in this theorem. Given four simple axioms that require only ordinal properties in the data for the binary relation \succ , we arrive at a theorem which guarantees the existence of functions ϕ , ϕ_1 , and ϕ_2 such that numerical scale values can be assigned to the stimulus objects in such a way that (1) the order among objects is preserved, (2) the levels of the factors on which the stimuli vary combine in an independent and additive fashion, and (3) the numerical scales have interval properties. Note that in (iii) above one is free to set the zero point of each scale, but the same unit value is applied to both ϕ_1 and ϕ_2 . It will be shown later how some mathematical psychologists have developed procedures for actually constructing the scales ϕ , ϕ_1 , and ϕ_2 on the basis of only the ordinal relationships among the stimuli in the data set.

We now proceed with a discussion of the three-factor simple polynomial models that were the foci of this research project. There are four simple models that we investigated. They are the familiar additive model, the multiplicative model, the distributive model, and the dual-distribution model. These can be presented in our ϕ notation as:

$$\phi(a_1, a_2, a_3) = \phi_1(a_1) + \phi_2(a_2) + \phi_3(a_3) \quad (2)$$

for the additive model,

$$\phi(a_1, a_2, a_3) = \phi_1(a_1) \cdot \phi_2(a_2) \cdot \phi_3(a_3) \quad (3)$$

for the multiplicative model,

$$\phi(a_1, a_2, a_3) = \phi_1(a_1) \cdot [\phi_2(a_2) + \phi_3(a_3)] \quad (4)$$

for the distributive model, and

$$\phi(a_1, a_2, a_3) = \phi_1(a_1) + [\phi_2(a_2) \cdot \phi_3(a_3)] \quad (5)$$

for the dual-distributive model.

Krantz and Tversky have previously discussed a number of ordinal properties that are necessary though not sufficient for these four models to hold. Several will be briefly summarized and illustrated here. The intent of this summary is not to present an axiomatization for each of the four models in Equations 2 - 5, but rather to describe a set of ordinal properties that may be used as diagnostic tools in differentiating among the four models as viable composition rules. It is implicit throughout this discussion that the common empirical situation with the scale values of the levels of the factors all being positive is assumed.

We begin with the fundamental property of independence which can be checked separately for each of the three factors. We say that

$$\begin{aligned} &A_1 \text{ is independent of } A_2 \text{ and } A_3 \text{ whenever} \\ &(a_1, a_2, a_3) \succsim (b_1, a_2, a_3) \text{ if and only if} \\ &(a_1, b_2, b_3) \succsim (b_1, b_2, b_3). \end{aligned} \quad (6)$$

Thus independence of A_1 asserts that if $a_1 \succsim b_1$ for some combination of levels of factors A_2 and A_3 , then this relation will hold for any other combination of levels of A_2 and A_3 . This property is clearly necessary for an additive model, as well as each of the other three models in Equations 3 - 5.

A second form of independence can also be examined in our three-factor models. The property, known as joint independence, states that

$$\begin{aligned} &A_1 \text{ and } A_2 \text{ are jointly independent of } A_3 \text{ whenever} \\ &(a_1, a_2, a_3) \succ (b_1, b_2, a_3) \text{ if and only if} \\ &(a_1, a_2, b_3) \succ (b_1, b_2, b_3). \end{aligned} \quad (7)$$

Joint independence of A_1 and A_2 with respect to A_3 indicates that if one combination of A_1 and A_2 is greater than another at a fixed level of A_3 , (i.e., $(a_1, a_2) > (b_1, b_2)$ at a_3), then the ordering should be preserved for any other level of the third factor (b_3). It is important to recognize that if joint independence holds for all pairs of factors, then this implies that independence holds for a single factor. However, if simple independence holds for all factors, this does not imply that joint independence will be satisfied for all pairs of factors.

We can, of course, state two other forms to the joint independence property for A_1 and A_3 of A_2 , and A_2 and A_1 of A_3 . If we again restrict our scale values for all factors to be positive, then it is clear that joint independence must hold in all three forms for the additive and multiplicative models. However, for the distributive model of the form $A_1 \cdot [A_2 + A_3]$ only A_2 and A_3 must be jointly independent of A_1 .

The third property is one that has already been discussed with respect to the Luce-Tukey axiomatization for the two-factor additive model. This is the property usually referred to as double cancellation or Luce-Tukey cancellation and is stated for factors A_1 and A_2 as

$$\begin{aligned} &\text{If } (a_1, b_2, a_3) \succ (b_1, c_2, a_3) \text{ and} \\ &(b_1, a_2, a_3) \succ (c_1, b_2, a_3) \text{ then,} \\ &(a_1, a_2, a_3) \succ (c_1, c_2, a_3). \end{aligned} \quad (8)$$

Note that double cancellation requires at least three levels of each of factors A_1 and A_2 , and deals with only two such factors at a time. Hence, it must be satisfied in Equations 2 - 5 when the scale values are all positive.

Up to this point there has not been presented a means of distinguishing between the distributive and dual-distributive models. The final two

properties attempt to do this. We first describe a property known as distributive cancellation.

Distributive cancellation is satisfied if and only if whenever

$$\begin{aligned} (a_1, b_2, a_3) &\sim (d_1, c_2, c_3), \\ (b_1, a_2, a_3) &\sim (c_1, d_2, c_3), \text{ and} \\ (d_1, d_2, c_3) &\sim (b_1, b_2, a_3), \text{ then} \\ (a_1, a_2, a_3) &\sim (c_1, c_2, c_3). \end{aligned} \tag{9}$$

It can be shown that this property is a necessary condition for the distributive model to hold. However, distributive cancellation also holds in an additive representation. Hence, it is important to note that while the property can be used to support a distributive representation, it cannot be used to reject additivity. It is not necessary for a dual-distributive representation, however, and can be used as a means to differentiate between these two models.

The final property to be discussed for our three-factor models is dual-distributive cancellation. Formally, we say that

$$\begin{aligned} \text{dual-distributive cancellation is satisfied if and only if} \\ (a_1, c_2, c_3) &\sim (c_1, d_2, b_3), \quad (a_1, e_2, e_3) \sim (d_1, b_2, e_3), \\ (d_1, a_2, a_3) &\sim (b_1, e_2, d_3), \\ (d_1, c_2, d_3) &\sim (e_1, d_2, a_3), \text{ and} \\ (c_1, e_2, e_3) &\sim (e_1, b_2, c_3), \text{ then} \\ (a_1, a_2, b_3) &\sim (b_1, b_2, c_3). \end{aligned} \tag{10}$$

Dual-distributive cancellation is comparable to distributive cancellation in that it is necessary for both a dual-distributive and additive representation. Hence, again it cannot be used to reject additivity. Since it is not necessary for a distributive representation, however, it can be used as a means of possibly distinguishing between a distributive and dual-distributive model. Note, however, that this property is extremely complex. It requires that five antecedent conditions from a 5x5x5 design be met in order for a test to even be possible. Hence, this property

suffers from being empirically very difficult to evaluate because of the size of the design that is required and because of the reduced likelihood of obtaining tests that meet all five antecedent conditions in the data.

Given this set of conditions it should be possible to evaluate each of the four polynomial models in Equations 2 - 5 for a set of observations obtained from a factorial design. In each of the axiom conditions only ordinal information is required in order to adequately test these properties. Thus it is sufficient to require each subject to merely present rank-order estimates to each of the stimulus combinations generated by combining levels of the factors. As was discussed earlier, in most applications of conjoint measurement methodology it is the additive representation with restriction to the positive case that is of interest. However, even for an additive model as small as $3 \times 3 \times 3$, both the testing procedures for the properties mentioned above and the actual scaling procedure for obtaining the numerical scale values become extremely impractical without the aid of a computer-based algorithm. In the next sections we will discuss several of the computer programs that were documented and generalized during this project.

IV. AXIOM TESTING PROGRAMS

In order to enhance the use of conjoint scaling techniques as useful methodological tools, six computer programs were generalized and documented for applied research situations. A brief description of each of the documented programs and their potential applications will now follow. We begin with two programs, CONJOINT (CONJOINT measurement property testing) and PCJM2 (Polynomial Conjoint Measurement, version 2), which were designed to help differentiate between the models in Equations 2 - 5.

The first attempt to develop a general diagnostic program for testing the conjoint measurement axioms was made by Holt and Wallsten⁸. Their program, CONJOINT, was designed to test each of the axioms mentioned above except dual-distributive cancellation. Later, Ullrich and Cummins⁹ developed a program, PCJM2, to do essentially the same thing as CONJOINT. There are, however, several differences between the programs which make both useful as diagnostic tools.

Both CONJOINT and PCJM2 allow one to test for independence among the factors, although the approach taken by each is somewhat different. CONJOINT tests for independence of factors by considering them two at a time. Independence for A_1 of A_2 would be checked by comparing the rank order of the cells for the levels of A_1 at each level of A_2 . Similarly, a check can be made for the independence of A_2 at each level of A_1 . A Kendall's Coefficient of Concordance (W) is computed in each case to check for independence. Thus, if independence is satisfied, then the rows (columns) should all be in the same rank order, yielding W values equal to 1.0. PCJM2 takes a different approach. This program actually searches for all possible tests of independence and counts the number of violations of the axiom. In addition, PCJM2 will show which cells have contributed to the total number of violations of the axiom.

Comparable procedures to those described above are used to test for joint independence of a pair of factors from the third (e.g., $A_1 \times A_2$ of A_3). As with independence, CONJOINT computes the W values; whereas PCJM2 actually computes the number of violations of the axioms and the cells involved in violations. One additional feature of CONJOINT not found in PCJM2 is that a check for sign dependence and joint sign dependence can also be made.

For the remaining factors the two programs are essentially identical. Both programs count the number of violations of double cancellation and distributive cancellation with each factor as the outside factor. Both will also show, if desired, which data cells were involved in violations. PCJM2 will also check for dual-distributive cancellation. However, since a $5 \times 5 \times 5$ design is necessary to test the axiom, this feature has limited practicality.

The remaining four programs examined in this project were nonmetric conjoint scaling techniques designed to fit a given data structure to either an additive, distributive or dual-distributive model. Since an additive model can be obtained from a multiplicative model by taking logarithms, these two models are essentially indistinguishable from a scaling standpoint. Hence, when we speak of an additive model we are allowing for the possibility of a multiplicative model as well, if we restrict the levels of our factors to the positive case. The four programs

to be discussed are NONMETRG¹⁰ (NON-METric ReGression), MONANOVA¹¹ (MONotonic Analysis of VARIance), DISTRIB¹² (DISTRIButive model testing), and DUALDIST¹³ (DUAL-DISTRibutive model testing).

Both NONMETRG and MONANOVA are used to fit data to an additive model via a nonmetric scaling procedure. Although the mechanism is not the same in each case, the goal is. In MONANOVA, a monotonic transformation of the data is found which will lead to estimates of the scale values for levels of the factors. These scale values are such that when they are combined via an additive composition rule, their joint effects "best" fit the original data. Just how the scaling is done will now be sketched. First, a random or initial configuration (i.e., an initial set of scale values for the levels of the factors) is generated or read by the program. After this configuration is suitably normalized, a set of "distances", d_j , can be calculated based on the additive rule. The program next uses a monotone regression subroutine written by Kruskal¹¹ to create "disparities", \hat{d}_j , which are "modified" distances subject to the constraint that they are monotonically ordered in the same way as their corresponding raw data values. Thus only the rank orders of the original data are used, not the data values themselves. To estimate how well the model is fitting the data, a goodness-of-fit measure called STRESS is computed. STRESS is the sum of squared discrepancies between the d_j and the \hat{d}_j normalized as shown in Equation 11 below.

$$S = \sqrt{\frac{\sum_{j=1}^n (d_j - \hat{d}_j)^2}{\sum_{j=1}^n (d_j - \bar{d})^2}} \quad (11)$$

where n is the number of stimuli and \bar{d} is the mean distance value. If the model were to fit the data perfectly, then the d_j and \hat{d}_j values would be identical and STRESS would be zero. The higher the STRESS value, the poorer the fit of the model to the data. Since a random configuration will usually yield a high STRESS value, a mechanism is needed to find a configuration that will produce a minimal value of this goodness-of-fit

measure. Kruskal¹¹ proposed in his nonmetric procedure that the method of gradients or steepest descent be used to find the configuration that will minimize STRESS. Based on this mathematical procedure, the MONANOVA program calculates new d_j that will reduce the STRESS. The program proceeds in an iterative fashion to do this until either a maximum number of iterations has been used or no significant improvement in fit can be obtained. Following the termination of the last iteration, the final configuration coordinates (i.e., the scale values of the levels of the factors) are printed as well as a history of the iterative procedure. From the coordinates the estimated scale values of joint effects of the factors are then produced according to the additive model.

NONMETRG, although it is a nonmetric procedure, does not directly attempt to find a monotonic transformation. The iterative procedure here is a one-step pairwise method. An initial random configuration of points is generated just as with MONANOVA, and distances are then computed according to the additive rule. The data are then ranked, and for every pair of stimuli (i.e., factor combinations) the difference in their ranks, $r_i - r_j$, in the data is compared with the difference in the corresponding distance values generated from the initial configuration, $d_i - d_j$. If these two differences are of the same sign, the distances are in the right order. If not, the order in the distance is incorrect. The iterative procedure in this program, then, is based on an attempt to change the configuration of points so as to reduce the number of discrepancies as illustrated above. This suggests a measure of goodness-of-fit different from STRESS. Johnson¹⁰, in his development of the NONMETRG procedure defined the measure as THETA, where,

$$\theta = \sqrt{\frac{\sum_{i < j} a_{ij} (d_i - d_j)^2}{\sum_{i < j} (d_i - d_j)^2}} \quad (12)$$

where $a_{ij} = +1$ if $\text{sign}(d_i - d_j) = \text{sign}(r_i - r_j)$. Thus THETA would be zero only if the pairwise order of the distances from the configuration and the ranks in the data are the same across all pairs of stimuli.

Johnson derived the numerical analysis procedure necessary to minimize THETA by finding the gradient for the partial derivatives of THETA with respect to W, (the stimulus configuration). On each iteration the gradient determines to what extent W will be modified in order to obtain a better THETA value. As with MONANOVA the iterative procedure is stopped either when the maximum number of iterations is reached or no significant improvement in THETA can be obtained.

Upon completion of the last iteration, NONMETRG will print the history of the iterative procedure, the final THETA value, and a Kendall's Tau value indicating the rank order correlation between the original data and the final additive scale values for the stimuli. The configuration of levels of the factors and the values of all of the additive combinations of these levels are then printed or punched.

The final two programs included in this project were DISTRIB and DUALDIST. These two programs attempt to fit a set of data from a factorial design to a distributive model or dual-distributive model respectively. Both programs were developed by Emery^{12,13} as very simple extensions of Kruskal's MONANOVA program described above. In fact, both programs are essentially identical in form and in the iterative procedure to MONANOVA except that the additive model is replaced by a distributive or dual-distributive model. All input parameters and printed output are comparable to MONANOVA. One feature that has been added to both models by Nygren¹⁴ is that the program can test all three forms of the models in one analysis. For example, for the distributive model all of the forms $A(B+C)$, $B(A+C)$, and $C(A+B)$ can be checked in each set of data.

V. RECOMMENDATIONS

Subjective assessment techniques for scaling the joint effects of several psychological variables have been of interest to social and behavioral scientists for many years. In practice, however, the scaling has been applied to a limited range of interesting situations for several reasons. First, the theoretical foundations of some procedures (e.g., regression analysis) make strong assumptions about distributions or level of measurement for the response scale. Second, some procedures were developed as unidimensional scaling techniques. Hence, their value

as investigative tools in the construction of scales for interesting multidimensional attributes are minimal. Third, a number of procedures become very difficult or impractical to administer for even moderate-size stimulus sets. Finally, and perhaps most importantly, the model that is being fit is usually limited to being a linear combination of the independent variables.

Conjoint measurement theory as proposed initially by Luce and Tukey and generalized by Krantz and Tversky offers one means of greatly extending subjective scaling applications to situations where the dependent variable or response measure is assumed to be multidimensional in nature. In addition, necessary conditions for diagnosing some of the interesting models have been developed. These conditions allow for validating the additive, distributive or dual-distributive models based on only the ordinal properties inherent in the data. Once the necessary axioms for a given model have been met in the data, it is possible to use one of the four iterative scaling programs described above to obtain the scaling solution.

It is important to emphasize that each of these scaling procedures are nonmetric. This requirement that the data need only be ordinal is of great theoretical and practical importance. Perhaps the greatest advantage of the nonmetric scaling techniques over many other procedures is that interval-scaled stimulus values can be obtained from this ordinal input. In practical terms this reduces the subject's task considerably, increases the ease with which the data can be collected, and expands the possibilities for ways in which similar data structures can be obtained and compared.

Despite these advantages to conjoint measurement methodology, interesting applications in the psychological literature have been few. This is primarily due to a concern stated earlier which became an objective of the present research. Systematic research on and documentation of the six conjoint scaling programs cited above and related techniques has lagged far behind theoretical developments. The manual of use, CPSCAL¹⁴, which has been developed during this project will begin to establish the necessary documentation of the programs. However, further research efforts are needed to enhance the usefulness of this technique.

There are several areas in which I propose to continue this research effort. First, the axiom testing programs CONJOINT and PCJM2, while clearly necessary for a systematic research effort aimed at analysis of the simple polynomial models in Equations 2 - 5 as possible descriptive models of subjective judgment, are not foolproof procedures. That is, they cannot distinguish among possible models which might fit a set of data 100% of the time. Indeed, their discriminability has never been systematically evaluated except in situations where unrealistic error-free data sets have been generated.

Further research in this area of axiom testing would entail two related directions. One endeavor would be to appropriately test the power of the axioms for discriminating among the models under different conditions. That is, it may be possible to determine such things as the optimal number of levels to include in an experimental design when a certain model is expected or the minimal number of replications of a judgment needed to establish reliable estimates of the rank order among the cells. This research would have both theoretical and practical implications. The other related direction of research in this area would be to attempt to develop other ordinal properties or variations of the existing properties which might prove to be better (i.e., more powerful) diagnostic tools in applied research.

A second area of continued research would entail the expansion of conjoint measurement methodology beyond simple three-factor models. This might entail examining two or three-factor models that include potential interaction effects among the factors or the examination of four-factor models and their associated properties. Both of these developments would have potential for expanding the applicability of conjoint measurement methodology as a subjective assessment technique.

REFERENCES

1. A. Tversky, "A General Theory of Polynomial Conjoint Measurement," Journal of Mathematical Psychology, Vol. 4, pp.1-20, 1967.
2. G. B. Reid, C. A. Shingledecker, and F. T. Eggemeier, "Application of Conjoint Measurement to Workload Scale Development," Human Factors Society Annual Proceedings, 25th Annual Meeting, Rochester, N. Y., 1981.
3. G. B. Reid, C. A. Shingledecker, T. E. Nygren, and F. T. Eggemeier, "The Development of Multidimensional Subjective Measures of Workload," Proceedings of the 1981 International Conference on Cybernetics and Society, October, 1981.
4. N. Moray, Mental Workload: Its Theory and Measurement, (Plenum Press, New York, 1979).
5. D. H. Krantz, "Measurement Structures and Psychological Laws," Technical Report MMPP 71-2, University of Michigan, Michigan Mathematical Psychology Program, 1971.
6. R. D. Luce and J. W. Tukey, "Simultaneous Conjoint Measurement: A New Type of Fundamental Measurement," Journal of Mathematical Psychology, Vol. 1, pp. 1-27, 1964.
7. D. H. Krantz, "Conjoint Measurement: The Luce-Tukey Axiomatization and Some Extensions," Journal of Mathematical Psychology, Vol. 1, pp. 248-277, 1964.
8. J. O. Holt and T. S. Wallsten, "A User's Manual for CONJOINT: A Computer Program for Evaluating Certain Conjoint-Measurement Axioms," Technical Report No. 42, University of North Carolina, L. L. Thurstone Psychometric Laboratory, October, 1974.
9. J. R. Ullrich and D. E. Cumming, "PCJM: A Program for Conjoint Measurement Analysis of Polynomial Composition Rules," Behavioral Science, Vol. 18, pp. 226-227, 1973.
10. R. N. Johnson, "Pairwise Nonmetric Multidimensional Scaling," Psychometrika, Vol. 38, pp. 11-18, 1973.
11. J. B. Kruskal, "Analysis of Factorial Experiments by Estimating Monotone Transformations of the Data," Journal of the Royal Statistical Society, Series B, Vol. 27, pp. 251-263, 1965.
12. D. R. Emery, "DIST: A Numerical Conjoint Measurement Program Designed to Scale Data to a Distributive Model in Three Dimensions," Journal of Marketing Research, Vol. 14, pp. 413-414, 1977.

13. D. R. Emery, "DULDST: A Numerical Conjoint Measurement Program Designed to Scale to a Dual-Distributive Model in Three Dimensions," Journal of Marketing Research, Vol. 14, pp. 558-559, 1977.
14. T. E. Nygren, "CPSCAL: An Introduction to Conjoint Measurement Methodology," unpublished manuscript, Ohio State University, 1981.

1981 USAF - SCEEE SUMMER FACULTY RESEARCH PROGRAM

Sponsored by the

AIR FORCE OFFICE OF SCIENTIFIC RESEARCH

Conducted by the

SOUTHEASTERN CENTER FOR ELECTRICAL ENGINEERING EDUCATION

FINAL REPORT

EVALUATION OF NASTRAN TO PREDICT THE DYNAMIC RESPONSE
OF REINFORCED CONCRETE

Prepared by: Dr. William W. Payne, Jr.

Academic Rank: Associate Professor

Department and University: Department of Civil Engineering
University of Alabama in Huntsville

Research Location: Air Force Engineering and Services Center
Engineering Research Division
Tyndall AFB, FL 32403

USAF Research Colleague: Capt Paul L. Rosengren, Jr.

Date: August 5, 1981

Contract No: F49620-79-C-0038

EVALUATION OF NASTRAN TO PREDICT THE DYNAMIC
RESPONSE OF REINFORCED CONCRETE

By

William W. Payne, Jr.

ABSTRACT

This report evaluates the ability of the finite element program NASTRAN to analyze reinforced concrete structures under dynamic loads. Experimental data from a quarter scale model test of an underground shelter was used to validate the computer projections.

NASTRAN is a general purpose structural analysis program containing several types of finite elements and several displacement analysis approaches. For this study five different computer models of reinforced concrete were used. The models were composed of the following elements:

1. Plate membrane elements.
2. Plate membrane and rod elements.
3. Plate bending elements.
4. Plate bending-membrane elements.
5. Plate bending-membrane and beam elements.

Static Analysis and Transient Analysis Approaches were used to evaluate the computer model.

Favorable results were obtained for the plate membrane and rod element model using the Transient Analysis Approach. Strain in the reinforcing rods, time to maximum strain, and time to return to zero strain were used to compare the experimental data to the computer predictions.

ACKNOWLEDGEMENTS

The author would like to express his appreciation to the Air Force Engineering and Services Center, the Engineering Research Division, Airbase Survivability Branch, and the Southeastern Center for Electrical Engineering Education for the opportunity to participate in the 1981 Summer Faculty Research Program. He would like to acknowledge the personnel of the Airbase Survivability Branch for their hospitality to him and his family, and the excellent working conditions the branch members provided.

He would like to thank Capt Paul Rosengren for suggesting this area of research and for his advice and his assistance. Also he would like to acknowledge the help of Maj Steve Hawn, Mr. Walt Buchholtz, and Mr. Ricky Griner. A special thanks goes to Mr. David R. Coltharp, Structural Mechanics Division, Waterways Experiment Station, for performing the scale model testing and supplying the experimental results.

I. INTRODUCTION

The United States Air Force is investigating ways of predicting the response of reinforced concrete in hardened structures due to blast (dynamic) loads. The dynamic loads are caused by the nearby explosion of conventional (non-nuclear) weapons. Current generation hardened structures are reinforced concrete construction, covered with layer(s) of soil, rock rubble, and/or a burster slab. The structures have boxy shapes with heavily reinforced concrete walls, floors, and roofs.

The Air Force hopes to reduce the costs of construction by improving the analysis and design techniques. Substantial savings can be made by reducing the amount of steel required in the shelters.

Present design and analysis procedures use "limit state" theory to determine the ultimate strength of the structure and idealize the structure as a single degree of freedom system to predict the required resistance. These assumptions neglect the interaction between the structural components such as between the roof and the supporting walls. Finite element techniques offer the best means of modeling the structural interaction between components and predicting the capacity of each component.

Commonly available structural analysis programs are not strictly applicable to this problem. Most programs do not contain nonlinear material behavior and provisions for soil elements, concrete-soil interaction, or steel-concrete interaction. The few programs that address these areas are designed for nuclear weapons where the loading has a long duration shock front. Conventional weapons have a short duration pressure wave that decreases rapidly with distance from the detonation.¹

Many investigations are being conducted attempting to accurately model reinforced concrete for use in finite element programs. Investigators are developing models of the concrete that will exhibit the nonlinear stress-strain behavior and the low tensile strength that result in cracking and loss

of stiffness in the reinforced concrete. More sophisticated models are including strain-rate effects and load histories so that repeated detonations can be modeled.⁵ Present design criteria for hardened structures does not call for repeated explosions due to conventional weapons.

Besides the modeling problems of concrete, the interaction between the reinforcing steel and concrete is not completely understood. An accurate reinforced concrete element must model the bond stress and friction from interlocking between the deformed reinforcing bars and the concrete.

Until a complete reinforced concrete model is developed, analysis techniques will be able to predict failure mechanisms related to the response of the complete structure only. For those explosions where the structure can respond as a unit, developing bending and membrane forces, finite element methods can model the response with sufficient accuracy. Structural response where the pressures are high enough to cause failure of a localized area can not be modeled.¹

11. OBJECTIVES

The main objective of this project was to determine if the finite element program NASTRAN is a useful tool in modeling the response of hardened reinforced concrete structures. The accuracy of the finite element model was of primary importance and results from tests on a quarter scale model of an underground structure were used to evaluate the computer predictions. The utility of the program was also judged on the usefulness of the output and the ease of input.

A secondary objective was to develop an understanding of the full capabilities of NASTRAN and to relate them to the problems associated with modeling reinforced concrete. This would allow identification of areas in NASTRAN that could be changed in order to improve its ability to model reinforced concrete.

III. FINITE ELEMENT MODELS AND RESULTS

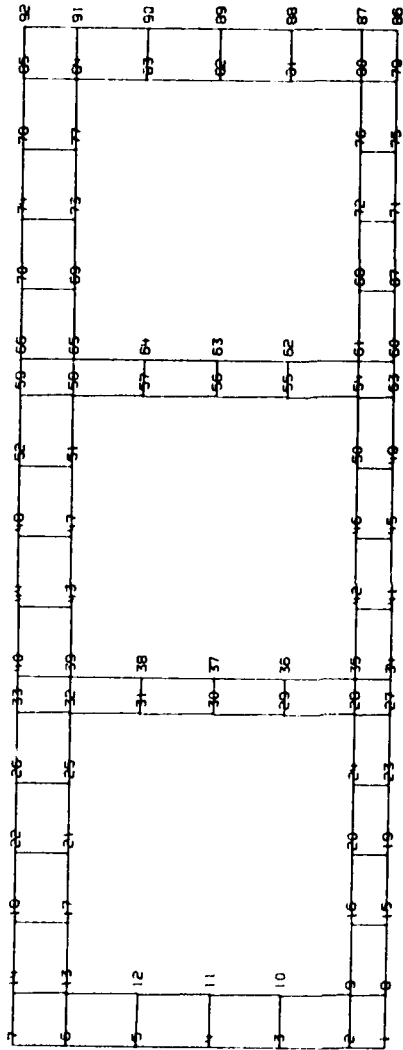
Introduction

NASTRAN (NASA STRuctural ANalysis) was developed to aid in the linear analysis of structures for the loading conditions associated with flight. Different static and dynamic analysis approaches are available and limited nonlinear capability is included. Nonlinear behavior may arise from changes in geometric shape or material properties.

To evaluate NASTRAN different finite element models of a quarter scale underground shelter were constructed and used in different static and dynamic analysis approaches. The finite element models were representative of the element types available in NASTRAN and were not intended to be sophisticated models of reinforced concrete, since an accurate reinforced concrete element does not exist. The models used were a combination of rod and plate elements in which the rods represented the reinforcing steel and the plates represented the concrete and a plate element alone that modeled both the steel and concrete.

The models were used in different analysis approaches and the predictions compared to the recorded data from the actual test. The computer projections were output in numerical and graphical form and the usefulness of the output evaluated. Because of the limited experimental data, the model predictions for maximum strain at specific locations of reinforcing steel, time to that maximum strain, and time to return to zero strain were used to judge the accuracy of the model.

The points used for evaluation were located on the top layer of reinforcing steel at the middle of the roof span and at the face of the interior wall (see Figure 7). The gage points are denoted by ET4 and ET5 for Test 1 and by ET2 and ET3 for Test 2. These points had the best experimental records for both Test 1 and Test 2.



STATIC ANALYSIS MEMBRANE ELEMENTS
LINEAR CONCRETE MATERIAL, GROSS SECTION PROPERTIES
UNDEFORMED SHAPE

Figure 1
Undeformed Shape for Membrane and Membrane-Rod Finite Element Model

A better measure of the accuracy of the model would have been deflections rather than strains. However, deflection data was unavailable. For the model composed of plates only, strain output from NASTRAN was not possible and some bias was introduced when converting deflections to strain.

The finite element models were used in two displacement analysis approaches, static and transient. The static approach used the static "equivalent" uniform loads provided in Reference 4. No mass effects are considered in static analysis. This analysis was used to develop a resistance-deflection function for each finite element model.

The transient analysis used a linear representation of the load history taken from the pressure-time traces in Reference 4. A grid point was placed at each pressure gage location (see Figure 7) for each finite element model. The loads could be applied directly to each grid point by assuming the pressure was uniformly distributed over one half the element length in both directions. The loads were stopped at the face of each wall.

Because the transient approach is a dynamic analysis, structural damping and nonstructural mass effects of the covering soil and burster slab can be included using NASTRAN. For this investigation, they were omitted except for the model composed of plate membrane and rod finite elements. Varying amounts of damping and nonstructural mass were added to the model in order to determine their effects. Damping and nonstructural mass were applied independently of each other.

No rational way of predicting the amount of structural damping is available, so the amounts used were chosen in an attempt to fine-tune the model. The denominator in the damping coefficient fraction is the second natural frequency from an eigenvalue analysis and the numerator was chosen to improve model response. A convenient way of converting this damping to percentage of critical damping was not found.

Some of the mass above the shelter roof acts with the roof and therefore affects the mass terms in the dynamic equilibrium equation. The nonstructural

mass of the concrete burster slab plus the covering soil and the nonstructural mass of the soil only was placed on the roof of the model. Since, no way of determining how much nonstructural mass acts with the shelter, these two amounts seem to be the logical choices.

The effects of damping and nonstructural mass were added to the Transient Analysis Approach on a model that included nonlinear loads. All NASTRAN dynamic approaches assume linear material properties. As the stress in the concrete increases, the concrete cracks in the tension zone and responds nonlinearly in the compression zone. Presently, the only way of inducing nonlinear behavior in the NASTRAN dynamic approaches is by including loads triggered by the displacements and/or velocities of grid points.

To represent the loss of stiffness in a reinforced concrete member due to cracking; nonlinear loads based on the resistance deflection function were applied in the direction of the blast loading. The load was equal to the difference between the NASTRAN elastic prediction (static analysis) for the resistance-deflection function and the resistance-deflection function as described in Reference 10. A detailed description of the resistance-deflection function is in Appendix 4.

The additional load used was assumed to start at the deflection where the finite element model strength and the ultimate moment strength from Reference 10 coincided. The load increased linearly to the maximum deflection of the shelter. This neglected the portion of the resistance-deflection function where the finite element model underestimated the flexural strength of the reinforced concrete structure.

The finite element models require certain geometric and material properties. Table 13, Appendix 3 contains the section properties of the quarter scale model. The table is repeated here for convenience.

Structural Element	Clear Span (in)	Thickness (in)	Flexural Depth (in)	Steel Area (in ²)
Roof	48	9	8	1.32 each face
Exterior Wall	48	9	8	1.32 each face
Interior Wall	48	6	*5	*0.66 each face
Floor	48	6	*5	*0.82 each face

* Assumed Values

The materials properties used for the concrete were:

$$E = 4.25 \times 10^6 \text{ psi}$$

$$G = 1.77 \times 10^6 \text{ psi}$$

$$\text{Poisson's Ratio} = 0.2$$

For the steel, the following material properties were used:

$$E = 29.0 \times 10^6 \text{ psi}$$

$$G = 11.2 \times 10^6 \text{ psi}$$

$$\text{Poisson's Ratio} = 0.3$$

In Appendices 1 and 2 are brief discussions of the NASTRAN analysis approaches and finite elements. The discussions deal only with those parts of the approaches and elements that are applicable to modeling reinforced concrete under blast loadings. More detailed information is available in references 12 and 13. Appendix 3 contains a description of the quarter scale model.

Plate Membrane Model

The initial model was composed of plate membrane elements (QDMEM2) representing both the steel and the concrete. The model was formed by passing two

parallel planes a unit distance apart through the cross section of the shelter. (See Figure 1) The nodes of each element were on the outer most concrete fiber, one-half the way between the planes. No attempt was made to model the reinforcing steel and the concrete material properties were used for all elements.

For this element, output of strain at the location of the reinforcing steel was not available. The difference in the horizontal displacements were converted to strain by dividing by the length of the elements. This was the strain on the outermost top and bottom concrete fibers. By assuming plane sections remain plane, these strains were converted to strain at the location of the reinforcing steel by using similar triangles. Since the grid mesh is very coarse, this strain was a crude average. In the Transient Analysis Approach, the time to maximum strain and the time to return to zero strain were assumed to occur at the time to maximum horizontal displacement and at the time to return to zero horizontal displacement, respectively.

The results from this model are in Tables 1 and 2. The maximum strain in the static and transient approaches is too small, particularly near the interior wall, and the time to zero strain is much too short for the transient approach. Nonlinear loads increase the strains and the time to return to zero strain; however, the loads did not improve the overall accuracy of the model.

The results from this model do not indicate membrane elements alone could successfully model a reinforced concrete shelter under blast loads. The structure has a thick roof with very short spans, so that inplane forces are predominant. If membrane elements alone could model a hardened shelter, they should work for this particular structure. As the vertical deflections increase or as the span of the roof lengthens, bending will become more important and the membrane model should become worse.

Plate Membrane and Rod Model

To improve the representation of reinforced concrete, rod elements (ROD) with linear steel properties were added to the membrane finite elements. The

ANALYSIS TYPE	Experimental	Static	Transient	Transient
MAXIMUM STRAIN % DIFFERENCE	1750×10^{-6}	1100×10^{-6} -37	1050×10^{-6} -40	2410×10^{-6} 37
TIME TO MAXIMUM STRAIN (SEC) % DIFFERENCE	2.5×10^{-3}	N/A	2.9×10^{-3} 18	4.0×10^{-3} 60
TIME TO ZERO STRAIN (SEC) % DIFFERENCE	8.5×10^{-3}	N/A	4.1×10^{-3} -52	5.4×10^{-3} -36

Notes:
Transient 1: Includes nonlinear loads

TABLE 1
Membrane Finite Element (QDMEM2) Model
vs Test 1 Results for Gage ET4

ANALYSIS TYPE	Experimental Test	Static	Transient	Transient 1
MAXIMUM STRAIN % DIFFERENCE	-2100×10^{-6}	-2090×10^{-6} -1	-2010×10^{-6} -4	-4150×10^{-6} 98
TIME TO MAXIMUM STRAIN (SEC) % DIFFERENCE	2.5×10^{-3}	N/A	3.0×10^{-3} 20	4.0×10^{-3} 60
TIME TO ZERO STRAIN (SEC) % DIFFERENCE	10×10^{-3}	N/A	4×10^{-3} -60	5.4×10^{-3} -46

Notes:
 Transient 1: Includes nonlinear loads

TABLE 2
 Membrane Finite Element (QDMEM2) Model
 vs Test 1 Results for Gage ET4

nodes for the membrane and rod elements were moved to the location of the reinforcing bars. An advantage of this model over the plate membrane model alone, is that although many new elements were added, the solution times should not be substantially increased because no additional nodes were added. The membrane elements represent the concrete between the top and bottom reinforcement. This neglects the concrete in compression outside the steel bars; however, includes the portion of the concrete in tension between the reinforcing steel layers.

This model worked very well up to the maximum strain using a transient analysis approach (see Tables 3 and 4). The percentage difference for the maximum strain and the time to maximum strain were small enough to be considered negligible. Even when the most sophisticated methods are used to determine material properties, the coefficient of variation for deflection predictions is in the order of 15 to 20 percent.³ For this case, the worse percentage difference (31 percent) should be considered excellent.

Since the results for Test 1 loads were so good, this model was used with the loads from Test 2. Results were excellent except for the maximum strain at the middle of the roof span (Table 8, gage ET2). The experimental results for the this gage are questionable. Normally, the first plastic hinge would form at this point and this section would have the largest strain in the roof. Therefore, the computer model is probably more accurate than Table 8 shows.

Nonlinear loads decreased the accuracy of the model by increasing the maximum strain and the time to maximum strain too much. The time to zero strain was improved.

The effects of nonstructural mass were investigated using this model and the results are in Tables 3 and 4. The amount of strain was greatly reduced and the response time of the structure increased. Even with only the weight of the soil applied to the roof, the model was much too stiff and slow to respond. A small amount of nonstructural mass could improve the response of the model; however, a rational way of determining the nonstructural mass is not available.

ANALYSIS TYPE	Experimental Test	Static	Transient	Transient 1	Transient 5	Transient 6
MAXIMUM STRAIN % DIFFERENCE	1750×10^{-6}	1770×10^{-6} 1	1640×10^{-6} -6	3700×10^{-6} 110	950×10^{-6} -46	820×10^{-6} -53
TIME TO MAXIMUM STRAIN (SEC) % DIFFERENCE	2.5×10^{-3}	N/A	3.0×10^{-3}	4.0×10^{-3}	6.0×10^{-3}	8.2×10^{-3}
TIME TO ZERO STRAIN (SEC) % DIFFERENCE	8.5×10^{-3}	N/A	4.2×10^{-3}	5.5×10^{-3}	10.0×10^{-3}	12.4×10^{-3}
			-51	-35	20	45

Notes:

Transient 1: Includes nonlinear loads

Transient 5: Includes nonlinear loads and the nonstructural mass of the soil only

Transient 6: Includes nonlinear loads and the nonstructural mass of the burster slab plus soil

TABLE 3

Membrane-Rod Finite Element (QDMEM2, ROD) Model
vs Test 1 for Gage ET4

ANALYSIS TYPE	Experimental Test	Static	Transient 31	Transient 1	Transient 5	Transient 6
MAXIMUM STRAIN % DIFFERENCE	-2100×10^{-6}	-2830×10^{-6} 35	-2760×10^{-6} 31	-5380×10^{-6} 156	-1330×10^{-6} -37	-990×10^{-6} -53
TIME TO MAXIMUM STRAIN (SEC) % DIFFERENCE	2.5×10^{-3}	N/A	2.9×10^{-3} 17	4.0×10^{-3} 60	7.1×10^{-3} 185	8.1×10^{-3} 225
TIME TO ZERO STRAIN (SEC) % DIFFERENCE	10×10^{-3}	N/A	4.0×10^{-3} -60	5.6×10^{-3} -44	10×10^{-3} 5	12.6×10^{-3} 26

Notes:

Transient 1: Includes nonlinear loads

Transient 5: Includes nonlinear loads and nonstructural mass composed of soil only

Transient 6: Includes nonlinear loads and nonstructural mass composed of burster slab plus soil

TABLE 4

Membrane-Rod Finite Element (QDMEM2, ROD)
Model vs Test 1 Results for Gage ET5

This model was also used to test the effects of structural damping. The results are shown in Tables 5, 6, 7, and 8. As the structural damping increased, the maximum strain and the time to maximum strain decreased, and the time to return to zero strain increased. Even though the amount of damping was chosen in an attempt to fine-tune the model, the results were no better than in the transient approach without nonlinear loads.

This model works particularly well up to the point of maximum strain. Beyond that time the model responds too quickly. By including the the proper amount of structural damping and nonstructural mass the model response could be improved for a longer time period.

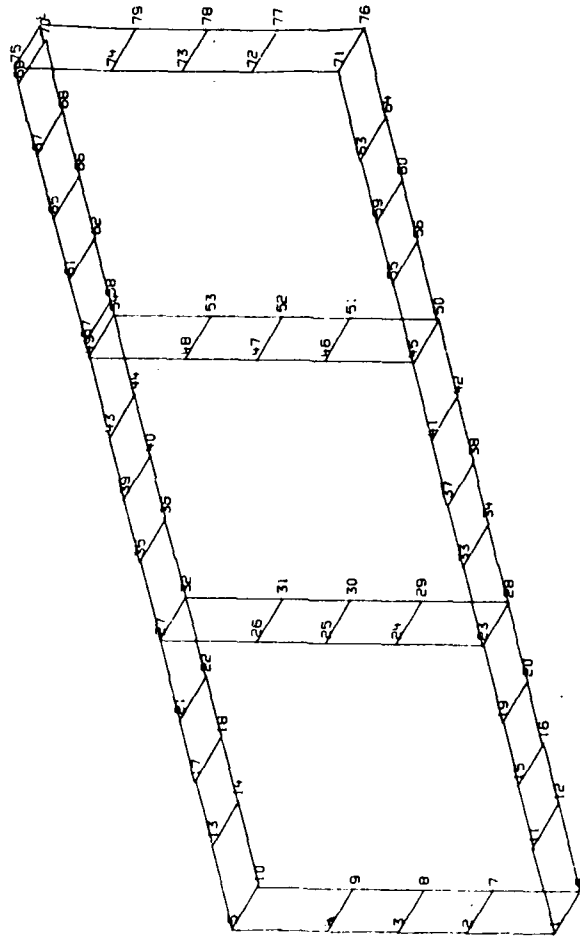
Plate Bending Model

A model was made of the shelter using plate bending elements (QDPLT) only. The model is formed by passing two parallel planes 12 inches apart through the shelter cross section, and the nodes of the elements are on the middle surface of the walls, roof, and floor (see Figure 2). The material properties used were for concrete. Bigg's moment of inertia for a cracked reinforced concrete section was used for the bending stiffness and the distance from the compression face to the centroid to the tension steel was used as the transverse shear thickness.²

The model was used in a static analysis approach only, because the elements require unrealistic boundary conditions. A plate bending element cannot resist inplane forces, so to be used as an element in a wall the vertical deflection of the wall must be completely constrained. Other finite elements do not require such restrictive boundary conditions and are more useful. This element may be employed as a roof element when used in combination with other element types. The roof should have a large span-to-depth ratio.

Plate Bending-Membrane Model

By using an element that can develop inplane forces, realistic boundary conditions can be used. A model using plate bending-membrane finite elements



TRANSIENT ANALYSIS BENDING - MEMBRANE AND BEAM ELEMENTS
LINEAR STEEL AND CONCRETE MATERIAL
UNDEFORMED SHAPE

Figure 2
Undeformed Shape for Plate Bending and
Plate Bending-Beam Finite Element Models

ANALYSIS TYPE	Experimental Test	Transient 1	Transient 2	Transient 3	Transient 4
MAXIMUM STRAIN % DIFFERENCE	1750×10^{-3}	3700×10^{-6} 110	3130×10^{-6} 79	1560×10^{-6} -11	1150×10^{-6} -34
TIME TO MAXIMUM STRAIN (SEC) % DIFFERENCE	2.5×10^{-3}	4.0×10^{-3} 61	4.0×10^{-3} 60	3.4×10^{-3} 34	2.4×10^{-3} 47
TIME TO ZERO STRAIN (SEC) % DIFFERENCE	8.5×10^{-3}	5.5×10^{-3} -35	5.4×10^{-3} -36	5.5×10^{-3} -36	10.7×10^{-3} 26

Notes:

- Transient 1: Includes nonlinear loads
- Transient 2: Includes nonlinear loads and damping coefficient 0.1/1719.592
- Transient 3: Includes nonlinear loads and damping coefficient 0.5/1719.592
- Transient 4: Includes nonlinear loads and damping coefficient 1.0/1719.592

TABLE 5

Membrane-Rod Finite Element (QDMEM2, ROD)
Model for Test 1 for Gage ET4

ANALYSIS TYPE	Experimental Test	Transient 1	Transient 2	Transient 3	Transient 4
MAXIMUM STRAIN % DIFFERENCE	-2100×10^{-3}	-5380×10^{-6} 156	-4620×10^{-6} 120	-2770×10^{-6} 32	-1750×10^{-6} -17
TIME TO MAXIMUM STRAIN (SEC) % DIFFERENCE	2.5×10^{-3}	4.0×10^{-3} 60	4.0×10^{-3} 58	3.8×10^{-3} 51	3.6×10^{-3} 45
TIME TO ZERO STRAIN (SEC) % DIFFERENCE	10×10^{-3}	5.6×10^{-3} -44	5.5×10^{-3} -45	5.5×10^{-3} -45	10.7×10^{-3} 7

Notes:

- Transient 1: Includes nonlinear loads
- Transient 2: Includes nonlinear loads and damping coefficient 0.1/1719.592
- Transient 3: Includes nonlinear loads and damping coefficient 0.5/1719.592
- Transient 4: Includes nonlinear loads and damping coefficient 1.0/1719.592

TABLE 6

Membrane-Rod Finite Element (QDMEM2, ROD) Model
vs Test 1 Results for Gage ET5

ANALYSIS TYPE	Experimental Test	Static	Transient 10	Transient 1	Transient 2	Transient 3
MAXIMUM STRAIN % DIFFERENCE	2700 x 10 ⁻⁶	3440 x 10 ⁻⁶ 27	2970 x 10 ⁻⁶ 10	8490 x 10 ⁻⁶ 214	4310 x 10 ⁻⁶ 60	2920 x 10 ⁻⁶ 8
TIME TO MAXIMUM STRAIN (SEC) % DIFFERENCE	3.0 x 10 ⁻³	N/A	2.6 x 10 ⁻³	3.6 x 10 ⁻³	2.6 x 10 ⁻³	3.3 x 10 ⁻³
TIME TO ZERO STRAIN (SEC) % DIFFERENCE	10.5 x 10 ⁻³	N/A	3.5 x 10 ⁻³	5.3 x 10 ⁻³	5.8 x 10 ⁻³	6.2 x 10 ⁻³
			-13	19	-12	10
			-67	-49	-45	-41

Notes:
 Transient 1: Includes nonlinear loads
 Transient 2: Includes nonlinear loads and damping = 0.5/1719.592
 Transient 3: Includes nonlinear loads and damping = 0.75/1719.592

TABLE 7
 Membrane-Rod Finite Element (QDMEM2, ROD) Model
 vs Test 2 for Gage ET3

ANALYSIS TYPE	Experimental Test	Static	Transient	Transient 1	Transient 2	Transient 3
MAXIMUM STRAIN % DIFFERENCE	-2250×10^{-6}	-5500×10^{-6} 144	-4820×10^{-6} 114	-12300×10^{-6} 446	-6690×10^{-6} 197	-5440×10^{-6} 142
TIME TO MAXIMUM STRAIN (SEC) % DIFFERENCE	2×10^{-3}	N/A	2.1×10^{-3}	3.7×10^{-3}	2.6×10^{-3}	2.5×10^{-3}
TIME TO ZERO STRAIN (SEC) % DIFFERENCE	9×10^{-3}	N/A	3.2×10^{-3}	5.3×10^{-3}	5.7×10^{-3}	6.1×10^{-3}
			-64	-41	-37	-32

Notes:

- Transient 1: Includes nonlinear loads
- Transient 2: Includes nonlinear loads and damping coefficient = 0.5/1719.592
- Transient 3: Includes nonlinear loads and damping coefficient = 0.75/1719.592

TABLE 8

Membrane-Rod Finite Element (QDMEM2, ROD) Model
vs Test 2 for Gage ET2

(QUAD1) was constructed in the same manner as for the plate bending model. Since the reinforcing steel was not being modeled, concrete material properties were used. Bigg's moment of inertia was used for bending stiffness, the distance from the compression fact to the centroid of the tension steel was used for the transverse shear thickness, and the total concrete thickness was used for the membrane shear thickness.²

For the accuracy required to analyze or design a shelter, the plate bending membrane model requires approximately the same number of nodes as a plate membrane element model. Because of the gross mesh size used in this project, extra nodes had to be added for the plate bending-membrane model. The stresses in each element are an average of the stresses within the element. This caused the element at the face of the interior wall to have small tensile strains rather than the large compression strains expected. Placing a small element at the face of the wall (see Figure 2) corrected this problem.

Tables 9 and 10 contain the results from the Static and Transient Analysis Approaches. The model is too flexible, does not reach the maximum strain soon enough, and returns to zero strain too quickly. Nonlinear loads worsen the predictions as would be expected for an overly flexible model.

A model composed of plate bending-membrane elements alone did not exhibit the kinds of characteristics necessary to model reinforced concrete. The flexibility of the model depends on the designer's choice for a moment of inertia. Also, input values for the transverse shear and membrane shear thickness are debatable. A better finite element model would have fewer and less critical choices.

Plate Bending - Membrane and Beam Model

By adding a beam (BAR) element to the bending-membrane model the importance of the value of the moment of inertia is reduced. The plate element was used to represent the concrete and was given concrete material properties.

ANALYSIS TYPE	Experimental Test	Static	Transient	Transient
MAXIMUM STRAIN % DIFFERENCE	1750×10^{-6}	3070×10^{-6} 75	2530×10^{-6} 44	4040×10^{-6} 131
TIME TO MAXIMUM STRAIN (SEC) % DIFFERENCE	2.5×10^{-3}	N/A	3.1×10^{-3}	3.9×10^{-3} 56
TIME TO ZERO STRAIN (SEC) % DIFFERENCE	8.5×10^{-3}	N/A	4.3×10^{-3}	5.7×10^{-3} -33

Notes:
Transient 1: Includes nonlinear loads

TABLE 9

Membrane-Bending Finite Element (QUAD1) Model
vs Test 1 Results for Gage ET4

ANALYSIS TYPE	Experimental Test	Static	Transient	Transient 1
MAXIMUM STRAIN % DIFFERENCE	-2100×10^{-6}	-5060×10^{-6} 141	-3970×10^{-6} 89	-6760×10^{-6} 222
TIME TO MAXIMUM STRAIN (SEC) % DIFFERENCE	2.5×10^{-3}	N/A	3.3×10^{-3} 30	4.0×10^{-3} 58
TIME TO ZERO STRAIN (SEC) % DIFFERENCE	10×10^{-3}	N/A	4.5×10^{-3} -55	6.0×10^{-3} -40

Notes:
Transient 1: Includes nonlinear loads

TABLE 10
Membrane-Bending Finite Element (QUAD1) Model
vs Test 1 Results for Gage ET5

The bending stiffness was the moment of inertia of the concrete between the center of gravity of the total section and the top layer of steel about the center of gravity of the total section (neglects concrete outside the steel layer). The transverse shear thickness was the distance from the compression face to the centroid of the tension steel and the membrane shear thickness was the distance between the steel layers.

Two beam elements were offset the proper distance in each direction, on each side of the middle surface of the plate. By releasing the the proper constraints only axial extension of each beam was allowed and bending was eliminated. Each beam had a cross-sectional area equal to one-half the reinforcing steel area in each layer and each element had the standard steel material properties.

The results from this model are in Tables 11 and 12. The model works well in a Transient Analysis Approach, without nonlinear loads. Good results are obtained at the mid-span of the roof; where bending forces predominate. Applying nonlinear loads increased the maximum strain and increased the time to maximum strain; however, did not improve the overall accuracy of the model. Near the interior support the model was too stiff even with nonlinear loads applied. As with all models this one returned to zero strain much too quickly.

The plate bending-membrane and beam model was the second most accurate model in this investigation. Indications are the model would be more accurate for longer span, thinner roof sections. The depth to span ratio of 3/16 is not small deflection plate theory and this model may be more applicable to full size structures.¹¹ The input requirements for this model are large because of the large number of elements; therefore, significant gains in accuracy would have to be achieved before this would be the model of choice.

Conclusions

The finite element program NASTRAN can be an extremely useful tool for analysing and designing hardened reinforced concrete shelters. When using a

ANALYSIS TYPE	Experimental Test	Static	Transient	Transient 1
MAXIMUM STRAIN % DIFFERENCE	1750 x 10 ⁻⁶	520 x 10 ⁻⁶ -70	370 x 10 ⁻⁶ -79	690 x 10 ⁻⁶ -61
TIME TO MAXIMUM STRAIN (SEC) % DIFFERENCE	2.5 x 10 ⁻³	N/A	2.8 x 10 ⁻³ 14	3.7 x 10 ⁻³ 46
TIME TO ZERO STRAIN (SEC) % DIFFERENCE	8.5 x 10 ⁻³	N/A	4.1 x 10 ⁻³ -52	5.3 x 10 ⁻³ -37

Notes:
Transient 1: Includes nonlinear loads

TABLE 11
Membrane-Bending and Rod Finite Element (QUAD1, BAR)
Model vs Test 1 Results for Gage ET4

ANALYSIS TYPE	Experimental Test	Static	Transient	Transient 1
MAXIMUM STRAIN % DIFFERENCE	-2100×10^{-6}	-1780×10^{-6} -15	-1690×10^{-6} -19	-2690×10^{-6} 28
TIME TO MAXIMUM STRAIN (SEC) % DIFFERENCE	2.5×10^{-3}	N/A	2.7×10^{-3} 10	3.4×10^{-3} 37
TIME TO ZERO STRAIN (SEC) % DIFFERENCE	10×10^{-3}	N/A	3.9×10^{-3} -61	5.2×10^{-3} -48

Notes:
Transient 1: Includes nonlinear loads

TABLE 12

Membrane-Bending and Rod Finite
Element (QUAD1, BAR) Model vs Test 1 Results for Gage ET5

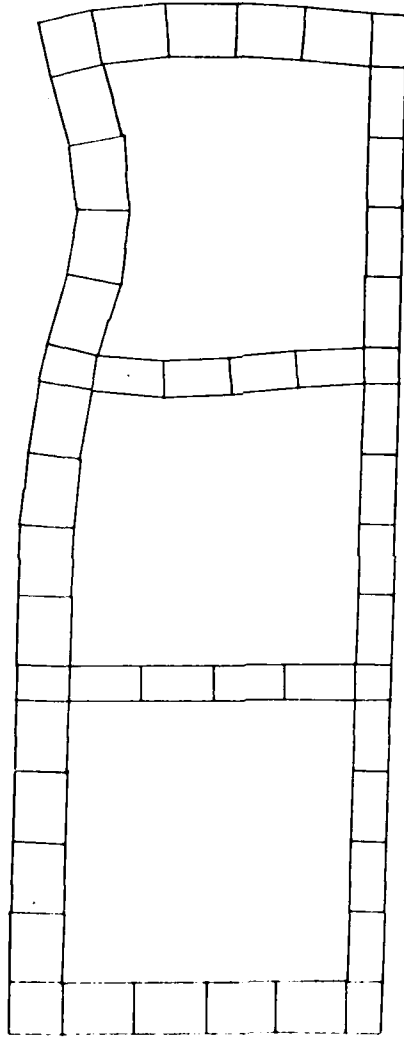
finite element model composed of plate membrane elements (QDMEM2) and rod elements (ROD) the structure is correctly modeled up to the maximum strain at the roof span center line and near interior support. Since the strains are accurately modeled it is reasonable to assume deflection are also successfully predicted.

Element stresses will not be correct because a linear stress-strain relationship is used by NASTRAN. Element forces are determined directly from the element displacement matrix and will be as accurate as the displacements. Deflection predictions of reinforced concrete members traditionally have a large degree of uncertainty and a prediction within 20% of the true deflection should be considered excellent.³ The large prediction error is related to material property and construction practices, so reductions in the size of the error can not be made by improving the mathematical modeling techniques.

Better modeling techniques will help improve the deflection predictions for repeated explosions, for pressures high enough to cause localized failures, and for time intervals that exceed the time to maximum strain. In particular, better techniques are needed in order to predict permanent set of a hardened structure. The areas that need improvement are in the finite element representation of reinforced concrete, the amount and type of structural damping in hardened structures and the amount of covering material that acts as nonstructural mass on the roof.

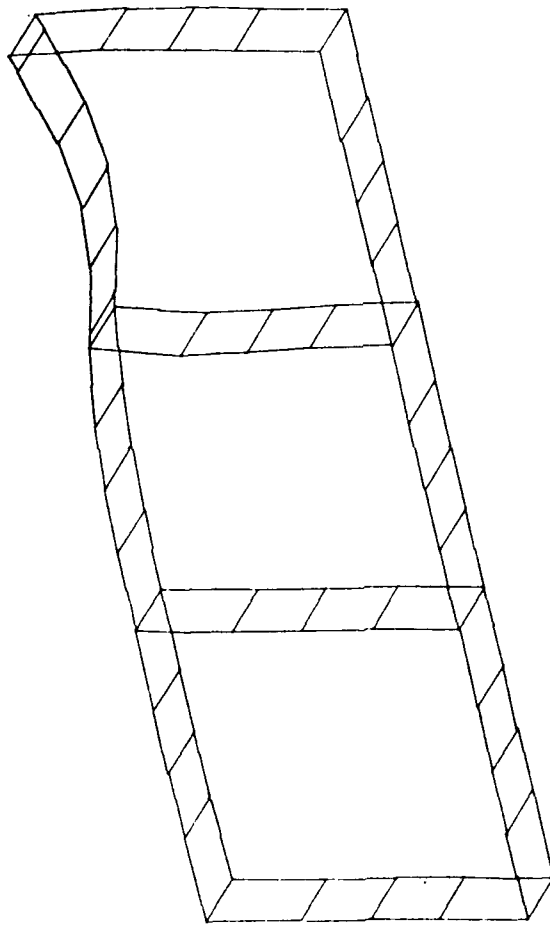
When dynamic analysis of a hardened structure is conducted huge amounts of output data are generated. By far the most functional form of output is graphical. Numerical output inundates the engineer with data and does not provide a feeling for how the structure is responding. The graphical capabilities of NASTRAN are a tremendous advantage. Undeformed plots (see Figures 1 and 2) and deformed plots (see Figures 3 and 4) may be made separately or superimposed. Plots of element stresses, strains and forces versus time (see Figure 5) and plots of grid point deflections, velocities, and accelerations versus time (see Figure 6) are available. Input loads versus time also can be plotted.¹³

5 1.7 6 8. MAX-DEF. = 0.26515114



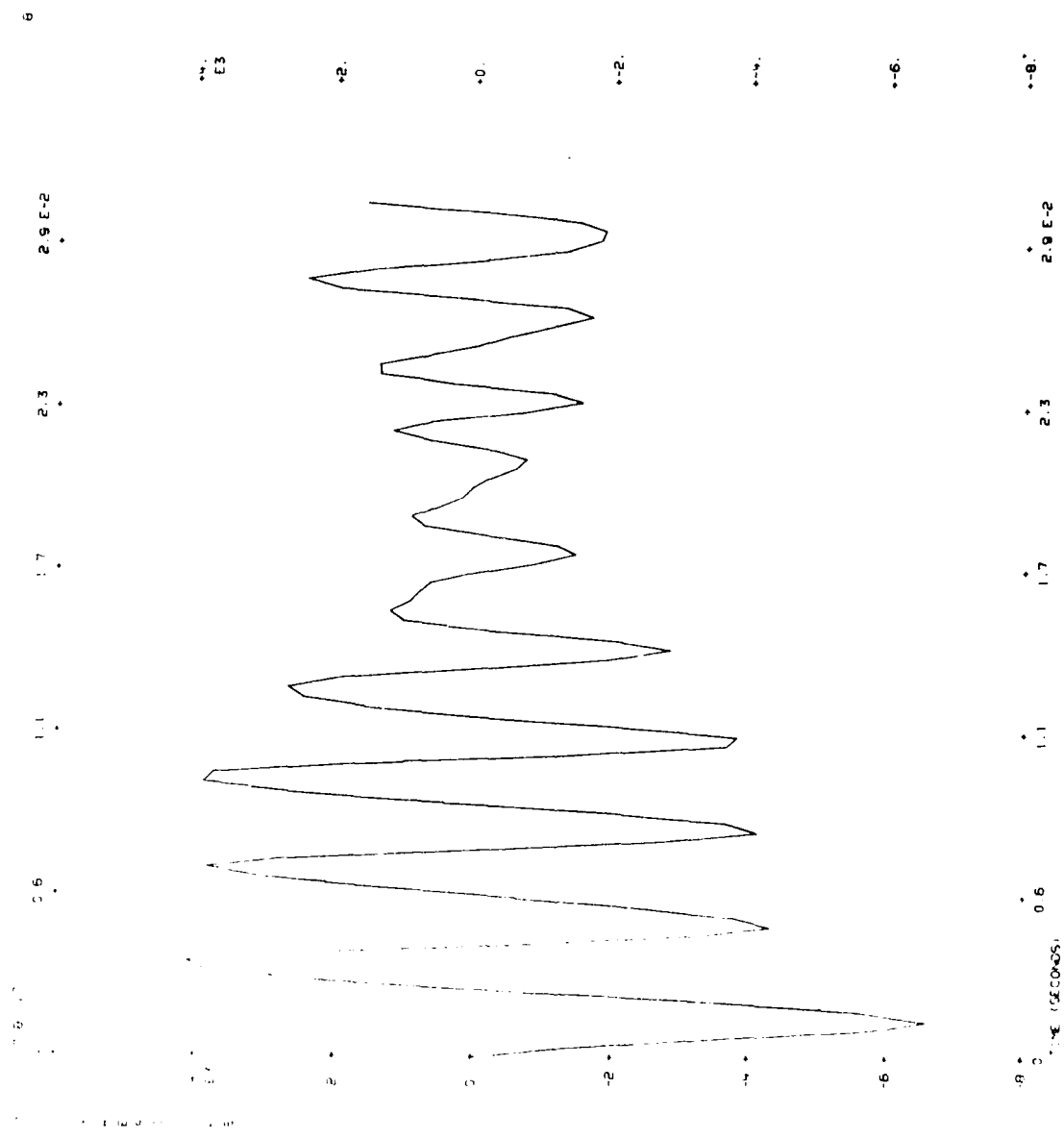
STATIC ANALYSIS MEMBRANE ELEMENTS
LINEAR CONCRETE MATERIAL, GROSS SECTION PROPERTIES
Q1CM TEST 1 AVERAGE PRESSURE = 1825 PSI
STATIC DEFOR. SUBCASE 1 LOAD 1

Figure 3
Nastran Plot of Deformed Membrane Model



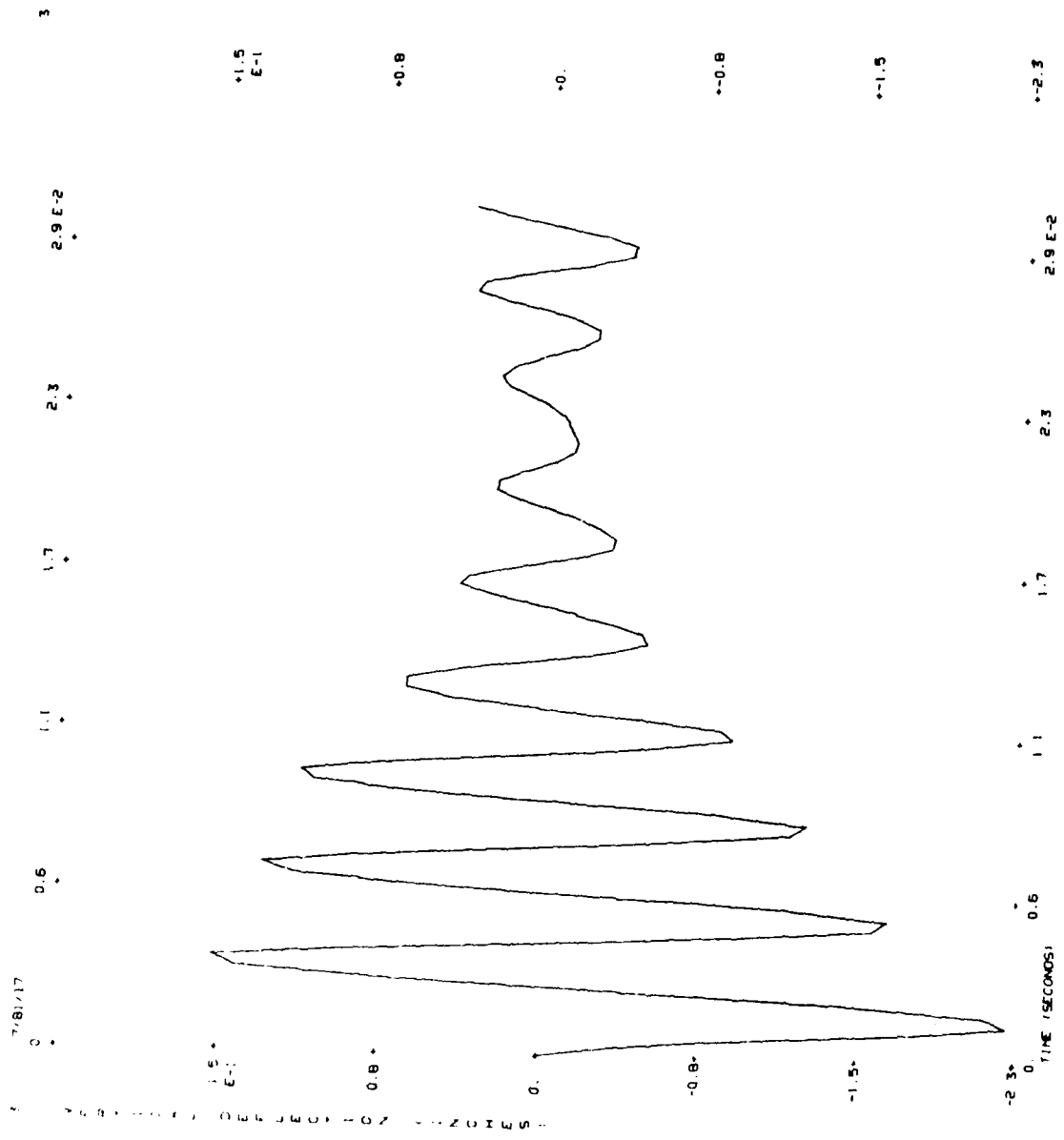
STATIC ANALYSIS BENDING - MEMBRANE ELEMENTS AND BEAM
 ELEMENTS, LINEAR STEEL AND CONCRETE MATERIAL
 CALCH TEST 1 AVERAGE PRESSURE = 1865 PSI
 STATIC DEFOR. SUBCASE 1 .LOAD 1

Figure 4
 Nastran Plot of Deformed Plate-Bending Model



TRANSIENT ANALYSIS - BENDING - MEMBRANE AND BEAR ELEMENTS
 LINEAR STEEL AND CONCRETE MATERIAL
 FIGURE 5

Typical Nastran Stress VS Time Plot



TRANSIENT ANALYSIS BENDING - MEMBRANE AND BEAM ELEMENTS
 LINEAR STEEL AND CONCRETE MATERIAL

Figure 6
 Typical Nastran Deflection VS Time Plot

Input for NASTRAN is tedious at best. A large number of cards must be punched for small problems and the number increases quickly as the number of elements increase. The format of the input cards is rigid, with input data restricted to certain fields. Where interactive computer service is available, input data could be written to disk as card images and properly formatted by simple user written programs. This relieves some of the monotony of inputting data but would not reduce the number of characters input.

IV. RECOMMENDATIONS

Results from the analyses performed during this project indicate NASTRAN in its present form is useful in analysing hardened reinforced concrete shelters up to the time of maximum strain. The test used in this project had a limited amount of useful data and more validation runs of NASTRAN should be made before the program is used for design of hardened structures. The test data needed for the validation run are:

- (1) blast pressures on the surface of the reinforced concrete member(s).
- (2) deflections and velocity of regularly spaced points on the outer surfaces of the reinforced concrete member(s).
- (3) strains at selected points on the tension and compression steel.

The boundary conditions on the test specimen should be instrumented so that any support movement can be determined and used in the analytic model. Any strain gage used on a concrete surface should use at least three inches long to eliminate bias from cracks and coarse aggregates.

The ability of NASTRAN to model reinforced concrete can be improved by adding nonlinear material behavior to the dynamic analysis approach. Nonlinear material behavior is available in a static approach (Piecewise Linear Analysis) and could be added to the dynamic approaches by changing the rigid formats.

To accurately predict structural response beyond the maximum strain, basic research into the nature of structural damping and nonstructural mass must be conducted. The limited analytic study in this project showed the computer model to be very sensitive to changes in nonstructural mass and structural damping. The surrounding and covering soil layers (including burster slab) act with the shelter as nonstructural mass and add structural damping. Since both phenomena are related, a nondimensional model study may be able to develop rational methods of determining structural damping and nonstructural mass for the specific configuration of a hardened structure.⁹

Intensive work is being done developing a reinforced concrete finite element and a good element should be available at any time.⁵ Most work is being done to model nuclear explosions and the finite element will have to be changed to properly model reinforced concrete subjected to a conventional weapon explosion. Whenever the model becomes available, it should be added to NASTRAN to improve its ability to predict the response of reinforced concrete structures.

The new element will contain strain/rate (or stress/rate) effects on material properties. Most of the data available on strain/rate effects is 23 years old or older and contains some questionable data. However, the information indicates gains in ultimate concrete strength are in the range 50 to 100%.^{6,7} An investigation into the strain/rate effect is needed and should lead to substantial cost savings in reinforced concrete shelters.

Investigation into the use of other general purpose finite elements programs should continue. Emphasis should be given to those programs that contain dynamic analysis capabilities that include structural damping and nonstructural mass. The programs should be able to be altered to take new finite elements. A most important consideration is the ability to generate graphical output. Lack of graphical output would seriously affect the program's ability for practical use.

V. REFERENCES

1. Baseheart, T. M., "The Response of Reinforced Concrete Structures to Near Field Explosions," USAF Summer Faculty Research Program, Vol 1, AFOSR, Bolling AFB, Washington, DC, 1980.
2. Biggs, J. M., Introduction to Structural Dynamics, McGraw-Hill Book Co, New York, NY, 1964.
3. Branson, D. E., Deformation of Concrete Structures, McGraw-Hill Book Co, New York, NY, 1977.
4. Coltharp, D. A., "Analysis of One-Quarter-Scale Model Test Results," Unpublished Report from USA Waterways Experiment Station, Structures Laboratory, Structure Mechanics Division, Vicksburg, MS.
5. Hegemier, G. A., "Evaluation of Material Models for MX Siting Vol II: Reinforced Concrete Models," SSS-R-80-4155, Systems, Science and Software, La Jolla, CA, November 1979.
6. Mindess, S., and Young, J. F., Concrete, Prentice-Hall, Inc., Englewood Cliffs, NJ, 1981.
7. Neville, A. M., Properties of Concrete, Pitman Publishing Limited, London, Great Britain, 1981.
8. Przemieniecki, J. S., Theory of Matrix Structural Analysis, McGraw-Hill Book Co., New York, NY, 1968.
9. Smith, J. H., and Vann, W. P., "Theoretical and Experimental Investigation of Buried Concrete Structures Vol I: Analysis and Experiment," AFOSR-TR-76-1070, AFOSR, Bolling AFB, Washington, DC, November 1975.
10. "Structures to Resist the Effects of Accidental Explosions," AFM 88-22, Departments of the Army, the Navy, and the Air Force, Washington, DC, June 1969.

11. Szilard, R., Theory and Analysis of Plates, Prentice-Hall, inc., Englewood Cliffs, NJ, 1974.
12. "The NASTRAN Theoretical Manual," NASA SP-221(05), National Aeronautics and Space Administration, Washington, DC, December 1980.
13. "The NASTRAN User's Manual," NASA SP-222(05), National Aeronautics and Space Administration, Washington, DC, December 1980.
14. Timoshenko, S. P., and Goodier, J. N., Theory of Elasticity, McGraw-Hill Book Co., New York, NY, 1934.
15. Venkayya, V. B., Eastep, F. E., and Johnson, J. R., "NASTRAN Beginner's Course," TM-FBR-76-121, Air Force Flight Dynamics Laboratory, Wright-Patterson AFB, OH, September 1976.
16. Wang, C. K., and Salmon, C. J., Reinforced Concrete Design, Harper and Row Publishers, New York, NY, 1979.

VI. APPENDICES

1) Displacement Approach Rigid Formats

Introduction

The NASTRAN (NASA STRuctural ANalysis) Computer Program is a general purpose structural analysis program intended for a wide range of applications. To meet this requirement NASTRAN contains different finite elements to represent common construction members and allows these elements to be combined to model more sophisticated construction materials. NASTRAN currently provides 15 different methods to determine displacements of a structure. Each method is referred to as a Displacement Approach Rigid Format and the user chooses the rigid format depending on the type of analysis required.¹⁵

To improve the generality of NASTRAN the program is divided into subprograms or modules that can be called independently of each other. A rigid format is a permanently stored sequence of subprograms calls which produce a particular kind of structural analysis. The user may alter the sequence of calls or develop a new sequence for unusual analysis problems.¹³

One of the subprograms available for use with any rigid format is the Plot Module. The plotting routines allow plotting of specific input and output data on a SC-4020 plotter, an Electronic Association Incorporated plotter, and most Calcomp plotters. Also a user may write his own plotter routines for use with NASTRAN.¹³

Some rigid formats yield large amounts of numerical output. Output in graphical form gives the engineer a better feeling for the response of the structure. Figures 1, 2, 3, 4, 5, and 6 are samples of the type of output available through the NASTRAN Plot Module. Undeformed structural plots aid in the detection of input errors in grid point coordinates and element connections.

For this investigation two rigid formats were used, Static and Transient. Also two other rigid formats, Piecewise Linear and Differential Stiffness may be useful. The remainder of this appendix is a brief discussion of those rigid formats, emphasizing the portions of those formats that are useful in analyzing hardened structures.

Static Displacement Approach Rigid Format

The Static Analysis Rigid Format is used to determine deformation, stresses, etc, due to very slowly applied loads. This rigid format is a good starting point in any analysis because the designer can check for input errors in the finite element model and for conceptual errors in the choice of elements and boundary conditions.

The loads may be concentrated at grid points, uniformly distributed over two dimensional finite elements and generated internally as body forces due to gravity. NASTRAN will compute the gravity loads from the mass matrix if the gravity acceleration vector is input. The mass matrix is composed of the element mass and any nonstructural mass applied to the element, for example, soil above an underground structure.¹² Different load factors may be applied to each load to aid in "limit state" design.

Solving the set of simultaneous equations generated by the finite element method uses large amounts of computer resources. The Static Analysis Rigid Format is set up to analyze the structure for different loading combinations and/or different boundary conditions without resolving the set of simultaneous equations. Each loading combination and each new set of boundary conditions is called a subcase.

Transient Approach Rigid Format

To solve structural dynamic problems the Transient Approach Rigid Format is used. This approach assembles the structural stiffness, mass, and damping matrices; generates time history load tables; and solves the differential

equations by a form of the Newmark Beta Method. The stiffness, mass, and damping matrices may be assembled by NASTRAN and/or directly input by the user.¹²

Because of the large number of load entries required for even a moderate size problem, NASTRAN provides four different functions, three linear functions and one power function, to input dynamic loads. In addition to those loads NASTRAN can generate nonlinear loads triggered by the deflections and/or velocities of grid points.¹² Nonlinear loads provide a means of modeling nonlinear material behavior.

Mass matrices are generated by either the Lumped Mass or Coupled Mass Methods. Some individual elements have restrictions on the method of mass matrix generation allowed. Also masses may be assigned directly to grid points.¹²

The Lumped Mass Method distributes the structural mass and nonstructural mass evenly between the nodes of the element. This yields a simpler model because there is no inertia coupling between grid points. In most cases the Lumped Mass Method will result in natural frequencies below the true value.¹²

The Coupled Mass Method, sometimes called "Consistent" Mass Method, yields an inertia coupling between grid points, i.e., the inertia properties of a grid point affect the inertia properties of adjacent grid points. The element mass matrix is dependent on the elastic properties of the element. This method normally yields natural frequencies above the exact results.¹²

The *damping matrix* is the sum of direct input damping coefficients from viscous damping elements, a percentage of the structure stiffness matrix, and a percentage of any/all element stiffness matrices. The user specifies the appropriate constants for NASTRAN to compute the damping matrix. If the input data is not specified, structural damping is neglected. Normally structural damping is expressed as a percentage of the critical damping.² NASTRAN does not contain a convenient way of expressing damping in this manner.

For this rigid format graphical output is particularly useful. Plots of element stresses and forces versus time, and grid point deflections and velocities versus time are available. Also deformed and undeformed structure plots are available in three dimensions.

Piecewise Linear Approach Rigid Format

Piecewise Linear Analysis is used to solve problems involving material plasticity. This rigid format is presently restricted to statically applied loads. Since the loads cannot be varied with time it is not applicable to the analysis of hardened structures in its present form and was not included in this investigation.

For the Piecewise Linear Approach the user specifies a material stress-strain table and the amount of load to be applied in each increment. The rigid format proceeds to determine the displacements and strain using the first load increment and the user specified elastic material properties (not the user provided stress-strain table). NASTRAN then uses extrapolation to determine the strain expected in the next load increment. With this projected strain a linear approximation for the modulus of elasticity for each element is calculated from the stress-strain table. A new stiffness matrix is assembled and the deflections and strains for the next load increment are determined. Deflections and strains are accumulated after each load increment. The rigid format repeats the sequence beginning with the extrapolation to estimate the next strain and continues until the total load has been applied.¹² Solving the simultaneous equations for each load increment requires huge amounts of computer resources. Choosing too many steps uses an unnecessary amount of computer resources; however, too few steps will make the solution inaccurate.

Piecewise Linear Analysis also generates large amounts of output data. The plotting capabilities of the plot modules provide output in a more useful form.

Differential Stiffness Approach Rigid Format

In some structural problems deformations occur that adversely affect the structures ability to carry the loads. In the design of tall steel buildings this is referred to as the P-Delta effect.

This rigid format introduces nonlinearity into the analysis caused by large deflections. The NASTRAN approach is an approximate analysis and may not be applicable to a particular problem, so that the use of this rigid format must be carefully reviewed. One important limitation is the applied loads remain fixed in direction and magnitude during the movement of the structure.¹²

In some hardened structures this rigid format may prove useful; however, when reinforced concrete is the construction material failure of the concrete will occur before the deflections affect the structural capacity.¹⁶ The Differential Stiffness Approach Rigid Format was not investigated in this report.

2) NASTRAN Finite Elements

Introduction

Only a few of the available finite elements were used in this investigation. This appendices list those elements and contains a brief description of the important element properties.

Plate Membrane Element

The NASTRAN plate membrane elements were developed by constructing the expression for strain energy using a linear variation in the inplane displacements. The basic element is triangular (TRMEM) and use is to form other quadrilateral elements. The quadrilateral elements are formed by either overlapping four triangular elements (QDMEM) or by connecting four triangular elements (QDMEM2) at the center point of the quadrilateral.¹²

The material properties for the elements may be anisotropic; however, only isotropic material was used in this investigation.¹⁴ For an isotropic material two of three material constants, modulus of elasticity, shear modulus, or Poisson's ratio must be specified.

The Lumped Mass Method for transferring structural and nonstructural mass to adjacent grid points is the only method available for membrane elements. The mass matrix and inplane stiffness for the elements are found by assigning one half the thickness of the quadrilateral element to each triangular element. Although the Coupled Mass Method cannot be used for structural models with membrane stiffness only, the method may be specified for elements with both bending and membrane stiffness. The terms in the mass matrix which correspond to inplane motions are computed by the Lumped Mass Method and the other mass terms will be computed by the Coupled Mass Method.¹²

The strains within this element are constant because the deflections were assumed to be linear, so the stresses are an average within each element. The state of stress for a nonoverlapping element is the average stress in the four triangular elements. A "shear flow" is calculated for the sides of each element. The "shear flow" is the change in the inplane force along the side divided by the length of the side.¹²

Rod Element

The rod element (ROD) developed for NASTRAN includes extensional and torsional properties only and is based on a linear deformation function. The elements are straight, loaded at the ends only, and have uniform geometric and material properties. The strains are constant for the element because of the linear deformation functions and the stresses are on average for the element.¹²

For dynamic analysis approaches the structural and nonstructural mass associated with each rod may be transferred to the adjacent grid points by the Lumped Mass or Coupled Mass Methods. For this element the coupled mass matrix

is the average of the pure lumped mass and the pure coupled mass matrices. This yields a much smaller error in the natural frequency than either the Lumped Mass or Coupled Mass Methods alone.¹²

Plate Bending Element

The basic NASTRAN plate bending element (TRPLT) is a triangle with three degrees of freedom, one translational and two rotational, at each node. The out-of-plane deflection is assumed to be the following incomplete third degree function.¹²

$$w = ax + by + cx^2 + dxy + ey^2 + fx^3 + gxy^2 + hy^3$$

The x^2y term is omitted because there are only eight independent deformations in the triangular element, and only eight constants can be determined in the out-of-plane deflection field. This displacement does not guarantee slope continuity on the edges of adjacent elements; however, elements which have slope continuity do not necessarily give better results.⁸

The plate bending element may be an anisotropic material and the user can specify material properties with respect any axis orientation. The program will rotate the properties into the proper coordinate system. As with the plate membrane element, two of the three material constants must be specified.¹³

The element may be assumed rigid in transverse shear. This decreases the magnitude of the element stiffness terms by an amount equal to the transverse shear stiffness.¹² In beam elements transverse shear stiffness is normally omitted because of its small size. In hardened structures transverse shear stiffness is important because of the thickness of the construction and should not be neglected.

The internal forces are determined at the center of gravity of the triangular element. A linear variation of strain through the thickness of the

plate is assumed, so stresses may be determined at any distance from the middle surface.¹²

The Lumped Mass and Coupled Mass Methods are available to create mass matrices for plate bending elements. The Lumped Mass Method places one third of the element mass at each node. In the Coupled Mass Method, the mass matrix of each element is calculated assuming a uniform mass density within the element. Thus the mass matrix is dependent on the bending properties of the plate element.¹²

A quadrilateral plate bending element (QDPLT) is formed by overlapping four triangular bending elements. The bending stiffness of each triangular element is one half the bending stiffness of the quadrilateral element. The mass matrix is formed by treating the quadrilateral as four triangular elements. The stresses are the average of the stresses in each triangular element.¹²

Plate Bending-Membrane Element

Small deflection theory for plates leads to independence between membrane (inplane) forces and bending (out-of-plane) forces.¹¹ NASTRAN forms a plate bending-membrane element by overlapping the quadrilateral membrane element, QDMEM (composed of four overlapping triangular elements), and the bending quadrilateral, QDPLT (composed of four overlapping elements). Two plate-bending membrane elements are formed; QUAD1 in which the different material properties may be specified for bending, membrane and transverse shear, and QUAD2 which assumes a solid homogeneous cross section.¹³

The mass matrices may be formed by using the Lumped Mass or Coupled Mass Method for the bending stiffness. The Lumped Mass Method will be used for the membrane stiffness.¹²

Element stresses are available at any location away from the middle surface. Also bending stresses of the plate combined with the membrane stresses are available.

Beam Elements

The beam element (BAR) is derived assuming a straight beam loaded only at the ends and having uniform geometric and material properties along its length. The directions of the principle axis may be selected by the user and the ends of the beam element may be offset from the grid point to which the beam is attached. The connection between the beam end and the corresponding grid point may be released for any degree of freedom provided one degree of freedom remains.¹²

The stiffness matrix includes extensional, torsional, and bending in two planes. The bending stiffness also include a contribution due to transverse shear.¹²

Internal forces and moments are computed on the ends of the element. Stresses at each end due to bending at users specified points may be determined along with the average axial stress and the maximum and minimum extensional stresses.¹²

Lumped Mass and Coupled Mass Methods are available to transfer structural and nonstructural mass to the adjacent grid points. The center of gravity is assumed to lie on the elastic axis and the inertia affects due to offset ends of beams are neglected. The Coupled Mass Method does not include the effect of transverse shear on the mass matrix.¹²

3) Quarter Scale Underground Shelter Test

The data used to judge the finite element models came from a one quarter scale model test of an underground shelter (see Reference 4). The tests were conducted in order to verify procedures for predicting shelter response and shelter loading caused by an explosion on a covering burster slab (see Figure 7). In all 14 tests were run and a large amount of data were collected. For this investigation only the interface stresses from pressure gages on the top of the roof and the strain in the reinforcing steel from Test 1 and Test 2

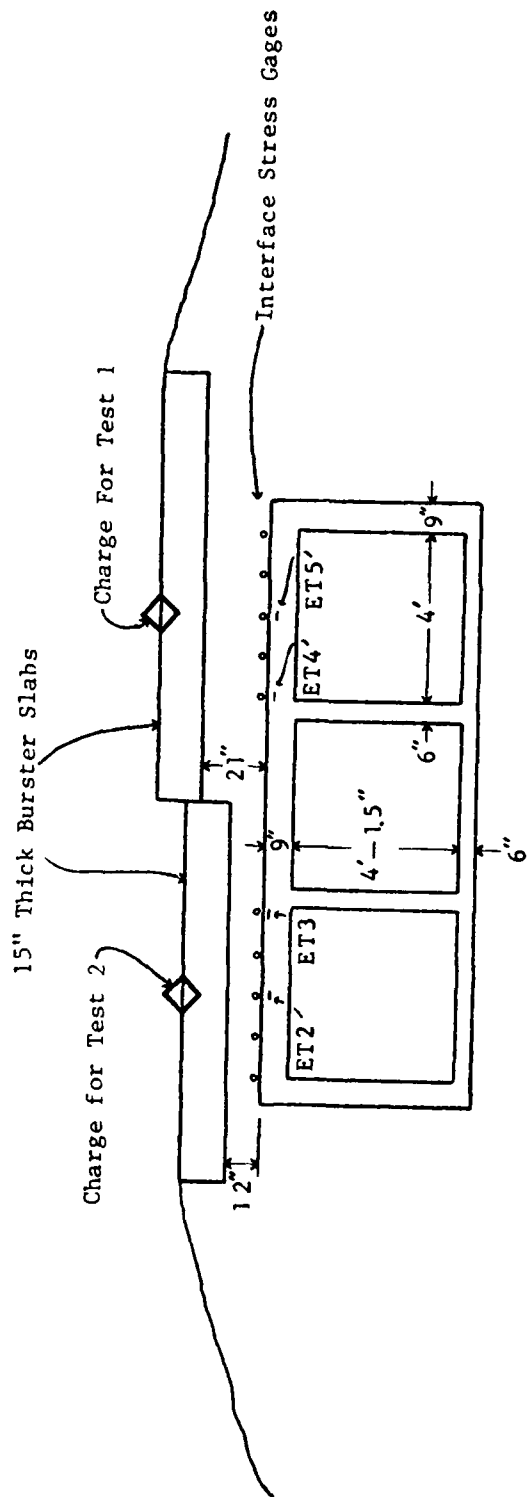


Figure 7
 Charge and Gage Locations for
 Test Shelter

SHELTER TEST 1
11 T33
200000. HZ CAL = 3809.

**

**

14291- 70 09/12/90 R0955

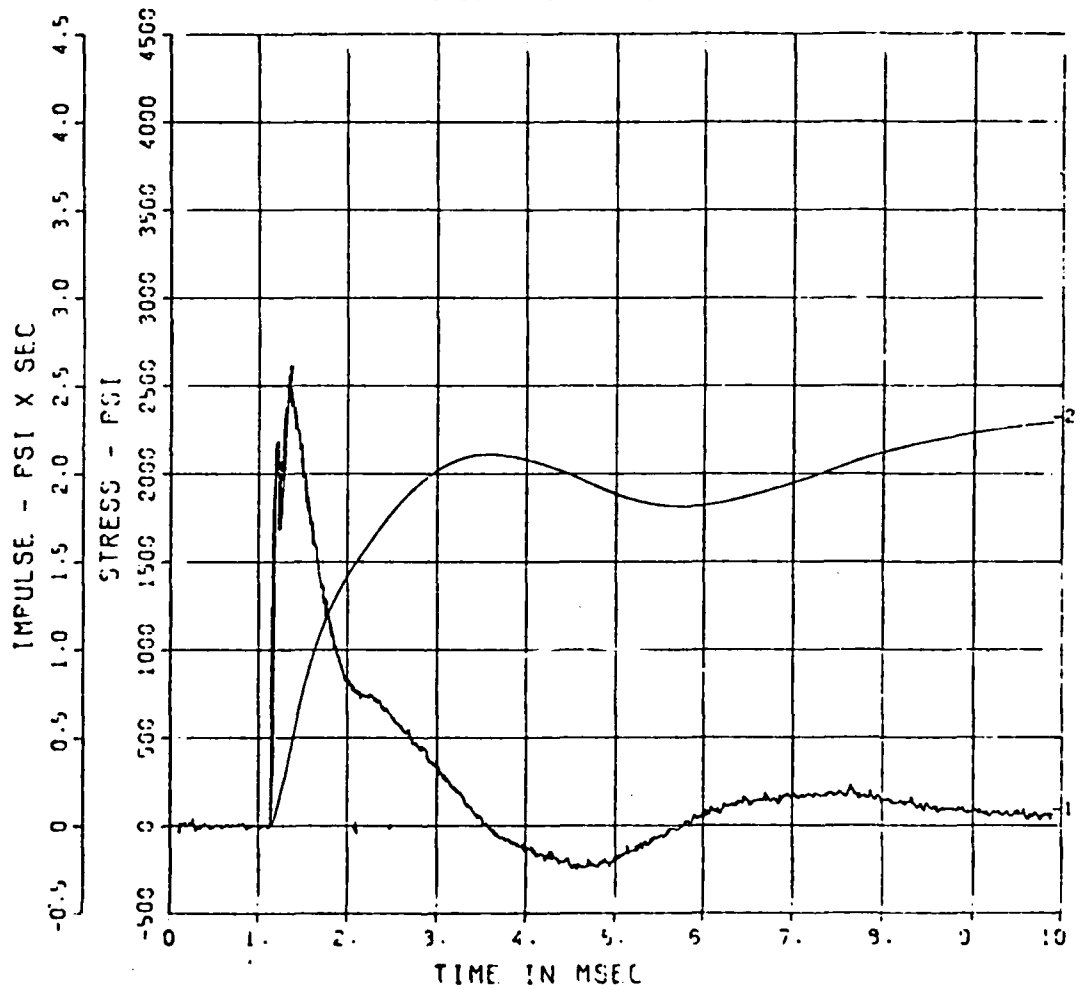


Figure 8
Typical Pressure-Time Curve from Shelter Test

SHELTER TEST 1

LT4

200000. HZ CAL= 2337.

LP4 70% CUTOFF= 30000. HZ

**

14201- 5 11/13/90 R0995

**

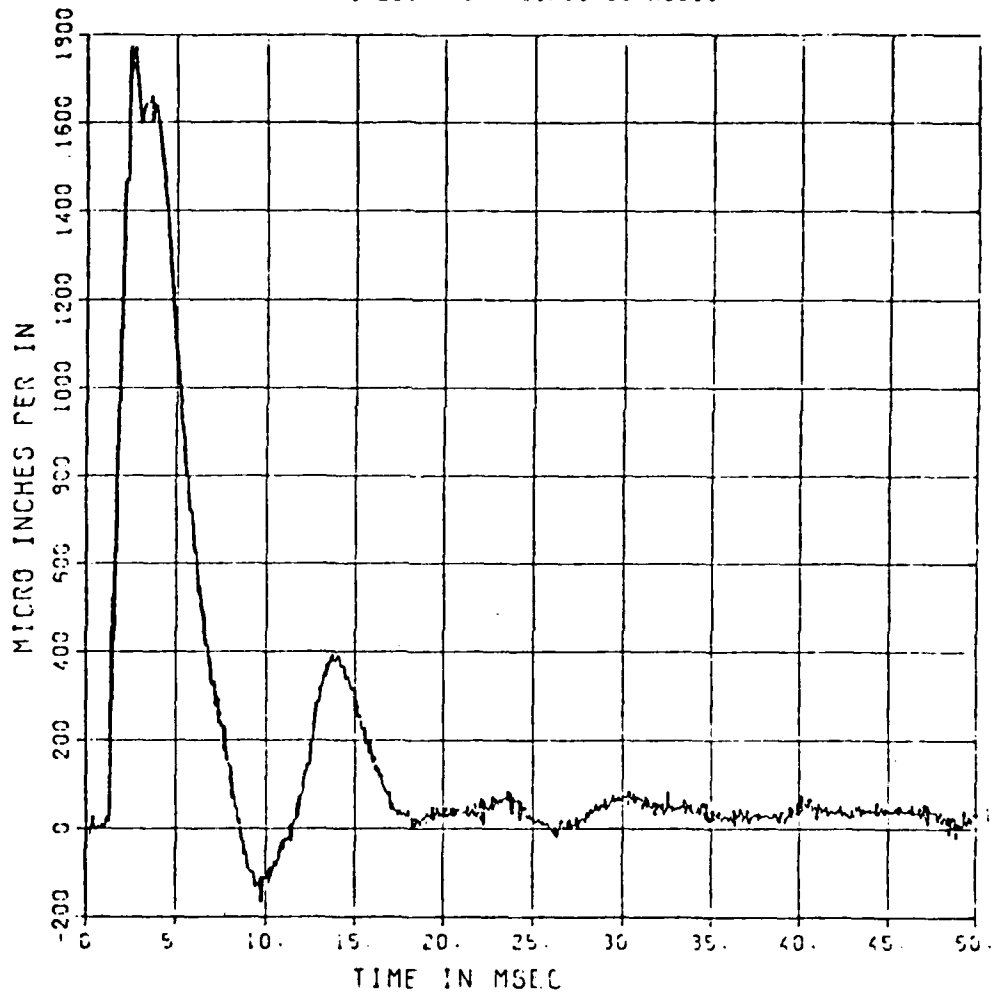


Figure 9
Typical Strain-Time Curve from Shelter Test

were used. A more detailed report on the test is being prepared and only preliminary data was available for this analysis.

Generally the pressure gages functioned well for both test and provided the loads for the finite element model. A typical pressure time curve is shown in Figure 8. The gage at the face of the exterior wall failed in Test 1 and the pressure from the gage at the face of the interior wall was substituted (see Figure 7).

The strain gage data was spotty because many gages failed under the high strain rates. Good strain data was available from Test 1 and 2 at the centerline of the roof span and at the face of the interior wall (see Figures 7 and 9). Since one gage was in a tension zone and the other was in a compression zone these two points were chosen to judge the accuracy of the computer models.

Table 13 contains the properties used in the finite element models. The section property data were incomplete and assumed values were used. The missing information was for the walls and floor so they should not be critical to the structural analysis.

The quarter scale test contained a weighted average for the interfaced pressure gages for each explosion. No information was given concerning how the weighted average was computed.⁴ This value was used for the Static Analysis Approaches.

4) Resistance-Deflection Functions

In response to externally applied loads a structural member deflects a sufficient amount to develop enough internal force to preserve equilibrium. These internal forces can be considered as an equivalent load, resistance, in the direction opposite the deflection. Since this equivalent load and the deflections are based on geometric and material properties, a graphical representation of resistance versus deflection can be drawn independently of the applied external loads.¹⁰

For a reinforced concrete member the initial response is elastic and the elastic response continues until the deflection is sufficient to cause first cracking in the tension zone. However, the nonlinearity induced by the initial cracks is neglectable and a linear resistance deformation function may be used until first yield in the reinforcing steel. After first yield in the reinforcing steel the response of a reinforced concrete member is termed elasto-plastic and sufficient cracking has occurred to require a reduced stiffness in order to model the response the reinforced concrete member. The upper limit of the elasto-plastic region is the formation of the first plastic hinge. From this point the members resistance will remain constant until incipient failure of the member occurs.¹⁰

The resistance deflection functions were calculated as described in Reference 10 except for the ultimate resistance of the reinforced concrete member. The equations given in Reference 10 to calculate the ultimate moment resistance of a reinforced concrete member neglect the contribution due to the compression concrete area. This would underestimate the strength of the concrete member in the elasto-plastic range. After enough rotation to cause crushing of the compression concrete area the equation given will accurately predict the ultimate capacity. The following equation was used to predict the ultimate capacity of the shelter.¹⁶

$$M_n = A_s f_y (d - a/2) - A'_s f'_s (d' - a/2)$$

in which

- A_s = tension steel area
- f_y = tension steel yield stress
- d = distance from compression face to centroid of tension steel
- d' = distance from compression face to centroid of compression steel
- A'_s = compression steel area
- f'_s = stress in compression steel
- a = depth of Whitney's stress block
- M_n = ultimate (nominal) moment

Concrete

$$E \approx 4.25 \times 10^6 \text{ psi}$$

$$G \approx 1.77 \times 10^6 \text{ psi}$$

$$\text{Poisson's Ratio} = 0.2$$

$$\text{Unit Weight} = 150 \text{ pcf}$$

$$\text{Unit Mass} = 0.000216 \text{ lb} \times \text{sec}^2/\text{in}^4$$

Steel

$$E = 29.0 \times 10^6 \text{ psi}$$

$$G = 11.2 \times 10^6 \text{ psi}$$

$$\text{Poisson's Ratio} = 0.3$$

$$\text{Unit Mass} = 0.000735 \text{ lb} \times \text{sec}^2/\text{in}^4$$

Soil

$$\text{Unit Weight} = 110 \text{ pcf}$$

Structural Element	Clear Span (in)	Thickness (in)	Flexural Depth (in)	Steel Area (in ²)
Roof	48	9	8	1.32 each face
Exterior Wall	48	9	8	1.32 each face
Interior Wall	48	6	*5	*0.66 each face
Floor	48	6	*5	*0.82 each face

* Assumed Values

TABLE 13
Material and Section Properties for Quarter Scale Model

1981 USAF - SCEEER SUMMER FACULTY RESEARCH PROGRAM

Sponsored by the

AIR FORCE OFFICE OF SCIENTIFIC RESEARCH

Conducted by the

SOUTHEASTERN CENTER FOR ELECTRICAL ENGINEERING EDUCATION

FINAL REPORT

AN ANALYSIS OF THE AVAILABILITY, ACCESSIBILITY

AND TIMELINESS OF COST DATA ASSOCIATED WITH

THE AFLC AIRCRAFT MODIFICATION SYSTEM WITH

EMPHASIS ON CLASS IV MODIFICATIONS

Prepared by: Dr. John E. Powell
Academic Rank: Professor
Department and University: School of Business
University of South Dakota
Research Location: Headquarters Air Force Logistics Command
Directorate Management Sciences (XRS)
Wright-Patterson AFB, Ohio 45433
USAF Research Colleague: Dr. William E. Dickison
Date: August 7, 1981
Contract No: F49620-79-C-0038

AN ANALYSIS OF THE AVAILABILITY, ACCESSIBILITY
AND TIMELINESS OF COST DATA ASSOCIATED WITH
THE AFIC AIRCRAFT MODIFICATION SYSTEM WITH
EMPHASIS ON CLASS IV MODIFICATIONS

by

John E. Powell

ABSTRACT

Modification of existing Air Force systems is receiving increased emphasis when faced with escalating costs of labor and materials associated with obtaining replacement systems. Approximately ninety percent of all modifications are designated Class IV and are concerned with safety of flight, mission essential and logistics as contrasted with Class V modifications which are designed to provide a new or improved capability. Approximately 80% of the Class IV modifications are IV-B, mission essential. It is not possible to budget all Class IV modifications required to maintain and update USAF aircraft. This research project looks at currently used allocation methods and observes several possible shortcomings. Suggestions are made for further research associated with the costing and prioritizing algorithms.

ACKNOWLEDGEMENT

The author would like to thank the Air Force Systems Command, the Air Force Office of Scientific Research and the Southeastern Center for Electrical Engineering Education for providing the opportunity to spend a very worthwhile and interesting summer at Headquarters, Air Force Logistics Command, Wright-Patterson Air Force Base, Ohio. The experience gained in the Management Science Division (XRSM) has been extremely rewarding.

Special thanks are given to Dr. William E. Dickison, XRSM Chief, for suggesting this area of research and for providing his guidance and expertise in bringing this project to fruition. Without his knowledge base, contacts, and accessibility this project would not have been completed.

Many other individuals provided information and support for this effort. Notable among these people are Mr. Billy Bishnow and Mr. Joe Loch.

I. INTRODUCTION:

The Air Force serves a continuing role of providing for operational readiness and capability of the aircraft and missiles within its inventory. To maintain a posture of being at the forefront of technological breakthroughs and innovations requires the obtaining of new systems or the updating of present systems through modifications.

Modification of existing systems is receiving a great deal of interest because of the perceived and/or actual cost savings realized when compared with the purchase of replacement systems. Considerable emphasis is placed on this approach in an effort to be good stewards of the resources assigned to the Air Force. This is particularly relevant during periods of high inflation when increasing labor and material costs force the acquisition price of new systems to increase many-fold over original equipment prices.

A modification is described as a change in the physical configuration or in the functional characteristics of a system or unit of equipment. There are five classifications numbered I - V, as described in AFR 57-4. This paper will be concerned only with Class IV modifications which account for approximately ninety percent of all modifications.

Class IV modifications are subdivided into three categories:

- 1) Class IV-A: modifications required to ensure safety of personnel, systems or equipment by eliminating physical hazards.
- 2) Class IV-B: modifications necessary to correct a deficiency including changes that affect reliability and maintainability.
- 3) Class IV-C: modifications required for improved logistics support.

II. OBJECTIVES OF THE RESEARCH EFFORT:

A major objective of this research effort was to develop a basic understanding of the Class IV modification process. As a result of

studying the present system, an ancillary objective was to determine possible areas for which further study might prove beneficial. Two computer models were studied and observations are made regarding possible enhancements.

The Class IV modification process is displayed on Figure 1. The left side of the flowchart shows the initiation and justification of a proposed Class IV modification by the using command. The justification must accompany the proposal to the approving authority. Among elements of information to be included are:

- a) Essentiality to mission accomplishment.
- b) Improved safety of operation.
- c) Compatibility with other approved and proposed modifications.
- d) Anticipated cost.
- e) Resultant increase or decrease in O&M requirements; systems effectiveness, reliability, survivability, vulnerability or maintainability.
- f) Requirement for training support.
- g) Requirement to modify trainers, training equipment, and simulators.
- h) Expected logistics support benefits.

An AFLC Form 775, USAF Class IV Modification Budgetary Requirement, must be prepared for each proposed modification. The operating commands conduct annual prioritization reviews by individual weapon system and forward AFLC Form 775s to AFLC for review and integrated prioritization. The ALCs prepare an AFLC Form 48, Configuration Control Board Item Record, to completely definitize the modification proposal. These Form 48s are normally prepared after modifications are programmed but they can be prepared concurrent with the Form 775s depending upon the urgency of the requirement. The Configuration Control Board (CCB) for an ALC reviews all modifications proposed by its command.

The AFLC CCB conducts periodic meetings to review and evaluate all Class IV modifications in accordance with current policy. They are to expedite safety modifications that could ground airborne systems or inactivate ground systems. When AFSC has engineering, development, or

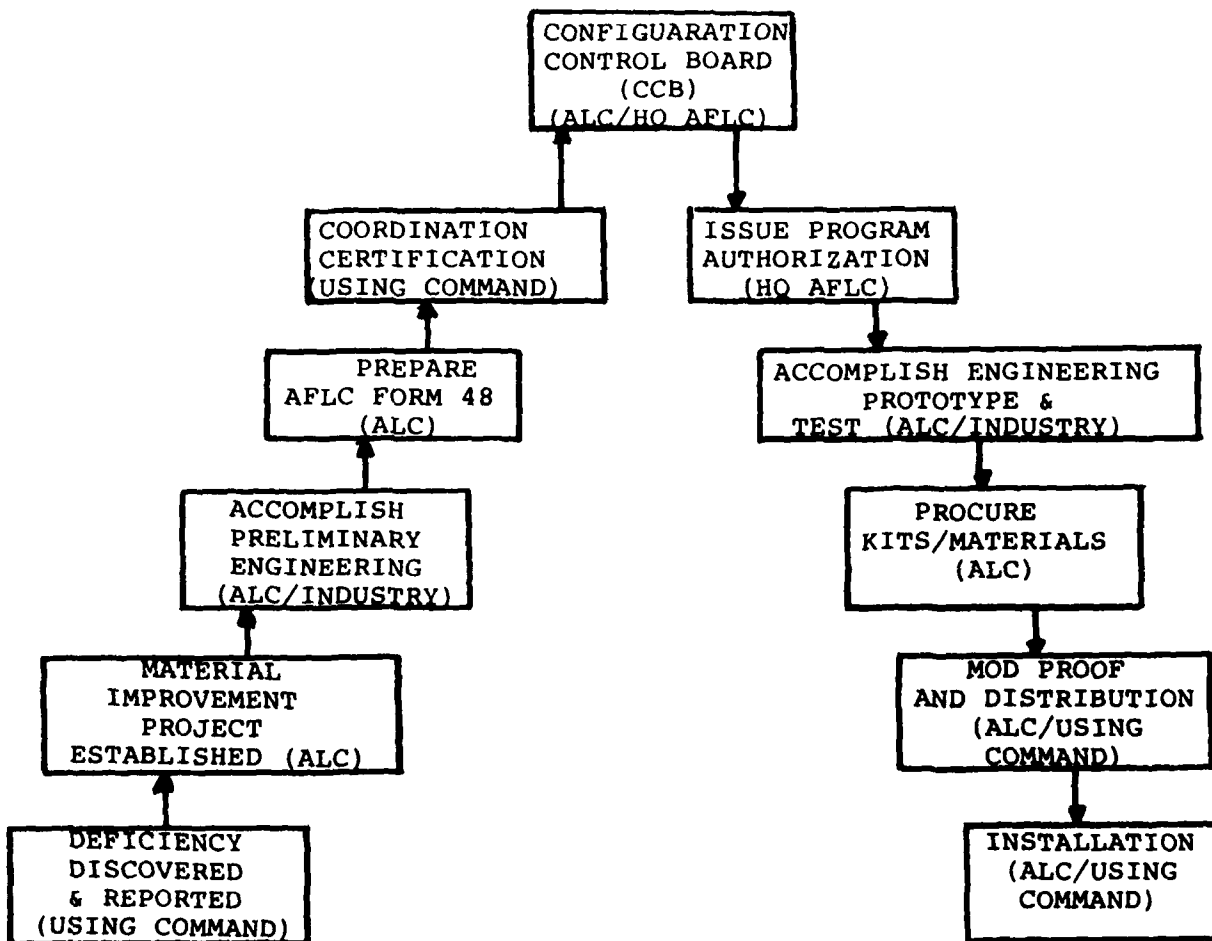


FIGURE 1: CLASS IV MODIFICATION PROCESS
(SUBJECT TO ESTABLISHED \$ LIMITS)

production tasks in support of an AFLC-managed modification program, AFLC helps prepare the technical specifications and makes the final decision, within dollar constraints, on program changes that affect equipment interfaces, costs and schedules. The Air Staff makes the final decision on all high cost modifications.

AFLC will prepare an integrated Class IV Modification Priority System which is an automated system that determines, for budgeting/funding purposes, the priority of aircraft Class IV modifications within and between Weapon Systems. The Modification Priority System is based on eighteen weighted parameters. A numerical value is assigned to each parameter and when all aircraft modifications are processed through the priority system, each modification accumulates a total point value. The modifications are then ranked from highest to lowest priority based on total points accumulated. It should be noted that simulator compatibility modifications carry the same priority as the associated Weapon System.

It is felt that the automated Class IV Modification Priority System helps to ensure that the most essential modifications receive funding in the Budget Year. The System is designed to provide an unbiased approach to the establishment of priorities for all operating commands' Class IV modifications. The parameters within the prioritization system are composed of modification process, cost and capability factors. Of crucial importance are the accuracy and timeliness of the data input to the model and the weightings applied to the model parameters. This importance is underscored by recognizing that not all Class IV modifications can be funded. For example, as noted in AFLMC Project 780303-1, there were 40 Class IV aircraft modifications not approved in the FY79 Modification Budget and 49 modifications not approved in the FY80 Modification Budget. Therefore, it is imperative that the Air Force apply the available budget effectively to obtain the most in safety, reliability, and maintainability from each modification dollar spent.

III. CLASS IV MODIFICATION MODELS OBSERVED:

In order that Class IV modifications compete on a consistent level, it is important that the most current data be utilized.² There are two models which might contribute at a significant level to this end. The first model is used for estimating development and procurement costs of aircraft while the second model is the Class IV Modification Prioritization System.

A computer model for Estimating Development and Procurement Costs of Aircraft (DAPCA-III) is a program developed by RAND which is intended to be useful to cost analysts and others who are concerned with the estimation and analysis of aircraft development and procurement costs.⁴ The model applies parametric estimating relationships to calculate the development and procurement costs of two major flyaway subsystems of the aircraft: airframe and engines. Avionics costs are included in the model but are not derived parametrically. The computer program calculates cumulative average, unit, and total flyaway costs for up to ten specified aircraft production quantities. Flight test costs are also calculated. A learning-curve slope is incorporated in order to obtain avionics production costs for specified aircraft quantities. The present system is run in batch mode.

The second computer model is the Class IV Modification Prioritization System.⁷ The objective of this program is to prioritize Class IV aircraft modifications both within and between weapon systems in a consistent manner. There are 18 parameters within the prioritization system which deal with modification process, cost and capability factors. A weight is assigned to each parameter so that as a modification is processed through the system it accumulates a total of all parameter values to provide the modification with a priority index. The modifications are ranked from highest to lowest based on this weighted index.

The weights built into the model were selected as a result of a sensitivity analysis process. Four different weighting systems were

analyzed using randomly selected Class IV modifications submitted for the FY80 budget. As a result of this analysis one of the weighting systems was selected and implemented.

In order to track and account for all aircraft modifications AFLC might consider establishing a computerized baseline of all aircraft as they currently exist and of all update changes as they occur. This could readily be accomplished through the CREATE network which is available at the ALCs as well as AFLC headquarters.

IV. OBSERVATIONS FOR POTENTIAL FUTURE STUDY:

Two potential areas worthy of further study are the computer model for Estimating Development and Procurement Costs of Aircraft (DAPCA-III) and the Class IV Modification Prioritization System. Observations will be made about each of these models.

The DAPCA-III model currently runs in batch mode and allows for the input of up to sixty four variables. These variables include: various costs (engineering, tooling, manufacturing and quality control), quantities (number of flight-test aircraft, airframe production quantities, number of engines), various learning curve slopes, labor hours, etc.

It is difficult to keep the model primed with current cost data. However, with the anticipated installation in the first quarter of 1982 of a significantly more powerful Central Processor Unit for the CREATE system, it should be possible to develop an on-line capability. This would allow developing in-house cost estimates of modifications and would afford the analyst an opportunity to "fine-tune" the model by iterating through different values of selected variables.

Rather than depend upon specific vendors to provide cost estimates for proposed modifications, the analyst can obtain current information relative to, e.g., engineering production salaries, through such sources as the Aerospace Industries Association of America, Inc. of

Washington, D.C. Using such independent data sources would enable the Air Force to develop their own cost estimates which can then be compared with those submitted by vendors.

The Class IV Modification Prioritization System lends itself to further study particularly in the area of the weights assigned to the eighteen parameters in the model. The current version is a result of analyzing four separate models where each was a slight variation of the others. For example, the four weighting systems are referred to as Method #1, Method #2, Method #3 and Method #4. Method #2 and Method #3 are identical to Method #1 except that one priority parameter value increased by a factor of 1.5 in Method #2 and by 3.0 in Method #3.

Further sensitivity analysis can be applied to this model to further explore the interactions of the parameters.

REFERENCES

1. S. Baily and R. Gilbertson, "Aircraft Modification Management Evaluation," ARINC Research Corporation, December 1980.
2. Elvis M. Baker, William H. Burgess and Albert F. Malkiewicz, "An Investigation of Cost Factors Relating to Class IV Aircraft Modifications," Thesis presented to AFIT, Air University, August 1973.
3. J. L. Birkler and J. P. Large, "A Method for Estimating the Cost of Aircraft Structural Modification, RAND, March 1981.
4. H. E. Boren, Jr., "A Computer Model for Estimating Development and Procurement Costs of Aircraft (DAPCA-III)," RAND, March 1976.
5. Allen Fatkin, "Generic Inflation Indexes for Weapon Systems," AFSC CAIG Research Report NR1, June 1980.
6. Frankie A. Kubecka, "Class IV Modifications: Problems in Improving Existing Weapon Systems and Equipment," Thesis, Air Command and Staff College, Maxwell AFB, May 1978.
7. R. Smith and T. Taylor, "Class IV Modification Prioritization System," AFLMC Project 780303-1, August 1979.
8. _____, "Improved Management of Air Force Modification Programs Can Save Millions," GAO Report to the Secretary of Defense, March 1981.
9. AFLCR 57-21, "Operational Requirements: Modification Program Approval," April 1979.
10. AFLCR 66-15, "Equipment Maintenance: Product Performance," July 1980.

11. AFR 57-4, "Operational Requirements: Modification Program Approval," December 1977 (Revision June 1981).
12. AFR 173-13, "Cost Analysis: USAF Cost and Planning Factors Regulation," February 1981.
13. _____, "Professional Income of Engineers (1980)," Engineering Manpower Commission, November 1980.
14. _____, "Component Support Cost System (CSCS)," Final Draft Users Manual, Prepared by the CSCS Project Office (HQ AFLC/LO (VAMOSC)), June 1981.

1981 USAF-SCEEE SUMMER FACULTY RESEARCH PROGRAM

Sponsored by the

AIR FORCE OFFICE OF SCIENTIFIC RESEARCH

Conducted by the

SOUTHEASTERN CENTER FOR ELECTRICAL ENGINEERING EDUCATION

FINAL REPORT

THE AIR FORCE WRIGHT AERONAUTICAL LABORATORIES

RESEARCH AND DEVELOPMENT PLANNING PROCESS

Prepared by:	Dr Robert H. Puckett
Academic Rank:	Professor
Department and University:	Department of Political Science Indiana State University
Research Location:	Air Force Wright Aeronautical Laboratories Integrated Plans Group
USAF Research Colleague:	Dr James T. Van Kuren
Date:	July 27, 1981
Contract No.:	F49620-79-C-0038

THE AIR FORCE WRIGHT AERONAUTICAL LABORATORIES
RESEARCH AND DEVELOPMENT PLANNING PROCESS

by
Robert H. Puckett

ABSTRACT

The AFWAL research and development planning process is investigated from the viewpoint of political science. Suggestions are offered concerning how AFWAL could interface more effectively with the external environment. The results of interviews with Air Force and Department of Defense officials in Washington, D.C., are presented. The contention is made that Air Force research and development planning must be integrated with (a) international political forecasts and (b) international context analysis. Suggestions for further research in this area are offered.

Acknowledgments

The author would like to thank the Air Force Systems Command, the Air Force Office of Scientific Research, and the Southeastern Center for Electrical Engineering Education for providing him with the opportunity of serving for ten weeks with the Integrated Plans Group at the Air Force Wright Aeronautical Laboratories, Wright-Patterson AFB, Ohio.

In particular, he would like to thank Dr. James T. Van Kuren, Robert H. Johnson, and Wilbert J. Uhl for their guidance and assistance.

I. INTRODUCTION:

For several years, I have been interested in the planning process. I have conducted research in the field of foreign policy planning. I have been an active participant in health resources planning, as a member of the Board of Directors of the Southern Indiana Health Systems Agency and its Project Review Committee.

My areas of teaching experience include international politics, American foreign policy, and American national security policy. I have been active in several professional groups dealing with military and national security issues.

With these interests, I felt that I could contribute--as a political scientist--to the defense research and development planning process. In particular, the Integrated Plans Group at the Air Force Wright Aeronautical Laboratories (AFWAL) offered me the opportunity to assess the functions, reports, and analyses of its planning efforts. The four Laboratories at AFWAL recently were reorganized under a central headquarters staff. This event necessitated developing the expertise to plan inter-laboratory projects and to aggregate all aspects of the operations of the Laboratories.

II. OBJECTIVES OF THE RESEARCH EFFORT

The two major goals of my research activities included efforts to analyze the AFWAL planning process from the viewpoint of a political scientist and to contribute my suggestions concerning how AFWAL could interface more effectively with the external environment.

In pursuing these objectives, I assessed internal AFWAL planning documents, read general works on technological forecasting and planning, and conducted interviews of Air Force and Department of Defense officials in Washington, D.C., about research and development planning activities.

III. AFWAL PLANNING

A. Introduction

As a political scientist reviewing the AFWAL research and development planning process, I was struck by the fact that it is almost entirely a budget-oriented system. I realize, of course, that program budgeting provides, in financial terms, planning infor-

mation and control as well as represents the objectives of the organization. But I expected to see unclassified reports, analyses, and briefings which related current and projected research and development efforts to the international context (political, economic, military, and ecological trends). It also would have been interesting to see assessments of the foreign policy implications of various military technology developments.

Other areas which could be emphasized to a greater degree would include background papers on technological forecasts concerning various types of military weapons, long-range corporate plans, establishing effective interface with the foreign policy and defense community (other than government and the aerospace industry), and cultivating relationships with more non-military Executive Branch and Congressional agencies.

B. Planning

Every organization must, of necessity, plan--relate current actions to prospective consequences and objectives. Through the most effective and efficient employment of available resources, the planner attempts to shape the future according to conscious preferences. It is essential that planning be responsive to the goals of the organization; this requires, as a first step, delineating corporate objectives and developing a consensus supporting them. These corporate goals must balance but not suppress the variety of interests of subdivisions within the organization.

Research and development planning involves considerable uncertainty--relating to cost, potential payoffs, and timing of projects. One of the planner's functions, then, is to help the decisionmakers choose the right risks. The planning process should not only attempt to solve technical problems but also to discover opportunities.

Comprehensive planning involves the following steps: (1) identify and assess opportunities, (2) recognize and examine problems, (3) clarify and analyze goals and objectives, (4) decide which goals and objectives are most important, (5) evolve programs of action, (6) allocate sufficient resources, and (7) develop and maintain acceptance and support for goals, objectives, and programs.

C. Integrated Planning

Integrated planning is essential for developing an AFWAL corporate plan, inasmuch as there are many distinct programs at each of the four Laboratories in addition

to several interlab programs. The objective is to develop a plan which: (1) aggregates all aspects of the operations of the four Laboratories (technical, financial resources, manpower, and facilities) in order to assess the relevance and sufficiency of the programs; (2) integrates strategic and operational planning; and (3) combines short, medium, and long-range time spans. The integrated planning incorporates technological forecasts (or "roadmaps") which establish the contribution and interrelationships of each exploratory, advanced, and engineering development in each program and project resources and time spans.

AFWAL integrated planning is documented in a format conducive to developing a master plan (Vanguard) of research and development needs and programs within the Air Force Systems Command. In systems analysis terms, each research and development activity is a "subsystem" performing a mission task.

From the viewpoint of political science, the weakness of AFWAL integrated planning is that the unclassified rationale of programs is not wholly multidimensional. It does not integrate the international political, economic, and ecological dimensions with Air Force estimates of military threats.

D. Corporate Planning

Corporate planning is the process of determining the long-range objectives of the organization. Inasmuch as all organizations have multiple goals, the problem of planning is to assure a proper balance among these objectives. This is difficult to do since resources are limited and estimating external threats is uncertain.

Corporate planners continually assess both system requirements and technological opportunities by projected forecasts. They assure that pertinent views are fairly presented; this lays the groundwork for managerial consensus-building within the organization.

The hierarchy of corporate goals is subject to frequent change, since external events alter the relative importance of objectives. Planners must rebalance the range of goals by taking account of shifts in external events and obligations. This requires a comprehensive understanding of hostile economic, political, and military threats and of foreign defense capabilities. Such analysis of the international context is important because these trends and events in world affairs impact on specific policy choices, programs, and organizational agendas.

In effect, corporate planning forecasts--and guides--the evolution of the institution itself. This includes an assessment of changing organizational structures,

shifting patterns of resources, inter-institution relationships, and adaptation to both domestic and foreign problems and opportunities.

E. Technological Forecasting

The AFWAL planning process incorporates technological forecasting into its program budgeting system. It predicts, in a given time frame, technical achievements that could be expected for a stated level of budgetary and manpower support. In particular, AFWAL integrated planning is a systems approach to research and development: it evolves targets for the growth of technological projects across two or more Laboratories by mapping out the elements of the projects and assessing the relationships between these elements.

The future contains an almost infinite number of technical threats and opportunities that could impact upon decisionmakers. Technological forecasting attempts to project those with the greatest probability and potential effects. This requires two types of projections: (1) potential needs and (2) stages of technological development.

Technological forecasting is crucial to defense research and development planning. Planners translate goals and missions into technological development projections to meet documented, probable, and possible technical threats. In turn, these forecasts are continually modified by the alternative courses of action presented by planners. At each decision point, the policymaker selects a technical solution he desires, having been informed by planners what obstacles must be overcome in order to achieve the results he seeks.

Technological forecasts feed back into estimates of the changing international environment, since technical innovation is influenced as to direction, timing, and application by external events. In essence, the technical future will be a part of the international environment. National technological development is a critical determinant of the economic, military, and political strength of countries and regions. Technological forecasts are important to defense decisionmakers, since they must be aware of significant shifts in the relative technological capacity of various nations and regions.

These predictions must be integrated with both long-range planning activities and political forecasts. It would be useful if AFWAL would develop both in-house and contracted forecast background papers. For example, one interesting study would be the foreign policy implications of the tendency to procure relatively few costly high technology weapons rather than larger numbers of less sophisticated ones. Another possibility would be an analysis of the impacts of natural resources denial on both military technological development and the international political position of the United States.

F. International Context Analysis

The function of planning is to achieve a proper balance among goals, in terms of current and projected resources allocated to these objectives, in the context of future external obligations and events. It is simply impossible to perform this task without continual analyses of the international context--political, economic, military, and ecological.

Over the past decades, revolutionary alterations in the international system have begun to appear. The growing interdependence of the system makes long-range planning imperative. It has become much more difficult to assess developments in a systems theory context because of the increasing complexity of interrelationships. Further, regional confrontations potentially become "flash points" which can trigger system-wide conflicts.

AFWAL planning continually assesses technical threats to our defense capabilities. This is done through technical threat scenarios and forecasts. These studies identify operational needs and deficiencies as well as suggest technical solutions in the near and long term. Options for future system designs and the prevention of technological surprise constitute the principal outcomes of such emphases.

The USAF Planning Concepts forecasts the future strategic environment, including political, social, scientific, technological, and military developments. However, sanitized portions of these assessments are not integrated into AFWAL unclassified planning documents. It seems to me that this is a very serious deficiency in AFWAL research and development planning.

International context analysis is based upon an assessment of the adversary's military and political intentions as well as his military capabilities. This must be the case since deterrence centers around intentions--not simply estimating enemy intentions but also influencing them.

AFWAL's capacity to engage in effective international context analysis would be enhanced by adding two planners to the staff: (1) a social scientist, who would assess international events and Congressional activities, prepare background papers on topics such as the impacts of international technology flows, and conduct literature searches and analyses in social science aspects of technology and in the fields of public administration and business management and (2) an intelligence analyst who would conduct briefings on international political and military developments and organize an intelligence report reading room for AFWAL personnel. In addition, perhaps some international context analyses and political forecast reports could be contracted out.

G. Analysis of Selected Internal Documents

After a review of unclassified internal planning and program documents, I concluded that AFWAL does an excellent job of presenting its programs--in budgetary and technological forecasting ("roadmaps") terms. However, the Program Book and the various briefings virtually ignore a central element of defense research and development planning: international context analysis.

Of course, this analysis is done at other levels of the Air Force and the entire defense structure. (Joint Intelligence Estimate for Planning; Joint Long Range Estimative Intelligence Document; Joint Strategic Capabilities Plan; Joint Long Range Strategic Study; Joint Strategic Objectives Plan; Joint Research and Development Objectives Document; USAF Planning Concepts; and AF SC Technology Planning Guide).

But I contend that it is essential for this analysis--couched is unclassified language--to be integrated into the rationale for AFWAL programs. The Program Book and various briefings seem disembodied, without narratives about the international political, military, and economic contexts of the technological programs being described. I shall cite some examples of the lack of international context analysis. The 1981 AFWAL Program Book could have been improved by adding more narrative--such as a "Security Framework Section," which, for example, could have discussed the security implications of avionics with regard to NATO defense, arms control, rapid deployment, and space defense. In addition to discussing the physical characteristics of strategic bombers, the report could have analyzed the arguments concerning the need for bombers in the late 1980's and beyond.

In the Avionics Laboratory Program Book description of high speed micro-signal processors, there could have been an analysis of the extent to which the processors would make Soviet submarines more vulnerable--and, assuming that the Soviets are developing this technology, to what extent would the US SLBM systems become vulnerable?

The Materials Laboratory Program Book neglected the opportunity to discuss the international political implications of the area of "critical/strategic materials" as well as of synfuels and fuels from alternative sources.

The December, 1980, Technical Objectives Document (FY 1982) of the Flight Dynamics Laboratory mentioned the importance of "USAF requirements" and "stated objectives," but it did not present any background on these needs. Neglecting to do so weakened the rationale in the document; an analysis of the international political and military contexts would have made the case more compelling.

In responses to technology need reports, there is no international context analysis when the "state-of-the-art/evaluation of technology need" is described. Here again, it would seem that the report would be enriched by such assessments.

The Tactical Night in Weather--An AFWAL Major Thrust (TMT) preliminary briefing paper is a good example of an integrated technology planning exercise. It assesses the interaction of related technologies and forecasts the future needs of research and technology to solve problems of tactical night/in weather attack aircraft. The rationale would have been more forceful, however, if there had been an unclassified narrative of the scenarios in which such aircraft could enhance U.S. strategic interests.

An external document--the Technology Base portion of the FY 82 RDT&F Posture Statement--discussed rapid solidification technology without expanding upon the very significant international political and economic implications of reducing our dependence on foreign sources of critical materials. In addition, its section on chemical warfare defense neglected to assess U.S.-Soviet postures on controlling chemical warfare capabilities. Thus, even higher level documents occasionally evade in-depth international context analysis.

IV. INTERFACE

In addition to its substantial interface with various military organizations and with NASA, AFWAL should begin a more extensive interface program with Congress, Executive Branch agencies, and the foreign policy and defense community. I will list some Congressional subcommittees and organizations with which AFWAL could establish some ongoing relationships--such as exchanging reports, establishing internship programs, and convening technology conferences.

U.S. Senate: (1) Appropriations Committee: (a) Defense Subcommittee; (2) Armed Services Committee: (a) Tactical Warfare Subcommittee and (b) Strategic and Theater Nuclear Forces Subcommittee; and (3) Commerce, Science, and Transportation Committee: (a) Aviation Subcommittee and (b) Science, Technology, and Space Subcommittee.

U.S. House of Representatives: (1) Appropriations Committee: (a) Defense Subcommittee; (2) Armed Services Committee: (a) Research and Development Subcommittee and (b) Procurement and Military Nuclear Systems Subcommittee; (3) Foreign Affairs Committee: (a) International Security and Scientific Affairs Subcommittee; (4) Public Works and Transportation Committee: (a) Aviation Subcommittee; and (5)

Science and Technology Committee: (a) Science, Research, and Technology Subcommittee, (b) Space Science and Applications Subcommittee, and (c) Transportation, Aviation, and Materials Subcommittee.

There are four Congressional organizations with which it would be useful for AFWAL to exchange reports and to establish internship programs. They include:

(1) General Accounting Office: (a) Defense Programs Planning and Analysis Staff; (b) Procurement, Logistics, and Readiness Division; and (c) International Division.

(2) Congressional Budget Office: (a) Assistant Director for National Security and International Affairs.

(3) Congressional Research Service: (a) Foreign Affairs and National Defense Division and (b) Science Policy Research Division.

(4) Office of Technology Assessment: (a) Energy, Materials, and International Security Division and (b) Science, Information, and Natural Resources Division.

In addition, AFWAL should increase its interface with Executive Branch agencies other than those in the defense community. For example:

(1) National Science Foundation: (a) Assistant Director for Scientific, Technological, and International Affairs: 1) Division Director, Science Resources Studies and 2) Division Director, Industrial Science and Technological Innovation and (b) Assistant Director for Engineering.

(2) Department of State: (a) Bureau of Oceans and International Environmental and Scientific Affairs: 1) Deputy Assistant Secretary for Science and Technology Affairs: a) Director, Office of Advanced Technology, b) Director, Office of Cooperation Science and Technology Programs and c) Director, Office of Science and Technology Support.

(3) Department of Transportation: (a) Office of Transportation Research and Technology and (b) Office of Technology Sharing.

(4) Department of Energy: (a) Assistant Secretary, Defense Programs.

AFWAL has substantial interface with the scientific and engineering communities and with the aerospace industry. I believe that it would be important to establish more contact with the foreign policy and defense community. I would suggest three key groups with which AFWAL could begin an interface program: (1) International Studies Association: (a) Military Studies Section; (2) American Society for Public Administration: (a) Section on National Security and Defense Administration; and (3) the Inter-University Seminar on Armed Forces and Society.

Interface with the foreign policy and defense community could take the form of periodic briefings, organizing professional meeting panels, and presenting papers at professional conferences.

A crucial component of interface is the internship experience: public involvement in AFWAL programs and AFWAL personnel on short-term assignments in other organizations. The summer faculty research program should be expanded with the inclusion of social scientists, business school professors, and financial planners. Staff personnel from Congressional committees as well as from the Congressional Research Service, Office of Technology Assessment, General Accounting Office, and Congressional Budget Office should be encouraged to serve short-term assignments in AFWAL.

A summer internship program for social science and business school graduate students--in addition to science and engineering graduate students--should be encouraged. In addition, AFWAL should institute a Congressional Fellow Program--in which AFWAL planners, scientists, and engineers could serve short-term assignments in Senate and House offices, on committee staffs, or on the staffs of the CRS, OTA, CBO, and GAO. Many Executive Branch agencies have Congressional Fellow Programs.

AFWAL should broaden the current foreign scientific exchange program of the Laboratories to include periodic exchanges of planners.

Civilian professional staff education is another area in which interface can be enhanced. The existing Sloan Fellowship program and Federal Executive Institute program should be used for the planning staff members. In addition, every effort should be made to include planners in periodic professional development courses (management, as well as national security issue, courses) at the Air University and the joint Service schools: National Defense University, National War College, Industrial College of the Armed Forces, and Armed Forces Staff College. AFWAL should consider hiring a public affairs officer to oversee existing interface programs as well as those additional ones suggested herein. This official also could arrange for periodic public television and cable television documentary programs about AFWAL activities.

V. SUMMARY OF RESULTS OF INTERVIEWS WITH AIR FORCE AND DEPARTMENT OF DEFENSE OFFICIALS IN WASHINGTON, D.C.

I interviewed 13 officials in the Air Force Systems Command, Air Force Office of Scientific Research, Defense Advanced Research Projects Agency, Office of the Under Secretary of Defense for Research and Engineering, and the Office of Deputy Chief of Staff of the Air Force for Research, Development, and Acquisition. There was a consensus among a majority of the respondents on the following aspects relating to research and development planning:

(1) It is essential for the Air Force to conduct in-house research in order to meet its future technological needs.

(2) Supporting a broad spectrum of research is the ideal, since we can never be sure about the payoff of each project.

(3) There are several difficulties involved in advocating R&D programs to the Air Force, DoD, and Congress:

(a) Effects of the domestic political environment during and immediately after the war in Southeast Asia were deleterious.

(b) Descriptions of R&D projects are too technical for Congressmen and their staffs. In addition, the narrative should describe accomplishments in terms of missions.

(c) Basic research programs are often delayed, since they do not seem to be compelling. This general area has been maligned by the "golden fleece" award. The public--and many top government officials--do not understand the nature of basic research.

(4) Long-range (or corporate) planning is not being done, and most respondents emphasized the inherent difficulty ~~of~~ moving in that direction. They agreed, however, that a set of long-term goals is essential to the rational allocation of resources for R&D.

(5) What passes for planning is basically programming and budgeting.

(6) International political forecasts should be folded into the R&D planning process, although there was disagreement about what level in the Air Force should be responsible.

(7) Various divisions of the Air Force should send briefing teams to professional and community groups to discuss the nature and payoffs of R&D. This is a very important long-term educational effort.

A number of interesting points were made by individual respondents. For example:

(1) Air Force Laboratories should concentrate R&D in those areas in which universities have little or no interest.

(2) Recent reports of AFOSR, DARPA, and the Rocket Propulsion Laboratory were cited as good examples of well-written--and well-received--explanations of R&D projects.

(3) The Air Force R&D planning process needs the input of social science analysis. For instance, DL should consider using some social scientists and intelligence analysts to look at future needs.

(4) A high-level advisory board should determine the most effective long-range mix of spending and activities in R&D for the Air Force.

(5) The Rocket Propulsion Laboratory was described as incorporating international political forecasts into its planning process.

(6) Informal educational sessions with Congressional staff analysts would be helpful in building long-term support for important R&D programs.

(7) The Air Staff is making some progress in developing a corporate plan, but AFSC may not succeed in fashioning one in the next couple of years.

VI. RECOMMENDATIONS

I would like to recommend that AFWAL:

(1) Relate current and projected research and development efforts to the international context (political, economic, military, and ecological trends).

(2) Prepare background papers on topics such as the foreign policy implications of various military technological developments, impacts of international technology flows, and technological forecasts.

(3) Concentrate more staff time on developing long-range corporate plans.

(4) Make the integrated planning process more multidimensional by enhancing the rationale for AFWAL programs. The unclassified narrative should integrate the international political, economic, and ecological dimensions with Air Force estimates of military threats.

(5) Hire a social scientist planner, who would:

(a) Monitor international events and Congressional activities,

(b) prepare background papers on topics such as the impacts on natural resource denial on both military technological development and the international political position of the United States; and

(c) *conduct literature searches and analyses in social science aspects of technology and in the fields of public administration and business management.*

(6) Hire an intelligence analyst who would present briefings on international political and military developments and organize an intelligence report reading room for AFWAL personnel.

(7) Establish effective interface with non-military Executive Branch agencies, Congress, and the private sector foreign policy and defense community:

(a) Develop some ongoing relationships--such as exchanging reports, establishing internship programs, and convening technology conferences--with a variety of Senate and House subcommittees listed in the text and with the General Accounting Office, Congressional Budget Office, Congressional Research Service, and Office of Technology Assessment,

(b) increase interface with the National Science Foundation, Department of State, Department of Transportation, and Department of Energy,

(c) create a pilot program of interrelationships with the American Society for Public Administration, International Studies Association, and Inter-University Seminar on Armed Forces and Society,

(d) expand the summer faculty research program,

(e) institute a Congressional Fellow program, in which AFWAL planners, scientists, and engineers could serve short-term assignments in Senate and House offices, on Committee staffs, or on the staffs of the CRS, OTA, CBO, or GAO,

(f) encourage Congressional staff members to serve internships in AFWAL,

(g) develop a summer internship program for social science and business school graduate students,

(h) broaden the current foreign scientific exchange program of the Laboratories to include periodic exchanges of planners,

(i) expand the civilian professional staff education program by encouraging planners to attend national security and management courses at the Air University and the joint Service schools, and

(j) hire a public affairs officer to oversee interface programs.

(8) Cooperate with follow-on research activities, including:

(a) A comprehensive survey of the political context of AFWAL's research and development programs. In particular, this would highlight the impact of the Air Force, Department of Defense, Congress, and Office of Management and Budget on AFWAL's activities, and

(b) a general study of political forecasting, which could then be incorporated into the ongoing process of constructing a plan for long-range research and development needs and programs. The research would develop a model of political forecasting--a series of variables which signal changes in the international system that could impact upon American national security.

ANNEX A INTERVIEW TRIP REPORT

1. Dr Bernard A. Kulp, Chief, Scientific Advisory Office, DL, AFSC

In discussing the role of Air Force Laboratories, Dr. Kulp emphasized the fact that a broad spectrum of research is the ideal. To accomplish that objective, 6.1 activities should be expanded in some Laboratories--but not necessarily in all of them. Research is not the forte of most industrial corporations, so the Air Force must conduct in-house research and support independent research in order to serve its needs.

Dr. Kulp discussed the difficulty of selling R&D programs to the Air Force and to Congress. There is no single source of the problem; rather, it is a package of problems. To some extent, it is based on the style of communication; although, that is certainly not the only difficulty. One important source has been the bad domestic political environment during the past ten years.

Most of the interview dealt with the planning process. Dr Kulp made some telling criticisms of planning efforts. First, it is politically necessary to demonstrate that we plan. In a real sense, it is "faddish," since Harvard Business School emphasizes it. Second, our planning is simply an extrapolation from where we are, rather than a truly innovative approach postulating the kinds of systems we will need in 10 or 15 years. Third, laboratory planning is basically programming and budgeting, rather than planning.

Dr Kulp agreed with me that there is virtually no emphasis on international political context analysis. He stated that Vanguard is not sensitive enough to that kind of analysis. The Air Staff should be pursuing it, although he was not aware of it being done. Currently, we go through cycles of political emphases: first Europe, then Southeast Asia, then the Middle East, etc. He agreed that political forecasts should be integrated with military plans into the Air Force structure plan.

Finally, he strongly supported space system planning and logistics system planning. He felt that the Laboratories have been much too reactive to these goals, and not innovative enough.

2. Col John J. Hargreaves, Director of Plans and Programs, DL, AFSC and D.B. Nichols, Chief, Laboratory Plans Division, DL, AFSC

Col Hargreaves felt that the current mix of spending and activities in R&D was well balanced. A broad spectrum of research is essential, since we never know what will pay off. He lamented the fact that it is harder to get money for basic research than for "glamor" systems. Our basic research program has been plagued by inflation and low levels of funding.

He emphasized that there are serious deficiencies in explaining R&D programs to Congress. Engineers talk in engineering terms; their reports are much too technical for Congressmen and their staffs. It is difficult to put your fingers on R&D payoffs. He argued that there should be more "tailoring" of the reports, briefings, and analyses. Recent reports of the Rocket Propulsion Laboratory, he said, have been well-tailored for purposes of explaining projects and have been well-received. In addition, he felt that the last AFOSR report to Congress was a good model of a document tailored for explaining research programs to Congress; the language was not overly technical.

Both Col Hargreaves and Mr Nichols agreed that we are not good at long-range planning, since we are almost completely driven by the budget cycle. The answer is not more basic research; rather, it is that not enough resources are allocated to long-range planning. No one is really thinking sufficiently about development planning for 10 to 15 years ahead.

They agreed that some social scientists are needed to contribute their expertise to the planning process. They lamented the fact that political forecasts built into the intelligence threat analysis are not involved in AFSC; there is no vehicle to filter down the forecasts, and they are not considered in technical planning. However, this kind of approach is emphasized in the Air War College and the joint Service Schools.

They stated that the laboratories should send briefing teams to community groups to discuss the industrial payoffs of R&D. AFSC has employed similar teams. However, any direct form of "lobbying" is frowned upon.

3. Maj Dale O. Condit, Executive, DCS/Plans and Programs, AFSC

Maj Condit emphasized that descriptions of R&D programs are much too technical; they should be packaged in language that could be understood by laymen.

In discussing the planning process, he said that its principal function is to determine gaps in technical needs to meet the perceived evolving threat. Everyone should

realize, though, that we have to invest some money in R&D that may never come to fruition.

Maj Condit stated that he had never thought much about the role of political forecasts. He agreed, though, that the Office of the Secretary of Defense must depend upon such forecasts, since it decides upon major new R&D investments. He felt that national goals incorporated political forecasts; the technology base, through, was at a lower level. It is aimed at creating the technology for Air Force needs.

4. Col Donald S. Fujii, Director of Science, DL, AFSC

Col Fujii argued that we need a high-level advisory board to look at the long-range mix of spending and activities in R&D for future Air Force needs. There is clearly a lack of focus in this area at the present time. R&D programs are weakened by recurring budget crises. That is why we need an Air Force staff policy on the proper mix. For research to be productive, there has to be predictability, not recurring increases and decreases in spending levels. Without a more structured policy of investment in research, we would be guilty of an unwise use of resources. He said that many top government officials really do not understand the nature of basic research. That is why long-range research goals must come from the Air Staff.

In response to a question about the technical nature of R&D reports, Col Fujii replied that that was a superficial way of looking at the problem. The real difficulty is that Congress does not understand the role of technology base. Instead of stating R&D accomplishments in purely technical language, they should be explained in mission terms. Realistically, it will take a long time to develop a more solid appreciation for technology base and basic research.

In a more superficial sense, of course, reports and briefings should be tailored to an audience of laymen. "Engineers live in another world," he said. They have to learn how to explain the projects in non-technical language and to describe accomplishments in terms of missions. Col Fujii was dubious about R&D seminars for Congressional staff: in the past, nothing very positive has come out of them.

In discussing long-range planning, Col Fujii stressed the role of two factors: (1) Vanguard requirements, which fold in intelligence information about threats, and (2) technology push; engineers can make the best judgments about what kind of technology the Air Force needs.

He stated that the intelligence people use political forecasts. These estimates do not filter down into technology planning, except in the case of the Rocket Propulsion

Laboratory. It incorporates them into its planning process. He felt that DL should perhaps consider using some intelligence analysts and social scientists to look at future roles.

5. Col Karl F. Lauenstein, Office of Congressional Affairs, CSL, AFSC

We discussed the interface of the Air Force R&D community with Congress. Col Lauenstein stated that we are good on "big money" projects, but it is very hard to sell smaller items in the R&D budget. Why? Because the descriptions of the projects are generally "opaque." Due to that fact, Congressional staff analysts often cut some projects that are difficult to understand. The descriptions should certainly be tailored for laymen. Ideally we are looking for advocates from Congressional staffs who can support various items in discussions with other staff members.

Panic develops when a project gets into trouble. By then it is usually too late, unless the program can be quickly and easily explained. It does no good simply to repeat the technical description.

Basic research is exceptionally difficult to sell, since it has been maligned by the "golden fleece" award, etc. Congressmen often believe that basic research programs can be delayed, since they do not seem to be compelling.

We get caught up in the annual budget cycle, he said. At that time, we do not prepare explanations of programs other than those we are directly requested to do. Instead, we ought to be more aggressive in convincing officials on the Air Staff to support various projects. In addition, Col Lauenstein felt that informal educational sessions with Congressional staff analysts would be helpful in building long-term support for important projects. That is a more constructive approach than just attempting to bail out those programs that are in jeopardy.

6. Col Thomas O. Millett, Corporate Planning Office, CCX, AFSC

Col Millett conceived of corporate planning as an emphasis on "macro-programming" and long-range resource planning. Once we develop a list of evolving programs, then we can plan resource allocations more effectively for 10 years ahead. AFSC is not moving fast toward developing a corporate plan, and he was rather pessimistic that it would succeed in the next two or three years. He did feel that the Air Staff is addressing macro questions and is closer to developing long-range planning. Currently we do some mid-range planning for programs, but we do not do a macro-analysis of all the resources

needed (budgetary, manpower, environmental costs, etc.). Somehow, he said, we have to get away from an overemphasis on programs.

He stressed that top leadership must support corporate planning if it is to be successful. An effective corporate plan would, ipso facto, improve our interface with Congress and the public.

Col Millett agreed that political forecasts should be built into the corporate plan. Perhaps, two or three international political scenarios could be employed.

7. Lt Col Donald L. Calvert, Chief, Plans and Programs Division, AFOSR

Lt Col. Calvert felt that the current mix of spending and activities in R&D is fairly good. Actually, during the past few years, we have had better luck with research than with some development projects. The domestic political climate has changed for the good, he said; Congress and the White House have supported R&D more wholeheartedly over the past four or five years.

For the first time, AFOSR held some educational sessions with Congressional staff personnel this year. He believed that this approach could prove to be useful. He stressed that AFOSR documents are in non-technical language.

There is some interface with the public, in terms of briefings to professional and civic meetings. Perhaps more are needed, he said.

Lt Col Calvert doubted that we could do much more than we are doing now in long-range research planning. AFOSR draws upon the scientific community in making long-term projections for research.

He said the AFOSR does not emphasize technological forecasts; they should be conducted by the Laboratories.

He agreed that political forecasts should be a consideration in the planning process. For example, demographic factors and their political implications would be crucial in the life sciences program of AFOSR.

8. Col Richard H. Hartke, Deputy Director, AFOSR

In relation to the mix of spending and activities in R&D, Col Hartke said that it differed for each laboratory. It depends upon the number of persons in each lab; that is the major limit. The quality of the labs differs; however, there are outstanding key scientists and engineers in each lab. One benefit of having Air Force labs is that scientists and engineers are freer to explore long-term projects and can be involved on the frontier of research.

He stressed that it is difficult to explain research to Congress, since it is really a host of very small programs without formal schedules or milestones that can be predicted firmly. The current report format is rather formal and does not adequately explain the projects. He felt that it is generally more effective to explain the proposals in person. There is one serious structural obstacle, though: Congress is always besieged by advocates. In the long run, it is important for AFOSR to demonstrate its credibility in justifying research programs.

Congressional staff personnel have visited some Laboratories. But technology is generally low on their agenda. The crucial problem they face is "how much is enough" for research.

AFOSR documents are distributed to the technical public community. Several times a year seminars on Air Force research are conducted at various universities for those interested in academic-oriented research programs. Col Hartke felt that these interface approaches were rather effective.

In discussing long-term planning, he stressed that probing for technological opportunities is the principal means of planning for the future. All lab chief scientists prepare reports on where the Air Force should go in terms of technology. Then the AFOSR directors put a plan together in seven separate areas. He mentioned the field of lasers as a good example of how investigating interesting physical phenomena can lead to potentially effective systems. He also argued that continuity of funding and keeping the best scientists and engineers are critical factors in effective long-term research planning.

In response to my question about political forecasting, Col Hartke recognized that they are important for Air Force doctrine. But the only experience he remembered was the recent major study on the year 2000; all Air Force labs participated in that project. He said that he would prefer to go to experts in each technical field and ask them what they think the future holds in their area--rather than depend upon a macro-plan which would set goals 10 to 20 years in advance.

9. Dr Richard A. Reynolds, Deputy Director, Defense Sciences Office, DARPA

Dr Reynolds stated that DARPA does not have much contact with Air Force Laboratories. In general, he felt that there was weak coupling between research activities and development projects. More integrated planning is needed.

He believed that DARPA fares well with Congress; he saw no problems at all in terms of format and justifications. He recalled no feedback that DARPA's reports were too technical.

Dr Reynolds viewed long-range planning as setting useful goals to accomplish. Although political forecasts are not incorporated in DARPA's reports, the Systems Sciences Division is working on advance warning technique analysis--which is part of international context analysis.

10. Lt Col Dibell and Lt Col Thomas M. Coyne, Directorate of Program Integration, Management Policy Division, Deputy Chief of Staff: RD&A, Air Force

These officers felt that both long-range planning and incorporating political forecasts into the R&D planning process would be quite difficult. They assumed that Air Force Intelligence should develop political forecasts, but they said that they were not aware that any such approaches have filtered through the various levels of the Air Force which are involved in R&D.

11. Col Paul Try, Director of Environmental and Life Sciences, Undersecretary of Defense for R&E

Col Try felt that the mix of spending and activities in R&D was about right. Most importantly, Air Force labs should concentrate on R&D in those areas in which universities have little or no interest. He sensed that the level of 6.1 funding in labs is satisfactory, but there is not enough money for basic research in universities. There should be basic research in a full spectrum of disciplines; he mentioned oceanography as an area where DoD has to do more.

In general, reports on R&D are too technical. Some research projects sound "flaky," but they do have defense applications. (for example, studying how to deal with clams which eat through pier pilings). But the fact remains that it is often difficult to convince people of the value of some research projects. The "golden fleece" award is a symptom of public wariness of research programs; then Congress reacts to those doubts. Research communities have to be better at public relations, he said.

Col Try had reservations about the benefits of long-range planning. It is useful, though, to illuminate goals and then mesh them with current programs. Program managers should be forced to plan more effectively by being influenced by long-range objectives. In practice, he realized that long-range planning is often relegated to a study group (similar to the one on the year 2000); that generally is the last ever heard about it.

In reference to the importance of political forecasting and international context analysis, Col Try was fairly enthusiastic. He argued that it was crucial to analyze such potential developments as: (1) How internal group conflicts in the Soviet Union might impact upon international conflict patterns, and (2) how political integration in Africa would affect mineral resource supplies in the future.

1981 USAF -SCEEE SUMMER FACULTY RESEARCH PROGRAM

Sponsored by the

AIR FORCE OFFICE OF SCIENTIFIC RESEARCH

Conducted by the

SOUTHEASTERN CENTER FOR ELECTRICAL ENGINEERING EDUCATION

FINAL REPORT

COUPLING REACTIONS AND REARRANGEMENTS OF 1,3,5-TRIAZINES

Prepared by: Dr. G. Fredric Reynolds

Academic Rank: Professor

Department and University: Department of Chemistry and Chemical Engineering
Michigan Technological University

Research Location: Frank J. Seiler Research Laboratory
United States Air Force Academy

USAF Research Colleague: Capt. Neal Ely

Date: July 29, 1981

Contract No: F49620-79-C-0038

COUPLING REACTIONS AND REARRANGEMENTS OF 1,3,5-TRIAZINES

by

G. Fredric Reynolds

ABSTRACT

Some unique chemistry of s-triazines is described involving the coupling of organic substrates containing acidic protons to the halogen sites on the triazine ring. In this manner, chains and rings of s-triazines can be formed. Rearrangements of oxygen-substituted s-triazine esters to nitrogen-substituted s-triazine esters are described, and a mechanism for the catalyzed rearrangement is proposed that is consistent with the kinetic data obtained.

Acknowledgement

The author wishes to express his appreciation to the Air Force Systems Command, the Air Force Office of Scientific Research and the Southeastern Center for Electrical Engineering Education for providing him with the opportunity of spending a profitable ten weeks at the Frank J. Seiler Research Laboratory, United States Air Force Academy. He would like to thank the officers and enlisted men of the Chemistry Division of the Seiler laboratory for their kind hospitality. In particular, he would like to thank Captain Neal Ely for much helpful discussion, and Mr. Lloyd Pflug for taking mass spectroscopy measurements.

I. INTRODUCTION:

1,3,5-triazines, or s-triazines, are one of the most useful classes of heterocyclic compounds. They have found use as effective herbicides such as 2-chloro-4,6-diethylamino-s-triazine¹ (simazine). Other substituted s-triazines are widely employed as dyestuffs, and the much used melamine-formaldehyde resins are formed from 2,4,6-triamino-s-triazines.² The high-explosive RDX is 1,3,5-trinitrohexahydro-s-triazine and is one of the most valuable explosives in munition formulations.³ Because of the application of substituted s-triazines in energetic materials, basic research on rearrangements and coupling of s-triazines has the potential of leading to useful products as explosives or explosive additives. For example, new compounds formed from the coupling of fluorinated s-triazines may have potential as high-energy explosive binders.

In order to couple reactive trihalo-s-triazines to organic substrates, the substrate must have acidic protons with an acid dissociation constant, K_a , of the order of 10^{-15} or greater. In this initial study, we used malonic ester for the substrate in which the protons are weakly acidic. Other potentially better substrates with larger values of K_a are given in the following table:

SOME DISSOCIATION CONSTANTS OF CARBON-HYDROGEN ACIDS⁴

<u>Acid</u>	<u>K_a (aq. 25°C)</u>
malonic ester	5×10^{-14}
NC-CH ₂ -CN	6.5×10^{-12}
CH ₃ COCH ₂ COOC ₂ H ₅	2.1×10^{-11}
CH ₃ COCH ₂ COOCH ₃	1×10^{-10}
CH ₃ COCH ₂ COCH ₃	1×10^{-9}
CH ₃ COCH ₂ COH	1.2×10^{-6}
C ₂ H ₅ OCOCH ₂ NO ₂	1.5×10^{-6}
CH ₃ COCH ₂ NO ₂	8.0×10^{-6}
HCOCH ₂ COH	1.0×10^{-5}
O ₂ N-CH ₂ -NO ₂	2.7×10^{-4}

Unfortunately, the most acidic substrate listed, dinitromethane, is an unstable liquid and explodes near the boiling point. In addition to reactions with acidic C-H compounds, most all halo-s-triazines can also couple reactively to N-H compounds such as anilines, and substituted amines,⁵ and these compounds, especially when nitrated, should have potential for use as explosives or explosive additives.

II. OBJECTIVES OF THE RESEARCH EFFORT:

One of the main objectives of the research effort was to find the conditions under which two or more s-triazine rings could be coupled together using malonic esters as the coupling substrate. Starting with 2,4,6-trichloro-s-triazine, one of the aims of the research was to prepare polymers of chlorinated s-triazine malonic esters. Once this was accomplished, similar procedures were to be used to couple 2,4,6-trifluoro-s-triazine to malonates and other compounds containing reactive hydrogen, since fluorinated s-triazines have greater potential for energetic material formulations. Because chlorinated s-triazines are less toxic and easier to handle than fluorinated s-triazines, reaction conditions were to be investigated for preparation of the chlorinated derivatives of s-triazine.

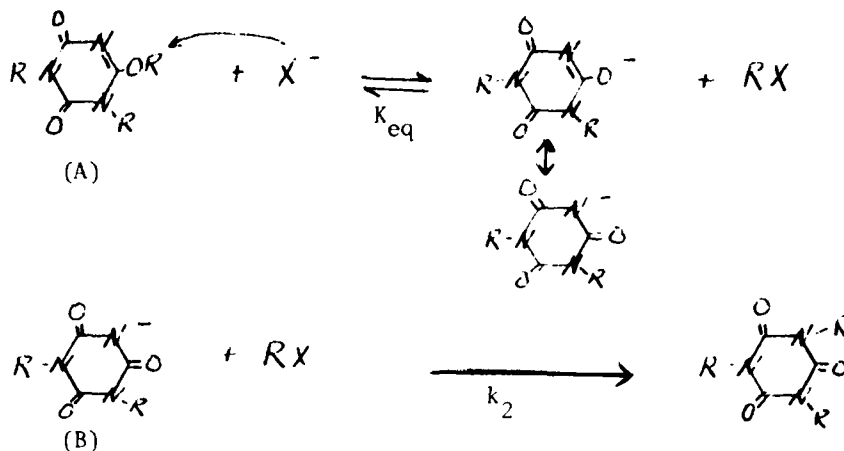
In addition to the main objective, some questions remained about the mechanism of rearrangement of oxygen-substituted s-triazine esters to nitrogen-substituted s-triazine esters, and a secondary objective was to elucidate the mechanism of this catalyzed rearrangement. In this type of rearrangement, substituents are transferred from the 2,4,6 positions of the s-triazine ring to the 1,3,5 positions of the ring due to a greater thermodynamic stability of the latter isomer. I discovered that it was unnecessary to carry out this type of rearrangement in the molten state since it will occur at relatively low temperatures in a solvent such as nitrobenzene when small amounts of tetraalkyl ammonium halides are used as catalysts. The role of the catalyst is to lower the activation energy of the rearrangement by providing a facile mechanism for the transfer of substituents from oxygen to nitrogen.

III. PROPOSED MECHANISM FOR THE O TO N REARRANGEMENT OF TRIAZINE ESTERS:

Kinetic data for the rearrangement of 2,4,6-trimethoxy-s-triazine to 1,3,5-trimethyl-2,4,6-trioxohexahydro-s-triazine and for the analogous benzyl ester showed that the rearrangement occurred over the period of several hours at a temperature of 150°C when catalyzed by small amounts of tetraalkyl ammonium halides. This rearrangement involves the transfer of three methyl or benzyl groups from oxygen to nitrogen, and in order to simplify the study of the reaction mechanism, the rearrangement was effected in which only one methyl or benzyl group was transferred. Thus, the mechanistic studies were carried out on the rearrangement of 1,3-dimethyl-6-methoxy-2,4-dioxo-1,2,3,6-tetrahydro-s-triazine to 1,3,5-trimethyl-2,4,6-trioxohexahydro-s-triazine and the corresponding benzyl analogue. The kinetic studies showed that the proposed mechanism for the reaction should explain the following points:

1. The rate of the reaction followed (pseudo) first order kinetics.
2. During the reaction, the catalyst concentration remains constant, but if a series of reactions are run using different catalyst concentrations, the reaction can be shown to depend on catalyst concentration. Thus the reaction is also first order in catalyst.
3. R_4NCI , R_4NBr and R_4NI are suitable catalysts while R_4NClO_4 is not. Thus the reaction involves nucleophilic attack by halide ion. The order of catalysis is chloride ion greater than bromide ion greater than iodide ion as expected for nucleophilic displacement in nitrobenzene solution.
4. While trimethyl and tribenzyl triazine esters rearrange readily, triethyl and triisopropyl esters do not, indicating steric hindrance of nucleophilic substitution on the carbon attached to oxygen in the triazine ester.
5. An important result is that when trimethyl and tribenzyl triazine esters are rearranged together, mixed nitrogen-substituted methyl and benzyl esters are formed. This result shows that the rearrangement proceeds by an intermolecular rather than an intramolecular mechanism.

The proposed mechanism for the catalyzed rearrangement in nitrobenzene solution which explains the five previous points is as follows:



Thus, the rate observed is: $\text{rate obs.} = k_2 (\text{B}) (\text{RX})$ (1)

but: $K_{\text{eq}} = \frac{(\text{B}) (\text{RX})}{(\text{A}) (\text{X}^-)}$ (2)

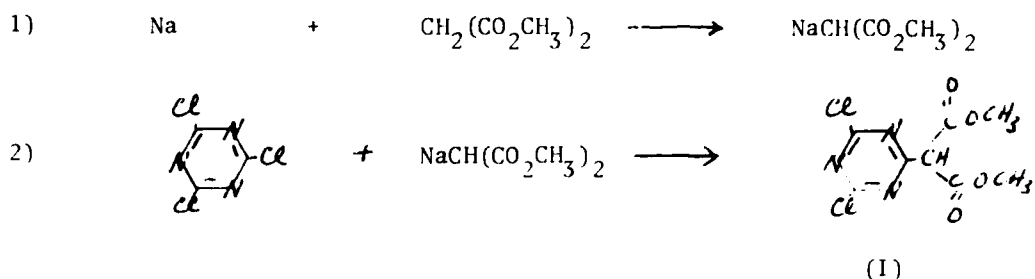
and: $\text{rate obs.} = k_2 K_{\text{eq}} (\text{A}) (\text{X}^-) = k_{\text{obs}} (\text{A})$ (3)

From equation (3), it can be seen that the proposed mechanism predicts that the catalyzed rearrangement will be pseudo first order in starting ester and that as the catalyst concentration is increased, the rate will increase to the first power.

IV. COUPLING OF TRIHALOTRIAZINES TO MALONIC ESTERS:

Trichloro-s-triazine was obtained commercially from Aldrich Chemical Company. Analysis of this material showed that it contained some impurities, and therefore it was purified by sublimation under reduced pressure and mild heating with a water bath before this material was used in reactions. Dimethylmalonate used in the reactions was purified by fractional distillation. The solvents p-dioxane and tetrahydrofuran were dried and distilled over sodium before use.

Preparation of s-triazine mono-substituted with malonic ester was carried out by the following two-step reaction:



The crude product (I) which was isolated as a viscous yellow oil is of interest because of its three reactive sites. Electrophilic substitution reactions can take place at the central carbon of the malonate group, and nucleophilic reactions can take place at the remaining two chlorinated sites on the s-triazine ring. Thus, coupling is possible between two or more molecules of compound I, although until this work coupling has never been observed for two molecules of this type.

The coupling reaction was attempted in four different ways during the course of this work; in each case followed by normal-phase liquid chromatography using silica gel and reverse-phase high-pressure liquid chromatography (HPLC) using C-18 coated silica gel to separate the products; followed by NMR and mass spectroscopy to identify the new materials isolated. These four methods were:

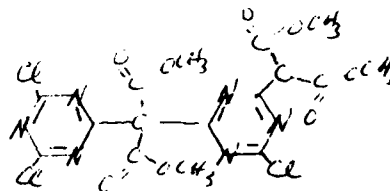
1. I (neat) + cyanuric chloride $\xrightarrow[\text{several days}]{40 - 60^\circ\text{C}}$
2. I + cyanuric chloride $\xrightarrow[\text{in dioxane overnight at b.p.}]{\text{metallic sodium}}$
3. I + cyanuric chloride $\xrightarrow[\text{in tetrahydrofuran overnight at b.p.}]{\text{metallic sodium}}$
4. I + cyanuric chloride $\xrightarrow[\text{in tetrahydrofuran overnight at b.p.}]{2,6\text{-di-}t\text{-butyl-4-methyl pyridine}}$

In each of the above cases, a portion of higher molecular weight material was obtained in addition to side products in which trace amounts of water reacted with the starting materials in the presence of base to hydrolyze the chloride groups on the s-triazine ring. The mass spectrum of one of the higher molecular weight fractions showed conclusively that the product was dimethylmalonate disubstituted with dichloro-s-triazine

having the structure (II), with a molecular weight of 426 based on chlorine mass of 35. In addition, the mass spectrum showed the presence of four chlorines based on the isotope ratios expected for the natural abundance of chlorine of masses 35 and 37. In addition to this evidence, the nuclear magnetic resonance spectrum of one of the higher molecular weight fractions indicated the presence of compound (III) expected from the dimerization of compound (I) in the presence of base.



(II)



(III)

Because the mass spectrometer has been inoperable recently, it has not been possible to verify compound (III) as yet, or to examine other higher molecular weight fractions.

V. RECOMMENDATIONS:

The rearrangement of oxygen-substituted s-triazines to nitrogen-substituted s-triazines stands as a completed work with a reasonable mechanism proposed for the catalyzed rearrangement in nitrobenzene solution. A related rearrangement problem in which at least one of the substituents is a nitro group could be undertaken. For example, mixed methoxy-nitro-s-triazine could be subjected to catalyzed rearrangement conditions to see if rearrangement would occur. This study could be of interest due to its relation to the explosive 1,3,5-trinitrohexahydro-s-triazine (RDX).

Of greater interest for future study is the coupling of halo-s-triazines, and in particular, fluorotriazines, to reactive substrates listed in the Table in the introduction of this report. Thus, the coupling of two or more rings and substrates should be pursued to find the reaction conditions necessary to maximize the formation of polymeric material. Under certain conditions, I feel cage molecules should form that would bond metallic ions inside the ring to the pi electrons of the conjugated triazine rings. In order to form these cages, the ends of four or more triazine-substrate molecules would have to be tied together by the elimination of a molecule of HCl by base.

The best candidates of the polymeric triazines for explosives or explosive additives would seem to be fluorinated triazines bonded to substrates containing nitro groups. For example, fluoro-s-triazine could be coupled to each end of nitro-guanidine, or perhaps fluoro-s-triazine coupled to guanidine and then the entire molecule subjected to nitration. Such molecules should prove to have interesting properties since nitro-guanidine itself is utilized in flashless explosives.⁶

REFERENCES

1. H. Gysin, Chem. Ind. (London), 1393 (1962).
2. J. Joule and G. Smith, Heterocyclic Chemistry, 2nd Edition, Van Nostrand Reinhold Co., N. Y., 1978, p. 125.
3. U.S. Army Material Command, Engineering Design Handbook, Explosive Series, "Properties of Explosives of Military Interest," 1967.
4. J. Leffler, The Reactive Intermediates of Organic Chemistry, Interscience, N. Y., 1956, p. 180.
5. E. Smolin and L. Rapoport, s-Triazines and Derivatives, Interscience, N. Y., 1967.
6. A. F. McKay, Chem. Rev., Vol. 51, 301 (1952).

1981 USAF - SCEE SUMMER FACULTY RESEARCH PROGRAM

Sponsored by the

AIR FORCE OFFICE OF SCIENTIFIC RESEARCH

Conducted by the

SOUTHEASTERN CENTER FOR ELECTRICAL ENGINEERING EDUCATION

FINAL REPORT

ADSORPTION OF TRICHLOROETHYLENE BY SOILS
FROM DILUTE AQUEOUS SYSTEMS

Prepared by: Richard O. Richter, PhD

Academic Rank: Assistant Professor

Department and

University: Civil and Environmental Engineering Department
Washington State University

Research

Location: Air Force Engineering and Services Center
Environics Division, Environmental
Engineering Branch

USAF Research

Colleague: Major Stephen G. TerMaath

DATE: August 24, 1981

Contract No: F49620-79-C-0038

ADSORPTION OF TRICHLOROETHYLENE BY SOILS
FROM DILUTE AQUEOUS SYSTEMS

by Richard O. Richter

ABSTRACT

The adsorption of trichloroethylene (TCE) onto inorganic soil fractions was studied to determine whether these materials might be significant sinks for chlorinated hydrocarbons. Results indicate that inorganic soils adsorbed TCE in the following order of capacity: goethite, kaolinite, amorphous manganese oxyhydroxide, montmorillonite. Organic peat and a soil from a TCE-contaminated aquifer were also used as adsorbents. As expected due to its organic carbon concentration, the peat had a greater capacity to remove TCE from solution. The aquifer soil had a capacity between that of kaolinite and manganese oxide. Freundlich adsorption isotherms were developed for the soils and K and $1/n$ values were determined.

Calculations using the isotherm equations for the inorganic soils and the octanol/water partitioning adsorption equation of Karickhoff indicate that when the amount of organic carbon in a composite soil is small compared to the clay content (less than 1 to 5), it is possible for the inorganic fraction to control the adsorption of TCE.

Further adsorption studies, both batch and column should be conducted to learn the behavior of halogenated hydrocarbons, such as TCE, in groundwater aquifers. The role of the inorganic soil fraction in the adsorption process should not be underestimated.

ACKNOWLEDGEMENTS

The author wishes to thank the Air Force Systems Command, the Air Force Office of Scientific Research, and the Southeastern Center for Electrical Engineering Education for providing him with the opportunity to spend an interesting and rewarding summer at the Air Force Engineering and Services Center, Tyndall AFB, FL. He would like to acknowledge all those in the Environics Division for their enthusiastic support and cooperation.

Special thanks go to Lt. Col. Michael G. MacNaughton and Lt. Col. Michael J. Ryan for their support; to Major Stephen G. TerMaath for his guidance in selecting this topic; to Mr. Thomas Stauffer for his aid in executing this project; and to the following senior NCOs for their support: Daniel Stork, Stacy Brown, and Charles Manikas.

Finally, he would like to thank Captain Joseph Zirrolli, Lieutenant Barbara Braun, and Dr. Robert Carlson for their stimulating conversations.

I. INTRODUCTION:

Many municipalities and individuals in the United States use groundwater as their sole source of drinking water; however, several factors have made it difficult to ascertain its quality with regard to toxic organics. While conventional pollution measurements, such as pH, BOD, and heavy metal concentrations are readily determined, organic contaminants require more sophisticated and costly analytical techniques. Due to the continuity of surface waters, it is easy to predict the extent of contamination; however, the transport of groundwater contaminants is often difficult to forecast due to the vagaries of the fluid's movement. Until recently, the coupling of these circumstances has prevented the realization of the extent to which organic chemicals are present in our groundwater. We are just now becoming aware that the industrial use and improper disposal of toxic organics, such as trichloroethylene, has led to the contamination of many groundwater sources of drinking water in the United States(1).

In the past, the Air Force used trichloroethylene (TCE) and other chlorinated hydrocarbons as degreasing solvents for aircraft parts. Due to problems in handling and disposal, TCE spills have occurred at several Air Force bases, resulting in the contamination of the underlying aquifers. At Wurtsmith AFB in Michigan, the Air Force is in the process of developing a decontamination scheme to cleanse the aquifer polluted by TCE leakage from a storage tank. Present plans call for the groundwater to be pumped out, the organic hydrocarbons to be removed by air stripping, and the water passed through activated carbon for polishing before discharge. A key assumption is that the aquifer soils have not adsorbed the TCE from solution and thus cannot release it back into the uncontaminated recharge water.

It is known that hydrocarbons will adsorb onto activated carbon and various soils (2, 3, 4, 5, 6). Most research has been directed toward the effect of the soil organic carbon content on the intensity and quantity of organic pollutants. While the organic soil fraction is a much stronger adsorbent than the inorganic fraction, in most cases the organic soil content is very small. In these instances, such as at Wurtsmith AFB, it may be that the

overwhelming quantity of inorganic soils acts as the main sink for adsorbed hydrocarbons. Unfortunately, little is known about the adsorption properties of the inorganic solids with respect to soluble organic pollutants. Clays, sands, and hydrous oxides are known adsorbents of inorganic solutes and ionic organics. These soil fractions need to be studied as to their adsorption with respect to organic hydrocarbons.

II. OBJECTIVES:

The primary objective of this project was to investigate the adsorption of a chlorinated hydrocarbon, trichloroethylene (TCE), onto inorganic soils. The effects of varying two parameters were to be studied: soil type and concentration. Several soil types were used: clays (montmorillonite and kaolinite), hydrous oxides (manganese and iron), organic peat, and a composite soil found at Wurtsmith AFB. The initial concentration of TCE was varied in order to determine the effects on adsorption and to generate adsorption isotherms. The initial TCE values ranged from 11 to 1,100 micrograms/liter (ug/l).

As a necessary side study, several experimental designs were attempted to determine an acceptable methodology for performing adsorption experiments. Both two-phase (solid, liquid) and three-phase (gas, liquid, solid) systems were evaluated.

III. EXPERIMENTAL PROCEDURES:

Materials Preparation

Trichloroethylene solutions were prepared from a saturated solution which is assumed to have an aqueous concentration of 1100 mg/l (4). Samples and standards were diluted from the stock solution immediately before use to minimize volatilization losses.

The soils used as adsorbents were washed several times with distilled water, dried at 100°C for one hour, put in a dessicator and brought to room

temperature, and passed through a sieve (no. 200) with 75 micron openings. The peat was commercial grade as were the kaolinite and montmorillonite. The hydrous oxides of iron and manganese were those used by Richter (7). The soil from Wurtsmith AFB was collected several feet below the top soil layer.

Trichloroethylene Measurement

The concentration of trichloroethylene in water was determined by using headspace gas chromatography (8). In this method, it is assumed that the concentration in the liquid phase is directly proportional to that of the TCE in the gas phase which is actually measured. Samples were equilibrated for 10 minutes on a wrist action shaker and 1.0 ml of head space gas was injected into the gas chromatograph (Perkin Elmer Model 900 with 10 feet of 10 percent SP-1000 on 100/120 supelcoport, operated isothermally at 100°C, and retention time of 2.5 minutes for TCE). Both of the following procedures relied on this technique to determine the residual soluble TCE concentration after adsorption.

Solid-Liquid Adsorption System

In this procedure, the solid adsorbent was placed in a 40 ml glass centrifuge tube with the liquid containing a known initial concentration of TCE. The bottle was completely filled to exclude any gas phase and sealed with aluminum foil to prevent contact with the teflon cap which could adsorb TCE. The bottles were then shaken for 18 hours to establish TCE equilibrium between the solid and liquid phases.

At equilibrium, the total mass of TCE, M_T , will be the sum of the masses in the two phases:

$$M_T = M_L + M_S \quad (1)$$

where:

M_L = mass in liquid (moles)

M_S = mass on solid (moles)

The total mass will be the product of the initial concentration in the liquid, C_0 (moles/liter), and the liquid volume, V_L (liter). The final mass in the liquid will be the product of the liquid equilibrium concentration, C_L , and liquid volume, V_L . substituting into equation (1) and solving for the mass adsorbed gives:

$$M_S = C_0 V_L - C_L V_L \quad (2)$$

Since C_0 and V_L are known, all that is required to determine the amount of TCE adsorbed is to find C_L . The tubes were centrifuged and 20 ml of centrifugate were removed and placed in a 40 ml head space bottle and sealed with a teflon cap. Standards were prepared and C_L was determined by head space gas chromatography. Thus, this procedure involved three steps: equilibration of the liquid phase with the solid phase, followed by centrifugation, and then equilibration of the separated liquid phase with a gas phase.

Solid-Liquid-Gas Adsorption System

Since the preceding experimental system required three steps, it was felt that a three-phase system could be utilized to save time and eliminate volatilization losses during transfer operations. If the solid, liquid, and gas phases are in equilibrium, it should be possible to calculate the amount adsorbed and the liquid concentration from the measured gas phase concentration.

For a closed, three-phase system, the total mass of TCE would be:

$$M_T = M_S + M_L + M_G \quad (3)$$

where:

$$M_G = \text{mass in gas (moles/liter)}$$

Using the universal gas law, the mass of gas for a given partial pressure, P' (atmos), of TCE will be:

$$M_G = P' V_G / RT \quad (4)$$

where:

V_G = gas volume (liter)
 R = universal gas constant
 (0.082 liter·atmos/mole·°K)
 T = temperature (°K)

From Henry's Law, the partial pressure can be related to the liquid concentration:

$$P' = HC_L \quad (5)$$

where:

H = Henry's Law constant

Gossett (9) found H equal to 8.62 liter·atmos/mole at 25°C. Substituting for the masses and solving for the mass adsorbed yields:

$$M_S = C_0V_L - C_LV_L - C_LV_GH/RT \quad (6)$$

Since all values are known except for C_L , determination of the mass of TCE adsorbed requires only the liquid equilibrium concentration. For this system, head space bottles of known volume (40 ml) were partially filled with known volumes of soil and TCE-containing liquid, leaving a given gas volume. The bottles were sealed with teflon septa and agitated for 18 hours. Head space gas chromatography was then performed directly on the samples, and the values of C_L and M_S calculated.

Adsorption Isotherms

Adsorption of solutes onto solids is a function of the amount of solid adsorbent and the concentration of adsorbate in solution. The two most common methods of presenting adsorption data are as isotherms described by Langmuir and Freundlich (10). The Langmuir isotherm is represented by the equation:

$$X = \frac{X_M b C}{1 + b C} \quad (7)$$

where:

X = mass adsorbed/mass solid (ug/g)

X_M = maximum value of X (ug/g)

b = constant based on data

C = equilibrium liquid concentration (ug/l)

Several linearizing procedures can be used to determine X_M and b for a given set of X vs C data.

The Freundlich isotherm uses the empirical relationship:

$$X = KC^{1/n} \quad (8)$$

Where:

K and n are constants

Generally, this isotherm is expressed logarithmically as:

$$\text{Log } X = \text{Log } K + (1/n)\text{Log } C$$

A plot of Log X vs Log C will have a slope of 1/n and an intercept of Log K.

Using either of the formulas and the constants determined experimentally for a given soil, it is possible to calculate the amount of TCE which would be adsorbed at a given equilibrium concentration.

IV. RESULTS & DISCUSSION:

Experimental Design

As described earlier, both two-phase (liquid, solid) and three-phase (liquid, solid, gas) systems were tried to determine which experimental procedure should be used in the adsorption isotherm studies. In the three-phase system, the bottles were sealed with teflon septa held in place by open, screw cap tops in order to allow direct sampling after equilibration. The two-phase systems were sealed with solid screw cap tops lined with aluminum foil.

For the three-phase system the head space concentration after 18 hours of mixing was the same for all samples and blanks which started with equal TCE concentrations. These values showed total mass losses of from 30 to 50 percent when compared to the initial TCE values. There are two possible reasons for the disappearance of the adsorbate. Trichloroethylene is highly volatile with an evaporative half-life of 19 minutes (5); therefore, even the slightest leak in the seal will result in large losses of the organic. The second possibility is that the teflon septa act as adsorbents for the TCE.

The two-phase system appeared to have little loss of TCE during agitation. Blanks that were mixed for 18 hours had the same final TCE values as were initially present, within the sensitivity of the analytical procedure. It should be noted that during the transfer of samples to head space bottles and the preparation of standards there may have been consistent evaporative losses which would result in actual concentrations lower than those assumed to have been present.

Due to the superiority of the solid-liquid system in minimizing TCE losses, it was selected as the experimental model for the adsorption isotherm studies. However, more work should be performed to ascertain whether evaporative losses are significant during transfer operations such as pipetting, and if necessary, an experimental procedure developed which would eliminate or minimize these losses.

Adsorption Isotherm Studies

Adsorption of aqueous trichloroethylene was found to vary considerably with the type of soil used. Tests with TCE in the presence of an iron oxyhydroxide, goethite, found the adsorption to be less than 0.1 ug/g at an initial TCE concentration of 100 ug/l. The changes in concentrations were too small to generate a significant adsorption isotherm.

An amorphous manganese oxyhydroxide was found to adsorb TCE at a significant level. Figure 1 shows the Freundlich isotherm for TCE on this manganese oxide. (It should be noted that all of the K-values and 1/n-values were

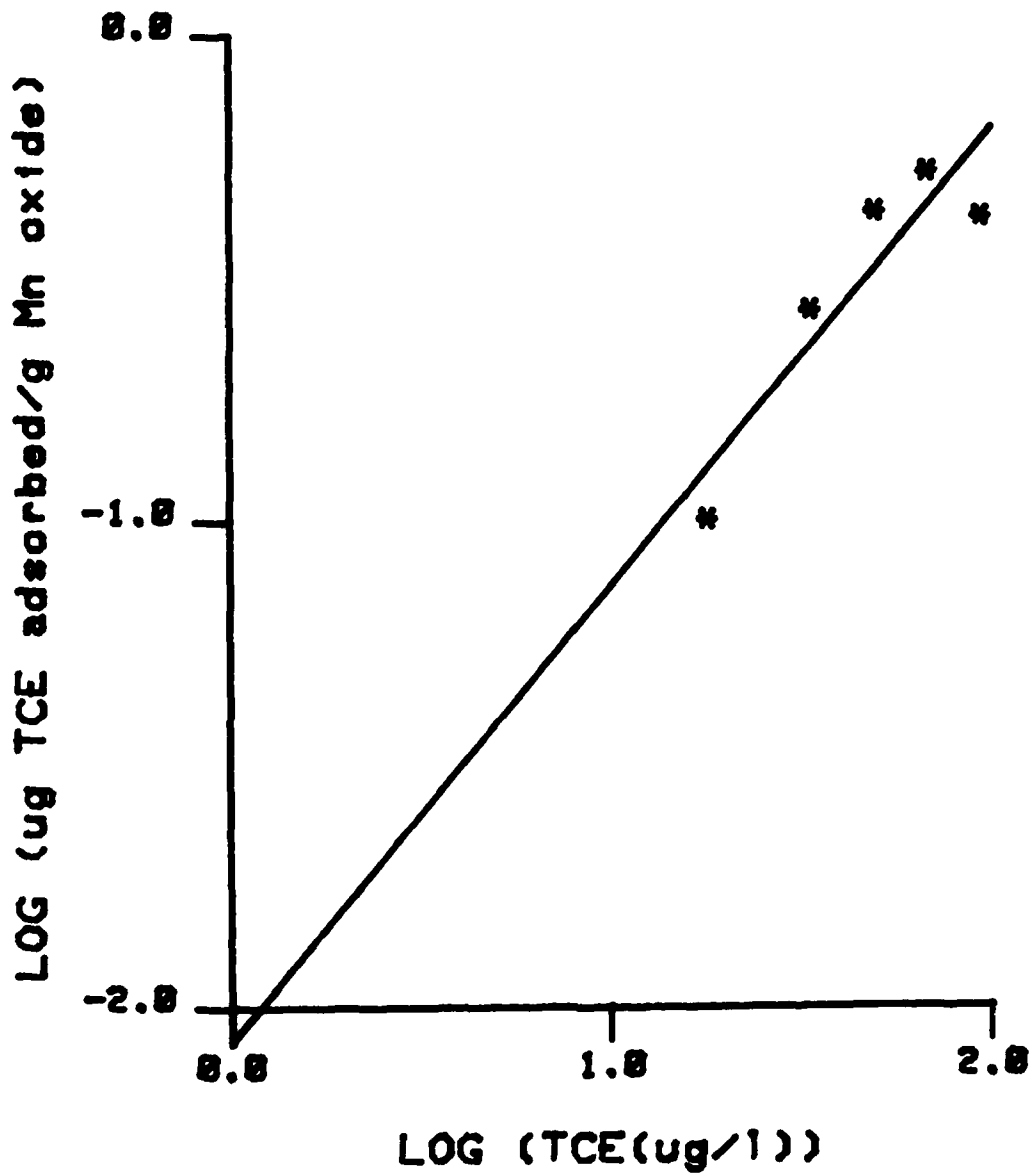


Figure 1. Freundlich isotherm of trichloroethylene adsorption by manganese oxide.

calculated using a least squares regression analysis for plots of Log_{10} (ug TCE adsorbed/g soil) versus Log_{10} (ug/l TCE at equilibrium). This latter point is important when comparing reported K's and 1/n's, as the K-values might vary depending upon units chosen for equilibrium concentration and adsorption.) The value of K was determined to be 0.0085 and 1/n was 0.938 with a correlation coefficient, r, of 0.907.

Kaolinite, a two layer clay, was found to have little capacity for the adsorption of trichloroethylene with the adsorption less than 0.2 ug/g at an equilibrium concentration of 100 ug/l. Adsorption was not sufficient at lower concentrations to generate an isotherm.

Montmorillonite, a three layer clay, adsorbed an order of magnitude more strongly than did kaolinite. Figure 2 is the Freundlich plot for TCE adsorption onto montmorillonite from which were derived a K of 0.0970 and a 1/n of 0.705 with a correlation coefficient of 0.968.

Organic peat was used as an adsorbent to act as a comparison for the inorganic soils tested. Figure 3 shows the large capacity for TCE which this soil has. The K-value was 0.148 and 1/n was 0.737 with a correlation coefficient of 0.990.

Figure 4 shows the Freundlich isotherm generated for TCE adsorption onto soil taken from Wurtsmith AFB, Michigan. The size fraction used in these experiments (≤ 75 microns) would consist of mostly clay and some organic matter. This soil had a K of 0.0759 and a 1/n of 0.324 with r equal to 0.774.

The Freundlich constants, K and 1/n, are summarized for the various soils in Table 1; for comparison, the values for activated carbon adsorption of TCE determined by the EPA (6) are also included. The last column represents the amount that would be adsorbed on the soil if the equilibrium concentration were 100. ug/l. For this concentration it can be seen that the order of adsorption capacity increases as: goethite, kaolinite, Wurtsmith soil, manganese oxide, montmorillonite, peat, and activated carbon.

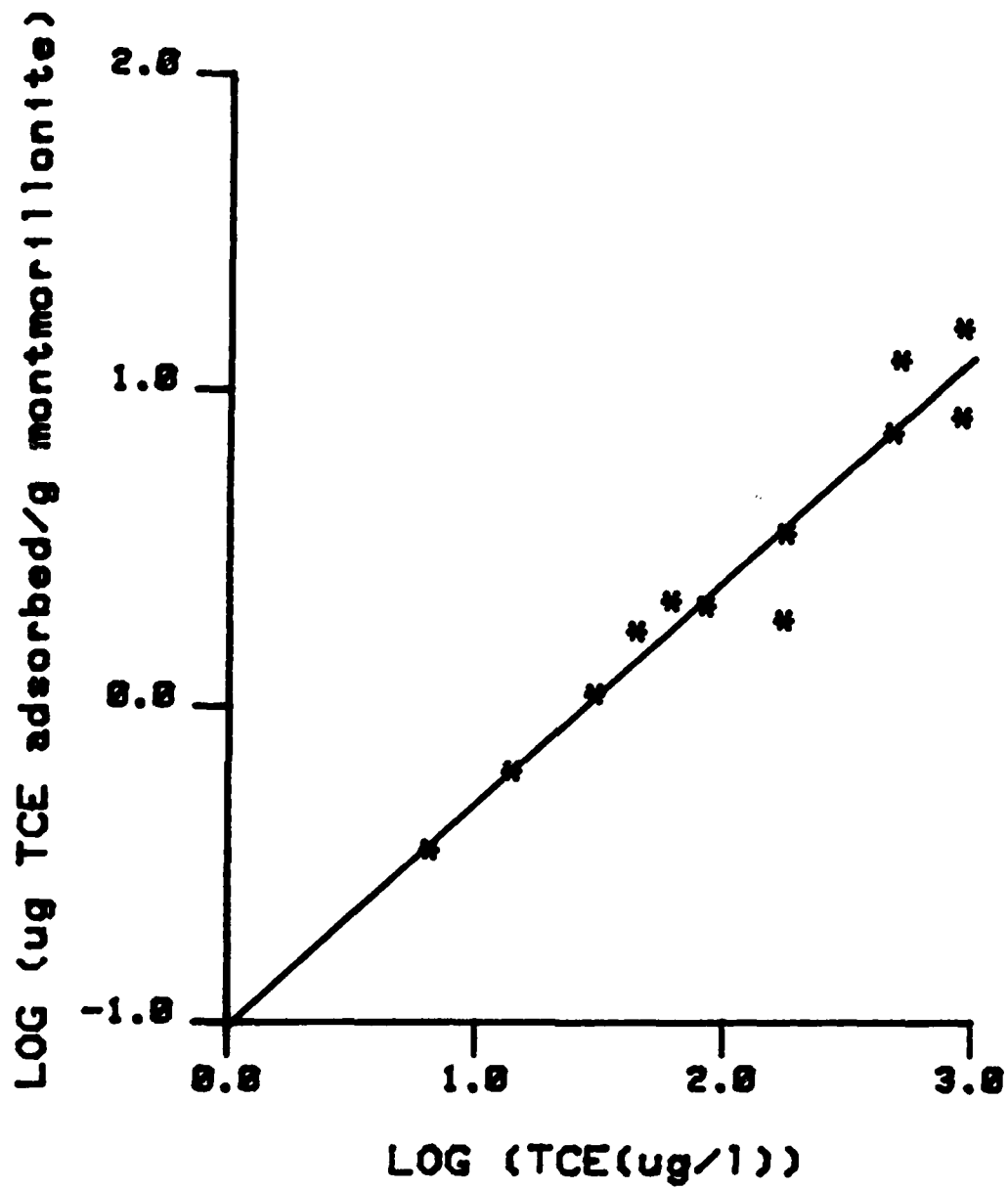


Figure 2. Freundlich isotherm of trichloroethylene adsorption by montmorillonite clay.

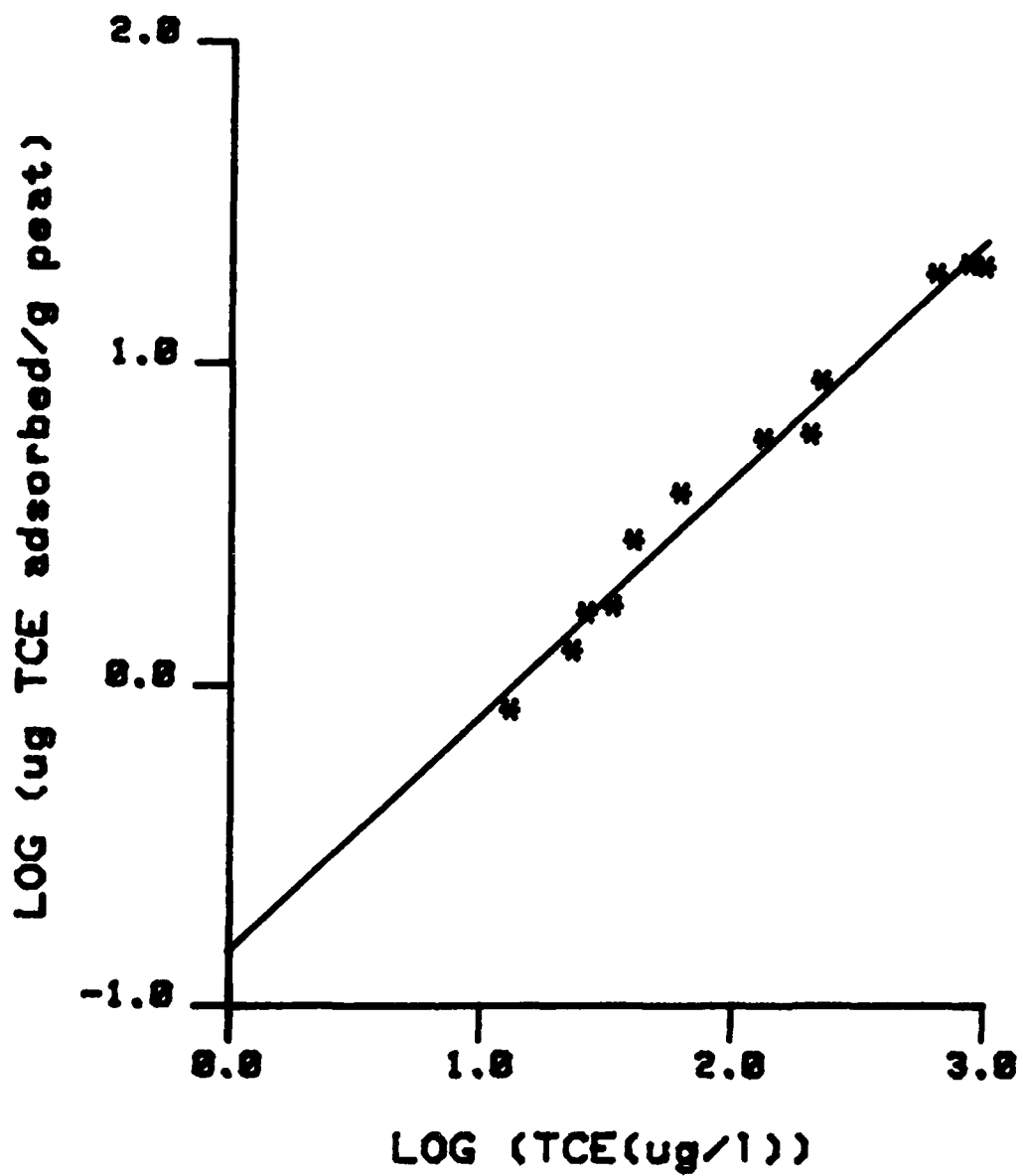


Figure 3. Freundlich isotherm of trichloroethylene adsorption by organic peat.

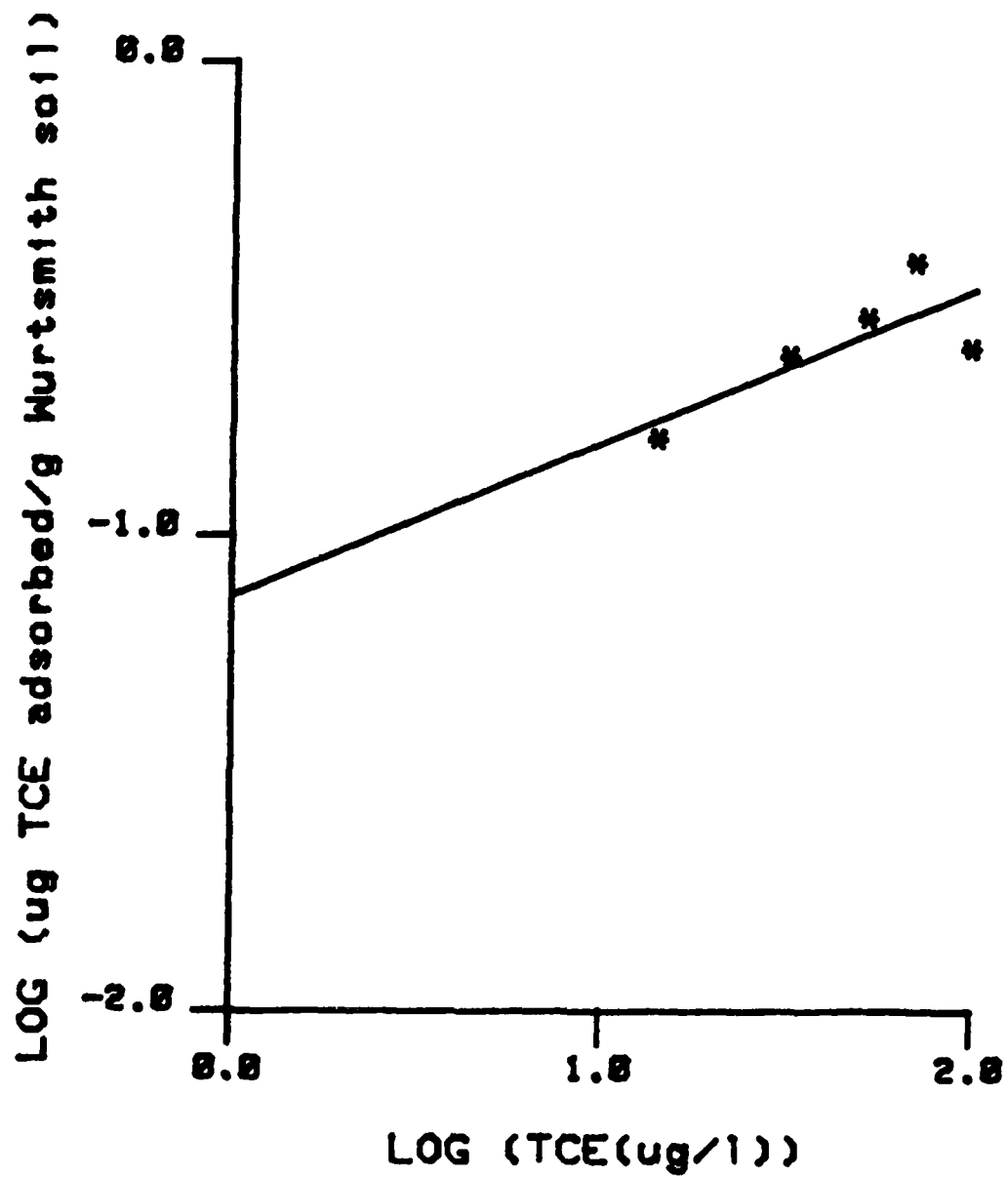


Figure 4. Freundlich isotherm of trichloroethylene adsorption by Wurtsmith AFB soil.

Table 1: Soil Adsorption Parameters for TCE.

Solid	K	1/n	r	X(ug/g at C=100 ug/l)
FeOOH	-	-	-	< 0.1
Mn _x O _y	0.0085	0.938	0.907	0.639
Kaolinite	-	-	-	< 0.2
Montmorillonite	0.0970	0.705	0.968	2.49
Peat	0.148	0.737	0.990	4.41
Wurtsmith AFB	0.0759	0.324	0.774	0.337
Activated Carbon (EPA)	377.	0.623	0.990	6640.

For the inorganic soils the increase in adsorption capacity resembles that of the increase in surface area. Since trichloroethylene is nonionic and only slightly polar, adsorption onto these soils is probably due to weak forces or hydrogen bonding rather than stronger electrostatic forces or even stronger chemical bonding.

The TCE was found to adsorb much more strongly onto the peat and activated carbon; that is, as the organic carbon content increased so did the amount of TCE adsorbed. This is supported by Karickhoff, Brown, and Scott (11) who demonstrated that hydrophobic compounds such as chlorinated hydrocarbons adsorbed in proportion to the organic carbon content of the soil. The largeness of the octanol/water partitioning coefficient of TCE, 195, is a good indicator that the compound will prefer the organic solid to remaining in solution.

Karickhoff et al (11) developed the following adsorption isotherm for soils of varying organic content:

$$X = 0.00063 K_{ow} f_{oc} C \quad (9)$$

where:

X = ug adsorbed/g soil
K_{ow} = octanol/water partitioning coefficient
f_{oc} = fraction organic carbon in soil
C = equilibrium concentration (ug/l)

For TCE, substituting for K_{ow} gives:

$$X = 0.123 f_{oc} C \quad (10)$$

For an equilibrium concentration of 100 ug/l and totally organic soil, the amount of TCE adsorbed would be 12.3 ug/g.

When compared to the inorganic soils used, it is evident that the organic fraction is important; however, as the carbon content of the soil decreases, the inorganic soil could actually control the amount of TCE adsorbed. For example, if the soil were composed of 5/6 montmorillinite and 1/6 organic carbon, the equations indicate that adsorption would be split evenly between the two solids; while if the organic carbon content were less, the clay would predominate in the removal of TCE from solution.

The possible affects of adsorption on the partitioning of TCE between the soil and groundwater can be seen by studying the Wurtsmith soil. The following values for the aquifer were assumed:

Soil bulk density = 2.5 kg/l
void volume = 50%
C = 100 ug/l, X = 0.337 ug/g.

For a total volume of 2.0 l, there would be 1.0 l of soil weighing 2,500 g and 1.0 l of water. This would result in 843 ug of TCE being adsorbed on the soil, or 8.4 times the amount in an equal volume of water. Due to the size distribution of the soil, the actual amount adsorbed would probably be less; however, the point is that the soil could act as a significant sink for the halogenated hydrocarbon.

V. CONCLUSIONS:

This project resulted in several conclusions regarding the adsorption of trichloroethylene onto inorganic soils.

1. When using volatile organics such as TCE, it is important to design the experiment to minimize evaporative losses due to either poor sealing or transfer of aqueous solutions.

2. Inorganic soils do adsorb chlorinated hydrocarbons to some extent. Adsorption increased in the following order: iron oxide, kaolinite, manganese oxide, montmorillonite, organic peat.

3. While organic carbon in the soils has a greater affinity for TCE, inorganic solid adsorption may be important when the organic fraction is relatively small, as may be the case in some aquifers.

4. The Wurtsmith AFB soil has an adsorption capacity of 0.34 ug/g when the equilibrium TCE concentration is 100 ug/l.

VI. RECOMMENDATIONS:

Based on this study several recommendations can be made for future investigations.

1. The effects of solution variables, such as pH, ionic strength, organic liquid concentrations, and temperature, on TCE adsorption should be ascertained. Controlled mixtures of various soil components could also be studied.

2. Adsorption/desorption studies should be conducted to determine whether the process is reversible. This will help in deciding whether the pumping out of aquifers will be sufficient to remove TCE, or whether the soils will act as sink/sources for organic pollutants.

3. Column studies would be helpful in ascertaining how TCE moves in aquifers. The effects of saturated and unsaturated flow should be studied due to the compound's volatility.

4. Regarding Wurtsmith AFB, both batch and column adsorption experiments should be conducted to study how TCE behaves in the aquifer. This will help in evaluating the present proposed clean-up scheme.

5. Future adsorption studies should use a method to directly measure TCE adsorption for comparison with that calculated due to disappearance from the solution phase. Recovery by organic solvent extraction should be considered.

REFERENCES

1. Petura, J. C., "Trichloroethylene and Methyl Chloroform in Groundwater: A Problem Assessment," J. American Water Works Association, 40, 200, (1981).
2. McCarty, P. L., Reinhard, M., and Rittman, B. E., "Trace Organics in Groundwater," Environmental Science and Technology, 15, 40, (1981).
3. Means, J. C., Wood, S. G., Hassett, J. J., and Banwart, W. L., "Sorption of Polynuclear Aromatic Hydrocarbons by Sediment and Soils," Environmental Science and Technology, 14, 1524, (1980)
4. US Environmental Protection Agency, Water Related Environmental Fate of 129 Priority Pollutants, EPA-440/4-79-029, (1979).
5. Dilling, W. L., Tefertiller, N. B., and Kallos, G. J., "Evaporation Rates and Reactivities of Methylene Chloride, Chloroform, 1, 1, 1 - Trichloroethane, Trichloroethylene, Tetrachloroethylene, and Other Chlorinated Compounds in Dilute Aqueous Solutions," Environmental Science and Technology, 9, 833, (1975).
6. US Environmental Protection Agency, Carbon Adsorption Isotherms for Toxic Organics, EPA-600/8-80-23, (1980).
7. Richter, R. O., "Attenuation of Heavy Metals in a Soil/Water System Underlying a Fly Ash Pond: With Emphasis on Nickel Adsorption by Hydrous Oxide," PhD Dissertation, Notre Dame, (1978).
8. Dietz, E. A., Jr., and Singley, K. F., "Determination of Chlorinated Hydrocarbons in Water by Head Space Gas Chromatography," Analytical Chemistry, 51, 1809, (1979).
9. Gossett, J. M., unpublished data.
10. Weber, W. J., Jr., Physicochemical Processes for Water Quality Control, Wiley Interscience, New York, 206-211, (1972).

11. Karickhoff, S. W., Brown, D. S., and Scott, T. A., "Sorption of Hydrophobic Pollutants on Natural Sediments," Water Research, 13, 241, (1979).

1981 USAF - SCEEE SUMMER FACULTY RESEARCH PROGRAM

Sponsored by the

AIR FORCE OFFICE OF SCIENTIFIC RESEARCH

Conducted by the

SOUTHEASTERN CENTER FOR ELECTRICAL ENGINEERING EDUCATION

FINAL REPORT

THE EFFECTS OF 2,3,7,8-TETRACHLORODIBENZO-p-DIOXIN (TCDD)

ON

TRIIODOTHYRONINE (T₃) BINDING TO RAT ISOLATED HEPATIC NUCLEI

Prepared by: Dr. John J. Riggs

Academic Rank: Assistant Professor

Department and University: Dept. of Physiology/Pharmacology
School of Vet. Med.
Tuskegee Institute
Tuskegee Institute, AL

Research Location: Air Force Aerospace Medical Research Laboratory
Toxic Hazards Division
Toxicology Branch
Wright-Patterson AFB, Ohio 45433

USAF Research Colleague: Dr. Melvin E. Andersen

Date: August 27, 1981

Contract No: F49620-79-C-0038

THE EFFECTS OF 2,3,7,8-TETRACHLORODIBENZO-p-DIOXIN (TCDD)
ON
TRIIODOTHYRONINE (T₃) BINDING TO RAT ISOLATED HEPATIC NUCLEI

by
JOHN J. RIGGS

ABSTRACT

The toxic effects caused by 2,3,7,8-tetrachlorodibenzo-p-dioxin (TCDD) are remarkably similar to those caused by certain long-chain perfluorinated fatty acids. The Air Force is interested in these chemicals because TCDD was a contaminant of herbicide formulations used in Vietnam and derivatives of the perfluorinated fatty acids are used today as surfactants in fire fighting foams. Their mechanisms of toxicity, in particular TCDD, remain unknown. Because of the structural similarity between TCDD and triiodothyronine (T₃), it was of interest to determine if TCDD antagonized the binding of T₃ to its nuclear receptor sites. Animals were treated with a single dose of TCDD (50 µg/kg IP) and sacrificed 7,9,14, and 21 days after treatment. The livers were removed, nuclei were isolated, incubated with 0.5 pM of radioactive T₃ solution alone or with increasing amounts of non-radioactive T₃ (1.0 to 1000 pM). In the control animal (acetone/corn oil) 6% of incubated T₃ was specifically bound to the Triton X-100 washed nuclei. Treated animals sacrificed at 7,9,14, and 21 days showed a decrease in specific T₃ binding of 65%, 80%, 98% and 98%, respectively. The data clearly showed a decrease in T₃ binding capacity in TCDD treated animals. A Scatchard plot showed a single class of T₃ binding sites, with an apparent association constant of $7.8 \times 10^8 \text{ M}^{-1}$, and a binding capacity of 1.36 picomoles T₃ for nuclei obtained from 0.25g of liver.

ACKNOWLEDGEMENT

The author would like to thank the Air Force Systems Command, the Air Force Office of Scientific Research, and the Southeastern Center for Electrical Engineering Education for providing him with the opportunity to spend a very fruitful and challenging summer at the Air Force Aerospace Medical Research Laboratory, Wright-Patterson AFB, Ohio. He would like to acknowledge the Laboratory, in particular the Toxic Hazards Division, for its hospitality and excellent working conditions.

Finally, he would like to give special thanks to Dr. Melvin E. Andersen for suggesting this interesting area of research and for his collaboration and guidance, and he would also like to acknowledge many helpful discussions with Dr. M. Paul Serve and Dr. Carl T. Olson.

I. INTRODUCTION

Personnel in the Toxicology Branch of the Air Force Aerospace Medical Research Laboratory pursue a variety of research efforts in the area of mammalian toxicology. This work is designed to evaluate the toxic potential of chemicals found in Air Force work environments. One of the major efforts at present is a broadbased program investigating the detailed molecular mechanisms responsible for the mammalian toxicity of halogenated aromatic and polyhalogenated aliphatic chemicals of special interest to the Air Force. These chemicals include chlorinated dibenzo-p-dioxins, contaminants of the phenoxyacetic acid herbicides, and perfluorinated fatty acids, surfactants used in fire fighting foams. Technical approaches for this program involve measuring alterations in structure and function of biological membranes and assessing the effects of these chemicals on endogenous hormone function.

2,3,7,8-Tetrachlorodibenzo-p-dioxin (TCDD) is formed as an unwanted contaminant in the synthesis of 2,4,5-trichlorophenol, which itself is used in the manufacture of 2,4,5-trichlorophenoxyacetic acid (2,4,5-T), related herbicides, and the germicide hexachlorobenzene.¹ TCDD is the most toxic and extensively studied isomer of the chlorinated dibenzo-p-dioxins.^{2,3} The (LD₅₀)₃₀ values for single oral doses range from 0.6 µg/kg in the guinea pig to 3000 µg of TCDD/kg in the hamster.

A variety of toxic effects has been observed in both humans and experimental animals exposed to TCDD. They include embryo and fetotoxicity,⁴ thymic atrophy, liver damage,⁵ reduced immunological responses,⁶ and chloracne.⁷ The most common toxic effect seen in all species exposed to TCDD is thymic atrophy and loss in body weight. Despite the numerous investigations over the past fifteen years, there are insufficient data to support a unified hypothesis explaining the mechanism, or mechanisms, responsible for TCDD lethality. Although various organs are involved in TCDD toxicity, damage to these organs does not appear to be sufficient to be the cause of death.

The thyroid hormone function was implicated in TCDD toxicity when Bastomsky⁷ reported a fourfold increase in biliary excretion of thyroxin (T₄) as its glucuronide conjugate after TCDD treatment. This reduced serum T₃ concentrations to 50% of normal, increased iodide uptake, increased serum

thyrotropin concentration, and produced goiters. These results and the fact that some of the symptoms of TCDD toxicity resemble those of the hypothyroid state prompted Neal *et al.*⁸ to examine the effects of TCDD on thyroid function. Neal *et al.*⁸ did find that daily injections of 200 µg/kg T₃ prolonged time-to-death. In this study, 200 µg T₃/kg/day was the highest concentration used and T₃ is a poorer choice for restoring thyroid function than would be T₄. The work of Neal *et al.*⁸ then cannot be considered conclusive evidence against a role for TCDD as a thyroid hormone antagonist. A more definitive answer to the question of the role of thyroid hormone antagonism by TCDD can be obtained by determining the effect of TCDD on the specific nuclear receptors for T₃. Therefore, it was of interest to examine specific T₃ binding by nuclei of treated rats at various times after treatment with TCDD.

II. OBJECTIVE

The objective of this study was to determine if 2,3,7,8-tetrachlorodibenzo-p-dioxin (TCDD) antagonized the binding of triiodothyronine (T₃) to its specific nuclear receptor sites in isolated rat liver nuclei.

III. METHODS AND MATERIALS

Normal, male Fischer 344 rats weighing between 200-250g were divided into two groups: Group I, vehicle control (acetone/corn oil); Groups II, dioxin treated, 50 µg/kg IP. Individual rats from Group II were sacrificed at days 7,9,14, and 21, respectively.

Animals were sacrificed, livers rapidly removed, weighed, and placed on ice. Livers were minced and subsequently homogenized in 0.32 M sucrose-3 mM MgCl₂ with a Potter-Elvehjem homogenizer. The homogenate was filtered through 8-ply gauze and centrifuged at 750 x g for ten minutes. The crude nuclear pellets were resuspended in 2.4M sucrose-3 mM MgCl₂ and centrifuged at 53,000 x g for forty-five minutes. The isolated nuclear pellets were resuspended in 10 ml of nuclear buffer [0.32M sucrose-3 mM MgCl₂, 20.0 mM TrisHCl (pH 7.85), 3.0 mM MgCl₂, 5.0 mM dithiothreitol, 2.0 mM EDTA, 25.0 mM KCl, and 5% glycerol (vol/vol)]. Aliquots of the nuclear suspension equivalent to 250 mg of liver were incubated in triplicate either with radioactive T₃ solution (0.5 pM) alone or with that plus increasing amounts of non-radioactive T₃ (1.0 to 1000 pM) in a volume of 1 ml of incubation medium for thirty minutes at 37°C. At the end of incubation, 1 ml of Triton X-100 in 0.32M sucrose-3 mM MgCl₂ was added to all tubes, which were placed in an ice bath for fifteen minutes. The nuclei were recovered by centrifugation at

10,000 x g for ten minutes, the supernant was aspirated, and the nuclear pellets were counted in a Packard Autogamma Counter. The counting rate of the pellets was determined as a measure of total radioactive triiodothyronine binding to the nuclei at each ligand concentration. Total nuclear binding was then corrected for nonspecific binding which was taken as the percent binding of radioactive triiodothyronine in the presence of a 1,000 molar excess of nonlabeled ligand. The difference between total and nonspecific binding was the percent of radioactive triiodothyronine bound to specific, low capacity, high affinity nuclear sites.

IV. RESULTS

After incubating isolated nuclei from a control animal with tracer T_3 (0.5 pM), 6% of the incubated T_3 was recovered in the Triton X-100 washed nuclear pellets which represented T_3 binding. Animals sacrificed at 7, 9, 14, and 21 days after TCDD treatment showed a progressive decrease in labeled T_3 binding when compared to control. The labeled T_3 recovered at 7 and 9 days after treatment decreased 65% (2.1) and 85% (1.2), respectively. The maximum decrease (98%) in T_3 binding occurred at 14 and 21 days. In each treated group, decreases in labeled T_3 binding paralleled the loss in body weight.

The results from this study showed that TCDD decreased the binding of labeled T_3 to its specific nuclear receptor sites with an abolition of binding occurring at 14 days. A Scatchard plot of data obtained from the control animal demonstrated a single class of binding sites for T_3 with an apparent association constant of $7.8 \times 10^8 M^{-1}$ and a binding capacity of 1.36 picomoles T_3 for nuclei obtained from 0.25g of liver.

V. RECOMMENDATION

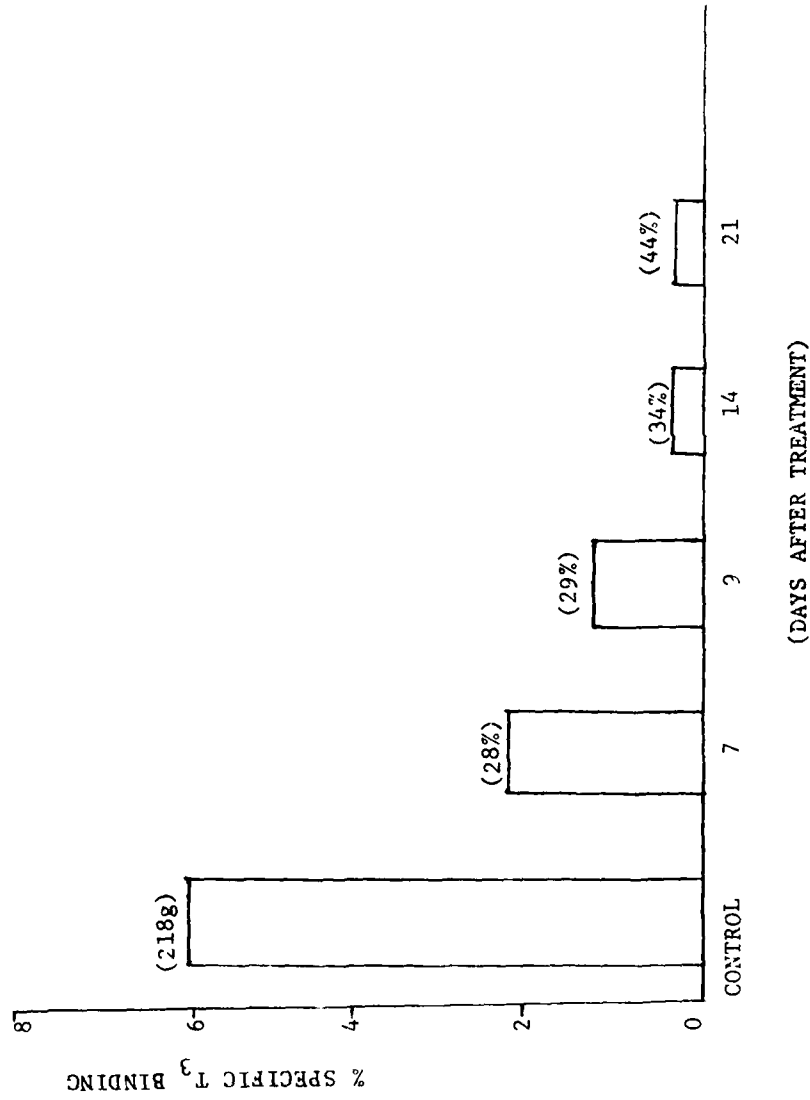
This method has demonstrated its use in assessing the effects of the chlorodibenzo-p-dioxin and other compounds on triiodothyronine (T_3) binding and these studies should be enlarged.

Other recommendations for follow-on research are: (1) to determine the time when the decrease in T_3 binding first occurs; (2) to determine the dose-effect relationship for this decreased binding; and (3) to increase the number of animals in each treated group.

REFERENCES

1. IARC Monographs on the Evaluation of the Carcinogenic Risk of Chemicals to Man, i.e., Some Fumigants, the Herbicide 2,4-D and 2,4,5-T, Chlorinated Dibenzodioxins and Miscellaneous Industrial Chemicals, Lyons, 1977.
2. Schwetz, B. A., Norris, J. M., Sparschu, G. K., Rowe, V. K., Gehring, P. J., Emerson, J. L., and Gerbig, G. C. Toxicology of chlorinated dibenzo-p-dioxins. Environmental Health Perspective, Vol. 5, pp. 87-100, 1973.
3. McConnell, E. E., Moore, J. A., Haseman, J. K., and Harris, M. W. The comparative toxicity of chlorinated dibenzo-p-dioxins in mice and guinea pigs. Toxicology and Applied Pharmacology, Vol. 44, pp. 335-356, 1978.
4. Neubert, D., Zeno, P., Rothenwallen, A. and Merker, H. J. A survey of the embryotoxic effects of TCDD in mammalian species. Environmental Health Perspective, Experimental Issue No. 5., pp. 67-80, 1973.
5. Guyton, B. N., Vos, J. G., Moore, J. A., Zinkle, J. G., and Bullock, B. C. Pathologic effects of 2,3,7,8-tetrachlorodibenzo-p-dioxin in laboratory animals. Environmental Health Perspective, Vol. 5, pp. 125-140, 1973.
6. Vos, J. G., Moore, J. A., and Zinkle, J. G. Effects of 2,3,7,8-tetrachlorodibenzo-p-dioxin on the immune system of laboratory animals. Environmental Health Perspective, Vol. 5, 149-162, 1973.
7. Bastomsky, C. H. Enhanced thyroxin metabolism and high uptake goiters in the rats after a single dose of 2,3,7,8-tetrachlorodibenzo-p-dioxin. Endocrinology, Vol. 101, pp. 292-296, 1977.
8. Neal, R. A., Beatty, P. W., and Gasiewicz, T. A. Studies of the mechanism of toxicity of 2,3,7,8-tetrachlorodibenzo-p-dioxin (TCDD). Annals of the New York Academy of Sciences. Vol. 320, pp. 204-213, 1979.

SPECIFIC BINDING OF T₃ TO ISOLATED HEPATIC NUCLEI FROM TCDD TREATED RATS



() = % decrease in body weight

FIGURE 1

1981 USAF - SCEEE SUMMER FACULTY RESEARCH PROGRAM

Sponsored by the

AIR FORCE OFFICE OF SCIENTIFIC RESEARCH

Conducted by the

SOUTHEASTERN CENTER FOR ELECTRICAL ENGINEERING EDUCATION

FINAL REPORT

VISUAL CUES IN THE SIMULATION OF LOW LEVEL FLIGHT

Prepared by: Dr. Edward J. Rinalducci, Ph.D.

Academic Rank: Professor

Department and University: School of Psychology
Georgia Institute of Technology

Research Location: Air Force Human Resources Laboratory/Operations Training
Division, Williams AFB, AZ 85224

USAF Research Colleague: Dr. Thomas Longridge, Ph.D.

Date: August 6, 1981

Contract No: F49620-79-C-0038

VISUAL CUES IN THE SIMULATION OF LOW LEVEL FLIGHT

by

Dr. Edward J. Rinalducci, Ph.D

ABSTRACT

Visual cues used by pilots to maintain altitude in low level flight simulation were examined. In particular, terrain texture in the form of black vs. white topped inverted cones, the presence or absence of vertical development, and the effects of rate of motion on terrain features were investigated using pilots who varied in flying experience. Less experienced pilots demonstrated increases in their mean altitude and RMS deviation with an increase in airspeed or with an increase in airspeed combined with a lack of vertical development in terrain features. Experienced pilots on the other hand, only showed increases in mean altitude and RMS deviation with an increase in airspeed. No differences were found between all black and white topped cones. Suggestions are made for application of research findings to CIG development and pilot training.

I.. INTRODUCTION:

Important visual factors are involved in flight simulation and the training of pilots. The various tasks especially required of U.S. Air Force pilots which involve these visual factors include formation flying and aerial refueling, low level flight, weapons delivery, and approach and landing. The research and objectives discussed in the following pages are primarily directed toward the various aspects of visual space perception and information processing relevant to visual flight simulation. These interests and objectives are commensurate with those of the Air Force Human Resources Laboratory located at Williams Air Force Base, AZ.

Depth perception has obvious relevance to visual flight simulation and the maintenance of altitude in flight. Outside the primary cue of retinal disparity there are the secondary cues of aerial perspective, linear perspective, retinal image and familiar size, texture gradient, motion parallax, streaming, interposition, height of an object in the visual field, light and shadows, as well as the physiological cues of accommodation and convergence (Graham, 1966; Harker and Jones, 1980). With regard to flight simulation some of these and related cues are more important than others especially when viewing a dynamic scene. Stenger, Zimmerlin, Thomas, and Braunstein (1981) and Harker and Jones (1980) in recent reports cite texture as a very important terrain feature in the dynamic simulator or flight environment and in the maintenance of low level flight. Unique terrain features and surface detail enables a pilot to keep track of his position and estimate altitude. Closely related to texture would be motion through the visual environment as influenced by airspeed. Motion would particularly effect the cues of motion parallax and streaming in actual flight and motion parallax in simulated flight.

The ASPT (Advanced Simulator for Pilot Training) at Williams Air Force Base provides an ideal environment for a visual scientist to study depth/distance cues in a realistic dynamic scene and still maintain considerable control over the visual cues. In addition, student pilots familiar with the operation of the simulator are available for participation in the research effort.

II. OBJECTIVES:

The main objective of the present project was to investigate the depth/distance cues employed in low altitude flight. Based on the on-going research efforts of Dr. E. L. Martin of AFHRL with regard to terrain features in the CIG display of the ASPT, it appeared that those features consisting of inverted tetrahedrons or cones with white tops showed some advantage over the all black cones in the maintenance of altitude in low level flight in the simulator. This finding seemed to suggest that a texture cue (in the form of contrast) was being employed by pilots in the simulator when using the cone terrain features. In addition, there had been some suggestion that vertical development of terrain features should also influence depth/distance judgments in flight (Harker and Jones, 1980). Therefore, the white triangular tops of the inverted cones were taken from the cones and placed, for all practical purposes, on the ground (OMSL) with the same spatial distribution as the inverted cones (average distribution for all terrain features used in study was a 1500 foot separation). Also, as differences in texture or surface detail should vary with rate of motion, it was decided that manipulation of airspeed should influence altitude maintenance.

Thus, the specific objectives of the study were to examine: (1) terrain texture in the form of all black vs. white topped cones; (2) the effects of the presence (or absence) of vertical development in terrain features; and (3) the effects of rate of motion on the maintenance of altitude in low level flight operations. An additional objective was realized by running an another group of subjects which had considerable flying experience. Thus, the effects of flying experience was also examined..

III. METHODS:

Subjects

Fourteen subjects participated in the first part of the study. However, the data for one subject was deleted leaving a total of 13. The data for the one deleted subject was contaminated due to the incorrect loading of the computer program which provided a flight path marker on the HUD. This gave the subject an additional reference for about half

of the trials. Inspection of the data indicated improved performance over the other subjects for the period during which the flight path marker was present and a degraded performance where it was absent. The subjects in the first phase of the study were all B-course pilots. B-course pilots are relatively inexperienced pilots (average flying time of 779 hours) who have recently completed UPT and are learning to fly the F-16. In the second part of the study, 6 T-course pilots were employed. T-course pilots are transitioning from other aircraft (e.g., F-4, F-111, etc.) to the F-16, and therefore, have more flying experience (average flying time of 1864 hours). All pilots had just completed at least 4 hours of training in the ASPT, F-16 cockpit. A total of 20 pilot subjects were employed in the entire study, however only the data from 19 subjects were used in the data analysis.

Apparatus

Fourteen subjects were run on the ASPT. This apparatus has been described in detail by Buckland, Monroe, and Mehrer (1980), but will be described briefly below.

The ASPT consists of two fully instrumented cockpits with wraparound visual systems. One cockpit is configured as the A-10 and the other as the F-16. The visual system consists of seven 36-inch CRTs (cathode-ray tube) which provide a visual field of + or - 150 degrees horizontally and + 110 to -40 degrees vertically.

The visual scenes are produced by computer image generation (CIG). A wide range of imagery is available with the present ASPT hardware and software. All objects and surfaces presented in the visual field consist of straight line segments or edges (2000 edges available). The CIG is updated 30 times per second in response to aircraft movement through the simulated environment.

The ASPT is able to record, store, and score various pilot performance parameters automatically. The measures discussed below, are sampled and stored 3.75 to 15 times/second depending on their nature.

The ASPT cockpits are also mounted on six-degree-of-freedom, hydraulically actuated motion platforms. Additional motion cues can be provided by 32-bellow pneumatic seats with variable tension lap belts. The motion systems were not active during the present study

Independent Variables

The major factors which were varied consisted of terrain texture and air speed. Terrain texture cues were varied by employing inverted tetrahedrons or cones which had either white tops or were all black and by employing white triangles on the ground. The cones were 35 feet high and had about a 10 foot base. The triangles had no height and also had a 10 foot base. The triangles essentially consisted of the tops or bases of the inverted cones. The cones provided vertical development, whereas this cue was removed in the case of the triangles. Both types of cones and the triangles were distributed with an average density or separation of 1500 feet. Thus, there were three terrain features all with the same distribution density: black cones with white tops, all black cones, and white triangles on the ground. In addition, there were two airspeeds: 300 KIAS and 540 KIAS. The difference in air speed provided a rate of texture motion which could produce differences in a depth cue such as motion parallax.

Altitude was to be maintained under all conditions at 200 feet AGL. Ground elevation was OMSL. The 200 foot altitude was chosen so as the various terrain features would be readily visible but still represent low level flight.

Experimental Design and Procedures

The experimental design used in the study was a 3 X 2 factorial design (3 terrain features X 2 airspeeds) with repeated measures on each variable producing a 3 X 2 within-subjects design. Each student pilot was run for a total of 15 trials (about 1 hour and 10 minutes in duration). The first three trials were practice trials and the student pilots were informed of their altitude throughout the trial in order to provide knowledge-of-results or feedback. The experimenter presented the aircraft's altitude every few seconds over the student pilot's headset. However, during the last 12 trials they were only told how close they came to the prescribed altitude at the end of the trial. Three of the six conditions were chosen at random for the 3 practice trials and during the following 12 trials the two trials for each

of the six conditions were distributed randomly.

Each student pilot received both a verbal and a written briefing prior to participation in the experiment. The student pilot was informed that he was to fly a prescribed course at an altitude of 200 feet and to maintain an airspeed of either 300 or 540 KIAS. The course consisted of three legs arranged at right angles. Each leg was seven miles long and two miles wide. An aiming tower measuring 450 feet was positioned at each end of a leg. A tone was presented through the student pilot's headset and served as a cue to initiate a left or right turn as required. The turn was a 90 degree heading change. The course is shown schematically in Fig. 1 (see Appendix).

Each pilot was initialized to the desired altitude at the beginning of each trial. In addition, whenever a pilot fell below or exceeded his prescribed airspeed by more than 40 KIAS an automated voice said "Low, Low", etc. or "High, High", etc. until the appropriate increases or decreases in airspeed were made.

All pilots were questioned immediately after participating in the experiment to determine their preference for the different terrain features (in rank order), and the different cues they used to maintain altitude.

Dependent Measures and Data Analysis

The ASPT has the capacity to record and store a wide variety of variables associated with low level flight simulation. Table 1 (see Appendix) shows the performance measures which were analyzed in this study. These include the mean altitude and RMS deviation from 200 feet for the total course, as well as the mean altitude and RMS deviation for level flight portions of the course and the turns. In addition, the number of terrain crashes for each of the six conditions were recorded.

IV. RESULTS

The results of both studies are presented in tabular form. Results of the MANOVAs (BMDX69X) and the values of omega squared for the B-course pilots are shown in Tables 2-7. Tables 8-13 present the mean values for altitude and RMS deviation (from 200 feet) for the entire course, for level

flight only, and for turns only for the same subjects. Table 14 shows the number of terrain crashes for each terrain feature and air speed combination. The results of the MANOVAs and the values of omega squared for the T-course pilots are shown in Tables 15 and 16, and the mean values for altitude and RMS deviation for the entire course are shown in Tables 17 and 18. See Appendix for all Tables.

Inspection of Tables 2-13 show that, in general, for the B-course or less experienced pilots, mean altitude and RMS deviation is most effected by the variables of airspeed and texture or terrain features. Tukey tests (p less than .01) showed that these values increased significantly with an increase in airspeed and when white triangles were used in place of either type of cone (all black or white top). These factors usually accounted for the largest amount of the total variance as shown by the values of omega squared. In addition, there was a significant subjects effect.

The results for the T-course or more experienced pilots are shown in Tables 15-18. Here, the only significant effects were for airspeed and subjects with texture being non-significant.

Table 14 shows the number of terrain crashes for each terrain feature-air speed combination. The results are shown for both B-course and T-course pilots (in parentheses). In general, the overwhelming number of terrain crashes for B-course pilots (16 out of 19) and T-course pilots (4 out of 5) occurred for the conditions which employed white triangles. For both groups most crashes occurred in the right turn (20 out of 24).

Finally, all subjects were interviewed immediately after participating in the experiment. As indicated above, they were questioned as to the cues they used in maintaining their altitude and their preferences (in rank order) of the three terrain features. For the B-course pilots, all save two preferred the white topped cones first, the all black cones second, and the white triangles third. Of the two who ranked the terrain features differently, one did not discriminate between the different cones and the other preferred the all black cones first followed by the white topped cones and then the triangles. However, the T-course pilots tended to choose the

all black cones first, the white topped cones second, and the triangles third. The other two T-course pilots reversed the order of cone preference. In all cases, the white triangles were least preferred by pilots.

With regard to the kinds of cues the pilots reported they used, several interesting and often similar comments were made by subjects from both groups (B- and T-course pilots). The main comments are briefly summarized as follows: (1) the HUD was used as a visual reference relative to the aiming towers or the horizon; (2) the use of peripheral vision and the rush; (3) the necessity of having vertically developed terrain features; (4) the relative height of the terrain features and the aiming towers; (5) the rate of movement of the terrain features; (6) the size of the white triangles; and (7) the use of the VVI on the HUD to provide an indication of altitude. Few differences were observed between the comments of B-course and T-course pilots.

V. DISCUSSION:

In general, the results obtained with both groups of subjects (B-course and T-course pilots) in the present study show that airspeed has the greatest effect on the dependent variables of mean altitude and RMS deviation. In other words, an increase in airspeed from 300 to 540 KIAS produced a significant increase in mean altitude and RMS deviation. However, less experienced pilots (B-course) also show significantly increased altitude and RMS deviation measures at the higher airspeed when there is a lack of vertical development in the terrain features (white triangles vs. cones). This effect was not found with the more experienced pilots (T-course), which may suggest that they are better able to utilize other cues in their visual environment (e.g., the VVI, the HUD frame, the windscreen frame, the combining glass of the HUD, etc.) in the absence of vertically developed terrain features. No significant effects were found when texture in the form of contrast was manipulated (all black vs. white topped cones) for either group. Thus, vertical development appears to be the most important terrain feature. This finding is emphasized when the data for terrain crashes are examined (see Table 14). As previously noted,

most of the crashes occurred when using the white triangles for both groups. This indicates that vertical development is also important to the more experienced as well as the less experienced pilots. The ability of a pilot to maintain altitude and RMS deviation with or without vertically developed terrain features in the CIG of the flight simulator might, with further study, be employed as a predictor of pilot success.

It was also noted that most crashes occurred when pilots attempted to make a right turn. This finding may be due to the difficulty many pilots experience in making right vs. left turns.

A significant subject effect with both B-course and T-course pilots may well be due to the differences in their flying experience. Pilots in both courses tended to vary (SD = 684 for B-course pilots and SD = 767 for T-course pilots for hours flown) both in the number of hours and the type of aircraft flown.

Finally, in that no significant differences were obtained with the two different types of cones, the one that is most edge efficient in the CIG display would be the most appropriate. As the all black cones are more edge efficient due to hidden contours than are the white topped cones, the black cones should be preferred as terrain features.

VI. RECOMMENDATIONS:

Implementation of Research Results

The results of the present research indicate that vertical development of terrain features is very important in the maintenance of altitude in low level flight simulation. This is particularly true for higher airspeeds (540 vs 300 KIAS). In addition, the use of vertically developed terrain features may be more important for less experienced pilots in maintaining altitude than for those with more experience. Thus, it would be more important to the less experienced pilot to have vertically developed terrain features in the CIG of the flight simulator. In addition, black cones due to their edge efficient nature when compared to white topped cones would be more desirable for CIG since no significant differences were found between them.

Suggestions for Follow-on Research

Several suggestions for follow-on research related to the visual

aspects of flight simulation and pilot training are described below.

First, it would seem to be useful to developers of simulator CIG that a study be undertaken to determine the optimal height for vertically developed terrain features (e.g., the inverted cones used in the present research effort). Another objective of such a study would be to determine whether or not there needs to be a particular mixture of object heights or only a single height. Data should be collected both in a static and a dynamic scene situation and with pilots and non-pilots. Although it has been generally assumed that pilot subjects would be more appropriate than non-pilot subjects for all phases of research having to do with flight training and simulation, it remains to be proven empirically. Proposed research in this area would provide the necessary empirical data. If the differences between pilots and non-pilots were found to be minimal or only a matter of degree then the use of large numbers of non-pilots would be more economical for preliminary research questions. This would allow for the elimination or isolation of certain cues in preliminary research and a more economical employment of pilot subjects. In addition, an advantage of the combined use of static as well as dynamic presentation of terrain features and depth cues would also be one of economy (static scenes such as those provided by photographic slides would be more economical than a dynamic presentation) and would provide empirical support of any real differences between the two modes of presentation. Here again, empirical evidence on this issue is lacking. Finally, those cues (e.g., vertical development, aerial perspective, texture gradient, velocity gradient, etc.) identified in the laboratory as effecting depth/distance judgments would eventually be incorporated into simulator CIG and tested using pilot observers. For example, altitude judgments using different heights of vertically developed terrain features could be investigated in the laboratory using slides for static scene presentation and using either motion pictures, video disk and monitor, or video projection for dynamic scenes. The findings could then be employed in the dynamic scene situation of the simulator for further examination. In the simulator mean altitude and RMS deviation measures could be obtained by flying a prescribed course using the vertically developed terrain features.

A related and important research problem concerns the more general question of the use of texture in CIG visual displays. In particular, are texture gradients or velocity gradients more important in conveying surface slant, distance, and curvature to observers (Stenger, et al, 1981)? If velocity gradients are relatively more important than texture gradients, recognizable texture elements may not be necessary as symbolic texture elements (such as those used in the present study) and approximate texture gradients may be sufficient. Basic psychophysical research in this area using static and dynamic scenes could be conducted using the methods referred to above in conjunction with a microcomputer for data sequencing, collection, and analysis.

Second, judgments of altitude using the method of magnitude estimation with the free modulus variation could be made using slides of the simulator visual display taken at different altitudes above the ground using different terrains and terrain features. A preliminary study has already been carried out by Dr. J. C. De Maio and this investigator. Power functions and slopes of the regression lines would be obtained for different terrain features and student pilots of varying experience as well as a large non-pilot population. By using subjects with a wide variety of flying experience as well as no experience, ability to judge altitude might be employed as a predictor of performance depending on the outcome of the investigation. The proposed study could be augmented by photographs taken from the HUD camera of an F-16 flying at different altitudes over a given terrain. Altitude judgments could then be made with both types of stimuli (CIG or actual terrain photographs) in order to determine if the power functions obtained are similar. Again, subjects should range from those with no flying experience to those who are relatively experienced. Direct scaling procedures such as magnitude estimation provide a potentially powerful and low cost technique for evaluating visual displays and CIG, but they will also need to be evaluated relative to the pilot-simulator approach.

Advantages to be obtained from such a study would have a direct impact on CIG development and pilot training. In the usual magnitude estimation study (direct scaling), if one plots sensation magnitude as a function of physical magnitude and obtains a linear function (a slope of 1 on a log-log plot) this would indicate a proportional relationship between sensation

magnitude of altitude and actual height above the ground. A slope of less than 1 implies a compressed function or a small increase in sensation with a large increase in physical magnitude. A slope greater than 1 would imply an expansive function in which there is a large increase in sensation magnitude with a small increase in physical magnitude. One obvious objective would be to determine if the altitude judgments made in the simulator are the same as those made in real world scenes (or CIG vs. photographs and actual flight conditions).

Pilots should be run in the simulator system in order to determine effects of the field of view (FOV) as provided by the peripheral visual input from the wraparound ASPT visual system. These observations and judgments should be made both in the static and the dynamic scene situation. It is conceivable that training involving the judgment of altitudes may transfer positively to both the simulator and the actual flight situation.

Third, a study needs to be initiated which would examine the role of aerial perspective in altitude judgments and the usefulness of this cue in flying tasks in general (Harker and Jones, 1980; Stenger, et al, 1981). Aerial perspective is regarded as a secondary or learned cue for the perception of depth or distance. It consists of a shift in hue, contrast, and saturation as a function of distance and elevation. Depending on the outcome of research related to this cue, the perceptual importance of aerial perspective might be increased or decreased in the simulator. Again, results in this area should have implications for the development of CIG and the training of flight personnel.

Aerial perspective could be employed in both static and dynamic scenes using photographic and/or CIG presentations. Stimuli would be presented using slide projection of a given terrain with varying amounts of aerial perspective. This would provide information in a static scene condition. Motion pictures or video disk could be used to present a dynamic scene condition. The observer would be requested to indicate height/distance at several times during a dynamic scene presentation. Both static and dynamic scenes would be taken from CIG presentations and from natural scenes. Observers should consist of those with varying degrees of flying experience including those with little or no experience. At the present time very little is known about this particular cue to depth perception and its

usefulness in flight activity.

A fourth area for follow-on research concerns the application of channel theory to the simulator environment and pilot training. Ginsburg (1978, 1980) has pointed out that there is considerable psychophysical and neurophysiological evidence supporting the notion that the visual system employs narrow band quasi-independent neural channels tuned to spatial frequencies of a certain bandwidth and orientation. Consistent with such data is the sustained/transient neural mechanism dichotomy (Breitmeyer and Ganz, 1976) which suggests that there are two parallel and complementary visual mechanisms; a sustained mechanism which is characterized by having high spatial resolving ability, a long latency, and a long integration time and a transient mechanism characterized by a high temporal resolving ability, a short latency, and a low spatial resolution. The transient system would be concerned with the detection, tracking, and attention-getting aspects of large moving objects. The sustained system would be more concerned with good acuity or high resolution.

One potential research area has to do with those simulators employing readily visible raster scan displays. With the advent of liquid-crystal light valves this problem may be alleviated in some, although perhaps not all simulator systems. In particular, the presence of a visible raster structure (as in the present ASPT) would tend to mask or prevent the detection of small objects or fine patterns. Thus, it would be useful to have information relating to the pilot's ability to detect large and small detail targets which are moving against a stationary background of a given spatial frequency (e.g., within the range of the simulator raster structure). Independent variables would include the spatial frequency (in cycles/degree or cpd) of the background field, the orientation of the sine-wave grating bars in the background field, the exposure time to the background field, the spatial frequency of the target grating, whether the target is moving or stationary, how fast the target is moving (degrees/second), and duration of target presentation. Dependent measures would include the overall shapes of the contrast sensitivity functions (CSF) and measures of visible persistence. The data could be obtained using a

microcomputer controlled display monitor system.

Data to be obtained from research in this area would contribute to the determination of what effects might be induced by a visible raster structure on the CSF and thus on the detection of complex objects (Ginsburg, 1978, 1980). In addition, data would be obtained on the effects of grating adaptation (as produced by the raster structure), grating orientation, and target movement on visible persistence (perceived duration of a visual stimulus as compared to its physical duration) (Long, 1980). These data in turn should relate to the frequent discrepancy between CIG update and CRT refresh rates. It should also be pointed out that research on spatial contrast sensitivity and visible persistence relates to the spatial resolution requirements and the limits of spatial resolution in the simulator display whether it is of a CRT raster scan nature or a liquid crystal light valve.

ACKNOWLEDGMENTS

I wish to express my appreciation to the members of the Air Force Human Resources Laboratory who were very helpful in the initiation and completion of the research effort reported here. I wish to thank, in particular, Dr. Thomas Longridge, Dr. Elizabeth Martin, and Dr. Joseph De Maio. I also wish to express my gratitude to Mr. Michael Harding, 2nd Lt. Abel Hammid, and Ms. Rebecca Brooks for their invaluable assistance in the data collection and the data analysis. I also wish to thank Mr. Thomas Farnon, Ms. Pamela Kosirog, Mr. William Brubaker, Mr. Steven Stephens, and all of the ASPT operators without whose cooperation and assistance this study would not have been possible. Finally, I would also like to express my appreciation to those F-16 pilots who willingly participated in this research project.

REFERENCES

Breitmever, B. B., and Ganz, L. Implications of sustained and transient channels for theories of visual pattern masking, saccadic suppression, and information processing. Psychological Review, 1976, 83, 1-32.

Buckland, G. H., and Monroe, E. G., and Mehrer, K. L. Flight simulator runway visual textural cues for landing. AFHRL-TR-79-81, August 1980.

Ginsburg, A. P. Visual information processing based on spatial filters constrained by biological data. AMRL-TR-79-129, Volumes I and II, December 1978.

Ginsburg, A. P. Specifying relevant spatial information for image evaluation and display design: an explanation of how we see objects. Proceedings of the Society for Information Display, 1980, 21/3, 219-227.

Graham, C. H. (Editor) Vision and visual perception. New York: Wiley, 1966.

Harker, G. S., and Jones, P. D. Depth perception in visual simulation. AFHRL-TR-80-19, August 1980.

Hennessy, R. T., and Cooles, H. D. Critical issues and visual system requirements for a V/STOL training research simulator. NAVTRAEQUIPCEN 78-C-0076-1, October 1980.

Long, G. M. Iconic memory: a review and critique of the study of short-term visual storage. Psychological Bulletin, 1980, 88, 785-820.

Stenger, A. J., Zimmerlin, T. A., Thomas, J. P., and Braunstein, M. Advanced computer image generation techniques exploiting perceptual characteristics. AFHRL-TR-80-61, February 1981.

APPENDIX

TABLE 1

Dependent Variables Used in Visual Cues Study

Total Course Altitude Dependent Measures

- (1) Total Course Mean Altitude (feet)
- (2) RMS deviation*

Level Altitude Dependent Measures

- (1) Mean Level Altitude (feet)
- (2) RMS deviation*

Turn Altitude Dependent Measures

- (1) Mean Turn Altitude (feet)
- (2) RMS deviation*

Terrain Crashes for Each Experimental Condition

*deviation in feet from a 200 foot reference

TABLE 2

Results of MANOVAs and Omega Squared Values for Total Course Mean Altitude

<u>Source</u>	<u>Degrees of Freedom</u>	<u>F</u>	<u>p level</u>
S (Subjects)	12	3.3996	.00071
A (Airspeed)	1	157.6789	.00000
B (Texture)	2	15.0721	.00003
SA	12	1.6726	NS
SB	24	2.3590	.00270
AB	2	11.8288	.00012
SAB	24	1.3167	NS

Omega Squared/S = .066

Omega Squared/A = .356

Omega Squared/B = .064

Omega Squared/SB = .074

Omega Squared/AB = .049

Total Variance Accounted for = .609

TABLE 3

Results of MANOVAs and Omega Squared Values for Total Course RMS Deviation

<u>Source</u>	<u>Degrees of Freedom</u>	<u>F</u>	<u>p level</u>
S	12	3.4490	.00063
A	1	127.4875	.00000
B	2	38.4251	.00000
SA	12	3.2787	.00096
SB	24	3.5919	.00004
AB	2	19.9981	.00001
SAB	24	2.7021	.00072

Omega Squared/S = .062

Omega Squared/A = .265

Omega Squared/B = .157

Omega Squared/SA = .157

Omega Squared/SB = .057

Omega Squared/AB = .080

Omega Squared/SAB = .086

Total Variance Accounted for = .837

TABLE 4

Results of MANOVAs and Omega Squared Values for Level Flight Mean Altitude

<u>Source</u>	<u>Degrees of Freedom</u>	<u>F</u>	<u>p level</u>
S	12	2.5010	.00800
A	1	76.6952	.00000
B	2	8.9092	.00057
SA	12	1.3735	NS
SB	24	1.7609	.03200
AB	2	7.8003	.00110
SAB	78	.9169	NS

Omega Squared/S = .061

Omega Squared/A = .242

Omega Squared/B = .053

Omega Squared/SB = .062

Omega Squared/AB = .046

Total Variance Accounted for = .464

TABLE 5

Results of MANOVAs and Omega Squared Values for Level Flight RMS Deviation

<u>Source</u>	<u>Degrees of Freedom</u>	<u>F</u>	<u>p level</u>
S	12	2.8286	.00320
A	1	53.3613	.00000
B	2	28.1642	.00000
SA	12	2.2340	.01700
SB	24	2.5209	.00140
AB	2	11.2513	.00016
SAB	24	1.7761	.00200

Omega Squared/S = .058

Omega Squared/A = .140

Omega Squared/B = .145

Omega Squared/SA = .040

Omega Squared/SB = .097

Omega Squared/AB = .055

Omega Squared/SAB = .050

Total Variance Accounted for = .585

TABLE 6

Results of MANOVAs and Omega Squared Values for Mean Altitude in Turns

<u>Source</u>	<u>Degrees of Freedom</u>	<u>F</u>	<u>p level</u>
S	12	3.998	.00018
A	1	150.2852	.00000
B	2	5.6762	.00530
SA	12	2.0398	.03100
SB	24	2.0505	.00950
AB	2	15.1466	.00003
SAB	24	2.1350	.00670

Omega Squared/S = .081

Omega Squared/A = .336

Omega Squared/B = .021

Omega Squared/SA = .028

Omega Squared/SB = .057

Omega Squared/AB = .064

Omega Squared/SAB = .061

Total Variance Accounted for = .648

TABLE 7

Results of MANOVAs and Omega Squared Values for RMS Deviation in Turns

<u>Source</u>	<u>Degrees of Freedom</u>	<u>F</u>	<u>p level</u>
S	12	4.0118	.00018
A	1	132.6463	.00000
B	2	22.7085	.00000
SA	12	2.6707	.00490
SB	24	2.4008	.00230
AB	2	14.7426	.00003
SAB	24	2.4919	.00160

Omega Squared/S = .075

Omega Squared/A = .275

Omega Squared/B = .090

Omega Squared/SA = .041

Omega Squared/SB = .069

Omega Squared/AB = .057

Omega Squared/SAB = .074

Total Variance Accounted for = .678

TABLE 8

Means for Total Altitude

	<u>Airspeed</u>	
	<u>300 KIAS</u>	<u>540 KIAS</u>
<u>White Triangles</u>	184.67422	325.42537
<u>All Black Cones</u>	181.56306	251.35844
<u>White Top Cones</u>	178.63768	241.35844

TABLE 9

Means for Total Course RMS Deviation

	<u>Airspeed</u>	
	<u>300 KIAS</u>	<u>540 KIAS</u>
<u>White Triangles</u>	69.71000	179.43349
<u>All Black Cones</u>	54.67442	91.64188
<u>White Top Cones</u>	56.71627	93.70199

TABLE 10

Means for Level Course Altitude

	<u>Airspeed</u>	
	<u>300 KIAS</u>	<u>540 KIAS</u>
<u>White Triangles</u>	188.36998	297.30613
<u>All Black Cones</u>	180.61845	238.01498
<u>White Top Cones</u>	188.81345	223.54767

TABLE 11

Means for Level Course RMS Deviation

	<u>Airspeed</u>	
	<u>300 KIAS</u>	<u>540 KIAS</u>
<u>White Triangles</u>	67.52399	135.45772
<u>All Black Cones</u>	52.86430	72.22788
<u>White Top Cones</u>	53.79326	72.73411

TABLE 12

Mean Altitude in Turns

	<u>Airspeed</u>	
	<u>300 KIAS</u>	<u>540 KIAS</u>
<u>White Triangles</u>	171.28680	401.36383
<u>All Black Cones</u>	188.53729	300.12997
<u>White Top Cones</u>	204.14268	287.40229

TABLE 13

Mean RMS Deviation in Turns

	<u>Airspeed</u>	
	<u>300 KIAS</u>	<u>540 KIAS</u>
<u>White Triangles</u>	80.73184	257.50613
<u>All Black Cones</u>	63.57426	139.19199
<u>White Top Cones</u>	72.13561	138.29910

TABLE 14

Terrain Crashes as a Function of Experimental Conditions

	<u>Airspeed</u>	
	<u>300 KIAS</u>	<u>540 KIAS</u>
<u>White Triangles</u>	9 (2)	7 (2)
<u>All Black Cones</u>		1
<u>White Top Cones</u>	1 (1)	1

(Values in parantheses refer to T-course pilots while all others are B-course pilots)

TABLE 15

Results of MANOVAs and Omega Squared Values for Total Course Mean Altitude

<u>Source</u>	<u>Degrees of Freedom</u>	<u>F</u>	<u>p level</u>
S	5	3.4305	.01200
A	1	15.8053	.00056
B	2	2.7343	NS
SA	5	.8644	NS
SB	10	.8319	NS
AB	2	2.5672	NS
SAB	10	1.0821	NS

Omega Squared/S = .117

Omega Squared/A = .142

Total Variance Accounted for = .259

TABLE 16

Results of MANOVAs and Omega Squared Values for Total Course RMS Deviation

<u>Source</u>	<u>Degrees of Freedom</u>	<u>F</u>	<u>p level</u>
S	5	3.3790	.01300
A	1	15.0883	.00068
B	2	1.4724	NS
SA	5	.9841	NS
SB	10	.4533	NS
AB	2	2.0138	NS
SAB	10	1.0802	NS

Omega Squared/S = .124

Omega Squared/A = .146

Total Variance Accounted for = .270

TABLE 17

Means for Total Course Altitude

	<u>Airspeed</u>	
	<u>300 KIAS</u>	<u>540 KIAS</u>
<u>White Triangles</u>	227.62916	244.31249
<u>All Black Cones</u>	212.40166	304.33999
<u>White Top Cones</u>	193.13500	246.25083

TABLE 18

Means for Total Course RMS Deviation

	<u>Airspeed</u>	
	<u>300 KIAS</u>	<u>540 KIAS</u>
<u>White Triangles</u>	84.43766	108.84358
<u>All Black Cones</u>	56.66975	140.53158
<u>White Top Cones</u>	55.31591	94.11016

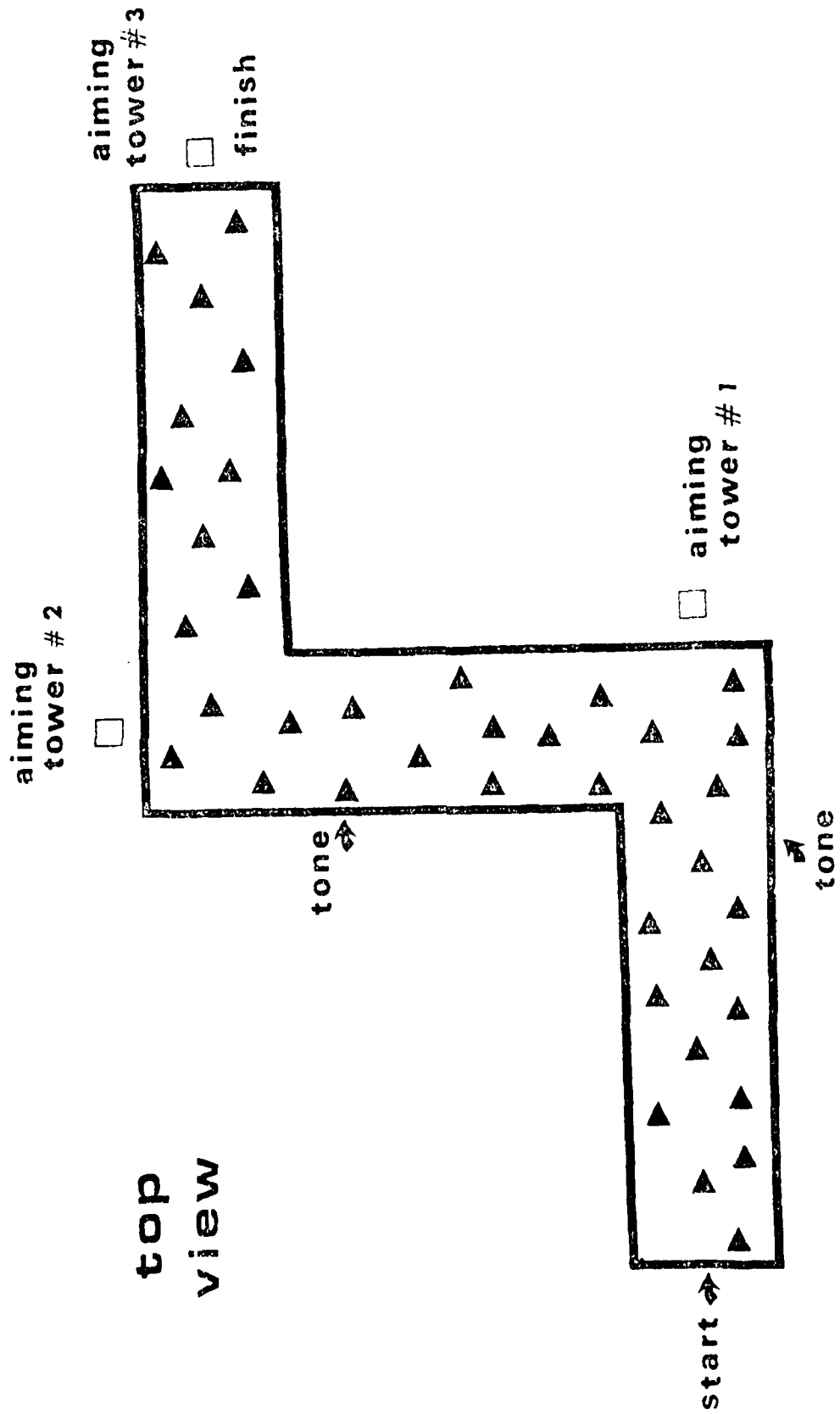


Fig. 1. Schematic diagram of prescribed course of flight.

1981 USAF SCEE SUMMER FACULTY RESEARCH PROGRAM

Sponsored by the

AIR FORCE OFFICE OF SCIENTIFIC RESEARCH

Conducted by the

SOUTHEASTERN CENTER FOR ELECTRICAL ENGINEERING EDUCATION

FINAL REPORT

A METALLURGICAL INVESTIGATION OF THE INTERNAL BRONZE

MANUFACTURING PROCESS OF Nb₃Sn SUPERCONDUCTING WIRE

Prepared by: Dr. John Melville Roberts

Academic Rank: Professor of Materials Science

Department and University: Department of Mechanical Engineering and Materials Science, Rice University

Research Location: Aerospace Power Division, Aero Propulsion Laboratory, AFWAL/POOS-2 WPAFB, Ohio 45433

USAF Research Colleague: Dr. Charles Oberly

Date: September 15, 1981

Contract No: F49620-79-C-0038

A METALLURGICAL INVESTIGATION OF THE INTERNAL BRONZE
MANUFACTURING PROCESS OF Nb₃Sn SUPERCONDUCTING WIRE

by

DR. JOHN MELVILLE ROBERTS

ABSTRACT

An introductory basic type of metallurgical investigation has been carried out on nominally 13 wt.% Sn bronze rods and Nb/bronze multifilamentary composite wires. These studies have included optical metallographic, scanning electron microscopy and x-ray microprobe techniques. Preliminary ageing studies of the quenched in metastable α phase in 13 wt.% Sn bronze have been made up to 220°C. This program of study was carried-out in an attempt to learn more about unwanted and often premature failures occurring in these Nb/bronze multifilamentary wires during manufacture. Defects such as voids, chemical inhomogeneities, tin rich phases and abnormally large and possibly discontinuous Nb filaments in these wires have been observed. The consequences of these defects upon the success of manufacturing high quality Nb₃Sn superconducting wire are briefly discussed. The concept of the "limiting bronze grain size" and possibly the "limiting sub-grain structure size" imposed upon the bronze matrix by the Nb filaments has been discussed and preliminary observations of these effects are presented. Numerous suggestions for further research in this area are offered. The concept of a new matrix alloy for the internal bronze process is suggested and it is pointed out higher temperature superconductors, i.e. better than Nb₃Sn, should be investigated.

Acknowledgement

The author would like to thank the Air Force Systems Command, the Air Force Office of Scientific Research and the Southeastern Center for Electrical Engineering Education for providing him with the opportunity to spend an interesting and sometimes exciting summer at the Aero Propulsion Laboratory, Wright-Patterson AFB, Ohio. He would like to thank in particular the splendid cooperation of Mr. John Leonard and Mr. Jim Ray of the Aero Propulsion Laboratory. The author also thanks and is deeply appreciative of the cordial cooperation of Mr. C. R. Underwood, Mr. Robert Lewis, Mr. Ed Harper and Mr. Fritz Deutscher of SRL (Materials Laboratory) WPAFB, Area B where the current investigation was dominantly carried-out.

I. INTRODUCTION

From my pre-summer site visit and from conversations with Dr. Charles Oberly and 2nd Lt. Douglass Scott Holmes during my first few days at WPAFB, the following background information on the nature of problems associated with the manufacture of Nb_3Sn superconducting wires employing the internal bronze process was established. The overall problem appeared to be one of manufacturing high electrical quality superconducting Nb_3Sn composite wires in sufficiently long lengths to be useful in the winding of superconducting magnets or generators. One specific problem area involved apparent embrittlement and unpredictable failures in the Nb/13wt.% Sn Bronze unreacted wires in the later stages of their manufacture i.e. in the last few wire drawing operations. There was some scant evidence that this may be an age hardening type of phenomena, at least in some of the failure cases.

At this stage the present author could envisage possible martensitic, and/or spinodal (continuous) and/or classical nucleation and growth types of phase transformations occurring in this (10-14 wt.%) Sn bronze alloy, which may or may not be strain induced. Dr. Oberly and 2nd Lt. Holmes did not know what a spinodal reaction was, so Dr. Roberts presented these two persons a lecture on spinodal reactions during his pre-summer site visit. The present author decided at this time some planned, systematic and structured ageing experiments on (10-14 wt.%) Sn bronze were needed in this field. To this end Dr. Roberts suggested to Holmes to cut out a piece from a homogenized bronze billet and swage and draw it to rod or wire form in preparation for the summer research effort. Rod of 0.010 in. dia. was made and available to Dr. Roberts upon his arrival at WPAFB for the summer period. Other metallurgical aspects contributing to possible attendant wire fabrication problems were perceived by the present author to be:

- (1) the role of porosity in the bronze cast billets;
- (2) the degree to which homogenization was complete in the homogenized bronze billets; and
- (3) the role of possible second phase particles existing either in a microscopically distributed state or in a macroscopically distributed state upon the success of wire fabrication.

During the present author's first week of the summer period (i.e. the week of May 18, 1981), he independently thought of and decided that the following metallurgical variables which appeared to be previously overlooked in this field needed thought, inspection and research in this particular wire manufacturing process. The effect of wire diameter (size effect) and niobium filament distribution upon the limiting grain size of the bronze needed to be studied. Possible secondary recrystallization effects, sub-grain defect structure details and grain texture effects upon the bronze ductility needed more attention. The present author informed 2nd Lt. Holmes and Dr. Oberly of his ideas at that time. For several weeks, Holmes asked me about the "limiting grain size effect", since he knew nothing about it; and I told him it was a simple analysis and I gave it to my undergraduate students as a homework assignment. Dr. Oberly chased down a copy of Reed-Hill¹ for me, which treats the effect in simple terms since it was not in the WPAFB library. I made the calculations on "the limiting grain size effect", showed Holmes my answers and told him it seems to be important. Anything Holmes has done on "the limiting grain size effect" came after this sequence of events. It seems rather important to report a chronological development of these events.

After reading various articles¹⁻²⁹, some contractor-WPAFB communications^{30,31} and reports^{32,33} for two weeks, I realized it was not possible for me to obtain a coherent metallurgical evaluation of this "state of the art process" with just this reading knowledge and discussions with Holmes. I then decided that it would be more productive for myself to simply carry out a straightforward basic metallurgical study of the 13 wt.% Sn bronze system and Nb filament/bronze matrix composite materials. I needed to do this for two reasons. First, this was a new field for me, so I could "get my feet wet" and get a good feel for this area of technology by actually carrying out preliminary studies. Second, it appeared to me the basic type of metallurgical studies this program required had not been undertaken previously in a systematic and thorough way. In any event, confirmation of what had been done or found would certainly be of some help.

II. OBJECTIVES OF THE RESEARCH EFFORT

The main objectives of this project were to investigate unwanted and often unexpected failures which occurred during the manufacturing of Nb₃Sn superconductor multi-filamentary wire. In order to do this, a planned program of study was carried out which included the following phases:

- (1) Perusal of technical reports and published papers by Dr. Roberts, so that the current investigator became familiar with the terminology of this field of technology.
- (2) Carrying out an investigative study of polishing and etching techniques to reveal the microstructure and geometric morphology of these superconducting multi-filamentary wires at various stages of their manufacture.
- (3) Employing (2) to study porosity, degree of homogeneity grain size and second phase presence in 13 wt % Sn Bronze in the following states, "as cast", "homogenized", "wrought" (in both the annealed or unannealed states), and "hot/cold swaged". Scanning electron microscopy (SEM) studies were planned to study the morphology of the microstructures as well as X-Ray Microprobe Analyses by EDS (Energy Dispersive Spectrum) to check chemical compositions at interesting microstructural features.
- (4) To carry out conventional quenching and ageing experiments upon 13 wt. % Sn bronze, in order to ascertain if a type of "age hardening" phenomena actually occurs in this alloy at temperatures and/or times which may be realized in the actual manufacturing process. It was planned to extend these studies to include investigating the effect of plastic prestrain upon any possible type of phase transformation which may occur in this 13 wt. % Cu bronze system at relatively low temperatures i.e. below 200°C.
- (5) To give some thought about designing a new Sn bearing alloy which would be predicted to be less susceptible to the formation of second phase particles, be easier to homogenize and possibly would not exhibit any form of a strain ageing transformation during the manufacture of Nb₃Sn wires.

III. EXPERIMENTAL PROCEDURES

A. Polishing and Etching Techniques. Suitable fine grinding of the bronze and Nb/bronze composite wires was carried out by successive use of 320 grit, 400 grit and 600 grit abrasive papers. This was followed by rough polishing with powdered diamond paste of 6 micron particle size. Final polishing was carried out employing 0.30 and 0.05 micron alumina solutions on the Vibromet wheels for various times. It is important to thoroughly clean the sample between each of the above steps to prevent carrying coarse particles into the finer particle polishing operations.

After some experimentation, a ferric chloride etch and a chromic acid etching solution used one after the other for various times with thorough cleaning in between each etching immersion was found to be satisfactory for the present studies. Due to time limitations, the present investigator did not explore electro-polishing and electro-etching techniques for these alloys, but this may be an even more fruitful avenue to explore and delineate microstructural features of interest. A great many other etching solutions for Cu and its alloys are suggested in Smithells⁵ and it is entirely possible an even better etching technique can be developed for these particular bronze/Nb composite wires. Studies to develop improved etching characteristics of these structures appears to be worthy of further investigation.

B. Mounting Techniques. Generally these types of samples can be mounted in bakelite or lucite type of mounting materials. It is highly recommended, all of these types of samples should be clear plastic lucite mounted. EDS analysis of the lucite material revealed no elements detectable with atomic numbers greater than those of Al or Na in the lucite.

A similar analysis of the bakelite mounting material revealed light hard (Silicon-rich) particles and the matrix or filler material between the Si-rich particles to contain Al, Cl and Ca. The Si-rich particles can dislodge and get onto and into the Nb/bronze filamentary wires and create artifacts in metallurgical studies. The softer Al, Cl and Ca phase of the bakelite can smear over the sample surface

and become entrapped at porosity holes or cavities, also creating an artifact appearance. With careful polishing and etching of lucite clear mounted samples, the present investigator was able to overcome these "artifact" effects.

C. Equipment Used. Many SEM (Scanning electron microscopy) photographs were taken on the Super III A ISI (Internatonal Scientific Instruments) microscope with the Robinson Collector. Under optimum operating conditions microstructural details to 100 \AA (Angstroms) resolution might be expected with this instrument. The assistance of Mr. John Leonard of the Technical Battery Group of the Aero Propulsion Lab, WPAFB in this phase of the work is greatly appreciated.

Most optical metallographic photographs were made on the Xenon source, Bausch and Lomb Metallograph located in the AFWAL Materials Laboratory, Bldg. 32, WPAFB under the overall supervision of Mr. C. R. Underwood. Specimen preparation equipments were all located with SRL, AFWAL, MATERIALS LAB, BLDG. 32, WPAFB again under the overall supervision of Mr. Underwood. These included the Vibromet tables, cut-off wheels, etc., and a carbon vacuum evaporator station.

Within the same laboratory section, microhardness readings were made on the Wilson Model MO serial 2469 microhardness tester. Mr. Richard Bacon of SRL in this same group was extremely helpful in carrying out x-ray microprobe studies on the ETEC MICROPROBE in this laboratory using EDS analysis. It should be recalled that a microprobe analysis employing this unit provides data for a volume of material generally $1 \times 1 \times 1$ (microns)³.

For the ageing studies, samples were encapsulated in quartz glass under an Argon atmosphere and annealed in Mr. Jim Ray's glass laboratory of the Aero Propulsion Lab, Bldg. 450, WPAFB. After annealing, the samples were quenched into an ice/water bath. Ageing studies above room temperature were conducted in a muffle furnace in the SRL laboratory group section noted above. The current investigator found Mr. Robert Lewis, Mr. Ed Harper and Mr. Fritz Duetscher of the SRL, AFWAL, MATERIALS LABORATORY to be helpful and cooperative at all times in my endeavors.

IV. MICROSTRUCTURES AND MICROPROBE RESULTS

A. Photomicrographs. Appendix A presents a photograph identification legend for the 58 (fifty-eight) pictures which form a part of this report. These 58 pictures show typical examples of the salient features of the results the present investigator studied during this summer program.

Pictures 1-11 are of the nominally 13 wt.% Sn homogenized bronze in the hot/cold worked state. Pictures 12-16 are of the nominally 13 wt.% non-homogenized bronze billet. Pictures 17 and 18 are of a bronze powder prepared by Holmes at WPAFB. Pictures 19-24 are of nominally 13 wt.% Sn homogenized bronze in the hot/cold worked state after having been silver soldered into brass plates. The hot/cold worked structure has obviously been exposed to a temperature of the order of 1000°C. Pictures 25-30 are of the nominally 13 wt.% Sn bronze billet in the homogenized state. Pictures 31-34 are of a nominally 12 wt.% Sn bronze rod (designated CC, see reference 30) cast by Cannon-Muskegon Corp. and processed by the IGC Corporation. This 0.073 in. in. dia. rod had cracked. Pictures 35 and 36 are of nominally 12 wt.% Sn bronze rod (designated Rod 3S, see reference 30) which did not exhibit cracks. Pictures 37 and 38 are of a multi-filamentary Nb/bronze sample designated "Bob Rose" by Holmes at WPAFB.

Pictures 39-58 are of multifilamentary Nb/bronze wires, showing numerous examples of transverse cross-sections of the wire and longitudinal (along the axis of the wire) sections. Pictures 39 and 46 for example show typically oversized Nb filaments in cross-section. Pictures 45 and 57 for example show typically oversized Nb filaments as detected in the longitudinal sections.

Tin-rich and tin-depleted microconstituents and porosity are readily identifiable in the non-homogenized casting. In all of the current investigators' studies, no positive identification could be made that the tin-rich regions were δ -phase as suggested by Holmes et al.⁸. This seems to be a point worthy of further detailed research. The homogenized billet exhibited dominantly a uniform microstructure, yet rather massive tin-rich regions could be found which had not been solutionized during homogenization. Picture 43 shows a typical example of the bronze grain size in the multifilamentary Nb/bronze wires.

The "limiting grain size" effect will be briefly described. This idea was originally developed by C. Zener and is explained by Reed-Hill¹. The Nb filaments in the bronze wire can be considered similar to second phase inclusions in a homogeneous primary phase matrix. These second phase filaments can put an upper limit on the grain size attainable in the primary phase upon annealing. During annealing and recrystallization, the strain free grains migrate and move into the strained matrix. After recrystallization is complete, grain coarsening can occur to lower grain boundary surface energy. In both processes, the migrating boundaries are interrupted at the second phase filaments, and the boundaries form curvatures and try and pull-away from the second phase obstacles. If the surface tension force is small due to a large radius of curvature of the migrating boundary, the boundary cannot overcome the restraining force of the inclusions. In this case the migrating strain free recrystallized grains cannot move into either the strained matrix or into other recrystallized grains to allow grain coarsening. Hence the grain size is limited by the second phase filaments. It can be readily shown that the limiting grain size R is given approximately by:

$$R = \frac{2}{n_s \pi r} \quad (1)$$

where n_s is the number of Nb filaments/cm² of cross-section of the wire, π has its usual meaning, r is the radius of the Nb filaments in cm, and R is the limiting grain size in cm. This form of analysis can be readily applied to the growth of the grains in the longitudinal direction of multifilamentary Nb/bronze wires. This analysis must be modified into a two dimensional problem, namely the longitudinal and radial directions of the wires. The effect of wire draw reduction and number of draws between anneals as well as the total prior thermal/mechanical history of the sample are parameters very important to understand in controlling this overall effect. In addition, when recrystallization is incomplete, the sub-grain structure recovery details must be taken into consideration. Finally, the mean free path in the bronze must also be considered to afford a total analysis of this phenomena with respect to the Nb/bronze multifilamentary wire manufacturing process. The present author will analyze in detail all the data he has on this effect in the light of the above comments and

prepare it for publication in the near future. There is little doubt that this effect comes into play in an important way in the final annealing and drawing process steps of the wires. Methods to circumvent this embrittling effect will be discussed in a forthcoming publication. The reasons why this effect is more critical in Nb/bronze wires as contrasted to Nb/Cu wires will also be presented.

As regards to the oversized and discontinuous Nb filaments found in cross-sections and in the longitudinal sections of the wires, the present investigator is currently considering their origin. It has been observed their frequent location is near the center of the overall wire, the fact that cavities are generally located at their ends and no second phase foreign particles have yet been found blocking their flow during drawing. The present author has some ideas as to explaining the origin of these "abnormally" large filaments which appear to be discontinuous. Presentation of these ideas must await a forthcoming publication.

The present investigator has intentionally not discussed in detail the 58 pictures of this report and the microprobe results. Firstly, this would be an enormous task at this time, and that must wait some time, probably of the order of 6 months or so, until the present author is ready to publish. Secondly, 2nd Lt. D. S. Holmes and Mr. Jim Reams of the Aerospace Power Division, AFWAL, WPAFB have both informed the present investigator that it is their opinion they want themselves and other so-called experts in this field, who have been at this game longer than I, to analyze these pictures. The microprobe raw data is with Mr. Richard Bacon, of SRL, AFWAL, Materials Laboratory. I do not care to present any of my detailed ideas on this matter, until I have had the opportunity to fully analyze my own data and present it publically.

In this way, my interpretation of my data and their interpretation of my data can be readily appraised and evaluated by others also interested in this field of study.

b. Consideration of a New Matrix Alloys for Nb₃Sn Superconductor Wires.

It is proposed a new Sn bearing alloy be considered which may be free intrinsically of some of the Nb/bronze manufacturing process

problems. After some reflection, the present author suggests a Ag/Sn (up to 10 wt. % Sn) may be a good viable candidate. Possibly a ternary Ag/Cu/Sn or even a quaternary Ag/Cu/Al/Sn may be even more attractive candidates. It is obvious a small scale research and development project would be required to investigate this idea in depth.

V. A PRELIMINARY AGEING STUDY IN 13wt% Sn BRONZE

Small 0.10 in. dia. specimens of 13 wt.% Sn bronze in the hot/cold swaged state were force fit into brass plates. The plates with the bronze samples were encapsulated in vicor glass tubes filled with an argon atmosphere. The composite plates were annealed and solution heat treated at 475°C for 4 hours and quenched into an ice/water bath. The variation of the Vickers microhardness of the bronze samples was monitored with long periods of ageing, up to several weeks, at 23, 100 and 220°C. Essentially no age hardening peak was found and essentially no significant change in the microhardness was detected.

To the resolution of optical metallographic techniques, no ϵ (epsilon) phase⁷ precipitation could be found in these quenched and aged samples. The results tell us that no apparent change in the ultimate tensile strength is occurring during these ageing treatments. These results suggest the manufacturers of Nb/bronze multifilamentary wires should anneal and rapid cool the material to 200°C and then slow cool to ambient temperature. Decomposition of the α phase with a possible attendant embrittling effect in the critical temperature region of 250 to 350°C could thus most likely be prohibited.

There is little doubt that the room temperature metastable α phase in Cu 13 wt. % Sn bronze does want to decompose under certain temperature, time and prestress conditions into more stable non-equilibrium or equilibrium products. At present, these particular conditions have not been established which cause possibly significant changes in yield stress, tensile strength, work hardening characteristics and electrical resistivity of the bronze matrix material. Further studies are planned to investigate the ageing characteristics of this particular alloy in greater depth.

VI. RECOMMENDATIONS

This work has stimulated the present Investigator to consider several avenues of research which could ultimately lead to significant technological "state of the art" advances in this manufacturing process.

More extensive studies should be made on etching, electropolishing and electroetching techniques in order to bring-out finer details of the microstructures of both the bronze and the niobium phases of these multifilamentary wires.

X-ray diffraction and transmission electron microscopy (TEM) analyses of the tin rich phases detected in the supposedly single phase α bronze should be made. These studies are needed to positively identify if these tin rich regions are δ , γ or β phase particles. Only when the phase is unambiguously identified can one understand fully its origin and hence try to eliminate its occurrence, since these are much harder and less ductile regions entrapped in the bronze.

There is a need to carry-out more extensive ageing studies of the 13 wt. % Sn bronze system. Slow cooled samples, in particular, from the annealing temperature range should be studied for any type of α phase decomposition with attendant changes in properties. The manufacturing process conditions which could induce α phase formation have not as yet been established. The properties which should be investigated are microhardness, yield stress, work hardening exponent and electrical resistivity. Phase identification techniques by whichever method is required for positive identification of any decomposition produced from the metastable α phase should be made. The effect of plastic prestrain upon any attendant α phase decomposition must be examined.

Detailed analysis of the true quality limits of the current Nb_3Sn superconducting multifilamentary wires produced by the internal bronze process must be examined in the light of the "limiting grain size" effect. The role of the "mean free bronze path" and possibly a "limiting sub-grain size" effect must also be considered.

Analytical studies should be initiated such that a viable mechanism or mechanisms can be identified which controls or causes the formation of abnormally large Nb filaments to occur in multifilamentary and ultra-fine Nb/bronze wires. These abnormally large filaments appear to represent discontinuous Nb filaments in the wires and their occurrence is far too

frequent. These filaments obviously create reduced electrical performance characteristics in the wire. They are also centers for the build-up of large internal stresses and strains and even cavities or microcracks in the wires. The latter can cause unexpected and unwanted mechanical failures of the wire during subsequent manufacturing operations. The study must be comprehensive enough and thorough enough so that one can ultimately say with considerable authority "I know how to produce those abnormally large filaments" or "I know how to eliminate their occurrence" or "I know the mechanism by which they formed."

It appears that a new Sn bearing matrix alloy such as Ag/Sn, a Ag/Sn/Cu or Ag/Sn/Cu/Al should be given some consideration for the production of Nb₃Sn superconducting wire by the internal bronze process. Such an alloy may have some intrinsic properties both in casting and hot/cold forming which could be superior to those of the high tin bronze presently in use.

The present investigator intends to study some samples of the Lakeshore Ceramic coating (SC2B) currently being considered for use on multifilimentary Nb₃Sn superconducting wires. These studies will be of the preliminary type to study the composition and microstructure of the various phases present. Electrical, thermal and mechanical property evaluations could follow the preliminary studies.

All of the above proposed recommendations for further study and analysis in this area of technology can be carried out at Rice University, with WPAFB through Dr. C. Oberly supplying material for samples from time to time. Some of the details of the above recommendations will be answered when I have completed a thorough analysis of my present results and have the work ready for publication.

Finally, a significant step forward in this field of technology would result if a higher temperature superconductor than Nb₃Sn were sought. It appears the Russians³⁴ are moving in this direction. To this investigator's knowledge there is not a serious effort going on at WPAFB to keep abreast and develop this highly potentially fruitful avenue of approach. Serious consideration should be given to such a project. As this investigator sees it, this could be accomplished by hiring one or two competent people in this field and an expendable materials budget.

In general, it is this investigator's opinion that WPAFB should do much more research and small scale development work at moderately low cost before jumping into the procurement of products in large quantities of items not yet fully developed from a good technological view point. It then becomes enormously expensive to patch-up the problems and failures at the latter and large scale stages.

APPENDIX A

PICTURE IDENTIFICATION LEGEND

APPENDIX A

A photograph identification legend is presented in this Appendix for 58 pictures. All magnifications reported are for 3½ x 4½ in. pictures prior to enlargement for reproduction purposes.

Picture 1	(Roberts No. 8)	Magnification	400x
Picture 2	(Roberts No. 85)	Magnification	720x
Picture 3	(Roberts No. 78(C))	Magnification	800x
Picture 4	(Roberts No. 96)	Magnification	800x
Picture 5	(Roberts No. 98)	Magnification	800x
Picture 6	(Roberts No. 99)	Magnification	800x
Picture 7	(Roberts No. 299)	Magnification	shown on picture
Picture 8	(Roberts No. 300)	Magnification	shown on picture
Picture 9	(Roberts No. 301)	Magnification	shown on picture
Picture 10	(Roberts No. 302)	Magnification	shown on picture
Picture 11	(Roberts No. 303)	Magnification	shown on picture
Picture 13	(Roberts No. 26)	Magnification	400x
Picture 13	(Roberts No. 36)	Magnification	1000x
Picture 14	(Roberts No. 215)	Magnification	500x
Picture 15	(Roberts No. 240)	Magnification	shown on picture
Picture 16	(Roberts No. 241)	Magnification	shown on picture
Picture 17	(Roberts No. 88)	Magnification	200x
Picture 18	(Roberts No. 89)	Magnification	800x
Picture 19	(Roberts No. 194)	Magnification	400x
Picture 20	(Roberts No. 198)	Magnification	800x
Picture 21	(Roberts No. 201)	Magnification	200x
Picture 22	(Roberts No. 204)	Magnification	800x
Picture 23	(Roberts No. 206)	Magnification	800x
Picture 24	(Roberts No. 239)	Magnification	shown on picture

Picture 25	(Roberts No. 16)	Magnification	200x
Picture 26	(Roberts No. 17)	Magnification	200x
Picture 27	(Roberts No. 223)	Magnification	300x
Picture 28	(Roberts No. 251)	Magnification	shown on picture
Picture 29	(Roberts No. 252)	Magnification	shown on picture
Picture 30	(Roberts No. 253)	Magnification	shown on picture
Picture 31	(Roberts No. 304)	Magnification	shown on picture
Picture 32	(Roberts No. 305)	Magnification	shown on picture
Picture 33	(Roberts No. 306)	Magnification	shown on picture
Picture 34	(Roberts No. 307)	Magnification	shown on picture
Picture 35	(Roberts No. 308)	Magnification	shown on picture
Picture 36	(Roberts No. 309)	Magnification	shown on picture
Picture 37	(Roberts No. 168)	Magnification	1200x
Picture 38	(Roberts No. 208)	Magnification	5000x
Picture 39	(Roberts No. 137)	Magnification	1000x
Picture 40	(Roberts No. 170)	Magnification	1200x
Picture 41	(Roberts No. 173)	Magnification	1200x
Picture 42	(Roberts No. 174)	Magnification	1200x
Picture 43	(Roberts No. 185)	Magnification	600x
Picture 44	(Roberts No. 243)	Magnification	shown on picture
Picture 45	(Roberts No. 244)	Magnification	shown on picture
Picture 46	(Roberts No. 245)	Magnification	shown on picture
Picture 47	(Roberts No. 247)	Magnification	shown on picture
Picture 48	(Roberts No. 248)	Magnification	shown on picture
Picture 49	(Roberts No. 249)	Magnification	shown on picture

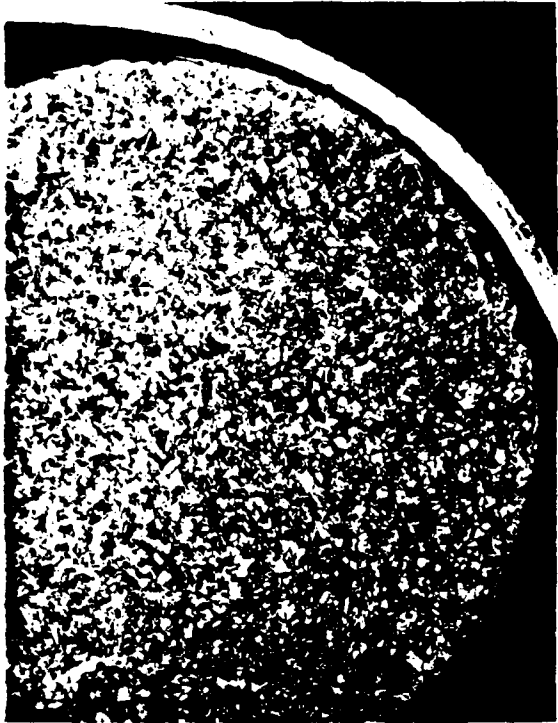
Picture 50	(Roberts No. 250)	Magnification	shown on picture
Picture 51	(Roberts No. 254)	Magnification	1000x
Picture 52	(Roberts No. 255)	Magnification	350x
Picture 53	(Roberts No. 257)	Magnification	1000x
Picture 54	(Roberts No. 259)	Magnification	1000x
Picture 55	(Roberts No. 262)	Magnification	1000x
Picture 56	(Roberts No. 286)	Magnification	1000x
Picture 57	(Roberts No. 297)	Magnification	shown on picture
Picture 58	(Roberts No. 298)	Magnification	shown on picture

REFERENCES

1. Robert E. Reed-Hill, Physical Metallurgy Principles, 2nd Edition, (D. Van Nostrand, New York, 1973), pp. 304-325.
2. M. Suenaga and A. F. Clark eds., Filamentary Al5 Superconductors, (Plenum Press, New York, 1980), various articles.
3. M. Tanenbaum and W. V. Wright eds., Superconductors (John Wiley and Sons, Inc., New York, 1962), various articles.
4. S. F. Cogan, D. S. Holmes, and R. M. Rose, "On the elimination of Kirkendall voids in superconducting composites", Appl. Phys. Lett., Vol. 35, pp. 557-559, 1979.
5. C. J. Smithells ed., Metals Reference Book, 5th Edition (Butterworth, London, 1976), pp. 326-327, 1310-1326, and 591-607.
6. S. F. Cogan, D. S. Holmes and R. M. Rose, "Microfilamentary superconducting composites by the external diffusion method: Nb₃Sn," J. App. Phys. Vol. 51, pp. 4332-4337, 1980.
7. M. Hansen, Constitution of Binary Alloys, Second Edition, (McGraw-Hill, New York, 1958) pp. 633-637.
8. D. S. Holmes, A. M. Adair, C. E. Oberly and J. C. Ho, "Bronze For Superconducting Wires: The Powder Metallurgy Approach," IEEE Trans. Magn. Mag. Vol. 17 (1), pp. 1-3, 1980.
9. H. H. Farrell and G. H. Gilmer, "Grain boundary diffusion and growth of intermetallic layers," J. App. Phys., Vol. 45, pp. 4025-4035, 1974.
10. J. C. Ho, C. E. Oberly, H. J. Garrett, M. S. Walker, B. A. Zietlin and J. W. Ekin, Advances in Cryogenic Engineering, Vol. 26, pp. 358-366, 1980.
11. N. F. Kennon, "Stabilization of the Beta Phase in Cu-15.1 at. % Sn", J. Met. Sci., Vol. 6, pp. 64-66, 1972.
12. W. Vandermeulen and A. Deruyttere, "Omega Phase in the Cu-16.5 At Pct Sn Alloy," Metall. Trans. Vol. 4, pp. 1659-1664, 1973.
13. L. H. Schwartz, S. Mahajan and J. T. Plewes, "Spinodal Decomposition in a Cu-9 wt % Ni - 6 wt % Sn Alloy," Acta Metall., Vol. 22, pp. 601-609, 1974.
14. I. A. Arbuzova, Yu. N. Koval, V. V. Martynov and L. G. Khandros, "Influence of Ageing on Hysteresis in a Copper-Tin Alloy During Martensitic Transformation," Phys. Met. Metallogr., Vol. 36, pp. 202-204, 1973.

15. J. T. Plewes, "High Strength Spinodal Cu Ni Sn Alloys by Thermo-mechanical Processing," Inst. Met. (London) Monogr. Rep. Ser. 36, Vol. 1, pp. 109-113, 1973.
16. L. H. Schwartz and J. T. Plewes, "Spinodal Decomposition in Cu-9 wt % Ni - 6 wt % Sn. A Critical Examination of Mechanical Strength of Spinodal Alloys," Acta Metall., Vol. 22, pp. 911-921, 1974.
17. S. Miura, Y. Morita and N. Nakanishi, "Superplasticity and Shape Memory Effect in Cu-Sn Alloys," Metall. Soc. of AIME Proc. (Penum Press, New York, 1975), pp. 389-405.
18. J. T. Plewes, "High-Strength Cu-Ni-Sn Alloys by Thermomechanical Processing," Metall. Trans., Vol. 6A, pp. 537-544, 1975.
19. W. Duerrschabel and H. Lederer, "Relaxation of Cold Work Hardening Copper Alloys," Metall. Vol. 30, pp. 1046-1049, 1976.
20. B. Ditchek and L. H. Schwartz, "On the Strength of Spinodal Alloys," Int. Confr. on Strength of Metals and Alloys, 4th Proc. Nancy, France, Vol. 3, pp 1319-1323, 1976.
21. V. K. Sorokin and V. K. Kalistov, "Investigation of the Mechanical Properties of Sintered Tin Bronze," Sov Powder Metall Met. Ceram. Vol. 15, pp. 231-233, 1976.
22. K. W. Sweatman and C. J. Thwaites, "The Development of an age-hardening tin bronze," Met. Congr. (Proc.) Aust. Inst. Met., pp. 83-96, 1975.
23. I. S. Servi, "Annealing Behavior of Copper-Tin-Oxygen Alloys," Trans. Met. Soc. AIME, Vol. 245, pp. 873-875, 1969.
24. E. D. Levine, "Electron Microprobe Observations of Grain Boundary Segregation in Equilibrated Copper-Tin Alloys," Scripta Met., Vol. 2, pp. 165-168, 1968.
25. R. E. Hanneman, "Comments on Electron Microprobe Observations of Grain Boundary Segregation in Equilibrated Copper-Tin Alloys," Scripta Met. Vol. 2, pp. 485-486, 1968.
26. W. Vandermeulen, "The Decomposition of the Gamma Phase of a Copper-27 wt % Tin Alloy", Mechanism of Phase Transformations in Crystalline Solids, Inst. of Met. (London), pp. 294-296, 1969.
27. I. A. Arbuzova, Yu N. Koval and V. V. Martynov, "Influence of Ageing on Hysteresis in a Cu-Sn Alloy During Martensitic Transformation," Phys. Met. Metallogr., Vol. 36, pp. 202-204, 1973.
28. O. Vohringer, "Dynamic Strain Aging in Alpha-Copper-Tin-Alloys," Z. Metallkunde, Vol. 58, pp. 317-320, 1967.

29. I. B. Mogarycheva, "Change in the Structural State of Copper 25.5 - 27.8 wt. % Tin Alloys During Natural Ageing," Fig. Metal Metalloved., Vol. 24, pp. 623-628, 1967.
30. Michael S. Walker's communication to Lt. Scott Holmes, "Partial Shipment of Deliverable Items," June 17, 1981.
31. T. Luhman, M. Suenaga, C. Klamut, and W. B. Sampson, Brookhaven National Laboratory, Quarterly Letter, Oct.-Dec. (FY 1981) titled "Fabrication and Properties of Conductors for Fusion Magnets."
32. M. S. Walker, B. A. Zietlin, R. E. Schwall, G. M. Ozeryansky and C. T. Nelson, "Manufacturing Technology of Multifilamentary Nb₃Sn Superconductors," IGC's 16th Interim. Tech. Report, June 23, 1980, Report no. 680-11.
33. M. S. Walker, B. A. Zietlin and C. T. Nelson, "Manufacturing Technology of Multifilamentary Nb₃Sn Superconductors," IGC's 17th Interim. Tech. Report, Nov. 25, 1980, Report No. 1280-3.
34. V. L. Ginzburg and D. A. Kirzhnits, eds., "High Temperature Superconductivity," (Plenum Pub. Corp., New York, 1981), in its entirety.



1



2



3



4



5



6



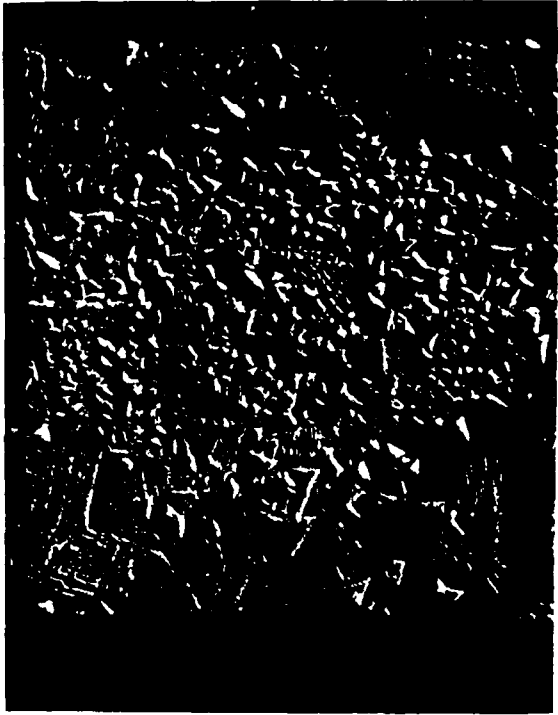
7



8



9



10



11



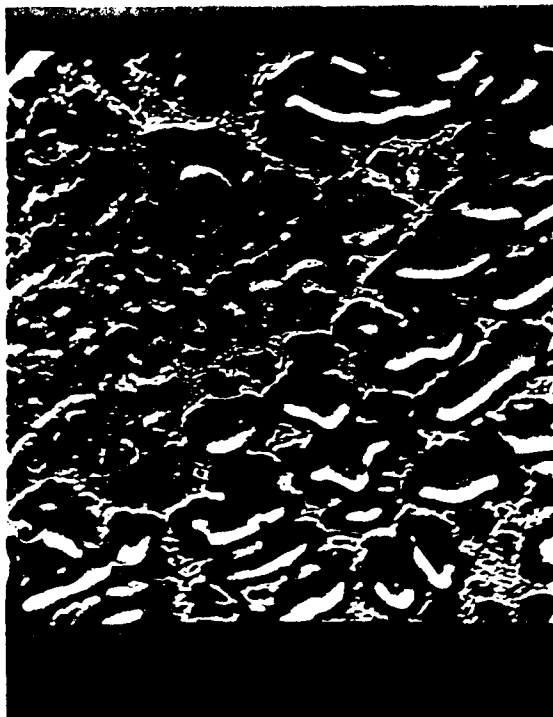
12



13



14



15



16



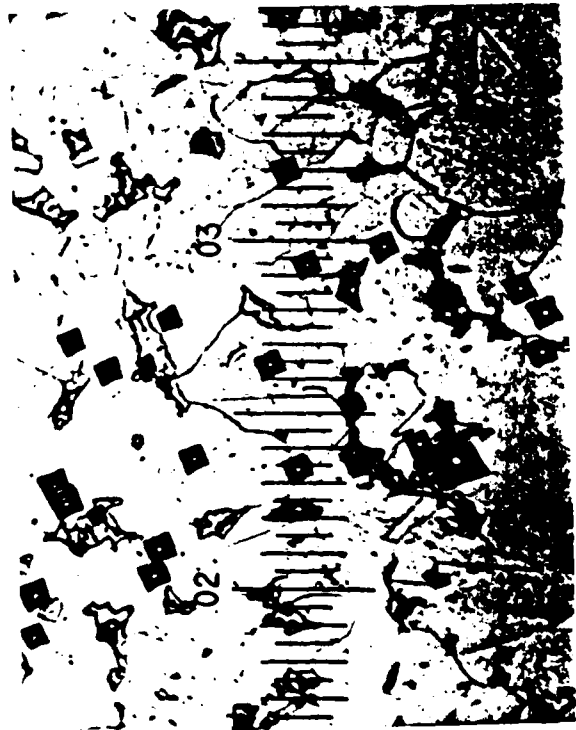
17



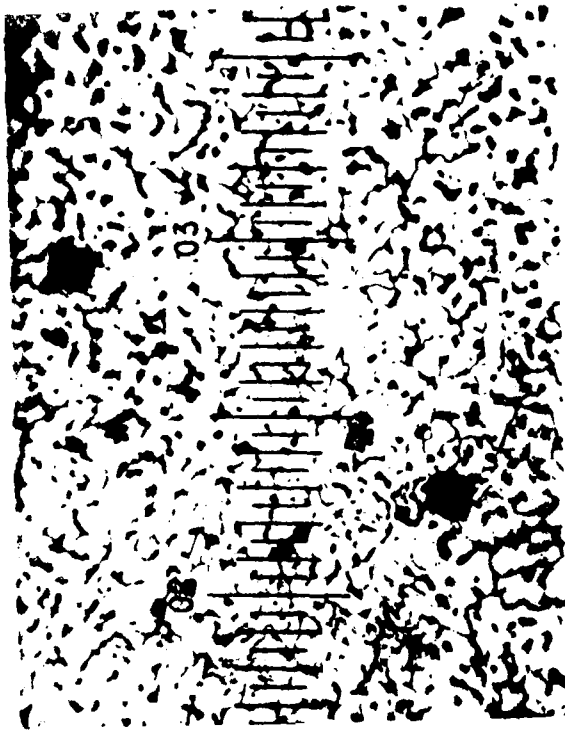
18



19



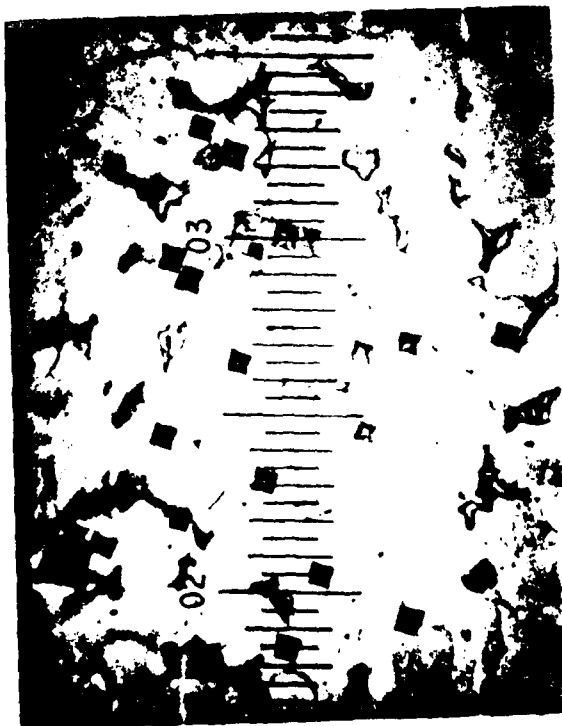
20



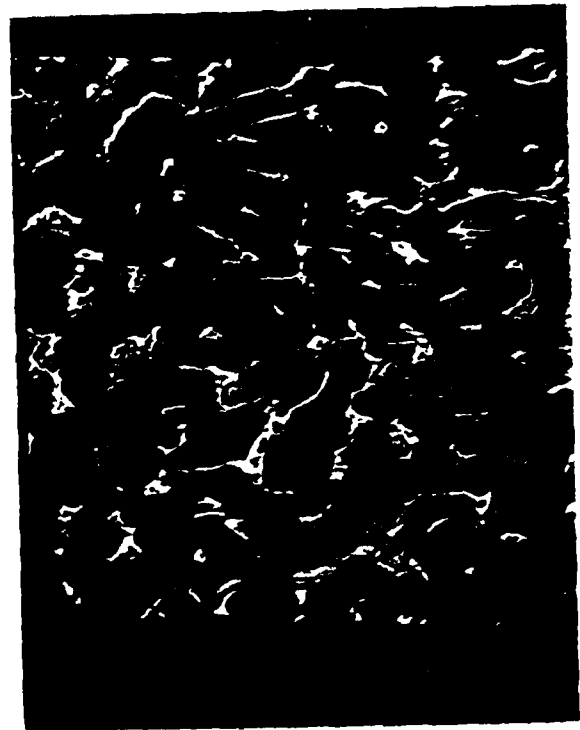
21



22



23



24



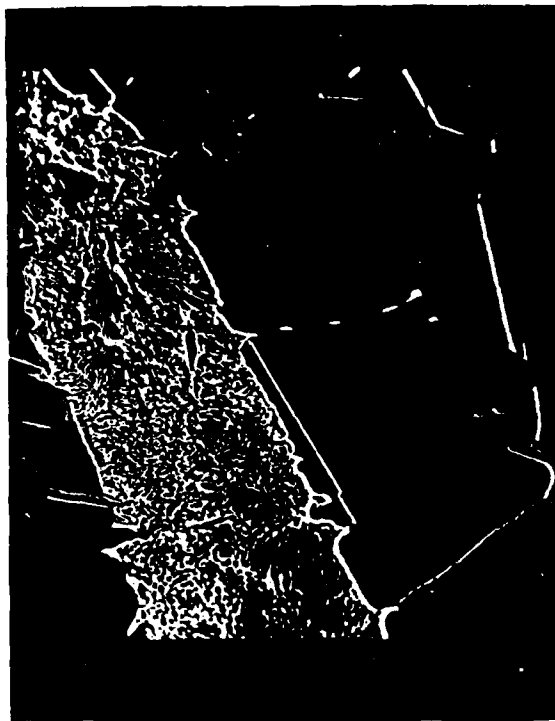
25



26



27



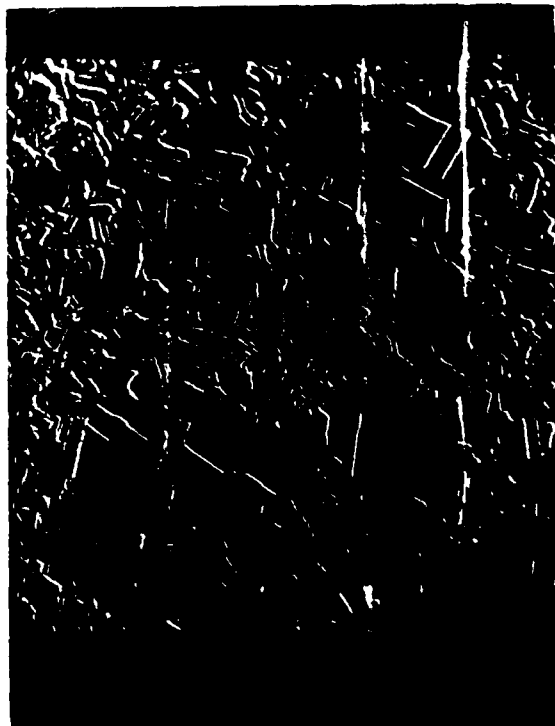
28



29



30



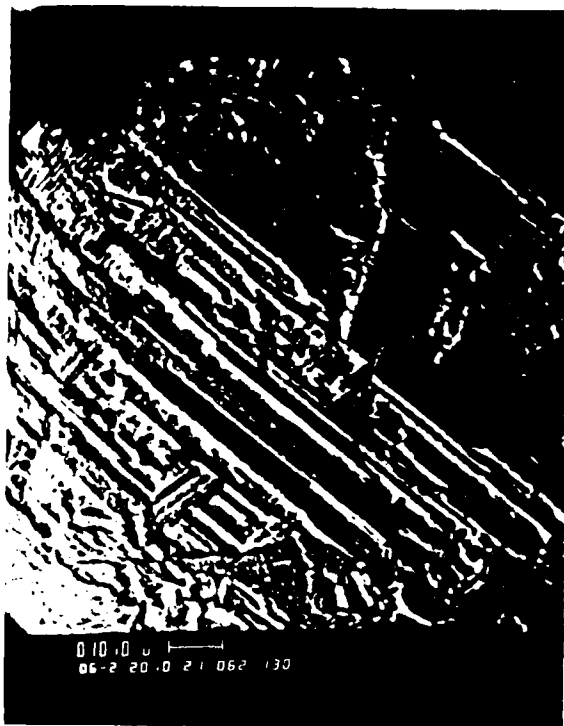
31



32



33



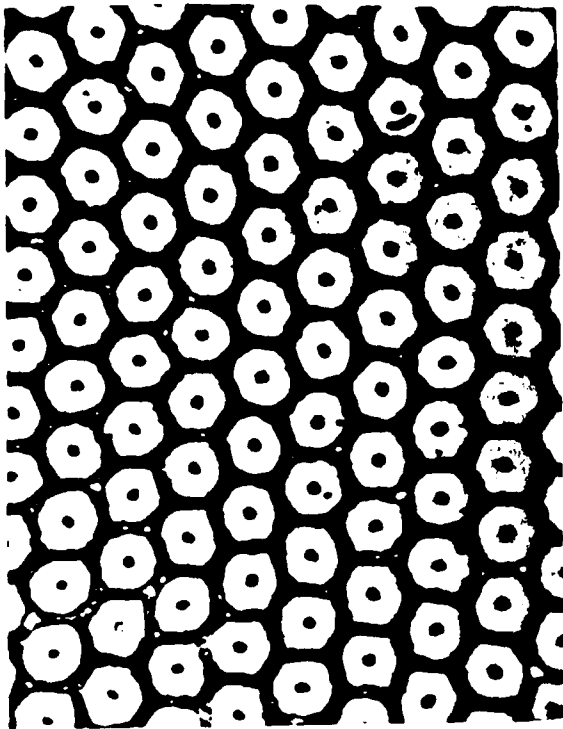
34



35



36



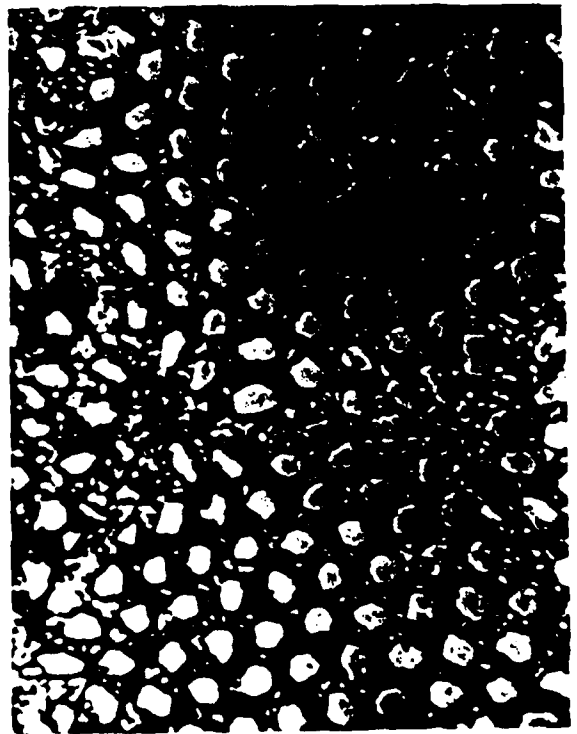
37



38



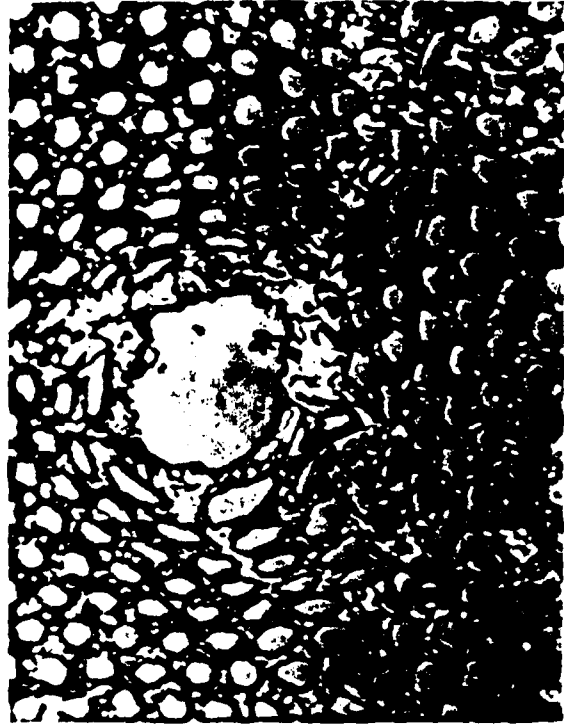
39



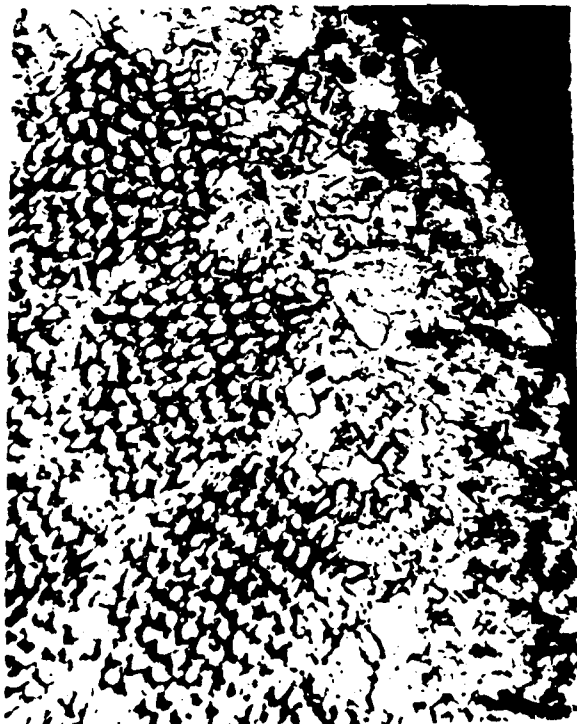
40



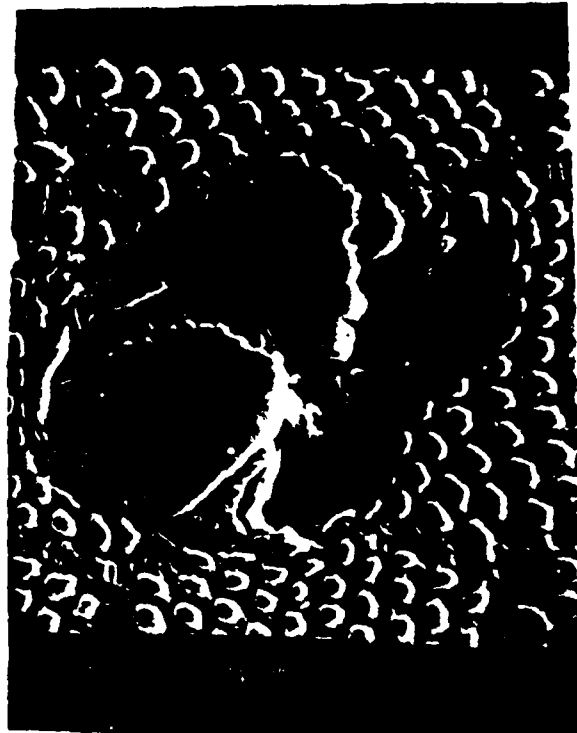
41



42



43



44



45



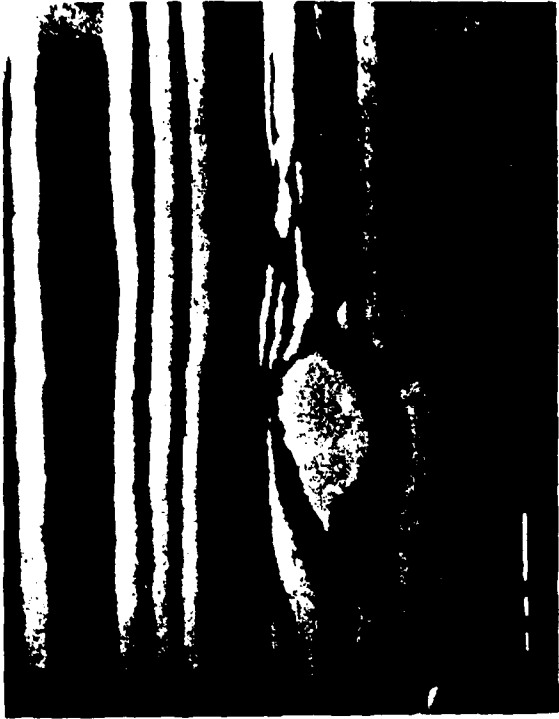
46



47



48



53



54



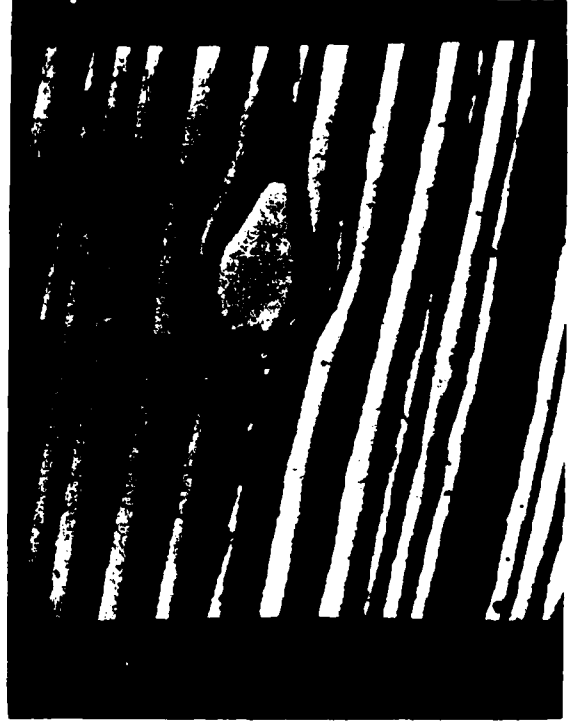
55



56



57



58

1981 USAF - SCEEE SUMMER FACULTY RESEARCH PROGRAM

Sponsored by the

AIR FORCE OFFICE OF SCIENTIFIC RESEARCH

Conducted by the

SOUTHEASTERN CENTER FOR ELECTRICAL ENGINEERING EDUCATION

FINAL REPORT

INVESTIGATION OF THE MECHANICAL PROPERTIES

OF LESS THAN 100% DENSE TITANIUM POWDER

METALLURGY COMPACTS

Prepared by:	Dr. Thomas A. Roth
Academic Rank:	Associate Professor
Department and University:	Department of Chemical Engineering Kansas State University
Research Location:	Air Force Wright Aeronautical Laboratory, Metals and Ceramics Division, Structural Metals Branch
USAF Research Colleague:	Dr. F.H. Froes
Date:	July 24, 1981
Contract No:	F49620-79-C-0038

INVESTIGATION OF THE MECHANICAL PROPERTIES
OF LESS THAN 100% DENSE TITANIUM POWDER
METALLURGY COMPACTS

by

Thomas A. Roth

ABSTRACT

A possible method to improve the mechanical properties of porous powder compacts by altering the surface condition of the compacts through the use of shot-peening to reduce surface porosity is used to study the tensile properties of elemental blend Ti-6Al-4V. The effects of a stress-relief treatment of the shot-peened material are considered. Tensile test data, along with studies of the porosity and microstructure, suggest improvement is to be found in the fatigue behavior of the material rather than in the tensile properties. Suggestions for further research examining the effect of shot-peening on the fatigue behavior of the less than 100% dense material are offered.

ACKNOWLEDGEMENTS

The author would like to thank the Air Force Systems Command, Air Force Office of Scientific Research, and the Southeastern Center for Electrical Engineering Education for the opportunity to perform this work at the Structural Metals Branch, Metals and Ceramics Division of the Air Force Wright Aeronautical Laboratory, Wright-Patterson AFB, Ohio.

Special thanks are extended to the author's effort focal point, Dr. F. H. (Sam) Froes, for his interest, assistance, encouragement, and hospitality during the course of this work. Thanks are also due to Dr. Danny Eylon of the Metcut-Materials Research Group and to his staff for their assistance in this effort. Al Jackson of Systems Research Laboratories and his staff are thanked for their aid and patience during the metallographic preparation and examination phases of the research.

I. INTRODUCTION

Titanium alloys are a very attractive choice for use in advanced Air Force systems because of their excellent strength-to-density characteristics combined with outstanding general corrosion resistance and fracture behavior. However, use has been restricted because of the cost of component fabrication; a result of initial high material cost and high fabrication costs for forging and machining. To circumvent these high costs, much effort has been put into near net shape techniques. Of these techniques, powder metallurgy offers a very attractive route not only to a more cost-effective approach but also to enhanced mechanical property levels.

Recent work at the Air Force Materials Laboratory has shown that the mechanical property levels of powder compacts can indeed be raised to levels which in some case exceed those of wrought material.⁽¹⁻⁴⁾ To achieve this, the powder metallurgy process must be carefully controlled during powder production, handling, compaction, and manipulation of the final microstructure.⁽⁴⁻⁶⁾ The mechanical properties equivalent to or exceeding those of the wrought material include the tensile properties of both compacts made by the elemental blend approach and those made from prealloyed powder. Fatigue behavior is, however, more sensitive to microstructural integrity, i.e., the presence of discontinuities such as pores and foreign particles, and often the values obtained are below wrought material levels. Values below wrought levels are found for elemental blend material; however, surprisingly material produced from prealloyed powder often exhibits fatigue levels equivalent to wrought material even when the density is less than 100%.

Since it is not possible to completely eliminate the discontinuities, microstructural control has been used to reduce the sensitivity of the compacted material to their presence.⁽³⁾ In the case of less than 100% dense compacts, some of the residual porosity would be expected to lie at the surface, especially after final shaping, as by machining. Porosity at the surface could thus contribute to the generally observed poor fatigue behavior. In another approach to reducing the sensitivity of the compacts to the presence of discontinuities, here

the pores and specifically the surface pores, to improve the mechanical properties, particularly the fatigue behavior, of less than 100% dense compacts through control of such surface porosity, a study has begun on the effects of shot-peening the surface of less than 100% dense compacts. This report discusses the initial findings of this ongoing study.

II. OBJECTIVES OF THE RESEARCH EFFORT

The main objective of this research was to provide additional insight into the ongoing Materials Laboratory studies of the mechanical property behavior of less than 100% dense powder compacts produced by both the elemental blend and the prealloyed techniques. The specific objective of this effort has been to study an attempt at improving the mechanical properties of elemental blend Ti-6Al-4V powder compacts by altering the surface condition of the compacts through the use of shot-peening in order to reduce the sensitivity of the material to the effects of porosity at the surface.

It was hoped that the influence of the pores on mechanical properties, both tensile and fatigue, could be defined and the overall behavior rationalized. The study of the effect of shot-peening on the tensile properties of elemental blend Ti-6Al-4V compacts has been completed and the results are the basis for this report. The study of the effect of shot-peening on the fatigue behavior is currently in its initial stages, i.e., the fatigue specimens are only now being fatigue tested. The fatigue behavior part of the investigation is considered below for follow-on work under the Recommendations Section of this report.

To carry out this study, optical and scanning electron microscopy techniques have been used. Fractographic analysis is expected to be a useful tool for the continuing study on the effects of shot-peening on the fatigue behavior. By correlating factors such as basic microstructure, pore characteristics, dislocation interactions, and fractographic features, it should be possible to rationalize the observed behavior, when the total investigation is completed.

III. MATERIALS

Ti-6Al-4V is an alpha-beta alloy at room temperature with moderate strength. It is currently the most widely used titanium alloy. The vast majority of titanium alloy powder metallurgy evaluation has been performed on Ti-6Al-4V in the annealed

condition.⁽⁷⁾ Because of its commercial significance and the solid understanding of its fundamental behavior, Ti-6Al-4V seems a good choice for study of variations and modifications of its treatment for property improvement.

For this work, Ti-6Al-4V powder compacts, with the composition given in Table I, were produced by Gould Laboratories from titanium sponge fines (-100 μm) and master alloy powder cold pressed and subsequently sintered at 2300^oF (1260^oC) 4 hrs. using the method discussed by Andersen and Eloff.⁽⁸⁾

Table I. Typical Chemical Analysis of the Elemental Blend Ti-6Al-4V

Al	V	O ₂	N ₂	H ₂	C	Fe	Na	Cl
6.2	4.1	0.24	0.016	0.002	0.02	0.18	0.10	0.12

This material is the same as used in a previous Materials Laboratory study⁽¹⁾ to evaluate the effect of microstructure on the mechanical properties of cold pressed and sintered elemental blend Ti-6Al-4V powder. The powder compacts used in the present work differ from the previously studied material in that they were shot-peened at two different intensities after being machined into the desired test bars, in the attempt to enhance the mechanical properties by improving the continuity of the surface by closing any surface pores. Additionally, some of the shot-peened compacts were subsequently stress-relieved in an attempt to remove the strain resulting from the shot-peening.

The details of the conditions of the material of this study are given in Table II.

Table II. Conditions of the Test Material

Group	Condition
I	Smooth test bars (as-pressed, sintered, and machined)
II	Shot-peened bars (0.006N Almen intensity)
III	Shot-peened bars (0.012N Almen intensity)

- IV Shot-peened bars
(0.006N Almen intensity)
Stress-relieved
(2 hrs. @ 1150^oF in vacuum)
- V Shot-peened bars
(0.012N Almen intensity)
Stress-relieved
(2 hrs. @ 1150^oF in vacuum)

IV. TENSILE PROPERTIES

Two specimens in each of the five conditions of Table II were tensile tested by Metcut Research Associates with the results as listed in Table III. The average of the two values obtained for specimens tested in the same condition is shown in parentheses. The results found in the prior study ⁽¹⁾ are shown for comparison as are values for wrought Ti-6Al-4V and typical minimum mechanical property specifications for the alloy.

The results shown in Table III indicate that, except for the yield strength, the material of this study satisfies the minimum mechanical property specifications. The tensile properties of this series of specimens are, however, well below those of the mill annealed wrought Ti-6Al-4V and have lower strength values, but greater ductility, than those reported in the prior study. ⁽¹⁾

The results shown in Table III also indicate that the shot-peening treatment has not improved the strength values of the material. No significant change in those values is to be noted other than a slight decrease in yield strength resulting from the shot-peening. Since it has been shown ⁽²⁾ that the tensile properties of powder compacts are not as dependent on the porosity as is the fatigue behavior, the similarity in the strength values of Table III for the specimens in the different conditions is not entirely unexpected.

The ductility of the material has certainly been reduced by the shot-peening. Surprisingly, the lighter peening (0.006N Almen intensity of Group II Specimens) is seen to have a greater effect in reducing the ductility than does the heavier peening (0.012N Almen intensity of Group III specimens).

Table III. Room Temperature Tensile Property Results
Compared to Prior Results and Wrought Ti-6Al-4V.

Specimen Condition	Specimen Number	U.T.S. (Ksi)	Y.S. (0.2%) (Ksi)	Elong. (%)	R.A. (%)
I	78-12	130.9	119.4	14.4	28.4
I	78-41*	129.8 (130.4)**	118.2 (118.8)	16.9 (15.6)	27.2 (27.8)
II	78-23	130.6	117.2	11.0	11.6
II	78-34*	130.6 (130.6)	117.4 (117.3)	12.9 (12.0)	17.4 (14.5)
III	78-19*	130.9	119.0	14.4	22.0
III	78-52	130.3 (130.6)	117.4 (118.2)	14.6 (14.5)	28.9 (25.4)
IV	78-14*	130.3	122.3	15.2	21.9
IV	78-24	131.2 (130.8)	120.8 (121.6)	16.4 (15.8)	26.8 (24.4)
V	78-5	130.9	120.1	13.8	18.0
V	78-10*	130.9 (130.9)	120.7 (120.4)	16.5 (15.5)	27.6 (22.8)
Prior Results ⁽¹⁾		137.6	126.4	14.8	24.6
Wrought, mill anneal ⁽¹⁾		141.5	134.0	16.7	44.1
Typical Minimum Mechanical Properties (MIL-T-9047)		130.0	120.0	10.0	25.0

* Specimens randomly selected for metallographic examination.

** The values in parentheses are the average for the two specimens tested in the same condition.

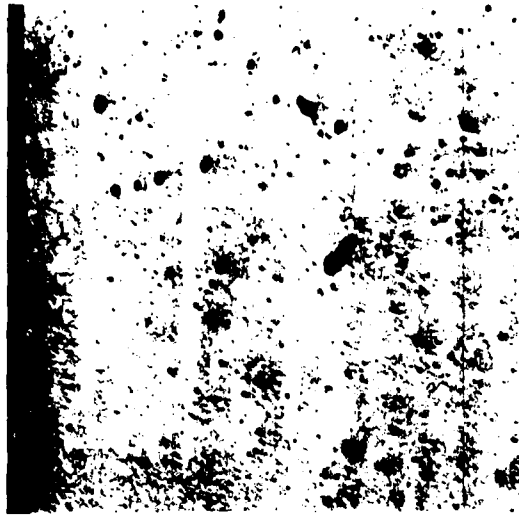
The stress-relieving treatment is seen to produce the desired result of raising the yield strength values, the per cent elongation values, and the lighter shot-peened per cent reduction of area value to near their original range. It has not been effective, however, for the one heavier shot-peened specimen (78-5). In fact, due to the greater scatter in duplicate results for the per cent reduction of area values, the stress-relief treatment produced an apparent decrease in the average per cent reduction of area value. Visual examination of the four stress-relieved specimens was sufficient to detect a discoloration of the surface suggesting the possibility for oxidation having played a role in the incomplete recovery of the per cent reduction of area values.

V. METALLOGRAPHY

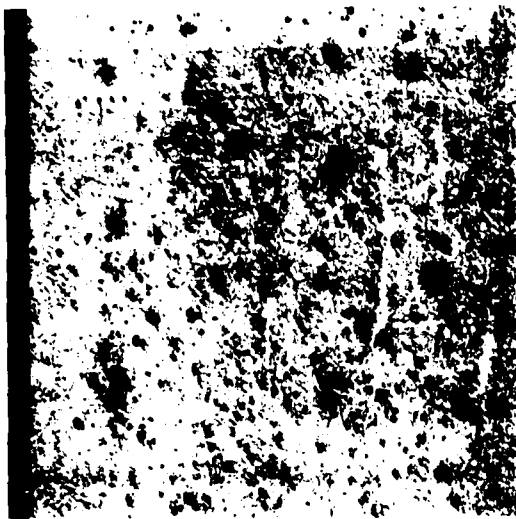
Upon return of the failed tensile test specimens, one fractured half of each of the specimens representing each of the five different conditions of Table II was randomly selected for metallographic examination. Each selected specimen was cut through the threaded grip area of the tensile bar in order to provide a length that could be contained in the mounting press. The remaining bar was then sectioned lengthwise in order to provide two halves of the same specimen for metallographic examination in the unetched as well as the etched condition. Each sectioned half thus obtained could be used to examine the surface edge and interior of the failed tensile test bar. After mounting, specimen preparation consisted of a series of grinding steps to 600 grit paper. Polishing through 6 μ diamond followed by 0.3 μ alumina produced an adequate metallographic finish. Etching solutions were Kroll's etch and a stain etch (10 ml KOH, 5 ml H₂O₂, 20 ml H₂O). Following examination of the entire prepared specimen area using optical microscopy, both bright field and polarized light, micrographs were obtained for typical and representative areas of each of the specimens in the etched and unetched conditions.

In Fig. 1, the unetched appearance of the specimens in the five conditions of Table II is shown. Fig. 2 shows the microstructure typical of these specimens.

As seen in Fig. 1, the pores remaining in the specimens are quite numerous and range from small to large in size, independent of specimen condition. In general, fewer larger pores are found near the surface of the specimens. A small band, on the order of 0.05 to 0.1mm, at the surface containing generally fewer pores compared to the interior is to be noted in each specimen.



(a)

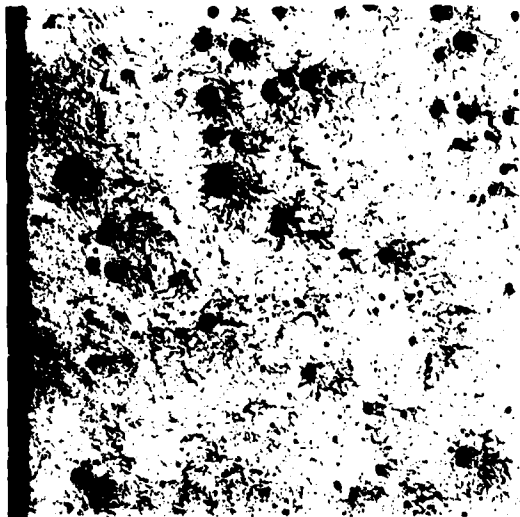


(b)

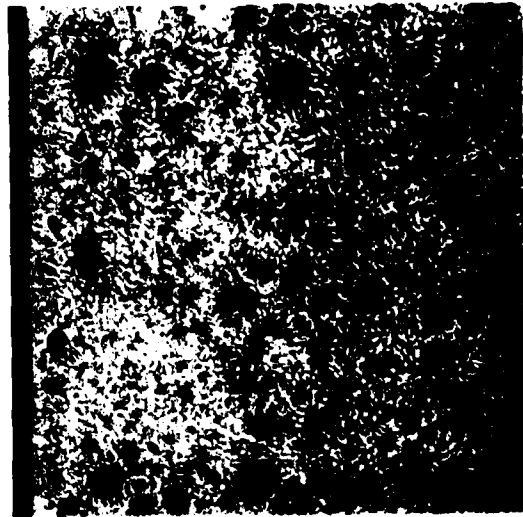


(c)

Figure 1. Porosity present in specimen of this study. Large pores, small pores, and some etching artifacts are evident. (a) Group I - smooth bar. (b) Group II - 0.006N shot-peened. (c) Group III - 0.012N shot-peened.



(d)

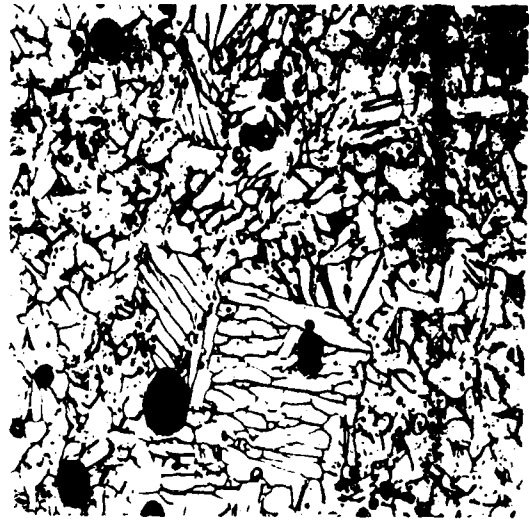


(e)

Figure 1 (con't.) (d) Group IV - 0.006N shot-peened, stress-relieved.
(e) Group V - 0.012N shot-peened, stress-relieved.
All at 100x.



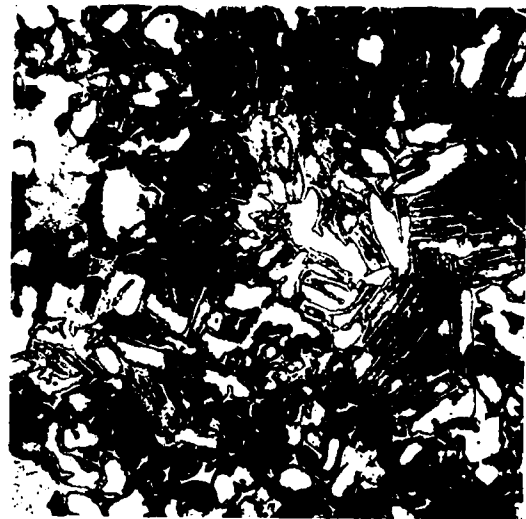
(a)



(b)



(c)



(d)

Figure 2. Microstructure typical of the Ti-6Al-4V specimens of this study. (a) and (b) Kroll's etch; 200x and 400x, respectively. (c) and (d) stain etch; 200x and 400x, respectively.

Pores at the surface are evident in Fig. 1(a). Although no pores are to be observed at the surface in the shot-peened specimens, Figs. 1(b)-(d), a small number of surface pores were observed in the complete examination of the shot-peened specimens. This is in agreement with results at Gould Laboratories⁽⁹⁾ which showed that the surface pores were not completely healed by peening. Some smaller pores are to be seen just beneath the surface of the shot-peened material, Figs. 1(b) and (c). Small surface cracks are seen in Figs. 1(d) and (e), the stress-relieved specimens. Examination at higher magnifications confirmed that these are indeed small cracks. Except as noted regarding the surface pores, none of these observations is unique to these particular micrographic areas as these phenomena were observed frequently in the complete examination of the specimens and the areas selected here are meant to be representative of these specimens.

The microstructural feature to be noted in Fig. 2, in addition to the pores, is a structure that consists of colonies of alpha plates, fine beta grains, and intergranular beta. This is especially evident in Figs. 2(c) and (d) where the stain etch used was selected because it stains the alpha and transformed beta leaving retained beta to appear white. These microstructural features are found to be characteristic of both the area at and just beneath the specimen surface, as well as within the interior, of each of the specimens regardless of condition. Shot-peening and the stress-relieving treatment would not be expected to have any effect on altering the microstructure and none was found.

The location of the larger pores is seen to be generally within alpha areas at the junction of beta boundaries, Fig. 2(c). The smaller pores, as seen in Fig. 2(d), are found mainly within alpha grains, occasionally at the alpha grain/beta boundary interface, and, only in a very few instances, within beta grains.

VI RECOMMENDATIONS

As noted above, the report has dealt only with the initial stages of a continuing effort to study the feasibility for improving the mechanical properties of elemental blend Ti-6Al-4V powder compacts by shot-peening in order to reduce or eliminate the detrimental effects of surface discontinuities in the form of pores. The main objective of this study is to consider the effect of the surface treatment on the fatigue behavior of the material. The fatigue behavior is also the most likely characteristic of the material to be effected by the shot-peening treatment. Froes et al.⁽¹²⁾ have used the interaction of the surface pores with dislocations to rationalize the observed differing behavior of elemental blend Ti-6Al-4V powder compacts under tensile and fatigue conditions. For tensile loading, they found

that the surface pores promote homogeneous slip, allowing large amounts of plastic deformation, and therefore, good ductility. For fatigue conditions, where crack initiation is the controlling factor in determining total fatigue life, the surface pores were found to result in non-homogeneous slip, leading to early crack initiation at the pores, and therefore, reduced fatigue performance. Should the shot-peening treatment be effective in closing the surface pores, the result of this treatment should be a marked improvement of the fatigue behavior of the powder compacts.

I therefore propose to continue this study attempting to improve the fatigue behavior of elemental blend Ti-6Al-4V powder compacts through the use of shot-peening to reduce the sensitivity of the material to the effects of surface porosity. As with the completed work reported here, optical and scanning electron microscopy, along with fractographic analysis, will be used to analyze the failed fatigue specimens of this same material currently being tested under fatigue conditions. It should be possible to rationalize the results of this follow-on research, along with that presented here, by correlating microstructure and pore characteristics, dislocation interactions, and fractographic features.

REFERENCES

1. Y. Mahajan, D. Eylon, R. Bacon, and F.H. Froes, "Microstructure Property Correlation in Cold Pressed and Sintered Elemental Ti-6Al-4V Powder Compacts," Proc. TMS-AIME Powder Metallurgy of Titanium Alloys Symposium, Edited by F.H. Froes and J.E. Smugeresky, Las Vegas, Nevada, February 1980, pp. 189-202.
2. F.H. Froes, D. Eylon, and Y. Mahajan, "The Effect of Microstructure and Microstructural Integrity on the Mechanical Properties of Ti-6Al-4V PM Products," Modern Developments in Powder Metallurgy, Vol. 12-14, 1981
3. D. Eylon, R.E. Omlor, and F.H. Froes, "Microstructure Control of Titanium Alloy PM Products for Mechanical Property Optimization," Titanium '80, Science and Technology, Edited by H. Kimura and O. Izumi, TMS-AIME Publications, Warrendale, PA, 1981, pp. 2205-2213.
4. F.H. Froes, D. Eylon, G.E. Eichelman, and H.M. Burte, "Developments in Titanium Powder Metallurgy," Journal of Metals, Vol. 32, No. 2, 1980, pp. 47-54.
5. C.A. Kelto, B.A. Kosmal, D. Eylon, and F.H. Froes, "Titanium Powder Metallurgy - A Perspective," Journal of Metals, Vol. 32, No. 8, 1980, pp. 17-25.
6. D. Eylon, R.E. Omlor, R.J. Bacon, and F.H. Froes, "Morphological and Microstructural Evaluation of Various Titanium Alloy Powders," Proc. TMS-AIME Powder Metallurgy of Titanium Alloys Symposium, Edited by F.H. Froes and J.E. Smugeresky, Las Vegas, Nevada, February 1980, pp. 71-81.
7. A.G. Jackson, J. Moteff, and F.H. Froes, "Dispersion Hardening of the Ti-5Al-2.5Sn Alloy Using a Powder Metallurgy Approach," Titanium '80 Science and Technology, Edited by H. Kimura and O. Izumi, TMS-AIME Publications, Warrendale, PA, 1981, pp. 2461-2470.
8. P.J. Andersen and P.C. Eloff, "Development of Higher Performance Blended Elemental P/M Ti Alloys," Proc. TMS-AIME Powder Metallurgy of Titanium Alloys Symposium, Edited by F.H. Froes and J.E. Smugeresky, Las Vegas, Nevada, February 1980, pp. 175-187.
9. P.C. Eloff, Private Communication, 1981.

1981 USAF - SCEEE SUMMER FACULTY RESEARCH PROGRAM

Sponsored by the

AIR FORCE OFFICE OF SCIENTIFIC RESEARCH

Conducted by the

SOUTHEASTERN CENTER FOR ELECTRICAL ENGINEERING EDUCATION

FINAL REPORT

APPLICATION OF TASK ANALYTIC TECHNIQUES TO THE DESIGN
OF A FLIGHT SIMULATOR INSTRUCTOR/OPERATOR CONSOLE

Prepared by: Dr. Charles D. Sanders

Academic Rank: Professor

Department and University: Department of Psychology
Coppin State College

Research Location: Air Force Human Resources Laboratory, Operations
Training Division, Williams Air Force Base, Arizona

USAF Research Colleague: Mr. Robert R. Woodruff

Date: August 18, 1981

Contract No: F49620-79-C-0038

Application of Task Analytic Techniques to the Design
of A Flight Simulator Instructor/Operator Console

by

Charles D. Sanders

ABSTRACT

Instructional Systems Development (ISD) has contributed to the efficiency and low cost of air flight training through the medium of the simulator. Task analysis is a component of ISD, and its application to the improvement of devices such as simulator instructor/operator consoles will continue to enhance the quality of flight training. Task analytic techniques are inextricably interwoven into the design of an instructor/operator console. The application involves the process, persons, and a machine within the context of a flight simulator. The tasks of the instructor and student are primary in the design process. The efficiency and economy of the task analytic process has implications for its use in the future developments of automated flight training.

Acknowledgement

The author would like to thank the Air Force Systems Command, the Air Force Office of Scientific Research and the Southeastern Center for Electrical Engineering Education for providing him with an opportunity to spend a very beneficial and interesting summer at the Human Resources Laboratory, Williams Air Force Base, Arizona. The hospitality of the staff was commendable, and the working conditions were excellent. Excellent rapport and esprit de corps existed among fellow Summer Faculty Research Associates.

Special recognition is in order for certain individuals due to their dedication and commitment to their work as well as the assistance which they gave me in the support of this project. Those individuals were Mr. Warren E. Richeson, Dr. Thomas H. Gray, and Mr. Robert R. Woodruff.

Special recognition is also in order for Dr. Warren D. Peele and Ms. Brenda S. Bomar of the Southeastern Center for Electrical Engineering Education.

Table of Contents

- I. Introduction
- II. Objectives
- III. Review of the Literature
 - Instructional Systems Development
 - The Military and Instructional Systems Development
 - Task Analysis
 - Instructor/Operator Console
- IV. Application of Task Analytic Techniques
- V. Recommendations
- VI. References
- VII. Appendices
 - Appendix A
 - Appendix B

Application of Task Analytic Techniques to the Design of a Flight Simulator Instructor/Operator Console

I. Introduction

The purpose of this study was to present findings from a review of literature on procedures related to the application of task analytic techniques to the design of an instructor/operator console. The study did not attempt to evaluate an existing simulator or its instructor/operator console parts, but it did present suggestions for their improvement generally. These recommendations were made after an extensive review of literature had been conducted. The study was not conducted for the purpose of designing theoretically or graphically, a new kind of instructor/operator console; however the findings may be useful to those involved in the technical design of instructor/operator consoles. The review of literature consisted of an examination and an extrapolation of the many aspects and factors associated with task analysis. An examination was made of the present use of task analysis by the Department of the Air Force and the military in general.

Emphasis was placed upon Instructional Systems Development (ISD) for the following reasons: (1) since the Air Force developed its first major instructional system in 1965, the systems approach to training has received considerable emphasis within the Department of Defense and in the civilian sector; and (2) task analysis is a major component of Instructional Systems Development.

A special section is devoted to ISD in the military due to the fact that the military has been a prime developer and consumer of instructional design and instructional technology. Some attention was given to the historical growth of the process as well as the rationale for certain aspects of growth. Special emphasis was given to the fact that the military has a specific mission in national defense and space exploration which requires efficiency and high standards of human performance. Increased efficiency of training simulators resulting from better-designed instructor/operator consoles (IOC) will come from application of ISD principles.

II. Objectives

The first major objective of this project was to conduct a review of the literature dealing with (1) flight simulator instructor/operator consoles, and (2) task analytic techniques to determine procedures whereby an instructor/operator console may be designed with sufficient regard to information and control requirements of the instructor pilot. The second major objective was to produce a document describing accepted task analytic techniques and how a task analytic technique or techniques might be utilized in instructor/operator console design.

The specific objectives that emerged from the major objectives were:

- (1) To review the literature on ISD in order to determine the role of task analysis in this overall design.
- (2) To portray through a literature review the accomplishments of the military in the field of ISD.
- (3) To present recommended principles and techniques for conducting a task analysis.
- (4) To present the present status of the instructor/operator console.
- (5) To make recommendations for applying a technique or techniques to deal with the possibility of improving information and control requirements of the instructor pilot.

III. Review of the Literature

Instructional Systems Development

Instructional Systems Development (ISD) is a planned and organized process for designing efficient training programs. It is a cyclical process involving team effort and it is goal-oriented and user-oriented. It is a primary function of professional educators and industrial or military trainers.

An instructional development system is both a philosophy and a set of tools. The basic objective of instructional design is to identify the concepts, principles, and skills to be taught so that scientifically validated information about human learning can be applied. Instructional design requires an orderly, sequential program of proficiency goals which are both specific and flexible. The task of designing instruction is not easy. It requires not only an in-depth knowledge of the particular skill to be taught, but also the ability to perceive the skill from each learner's point of view. An instructor should specify the final proficiency requirements in specific observable terms; assess the learner's current repertoire which is relevant to the desired outcome; and design a program consisting of a series of steps from current status to desired proficiency. In some cases it may be necessary to design a preparatory program for those learners whose current repertoires are inadequate.

ISD in the Military

The military has been the greatest developer and consumer of instructional design. Training effectiveness and efficiency are highly important in the military arena, and considerable emphasis is given to efforts which are intended to increase effectiveness and efficiency. Training programs applied in the context of the ISD approach had not been developed to any large extent prior to the 1950's; however, ISD is an outgrowth of the Systems Approach to Training (SAT). Investigations on learning and instruction were conducted by the process of research in psychological laboratories.

World War II created a need to increase the effectiveness and efficiency of military training. Psychologists were brought into the military and were given the assignment of designing such training. The period represented a dramatic increase in the areas of instructional technology and instructional design. Briggs (1977) feels that probably the most interesting of all longer-term training is that of aircrew flight training. Psychologists adapted their traditional laboratory equipment to devise selection tests, after which the equipment was further transformed into various types of training devices. After a short period of time, special-purpose equipment was designed to train equipment operators and maintenance personnel. These personnel were taught not only to operate, but also to repair and service the equipment. Initial research on the use of film in instruction began during this period. In the military environment, according to Briggs (1977), the validity of training is paramount to the success of a mission; that is, poor instruction yields poor performance.

Many resources are utilized for the design of instruction -- military personnel; civilians employed by the military; and contracts with universities, research laboratories, and private companies. The designer makes important decisions relative to cost-effectiveness. The designer is always aware of the fact that training programs are related to the national defense or space exploration and they must meet extremely high standards of human performance.

Training begins with the development of individual skills; then groups or crews are trained together. Each person is dependent on the other. Training aids, training devices, and simulators contribute to the learning effort. The command and control structure for learning in the military is direct and firm. Control implies that planned objectives are met and objectives are valid.

Task Analysis

Task analysis is the process of breaking down a task into its component parts. The components parts are referred to as subtasks. After the

subtasks have been identified, precise determinations are made about the skills and knowledges a learner needs to become proficient in performing each subtask.

Task analysis involves the application of scientifically validated principles of human learning to the teaching of concepts, principles, and skills. There are certain advantages that accrue from the use of task analysis: (1) students are taught the best procedures for doing things; (2) nothing irrelevant or erroneous is taught; (3) no gaps exist; (4) material will be presented in well-organized instructional units, incorporating the most effective conditions under which students learn; and (5) students are more likely to learn if the material is presented in the correct sequence. Task analysis can be applied to many situations and tasks other than those related to training systems.

There are two broad classes of tasks: action and cognitive. Action tasks, in the majority of instances, involve clearly defined observable steps. The steps can be broken down into subtasks and sequenced. Cognitive tasks are performed mentally, and the activity is generally not observable. Cognitive tasks involve such activities as deciding, evaluating, and discriminating. Some tasks of a cognitive nature are fixed sequence in orientation, and they may be described by using a flow diagram, but cognitive tasks that don't lend themselves to the flow chart may be described by outline or narrative form.

Since action tasks are more adaptable to sequencing, attention is given to the kinds of action tasks. The two major kinds of action tasks are fixed sequence and variable sequence. Fixed sequence action tasks may branch and return to the mainstream of action. The absence of the normal feedback is a cue for a different sequence of actions. In some cases, the task has branches and the action may be followed by two or more cues signaling different intervening activities. These action tasks are of a variable sequence nature. Variable sequence action tasks cannot be described completely in a fixed sequence of actions. Generally, variable sequence action tasks do not involve a series of discrete actions elicited by

particular cues. The cues are constantly changing, and for this reason the actions resulting therefrom are referred to as variable sequence. Variable sequence action tasks can be described by dividing the task into subtasks and using outlines, narrative descriptions, and flow diagrams. Usually, one or more fixed sequence subtasks are involved in variable sequence action tasks. It is important to be able to recognize fixed sequence tasks among variable sequence ones.

Flow diagrams are methods of representing fixed sequence tasks in schematic or diagrammatic form. Flow diagrams assist in visualizing the structure of a task. It is a method for clarifying relationships among actions, cues and feedback. If flow charting were not used, the clarifying of the sequences might become obscure and possibly overlooked. The steps in a task are represented by a set of symbols. The shape of the symbol used depends on the function being performed. The symbols used in flow diagramming have not been standardized; however, the symbols used in computer programming are commonly used.

Davis, et. al. (1974) developed a Task Description Checklist that could be used as a summary of steps useful in performing a task analysis. It also provides guidelines for the points at which flow diagrams should be used. The steps are as follows: (1) if you are an expert in performing the task, go directly to No. 2. if you are not an expert, learn how the task is performed; (2) break the tasks down into subtasks using action verbs such as operate, decide, ask, lift, etc.; (3) identify those subtasks which are fixed sequence, and describe them using flow diagrams; (4) do not attempt to describe subtasks which involve preference, taste, or values, and avoid subtasks which cannot be broken down into more discrete steps; and (5) describe all remaining subtasks using either a narrative form or outline. This checklist is a significant guide in performing the task analysis process.

DeVries, Eschenbrenner, and Ruck (1980) did an extensive and intensive study of task analysis for the United States Air Force which resulted in the Task Analysis Handbook. From a comparative point of view, the principles

and practices recommended by the researchers cited above coincide precisely with those of DeVries, Eschenbrenner, and Ruck (1980).

DeVries and his co-authors begin their study with an overview of ISD with an emphasis on an analysis of the system; definition of education training requirements; development of objectives and tests; planning, development, and validating instruction; and conducting and evaluating instruction. Task analysis and its component parts were defined. Three major acronyms were used: STS, CTS, and PPR. STS is the acronym for Specialty Training Standard; CTS is Course Training Standard; and PPR is Preliminary Performance Requirement. The STS or CTS is a contract between the Air Training Command and the Wing Command. It specifies what must be taught at the appropriate level in each course. Figure I-3 (Appendix A) is significant in that it is a schematic design of all steps used in task analysis. The DeVries study does caution one to be aware of the fact that task analysis may be defined in simple terms, but as a process, it is quite complex.

The DeVries study emphasizes the importance of preliminary performance requirements, identification of subtasks, identification of supporting skills and knowledges, examination of training standards, converting task performance and task knowledge statements into behavioral requirements, documentation of preliminary performance requirements, task observation, and specifying proficiency levels.

Identification and delineation of subtasks are critical in the task analysis process, and this area received substantial treatment in the DeVries study. It was concluded that a subtask has all of the characteristics of a task except independence. Each task is independent of other tasks. Each subtask is dependent upon other subtasks. A subtask essentially does not exist outside of the group of subtasks that make up a task. Tasks are usually not components of a procedure, but subtasks are always components of a procedure. Subtasks are important for the instructional designer preparing detailed and meaningful instruction. In identifying subtasks, one must determine whether or not there is a logical

breakdown of the task, a measurement capability of the subtasks, and the statement of all steps needed to perform the task.

The two best methods or techniques used in the identification of subtasks are the document study and task observation. It is recommended that while one is in the process of identifying subtasks which comprise a procedural task, it is often useful to observe a subject matter specialist perform the task under either simulated or actual job performance conditions. Task observation should take place in the job environment. The task observer should list the steps and indicate how the steps are performed. The document study should use the following steps: (1) select the document to be used; (2) review all documents for content, sequencing and relevant technical data; (3) become knowledgeable of terminology; and (4) sort selected documents according to the types of information. The selected documents should include information such as system requirements and functions data; listings of duties, tasks, and subtasks; task data; descriptions of task activities and performance standards; and listings of supporting skills and knowledges.

Several diagrams, tables, charts, and lists were taken from the volume titled Task Analysis Handbook by DeVries, Eschenbrenner, and Ruck (1980). These schema appear in Appendix A. These schema were selected in order to make knowledge of procedures readily available in an illustrated manner. The following procedures or processes are illustrated: (1) the ISD model; (2) hierarchy of performances, titles, and definitions; (3) STS/CTS proficiency levels; (4) task analysis process; (5) behavioral statement list form; (6) verb forms for task performance items; (7) verbs for each type of knowledge item; (8) types of conditions for preliminary performance ratings; (9) standards for preliminary performance ratings; (10) sample task diagram of a fixed sequence procedural task; (11) sample task diagram of variable sequence procedural task; (12) sample chart of documents used for document study; (13) appropriate and inappropriate levels of detail for specifying subtasks; (14) sample of task observation results; (15) a complete sample of a task diagram of a fixed sequence procedural task; (16) types of physical skills; (17) types of manipulative skills; (18) types of supporting

knowledges; (19) a task diagram of a fixed sequence, oriented task; (20) a task analysis documentation form; (21) a task diagram of a variable sequence, nonequipment oriented task; (22) a completed task analysis documentation form of a variable sequence, nonequipment-oriented task; (23) a task diagram of a variable sequence, equipment-oriented task.

Instructor/Operator Console

Research indicates that many flight simulator consoles in use today were not designed according to the task analysis procedures described in this study. Some of the design requirements were established by subjective opinion, past experience, and space and equipment constraints. The improvement of simulation quality and pilot training is related to instructor facilities.

Task analysis procedures may be used in the improvement of IOC's by the use of the following methods: (1) delineation of the instructional tasks and activities; (2) construction of a typical sequence of instructional tasks; (3) a definition of typical instructor tasks or activities and a breakdown of those tasks in terms of units of time required for completion, and (4) the consideration of student learning activities into an integrated student oriented syllabus.

The study by Gray, Chun, Warner, and Eubanks (1981) is a model of some advanced techniques using principles of task analysis. Some of the design concepts of the model are shown in Appendix B. The IOC was designed to simplify operational requirements and provide the maximum of A-10 training capability. With a minimum amount of training, the IP can provide the operator functions and the training functions. The A-10 IOC was designed to accommodate one person, the IP. Proposed utilitarian factors and design features will cause further adjustments relative to the location of the console. Further developments in automation will also have an effect on IOC design.

IV. Application of Task Analytic Techniques

The design and use of an IOC are related to functions of the instructor, the student, instructional support features, and training tasks. Specific areas in which task analysis techniques can be used include individualization of instruction; productive, economic and efficient use of student and instructor time; standardization of training; control of the simulated environment and aircraft conditions; diagnosis of student learning problems; focus of instruction; and provision for immediate feedback.

The task analytic techniques most adaptable to the IOC functions stated above would include a statement of preliminary performance requirements of a given task, identification of subtasks, identification of supporting skills and knowledges related to the subtasks, examination of training standards, conversion of task performance and task knowledge statements into behavioral requirements, documentation of preliminary performance requirements, task observation, and specification of proficiency levels.

Computer aided instruction and computer managed instruction have further possibilities in the future design of IOC's and computer applications make extensive use of task analysis techniques. SAINT (Systems Analysis of Integrated Network of Tasks) was developed at the Aerospace Medical Research Laboratory, Wright-Patterson Air Force Base, Ohio. SAINT is a model, in network form, of sets of tasks performed during the course of a mission. The following computer-based, automated activities have further implications for the application of task analytic techniques: automated adaptive training, automated demonstrations, automated coaching, automated controllers, automated cuing, automated performance measurement, and programmed mission scenarios.

Finally, task analytic processes emerge from a system; in a similar manner, the instructor operator console should be designed using the ISD approach. Automation in pilot training will continue in the future; therefore, the efficiency and low-cost aspects of the task analytic process will justify its continued application in the pilot training efforts.

V. Recommendations

The application of task analytic techniques to the design of an instructor/operator console should continue to be an effective development effort since computer-based, multimedia, and individualized instructional systems have proved to be beneficial in military training. Continuation of this process will yield current results of substantial savings in training time and more efficient utilization of resources.

The present capability of the instructor/operator console is adequate; yet, on the other hand, additional refinement could increase capability and cost effectiveness. The progressive development of the product is related to the ISD approach. According to Baker and Schutz (1971), one always has the next generation product underway before the current generation is developed.

It is further recommended that another component be added to the CAI/CMI-related instructor/operator console. The designation for the process would be the CAI/CMI/LCI Instructor/Operator Console. LCI is the acronym for *Learner-Controlled Instruction*. LCI is a method in which each learner develops his own sequence of learning. The LCI approach will need a great deal of study before it can be fully implemented in flight training.

VI. References

- Armstrong, G., Denton, J. J. and Savage, T. R. Instructional Skills Handbook. Englewood Cliffs, New Jersey: Educational Technology Publications, 1978.
- Baker, R. L., and Schutz, R. E. Instructional Product Development. New York: Van Nostrand Reinhold Company, 1971.
- Briggs, L. J. (Editor) Instructional Design, Principles and Application. Englewood Cliffs, New Jersey: Educational Technology Publications, 1977.
- Brown, J. S., Burton, R., Dekleer, J., and Benhaim, N. "Intelligent" Computer Assisted Instruction (CAI) Applications. Lowry Air Force Base, Colo.: AFHRL-TR-76-67. Air Force Human Resources Laboratory, Technical Training Division, October 1976.
- CAE Electronics Ltd. Instructor-Simulator Interface Design. AFHRL-TR-80-48(I). Williams Air Force Base, AZ: Air Force Human Resources Laboratory, Operations Training Division, April 1981.
- Caro, P. W., Pohlmann, L. D., and Isley, R. N. Development of Simulator Instructional Feature Design Guides (U). Seville-TR-79-12. Pensacola, Fl.: Seville Research Corporation, October 1979.
- Chauhan, S. S. Innovations in Teaching-Learning Process. New Delhi, India: VIKAS Publishing PVT LTD, 1979.
- Davis, R. H., Alexander, L. T. and Yelon, S. L. Learning System Design, An Approach to the Improvement of Instruction. New York: McGraw-Hill, 1974.
- DeVries, P. B., Jr., Eschenbrenner, A. J., and Ruck, H. W. Task Analysis Handbook. AFHRL-TR-79-45 (11). Brooks Air Force Base, TX: Air Force Human Resources Laboratory, Manpower and Personnel Division, July 1980.

Elworth, C. Instructor/Operator Display Evaluation Methods. AFHRL-TR-79-41. Williams Air Force Base, AZ: Air Force Human Resources Laboratory, Operations Training Division, March 1981.

Eschenbrenner, A. J., Jr., Devries, P. B. Jr., Miller, J. T., and Ruck, R. W. Methods for Collecting and Analyzing Task Analysis Data. AFHRL-TR-79-45 (1). Brooks Air Force Base, TX: Air Force Human Resources Laboratory, Manpower and Personnel Division, July 1980.

Faconti, V., Mortimer, C. P. L., and Simpson, D. W. Automated Instruction and Performance Monitoring in Flight Simulator Training. AFHRL-TR-69-29. Wright-Patterson Air Force Base, Ohio: Air Force Human Resources Laboratory, Training Research Division, February 1970.

Faconti, V. and Epps, R. Advanced Simulation in Undergraduate Pilot Training: Automatic Instructional System. AFHRL-TR-75-59 (V). Williams Air Force Base, AZ: Air Force Human Resources Laboratory, Flying Training Division, October 1975.

Gray, H., Chun, E. K., Warner, H. D., and Eubanks, J. L. Advanced Flight Simulator: Utilization in A-10 Conversion and Air-to-Surface Attack Training. AFHRL-TR-80-20. Williams Air Force Base, AZ: Air Force Human Resources Laboratory, Operations Training Division, January 1980.

Gray, I. H., and Fuller, R. R. Effects of Simulator Training and Platform Motion on Air-to-Surface Weapons Delivery Training. AFHRL-TR-77-29. Williams Air Force Base, AZ: Air Force Human Resources Laboratory, Flying Training Division, July 1977.

Haddan, E. E. Evolving Instruction. New York: Macmillan, 1970.

Lintz, L. M., Tate, T., Pflasterer, D. C., Nix, C. J., Klem, T. G., and Click, L. E. Low-Cost Computer-Aided Instruction/Computer-Managed Instruction (CAI/CMI) System: Feasibility Study. AFHRL-TR-79-42. Brooks Air Force Base, TX: Air Force Human Resources Laboratory, Technical Training Division, December 1979.

Mager, R. F. Preparing Instructional Objectives. Belmont, California: Fearon/Lear Siegler, 1962.

McCombs, B. L., Marco, R. A., Sprouts, M. W., and Eschenbrenner, A. J. Media Adjunct Programming, An Individualized Media-Managed Approach to Academic Pilot Training. AFHRL-TR-73-71(11). Williams Air Force Base, AZ: Air Force Human Resources Laboratory, Flying Training Division, January, 1974.

Miller, R. M., Swink, J. R., and McKenzie, J. F., Jr., Instructional Systems Development (ISD) in Air Force Flying Training. AFHRL-TR-78-59. Williams Air Force Base, AZ: Air Force Human Resources Laboratory, Flying Training Division, December, 1978.

Sample, A. S., Cotton, J. C., and Sullivan, D. J. Aircrew Training Devices: Instructional Support Features. Wright-Patterson Air Force Base, Ohio: Air Force Human Resources Laboratory, Logistics and Technical Training Division, January 1981.

Smith, J. F. and Flexman, R. E. An Instructional Manual for Using Performance Record Sheets Designed for Primary Pilot Training. AFHRL-TR-72-11. Williams Air Force Base, AZ: Flying Training Division, March 1972.

Stallings, L. M. Motor Skills, Development and Learning. Dubuque, Iowa: William C. Brown, 1973.

Steinkerchner, R. E. and Gerard, D. M. Computer Assisted Instruction in Air Force Medical Training: Preliminary Findings. AFHRL-TR-77-17. Lowry Air Force Base, Colo.: Air Force Human Resources Laboratory, Technical Training Division, May 1977.

Wood, M. E. and Gerlach, V. S. Transfer from Audiovisual Pretraining to a Continuous Perceptual Motor Task. AFHRL-TR-74-8. Williams Air Force Base, AZ: Air Force Human Resources Laboratory, Flying Training Division, March 1974.

Woodruff, R. R., Smith, J. F., and Morris, R. A. Use of the T-4G Simulator in USAF Undergraduate Pilot Training (UPT), Phase I. AFHRL-TR-74-61. Williams Air Force Base, AZ: Air Force Human Resources Laboratory, Flying Training Division, July 1974.

Woodruff, R. R., Smith, J. F., Fuller, J. R., and Weyer, D. C. Full Mission Simulation in Undergraduate Pilot Training: An Exploratory Study. AFHRL-TR-76-84. Williams Air Force Base, AZ: Air Force Human Resources Laboratory, Flying Training Division, December 1976.

VII. Appendices

Appendix A

Appendix B

Appendix A

Task Analysis

Procedures

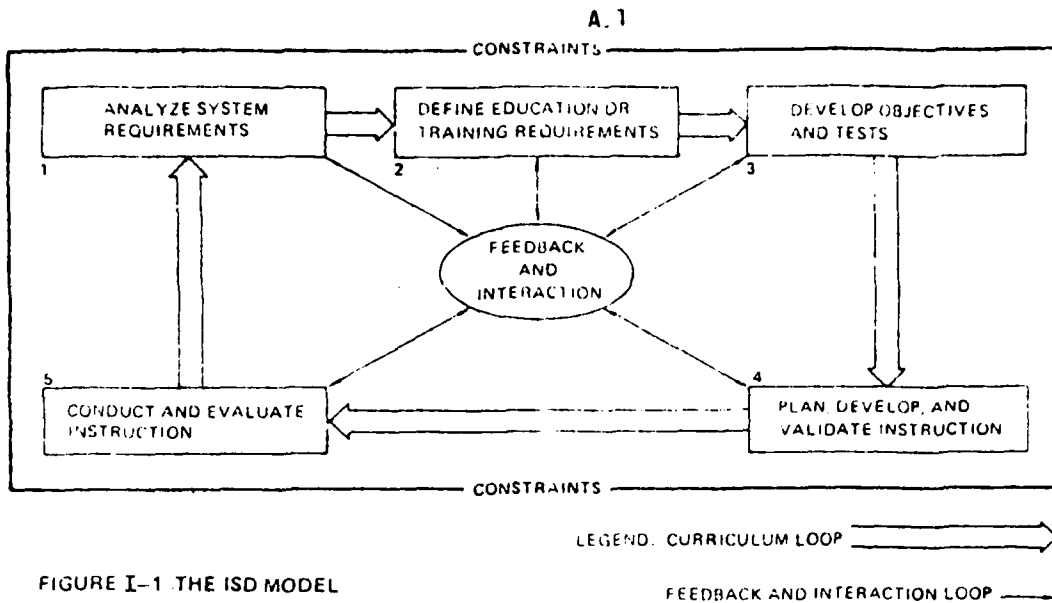


FIGURE I-1 THE ISD MODEL

DeVries, et. al. (1980) P.8.

A.2

HIERARCHY OF PERFORMANCES, TITLES, AND DEFINITIONS

• Job	The duties and tasks performed by the person who fills a position.
• Duty	One of the large segments of closely related tasks performed during a person's job.
• Task	Part of a duty; an action performed for its own sake, a specific action, with verb and object, resulting in a meaningful product or service; an observable and time-rateable action independent of other actions under the duty.
• Subtask	A major step in performing the task; dependent on other subtasks.
• Supporting Skills	Manipulative skills or mental skills which allow consummation of a given action; very small, interdependent activities.
• Supporting Knowledges	Mental conditions or capabilities which enable a person to act intelligently and purposefully.

DeVries, et. al. (1980), P. 12.

STS/CTS PROFICIENCY LEVELS

PROFICIENCY CODE KEY		
	SCALE VALUE	DEFINITION: The Individual
TASK PERFORMANCE LEVELS	1	Can do simple parts of the task. Needs to be told or shown how to do most of the task. (EXTREMELY LIMITED)
	2	Can do most parts of the task. Needs help only on hardest parts. May not meet local demands for speed or accuracy. (PARTIALLY PROFICIENT)
	3	Can do all parts of the task. Needs only a spot check of completed work. Meets minimum local demands for speed and accuracy. (COMPETENT)
	4	Can do the complete task quickly and accurately. Can tell or show others how to do the task. (HIGHLY PROFICIENT)
TASK KNOWLEDGE LEVELS	a	Can name parts, tools, and simple facts about the task. (NOMINCLATURE)
	b	Can determine step by step procedures for doing the task. (PROCEDURES)
	c	Can explain why and when the task must be done and why each step is needed. (OPERATING PRINCIPLES)
	d	Can predict, identify, and resolve problems about the task. (COMPLETE THEORY)
SUBJECT KNOWLEDGE LEVELS	A	Can identify basic facts and terms about the subject. (FACTS)
	B	Can explain relationship of basic facts and state general principles about the subject. (PRINCIPLES)
	C	Can explain facts and principles and draw conclusions about the subject. (ANALYSIS)
	D	Can evaluate conditions and make problem decisions about the subject. (EVALUATION)
EXPLANATIONS		
<p>* A task knowledge scale value may be used alone or with a task performance scale value to define a level of knowledge for a specific task. (Examples: b and 1b)</p> <p>** A subject knowledge scale value is used alone to define a level of knowledge for a subject not directly related to any specific task, or for a subject common to several tasks.</p> <p>† This mark is used alone instead of a scale value to show that no proficiency training is provided in the course, or that no proficiency is required of this skill level.</p> <p>> This mark is used alone in course columns to show that training is not given due to limitations in resources.</p>		

DeVries, et. al., (1980) P.24.

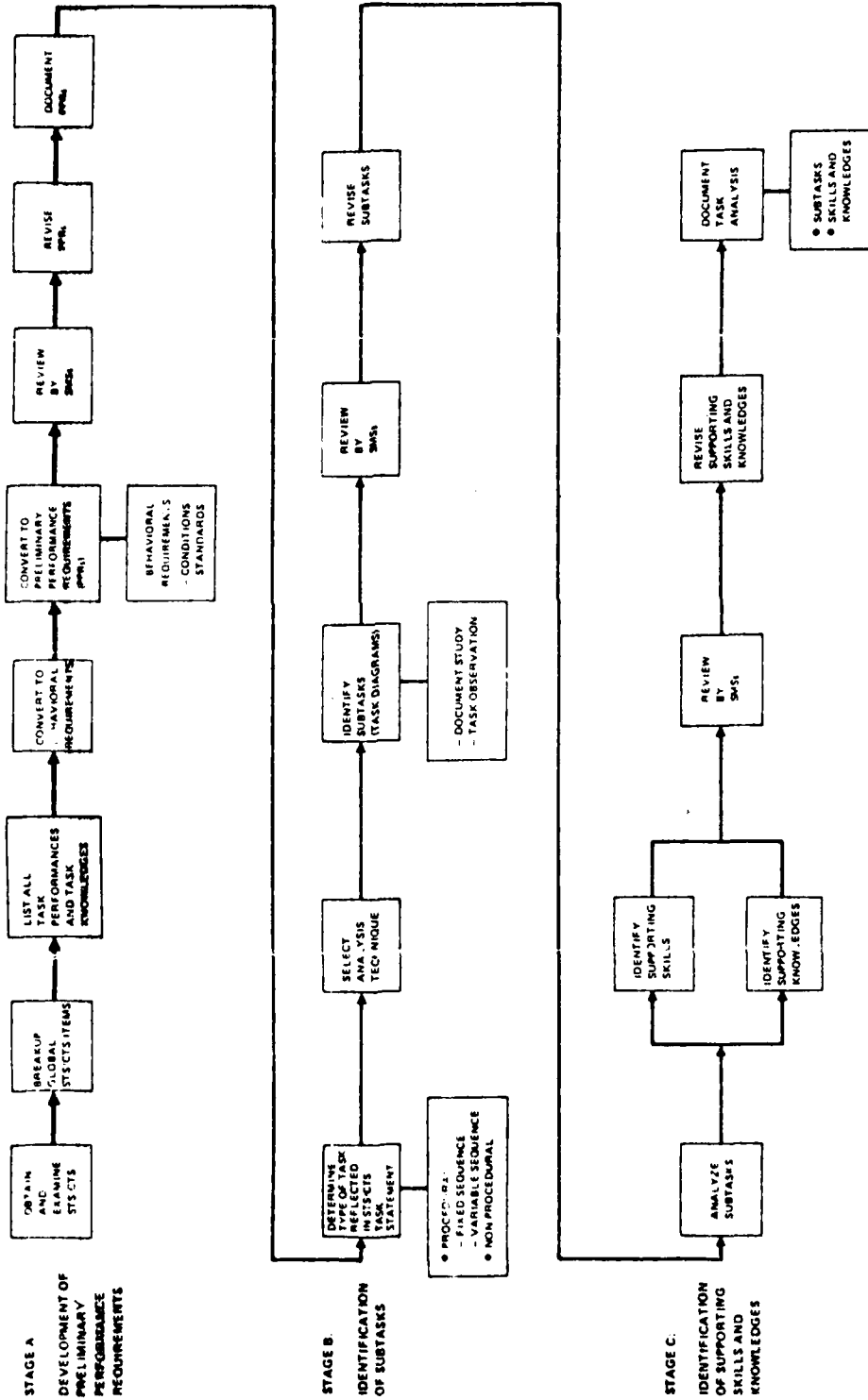


FIGURE I-3 TASK ANALYSIS PROCESS

A.5

Analyst _____ Course No. _____ STS/CTS No. _____

Dated _____ Page _____ of _____

STS/CTS REF.	PROF CODE	STS/CTS TASK STATEMENT	BEHAVIORAL REQUIREMENT

BEHAVIORAL STATEMENT LIST FORM

DeVries, et. al., 1980
Figure A-1, P. 27.

EXAMPLES OF ACTION VERBS FOR TASK PERFORMANCE ITEMS

Adjust	Manipulate
Administer	Mark
Assemble	Measure
Calibrate	Operate
Check	Place
Collate	Position
Complete	Prepare
Disassemble	Print
Display	Probe
Execute	Process
Fillout	Record
Guide	Remove
Handle	Repair
Initiate	Replace
Inspect	Troubleshoot
Interlock	Use
Interview	Weigh
Load	

DeVries, et. al. (1980)

Table A-3, P. 29.

EXAMPLES OF ACTION VERBS FOR EACH TYPE OF KNOWLEDGE ITEM

INFORMATION	MENTAL SKILL
Define	Analyze
Describe	Apply (a rule)
Enumerate	Calculate
Explain	Classify
Express	Compare
Identify	Compute
Label	Contrast
List	Demonstrate
Name	Derive
Recall	Discriminate
Recite	Evaluate
Recount	Forecast
Relate	Generate (a solution)
Repeat	Predict
Select	Prove
Show	Solve
State	
Tell	
Write	

DeVries, et. al (1980)
Table A-4, P. 31.

TYPES OF CONDITIONS FOR PPRs

9-1837

SIMULATED OR REAL LIFE SITUATIONS	If you remember that PPRs specify what the student will do during instruction in a training situation, then you will realize that the real-life performance is not always possible in the course. For example, there are numerous trainers and simulators designed to simulate an aircraft or other system; however, they usually simulate real life performance. In addition, some tasks which are decision making in nature can be simulated. For example, if the task is to isolate a malfunction in an electrical system, in some cases the student can be given some malfunction results and be required to use diagrams and schematics to isolate the malfunction. In this example, your objective should make clear that the student is working with diagrams and schematics instead of actual equipment.
EQUIPMENT	Another important condition that applies to many PPRs is equipment such as special tools or devices the student must use when he performs the objectives. If it is commonly understood that certain tools will be used, then it is not necessary to specify them. However, it is not wrong if you do so. In many cases, special tools or equipment are required and should be specified as a condition. Example: "Given GRBT testing meter . . ." "Given toolkit 12-1 . . ."
PROCEDURAL AIDS	There are many tasks which require the student to follow procedural aids. Two examples of such aids are checklists and TOs. Many of the tasks in your course might require the appropriate TO as one of the conditions. Hence, an objective might read, "Using TO . . ." or "Given TO . . ."
REFERENCES	There are some tasks or knowledge-demonstrating activities that are not accomplished from memory -- the students, like the man on the job, must use a reference. So if the task or activity requires direction from a manual or other publication (other than TO which is considered a procedural aid) then your objectives must include it as a reference. Example: ". . . using AFM XX XX . . ."
SUPERVISION	During the student performance of the objectives, it is understood that an instructor will be present to evaluate. In this sense, supervision is always present. But for some tasks, it might be desirable to allow the instructor to provide limited assistance or correction. This is compatible with what actually happens on the job, since a supervisor must see that a task is performed correctly. And in order to assure a good finished production, it is necessary for him to make corrections from time to time. Sometimes the same is acceptable in a training situation, especially with the higher proficiency levels. For example, if the student makes certain mistakes he might endanger himself, damage equipment, or cause an unnecessary delay (especially if other students are waiting to use the same equipment). In such situations, limited supervision can become a condition. This may be written as "Given limited instructor assistance . . ." ". . . with limited instructor supervision."
OTHER ENVIRONMENTAL CONDITIONS	Sometimes the student can be provided the actual equipment but must do something to it in an environment or situation different from that encountered on the job. For example, on the job a certain component is repaired in the aircraft, but in the training situation it must be repaired on a workbench. Another example would be to require the student to park a jeep on concrete, but in real life the jeep might be parked in snow, mud, ice, or on concrete. You should always specify any environmental conditions in the training situation.

TYPES OF STANDARDS FOR PPRS

DESCRIBE STANDARDS BY	EXAMPLES
Specifying Degree of Accuracy	-- Solve at least 18 of 21 problems correctly -- Match 25 of 28 items correctly -- Perform at least 14 of 16 steps correctly
Specifying Degree of Supervision	-- Instructor may not make more than 3 corrections -- The student may ask no more than 3 questions pertaining to procedures
Specifying Quality of Finished Product	-- Adjustment must produce a meter reading of "0" -- The engine must run smoothly at 4500 rpm -- All panels must light up when master switch is turned on
Specifying Content of Finished Product	-- Write a report to include at least three recommended solutions
Specifying Time Limits	-- Within five minutes
Referring to Standards Prescribed Elsewhere	-- In accordance with (IAW) Technical Order (TO)
Implying Standard of No Error	-- Student will perform without error

DeVries, et. al. (1980)
Table A-6, P. 35.

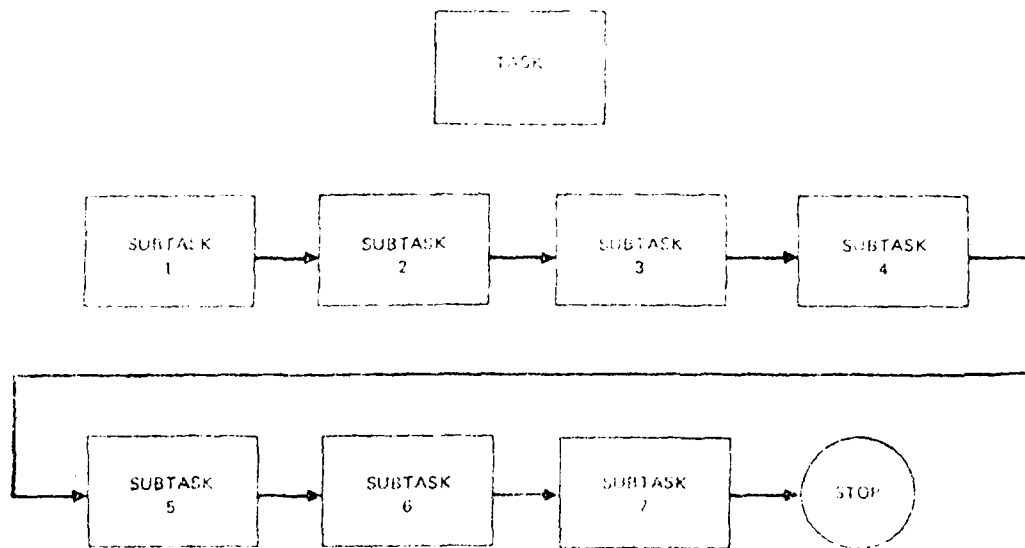
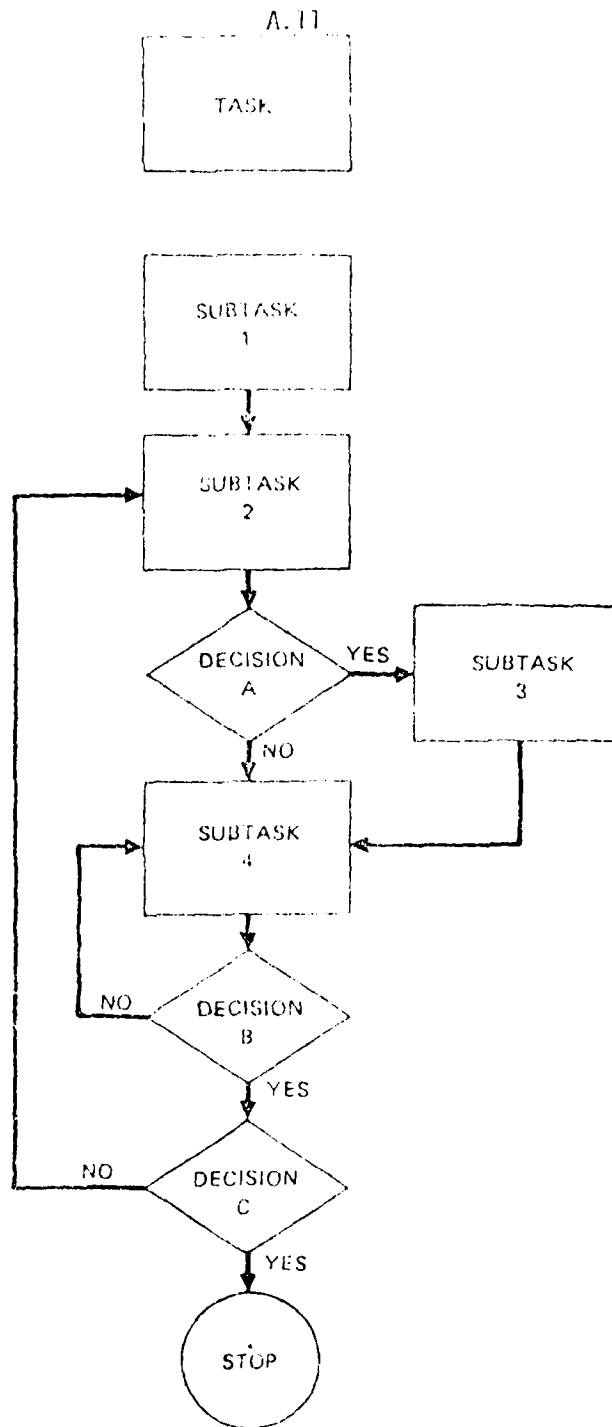


FIGURE B-1 SAMPLE TASK DIAGRAM (FIXED SEQUENCE PROCEDURAL TASK)

DeVries, et. al. (1980) P. 41.



SAMPLE TASK DIAGRAM (VARIABLE SEQUENCE PROCEDURAL TASK)

DeVries, et. al. 1980, P. 42.

Figure B-2

A.12

DOCUMENTS USED FOR DOCUMENT STUDY

NAME OF DOCUMENT	WHERE PROCURED	SYNOPSIS	USE
System Planning Data SOM, Feasibility Studies, PMD, and Test Plans	Obtain from contractor through System Program Office (SPO) Major Command	Provides information on equipment systems undergoing modification or development (aircraft) missiles detection and warning systems)	Provides information on Systems mission and performance characteristics Concepts, policies, and/or procedures for system activation, operation, maintenance, and support
Contractor Data blueprints, drawings, block diagrams, specifications and standards, reports and test, purchased through SPO (AFR 80-14)	Obtain from contractor through SPO Major Command	Describes in functional terms the subsystems, equipment, or components required to achieve system objectives	<p>Management responsibilities</p> <p>Provides Performance and design requirements equipment personnel functions Support equipment, operation, and maintenance Subsystems equipment and personnel Personnel performance requirements Personnel training, training equipment, and technical data requirement</p>

APPROPRIATE AND INAPPROPRIATE LEVELS OF DETAIL FOR SPECIFYING SUBTASKS

FAR TOO DETAILED	TOO DETAILED	ADEQUATE DETAIL	POSSIBLY TOO LITTLE DETAIL
Turn left and face tool kit	Open tool kit.	Use small screwdriver to adjust potentiometer P-3 from underside of chassis	Adjust P-3 until VTVM reads 20-22 VDC.
Grasp tool kit by lifting catch.	Pick out small screwdriver.		
Open tool kit by swinging lid up.	Grasp by handle with right hand	Turn P-3 slowly to the right until VTVM reads 20-22 VDC.	
Remove small parts tray.	Hold chassis with left hand so that underside faces you.		
Find small screwdriver at left rear of tool kit.	Insert screwdriver in hole for potentiometer P-3 (next to transformer).		
Grasp screwdriver by handle with right hand.	Turn P-3 1/3 turn to right.		
Remove screwdriver from tool kit.	Observe that VTVM reading is between 20-22 VDC.		
Turn right and face work bench.	Readjust P-3 (no more than 1/3 turn in either direction) until VTVM reads 20-22 VDC.		
	Remove screwdriver from P-3.		
	Lower chassis		
	Return small screwdriver to tool kit		

DeVries, et. al. (1980)
Table B-2, P. 49.

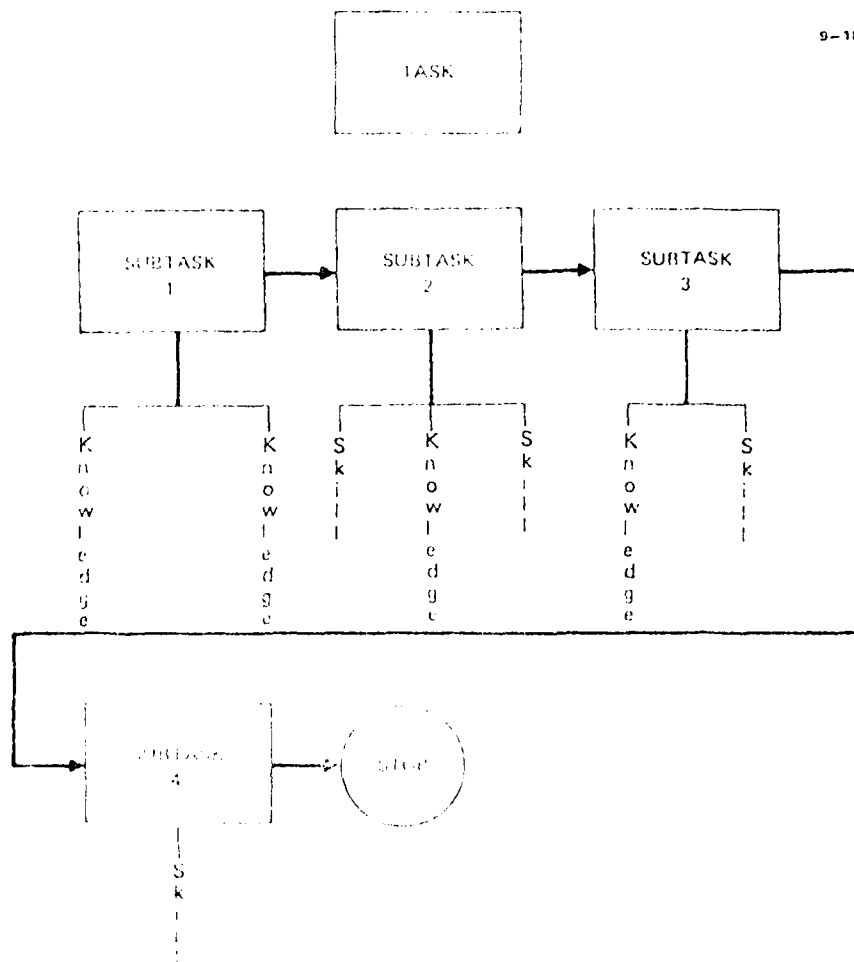
SAMPLE TASK OBSERVATION RESULTS

DUTY: Adjust Laboratory Equipment

TASK: Perform pre-operational check on the MV-1 Generator

STEPS PERFORMED	HOW PERFORMED
1. Turn master switch to "Standby" position 2. Adjust voltage to 150 VDC. 3. Turn masters switch to "Manual" or "Automatic" position. 4. Turn "Ready" switch to ready position 5. Turn "Operate" switch to "On" position.	1. Depress "Standby" button 2. Turn "Line Adjust" knob clockwise. 3. Decision: Turn to "Manual" position when the ammeter indicates a fluctuation in line voltage. 4. Depress "Ready" switch. 5. Throw knife switch to "On."

DeVries, et. al. (1980)
 Table 3, P. 52.



SAMPLE COMPLETE TASK DIAGRAM (FIXED SEQUENCE PROCEDURAL TASK)

DeVries, et. al. (1980
Figure C-1, P. 55

TYPES OF PHYSICAL SKILLS

PHYSICAL PROFICIENCY	EXAMPLE
<p>Strength</p> <p>Explosive - exerting maximum energy in one instantaneous act.</p> <p>Dynamic - moving or supporting the weight of the body.</p> <p>Static - continuously exerting a maximum force for a brief period of time.</p>	<p>Broad jumping</p> <p>Rope climbing</p> <p>Lifting weights</p>
<p>Flexibility</p> <p>Dynamic - making repeated, rapid, flexing movements in which muscles must recover from the strain quickly.</p>	<p>Deep-knee bends</p>
<p>Speed</p> <p>Changing directions.</p> <p>Running</p> <p>Limb movement - moving arms or legs as rapidly as possible.</p>	<p>Dodging runs</p> <p>Short and medium dashes</p> <p>Rapidly inflating a tire with a hand pump</p>
<p>Balance</p> <p>Static - maintaining bodily equilibrium in some fixed position.</p> <p>Dynamic - maintaining balance while performing a task</p> <p>Balancing objects</p>	<p>Standing on one foot</p> <p>Rail walking</p> <p>Loading equipment in overhead racks</p>
<p>Coordination</p> <p>Multi-Limb - Coordinating the simultaneous movement of two hands two feet, or hands and feet in operating various devices.</p> <p>Gross body - controlling gross activity of the whole body.</p>	<p>Driving a car</p> <p>Jumping rope</p>
<p>Endurance</p> <p>Maintaining maximum effort over long periods of time.</p>	<p>Doing as many pullups as possible</p>

DeVries, et. al. (1980)

Table C-1, P. 57.

TYPES OF MANIPULATIVE SKILLS

MANIPULATIVE PROFICIENCY	EXAMPLE
Control precision - making fine, highly controlled muscular adjustment	Turning the jets of a carburetor
Multi-limb coordination - coordinating the movements of a number of limbs simultaneously	Controlling rudder and manipulating throttle
Response orientation - making the correct movement in relation to the correct input, especially under high-speed conditions.	Emergency braking (as opposed to incorrectly depressing the clutch)
Reaction time - speed with which an individual is able to respond to an input when it appears.	Applying brakes at stop signal soon enough to stop
Rate control - making continuous, anticipatory motor adjustments relative to changes in speed and in direction of a continuously moving object	Tracking a target on a display
Manual dexterity - making skillful, well-directed arm-hand movements	Planning a board or otherwise working with hand tools
Finger dexterity - making skillful, controlled manipulations of tiny objects, primarily using the fingers.	Repairing a watch
Arm-hand steadiness - making precise arm-hand positioning movements when strength and speed are minimized.	Assembling a printed circuit board

DeVries, et. al. (1980)
Table C-2, P. 58.

TYPES OF SUPPORTING KNOWLEDGES

Primarily Factual Knowledges

- Terms, jargon, codes
- Names and location of objects, aids, and inputs
- Procedures for emergency situations
- Identification or recognition of objects or signals
- Interpretation of symbols, signals, or instructions
- Functional or organizational relationships
- Precautions

Knowledges Prerequisite to Skilled Performance

- Procedures for sets of activities
- Procedures for calculations
- Procedures for use of tools or test instruments

Complex Knowledges - Often Related to Complex Decisions

- Problem solution, diagnosis, or procedures for troubleshooting
- Anticipation of later conditions from earlier conditions
- Planning
- Strategies or tactics
- Inventions or improvisations

"Theory" Knowledges

When possible, don't identify the need for "theory" as a knowledge.

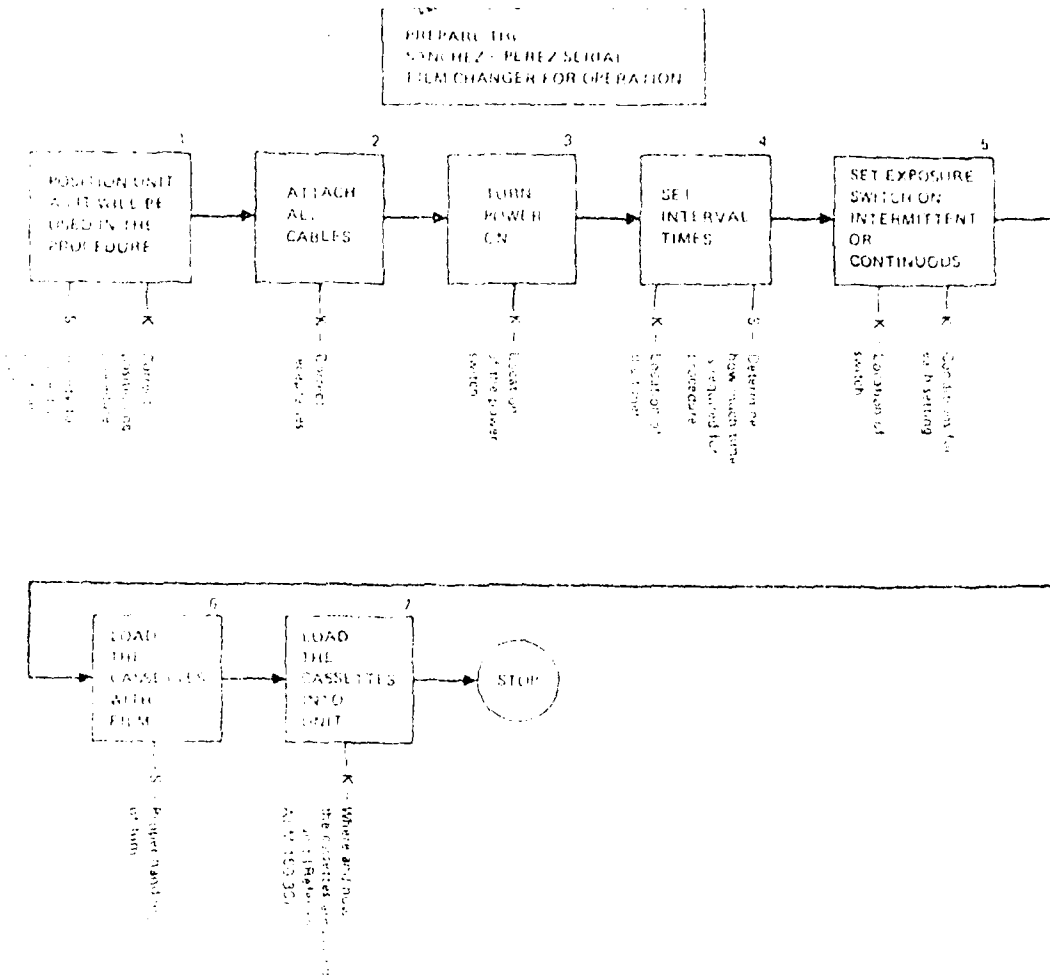
Instead, identify:

- Appropriate rules of thumb-principles which relate directly to the tasks
- Specific inputs which require the knowledge
- Proper action(s) indicated by the knowledge

DeVries, et. al. (1980)

Table C-3, P. 60.

A.19



TASK DIAGRAM (FIXED SEQUENCE, EQUIPMENT ORIENTED TASK)

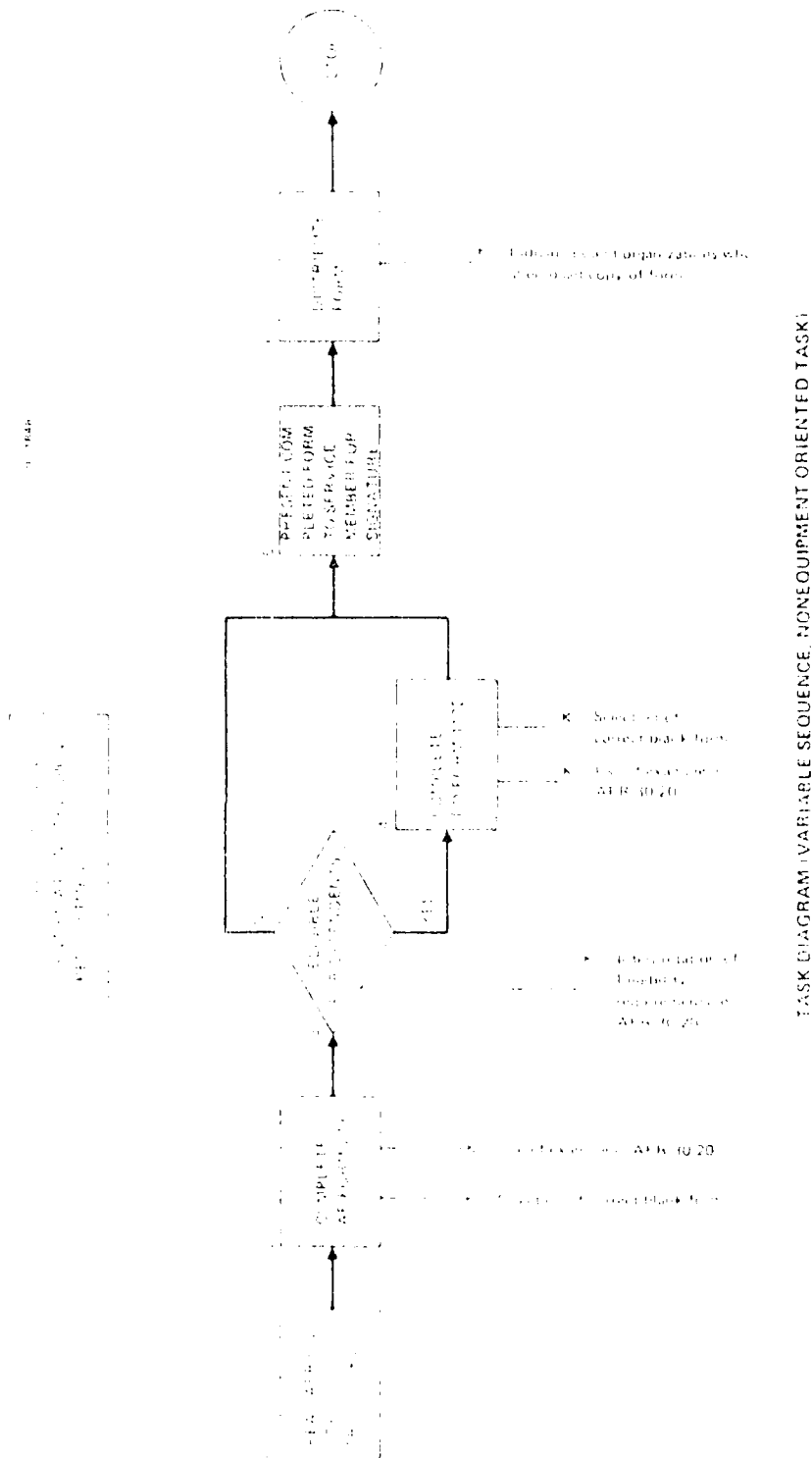
DeVries, et. al. (1980) P.62.

TASK ANALYSIS DOCUMENTATION FORM

STS/CTS TASK STATEMENT PREPARE THE SANCHEZ - PEREZ SERIAL FILM CHANGER FOR OPERATION CHANGER FOR OPERATION		Course No. 3ABR90330 STS/CTS No. 903XD Dated: Nov 1976 Duty: Special Radiographic Procedures Date: 15 Sept 1978 Page 1 of 1 Analyst: Brown STS/CTS REF: 15:(6) Prof Code: a		
BEHAVIOR PREPARE THE SANCHEZ PEREZ SERIAL FILM CHANGER FOR OPERATION CONDITIONS GIVEN THE NECESSARY EQUIPMENT STANDARDS IN ACCORDANCE WITH AIR FORCE MANUAL 160-30 REFERENCES AFM 160 30				
STEP NO	STEP (SUBTASK/DECISION QUESTION)	DECISIONS		GO TO STEP
		YES	NO	
1	Position the unit as it will be used in the procedure			2
2	Attach all cables			3
3	Turn power on			4
4	Set interval time			5
5	Set exposure switch on intermittent or continuous			6
6	Load the cassettes with film			7
7	Loading the cassettes into the unit			STOP
		SUPPORTING SKILLS AND KNOWLEDGES		
		K - Correct positioning procedures S - Ability to correctly position the unit K - Correct receptables K - Location of the power switch K - Location of the timer S - Determine how much time is needed K - Location of switch K - Conditions for each setting S - Proper handling of film K - Where and how the cassettes are placed in the unit (refer to AFM 160-30)		

COMPLETED TASK ANALYSIS DOCUMENTATION FORM
 (FIXED SEQUENCE, EQUIPMENT - ORIENTED TASK)

A.21



DeVries, et. al. (1980)
 Figure C-4, P. 65.

TASK ANALYSIS DOCUMENTATION FORM

<p>STS/CTS TASK STATEMENT: Process application for identification card upon reenlistment</p>		<p>Course No: 3ABR73230 Dated:</p>			
<p>BEHAVIOR: Process application for identification card upon reenlistment</p>		<p>STS/CTS No: 732X0</p>			
<p>CONDITIONS: Given AFR 30-20, Blank AF Form 279, and and DD Form 1172 and using a reenlistment situation</p>		<p>Duty: Quality Force</p>			
<p>STANDARDS: Will perform with 100% accuracy</p>		<p>Date: 02 July 1978 Page 1 of 1</p>			
<p>REFERENCES: AFR 30-20</p>		<p>Analyst: John Doe</p>			
		<p>STS/CTS REF: 8:(1) Prof Code 1b</p>			
STEP NO.	STEP (SUBTASK/DECISION QUESTIONS)	DECISIONS		GO TO STEP	SUPPORTING SKILLS AND KNOWLEDGES
		YES	NO		
1	Read AFR 30-20 for procedures			2	K - Selection of correct blank form
2	Complete AF Form 279			3	K - Use of examples in AFR 30-20
3.	Eligible for dependents?	4	5	5	K - Interpretation of AFR 30-20
4.	Complete DD Form 1172			5	S - Selection of correct blank form
5.	Present completed form to service member upon reenlistment for signature			6	K - Use of example in AFR 30-20
6.	Distribute Form			STOP	K - Use of example in AFR 30-20
<p>K - Individuals and organizations should get copy of form</p>					

COMPLETED TASK ANALYSIS DOCUMENTATION FORM
(VARIABLE SEQUENCE, NONEQUIPMENT-ORIENTED TASK)

DeVries, et. al. (1980)
Figure C-5. P. 66

DOCUMENTS USED FOR DOCUMENT STUDY (Continued)

Commercial Texts	Base library, section library, civilian library, local purchase through supply channels	Covers an array of subject matter in any detail necessary	Determines and provides Skills Knowledge Teaching points Performance Standards Conditions Duties Responsibilities
Air Force Regulatory Publications (Regs, Manuals, Pamphlets)	Normal Air Force publication channels	Gives policies, procedures and specific instructions on how duties and tasks are to be accomplished	Gives detailed listings of Duties Tasks Subtasks Performance standard
Procedural Publications (TOs, TMs)	Consult TO 00-5-2	Gives specific instructions on how duties and tasks are to be accomplished	Gives detailed listings of Duties Tasks Subtasks Performance standard Sequencing

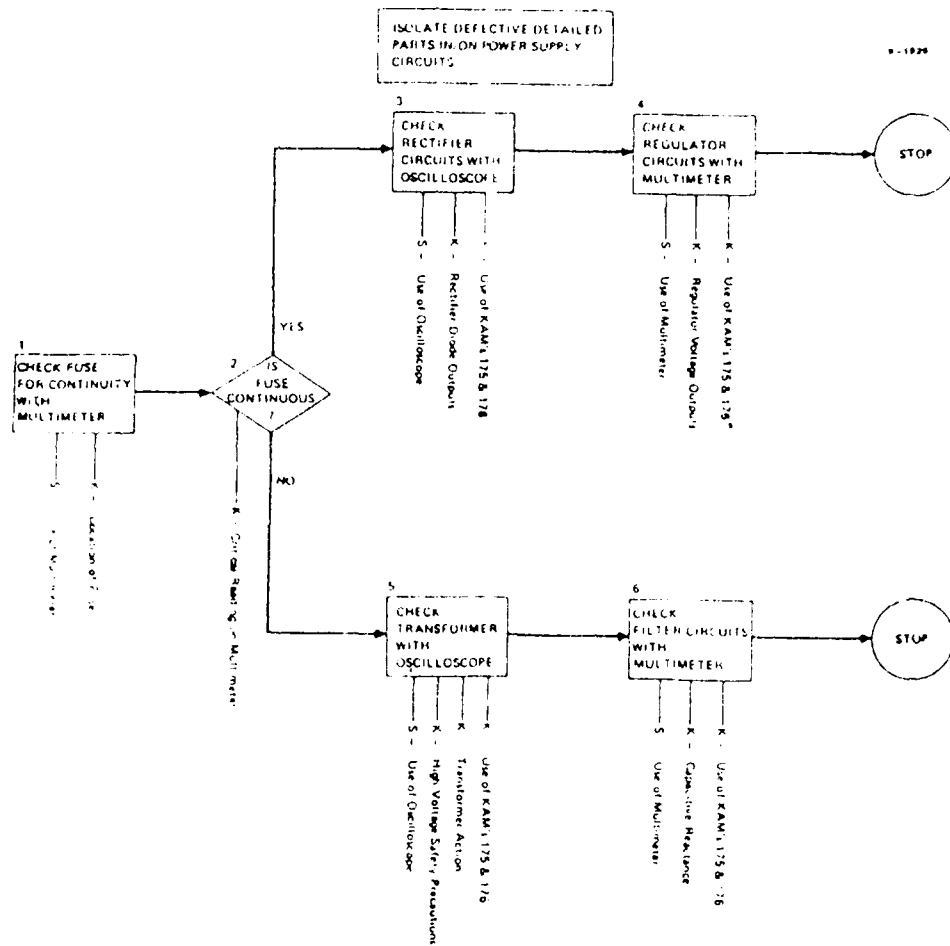
DeVries, et. al. (1980)
Table B-1, P. 48.

DOCUMENT USED FOR DOCUMENT STUDY (Continued)

Plan of Instruction	ATC Prime Technical Training Center	An ATC course control used for course development, implementation, and operation	Gives Specific objectives Training times by lesson STS/CTS correlation by objective Listing of instructional materials Audiovisual aids Training equipment Training methods Instructional guidance
Lesson Plan	ATC Prime Technical Center	A guide for teaching used by the instructor for effective attainment of objectives	Contains a list of Objectives Teaching steps Other pertinent information deemed necessary by instructors
Course Training Literature	Appropriate activity conducting training	Identifies actual skills and knowledge being taught to the student. The training literature is what the student is receiving in training	Provides Task Subtasks Activities Performance standards
Career Development Course (CDC)	ECI Gunter AFS, AL	Provides a complete training program for all knowledges required for a given AFC	Provides Skills Knowledges Teaching points Standards
Officer Classification Manual (AFR 36-1) and Airman Classification Manual (AFR 39-1)	Air Force publications channel	Defines the total job content	Provides Duties Responsibilities Qualifications

DOCUMENTS USED FOR DOCUMENT STUDY (Continued)

Occupational Survey Reports (OSR)	ATC/OMY Randolph AFB, TX	Provides a detailed listing of what man's role is in the mission	Gives listing of Duties Tasks Subtasks Task Data Number of performing Percent performing Training Emphasis Learning difficulty Time spent
Air Training Command (ATC) Course Control Documents	ATC Prime Technical Training Center	The following listed documents are used by USAF ATC. Other government agencies probably have similar documents	These documents are consulted when systems are being revised or lateral courses are being developed
Course Chart (C C)	ATC Prime Technical Training Center	An ATC Qualitative course control document	Gives Course identity Length Security classification Major items training equipment Summary of subject matter taught by blocks and units of instruction



TASK DIAGRAM (VARIABLE SEQUENCE, EQUIPMENT ORIENTED TASK)

DeVries, et. al. (1980)
 Figure C-6, P 67.

Appendix B

Instructor/Operator

Consoles

B.1

A-10 IO Instructional and Operational Task Capability Outline

The IOS design incorporates the capability to conduct all facets of A-10 flight training. The instructional and operational tasks which the IOS can support are categorized as follows:

- A. Simulator Operations
 - 1. Application of power to the simulator
 - 2. Control loading system control
 - 3. System initialization
 - 4. Communications
 - 5. System shutdown and emergency stop
- B. Monitoring, Evaluating, and Controlling Student Performance
 - 1. Conversion training
 - a. ground cockpit checks
 - b. takeoff, climb and level-off
 - c. normal and closed patterns
 - d. normal flight maneuvers
 - e. abnormal flights and spins
 - f. basic airwork and aerobatics
 - g. radio and instrument navigation
 - h. formation flight
 - i. visual and ground controlled approaches and landings
 - 2. Surface attack training
 - a. weapons loading
 - b. target approach-dive angle and ground path
 - c. bomb delivery
 - d. strafe
- C. Utilization of IOS Training Features
 - 1. Conventional training features
 - a. malfunction insertion
 - b. flight controls monitoring--stick and throttle position

- c. hardcopy
- d. automated student performance scoring
- e. crash override and reset
- f. aircraft environmental control
- 2. Specialized training features
 - a. video and voice recording and playback
 - b. initial condition reset
 - c. position freeze and reset
 - d. manual aircraft configuration and position setup
 - e. repeater heads-up display (HUD)
- D. IOS Configuration and Environment Control
 - 1. CRT page assignment
 - 2. IOS speaker and aircraft sound control
 - 3. IOS lighting control
 - 4. CCTV control
 - 5. Visual scene select

Gray, et. al. (1981) PP. 36-38.

INSTRUCTIONAL SUPPORT FEATURE INVENTORY

1. Event Definition and Control

- a. Pre-session audio-visual demonstrations
- b. Simulator initialization procedures
- c. Automated demonstration(s)
- d. Pre-programmed (canned) mission events
- e. On-line programmable mission events
- f. On-line capability for establishing event initial conditions
- g. Auto malfunction/emergency insertion-removal; and capability to add additional malfunctions/emergencies
- h. Manual malfunction/emergency insertion-removal; and capability to add additional malfunctions/emergencies
- i. Dedicated controls (functional groupings)
- j. Keyboards
- k. Joy sticks and related controls
- l. CRT data entry/selection formats (touch panel, other)
- m. Threat control
- n. Environment control (rough air, etc.)
- o. Task difficulty control
- p. Freeze
- q. Reset
- r. Record and replay

2. Event Monitoring

- a. Repeater instruments (functional groupings)
- b. Electronic pictorial/analog display(s)
- c. Other performance and event monitoring displays
- d. Mechanical plotter
- e. Closed circuit TV, and record/playback capabilities
- f. Other video monitoring capabilities, and record/playback capabilities
- g. Hard copy output

3. Instructor/Operator - Student Communication
 - a. Usual methods of communicating with student work station
 - b. Cockpit-mounted alphanumeric displays
 - c. Cockpit-mounted responder controls
 - d. Computer generated voice
 - e. Automated speech understanding
 - f. Simulator-mounted audio-visual instructional devices
4. Automated Support
 - a. Automated performance measurement
 - b. On-line performance monitoring and alerting
 - c. Automated scoring
 - d. Automated learning problem diagnosis
 - e. Automated coaching
 - f. Automated cuing
 - g. Automated performance norm data files
 - h. Computer managed instruction

INSTRUCTIONAL SUPPORT FEATURE SURVEY ELEMENTS

1. Description
 - a. Manufacturer and date
 - b. Functional description
 - c. Modes of operation
 - d. Man-machine interface
 - e. Representative operating procedures
 - f. Difficulty of use
 - g. Factors affecting operability (ease/complexity and time)
 - h. Planned design changes
 - i. Desirable design changes
 - j. Local modifications made and date (hardware and software)
 - k. Contracted modifications and date
 - l. Reasons for modifications
 - m. Perceived benefits from modifications
 - n. Training evaluations of modifications
 - o. Surveyor's assessments

2. Training Applications

- a. Present training applications (tasks)
- b. Training content involved (tasks)
- c. Specific student learning and/or performance problems
- d. Instructional uses originally designed to support
- e. Reasons for additions/deletions to uses
- f. Training evaluations performed
- g. Planned changes to training that could affect applications
- h. Suggestions for other applications
- i. Surveyor's assessment

3. Utilization

- a. Job performance aids and user assists available
- b. Perceived values of the feature
- c. Perceived drawbacks of the feature
- d. Frequency of use
- e. Reliability
- f. Procedures and forms to report maintenance problems
- g. Factors influencing feature utilization
 - (1) Training requirements
 - (2) Perceived benefits
 - (3) Perceived drawbacks
 - (4) Design/implementation
 - (5) Schedule considerations
 - (6) Instructor training
 - (7) Attitudes toward simulation
 - (8) Other
- h. Characterize impacts of feature on ATD utilization
- i. Essentiality

Cite representative uses of the feature that fall into the following categories.

 - (1) Highly essential. The feature is required to accomplish simulator training
 - (2) Moderately essential. The feature aids in accomplishing simulator training, but it would be possible to get along without it.

- (3) Marginally essential. The feature is convenient for simulator training, but it would be easy to get along without it.
- (4) Totally non-essential.
- j. Surveyor's assessments

SURVEY ELEMENTS UNIQUE TO CERTAIN FEATURES

1. Record and Replay
 - a. Where is replay accomplished?
 - (1) in cockpit
 - (2) remote (location and content)
 - (3) availability of augmented feedback during replay (e.g., scoring and diagnostics)
 - b. How much of the mission can be replayed?
2. Freeze
 - a. Can freeze be operated during replay?
3. Video Display
 - a. Description (field of view, size, resolution, color, number)
 - b. Record/replay capabilities
4. Automated Demonstrations
 - a. Capabilities and procedures for constructing/modifying canned scenarios
 - (1) On-line (who and how)
 - (2) Off-line (who and how)
 - b. Difficulties in developing and using canned scenarios
 - (1) Development
 - (2) Call-up and use
5. Automated Performance Measurement
 - a. Descriptive data
 - (1) Manufacturer and delivery date
 - (2) Add-on to simulator?
 - (3) Production or R&D feature/capability?
 - (4) Describe any in-house modifications
 - (5) Describe any on-going APM R&D
 - (6) Obtain system and R&D documentation
 - (7) Identify R&D point of contact (name, organization, telephone)

b. Characteristics

- (1) Parameters that can be measured (total set)
- (2) How are the parameters designated (procedures)
on-line
off-line
- (3) How are performance tolerances set?
on-line
off-line
- (4) How is measurement start and stop designated?
on-line
off-line
- (5) Are any mathematical transforms performed?
- (6) How and when are the measures displayed?
- (7) Utility of measures for quantifying proficiency (criteria used)
(use of measurement outputs when completing student grade forms?)
- (8) Diagnostic value of the measures
- (9) Utility of the measurements for training quality control
- (10) Desirable improvements
- (11) Other applications

6. Automated Scoring

- a. Describe/define the combining of measures into scores
- b. Describe/define scoring criteria used
- c. Describe intended uses of the scores
- d. Utility of performance scores for training quality control
- e. Use of scores when completing student grade forms

7. Automated Adaptive Training (AAT)

- a. Descriptive Data
 - (1) Manufacturer and delivery date
 - (2) Add-on
 - (3) Production of R&D feature/capability
 - (4) Describe any in-house modifications
 - (5) Describe any related R&D activities
 - (6) Obtain system and R&D documentation
 - (7) Identify R&D point of contact (name, organization, telephone)

b. Characteristics

- (1) Describe adaptive logic structure(s) used
- (2) Describe automated measurement/scoring used
- (3) Describe on-site modifications and reasons
- (4) Training impacts of modifications
- (5) Effects of AAT system on:
 - (a) Student progress through automated portions of syllabus
 - (b) Student proficiency
 - (c) Training quality control (portions of syllabus involved)
- (6) Effect of AAT on instructor involvement
- (7) Effect of AAT on operator involvement
- (8) Student acceptance of AAT
- (9) Instructor acceptance

8. Computer Managed Instruction

a. Descriptive Data

- (1) Name and acronym
- (2) Developer and installation date
- (3) Cognizant organization and symbol
- (4) Obtain documented description of the system
- (5) Training supported (academics, simulator, inflight)

b. Characteristics

- (1) Describe how it is used (general)
- (2) Input data sources
- (3) Simulator training objectives tracked
- (4) Inflight training objectives tracked
- (5) Utility in determining simulator session training content
- (6) Utility in determining flight training content
- (7) Utility in scheduling simulator sessions
- (8) Utility in scheduling training flights
- (9) Impacts on training quality control

INSTRUCTOR/OPERATOR STATION DESIGN

1. Present configuration

a. Device designation and type

- b. Linked mode operation
 - c. Location(s) relative to student workstation
 - d. Present opportunities for dynamic observation
 - e. Functions performed (at each location)
 - f. Instructors/operators assigned to each location
 - g. Instructor/operator interaction
 - h. Ease/difficulty of coordination
 - i. Perceived benefits of present configuration
 - j. Perceived drawbacks of present configuration
 - k. Suggested design modifications (and reasons)
2. General Perceptions and Suggestions:
- a. Types of training where direct observation is perceived as necessary
 - b. Types of training where direct observation is perceived as desirable
 - c. Student skill level impacts on instructor/operator station locations
 - d. Device type (CPT, OFT, WST, etc.) impacts on instructor/operator station locations
 - e. Perceived general benefits and drawbacks of in-cockpit location
 - f. Perceived general benefits and drawbacks of remote location
 - g. Advantages/disadvantages of designing student workstations to incorporate an instructor/operator station if it meant that the student's workstation environment might not appear exactly as in the aircraft
3. Background
- a. Interviewer's prior experience with remote and/or in-cockpit instructor stations.
 - (1) As a student (weapon system, device, dates)
 - (2) As an instructor (weapon system, device, dates)

DEVICE OPERATIONS

1. Surveyor's Assessments
- a. Instructor status/morale
 - b. Adequacy of instructor training
 - c. Problems noted
 - d. Desirable points noted
 - e. Implications for other programs

2. Typical Device Operator Characteristics
 - a. Rank
 - b. Years in service
 - c. Number of months at this assignment
 - d. Duration of this assignment in months
 - e. Prior device operator experience
 - f. Operator selection criteria/procedures
 - g. Continuity in operator staff
3. Device Operator Job Characteristics
 - a. Hours worked per week, training support activities
 - b. Hours worked per week, other activities
 - c. Device utilization activities description
 - d. Other activities description
4. Device Operator Training
 - a. Schools attended
 - b. Factory training for this job
 - c. Local program for operator training
 - (1) Topics covered
 - (2) Program description
 - (3) Program duration
 - (4) Role of formal instruction
 - (5) Role of on-the-job training
 - (6) OJT supervision
 - (7) Criteria for completing training
 - d. Perceived value of school training for this job
 - e. Perceived value of factory training for this job
 - f. Perceived value of local training for this job
 - g. Planned changes in operator training program
 - h. Suggested changes to operator training program
5. Surveyor's Assessments
 - a. Operator status/morale
 - b. Adequacy of operator training
 - c. Problems noted
 - d. Desirable points noted
 - e. Implication for other programs

1981 USAF - SCEEE SUMMER FACULTY RESEARCH PROGRAM

Sponsored by the

AIR FORCE OFFICE OF SCIENTIFIC RESEARCH

Conducted by the

SOUTHEASTERN CENTER FOR ELECTRICAL ENGINEERING EDUCATION

FINAL REPORT

STUDY OF DYNAMIC BEHAVIOR OF A BLUFF-BODY DIFFUSION FLAME IN THE APL
COMBUSTION TUNNEL FACILITY

Prepared by: Dr. Sarwan S. Sandhu
Academic Rank: Assistant professor
Department and University: Department of Chemical Engineering
University of Dayton
Research Location: Air Force Aero Propulsion Laboratory,
Wright-Patterson Air Force Base, Ohio
USAF Research Colleague: Dr. W. M. Roquemore
Date: July 20, 1981
Contract No: F49620-79-C-0038

STUDY OF DYNAMIC BEHAVIOR OF
A BLUFF-BODY DIFFUSION FLAME IN THE APL
COMBUSTION TUNNEL FACILITY

by

Sarwan S. Sandhu

ABSTRACT

An experimental study to gain insight into the dynamic behavior of the combustion process in the APL combustion tunnel facility has been initiated with the intent of utilization of information attained from such a study to develop a mathematical model for the prediction of combustion process in a combustor of the APL combustor type. From the preliminary data acquired dependence of fireball frequency and velocity on air/fuel flow rates, effect of axial location on the frequency, and, fireball and nonemitting region number distribution versus time length are presented. A qualitative global mechanism for relative increase or decrease in fireball frequency is proposed.

ACKNOWLEDGEMENTS

The author would like to thank the Air Force Office of Scientific Research and Southeastern Center for Electrical Engineering for providing him with the opportunity to spend a very worthwhile, interesting and idea stimulating summer at the Air Force Aero Propulsion Laboratory, Wright-Patterson Air Force Base, Ohio. He would particularly like to thank Dr. W. M. Roquemore for stimulating, new idea development discussions, colleague friendship and understanding. He would also like to acknowledge the technical assistance of Mr. Ronald Britton in acquisition of spectrophotometer data and analysis. His thanks are also due to Mr. Melvin Russel and Mr. Curtis Reeves for assistance in performing experiments and drawing plots respectively. Finally, the expert typing skill of Mrs. Mary Lu Kinzeler and Miss Charlyn Wehner is appreciated.

I. INTRODUCTION

The APL combustion tunnel facility consists of a cylindrical duct with a concentric centerbody that has a flat end face. Fuel is injected at the center of the centerbody face through an orifice, and air flows through the annular passage between the outer duct and the centerbody. The centerbody acts as a bluff-body to air flow. Air flow separation at the centerbody leads to vortex formation and shedding. Interaction between air vortices and fuel jet is likely to occur. Near the centerbody face fuel and annular air jets compete for entrainment of fluid leading to a complex pattern of mixing between fuel and air. Fuel and oxidant mixing could occur via molecular diffusion, small and large scale air turbulence interaction with fuel jet. With increasing distance from centerbody, fuel jet slows down because of mass entrainment from its surroundings. For a spatial region where fuel jet velocity becomes comparable to mean air flow velocity, an "air ball" could penetrate into fuel stream. Interaction between three dimensional air vortices and fuel stream could lead to the situation where an oxidant containing eddy could envelope or be enveloped by fuel. Such interaction and mixing phenomena lead to formation of moving "fireballs" of complex structure. Understanding of such moving fireball phenomenon was thought to be essential to search for a relationship between this phenomenon and overall combustion process. This motivated us to study the dynamic behavior of the bluff-body diffusion flame (C_3H_8 /air) in the APL combustion tunnel facility. Results of the experimental study were thought to give deeper insight into the combustion process occurring in the APL combustor. Experimental results related to dynamic behavior of a combustor of the APL tunnel combustor type are essential for the development and testing of appropriate mathematical models to predict combustion efficiency and pollutant emissions.

II. OBJECTIVES

Objectives of this short duration study were:

1. Initiation of an experimental program to understand the formation and disappearance of "moving fireballs" and determine their relationship, if any, with the bluff-body vortex shedding phenomenon in a bluff-body diffusion flame combustor of the APL tunnel combustor type.
2. To refine and gain experience with experimental techniques, for example, spectrophotometry to record local time varying flame emission data related to understanding of the above mentioned moving "fireball" phenomenon.

III. EXPERIMENTAL

APL COMBUSTION TUNNEL FACILITY

A sketch of the APL combustor is shown in Fig. 1. It is consisted of a cylindrical duct with a concentric centerbody having a flat end face. Fuel is injected into the combustor proper at the center of the centerbody through a 4.8mm diameter tube, and air is introduced through the annular passage between the outer duct and the centerbody. The diameter and length of the centerbody are 14 and 79cm respectively. The upstream surface of the centerbody is aerodynamically shaped to minimize disturbances in the annulus air flow. A 31.8 mm long square-cell honeycomb flow straightener with a cell size of 4.8 by 4.8 mm and two 16 mesh screens are mounted in the annulus. The inside diameter of the duct is 25.4cm. The duct has viewing ports that provide both optical and conventional probe access to important combustion regions. Additional facility details may be found in Ref. 1.

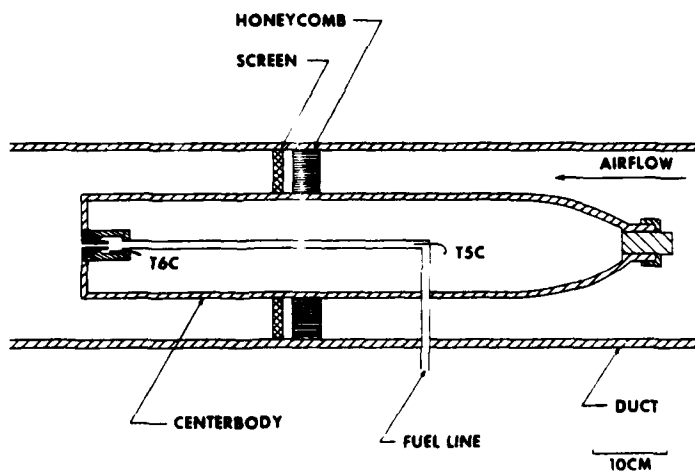


Fig. 1 Sketch of the RPL Combustor

TABLE. TEST FLOW RATE CONDITIONS

Flow Rate kg/s	Air			Fuel			Exhaust Temp. (K)	Flame Length (cm)	
	Duct Flow Velocity m/s	$Re \times 10^{-5}$	Annulus Velocity m/s	Flow Rate kg/hr	Injection Velocity m/s	Total		Blue	
0.5	8.4	1.4	12.1	4.0	35.4	150	410		
	8.4		12.0	8.0	74.0	180+	498	22	
	8.4		12.0	12.0	110.9	180+	598	33	
1.0	16.7	2.8	2.4	6	58.4	130	391		
			23.9	8	78.8		410	20	
			24.0	13	127.8		464	39	
1.5	25.0	4.1	35.9	10.0	103.4	150	397	30	
	25.0		35.8	13.1	136.4		417	38	
	25.0		35.9	16.0	160.2		438	46	
2.0	33.2	5.5	47.6	13.0	135.2	140	396	140	
	33.5		48.1	16.0	159.8	160	410	160	
	33.5		48.0	18.0	183.7	170	421	170	

Test conditions

Air and fuel flow rate combinations selected and other pertinent information are tabulated above.

Experimental techniques

High speed cine photography, spectrophotometers and pressure transducers were employed to study the dynamic behavior of the combustion system with regard to the determination of fireball-length, velocity and frequency and pressure fluctuations as function of combustor axial length, fuel and air flow rates. Spectrophotometers were tuned to CH^{*} emission ($\lambda=4315^{\circ}\text{A}$). Signals from the spectrophotometers and pressure transducers were recorded using high speed chart recorder and oscilloscope. A Fourier transform frequency analyzer, Nicolet 660A, was also employed for the determination of fireball frequency.

IV. RESULTS AND DISCUSSION

*Effect of flow rates on fireball frequency

Figs. 2 and 3 show the dependence of fireball frequency (determined by means of spectrophotometers tuned to CH^{*} emission) on air and fuel flow rates at two axial distances measured from the face of the centerbody. In general, at each location fireball frequency increases with increase in fuel flow rate for a fixed air flow rate. An overall general comment on the dependence of the frequency on air flow rate cannot be made. However, it appears that the frequency decreases with increase in air flow rate at axial location of 116cm except for air flow rate of 0.5kg/s. This can be explained in terms of higher mixing rates of fuel and air due to enhanced turbulence generated by higher air flow rates. Effect of air flow rate on bluff-body vortex shedding frequency, higher fuel consumption rate because of higher fuel/air mixing rate, and coalescence of fireballs may be responsible for this trend. Similar trend is observed for air flow rates of 1.5 and 2.0kg/s at axial location of 61cm.

*Effect of flow rates on fireball velocity

Figs. 4 and 5 show the dependency of fireball velocity on air and fuel flow rates at an axial location of 61cm from the centerbody face.

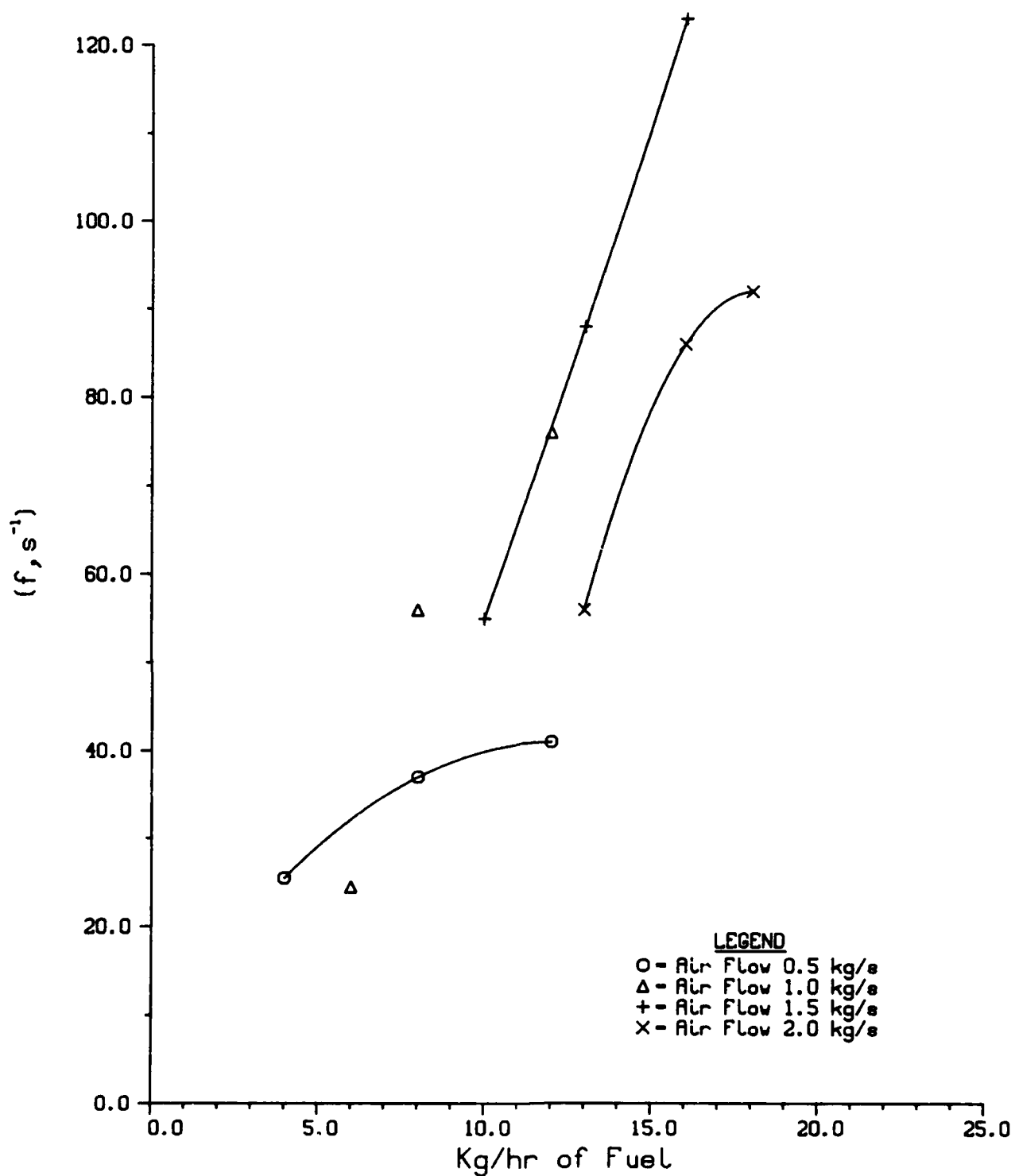


Fig. 2 Fireball Frequency (Oscilloscope Data) versus Fuel Flow Rate , Z = 61 cm

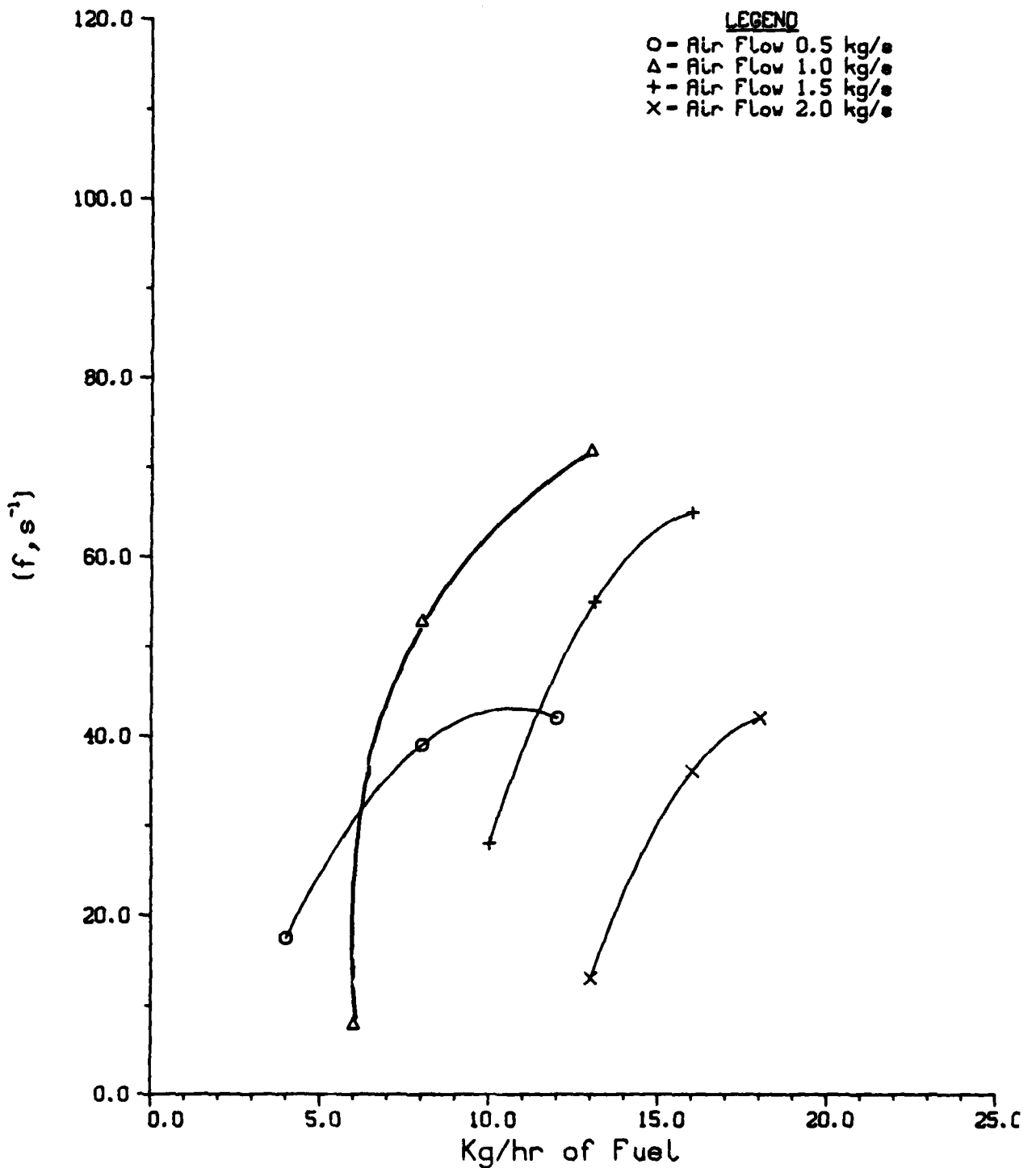


Fig. 3 Fireball Frequency (Oscilloscope Data) versus Fuel Flow Rate, Z = 116 cm

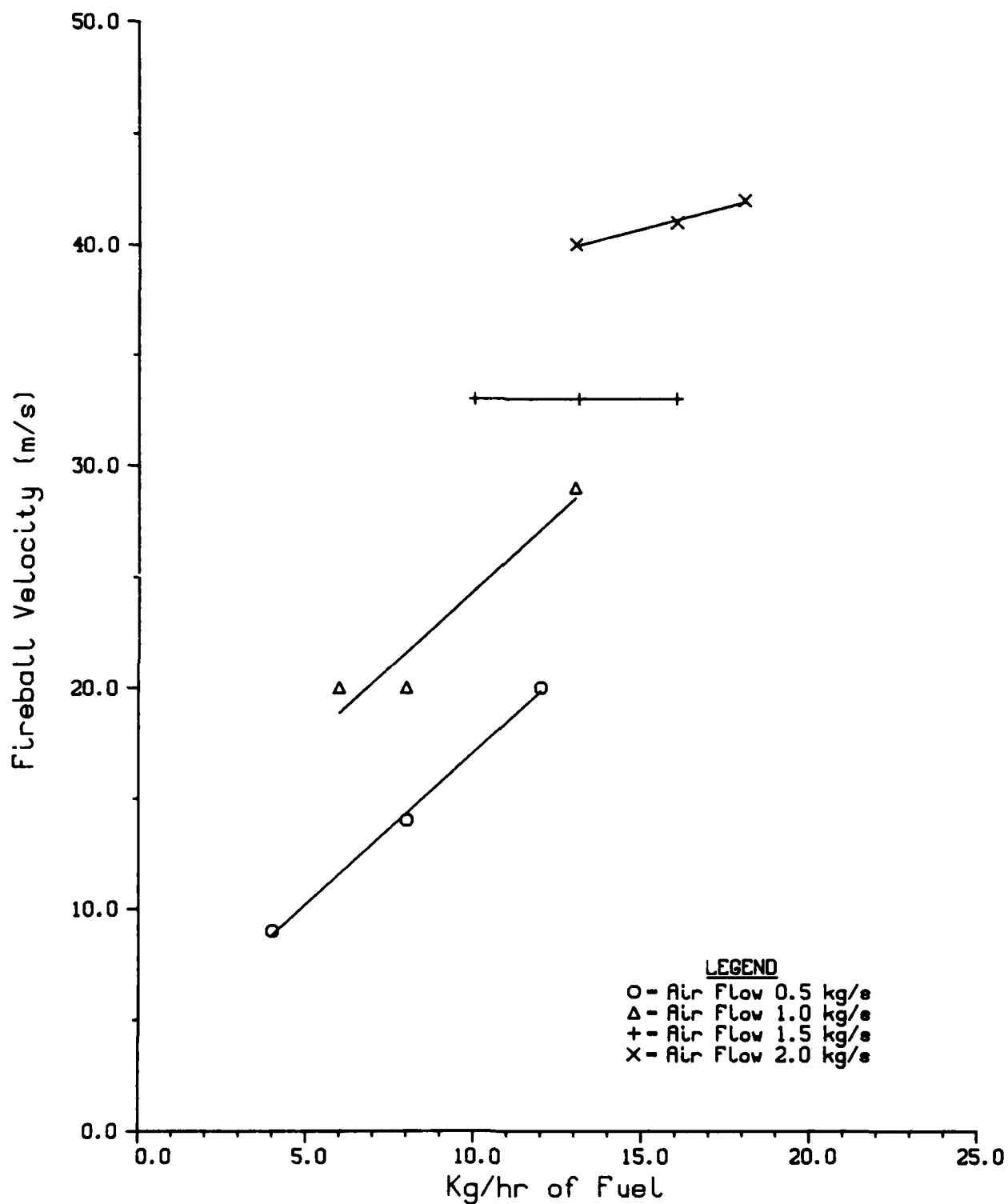


Fig. 4 Fireball Velocity (Film Data) versus Fuel Flow Rate, Z = 61 cm

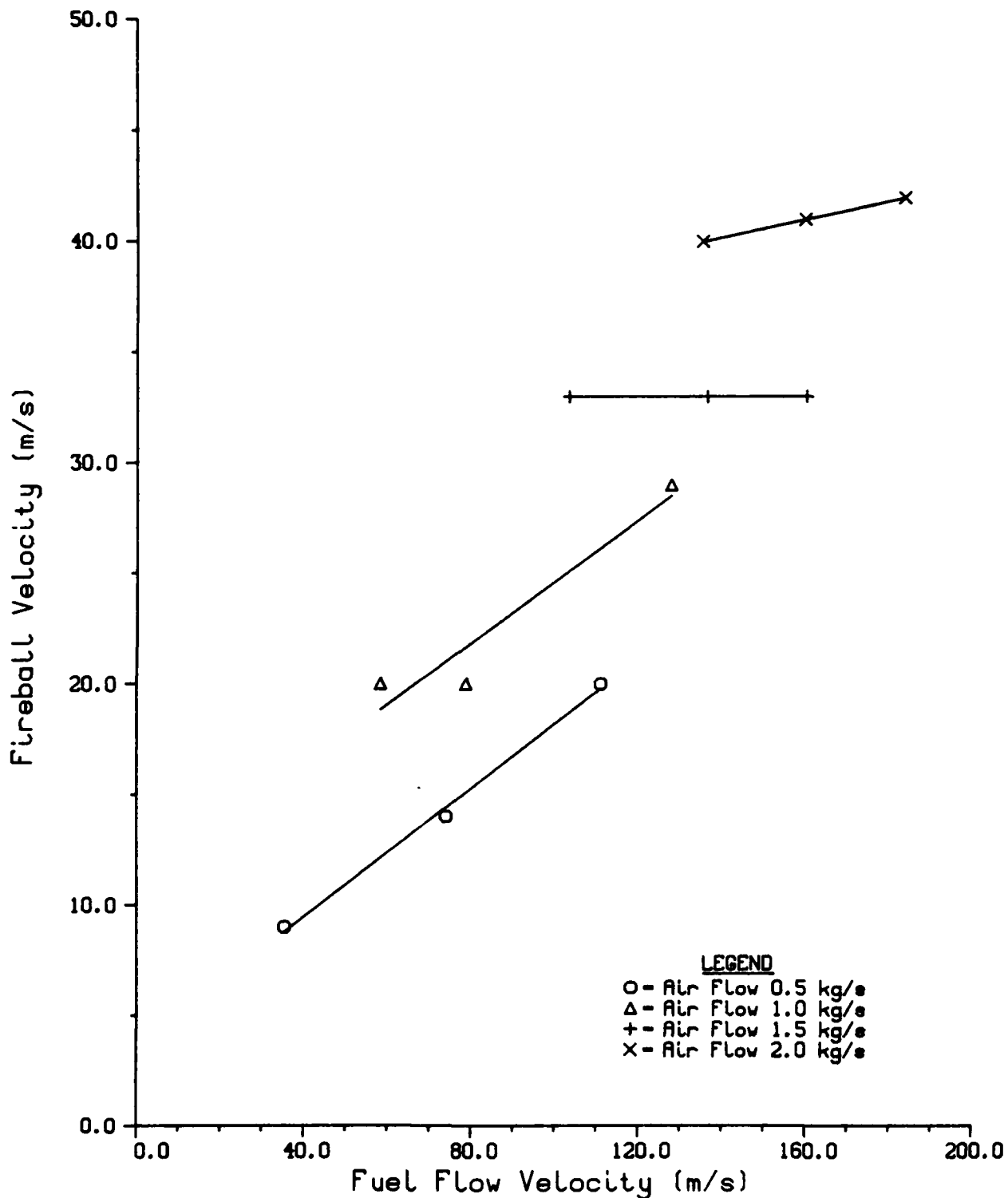


Fig. 5 Fireball Velocity versus Fuel Flow Rate , Z = 61 cm

From Fig. 4 , it is apparent that fireball velocity increases linearly with increase in fuel flow rate at each fixed air flow rate except that of 1.5kg/s - where it is invariant with respect to fuel flow rate over the fuel flow rate range investigated. At a fixed fuel flow rate fireball velocity also increases with increase in air flow rate. This linear trend may be interpreted on global basis as follows. A fireball resulting from interaction between air and fuel streams gains its "initial" axial momentum from these streams. Fireball initial inertial force in the axial direction is higher for the increase in the combined axial inertial force of both the fluid streams. Thus, an increase in either of the two fluid streams would result in higher fireball initial force, and hence, in an increased fireball velocity. Fig. 5 shows the similar effect of flow rates on fireball velocity. At air flow rate of 1.5kg/s fireball velocity invariation with fuel flow rate requires deeper insight for such a behavior.

• Effect of axial location on fireball frequency

Figures 6 and 7 show the effect of axial location on fireball frequency at two air/fuel flow rate combinations. For air flow rate of 1kg/s and fuel flow rate of 8 kg/hr fireball frequency decreases with increase in the down-stream distance from the centerbody face over the axial distance range of 40 - 65 cm distance. Decrease in the fireball frequency with increase in the distance may be explained in terms of quenching of combustion reactions, extinction of flame due to lack of sufficient amount of fuel to sustain flame reactions, and coalescence of fireballs.

Dependence of the fireball frequency upon the axial distance for air and fuel flow rates of 2kg/s and 13kg/hr respectively appears to be more complicated over the distance range investigated (Figure 7). Average fireball frequency increases from 71 s^{-1} to 102 s^{-1} over the axial distance of 5cm from $Z=0$ to Z (axial distance) = 5cm; decreases from 102 to 79 s^{-1} over 10cm distance from $Z=5$ to $Z=15\text{cm}$. It again increases from 79 to 104 s^{-1} over distance of 5cm from $Z=15\text{cm}$ to $Z=20\text{cm}$; remains constant from $Z=20\text{cm}$ to $Z=25\text{cm}$. It decreases from 104 s^{-1} to 74 s^{-1} over distance of 30cm from $Z=25$ to $Z=55\text{cm}$, increases

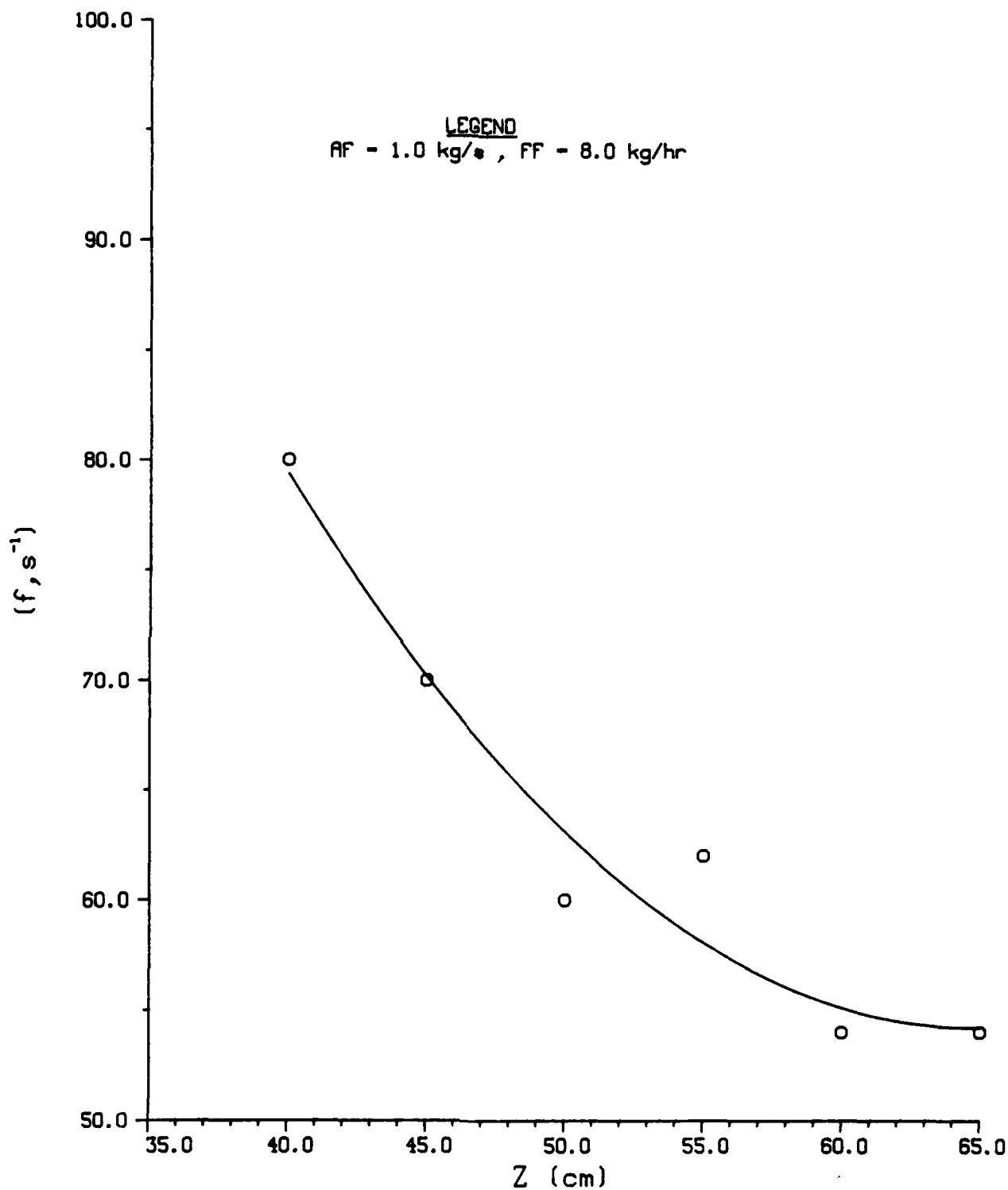


Fig. 6 Fireball Frequency versus Axial Distance from the Face of the Centerbody

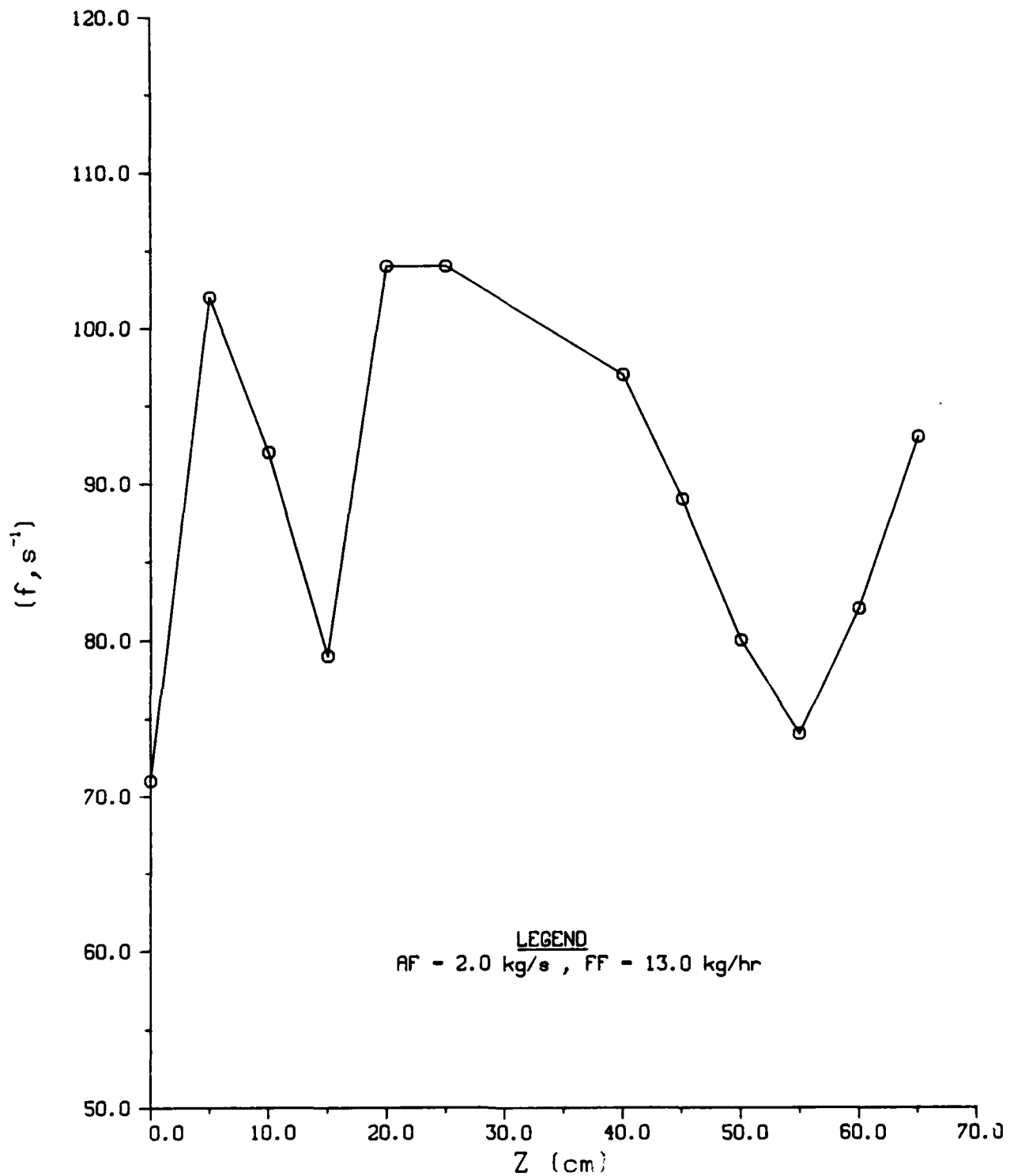


Fig. 7 Fireball Frequency versus Axial Distance Measured from the Face of the Centerbody (Ave. Data)

from 90 to 93 s⁻¹ from Z=55 to Z=65cm. Interpretation of decrease in fireball frequency with distance is similar to the one given for the run where air flow and fuel flow rates were 1kg/s and 8 kg/hr respectively. Increase in frequency with distance may be generally interpreted in terms of fireball splitting, greater number of different regions of same large structure fireball appearing as flame, and generation of new ones in a previously nonemitting and noncombusting moving gas region.

Fireball and nonemitting region number distribution versus normalized fireball "base" time length

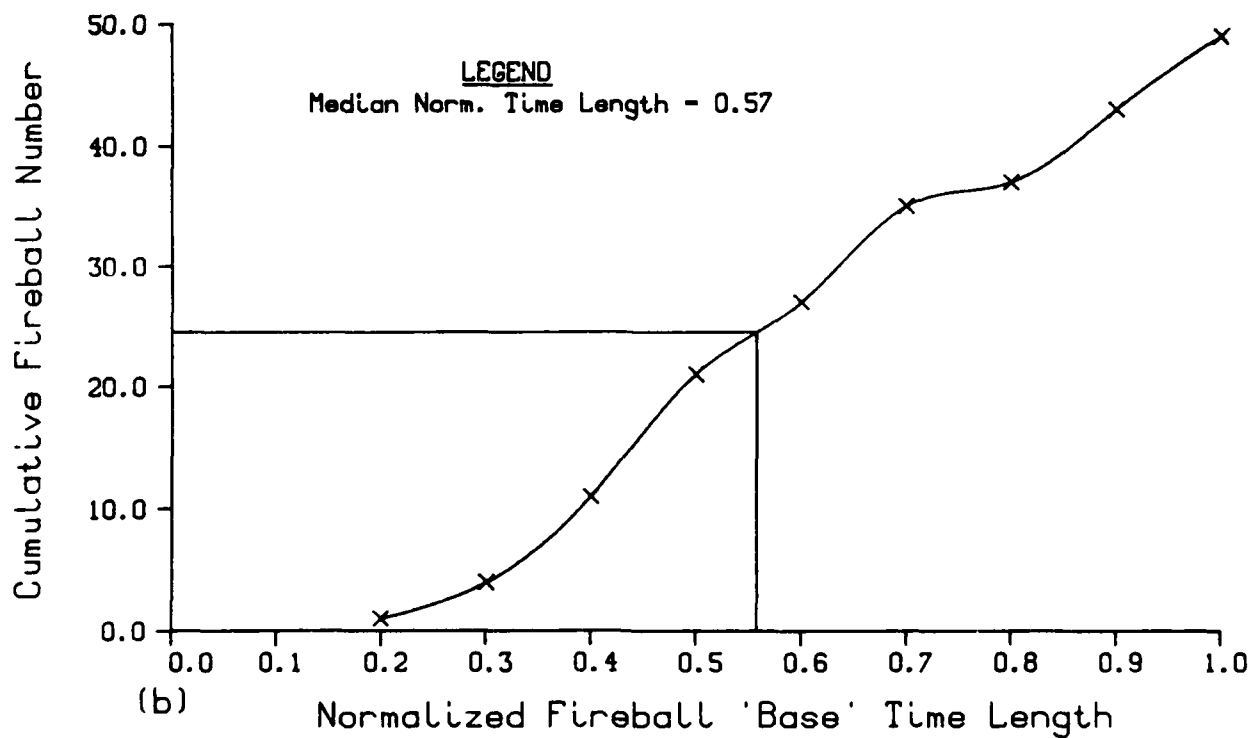
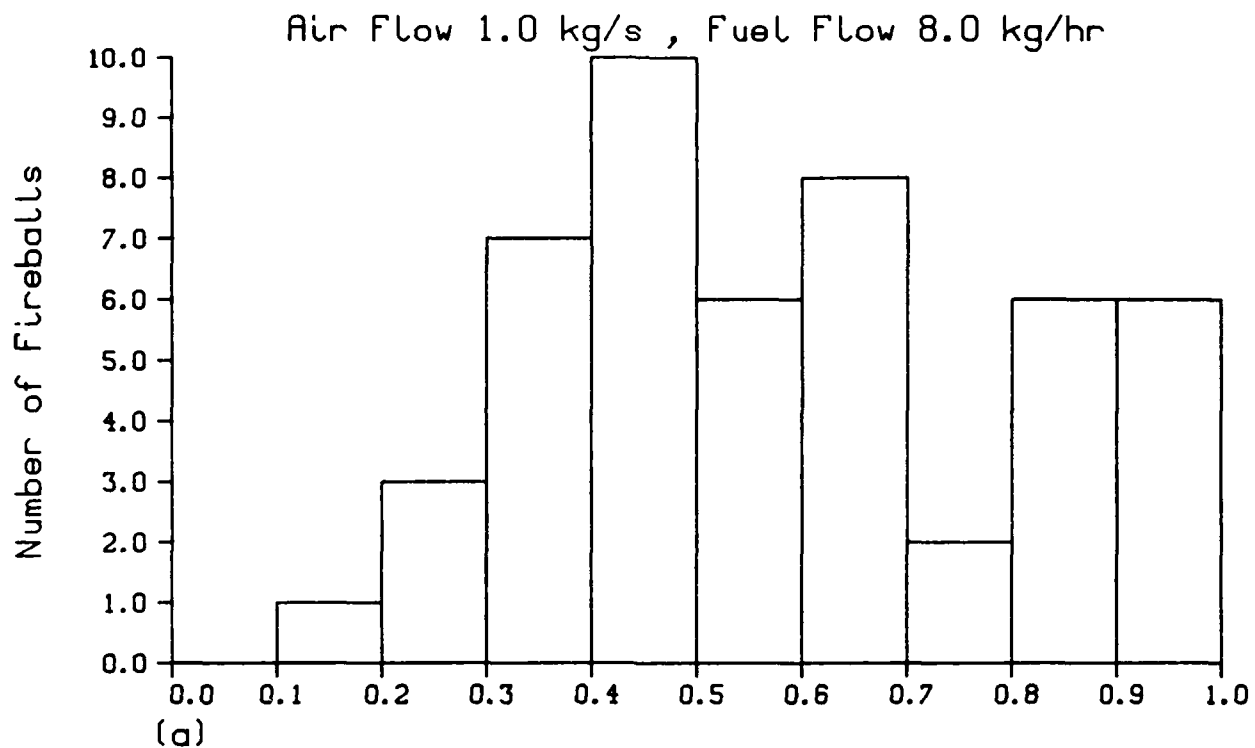
Figs. 8 and 9 show the number distribution of fireballs and nonemitting regions as function of peak "base" time normalized with respect to maximum of 0.0216 s. The data for these plots were acquired by means of spectrometer, and associated electronic and recording systems at axial location, Z of 60cm for air and fuel rates of 1kg/s and 8 kg/hr respectively. Average normalized fireball base time and nonemitting region base time lengths are 0.59 and 0.26 respectively. Median values are 0.57 and 0.22 for fireballs and nonemitting gas regions respectively. The fireball time length is about 2.3 times the nonemitting region time length on the average. From peak chart recordogram, it became apparent that a number of fireballs are not separated by nonemitting regions. 1 and 2 in two slices of the peak chart recordogram in Fig. 10 are examples of probable fireball coalescence or different regions of same large structure fireball being at different reaction stages.

S_S number versus Re_b

S_S and Re_b numbers are defined as follows:

$$S_S = \frac{\text{fireball frequency} \times \text{bluff-body diameter}}{\text{Duct Fluid Flow Velocity}}$$

$$= \frac{f_b D_b}{U_o}$$



Normalized Fireball 'Base' Time Length
Fig. 8 Fireball Number Distribution versus
Normalized Fireball 'Base' Time Length

Air Flow 1.0 kg/s , Fuel Flow 8.0 kg/hr

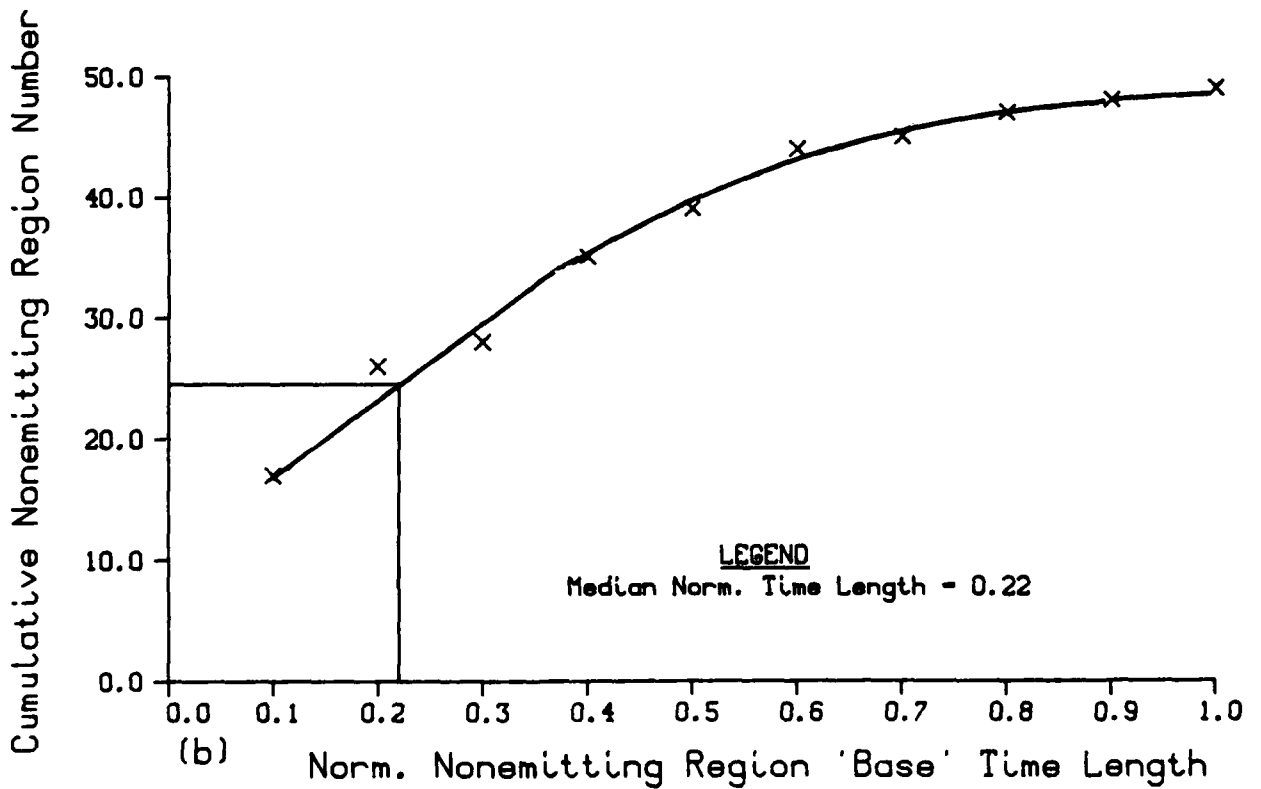
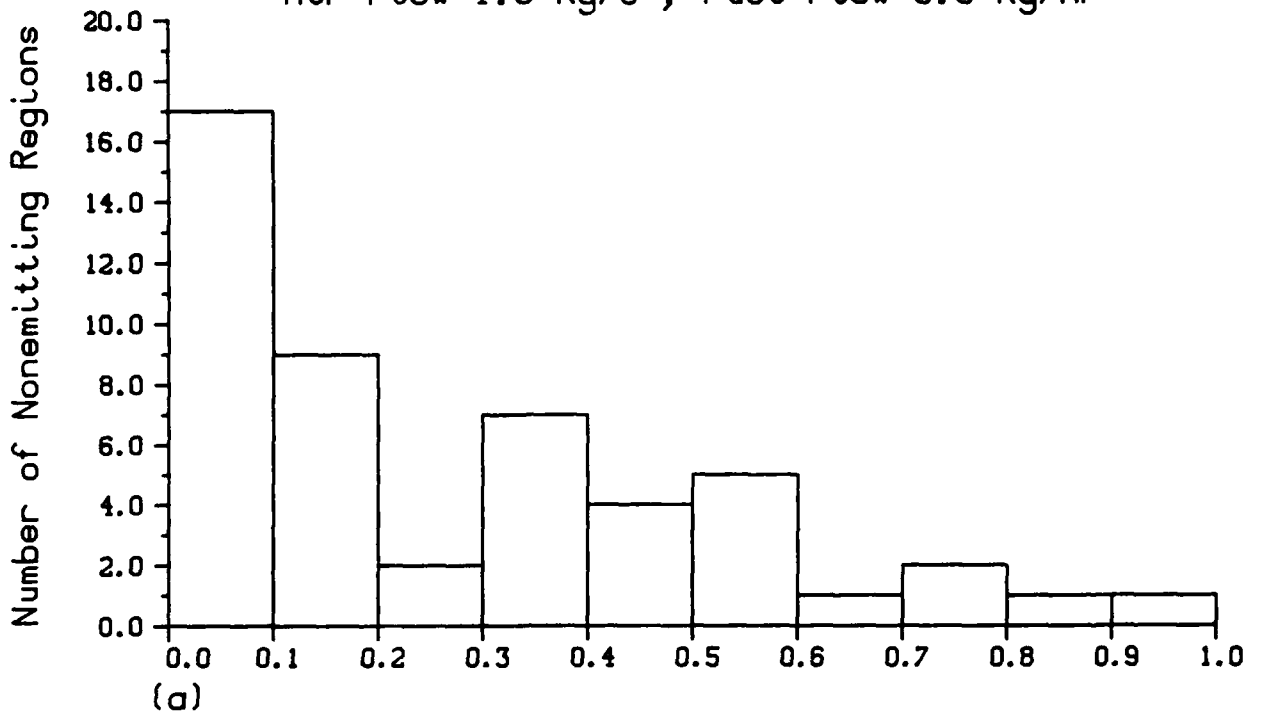


Fig. 9 Nonemitting Region Distribution versus Normalized Nonemitting Region 'Base' Time Length

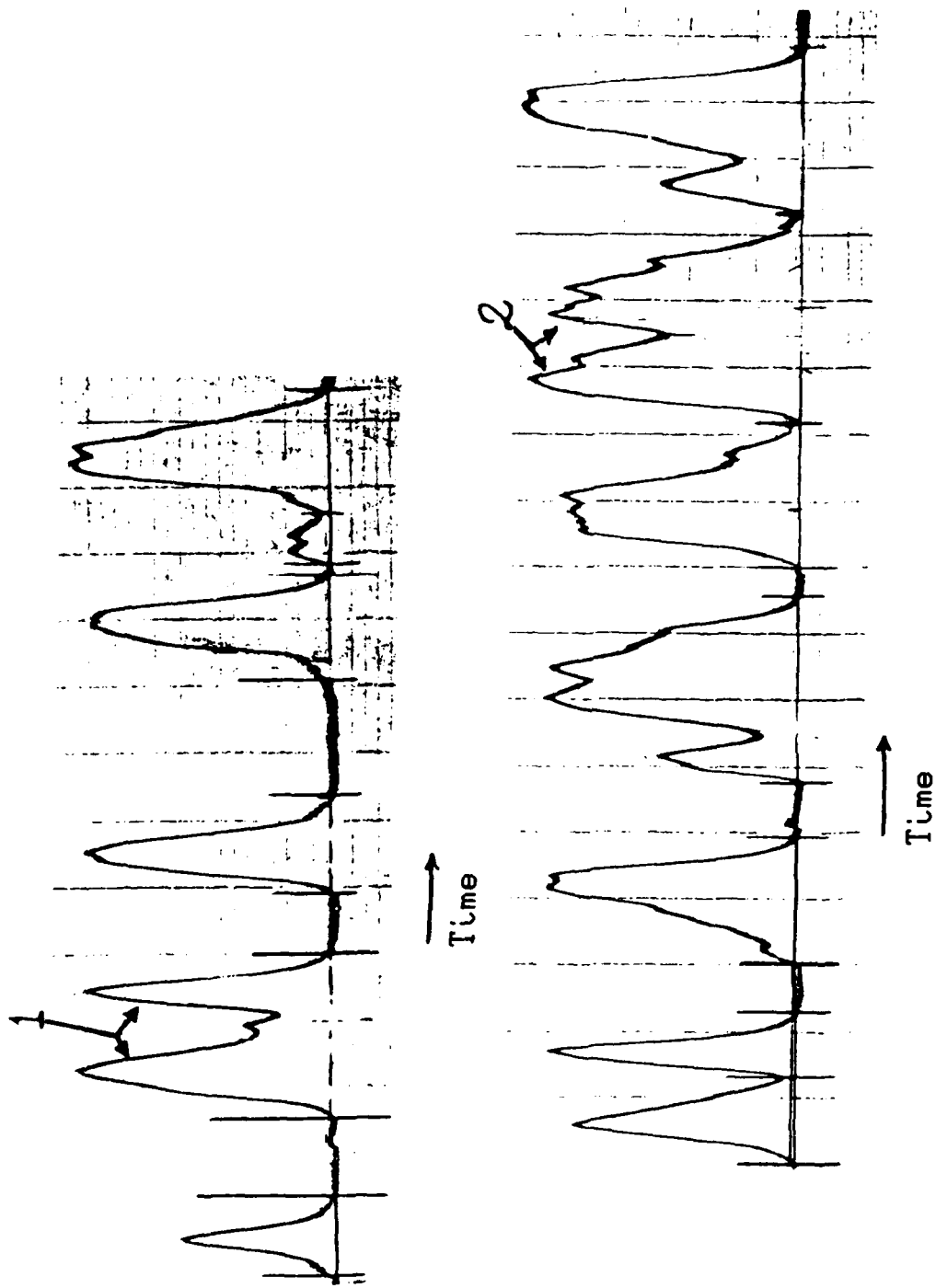


Fig. 10 Peak Chart Recordogram of CH^m Emissions at Axial Distance of 60 cm from Centerbody Face for Air and Fuel Rates of 1 kg/s and 8 kg/hr Respectively
FIG10

Re_D (Reynolds number based on bluff-body diameter) =
centerbody diameter x duct fluid flow velocity

$$\frac{D_D U_0}{\nu}$$

Fig. 11 shows plots of S_G number versus Re_D for two Z (axial distance from the face of centerbody) locations. At $Z=61\text{cm}$, S_G number appears to remain constant with respect to Re_D . For constant S_G number with increase in Re_D or average duct fluid flow velocity frequency of approaching fireballs, f_D also increases. This trend, however, is not found at $Z=116\text{cm}$ where S_G number decreases with increase in Re_D . This implies that f_D decreases with increase in Re_D . This further means that the approaching fireball frequency should either decrease or remain invariant.

V. A GLOBAL PROPOSED MECHANISM FOR RELATIVE INCREASE OR DECREASE IN FIREBALL FREQUENCY f_D AT TWO AXIAL LOCATIONS OF THE APL TUNNEL COMBUSTOR

Splitting, greater number of different regions of same large structured fireball becoming chemically active in accordance with the flame conditions and "birth" of new ones in a previously nonemitting and noncombusting moving gas region between two adjacent fireballs could lead to higher approaching fireball frequency. Quenching of combustion reactions in a fireball, extinction of flame due to lack of sufficient amounts of reactants (fuel and air) to sustain flame reactions, and coalescence of fireballs could lead to decrease in the fireball frequency. Equal number of "death" and "birth" rates of fireballs between two axial locations would lead to invariance of fireball frequency with respect to axial distance.

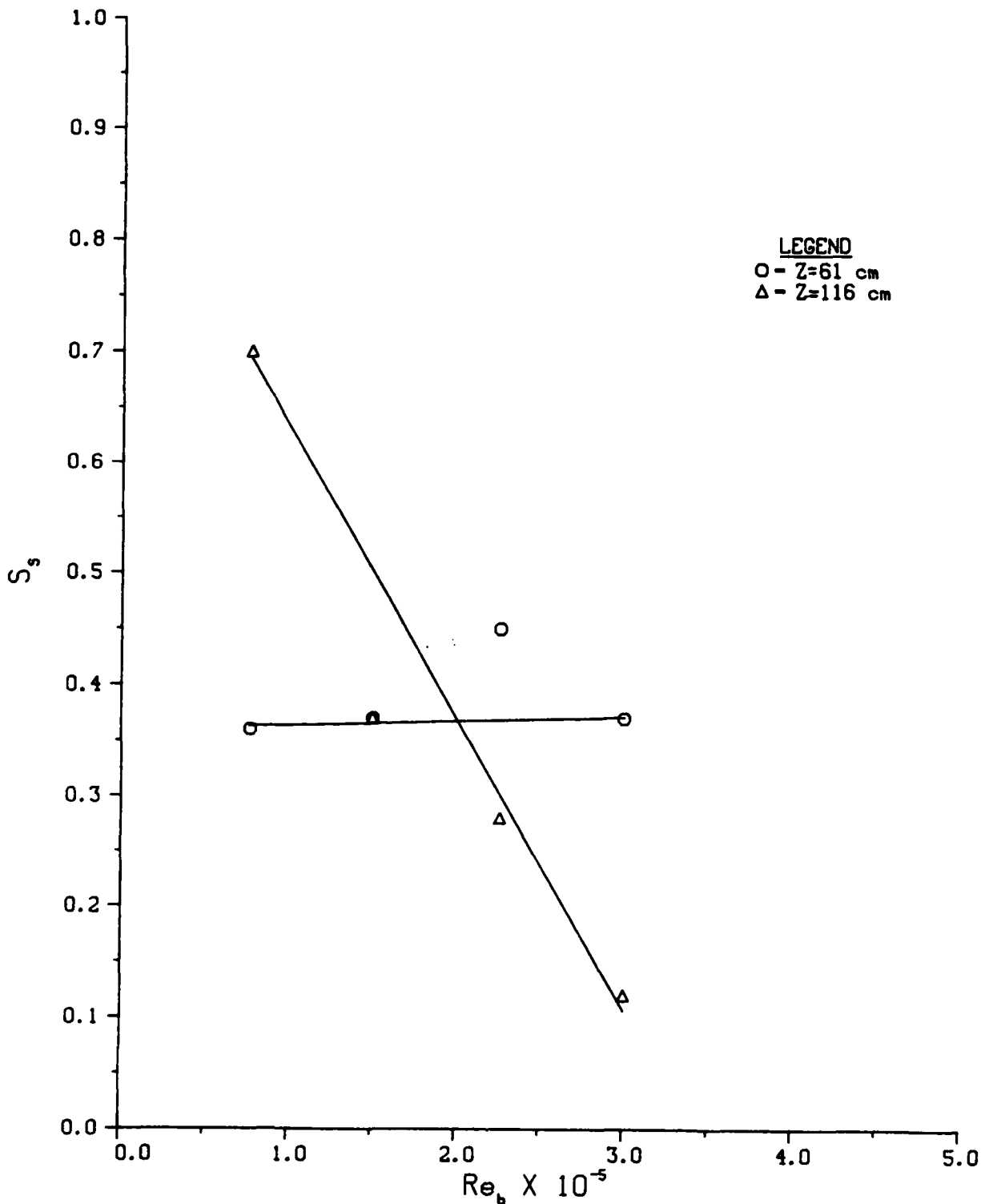


Fig. 11 $S_s (-f_b D_b / U_0)$ versus $Re_b (-D_b U_0 / \nu)$

VI. RECOMMENDATIONS

1. On finding suitable applicability of the refined experimental techniques for the study of the dynamic behavior of the bluff-body diffusion flame combustor by way of acquisition of the reasonably satisfactory preliminary data, a carefully planned parametric investigation of the combustion process in the APL combustor should begin. A series of experiments to record flame emission and static pressure data should be performed as function of axial location and fuel/air flow rate combination. At each air flow rate, a fuel flow rate range from lean to rich flame blow-off limit should be investigated. In fact, to observe the effect of fuel jet penetration through the recirculation zone located immediately downstream of the bluff-body upon the moving "fireball" phenomenon fuel tubes of different diameters should be employed keeping the same air/fuel mass flow rate combination. At each air/fuel flow rate combination total flame length as well as exhaust gaseous species and particulate matter concentrations, and temperature should also be advisably determined. To achieve the final aim of developing mathematical models to predict combustion and pollutant emissions information regarding time varying local gaseous species concentration, temperature, pressure and velocity profiles at each axial location should also be determined at each air/fuel flow rate combination.
2. To gain insight into the relationship between the bluff-body vortex shedding and "fireball" phenomena in the diffusion flame laser light scattering technique may be employed to study the vortex shedding phenomenon in the cold flow operated system with a range of air/fuel (C_3H_8) flow rate combinations simulated by air/ CO_2 flow rate combinations. Further, laser high speed schlieren photography may be employed to complement the desired information regarding the dynamic behavior of the combustor at a number of air/fuel flow rate combinations.

REFERENCE

1. Roquemore, W. M. et al. "Preliminary evaluation of a combustor for use in modeling and diagnostics development," ASME Publication 80-GT-93, Mach, 1980.

JOURNAL ARTICLES STUDIED

1. Lightman, A. J. et al. "Velocity measurements in a bluff-body diffusion flame," AIAA 15th Thermophysics conference, Snowmass, Colorado, July, 1980.
2. Pitz, R. W., and Daily, J. W., "Experimental study of combustion in a turbulent free shear layer formed at a rearward facing step," AIAA 19th Aerospace Sciences Meeting, St. Louis, Missouri, January, 1981.
3. Keller, J. O. et al. "Mechanism of instabilities in turbulent combustion leading to flashback," AIAA 19th Aerospace Sciences Meeting, St. Louis, Missouri, January, 1981.
4. Hurle, I. R. et al. "Sound emission from open turbulent premixed flames," Proc. Roy. Soc. A 303, 409-427 (1980).
5. Mehta, G. K. et al. "Correspondence between ions and light emitting radicals in turbulent flames," Western States Section, The Combustion Institute, Spring Meeting, University of California, Irvine, April, 1980.
6. Price, R. B. et al. "Optical studies of the generation of noise turbulent flames," The Combustion Institute Symposium.
7. Cohen, L. S. and Director, M. N., "Transport processes in the two-dimensional near wake," AIAAJ, 13, 969-970, 1975.
8. Bloom, M. S. and Gerrard, J. H. "Measurements on turbulent vortices in a cylinder wake," Proc. Roy. Soc. A, 294, 319-342, 1966.
9. Perry, A. E. and Linn, T. T., "Coherent structures in coflowing jets and wakes," J. Fluid Mech., 88, 451-463, 1978.
10. Sarpkaya, T., "Vortex - induced oscillations," J. O. Applied Mechanics, 46, 241 - 258, 1979.

It is mentioned that the above recommendations would partly constitute the theme for proposal for follow-on research.

11. Crow, S. C., and Champagne, F. H., "Orderly structure in jet turbulence," *J. Fluid Mech.*, 48, 547-591, 1971.
12. Shivashankara, B. N. et al., "Evaluation of combustion noise scaling laws by an optical technique," *AIAAJ*, 13, 623-627, 1975.

1981 USAF - SCEE SUMMER FACULTY RESEARCH PROGRAM

Sponsored by the

AIR FORCE OFFICE OF SCIENTIFIC RESEARCH

Conducted by the

SOUTHEASTERN CENTER FOR ELECTRICAL ENGINEERING EDUCATION

FINAL REPORT

SHEAR-WAVE VELOCITY STRUCTURE DETERMINED

FROM ANALYSIS OF RAYLEIGH-WAVE GROUP-VELOCITY DISPERSION

Prepared by: Dr. Gerald W. Simila
Academic Rank: Assistant Professor
Department and University: Department of Geological Sciences
California State University, Northridge
Research Location: Air Force Weapons Laboratory
Civil Engineering Research Division

USAF Research Colleague: Captain Brian W. Stump, Ph.D.
Date: September 16, 1981
Contract No: F49620-79-C-0038

SHEAR-WAVE VELOCITY STRUCTURE DETERMINED
FROM ANALYSIS RAYLEIGH-WAVE GROUP-VELOCITY DISPERSION

by

Gerald W. Simila

ABSTRACT

The moving window technique has been utilized successfully to extract group-velocity dispersion data from high-explosive ground motion records. Fundamental Rayleigh-wave group-velocities (225-264 m/sec) have been determined for period range 50-164 msec. The Haskell method has been used to model the dispersion data. The resulting shear-wave velocity distribution for the McCormick Ranch test site is $V_s = 244-400$ m/sec for depth range 0 - 22 m. In addition, possible body wave dispersion has been observed. Suggestions for further research in this area are presented.

ACKNOWLEDGEMENT

The author would like to thank the Air Force Systems Command, the Air Force Office of Scientific Research and the Southeastern Center for Electrical Engineering Education for providing him with the opportunity to spend a very worthwhile and interesting summer at the Air Force Weapons Laboratory, Kirtland AFB, New Mexico. He would like to acknowledge the laboratory, specifically Civil Engineering Research Division, for its cooperation and hospitality.

Finally, he would like to thank Capt Brian Stump, Ph.D., for his collaboration and suggestions in this research project. Also, he wishes to acknowledge the helpful discussions with Dr Bob Reinke and computer programming consultations with Mr Tony Tagliaferro.

I. INTRODUCTION:

The determination of ground response to high-explosive detonations is an important problem in the design of military structures. Specifically, the Air Force is interested in the strong-motion seismic waveforms generated by explosion sources. In addition, the determination of the geologic structure of the site is necessary to understand and model the generated waveforms.

The present project is involved with a specific technique to process the explosion waveforms and extract information that will yield inference regarding the local geologic structure. In general, two types of waves are generated by explosions: body and surface waves. A specific surface wave, called Rayleigh, is a combination of two body wave particle motions, the compressional (P) and shear (S). Rayleigh waves generally exhibit dispersion which means that the frequency content of the waveform is a function of the P and S wave velocity associated with the geologic media. Initially, this project utilizes a signal processing technique to determine the dispersive character of Rayleigh waves generated from high-explosive tests.

In studying surface waves, one must differentiate between the group and phase velocity of the waveforms. For a nondispersive media, the group velocity is equivalent to the phase velocity, and the seismic pulse propagates from the source without a change in shape. In the case of a dispersive media, each component of the wave motion travels with its own characteristic velocity, the phase velocity. In addition, the group velocity is the velocity associated with a packet of waves of a given frequency¹.

The group velocity controls the waveform observed on a seismogram. The group velocity (U) is a function of period (T), and is related to the phase velocity (C) by the expression:

$$\begin{aligned} U &= C + k \, dC/dk & (1) \\ &= - C - \lambda \, dC/d\lambda \end{aligned}$$

$$\text{where } k = 2\pi/CT$$

Now, the group velocities of the dispersed waveform can be calculated by the simple equation:

$$U_R(T) = \frac{x}{t} \quad \begin{array}{l} \text{where } x = \text{distance} \\ t = \text{travel time} \\ T = \text{wave period} \end{array} \quad (2)$$

Various digital processing techniques have been applied to surface waves to determine group-velocity dispersion curves. The specific approach used in this investigation is the moving-window technique² to determine Rayleigh-wave group velocities. The method is a frequency-time analysis which calculates a two-dimensional array of Fourier amplitudes as a function of wave period. The group-velocity dispersion curve is traced through the Fourier amplitude maximum for each period.

Strong-motion seismic records from a series of high-explosive tests at McCormick Ranch, New Mexico, in 1978-79, are analyzed for group velocities. The Haskell method³ is used to generate theoretical Rayleigh-wave group-velocity dispersion curves. The observed and theoretical group velocities are matched by a trial and error approach for a selected set of velocity models. The best-fitting models are also constrained by seismic refraction observations.

II. OBJECTIVES:

The main objective of this research project was to investigate initially the application of the moving-window technique to near source high-explosive ground motion data. After the group-velocity dispersion curves were determined, the Haskell formulation was used to calculate group velocities for shear-wave velocity models. Various models were selected which provided close agreement between the observed and calculated dispersion curves.

The specific objectives for this investigation were:

- (1) Apply the moving-window technique to determine Rayleigh-wave group-velocity dispersion curves.
- (2) Model the observed group velocities, using the Haskell formulation for a select set of geologic model parameters.

(3) Compare the models derived from dispersion observation with the reported seismic refraction models.

This investigation presents the first known attempt to evaluate high-explosion ground motion data for Rayleigh-wave group-velocity dispersion using the moving window technique.

III. OBSERVATIONS

The data used in this investigation were strong-motion seismic records from a series of high-explosive tests in 1978-79 at McCormick Ranch, New Mexico (see Figure 1). The data were recorded by vertical accelerometers (Endevco Model series 2260) and recorded on magnetic tape. The analog acceleration recordings were sampled at a rate of 2000 samples per sec with an antialias filter at 400 Hz. The data were recorded at distance ranges of 6.55 to 228.6 m⁴.

The Pre-Multiple Burst (PMB) high-explosive program was conducted by the AFWL in September, 1978. A series of small bursts, both buried and above ground, with single and multiple-charge configurations were performed⁵. Another series of high-explosive tests were conducted in 1979. The tests, Pre-Hybrid Gust (PHG), involved single burst covered and surface tangent bursts along with hexagonal array multi-bursts equivalents⁶. The data from these experiments were chosen to determine Rayleigh-wave group-velocity dispersion, and compare the velocity models determined by previous geophysical studies⁴.

IV. DATA ANALYSIS TECHNIQUE

The moving window analysis technique can resolve broad frequency band recordings of multi-mode transient signals. Fourier spectral amplitudes as functions of period and group arrival time are interpreted in terms of Rayleigh-wave group velocity associated with each of the individual modes of propagation. The Rayleigh surface waves are analyzed for the fundamental and first-higher modes.

The analysis begins with the extraction of a section of a digitized

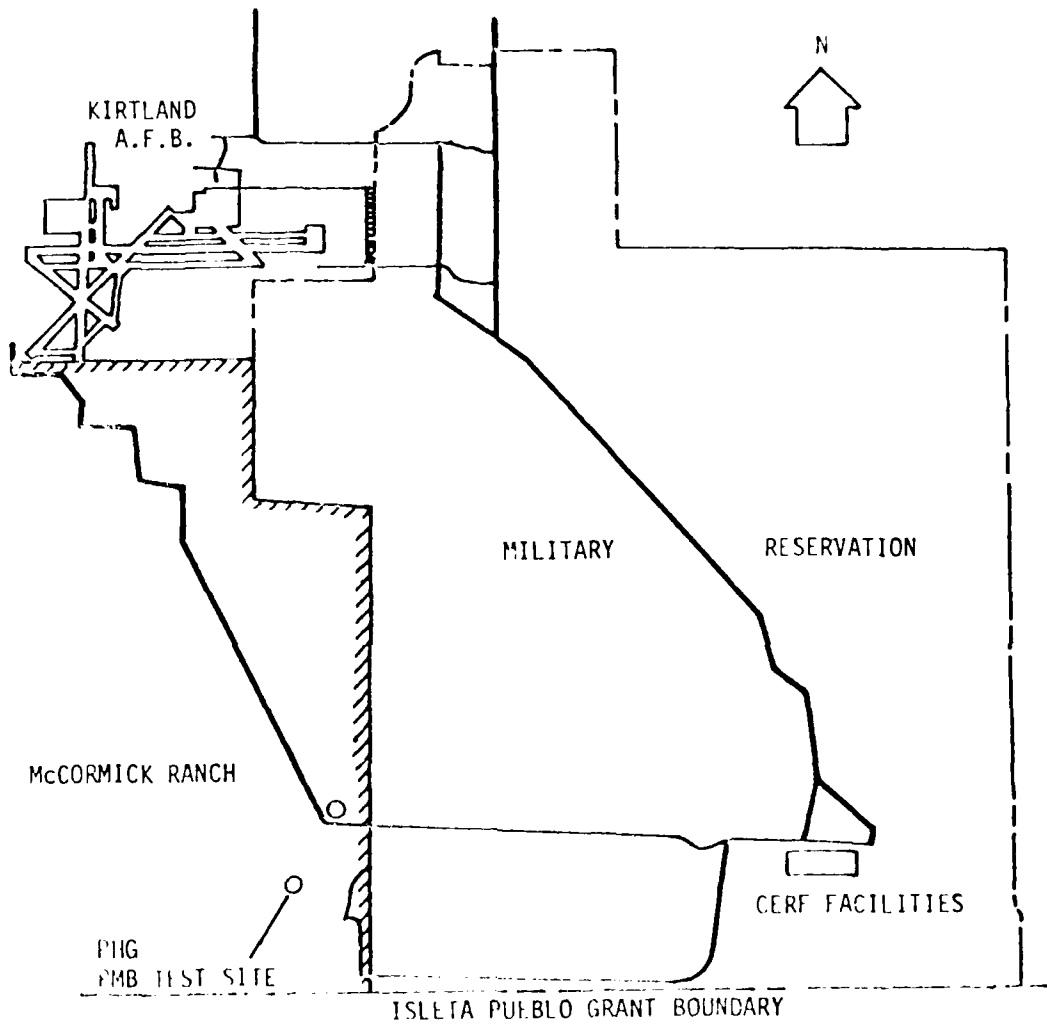


Figure 1 General map of the PMB and PHG test sites (Brown,1980).

seismogram $f(t)$ using a rectangular time window $w(t)$ centered at a time t_n which corresponds to a group velocity $U_n(T)$. The length of the extracted segment is variable, but is proportional to the product of a fixed window factor W and the current wave period of analysis T_n . The representation is:

$$\begin{aligned} w(t) &= 1 & t_n - \frac{1}{2} WT_n < t < t_n + \frac{1}{2} WT_n \\ w(t) &= 0 & \text{otherwise} \end{aligned} \quad (3)$$

and $s(t) = f(t) \cdot w(t)$.

Experimental analyses have indicated that reliable results are obtained when the window length (W) is 4-6 times the period.

The next step in the moving window analysis is the multiplication of the windowed seismogram by a modulating symmetrical function $q(t)$ centered at times corresponding to a particular group velocity in a series of equally spaced velocities. The resulting time series is $h(t) = g(t) \cdot s(t)$. Several types of modulating functions can be used, and a common function which has been applied is $q(t) = \cos^2(\pi t/WT)$.

Multiplication of the specified time series by a window function is equivalent to convolution of the corresponding spectra in the frequency domain, and each spectral component of the time series will possess a shape resembling that of the Fourier transform of the applied window. The purpose of the modulation function is to give greater weight to that portion of the seismogram which corresponds to the group velocity of interest. Modulation also diminishes the side lobes in the frequency domain produced by analysis of a truncated signal. The final step of the moving window analysis involves taking the Fourier transform of the prepared signal $h(t)$ to extract the spectral amplitudes and phases².

The data are then displayed and contoured on a two-dimensional plot of the spectral amplitude values as a function of group velocity versus wave period. The dispersion curve is traced through the amplitude maxima for each period. The general result is illustrated in Figure 2 in the form of contour lines for selected amplitude values. The amplitude maxima which represent the group velocity data are indicated by dots. The contours represent amplitude values (zero to Z) that are

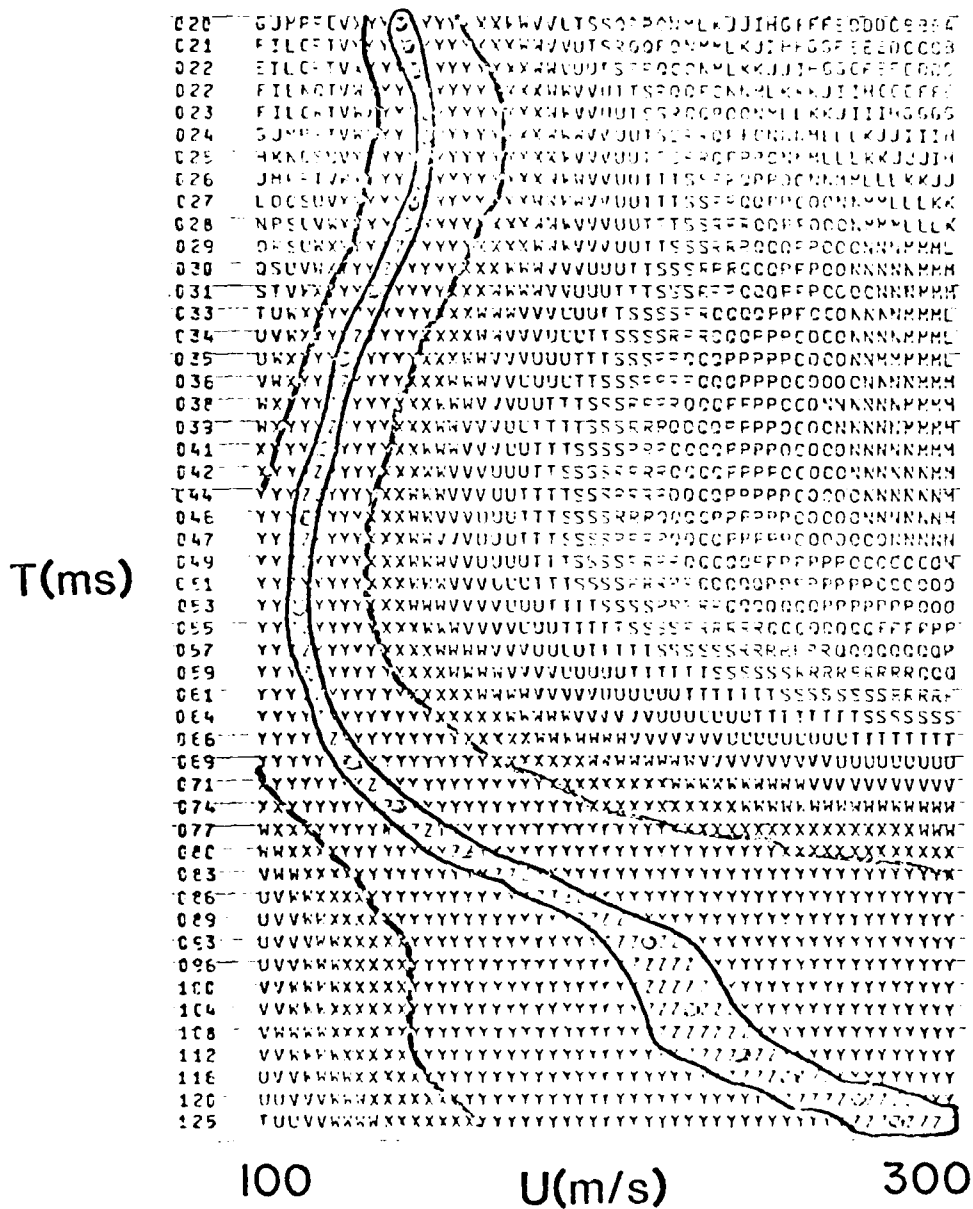


Figure 2. Example of output from moving window analysis, T=period in millisecc (ms) and group velocity U(m/sec).

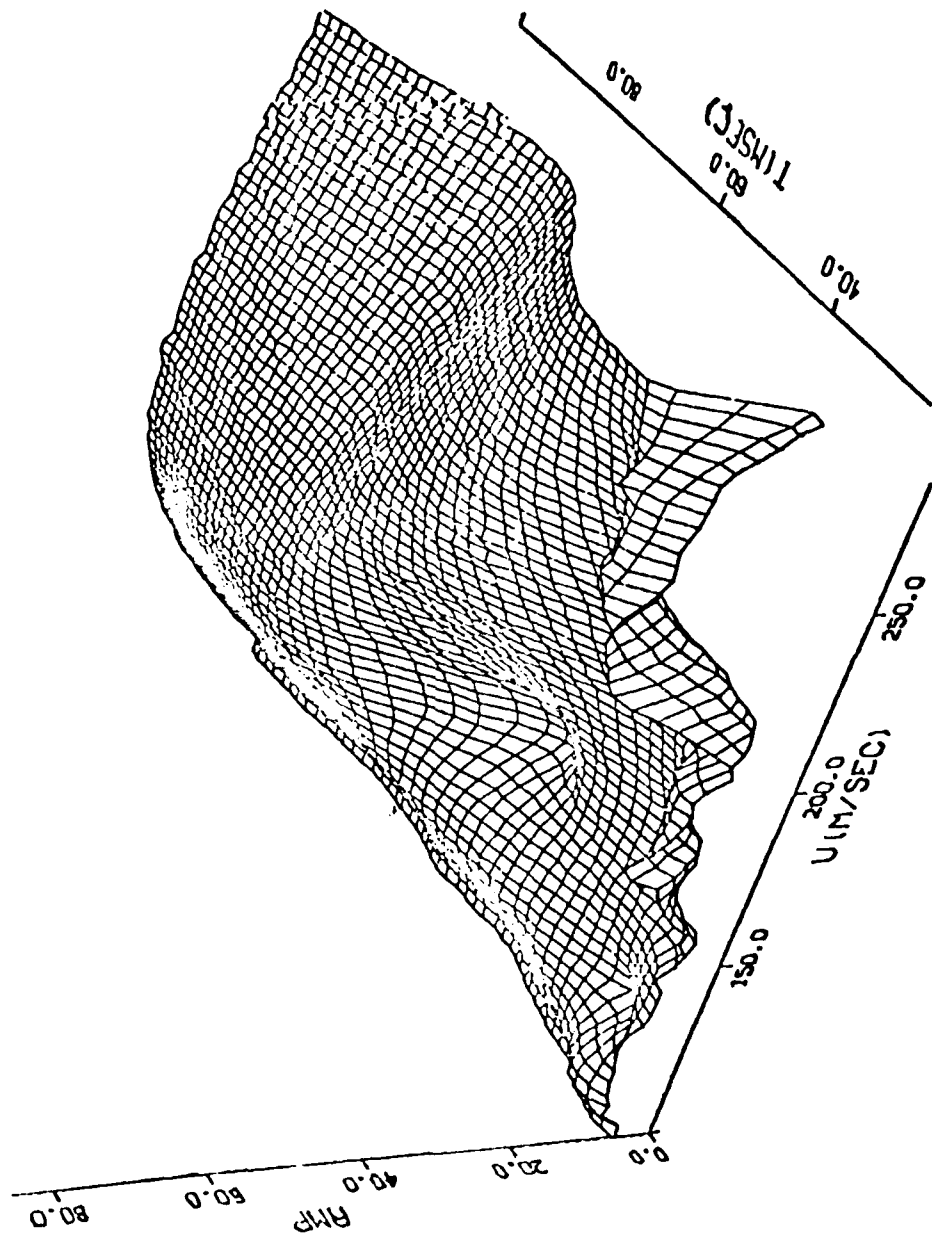


Figure 3. Three-dimensional plot of moving window output for period, group velocity, and amplitude.

normalized with respect to the maximum value at each period rather than absolute levels. An example of a three-dimensional plot of amplitude, group velocity, and period is shown in Figure 3 which also illustrates the dispersion of the amplitude maxima.

V. RESULTS

The dispersion data for the PMB tests are presented for the ground motion observations at distance ranges of 73.2 m and 228.6 m. Representative time series for these distances are presented in Figures 4 and 5, respectively. The results from the moving window analysis are presented in Figures 6, 7, 8, 9, and 10. The group-velocity dispersion data are shown in Figure 11. The Rayleigh-wave dispersion curves indicate group velocities $U=224-264$ m/sec for period range $T=50-164$ msec. These data are interpreted as fundamental mode dispersion from the recordings at a distance of 228.6 m. The first higher-mode dispersion data were determined from recordings at a distance of 73.2 m. The associated group velocity range is 260-300 m/sec for periods of 25-59 msec. The various symbols represent different high-explosive tests for the same distance.

Ground motion records from the PHG test series are presented in Figures 12, 13, 14, and 15 representing distances of 10.9, 14.6, 18.4 and 35.8 m, respectively. The corresponding group-velocity dispersion data are shown in Figure 16. The pattern of dispersion for recordings at distances of 10.9 and 14.6 m is characterized by a monotonic decrease for velocity range 260 to 108 m/sec with period range $T=20-100$ msec. The time records exhibit the long period waveform usually identified as the "spall" wave associated with explosions. Stump⁷ has modeled these specific waveforms, and concluded that Rayleigh-waves can generate tensile stress components in the vertical direction which may produce the spall waveform. Consequently, the observed dispersion pattern probably represents the spall phase, but may also include dispersion from body waves at the short periods.

The group-velocity data recorded at 18.4 m shows dispersion repre-

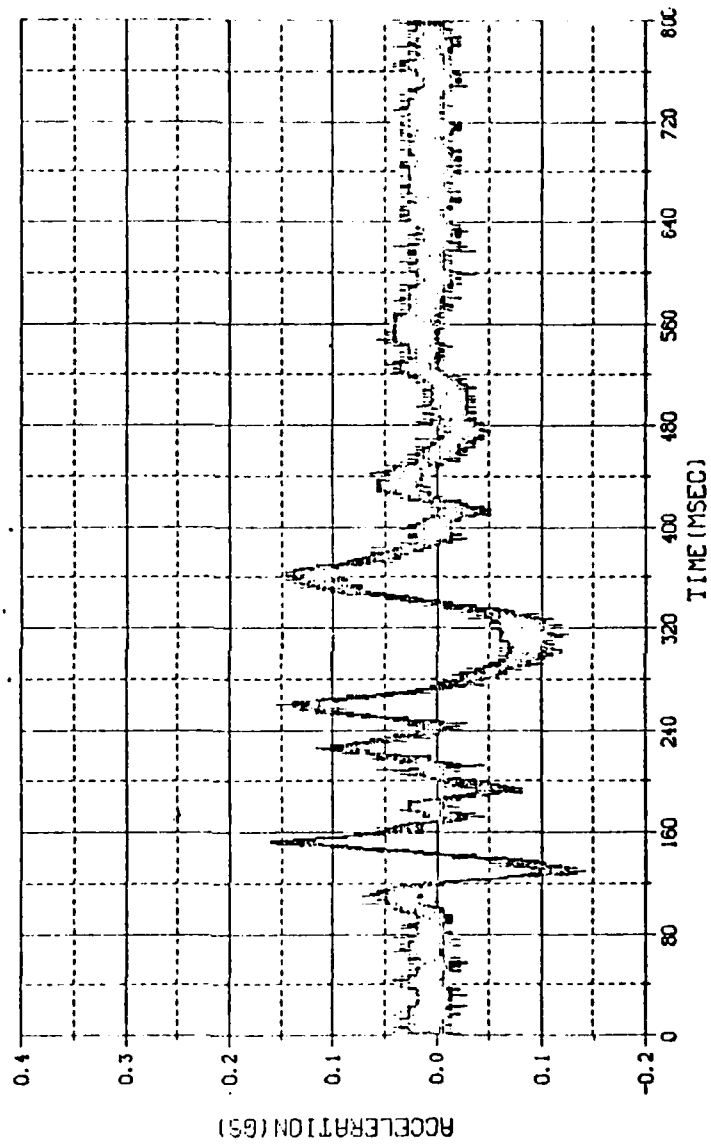


Figure 4. PMB ground motion record at distance of 73.2 m.

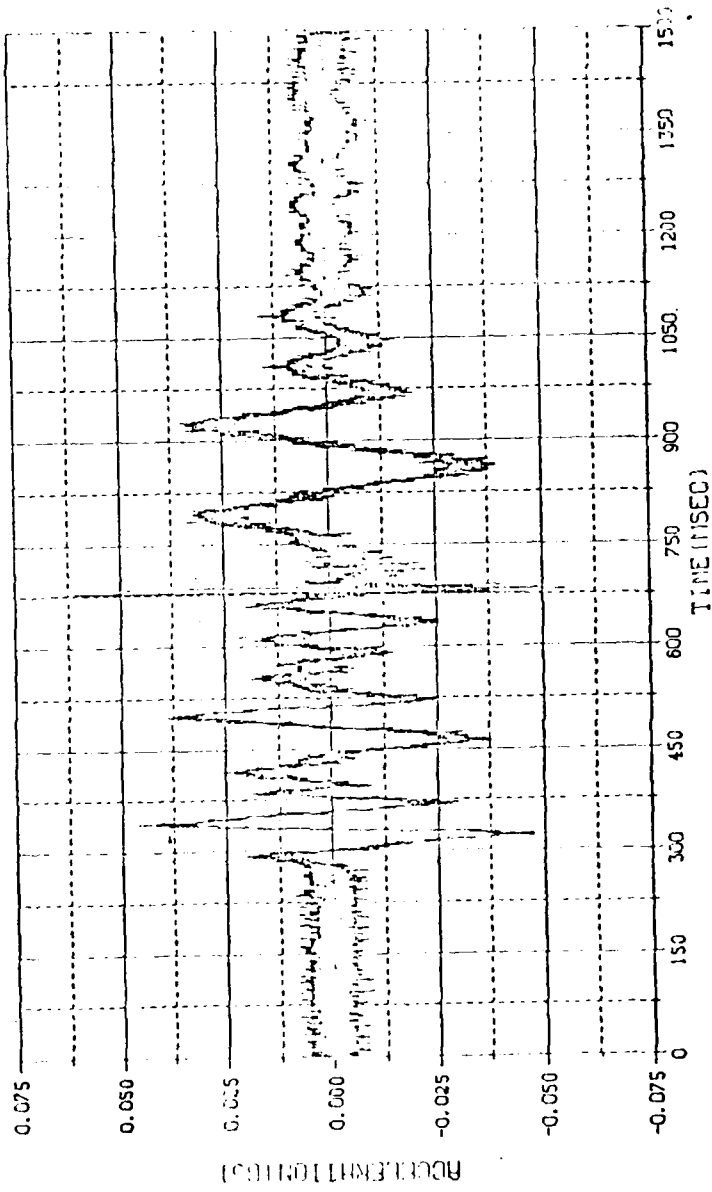


Figure 5. PMB ground motion record at distance 228.6 m.

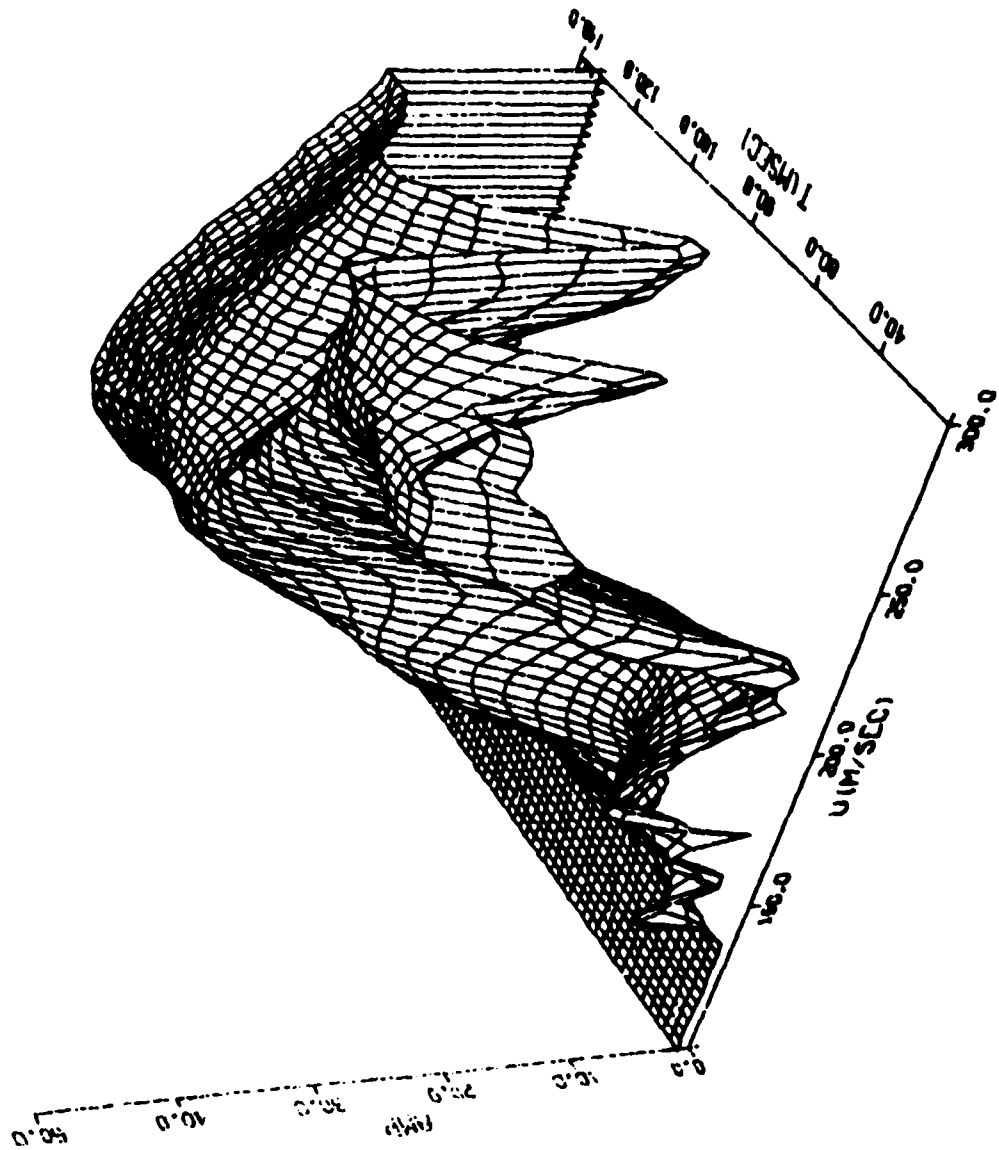


Figure 6. Moving window technique results for PM9-06 recorded at a distance of 73.2 m.

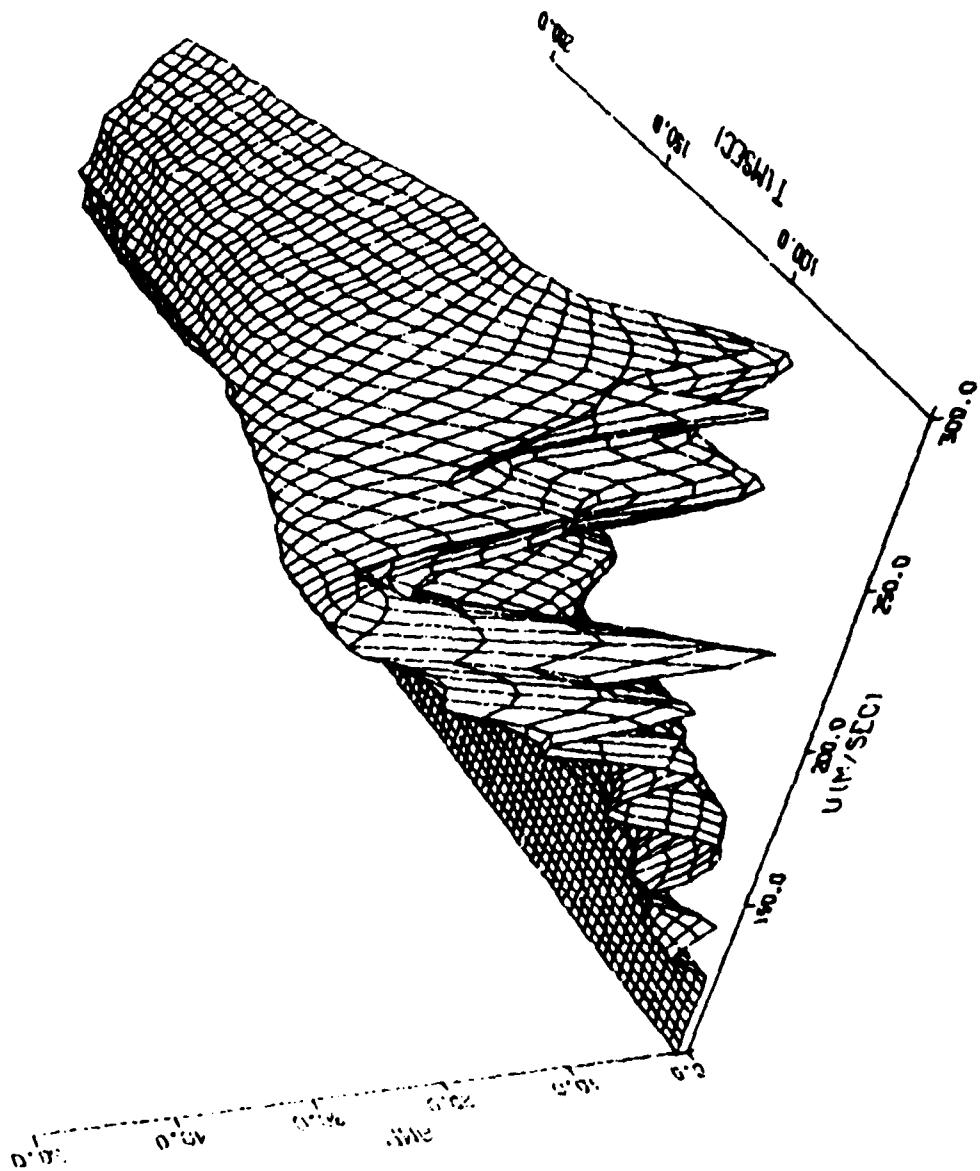


Figure 7. Moving window technique results for PMB-03 recorded at a distance of 228.6 m.

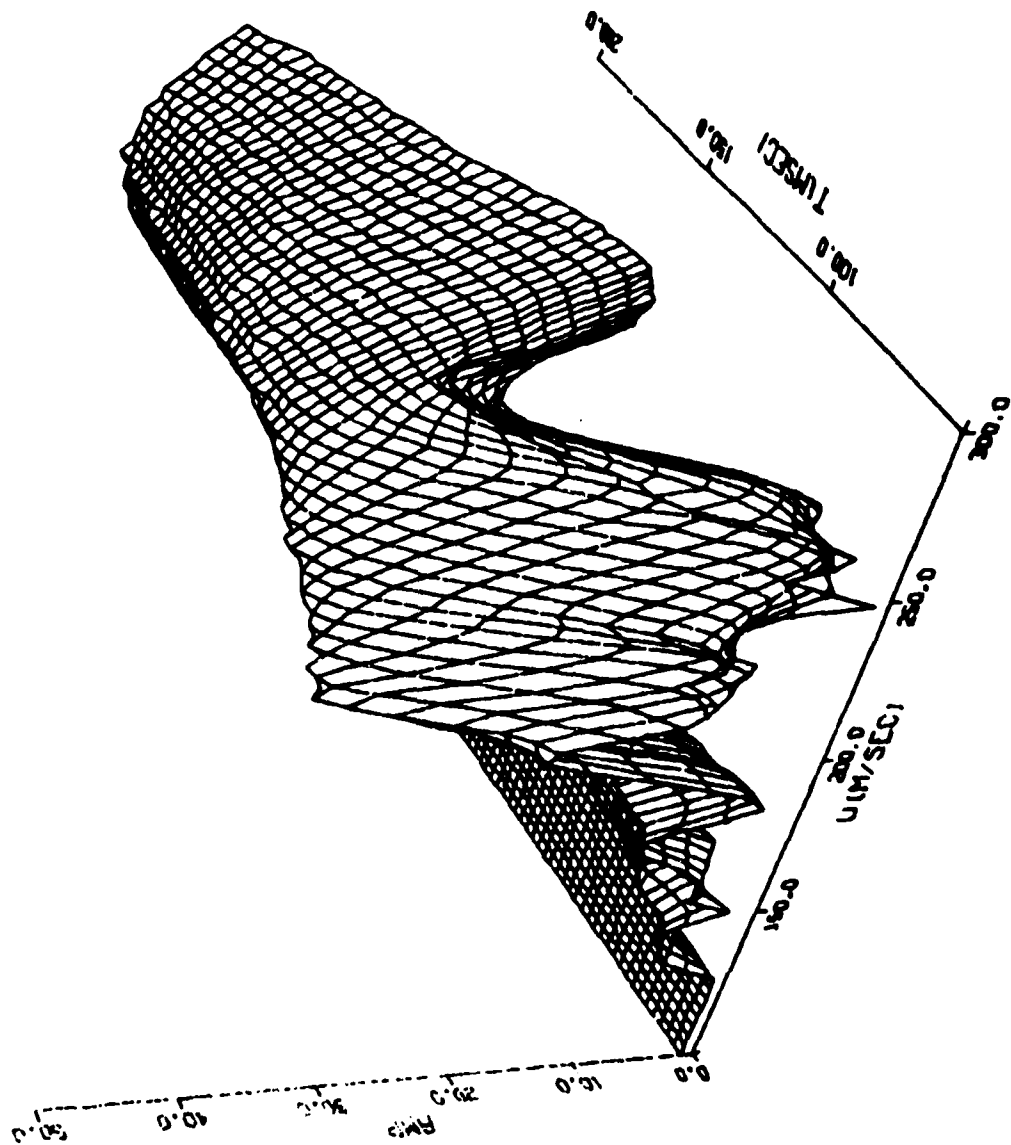


Figure 8. Moving window technique results for PMB-04 recorded at a distance of 228.6 m.

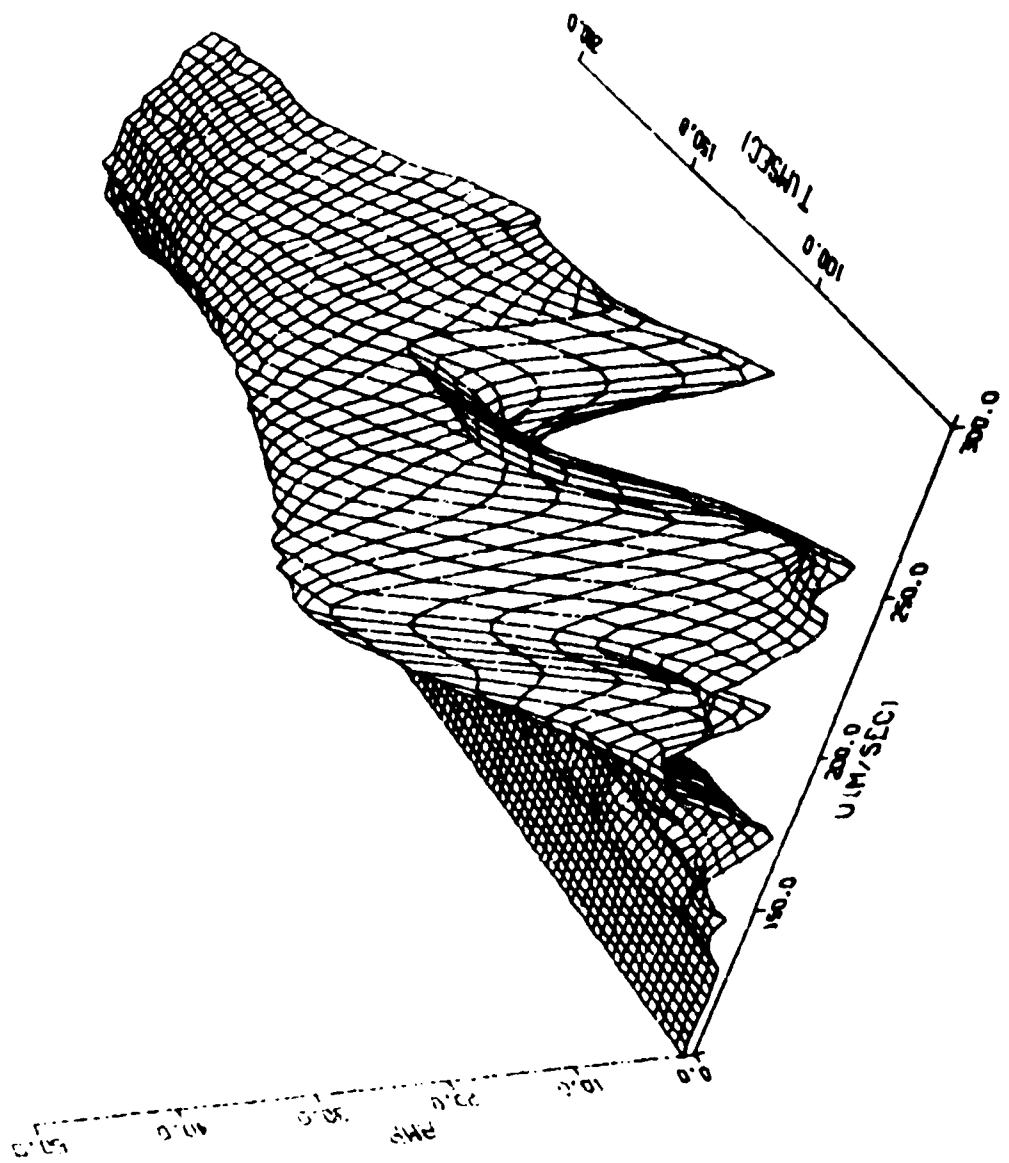


Figure 9. Moving window technique results for PIR-06 recorded at a distance of 228.6 m.

AD-A113 709

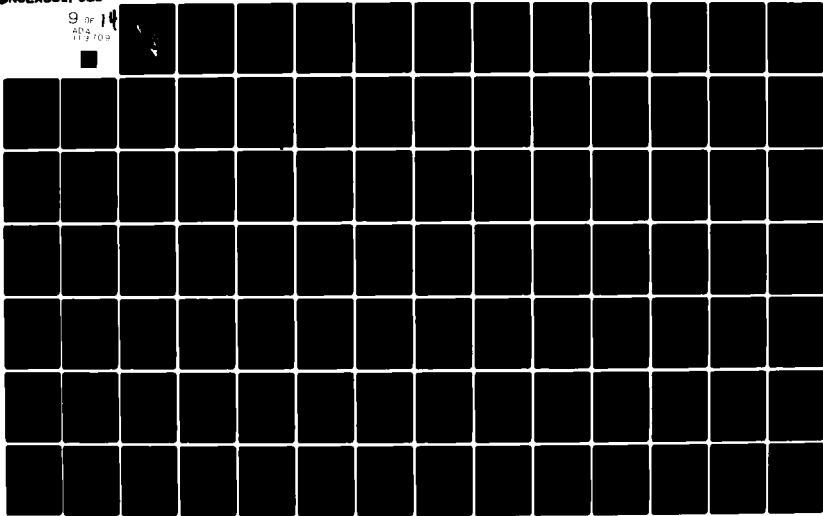
SOUTHEASTERN CENTER FOR ELECTRICAL ENGINEERING EDUCAT--ETC F/S 5/1
USAF SUMMER FACULTY RESEARCH PROGRAM. 1981 RESEARCH REPORTS. VO--ETC(U)
OCT 81 W D PEELE F49620-79-C-0038

AFOSR-TR-82-0226

NL

UNCLASSIFIED

9 of 14
404
117 709



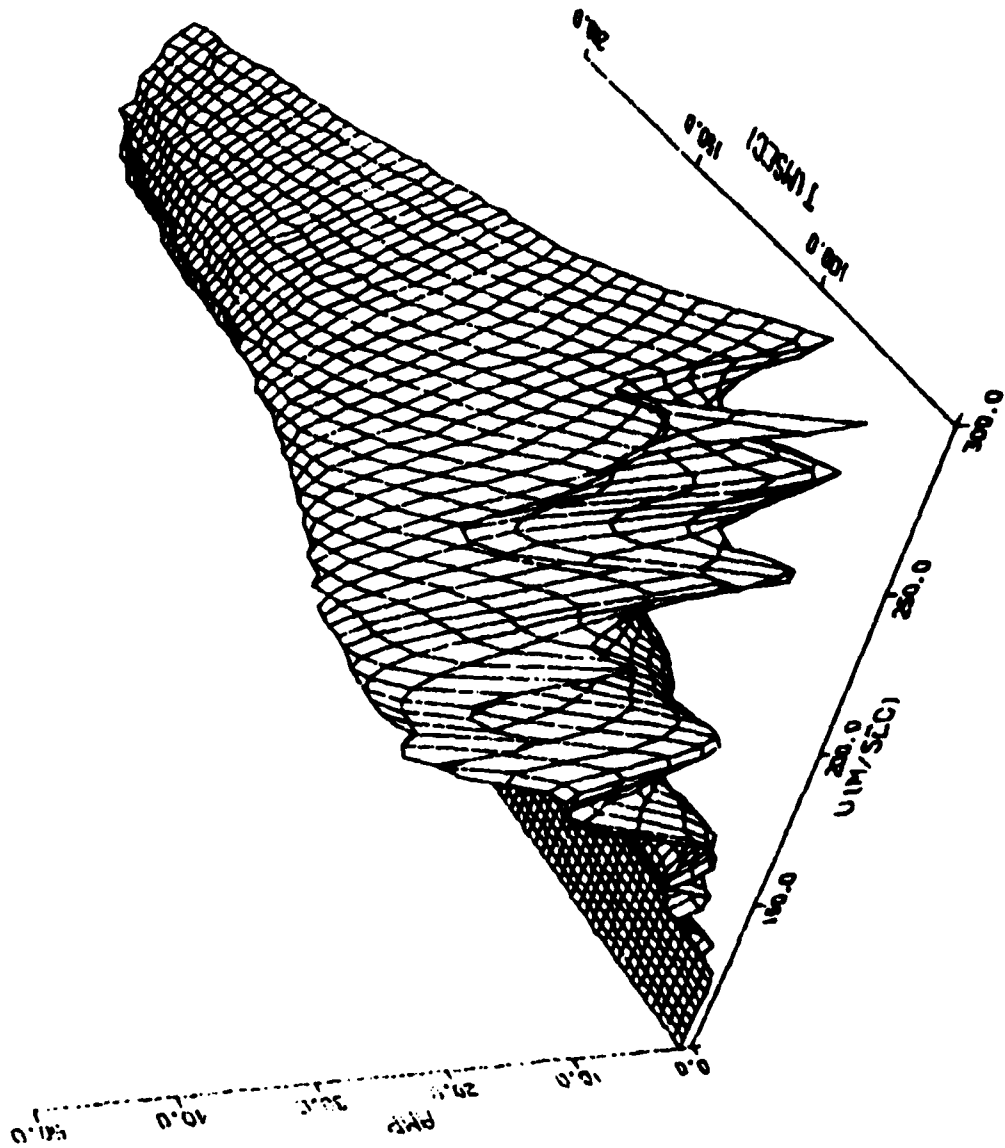


Figure 10: Moving window technique results for PMP-08 recorded at a distance of 228.6 m.

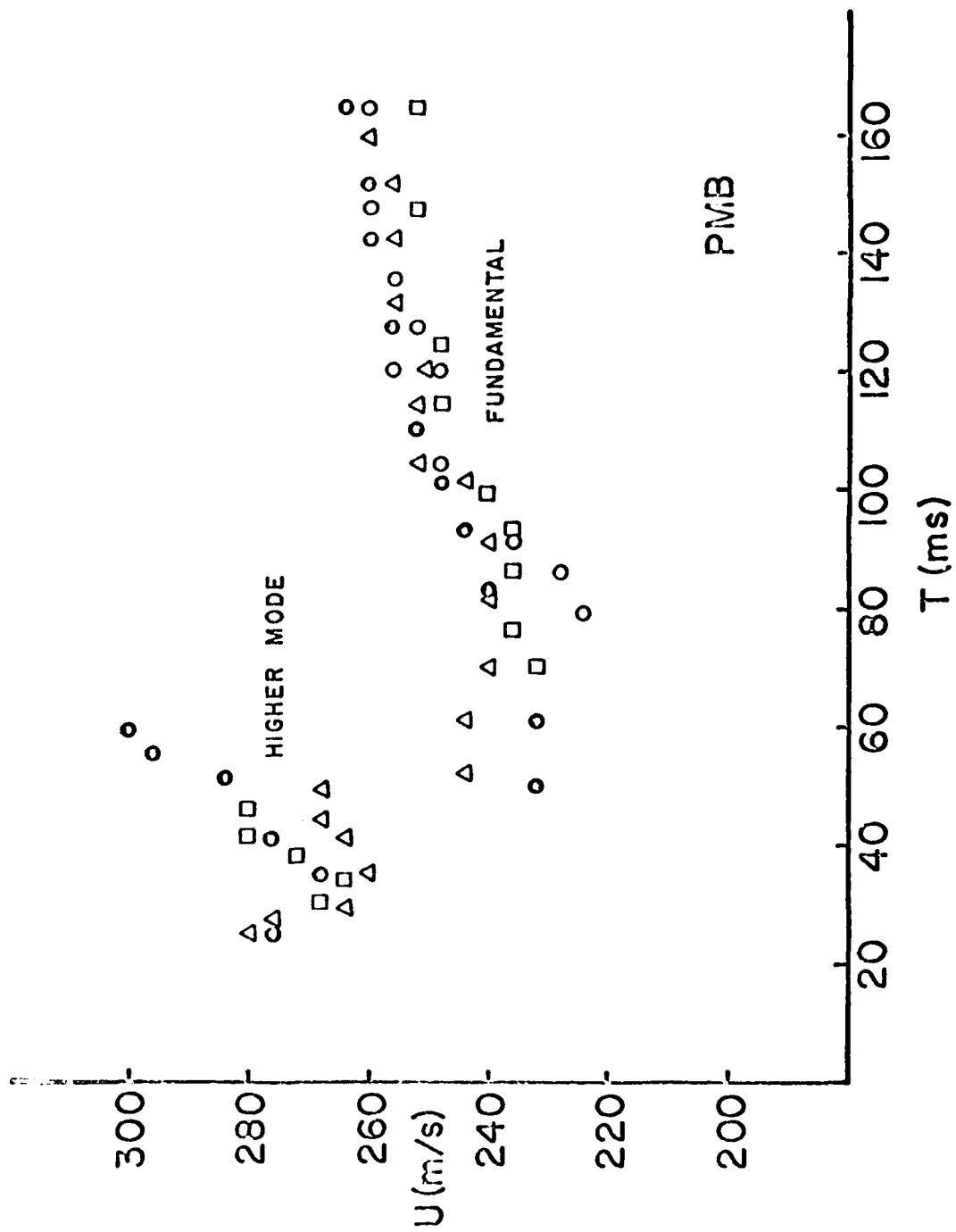


Figure 11. Rayleigh-wave group-velocity dispersion for PMB data set.

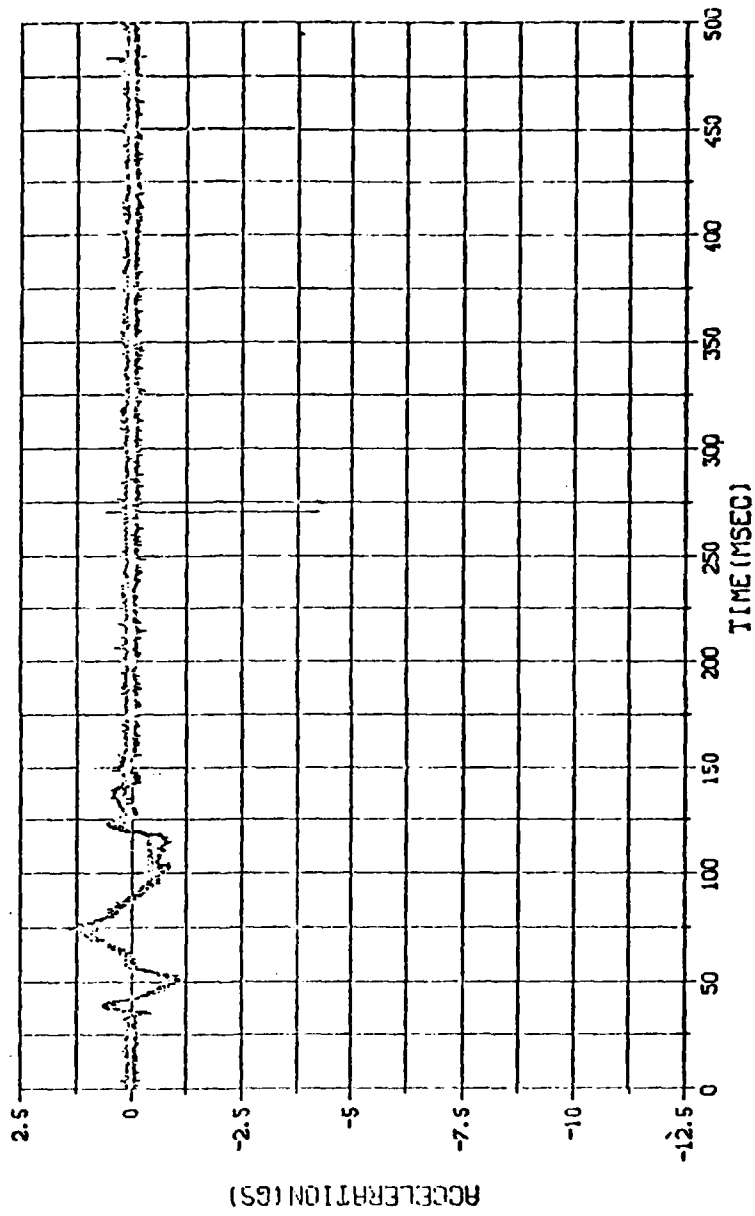


Figure 12. PHG ground motion record at distance 10.9 m.

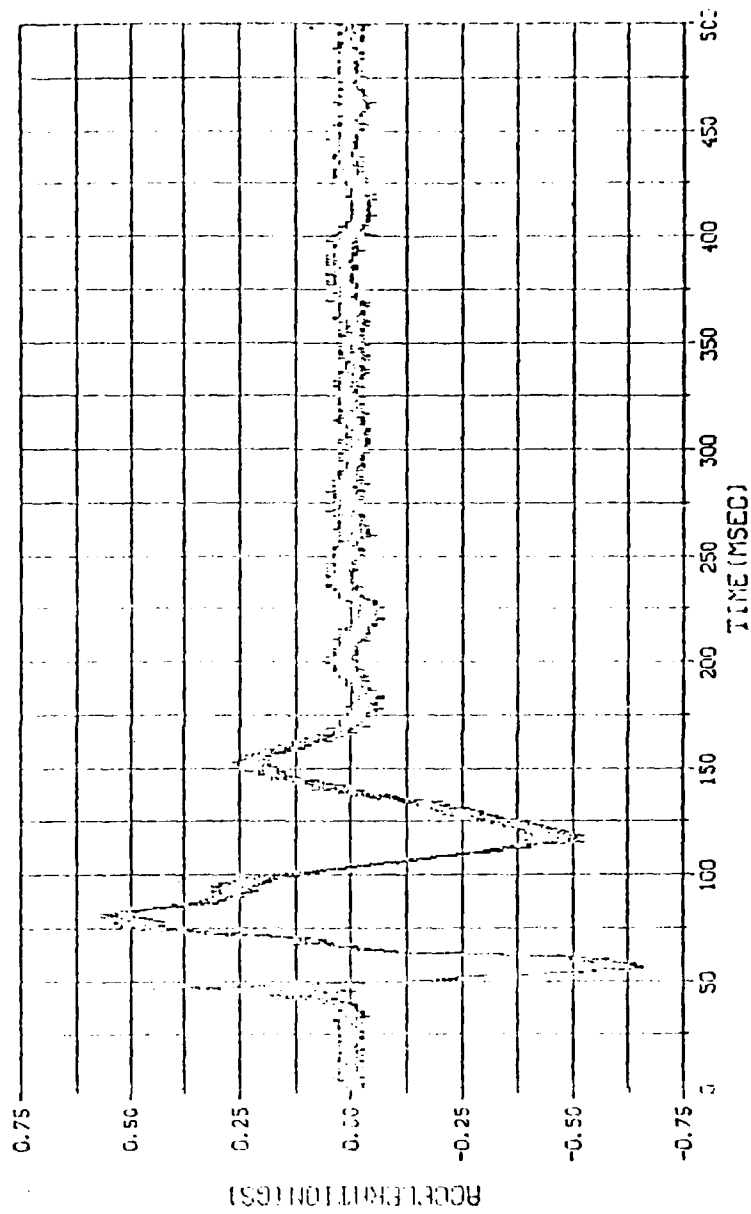


Figure 13. PHG ground motion record at distance 14.6 m.

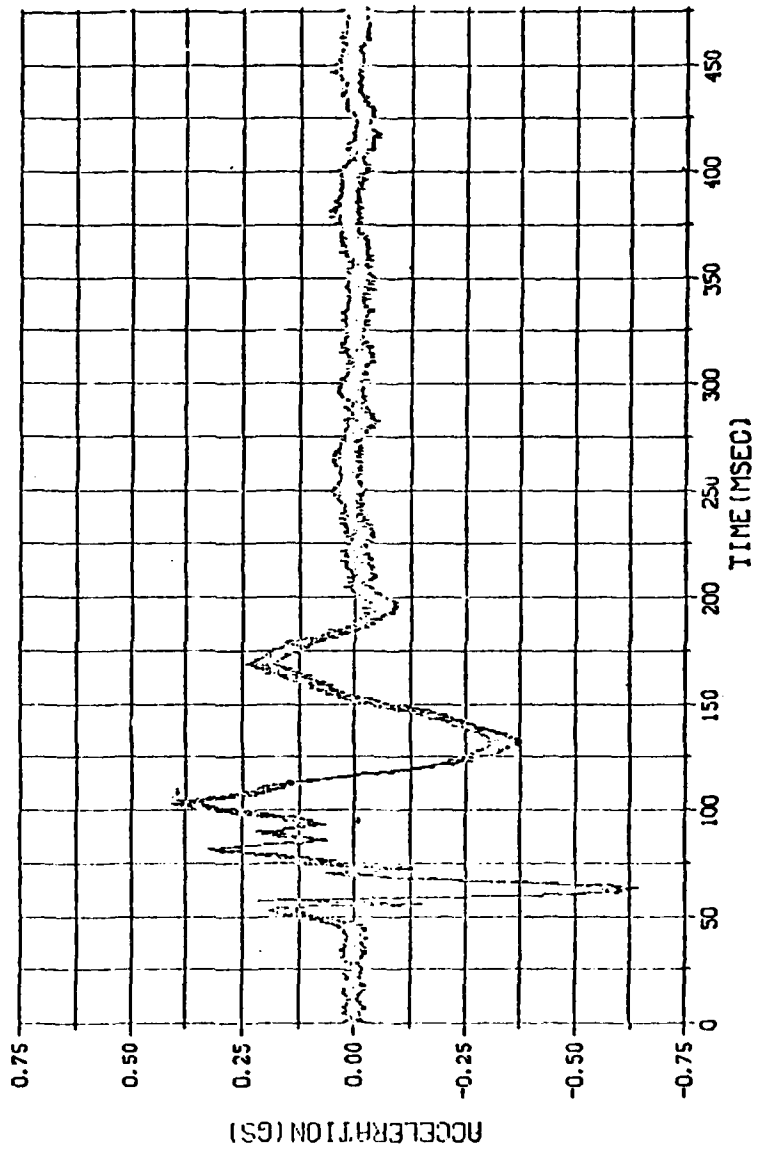


Figure 14. PHG ground motion record at distance 18.4 m.

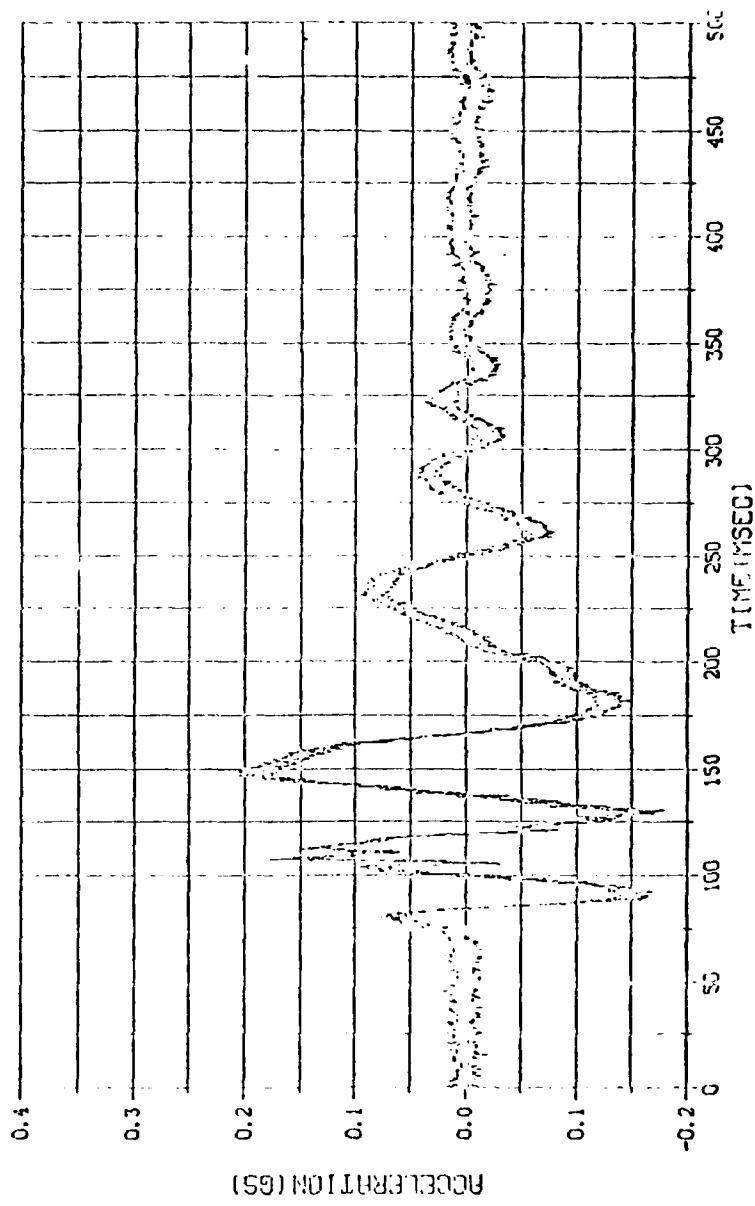


Figure 15. PHG ground motion record at distance 35.8 m.

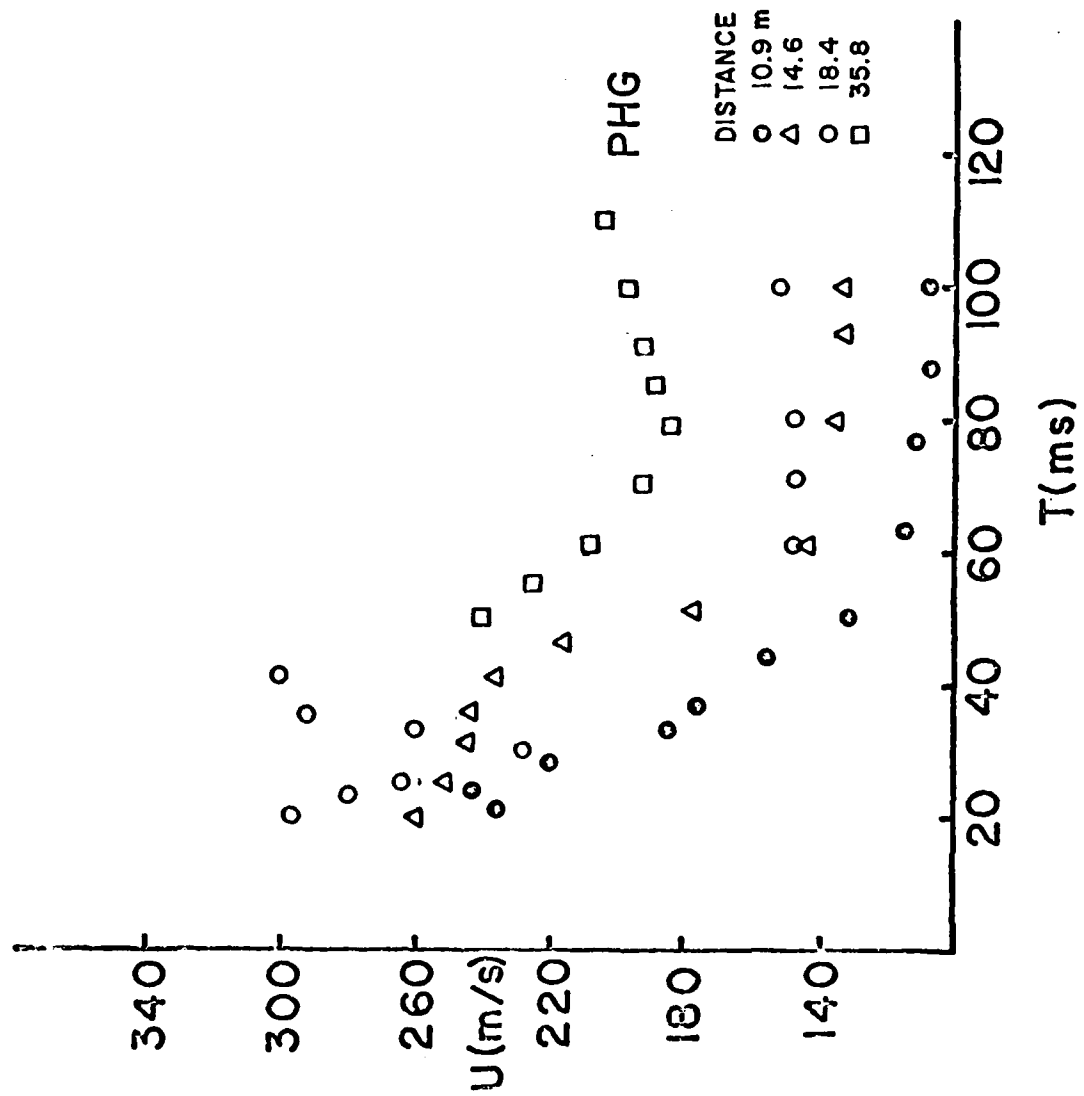


Figure 16. Rayleigh-wave group-velocity dispersion for PHG data set.

senting either a higher-mode Rayleigh-wave or possible body wave. The longer period dispersion may still represent the spall phase at this distance. At the distance of 35.8 m, the dispersion pattern is typical for a fundamental Rayleigh-wave mode. The associated group velocities are 240-200 m/sec with T=50-110 msec. These velocities are approximately 20% slower at T=80 msec than those observed from the PMB data even though the test site is the same.

Theoretical dispersion curves are generated to match the observed Rayleigh-wave group velocities by utilizing the Haskell method³. The technique requires a model with parallel layers to simulate the near-surface geologic structure. The input elastic parameters are P- and S-wave velocities, density, and layer thickness. The Haskell method is used with a trial and error approach of selecting model parameters to generate dispersion curves which match the observed data. Consequently, several models will produce satisfactory data fits. Two crustal velocity models have been determined for the McCormick Ranch from previous geophysical studies⁴. The model parameters are presented in Table 1.

The dispersion curves from the PMB data set and theoretical models are presented in Figure 17. The dispersion curves from the two models provide an approximate upper and lower bound for the observed data in the period range of 100-160 msec. Good agreement of the data sets occur for the periods T=70-90 msec. In general, at a depth of $0.4 \lambda_R$ (wavelength of the Rayleigh waves). The shear wave velocity has the greatest effect on the value of the group velocity at the given period. Thus, if the period is 160 msec, the Rayleigh waves are influenced by a corresponding depth of about 22 m. Consequently, the group-velocity dispersion data are limited in the resolution of the model depth and associated shear-wave velocity distribution.

In conclusion, fundamental-mode Rayleigh-wave group-velocity dispersion has been determined from high-explosive ground-motion records by using the moving window technique. The shear-wave velocity for the McCormick Ranch test site is approximately 244-400 m/sec for depths 0 to 22 m. These results provide important information for the propagation path required for the synthetic modeling of ground motion records.

TABLE 1
VELOCITY MODEL PARAMETERS

<u>Model</u>	<u>V_p(m/s)</u>	<u>V_s(m/s)</u>	<u>ρ (gm/cc)</u>	<u>h(m)</u>
M1	366	244	1.80	4
	671	366	1.90	10
	823	366	2.00	10
	1130	610	2.10	-
M2	366	244	1.80	4
	671	366	1.90	10
	823	400	1.90	-

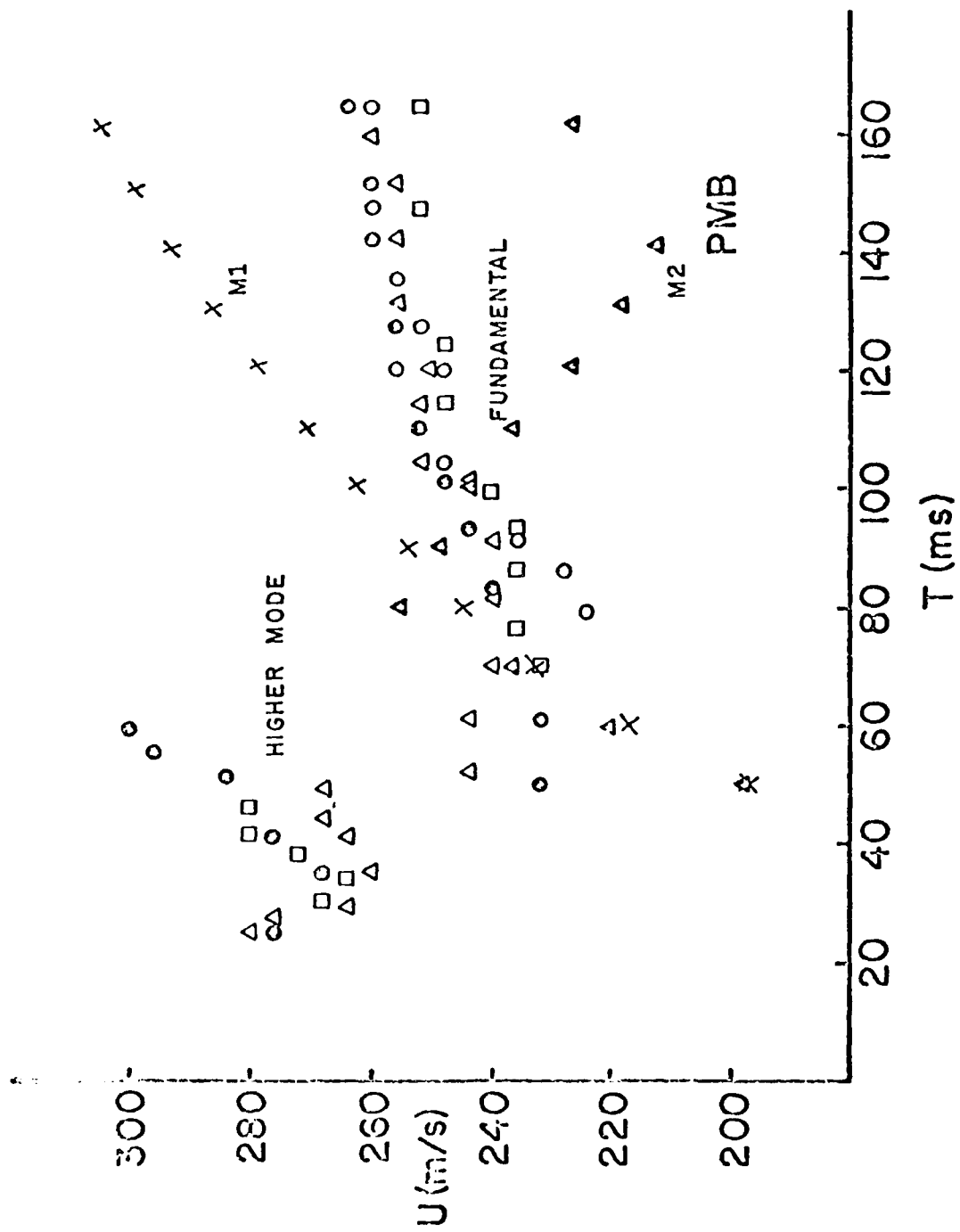


Figure 17. Dispersion curves for PMB data set and theoretical models M1 and M2.

REFERENCES

1. Kovach, R. L., "Seismic Surface Waves and Crustal and Upper Mantle Structure", Reviews of Geophysics and Space Physics, Vol. 16, pp. 1-13, 1978.
2. Landisman, M., A. Dziewonski, and Y. Sato, "Recent Improvements in the Analysis of Surface Wave Observations", Geophys. J. R. astr. Soc., Vol. 17, pp. 369-403, 1969.
3. Haskell, N. A., "The Dispersion of Surface Waves on Multilayered Media", Bull. Seis. Soc. Amer., Vol. 43, pp. 17-34, 1953.
4. Stump, B. W. and R. E. Reinke, "Geophysical Studies at McCormick Ranch, New Mexico and the Importance of Spall Waveforms in High-Explosive Testing", Technical Report (in preparation), Air Force Weapons Lab, Kirtland AFB, 1981.
5. Brown, R. W., "Pre-Multiple Burst (PMB II-78) Data Report", AFWL-TR-79-206, Air Force Weapons Lab, Kirtland AFB, 1980.
6. Babcock, S., "Prehybrid Gust Phase II Quick Look Report" CERF-AG-27, Engineering Research Institute, Univ. of New Mexico, 1980.
7. Stump, B. W., "Source Characterization of Bermed Surface Bursts", Technical Report (in preparation), Air Force Weapons Lab, Kirtland AFB, 1981.

VI. RECOMMENDATIONS

The moving window analysis technique has proved successful in extracting Rayleigh-wave group-velocity dispersion data from high-explosive ground motion data. Some of the results indicate that the body waves may also exhibit dispersion, and that the spall phase has minor dispersion. The forward Haskell modeling process produced two satisfactory shear-wave velocity models, but details of the model parameters were not resolved.

Based on these results from the present research, I propose the following recommendations for future research:

- 1) Resolve the detailed shear-wave velocity distribution by using an iterative inversion technique to model the dispersion data rather than the forward trial and error approach.
- 2) Investigate the possible body-wave dispersion character by utilizing the moving window technique for a high frequency range (less than 20 msec). Also investigate whether dispersion occurs as a function of depth of recorder.

OPERATING VARIOUS SUBSYSTEMS OF THE TOTAL
SIMULATION SYSTEMS FOR FLIGHT TRAINING

by

Dr. Vina Sloan

ABSTRACT

In order for these results to be valid, it is necessary for the configuration and performance of the subsystems involved be known and to remain constant during the research project so that measured performance variation can be correctly attributed to subjects performance variations. In addition, that configuration control should be maintained over the entire system so that intellegent decisions can be made regarding the allocation of resources and establishment of priorities for the development of the system. This refers and is directed toward establishing these configuration control policies.

* This report may be obtained by request from AFHRL/OTF,
Williams AFB, AZ 85224.

1981 USAF - SCEEE SUMMER FACULTY RESEARCH PROGRAM

Sponsored by the

AIR FORCE OFFICE OF SCIENTIFIC RESEARCH

Conducted by the

SOUTHEASTERN CENTER FOR ELECTRICAL ENGINEERING EDUCATION

FINAL REPORT

ENHANCING CAREER DEVELOPMENT AT THE AIR FORCE ROCKET

PROPULSION LABORATORY

Prepared by:	Dr. Russ Smith
Academic Rank:	Assistant Professor
Department and University:	Department of Political Science North Texas State University
Research Location:	Air Force Rocket Propulsion Laboratory, Edwards Air Force Base, California
USAF Research Colleagues:	Ms. Margret Waldie and Dr. J. Daniel Stewart
Date:	5 August, 1981
Contract No.:	F49620-79-C-0038

ENHANCING CAREER DEVELOPMENT AT THE AIR FORCE ROCKET

PROPULSION LABORATORY

by

Russ Smith

ABSTRACT

The importance of an effective career development program for an R & D organization, especially for a major Air Force laboratory is investigated. There was widespread interest in an enhanced program at the Rocket Propulsion Laboratory. An exhaustive analysis of top management's concerns, capabilities and constraints of the military and civilian personnel systems, supervisors' and managers' criteria for selection, promotion and transfer, and employees' expectations of a career development program was conducted. This research led to the generation of twenty-five recommendations. Suggestions for further research in this area are offered.

Acknowledgement:

The author would like to thank the Air Force Systems Command, the Air Force Office of Scientific Research and the Southeastern Center for Electrical Engineering Education for providing him with the opportunity to spend an intellectually stimulating summer at the Air Force Rocket Propulsion Laboratory. He would like to especially acknowledge the assistance and support provided by the Laboratory Command Section personnel.

The author would like to thank Ms. Margret Waldie of the Civilian Personnel Office for her invaluable assistance throughout the course of the project. The author would also like to thank Dr. J. Daniel Stewart for faciitating the research and for his collaboration and guidance. Finally, he would like to acknowledge the extensive information provided by numerous Laboratory personnel, especially Mr. Eugene Haberman and Ms. Sharrie Spicher, of the Civilian Personnel Office.

I. Introduction:

"Career development" encompasses a variety of concerns important to the successful operation of any large organization, especially research and development ones. Among the more important concerns in career development we may include professional obsolescence (of engineers, scientists and managers), employee turnover (due to a perceived lack of opportunities for growth), and human resources planning (anticipating future needs of the organization).

Top management of the Air Force Rocket Propulsion Laboratory (RPL) concluded in 1979 that there was a need to enhance career development and established it as an objective in RPL's 1981 Operational Plan.¹ An Organizational Assessment Survey conducted by the Air Force Leadership Management and Development Center (LMDC) underscored employees' concerns about career development: in the 1981 survey, the factor "Advancement/Recognition" for RPL was 3.79; at a "similar" AF Laboratory this score was 4.11.* This score was also much lower than the scores for all other measures of job satisfaction at RPL.

Several organizations or individuals have recognized either the need to be aware of individuals' perceptions of career development opportunities in an organization (because of their effect on productivity and behavior) or its utility to the organization. Thompson and Dalton noted that the lack of career development in R & D organizations hastened the obsolescence of professionals and managers and gave employees the mistaken belief that career development only meant promotions.¹¹ Gautschi argued that engineers became dissatisfied with an organization when their only career development option was to become a manager, with infrequent opportunities to use engineering expertise.²

*These scores are based on individuals' responses to several items, with values ranging from 1 (low) to 7 (high). The items were then averaged for each person to generate an individual's factor score; the values reported here are lab-wide mean scores.

The Dahlgren Laboratory of the Surface Naval Weapons Center recognized the importance of a career development program in providing talented executive personnel. The Laboratory's program makes extensive use of lateral moves by its mid-level managerial personnel to "groom" them for top management positions.⁷ Other organizations, including R&D organizations, have also established career development programs to prepare people for higher level positions or to enhance job satisfaction.^{5,8} Finally, the USAF has a sophisticated system for the training, development, procurement and utilization of officers, based on a complex career development plan for this force.¹²

RPL decided in early 1981 to use the Office of Scientific Research's Summer Faculty Research Program to get someone to help local personnel create an RPL career development program.

II. Objectives:

The main objective of this project was to develop a set of recommendations for enhancing career development for RPL employees. The Laboratory's Program Council (i.e., top management) would then review these and decide whether to implement them. Implicitly, the researcher was also to examine the results of the Organizational Assessment Package (OAP) survey to ascertain the relationship between measures of job satisfaction and measures of attitudes about the career development program at RPL.

Early in the project, a decision was made to gather additional data to use in developing the recommendations. Four kinds of additional data were identified; top management's concerns about career development; the capabilities and constraints inherent in the military and civilian personnel systems; supervisors' and managers' criteria for selection, promotion and transfer; and individuals' expectations of how to achieve successful careers.

III. Approaches:

The objectives were obtained by a variety of methods. A team was created, involving the researcher and Ms. Margret Waldie (Training and Development Specialist) and Ms. Sharrie Spicher (Classification Specialist), both of the Civilian Personnel Office, Edwards AFB. The team informally included Dr. J. D. Stewart, Special Assistant, Research and Technology Management, RPL.

Processing the OAP survey entailed simply an examination of statistical relationships between measures of job satisfaction and measure of attitudes about the career development program at RPL. Due to limitations in analytical capabilities at LMDC, analysis was limited to univariable and bivariate frequency distributions, Pearson's r correlations, and stepwise linear regression (using dummy variables). The bivariate and multivariate (linear, additive) analyses produced no statistically significant associations between the two sets of measures.

Top management's concerns about career development were ascertained through the use of interviews. The Director, Chief Scientist and three division heads were asked to identify their concerns about career development. These interviews indicated concerns that: 1) employees perceive that lateral moves and intensified training, in addition to promotions, constitute career development; 2) employees perceive that they have primary responsibility for their own development; 3) employees should not be given unrealistic (or unattainable) expectations about career development due to data gathering or analysis (i.e., as side effects); and 4) implementation of any recommendations would be the responsibility of the Program Council or someone they designate.

Supervisors' and managers' criteria for selection, promotion and transfer were obtained in a survey sent to all section or higher level personnel; the response rate was 51%. Among a variety of criteria, the most important were formal educational background, related prior work experience, enthusiasm for the position, and communication skills.

Employees at RPL were designated as being in one of seven "career groups" (sets of allied career fields); officers, enlisted technicians (mechanics, etc.), enlisted support (clericals, etc.), scientists and engineers, General Schedule technicians (electronic engineer technicians, etc.) General Schedule support (clericals, etc.), and Wage Grade technicians (machinists, etc.). A "sample" of twelve to sixteen people was drawn from each group, stratified by level of experience/responsibility and division. Each "sample" then participated in an information-gathering workshop based on the Nominal Group Technique. Basically, people shared with each other, then rank-ordered the criteria which they believed would help someone develop within the career group. These groups of employees stressed the need for more training (especially among technicians), more information about career development, and more opportunities to show their abilities or growth potential to management.

Finally, the research team pooled the data noted above plus their own knowledge about career development done elsewhere and the capabilities and constraints of the military and civilian personnel systems to create recommendations for enhancing career development at RPL. These recommendations were presented to the Program Council on 5 August, 1981.

IV. Recommendations for Enhancing Career Development:

The numerous recommendations proposed here are designed to address career development concerns expressed by top management, supervisors and managers, and a variety of employees. The primary consideration was to help RPL make the best use of its human resources in achieving its goals.

The recommendations are presented in the order of their apparent ease and cost of implementation. Recommendations in the first group should be the easiest and least costly way to enhance career development at RPL. All of the recommendations, if

implemented, would make RPL the only organization to do as much to efficiently utilize human resources while showing an interest in its employees' career development.

Many of the recommendations provide ancillary payoffs, principally with regard to employee job satisfaction and sense of recognition. Since the Hawthorne studies of the 1930s, researchers have noted the tremendous effect of achieving "psychological success" (a feeling of having accomplished a difficult task or job) on productivity, behavior on the job, and job satisfaction.^{3,4,6,7,8,9,10,11} Implementation of these recommendations would demonstrate to employees top management's concern for employees while helping top management efficiently use its human resources.

Group 1: Minor Changes/Minimal Cost to RPL:

1. **MANAGER MENTORS:** Mid-level managers volunteer to serve as mentors for newly-appointed supervisors/managers, to help them learn RPL's expectations of managers. Two or three people would be designated for a six month period. Such work might be noted in later promotions.
2. **CIVILIAN SPONSORS:** Mid-level non-managers volunteer to serve as sponsors for new civilian employees, to facilitate their adjustment to RPL. One or two people per career group would be designated for a six month period. Such work might be noted in later promotions.
3. **DIVISION TRAINING OFFICERS:** Senior managers volunteer to serve as DTOs, providing information about training opportunities to employees in the divisions, assisting in career counseling, and (in quarterly meetings), developing recommendations to the Program Council for future training needs. One person per division would be designated for a year. Such work might be noted for later promotions.

4. HUMAN RESOURCES COMMITTEE: Senior managers volunteer to serve on a Human Resources Committee to: a) share with each other the anticipated openings/personnel needs in their divisions; b) share with each other the names of people ready for/interested in position changes; c) share this information with their parent divisions; and d) gather this information from their parent divisions. One person per division (not the DTO) would be designated to serve for a year. Such work might be noted for later promotion.
5. BRIEFING ON CAREER CHANGES: Military and Civilian Personnel Office (MPO/CPO) personnel would brief, every six months, anyone interested in changing AFSC codes, cross-training, or moving into new career fields.
6. BRIEFING ON CAREER DEVELOPMENT FOR SUPERVISORS OF WAGE GRADE EMPLOYEES: CPO would brief supervisors of Wage Grade employees about training opportunities available for such people, answer questions, and help with related paperwork. Mandatory participation for first-level supervisors of such employees.
7. BRIEFING ON CAREER DEVELOPMENT FOR SUPERVISORS OF ENLISTED PERSONNEL: MPO would brief supervisors (especially civilians) of enlisted personnel about training opportunities available; help with related paperwork, and clarify the special needs of such people (e.g., awards). Mandatory participation for first-level supervisors of such employees.
8. BRIEFING ON THE CIVILIAN PERSONNEL SYSTEM: CPO would brief all interested employees on aspects of/changes in the civilian personnel system, answer questions, and help with related paperwork. Participation would be voluntary.
9. CAREER DEVELOPMENT OPPORTUNITIES FOR AF PERSONNEL: MPO would brief all interested people on aspects of/changes in the military personnel system, answer questions, and help with related paperwork. Participation would be voluntary.

10. **RPL TRAINING POLICY GUIDELINES:** A team of representatives of top management, RPL employees and MPO/CPO employees would codify RPL's training policies, including eligibility requirements, sample forms, etc. A copy of the guidelines would be kept with each division.
11. **POSITION SWAPPING:** When key positions are vacant because they require a specific type of employee (i.e, military or civilian) and none are available, RPL would temporarily detail a person to that position or would exchange the position for one of the other type.

Group 2: Major Changes/Minimal Cost to RPL:

12. **COLLEGE EDUCATION:** Increase availability of undergraduate college courses offered on-site, especially non-job-related courses.
13. **CLERICAL ORIENTATION:** Newly-hired clerical employees would spend their first week at RPL assigned to a senior secretary to learn RPL's procedures and expectations of clericals, after which they would be assigned to the Administrative Section.
14. **SIX MONTH TRAINING PLAN:** New people would be assisted by someone at RPL in developing training goals to be accomplished during their first six months at RPL.

Group 3: Major Changes/Increased Cost to RPL:

15. **RPL AWARDS:** A team comprised of representatives of top management and employees would design RPL awards (and procedures to give them). The awards could include certificates for special duties, completion of self-improvement efforts, contributions to special projects, etc.
16. **SUPERVISOR TRAINING PROGRAM:** Every two months, a different group of first-level supervisors would be given training in career development enhancing behaviors, such as: a) how to enrich jobs; b) how to do informal, short-

term goal-setting; c) how to be assertive when giving feedback on performance; d) how to give people support (i.e., "stroking") for their self-improvement efforts.

17. **MANAGER ROTATION:** Treat all supervisory/managerial jobs as interdisciplinary (where possible) to facilitate lateral movement of people in a "management track."
18. **ADVANCED TECHNICAL TRACK:** Treat all advanced technical jobs (AFSC codes 2600, 2800 or CPO codes 800, 1300, GS-13 to GS-15) as Research General Engineer/Physical Scientist positions. These may then be filled by most engineers or scientists, increasing the number of advanced non-managerial positions in the Lab.
19. **TEMPORARY DETAILS:** As a corollary to Item 11, when RPL needs a key position filled, temporarily detail a qualified person (for up to 120 days) to the position. Moves should be to fill RPL needs, thereby obviating the need for competition for such positions; where possible, assignments should be to different divisions.
20. **INCREASED OFF-SITE TRAINING:** Provide more opportunities, especially to technical personnel, to go off-site to other organizations for training (e.g., other labs, other bases, contractors). (More opportunities for technicians were indicated during data gathering as very great needs among those personnel).
21. **ENHANCING IDPS:** Redefine the Individual Development Plan (IDP) process so RPL can use it in determining training needs, budgeting and human resource planning. Also, people might view the process as more meaningful if IDPs were used to help select people for participation in Items 5, 11, 12, 14, 17, 18, 19, and 20.

Group 4: Major Changes/Greatest Cost to RPL:

22. **RPL TRAINING & DEVELOPMENT COORDINATOR (TDC):** Create a position with Lab-wide responsibility for coordinating training and development acti-

vities at RPL. The person would play a key role in implementing or facilitating most of the recommendations proposed here.

23. FEEDER PROGRAMS: Use existing programs to help employees become scientists and engineers, to help meet RPL's personnel needs. The TDC would help RPL employees enter feeder programs.
24. CAREER PLANNING WORKSHOP: Small groups of employees may volunteer to participate in career planning workshops in which they: a) are informed about top management's expectations and opportunities at RPL; b) participate in a planning exercise (e.g., "Exercises Future")¹³; and c) set short- and long-term goals in their IDPs.⁸
25. RPL TRAINING AND DEVELOPMENT CENTER: Designate a permanent space as a T & D Center which; a) is staffed full-time by the TDC; b) is conveniently located so all Lab personnel can use it; has information on military and civilian training programs, application forms, etc.; d) has self-placed learning equipment (VCRs, books, et.) and a list of "resource people" who will answer questions which arise during one's self-study; and e) information and forms for college and vocational education courses.

In addition to implementing these recommendations, there are two other activities RPL may do or sponsor. The first activity is a more thorough analysis of the OAP survey data, including non-linear and non-additive multivariate statistics for ordinal-scale data. An interactive analysis, for example, may reveal relationships in the data that were suppressed by stepwise regression analysis.

Second, after some time has passed (perhaps a year), there should be a follow-up investigation of the effects of the implemented recommendations on self-improvement activities, performance, and attitudes about career development opportunities at RPL. At the very least, inspection of turnover data and another OAP survey could be used. Any more rigorous research might require outside help.

REFERENCES

1. Air Force Rocket Propulsion Laboratory, Management Improvement Plan and Assessment, (Edwards AFB, CA., February, 1981).
2. T. F. Gautschi, "Dual Ladder Career Paths," Design News, Vol. 36, pp. 280-281, 1980.
3. W. F. Glueck, "Career Management of Managerial, Professional and Technical Personnel," in Manpower Planning and Programming, E. Burack and J. Walker, eds., (Boston: Allyn & Bacon, Inc., 1972), pp. 239-256.
4. D. T. Hall and F. S. Hall, "What's New in Career Management," Organization Dynamics, Vol. 5, pp. 17-33, 1976.
5. Internal Revenue Service, Technical's Career System Handbook, (Washington: Department of the Treasury, October, 1973), IRM 18 (12) 7.
6. H. G. Kaufman, "Relationship of Early Work Challenge to Job Performance, Professional Contributions, and Competence of Engineers," Journal of Applied Psychology, Vol. 59, pp. 377-379, 1974.
7. P. L. Martin, "The Peripatetic Manager: Executive Rotation at Dahlgren Laboratory," Defense Management Journal, Vol. 15, pp. 6-13, 1979.
8. J. A. Miller, B. M. Bass, and W. L. Mihal, An Experiment to Test Methods of Increasing Self-Development Activities Among Research and Development Personnel, Technical Report 43, (Management Research Center, University of Rochester, Rochester, N.Y., February, 1973).
9. E. H. Schein, "The Individual, the Organization, and the Career: A Conceptual Scheme," Journal of Applied Behavioral Psychology, Vol. 7, pp. 401-26, 1971.
10. D. E. Super and D. T. Hall, "Career Development: Exploration and Planning," Annual Review of Psychology, Vol. 29, pp. 373-404, 1978.
11. P. H. Thompson and G. W. Dalton, "Are R & D Organizations Obsolete?" Harvard Business Review, Vol. 54, pp. 105-116, 1976.

12. U. S. Air Force, Officer Career Development, AFM 36-23 (Washington, D.C., December, 1979).
13. J. Vaughn, Exercise Future: A Program of Exercises for Management and Organization Development, 3d Rev. Ed., (Pittsburgh, Instad Ltd., 1974).

1981 USAF - SCEEE SUMMER FACULTY RESEARCH PROGRAM

Sponsored by the

AIR FORCE OFFICE OF SCIENTIFIC RESEARCH

Conducted by the

SOUTHEASTERN CENTER FOR ELECTRICAL ENGINEERING EDUCATION

FINAL REPORT

DEVELOPMENT OF A COMPUTER ALGORITHM FOR THE AUTOMATIC DETERMINATION OF
SPACE VEHICLE POTENTIAL UTILIZING ELECTROSTATIC ANALYZER MEASUREMENTS.

Prepared by: Dr. Stanley L. Spiegel
Academic Rank: Assistant Professor
Department and University: Department of Mathematics
University of Lowell
Research Location: Air Force Geophysics Laboratory
Space Physics Division, Spacecraft Environment Branch
USAF Research Colleague: Mr. Herbert A. Cohen
Date: 10 September 1981
Contract No: F49620-79-C-0038

DEVELOPMENT OF A COMPUTER ALGORITHM FOR THE AUTOMATIC DETERMINATION OF SPACE
VEHICLE POTENTIAL UTILIZING ELECTROSTATIC ANALYZER MEASUREMENTS.

by

Stanley L. Spiegel

ABSTRACT

A real time technique for determining space vehicle potential using electrostatic analyzer (ESA) positive ion count data has been developed. The method involves examining the count ratios in adjacent ESA energy channels and searching for a precipitous increase in this ratio with increasing energy, or alternatively for a statistically significant increase in the plasma distribution function, derivable from the ion counts. The satisfaction of either condition indicates charging to the level of the higher ESA channel. Tests of the algorithm, using data from the P78-2 satellite have shown excellent agreement with independent estimates of vehicle potential. Hence the algorithm appears suitable to be employed with an ESA of appropriate design for the purpose of automatically activating discharge mechanisms should vehicle potential exceed some critical value.

Acknowledgement

I would like to express my appreciation to the Air Force Systems Command, the Air Force Office of Scientific Research and the Southeastern Center for Electrical Engineering Education for support to work on a challenging and important problem this summer at the Air Force Geophysics Laboratory, Hanscom AFB, MA. Thanks are due especially to Mr. Herbert A. Cohen of the Spacecraft Environment Branch for suggesting this research topic, and for his continuing interest and guidance. I should also like to acknowledge the pleasurable and helpful interactions with Mr. William Huber, 1st Lieutenant Allen Chesley, and Captain David Hardy, that were of significant assistance in this research.

I. INTRODUCTION:

The problem of spacecraft charging at high altitudes is an important one for Air Force applications; indeed a major effort (SCATHA Project) has been undertaken to understand this phenomenon. Quite simply, when a space vehicle at geosynchronous orbit, interacting with its plasma environment, acquires a high negative potential (of the order of 1/2 kilovolt), it is possible that onboard instrumentation will be damaged by electrical discharge between differentially charged components of the spacecraft. Thus it is important to activate a discharge mechanism as soon as a dangerously high potential develops. This means it is important to have a reliable, real time method of determining the vehicle potential, or more specifically, whether or not the critical potential has been reached or exceeded. An algorithm incorporating an onboard microprocessor to analyze data obtained by the vehicle, and determine the extent of charging, is desirable. Computational simplicity and speed are important considerations in design of such an algorithm. Preliminary work by the author¹ indicated that electrostatic analyzer (ESA) positive ion count data, of the type provided by the SC9 experiment of the P78-2 satellite, could serve as input to an algorithm designed to fulfill the aforementioned objectives. The continued development and testing of this method are described below.

II. OBJECTIVES:

One main objective of this effort was to examine in greater detail an algorithm of the type previously devised by the author (Spiegel 1980). This algorithm examined the positive ion counts in adjacent ESA energy channels and reported vehicle charging if an empirically determined critical high-to-low channel count ratio was reached or exceeded. It was

planned that this algorithm would be tested on SC9 count data from a wide variety of ambient conditions to determine its continued success at estimating vehicle potential.

A second objective was to develop an approach which utilized ion count data to compute the ion distribution function. It was expected on physical grounds that the shape of this distribution function could serve as an indicator of vehicle potential. Further, it was hoped that this type of algorithm would be less instrument dependent than one which analyzed the counts themselves, whose channel to channel variations depends heavily on instrument design. This algorithm would also be tested on a wide variety of data.

An additional objective was to determine criteria regarding the number of ion counts necessary to guard against spurious reports of charging owing to random fluctuations in count rates.

A further goal was to see whether the algorithms could work successfully on ion count data from a differently designed ESA, that of the SC5 experiment onboard the P78-2 satellite.

A final objective was to attempt to determine desirable characteristics for an ESA designed for the task of detecting critical charging.

III. THE COUNTS ALGORITHM

One of the instruments aboard the P78-2 satellite, associated with the SC9 experiment, is a high resolution electrostatic analyzer. Among other functions, this instrument counts the number of positive and negatively charged particles (protons and electrons) incident upon it in each of 64 exponentially spaced energy channels that span the energy range 0 to 81 keV, during sequential 250 m sec time intervals. The 64 energy channels have mid-channel energies given (in eV) by:

$$E(I) = 16.1(1.145)^I - 21 + \frac{28}{I+129}, I = 0, 1, \dots, 63$$

(1)

and the ratio of channel width to mid-channel energy is essentially constant at about 20% over the entire spectrum. There is very little overlap in energy response between adjacent channels. Hence the SC9 ESA provides high resolution in particle number flux during each 16 sec sweep through its 64 channels.

When the spacecraft is at zero potential with respect to the ambient plasma, the ESA design is such that the number of positive ion counts per channel shows a modest increase with energy over most of the 64 channel energy range. But when the spacecraft has acquired a negative potential with respect to the plasma, positive ions approaching the instrument will be accelerated by this potential difference. As a result, the number of ion counts in energy channels below the level of charging would ideally drop to zero and there would be an increase in the number of counts in the channel at and just above the level of charging. Examination of SC9 ion count data shows this effect quite clearly: while for various reasons, the zero count rate is not exactly achieved, the presence of spacecraft charging is characterized by a very low count rate in all channels up to a certain energy followed by a sharp increase in counts in the next several channels. A graph of counts vs energy resembles a step function during vehicle charging, in contrast to the slow rise associated with the uncharged state. The so called counts algorithm utilizes this phenomenon to determine the spacecraft potential.

The algorithm consists of examining the counts in adjacent energy channels to determine if the upper-to-lower energy count rate has reached or exceeded some empirically determined critical value that will distinguish between a charged and uncharged spacecraft. Since the particle counts are a random event (Poisson process), it is necessary to require that some minimal number of counts be obtained in order for the count rate to be used to diagnose charging. (Otherwise, random fluctuations would result in spurious reports of charging at low count rates.) This minimal number of counts is also empirically determined. Based on data from several days during which the spacecraft was negatively charged part of the time, a critical count ratio of 4.5 with a threshold requirement of at least 90 counts in the upper energy channel, were found to give good results. The results are improved by the following refinement: if the aforementioned criteria are satisfied (indicating vehicle charging), the next higher energy channel is examined to see whether there is a substantial further increase in counts (by a factor of two or more). If so, the level of charging is taken to be at this higher energy level, rather than the level of the initial precipitous increase.

This counts algorithm, with the above parameter values, has been tested on SC9 data from some 30 time intervals on different days, encompassing a variety of plasma environments. Its success, as measured by the fraction of time its predicted vehicle potential is within 20% of independent estimates of potential often exceeds 90%. A day by day summary of these results is tabulated Section IV below. Further testing may lead to adjustments in the count ratio

and threshold parameters to give even better results. (It should be remembered that for the purpose of triggering a vehicle discharge mechanism, a better measure of the algorithm's success is the fraction of time it correctly detects that a critical vehicle potential has or has not been reached; this analysis remains to be performed.)

In any event, the counts algorithm has proven to serve as a reasonably accurate voltmeter in its present form. It is quite suitable for real time implementation on a spacecraft microprocessor, requiring relatively little computation and data storage. One drawback is the ad hoc way in which the parameters are determined. It is reasonable to question whether the optimal critical count ratio should vary with the channel pair being compared. And since the count rate per channel of itself has no direct physical significance (being a function of ESA design as well as plasma properties) it is difficult to establish count ratio and threshold requirements in a physically and statistically meaningful way. Hence a major effort was made to develop an algorithm based on a physically significant quantity derivable from the SC9 ion counts: the plasma distribution function.

IV. THE DISTRIBUTION FUNCTION ALGORITHM

The distribution function gives the particle density in phase space (a six dimensional space in which a particle is described by three spatial coordinates and the corresponding three momentum coordinates). If the positive ion distribution function were known, then for an ESA with known sensitivity and energy response characteristics, one could calculate the count rate to be expected over a given energy interval. The computation can be readily reversed, so that with a measured spectrum of counts per unit time over a series of energy intervals, one can compute the positive ion distribution function. Its average value for protons over energy interval

$\Delta E(I)$ associated with the I th energy channel is given by

$$F(I) = \frac{5.45 \times 10^5 \cdot C(I)}{E(I) \cdot \Delta E(I) \cdot G(I)} \quad (2)$$

where $G(I)$ is the so called geometric factor of the ESA, a function of instrument design and efficiency which is determined by careful calibration for each individual channel. The numerical factor is chosen so that if $C(I)$ is given in counts per second, $E(I)$ and $\Delta E(I)$ in eV, and $G(I)$ in cm^2 -steradian, $F(I)$ will be in its customary units of sec^3/km^6 .

Now it is known that on physical grounds the distribution function is a decreasing function of energy, regardless of plasma temperature (or temperatures if more than one population is present). However, if the spacecraft is at a negative potential with respect to the plasma, the positive ion energy spectrum will be shifted by an amount equal to the vehicle potential. Thus the distribution function as measured by the ESA will be quite small (ideally zero) until the channel corresponding to vehicle potential is reached, at which point the computed distribution function will show a significant increase. (This is of course in keeping with Eq (2) and the count rate spectrum discussed in Sec. III). Hence the observation of an increase in distribution function with energy can serve as an indication of spacecraft charging.

Since the distribution function is derived from a randomly fluctuating count rate and imprecisely known instrument parameters, it is necessary to insure that any computed increase in distribution function be statistically significant. Thus the criterion for determining that the vehicle is charged is that $F(I+1) - F(I)$ exceed zero by some number of standard deviations of the distribution function difference. To compute this, one must first

compute the standard deviation in $F(I)$.

For the SC9 ESA, it can be shown that the denominator on the right hand side of (IV.1) can be rewritten in a form dependent only on $E(I)$, so that (2) becomes:

$$F(I) = \frac{1.70 \times 10^9 \cdot C(I)}{\left[1 + \frac{2}{1 + (E(I)/1500)^3}\right] [E(I)]^2} \quad (3)$$

On the assumption that the count rate is a Poisson process, its standard deviation is $C(I)^{1/2}$, and its fractional standard deviation (FSD) is $C(I)^{-1/2}$. To determine the standard deviation of the denominator in (3), one must make an assumption concerning the precision of $E(I)$. A probable error of one or two percent seems reasonable, hence an FSD of about 0.02 is assumed. This implies an FSD in $(E(I))^2$ of about 0.04. For values of $E(I)$ in the region of interest for critical charging (about 1/2 kilovolt) the FSD of the remaining factor in the denominator is negligible. Thus the FSD in $F(I)$ is approximately

$$\text{FSD}(F(I)) \doteq [(0.04)^2 + (C(I)^{-1/2})^2]^{1/2} \doteq [0.002 + C(I)^{-1}]^{1/2} \quad (4)$$

Finally, the standard deviation in $F(I+1) - F(I)$ is given by:

$$\text{SD}(F(I+1) - F(I)) = \left[\left(0.002 + \frac{1}{C(I+1)}\right) F(I+1)^2 + \left(0.002 + \frac{1}{C(I)}\right) F(I)^2 \right]^{1/2} \quad (5)$$

Hence the criterion for determining that the vehicle is charged is that

$$F(I+1) - F(I) \geq \gamma \cdot \text{SD}(F(I+1) - F(I)) \quad (6)$$

where γ , the standard deviation factor, is a positive constant. The choice $\gamma = 4$ has been found to give good results. In general, a high value of γ

will reduce the fraction of the time the algorithm will falsely report charging (to less than $1/\gamma^2$ of the time by Chebyshev's theorem), but this will be at the expense of increasing the number of times the algorithm will miss genuine charging. An additional condition is that if charging is detected at a given channel (I+1), F(I+2) is computed and if F(I+2)-F(I+1) exceeds F(I+1)-F(I), the potential is taken to be at E(I+2) instead of E(I+1).

This distribution function algorithm has been tested on the same data base as the counts algorithm described above, for the choice of $\gamma=4$. Its success at estimating vehicle potential to within 20% is indicated in the following table:

<u>Day</u>	<u>Counts Algorithm</u>	<u>Distribution Function Algorithm</u>
79086	.92	.93
79087	.86	.92
79098	.95	1.00
79100	.93	.95
79104	.96	.99
79105	.92	.97
79106	.97	.95
79108	.86	.96
79114	.71	.86
79117	.72	.93

<u>Day</u>	<u>Counts Algorithm</u>	<u>Distribution Function Algorithm</u>
79118	.92	.93
79120	.91	.94
79127	.91	.98
79241	.72	.81
79267	.80	.91
79270	.98	.93
79271	.85	.88
79272	.98	.90
79273	.80	.89
79274	.95	.96
79276	.97	.93
79277	.95	.98
79278	.99	.99
79283	.90	.99
79285	.97	1.00
79286	.93	.99
79294	1.00	1.00
79302	.99	.98
79305	.98	.99
80164	1.00	1.00
Overall:	.91	.95

It is seen that both algorithms are often quite successful at estimating vehicle potential, although on occasion, the success rate drops to below 80%. The distribution function algorithm appears to be superior in its present form, and can be expected to give better results when certain contemplated refinements are implemented in the program. It has advantages over the counts algorithm in that there is no need to consider ad hoc (possibly variable) critical count ratios and minimum count rates. The fundamental distribution function criterion is physically reasonable and statistical methods are employed to reduce the risk of spurious results. The computational and storage requirements of this method are greater than for the counts algorithm but are not excessive. Unfortunately, without a detailed knowledge of the statistics of ion distribution functions, and of ESA calibrations, the optimal value for γ must be empirically determined.

V. THE USE OF SC5 DATA

A second ESA associated with the SC5 experiment also supplied positive ion count data, and the algorithms described above were tested on this data as well. The SC5 instrument provided much poorer energy resolution, with only eight energy channels covering the range 0 to 50 keV. Moreover, the ESA calibration curves showed considerable overlap in the response curves for the various channels. The count rates per channel tended to be much lower (and hence exhibited greater variability) than for the SC9 ESA. This variability was satisfactorily smoothed by averaging over up to sixteen 200 m sec time intervals. However, neither algorithm was able to perform nearly as well with the SC5 data as with the SC9 data in estimating vehicle potential.

To explore the impact of the reduced number of channels, the SC9 data was summed into eight energy "bins" corresponding in energy range to the SC5 channels. Using this summed data, the counts and distribution function algorithms

gave excellent estimates of vehicle potential (to within the reduced resolution of the eight bins). Hence the poor showing with the SC5 data seems attributable to the lack of channel separation. Increases in count rates or distribution function typical of vehicle charging are harder to detect when such effects may be smeared over adjacent channels. Good channel separation is important for these charge detection algorithms to work well.

VI. RECOMMENDATIONS

The results obtained thus far have been highly encouraging, especially with regard to the use of either algorithm with positive ion count data from an SC9 type ESA. I believe the distribution function algorithm should be chosen for further development. Refinements such as refusing to report charging unless indicated on two successive sweeps of the instrument, should be implemented and tested. A study of the types of plasma environment to be found at the vehicle orbit would be useful in theoretically determining the optimal standard deviation factor γ . Meanwhile, further testing is needed to determine that value empirically. Clearly any evaluation of algorithm performance depends on how well the true satellite potential can be independently determined. Hence any improvement in the latter estimates would be most welcome.

The usefulness of these algorithms for SC5 data remains to be determined. It is possible that the various charge detection criteria can be modified so that vehicle potential can be estimated with satisfactory accuracy even with considerable channel overlap. Tests in which the distribution function algorithm has been modified to search for a smaller than expected decrease (rather than a significant increase) in distribution

function have shown improved results in a limited number of trials. With a better understanding of the ESA responses to a variety of ambient plasmas, it should be possible to find optimal criteria for charge detection with this type of instrument.

REFERENCE

1. S. L. Spiegel, "Design of a Computer Algorithm to Measure Satellite Surface Charging," Technical Report to Tri-Con Associates, Inc., Cambridge, MA, 1980.

1981 USAF - SCEEE SUMMER FACULTY RESEARCH PROGRAM

Sponsored by the

AIR FORCE OFFICE OF SCIENTIFIC RESEARCH

Conducted by the

SOUTHEASTERN CENTER FOR ELECTRICAL ENGINEERING EDUCATION

FINAL REPORT

PLASTIC ROTATING BAND LOADS AND SLIDING RESISTANCE FORCES

Prepared by:	Dr. A. Kent Stiffler
Academic Rank:	Associate Professor
Department and University:	Department of Mechanical Engineering Mississippi State University
Research Location:	Air Force Armament Laboratory, Direct Fire Weapons Division (DLD), Ballistics Branch (DLDL)
USAF Research Colleague:	Otto K. Heiney
Date:	August 7, 1981
Contract No:	F49620-79-C-0038

PLASTIC ROTATING BAND LOADS AND SLIDING RESISTANCE FORCES

by

A. Kent Stiffler

ABSTRACT

A theory is presented for the determination of the projectile resistance forces in interior ballistics. Emphasis is placed on the engraving process for plastic rotating bands. It is proposed that the normal contact stress is constant during engraving and is given by the material flow pressure. Normal loads and friction forces are dependent on the growth of the contact area. The theory is in agreement with experimental data.

The contact stress following the engraving process can be changed by several dynamic sources: (1) projectile spin; (2) projectile compression from acceleration; (3) gas pressure on the barrel wall; (4) rotating band wear. These sources are examined to establish post-engraving contact stresses.

Suggestions for further research on high velocity friction coefficients are offered.

ACKNOWLEDGMENT

The author would like to thank the Air Force Systems Command, the Air Force Office of Scientific Research, and the Southeastern Center for Electrical Engineering Education for the opportunity to spend a summer at the Air Force Armament Laboratory, Eglin AFB, FL. He is particularly indebted to Otto Heiney for his topic suggestion, collaboration, and unbounded energy for tackling the problems at hand. Finally, the author would like to acknowledge the helpful discussions with Dale Davis.

I. INTRODUCTION

The basic interior ballistic problem of closed breech gun systems is to determine the energy release and corresponding pressure generated by the burning propellant in a variable volume, ultimately to establish the muzzle velocity of the projectile (1). The present approach to this problem basically involves an energy balance in which the energy input from the propellant is equated to the translational energy of the projectile plus losses. Losses during the projectile travel down the gun barrel can be ascribed to three sources: kinetic energy of unburned propellant and of hot gases, rotating band frictional effects, and heat transfer from hot gases to the gun. Presently these losses are lumped together and, based upon qualitative arguments in the literature, are assumed to be proportional to the projectile kinetic energy. The proportionality constant is evaluated from experimental tests.

In the past, rotating bands have been made from gilding metal (bronze); however, recent success (2) with nylon bands at AFATL suggest that they will be used extensively in the future. Plastic bands not only improve gun barrel life, but reduce the frictional forces as well. Furthermore, there is evidence (3) that these bands melt during the engraving process. It is speculated that a layer of plastic is deposited along the barrel which interferes with heat losses to the gun. Plastic band performance has altered existing velocity predictive codes to the extent that previous approximations to losses are no longer valid. A better understanding of the band-rifling contact area is needed.

II. OBJECTIVES OF THE RESEARCH EFFORT

Frictional behavior in internal ballistics is exceedingly complex due to the large loading forces, high sliding velocities, and the nature of the dynamically changing interface between the projectile and barrel. Montgomery

(3) has shown that even pin-disk friction experiments may not be adequate to describe the coefficient of friction under the above conditions, particularly since band melt occurs. As a long range objective, it would be desirable to develop a high velocity-load friction model which is applicable to ballistics. But, this model would require some understanding of the normal (loading) forces between surfaces. A review of the literature shows that this information is only available from a few ad hoc experimental strain measurement studies (4). Thus, the objective of this research effort is:

- (a) to develop an equation for the normal loads between the projectile rotating band and gun barrel;
- (b) to develop a resistance force model for the engraving process.

III. PROJECTILE FORCES

After the projectile band is engraved, the projectile is accelerated down the barrel by gas pressure P_g at it's base. The projectile is loaded at the bands by a force normal to the rifling top (land) W_N caused by the compressive stress between band and rifling, and by a force normal to the rifling side W_s caused by the projectile spin. These forces in turn produce frictional sliding forces on the surfaces, F_N and F_s respectively. If the rifling twist is aligned at θ to the axial direction x , the following equations can be written for the projectile acceleration:

$$m\ddot{x} = P_g A_B - F_x \quad (1)$$

$$I\ddot{\alpha} = \frac{d_B}{2} F_y \quad (2)$$

where

$$F_x = W_s \sin\theta + (F_N + F_s) \cos\theta \quad (3)$$

$$F_y = W_s \cos\theta + (F_N + F_s) \sin\theta \quad (4)$$

In general, the spin forces can be neglected in Equation (1) and the axial resistance force is

$$F_x \approx \mu_n W_n \cos \theta \quad (5)$$

During the engraving process, the band is pushed through a forcing cone of total angle ϕ . The net effect of this process is to place the normal load and friction force on the band surface at an angle $\phi/2$. Thus, the engraving resistance force for small rifle twist is

$$F_x = W_n (\mu_n \cos \phi/2 + \sin \phi/2) \quad (6)$$

IV. QUASI-STATIC ENGRAVING THEORY

Much of the engraving force data in the literature show considerable variation in force-displacement curves because there is little uniformity in the rotating band, forcing cone, and barrel groove dimensions (4)(5). Bronze bands compound the problem because material of the same composition can vary by a factor of two depending on the degree of work hardening. It is imperative then to focus on the projectile-barrel geometry and band properties. Figure 1 shows the band and gun dimensions for 20mm projectiles used in an excellent experimental study by Cross (6) to determine rifling design parameters in conjunction with plastic bands. This study will be used later for the experimental data to verify the theory.

Let the engraving process begin with point contact between the band and forcing cone. Before the projectile moves, the material at this point must yield or flow. As movement commences, additional material begins to flow as it is pushed and/or squeezed to the rear of the band. A simple calculation will show that only a small fraction of the material is actually taken up in strain. The following model of the engraving process is proposed.

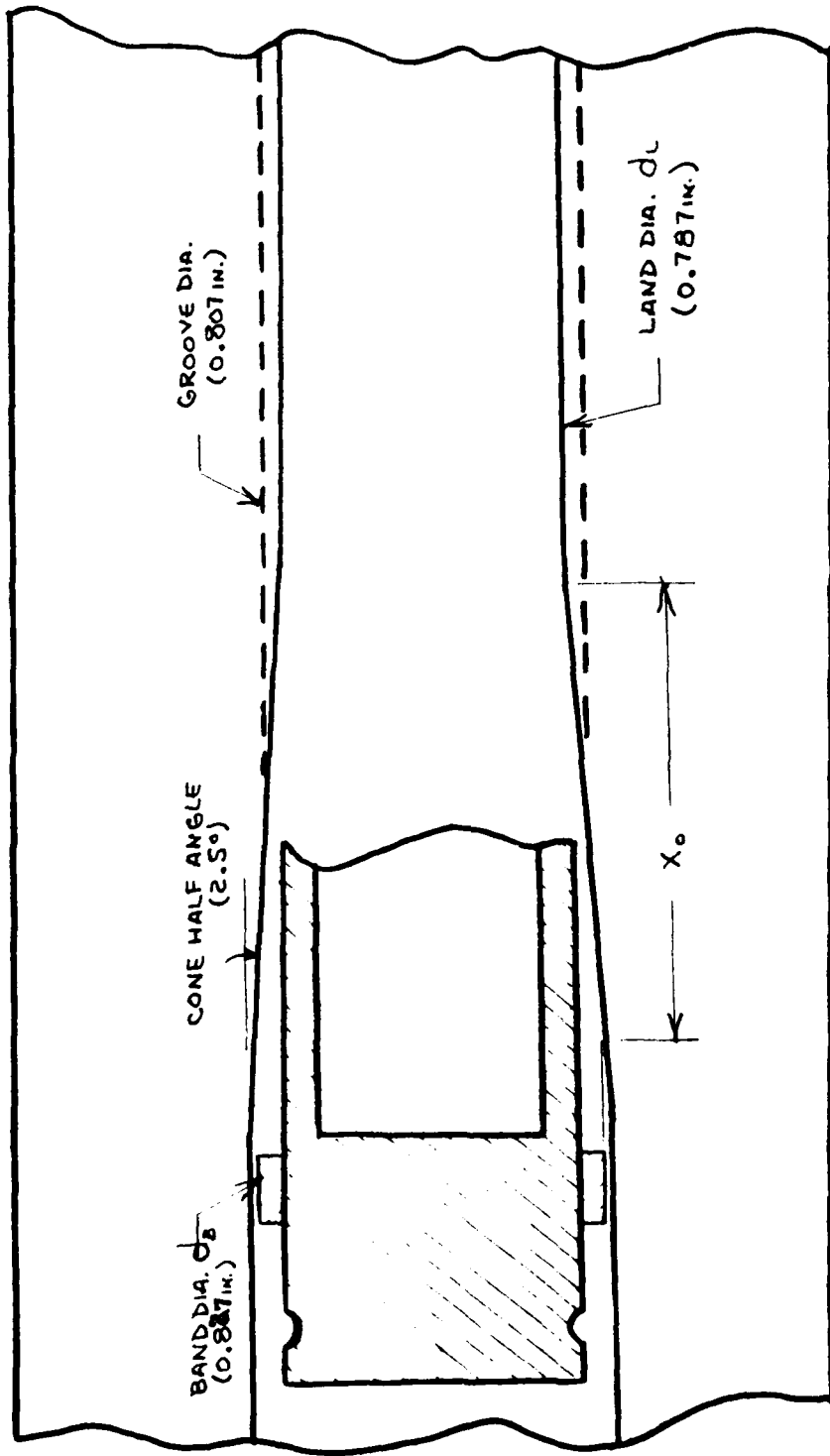


Figure 1. Engraving Geometry

(1) It is assumed that the stress between band and cone surface remains constant and is given by the material flow pressure σ_F under quasi-static conditions. Then,

$$F_x = \sigma_F A (\mu_N \cos \phi/2 + \sin \phi/2) \quad (7)$$

where A is the contact area.

(2) The engraving force increase with displacement is caused by the growth in contact area.

Based upon these principles, several regimes develop in the force-displacement curves.

Regime I

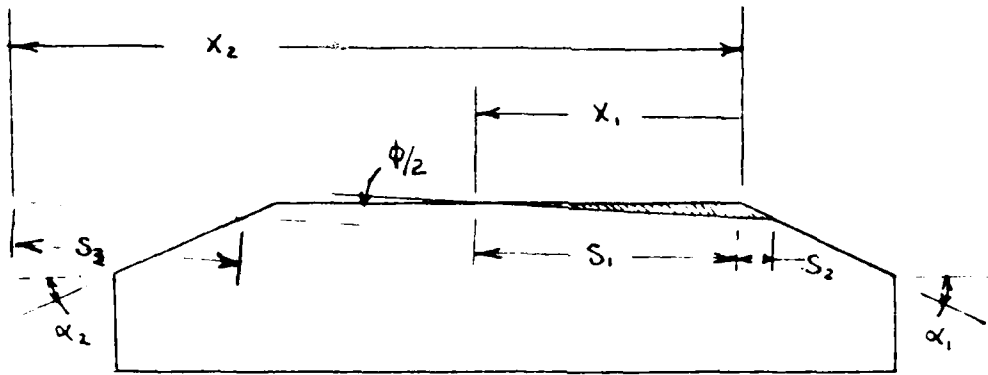
In the case to be considered, the band diameter exceeds the groove diameter and contact will occur over the circumference including band and groove. The force and area will increase linearly as the band moves into the fixed cone angle. If the band diameter is less than the groove diameter, initial contact will occur on the land width. Later, contact may take place on the groove, enhanced by the tendency of flowing band material to enter the groove. Thus, the displacement curve may be broken by an initial shallower slope.

The geometry of the test rotating band is given in Figure 2. A typical displacement will expose a band contact length $s_1 + s_2$. Then

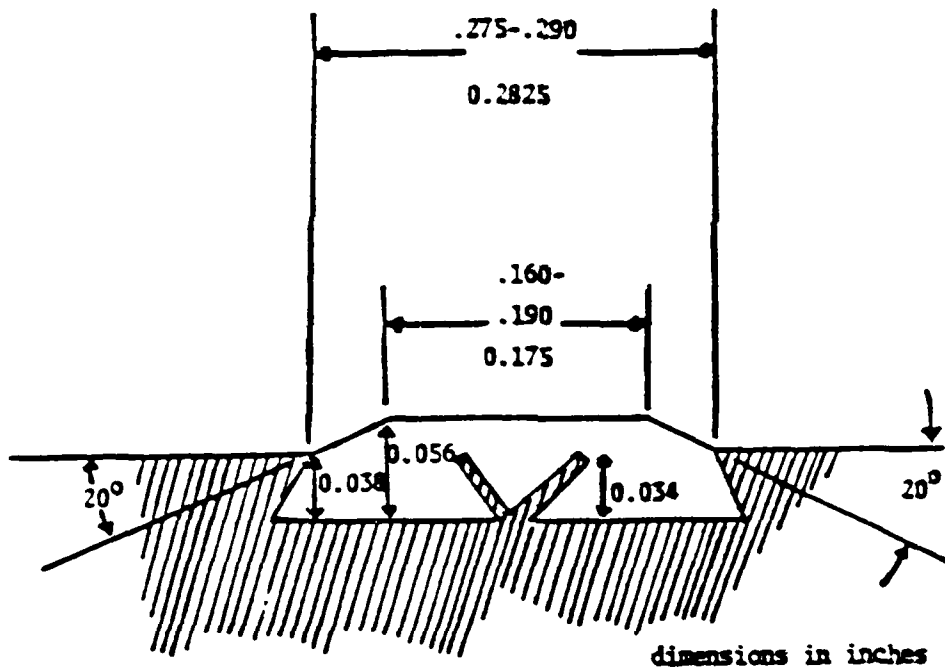
$$A = \pi d_b (s_1 + s_2) \quad 0 \leq x \leq l_1 \quad (8)$$

After the cone cuts through the band top surface, it will continue to add contact length but at a much lower rate as the back side bevel is cut:

$$A = \pi d_b (s_1 + s_2 - s_3) \quad l_1 \leq x \leq l_2 \quad (9)$$



(a) Contact Area Development



(b) Dimensions

Figure 2. Band Characteristics

This rate will continue until the cone cuts its way to the bevel base at l_2 or until the end of the cone is reached at

$$x_0 = (d_s - d_L) / 2 \tan \phi/2 \quad (10)$$

Regime II

After the cone has cut through the vertical sides of the band, no further increase in the area is possible. the force will remain constant until the forward point of the band reaches the end of the cone:

$$A = A_{MAX} \quad l_2 \leq x \leq x_0 \quad (11)$$

where A_{MAX} is found from Equation (9) at $x=l_2$. At this point the contact length is s_c .

Regime III

As the band proceeds into the straight section, its contact area changes from slope $\phi/2$ to zero slope. Therefore, the $W \sin \phi/2$ component of the force is gradually lost. The force must decay linearly until the entire band length is in the straight section.

$$F_x = F_x|_{x=x_0} - W \sin \phi/2 (x-x_0) \quad x_0 \leq x \leq x_0 + S_c \quad (12)$$

It is very likely that Regimes I and III overlap slightly to eliminate Regime II.

Regime IV

When the band is completely through the cone section, the force becomes constant.

$$F_x = \sigma_F A_{MAX} \mu_N \quad (13)$$

Once the basic contact area is determined, it remains to establish the quasi-static flow pressure and the coefficient of friction. Properties for the band material, 20% glass filled polyethersulphone, can be found in the literature (7)(8): σ_u (tension) = 20,000 psi; σ_u (compression) = 20,000 psi; σ_s (shear) = 11,000 psi. Based upon the following failure theories,

$$\sigma_F = \sigma_u \text{ (RANKINE)} = 20,000 \text{ psi}$$

$$\sigma_F = 2\sigma_s \text{ (TRESCA)} = 22,000 \text{ psi}$$

$$\sigma_F = \sqrt{3} \sigma_s \text{ (VON MISES)} = 19,000 \text{ psi}$$

the quasi-static flow pressure is taken as $\sigma_F = 20,000$ psi.

The coefficient of friction for nylon on steel (all polyethersulphone properties are almost identical to nylon) under normal loading, less than 100 psi, is listed in a number of sources as $\mu = 0.30 - 0.34$. However, under extreme loading and low velocities, it drops to a value of $\mu = 0.10 - 0.15$ (9).

The above theory is compared with quasi-static engraving data (6) in Figure 3. Using a coefficient of friction $\mu_N = 0.14$, the agreement is quite good. Two discrepancies are noted:

- (i) The theory models the cone section with an abrupt entry into the straight section. In practice, this sharp edge is rounded so that the band entry and resulting force curve is smooth.
- (ii) The experimental force gradually drops after the band has completed its move into the straight section. The reason is that material creeps from the high stress contact region. The phenomenon would not be present during dynamic conditions.

V. DYNAMIC ENGRAVING THEORY

The fundamental difference between quasi-static and dynamic conditions is the velocity sensitivity of the material mechanical properties and the coefficient of friction. Thus, their static values must be replaced by their dynamic counterparts σ'_F and μ'_N respectively.

When a material suffers impact, initial strains depend on the strain propagation velocity; large strains propagate at lower velocities than small strains. A maximum impact velocity exists above which the large plastic strains being generated cannot propagate as rapidly as the material is loaded, and brittle fracture occurs immediately (10). This critical velocity is between 100 - 200 ft/sec. and the corresponding increase in strength ranges from 20% - 50% for various metals (11). No corresponding information could be found for glass-filled polymers; however, their static failure strains are similar to metals.

In general, the coefficient of friction decreases with velocity. Above a certain PV (pressure x velocity) the coefficient of friction drops to a value substantially less than 0.1 and remains constant. This critical PV value for bronze rotating bands is approximately 4×10^6 (psi)(fps), and Montgomery (3) identifies this equilibrium region with material melting. Since polymers melt at much lower temperatures than bronze, it is probable that most of the band engraving takes place in this equilibrium region.

In reference (6) dynamic tests were conducted at 50 m/sec and 130 m/sec. No difference was observed in the peak force during the engraving process, suggesting uniform values for the dynamic flow pressure and coefficient of friction. The results of one dynamic test (50 m/sec) was converted from a time base to a displacement base and compared with the quasi-static test data, Figure 3. Assuming the contact area remains the same at equivalent locations,

$$\frac{F_x(\text{DYNAMIC})}{F_x(\text{STATIC})} = \frac{(\mu'_N + \sin \phi/2) \sigma'_F}{(\mu_N + \sin \phi/2) \sigma_F} \quad (14)$$

for the engraving process. After the band enters the straight section, the dynamic flow pressure drops to the quasi-static flow pressure and

$$\frac{F_x(\text{DYNAMIC})}{F_x(\text{STATIC})} = \frac{\mu'_N}{\mu_N} \quad (15)$$

Now $\mu_N = 0.14$ from the static test results. Therefore, using the ratio of forces for the post-engraving region of the data,

$$\mu'_N = 0.02 \quad (16)$$

Since the contact pressure and velocity are constant over the entire engraving process, this value of friction coefficient can be used in Equation (14).

From the data in Figure 3,

$$\sigma'_F = 0.98 \sigma_F \approx \sigma_F \quad (17)$$

Apparently the static and dynamic flow pressures for glass-filled plastic are similar based upon this single test. Confirmation of this fact is needed.

The dynamic test data in Figure 3 show a slight delay in peak force, causing a more rapid drop to steady values when compared with the quasi-static data. It is attributed to a delay in material removal from the back of the band.

The above dynamic flow pressure and coefficient of friction should be representative over the velocity range encountered during an engraving process with plastic bands.

VI. POST ENGRAVING THEORY

As the projectile leaves the engraving region, the resistance force is given by Equation (13). The coefficient of friction is expected to remain reasonably constant. Although the stress at this point is the flow pressure,

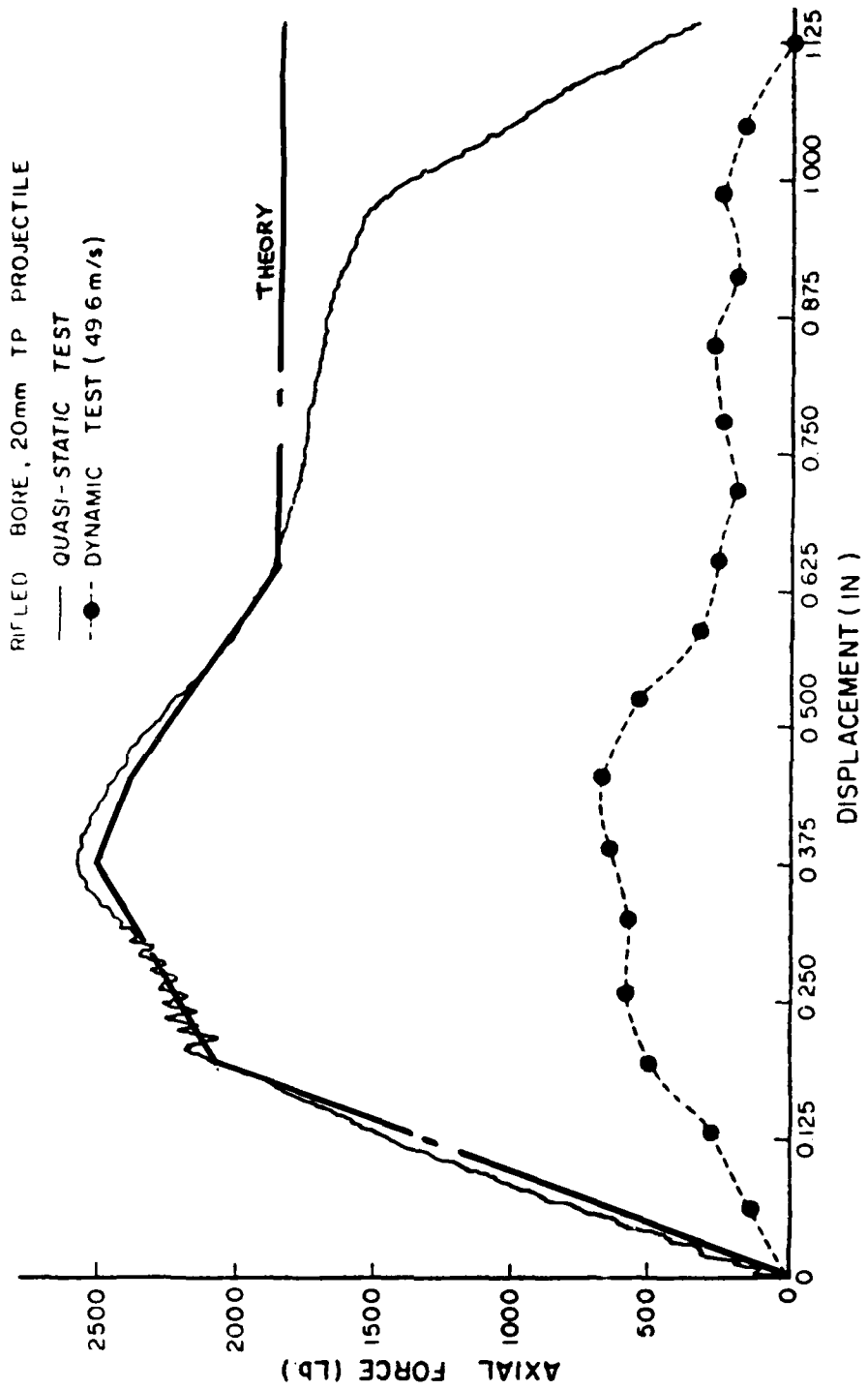


Figure 3. Comparison of Quasi-Static and Dynamic Results for 5-degree Rifled Forcing Cone, Avlon® TP Projectile

the stress will change as the projectile proceeds down the barrel. The stress will be decreased by (a) the gas pressure increasing the inner radius of the barrel and (b) the wear of the bands. The stress will be increased by the projectile radius change due to (a) spin and (b) compression from the acceleration. Expressions for these strains can be found in Timoshenko and Goodier (12). Thus,

$$\sigma = \sigma_F - k_1(P_B - P_{Be}) + k_2(\dot{x}^2 - \dot{x}_e^2)$$

where k_1 and k_2 are elastic constants and P_{Be} and \dot{x}_e are the gas pressure and projectile velocity at the end of the engraving process.

Further details of this report can be found in reference (13).

VII. RECOMMENDATIONS

The author has presented for the first time a theory of engraving which gives structure to the resistance force-displacement curves in interior ballistics. The theory illustrates the need to consider geometrical details and serves to isolate the dynamic flow pressure and coefficient of friction as the main parameters. These parameters require better definition in the range of ballistic loads and velocities.

The friction coefficient is particularly important since band melting occurs over most of the projectile displacement. A sound approach to the problem would be to model the band as a film bearing. Since the normal load is known as a result of this study, film bearing theory would give an accurate description of both the resistance force and the melt layer thickness. The latter would establish the band wear for the post-engraving model and contribute to the solution of the heat transfer problem.

Finally, it is recommended to apply the engraving theory to the 30mm projectiles used in the GAU-8 gun. These projectiles have double plastic bands which are located over the hollow portion of the projectile. The

results of reference (6) indicate that HEI 20mm projectiles (hollow-based) produce a smaller peak axial force during impact than solid-based projectiles. This is attributed to the flexing beneath the band seat. Thus, the theory must be modified to correct for radial displacements during the engraving process. In addition, it is believed that these corrections will influence the apparent dynamic flow pressure found from the tests in reference (6).

REFERENCES

1. Heiney, O.K., "Ballistics Applied to Rapid-Fire Guns", Interior Ballistics of Guns, Progress in Astronautics and Aeronautics, Vol. 66, 1979.
2. Davis, D.M., "Review of the Air Force Program in Gun Barrel Life", Proceedings of the Tri-Service Gun Tube Wear and Erosion Symposium, U.S. Army Armament Research and Development Command, Dover, NJ, March 29-31, 1977, p. I(100)-I(119).
3. Montgomery, R.S., "Surface Melting of Rotating Bands", Wear, Vol. 38, 1976, p.235-243.
4. Hartman, W.F. and Stirbis, P.P., "Rotating Band Pressures and Engraving Forces in 155mm Artillery Shells", ASME Trans., Journal of Engineering Materials and Technology, April, 1973, p.124-129.
5. Heiney, O.K., et al., "Experimental Interior Ballistic Variability Phenomena in the 30mm GAU-8 Gun", Final Report, AFATL-TR-79-64, August, 1979, p. 1-15.
6. Cross, L.A., "Optimum Gun Barrel Rifling Designs for High Performance Aircraft Gun Systems", Final Report, AFATL-TR-80-83, June, 1980, p. 1-224.
7. The International Plastics Selector, 1977, Cordura Publications, Inc.
8. Modern Plastics Encyclopedia, 1978-79, McGraw-Hill Book Co.
9. Clauss, F.J., Solid Lubricants and Self-Lubricating Solids, Academic Press, 1972.
10. Johnson, W., Impact Strength of Materials, London, Edward Arnold, 1972.
11. Rothbart, E.W. editor, Mechanical Design and Systems Handbook, McGraw-Hill Book Co., 1964, p. 16-27.
12. Timosenko, S.P. and Goodier, J.N., Theory of Elasticity, 3rd ed., McGraw-Hill Book Co., 1970.
13. Stiffler, A.K., "Rotating Band Loads and Friction Forces in Interior Ballistics", to be submitted to the International Journal of Engineering Science.

1981 USAF - SCELE SUMMER FACULTY RESEARCH PROGRAM

Sponsored by the
AIR FORCE OFFICE OF SCIENTIFIC RESEARCH

Conducted by the
SOUTHEASTERN CENTER FOR ELECTRICAL ENGINEERING EDUCATION

FINAL REPORT

BINARY AND TERNARY COMPOSITIONS AND THEIR PHYSICAL PROPERTIES

Prepared by:	Dr. Lawrence Suchow
Academic Rank:	Professor of Chemistry
Department and University:	Department of Chemical Engineering and Chemistry, New Jersey Institute of Technology
Research Location:	Materials Technology Branch, Solid State Sciences Division, Rome Air Development Center, Hanscom AFB, Mass. (RADC/ESM).
USAF Research Colleagues:	John K. Kennedy and Robert C. Marshall
Date:	August 3, 1981
Contract No:	F49620-79-C-0038

BINARY AND TERNARY COMPOSITIONS AND THEIR PHYSICAL PROPERTIES

by

Lawrence Suchow

ABSTRACT

Literature studies have been made on (1) compositions with the nickel arsenide structure, (2) growth of large, untwinned crystals of cadmium telluride, and (3) preparation of mercury cadmium telluride thin films. Area 1 will be the basis for an Air Force minigrant proposal for follow-on research. Laboratory research recommendations are also made in areas 2 and 3. A fourth area of endeavor has led to a new explanation of the effectiveness of adding impurities as a means of growing dislocation-free indium phosphide crystals from the melt. A paper on this topic will be submitted for publication, and a recommendation for use of the explanation in designing laboratory experiments is given.

ACKNOWLEDGMENTS

The author wishes to take this opportunity to thank the Air Force Systems Command, the Air Force Office of Scientific Research, and the Southeastern Center for Electrical Engineering Education for making possible a useful and stimulating 10-week stay at the Materials Technology Branch, Solid State Sciences Division, Rome Air Development Center, Hanscom Air Force Base, Massachusetts. He also wants to thank his immediate hosts, John K. Kennedy and Robert C. Marshall, for long and fruitful discussions. Others with whom valuable discussions were held included Joseph Adamski, Brian Ahern, Dr. (2nd Lt.) Thomas Erstfeld, Jane Horrigan, and Dr. Kenneth Quinlan. The author is grateful to Susan Iozzo for maintaining her good humor during much difficult typing.

I. INTRODUCTION:

The author has had long and varied experience in the area of solid state inorganic chemistry (or inorganic materials science). The Materials Technology Branch of the Solid State Sciences Division, Rome Air Development Center, Hanscom AFB, Mass. (RADC/ESM) has long been interested in inorganic materials, especially those with interesting and useful electrical and optical properties.

The author has had specific experience over the last several years in the area of sputtered thin films of mercury cadmium telluride for possible use as infrared detectors. RADC/ESM has not had direct experience in this field but has been working with single crystals and thin films with the same structure (zincblende) as (Hg,Cd)Te. RADC/ESM is interested in the possibility of attacking the problem of growth of large, untwinned single crystals of CdTe for use as substrate material for growth of thin films of (Hg,Cd)Te. It is also interested in the possibility of growth of such films by vapor phase epitaxy.

It was these common interests which served to bring RADC/ESM and the author together.

II. OBJECTIVES OF THE RESEARCH EFFORT:

The initial goals involved evaluation of the literature in three areas of binary and ternary compounds with such evaluation expected to lead to proposals for research which could be carried out at New Jersey Institute of Technology, at Hanscom AFB, or perhaps jointly.

The three areas were:

(1) Preparation and study of physical properties of solid solutions between compounds crystallizing in the hexagonal nickel arsenide structure. Among the known compounds of this type are both metals and semiconductors.

(2) Growth of large, untwinned single crystals of CdTe which would, for example, be suitable for use as substrates for (Hg,Cd)Te thin films.

(3) Preparation of thin films of (In,Ga)Te by sputtering, evaporation, liquid phase epitaxy, vapor phase epitaxy, and any other possible methods.

It was also expected that the author would be able to observe and discuss other projects at RADC/ESM. As a consequence of this, he became interested in preparation of dislocation-free single crystals of InP, studied the literature on this topic, reappraised earlier explanations, and proposes a better explanation.

Rather lengthy reports have been written on the studies listed above. Copies have been presented to John K. Kennedy and Robert C. Marshall of RADC/ESM and will only be summarized here. More detailed information is available from the author.

III. COMPOSITIONS WITH THE NICKEL ARSENIDE STRUCTURE

Nickel arsenide crystallizes on a hexagonal lattice in which the As atoms are arranged in hexagonal close-packed fashion with Ni atoms in all of the octahedral interstices and each As is surrounded by a trigonal prism of Ni atoms.⁽¹⁻⁴⁾ A large number of additional compounds crystallize in this structure. Most, like NiAs itself, are metallic because of the d-orbital overlap along the c-axis, and in such cases the c/a axial ratio is found to be considerably less than the ideal value of 1.63 expected for hexagonal close packing. When, however, the ratio is close to 1.63, the compounds are semiconductors. Solid solutions of two types are proposed:

(1) Those between two binary compounds of which one is a semiconductor and the other a metal.

(2) Those between two binary compounds, either semiconductors or metals, which contain the same metallic element but in different oxidation states (at least nominally).

Electrical and optical properties of such solid solutions would be interesting and perhaps useful. Some may prove to have application as

infrared detectors (as in the case of HgTe (semimetal) -CdTe(semiconductor)).

"Solid Solutions with the Nickel Arsenide Structure and Their Physical Properties: A Literature Study and Research Proposal", an 8-page single-spaced report with 12 references, dated July 20, 1981, has been written and will be the basis for an Air Force minigrant proposal.

IV. GROWTH OF LARGE, UNTWINNED SINGLE CRYSTALS OF CADMIUM TELLURIDE

The best possible substrate for (Hg,Cd)Te thin films for infrared detection is monocrystalline cadmium telluride. For this application, large, twin-free crystals are required but are not easily, if at all, grown. A literature search has uncovered previous attempts to accomplish this, and key references are 5-8.

Much of the literature deals with controlling thermal conditions during melt-growth as a means of preparing large, untwinned single crystals of CdTe and some investigators claimed success years ago, but it seems fair to conclude that it has not been possible to reduce these methods to *commercial practice or else such CdTe crystals would be readily available for purchase*. The present author, partly as a result of his consideration this summer of growth of dislocation-free InP crystals (See Section VI below), proposes a systematic study of intentional impurity addition for possible reduction or elimination of twinning in CdTe crystals grown by the Bridgman-Stockbarger method.

This work has resulted in "Toward Growth of Large, Untwinned Cadmium Telluride Crystals: A Literature Study and a Research Proposal", an 8-page single-spaced report with 26 references, dated July 24, 1981.

V. PREPARATION OF (Hg,Cd)Te THIN FILMS

This study has resulted in "Mercury Cadmium Telluride Thin Films: A Literature Survey", a 24-page, single-spaced report with 68 references, dated June 11, 1981. It covers liquid phase epitaxy, current-controlled liquid phase epitaxy (electroepitaxy), thermal evaporation, sputtering, implantation, vapor phase epitaxy (including growth from gaseous elemental species, chemical vapor transport, and alkyl vapor growth), and molecular

beam epitaxy. This report was designed to be a working guide as a takeoff point for new studies and so contains no research proposals, but oral recommendations for research in the area of open-tube chemical vapor transport for vapor phase epitaxy have been made to RADC/ESM personnel. These deal with chemical vapor transport in multizone furnaces. For example, (Hg,Cd)Te solid solutions or, perhaps better, HgTe and CdTe separately at different temperatures could be reacted with HI, I₂, HCl, or Cl₂ (with H₂ perhaps and/or a noble carrier gas like Ar or He). Alternatively one could start with the diiodides or dichlorides of Hg, Cd, and Te and pass H₂ and Ar or He over them in the multizone furnace. The halides cited here have low or relatively low boiling points so that desired vapor pressures at low temperatures would be easily available. Additional time and thought would be required to firm up this recommendation.

Some key references are 9-19.

VI. DISLOCATION-FREE INDIUM PHOSPHIDE CRYSTALS

References 20-24 deal with preparation of dislocation-free single crystals of indium phosphide by heavy doping with certain impurities; attempts were made by the authors to explain the observed effects on the basis of bond energies and formation of fine precipitates. A careful analysis has shown, however, that there are errors in References 20 and 21. A much more consistent explanation is based on the relative atomic radii of host and impurity atoms. A rough draft of a paper dealing with this reappraisal has been written and it is anticipated that it will be submitted for publication shortly. The new explanation leads to a suggestion for growing dislocation-free and precipitate-free InP crystals.

VII. RECOMMENDATIONS

1. NiAs structure solid solutions should be prepared and studies made of their electrical and optical properties. New useful materials may well result from this study. This is the project chosen for the author's Air Force minigrant proposal.
2. A systematic study should be made of the effect of intentionally-added impurities on twin concentration in melt-grown cadmium telluride. The author is willing to undertake this himself if funds are provided.
3. The author intends to continue his work (with R. Cornely) on sputtered thin films of (Hg,Cd)Te. In addition, he recommends open-tube chemical vapor transport studies aimed at depositing thin films by vapor phase epitaxy, and will consider undertaking the work himself if there is a possibility of funding.
4. In designing experiments to prepare dislocation-free and precipitate-free InP crystals, the author's explanation of the effect of impurities can probably be profitably employed.

REFERENCES

1. A.F. Wells, Structural Inorganic Chemistry, 4th ed., Oxford University Press, London (1975);
2. W.B. Pearson, The Crystal Chemistry and Physics of Metals and Alloys, Wiley-Interscience, New York (1972).
3. R.W.G. Wyckoff, Crystal Structures, Wiley-Interscience, New York (1963).
4. A. Kjekshus and W.B. Pearson, "Phases with the Nickel Arsenide and Closely-Related Structures", Chap. 3 of Progress in Solid State Chemistry, Vol. 1, ed. by H. Reiss, The Macmillan Company, New York (1964).
5. M.R. Lorenz, "Thermodynamics, Materials Preparation and Crystal Growth" Chapter 2 of Physics and Chemistry of II-VI Compounds, edited by M. Aven and J.S. Prener, North-Holland Publishing Co., Amsterdam (1967).
6. Proceedings of the International Symposium on Cadmium Telluride, Strasbourg, France, 1971; ed. by P. Siffert and A. Cornet, published by Centre de Recherches Nucleaires.
7. Proceedings of the 2nd International Symposium on Cadmium Telluride: Physical Properties and Applications, 1976, Strasbourg, France; published in the February 1977 issue of Revue de Physique Appliquee (Vol. 12, No. 2).
8. N.R. Kyle, J. Electrochem. Soc. 118, 1790-1797 (1977).
9. T.C. Harman, J. Electronic Materials 8, 191-200 (1979)
10. P.E. Vanier, F.H. Pollak, and P.M. Raccah, J. Electronic Materials 9, 153-164 (1980).
11. J. Piotrowski, Electron Technol. 5 (2), 87-89, Institute of Electron Technology, Warsaw (1972).
12. R.H. Corneiy, L. Suchow, T. Gabara, and P. Diodato, IEEE Transactions on Electron Devices ED-27, 29-32 (1980).
13. N.A. Foss, J. Appl. Phys. 39, 6029-6031 (1968).
14. P. Vohl and C.M. Wolfe, J. Electronic Materials 7, 659-678 (1978).

15. Z. Golacki and J. Makowski, J. Crystal Growth **47**, 749-750 (1979).
16. H. Wiedemeier, D. Chandra, P.H. Yang, and W.J. Koniowka, oral paper at the Fifth International Conference on Vapor Growth and Epitaxy and the Fifth American Conference on Crystal Growth, Coronado, California, July 24, 1981.
17. H.M. Manasevit and W.I. Simpson, J. Electrochem. Soc. **118**, 644-650 (1971).
18. T.F. Kuech and J.O. McCaldin, J. Electrochem. Soc. **128**, 1142-1144 (1981).
19. J.P. Faurie, oral paper at NATO Cadmium Mercury Telluride Workshop, Grenoble, France, April 23-24, 1981.
20. Y. Seki, J. Matsui, and H. Watanabe, J. Appl. Phys. **47**, 3374-3376 (1976).
21. Y. Seki, H. Watanabe, and J. Matsui, J. Appl. Phys. **49**, 822-828 (1978).
22. S. Mahajan, W.A. Bonner, A.K. Chin, and D.C. Milier, Appl. Phys. Lett. **35**, 165-168 (1981).
23. G.T. Brown, B. Cockayne, and W.R. MacEwan, J. Crystal Growth **51**, 369-372 (1981).
24. J. Matsui, H. Watanabe, and Y. Seki, J. Crystal Growth **46**, 563-568 (1979).

1981 USAF-SCEEE Summer Faculty Research Program
Sponsored by the
Air Force Office of Scientific Research
Conducted by the
Southeastern Center for Electrical Engineering Education

Final Report

A System Dynamics Model of the Acquisition Process

Prepared by: Dr. Patrick J. Sweeney
Academic Rank: Associate Professor
Department and Engineering Management Department
University: University of Dayton
Research Location: Air Force Business Research Management Center
USAF Research Colleague: Captain Michael Tankersley
Date: July 24, 1981
Contract No: F49620-79-C-0038

A SYSTEM DYNAMICS MODEL
OF THE ACQUISITION PROCESS

by

Patrick J. Sweeney

ABSTRACT

Numerous instances have been reported concerning cost overruns, delivery delays, and substandard performance characteristics of acquisitions in government and industry. The dynamic models in this report assess portions of the acquisition process as dynamic feedback systems. The report includes sub-models of the Technology, Weapon System, Financial, Resources, Production and Operations Sectors. Additional work will include the Need, Political, Allied, and Enemy Sectors. Continuations of the effort will include bringing the ten sub-models together into one major model. The model should then be tested and validated. The final result will be an all inclusive dynamic computer simulation model of the functioning acquisition system in the Department of Defense. This model can then be used as a policy evaluation mechanism.

7

Acknowledgement

The author wishes to thank the Air Force Business Research Management Center, the Air Force Office of Scientific Research, and the Southeastern Center for Electrical Engineering Education for providing him with the opportunity to spend a very worthwhile and interesting summer at Wright-Patterson AFB, Ohio. He wishes to acknowledge the excellent support and hospitality of Captain Michael Tankersley and Colonel William Cheney of the Air Force Business Research Management Center.

Table of Contents

	<u>Page</u>
I. Introduction	
II. Objective.	
III. Models	
A. Technology	
B. Weapon System.	
C. Financial.	
D. Resources.	
E. Production	
F. Operations	
IV. Result and Conclusions.	
A. Results	
1. Technology.	
2. Weapon System	
3. Financial	
4. Resources	
5. Production.	
6. Operations.	
B. Conclusions	
V. Recommendations.	
Appendix I Programs	
A. Technology	
B. Weapon System.	
C. Financial.	
D. Resources.	
E. Production	
F. Operations	
Appendix II Definition of Terms	
Appendix III References.	

I. Introduction

The weapon system acquisition process is an important element of national policy, but unfortunately the affects of varying acquisition policies are not well understood. The current process has evolved over the years into an extremely complex system of decision points, budget and resource constraints, operational needs, and political expediencies.

Due to the complexities of the weapon system acquisition process, decision makers are often unaware of the impact of policy changes on the acquisition results. As stated by Dr. Forrester of MIT, the mind is capable of handling only a limited number of variables simultaneously. Therefore only by use of a computing device can man understand all of the interactions of a multitude of changing variables upon system performance. If better acquisition policies are to be developed, it is imperative that the affects of these changes in all parts of the process be known before they are implemented. An accurate and operating computer simulation of the entire acquisition process would be a giant step forward towards understanding the system and designing improved policies.

The acquisition process was generally modeled by Ms Susan A. Kaffenberger and Captain David P. Martin while they were graduate students at the Air Force Institute of Technology's School of Systems and Logistics. Under the tutelage of Lt Col (Dr.) Thomas D. Clark they were able to generally identify the structure and influences of the components and variables within the DOD acquisition process. This model included ten sectors, technology, need, weapon system development (R&D), enemy capability, allied capability, political, financial, operational, production, and resources. Because of the magnitude and variety of sectors included in this model it is possible that this work could be used as the basis for a Defense Department policy evaluation device. Unfortunately, the authors were unable to complete the required testing and validation of their model.

In this study the sectors of technology, weapon system development, financial, resources, production, and operations have been remodeled and validated for expected results as a function of changing variables. When the other four sectors have been modeled, the ten sub-models should be integrated into a single model. Then when tested and validated this model could be used as a policy analysis device for Defense Department policy makers.

II. Objective

The objective of this effort was to model all ten sectors and to confirm that the models respond to stimuli in the expected fashion. Due to the complexities of the weapon systems acquisition processes only six sector or sub-models (technology, weapn system development, financial, resources, production and operations) were designed and tested.

The objective of the total effort, which is beyond the scope of this ten week study with the AFBRMC, is to completely test all ten sub-models and to integrate the ten into a single acquisition model that can be used as a policy evaluation mechanism.

III. Models

The following sections provide the rationale, the flow diagrams, the graphed functions, the equations, and the definitions of terms for each of the sub-models.

It has been assumed by the author that the reader is both familiar with the Defense Department acquisition process and system dynamics. Several Defense Department documents including DODD 5000.1 and 5000.2 plus OMB Circular A-109 generally outline the process. Forrester's "Industrial Dynamics" explains fully the rationale, equations, and flow diagrams used in system dynamics.

A. Technology

This model addresses the state of the art of technology and can be used in very specific terms such as engine technology or in much broader terms such as the total technological base of the United States. This particular model has only one level equation, Technology (TECH), and is used to measure the state-of-technology over time.

Previous work has shown that technological change occurs when pressures in one form or another are applied from within or from outside the technology or scientific community. This technological change is also a function of the complexity of the technology. That is, the more complex the technology the slower the change rate. It is also noted that searching for new advances can be spurred on by increased outside pressure but that is not a linear function.

The Technology Sector flow diagram is shown in Figure 1. This figure also shows the basic curves used for the variables, Technical Complexity Factor (TCF), Technical Pressure (TP), Search for New Technology (SNT), and the Technical Discovery Factor (TDF).

The equations and definitions of terms are shown in Figure 2.

B. Weapon System Development

The weapon system development sub-model consists of six basic levels. It is these six variables that are used to measure the progress, cost, and value of the weapon system under development. These levels and their interactions are shown in Figure 3.

Figure 4 shows the flow diagrams for the actual progress level (AP1). The actual progress is a function of technical effectiveness (TE1), the program (PGM1), and the change in actual progress (CAPRS1). The technical effectiveness is a function of the technical complexity of the system under development (TCF) and the management effectiveness (ME1) of the management team. The program is affected by the schedule (SCHED1), the time since milestone zero (TSMSO), the outside pressure (PRESS1), the revised time to milestone one (RTTMS1), and the decision control point (DCP1). The change in actual progress is affected by a funds limiting factor (FLF) and a desired change in the actual progress rate (DCAPR1).

The reported schedule compliance (SF1) and cost compliance factors (CF1) are a function of the planned progress (PF1) and the perceived actual progress (PAT1).


```

* TECH*****
L TECH.K=TECH.J+DT*(TIR.JK-TLR.JK)
N TECH=TECHC
C TECHC=100
C GROWTH=.005
C RDOC=1
C SUM=.001
C RPFT=1
    TECH      TECHNOLOGY AVAILABLE
    TIR      TECHNOLOGY INPUT RATE
    TLR      TECHNOLOGY LOSS RATE
R TIR.KL=TECH.K*(GROWTH+TDFS.K)
A TDFS.K=SMOOTH(TDF.K,TDFD)
C TDFD=24
    TIR      TECHNOLOGY INPUT RATE
    TECH      TECHNOLOGY AVAILABLE
    GROWTH    GROWTH FACTOR
    TDFS      TECHNOLOGY DISCOVERY FRACTION (SMOOTHED)
    TDF       TECHNOLOGY DISCOVERY FRACTION
    TDFD      TECHNOLOGY DISCOVERY FRACTION
A TDF.K=TABHL(TDFT,SNT.K,0,.1,.025)
T TDFT=.001/.005/.01/.015/.02
A TSP.K=TP.K+OP.K
    TDF       TECHNOLOGY DISCOVERY FRACTION
    SNT       SEARCH FOR NEW TECHNOLOGY
    TDFT      TECHNOLOGY DISCOVERY FRACTION
    TSP       TOTAL SEARCH PRESSURE
    TP        TECHNOLOGY PRESSURE
    OP        OTHER PRESSURE
A TP.K=TABHL(TPT,TECH.K,0,100,25)
T TPT=1/.75/.5/.25/.001
A OP.K=(SUM(RDOC)/ECON)*RPFT
C ECCN=1
    TP        TECHNOLOGY PRESSURE
    TPT       TECHNOLOGY PRESSURE IN TIME
    TECH      TECHNOLOGY AVAILABLE
    OP        OTHER PRESSURE
    RDOC      RESEARCH DOLLARS ON CONTRACT
    ECON      ECONOMIC BASELINE
    RPFT      RESOURCES PRESSURE FOR TECHNOLOGY
A SNT.K=TABHL(SNTT,TSP.K,0,2,.5)
T SNTT=.001/.025/.05/.075/.1
    SNT       SEARCH FOR NEW TECHNOLOGY
    SNTT      SEARCH FOR NEW TECHNOLOGY
    TSP       TOTAL SEARCH PRESSURE

```

FIGURE 2. TECHNOLOGY SECTOR EQUATIONS AND DEFINITION OF TERMS

```

R   TLR.KL=TECH.K*TLF.JK
R   TLF.KL=SMOOTH(GROWTH,TLFL)
C   TLFD=120
    TLR      TECHNOLOGY LOSS RATE
    TECH     TECHNOLOGY AVAILABLE
    TLF      TECHNICAL LOSS FACTOR
    GROWTH   GROWTH FACTOR
    TLFD     TECHNOLOGY DISCOVERY FACTOR
A   TCF.K=TABHL(TCFT,TECHCR.K,3,.2,.05)
T   TCFT=2/1.5/1/.05/.001
A   TECHCR.K=(TIR.JK-TLP.JK)/TECH.K
    TCF      TECHNICAL COMPLEXITY FACTOR
    TCFT     TECHNICAL COMPLEXITY FACTOR IN TIME
    TECHCR   TECHNOLOGY CHANGE RATE
    TIR      TECHNOLOGY INPUT RATE

```

```

    TLR      TECHNOLOGY LOSS RATE
    TECH     TECHNOLOGY AVAILABLE
PLOT TECH=T/TIR=I/TLR=L/TLF=F/TECHCR=C
PLOT TDFS/TDF/TSP/TP/OP/SNT/TCF
X   /TECHCR=C
PRINT TECH/TIR/TLP/TLF
SPEC DT=1/LENGTH=120/PLTPERES/PPTPLER=0
RUN  STD#

```

FIGURE 2. (CONTINUED)

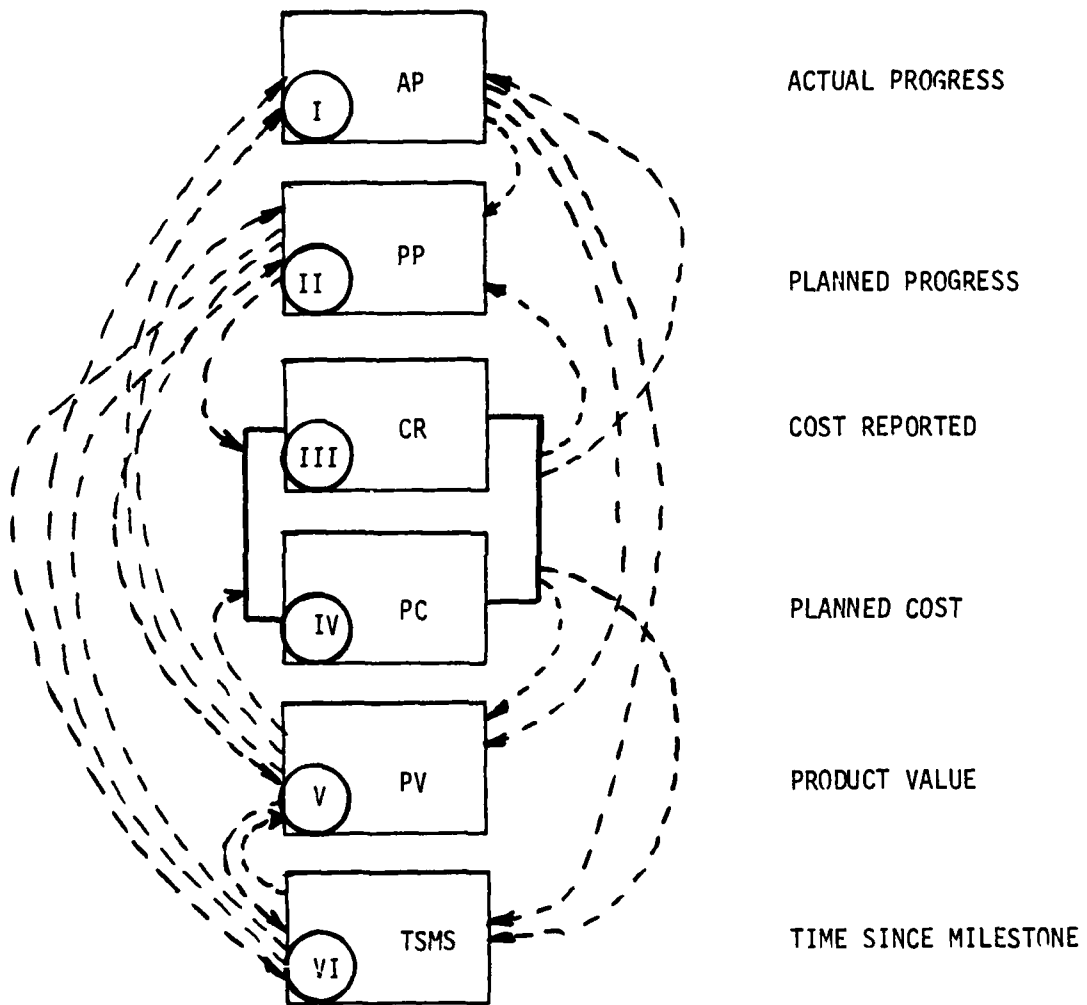


FIGURE 3. WEAPON SYSTEM DEVELOPMENT
LEVEL INTERACTIONS

During this effort a particular interest in management effectiveness was indicated and therefore a specific set of equations were developed for this factor. The author believes that motivation (MOD) and effectiveness (E1) constitute management effectiveness (ME1). Effectiveness was tied to average years in R&D, rank or grade, and education. These particular functions are shown in Figure 5.

The planned progress (PP1) level and the actual progress (AP1), actual to planned (PRAP1), are shown in Figure 6. This reflects that the plan is affected by the schedule.

The costs reported level shows that reported costs (CR1) are affected by the desired cost factor (DCFS1), the cost estimating error (CE1), the programs (PGM1), and a production to cost ratio (PTCR). The cost ratio planned to actual (CRPA1) which is a significant variable is identified on Figure 7 along with the entire cost reported sector.

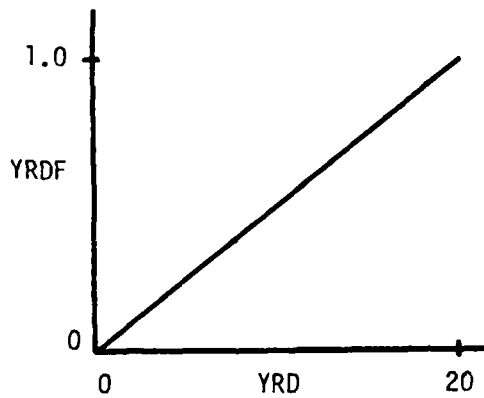
The flow diagram for planned costs (PC) is shown in Figure 8. These costs are affected by the planned program (PPGM1), the funds available factor (FAF1), the funds limitations factor (FLF), the inclination to approve funds (ITAF1), the cost ratio planned to actual (CRPA1), the U.S. urgency factor (URURGF), the mission importance factor (MAIMPF), times since the last milestone (TSMO) and the revised time to the next milestone (RTTMS1).

The product value (PV1) is shown in Figure 9. Product value is a function of the planned program (PPGM1), the cost ratio (CRPA1), the progress ratio (PRAD1).

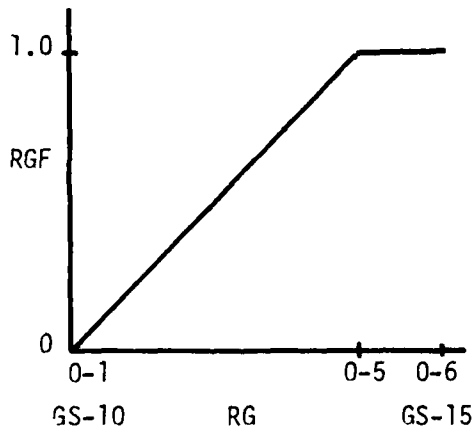
The time since milestone zero level is merely a time counter and is shown in Figure 10.

The table functions are shown in Figure 11. These graphics show the functions of the program (PGM1), the perceived actual progress table function (PAT1), the planned progress table functions (PPIT), the cost factor (CF1), the schedule factor (SF1), the planned program (PPGMIT), the pressure for increased funds (PIF1), the funds increase decisions (FID1), and the funds availability (FA1).

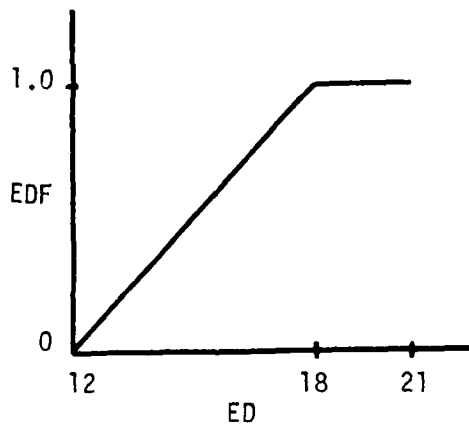
It must be noted that the above explanation and flow diagrams represent only one phase of the weapon systems development, say the conceptual phase. In order to accommodate additional phases the equations are merely replicated and the number 1 (one) is changed to two (2), three (3), etc. The program equations in this pilot effort can accommodate a two phase development program. Additional phases can easily be added. The equations are shown in Figure 12.



AVERAGE YEARS
IN R & D



AVERAGE RANK
OR GRADE



AVERAGE YEARS
OF EDUCATION

FIGURE 5. MANAGEMENT EFFECTIVENESS CURVES

II

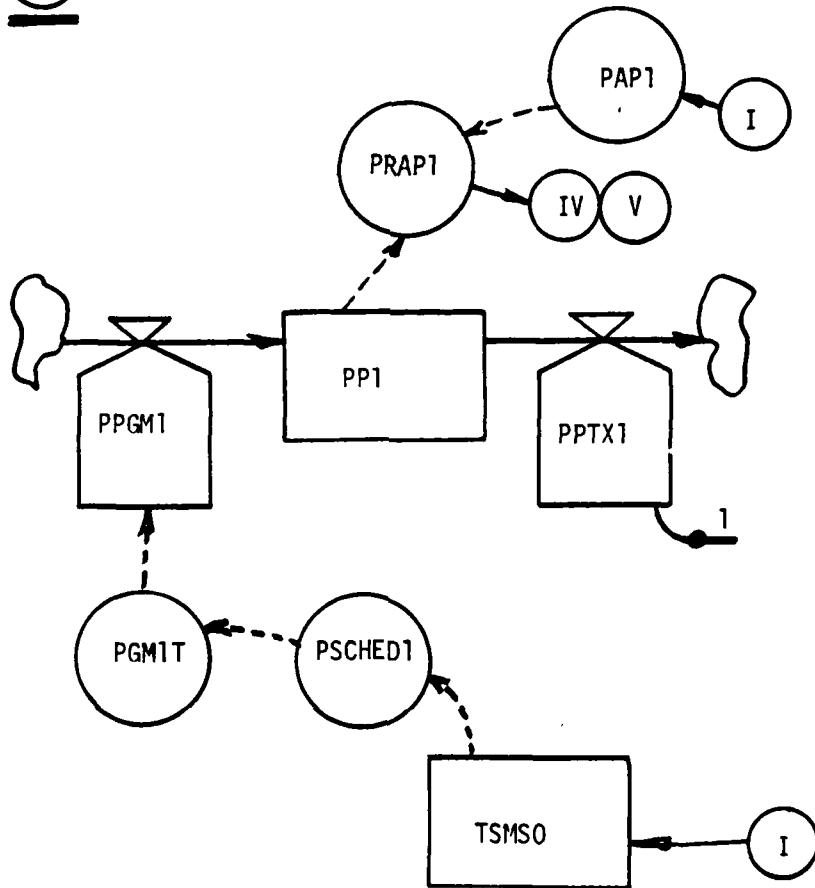


FIGURE 6. PLANNED PROGRESS

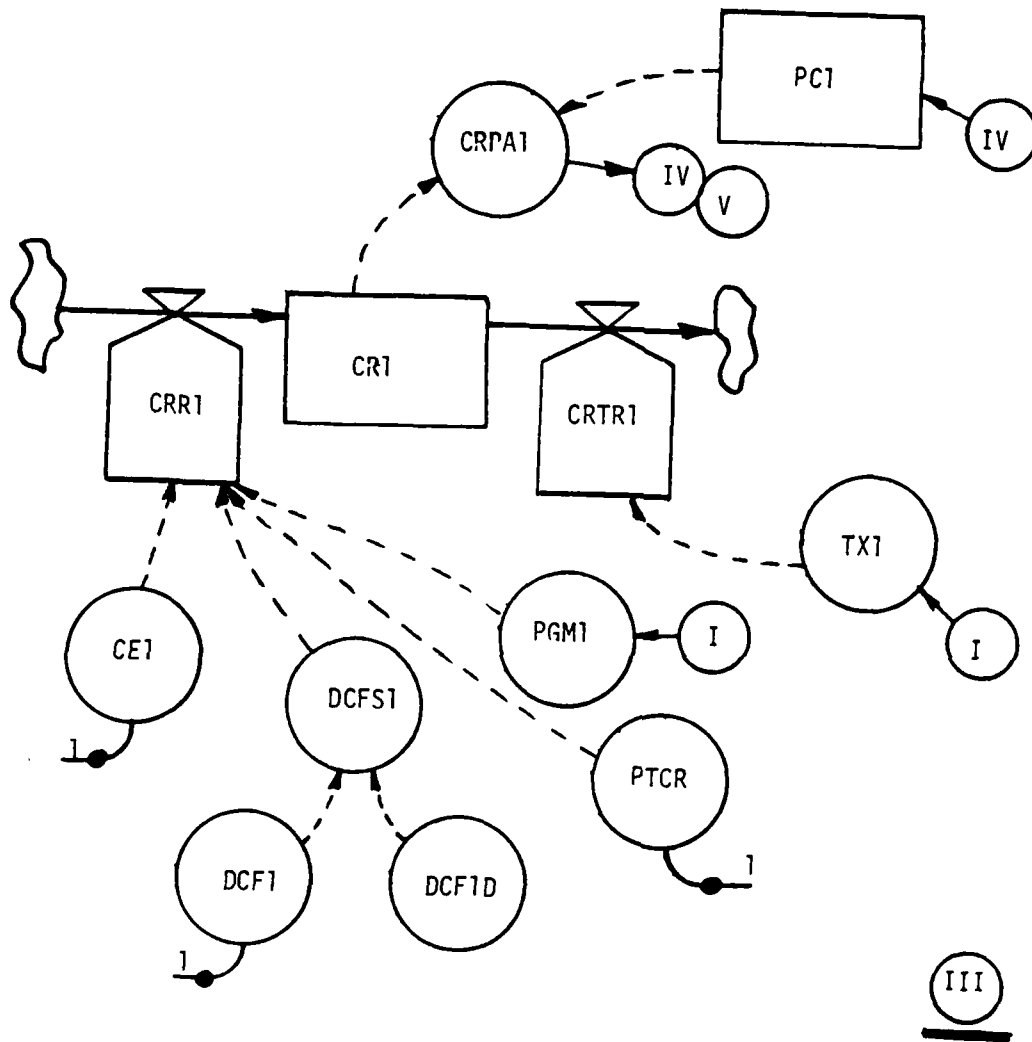
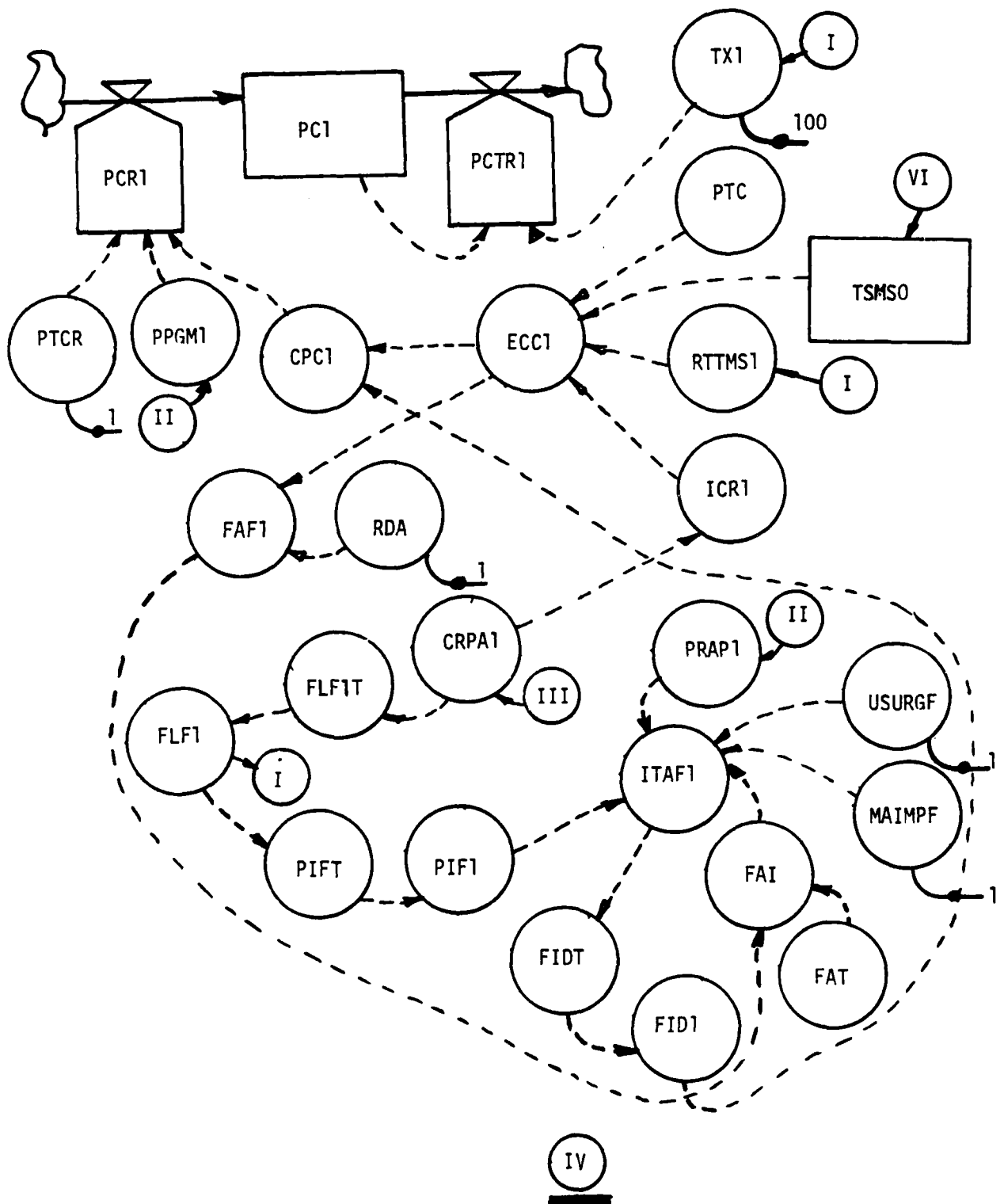


FIGURE 7. COSTS REPORTED



IV
FIGURE 8. PLANNED COSTS

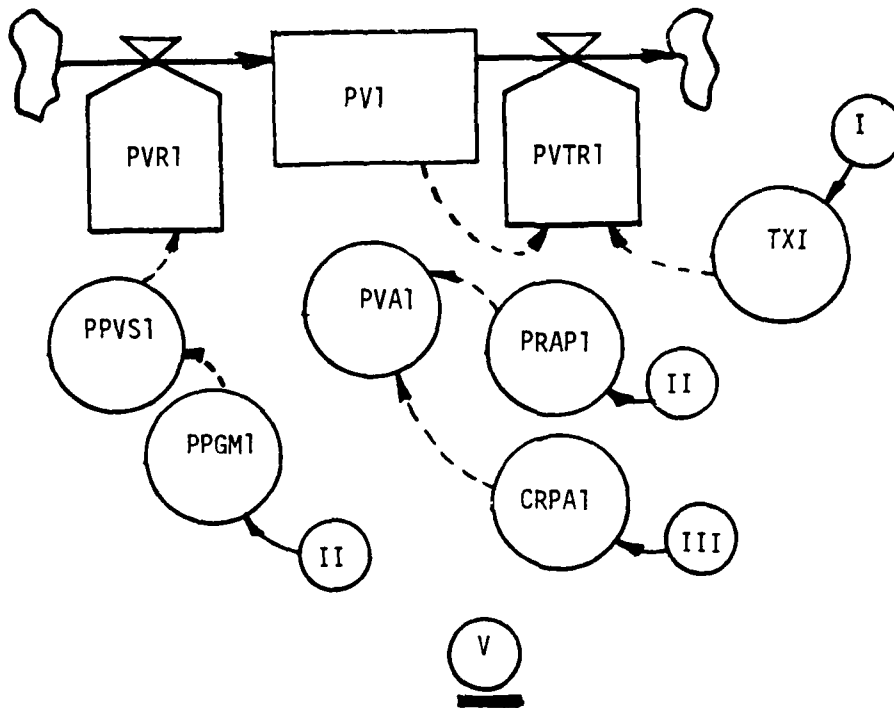


FIGURE 9. PRODUCT VALUE

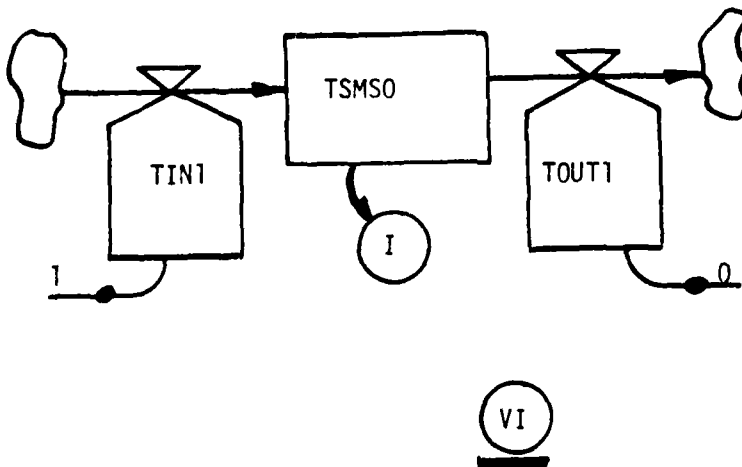


FIGURE 10. TIME SINCE MILESTONE ZERO

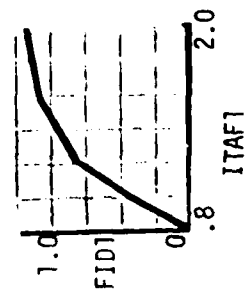
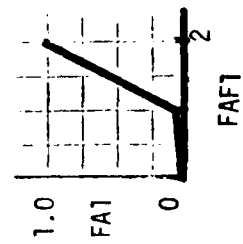
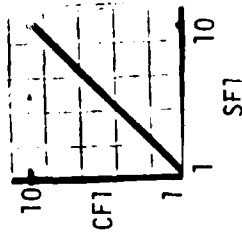
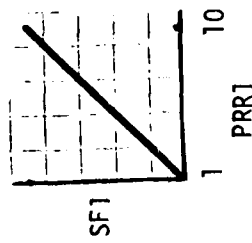
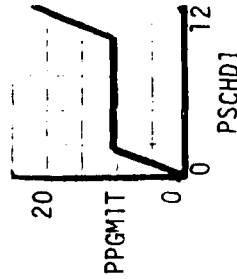
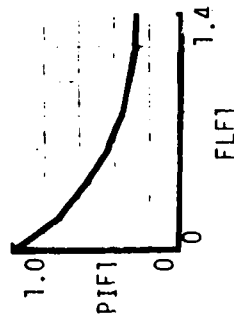
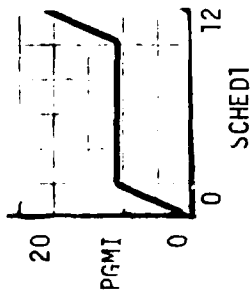
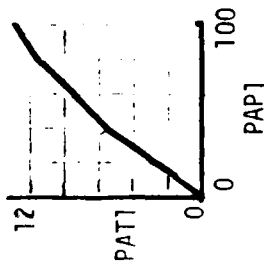
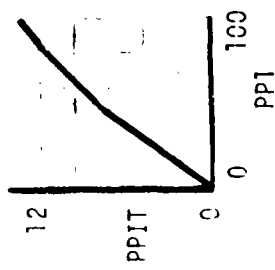


FIGURE 11. WEAPON SYSTEM DEVELOPMENT CHARTS

```

NOTE*****WEAPON SYSTEM DEVELOPMENT*****
NOTE*****PHASE1*****
L  AP1.K=AP1.J+DT(APR1.JK-ATR1.JK)
    AP1          ACTUAL PROGRESS
    APR1         ACTUAL PROGRESS RATE(PROGRESS/TIME)
N  AP1=0
R  ATR1.KL=0
R  APR1.KL=APRR11.K
N  APRR11=0
A  APRR11.K=TE1.K*PGM1.K*CAPRS1.K
    AP1          ACTUAL PROGRESS RATE(PROGRESS/TIME)
    TSMSO        TIME SINCE MILESTONE C
    TIN1         TIME IN PHASE 1
    TOUT1        TIME OUT OF PHASE 1
    TE1          TECHNICAL EFFECTIVENESS
    PGM1         PROGRAM
    CAPRS1       CHANGE IN ACTUAL PROGRESS RATE(SMOOTHED)
A  CAPRS1.K=DELAY3(CAPR1.K,CAPRD1)
    CAPRS1       CHANGE IN ACTUAL PROGRESS RATE(SMOOTHED)
    CAPR1        CHANGE IN ACTUAL PROGRESS RATE
    APRD1        ACTUAL PROGRESS RATE DELAYED
C  CAPRD1=1
A  CAPR1.K=FLF1.K*DCAPR1.K
    CAPR1        CHANGE IN ACTUAL PROGRESS RATE
    FLF1         FUNDS LIMIT FACTOR
    DCAPR1       DESIRED CHANGE IN ACTUAL PROGRESS RATE
A  DCAPR1.K=DCAPR1C
C  DCAPR1C=1
A  TE1.K=TCF*ME1.K
    TE1.K        TECHNICAL EFFECTIVENESS
    ME1          MANAGEMENT EFFECTIVENESS
C  TCF=1
A  ME1.K=E1.K*MOD
C  MOD=1
    ME1          MANAGEMENT EFFECTIVENESS
    EI           MANAGEMENT EFFECTIVENESS FACTOR
A  E1.K=YRDF1.K*RGF1.K*EDF1.K
    YRDF1        YEARS OF R&D (AVERAGE)
    RGF1         RANK OR GRADE (AVERAGE)
    EDF1         EDUCATION (AVERAGE)
A  ED1.K=ED1C
C  ED1C=18
A  RG1.K=RG1C
C  RG1C=5
A  YRD1.K=YRD1C
C  YRD1C=23
A  EDF1.K=TABHL(EDF1T,ED1.K,12,21,1)
T  EDF1T=0/.16/.33/.5/.66/.83/1/1/1/1
A  RGF1.K=TABHL(RGF1T,RG1.K,1,6,1)
T  RGF1T=0/.25/.5/.75/1/1
A  YRDF1.K=TABHL(YRD1FT,YRD1.K,0,20,5)
T  YRD1FT=0/.25/.5/.75/1.0
A  PGM1.K=TABHL(PGM1T,SCHED1.K,0,12,1)
A  SCHED1.K=TSMSO.K
    PGM1         PROGRAM
    PGM1T        PROGRAM
    SCHED1       SCHEDULE
    TSMSO        TIME SINCE MILESTONE C
A  PAPI.K=DELAY1(AP1.K,APD1)
C  APD1=.05

```

FIGURE 12. WEAPON SYSTEM DEVELOPMENT EQUATIONS AND DEFINITIONS

```

PAP1      PERCEIVED ACTUAL PROGRESS
API       ACTUAL PROGRESS
APD1      ACTUAL PROGRESS DELAY
A RTTMS1.K=(TSMSO.K-PAT1.K+TTMS1.K)*PRESS1
RTTMS1    REVISED TIME TIL MILESTONE ONE
TSMSO     TIME SINCE MILESTONE 0
PAT1      --
TTMS1     TIME TIL MILESTONE 1
PRESS1    ---
A PRR1.K=(PP1T.K-PAT1.K+RTTMS1.K)/TTMS1.K
PRR1      PROGRESS RATE REQUIRED
PP1T      PLANNED PROGRESS TIME
RTTMS1    REVISED TIME TIL MILESTONE 1
TTMS1     TIME TIL MILESTONE 1
A PAT1.K=TABHL(PAT1T,PAP1.K,0,100,20)
A PP1T.K=TABHL(PP1TT,PP1.K,0,100,20)
T PP1TT=0/3/5.5/7.6/9.8/11
T PAT1T=0/3/5.5/7.6/9.8/11
C PRESS1=1
PAT1T     PERCEIVED ACTUAL PROG FACTOR
PAP1      PERCEIVED ACTUAL PROGRESS
PP1T      PLANNED PROGRESS TIME
PP1TT     PLANNED PROGRESS TIME
PP1       PLANNED PROGRESS
A TTMS1.K=12-TSMSO.K
A CF1.K=TABHL(CFT1,SF1.K,1,10,1)
T CFT1=1/10
CF1       COST FACTOR
CFT1      COST FACTOR IN TIME
SF1       SCHEDULE FACTOR
A SF1.K=TABHL(SFT1,PRR1.K,1,10,10)
T SFT1=1/10
SF1       SCHEDULE FACTOR
SFT1      SCHEDULE FACTOR IN TIME
PRR1      PROGRESS RATE REQUIRED
L PP1.K=PP1.J+DT(PPGM1.JK-PPTX1.JK)
N PP1=.01
R PPTX1.KL=0
PP1       PLANNED PROGRESS
PPGM1     PLANNED PROGRESS RATE
PPTX1     PLANNED PROGRESS TRANSFER RATE
R PPGM1.KL=TABHL(PGM1T,PSCHD1.K,0,12,1)
T PGM1T=0/4.165/8.33/8.33/8.33/8.33/8.33/8.33/8.33/
X 8.33/8.33/12.495/16.66
A PSCHD1.K=TSMSO.K
PPGM1     PLANNED PROGRESS RATE
PGM1T     PROGRAM
PSCHD1    PLANNED SCHEDULE
L CR1.K=CR1.J+DT*(CRR1.JK-CRTR1.JK)
N CR1=CR1C
C CR1C=.01
CR1       COST REPORTED
CRR1      COST REPORTING RATE
CRTR1     COST REPORTING TRANSFER RATE
R CRR1.KL=CE1*DCFS1.K*PGM1.K/PTCR
C CE1=1
CRR1      COST REPORTING RATE
CE1       COST ESTIMATING FACTOR
DCFS1     DESIRED COST FACTOR(SMOOTHED)
PGM1      PROGRAM

```

FIGURE 12. (CONT 1)

```

      PTCR      PRODUCTION TO COST RATIO
A  DCF1.K=SMOOTH(DCF1.K,DCF1D)
C  DCF1D=1
C  PTCR=1
      DCF1     DESIRED COST FACTOR (SMOOTHED)
      DCF1     DESIRED COST FACTOR
      DCF1D    DESIRED COST FACTOR DELAY
      PTCR     PRODUCTION TO COST RATIO
R  CRTR1.KL=CR1.K*TX1.K
A  DCF1.K=DCF1C
C  DCF1C=1
      CRTR1    COST REPORTING TRANSFER RATE
      CR1      COST REPORTED
      TX1      TRANSFER SWITCH 1
      DCF1     DESIRED COST FACTOR
      DCF1C    DESIRED COST FACTOR
L  PC1.K=PC1.J+DT*(PCR1.JK-PCTR1.JK)
N  PC1=PC1C
C  PC1C=.01
      PC1      PLANNED COST
      PCR1     PLANNED COST RATE
      PCTR1    PLANNED COST TRANSFER RATE
R  PCR1.KL=(PPGM1.JK/PTCR)*(TTMS1.K/RTTMS1.K)+CPC1.K
R  PCTR1.KL=0
      PCR1     PLANNED COST RATE
      PPGM1    PLANNED PROGRAM RATE
      PTCR     PRODUCTION TO COST RATIO
      TTMS1    TIME TIL MILESTONE 1
      RTTMS1   REVISED TIME TIL MILESTONE 1
      CPC1     CHANGE IN PLANNED COST
      PCTR1    PLANNED COST TRANSFER RATE
      PRAP1    PROGRESS RATIO,ACTUAL TO PLANNED
      PAPI     PERCIEVED ACTUAL PPROGRESS
      PPI      PLANNED PROGRESS
      CRPA1    COST RATIO,PLANNED TO ACTUAL
      PC1      PLANNED COST
      CR1      COST REPORTED
A  PRAP1.K=PAPI.K/PP1.K
A  CRPA1.K=PC1.K/CR1.K
A  FLF1.K=TABHL(FLFIT,CRPA1.K,0,2,1)
T  FLFIT=0/1/2
      PRAP1    PROGRESS RATIO,ACTUAL TO PLANNED
      PAPI     PERCIEVED ACTUAL PPROGRESS
      PPI      PLANNED PROGRESS
      CRPA1    COST RATIO,PLANNED TO ACTUAL
      PC1      PLANNED COST
      CR1      COST REPORTED
      FLF1     FUNDS LIMIT FACTOR
      FLFIT    FUNDS LIMIT FACTOR IN TIME
A  PIF1.K=TABHL(PIFT,FLF1.K,0,1.4,.2)
T  PIFT=1/.72/.57/.45/.38/.32/.28/.25
A  IYAF1.K=FA1.K*PIF1.K*PRAP1.K+USURGF.K*MAIMPF
      PIF1     PRESSURE FOR INCREASED FUNDS
      PIFT     PRESSURE FOR INCREASED FUNDS IN TIME
      FLF1     FUNDS LIMIT FACTOR
      ITAF1    INCLINATION TO IMPROVE FUNDS
      FA1      FUNDS AVAILABILITY
      PIF1     PRESSUPE FOR INCEASED FUNDS
      PPAP1    PROGRESS RATIO,ACTUAL TO PLANNED
      USURGF   US URGENCY FACTOR

```

MAIMPF MISSION AREA IMPORTANCE FACTOR
 A $FID1.K = TABHL(FIDT, ITAF1.K, .8, 2, .2)$
 T $FIDT = 0/.375/.62/.75/.86/.92/.96$
 A $CPC1.K = FID1.K * ECC1.K$
 FID1 FUNDS INCREASE DECISION
 FIDT FUNDS INCREASE DECISION IN TIME
 ITAF1 INCLINATION TO APPROVE FUNDS
 CPC1 CHANGE IN PLANNED COST
 ECC1 ESTIMATED CHANGE IN COST
 A $ECC1.K = CLIP(ICR1.K, 0, ICR1.K, 0) * (TSMSO.K + RTTMS1.K) * PTC$
 C $PTC = 100$
 ICR1 INCREASE IN COST
 TSMSO TIME SINCE MILESTONE 0
 RTTMS1 REVISED TIME TIL MILESTONE 1
 PTC PRODUCTION TO COST
 A $ICR1.K = 1 - (1/CRPA1.K)$
 A $FAF1.K = ECC1.K / RDA.K$
 A $RDA.K = RDAC$
 C $RDAC = 1$
 ICR1 INCREASE IN COST
 CRPA1 COST RATIO, PLANNED TO ACTUAL
 FAF1 FUNDS AVAILABILITY FACTOR
 ECC1 ESTIMATED CHANGE IN COST
 RDA RESEARCH DOLLARS APPROPRIATED
 RDAC RESEARCH DOLLARS APPROPRIATED
 A $FA1.K = TABHL(FAT, FAF1.K, 0, 1, 2)$
 T $FAT = 0/.001/1$
 FA1 FUNDS AVAILABILITY
 FAT FUNDS AVAILABLE TABLE
 FAF1 FUNDS AVAILABILITY FACTOR
 L $PV1.K = PV1.J + DT(PVR1.JK - PVTR1.JK)$
 N $PV1 = 0$
 R $PVR1.KL = PPVS1.K * PVA1.K$
 A $PPVS1.K = PPGM1.JK$
 A $PVA1.K = PRAP1.K * CRPA1.K$
 R $PVTR1.KL = PV1.K * TX1.K$
 PV1 PRODUCT VALUE
 PVR1 PRODUCT VALUE RATE
 PVTR1 PRODUCT VALUE TRANSFER RATE
 PPVS1 PLANNED PRODUCT VALUE (SMOOTHED)
 PVA1 PRODUCT VALUE ADJUSTOR
 PPGM1 PLANNED PROGRAM RATE
 PRAP1 PRODUCT RATIO, ACTUAL TO PLANNED
 CRPA1 COST RATIO, ACTUAL TO PLANNED
 PVTR1 PRODUCT VALUE TRANSFER RATE
 TX1 TRANSFER SWITCH 1
 L $TSMSO.K = TSMSO.J + DT(TIN1.JK - TOUT1.JK)$
 N $TSMSO = 0$
 R $TOUT1.KL = 0$
 R $TIN1.KL = 1$
 A $DCP1.K = SWITCH(0, 1, RTTMS1.K)$
 A $TX1.K = SWITCH(1, 0, DCP1.K)$
 A $USURGF.K = USURGFC$
 C $USURGFC = 1$
 C $MAIMPF = 1$
 DCP1 DECISION COORD PAPER 1
 RTTMS1 REVISED TIME TIL MILESTONE 1
 TX1 TRANSFER RATE
 DCP1 DECISION COORD PAPER1
 USURGF US URGENCY FACTOR

```

      USURGFC   US URGENCY FACTOR
NOTE*****PHASE2*****
L   AP2.K=AP2.J+DT*(APF2.JK-ATR2.JK)
N   AP2=0
R   ATR2.KL=0
R   APR2.KL=APRR22.K*CLP.K
N   APRR22=0
A   APRR22.K=TE2.K*PGM2.K*CAPRS2.K
A   CAPRS2.K=DELAY3(CAPR2.K,CAPRU2)
C   CAPRD2=1
A   CAPR2.K=FLF2.K*DCAPR2.K
A   DCAPR2.K=DCAPR2C
C   DCAPR2C=1
A   TE2.K=TCF*ME2.K
A   ME2.K=E2.K*MOD
A   E2.K=YRDF2.K*RGF2.K*EDF2.K
A   ED2.K=ED2C
C   ED2C=18
A   RG2.K=RG2C
C   RG2C=5
A   YRD2.K=YRD2C
C   YRD2C=20
A   EDF2.K=TABHL(EDF1T,ED2.K,12,21,1)
A   RGF2.K=TABHL(RGF1T,RG2.K,1,6,1)
A   YRDF2.K=TABHL(YRD1FT,YRD2.K,0,20,1)
A   PGM2.K=TABHL(PGM2T,SCHED2.K,0,12,1)
A   SCHED2.K=TSMS1.K
A   PAP2.K=DELAY1(AP2.K,APD2)
C   APD2=.05
A   RTTMS2.K=(TSMS1.K-PAT2.K+TTMS2.K)*PRESS2
A   PRR2.K=(PP2T.K-PAT2.K+RTTMS2.K)/RTTMS2.K
A   PAT2.K=TABHL(PAT2T,PAP2.K,0,100,20)
A   PP2T.K=TABHL(PP2TT,PP2.K,0,100,20)
T   PP2TT=0/3/5.5/7.6/9.8/11
T   PAT2T=0/3/5.5/7.6/9.8/11
C   PRESS2=1
A   TTMS2.K=12-TSMS1.K
A   CF2.K=TABHL(CFT2,SF2.K,1,10,1)
T   CFT2=1/10
A   SF2.K=TABHL(SFT2,PRR2.K,1,10,1)
T   SFT2=1/10
L   PP2.K=PP2.J+DT*(PPGM2.JK-PPTX2.JK)
N   PP2=.01
R   PPTX2.KL=0
R   PPGM2.KL=TABHL(PGM2T,PSCHD2.K,0,12,1)*CLPP.K
T   PGM2T=0/4.165/8.33/8.33/6.33/8.33/8.33/8.33/8.33/
X   8.33/8.33/12.495/16.66
A   PSCHD2.K=TSMS1.K
L   CR2.K=CR2.J+DT*(CRR2.JK-CRTR2.JK)
N   CR2=CR2C
C   CR2C=.01
R   CRR2.KL=(CE2*DCFS2.K*PGM2.K/PTCR)*CLP.K
C   CE2=1
A   DCFS2.K=SMOOTH(DCF2.K,DCF2D)
C   DCF2D=1
R   CRTR2.KL=CR2.K*TX2.K
A   DCF2.K=DCF2C
C   DCF2C=1
L   PC2.K=PC2.J+DT*(PCR2.JK-PCTR2.JK)
N   PC2=PC2C

```

FIGURE 12. (CONT 4)

```

C   PC2C=.01
R   PCR2.KL=(PPGM2.JK/PTCR)*(TTMS2.K/RTTMS2.K)+CPC2.K
R   PCTR2.KL=0
A   PRAP2.K=PAP2.K/PP2.K
A   CRPA2.K=PC2.K/CR2.K
A   FLF2.K=TABHL(FLF2T,CRPA2.K,0,2,1)
T   FLF2T=0/1/2
A   PIF2.K=TABHL(PIFT,FLF2.K,0,1.4,.2)
A   ITAF2.K=FA2.K*PIF2.K*PRAP2.K+USURGF.K*MAIMPF
A   FID2.K=TABHL(FIDT,ITAF2.K,.8,2,.2)
A   CPC2.K=FID2.K*ECC2.K
A   ECC2.K=CLIP(ICR2.K,0,ICR2.K,0)*(TSMS1.K+RTTMS2.K)/PTC
A   ICR2.K=1-(1/CRPA2.K)
A   FAF2.K=ECC2.K/RDA.K
A   FA2.K=TABHL(FAT,FAF2.K,0,.4,.05)
L   PV2.K=PV2.J+DT(PVR2.JK-PVTR2.JK)
N   PV2=0
R   PVR2.KL=PPVS2.K*PVA2.K
A   PPVS2.K=PPGM2.JK
A   PVA2.K=PRAP2.K*CRPA2.K
R   PVTR2.KL=PV2.K*TX2.K
L   TSMS1.K=TSMS1.J+DT(TIN2.JK-TOUT2.JK)
N   TSMS1=0
R   TOUT2.KL=0
R   TIN2.KL=1*CLP.K
A   DCP2.K=SWITCH(0,1,RTTMS2.K)
A   TX2.K=SWITCH(1,0,DCP2.K)
A   PP11.K=MIN(PP1.K,100)
A   PP22.K=MIN(PP2.K,100)
A   AP11.K=MIN(AP1.K,100)
A   AP22.K=MIN(AP2.K,100)
A   CR11.K=MIN(CR1.K,100)
A   CR22.K=MIN(CR2.K,100)
A   PC11.K=MIN(PC1.K,100)
A   PC22.K=MIN(PC2.K,100)
A   PV11.K=MIN(PV1.K,100)
A   PV22.K=MIN(PV2.K,100)
A   CLP.K=CLIP(1,0,PAP1.K,100)
A   CLPP.K=CLIP(1,0,PP1.K,100)
SPEC DT=.05
SPEC LENGTH=24
SPEC PLTPER=1
SPEC PRTPER=0
PLOT      AP11,AP22,PP11,PP22
X   CR11,PC11,CR22,PC22,PV11,PV22
PRINT CAPRS1,ME1,TE1,APR1,AP1,PAP1,PAT1
PRINT RTTMS1,TTMS1,SF1,CF1,PGM1,PPGM1,CF2
PRINT PP1,PRAP1,DCFS1,CRR1,CR1,CRPA1,PP1T
PRINT PCR1,PC1,CPC1,ECC1,PIF1,ITAF1,FAF1
PRINT DCP1,TX1,PVA1,PVR1,PV1,TX2,PVA2,PVR2,PV2,DCP2
PRINT PP1T,PAT1,PRR1,ICR1,ECC1,FAF1,FA1,ITAF1,
PRINT FID1,CPC1,PCR1,PC1
PLOT SF1,CF1/RTTMS1,TTMS1/CRPA1,PRAP1/ITAF1/CPC1
PLOT SF2,CF2/RTTMS2,TTMS2/CRPA2,PRAP2/ITAF2/CPC2

```

FIGURE 12. (CONT 5)

C. Financial

The Financial Model is composed of three segments (R&D, Investment, and O&S) and two competitors (the weapon system of interest and all other weapon systems). Moneys are programed and dispersed by the Department of Defense to specific weapon systems and to the particular segments within that system. The explanations and flow diagrams are specific to the R&D segment. However, both the Investment (new weapon system procurements) and the O&S (logistics) are virtual replicas of the R&D explanations and flow diagrams.

Figure 13 shows the flow diagram of the Financial Sector Sub-Model. This figure depicts primarily the R&D sector and consists of three levels - Defense Department Requested Budget (DDRB), Five Year Defense Plan for R&D (FYDP1), and the R&D Dollars Requested in the Budget (RDRB). If the Investment and O&S areas were included the levels of FYDP2 (Five Year Defense Plan for Investment), FYDP3, (Five Year Defense Plan for O&S), IDRB (Investment dollars requested in the budget), and ORDB (O&S dollars requested in the budget) would be included. Also note that dollars to specific weapon systems compete with all other systems in the DOD program and a complete replication of Figure 13 for all of the above levels would be necessary to completely flow chart this sub-model.

Funds to specific weapon systems and to specific portions of these weapon systems are constrained by the FYDP, the DDRB, and the pressures from competing systems. The moneys flow from DDRB and at the same time exert pressure on the weapon system management to expend these funds. The model includes a government support factor (GSPT __) for all three sectors. This factor influences the spending of the allocated funds. Also included is a support factor (__ SUPP) that enables upper level managers to divert funds from one system to another. From time to time during the weapon life additional or supplemental funding is funded to programs. A pulse function (__ PUL) handles all three types of moneys - R&D, Investment, or O&S.

The model is so designed that funds can be transferred from program to program, government support can be varied significantly, support for specific segments can be applied, and supplemental funding can be added to any segment and/or any weapon system.

The specific affects of overall government support to, say R&D, (GSPTRD) and the affect on the government support for the R&D of a specific weapon system is shown on Figure 14.

The affects of support to R&D (RDSUPP) and the specific weapon system R&D effort (RDRBX) is shown in Figure 15.

The equations for the Financial Section Sub-Model are shown on Figure 16.

D. Resources

The Resource Factor Sub-Model deals with the problems of world-wide and US natural resources that are utilized in defense production programs. The strategic materials reserves of the US are vital to defense programs for without certain minerals or materials the US would be unable to produce the required weapon systems for national defense.

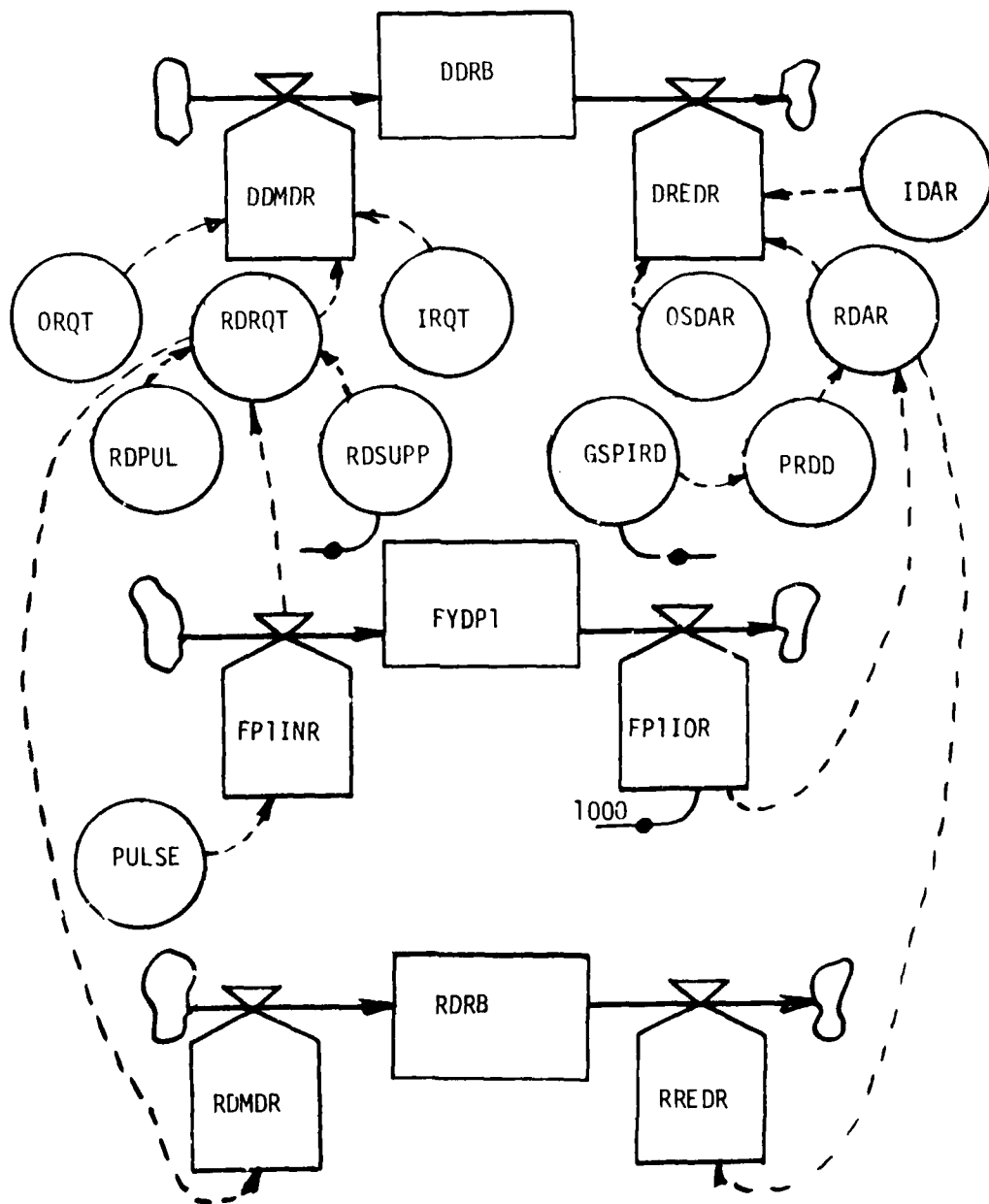


FIGURE 13. FINANCIAL SECTOR

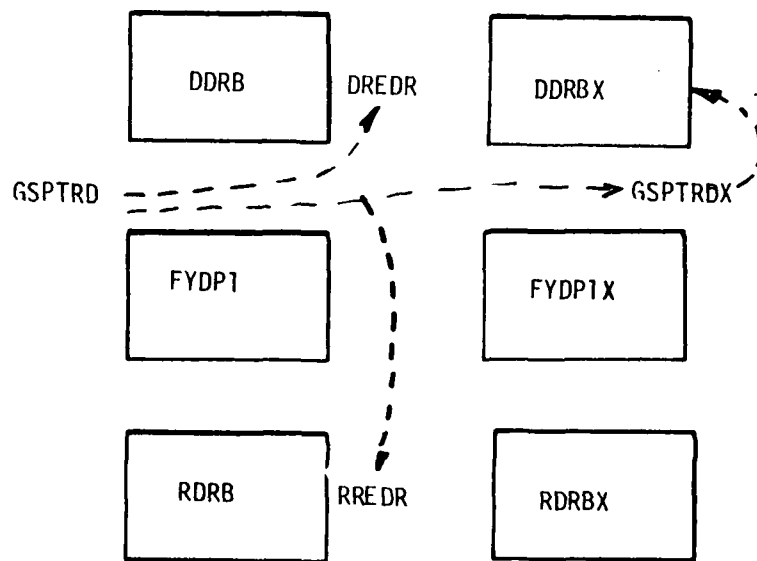


FIGURE 14. EFFECTS OF GSPTRD ON
GSPTRDX

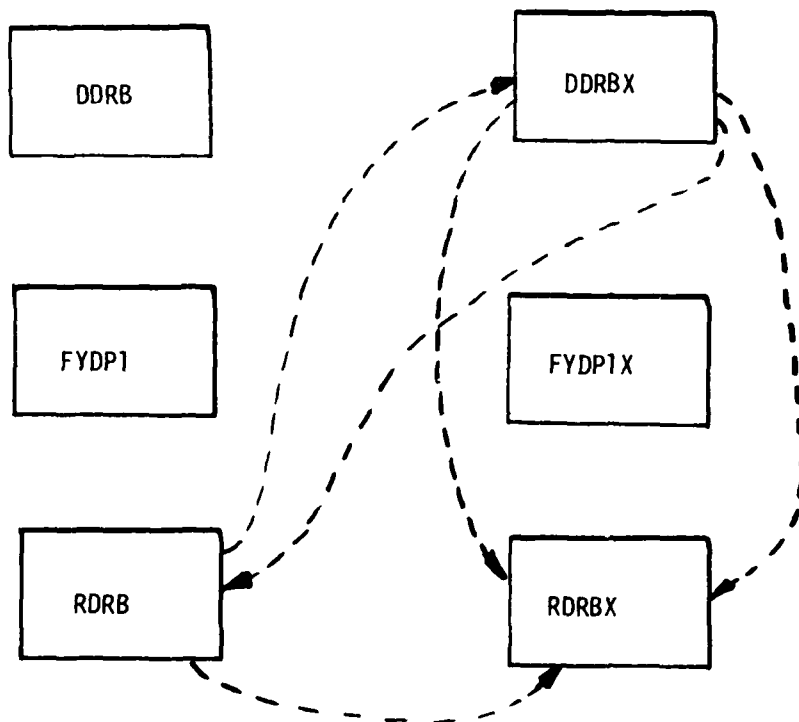


FIGURE 15. R&D MONEY FLOW

```

*****BUDGET FOR WEAPON SYSTEM OF INTEREST*****
*****THE FOLLOWING EQUATIONS RELATE TO THE
*****WEAPON SYSTEM OF INTEREST
L  FYDP1X.K=FYDP1X.J+DT(FP1INRX.JK-FP1ORX.JK)
L  FYDP2X.K=FYDP2X.J+DT(FP2INRX.JK-FP2ORX.JK)
L  FYDP3X.K=FYDP3X.J+DT(FP3INRX.JK-FP3ORX.JK)
N  FYDP1X=120
N  FYDP2X=360
N  FYDP3X=600
- FYDP1X      R&D EXPENDITURES PLANNED IN THE FYDP
- FP1INRX     R&D COSTS FUNDED FROM THE FYDP
- FP1ORX      R&D COSTS FUNDED FROM THE FYDP
- FYDP2X      INVESTMENT EXPENDITURES PLANNED IN THE FYDP
- FP2INRX     INVESTMENT COSTS INPUT TO THE FYDP
- FP2ORX      INVESTMENT COSTS FUNDED FROM THE FYDP
- FYDP3X      O&S EXPENDITURES PLANNED IN THE FYDP
R  FP1INRX.KL=0+PULSE(120/DT,12,12)
R  FP2INRX.KL=C+PULSE(360/DT,12,12)
R  FP3INRX.KL=0+PULSE(600/DT,12,12)
R  FP1ORX.KL=10
R  FP2ORX.KL=30
R  FP3ORX.KL=50
- FP1INRX     R&D COSTS FUNDED FROM THE FYDP
- FP2INRX     INVESTMENT COSTS INPUT TO THE FYDP
- FP3INRX     O&S COSTS INPUT TO THE FYDP
- FP1ORX      R&D COSTS FUNDED FROM THE FYDP
- FP2ORX      INVESTMENT COSTS FUNDED FROM THE FYDP
- FP3ORX      O&S COSTS FUNDED FROM THE FYDP
R  RDPULX.KL=0+PULSE(120/DT,12,12)
R  INVPULX.KL=0+PULSE(360/DT,12,12)
R  OSPULX.KL=0+PULSE(600/DT,12,12)
L  DDRBX.K=DDRBX.J+DT(DDMDRX.JK-DREDRX.JK)
N  DDRBX=1200
- RDPULX      R&D PULSE
- INVPULX     INVESTMENT PULSE
- OSPULX      O&S PULSE
- DDRBX       DOD DOLLARS REQUESTED IN THE BUDGET
- DDMDRX      DEFENSE DEMAND RATE
- DREDRX      DEFENSE DEMAND REDUCTION RATE
R  DDMDRX.KL=RDRQTX.K+IRQTX.K+ORQTX.K+
X  RDARX.JK*(1-GSPTRDX.K)+IDARX.JK(1-GSPTINXV.K)+
X  OSCARX.JK(1-GSPTOSX.K)
- DDMDRX      DEFENSE DEMAND RATE
- RCRQTX      R&D FUNDS REQUIREMENT
- IRQTX       INVESTMENT FUNDS REQUIREMENT
- ORQTX       O&S FUNDS REQUIREMENT
- RDARX       R&D ALLOCATION RATE
- GSPTRDX     GOVERNMENT SUPPORT FOR R&D PROGRAMS
- IDARX       INVESTMENT ALLOCATION RATE
- GSPTINXV    GOVERNMENT SUPPORT FOR INVESTMENT
- OSDARX      O&S ALLOCATION RATE
- GSPTOSX     GOVERNMENT SUPPORT FOR O&S
R  DREDRX.KL=RDARX.JK+IDARX.JK+OSDARX.JK
A  RDRQTX.K=RDPULX.JK+RDSUPPX.K
A  IRQTX.K=INVPULX.JK+INSUPPX.K
A  ORQTX.K=OSPULX.JK+OSSUPPX.K
- DREDRX      DEFENSE DEMAND REDUCTION RATE
- RDARX       R&D ALLOCATION RATE
- IDARX       INVESTMENT ALLOCATION RATE
- OSDARX      O&S ALLOCATION RATE

```

FIGURE 16. FINANCIAL

```

-RDRQTX      R&D FUNDS REQUIREMENT
-RDPULX      R&D PULSE
-RDSUPPX     R&D SUPPLEMENTAL REQUEST
-IRQTX      INVESTMENT FUNDS REQUIREMENT
-INVPUX     INVESTMENT PULSE
-INSUPPX     INVESTMENT SUPPLEMENTAL REQUEST
-ORQTX      O&S FUNDS REQUIREMENT
-OSPULX     O&S PULSE
=OSSUPPX    O&S SUPPLEMENTAL REQUEST
A  RDSUPPX.K=RDSUPPXC+PTX.K*RDSUPPC
A  INSUPPX.K=INSUPPXC+PTX.K*INSUPPC
A  OSSUPPX.K=OSSUPPXC+PTX.K*OSSUPPC
C  RDSUPPXC=0
C  INSUPPXC=0
C  OSSUPPXC=0
-RDSUPPX     R&D SUPPLEMENTAL REQUEST
-INSUPPX     INVESTMENT SUPPLEMENTAL REQUEST
-OSSUPPX     O&S SUPPLEMENTAL REQUEST
-RDSUPPXC-R&D SUPPLEMENTAL REQUEST CONSTANT
-INSUPPX     INVESTMENT SUPPLEMENTAL REQUEST CONSTANT
-OSSUPPX     O&S SUPPLEMENTAL REQUEST CONSTANT
*****THE ABOVE THREE EQUATIONS SHOULD BE IN DOLLARS/PERIOD
*****FOR THE RD, INV, AND OS VALUES 10, 30, AND 60 REPRESENT
*****100%
R  RDARX.KL=PRDDX.K*FP1ORX.JK
R  IDARX.KL=PINVDX.K*FP2ORX.JK
R  OSDARX.KL=POSDX.K*FP3ORX.JK
A  PRDDX.K=GSPTROX.K
A  PINVDX.K=GSPTINX.K
A  POSDX.K=GSPTOSX.K
=RDARX      R&D ALLOCATION RATE
-PRDDX      PRESSURE FOR R&D DOLLARS
=FP1ORX     R&D COSTS FUNDED FROM THE FYDP
-IDARX      INVESTMENT ALLOCATION RATE
-PINVDX     PRESSURE FOR INVESTMENT DOLLARS
-FP2ORX     INVESTMENTS COSTS FUNDED FROM THE FYDP
-OSDARX     O&S ALLOCATION RATE
-POSDX      PRESSURE FOR O&S DOLLARS
-FP3ORX     O&S COSTS FUNDED FROM THE FYDP
-GSPTRDX    GOVERNMENT SUPPORT FOR R&D PROGRAMS
-GSPTINX    GOVERNMENT SUPPORT FOR INVESTMENT
-GSPTOSX    GOVERNMENT SUPPORT FOR O&S
A  GSPTROX.K=GSPTROXC+CLIP(0,MAIMPFX*GSPTROXC-1,1-MAIMPFX,0)
A  GSPTINX.K=GSPTINXVC+CLIP(0,MAIMPFX*GSPTINXVC-1,1-MAIMPFX,0)
A  GSPTOSX.K=GSPTOSXC+CLIP(0,MAIMPFX*GSPTOSXC-1,1-MAIMPFX,0)
C  GSPTROXC=1
C  GSPTINXVC=1
C  GSPTOSXC=1
-GSPTRDX    GOVERNMENT SUPPORT FOR R&D PROGRAMS
-GSPTRDXC   GOVERNMENT SUPPORT FOR R&D PROGRAMS CONSTANT
-MAIMPFX    MISSION AREA IMPORTANCE FACTOR
-GSPTRDXC   GOVERNMENT SUPPORT FOR R&D PROGRAMS CONSTANT
-GSPTINXVC  GOVERNMENT SUPPORT FOR INVESTMENT CONSTANT
-GSPTOSXC   GOVERNMENT SUPPORT FOR O&S CONSTANT
*****THE ABOVE GOVERNMENT SUPPORT SHOULD BE IN %, FOR
*****EXAMPLE; 1.2=20%
C  MAIMPFX=1
L  RDRBX.K=RDRBX.J+DT(RDMRX.JK-PRDRX.JK)
L  IDRBX.K=IDRBX.J+DT(IDMRX.JK-IREDRX.JK)
L  ODRBX.K=ODRBX.J+DT(ODMRX.JK-OREDRX.JK)

```

FIGURE 16. (CONT 1)

```

N   RDRBX=120
N   IDRBX=360
N   ODRBX=600
    -MAIMPFX   MISSION AREA IMPORTANCE FACTOR
    -RDRBX    R&D DOLLARS REQUESTED IN THE BUDGET
    -RDMDRX   R&D DEMAND RATE
    -RREDRX   R&D DEMAND REDUCTION RATE
    -IDRBX    INVESTMENT DOLLARS REQUESTED IN THE BUDGET
    -ICMDRX   INVESTMENT DEMAND RATE
    -IREDRX   INVESTMENT DEMAND REDUCTION RATE
    -ODRBX    O&S DOLLARS REQUESTED IN THE BUDGET
    -ODMDRX   O&S DEMAND RATE
    -OREDRX   O&S DEMAND REDUCTION RATE
R   RDMDRX.KL=RDRQTX.K
R   IDMDRX.KL=IRQTX.K
R   ODMDRX.KL=ORQTX.K
R   RREDRX.KL=RDARX.JK
R   IREDRX.KL=IDARX.JK
R   OREDRX.KL=OSDARX.JK
    -RCMDRX   R&D DEMAND RATE
    -RDRQTX   R&D FUNDS REQUIREMENT
    -IDMDRX   INVESTMENT DEMAND RATE
    -IRQTX    INVESTMENT FUNDS REQUIREMENT
    -ODMDRX   O&S DEMAND RATE
    -ORQTX    O&S FUNDS REQUIREMENT
    -RREDRX   R&D DEMAND REDUCTION RATE
    -RDARX    R&D ALLOCATION RATE
    -IREDRX   INVESTMENT DEMAND REDUCTION RATE
    -IDARX    INVESTMENT ALLOCATION RATE
    -OREDRX   O&S DEMAND REDUCTION RATE
    -OSDARX   O&S ALLOCATION RATE
    *****BUDGET FOR ALL OTHER WEAPON SYSTEMS*****
    *****THE FOLLOWING EQUATIONS RELATE TO THE
    *****OTHER WEAPON SYSTEMS IN THE DOD PROGRAM.
L   FYDP1.K=FYDP1.J+DT(FP1INR.JK-FP1OR.JK)
L   FYDP2.K=FYDP2.J+DT(FP2INR.JK-FP2OR.JK)
L   FYDP3.K=FYDP3.J+DT(FP3INR.JK-FP3OR.JK)
N   FYDP1=12000
N   FYDP2=36000
N   FYDP3=60000
    -FYDP1    R&D EXPENDITURES PLANNED IN THEFYDP
    -FP1INR   R&D COSTS FUNDED FROM THE FYDP
    -FP1OR    R&D COSTS FUNDED FORM THE FYDP
    -FYDP2    INVESTMENT EXPENDITURES PLANNED IN THE FYDP
    -FP2INR   INVESTMENT COSTS INPUT TO THE FYDP
    -FP2OR    INVESTMENT COSTS JUNDED FROM THE FYDP
    -FYDP3    O&S EXPENDITURES PLANNED IN THE FYDP
    -FP3INR   O&S COSTS INPUT TO THE FYDP
    -FP3OR    O&S COSTS FUNDED FROM THE FYDP
R   FP1INR.KL=0+PULSE(12000/DT,12,12)
R   FP2INR.KL=0+PULSE(36000/DT,12,12)
R   FP3INR.KL=0+PULSE(60000/DT,12,12)
R   FP1OR.KL=1000
R   FP2OR.KL=3000
R   FP3OR.KL=5000
    -FP1INR   R&D COSTS FUNDED FORM THE FYDP
    -FP2INR   INVESTMENT COSTS INPUT TO THE FYDP
    -FP3INR   O&S COSTS INPUT TO THE FYDP
    -FP1OR    R&D COSTS FUNDED FORM THE FYDP
    -FP2OR    INVESTMENT COSTS FUNDED FROM THE FYDP

```

```

- FP3OR      O&S COSTS FUNDED FORM THE FYDP
R  RDPUL.KL=0+PULSE(12000/DT,12,12)
R  INVPUL.KL=0+PULSE(36000/DT,12,12)
R  OSPUL.KL=0+PULSE(60000/DT,12,12)
L  DDRB.K=DDR.B.J+DT(DDMDR.JK-DREDR.JK)
N  DDRB=120000
- RDPUL      R&D PULSE
- INVPUL     INVESTMENT PULSE
- OSPUL      O&S PULSE
- DDRB       DEFENSE DOLLARS REQUESTED IN THE BUDGET
- DDMDR      DEFENSE DEMAND RATE
- DREDR      DEFENSE DEMAND REDUCTION RATE
R  DDMDR.KL=RDRQT.K+IRQT.K+ORQT.K
R  DREDR.KL=RDAR.JK+IDAR.JK+OSDAR.JK
A  RDRQT.K=RDPUL.JK+RDSUPP.K
A  IRQT.K=INVPUL.JK+INSUPP.K
A  ORQT.K=OSPUL.JK+OSSUPP.K
A  RDSUPP.K=RDSUPPC+PTX.K*RDSUPPC
A  INSUPP.K=INSUPPC+PTX.K*INSUPPC
A  OSSUPP.K=OSSUPPC+PTX.K*OSSUPPC
A  PTX.K=CLIP(MAIMPFX*DDR.B.K/DDR.B.K,0,0,1-MAIMPFX)
C  RDSUPPC=0
C  INSUPPC=0
C  OSSUPPC=0
- DDMDR      DEFENSE DEMAND RATE
- RDRQT      R&D FUNDS REQUIREMENT
- IRQT       INVESTMENTS FUND REQUIREMENT
- ORQT       O&S FUNDS REQUIREMENT
- DREDR      DEFENSE DEMAND REDUCTION RATE
- RDAR       R&D ALLOCATION RATE
- IDAR       INVESTMENT ALLOCATION RATE
- OSDAR      O&S ALLOCATION RATE
- RDRQT      R&D FUNDS REQUIREMENT
- RDSUPP     R&D SUPPLEMENTAL REQUEST
- IRQT       INVESTMENTS FUND REQUIREMENT
- INSUPP     INVESTMENT SUPPLEMENTAL REQUEST
- ORQT       O&S FUNDS REQUIREMENT
- OSSUPP     O&S SUPPLEMENTAL REQUEST
- PTX        PERCENTAGE
- MAIMPFX    MISSION AREA IMPORTANCE FACTOR
- DDRBX      DOD DOLLARS REQUESTED IN THE BUDGET
- DDRB       DOD DOLLARS REQUESTED IN THE BUDGET
- RDSUPPC    R&D SUPPLEMENTAL REQUEST CONSTANT
- INSUPPC    INVESTMENT SUPPLEMENTAL REQUEST CONSTANT
- OSSUPPC    O&S SUPPLEMENTAL REQUEST CONSTANT
*****THE ABOVE THREE EQUATIONS SHOULD BE IN DOLLARS/
*****PERIOD.  FOR THE RD,INV,AND OS VALUES 1000,3000, AND
*****6000 REPRESENT 100%.
R  RCAR.KL=PRDD.K*FP1OR.JK
R  IDAR.KL=PINVD.K*FP2OR.JK
R  OSDAR.KL=POSD.K*FP3OR.JK
A  PRDD.K=GSPTRD
A  PINVD.K=GSPTINV
A  POSD.K=GSPTOS
C  GSPTRD=1
C  GSPTINV=1
C  GSPTOS=1
- RDAR       R&D ALLOCATION RATE
- FP1OR      R&D COSTS FUNDED FROM THE FYDP
- IDAR       INVESTMENT ALLOCATION RATE

```

FIGURE 16. (CONT 3)

```

-FP2OR      INVESTMENT COSTS FUNDED FROM THE FYDP
-OSDAR      O&S ALLOCATION RATE
-FP3OR      O&S COSTS FUNDED FROM THE FYDP
-PRDD       PRESSURE FOR R&D DOLLARS
-GSPTRD     GOVERNMENT SUPPORT FOR R&D PROGRAMS
-PINVD      PRESSURE FOR INVESTMENT DOLLARS
-GSPTIVN    GOVERNMENT SUPPORT FOR INVESTMENT
-POSD       PRESSURE FOR O&S DOLLARS
-GSPTOS     GOVERNMENT SUPPORT FOR O&S
*****THE ABOVE GOVERNMENT SUPPORT SHOULD BE IN %. FOR
*****EXAMPLE; 1.2=20%.
L  RDRB.K=RDRB.J+DT(RDMDR.JK-RREDR.JK)
L  IDRB.K=IDRB.J+DT(IDMDR.JK-IREDR.JK)
L  ODRB.K=ODRB.J+DT(ODMDR.JK-OREDR.JK)
N  RDRB=12000
N  IDRB=36000
N  ODRB=60000
-RDRB       R&D DOLLARS REQUESTED IN THE BUDGET
-RDMDR      R&D DEMAND RATE
-RREDR      R&D DEMAND REDUCTION RATE
-IDRB       INVESTMENT DOLLARS REQUESTED IN THE BUDGET
-IDMDR      INVESTMENT DEMAND RATE
-IREDR      INVESTMENT DEMAND REDUCTION RATE
-ODRB       O&S DOLLARS REQUESTED IN THE BUDGET
-ODMDR      O&S DEMAND RATE
-OREDR      O&S DEMAND REDUCTION RATE
R  RDMDR.KL=RDRQT.K
R  IDMDR.KL=IRQT.K
R  ODMDR.KL=ORQT.K
R  RREDR.KL=RDAR.JK+RDARX.JK
R  IREDR.KL=IDAR.JK+IDARX.JK
R  OREDR.KL=OSDAR.JK+OSDARX.JK
-RDRQT      R&D FUNDS REQUIREMENT
-IRQT       INVESTMENT FUNDS REQUIREMENT
-ORQT       O&S FUNDS REQUIREMENT
-RDAR       R&D ALLOCATION RATE
-RDARX      R&D ALLOCATION RATE
-IDAR       INVESTMENT ALLOCATION RATE
-IDARX      INVESTMENT ALLOCATION RATE
-OSDAR      O&S ALLOCATION RATE
-OSDARX     O&S ALLOCATION RATE
*****ALL INITIAL VALUES (N) MUST BE ESTABLISHED FOR
*****EACH DIFFERENT WEAPON SYSTEM AND THE DOD SYSTEM.
SPEC DT=.5
SPEC LENGTH=36
SPEC PLTPER=1
SPEC PRTPER=0
PLOT FYDP1,RDRB/FYDP2,IDRB/FYDP3,ODPB/DDRB
PLOT FYDP1X,RDRBX/FYDP2X,IDRBX/FYDP3X,ODRBX/DDRB/DDRBX

```

FIGURE 16. (CONT 4)

The resource model consists of two levels, total world resources (TOTRES) and US resources (USRES). The total resources are effected by the quantity and quality of the searching effort (SEARCH) and the success of that effort in discoveries (DISCOV).

The use of world resources (TRUSE) is controlled by the world growth rates in industrialization and subsequently the use rate world-wide. The US can draw upon world resources and US resources and can allocate varying proportions to defense related programs. The ability to make more efficient use of US natural resources, to obtain a greater percentage of world resources, and the effects of conservation programs are included in the model.

The flow diagram of the Resource Sector Sub-Model is shown in Figure 17 and the table functions in Figure 18. The tables include the discovery factor (DISCOV), the search factor (SEARCH), the growth factor (GROWTH), the desire to conserve (DTC), the technical improvement factor (TECHIF), the pressure for technology (RPFT), the resource percentage for defense (RADPP), and the resources available for defense production (RPUSDP).

The equations for the resource sector are shown in Figure 19.

E. Production

The Production Sector Sub-Model consists of three levels, Weapon Systems in Production (WSP), Weapon Systems in Transit (WSIT), and Total Weapon Systems Produced (TWSP). The production capacities of the US are affected by many variables such as facilities, labor force, technology, etc. In this model the author has used only natural resources as a constraint in production. The other factors can easily be added at a later time. The production is primarily affected by the programmed effort (PGMXX), the managerial expertise of the production team (TEX), the learning curve function (LCF), and managements desire to change the production schedule of the effort (CPTS). The weapon systems in transit are controlled by the production rate (WSPR) and the time required to move the weapon system from the plant to an operational unit (WSTT).

In addition to the above, the production sector is very similar to the weapon system development sub-model. The problems of cost, schedule, and performance are even more pronounced in this part of the acquisition process. A ten percent overrun in R&D may not be too significant but 10% in a multi-billion dollar effort can add up to many dollars. The model includes the levels of planned costs (PCX), the costs reported (CRX), the planned progress (PPX), the product value (PV), and the time counter, time since milestone X (TSMXOX).

The flow diagram of the Production Sector Sub-Model is shown in Figure 20, learning curve factor (LCF) in Figure 21, and the equations in Figure 22.

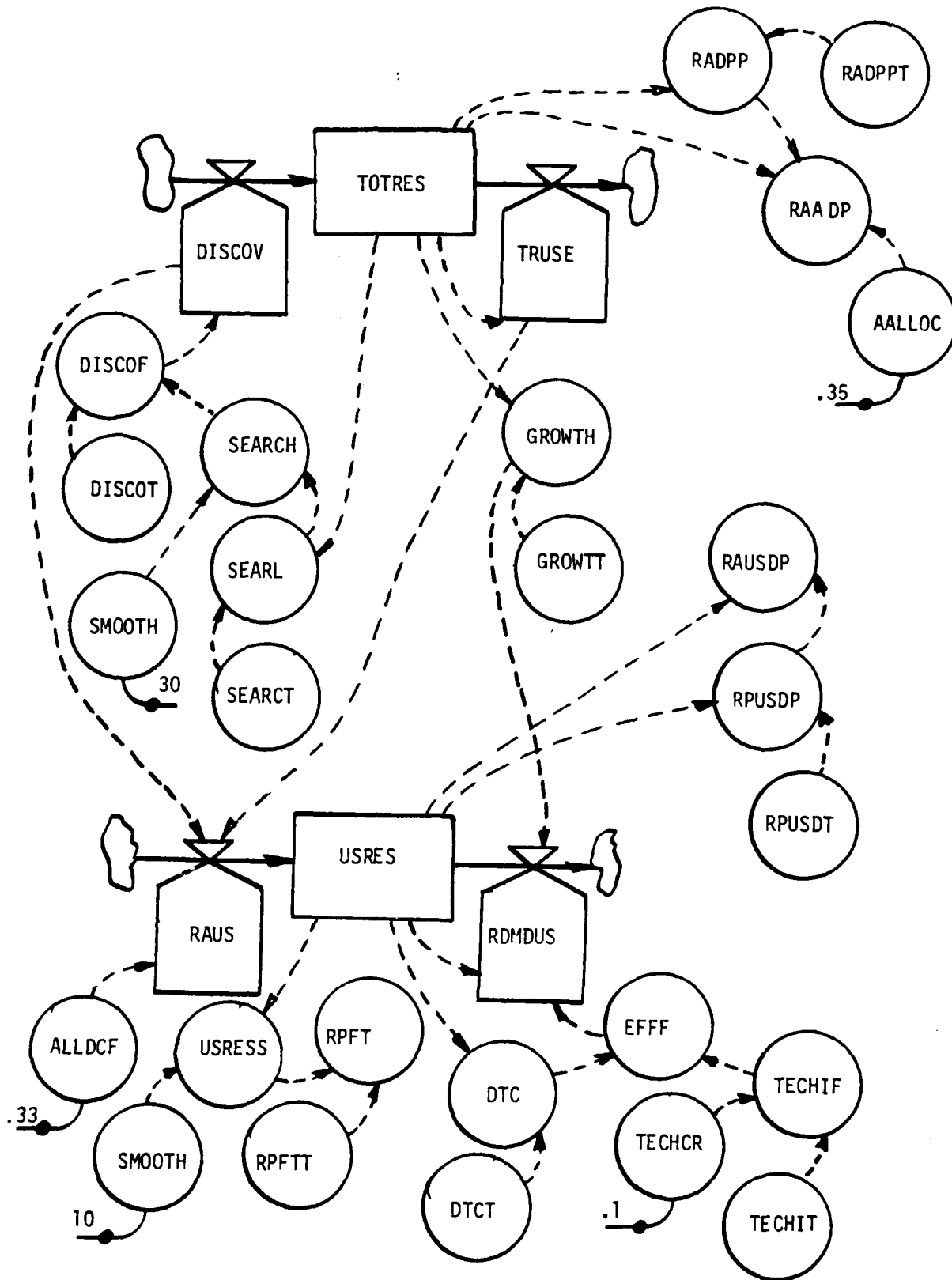


FIGURE 17. RESOURCE SECTOR

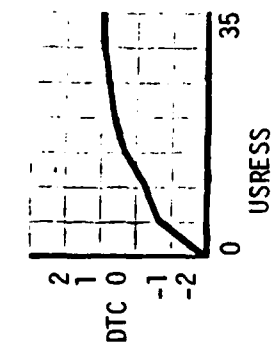
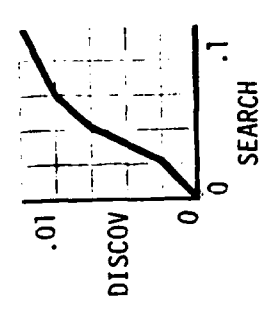
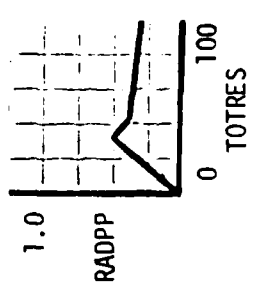
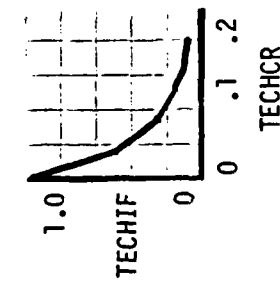
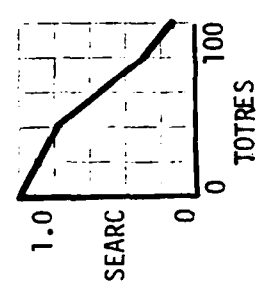
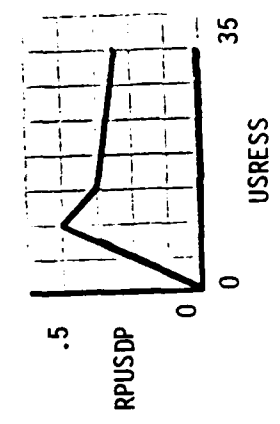
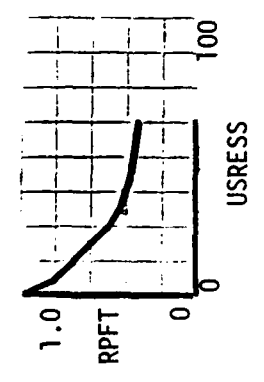
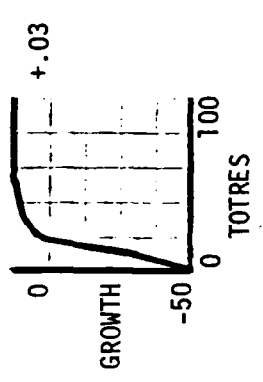


FIGURE 18. RESOURCE CHARTS

```

*****RESOURCES*****
L  TOTRES.K=TOTRES.J+DT*(DISCOV.JK-TRUSE.JK)
N  TOTRES=TOTRSC
C  TOTRSC=100
    TOTRES-TOTAL RESOURCES
    TOTRSC-TOTAL RESOURCES INITIAL VALUE
R  DISCOV.KL=DISCOF.K*TOTRES.K
A  DISCOF.K=TABHL(DISCOT,SEARCH.K,0,.1,.02)
    DISCOV-DISCOVERY RATE
    DISCOF-DISCOVERY FACTOR
    DISCOT-DISCOVERY TABLE
    SEARCH-SEARCH FOR RESOURCES (SMOOTHED)
T  DISCOT=.0/.002/.006/.008/.009/.01
A  SEARCH.K=SMOOTH(SEARC.K,30)
    SEARC-SEARCH FOR RESOURCES
A  SEARC.K=TABHL(SEARCT,TOTRES.K,0,100,20)
T  SEARCT=1/.9/.8/.55/.3/.15
R  TRUSE.KL=GROWTH.K*TOTRES.K
    TRUSE-TOTAL RESOURCE USE
    GROWTH-GROWTH FACTOR
A  GROWTH.K=TABHL(GROWTT,TOTRES.K,0,100,10)
T  GROWTT=-50/-30/-15/-6/-1/0/.007/.018/.025/.03/.03
    GROWTT-GROWTH FACTOR TABLE
L  USRES.K=USRES.J+DT*(RAUS.JK-RDMOUS.JK)
    USRES-US RESOURCES
    RAUS-RESOURCE ALLOCATION FOR THE US
    RDMOUS-RESOURCE DEMAND IN THE US
    USRESC-US RESOURCES INITIAL VALUE
N  USRES=USRESC
C  USRESC=33
R  RAUS.KL=(DISCOV.JK-TRUSE.JK)*ALLOCF
C  ALLOCF=.33
    ALLOCF-ALLOCATION FRACTION
R  RDMOUS.KL=(GROWTH.K-(EFFF.K/100))*USRES.K
    EFFF-EFFICIENCY
A  EFFF.K=DTC.K+TECHIF.K
    DTC-DESIRE TO CONSERVE
    TECHIF-TECHNICAL IMPROVEMENT FACTOR
A  USRESS.K=SMOOTH(USRES.K,10)
A  DTC.K=TABHL(DTCT,USRESS.K,0,35,5)
    DTCT-DESIRE TO CONSERVE TABLE
T  DTCT=-2./-.75/-.15/.4/.7/.9/1./1.0
A  TECHIF.K=TABHL(TECHIT,TECHCR.K,0,.2,.04)
    TECHIT-TECHNICAL IMPROVEMENT TABLE
    TECHCR-TECHNOLOGY CHANGE RATE
A  TECHCR.K=TECHCRC
C  TECHCRC=.1
    TECHCRC-TECHNOLOGY CHANGE RATE CONSTANT
T  TECHIT=1/.5/.25/.15/.07/.04
A  RPFT.K=TABHL(RPFTT,USRESS.K,0,100,10)
    RPFT-RESOURCES PRESSURE FOR TECHNOLOGY
    RPFTT-RESOURCES PRESSURE FOR TECHNOLOGY TABLE
    USRESS-US RESOURCES (SMOOTHED)
T  RPFTT=1/.8/.7/.6/.5/.45/.41/.39/.38/.36/.35
A  RADPP.K=TABHL(RADPPT,TOTRES.K,0,100,10)
    RADPP-RESOURCES AVAILABLE FOR DEFENSE PRODUCTION
    RADPPT-RESOURCES AVAILABLE FOR DEFENSE PROD TABLE
T  RADPPT=0/.1/.25/.4/.35/.32/.3/.28/.27/.26/.25
A  RAAOP.K=TOTRES.K*RADPP.K*AALLOC
    RAAOP-RESOURCES ALLOWED FOR ALLIED DEF. PROD.

```

FIGURE 19. RESOURCES

```
          AALLOC-ALLIED ALLOCATION PERCENTAGE
C   AALLOC=.35
A   RAUSD $P.K=USRES.K*RPUSD $P.K
      RPUSD $P-RESOURCES % FOR DEFENSE PRODUCTION
A   RPUSD $P.K=TABHL(RPUSD $T,USRES.K,0,35,5)
      RPUSD $P $T-RESOURCES % FOR DEF. PROD. TABLE
T   RPUSD $T=0/.2/.4/.3/.28/.27/.26/.25
SPEC DT=.05
SPEC LENGTH=36
SPEC PLTPER=2
SPEC PRTPER=0
PLOT TOTRES/USRES/DISCOV/GROWTH/USRESS/RAUSD $P/RPFT/EEEE/RAAD $P
PRINT TOTRES,USRES,DISCOV,GROWTH,USRESS,RAUSD $P,RPFT,RAAD $P$$$$$$$$$$$$ 
```

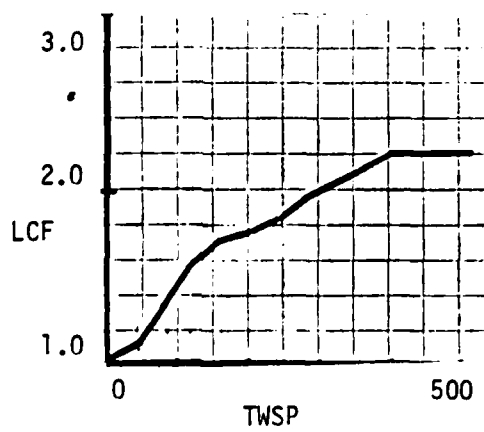



FIGURE 21. LEARNING CURVE

```

NOTE*****PRODUCTION*****
L  WSP.K=WSP.J+DT(WSPIR.JK-WSPR.JK)
    WSP      WEAPON SYSTEM PRODUCTION
    WSPIR    WEAPON SYSTEM PRODUCTION RATE INPUT
    WSPR     WEAPON SYSTEM PRODUCTION RATE (OUT)
N  WSP=0
R  WSPIR.KL=MIN(PGMXX.K,RCWS.K)
    PGMXX    PROGRAM
    RCWS     RESOURCE CONSTRAINT ON WEAPON SYSTEMS
A  PGMXX.K=PGMX.K*PPRC
    PPRC     PLANNED PROGRESS RATE
C  PPRC=5
R  WSPR.KL=DELAY3(WSPIR.JK,PRODT.K)
    PRODT    PRODUCTION TIME
A  RCWS.K=RAUSDP.K*WSRCF
    RAUSDP   RESOURCES AVAILABLE FOR US DEF. PROD.
    WSRCF    WEAPON SYSTEM RESOURCES CONVERSION FACTOR
A  RAUSDP.K=RAUSDPC
C  RAUSDPC=100
C  WSRCF=1
A  PRODT.K=PRODTDC/PRODTA.K
    PRODTA   PRODUCTION TIME ADJUSTOR
A  PRODTA.K=LCF.K*TEX.K*CPTS.K
    LCF      LEARNING CURVE FACTOR
    TEX     TECHNICAL EFFECTIVENESS
    CPTS    CHANGE IN PRODUCTION TIME (SMOOTHED)
A  CPTS.K=SMOOTH(CPTT.K,CPTD)
    CPTT    CHANGE IN PRODUCTION TIME TABLE
    CPTD    CHANGE IN PRODUCTION TIME DELAY
A  CPTT.K=CPT.K
C  CPTD=1
A  CPT.K=PRODTD.K/PRODTDC
    PRODTD   PRODUCTION TIME DESIRED
    PRODTDC  PRODUCTION TIME PLANNED
A  PRODTD.K=PRODTDC*TEX.K
C  PRODTDC=12
A  LCF.K=TABHL(LCFT,TWSP.K,0,520,40)
    LCFT     LEARNING CURVE FACTOR TABLE
    TWSP     TOTAL WEAPON SYSTEMS PRODUCED
T  LCFT=1/1.15/1.35/1.57/1.69/1.78/1.87/1.96/2.02/2.11/2.2/2.2/2.2
X  /2.2
A  RWSP.K=NWSP-TWSP.K
    RWSP     REMAINING WEAPON SYSTEMS TO PRODUCE
    NWSP     NUMBER OF WEAPON SYSTEMS PRODUCED
    TWSP     TOTAL WEAPON SYSTEMS TO PRODUCE
C  NWSP=422
L  TWSP.K=TWSP.J+DT(WSPR.JK-RR.JK)
    RR      RETIREMENT RATE
N  TWSP=0
R  RR.KL=0
L  WSIT.K=WSIT.J+DT(WSPR.JK-WSDR.JK)
    WSIT    WEAPON SYSTEMS IN TRANSIT
    WSPR    WEAPON SYSTEM PRODUCTION RATE
    WSDR    WEAPON SYSTEM DELIVERY RATE
N  WSIT=0
R  WSDR.KL=DELAY3(WSPR.JK,WSTT)
    WSTT    WEAPON SYSTEM TIME IN TRANSIT
C  WSTT=2
L  APX.K=APX.J+DT(APRX.JK-ATPX.JK)
NOTE:FOR THE REMAINING DEFINITIONS REFER TO THE WEAPON SYSTEM

```

FIGURE 22. PRODUCTION EQUATIONS AND DEFINITIONS

NOTE: DEVELOPEMENT MODEL EQUATIONS.

```

N   APX=0
R   ATRX.KL=0
R   APRX.KL=APRRXX.K
N   APRRX=0
A   APRRX.K=TEX.K*PGMX.K*CAPRSX.K
A   CAPRSX.K=DELAY3(CAPRX.K,CAPRDX)
C   CAPRDX=1
A   CAPRX.K=FLFX.K*DCAPRX.K
A   DCAPRX.K=DCAPRXC
C   DCAPRXC=1
A   TEX.K=MEX.K/TCF
C   TCF=1
A   MEX.K=EX.K*MOD
A   EX.K=EXC
C   EXC=1
C   MOD=1
A   PGMX.K=TABHL(PGMXT,SCHEDX.K,0,60,5)
A   SCHEDX.K=TSMSXO.K
A   PAPX.K=DELAY1(APX.K,WSPDX)
C   WSPDX=.05
A   RTTMSX.K=(TSMSXO.K-PATX.K+TTMSX.K)*PRESSX
A   PRRX.K=(PPXT.K-PATX.K+RTTMSX.K)/TTMSX.K
A   PATX.K=TABHL(PATXT,PAPX.K,0,100,20)
A   PPXT.K=TABHL(PPXTT,PPX.K,0,100,20)
T   PPXTT=0/3/5.5/7.6/9.8/11
T   PATXT=0/3/5.5/7.6/9.8/11
C   PRESSX=1
A   TTMSX.K=60-TSMSXO.K
A   CFX.K=TABHL(CFTX,SFX.K,0,10,5)
T   CFTX=1/5/10
A   SFX.K=TABHL(SFTX,PRRX.K,0,10,5)
T   SFTX=1/5/10
L   PPX.K=PPX.J+DT*(PPGMX.JK-PPTXX.JK)
N   PPX=.01
R   PPTXX.KL=0
R   PPGMX.KL=TABHL(PGMXT,PSCHDX.K,0,60,5)
T   PGMXT=0/.833/1.66/1.66/1.66/1.66/1.66/1.66/1.66/
X   1.66/1.66/2.499/3.332
A   PSCHDX.K=TSMSXO.K
L   CRX.K=CRX.J+DT*(CRRX.JK-CRTRX.JK)
N   CRX=CRXC
C   CRXC=.01
R   CRRX.KL=(CEX/TEX.K)*DCFSX.K*PGMX.K/PTCR
C   CEX=1
A   DCFSX.K=SMOOTH(DCFX.K,DCFXD)
C   DCFXD=1
C   PTCR=1
R   CRTRX.KL=0
A   DCFX.K=DCFXC
C   DCFXC=1
L   PCX.K=PCX.J+DT*(PCRX.JK-PCTRX.JK)
N   PCX=PCXC
C   PCXC=.01
R   PCRX.KL=(PPGMX.JK/PTCR)+CPCX.K
R   PCTRX.KL=0
A   PRAPX.K=PAPX.K/PPX.K
A   CRPAX.K=PCX.K/CRX.K
A   FLFX.K=TABHL(FLFXT,CRPAX.K,0,2,1)
T   FLFXT=0/1/2

```

```

A   PIFX.K=TABHL(PIFT,FLFX.K,0,1.4,.2)
T   PIFT=1/.72/.57/.45/.38/.32/.28/.25
A   ITAFX.K=FAX.K*PIFX.K*PRAPX.K+USURGF.K*MAIMPF
A   FIDX.K=TABHL(FIDT,ITAFX.K,.8,2,.2)
T   FIDT=0/.375/.62/.75/.86/.92/.96
A   CPCX.K=FIDX.K*ECCX.K
A   ECCX.K=CLIP(ICRX.K,0,ICRX.K,0)*(TSMSX0.K+RTTMSX.K)/PTC
C   PTC=100
A   ICRX.K=1-(1/CRPAX.K)
A   FAFX.K=ECCX.K/RDAX.K
A   RDAX.K=RDAXC
C   RDAXC=1
A   FAX.K=TABHL(FATX,FAFX.K,0,1,.5)
T   FATX=0/.001/1
L   PVX.K=PVX.J+DT(PVRX.JK-PVTRX.JK)
N   PVX=0
R   PVRX.KL=PPVSX.K*PVAX.K
A   PPVSX.K=PPGMX.JK
A   PVAX.K=PRAPX.K*CRPAX.K
R   PVTRX.KL=0
L   TSMSX0.K=TSMSX0.J+DT(TINX.JK-TOUTX.JK)
N   TSMSX0=0
R   TOUTX.KL=0
R   TINX.KL=1
A   USURGF.K=USURGFC
C   USURGFC=1
C   MAIMPF=1
A   PPXX.K=PPX.K*(PPRC/5)*(12/PRODTDC)
A   CRXX.K=CRX.K*(PPRC/5)*(12/PRODTDC)
A   PCXX.K=PCX.K*(PPRC/5)*(12/PRODTDC)
A   PVXX.K=PVX.K*(PPRC/5)*(12/PRODTDC)
SPEC DT=.05
SPEC LENGTH=60
SPEC PLTPER=3
SPEC PRTPER=0
PLOT PPXX,CRXX,PCXX,PVXX/WSP/TWSP/WSIT/RWSP/LCF
PRINT CAPRSX,CAPRDX,CAPRX,DCAPRX,TEX
PRINT MEX,EX,PGMX,SCHEDX,PAPX,RTTMSX,PRRX
PRINT PATX,PPXT,CFX,SFX,PPX,PPTXX,PPGMX,PSCHDX
PRINT CRX,CRRX,DCFSX,CRTRX,DCFX,PCX,PCRX,PCTRX
PRINT PRAPX,CRPAX,FLFX,PIFX,ITAFX,FIDX,CPCX,ECCX
PRINT ICRX,FAFX,PVX,PVRX,PPVSX,PVAX,PVTRX

```

FIGURE 22. (CONT 2)

F. Operations

The Operations Sector Sub-Model consists of three levels, the Weapon Systems Operational (WSO), the Weapon Systems Not Operational (WSN), and the Average Number of Weapon Systems Available (AWSA).

The weapon systems operational and weapon systems not operational levels are affected by the weapon system deficiency rate (WSSDR) or out of commission rate and the Weapon System Maintenance Rate (WSMR). The WSO is also affected by the delivery rate (WSDR) and the retirement rate (WSRR). The weapon system delivery rate although constant in this model is affected by the delivery rate from the production sector. The maintenance rate is affected by the number of systems not operational, the available O&S dollars (OSDAM), and the other O&S requirements (OSR). The deficiency rate (WSSDR) is affected by WSO, the use rate (USE), and the mean time between failure (MTBF). The operations plan (OPLAN), the technical effectiveness of the design (TE4D), and the operational readiness factor (WSORF) all affect the weapon systems operational. The average weapon system available (AWSA) is a counter. Figure 23 shows the flow diagram of the Operational Sector Sub-Model.

Figure 24 shows the applicable table functions for the operational sector. These include pressure for support (PFOS), O&S dollars available (OSDAM), the operations plan (OPLAN), the weapon system OR factor (WSORF), the mean time between failures age multiplier (MTBFM), the weapon system retirement factor (WSRF) and the need factor (ND).

Figure 25 shows the equations of the Operational Sector.

IV. Results and Conclusions

A. Results

The results shown below are the final product of computer runs of the various sub-models. In each case the basic model is depicted as defined by the appropriate listing of equations and its behavior is explained. Next constant or table changes were made to the basic program which was then rerun. These rerun results are also depicted and explained.

1. Technology

Figure 26 shows the basic Technology run. In this case technology (T), technology input and loss (I,L) all show constant increase with time. The technology base grows from a given 100 percent to 115 percent in 120 months. In this run the technical loss factor (F) and the technical change rate (R) remained constant. On Figure 27 all factors remained constant for the 120 month run period.

Figure 28 shows the technology model with a doubled growth rate at 1.0%. This very small increase in growth from .005 to .01 shows the typical compounding effect on the overall technology and increased it to 119 from 115 on the basic run.

Figure 29 shows the effect of increasing the pressure on R&D by increasing RDOC from 1 to 2. Although this constant is doubled, its affect is quite small and results in a technology level of 116. Figure 30 shows the increase on total search pressure (TSP), other pressures (OP), and the search for new technology (SMT). A similar result could be expected if economy (ECON), resource pressure for technology (RPFT), or SUM were increased similarly.

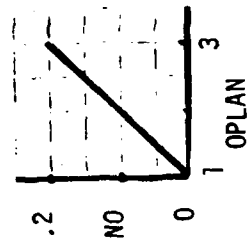
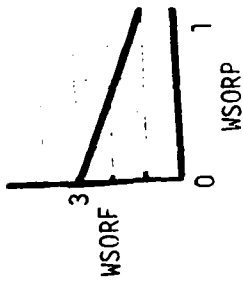
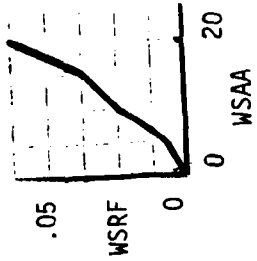
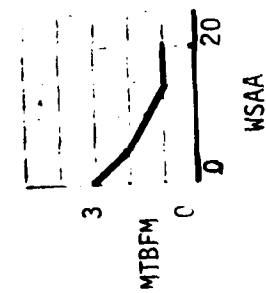
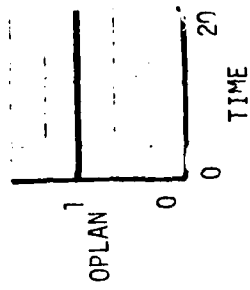
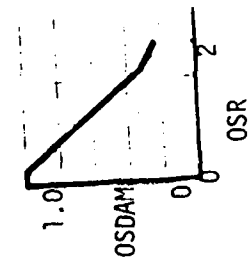
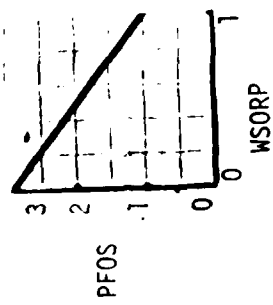


FIGURE 24. WEAPON SYSTEM OPERATION CHARTS

NOTE *****WEAPON SYSTEM OPERATIONS SECTOR*****
NOTE*****OPS2*****

L $WSO.K = WSOC.J + DT * (WSMR.JK + WSDR.JK - WSSDR.JK - WSPR.JK)$
N $WSO = WSOC$
C $WSOC = 1800$
WSO WEAPON SYSTEMS OPERATIONAL
WSMR WEAPON SYSTEM MAINTENANCE RATE
WSDR WEAPON SYSTEM DELIVERY RATE
WSSDR WEAPON SYSTEM DEFICIENCY RATE
WSRR WEAPON SYSTEM RETIREMENT RATE

R $WSMR.KL = WSORP.K * OSF.K * WSN.K$
WSORP WEAPON SYSTEM OR PERCENT
OSF O&S FACTOR
WSN WEAPON SYSTEMS NOT OPERATIONAL

R $WSDR.KL = WSDRC.K$
A $WSDRC.K = WSDRCC$
C $WSDRCC = 100$

L $WSN.K = WSN.J + DT * (WSSDR.JK - WSMR.JK)$
A $WST.K = WSO.K + WSN.K$
N $WSN = WSNC$
C $WSNC = 200$

R $WSSDR.KL = USE.K / MTBF.K$
USE USE
MTBF MEAN TIME BETWEEN FAILURES

A $WSORP.K = WSO.K / (WSN.K + WSO.K)$
A $OSR.K = OSCF * (1 - WSORP.K)$
OSCF O&S COST FACTOR

C $OSCF = .1$

A $PFOS.K = TABHL(PFOST, WSORP.K, 0, 1, .5)$
PFOS PRESSURE FOR O&S
PFOST PRESSURE FOR O&S TABLE

T $PFOST = 3/2/1$

A $OSF.K = OSDAM.K * PFOS.K$
OSDAM O&S DOLLARS AVAILABLE MULTIPLIER

A $OSDAM.K = TABHL(OSDAMT, OSR.K, 0, 2, .2)$
T $OSDAMT = 1.0/.98/.9/.82/.7/.5/.38/.29/.26/.24/.22$

A $USE.K = WSORF.K * (WSO.K) * OPLAN.K$
WSORF WEAPON SYSTEM OR FACTOR
OPLAN OPERATING PLAN

A $OPLAN.K = TABHL(OPLANT, TIME.K, 0, 20, 2)$
OPLANT OPERATING PLAN TABLE

T $OPLANT = 1/1/1/1/1/1/1/1/1/1/1$

T $WSORFT = 3/2/1$
WSORFT WEAPON SYSTEM OR FACTOR TABLE

A $WSORF.K = TABHL(WSORFT, WSORP.K, 0, 1, .5)$

A $MTBF.K = MTBFC * TE4D.K * MTBFM.K$
MTBFC MEAN TIME BETWEEN FAILURES CONSTANT
TE4D TECHNICAL EFFECTIVENESS DESIGNED (SMOOTHED)
MTBFM MEAN TIME BETWEEN FAILURES MULTIPLIER

C $MTBFC = 4$

A $TE4D.K = SMOOTH(TTE.K, 5)$
TTE TOTAL TECHNICAL EFFECTIVENESS

C $TTEC = 1$

A $TTE.K = TTEC$

A $MTBFM.K = TABHL(MTBFMT, WSAA.K, 0, 20, 5)$
WSAA WEAPON SYSTEM AVERAGE AGE

T $MTBFMT = 3/2/1.5/1$

A $TM.K = TMC$
TM TIME MULTIPLIER

C $TMC = 1$

FIGURE 25. OPERATIONS, EQUATIONS AND DEFINITIONS

```

A   WSRRR.K=(WSRF.K)*(WST.K)+(ATTR*USE.K)-ND.K*WST.K
    WSRRR      WEAPON SYSTEM RETIREMENT RATE AVERAGE
    WSRF       WEAPON SYSTEM RETIREMENT FRACTION
    WST        WEAPON SYSTEMS TOTAL
    ATTR       ATTRITION RATE
    ND         NEED
R   WSRR.KL=MAX(WSRRR.K,0)
C   ATTR=.01
A   WSRF.K=TABHL(WSRFT,WSAA.K,0,20,5)/TM.K
T   WSRFT=0/.007/.02/.03/.05
A   ND.K=TABHL(NDT,OPLAN.K,1,3,1)
T   NDT=0/.1/.2
L   AWSA.K=AWSA.J+DT(WSAR.JK-WSARR.JK)
    AWSA       ACCUMULATED WEAPON SYSTEM AGE
    WSAR       WEAPON SYSTEM AGE RATE
    WSARR      WEAPON SYSTEM AGE RETIREMENT AND RESTORATION
N   AWSA=21000
R   WSAR.KL=WSDRCC+AWSA.K*(2290/WST.K)-AWSA.K
R   WSARR.KL=WSRR.JK*20
A   WSAA.K=AWSA.K/WST.K
SPEC DT=.5
SPEC LENGTH=30
SPEC PLTPER=1
SPEC PRTPER=0
PLOT WSO,WSN,WST/WSRR/WSSDR/WSMR/WSORP/USE/MTBF/OSDAM
PRINT WSO,WSN,WST,WSRR,WSSDR,WSMR,WSORP,USE,MTBF,OSDAM

```

FIGURE 25. (CONT 1)

Figure 31 shows that there is no affect when changing the delay of the technical loss factor from 120 to 60 months.

Figure 32 and 33 show that changing the shape of this table function, Technical Pressure (TP), has little affect on the overall results.

The technical discovery factor (TDF), however, is quite sensitive to changing table parameters. This is shown on Figures 34 and 35. Increasing the TDF results in an increase in technology (117) and a decrease in TDF shows a decrease to 113.

The search for new technology (SNT) and technology complexity factor (TCF) table functions were changed and run, however, neither showed significant changes in the technology base over the 120 month period.

2. Weapon System Development

This model was designed to accommodate a two cycle weapon system development program. More cycles could easily be added as explained earlier. In each cycle the time to completion was planned to be 12 months and completion is shown as 100% on the graphics. The planned costs and product value are also targeted at 100% and 12 months.

The basic run, Figure 36, shows that the actual progress (AP,0,1) the planned progress (PP,2,3), costs reported (CR,4,6), planned costs (PP,5,7) and product value (PV,8,9) all follow a linear course to 100% at the twelve month period for phase I and at the 24 month period for phase II. The double digit numbers in the legend (11,22) denote phase I and II respectively. This result shows that if everything goes as planned everything will be at 100% at the appropriate 12 month period. Note that each phase starts with all values at 0 and finishes at 100% twelve months later.

Figure 37 shows that when the management team's motivation declines from 1.0 to 0.5 each phase will require 19 months for completion. However, the costs reported will be at 100% of planned at the twelve month period. This shows that poor management will take longer and cost more than good management. The product value does not reach 100% until the first phase is complete at the 19 month point.

Figure 38 shows just the opposite of Figure 37. In this case the team is highly motivated at 1.5. This results in phase I completion at 10 months. During phase I the costs reported tracked the planned costs. This results in a program completion ahead of schedule and below costs. Phase II shows some interesting results as the costs reported exceeds both planned costs and the planned program and these all exceed the actual progress. For phase II product value lags all others. The completion time for phase II is at the 23 month point which means that phase II required 13 months. This is an interesting result that will require further scrutiny.

Figure 39 shows the impact of reducing the experience rank, and education of the management team. In this case education was lowered from 18 to 16 years, rank from 0-4 to 0-3, and R&D experience from 20 to 10 years. This change drastically affected the program. The 12 month phase I effort became 24 months long and the budget was expended at 12 months. Actually 100% of the budget was expended when only 30% of the program was completed.

PAGE 19 FILE TECH TECH*****
 TDFS=C, TDF=1, TSP=2, IP=3, OP=4, SNT=5, TCF=6, TECHCR=C

U7/13/R1

	5.A	10.A	15.A	20.A
.0				
.0	1.A	2.A	3.A	4.A 2
.0	.5A	1.A	1.5A	2.A 345
1.869	1.869	1.87	1.87	1.971 6
12.9A	12.95A	13.A	13.05A	13.1A C
.0	-6-	-2-	-0-	-C-
C	.	2 5	0	6 01,234
C	.	2 5	0	6 01,234
C	.	2 5	0	6 01,234
C	.	2 5	0	6 01,234
C	.	2 5	0	6 01,234
C	.	2 5	0	6 01,234
C	.	2 5	0	6 01,234
C	.	2 5	0	6 01,234
C	.	2 5	0	6 01,234
C	.	2 5	0	6 01,234
50.C	-	-2-	-0-	-6 01,234
C	.	2 5	0	6 01,234
C	.	2 5	0	6 01,234
C	.	2 5	0	6 01,234
C	.	2 5	0	6 01,234
C	.	2 5	0	6 01,234
C	.	2 5	0	6 01,234
C	.	2 5	0	6 01,234
C	.	2 5	0	6 01,234
C	.	2 5	0	6 01,234
100.C	-	-2-	-0-	-6 01,234
C	.	2 5	0	6 01,234
C	.	2 5	0	6 01,234
C	.	2 5	0	6 01,234
C	.	2 5	0	6 01,234
C	.	2 5	0	6 01,234

FIGURE 35. TECHNOLOGY. TDFT = .01/.08/.18/.19/.2 (B)

PAGE 6 FILE WEAPSYS 07/13/61
 AP11=0, AP22=1, PP11=2, PP22=3, CP11=4, PC11=5, CR22=6, PC22=7, PV11=8, PV22=9

	.0	50.	100.	150.	200.	
.00						0123456789
10						0245,136789
1 0						02458,13679
1 02						13679,245,08
1 60						0245,13679
1 602						13679,245
1 8 0						0245,13679
1 8 0 P02						13679,245
1 8 0						0245,13679
1 8 02						13679,245
10.1						0245,13679
1						13679,24,05
1						13679,245
1						02458,13679
.91						02458,1367
.91						02458,1367
.913						02458,367
.91						02458,1367
.913						02458,367
.9 1.						02458,1367
20.						02458,367
.9 1						02458,1367
.9 13						02458,367
.9 13						02458,367
.9 13						02458,36,17
.9 170						02458,36,17

FIGURE 36A. WEAPON SYSTEM DEVELOPMENT. BASIC (A)

PAGE 10 FILE WEAPSYS 07/14/81
 AP11=0,AP22=1,PP11=2,PP22=3,CR11=4,PC11=5,CR22=6,PC22=7,PV11=8,PV22=9

.0	50.	100.	150.	200.
.00				0123456789
02	.	.	.	0136789,245
0 2	.	.	.	0136789,245
10 2	.	.	.	13679,245,08
10 2	.	.	.	13679,245,08
180 2	.	.	.	13679,245
1 0 2	.	.	.	13679,245,08
1 0 2	.	.	.	13679,245,08
1 80 2	.	.	.	13679,245
1 0 2	.	.	.	13679,245,08
10.1 -80 2	.	.	.	13679,245,08
1 0 52	.	.	.	13679,24,08
1 80 2	.	.	.	13679,245
1 80 2	.	.	.	13679,245
1 0 2	.	.	.	13679,245,08
1 0 2	.	.	.	13679,245,08
1 0 2	.	.	.	13679,245,08
1 80 2	.	.	.	13679,245
1 80 2	.	.	.	13679,245
20.1 -0 2	.	.	.	13679,245,08
1 0 2	.	.	.	13679,245,08
1 80 2	.	.	.	13679,245
1 80 2	.	.	.	13679,245
1 80 2	.	.	.	13679,245

FIGURE 39. WEAPON SYSTEM DEVELOPMENT
 EDIC = 16, RGIC = 3, YRDIC = 10

Figure 40 shows the effect of combining high motivation (See Figure 38) and low experience (See Figure 39). This highly motivated but low experience team is able to bring in phase I in 18 months. This reflects that the model is responsive to a number of modeling changes simultaneously.

Figure 41 shows the effects of changing the actual progress perceived delay (APDI) from 0.05 to 1 for phase I only. The actual progress and costs reported follow the plan, for only a perception not the actual performance variable was changed. This perceived effect shows up in product value which lags throughout phase I and reaches 100% at the 15 month time point. Figure 42 shows that increasing APDI to 2 results in a continued change in product value to 100% at 16 months.

Increasing the cost estimating error factor from 1 to 1.5 is shown on Figure 43. This has a drastic effect and shows increased costs reported and reduced actual progress and product value. This shows the drastic impact of not knowing what costs are actually incurred during the development of a weapon system.

Many other runs of this weapon system development sub-model were accomplished. Nearly every constant and table was altered and evaluated. In each case the results were as expected, with the exception of the cost and schedule factors. These factors are used to forecast the program progress. Additional work needs to be done here if it is later determined that these factors can contribute to improved program management.

3. Financial

The Defense Department generally operates from a five year defense plan (FYDP). This entails a 60 period time frame of 5 fiscal years of 12 months each. In order to simplify the computer results the author has limited the output to 36 months or 3 fiscal years. Adding the two years is an easily accomplished feat.

Figure 44 shows the basic financial sector sub-model run. In this model the defense funds requested for all weapon systems R&D is (RDRB), for investment is (IDRB), and for O&S is (ODRB). The five year defense plan for R&D is coded, (FYDP1), for investment (FYDP2), and for O&S (FYDP3). The DOD requested budget shows a steady decline over each of the twelve month fiscal year periods.

Figure 45 shows a similar result for the weapon system of interest. This shows that if there are no changes to the plan all budgeted items proceed as scheduled. The FYDP1 moneys for example track the expenditure of R&D dollars.

Figure 46 and 47 show the affects of increasing government R&D support (GSPTRDX), effort not dollars, to a specific weapon system. They show that the overall DOD picture does not change (Figure 46). However, for the weapon system of interest (Figure 47) gross over spending is apparent on this weapon system. In fact when changing GSPTRDX from 1, the original value, to 1.5 three years of funds are expended in 2 years.

Figure 48 and 49 show a similar result if the interest, GSPTD, is at the DOD level only. The research budget at DOD is overspent.

Figure 50 and 51 show the effects of adding dollars (RDSUPXC) to the research budget of a specific program. Unless more government support (effort) is exerted the program will not spend all of its newly acquired R&D money.

PAGE 10 FILE WEAPSYS 07/15/81
 AP11=0,AP22=1,PP11=2,PP22=3,CR11=4,PC11=5,CR22=6,PC22=7,PV11=8,PV22=9

	.0	50.	100.	150.	200.
.00					0123456789
10					0245,136789
180					0245,13679
1 8 02					13679,245
1 8 0					0245,13679
1 8 02					13679,245
1 8 0					0245,13679
1 8 02					13679,245
1 8 0					0245,13679
1 8 02					13679,245
10.1					0245,13679
1					13679,24,05
1					13679,245
1					0245,13679
1					0245,13679
.91					02458,1367
. 913					02458,36,17
. 13					02458,367,19
. 913					02458,36,17
. 913					02458,367
20.					02458,36,17
. 913					02458,367
. 9 13					02458,36,17
. 913					02458,367
. 9 13					02458,367

FIGURE 41. WEAPON SYSTEM DEVELOPMENT. APDI = 1

PAGE 10 FILE WEAPSYS 07/16/81
 AP11=0,AP22=1,PP11=2,PP22=3,CR11=4,PC11=5,CR22=6,PC22=7,PV11=8,PV22=9

.00	50.	100.	150.	200.
100123456789
180 40245,136789
1 80 2 4025,13679
1 8 0 2 413679,25
1 8 0 2 413679,25
1 8 0 2 413679,25
1 8 0 2 413679,25
1 8 0 2 413679,25
1 8 0 2 413679,25
1 8 0 2 413679,25
10.1	8 - - 0 - - 2 - - 4 - -	4 - - 4 - - 4 - -		.13679,25
1	8 8 0 0 52	4		.13679
1	8 8 0 0	2		.13679,245
1	8 8 0 0	2		.13679,245
1	8 8 0 0	2		.13679,245
1	8 8 0 0	0		.0245,13679
1	8 8 0 0	0		.0245,13679
.91	8 8 8	0		.0245,1367
.91	8 8 8	0		.0245,1367
20.	913 8 0	0		.0245,367
.	913	0		.02458,1367
.	9 1.	0		.02458,367
.	913	0		.02458,1367
.	9 1	0		.02458,367
.	9 1	0		.02458,1367

FIGURE 43. WEAPON SYSTEM DEVELOPMENT. CEI = 1.5

PAGE 14 FILE 5UDX4 07/12/84
 FYDPX=3, RCPBX=1, FYCPRX=2, ICKRYS=3, FYCPRZY=4, CDPYEF, CDPRE=5, CDRPRT=7

Code	500.	1000.	100.	200.	300.	400.	500.	600.	700.	800.	900.	01
00	50.	100.	100.	200.	300.	400.	500.	600.	700.	800.	900.	01
01	100.	200.	300.	400.	500.	600.	700.	800.	900.	1000.	1500.	01
02	200.	400.	600.	800.	1000.	1500.	2000.	2500.	3000.	3500.	4000.	01
03	300.	600.	900.	1200.	1500.	2000.	2500.	3000.	3500.	4000.	4500.	01
04	400.	800.	1200.	1600.	2000.	2500.	3000.	3500.	4000.	4500.	5000.	01
05	500.	1000.	1500.	2000.	2500.	3000.	3500.	4000.	4500.	5000.	5500.	01
06	600.	1200.	1800.	2400.	3000.	3600.	4200.	4800.	5400.	6000.	6600.	01
07	700.	1400.	2100.	2800.	3500.	4200.	4900.	5600.	6300.	7000.	7700.	01
08	800.	1600.	2400.	3200.	4000.	4800.	5600.	6400.	7200.	8000.	8800.	01
09	900.	1800.	2700.	3600.	4500.	5400.	6300.	7200.	8100.	9000.	9900.	01
10	1000.	2000.	3000.	4000.	5000.	6000.	7000.	8000.	9000.	10000.	11000.	01
11	1100.	2200.	3300.	4400.	5500.	6600.	7700.	8800.	9900.	11000.	12100.	01
12	1200.	2400.	3600.	4800.	6000.	7200.	8400.	9600.	10800.	12000.	13200.	01
13	1300.	2600.	3900.	5200.	6500.	7800.	9100.	10400.	11700.	13000.	14300.	01
14	1400.	2800.	4200.	5600.	7000.	8400.	9800.	11200.	12600.	14000.	15400.	01
15	1500.	3000.	4500.	6000.	7500.	9000.	10500.	12000.	13500.	15000.	16500.	01
16	1600.	3200.	4800.	6400.	8000.	9600.	11200.	12800.	14400.	16000.	17600.	01
17	1700.	3400.	5100.	6800.	8500.	10200.	11900.	13600.	15300.	17000.	18700.	01
18	1800.	3600.	5400.	7200.	9000.	10800.	12600.	14400.	16200.	18000.	19800.	01
19	1900.	3800.	5700.	7600.	9500.	11400.	13300.	15200.	17100.	19000.	20900.	01
20	2000.	4000.	6000.	8000.	10000.	12000.	14000.	16000.	18000.	20000.	22000.	01
21	2100.	4200.	6300.	8400.	10500.	12600.	14700.	16800.	18900.	21000.	23100.	01
22	2200.	4400.	6600.	8800.	11000.	13200.	15400.	17600.	19800.	22000.	24200.	01
23	2300.	4600.	6900.	9200.	11400.	13600.	15800.	18000.	20200.	22400.	24600.	01
24	2400.	4800.	7200.	9600.	11800.	14000.	16200.	18400.	20600.	22800.	25000.	01
25	2500.	5000.	7500.	10000.	12200.	14400.	16600.	18800.	21000.	23200.	25400.	01
26	2600.	5200.	7800.	10400.	12600.	14800.	17000.	19200.	21400.	23600.	25800.	01
27	2700.	5400.	8100.	10800.	13000.	15000.	17200.	19400.	21600.	23800.	26200.	01
28	2800.	5600.	8400.	11200.	13400.	15200.	17400.	19600.	21800.	24000.	26600.	01
29	2900.	5800.	8700.	11600.	13800.	15400.	17600.	19800.	22000.	24200.	27000.	01
30	3000.	6000.	9000.	12000.	14200.	15600.	17800.	20000.	22200.	24400.	27400.	01
31	3100.	6200.	9300.	12400.	14600.	15800.	18000.	20200.	22400.	24600.	27800.	01
32	3200.	6400.	9600.	12800.	15000.	16000.	18200.	20400.	22600.	24800.	28200.	01
33	3300.	6600.	9900.	13200.	15400.	16200.	18400.	20600.	22800.	25000.	28600.	01
34	3400.	6800.	10200.	13600.	15800.	16400.	18600.	20800.	23000.	25200.	29000.	01
35	3500.	7000.	10500.	14000.	16200.	16600.	18800.	21000.	23200.	25400.	29400.	01
36	3600.	7200.	10800.	14400.	16600.	16800.	19000.	21200.	23400.	25600.	29800.	01
37	3700.	7400.	11100.	14800.	17000.	17000.	19200.	21400.	23600.	25800.	30200.	01
38	3800.	7600.	11400.	15200.	17400.	17200.	19400.	21600.	23800.	26000.	30600.	01
39	3900.	7800.	11700.	15600.	17800.	17400.	19600.	21800.	24000.	26200.	31000.	01
40	4000.	8000.	12000.	16000.	18200.	17600.	19800.	22000.	24200.	26400.	31400.	01
41	4100.	8200.	12300.	16400.	18600.	17800.	20000.	22200.	24400.	26600.	31800.	01
42	4200.	8400.	12600.	16800.	19000.	18000.	20200.	22400.	24600.	26800.	32200.	01
43	4300.	8600.	12900.	17200.	19400.	18200.	20400.	22600.	24800.	27000.	32600.	01
44	4400.	8800.	13200.	17600.	19800.	18400.	20600.	22800.	25000.	27200.	33000.	01
45	4500.	9000.	13500.	18000.	20200.	18600.	20800.	23000.	25200.	27400.	33400.	01
46	4600.	9200.	13800.	18400.	20600.	18800.	21000.	23200.	25400.	27600.	33800.	01
47	4700.	9400.	14100.	18800.	21000.	19000.	21200.	23400.	25600.	27800.	34200.	01
48	4800.	9600.	14400.	19200.	21400.	19200.	21400.	23600.	25800.	28000.	34600.	01
49	4900.	9800.	14700.	19600.	21800.	19400.	21600.	23800.	26000.	28200.	35000.	01
50	5000.	10000.	15000.	20000.	22200.	19600.	21800.	24000.	26200.	28400.	35400.	01

FIGURE 49. FINANCIAL. GSPTD = 1.5 (B)

Adding R&D dollars at DOD by increasing support (RDSUPP) from 1.0 to 1.5 shows little change, see Figure 52A & 52B.

Changing both support and dollars is the best of all worlds. When additional dollars are available the government managers should exert more support to these areas. After many runs it was determined that an increase in RDSUPP of 500 could be balanced by a GSTRD of 1.5. This is shown in Figure 53 and 54. Note that this is a similar result to Figure 44, the basic run. However, the above policies have a striking affect on the weapon system of interest, see Figure 55. In this case GSPTRDXC should be increased to keep up with the newly acquired funds. This is shown in Figure 56.

If a specific weapon system receives an increased priority (MAIMPF), this will spur the managers to increase spending which will require additional funding. Priorities cannot be raised without increasing funds or the priority increase is meaningless. Figure 57 shows the affect of changing priority on the weapon system of interest (MAIMPF), and government support (dollars).

In most of the above cases the changes have been made in the R&D area only. Similar results can be obtained by varying the constants in the investment and O&S areas.

The model is sensitive to managerial support (effort), additional funding (dollars), and changing priorities.

4. Resources

The primary function of the resources sub-model is to feed in as an input to the production sector sub-model. If resources are unlimited then resources become non-constraints in the acquisition process. If however, there are shortages or reduced DOD allocations then the defense production capability of the US could be significantly affected.

Figure 58 is the basic run of the resource model. It shows that as world resources (TOTRES) dwindle so do the resources available for defense production (RAUSDP). Changing US allocations (RAUS), the percent of resources available for defense production (RPUSDP), improving efficiency (EFFF), altering the desire to conserve (DTC), or changing the pressures for new technology (RPFT) all show the appropriate responses on the model.

In the interest of brevity only the discovery rate (DISCOT) and the allocation fraction (ALLOC) changes are shown graphically. Figure 59 shows the affect of improving the discovery rate of new resources. This shows a significant increase in world resources (TOTRES) and a subsequent increase in the resources available for defense production. Figure 60 shows an increase from .33 to .5 in the allocation of world resources to the US although as expected world resources remain unchanged, the US resources for defense production actually decrease at the 36 year point from 4 to 2.8. This is due to the low efficiency factor and a limited desire to conserve. Just increasing total US resources will not guarantee increase resources for defense.

PAGE 11 FILE BUCX4 07/14/91
 FYDP1X=0,CDFFX=1,FYDP2X=2,ICRFX=3,FYDP2X=4,CDFFX=5,CDFFX=6,CDFFX=7

	50.	100.	150.	200.	250.	300.	350.	400.	450.	500.	550.	600.	650.	700.	750.	800.	850.	900.	950.	1000.
10.	6	6	6	6	6	6	6	6	6	6	6	6	6	6	6	6	6	6	6	6
20.	6	6	6	6	6	6	6	6	6	6	6	6	6	6	6	6	6	6	6	6
30.	6	6	6	6	6	6	6	6	6	6	6	6	6	6	6	6	6	6	6	6

FIGURE 57B. FINANCIAL. MAIMPF = 1.1

PAGE 2 FILE RES 07/14/81
 TOTRES=0,USRES=1,OISCOV=2,GROWTH=3,USRESS=4,RAUSDP=5,RPFT=6,EFFF=7,RAADP=8

60.	70.	80.	90.	100.
.0	10.	20.	30.	40. 1
.65	.75	.85	.95	1.05 2
.0	10.A	20.A	30.A	40.A 3
.0	10.	20.	30.	40. 4
1.	3.	5.	7.	9. 5
.55	.6	.65	.7	.75 6
.5	.7	.9	1.1	1.3 7
5.	6.	7.	8.	9. 8
.0	6		3	-2-58 - 0 14,27
.	6	.	312 4	78
.	6	.	21 3 0 8	. 78
.	6	.	2 1 035 4	. 045
.	6	.	2 1 0 3 8 4	. 48
.	6	.	2 1 0 3 8 4	. 35
.	6	2	0 3 8 4	. 01,35
.	6	2	0 3 8 4	. 38
.	6	62	0 1 5 3 4	. 35
.	6	2	60 1 538 4	. 35
.	6	2	0 1 6 38 4	. 35
.	6	2	0 1 38 6 4	. 35
20.	-2-	-0-	-1-	-38-4 -67 - - - - -
.	2	0	1 38. 4 7	. 35
.	2	0	1 38. 4	. 35,47
.	2	0	1 38. 4	. 35,47
.	2	0	1 35874.	. 37,58
.	2	0	1 3 5 4	. 58
.	2	0	71 3 5 4	. 45
.	2	0	7 1 3 8 4	. 48
.	2	0	7 1 3 4 5	. 48
.2	0 7	.	13 45	. 6 . 58

FIGURE 58. RESOURCES. BASIC RUN

PAGE 4 FILE RES 07/14/81
 TOTRES=0,USRES=1,DISCOV=2,GROWTH=3,USRESS=4,RAUSDP=5,RPFT=6,EFFF=7,RAADP=8

60.	70.	80.	90.	100.	0
.0	10.	20.	30.	40.	1
.65	.75	.85	.95	1.05	2
.0	10.A	20.A	30.A	40.A	3
.0	10.	20.	30.	40.	4
.0	3.	6.	9.	12.	5
.4	.5	.6	.7	.8	6
.0	.5	1.	1.5	2.	7
5.	6.	7.	8.	9.	8
.0	-	-	-	-	0 14
.	.	6	7	5	- 1 2 4 80
.	.	6	5	12	3 0 8
.	.	6.	5	1	03.48
.	.	52	1	7	0 3 4.
.	.	2	5	1	607 3 84
.	.	2	51	0	7 6 34
.	.	2	51	0	. 7 3846
.	.2	10	.7	34	6
20.	2.	05	7.34	6	6
-	-	-	-	-	-
2	2	01	5	7	38.
.	2	01	57	438	.
.	2	01	5	438	.
.	2	01.5	4	38	.
.	2	01.5	4	38	.
.	2	07	15	4	38
.	2	0	15	4	38
.2	7	0	15	4	38
.

FIGURE 60. RESOURCES. ALLOC = 0.5

5. Production

The production sector sub-model addresses the defense production of the US. The primary level is the total weapon systems produced (TWSP).

Figure 61 shows the basic run of the model and includes the planned program (PPXX), the cost reported (CRXX), the planned cost (PCXX), the product value (PVXX), the weapon system production level (WSP), the total weapon systems produced (TWSP), the weapon systems in transit (WSIT), and the learning curve factor (LCF). From this figure it can be noted that when the program proceeds as planned the planned and actual parameters track very well and are complete (reach 100%) at the planned 60 month point. The changing learning curve can also be noted on Figure 61.

When the management-production team motivation is reduced from 1.0 to 0.5 the total weapon systems produced drops from 400 to 175, see Figure 62. Costs reported exceed the planned costs and the product value remains very low. Increasing the technical complexity factor (TCF) from 1 to 2 causes a similar result, see Figure 63A.

Decreasing the production time (PRODTDC) from 12 to 9 months is reflected an increase in weapon system produced. The planned program reaches 100% in approximately 48 months rather than 60, see Figure 63B.

Figure 64 shows the affects of extremely limited resources and production falls to 2 units.

Other runs were accomplished that show similar results with the production sector sub-model.

6. Operations

The operations sector sub-model is highlighted by the level of weapon systems operational, which is some measure of the defense capability of the US Defense Department.

Figure 65 is the basic run. This graphic shows that as MTBF increases so also does the availability of weapon systems. In this basic run the weapon systems not operational remains relatively constant, for as the use increases, the MTBF increases, the total weapon systems increase, and the maintenance capability also increases.

Figure 66 shows the effects of increasing the weapon system delivery rate (WSDRC) from 100 to 150. The WSO increases from 3000 to 4300 and use increases significantly. The MTBF improves much sooner in the program. The fleet also develops a "younger" average age.

Figure 67 shows the affects of changing the O&S cost factor (OSCF) from 0.1 to 0.2. As expected no perceivable change can be seen.

Figure 68 shows a change in MTBFC from 4 to 6. The only change is a slight reduction in the weapon systems not operational (WSN) and an improvement in MTBF.

Increasing to total technical effectiveness (TTE) of the design results in an increase in the operational systems (WSO) to 3400. The MTBF is significantly improved from 12 in the basic run to 24 in this run, see Figure 69.

When the time multiplier (TM) is doubled to 2, the WSO increases to 3400 at the 30 year point. This shows the impact of reducing the number of systems retired each year, see Figure 70. Also noted is an increase in the WSN due to the aging of the fleet.

PAGE 4 FILE PRODY 07/14/81
 PPXX=0,CRXX=1,PCXX=2,PVXX=3,WSP=4,TWSP=5,WSIT=6,RWSP=7,LCF=8

.00	50.	100.	150.	200.	0123456
0 4	8	7	.	.	.
50	8	7	.	.	012356
5 0	84	7	.	.	0123,56
.5 0 6	8	4	.	.	01236
.5 0	6	7	.	.	0123
.5 0	.8	7	.	.	0123
.5 0	6 8	7	.	.	0123
.5 0	.8 6	7	.	.	0123
.5 0	.8	6 7	.	.	0123
.5 0	.8 7	6	.	.	0123
30.	5 0	7 8	.	.	0123
.	530.	7 8	.	.	012
.	0 7	8 64	.	.	01235
.	730	64.	.	.	0125,68
.	7 . 05	64.	.	.	0123,48
.	7 . 305	4 8.	.	.	012,46
.	7 . 0 5 46 8	.	.	.	0123
.	7 . 30 46 .8	.	.	.	012,45
.	7 . 30 54 .8	.	.	.	012,56
59.997	7 . 0 56 48	.	.	.	0123
		-30 58-6- 4			012

FIGURE 61. RESOURCES. BASIC RUN

PAGE 6 FILE PRODY 07/20/81
 PPXX=0,CRXX=1,PCXX=2,PVXX=3,WSP=4,INSP=5,MSIT=6,RWSP=7,LCF=8

.0	50.	100.	150.	200.	0123
.0	100.	200.	300.	400.	4
.0	50.	100.	150.	200.	5
.0	5.	10.	15.	20.	6
50.	150.	250.	350.	450.	7
1.	1.2	1.4	1.6	1.8	8
.00					01234568
04	7
301	7
3 0 14	7
3 0 1 4	7
53 0 1 4	7
.36 0 1 .4	7
.3 6 0 .1 4	7
.35 6 0 .1 4	7
.3 5 6 0 .1 4	7
30.- 3 5 - - 6 0 - - - - -1- -4- - - - -7 - -					
. 3 5 85 06.		1 . 4	.	.	7
. 3 85 06		.1 4	.	.	7
. 3 85 0 6		. 1 4	.	.	7
. 3 5 0 6		. 1 4	.	.	7
. 3 50 6		. 1 . 7	.	.	7
. 3 0 5 8 . 6		. 4 17.	.	.	7
. 3 0 0 6 74 .1		. 6 74 .1	.	.	7
. 3 0 0 5 84.6 1		. 5 84.6 1	.	.	7
. 3 0 0 7 54 8 6 1		. 7 54 8 6 1	.	.	7
59.99- - 3 - - - - -70 - - - - -4 - -5-8- 6 1 02					

FIGURE 63A. PRODUCTION. TCF = 2

The operational arena is affected by attrition (ATTR) and when increased from .01 to .02 shows a decline in the WSO and weapon systems total, see Figure 71. The use rate is also significantly reduced and the weapon systems not operational increases significantly.

When the operations plan reflects a doubling of effort over a limited period, the use rate during this period increases appropriately. The WSN during this same period also increases, see Figure 72.

This sub-model behaved in the expected manner for all test runs. Further work on the model should include a better estimator for the average fleet age.

B. Conclusions

This modeling effort was an overwhelming success. Although the scope was reduced from the planned ten sub-models to six, the most important models are up and operating effectively. The models of Technology, Weapon System Development (R&D), Financial, Resources, Production, and Operations define a great majority of the acquisition process as perceived by a system program office. The sub-models of Political, Allied Capability, Enemy Capability, and Need represent the higher echelon portions of the acquisition process.

There are many factors that affect the acquisition process. The six sub-models include many of these factors, but definitely not all of the possible combinations. By working with DOD system managers the additional factors can be identified and can be added into the models in the appropriate fashion. Having an operating model of the system enables the modeler to easily add new parameters, change relationships, and to test the new version of the models.

No significant insights into the acquisition process were discovered during this modeling effort. However, after completing the other four sub-models and integrating all ten into a single acquisition model, this comprehensive model should prove to be quite interesting. The counter-intuitiveness of this complex system will surely be evident when different policies are evaluated using the acquisition process model.

This may be one of the first attempts at dynamically modeling the acquisition process. The author is more convinced now than at the beginning of this work that continued effort in this arena will result in a better understanding of major system acquisitions and improved policies for the Department of Defense.

V. Recommendations

The work on the weapon system acquisition process model should continue. This study has demonstrated the feasibility of dynamic modeling in the acquisition arena.

The remaining effort can logically be divided into five separate phases:

- 1) Complete the work on the remaining four sub-models of Political, Allied Capability, Enemy Capability and Need. The author has accomplished some preliminary work on this phase.
- 2) Combine all ten sub-models into one comprehensive weapon system acquisition process model. Complete a computer test and sensitivity analysis of the model.

3) Through the good office of the AFBRMC obtain access to two or three small R&D type programs at WPAFB and validate the constants, tables, and relationships within the model. Programs such as The Cruise Missile or other simple weapon system would probably be ideal for this phase 3 validation.

4) Again with the aid of the AFBRMC obtain access to a major weapon system such as the F-15 or F-16 and validate the model as was suggested in phase 3.

5) With the experience and data bases obtained in the previous phases, phase 5 would consist of developing improved policies for the weapon system acquisition process. Policies similar to the initiatives of Secretary Calucci could be tested and validated prior to implementations.

It is recommended that the work continue because of its demonstrated high potential as a policy analysis tool and because of the rather low budget required to complete this endeavor.

APPENDIX I.
MODEL EQUATIONS

1. TECHNOLOGY
MODEL

```

FILE TECH  TECH*****
*  TECH*****
L  TECH.K=TECH.J+DT*(TIP.JK-TLR.JK)
N  TECH=TECHC
C  TECHC=100
C  GROWTH=.005
C  RDOC=1
C  SUM=.001
C  PPFT=1
R  TIR.KL=TECH.K*(GROWTH+TDFS.K)
A  TDFS.K=SMOOTH(TDF.K,TDFD)
C  TDFD=24
A  TDF.K=TABHL(TDFT,SNT.K,0,.1,.025)
T  TDFT=.001/.005/.01/.015/.02
A  TSP.K=TP.K+OP.K
A  TP.K=TABHL(TPT,TECH.K,0,100,25)
T  TPT=1/.75/.5/.25/.001
A  OP.K=(SUM(RDOC)/ECON)*PPFT
C  ECON=1
A  SNT.K=TABHL(SNTT,TSP.K,0,2,.5)
T  SNTT=.001/.025/.05/.075/.1
R  TLR.KL=TECH.K*TLF.JK
R  TLF.KL=SMOOTH(GROWTH,TLFD)
C  TLFD=120
A  TCF.K=TABHL(TCFT,TECHC.K,0,.2,.05)
T  TCFT=2/1.5/1/.05/.001
A  TECHCR.K=(TIP.JK-TLR.JK)/TECH.K
PLOT TECH/TIR/I/TLR/L/TLF/F/TECHCR/R
PLOT TDFS/TDF/TSP/TP/OP/SNT/TCF
X   /TECHCR=C
PRINT TECH/TIR/TLR/TLF
SPEC DT=1/LENGTH=120/PLTPEP=5/PRTPER=6
RUN  STD#

```

2. WEAPON SYSTEM DEVELOPMENT
MODEL

FILE WEAPSYS 07/14/61

```
NOTE*****WEAPON SYSTEM DEVELOPMENT*****
NOTE*****PHASE I*****
L AP1.K=AP1.J+DT(APR1.JK-ATR1.JK)
N AP1=0
R ATR1.KL=0
R APR1.KL=APRR11.K
N APRR11=0
A APRR11.K=TE1.K*PGM1.K*CAPRS1.K
A CAPRS1.K=DELAY3(CAPR1.K,CAPRD1)
C CAPRD1=1
A CAPR1.K=FLF1.K*DCAPR1.K
A DCAPR1.K=DCAPRIC
C DCAPRIC=1
A TE1.K=TCF*ME1.K
C TCF=1
A ME1.K=E1.K*MOD
C MOD=1
A E1.K=YRDF1.K*RGF1.K*EDF1.K
A ED1.K=ED1C
C ED1C=18
A RG1.K=RG1C
C RG1C=5
A YRD1.K=YRD1C
C YRD1C=20
A EDF1.K=TABHL(EDFIT,ED1.K,12,21,1)
T EDFIT=0/.16/.33/.5/.66/.83/1/1/1/1
A RGF1.K=TABHL(RGFIT,RG1.K,1,6,1)
T RGFIT=0/.25/.5/.75/1/1
A YRDF1.K=TABHL(YRDFIT,YRD1.K,0,20,5)
T YRDFIT=0/.25/.5/.75/1.0
A PGM1.K=TABHL(PGM1T,SCHED1.K,0,12,1)
A SCHED1.K=TSMSO.K
A PAP1.K=DELAY1(AP1.K,APD1)
C APD1=.05
A RTTMS1.K=(TSMSO.K-PAT1.K+TTMS1.K)*PRESS1
A PRR1.K=(PP1T.K-PAT1.K+RTTMS1.K)/TTMS1.K
A PAT1.K=TABHL(PAT1T,PAP1.K,0,100,20)
A PP1T.K=TABHL(PP1TT,PP1.K,0,100,20)
T PP1TT=0/3/5.5/7.6/9.8/11
T PAT1T=0/3/5.5/7.6/9.8/11
C PRESS1=1
A TTMS1.K=12-TSMSO.K
A CF1.K=TABHL(CFT1,SF1.K,1,10,1)
T CFT1=1/10
A SF1.K=TABHL(SFT1,PRR1.K,1,10,10)
T SFT1=1/10
L PP1.K=PP1.J+DT(PPGM1.JK-PPTX1.JK)
N PP1=.01
R PPTX1.KL=0
R PPGM1.KL=TABHL(PGM1T,PSCHD1.K,0,12,1)
T PGM1T=0/4.165/8.33/8.33/8.33/8.33/8.33/8.33/8.33/
X 8.33/8.33/12.495/16.66
A PSCHD1.K=TSMSO.K
L CR1.K=CR1.J+DT*(CRR1.JK-CRTR1.JK)
N CR1=CRIC
C CRIC=.01
R CRR1.KL=CE1*DCFS1.K*PGM1.K/PTCP
C CE1=1
```

FILE WEAPSYS 07/14/81

A DCF1.K=SMOOTH(DCF1.K,DCF10)
C DCF10=1
C PTCR=1
R CRTR1.KL=CR1.K*TX1.K
A DCF1.K=DCF1C
C DCF1C=1
L PC1.K=PC1.J+DT*(PCP1.JK-PCTR1.JK)
N PC1=PC1C
C PC1C=.01
R PCR1.KL=(PPGM1.JK/PTCR)+CPC1.K
R PCTR1.KL=J
A PRAP1.K=PAP1.K/PP1.K
A CRPA1.K=PC1.K/CR1.K
A FLF1.K=TABHL(FLF1T,CPPA1.K,U,2,1)
T FLF1T=0/1/2
A PIF1.K=TABHL(PIFT,FLF1.K,U,1.4,.2)
T PIFT=1/.72/.57/.45/.38/.32/.28/.25
A ITAF1.K=FA1.K*PIF1.K*PRAP1.K+USURGF.K*MAIMPF
A FID1.K=TABHL(FIDT,ITAF1.K,.8,2,.2)
T FIDT=0/.375/.62/.75/.86/.92/.96
A CPC1.K=FID1.K*ECC1.K
A ECC1.K=CLIP(ICR1.K,0,ICR1.K,0)*(TSMSO.K+RTTMS1.K)*PTC
C PTC=100
A ICR1.K=1-(1/CRPA1.K)
A FAF1.K=ECC1.K/RDA.K
A RDA.K=RDAC
C RDAC=1
A FA1.K=TABHL(FAT,FAF1.K,0,1,2)
T FAT=0/.001/1
L PV1.K=PV1.J+DT(PVR1.JK-PVTR1.JK)
N PV1=0
R PVR1.KL=PPVS1.K*PVA1.K
A PPVS1.K=PPGM1.JK
A PVA1.K=PRAP1.K*CRPA1.K
R PVTR1.KL=PV1.K*TX1.K
L TSMSO.K=TSMSO.J+DT(TIN1.JK-TOUT1.JK)
N TSMSO=0
R TOUT1.KL=0
R TIN1.KL=1
A DCP1.K=SWITCH(0,1,RTTMS1.K)
A TX1.K=SWITCH(1,0,DCP1.K)
A USURGF.K=USURGFC
C USURGFC=1
C MAIMPF=1

NOTE *****PHASE2*****

L AP2.K=AP2.J+DT(APR2.JK-ATR2.JK)
N AP2=0
R ATR2.KL=0
R APR2.KL=APRR22.K*CLP.K
N APRR22=0
A APRR22.K=TE2.K*PGM2.K*CAPRS2.K
A CAPRS2.K=DELAY3(CAPR2.K,CAPRD2)
C CAPRD2=1
A CAPR2.K=FLF2.K*DCAPR2.K
A DCAPR2.K=DCAPR2C
C DCAPR2C=1
A TE2.K=TCF*ME2.K
A ME2.K=E2.K*MOD

FILE *!APSYS

U7/14/61

```
A E2.K=YRDF2.K*RGF2.K*FDI2.K
A ED2.K=ED2C
C ED2C=18
A RG2.K=RG2C
C RG2C=5
A YRD2.K=YRD2C
C YRD2C=20
A FDF2.K=TABHL(EDF1T,LD2.K,12,21,1)
A RGF2.K=TABHL(RGF1T,RG2.K,1,0,1)
A YRDF2.K=TABHL(YRD1T,YRD2.K,0,20,1)
A PGM2.K=TABHL(PGM2T,SCHFD2.K,0,12,1)
A SCHED2.K=TSMS1.K
A PAP2.K=DELAY1(AP2.K,APD2)
C APD2=.05
A RTMS2.K=(TSMS1.K-PAT2.K+TTMS2.K)*PRESS2
A PRR2.K=(PP2T.K-PAT2.K+RTMS2.K)/RTMS2.K
A PAT2.K=TABHL(PAT2T,PAP2.K,0,100,20)
A PP2T.K=TABHL(PP2TT,PP2.K,0,100,20)
T PP2TT=0/3/5.5/7.6/9.8/11
T PAT2T=0/3/5.5/7.6/9.8/11
C PRESS2=1
A TTMS2.K=12-TSMS1.K
A CF2.K=TABHL(CFT2,SF2.K,1,10,1)
T CFT2=1/10
A SF2.K=TABHL(SFT2,PRR2.K,1,10,1)
T SFT2=1/10
L PP2.K=PP2.J+DT*(PPGM2.JK-PPTX2.JK)
N PP2=.01
R PPTX2.KL=0
R PPGM2.KL=TABHL(PGM2T,PSCHD2.K,0,12,1)*CLPP.K
T PGM2T=0/4.165/8.33/8.33/8.33/8.33/8.33/8.33/8.33/
X 8.33/8.33/12.495/16.66
A PSCHD2.K=TSMS1.K
L CR2.K=CR2.J+DT*(CRR2.JK-CRTR2.JK)
N CR2=CR2C
C CR2C=.01
R CRR2.KL=(CE2*DCFS2.K*PGM2.K/PTCR)*CLP.K
C CE2=1
A DCFS2.K=SMOOTH(DCF2.K,DCF2D)
C DCF2D=1
R CRTR2.KL=CR2.K*TX2.K
A DCF2.K=DCF2C
C DCF2C=1
L PC2.K=PC2.J+DT*(PCR2.JK-PCTR2.JK)
N PC2=PC2C
C PC2C=.01
R PCR2.KL=(PPGM2.JK/PTCR)+CPC2.K
R PCTR2.KL=0
A PRAP2.K=PAP2.K/PP2.K
A CRPA2.K=PC2.K/CR2.K
A FLF2.K=TABHL(FLF2T,CRPA2.K,0,2,1)
T FLF2T=0/1/2
A PIF2.K=TABHL(PIFT,FLF2.K,0,1.4,.2)
A ITAF2.K=FA2.K*PIF2.K*PRAP2.K+USURGF.K*MAIMPF
A FIU2.K=TABHL(FIDT,ITAF2.K,.8,2,.2)
A CPC2.K=FIU2.K+ECC2.K
A ECC2.K=CLIP(ICR2.K,0,ICR2.K,0)*(TSMS1.K+RTMS2.K)/PTC
A TCR2.K=1-(1/CRPA2.K)
```

```

FILE WEAPSYS      U7/14/61
A   FAF2.K=ECC2.K/RUA.K
A   FA2.K=TABHL(FAT,FAF2.K,0,.4,.05)
L   PV2.K=PV2.J*DT(PVK2.JK-PVTR2.JK)
N   PV2=0
R   PVR2.KL=PPVS2.K*PVA2.K
A   PPVS2.K=PPGM2.JK
A   PVA2.K=PRAP2.K*CRPA2.K
R   PVTR2.KL=PV2.K*TX2.K
L   TSMS1.K=TSMS1.J*DT(TIN2.JK-TOUT2.JK)
N   TSMS1=0
R   TOUT2.KL=J
R   TIN2.KL=1*CLP.K
A   DCP2.K=SWITCH(0,1,RTTMS2.K)
A   TX2.K=SWITCH(1,0,DCP2.K)
A   PP11.K=MIN(PP1.K,100)
A   PP22.K=MIN(PP2.K,100)
A   AP11.K=MIN(AP1.K,100)
A   AP22.K=MIN(AP2.K,100)
A   CR11.K=MIN(CR1.K,100)
A   CR22.K=MIN(CR2.K,100)
A   PC11.K=MIN(PC1.K,100)
A   PC22.K=MIN(PC2.K,100)
A   PV11.K=MIN(PV1.K,100)
A   PV22.K=MIN(PV2.K,100)
A   CLP.K=CLIP(1,0,PAP1.K,100)
A   CLPP.K=CLIP(1,0,PP1.K,100)
SPEC DT=.05
SPEC LENGTH=24
SPEC PLTPER=1
SPEC PRTPER=0
PLOT      AP11,AP22,PP11,PP22
X   CR11,PC11,CR22,PC22,PV11,PV22
PRINT CAPRS1,ME1,TE1,APR1,AP1,PAP1,PAT1
PRINT RTTMS1,TTMS1,SF1,CF1,PGM1,PPGM1,CF2
PRINT PP1,PRAP1,DCFS1,CRR1,CR1,CRPA1,PP1T
PRINT PCR1,PC1,CPC1,ECC1,PIF1,ITAF1,FAF1
PRINT DCP1,TX1,PVA1,PVR1,PV1,TX2,PVA2,PVR2,PV2,DCP2
PRINT PP1T,PAT1,PRR1,ICR1,ECC1,FAF1,FA1,ITAF1,
PRINT FID1,CPC1,PCR1,PC1
PLOT SF1,CF1/RTTMS1,TTMS1/CRPA1,PRAP1/ITAF1/CPC1
PLOT SF2,CF2/RTTMS2,TTMS2/CRPA2,PRAP2/ITAF2/CPC2

```

3. FINANCIAL
MODEL

FILE BUDX4

07/14/81

NOTE*****BUDGET FOR WEAPON SYSTEM OF INTEREST*****

NOTE*****THE FOLLOWING EQUATIONS RELATE TO THE

NOTE*****WEAPON SYSTEM OF INTEREST

L FYDP1X.K=FYDP1X.J+DT(FP1INRX.JK-FP1ORX.JK)

L FYDP2X.K=FYDP2X.J+DT(FP2INRX.JK-FP2ORX.JK)

L FYDP3X.K=FYDP3X.J+DT(FP3INRX.JK-FP3ORX.JK)

N FYDP1X=120

N FYDP2X=360

N FYDP3X=600

NOTE-FYDP1X R&D EXPENDITURES PLANNED IN THE FYDP

NOTE-FP1INRX R&D COSTS FUNDED FROM THE FYDP

NOTE-FP1ORX R&D COSTS FUNDED FROM THE FYDP

NOTE-FYDP2X INVESTMENT EXPENDITURES PLANNED IN THE FYDP

NOTE-FP2INRX INVESTMENT COSTS INPUT TO THE FYDP

NOTE-FP2ORX INVESTMENT COSTS FUNDED FROM THE FYDP

NOTE-FYDP3X O&S EXPENDITURES PLANNED IN THE FYDP

R FP1INRX.KL=0+PULSE(120/DT,12,12)

R FP2INRX.KL=0+PULSE(360/DT,12,12)

R FP3INRX.KL=0+PULSE(600/DT,12,12)

R FP1ORX.KL=10

R FP2ORX.KL=30

R FP3ORX.KL=50

NOTE-FP1INRX R&D COSTS FUNDED FROM THE FYDP

NOTE-FP2INRX INVESTMENT COSTS INPUT TO THE FYDP

NOTE-FP3INRX O&S COSTS INPUT TO THE FYDP

NOTE-FP1ORX R&D COSTS FUNDED FROM THE FYDP

NOTE-FP2ORX INVESTMENT COSTS FUNDED FROM THE FYDP

NOTE-FP3ORX O&S COSTS FUNDED FROM THE FYDP

R RDPULX.KL=0+PULSE(120/DT,12,12)

R INVPULX.KL=0+PULSE(360/DT,12,12)

R OSPULX.KL=0+PULSE(600/DT,12,12)

L DDRBX.K=DDRBX.J+DT(DDMDRX.JK-DPREDRX.JK)

N DDRBX=1200

NOTE-RDPULX ---

NOTE-INVPULX ---

NOTE-OSPULX ---

NOTE-DDRBX DOD DOLLARS REQUESTED IN THE BUDGET

NOTE-DDMDRX DEFENSE DEMAND RATE

NOTE-DREDRX DEFENSE DEMAND REDUCTION RATE

R DDMDRX.KL=RDRQTX.K+IRQTX.K+ORQTX.K+

X RDARX.JK*(1-GSPTRDX.K)+IDARX.JK*(1-GSPTINX.K)+

X OSDARX.JK*(1-GSPTOSX.K)

NOTE-DDMDRX DEFENSE DEMAND RATE

NOTE-RDRQTX R&D FUNDS REQUIREMENT

NOTE-IRQTX INVESTMENT FUNDS REQUIREMENT

NOTE-ORQTX O&S FUNDS REQUIREMENT

NOTE-RDARX R&D ALLOCATION RATE

NOTE-GSPTRDX GOVERNMENT SUPPORT FOR R&D PROGRAMS

NOTE-IDARX INVESTMENT ALLOCATION RATE

NOTE-GSPTINX GOVERNMENT SUPPORT FOR INVESTMENT

NOTE-OSDARX O&S ALLOCATION RATE

NOTE-GSPTOSX GOVERNMENT SUPPORT FOR O&S

R DREDRX.KL=RDARX.JK+IDARX.JK+OSDARX.JK

A RDRQTX.K=RDPULX.JK+RDSUPPX.K

A IRQTX.K=INVPULX.JK+INSUPPX.K

A ORQTX.K=OSPULX.JK+OSSUPPX.K

NOTE-DREDRX DEFENSE DEMAND REDUCTION RATE

NOTE-RDARX R&D ALLOCATION RATE

FILE BUDX4

07/14/81

NOTE-IDARX INVESTMENT ALLOCATION RATE
NOTE-OSDARX O&S ALLOCATION RATE
NOTE-RDRQTX R&D FUNDS REQUIREMENT
NOTE-RDPULX ---
NOTE-RDSUPPX R&D SUPPLEMENTAL REQUEST
NOTE-IRQTX INVESTMENT FUNDS REQUIREMENT
NOTE-INVPULX ---
NOTE-INSUPPX INVESTMENT SUPPLEMENTAL REQUEST
NOTE-ORQTX O&S FUNDS REQUIREMENT
NOTE-OSPULX ---
NOTE=OSSUPPX O&S SUPPLEMENTAL REQUEST
A RDSUPPX.K=RDSUPPXC+PTX.K*RDSUPPC
A INSUPPX.K=INSUPPXC+PTX.K*INSUPPC
A OSSUPPX.K=OSSUPPXC+PTX.K*OSSUPPC
C RDSUPPXC=0
C INSUPPXC=0
C OSSUPPXC=0
NOTE-RDSUPPX R&D SUPPLEMENTAL REQUEST
NOTE-INSUPPX INVESTMENT SUPPLEMENTAL REQUEST
NOTE-OSSUPPX O&S SUPPLEMENTAL REQUEST
NOTE-RDSUPPXC-R&D SUPPLEMENTAL REQUEST CONSTANT
NOTE-INSUPPX INVESTMENT SUPPLEMENTAL REQUEST CONSTANT
NOTE-OSSUPPX O&S SUPPLEMENTAL REQUEST CONSTANT
NOTE*****THE ABOVE THREE EQUATIONS SHOULD BE IN DOLLARS/PERIOD
NOTE*****FOR THE RD,INV,AND OS VALUES 10,30,AND 60REPRESENT
NOTE*****100%
R RDARX.KL=PRDDX.K*FP10RX.JK
R IDARX.KL=PINVDX.K*FP20RX.JK
R OSDARX.KL=POSDX.K*FP30RX.JK
A PRDDX.K=GSPTROX.K
A PINVDX.K=GSPTINX.K
A POSDX.K=GSPTOSX.K
NOTE=RDARX R&D ALLOCATION RATE
NOTE=PRDDX PRESSURE FOR R&D DOLLARS
NOTE=FP10RX R&D COSTS FUNDED FROM THE FYDP
NOTE-IDARX INVESTMENT ALLOCATION RATE
NOTE-PINVDX ---
NOTE=FP20RX INVESTMENTS COSTS FUNDED FROM THE FYDP
NOTE=OSDARX O&S ALLOCATION RATE
NOTE=POSDX PRESSURE FOR O&S DOLLARS
NOTE=FP30RX O&S COSTS FUNDED FROM THE FYDP
NOTE=GSPTROX GOVERNMENT SUPPORT FOR R&D PROGRAMS
NOTE=GSPTINX GOVERNMENT SUPPORT FOR INVESTMENT
NOTE=GSPTOSX GOVERNMENT SUPPORT FOR O&S
A GSPTROX.K=GSPTROXC+CLIP(0,MAIMPFX*GSPTROXC-1,1-MAIMPFX,0)
A GSPTINX.K=GSPTINXVC+CLIP(0,MAIMPFX*GSPTINXVC-1,1-MAIMPFX,0)
A GSPTOSX.K=GSPTOSXC+CLIP(0,MAIMPFX*GSPTOSXC-1,1-MAIMPFX,0)
C GSPTROXC=1
C GSPTINXVC=1
C GSPTOSXC=1
NOTE=GSPTROX GOVERNMENT SUPPORT FOR R&D PROGRAMS
NOTE=GSPTROXC GOVERNMENT SUPPORT FOR R&D PROGRAMS CONSTANT
NOTE=MAIMPFX MISSION AREA IMPORTANCE FACTOR
NOTE=GSPTROXC GOVERNMENT SUPPORT FOR R&D PROGRAMS CONSTANT
NOTE=GSPTINXVC GOVERNMENT SUPPORT FOR INVESTMENT CONSTANT
NOTE=GSPTOSXC GOVERNMENT SUPPORT FOR O&S CONSTANT
NOTE*****THE ABOVE GOVERNMENT SUPPORT SHOULD BE IN %, FOR
NOTE*****EXAMPLE; 1.2=20%

FILE BUDX4 Q7/14/81

C MAIMPFX=1
L RDRBX.K=RDRBX.J+DT(RDMORX.JK-RREDRX.JK)
L IDRBX.K=IDRBX.J+DT(IDMORX.JK-IPEDRX.JK)
L ODRBX.K=ODRBX.J+DT(ODMORX.JK-OREDRX.JK)
N RDRBX=120
N IDRBX=360
N ODRBX=600
NOTE-MAIMPFX MISSION AREA IMPORTANCE FACTOR
NOTE-RDRBX R&D DOLLARS REQUESTED IN THE BUDGET
NOTE-RDMORX R&D DEMAND RATE
NOTE-RREDRX R&D DEMAND REDUCTION RATE
NOTE-IDRBX INVESTMENT DOLLARS REQUESTED IN THE BUDGET
NOTE-IDMORX INVESTMENT DEMAND RATE
NOTE-IPEDRX INVESTMENT DEMAND REDUCTION RATE
NOTE-ODRBX O&S DOLLARS REQUESTED IN THE BUDGET
NOTE-ODMORX O&S DEMAND RATE
NOTE-OREDRX O&S DEMAND REDUCTION RATE
R RDMORX.KL=RDRQTX.K
R IDMORX.KL=IRQTX.K
R ODMORX.KL=ORQTX.K
R RREDRX.KL=RDARX.JK
R IPEDRX.KL=IDARX.JK
R OREDRX.KL=OSDARX.JK
NOTE-RDMORX R&D DEMAND RATE
NOTE-RDRQTX R&D FUNDS REQUIREMENT
NOTE-IDMORX INVESTMENT DEMAND RATE
NOTE-IRQTX INVESTMENT FUNDS REQUIREMENT
NOTE-ODMORX O&S DEMAND RATE
NOTE-ORQTX O&S FUNDS REQUIREMENT
NOTE-RREDRX R&D DEMAND REDUCTION RATE
NOTE-RDARX R&D ALLOCATION RATE
NOTE-IPEDRX INVESTMENT DEMAND REDUCTION RATE
NOTE-IDARX INVESTMENT ALLOCATION RATE
NOTE-OREDRX O&S DEMAND REDUCTION RATE
NOTE-OSDARX O&S ALLOCATION RATE
NOTE*****BUDGET FOR ALL OTHER WEAPON SYSTEMS*****
NOTE*****THE FOLLOWING EQUATIONS RELATE TO THE
NOTE*****OTHER WEAPON SYSTEMS IN THE DOD PROGRAM.
L FYDP1.K=FYDP1.J+DT(FP1INR.JK-FP1OR.JK)
L FYDP2.K=FYDP2.J+DT(FP2INR.JK-FP2OR.JK)
L FYDP3.K=FYDP3.J+DT(FP3INR.JK-FP3OR.JK)
N FYDP1=12000
N FYDP2=36000
N FYDP3=60000
NOTE-FYDP1 R&D EXPENDITURES PLANNED IN THEFYDP
NOTE-FP1INR R&D COSTS FUNDED FROM THE FYDP
NOTE-FP1OR R&D COSTS FUNDED FORM THE FYDP
NOTE-FYDP2 INVESTMENT EXPENDITURES PLANNED IN THE FYDP
NOTE-FP2INR INVESTMENT COSTS INPUT TO THE FYDP
NOTE-FP2OR INVESTMENT COSTS JUNDED FROM THE FYDP
NOTE-FYDP3 O&S EXPENDITURES PLANNED IN THE FYDP
NOTE-FP3INR O&S COSTS INPUT TO THE FYDP
NOTE-FP3OR O&S COSTS FUNDED FROM THE FYDP
R FP1INR.KL=0+PULSE(12000/DT,12,12)
R FP2INR.KL=0+PULSE(36000/DT,12,12)
R FP3INR.KL=0+PULSE(60000/DT,12,12)
R FP1OR.KL=1000
R FP2OR.KL=3000

FILE BUDX4 07/14/81

R FP3OR.KL=5000
NOTE-FP1INR R&D COSTS FUNDED FROM THE FYDP
NOTE-FP2INR INVESTMENT COSTS INPUT TO THE FYDP
NOTE-FP3INR O&S COSTS INPUT TO THE FYDP
NOTE-FP1OR R&D COSTS FUNDED FROM THE FYDP
NOTE-FP2OR INVESTMENT COSTS FUNDED FROM THE FYDP
NOTE-FP3OR O&S COSTS FUNDED FROM THE FYDP
R ROPUL.KL=0+PULSE(12000/DT,12,12)
R INVPUL.KL=0+PULSE(36000/DT,12,12)
R OSPUL.KL=0+PULSE(60000/DT,12,12)
L DDRB.K=DDR.B.J+DT(DDMDR.JK-DREDR.JK)
N DDRB=120000
NOTE-RDPUL ---
NOTE-INVPUL ----
NOTE-OSPUL ---
NOTE-DDRB DEFENSE DOLLARS REQUESTED IN THE BUDGET
NOTE-DDMDR DEFENSE DEMAND RATE
NOTE-DREDR DEFENSE DEMAND REDUCTION RATE
R DDMDR.KL=RDRQT.K+IRQT.K+ORQT.K
R DREDR.KL=RDAP.JK+IDAR.JK+OSDAR.JK
A RDRQT.K=RDPUL.JK+RDSUPP.K
A IRQT.K=INVPUL.JK+INSUPP.K
A ORQT.K=OSPUL.JK+OSSUPP.K
A RDSUPP.K=RDSUPPC+PTX.K*RDSUPPC
A INSUPP.K=INSUPPC+PTX.K*INSUPPC
A OSSUPP.K=OSSUPPC+PTX.K*OSSUPPC
A PTX.K=CLIP(MAIMPFX*DDR.B.K/DDR.B.K,0,0,1-MAIMPFX)
C RDSUPPC=0
C INSUPPC=0
C OSSUPPC=0
NOTE-DDMDR DEFENSE DEMAND RATE
NOTE-RDRQT R&D FUNDS REQUIREMENT
NOTE-IRQT INVESTMENTS FUND REQUIREMENT
NOTE-ORQT O&S FUNDS REQUIREMENT
NOTE-DREDR DEFENSE DEMAND REDUCTION RATE
NOTE-RDAP R&D ALLOCATION RATE
NOTE-IDAR INVESTMENT ALLOCATION RATE
NOTE-OSDAR O&S ALLOCATION RATE
NOTE-RDRQT R&D FUNDS REQUIREMENT
NOTE-RDPUL ---
NOTE-RDSUPP R&D SUPPLEMENTAL REQUEST
NOTE-IRQT INVESTMENTS FUND REQUIREMENT
NOTE-INVPUL ---
NOTE-INSUPP INVESTMENT SUPPLEMENTAL REQUEST
NOTE-ORQT O&S FUNDS REQUIREMENT
NOTE-OSPUL ---
NOTE-OSSUPP O&S SUPPLEMENTAL REQUEST
NOTE-PTX ---
NOTE-MAIMPFX MISSION AREA IMPORTANCE FACTOR
NOTE-DDRBX DOD DOLLARS REQUESTED IN THE BUDGET
NOTE-DDRE DOD DOLLARS REQUESTED IN THE BUDGET
NOTE-RDSUPPC R&D SUPPLEMENTAL REQUEST CONSTANT
NOTE-INSUPPC INVESTMENT SUPPLEMENTAL REQUEST CONSTANT
NOTE-OSSUPPC O&S SUPPLEMENTAL REQUEST CONSTANT
NOTE*****THE ABOVE THREE EQUATIONS SHOULD BE IN DOLLARS/
NOTE*****PERIOD. FOR THE PD,INV,AND OS VALUES 1000,3000, AND
NOTE*****6000 REPRESENT 100%.
R RDAR.KL=PRDU.K*FP1OR.JK

FILE BUDX4 07/14/81

R IDAR.KL=PINVD.K*FP20R.JK
R OSDAR.KL=POSD.K*FP30R.JK
A PRDD.K=GSPTRO
A PINVD.K=GSPTINV
A POSD.K=GSPTOS
C GSPTPD=1
C GSPTINV=1
C GSPTOS=1
NOTE-RDAR R&D ALLOCATION RATE
NOTE-FP10R R&D COSTS FUNDED FROM THE FYDP
NOTE-IDAR INVESTMENT ALLOCATION RATE
NOTE-FP20R INVESTMENT COSTS FUNDED FROM THE FYDP
NOTE-OSDAR O&S ALLOCATION RATE
NOTE-FP30R O&S COSTS FUNDED FROM THE FYDP
NOTE-PRDD PRESSURE FOR R&D DOLLARS
NOTE-GSPTRO GOVERNMENT SUPPORT FOR R&D PROGRAMS
NOTE-PINVD ---
NOTE-GSPTINV GOVERNMENT SUPPORT FOR INVESTMENT
NOTE-POSD PRESSURE FOR O&S DOLLARS
NOTE-GSPTOS GOVERNMENT SUPPORT FOR L&S
NOTE*****THE ABOVE GOVERNMENT SUPPORT SHOULD BE IN %. FOR
NOTE*****EXAMPLE; 1.2=20%.
L RDRB.K=RDRB.J+DT(RDMDR.JK-RREDR.JK)
L IDRB.K=IDRB.J+DT(IDMDR.JK-IREDR.JK)
L ODRB.K=ODRB.J+DT(ODMDR.JK-OREDR.JK)
N RDRB=12000
N IDRB=36000
N ODRB=60000
NOTE-RDRB R&D DOLLARS REQUESTED IN THE BUDGET
NOTE-RDMDR R&D DEMAND RATE
NOTE-RREDR R&D DEMAND REDUCTION RATE
NOTE-IDRB INVESTMENT DOLLARS REQUESTED IN THE BUDGET
NOTE-IDMDR INVESTMENT DEMAND RATE
NOTE-IREDR INVESTMENT DEMAND REDUCTION RATE
NOTE-ODRB O&S DOLLARS REQUESTED IN THE BUDGET
NOTE-ODMDR O&S DEMAND RATE
NOTE-OREDR O&S DEMAND REDUCTION RATE
R PDMDR.KL=RDROT.K
R IDMDR.KL=IRQT.K
R ODMDR.KL=ORQT.K
R RREDR.KL=RDAR.JK+RDARX.JK
R IREDR.KL=IDAR.JK+IDARX.JK
R OREDR.KL=OSDAR.JK+OSDARX.JK
NOTE-RDROT R&D FUNDS REQUIREMENT
NOTE-IRQT INVESTMENT FUNDS REQUIREMENT
NOTE-ORQT O&S FUNDS REQUIREMENT
NOTE-RDAR R&D ALLOCATION RATE
NOTE-RDARX R&D ALLOCATION RATE
NOTE-IDAR INVESTMENT ALLOCATION RATE
NOTE-IDARX INVESTMENT ALLOCATION RATE
NOTE-OSDAR O&S ALLOCATION RATE
NOTE-OSDARX O&S ALLOCATION RATE
NOTE*****ALL INITIAL VALUES (N) MUST BE ESTABLISHED FOR
NOTE*****EACH DIFFERENT WEAPON SYSTEM AND THE DOD SYSTEM.
SPEC DT=.5
SPEC LENGTH=36
SPEC PLTPER=1
SPEC PRTPER=0

4. RESOURCES
MODEL

FILE RES 07/14/81

NOTE *****RESOURCES*****

L TOTRES.K=TOTRES.J+DT*(DISCOV.JK-TRUSE.JK)

N TOTRES=TOTRSC

C TOTRSC=100

R DISCOV.KL=DISCOF.K*TOTRES.K

A DISCOF.K=TABHL(DISCOT,SEARCH.K,0,.1,.02)

T DISCOT=.0/.002/.006/.008/.009/.01

A SEARCH.K=SMOOTH(SEARC.K,30)

A SEARC.K=TABHL(SEARCT,TOTRES.K,0,100,20)

T SEARCT=1/.9/.8/.55/.3/.15

R TRUSE.KL=GROWTH.K*TOTRES.K

A GROWTH.K=TABHL(GROWTT,TOTRES.K,0,100,10)

T GROWTT=-50/-30/-15/-6/-1/0/.007/.018/.025/.037/.03

L USRES.K=USRES.J+DT*(RAUS.JK-RMDUS.JK)

N USRES=USRESC

C USRESC=33

R RAUS.KL=(DISCOV.JK-TRUSE.JK)*ALLOCF

C ALLOCF=.33

R RMDUS.KL=(GROWTH.K-(EFFF.K/100))*USRES.K

A EFFF.K=DTC.K+TECHIF.K

A USRESS.K=SMOOTH(USRES.K,10)

A DTC.K=TABHL(DTCT,USRESS.K,0,35,5)

T DTCT=-2./-.75/-.15/.4/.7/.9/1./1.0

A TECHIF.K=TABHL(TECHIT,TECHCR.K,0,.2,.04)

A TECHCR.K=TECHCRC

C TECHCRC=.1

T TECHIT=1/.5/.25/.15/.07/.04

A RPFT.K=TABHL(RPFTT,USRESS.K,0,100,10)

T RPFTT=1/.8/.7/.6/.5/.45/.41/.39/.38/.36/.35

A RADPP.K=TABHL(RADPPT,TOTRES.K,0,100,10)

T RADPPT=0/.1/.25/.4/.35/.32/.3/.28/.27/.26/.25

A RAADP.K=TOTRES.K*RADPP.K*AALLOC

C AALLOC=.35

A RAUSDP.K=USRES.K*RPUSDP.K

A RPUSDP.K=TABHL(RPUSDT,USRES.K,0,35,5)

T RPUSDT=0/.2/.4/.3/.28/.27/.26/.25

SPEC DT=.05

SPEC LENGTH=36

SPEC PLTPER=2

SPEC PRTPER=0

PLOT TOTRES/USRES/DISCOV/GROWTH/USRESS/RAUSDP/RPFT/EFFF/RAADP

PRINT TOTRES,USRES,DISCOV,GROWTH,USRESS,RAUSDP,RPFT,PAADP

5. PRODUCTION
MODEL

FILE PRODY 07/10/81

NOTE*****PRODUCTION*****

L WSP.K=WSP.J+DT(WSPIR.JK-WSPR.JK)
N WSP=0
R WSPIR.KL=MIN(PGMXX.K,RCWS.K)
A PGMXX.K=PGMX.K*PPRC
C PPRC=5
R WSPR.KL=DELAY3(WSPIR.JK,PRODT.K)
A RCWS.K=RAUSDP.K*WSRCF
A RAUSDP.K=RAUSDPC
C RAUSDPC=100
C WSRCF=1
A PRODT.K=PRODTDC/PRODTA.K
A PRODTA.K=LCF.K*TEX.K*CPTS.K
A CPTS.K=SMOOTH(CPTT.K,CPTD)
A CPTT.K=CPT.K
C CPTD=1
A CPT.K=PRODTD.K/PRODTDC
A PRODTD.K=PRODTDC*TEX.K
C PRODTDC=12
A LCF.K=TABHL(LCFT,TWSP.K,0,520,40)
T LCFT=1/1.15/1.35/1.57/1.69/1.78/1.87/1.96/2.02/2.11/2.2/2.2/2.7
X /2.2
A RWSP.K=NWSP-TWSP.K
C NWSP=422
L TWSP.K=TWSP.J+DT(WSPR.JK-RR.JK)
N TWSP=0
R RR.KL=0
L WSIT.K=WSIT.J+DT(WSPR.JK-WSDR.JK)
N WSIT=0
R WSDR.KL=DELAY3(WSPR.JK,WSTT)
C WSTT=2
L APX.K=APX.J+DT(APRX.JK-ATRX.JK)
N APX=0
R ATRX.KL=0
R APRX.KL=APRRXX.K
N APRRX=0
A APRRX.K=TEX.K*PGMX.K*CAPRSX.K
A CAPRSX.K=DELAY3(CAPRX.K,CAPROX)
C CAPROX=1
A CAPRX.K=FLFX.K*DCAPRX.K
A DCAPRX.K=DCAPRXC
C DCAPRXC=1
A TEX.K=MEX.K/TCF
C TCF=1
A MEX.K=EX.K*MOD
A EX.K=EXC
C EXC=1
C MOD=1
A PGMX.K=TABHL(PGMXT,SCHEDX.K,0,60,5)
A SCHEDX.K=TSMSX0.K
A PAPX.K=DELAY1(APX.K,WSPDX)
C WSPDX=.05
A RTTMSX.K=(TSMSX0.K-PATX.K+TTMSX.K)*PRESSX
A PRRX.K=(PPXT.K-PATX.K+RTTMSX.K)/TTMSX.K
A PATX.K=TABHL(PATXT,PAPX.K,0,100,20)
A PPXT.K=TABHL(PPXTT,PPX.K,0,100,20)
T PPXTT=0/3/5.5/7.6/9.8/11
T PATXT=0/3/5.5/7.6/9.8/11

FILE PRODY 07/10/81

```
C PRESSX=1
A TTMSX.K=60-TSMSXD.K
A CFX.K=TABHL(CFTX,SFX.K,0,10,5)
T CFTX=1/5/10
A SFX.K=TABHL(SFTX,PRRX.K,0,10,5)
T SFTX=1/5/10
L PPX.K=PPX.J+DT(PPGMX.JK-PPTXX.JK)
N PPX=.01
R PPTXX.KL=0
R PPGMX.KL=TABHL(PGMXT,PSCHDX.K,0,60,5)
T PGMXT=0/.833/1.66/1.66/1.66/1.66/1.66/1.66/1.66/1.66/
X 1.66/1.66/2.499/3.332
A PSCHDX.K=TSMSXD.K
L CRX.K=CRX.J+DT*(CRRX.JK-CRTRX.JK)
N CRX=CRXC
C CRXC=.01
R CRRX.KL=(CEX/TEX.K)*DCFSX.K*PGMX.K/PTCR
C CEX=1
A DCFSX.K=SMOOTH(DCFX.K,DCFxD)
C DCFxD=1
C PTCR=1
R CRTRX.KL=0
A DCFX.K=DCFXC
C DCFXC=1
L PCX.K=PCX.J+DT*(PCPX.JK-PCTRX.JK)
N PCX=PCXC
C PCXC=.01
R PCRX.KL=(PPGMX.JK/PTCR)+CPCX.K
R PCTRX.KL=0
A PRAPX.K=PAPX.K/PPX.K
A CRPAX.K=PCX.K/CRX.K
A FLFX.K=TABHL(FLFXT,CRPAX.K,0,2,1)
T FLFXT=0/1/2
A PIFX.K=TABHL(PIFT,FLFX.K,0,1.4,.2)
T PIFT=1/.72/.57/.45/.38/.32/.28/.25
A ITAFX.K=FAX.K*PIFX.K*PRAPX.K+USURGF.K*MAIMPF
A FIDX.K=TABHL(FIDT,ITAFX.K,.8,2,.2)
T FIDT=0/.375/.62/.75/.86/.92/.96
A CPCX.K=FIDX.K*ECCX.K
A ECCX.K=CLIP(ICRX.K,0,ICRX.K,0)*(TSMSXD.K+RTTMSX.K)/PTC
C PTC=100
A ICRX.K=1-(1/CRPAX.K)
A FAFX.K=ECCX.K/RDAX.K
A RDAX.K=RDAXC
C RDAXC=1
A FAX.K=TABHL(FATX,FAFX.K,0,1,.5)
T FATX=0/.001/1
L PVX.K=PVX.J+DT(PVRX.JK-PVTRX.JK)
N PVX=0
R PVRX.KL=PPVSX.K*PVAX.K
A PPVSX.K=PPGMX.JK
A PVAX.K=PRAPX.K*CRPAX.K
R PVTRX.KL=U
L TSMSXD.K=TSMSXD.J+DT(TINX.JK-TOUTX.JK)
N TSMSXD=0
R TOUTX.KL=0
R TINX.KL=1
A USURGF.K=USURGFC
```

FILE PRODY 07/10/81

C USURGFC=1
C MAIMPF=1
A $PPXX.K=PPX.K*(PPPC/5)*(12/PRODTDC)$
A $CRXX.K=CRX.K*(PPRC/5)*(12/PRODTDC)$
A $PCXX.K=PCX.K*(PPPC/5)*(12/PRODTDC)$
A $PVXX.K=PVX.K*(PPPC/5)*(12/PRODTDC)$
SPEC DT=.05
SPEC LENGTH=60
SPEC PLTPER=3
SPEC PRTPER=0
PLOT PPXX,CRXX,PCXX,PVXX/WSP/TWSP/WSIT/RWSP/LCF
PRINT CAPRSX,CAPROX,CAPRX,DCAPRX,TEX
PRINT MEX,EX,PGMX,SCHEDX,PAPX,RTMSX,PRRX
PRINT PATX,PPXT,CFX,SFX,PPX,PPTXX,PPGMX,PSCHDX
PRINT CRX,CRRX,DCFSX,CRTRX,DCFX,PCX,PCRX,PCTRX
PRINT PRAPX,CRPAX,FLFX,PIFX,ITAFX,FIDX,CPCX,ECCX
PRINT ICRX,FAFX,PVX,PVRX,PPVSX,PVAX,PVTRX

6. OPERATIONS
MODEL

```

FILE OPS2          07/10/81
NOTE *****WEAPON SYSTEM OPERATIONS SECTOR*****
NOTE*****GPS2*****
L   WSO.K=WSO.J+DT*(WSMR.JK+WSDR.JK-WSSDR.JK-WSRR.JK)
N   WSO=WSOC
C   WSOC=1800
R   WSMR.KL=WSORP.K*OSF.K*WSN.K
R   WSDR.KL=WSDRC.K
A   WSDRC.K=WSDRCC
C   WSDRCC=100
L   WSN.K=WSN.J+DT*(WSSDR.JK-WSMR.JK)
A   WST.K=WSO.K+WSN.K
N   WSN=WSNC
C   WSNC=200
R   WSSDR.KL=USE.K/MTBF.K
A   WSORP.K=WSO.K/(WSN.K+WSO.K)
A   OSR.K=OSCF*(1-WSORP.K)
C   OSCF=.1
A   PFOS.K=TABHL(PFOST,WSORP.K,0,1,.5)
T   PFOST=3/2/1
A   OSF.K=OSDAM.K*PFOS.K
A   OSDAM.K=TABHL(OSDAMT,OSR.K,0,2,.2)
T   OSDAMT=1.0/.98/.9/.82/.7/.5/.38/.29/.26/.24/.22
A   USE.K=WSORF.K*(WSO.K)*OPLAN.K
A   OPLAN.K=TABHL(OPLANT,TIME.K,0,20,2)
T   OPLANT=1/1/1/1/1/1/1/1/1/1/1
T   WSORFT=3/2/1
A   WSORF.K=TABHL(WSORFT,WSORP.K,0,1,.5)
A   MTBF.K=MTBFC*TE4D.K*MTBFM.K
C   MTBFC=4
A   TE4D.K=SMOOTH(TTE.K,5)
C   TTEC=1
A   TTE.K=TTEC
A   MTBFM.K=TABHL(MTBFMT,WSAA.K,0,20,5)
T   MTBFMT=3/2/1.5/1
A   TM.K=TMC
C   TMC=1
A   WSRRR.K=((WSRF.K)*(WST.K))+(ATTR*USE.K)-ND.K*WST.K
R   WSRR.KL=MAX(WSRRR.K,0)
C   ATTR=.01
A   WSRF.K=TABHL(WSRFT,WSAA.K,0,20,5)/TM.K
T   WSRFT=.007/.02/.03/.05
A   ND.K=TABHL(NDT,OPLAN.K,1,3,1)
T   NDT=0/.1/.2/.3
L   AWSA.K=AWSA.J+DT(WSAR.JK-WSARR.JK)
N   AWSA=21000
R   WSAR.KL=WSDRCC+AWSA.K*(2290/WST.K)-AWSA.K
R   WSARR.KL=WSRR.JK*20
A   WSAA.K=AWSA.K/WST.K
SPEC DT=.5
SPEC LENGTH=30
SPEC PLTPER=1
SPEC PRTPER=0
PLOT WSO,WSN,WST/WSRR/WSSDR/WSMR/WSORP/USE/MTBF/OSDAM
PRINT WSO,WSN,WST,WSRR,WSSDR,WSMR,WSORP,USE,MTBF,OSDAM

```

APPENDIX II.
DEFINITION
OF
TERMS

DEFINITION OF TERMS

NOTE*THIS LIST OF DEFINITIONS INCLUDES ALL OF THE TERMS
USED IN THE SIX SECTOR SUB-MODELS OF THIS REPORT AND
SOME SUGGESTED TERMS FOR THE REMAINING FOUR SUB-
MODELS NEEDED TO COMPLETE THE ACQUISITION PROCESS
MODEL.

AAGE AVERAGE AGE OF ALLIED WEAPONS
AALOC ALLIED ALLOCATION PERCENT
ABF AREA BENEFITS FACTOR
ACAP ALLIED CAPABILITY
ACAPDP ALLIED CAPACITY FOR DEFENSE PRODUCTION
ACBWS ALLIED COST TO BUY WEAPON SYSTEMS
ACOWS ALLIED COST FOR ALLIED WEAPON SYSTEMS
ACOMWS ALLIED COST FOR MIXED WEAPON SYSTEMS INVENTORY
ACOPR ALLIED COPRODUCTION REQUEST
ACOSWS ALLIED COST PER WEAPON SYSTEM
ACOWS ALLIED COST FOR US WEAPON SYSTEMS
ACPWS ALLIED CAPABILITY PER WEAPON SYSTEM
ADECB ALLIED DECISION TO BUY
ADECP ALLIED DECISION TO PRODUCE
ADEF ALLIED DEFICIENCY
ADELR ALLIED DELAY RATE IN PRODUCTION
ADESWF ALLIED DESIRE FOR WEAPON SYSTEMS
ADIF ALLIED DIFFERENCE IN CAPABILITY
ADPCT ALLIED PERCENTAGE OF DEFICIENCY
ADVOC ADVOCACY FACTOR
ADWSL ALLIED DESIRED WEAPON SYSTEMS LEVEL
AFMSDR ALLIED FOREIGN MILITARY SALES DELIVERY RATE
AGEF AGE FACTOR
AGEM AGE MULTIPLIER
AGER ALLIED AGE RATE
AGNP ALLIED GROSS NATIONAL PRODUCT
AGNPGF ALLIED GNP GROWTH FACTOR
AGNPGR ALLIED GNP GROWTH RATE
AINT ALLIED INTENT
AINTF ALLIED INTENT FACTOR
ALLOCF ALLOCATION FRACTION
ALRADJ ALLIED LONG-RANGE ADJUSTMENT RATE
AMPCT ALLIED PERCENTAGE OF WEAPONS REPAIRED
AMSBR FOREIGN MILITARY SALES BY RATE
APACC ALLIED PRODUCTION ACCELERATOR
APD ACTUAL PROGRESS DELAY
APGNPD ALLIED PERCENT OF GNP TO DEFENSE
APLAN ALLIED PLANNED PRODUCTION
APPC ALLIED PROJECTED PRODUCTION CAPACITY
APRF APPROPRIATION RATE FRACTION
APRFA APPROPRIATION FRACTION ADJUSTOR

APRODT AVERAGE PRODUCTION TIME
 APR1 ACTUAL PROGRESS RATE
 APR2 ACTUAL PROGRESS RATE
 APR3 ACTUAL PROGRESS RATE
 APR4 ACTUAL PRODUCTION RATE
 APSWS ALLIED PERCENTAGE OF STANDARDIZED WEAPON SYSTEMS
 APTHR ALLIED PERCEIVED THREAT
 APTR1 ACTUAL PROGRESS TRANSFER RATE
 APTR2 ACTUAL PROGRESS TRANSFER RATE
 APTR3 ACTUAL PROGRESS TRANSFER RATE
 AP1 ACTUAL PROGRESS
 AP2 ACTUAL PROGRESS
 AP3 ACTUAL PROGRESS
 AQF ALLIED QUALITY FACTOR
 ARETC ALLIED RETIREMENT CONSTANT
 ARUCWS ALLIED RESOURCE UNIT CONSTRAINT PER WEAPON SYSTEM
 ASDEV ALLIED SCHEDULE DEVIATION
 ASTINV ALLIED STANDARDIZED INVENTORY
 ASTR ALLIED STANDARDIZATION TRANSFER RATE
 ATXR ALLIED TRANSFER RATE
 AUPCT ALLIED PERCENTAGE OF WEAPONS USED
 AURG ALLIED URGENCY--TIME TO FIRST DEFICIENCY
 AURGF ALLIED URGENCY FACTOR
 AWSA ACCUMULATED WEAPON SYSTEM AGE
 AWSDR ALLIED WEAPON SYSTEMS DELIVERY RATE
 AWSM ALLIED WEAPON SYSTEMS NON-OPERATIONAL
 AWSMR ALLIED WEAPON SYSTEMS MAINTENANCE RATE
 AWSN ALLIED WEAPON SYSTEMS NON-OPERATIONAL
 AWSO ALLIED WEAPON SYSTEMS OPERATIONAL
 AWSP ALLIED WEAPON SYSTEMS IN PRODUCTION
 AWSPR ALLIED WEAPON SYSTEMS PRODUCTION RATE
 AWSRR ALLIED WEAPON SYSTEMS RETIREMENT RATE
 AWSUR ALLIED WEAPON SYSTEMS USE RATE
 BRF BUDGET REDUCTION FACTOR
 BUD BUDGET
 CAPRD CHANGE IN ACTUAL RATE DELAY
 CAPRS1 CHANGE IN ACTUAL PROGRESS RATE (SMOOTHED)
 CAPRS2 CHANGE IN ACTUAL PROGRESS RATE (SMOOTHED)
 CAPRS3 CHANGE IN ACTUAL PROGRESS RATE (SMOOTHED)
 CAPP1 CHANGE IN ACTUAL PROGRESS RATE
 CAPP2 CHANGE IN ACTUAL PROGRESS RATE
 CAPP3 CHANGE IN ACTUAL PROGRESS RATE
 CE1 COST ESTIMATING ERROR
 CE2 COST ESTIMATING ERROR
 CE3 COST ESTIMATING ERROR
 CE4 COST ESTIMATING ERROR
 CF1 COST FACTOR
 CF2 COST FACTOR
 CF3 COST FACTOR
 CF4 COST FACTOR
 CMS1 CHANGE IN MILESTONE 1
 CMS2 CHANGE IN MILESTONE 2
 CMS3 CHANGE IN MILESTONE 3
 CMS4 CHANGE IN SCHEDULE
 CNRD COST FOR R&D ON NEW WEAPON SYSTEM
 COFAC COPRODUCTION FACTOR
 COMP COMPUTED TRADEOFF FACTOR
 CONGSC CONGRESSIONAL SUPPORT CONSTANT
 CONGSF CONGRESSIONAL SUPPORT FACTOR
 COST COST FOR OPTION

COSTF COST FACTOR FOR ALTERNATIVE
 COST1 COST OF ALTERNATIVE 1
 COST2 COST OF ALTERNATIVE 2
 COST3 COST OF ALTERNATIVE 3
 COST4 COST OF ALTERNATIVE 4
 CPARS2 CHANGE IN ACTUAL PROGRESS RATE(SMOOTHED)
 CPC CHANGE IN PLANNED COSTS
 CPC1 CHANGE IN PLANNED COST
 CPC2 CHANGE IN PLANNED COST
 CPC3 CHANGE IN PLANNED COST
 CPC4 CHANGE IN PLANNED COST
 CPT CHANGE IN PRODUCTION TIME
 CPTD CHANGE IN PRODUCTION DELAY
 CPTS CHANGE IN PRODUCTION TIME(SMOOTHED)
 CP1 COST PENALTY
 CP2 COST PENALTY
 CP3 COST PENALTY
 CP4 COST PENALTY
 CRPA1 COST RATIO, PLANNED TO ACTUAL
 CRPA2 COST RATIO, PLANNED TO ACTUAL
 CRPA3 COST RATIO, PLANNED TO ACTUAL
 CRPA4 COST RATIO, PLANNED TO ACTUAL
 CRR1 COST REPORTING RATE
 CRR2 COST REPORTING RATE
 CRR3 COST REPORTING RATE
 CRR4 COST REPORTING RATE
 CRTR1 COST REPORTING TRANSFER RATE
 CRTR2 COST REPORTING TRANSFER RATE
 CRTR3 COST REPORTING TRANSFER RATE
 CRTR4 COST REPORTING TRANSFER RATE
 CR1 COST REPORTED
 CR2 COST REPORTED
 CR3 COST REPORTED
 CR4 COST REPORTED
 CWF COST WEIGHT FACTOR
 CWSF COST WEIGHTED SUPPORT FACTOR
 DC DECISION CONTROL FOR OPTIONS
 DCAPR1 DESIRED CHANGE IN ACTUAL PROGRESS RATE
 DCAPR2 DESIRED CHANGE IN ACTUAL PROGRESS RATE
 DCAPR3 DESIRED CHANGE IN ACTUAL PROGRESS RATE
 DCAPR4 DESIRED CHANGE IN ACTUAL PRODUCTION RATE
 DCFD DESIRED COST FACTOR DELAY
 DCFS1 DESIRED COST FACTOR(SMOOTHED)
 DCFS2 DESIRED COST FACTOR(SMOOTHED)
 DCFS3 DESIRED COST FACTOR(SMOOTHED)
 DCFS4 DESIRED COST FACTOR(SMOOTHED)
 DCF DESIRED COST FACTOR
 DCFX0 DESIRED COST FACTOR DELAY
 DCP1 DECISION COORD POINT 1
 DCP2 DECISION COORD POINT 2
 DCP3 DECISION COORD POINT 3
 DDMOR DEFENSE DEMAND RATE
 DDRB DOD DOLLARS REQUESTED IN THE BUDGET
 DEF FEDERAL DEFICIT
 DISCOF DISCOVERY FRACTION
 DISCOV DISCOVERY RATE
 DISTK DISTRIBUTION CONSTANT
 DNNWS DESIRED NUMBER OF NEW WEAPON SYSTEMS
 DNOWS DESIRED NUMBER OF LOD WEAPONS SYSTEMS
 DODD DOD DOLLARS APPROPRIATED

DGDSP SUPPORT FOR DOD IN GENERAL
 DDMO DOD DEMAND FOR DOLLARS
 DORR DESIRED OR RATE
 DPR1 DESIRED PROGRESS RATE
 DPR2 DESIRED PROGRESS RATE
 DPR3 DESIRED PROGRESS RATE
 DREDR DEFENSE DEMAND REDUCTION RATE
 DSWI DOLLAR SWITCH
 DTC DESIRE TO CONSERVE
 DTL1 DESIRED TIME LATE
 DTL2 DESIRED TIME LATE
 DTL3 DESIRED TIME LATE
 DTL4 DESIRED TIME LATE
 DWSPR DESIRED WEAPON SYSTEM PRODUCTION RATE
 D1 DECISION FOR ALTERNATIVE 1
 D2 DECISION FOR ALTERNATIVE 2
 D3 DECISION FOR ALTERNATIVE 3
 D4 DECISION FOR ALTERNATIVE 4
 EADJ ENEMY ADJUSTMENT RATE
 EALLOC ENEMY ALLOCATION
 ECAP ENEMY CAPABILITY
 ECAPWS ENEMY CAPABILITY PER WEAPON SYSTEM
 ECC1 ESTIMATED CHANGE IN COST
 ECC2 ESTIMATED CHANGE IN COST
 ECC3 ESTIMATED CHANGE IN COST
 ECC4 ESTIMATED CHANGE IN COST
 ECON ECONOMIC BASELINE
 EDEF ENEMY DEFICIENCY
 EDELR ENEMY PRODUCTION DELAY FACTOR
 EDESWF ENEMY DESIRE FOR WEAPONS FACTOR
 EDIF ENEMY DIFFERENCE IN CAPABILITY
 EDWSL ENEMY DESIRED WEAPON SYSTEMS LEVEL
 EFFF EFFICIENCY FACTOR
 EINT ENEMY INTENT
 EINTF ENEMY INTENT FACTOR
 ELF1 ESTIMATED LATE FACTOR
 ELF2 ESTIMATED LATE FACTOR
 ELF3 ESTIMATED LATE FACTOR
 ELF4 ESTIMATED LATE FACTOR
 ELYRM ELECTION YEAR MULTIPLIER
 EMPCT ENEMY PERCENTAGE OF WEAPONS REPAIRED
 EPACC ENEMY PRODUCTION ACCELERATOR
 EPLAN ENEMY PLANNED PRODUCTION
 EPTHR ENEMY PERCEIVED THREAT
 EUPCT ENEMY PERCENTAGE OF WEAPON SYSTEMS USED
 EURG ENEMY URGENCY--TIME TO FIRST DEFICIENCY
 EURGF ENEMY URGENCY FACTOR
 EWGT URGENCY WEIGHTING TABLE
 EWSDR ENEMY WEAPON SYSTEMS DELIVERY RATE
 EWSMR ENEMY WEAPON SYSTEMS MAINTENANCE RATE
 EWSN ENEMY WEAPON SYSTEMS NON-OPERATIONAL
 EWSO ENEMY WEAPON SYSTEMS OPERATIONAL
 EWSP ENEMY WEAPON SYSTEMS PRODUCTION
 EWSPR ENEMY WEAPON SYSTEMS PRODUCTION INPUT RATE
 EWSRR ENEMY WEAPON SYSTEMS RETIREMENT RATE
 EWSUR ENEMY WEAPON SYSTEMS USE RATE
 FAF1 FUNDS AVAILABILITY FACTOR
 FAF2 FUNDS AVAILABILITY FACTOR
 FAF3 FUNDS AVAILABILITY FACTOR
 FAF4 FUNDS AVAILABILITY FACTOR

FA1 FUNDS AVAILABILITY
 FA2 FUNDS AVAILABILITY
 FA2 FUNOS AVAILABILITY
 FA4 FUNDS AVAILABILITY
 FBRQMT FEDERAL BUDGET REQUIREMENTS
 FDAR D&D APPROPRIATION RATE
 FID1 FUNDS INCREASE DECISION
 FID2 FUNDS INCREASE DECISION
 FID3 FUNDS INCREASE DECISION
 FID4 FUNDS INCREASE DECISION
 FLF1 FUNDS LIMIT FACTOR
 FLF2 FUNDS LIMIT FACTOR
 FLF2 FUNDS LIMIT FACTOR
 FLF4 FUNDS LIMIT FACTOR
 FLTAGE COMBINED AGE OF ALLIED FLEET
 FMSA FOREIGN MILITARY SALES AGREEMENTS
 FMSBR FOREIGN MILITARY SALES BUY RATE
 FP1INR R&D COSTS FUNDED FROM THE FYDP
 FP1OR R&D COSTS FUNDED FROM THE FYDP
 FP2INR INVESTMENT COSTS INPUT TO THE FYDP
 FP2OR INVESTMENT COSTS FUNDED FROM THE FYDP
 FP3INR O&S COSTS INPUT TO THE FYDP
 FP3OR O&S COSTS FUNDED FROM THE FYDP
 FREV FEDERAL REVENUES
 FYDP FIVE YEARD DEFENSE PLANS FOR FUNDS
 FYDP1 R&D EXPENDITURES PLANNED IN THE FYDP
 FYDP2 INVESTMENT EXPENDITURES PLANNED IN THE FYDP
 FYDP3 O&S EXPENDITURES PLANNED IN THE FYDP
 FYTIME FISCAL YEAR TIME
 FYTIN FISCAL YEAR TIME IN
 FYTOUT FISCAL YEAR TIME OUT
 FYTX FISCAL YEAR TRANSFER
 GNP GROSS NATIONAL PRODUCT
 GNPGR GNP GROWTH RATE
 GROWTH GROWTH FACTOR
 GSPTIN GOVERNMENT SUPPORT FOR INVESTMENT
 GSPTOS GOVERNMENT SUPPORT FOR O&S
 GSPTRD GOVERNMENT SUPPORT FOR R&D PROGRAMS
 ICR INCREASE IN COST
 IDA INVESTMENT DOLLARS APPROPRIATED
 IDAR INVESTMENT ALLOCATION RATE
 IDMDR INVESTMENT DEMAND RATE
 IDOC INVESTMENT DOLLARS ON CONTRACT
 IDOR INVESTMENT DOLLARS OBLIGATION RATE
 IDOSWI INVESTMENT DOLLARS OBLIGATION SWITCH
 IDPR INVESTMENT DOLLARS PAYMENT RATE
 IDPRD INVESTMENT DOLLARS PAYMENT RATE DELAY
 IDPP2D INVESTMENT DOLLARS PAYMENT RATE DELAY
 IDPSWI INVESTMENT DOLLARS PAYMENT SWITCH
 IDR8 INVESTMENT DOLLARS REQUESTED IN THE BUDGET
 INSUPP INVESTMENT SUPPLEMENTAL REQUEST
 IPF INVESTMENT PROGRAM FUNDING
 IREDR INVESTMENT DEMAND REDUCTION RATE
 IRPR INVESTMENT REPROGRAMMING RATE
 IRQT INVESTMENT FUNDS REQUIREMENT
 ISUP AMOUNT OF SUPPLEMENT FOR INVESTMENT
 ITAF1 INCLINATION TO APPROVE FUNDS
 ITAF2 INCLINATION TO APPROVE FUNDS
 ITAF3 INCLINATION TO APPROVE FUNDS
 ITAF4 INCLINATION TO APPROVE FUNDS

LCF LEARNING CURVE FACTOR
 LCRR LEARNING CURVE RELEASE RATE
 LFL1 FUNDS LIMIT FACTOR
 LOELF ESTIMATED LATE FACTOR
 LPF LOBBYIST PRESSURE FACTOR
 LTF LEAD TIME FACTOR
 MAIMPF MISSION AREA IMPORTANCE FACTOR
 ME1 MANAGEMENT EFFECTIVENESS
 ME2 MANAGEMENT EFFECTIVENESS
 ME3 MANAGEMENT EFFECTIVENESS
 ME4 MANAGEMENT EFFECTIVENESS CONSTANT
 MODC MODIFICATION COST
 MODF MODIFICATION FACTOR
 MODK MODIFICATION CONSTANT INCREASE IN CAPABILITY
 MTBF MEAN TIME BETWEEN FAILURES
 MTBFC MTBF INITIAL CONSTANT
 MTBFM MTBF AGE MULTIPLIER
 NALS NUMBER OF ALLIED WEAPON SYSTEMS
 NCPWS NEW CAPABILITY PER WEAPON SYSTEM
 NODMD NON-DOD DEMAND FOR DOLLARS
 NODDD NON-DOD DOLLARS APPROPRIATED
 NEWORR NEW OR RATE
 NUSWS NUMBER OF US WEAPON SYSTEMS PLANNED
 NWSO NEW WEAPON SYSTEMS DESIRABILITY
 NWSO NEW WEAPON SYSTEMS PERFORMANCE FACTOR
 ODMDR O&S DEMAND RATE
 ODRB O&S DOLLARS REQUESTED IN THE BUDGET
 OP OTHER PRESSURE
 OPLAN OPERATING PLAN
 OREDR O&S DEMAND REDUCTION RATE
 ORQT O&S FUNDS REQUIREMENT
 OSA O&S AVAILABLE
 OSAD O&S AVAILABLE DEFICIT
 OSASWI O&S AVAILABLE SWITCH
 OSCF O&S COST FACTOR
 OSDA O&S DOLLARS APPROPRIATED
 OSDAM O&S DOLLARS AVAILABLE MULTIPLIER
 OSDAR O&S ALLOCATION RATE
 OSDI O&S DEFICIT IMPORTANCE
 OSDOR O&S DOLLAR OBLIGATION RATE
 OSDRAD O&S DOLLARS REALLOCATION DECISION
 OSDSWI O&S DOLLARS SWITCH
 OSDWSI O&S DOLLARS APPROPRIATED
 OSEP O&S EXPENSE RATE
 OSERD O&S EXPENSE REPORTING DELAY
 OSF O&S FACTOR
 OSR O&S REQUESTED
 OSRAR O&S REALLOCATION RATE
 OSSUPP O&S SUPPLEMENTAL REQUEST
 OSUP AMOUNT OF SUPPLEMENT FOR O&S
 OSUPP O&S SUPPLEMENTAL REQUEST
 PAPA PERFORMANCE RATIO PLANNED TO ACTUAL
 PAP1 PERCEIVED ACTUAL PROGRESS
 PAP2 PERCEIVED ACTUAL PROGRESS
 PAP3 PERCEIVED ACTUAL PROGRESS
 PASTP1 PAST PROGRESS 1
 PASTP2 PAST PROGRESS 2
 PASTP3 PAST PROGRESS 3
 PASTR1 PAST PROGRESS TRANSFER RATE
 PASTR2 PAST PROGRESS TRANSFER RATE

PASTR3 PAST PROGRESS TRANSFER RATE
 PBN0 PERCENT BUDGET TO NON-000
 PCR1 PLANNED COST RATE
 PCR2 PLANNED COST RATE
 PCR3 PLANNED COST RATE
 PCR4 PLANNED COST RATE
 PCTR1 PLANNED COST TRANSFER RATE
 PCTR2 PLANNED COST TRANSFER RATE
 PCTR3 PLANNED COST TRANSFER RATE
 PCTR4 PLANNED COST TRANSFER RATE
 PC1 PLANNED COST
 PC2 PLANNED COST
 PC2 PLANNED COST
 PC3 PLANNED COST
 PC4 PLANNED COST
 PF05 PRESSURE FOR O&S
 PGM1 PROGRAM
 PGM2 PROGRAM
 PGM3 PROGRAM
 PGM4 PROGRAM
 PGNPG PERCENT GNP TO THE GOVERNMENT
 PID PRESSURE FOR INVESTMENT DOLLARS
 PIF1 PRESSURE FOR INCREASED FUNDS
 PIF2 PRESSURE FOR INCREASED FUNDS
 PIF3 PRESSURE FOR INCREASED FUNDS
 PIF4 PRESSURE FOR INCREASED FUNDS
 PLADJ PLAN ADJUSTMENT RATE
 PLAN PLANNED FORCE LEVEL
 POSD PRESSURE FOR O&S DOLLARS
 PPD PLANNED PROGRESS DELAY
 PPGM PLANNED PROGRAM RATE
 PPR PLANNED PROGRESS RATE
 PPTX1 PLANNED PROGRESS TRANSFER RATE
 PPTX2 PLANNED PROGRESS TRANSFER RATE
 PPTX3 PLANNED PROGRESS TRANSFER RATE
 PPTX4 PLANNED PRODUCTION TRANSFER RATE
 PPVS1 PLANNED PRODUCT VALUE(SMOOTHED)
 PPVS2 PLANNED PRODUCT VALUE(SMOOTHED)
 PPVS3 PLANNED PRODUCT VALUE(SMOOTHED)
 PPVTR1 PAST PRODUCT VALUE TRANSFER RATE
 PPVTR2 PAST PRODUCT VALUE TRANSFER RATE
 PPVTR3 PAST PRODUCT VALUE TRANSFER RATE
 PPVTR4 PAST PRODUCT VALUE TRANSFER RATE
 PPV1 PAST PRODUCT VALUE
 PPV2 PAST PRODUCT VALUE
 PP1 PLANNED PROGRESS
 PP2 PLANNED PROGRESS
 PP3 PLANNED PROGRESS
 PP4 PLANNED PROGRESS
 PRAP PROGRESS RATIO, ACTUAL TO PLANNED
 PRDD PRESSURE FOR R&D DOLLARS
 PRESSC PRESIDENTIAL SUPPORT CONSTANT
 PRESSF PRESIDENTIAL SUPPORT FACTOR
 PROD PRESSURE FOR R&D DOLLARS
 PRODT PRODUCTION TIME
 PRODTA PRODUCTION TIME ADJUSTOR
 PRODTD PRODUCTION TIME DESIRED
 PRR1 PROGRESS RATE REQUIRED
 PRR2 PROGRESS RATE REQUIRED
 PRR3 PROGRESS RATE REQUIRED

PSCHD PLANNED SCHEDULE
 PSDD POPULAR SUPPORT FOR DOD
 PSE1 PRESSURE FOR SCHEDULE EXTENSION
 PSE2 PRESSURE FOR SCHEDULE EXTENSION
 PSE3 PRESSURE FOR SCHEDULE EXTENSION
 PSE4 PRESSURE FOR SCHEDULE EXTENSION
 PSTPP1 PAST PLANNED PROGRESS
 PSTPP2 PAST PLANNED PROGRESS
 PSTPP3 PAST PLANNED PROGRESS
 PSTPT1 PAST PLANNED PROGRESS TRANSFER RATE
 PSTPT2 PAST PLANNED PROGRESS TRANSFER RATE
 PSTPT3 PAST PLANNED PROGRESS TRANSFER RATE
 PTCR PRODUCTION TO COST RATIO
 PVA PRODUCT VALUE ADJUSTOR
 PVR1 PRODUCT VALUE RATE
 PVR2 PRODUCT VALUE RATE
 PVR3 PRODUCT VALUE RATE
 PVTRA PRODUCT VALUE TRANSFER RATE
 PVTR1 PRODUCT VALUE TRANSFER RATE
 PVTR2 PRODUCT VALUE TRANSFER RATE
 PVTR3 PRODUCT VALUE TRANSFER RATE
 PV1 PRODUCT VALUE
 PV2 PRODUCT VALUE
 PV3 PRODUCT VALUE
 PWSF PERFORMANCE WEIGHTED SUPPORT FACTOR
 QOL QUALITY OF LIFE
 RAADP RESOURCES AVAILABLE FOR ALLIED DEFENSE PRODUCTION
 RADPP RESOURCES AVAILABLE % FOR DEFENSE PRODUCTION
 RAEDP RESOURCES AVAILABLE FOR ENEMY DEFENSE PRODUCTION
 RAPI REMAINING ACTUAL PROGRESS
 RAP2 REMAINING ACTUAL PROGRESS
 RAP3 REMAINING ACTUAL PROGRESS
 RAUS RESOURCES ALLOCATION FOR THE US
 RAUSDP RESOURCES ABAILABLE FOR US DEFENSE PRODUCTION
 RCWS RESOURCE CONSTRAINED WEAPON SYSTEMS
 RDA RESEARCH DOLLARS APPROPRIATED
 RDAR R&D ALLOCATION RATE
 ROMDR R&D DEMAND RATE
 ROMDUS RESOURCE DEMAND IN US
 RDOC RESEARCH DOLLARS ON CONTRACT
 RDOOR RESEARCH DOLLARS OBLIGATION RATE
 RDOSWI RESEARCH DOLLARS OBLIGATION SWITCH
 RDPR RESEARCH DOLLARS PAYMENT RATE
 RDPPD RESEARCH DOLLARS PAYMENT RATE DELAY
 RDPSWI RESEARCH DOLLARS PAYMENT SWITCH
 RDRR R&D DOLLARS REQUESTED IN THE BUDGET
 RDRQT R&D FUNDS REQUIREMENT
 RDRIT R&D FUNDS REQUIREMENT
 RDSUPP R&D SUPPLEMENTAL REQUEST
 RESCF RESOURCE COST FACTOR
 RPF RESEARCH PROGRAM FUNDING
 RPFT RESOURCES PRESSURE FOR TECHNOLOGY
 RPODT PRODUCTION TIME
 RPUSDP RESORCES % FOR US DEFENSE PRODUCTION
 RREDR R&D DEMAND REDUCTION RATE
 RRRR RESEARCH REPORGRAMMING RATE
 RSUP AMOUNT OF SUPPLEMENT FOR R&D
 RTTMS1 REVISED TIME TIL MILESTONE 1
 RTTMS2 REVISED TIME TIL MILESTONE 2
 RTTMS3 REVISED TIME TIL MILESTONE 3

RTTPCC REVISED TIME TIL PRODUCTION CONTRACT COMPLETE
RWSP REMAINING WEAPON SYSTEMS TO PRODUCE
SCDM SCHEDULE MULTIPLIER
SCD1 SCHEDULE EXTENSION DECISION
SCD2 SCHEDULE EXTENSION DECISION
SCD3 SCHEDULE EXTENSION DECISION
SCD4 SCHEDULE EXTENSION DECISION
SCHED SCHEDULE
SCHEDP SCHEDULED PRODUCTION
SCHF SCHEDULE DECISION FACTOR FOR ALTERNATIVES
SEARC SEARCH FOR RESOURCES
SEARCH SEARCH FOR RESOURCES(SMOOTHED)
SEA1 SCHEDULE EXTENSION ADJUSTOP
SEA2 SCHEDULE EXTENSION ADJUSTOR
SEA3 SCHEDULE EXTENSION ADJUSTOR
SEA4 SCHEDULE EXTENSION ADJUSTOR
SEF SCHEDULE WEIGHT FACTOR
SF1 SCHEDULE FACTOR
SF2 SCHEDULE FACTOR
SF3 SCHEDULE FACTOR
SF4 SCHEDULE FACTOR
SNT SEARCH FOR NEW TECHNOLOGY
SORR DESIRED OR RATE
SPTHR SMOOTHED PERCEIVED THREAT
SP1 SCHEDULE PENALTY
SP2 SCHEDULE PENALTY
SP3 SCHEDULE PENALTY
SP4 SCHEDULE PENALTY
STDF STANDARDIZATION FACTOR
SWF SCHEDULE WEIGHT FACTOR
T TIME
TCF TECHNICAL COMPLEXITY FACTOR
TC1 TOTAL COST
TC2 TOTAL COST
TC3 TOTAL COST
TC4 TOTAL COST
TDF TECHNOLOGY DISCOVERY FRACTION
TDFD TECHNOLOGY DISCOVERY FRACTION DELAY
TDFS TECHNOLOGY DISCOVERY FRACTION SMOOTHED
TECH TECHNOLOGY AVAILABLE
TECHCR TECHNOLOGY CHANGE RATE
TECHIF TECHNICAL IMPROVEMENT FACTOR
TE1 TECHNICAL EFFECTIVENESS
TE2 TECHNICAL EFFECTIVENESS
TE3 TECHNICAL EFFECTIVENESS
TE4 TECHNICAL EFFECTIVENESS
TE4D TECHNICAL EFFECTIVENESS DESIGNED(SMOOTHED)
TICP TIME IN CONCEPTUAL PHASE
TIFSD TIME IN FULL-SCALE DEVELOPMENT
TIN1 TIME IN PHASE 1
TIN2 TIME IN PHASE 2
TIN3 TIME IN PHASE 3
TIN4 TIME IN PRODUCTION
TIP TIME IN PRODUCTION
TIR TECHNOLOGY INPUT RATE
TIVP TIME IN DEVELOPMENT PHASE
TLF TECHNICAL LOSS FACTOR
TLFD TLF DELAY
TLR TECHNOLOGY LOSS RATE
TL1 TIME LATE

TM TIME MULTIPLIER
 TOTRES TOTAL RESOURCES
 TOUT1 TIME OUT OF PHASE 1
 TOUT2 TIME OUT OF PHASE 2
 TOUT3 TIME OUT OF PHASE 3
 TP TECHNOLOGY PRESSURE
 TPC0 TOTAL PLANNED COST OBLIGATED
 TPC1 TOTAL PLANNED COST
 TPC2 TOTAL PLANNED COST
 TPC3 TOTAL PLANNED COST
 TPC4 TOTAL PLANNED COSTS
 TPG1 TOTAL PROGRESS GOAL
 TPG2 TOTAL PROGRESS GOAL
 TPG3 TOTAL PROGRESS GOAL
 TPG4 TOTAL PROGRESS GOAL
 TPIC TOTAL PLANNED COSTS
 TPRC TOTAL PLANNED RESEARCH COSTS
 TRUSE TOTAL RESOURCE USE
 TSMS TIME SINCE MILESTONE
 TSMS0 TIME SINCE MILESTONE 0
 TSMS1 TIME SINCE MILESTONE 1
 TSMS2 TIME SINCE MILESTONE 2
 TSMS3 TIME SINCE MILESTONE 3
 TSP TOTAL SEARCH PRESSURE
 TTE TOTAL TECHNICAL EFFECTIVENESS
 TTMS1 TIME TIL MILESTONE 1
 TTMS2 TIME TIL MILESTONE 2
 TTMS3 TIME TIL MILESTONE 3
 TTPCC TIME TIL PRODUCTION CONTRACT COMPLETE
 TWC1 TIME WEIGHTED COST
 TWC2 TIME WEIGHTED COST
 TWC3 TIME WEIGHTED COST
 TWC4 TIME WEIGHTED COST
 TWSP TOTAL WEAPON SYSTEM PRODUCED
 TX1 TRANSFER SWITCH 1
 TX2 TRANSFER SWITCH 2
 TX3 TRANSFER SWITCH 3
 TX4 TRANSFER SWITCH 4
 UADEF US/ALLIED COMBINED DEFICIENCY
 USCAP US CAPABILITY
 USCOPIA US COPRODUCTION AGREEMENT
 USCPWS US CAPABILITY PER WEAPON SYSTEM
 USDEF US DEFICIENCY
 USDEFW US DESIRABILITY TO BUILD WEAPONS
 USDIFF US DIFFERENCE IN CAPABILITY
 USDPCT PERCENT OF DEFICIENCY
 USDWSL US DESIRED WEAPON SYSTEMS LEVEL
 USE USE
 USINT US INTENT
 USPTHR US PERCEIVED THREAT
 USRES US RESOURCES
 USRESS US RESOURCES (SMOOTHED)
 USRUGF US URGENCY FACTOR
 USURG US URGENCY
 USURGF US URGENCY FACTOR
 VALT VALUE OF ALTERNATIVES
 WSAA WEAPON SYSTEM AVERAGE AGE
 WSAR WEAPON SYSTEM AGE RATE
 WSARR WEAPON SYSTEM AGE RESTORATION AND RETIREMENT RATE
 WSD WEAPON SYSTEM DEVELOPMENT DECISION

WSDR WEAPON SYSTEM DELIVERY RATE
WSD1 WEAPON SYSTEM DEVELOPMENT DECISION 1
WSD2 WEAPON SYSTEM DEVELOPMENT DECISION 2
WSD3 WEAPON SYSTEM DEVELOPMENT DECISION 3
WSD4 WEAPON SYSTEM DEVELOPMENT DECISION 4
WSFAI WEAPON SYSTEMS FOR ALLIED INVENTORIES
WSIT WEAPON SYSTEMS IN TRANSIT
WSMR WEAPON SYSTEM MAINTENANCE RATE
WSN WEAPON SYSTEMS NOT OPERATIONAL
WSO WEAPON SYSTEM OPERATIONAL
WSORF WEAPON SYSTEM OR FACTOR
WSORP WEAPON SYSTEM OR PERCENT
WSP WEAPON SYSTEM PRODUCTION
WSPIR WEAPON SYSTEM PRODUCTION INPUT RATE
WSPR WEAPON SYSTEM PRODUCTION RATE
WSPRR WEAPON SYSTEM PRODUCTION RATE REQUIRED
WSRCF WEAPON SYSTEM TO RESOURCES CONVERSION FACTOR
WSRF WEAPON SYSTEMS RETIREMENT FRACTION
WSRR WEAPON SYSTEMS RETIREMENT RATE
WSSDR SYSTEM DEFICIENCY RATE

APPENDIX III

REFERENCES

REFERENCES

- Abell, John B., "Resources To Readiness: The Tactical-Fighter Case," Defense Management Journal, Second Quarter, 1981.
- Augustine, Norman R. "Augustine's Laws and Major System Development". Defense Systems Management Review, Spring, 1979.
- Babiarz, Anthony S., and Gredras, Pekar W. A Model to Predict Final Cost Growth in a Weapon System Development Program. Unpublished master's thesis, SLSR 49-75B, School of Systems and Logistics, Air Force Institute of Technology (AU), Wright-Patterson AFB, OH, 1975.
- Burt, J. M., "Planning and Dynamic Control of Projects Under Uncertainty", Management Science, Vol 24. Nov., 1977.
- Busse, Daniel E., A Cost Performance Forecasting Model, ACSC-0370-77 Air Command and Staff College, Maxwell AFB, AL. May, 1977. AD/B019-568L.
- Cheslow, Richard T. and Dever James R. "Acquisition Costing in the Federal Government." Defense Systems Management Review. Autumn, 1979. Vol 2 No. 4.
- Clark, James C., Centralized Control: The Missing Ingredient in Multi-Service System Acquisition Management. ACSC-0415-79. Air Command and Staff College, Maxwell AFB, AL. May, 1979. AD/B038-740L.
- Core, George N., Analysis of the Effectiveness of the Preproduction Evaluation Contract in Preventing Cost Overruns. CARCOM Intern Training Center, Texarkana, TX. May, 1976. AD/A024-818.
- Corley, Parris L. and Roscoe, Arthur J., Cost Control in Air Force Systems Acquisition. ACSC-5560 Air Command and Staff College, Maxwell AFB, AL. April, 1975. AD/B003-9366.
- Davis, Guy W. The Dilemma of Uncertainties Associated with Cost Estimating in the Project Management Office, Defense Systems Management College, Ft. Belvoir, VA. May, 1976. LD-36420A.
- Defense Documentation Center, Cost Effective Analysis; Report Bibliography, DDC/B1B-78/01, Alexandria, VA. Apr., 1978. AD/A052-400.
- Defense Technical Information Center, Cost Effectiveness Analysis, A DTIC Bibliography. report bibliography July 73-Feb 80, Alexandria, VA. July 1980. AD/A087 800.
- Drake, Hudson B. "Major DOD Procurements at War With Reality" Harvard Business Review Jan-Feb, 1970.

- Ellsworth, Roger W. USAF RDT & E Cost Growth: A Perspective, 630-79, Air Command Staff College, Maxwell AFB, AL. Apr, 1979. LD-45086A.
- Forrester, Jay W., "A National Model for Understanding Social and Economic Change," Simulation Today, April 1975.
- Freeman, Rowland G., III. "Major Systems Developed: Lessons Learned." Program Manager's Newsletter, Jan/Feb, 1979.
- Gibson, Robert G. "Concurrency". Defense Systems Management Review. Autumn, 1979, Vol 2. No. 4.
- Gordon, Harvey J. "The Role of the contract in Systems Acquisition." Defense Systems Management Review. Winter, 1980. Vol 3 No. 1
- Grimm, Richard W., Using Cost Analysis to Break the Overrun Habit. Defense Systems Management College, Ft. Belvoir, VA. May, 1977. AD/A042-935.
- Hart, Steven L. and Ising, Terry R. 1977-1990 Technology Effects on NAVAIR Acquisition Management Concepts, NAFI-TR-2183, Naval Avionics Facility Indianapolis, IN. May, 1977. AD/B018-391L.
- Harvey, Thomas E. "Concurrency Today in Acquisition Management" Defense Systems Management Review Winter, 1980. Vol. 3 No. 1.
- Higgins, J. Alan. An Outlook on Future Weapon Systems Acquisition, Defense Systems Management College, Ft. Belvoir, VA. Nov., 1977. LD-41076A.
- Hill, Vaughn E. and Martin, Paul L. Life Cycle Costing: Its Promise and Problems. Air War College #5995, Maxwell AFB, AL. April 1976. LD-35957A.
- Holland, Robert L., Role Definition in the Decision Making process of Weapon Systems Acquisitions. Unpublished Master's thesis, Air Force Institute of Technology, Wright-Patterson AFB, OH. Dec, 1970. LD-26233.
- International Maritime Associates, Inc., A Study of Ship Acquisition Cost Estimating in the Naval Sea Systems Command, Executive Summary, Washington, D.C., Oct, 1977, AD/A046-976.
- Jones, Julius E. An Analysis of Incentive Contracts With Respect To Risk. US Army Command and General Staff College, Ft. Leavenworth, KS. June 1971. LD-27535.
- Kelley, Albert J. "Can Weapon System procurement be Managed?" Defense Systems Management Review Autumn 1977.
- Large, Joseph P., Bias in Initial Cost Estimates: How Low Estimates Can Increase the Cost of Acquiring Weapon Systems. R-1467-PA/E. RAND Corporation, Santa Monica, Ca., July 1974.
- Launer, Robert L. et al. Cost-Growth-Effects of Contract Size, Duration, Inflation, and Technology Level. Army Procurement Research Office, Ft. Lee, VA. May 1972. AD/746-620.

- Leon, Hayden L. Jr. The Ship Acquisition Process: An Inter-organizational Perspective. Unpublished Master's thesis, Naval Post Graduate School, Monterey, CA. March 1976. LD-36971A.
- Lewis, Edwin H. and Pearson, Eugene, D. The Air Force Cost Estimating Process: The Agencies Involved and Estimating Techniques Used. Unpublished thesis, Air Force Institute of Technology, Wright-Patterson AFB, OH. June, 1977. LD-39962A.
- Lilce, Ralph W., Total Risk Assessing Cost Estimate (TRACE): An Evaluation. US Army Reserach and Development Command. St. Louis, MO. Feb, 1979. LD-44065A.
- Lincoln, James B. Managing Total Acquisition Time: A New Priority for Major Weapon Systems. Defense Systems Management College, Ft. Belvoir, VA. May, 1977.
- Magee, Terry E. Differences in Aircraft Acquisition Management Practices Between the Air Force and the Navy. Unpublished thesis. Naval Postgraduate School, Monterey, CA: 1977 AD/A042-303.
- March, Robert T. "The Impact of Today's Electronics Technology on Systems Acquisition." Defense Systems Management Review, Summer 1979.
- Mariutto, William F., Managing Cost Overrun Engineering Change Proposals. Army Material Command, Texarkana, TX. Apr., 1975. AD/A009-183.
- Marks, Kenneth E. An Appraisal of Models Used in Life Cycle Cost Estimation for USAF Aircraft Systems. Santa Monica, CA: 1978. Rand Corporation.
- Martin, David P, and Kaffenberger, Susan A. A Dynamic Policy Model of the Department of Defense Acquisition process. Unpublished thesis. Air Force Institute of Technology, Wright-Patterson AFB, OH June, 1979. LD-44970A.
- McIver, D. W. et al A Proposed Strategy for the Acquisition of Avionics Equipment. R-1499-PR. RAND Corporation, Santa Monica, CA. Dec, 1974.
- McLeod, Hugh S., The Accuracy of Air Force Weapon System Cost Estimates as a Function of Time. Unpublished Master's thesis. Air Force Institute of Technology, Wright-Patterson AFB, OH June, 1976. AD/A030-240.
- Metcalf, Joseph. Cost Overruns in Military Hardware: An Analysis of Cause. US Army War College. Carlisle Barracks, PA. March, 1971. LD-26399.
- Mills, Brian S. Understanding and Evaluating Life Cycle Cost Models (second edition). Air Force Systems Command, Wright-Patterson AFB. OH. March, 1977. LD-45159A.
- Moeller, William G. et al. Accelerating the Decision Process in Major System Acquisition, Washington: Logistics Management Institute, 1979.

- Moeller, William G. Affordability For Major System Acquisitions
Washington: Logistics Management Institute, 1980.
- Montgomery, Douglas C., et al. Application of Decision/Risk Analysis
in Operational Tests and Evaluation, Georgia Institute of
Technology, GA, Sept., 1975. AD/A024-205.
- Morris, Maynard B. and Fred A. Franke, "A Methodology for the
Determination of Manufacturing Personnel Requirements
within the Aeronautical Systems Division," Unpublished
Thesis, AFIT (LSSR-9-78B), September 1978.
- Nelson, J. R. Performance/Schedule/Cost Tradeoffs and Risk Analysis
for the Acquisition of Aircraft Turbine Engines: Applications
of R-1288-PR Methodology. R-1781-PR. RAND Corporation, Santa
Monica, CA June, 1975.
- Oder, F. C. E. "Affordability and the Acquisition of Major Defense
Systems". Defense Systems Management Review Autumn 1977.
- Osterhus, Damond L. and Lawson, Diann. A Conceptual Model of the
Department of Defense Major System Acquisition Process.
Unpublished thesis, Air Force Institute of Technology,
Wright-Paterson AFB, OH. June 1978. LD-43088A.
- Ostronski, George et al, Simplifying Contracts for Commercial
Systems: A Case Study of DOD Acquisition of Commercial Systems
and Components, Don Sowle Assoc., Inc. Arlington, VA.
Jan., 1980. LD-46487A.
- Padgett, Thomas C. An Examination of the Relationships Between
Inflation and Cost Overruns in Defense contracts and the
Adequacy of Various Types of Price Indexes in Explaining these
Relationships. Unpublished dissertation, Air Force Business
Research Management Center, Wright-Patterson AFB, OH. March, 1975
LD-31618A.
- Pearce, Michael A., Prototyping: A Strategy for the Acquisition
of Naval Aircraft. Defense Management Systems College, Ft.
Belvoir, VA. Nov., 1976. AD/A035-357.
- Perry, Robert et al. Systems Acquisition Strategies, R-733-PR/ARPA,
RAND Corporation, Santa Monica, CA. June, 1971. AD/746-620.
- Perry, Robert L. et al, System Acquisition Experience RM-6072-PR,
RAND Corp., Santa Monica, CA. Nov., 1969.
- Quade, E. S.; A Critique of Cost-Effectiveness. P-5524. RAND
Corporation, Santa Monica, CA. Nov., 1975. AD/A022-195.
- Richardson, John H. "Defense Systems Acquisition: Working Toward
Improving Process." Program Managers Newsletter, Oct 1977.
- Sellers, Benjamin R. Competition in the Acquisition of Major Weapon
Systems. Unpublished thesis. Naval Postgraduate School,
Monterey, CA 1979. AD/A078-268.
- Sherman, Harold A. and Peter C. Gardiner, "A Methodology for
Managing Delays and Disruptions in the System Acquisition
Process," Proceedings of The Management of Risk and
Uncertainty in the Acquisition of Major Problems, US Air
Force Academy, February 1981.

- Sidney, W. A. The Defense Systems Acquisition and Review Council: A Study of Areas of Consideration Affecting the Functions and Process of Defense Major Systems Acquisition. Unpublished report, University of Southern California, Los Angeles, CA. Sept, 1976. LD-9210A.
- Simpson, F. S. Measurement of Technical Performance in Weapon System Development Programs: A Subjective Probability Approach. RM-5207-ARPA. Santa Monica, California: The RAND Corporation, 1968.
- Smith, Giles K. Air Force Acquisition Options For the 1980s: a Briefing on Study Plans. RAND Corporation, Santa Monica, CA. 1979 N-124-AF.
- Spencer, David T. "Alternatives for Shortening the Acquisition Process." Defense Systems Management Review. Autumn, 1979 Vol. 2 No. 4.
- Stanley, William L. and Miller, Michael D. Measuring Technological Change in Jet Fighter Aircraft. R-2249-AF. RAND Corporation, Santa Monica, CA, Sep., 1979.
- Stiles, Charles. "Formulating Improved Figures of Merit in Aircraft Acquisition." Defense Management Journal, 1st Qtr 1980, p. 56-60.
- Tateyana, Joseph T., A Defense Systems Acquisition Management Taxonomy and Inventory of Official Acquisition Management Documents. Defense Systems Management College. Ft. Belvoir, VA, May, 1977. AD/A044-958.
- USAF, HQ USAF (AF/SA), "Guidelines for Documenting Computer Simulation Models," 1981.
- US Army Material Development and Readiness Command, Acquisition Strategy Development, in-house study, Alexandria, VA. Sept., 1980. LD-46766.
- US Congress House, Inaccuracy of Department of Defense Weapons Acquisition Cost Estimates. Report of the Committee, 96th Cong., 1st sess. Nov. 16, 1979. H. Rept. 96-656. Washington: US Govt. Print Off., 1979.
- US General Accounting office, FAA Has Not Gone Far Enough With Improvements to its Planning and Acquisition Processes. PSAD-80-42. Washington, DC, June 4, 1980.
- US General Accounting Office. Impediments to Reducing the Costs of Weapons Systems, PSAD-80-6. Washington, DC, November 8, 1979.
- US General Accounting Office. Issues Identified in 21 Recently Published Major Weapon System Reports. PSAD-80-43. Washington, DC, June 12, 1980.
- White, Richard P. and Myers, Myron G. Competition in DOD Acquisitions. Logistics Management Institute, Washington, DC, May, 1979. LD-45320A.

1981 USAF - SCEE SUMMER FACULTY RESEARCH PROGRAM

Sponsored by the

AIR FORCE OFFICE OF SCIENTIFIC RESEARCH

Conducted by the

SOUTHEASTERN CENTER FOR ELECTRICAL ENGINEERING EDUCATION

FINAL REPORT

ANALYSIS OF MAINTENANCE DECISIONS AT LOWER

ECHELON LEVELS INVOLVING JET AIRCRAFT ENGINES

Prepared by: Dr. Charles J. Teplitz

Adademic Rank: Assistant Professor

Department and University: School of Business
State University of New York at Albany

Research Location: Air Force Human Resources Laboratory, Logistics
and Technical Training Division, Logistics Research
Branch, Logistics Acquisition Section

USAF Research Colleague: Mr. Russell M. Genet

Date: August 26, 1981

Contract No: F49620-79-C-0038

ANALYSIS OF MAINTENANCE DECISIONS AT LOWER
ECHELON LEVELS INVOLVING JET AIRCRAFT ENGINES

by

Charles J. Teplitz

ABSTRACT

The existence of diagnostic errors in the decision processes of jet aircraft engine maintenance is investigated. The sources of such errors and their remedies have often gone undiscovered. The effort discussed in this paper was designed (1) to provide a conceptual framework for the analysis of decisions in the maintenance process on jet aircraft, (2) to illustrate the interactions between various factors affecting maintenance decisions, and (3) to identify some major sources of diagnostic errors. Using a simulation model of the maintenance process, insight was gained into the causes and effects of diagnostic errors on jet aircraft maintenance. Suggestions for further research in this area are offered.

ACKNOWLEDGEMENT

The author would like to thank the Air Force Systems Command, the Air Force Office of Scientific Research and the Southeastern Center for Electrical Engineering Education for providing him with the opportunity to spend a most interesting and educational summer at the Human Resources Laboratory, Wright-Patterson AFB, Ohio. He would like to thank Mr. Russell M. Genet for suggesting this area of research and for his expert guidance. He would also like to acknowledge the assistance of Mr. Alan E. Herner, Mr. Terry M. Miller, and Capt Gordon W. Spray.

I. INTRODUCTION

The Logistics Acquisition Section of the Human Resources Lab (HRL) at Wright-Patterson Air Force Base has been investigating the relationship between jet aircraft maintenance costs and sortie generation. One determination of this investigation was the need for an adequate spares inventory. If an aircraft requires a replacement part, the existence of an adequate spares inventory facilitates rapid replacement of the defective item, thereby reducing turnaround time.

In examining the level of spares inventories, the question arises: Can we reduce the level of inventory without jeopardizing operational readiness? To answer this, it is necessary to determine why current levels are what they are. The primary reason for current levels of spares can be directly linked to past usage rates: experience. Based on records of this and other aircraft, inventory requirements, for a given level of service, can easily be determined. Our effort at HRL has been to determine whether these historical rates of usage are equivalent to expected rates, or somewhat higher. More specifically, is it possible that items have been replaced earlier than truly necessary?

Consider the situation when a line replaceable unit (LRU) is removed from an aircraft at the flight line, sent to the intermediate shop for repair, and returned to the flight line, without any maintenance performed, as a good unit. At the time the LRU was removed, it was replaced by an item from the spares inventory. As was later discovered; the LRU should never have been pulled, the replacement item should never have been pulled from spares inventory, and therefore, the spares inventory need not have been kept at such a high level. This relationship between diagnostic performance and spares inventory lead to the analysis to be described in this report.

The existence of diagnostic errors on maintenance decision process is well documented.^{1,2,3} The sources of errors within a representative maintenance network can be attributed almost exclusively to the following elements:

- 1) Technical personnel
- 2) Test equipment
- 3) Aircraft equipment instability
- 4) Poorly designed testing procedures

Each of these critical elements can be uniquely described by corresponding mean and variance estimates that describe their long-term performance. For example, a specific technician or operator may consistently declare marginally good equipment items as failed units. Conversely, he may mistakenly find failed items to be usable and return them to supply for future use in the active inventory. This particular equipment item, presumed to be usable, may unfortunately lead to a subsequent aborted sortie or premature failure.

The problem facing the Air Force is not one of trying to realize an ideal decision process, but one of identifying the important sources of decision errors, arranging to reduce or circumvent these sources in currently fielded systems, and designing around them in future systems.

II. OBJECTIVES

The main objective of this project was to develop a means by which the analyst, in the field, could determine if diagnostic errors were being made during the maintenance processes. While developing a procedure for jet engine maintenance, we were designing it to be applicable to any aircraft maintenance process.

A secondary objective was the development of a technique to isolate the causes of diagnostic errors committed. Our specific objectives were:

- (1) To model a general, or typical, aircraft maintenance process, covering flight-line maintenance and intermediate repair shop maintenance.
- (2) To incorporate this model into a computerized simulation, similar to that developed by Spray⁴, in order to track the jet engine (and its components) over time.
- (3) To determine methods by which these errors can be determined from field data.
- (4) To determine the sources of the errors and possible remedies.
- (5) To examine the potential impacts of the classic Type I and Type II errors, shown in Figure 1. (Note: the hypothesis being that the item is truly bad.)

		True State	
		(GOOD)	(BAD)
Observed State	(GOOD)	Correct Decision	Type I Error
	(BAD)	Type II Error	Correct Decision

FIGURE 1 - CLASSIC TYPE I AND TYPE II ERRORS

III. SIMULATION MODEL

Figure 2 depicts a simple model of the jet aircraft maintenance process. This model demonstrates only key actions which could result during pre-flight, thru-flight or post-flight inspections.

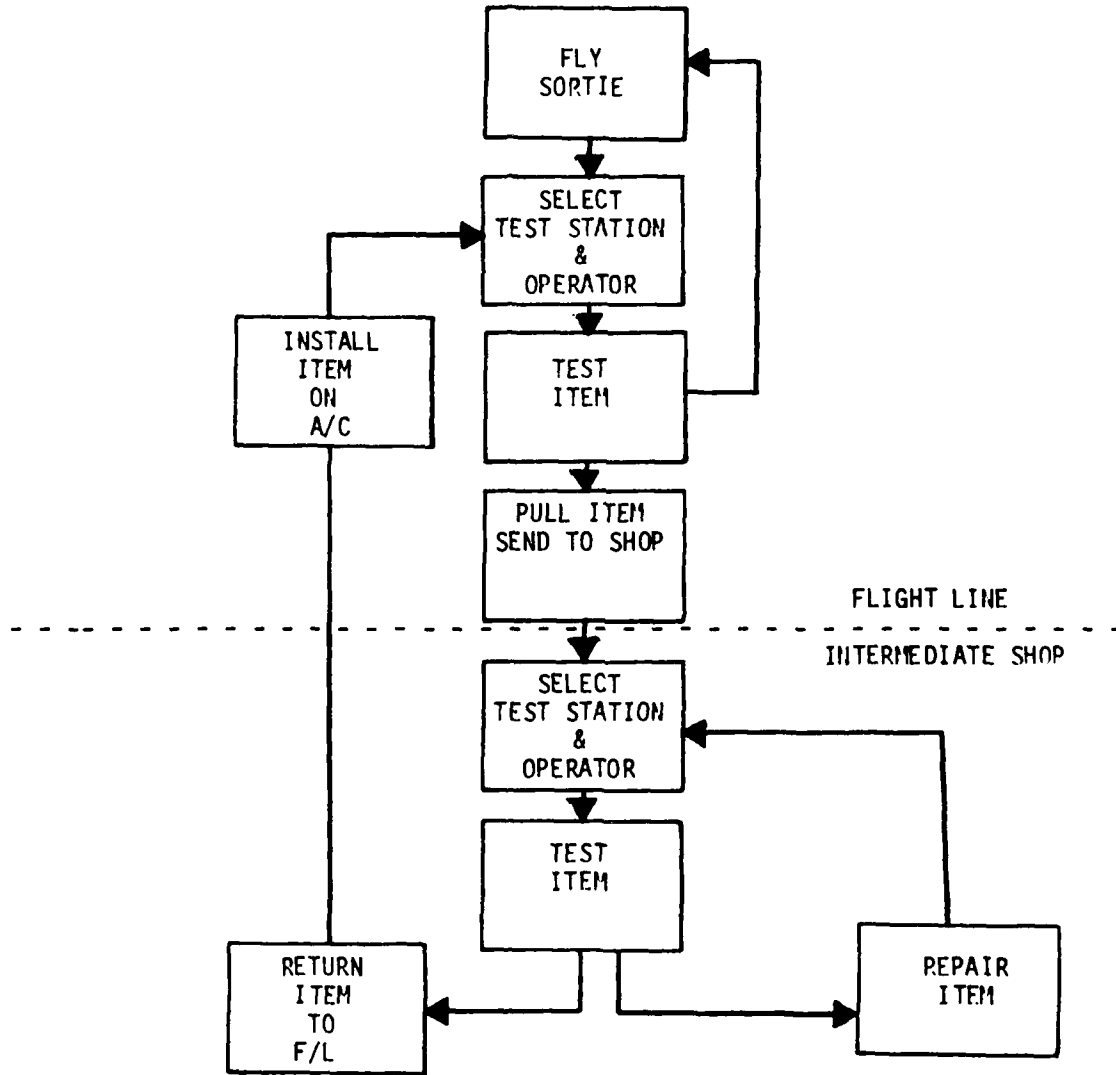


FIGURE 2 - MODEL OF MAINTENANCE PROCESS

This model was then programmed as a simulation model examining the diagnostic decisions regarding a single LRU of a jet engine. As our "simulated" aircraft flew, this component would be degraded, just as its true life counterpart. If, after a flight, the component had not degraded beyond a preset limit, then we would expect it to pass the post-flight inspection. Otherwise, we would expect it to fail the post-flight.

The step-by-step procedure of the simulation is listed below.

- STEP 1: INITIALIZE. Initialize network. Go to Step 2.
- STEP 2: FLY SORTIE. Increase flight time and degradation of components. If flying time or degradation limits exceeded, go to Step 3. Otherwise, go to Step 4.
- STEP 3: MODIFY TRUE VALUES. Change measured component characteristic to failure level. Set component status to "Failure". Go to Step 4.
- STEP 4: TEST LOCATION DETERMINATION. If flight-line test to be performed, go to Step 5. If shop test to be performed, go to Step 7.
- STEP 5: SELECT FLIGHT-LINE STATION AND OPERATOR. Determine flight-line test station and operator to perform test. Go to Step 6.
- STEP 6: TEST COMPONENT. If observed value of component characteristic is within cutting range and no other components need testing, go to Step 2. If other components need testing, go to Step 5. If observed value outside cutting range; pull engine, send to shop. Go to Step 7.
- STEP 7: SELECT SHOP STATION AND OPERATOR. Determine shop test station and operator to perform test. Go to Step 8.
- STEP 8: TEST COMPONENT. If observed value of component is within cutting range and no other components need testing, go to Step 10. If other components need testing, go to Step 7. If observed value outside cutting range, go to Step 9.

STEP 9: REBUILD COMPONENT. Repair or replace component. Change measurable component characteristic to "Repaired" level. Reset component flight time to zero. If measurable component characteristic within required range, set component status to "Good". Go to Step 7.

STEP 10: INCREASE COUNTER. If iteration counter less than maximum limit, ship engine to flight line, go to Step 11. Otherwise, go to Step 12.

STEP 11: INSTALL. Install engine on aircraft. Go to Step 5.

STEP 12: STOP. Iteration limit exceeded.

The simulation assumed the existence of two independent test stations on the flight line and two at the intermediate shop. Each station had its own test bias due to, perhaps, lack of calibration. Each also had some random noise associated with performing a test. This noise combined with the fixed bias caused each station to respond differently to a given situation.

The simulation also assumed the existence of two operators at each location capable of working at either of the two test stations. Each operator was also biased by some fixed amount, perhaps due to inconsistent training. The operator also had random noise obscuring his observation. This noise combined with the fixed bias caused each operator to respond differently to a given situation.

Once running smoothly, the simulation was adjusted to follow a randomized block factorial design. This was accomplished by requiring that every operator test the item twice at every station. Thus, instead of being tested once, the item was tested eight times for each single test required. This procedure allowed for two types of analyses. First, by requiring each operator to replicate each test, the reliability (repeatability) could be measured. Second, by having all operators test an item at all stations, the relative biases of operators and stations could be determined statistically without prior knowledge of the individual biases. The effects of these procedures will be discussed next.

IV. SAMPLE ANALYSIS

Table 1 shows a summary table for the situation where all operators are instructed to accept, as good, any item they observe which measures between 68 and 76, inclusive. All that can be seen directly from Table 1 is that the operators are not perfectly reliable, i.e., they change their decisions occasionally. Also, we can see that not all decisions are correct, based on the true quality shown in the last column. (It should be noted that, in reality, true quality and value are rarely known. However, it is possible during experimentation, to know these values with relative certainty.)

ITEM	STATION 1 OPERATOR 1		STATION 1 OPERATOR 2		STATION 2 OPERATOR 1		STATION 2 OPERATOR 2		TRUE VALUE	TRUE QUALITY
	TEST	RETEST	TEST	RETEST	TEST	RETEST	TEST	RETEST		
1	F	F	P	P	P	P	F	P	76	GOOD
2	P	P	P	P	P	P	P	P	74	GOOD
3	P	P	F	P	F	P	P	P	72	GOOD
4	P	P	P	P	P	F	P	P	70	GOOD
5	P	P	P	F	P	P	F	F	68	GOOD
6	F	F	F	P	P	P	F	F	66	BAD
7	P	P	P	F	F	F	P	P	64	BAD
8	F	F	F	F	P	F	F	F	62	BAD
9	F	F	F	P	F	P	F	F	60	BAD
10	F	F	F	F	F	F	F	F	58	BAD

P=Pass (Acceptable)
F=Fail (Unacceptable)

TABLE 1 - SAMPLE FIELD DATA

From Table 1 we can derive Table 2, measures of consistency, and Table 3, quality of decisions. In Table 2a, we see that overall, 75 percent of all decisions are maintained after a retest. Our example demonstrates a relatively reliable test situation. Looking closer, however, we see that the two test stations (Table 2b and 2c) are not perfectly reliable, but they do have identical consistency coefficients. This would indicate that while each station may be out of calibration (biased), they are biased equally. This indicates that while each station may result in erroneous decisions, we have no predisposition as to which station we want to run a specific test.

a. OVER ALL

		RETEST		
		P	F	
E S T	P	16	4	40
	F	6	14	

Consistency = $30/40 = .75$

b. STATION 1
ALL OPERATORS

		RETEST		
		P	F	
E S T	P	8	2	20
	F	3	7	

Consistency = $15/20 = .75$

c. STATION 2
ALL OPERATORS

		RETEST		
		P	F	
E S T	P	8	2	20
	F	3	7	

Consistency = $15/20 = .75$

d. OPERATOR 1
ALL STATIONS

		RETEST		
		P	F	
E S T	P	9	2	20
	F	2	7	

Consistency = $16/20 = .80$

e. OPERATOR 2
ALL STATIONS

		RETEST		
		P	F	
E S T	P	7	2	20
	F	4	7	

Consistency = $14/20 = .70$

TABLE 2 - CONSISTENCY (Repeatability)

Tables 2d and 2e, however, demonstrate that the two operators have different consistency coefficients. This indicates the operators are biased differently. This could result from unequal training or experience. Whatever the cause, the two operators will occasionally differ in their opinion of an item's quality. The existence of such a situation could possibly be remedied by further training, by replacing one or both operators, or by some other managerial technique.

	Overall	Station 1 All Operators	Station 2 All Operators	Operator 1 All Stations	Operator 2 All Stations
Correct Decisions	60/80=.750	31/20=.775	29/40=.725	30/40=.75	30/40=.75
Pass Good Item	31/40=.775	16/20=.800	15/20=.750	16/20=.80	15/20=.75
Fail Bad Item	29/40=.725	15/20=.750	14/20=.700	14/20=.70	15/20=.75
Incorrect Decisions					
Pass Bad Item	11/40=.275	5/20=.250	6/20=.300	6/20=.30	5/20=.25
Fail Good Item	9/40=.225	4/20=.200	5/20=.250	4/20=.20	5/20=.25

TABLE 3 - QUALITY OF DECISIONS
(Proportions)

Table 3 initially indicates that 75 percent of all decisions made are correct. This may or may not be an acceptable level. The acceptable level would be set such that the cost of errors is weighed against the cost of reducing such errors. This analysis is beyond the scope of the current effort.

Table 3 does indicate that Station 1 tends to be more accurate in its decisions than Station 2. Keeping in mind that the biases on the two stations are identical (see Table 2), we must conclude that the random noise on Station 1 has a tighter distribution than that of Station 2. With this knowledge, we can now examine both stations to determine why we have this disparity and what can be done to remedy the situation.

Table 3 also demonstrates another interesting situation. While both operators make accurate decisions 75 percent of the time, Operator 1 is better at spotting truly good items, while Operator 2 is better at spotting truly bad items. We were already aware of some discrepancy in bias between the two operators, now we see that this discrepancy affects their ability to corroborate each other's decisions. So while, on the surface, the two operators seem identical, we now see an area requiring corrective action.

If we are interested in improving the quality of decisions and reliability of operators while not performing any managerial effort to improve operators or stations, a method does exist. By setting cutting scores differently for each station, differences in biases can be artificially removed. Or, since in our example station biases are equal, we could give different operators their

own cutting scores. For example, if Operator 2 was instructed to pass any item measured between 66 and 76, instead of 68 and 76, he would most likely pass more items than before. This would probably improve his ability to spot truly good items, but at the expense of erroneously passing truly bad items. If this is our goal, it can be achieved in this way.

Expanding on this idea, we reran the simulation five times, each time varying the acceptable ranges. (No effort was made to vary the range for an individual station or operator.) This procedure enabled us to determine the cutting range which would optimize a particular criterion. For example, if, due to cost considerations, we wished to maximize the overall number of correct diagnoses on truly good items, a cutting range of 66-74 yielded the best solution. If, on the other hand, we wanted to maximize the overall number of correct diagnoses on truly bad items, a cutting range of 61-69 yielded the best solution.

In essence, a cutting range can be determined which averages out the biases and random noise for all combinations of stations and operators. While this does not remedy the causes of these biases, it does improve consistency of diagnosis throughout the process. Figure 3 shows the cost curves generated for the two objectives just described. Further description of this capability can be found in Spray⁵.

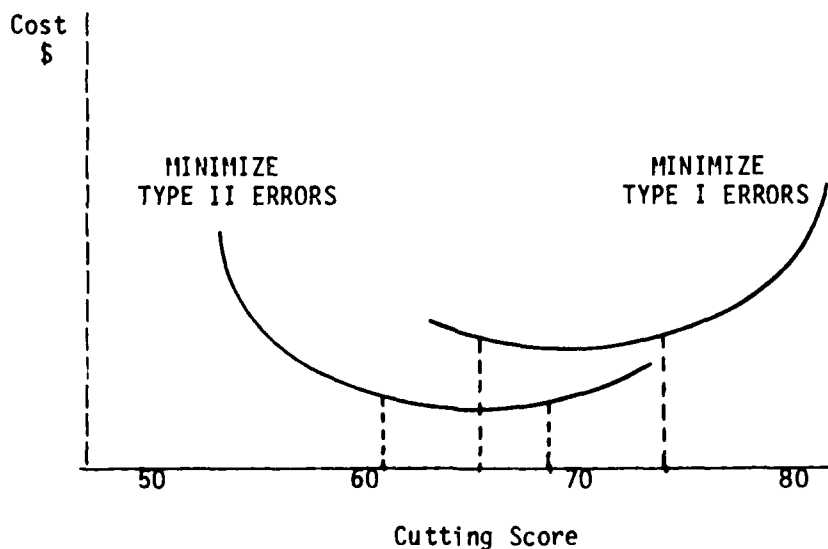


FIGURE 3 - OPTIMAL CUTTING SCORE WITH OPERATOR VARIANCE EFFECTS

V. RECOMMENDATIONS

The simulation of aircraft maintenance decisions has provided Human Resources Laboratory with a conceptual framework for analyzing a maintenance process. Our aim was to identify and illustrate interactions between various factors and to determine the probable sources of diagnostic errors.

While the simulation was a simplified model of a real process, it did provide us with the insight needed to further investigate means of reducing diagnostic errors. We found that diagnostic errors stem from a number of both simple and complex situations. Station bias and noise and operator bias and noise often combine unfavorably to lead to inaccurate maintenance decisions. Most biases, if accurately measured, can be reduced through better training, feedback and calibration. It is the determination of the existence of bias in the field that requires further study.

A promising method of determining biases includes the development of a simulation "game". This method, to be developed on a portable mini-computer, will permit test operators in the field to diagnose simulated items. The operator will receive information regarding maintenance history of the item, status of flight-line clocks and feedback as to the quality of their previous decisions on this item. It is hoped that this added information will serve to reduce operator bias. Additionally, their responses will enable us to accurately determine each operator's bias. Once discovered, we hope to find appropriate methods of reducing the bias, e.g., improved training, improved technical manuals, etc.

Once diagnostic error rates are reduced, a second recommendation for follow-on research is to analyze spares inventories in an effort to reduce required levels. With fewer erroneous replacements, less spares need be kept on hand. Multiplied across the entire spares pipeline, the effect will be to reduce support costs while maintaining or improving the operational readiness of the aircraft.

REFERENCES

1. Genet, R.M., "Future Logistics Management and Complex Equipment Item Tests," Proceedings of the Third Logistics Management Symposium, Washington, D.C., October 1973.

2. Neville, A.R. and R.M. Genet, "Testing the Tests, or the Quality of Diagnostic and Functional Tests," Proceedings of the German Institute of Navigation (DGON), Heidelberg, Germany, April 1974.
3. Genet, R.M., "Avionics Cost Reduction Through Improved Tests," Proceedings of the 1973 National Electronics Conference (NAECON), IEEE, May 1973.
4. Spray, G.W., "A Simulation Approach for Evaluation of Decision Errors in Maintenance Processes," PRAI PR Report, April 1976.
5. Spray, G.W., "Computer Simulation of Diagnostic Errors with a Simplified Maintenance Network." LRLA Technical Report (forthcoming).

1981 USAF - SCEEE SUMMER FACULTY RESEARCH PROGRAM

Sponsored by the

Air Force Office of Scientific Research

Conducted by the

Southeastern Center for Electrical Engineering Education

FINAL REPORT

A Study of the Interaction of Hydrazine, Methylhydrazine and Unsym-
dimethylhydrazine with Porphyrins, Metalloporphyrins, and some Metal
Coordination Compounds

Prepared by: Dr. Albert N. Thompson, Jr.
Academic Rank: Assistant Professor
Department and University: Department of Chemistry
Fayetteville State University*
Research Location: U.S. Air Force School of Aerospace Medicine
Crew Technology Division, Crew Environments
Branch (VNL)
USAF Research Colleague: Dr. Hubert G. Lovelady
Date: October 8, 1981
Contract No: F49620-79-C-0038

* Address Sept 81, Dept. of Chemistry, Spelman College, AtL., GA 30314

A Study of the Interaction of Hydrazine Methylhydrazine and Unsym-dimethylhydrazine with Porphyrins, Metalloporphyrins, and some Metal Coordination Compounds

by

Albert N. Thompson

Abstract

Hydrazine, Methylhydrazine and Unsym-dimethylhydrazine have been shown to react favorably with some porphyrins, metalloporphyrins and first transition series metal coordination compounds. The reaction of the hydrazines with certain porphyrins suggests an initial acid-base reaction followed by an oxidation reduction process. An oxidation reduction reaction is also observed for the reaction of the hydrazines with the metalloporphyrins and the transition metal compounds. The metals in both the metalloporphyrins and the metal compounds are reduced by the hydrazines to lower oxidation states.

Suggestion for follow up research in the area of hydrazine chemistry are given.

Acknowledgement

The author would like to thank the Air Force School of Aerospace Medicine, the Air force Office of Scientific Research and The Southeastern Center for Electrical Engineering Education for providing him with the opportunity to spend a very useful and rewarding summer at the Crew Technology Division and Environmental Branch (VNL), Brooks AFB, TX. He would like to acknowledge the sincere efforts of Dr. Richard L. Miller, Chief of Environments Branch, and his staff for providing him with excellent facilities and unreserved hospitality.

Finally, he would like to thank Dr. Hubert G. Lovelady for his sponsorship, guidance and also gratitude to him for interfacing his research efforts with those of the author.

I. INTRODUCTION

The detection and separation of Hydrazine (H), Methylhydrazine (MH), and Unsymdimethylhydrazine (UDMH) as well as reliable quantitative methods of determining the presence of hydrazine and its derivatives is still a major priority to researchers. Occupational exposure to hydrazines needs constant environmental monitoring. In recent years hydrazine and its derivatives have experienced increased use in industry as antioxidants, reducing agents pharmacological agents, and as rocket fuels.

It has been determined that hydrazine and its derivatives are carcinogenic and/or cancer suspect agents and that they should be monitored as such. Therefore extensive efforts have been initiated to develop and improve monitoring systems used to identify and measure each hydrazine separately and in mixtures.

Several analytical procedures for the detection of hydrazine and its derivatives have been developed and are in use today. Many of these techniques are based on the strong reducing properties of hydrazine. Many of these are only adequate if the test sample is free of interfering agents. Derivatives that can be monitored using relatively common and inexpensive UV-visible spectroscopy are formed from the reaction of hydrazine and its derivatives with salicylaldehyde, indanedione, p-dimethylaminobenzaldehyde, 1,2-naphthoquinone-4 sulfonate, 2,3-dichloro-1,4-naphthoquinone, 2-furaldehyde, and benzaldehyde. Several of the above laboratory procedures involve very time consuming preparations and their reliability is at times suspect.

In this study several porphyrins, metalloporphyrins and metal coordination compounds (such as Fe (III), Fe (II), Cr (VI) and Co (III) compounds) were reacted with hydrazine, methylhydrazine and Unsymdimethylhydrazine. Some of these reactions resulted in producing some physical observations such as spectral unique to the individual hydrazine derivatives when reacted with the compounds mentioned in this study.

II. OBJECTIVES

The primary objective of this project was to determine the feasibility and also the usefulness of synthesizing additional hydrazine coordination compounds and/or complexes. These derivatives could possibly be used in the detection and monitoring of hydrazine and its common derivatives, methylhydrazine, and unsym-dimethylhydrazine.

Initially macrocyclic porphyrins and metalloporphyrins were reacted with hydrazine and the hydrazine derivatives. Additionally the interaction of the hydrazines with metal coordination compounds was investigated. As a result of these interactions the following investigations will be carried out:

1. Efforts will be made to determine if any physical changes occurred as a result of interactions.
2. If any observations are confirmed e.g. color changes, spectrophotometric data will be collected to determine if reaction products are formed and the extent of the formation of products when possible.
3. Application of liquid chromatographic methods will be used to determine the usefulness of this technique in the separation and identification of mixtures of the hydrazine interaction products, especially in those products which produce no useful UV or visible spectra.

III. The reaction of the hydrazine derivatives with porphyrins and metalloporphyrins.

Investigations were undertaken to determine the nature of the reaction between water soluble porphyrins (Fig 1) for example Tetrakis trimethylaminotetraphenyl porphyrin iodide. Studies were carried out in acid, neutral, and base media. In acidic solution the diacid porphyrin exhibits a characteristic green color which is transformed into a free base red color compound upon the addition of hydrazine. Hydrazine which is a good reducing agent is capable of transforming the porphyrin in neutral and acid media to its dihydro form (one of the unsaturated bonds on the macrocyclic ring of the porphyrin is reduced to a saturated bond by the addition of two hydrogen atoms) (Fig 1). Background literature and spectrum analysis (Fig 2) indicates that due to the ability of hydrazine to act as a base toward Lewis acids, it can neutralize the diacid form of the porphyrin (green) to the free base form (red). Upon the addition of ammonia to the diacid species a similar transition occurs but to a greater degree than when equal amounts of hydrazine are added. The Lewis base activity of hydrazines are known to be less than that of ammonia, therefore these results are expected and are predictable.

Several non water-soluble metalloporphyrins were synthesized. One reversible reaction was observed as a result of the reaction of Tetra (4-N-methyl-pyridyl) porphyrin tosylate with hydrazine. No reversible reactions were, observed with the reaction of this porphyrin with methylhydrazine and unsym-dimethylhydrazine.^{7,8}

Iron (III), Zinc (II) and Cobalt (III) - Porphyrins were reacted with hydrazine, methylhydrazine and unsym-dimethylhydrazine. The reaction of Co (III) porphyrin with the hydrazines overall was more useful in the water soluble class and Zn (II) porphyrin was more useful in the non-water soluble class. Overall more productive results were obtained from Co (III) porphyrin. Three derivatives were formed as a result of the reaction of H, MH, and UDMH with

water soluble Co (III) Tetrakis (trimethyl aminotetraphenyl) porphyrin iodine (Co (III) TAPP I⁻). Visible spectra confirms the formation of hydrazine derivatives with this porphyrin. Though the spectra of the three hydrazine derivatives resulting from the reaction with Co (III) porphyrin in terms of individual absorption maximums are not as dissimilar as one would ideally want, further spectrum calculations and collected information from each individual spectrum can be used for determining amounts of each derivative present in mixtures.^{9,10}

The Zn (II) Tetraphenyl porphyrin (Zn TAPP) reacted only with hydrazine in pyridine solvent. No reaction was observed with other hydrazine derivatives.¹¹ In the case of Fe (III) TAPP, all three hydrazine derivatives reacted. The resulting visible spectra was much less characteristic and unique than the spectra of the Co (III) porphyrin hydrazine products.¹²

IV. The reaction of the Hydrazine derivatives with first transition series metal compounds.

Several metallic salts were reacted with hydrazine (H), methylhydrazine (MH), and unsym-dimethylhydrazine (UDMH). Preliminary spot tests were carried out on salts of Cr (VI), Fe (II), Co (III) and Fe (III) that were reacted with H, MH and UDMH. There were several positive reactions resulting from these tests.^{13,17}

At this point it was determined that several of the compounds formed could not be used as possible species for colorimetric determination. Some formed insoluble precipitates or either their color complexes with the hydrazines were not distinguishable.^{18,19}

Useful results were obtained from the reaction of sodium tripentacyanoamino ferrate (SPF) and potassium ferricyanide with hydrazine and its derivatives. These redox reactions resulted in the formation of distinctively different colored compounds representing the reaction of each of the hydrazines with the Iron compounds. As in the case of the Co (III) porphyrin reaction with hydrazines, individual absorption spectra are as dissimilar as one would ideally want. These reactions are not kinetically rapid, but as a result of extensive kinetic studies ideal reaction conditions can possibly be obtained.⁹

Preliminary thin-layer chromatographic and liquid chromatographic results indicate identification and separation of mixtures of these products is feasible (Figures 3 and 4).

V. RECOMMENDATIONS

After extensive studies and observations of the reaction of the hydrazines with several porphyrins, metalloporphyrins and transition metal compounds, the reactions of hydrazine and its common derivatives methylhydrazine and dimethylhydrazine with Tetra (4-N-methyl-pyridyl) porphyrin tosylate, Co (III) Tetrakis (trimethylamino tetraphenyl) porphyrin iodide, potassium ferricyanide, and sodium tripentacyanoaminoferrate warrant further investigations concerning their probable applications in the detection and quantitative measurement of hydrazine and its derivatives. New studies on these reactions should involve the investigation of these reactions as reaction parameters are varied. Temperature dependence kinetic studies at this point have the highest priority, especially for those reactions that do not proceed in a reasonable analytical time period.

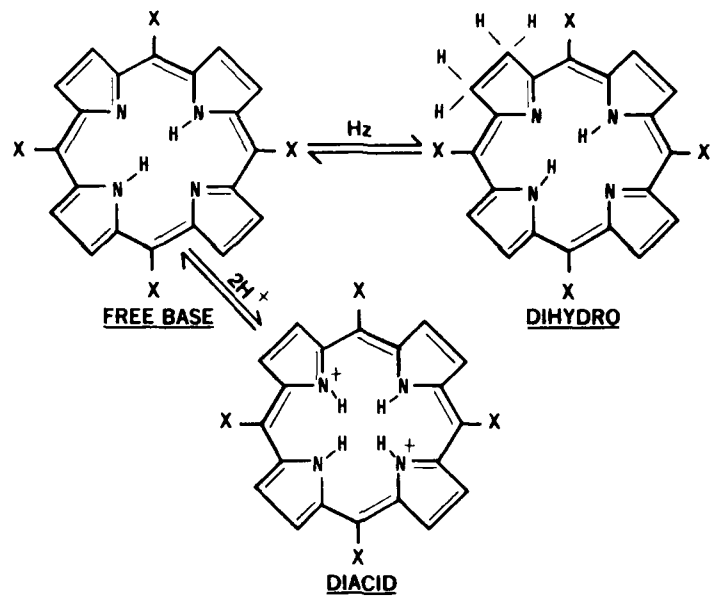
Additionally, due to the number of reactions investigated, time did not permit as much work in liquid chromatographic studies as one would need to confidently utilize this method as an investigative tool.

Therefore follow up experimentation will involve more extensive chromatographic studies, in addition to reaction parameter studies.

REFERENCES

1. Leonard C. Bailey and Thomas Medwick, "Spectrophotometric Determination of Hydrazine and 1,1-Dimethylhydrazine, Separately or in Admixture," Anal. Chem. ACTA., Vol. 35, pages 330-336, (1966).
2. L.A. Dee, "Gas Chromatographic Determination of Aqueous Trace Hydrazine and Methylhydrazine as corresponding Pyrazoles," Anal. Chem., Vol. 43, No. 11, (1971).
3. Hugh E. Malone, "The Determination of Hydrazine-Hydrazide Groups," (Pergamon Press, New York, 1970).
4. W. Peter Hambright, in "Porphyrins and Metalloporphyrins," (Elsevier, Amsterdam, 1975)
5. A. Adler, F.R. Longo, J. Goldmacher, et al., "A Simplified Synthesis for meso-Tetra-phenylporphin," J. Org. Chem., Vol. 32, page 476, (1967).
6. N. Data-Gupta and T.J. Bardos, "Synthetic Porphyrins I. Synthesis and Spectra of some para-substituted meso-Tetraphenyl porphyrins," J. Hetero. Chem., Vol. 3, pages 495-502, (1966).
7. P. Hambright, A. Adabi, J. Reid and D. Maitland, "Rapid Spot Test for Stannous Tin Levels in ^{99m}Tc kits," J. of Nucl. Med. Tech., Vol. 5, pages 88-89, (1977).
8. A. Micheal Zimmer and Stewart Spies, "The Paper Spot Test: A Rapid Method for Quantitating Stannous Concentrations in Radiopharmaceutical Kits," J. Nucl. Med., Vol. 22, pages 465-467, (1981).
9. M. Krishnamurthy, "Synthesis and Characterization of a New Water-Soluble Porphyrin," Indian J. Chem.
10. Albert N. Thompson and M. Krishnamurthy, "Peripheral charge effects on the Kinetics of Zn (II)-Porphyrin System," J. Inorg. Nucl. Chem., Vol. 41, pages 1251-1255, (1979).
11. A.N. Sidorov, "A spectral Examination of Photoreduction of Zinc Tetraphenylporphine," Dokl. Akad. Nauk. SSSR, Vol. 158, pages 973-976, (1964).
12. Albert N. Thompson and M. Krishnamurthy, "Studies on Reactions of Imidazole with Two Iron (III) Porphyrin Dimers in Aqueous Solution," Inorg. Chim ACTA., Vol. 34, pages 145-150, (1979).
13. P. Barz and H.P. Fritz, "Studies on Biochemically effective liqand Systems V. Complex-Chemical and Physico-Chemical Studies on 1,2 dimethylhydrazine," Z. Naturforsch B., Vol. 27, pages 1131-1136, (1972).
14. V. Ramanujam, et al., "Oxidation of Hydrazine by Cr (VI) Oxide Kinetic and Mechanistic studies in the Presence of complexing Agents," Inorg. Chem. ACTA., Vol. 31, pages 133-139, (1975).

15. V. Zhilinskaya et al. "Synthesis and Study of Sodium Penta-cyanoazidoferrate," Zh. Neorg. Khim., Vol. 19, pp 2186-2190, (1974).
16. A.N. Sergeeva et al. "Iron (II) cyanide complexes with nitrogen - containing ligands" Zh. Neorg. Khim., Vol. 20, pp 1925-1928, (1975).
17. S. Mannen and H.A. Hano, "STOICHIOMETRY of the Oxidation of Arylhydrazines with Ferricyanide" Tetrahedron, Vol. 29, pp 3497-3502, (1973).
18. J.E. Huheey. Inorganic Chemistry, (Harper and Row, pp 511, New York, 1978).
19. F.A. Cotton and G. Wilkinson, Advanced Inorganic Chemistry, (Wiley Interscience, pp 689, New York, 1980).
20. H. McKennis and A. Yard, "Determination of Methyl hydrazine," Anal. Chem., Vol. 26, pp 1960-1963, (1954).
21. M. Schmall et al., "Colorimetric Determination of Ascorbic Acid," Anal. Chem., Vol. 26, pp 1521-1522, (1954).
22. J. Yoe and R. Grob, "Colorimetric Determination of Boron with Tetrabromochrysolin," Anal. Chem., Vol. 26, pp 1465-1468, (1954).



X = PHENYL GROUPS AND/OR PHENYL DERIVATIVES THAT HAVE IONIC GROUPS ATTACHED

Figure 1

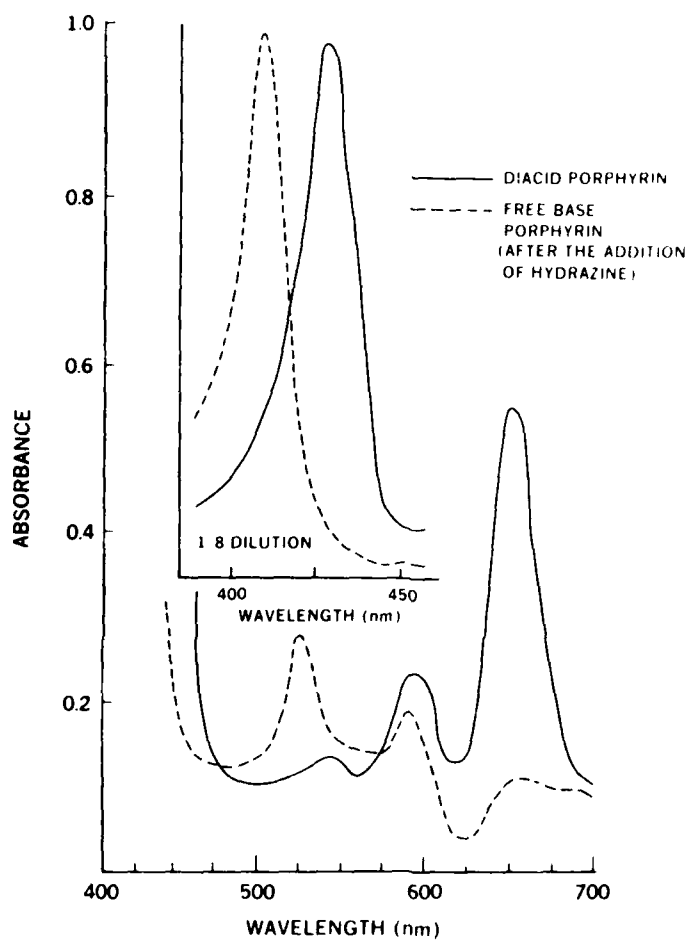


Figure 2

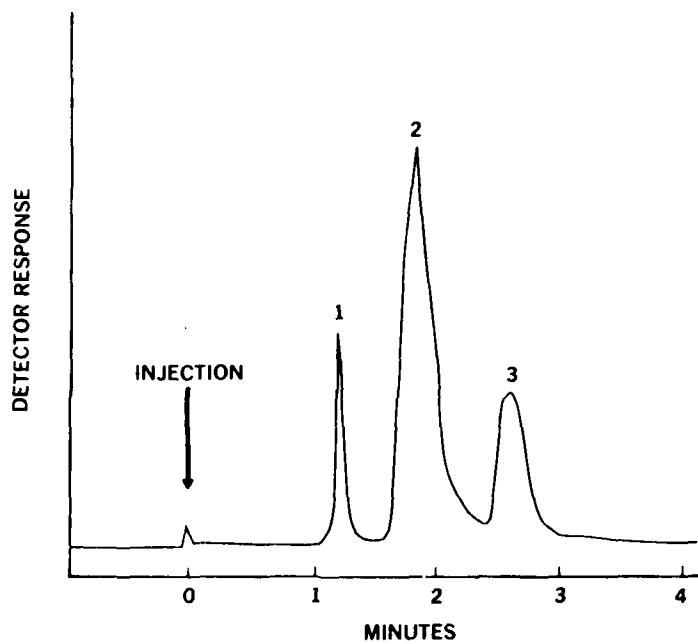


Fig 3. Sodium Tripenta-Cyanoamino Ferrate (SPF) Derivatives

1. SPF Hydrazine
2. SPF Methylhydrazine
3. SPF Dimethylhydrazine

HPLC Condition

4. 20 cm/min
5. 50 ml/hr flowrate
6. 66% acetonitrile in H₂O
7. Column: Micro Pak CN-10

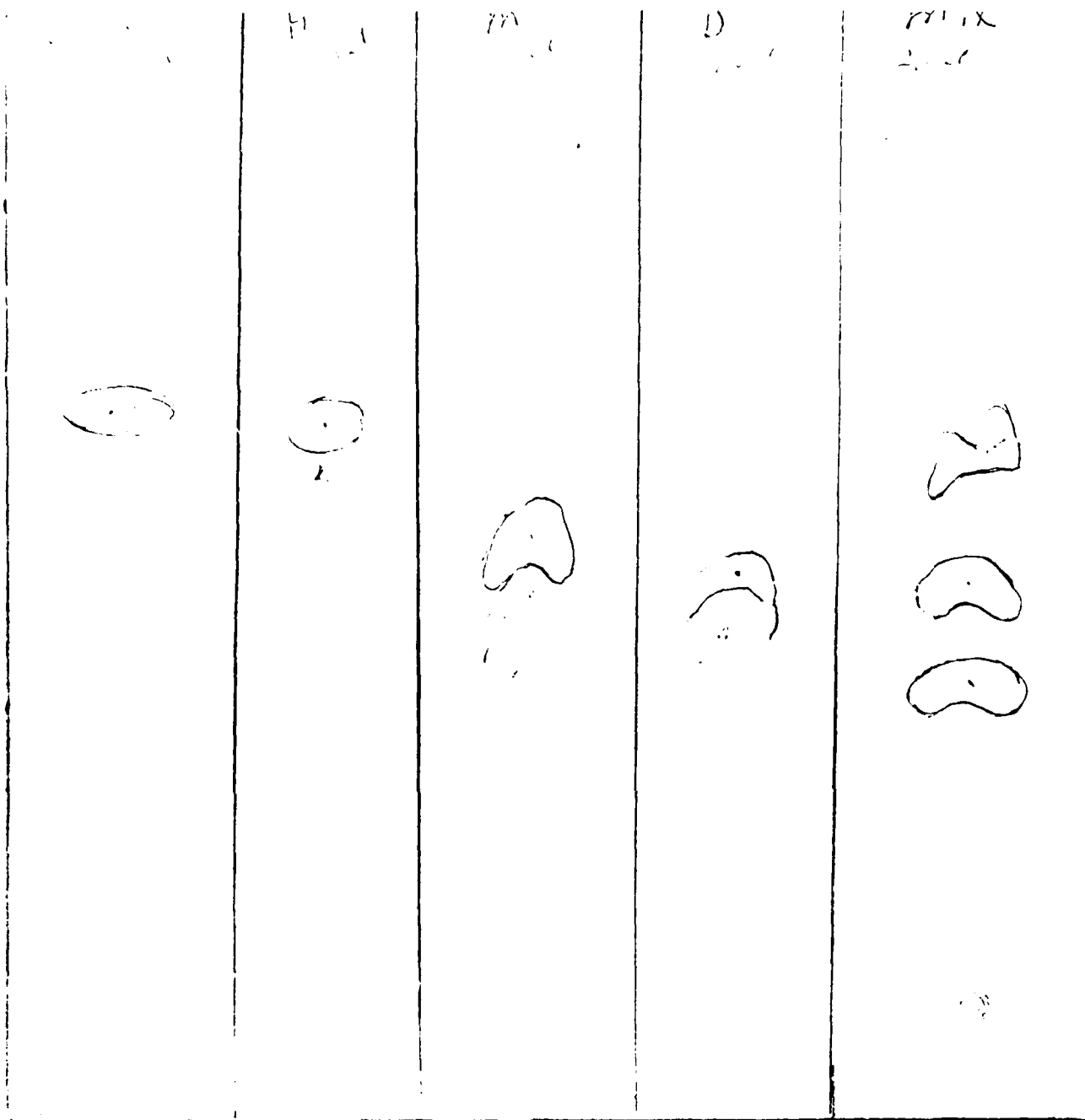


Fig 4. Preliminary Conditions for Thin-Layer Chromatographic

1. 2 hours
2. 80 Methanol
3. Rf Values
 1. SPF = 0.72
 2. SPF = 0.71
 3. SPF-MMHZ = 0.57
 4. SPF-UDMHZ = 0.52

1981 USAF - SCEE SUMMER FACULTY RESEARCH PROGRAM

Sponsored by the

AIR FORCE OFFICE OF SCIENTIFIC RESEARCH

Conducted by the

SOUTHEASTERN CENTER FOR ELECTRICAL ENGINEERING EDUCATION

FINAL REPORT

GaAs MESFET MODELING

Prepared by:	Dr. Arthur R. Thorbjornsen
Academic Rank:	Associate Professor
Department and University:	Department of Electrical Engineering The University of Toledo
USAF Research Colleague:	Dr. Chern Huang
Date:	September 11, 1981
Contract No:	F49620-79-C-0038

GaAs MESFET MODELING

by

Arthur R. Thorbjornsen

ABSTRACT

A mathematical model of a GaAs MESFET has been incorporated into a standard integrated circuit analysis program (SPICE2G). Because of their proprietary nature, it is difficult to obtain a copy of a circuit analysis program that contains a built-in MESFET model. This report contains detailed information on how holders of the SPICE2G program may modify their program to include a GaAs MESFET model. The model is valid for nonlinear DC analysis, linear AC small signal analysis, and nonlinear transient analysis. The results of several example circuit simulations are given. Some directions for future research are also given.

ACKNOWLEDGMENTS

The author would like to express his sincere gratitude to the U.S. Air Force Systems Command, the Air Force Office of Scientific Research, and the Avionics Laboratory at Wright-Patterson Air Force Base for the opportunity to participate in the 1981 USAF Summer Faculty Research Program. The interest, encouragement, and suggestions of the Effort Focal Points, Capt J.B. Rawlings and Mr James Skalski, are greatly appreciated. Special thanks are due to my research colleague, Dr Chern Huang, who worked with me on a day-to-day basis. Thanks are also due to 1st Lt Joseph Tatman, Mr Fredric Stormont, Mr Roy Newman, and 2nd Lt Bruce Pecor for their assistance.

I. INTRODUCTION

A type of semiconductor device that is currently the subject of considerable research and development is the GaAs (gallium-arsenide) MESFET (metal-semiconductor field-effect-transistor). The reason for the interest in this device is its potential for high-speed and high-frequency operation since GaAs has an electron mobility that is about 5.5 times greater than that of silicon at relatively low levels of electric field strength [1]. Therefore, a GaAs device should be capable of operating at speeds or frequencies about 5.5 times greater than an equivalent silicon device. The ability to fabricate such a device in integrated circuit form means that there will be numerous applications of the GaAs MESFET in avionics systems.

The GaAs MESFET is constructed like a silicon JFET except that the gate junction is a Schottky barrier junction formed by applying metal directly on the semiconductor surface [2].

When designing integrated electronic circuits it is necessary to make use of computer-aided circuit analysis and design programs because of the size and complexity of the circuits involved. Furthermore, in the case of high frequency IC's, a circuit analysis program is necessary for simulation because discrete breadboard circuits cannot be built which accurately reproduce an integrated circuit.

In order to accurately analyse an electronic circuit a circuit analysis program must contain models of various electronic devices that faithfully simulate those devices over a wide range of conditions. One of the most ubiquitous and versatile circuit analysis programs is SPICE2 (Simulation Program with Integrated Circuit Emphasis) which was developed at the University of California, Berkeley [3]. SPICE2 contains models for the bipolar junction transistor, the junction field effect transistor, and the metal-oxide-semiconductor field effect transistor, but not for the MESFET.

II. OBJECTIVES OF THE RESEARCH EFFORT

The objectives of this research effort at the Avionics Laboratory at Wright-Patterson Air Force Base were as follows: (1) to study the available technical literature on GaAs MESFET modeling and to select a suitable model for inclusion in a circuit analysis program; (2) to incorporate the selected model into the ASPEC program (Advanced Simulation Program for Electronic Circuits), which is in use at the Avionics Laboratory; and (3) to try to acquire a version of the SPICE2G program that contains a MESFET model, or to acquire a copy of the standard SPICE2G program and incorporate a MESFET model into it. In addition I was to spend some time in the Integrated Circuits Laboratory in the Avionics Lab to observe the fabrication of GaAs MESFET integrated circuits.

III. PREVIOUSLY DEVELOPED MESFET MODELS

The type of MESFET model that is to be selected and incorporated into a circuit analysis program is one of the so-called one-dimensional equivalent circuit models. In the one-dimensional model it is assumed that voltage changes take place only along the path from source to drain, under the gate. More accurate, two-dimensional models exist but the amount of computer time and storage necessary for two-dimensional simulations would be prohibitive for inclusion of such a model into a general circuit analysis program [1, 4].

Among the GaAs MESFET models that were considered are those of Curtice [4]; Hartgring, Oldham, and Chiu [5]; and Van Tuyl and Liechti [6]. The model of Hartgring, et al, is a modification of the JFET model used in the SPICE2G program. The model of Van Tuyl and Liechti includes a time delay to simulate the gate transit time of majority carriers and also includes a nonlinear resistance which produces a better match between computed and measured I-V values in the linear region of operation than can be obtained using the SPICE2G JFET model. Curtice essentially has incorporated the features of Van Tuyl and Liechti's model but with a simpler equivalent circuit.

The model chosen for this work is the Curtice model which is shown in Figure 1. C12 and C13 are fixed capacitors but C23 is a junction capacitance dependent on V23. The dependent current source has a governing equation, in the normal mode, given by

$$\begin{aligned}
 I_D &= 0, & V_{23} - V_T &\leq 0 \\
 &= (\text{BETA}) \cdot (V_{23} - V_T)^2 \cdot [1 + (\text{LAMBDA}) \cdot V_{13}] \cdot \text{TANH}[(\text{ALPHA}) \cdot V_{13}], & 0 < V_{23} - V_T
 \end{aligned}
 \tag{1}$$

Where LAMBDA is a constant channel length modulation parameter and ALPHA is a constant which is determined experimentally to assure a good fit between measured and computed values in the linear region. BETA is the slope of the linear region of a curve of $\sqrt{I_D}$ vs VGS and VT is the value of VGS at which a linear extension of this curve intersects the VGS axis, as shown in Figure 2. T is the gate transit time which is the amount of time delay between a change in gate to source voltage and the resultant change in drain current. The effect of this time delay may be included by the approximation suggested by Curtice in the equation below.

$$I_D[V_{23}(t-T), V_{13}(t)] \cong I_D[V_{23}(t), V_{13}(t)] - T \frac{dI_D}{dt}
 \tag{2}$$

An advantage of the Curtice model is that it can be incorporated into SPICE2 without changing the topology of the JFET model that is built into SPICE2, and thus, making the program modification quite simple. The SPICE2 JFET model, shown in Figure 3, has a drain current given, in the normal mode, by

$$\begin{aligned}
 I_D &= 0, & V_{23} - V_T &\leq 0 \\
 &= (\text{BETA}) \cdot (V_{23} - V_T)^2 \cdot [1 + (\text{LAMBDA}) \cdot V_{13}], & 0 < V_{23} - V_T \leq V_{13} \\
 &= (\text{BETA}) \cdot (V_{13}) \cdot [2 \cdot (V_{23} - V_T) - V_{13}] \cdot [1 + (\text{LAMBDA}) \cdot V_{13}], & 0 < V_{13} < V_{23} - V_T.
 \end{aligned}
 \tag{3}$$

IV. INCORPORATION OF THE MESFET MODEL.

A. ASPEC

The ASPEC circuit analysis program which resides in the Avionics Laboratory's DEC-10 computer was to have the MESFET model incorporated into it first. The details for modifying the ASPEC program were devised and actually carried out as described in the next section. However, there were problems of convergence with the ASPEC program so its use was abandoned.

B. SPICE2G

It was not possible to obtain a copy of the SPICE2G program containing the MESFET model. A copy of the standard SPICE2G program was obtained about midway through the summer research period and loaded into the DEC-10 computer. The program modifications to SPICE2G were made only in subroutine JFET. These changes involved "removing" some elements from the JFET model by forcing certain current, conductance, and capacitance values to be zero and modifying the equation for the dependent current source to be of the form of equation (2).

A novel technique was developed for incorporating the gate transit time delay into the MESFET model. This technique involves the use of a lossless transmission line to provide the desired time delay. As long as the transmission line has a high enough characteristic impedance, Z_0 , and is terminated in Z_0 , then its presence in the equivalent circuit will cause no adverse effects on the circuit. A lossless transmission line is one of the elements that are already incorporated into the SPICE2G program. The proper value of Z_0 must be determined by trial and error.

Another feature made use of in SPICE2G is the subcircuit capability, which obviates the need to repeat sets of data statements when a subcircuit is used more than once in a circuit. Figure 4 shows the subcircuit used to

represent Curtice's MESFET model. The dotted line surrounds the part of the subcircuit contained in the original JFET subroutine. The X's indicate those elements that have been removed from the JFET subroutine. The short circuits around RD and RS indicate that those elements have zero (default) values in the JFET description.

One parameter in equation (1) that is not a part of equation (3) is the parameter ALPHA. In order to read in a value of ALPHA, without having to make major changes in the SPICE2G program, use was made of one of the parameters for the removed diodes in the original JFET model. The zero-bias junction capacitance for the gate-to-drain diode is used to read in the value of ALPHA.

A typical set of input data for the MESFET subcircuit used in the modified version of SPICE2G is shown in Figure 5.

One limitation that must be kept in mind is the fact that the model for an ordinary JFET is inoperative while the MESFET model is incorporated in SPICE2G. However, it is very unlikely that JFETs and MESFETs would be constructed together in one integrated circuit, so there is no real problem. If it is necessary to simulate JFETs and MESFETs at the same time one can create a MESFET subcircuit for the JFET. In this case the MESFET parameters, particularly ALPHA, will have to be chosen to accurately represent a JFET.

V. EXAMPLES OF CIRCUIT SIMULATIONS

The modified SPICE2G program, called MSPICE, has been used successfully to simulate circuits containing GaAs MESFETs.

A. BFL Gate DC Transfer Curve.

The Buffer FET Logic (BFL) gate shown in Figure 6 was analyzed using MSPICE to produce a DC transfer characteristic. The MESFET device parameters used are from Curtice's paper [4] and are listed in Figure 5.

The solid line in Figure 7 is the DC transfer curve for one BFL gate while the dotted line is for four cascaded BFL gates. Both curves behave as expected.

B. BFL Gate Pulse Response.

With a voltage pulse applied to the input of the buffer FET logic gate of Figure 6, the output voltage shown in Figure 8 is obtained. As one can see, the output change occurs about 95 picoseconds after the input change, which demonstrates the extremely high-speed switching capabilities of the GaAs MESFET.

VI. RECOMMENDATIONS

A model for the GaAs MESFET has been incorporated into the SPICE2G circuit analysis program. The model includes the gate transit time effect which is incorporated by means of a novel technique involving a lossless transmission line. The modified SPICE2G program (MSPICE) has been tested by performing simulations of practical digital MESFET circuits and has been found to produce reliable and accurate analyses.

The MSPICE program is a valuable tool for use in the design and analysis of MESFET circuits and can be made use of at the Avionics Laboratory in the ongoing GaAs MESFET research and development programs. Should other Air Force organizations require a copy of the MSPICE program it can be obtained from the Avionics Laboratory at Wright-Patterson Air Force Base. If such organizations already have a copy of SPICE2G, they can convert it to MSPICE merely by obtaining a copy of the modified JFET subroutine and merging the modified JFET subroutine into their SPICE2G program in a link edit operation.

There are several areas of research that would logically follow the work reported here. One area of research would be to compare the measured data from MESFET integrated circuits with MSPICE simulation data. In this way the MESFET model could be "fine-tuned" by making modifications to the MESFET subcircuit. These modifications would consist of the addition of discrete elements, perhaps to simulate device parasitics.

Another area of research would involve the use of the MSPICE program to simulate circuits containing hypothetical MESFET devices with a goal of future development of MESFET devices having parameter values that would produce circuits with certain desired characteristics, such as small gate delay, a particular pulse response shape, etc.

Still another topic of research is the development of a computerized method for generating realistic sets of MESFET parameter values for use in Monte Carlo analyses. By realistic it is meant that the generated parameter values will have the same distribution shapes and correlations as do measured parameter values. Such a parameter value generator, coupled with the MSPICE program, would allow one to perform Monte Carlo analyses which would result in estimates of circuit yield and statistical measures of circuit performance.

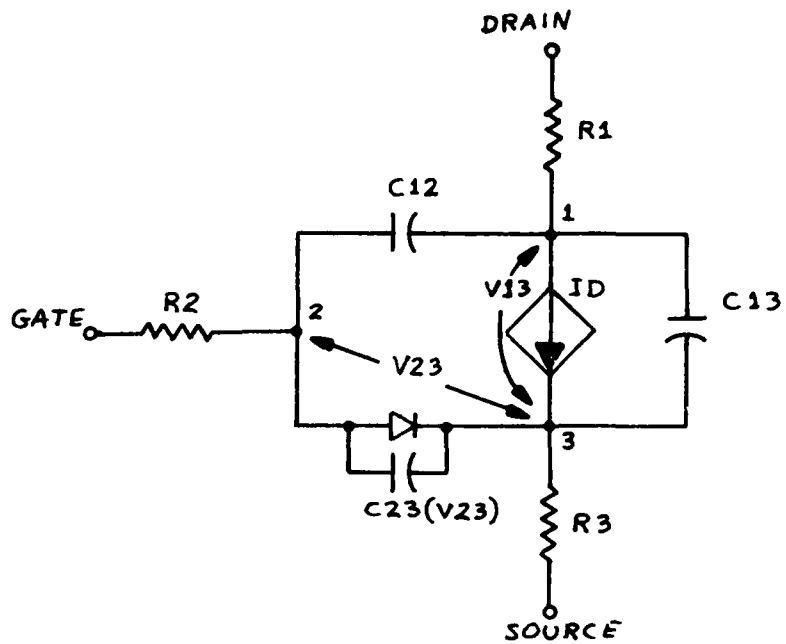


Figure 1: Curtice's GaAs MESFET model.

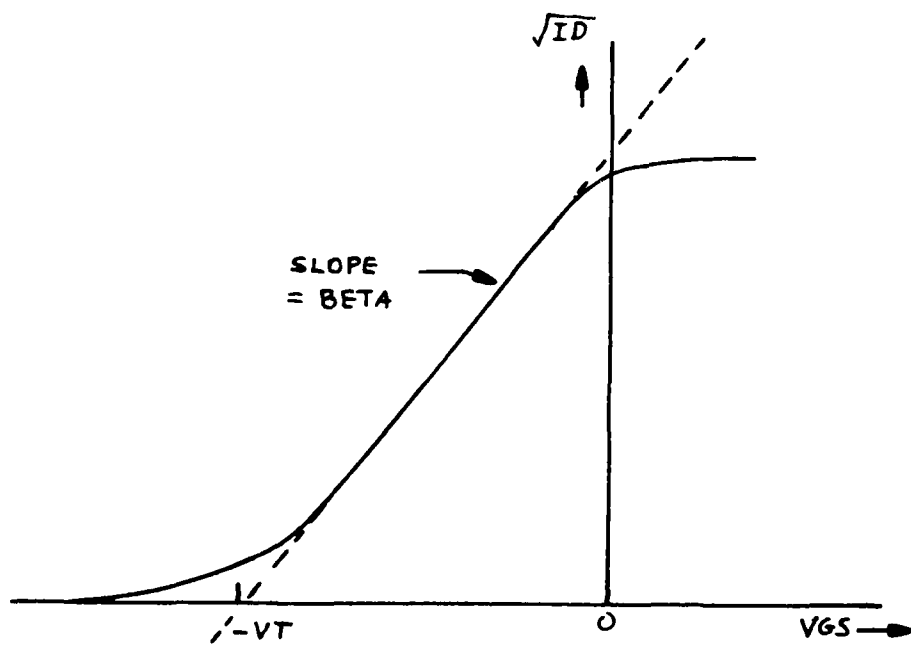


Figure 2: Curve of $\sqrt{I_D}$ vs V_{GS} .

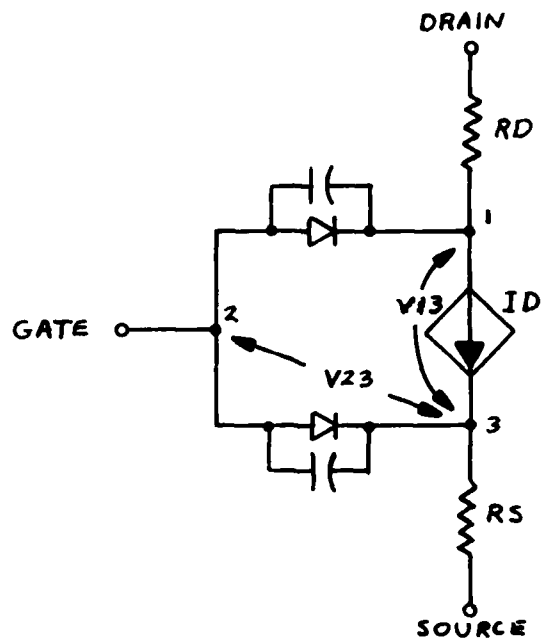


Figure 3: JFET model used in SPICE2.

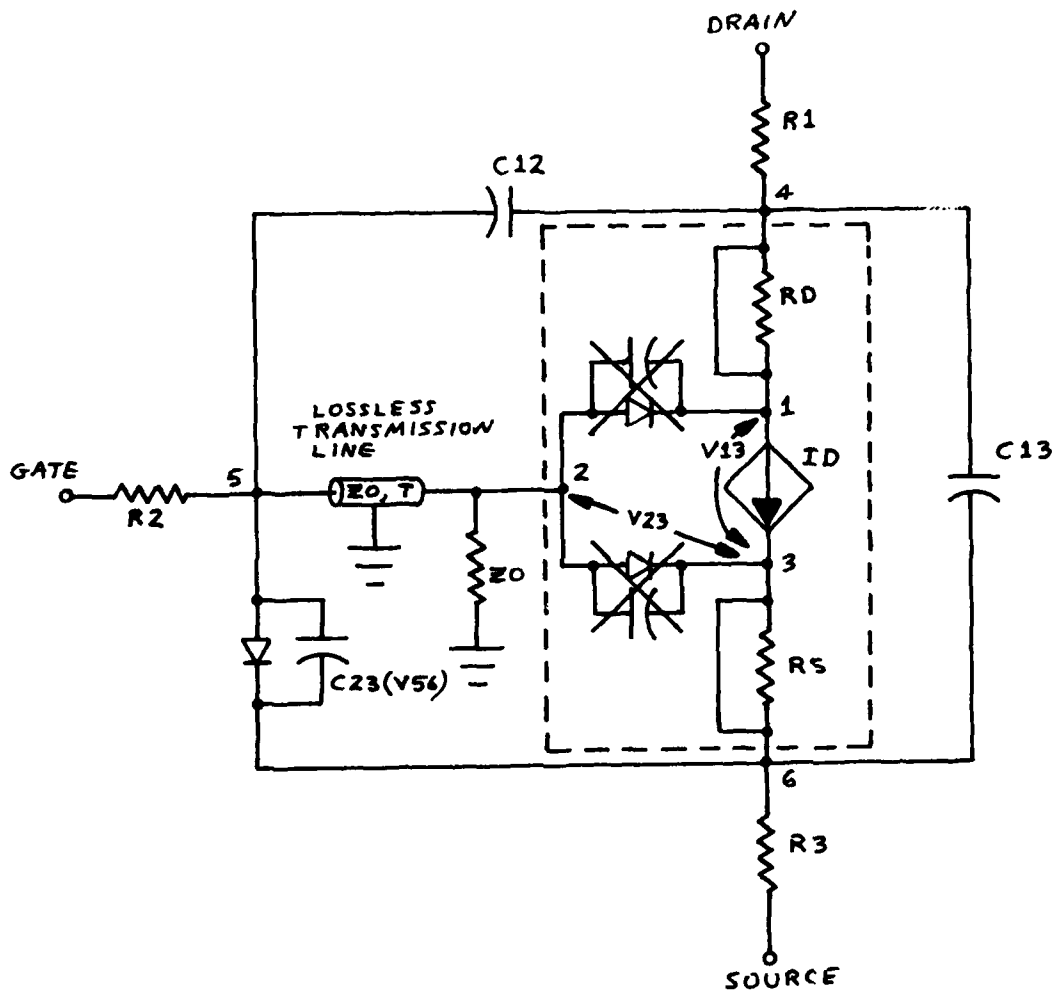


Figure 4: MESFET subcircuit used in SPICE2G.

```

-
-
-
XLOAD 3 2 2 MESFET
XINVRTR 2 1 0 MESFET
-
-
.SUBCKT MESFET 4 2 5
R1 4 1 3.0
R3 3 6 3.0
C12 5 1 0.03PF
C13 1 3 0.1PF
TLINE 5 0 2 0 ZO=100K TD=10PS
RLOAD 2 0 100K
DGS 5 3 DIODEGS
.MODEL DIODEGS D EG=0.69 VJ=0.7 CJO=0.5PF
JMESFET 1 2 3 VCIS
.MODEL VCIS NJF VTO=-2.63 BETA=13.1MA CGD=2.3
.ENDS MESFET
-
-

```

Figure 5: MESFET subcircuit input data for SPICE2G.

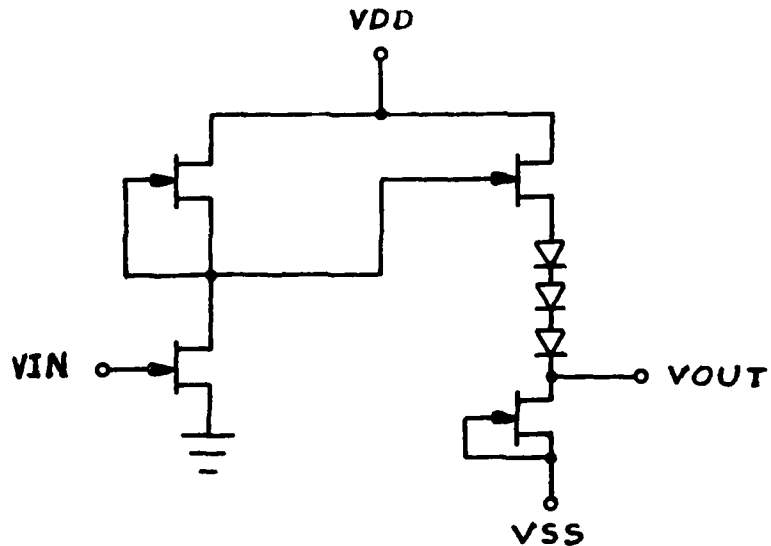


Figure 6: BFL gate.

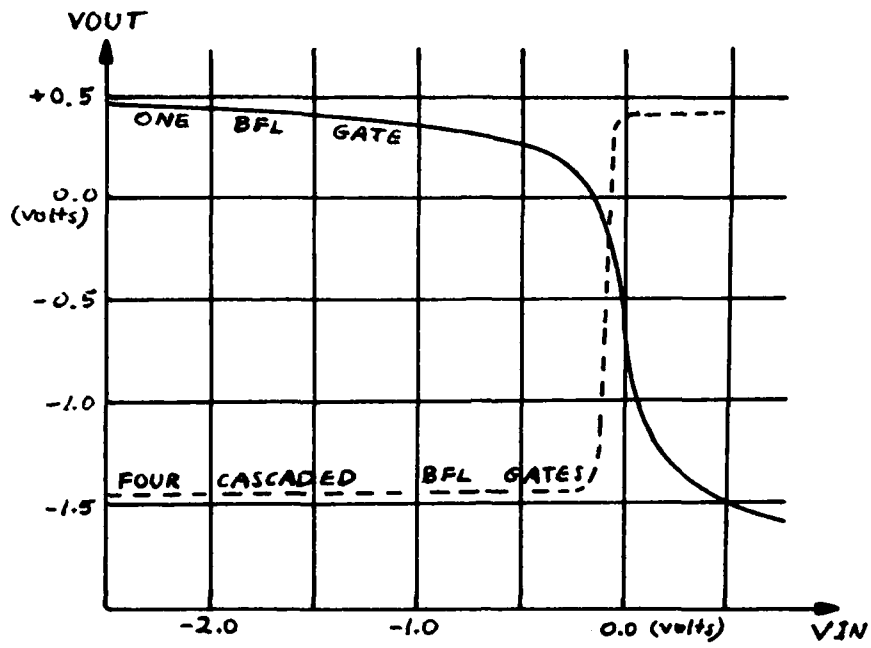


Figure 7: BFL gate DC transfer curves.

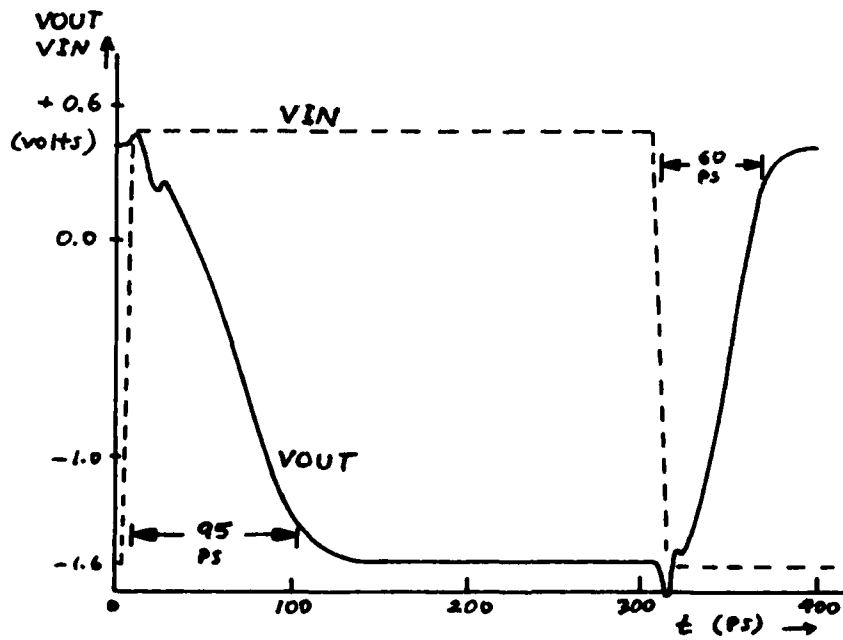


Figure 8: Pulse response of BFL gate.

REFERENCES

1. Lawrence Livermore National Laboratory, "Predicting Integrated-Circuit Performance," Energy and Technology Review, August 1981, pp. 1-11.
2. S.M. Sze, Physics of Semiconductor Devices, New York, Wiley-Interscience, 1969, p. 410.
3. L.W. Nagel, "SPICE2: A Computer Program to Simulate Semiconductor Circuits," Electronics Research Lab., Col. Eng., Univ. California, Berkeley, Memo. ERL-M520, May 1975.
4. W.R. Curtice, "A MESFET Model for Use in the Design of GaAs Integrated Circuits," IEEE Trans. on Microwave Theory and Techniques, May 1980, pp. 448-456.
5. C.D. Hartgring, W.G. Oldham, and T.Y. Chiu, "A MESFET Model for Circuit Analysis," Solid State Electronics, Vol. 23, 1980, pp. 121-126.
6. R.L. Van Tuyl and C.A. Liechti, "Gallium Arsenide Digital Integrated Circuits," Air Force Avionics Lab., AFWAL, WPAFB, Tech. Rept. AFAL-TR-74-40, March 1974.

1981 USAF - SCEE SUMMER FACULTY RESEARCH PROGRAM

Sponsored by the
AIR FORCE OFFICE OF SCIENTIFIC RESEARCH

Conducted by the

SOUTHEASTERN CENTER FOR ELECTRICAL ENGINEERING EDUCATION

FINAL REPORT

COVERING PROBLEMS IN

C³ I SYSTEMS

Prepared by: Richard Van Slyke
Academic Rank: Professor
Department and University: Electrical Engineering and
Computer Science Department Stevens Institute of Technology
Research Location: Electronics Systems Division,
Deputate of Development Plans.
USAF Research Colleague: Dr. Donald Brick
Date: September 8, 1981
Contract No.: F49620-79-C-0038

COVERING PROBLEMS IN

C³I SYSTEMS

by

Richard Van Slyke

ABSTRACT

A common problem in the study, design, and deployment of Command, Control, Communications, and Intelligence (C³I) Systems is minimizing the cost of satisfying various kinds of coverage requirements. Two examples are repeater coverage for terminals in tactical radio networks and radar surveillance. Mathematical techniques for finding optimal coverings have been well studied by the Operations Research community. Unfortunately, previously developed techniques ignore requirements of particular concern to the Air Force. Most important of these is the need for redundant coverage to provide reliability and to reduce vulnerability to attack. Also of concern is the need for algorithms that have guaranteed computation time requirements for use in real time applications. New algorithms for finding coverings satisfying these requirements are described. The results of extensive testing are reported. An experimental computer implementation is described. Finally, these techniques are applied to radio repeater location in tactical communication networks in Western Germany.

ACKNOWLEDGEMENTS

I am indebted to the Air Force Systems Command, the Air Force Office of Scientific Research, and the Southeastern Center for Electrical Engineering Education for the opportunity to pursue these investigations during a most productive summer at the Electronics System Division, Hanscom Air Force Base. The Deputy for Development Plans, Colonel Ernest Hatchell, Jr. and his staff were very hospitable in providing facilities for my research. Dr. Don Brick was most helpful in providing guidance in the applications of my research and in introducing me to the activities of ESD related to my work. Mr. Otto Wech and Dr. Steven Sussman (MITRE, Bedford) gave freely of their time to describe their work and to give suggestions for mine. Finally, none of this would have been possible without the generous assistance of Andy Clapp, Dick Wagner, Ed Le Clair, Karen Hincman, and the others of the CONCAP facility at MITRE Bedford for providing access to their PDP 11-70 system and patient instruction in its use.

I first worked on the problems described here while directing a project at the Network Analysis Corporation (NAC) for the Defense Department's Advanced Research Projects Agency [NAC, 1974]. Professor Roger Wets of the University of Kentucky as consultant to NAC was primarily responsible for the results in [NAC, 1974], and many of the results in this report are extensions of his work.

I. Introduction:

Future military Command, Control, Communications, and Intelligence (C³I) Systems will be more highly dispersed than at present for survivability purposes. This will of necessity give rise to new and difficult technical problems for which novel design and analysis techniques will be needed. One such, is the frequent requirement of these C³I systems for the provision of coverage. Two important examples are the coverage of communicating entities by communication systems and the coverage of (potential) targets by weapon systems or surveillance/reconnaissance.

To be more specific, consider a number of tactical radio terminals which are deployed in such a way that the origin and destination terminals cannot communicate directly; thus, messages must be relayed. Often this is accomplished by designating some radio terminals as "repeaters". A repeater accepts certain messages and retransmits them to each other and to the destination terminals.

Sufficient repeaters must be assigned and correctly located to guarantee that each terminal can communicate with at least one repeater. Determining the optimal number of repeaters, their location, and the assignment of terminals to repeaters can be given standard formulations as "set covering" [Garfinkel and Nemhauser, 1972], "p-median," and "mini-max" location problems [Handler and Mirchandani, 1979]. However, there are factors of significant importance in Air Force applications which are not adequately covered by these models.

First, it is extremely important in military applications that communication systems be highly redundant. This can be modeled by requiring that each terminal have access to several repeaters. On the other hand, even if cost is no object, one does not want to use all possible repeaters since each active, redundant repeater reduces network capacity. Thus, upperbounds on the number of repeaters

accessible by a terminal may be required or an upperbound on the total number of repeaters in a network may be imposed.

A second generalization is required to deal with applications in which assignments must be made in real time. This rules out all known exact algorithms and many heuristics because there are no practical bounds on their computation time [Garey and Johnson, 1979,p.222]. Thus bounded time heuristics must be developed along with estimates and/or bounds for their accuracy.

PAVE MOVER which is an airborne system designed to detect and track moving ground targets behind enemy lines and to guide missile and aircraft attacks to these targets is a second application of "covering". The detection of targets is dependent on the radar coverage behind enemy lines by airborne phased array radar. Because the radar plane (over friendly territory) is at some distance from the locations of potential targets (behind enemy lines) the scan is usually at a small angle relative to the horizon. Thus, there is a significant "terrain masking" where areas behind enemy lines are shadowed by topographical features between the radar and the area. Because of terrain masking and radar range considerations each potential flight path of a PAVE MOVER radar aircraft will cover only some of the potential target sites. Thus, in deployment planning, flight paths must be assigned in such a way that all the significant potential target sites are scanned by at least one flight path. However, not all areas behind enemy lines are equally important so that critical sites such as mountain passes, and the more passable areas should be assigned more coverage than relatively less passable areas such as swamps. (Radar "terrain masking" has played a pivotal role in recent discussions of the utility of AWACS aircraft in potential Arab-Israeli conflicts [N.Y. Times, 1981].)

In both these examples there is a set of potential coverers from which an optimal subset is required which

covers a given set of points. Schematically we can represent the situation as a bipartite graph. See Figure 1.1 where the bottom row of nodes represents the entities which must be covered and the top row of nodes represents the covering entities. The directed arcs connecting these two sets of nodes indicate which of the bottom nodes are covered by each of the top nodes. For example, node R1 covers nodes T1, T2 and T5 in Figure 1.1. In the first example, the covering nodes R1 to R4 represent potential repeaters sites to serve potential terminal locations T1 to T8. Arcs indicate which terminals can communicate using which repeaters. In the second example R1 to R4 represent possible PAVE MOVER radar plane flight paths and nodes T1 to T8 potential target locations. An arc connecting node R1, for example, to node T5 indicates that the PAVE MOVER radar can "see" potential target location T5 during the flight path represented by node R1.

To simplify discussion we shall use the terminology of the repeater location problems; for example, in Figure 1.1 we will call nodes R1 - R4 repeaters and nodes T1 - T8 terminals.

The case in which it is required that each terminal be covered at least once has been thoroughly studied (e.g., [Garfinkel and Nemhauser, 1972]). These problems are quite difficult and in fact are included in an important class of problems (NP-Hard) which are believed to be computationally intractable, in general [Garey and Johnson, 1979] (See especially p.222).

Thus, to solve problems where the number of repeaters and terminals are much greater than 20 or 30 heuristics must be resorted to. One particular class of heuristics, the "greedy heuristics", have been analyzed theoretically and bounds on their performance established [Chvatal, 1979], [Johnson, 1974], [Lovasz, 1975]. Fortunately, while these worst case bounds are very weak, in practice heuristics

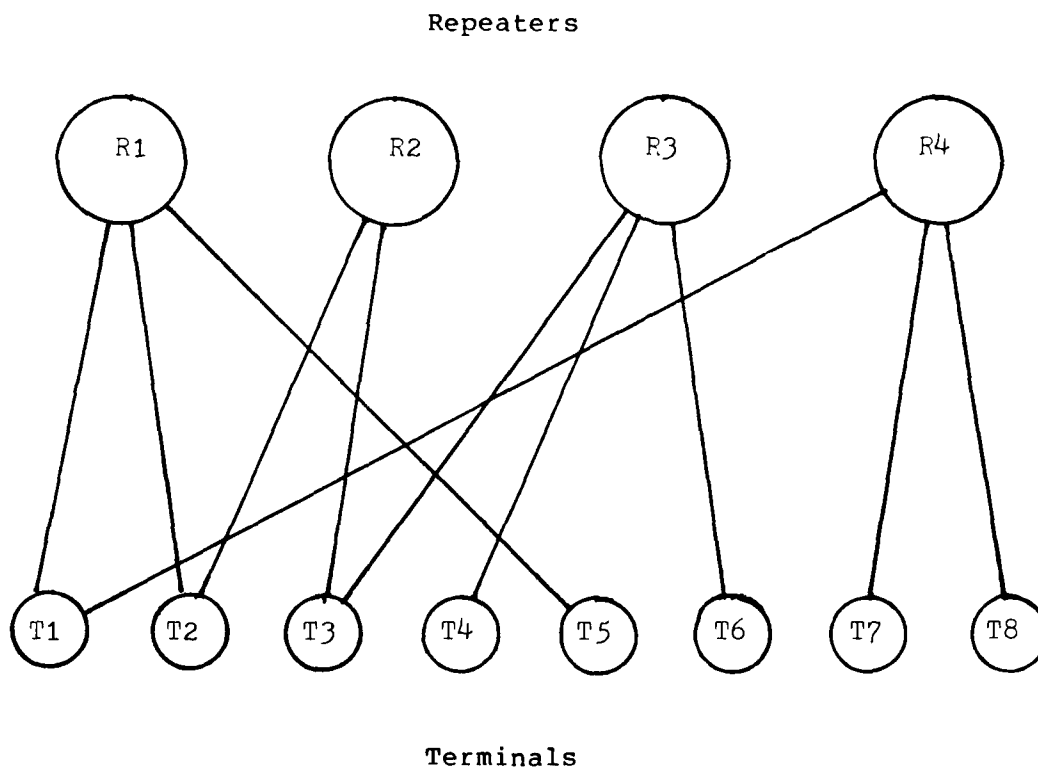


Figure 1.1: Schematic of Covering Problem

perform quite well (see Section 6).

Since, for example in the radio repeater application repeaters and terminals could number in the hundreds and, in PAVE MOVER the number of potential target sites ("terminals") could run in the thousands, heuristics are important in the applications considered here.

The novel aspect we consider is the extension of the simple set covering problem to the K-covering problem or more generally the K(I) covering problem in which it is required that each node I be covered by K(I) repeaters. Except for one set of theoretical studies [Fulkerson, 1962, pp. 89-90] [Ryser, 1963, p.77] of the "width" of 0-1 matrices and some preliminary work by Professor Roger Wets of the University of Kentucky and myself for the Network Analysis Corporation to apply to the DARPA Packet Radio Network in the early 70's [NAC, 1974] these problems have not been studied to my knowledge.

In Section II we give the objectives of our studies. The remainder of this report can be divided into two parts in the first part the mathematical properties of K-Cover problems are characterized, heuristic and exact algorithms for them described, and the formulation and results of tests of algorithm effectiveness reported (Sections III to X). In the second part the application of these techniques to radio repeater computations is described and a simplified case study of Air Force tactical radio communications in Central Europe is given (Section XI).

Finally, we close the report with recommendations (Section XII) for further activities in the study of covering problems, and more generally for the study of techniques for the design and analysis of communications systems based on new technologies such as satellites used in a random access mode, local area networks, and broadcast radio in which communications is broadcast rather than point-to-point.

II. Objectives of the Research Effort

The basic objective was to develop, evaluate, implement, and exercise optimization techniques for the assignment of covering entities to entities requiring coverage with particular emphasis on, and application to, tactical communication broadcast networks and radar surveillance.

III. Mathematical Models

Depending on the application different mathematical formulations of set covering problems are more useful. In this section we give these formulations and relate them

III.1 Simple Covering Problem

III.1.1 Set Theoretic Form

Given:

1. A finite set $T = \{t_1, t_2, \dots, t_M\}$
2. A family $R = \{R_1, R_2, \dots, R_N\}$

Find:

A subfamily $R^* \subseteq R$ with minimum cardinality that covers T :

i.e., Minimize $|R^*|$

Subject to $R^* \subseteq R$

and $\bigcup_{R_J \in R^*} R_J = T$

III.1.2 Matrix Form

Then given $A = \{A(I, J)\}$ where $A(I, J) = 1$ if $t_I \in R_J$ and 0 otherwise, we have:

Minimize $\sum X(J)$

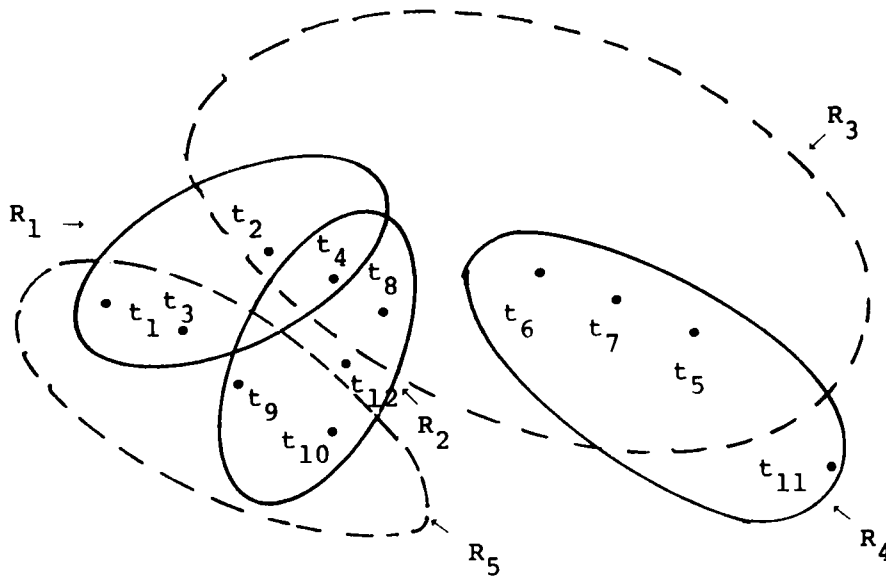
Such that $\sum_J A(I, J) X(J) \geq 1$

$X(J) \in \{0, 1\}$

III.1.3 Bipartite Graph Form

Consider two sets of nodes $R = \{r_1, r_2, \dots, r_N\}$ and $T = \{t_1, t_2, \dots, t_M\}$. Node r_J is connected to t_I with an edge if and only if $t_I \in R_J$.

Find the subset, R^* , of R with minimum cardinality such that every node in T is incident to at least one edge which is also incident to a node in R^* . Figure 3.1 illustrates the three formulations for a specific example.



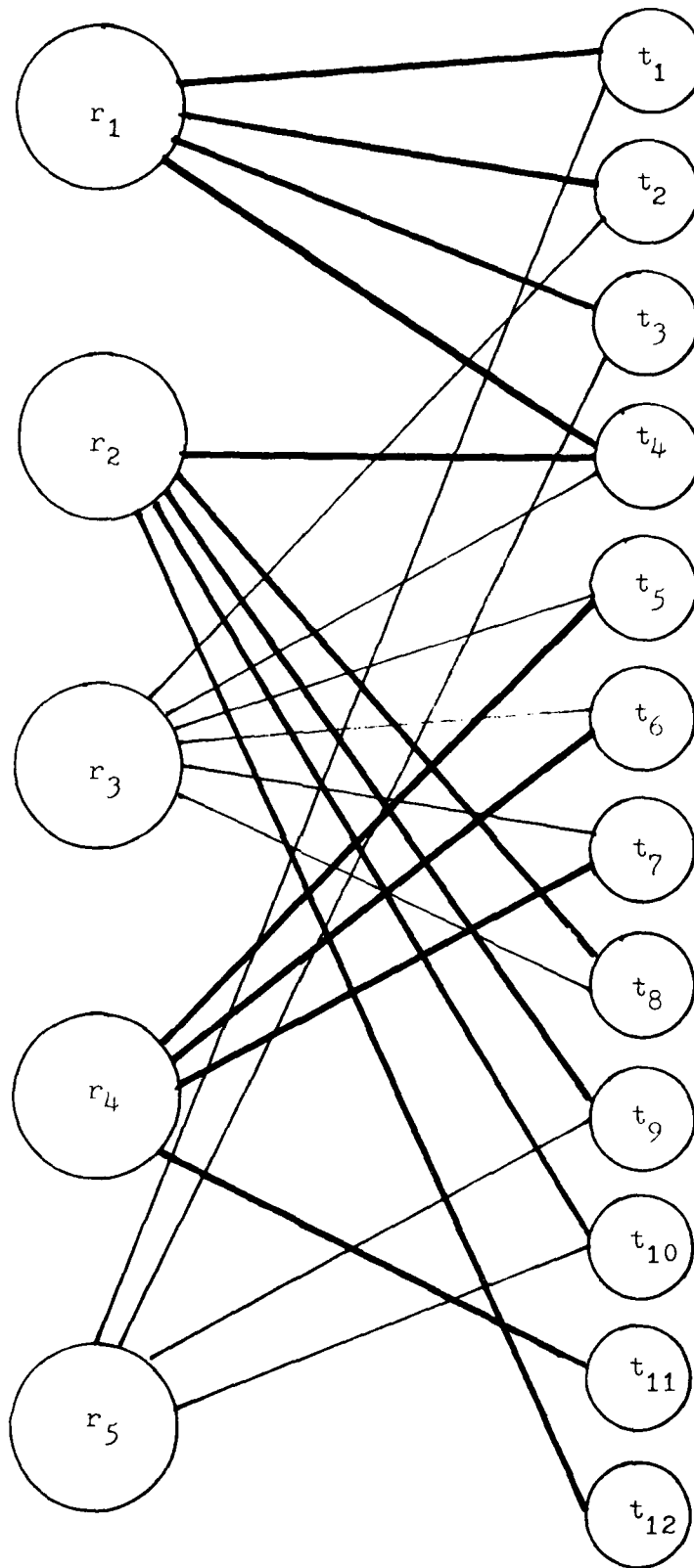
(a) Set Theoretic Formulation

$$\begin{array}{ll}
 \text{Minimize} & X(1) + X(2) + X(3) + X(4) + X(5) \\
 \text{Such that} & X(1) + X(5) \geq 1 \\
 & X(1) + X(3) \geq 1 \\
 & X(1) + X(5) \geq 1 \\
 & X(1) + X(2) + X(3) \geq 1 \\
 & X(3) + X(4) \geq 1 \\
 & X(3) + X(4) \geq 1 \\
 & X(3) + X(4) \geq 1 \\
 & X(2) + X(3) \geq 1 \\
 & X(2) + X(5) \geq 1 \\
 & X(2) + X(5) \geq 1 \\
 & X(4) \geq 1 \\
 & X(2) \geq 1
 \end{array}$$

$$X(j) \in \{0, 1\}$$

Optimal solution: $X(1)=X(2)=X(4)=1; X(3)=X(5)=0$

(b) Matrix Formulation



(c) Bipartite Graph Formulation

Figure 3.1: Representations of Simple Setcovering Problems

III.2 Weighted Covering Problem

III.2.1 Set Theoretic Form

Given:

1. A finite set $T = \{t_1, t_2, \dots, t_M\}$
2. A family $R = \{R_1, R_2, \dots, R_N\}$ of subsets of T
3. A cost c_J for each R_J in R

Find:

A subfamily $R^* \subseteq R$ with minimum cost

that covers T ;

i.e.,

$$\text{Minimize } \sum_{R_J \in R^*} c_J$$

III.2.2 Integer Programming Form

$$\text{Minimize } \sum c(J)X(J)$$

$$\text{Such that } \sum_J A(I, J)X(J) \geq 1 \quad I=1, \dots, M$$

$$X(J) \in \{0, 1\} \quad J=1, \dots, N$$

III.2.3 Bipartite Graph Form

Consider two sets of nodes $R = \{r_1, r_2, \dots, r_N\}$ and $T = \{t_1, t_2, \dots, t_M\}$ where the nodes in R have weights c_I for r_I . Node r_I is connected to t_J with an edge if and only if $t_J \in R_I$.

Find the subset R^* of R with minimum total weight

$\sum_{r_J \in R^*} c_J$ such that every node in T is incident to

at least one edge which is also incident to a node in R^* .

III.3 Simple $K(i)$ -Covering Problems

III.3.1 Set Theoretic Form

Given:

1. A finite set $T = \{t_1, t_2, \dots, t_M\}$
2. A family $R = \{R_1, R_2, \dots, R_N\}$ of subsets of T
3. A covering requirement $K(I)$ for the I th node of T

Find:

A subfamily $R^* \subseteq R$ of minimum cardinality such that each element t_I of T belongs to $K(I)$ members of R^* .

III.3.2

$$\begin{aligned} & \text{Minimize} && \sum J X(J) \\ & \text{Such that} && \sum A(I, J) X(J) \geq K(I) \quad I=1, \dots, M \\ & && J \\ & && X(J) \in \{0, 1\} \end{aligned}$$

III.3.3 Bipartite Form

Consider two sets of nodes $R = \{r_1, r_2, \dots, r_N\}$ and $T = \{t_1, t_2, \dots, t_M\}$ where r_I is connected to t_J by an edge if $t_J \in R_I$.

Find the subset R^* of R with minimum cardinality such that node t_I is incident to at least $K(I)$ edges which are also incident to nodes in R^* .

III.4 Weighted $K(I)$ -Covering Problems

The weighted covering problem and the $K(I)$ -covering problems can be combined in the obvious way.

IV. Relation of K(I)-Covering Problems to Other Problems

IV.1 Complexity

The simple covering problem is a special case of the K(I)-covering problem and the K(I)-covering problem is a special case of integer programming. The decision problems associated with both the simple covering problem and integer programming are NP complete [Garey and Johnson, 1979]; therefore the decision problem associated with the K(I)-covering problem is NP complete. Thus the K(I)-covering problem is in the same class of apparently intractible combinatorial problems as virtually every other interesting combinatorial optimization problem--at least as measured in the sense of worst case asymptotic running time.

IV.2 K(I)-Cover Problems are 1-Cover Problems

The K(I)-cover problems are related to the 1-cover problems even more directly. K(I)-cover problems can be solved as 1-cover problems. This result, due to Roger Wets, was reported without proof in [NAC,1974]. We give the following constructive proof.

Consider a weighted K(I)-cover problem in the bipartite form. The bipartite graph B is defined by a set of repeaters $\{R_1, \dots, R_N\}$ with weights $\{C(1), \dots, C(N)\}$, and a set of terminals $\{T_1, \dots, T_M\}$ with requirements $\{K(1), \dots, K(M)\}$. We seek to find a subset $R^* \subseteq R$ such that the weighted sum

$$\sum_{R \in R^*} C(R)$$

is minimized subject to the requirement that each node T_i be adjacent to at least $K(i)$ nodes of R^* .

Now consider a new set $T' = \bigcup_I T(I)$ where each individual

T_i in T is expanded into a set of nodes, $T(I)$ in T' .

Let $R(I) = \{R_j : (R_j, T_i) \text{ is an edge of the original graph}\}$. Now we let $T(I) = \{ \langle I, S \rangle : S \subseteq R(I) \text{ and } |S| = K(I) - 1 \}$; then

$$|T(I)| = \binom{|R(I)|}{K(I)-1}. \text{ We then have}$$

$$|T'| = \sum |T(I)| = \sum \binom{|R(I)|}{K(I)-1}$$

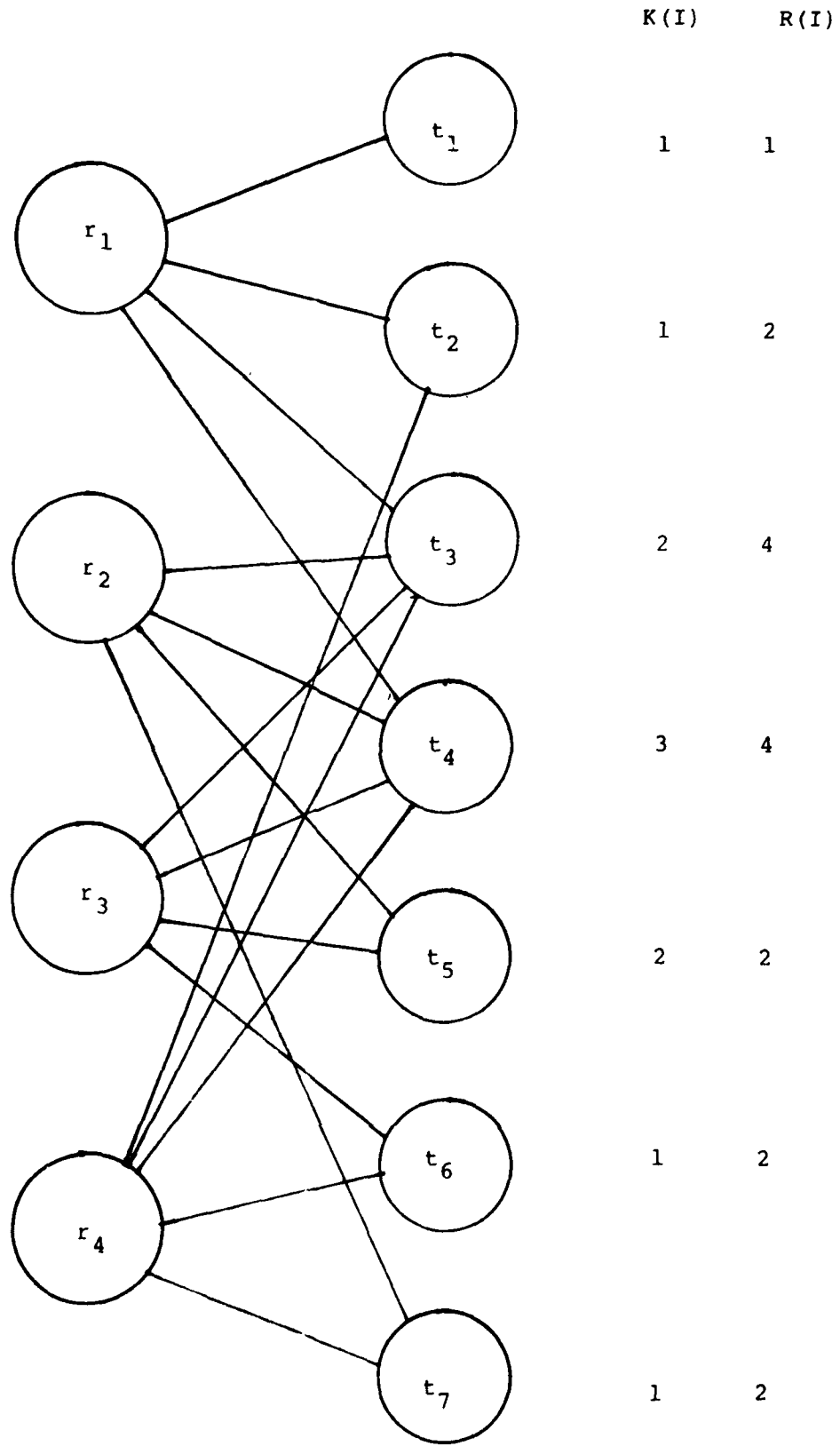


Figure 4.1(a): Mapping From K(I)-Cover to 1-Cover

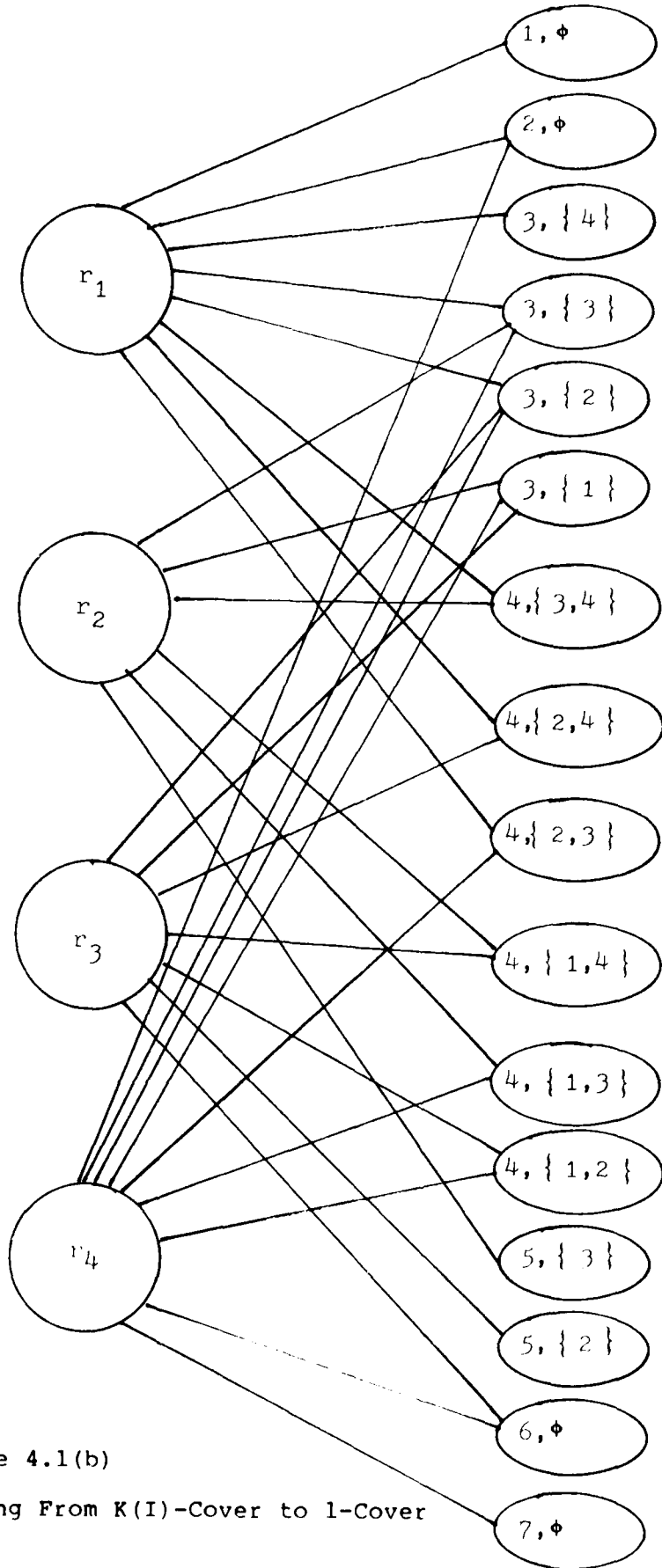


Figure 4.1(b)

Mapping From $K(I)$ -Cover to 1-Cover

The new bipartite graph B' has as its node sets R and T' . $(RJ, \langle I, S \rangle)$ is an edge of B' if (RJ, TI) is an edge in B and $RJ \notin S$.

We now show that R^* is an optimal weighted $K(I)$ -cover for the first problem if and only if R^* is an optimal weighted $(1-)$ cover for the second.

First suppose R^K is a $K(I)$ -cover for B . Now consider the node $\langle I, S \rangle$ in T' . $|R^K \cap R(I)| \geq K(I)$ since R^K satisfies the constraints. Hence, there exists $R \in (R^K \cap R(I)) - S$ since $|S| = K(I) - 1$. Then R is adjacent to $\langle I, S \rangle$ in B' since $R \notin S$. Hence any $K(I)$ cover for B leads to an one-cover for B' .

Now suppose R' is a one-cover for B' . Consider $TI \in T$. It corresponds to $T(I)$ in T' which consists of $\binom{|R(I)|}{K(I)-1}$ nodes of the form $\langle I, S \rangle$ with $S \subseteq R(I)$ and $|S| = K(I) - 1$. Let R^1 be any element of $R' \cap R(I)$. It is not adjacent to $\binom{|R(I)|-1}{K(I)-2}$ nodes corresponding to the sets S which contain R^1 . Of these $\binom{|R(I)|-2}{K(I)-3}$ are not adjacent to R^2 ,

where R^2 is a second element in $R' \cap R(I)$. Thus, in order to remove all the $\langle I, S \rangle$, we need $R^1, R^2, \dots, R^{K(I)}$. That is, I must be covered $K(I)$ times.

Therefore, there is a 1-1 correspondence between $K(I)$ covers in B and 1-covers in B' . Since the weighted sum is the same in each case, the two problems are theoretically equivalent. As we will soon see, they are not, however, computationally

IV.3 Differences

Consider the weighted covering problem in matrix form as defined in Section III.2. We can assume without loss of generality that the $c(J) > 0$ (For if $c(J) \leq 0$ we can simply set $x(J) = 1$ and solve the resulting reduced problem).

$$\text{Minimize } \sum c(J)X(J) \quad (1)$$

$$\text{Such That } \sum A(I, J)X(J) \geq 1 \quad (2)$$

$$X(J) \in \{0, 1\} \quad (3)$$

We can relax (3) to $X(J) \geq 0$, $X(J)$ integer since $X(J) > 1$ will not satisfy any more constraints than $X(J) = 1$ and will cost more. This is not the case for $K(I)$ -covering problems.

Further, if $A(I, J) \geq A(I, J')$ for $i = 1, \dots, M$ and $c(J) \leq c(J')$ then column J' can be ignored for the weighted covering problem but not for $K(I)$ -covering problems. However, we can require that $X(J) = 1$ before we need to consider $X(J')$.

Another difference shows up in the mathematical notation used to describe the problems. For weighted covers the set theoretic descriptions given in Sections III.1.1 and III.2.1 are particularly simple because we only require that the union of the sets chosen cover T . But for $K(I)$ -covers we cannot use the ordinary set union because the union operation results in only one copy of a $t \in T$ no matter how many times (> 0) it is covered.

V. Implicit Enumeration

In this section we review general implicit enumeration algorithms in order to define terms and to allow us to indicate the special characteristics of K-cover problems that we used.

Suppose we are minimizing an arbitrary function $f(x_1, x_2, \dots, x_n)$ of boolean variables $x_j \in \{0, 1\}$, $j=1, \dots, n$ subject to constraints $x \in X$. We will be interested in partial restrictions of f where some of the variables are fixed at value 1, others at value 0, and the remainder free to be 0 or 1. A partial restriction will be defined by $R = \langle S_0, S_1, S_f \rangle$ where S_0, S_1 , and S_f partition $\{1, \dots, n\}$ and $j \in S_0$ implies $x_j = 0$, $j \in S_1$ implies $x_j = 1$, and $j \in S_f$ indicates that we are free to choose x_j to be 0 or 1. A restriction $R = \langle S_0, S_1, S_f \rangle$ refines R' (or R' is a refinement of R) if $S_0' \supseteq S_0$, $S_1' \supseteq S_1$, and $S_f' \supseteq S_f$.

In general, implicit enumeration starts with an upper bound, \bar{z} , on the Minimum of $f(x)$ which may initially be $+\infty$ if no bound is immediately obvious. In other cases any 'feasible' solution (i.e., any $\bar{x} \in X$) given by a 'starting point function' can be used to give an upper bound. We also start with $S_0 = S_1 = \emptyset$, $S_f = \{1, \dots, n\}$. At the general step we have a collection, P , of partial restrictions. We choose one from P to be considered next using a 'restriction choice rule.' Initially, of course, we start with $P = \{R\}$ where R is the empty restriction $R = \langle \emptyset, \emptyset, \{1, \dots, n\} \rangle$. If P is empty we are done and \bar{z}, \bar{x} is the optimal solution.

We assume that we have a function $U(R)$ which gives an upper bound for the value of f for all $x \in X$ with $x_j = 0$ for $j \in S_0$, $x_j = 1$ for $j \in S_1$, and the remaining x_j at 0 or 1, as well as a boolean vector x which achieves the bound. If there exists no $x \in X$ satisfying S_0 and S_1 then $U(R)$ is set to $+\infty$.

We also assume we have available to us a function $L(R)$, of the restriction R which gives us a lower

bound for $x \in X$; $x_j = 0, j \in S_0$; $x_j = 1, j \in S_1$; $x_j = 0$ or $1, j \in S_f$. If there is no $x \in X$ satisfying S_0, S_1 , then we set $L(R) = +\infty$ and if there is no finite lower bound for f on X we set $L(R) = -\infty$.

At this point several cases may obtain:

1. If $L(R) \geq \bar{z}$ then we need consider R no more nor any of its refinements since the best that can be achieved is $L(R)$ and we already have \bar{z} in hand. In this case we say that R is 'fathomed.' This is particularly the case if R is infeasible and $L(R) = +\infty$.

2. If $L(R) < \bar{z}$ then we consider $U(R)$. If $U(R) < \bar{z}$ we replace \bar{x} by x^U obtained from $U(R)$. In either case we choose an index j' in S_f using a 'branching variable choice rule.' This gives rise to two new restrictions $R^0 = \langle S_0 \cup \{j'\}, S_1, S_f - \{j'\} \rangle$ and $R^1 = \langle S_0, S_1 \cup \{j'\}, S_f - \{j'\} \rangle$, which are added to P replacing the original restriction R . We then choose a new restriction from P and continue.

This is not the most general implicit enumeration framework but it will do for our purposes.

To summarize, in order to specify a particular implicit enumeration algorithm of this class we must specify:

- (i) a starting point function
- (ii) a restriction choice rule
- (iii) an upper bound function
- (iv) a lower bound function
- (v) a branching variable choice rule.

Let us start with the restriction choice rule. Throughout this report we assume a very particular rule. After considering a partial restriction, R , if it is not fathomed we will always consider next the refinement R' in which the variable chosen by the branching variable rule is fixed at one. If the

restriction R is fathomed we next consider the last variable fixed at one and fix it at zero. There are two reasons for this. First, the bookkeeping is considerably simplified for this rule. All that is needed is a stack of numbers n_1, n_2, \dots where each n_i is a variable index or the negative of one. Initially the stack is empty. Then the column rule is invoked to determine the next variable, j , to be branched on. Then $n_1=j$ is added to the stack. In general, suppose the stack is n_1, n_2, \dots, n_k for the restriction currently being considered; then $S_0 = \{-n_i : n_i < 0\}$ and $S_1 = \{n_i : n_i > 0\}$. If the current restriction is not fathomed then a new column j is determined by the column choice rule and j is 'pushed' onto the stack with $n_{k+1}=j$. If the restriction is fathomed, n_k is deleted ('popped') from the stack. If $n_k > 0$ then n_k is set to $-n_k$ and returned to the stack indicating that x_{n_k} is fixed at 0 instead of 1.

If $n_k < 0$ it is deleted and another element is popped from the stack. When the stack is empty the problem has been solved.

The second reason for the particular choice rule is that whenever a restriction is refined in a push operation another repeater is added. Thus, as soon as a restriction becomes feasible using S_1 as its repeaters all its refinements are feasible and the solution value can be no better. So any feasible restriction is fathomed and need not be considered further. This is not the case, for example, with arbitrary boolean optimizations but depends on the fact that f is monotone non-decreasing in x , and that $x \in X$ and $x \leq x'$ implies $x' \in X$. Let us call problems with these properties monotone. All the set-covering problems we defined in Section III are essentially monotone (for weighted problems if $c_j \leq 0$ the associated variable can immediately be set to 1 and the resulting reduced problem is monotone). Monotone

problems together with the restriction choice rule we use also have the property that if a restriction on the stack is infeasible we're done because the only way we can make the restriction feasible is to change at least one variable which is fixed at 0 to be 1. But all such restrictions have already been fathomed because we fix the variables at 1 first. Thus, the rule we describe is an end-order tree traversal [Knuth I, 1973] of the binary decision tree resulting from the boolean variables always being branched on by fixing the variables at one first.

The starting point function and the upper bound solutions are provided by heuristics which produce feasible solutions, if any exist, which are not necessarily optimal. The heuristic procedures for the two purposes do not necessarily need to be the same; in fact, our experiments indicate that different ones may be more effective (See Section VI). For the most part we considered 'myopic' heuristics. These heuristics pick one variable value at a time choosing the variable only on the basis of most improving the current situation with little or no consideration of the future implications of the choice. The criterion for measuring 'improvement' gives rise to different heuristics. Clearly one step of such heuristics can be used for the column choice rule. It is not immediately clear that improvement towards optimality is the most important factor in choosing the branching column, for it is most often the case that an optimal solution is found quickly and the major part of the work is in establishing the optimality. Thus, perhaps, the objective of the column choice should be to speed the proof process. Choice rules are described in Section VI.

The final ingredient that must be specified is the lower bound. This is often, and in this report exclusively, done by solving a relaxation of the given problem. If the problem is: Minimize $f(x)$ subject to $x \in X$, then a relaxation is Minimize $f'(x)$ subject to $x \in X'$ where f' and X' have the properties $X \subseteq X'$, and $f(x) \geq f'(x)$ for $x \in X$. Relaxations for coverings are discussed in detail in Section VII.

VI. Heuristics

VI.1 Introduction

Set covering problems are difficult. For example, they are known to be NP complete [Garey and Johnson, 1979]. Therefore, for practical applications, heuristics are strongly implied. Heuristics besides being of interest in their own right, perform important functions in exact implicit enumeration algorithms. They can be used to:

- (1) provide an initial solution
- (2) provide upper bounds on partial restrictions, and
- (3) be used in determining branching variables

(See Section V).

'Myopic' or 'greedy' heuristics which only look at immediate gains at each step have been studied in the 1-cover case. We review the results in Section VI.2. In 1974 Roger Wets and I studied heuristics for the K-covering problem. This work is extended in Section VI.3. Section VI.4 gives the results of computational experiments. Finally, in Section VI.5 a heuristic based on linear programming relaxations is described.

VI.2 One-Covering

Consider the simple one-covering problem in the set-theoretic formulation (See Section III.1). A simple recursive algorithm to estimate an optimal $J^* \subseteq \{1, \dots, n\}$ so that $\{R_j\}_{j \in J^*}$ is an optimal cover is:

1. Choose j_1 so that $|R_{j_1}|$ is a maximum for $j=1, \dots, n$.
2. Let $T^1 = T - \{R_{j_1}\}$ and $R^1 = \{R_j : j \neq j_1\}$.

Apply the above to the reduced problem defined by T^1, R^1 , etc. Break ties arbitrarily. This algorithm is called a 'greedy algorithm' because at each step the element j is chosen which, at that step, covers the most elements of T without considering how future choices will be affected.

D.S. Johnson [1974] and L. Lovasz [1975] have derived a bound for the performance of the greedy heuristic.

Theorem: ([Johnson, 1974], [Lovasz, 1975])

Let $z^* = |R^*|$ for the optimal cover R^* and let $z = |R^h|$ for a cover returned by the greedy heuristic. Then $z/z^* \leq (1 + 1/2 + 1/3 + \dots + 1/d) < 1 + \log d$ where $d = \max_i |J(i)|$ for $J(i) = \{j : i \in R_j\}$.

For repeater location problems in which the area covered increases with increases in the number of potential repeater sites and the number of terminals grows more or less proportionally we can expect d to increase relatively slowly with respect to the problem size. So while $\log d$ diverges in d , in many practical situations it grows rather slowly.

Chvatal [1979] obtained a similar result for greedy algorithms applied to the weighted one-covering problem. The greedy algorithm he considered is:

1. Choose j_1 so that $|R_{j_1}|/c_{j_1}$ is maximized (we assume $c_j > 0$; if $c_j \leq 0$ for any j we choose j immediately before beginning the heuristic).

2. Let $T^1 = T - \{R_{j_1}\}$ and $R^1 = \{R_j : j \neq j_1\}$.

The above is then applied to the problem defined by T^1 and R^1 to obtain j_2 , etc. When $T^1 = \emptyset$ we stop. Let c' be the total 'cost' resulting from an application of the heuristic and c^* be the optimal total cost, then we have:

Theorem: ([Chvatal, 1979])

$$c'/c \leq 1 + 1/2 + 1/3 + \dots + 1/d < 1 + \log d.$$

Notice that in the weighted 1-cover problem 'greed' is somewhat ambiguous because we want to do two things at once. We want to cover points of T and we want to minimize cost. As a greedy selector Chvatal's interest in a covering set R_j is measured by the ratio of the number of new points of T covered to the cost of the set. For the weighted $K(I)$ -covering problem we will be trading off three aspects: the cost of the covering set, the number of elements covered, and the size of the requirements for the points in T that are covered.

VI.3 $K(I)$ -Covering

Roger Wets and I addressed [NAC, 1974] the problem of repeater location for DARPA's Packet Radio System [Kahn et al, 1978]. The idea of using $K(I)$ -cover algorithms was introduced to help provide sufficient reliability of communication. Since the problems contemplated were large, heuristics were developed. The basic philosophy behind the heuristics was that terminals are critical if they are covered by few of the R_j relative to the requirement K_i and potential repeater sites were desirable if they cover many terminals. Consider the weighted $K(I)$ -cover problem in integer programming form:

$$\begin{array}{ll} \text{Minimize} & \sum C(J) X(J) \\ \\ \text{Such That} & \sum A(I, J) X(J) \geq K(I) \quad I=1, \dots, M \\ & X(J) \in \{0, 1\} \quad J=1, \dots, N \end{array}$$

The heuristics we define will all be of the same form. We choose a repeater R_J corresponding to $X(J)=1$. Then a new (smaller) weighted cover problem is obtained by removing column J and $X(J)$ from the problem and adjusting $K(I)$ to $\text{Max. } \{K(I)-A(I,J), 0\}$. The rule is then applied to the new problem to obtain a new J and the process is repeated.

Each rule is based on choosing the column J with the greatest weight where the weight for column J is a sum of row weights. Let $R(I)=\sum_J A(I,J)$, $R^*(I)=\sum_J A(I,J)-K(I)$.

Four weights introduced by Wets [NAC,1974] are:

$$W1(J) = \frac{1}{C(J)} \sum (K(I)/R^*(I)) A(I,J)$$

$$W2(J) = \frac{1}{C(J)} \sum (K(I)/R(I)) A(I,J)$$

$$W3(J) = \frac{1}{C(J)} \sum (1/R^*(I)) A(I,J)$$

$$W4(J) = \frac{1}{C(J)} \sum (1/R(I)) A(I,J)$$

Empirical studies were run on problems ranging from $M=5, N=5$ to $M=400, N=400$. Also an example was based on the area of a Packet Radio Test Bed in Palo Alto California with $N=42$ and $M=180$.

For this study we added a 'Bayesian' column choice rule given by

$$W5(J) = \frac{1}{C(J)} \prod \left(1 - \frac{R^*(I)}{R(I)} \right)$$

To motivate $W5$ suppose for each I we assume each of the $\binom{R(I)}{K(I)}$ possibilities are equally likely; i.e., that each $J \in R_I = \{J: A(I,J)=1\}$ has 'probability' $K(I)/R(I)$ of being 1. If we assume all the 'events' are independent

we get the probability of J being chosen as the expression in brackets for $W5(J)$. For purposes of comparison we also tested $W6$ given by:

$$W6(J) = \sum_I A(I, J)$$

which corresponds to the greedy algorithm for the one-cover problem (see Section VI.2).

VI.4 Computational Experiments

A number of experiments were conducted to compare the performance of the six heuristics defined in Section VI.3.

In the first series each of the six heuristics were applied to the same sequence of 50 randomly generated problems using the geometric test problem generator RNDMAG (See Section IX). All the problems had 25 columns and 25 rows. The experiments were run with covering factors of $K=2$ and $K=5$. The problems were also solved exactly by implicit enumeration using each heuristic for the initial solution, for upperbounds, and for the column choice rule (see Section V). Two figures of merit were considered: (1) The fraction of the 50 problems for which the heuristic gave the optimal solution and (2) the average number of fathoms in the implicit enumeration procedure when using the heuristic. Table 6.1 gives the results. The second series of runs was to apply the six heuristics to 50 randomly generated test problems using the test problem generator RNDMA (see Section IX). These problems had 50 columns and rows with density $1/3$. Coverage requirements of $K=2$ and $K=5$ were considered. The results of these runs are summarized in Table 6.2.

In the third series, 100 problems, each with 50 rows and 50 columns were generated by RNDMAG. These problems were then solved by each of the six heuristics. The results are summarized in Table 6.3. Since exact computation is prohibitively expensive the 'correct solution' is actually the best of the six solutions produced by the heuristics.

Table 6.1

Heuristics Performance on 50 "Geometrically" Random 25 x 25 Problems

Heuristic	% Correct	K=2	K=5
		Average No. of Attempted Fathoms	Average No. of Attempted Fathoms
1.	86	62.84	98
2.	84	74.00	94
3.	84	58.96	94
4.	80	79.32	92
5.	84	68.12	94
6.	60	111.20	82

Table 6.2

Heuristic Performance on 50 Random 20 x 20 Problems

Heuristic	% Correct	K=2	K=5
		Average No. of Attempted Fathoms	Average No. of Attempted Fathoms
1.	76	49.80	92
2.	74	57.26	88
3.	64	48.52	90
4.	64	59.04	90
5.	76	52.32	90
6.	48	76.48	90

Table 6.3

Heuristic Performance on 100 "Geometrically" Random 50 x 50 Problems

Heuristic	K=2		K=5	
	% "Correct"	% off by > 1	% "Correct"	% off by >1
1.	86	0	87	0
2.	82	0	75	0
3.	68	3	38	14
4.	70	4	21	27
5.	83	0	74	0
6.	54	4	22	34

Table 6.4

100 50 x 50 Random Problems

Heuristic	K=2		K=5	
	% "Correct"	% off by > 1	% "Correct"	% off by >1
1.	95	0	96	0
2.	92	0	84	1
3.	73	0	36	9
4.	70	2	24	32
5.	94	0	90	1
6.	63	5	20	30

Table 6.5

50

100 x 100 Random Problems

Heuristic	K=2		K=5	
	% "Correct"	% off by > 1	% "Correct"	% off by >1
1.	100	0	88	0
2.	98	0	92	0
3.	68	2	22	30
4.	68	4	18	42
5.	100	0	90	0
6.	100	0	20	36

Besides calculating the percentage of 'correct solutions' for each heuristic the percentage of time each heuristic differs by more than one from the best observed solution was also tabulated.

Finally, Tables 6.4 and 6.5 give results for 100 problems of size 50 by 50, and 50 problems of size 100 by 100 generated by RNDMA with density $1/3$ in all cases.

From these experiments we observe that Heuristic 1 almost universally does best (the one exception is size 100 problems with $K=5$ generated by RNDMA) followed closely by Heuristics 2 and 5. The remaining heuristics performed substantially worse. The differences between the best three heuristics and the worst three grow more pronounced as the problems get larger. These observations hold for both the geometrically random and the random 0-1 problems.

Surprising, however, is the fact that Heuristic 3 performs best in all cases as part of the implicit enumeration algorithm. Heuristics can be used in three ways in implicit enumeration algorithms: (i) as an initial solution, (ii) as an upperbound on partial restrictions, and (iii) to choose branching variables. Since Heuristics 1, 2, and 5 seem to give better solutions, these results seem to indicate that Heuristic 3 performs best when used as a branching variable decision rule.

VI.5 Lower Bounds

The heuristics defined in Sections VI.2 and VI.3 give upper bounds on the number of repeaters and the sum of weights respectively for the simple and weighted covering problems. It is useful to have a lower bound also, especially for use in implicit enumeration algorithms. A simple bound is to relax the integer programming form of the covering

problem to a linear programm. The relaxation of the weighted K-cover problem is :

$$\text{Minimize } \sum C(J)X(J)$$

$$\text{Such That } \sum A(I,J)X(J) \geq K(I) \quad I=1, \dots, M$$

$$0 \leq X(J) \leq 1 \quad J=1, \dots, N$$

This provides a lower bound for the weighted K(I) cover problem. This lower bound was obtained by relaxing the constraint X(J) be 0 or 1 to $0 \leq X(J) \leq 1$. In fact, the result of Lovasz [1975] on the greedy heuristic is that $z/z^L \leq (1+1/2+1/3+\dots+1/d) < 1 + \log d$ where z^L is the solution to the linear programming relaxation. This result is stronger than the result given in Section VI.2.

Heuristics to generate good feasible solutions can be based on the linear programming relaxation plus the heuristics described in Section VI.3. First, the linear programming relaxation is solved. For variables in the relaxation which are at the lower bound 0 the corresponding problem in the original problem is also set to 0. For variables in the linear programming relaxation which are at upper bound 1 the corresponding variables in the original covering problem is set to 1. The problem is then reduced by removing all the variables assigned in this way and appropriately adjusting the K(I). Then one of the previous heuristics is applied to the remaining reduced problem.

Toregas et al [1971] found that if the objective function, z^L , for the linear programming relaxation of the simple set-covering problem is not integer then adding the constraint $\sum X(J) \geq [z^L]$ where $[z^L]$ is the least integer greater or equal to z^L resulted in an all integer solution in all cases they studied (see also Section VII). With this approach, no heuristics are needed to assign values to variables which were fractional in the LP solution.

VII. Relaxations

Consider a generalized optimization problem of minimizing a function $f(x)$ over all x belonging to a constraint set X . If $f'(x) \leq f(x)$ for all $x \in X$ and $X' \subset X$ then the problem of minimizing $f'(x)$ subject to $x \in X'$ is called a relaxation of the first problem. Relaxations are of interest for two reasons which are summarized in the following theorems.

Theorem 7.1: If x' solves the relaxed problem then the $f'(x') \leq f(x)$ for any $x \in X$.

That is, a solution to the relaxed problem is a lower bound to feasible solutions to the original.

Theorem 7.2: If x' solves the relaxed problem (i) $x' \in X$, and (ii) $f'(x') = f(x')$ then x' solves the original problem.

The proofs of these results are trivial.

For the $K(I)$ -cover problem we will consider relaxations which only relax the constraints; i.e., $f=f'$. We will consider four types of relaxations:

1. linear programming relaxations
2. constraints subset relaxations
3. constraint sums relaxations, and
4. 0-1 matrix relaxations.

We consider the $K(I)$ -cover problem in matrix form.

$$\text{Minimize} \quad \sum_J X(J) \quad (1)$$

J

$$\text{Such That} \quad \sum_J A(I,J) X(J) \geq K(I) \quad I=1, \dots, M \quad (2)$$

J

$$X(J) \in \{0, 1\} \quad J=1, \dots, N \quad (3)$$

VII.1 Linear Programming (LP) Relaxations

The LP relaxation is obtained by relaxing constraint (3) to allow fractional values of $X(J)$ besides the values 0 and 1. Then the problem becomes:

$$\text{Minimize} \quad \sum_{J} X(J) \quad (1)$$

$$\text{Such That} \quad \sum_{J} A(I,J) X(J) \geq K(I) \quad I=1, \dots, M \quad (2)$$

$$0 \leq X(J) \leq 1 \quad J=1, \dots, N \quad (4)$$

which is a linear program.

Upon solving the LP relaxation to obtain $X^*(J)$ $J=1, \dots, N$ using a method such as the simplex method we can have one of three results:

Case 1: All the $X^*(J)$ are 0 or 1. In this case, X^* solves the original problem by Theorem 7.2.

Case 2: Some of the $X^*(J)$ are fractional and $\sum X^*(J)$ is non-integer. In this case, we can add the constraint

$$\sum X(J) \leq [z^*] \quad (5)$$

where $[z^*]$ is the least integer greater or equal to z^* . Then the LP (1), (2), (3), (4), and (5) can be solved. For ordinary set-covering problems ($K(I)=1$ $I=1, \dots, M$) good results have been reported by [Toregas et al, 1971]. In almost all cases, the addition of the constraint (5) was sufficient for an all integer solution.

Case 3: Some of the $X^*(J)$ are fractional $\sum X^*(J)$ is integer, then all we can say is that $\sum X^*(J)$ is a lower bound for feasible solutions of the original problem.

By the duality theory of linear programming weights $\pi(I)$ for the M constraints of (2) and $\sigma(J)$ for the N upper bound constraints of (4) can be found which satisfy:

$$\sum_I \pi(I)A(I,J) - \sigma(J) \leq 1 \quad J=1, \dots, N \quad (6)$$

$$\pi(I) \geq 0 \quad I=1, \dots, M \quad (7)$$

$$\sigma(J) \geq 0 \quad J=1, \dots, M \quad (8)$$

$$\text{and which maximize } w = \sum \pi(I)K(I) - \sum \sigma(J) \quad (9)$$

subject to (6), (7), and (8).

VII.2 Constraints Subset Relaxations

A relaxation of (1), (2), and (3) can be obtained quite simply by considering a subset of the rows of (2). Because, in general, computation required in solving a $K(I)$ -covering problem increases much more than linearly with the number of constraints, one can solve many more than r problems with $1/r$ th of the constraints of (2). In many practical problems many of the terminals T_I $I=1, \dots, M$ are irrelevant in determining an optimal solution and relatively few are critical (e.g., when $K(I)$ is large compared to $\sum A(I,J)$). The problem, of course, is to determine which subset of the constraints to use. Artificial examples can be constructed in which all the constraints must be used. Consider a circle of unit diameter with an even number of points (>2) located at equi-spaced intervals around its circumference. The covers ($M=N$) are located at the same points. One point can cover another if they are strictly less than one unit apart. With all points (constraints) considered two covering points are required. If any point is not considered one point can cover all the others. This relaxation and the above example were proposed by Handler [Handler and Mirchandani, 1979, p. 133 and p. 146].

Trivial subcases of this relaxation occur when a row I has exactly $K(I)$ values of J for which $A(I,J)=1$. Then all the covers J for which $A(I,J)=1$ must be chosen and the problem can be reduced accordingly. Similarly, if $A(I,J)$ is one for all J in some row I the constraint I can be ignored.

VII.3 Constraints Sums Relaxations

For any $\pi(I) \geq 0$ $I=1, \dots, M$ we can replace (2) by a weighted sum of its constraints and obtain a relaxation. That is, we consider the relaxation:

$$s(\pi) = \text{Minimum } s = \sum X(J)$$

$$\text{Such That } \sum_{J \text{ I}} (\sum \pi(I) A(I,J)) X(J) \geq \sum_I \pi(I) K(I) \quad (10)$$

$$X(J) \in \{0, 1\} \quad (3)$$

This relaxation is trivially solved. Let $D(J) = \sum_I \pi(I) A(I,J)$

and $D(J_1), D(J_2), \dots, D(J_N)$ be the $D(J)$'s sorted in decreasing order. Then we can determine the optimal value $s(\pi)$ of s by the following simple algorithm.

- Step 0: $s := 0$
Sort the $D(J)$ in decreasing order
 $D(J_1) \geq D(J_2) \geq \dots \geq D(J_N)$
 $I := 1$, and $K := \sum_I \pi(I) K(I)$
- Step 1: If $K \leq 0$ stop. Current value of s is optimal.
Otherwise go to Step 2.
- Step 2: $s := s+1$, $K := K - D(J_I)$, $I := I+1$
Go to Step 1

The most straight forward relaxations of this type are the ones corresponding to $\pi(I) \in \{0,1\}$. That is, 'surrogate' constraints obtained simply by adding together a subset of the original constraints. Another fruitful source of particularly good multipliers are the dual variables of the LP relaxation [Garfinkel and Nemhauser, 1972, Section 4.7].

VII.4 0-1 Matrix Relaxations

This relaxation is motivated by the work on 0-1 matrices by Fulkerson [Ford and Fulkerson, 1962] and Ryser [1963]. Consider the simple $K(I)$ -cover problem in matrix form. It basically requires us to pick a subset of minimum cardinality from the columns of a given 0-1 matrix so that the sum of row I for these columns is at least $K(I)$. The relaxation that we consider is to allow all 0-1 matrices with the given row and column sums and pick the matrix which gives us the least number of required columns. This relaxation is at least as strong as the sum of rows relaxations and can be stronger.

Before we describe the construction of the relaxation we must introduce the notion of a conjugate sequence. Let $S(J) \ J=1, \dots, N$ be a sequence of positive integers. The conjugate sequence $S^*(I) \ I=1, \dots, M$ is given by $S^*(I) = |\{J: S(J) \geq I\}|$. Pictorially, the conjugate sequence can be represented by the row sums of the matrix in which the J th column has ones in rows 1 to $S(J)$ and 0's elsewhere for $J=1, \dots, N$. We now state a theorem of Gale, Ryser, and Fulkerson [Ford and Fulkerson, 1962, p. 81] transposed and put in our notation.

Theorem: Let $S(J) \ J=1, \dots, N; K(I) \ I=1, \dots, M;$ be two sets of non-negative integers where $K(1) \geq K(2) \geq \dots \geq K(M)$. Then there is an M by N 0-1 matrix satisfying

$\sum_{A(I,J)} \leq S(J) \quad J=1, \dots, N$ and

I

$\sum_{A(I,J)} \geq K(I) \quad I=1, \dots, M$

J

if and only if

I

I

$\sum_{K(II)} \leq \sum S^*(II) \quad I=1, \dots, M.$

l

l

Before we describe the relaxation let us consider some examples.

Consider the case with $M=6, N=6, S=(3,3,3,3,3,3),$

$K=(6,1,1,1,1,1).$ In this case the minimum number of columns

required, L^* , is 6 and all columns must be chosen in order

to cover the row with largest requirement ($K(1)=6$). Note that

$6 \times 3 = 18$ ones are used while only $11=6+1+1+1+1+1$ are needed.

As a second example consider $S=(3,3,3,3,3,3),$ and

$K=(2,2,2,2,2,1).$ In this case $L^*=4$ which can be recognized by

by the fact that $11=\sum K(I)$ ones are needed and it takes at least

4 columns to provide them. This is simply the constraints sum

bound described in Section VII.3. But there are intermediate

cases. Consider $M=3, N=4$ with $S=(3,3,1,1)$ and $K=(3,3,1).$ $K(1) = 3$

implies $L^* \geq 3,$ and $\sum K(I) = 7$ also implies $L^* \geq 3.$ However,

$L^*=4$ is, in fact, required which can be recognized by using

the theorem.

We now turn to an algorithm for computing L^* with given row and column sums.

I

Step 0: Compute $KS(I) = \sum K(II)$

l

$S^*(I) = |\{J: S(J) \geq I\}|$

$I := 1, L = KS(I), TEST = L$

Step 1: $I := I + 1$

If $I > M$ terminate L is the solution

$TEST := TEST + \min \{S^*(I), L\}$

Step 2: If $TEST < KS(I)$ go to Step 3
Else go to Step 1

Step 3: $L := L+1$, $TEST = TEST + \text{Min} \{S^*(L), I\}$
Go to Step 2

Discussion:

The test in Step 2 checks the necessary and sufficient condition in the theorem for I when using only the L largest columns. If the test fails that means we need more columns. They are added in Step 3.

We have not shown that the matrix generated to satisfy the requirements $K(I)$ can be extended to satisfy the current row sums $R(I)$ of the original matrix but we conjecture that in fact we can.

Example:

Consider $M=6$, $N=10$, $S=(6,6,1,1,1,1,1,1,1,1)$,
 $K=(8,3,3,2,1,1)$. Then $KS=(8,11,14,16,17,18)$,
 $S^*=(10,2,2,2,2,2)$.

$I=1$ $L=8$, $TEST=8$

$I=2$ $TEST=8+\text{Min}(2,8) = 10$
 $TEST=10 < KS(2)=11$
 $L=9$, $TEST=TEST + \text{Min}(1,2) = 11$
 $TEST=11 \geq KS(2) = 11$

$I=3$ $TEST=11 + \text{Min}(2,9) = 13$
 $TEST=13 < KS(3)=14$
 $L=10$
 $TEST=TEST + \text{Min}(1,3) = 14$
 $TEST=14 \geq KS(3) = 14$

I=4 TEST=14 + Min (2,10) = 16
 TEST=16 \geq KS(4) = 16

 I=5 TEST=16 + Min (2,10) = 18
 TEST=18 \geq KS(5) = 17

 I=6 TEST=18 + Min (2,10) = 20
 TEST=20 \geq K(6) = 18
 Terminate L*=10.

VII.5 Experiments

Since there was no convenient linear programming subroutine available on the computer facilities used for this study, no LP relaxations were implemented. Two relaxation routines were coded. In the first relaxation routine two estimates were made and the best of them was used. First, the equation with the largest residual requirement was considered, and since at least a number of repeaters equal to the largest residual requirement must be chosen that gives a lower bound. The other lower bound was to use the 'surrogate' constraint (Section VII.3) with (I)=1 for all I.

The second relaxation routine implemented the 0-1 matrix relaxation described in Section VII.4. Using the random 0-1 matrix generator RNDMA 100 20 by 20 problems with K=5 and density of 1/3 were run; 100 6 by 12 problems with K=4 and density .6 were run; and 4 problems of size 50 by 25 with K=12 and density .5 were run. One of the latter ran for 1,287 fathoms. Using the geometric test problem generator RNDMAG 100 25 by 25 problems with K=5 were run. In not one of these cases did the relaxation described in Section VII.4 provide any improvement over the first relaxation. This is startling since very easy examples can be constructed for which the second relaxation provides improvements. The

example given in Section VII.4 is one such. Nevertheless, literally thousands of problems arising from randomly generated test problems and the implicit enumeration applied to them did not give rise to one such case. This is a very intriguing point worth further investigation.

VIII. Branching Rules

As discussed in Section V the branching rule is used to determine which variable to fix at value 1 in order to refine a partial restriction. As was also pointed out any of the 'myopic' heuristics discussed in Section VI can be modified for use as column choice rules. However, recognizing that much of the work in implicit enumeration is spent in verifying the optimality of an optimal solution rather than initially finding it, we investigated choice rules to try to speed the validation process. Empirical results were not too encouraging however.

VIII.1 The Entropy Rule

It seems reasonable that we would like to pick a column to branch on that most reduces ones uncertainty as to what column to pick. For row I, if K(I) is the current requirement and R(I) is the number of ones in row I corresponding to free variables, there are $\binom{R(I)}{K(I)}$ ways the constraint can be satisfied. We then consider as a reasonable way to pick the column to branch on as:

$$\text{Max } \sum_J A(I,J) \binom{R(I)}{K(I)}.$$

In other words we try to pick the column which is associated with the most uncertainty. Another approach is to weight each row by the number of possibilities to be guaranteed to be reduced. That is, if we fix a column J to be 'in' (X(J)=1) the new number of possibilities is $\binom{R(I)-1}{K(I)-1}$ and $\binom{R(I)-1}{K(I)}$ if J is excluded (X(J)=0). We then define W(I) by:

$$W(I) = \text{Min.} \left[\binom{R(I)-1}{K(I)-1}, \binom{R(I)-1}{K(I)} \right]$$

and choose J to maximize $\sum_I A(I,J)W(I)$.

Note: $\binom{R(I)}{K(I)}$ by the principle of inclusion/exclusion is

$$\binom{R(I)-1}{K(I)-1} + \binom{R(I)-1}{K(I)}.$$

Thus, if we take a Bayesian point of view that $x(J) = 0$ or 1 is equally likely then:

$$\frac{1}{2} \binom{R(I)}{K(I)}$$

can be looked at as the average of $\binom{R(I)-1}{K(I)}$ and $\binom{R(I)-1}{K(I)-1}$.

So we let $W(I) = \binom{R(I)}{K(I)}$ in our experiments.

VIII.2 Results of Experiments

The entropy rule described above was tested against branching rules based on the 'myopic' heuristics described in Section VI. For comparison purposes a random choice rule was also tested. Random problems were generated using the two test problem generators described in Section IX. The entropy choice rule performed quite poorly. It did worse than all the heuristics and only outperformed the random choice rule.

IX. Test Problem Generators

In order to test the set covering algorithms and their variants in an unbiased and systematic way two test problem generators were constructed. The first, RNDMA, constructs random 0-1 matrices where each matrix element has the same probability of being a 0 or 1 (with one exception which will be described later). While this is the most obvious approach to generating problems it can be quite misleading if the application does not give rise to the same distribution of problems. In particular, problems such as repeater location problems and the PAVE MOVER radar problem which arise in a geometric context can have a quite different distribution of problem instances which in turn may dramatically effect the average performance of algorithms. To avoid this problem, a second geometric random problem generator, RNDMAG, was constructed.

IX.1 RDNMA

The input to this test problem generator is N , the number of potential repeater locations; M , the number of terminals; FE , the density of ones in the constraint matrix; and $K(I)$, $I=1\dots,M$, the coverage requirement for terminal I . The test problem generator first computes the number of ones, NE , as $FE * M * N$ (rounded down) and checks to make sure that there are matrices of the type required; i.e., that $NE \geq \sum K(I)$. Feasibility is guaranteed by first assigning $K(I)$ ones to row I at random. The remaining $NE - \sum K(I)$ ones are then assigned at random to the matrix locations that do not already have ones. If all the $K(I)$ are the same then each location in the matrix has the same probability of being assigned a one if the $K(I)$ are different the rows with the larger $K(I)$ have higher probabilities for containing ones. The selection sampling technique described in [Knuth II, 1969, Algorithm S, Section 3.4.2] is used in both cases. The output is a data file for use by the set covering algorithms.

IX.2 RNDMAG

The geometric test problem generator takes as input the number of potential repeater sites, N . It assumes that the terminal sites and the potential repeater sites are the same ($M=N$). It also takes as input $K(I)$ the requirement at each terminal site I , $I=1, \dots, N$. N random points are chosen in the unit square. The shortest radius R is determined by the program so that each terminal I is within R of $K(I)$ of the terminals. That is, the smallest radius is chosen which still is feasible with respect to the requirements $K(I)$. Then location I is said to cover all points at a distance R or less from I (excluding I). Note that at least one terminal I (row of the A matrix) has exactly $K(I)$ potential covers so that all of these must be chosen.

X. Software Implementation

X.1 Program Description

An experimental program implementing the K(I)-Cover algorithms was coded in Fortran IV and runs on both DEC PDP11-70 and DEC-10 computers. It was constructed modularly so the various options for relaxations and heuristics could be tested. The two random problem generators described in Section IX were also constructed. The resulting program is less than optimally efficient for two reasons. The first is that in order to be an effective test bed for algorithmic alternatives the program was broken into a number of subprograms and the information passed was of necessity the union of the requirements for all the options. Also extensive but computationally expensive debugging and statistics collection code was included. However, a more drastic inefficiency was the result of the data structure used for the algorithms. For ease of implementation the constraint matrix $A = \{A(I,J)\}$ was stored explicitly in MXN storage locations. This was both extravagant of space and computationally expensive, especially for sparse matrices. The only two operations used on the matrices are (1) examining the rows I for a given column J for which $A(I,J) = 1$ and (2) examining the columns I for a given row I such that $A(I,J) = 1$. Moreover the $A(I,J)$'s are fixed data and are not modified during the solution process. This suggests the following data structure which will be used in the next version of the program. In successive memory locations $D(L)$, $L=1, \dots, NE$ (where NE is the number of non-zero elements) the rows in which $A(I,J) = 1$ will be listed for $J = 1, 2, \dots, N$. A pointer $PJ(J)$ will point to the last entry for column J . Thus to scan the rows for which $A(I,J) = 1$, one need only read the entries in D from $L = PJ(J-1) + 1$ to $PJ(J)$. The rows of A will be kept in a list structure. That is, we let $H(I)$ be the header of a list containing all the column numbers

corresponding to non-zero elements in the Ith row of A. If the matrix is sparse:

$NE + N + M + 2NE \leq M \times N$ or equivalently $NE \leq (M \times N - N - M)/3$ (assuming each data element takes the same space) memory is saved and in any case computation saved as we explore in the next subsection. But first an example.

EXAMPLE:

Consider A given by:

$$A = \begin{pmatrix} 0 & 0 & 0 & 1 \\ 1 & 1 & 0 & 0 \\ 0 & 1 & 1 & 0 \end{pmatrix}$$

Then $M=3$, $N=4$, $NE=5$.

$D=(2,2,3,3,1)$, $PJ=(1,3,4,5)$

The list structure for the row elements is given by:

H(1) → 4
H(2) → 1 2
H(3) → 2 3

X.2 Computational Complexity

X.2.1 Heuristics

All the greedy heuristics described in Section VI have the same asymptotic order of complexity.

The first step is to compute the row sums $R(I)$. This has complexity of order NE .

Then each time we need to choose a column we must first compute the row weights, which given the $R(I)$ is of order 1.

Then for each column J the weights are summed for rows I such that $A(I,J) = 1$. For all the rows each non-zero element appears in a sum. Thus, the order of this part is also NE . Then, the $R(I)$'s must be adjusted which takes work of the order $NE(J^*)$ where J^* is the chosen column and $NE(J^*)$ is the number of non-zero elements in column J^* . An upper bound on all this is order $NE \times Z$ where Z is the number of columns chosen by the heuristic. This in turn is of less order than $NE \times N$. When A is stored explicitly all NE 's become $M \times N$ so that the order is dominated by $M \times N \times N$.

X.2.2 Relaxation

The three relaxations described in Sections VII.2, and VII.3 were implemented. The first was based on the observation that if $K(I^*)$ is the largest residual requirement then $Z \times K(I^*)$ is necessary. Finding $K(I^*)$ is order M . The second relaxation consists of considering the constraint obtained by summing all the constraints of the original problem. Obtaining the coefficients in the sum constraint takes order NE . Solving the constraint requires order $Z \log N$ plus order N arising from a partial sort (using, for example, Heapsort [Knuth III, 1973, Sect. 5.2]) of the coefficients of the sum constraint to find the smallest Z so that the Z largest coefficients of the sum constraint are more than the sum of the residual requirements. That is, Z is the upper bound given by the relaxation. Since we don't know Z a priori we can bound the work by order $NE + order N \log N$.

The final relaxation that was implemented was the 0-1 matrix relaxation described in Section VII.4. The computations needed in this case are: (i) sort the residual requirements $K(I)$ which takes order $M \log M$, (ii) compute the column sums $S(J)$ which takes work of order N since $S(J) = PJ(J) - PJ(J-1)$, (iii) compute the conjugate sequence $SC(I)$. The last computation can be carried out by first sorting the

$S(J)$. However, a more efficient method is to use Heapsort to partially sort the $S(J)$ starting with the largest and only compute the $SJ(I)$ which are needed, of which there are at most z , the bound calculated by the relaxation. The work required is order $Z \log N$ plus order N to form the heap. The actual calculations implied by Steps 1 to 3 in Section 7.4 can be done in order $\text{Max}(M, Z)$. The total work is then dominated by order $\text{Max}(M \log M, Z \log N)$ which is in turn bounded by order $\text{Max}(M \log M, N \log N)$.

XI. Air Force Tactical Radio in West Germany

A simplified West Germany Tactical Radio network analysis was performed to illustrate the use of the covering models described in Sections III to X. Because a number of strongly simplifying assumptions were made the results should be considered as indicative rather than conclusive. However, the analysis does clearly show the role that covering analysis can play in a careful and detailed design. Among the simplifications was choosing as a propagation model one that depends purely on distance. Conceptually there is no problem with including more accurate propagation models including factors such as topography, terrain, frequency dependencies, antenna height and placement, antenna orientation with respect to the FEBA, and jamming; however, the practical difficulties precluded the use of a more sophisticated model in the time available. The nodes in the tactical communication network were obtained from a MITRE report [Brown et al, 1979] which was in turn based on projections by [USAFE, 1978]. The MITRE study was designed to investigate the vulnerability of communications using the AN/TRC-170 tropospheric scatter radio terminal family. Since this is only a projected network one cannot be overly confident of results based on this choice of network locations. Moreover, in order to reduce the vulnerability of ground-to-ground communications it seems desirable to disperse the tactical communications functions into a highly-distributed network in order to decrease the dependence on critical nodes and paths. To the extent that this is carried out, the nodes to support the same functions will be more numerous and more widely distributed.

XI.1 The Problem Considered

Tactical radio network requirements are strongly influenced by the need for mobility of some of the network sites, and in the uncertainty of where others will be. For example, the FACP (Forward Air Control Post) locations are

hypothetical since the FACP's are relatively mobile and can be ready to move in an hour. Therefore, it is necessary to provide network coverage to many more locations than may ultimately be on the network. We are considering a two-level hierarchical network in which, at the lowest level, potential sites are connected to repeaters or backbone switches by radios with omni-directional or steered beam antennas which can communicate in a number of directions. It should be noted that the AN/TRC-170 radio terminal is not such a radio; but is rather designed to implement point-to-point channels. A description of a steered beam radio proposal can be found in [Sussman, 1980]. We are interested in determining how many repeaters are required to provide a given level of coverage where the "level" of coverage is measured by redundancy; i.e., how many repeater sites can serve each location. The redundancy is a design parameter to help make the network robust with respect to propagation difficulties, jamming, repeater failure or destruction, and other factors which make a particular terminal repeater connection unavailable. We do not consider how the repeaters (backbone switches) themselves are interconnected. (For design and analysis methods for the backbone see [NAC,1974].) We assume that the repeater locations will be known in advance of hostilities and will be well sited so that high efficiency point-to-point channels using directional antennas can be used. These repeaters then provide area coverage to other sites including those which are only potential sites. We considered the 49 sites used in [Brown et al, 1979] and shown in Figure 11.1. To avoid the modelling and data problems associated with propagation models we considered that propagation is characterized by a "range" and two points with great circle distance less than the range can communicate and otherwise cannot. The covering analysis does not depend on this assumption which was only made for convenience in this illustrative example. Repeaters can potentially be placed at

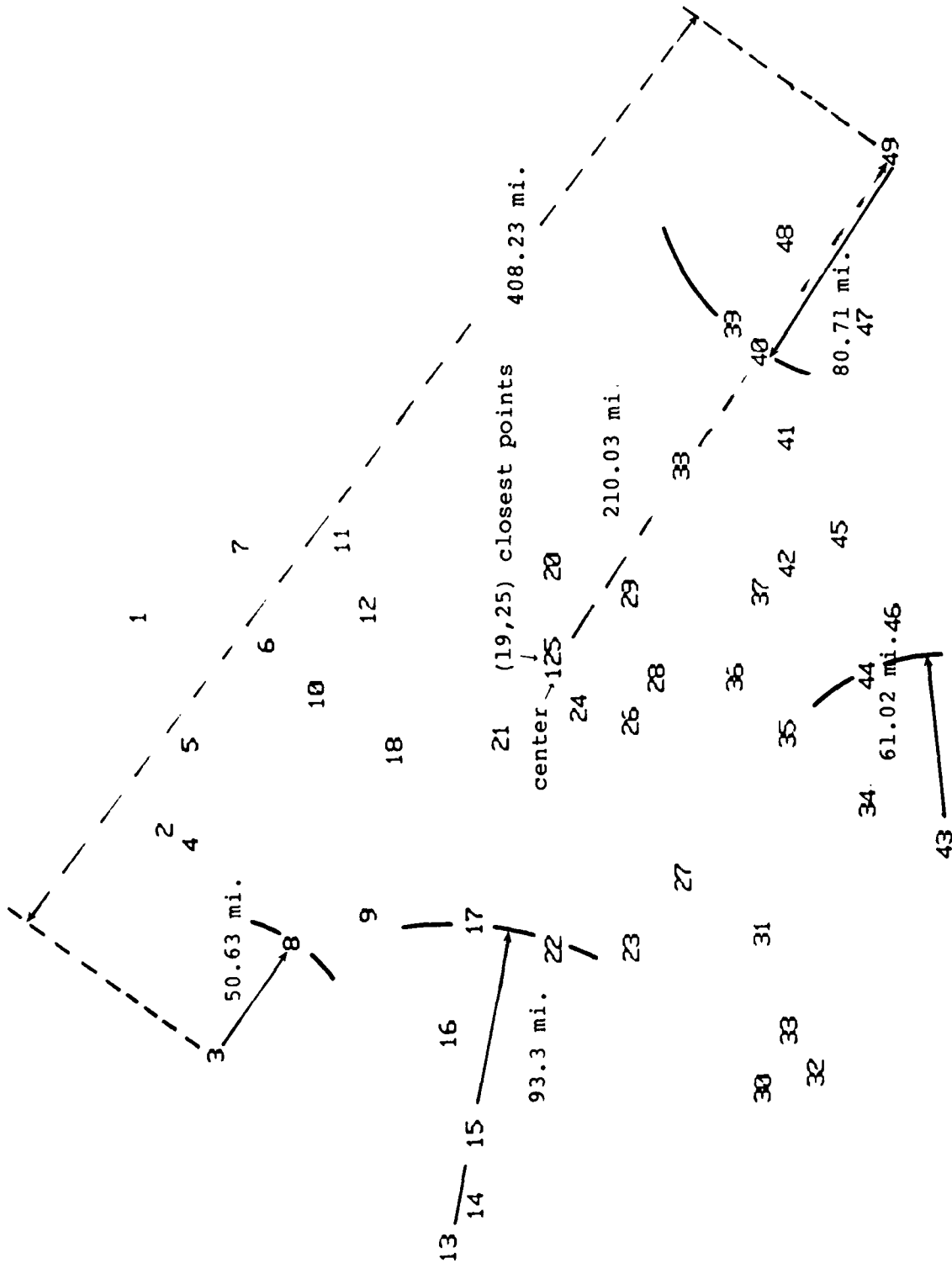


Figure 11.1: West German Locations

any of the 49 sites. Each site must be capable of communicating with K repeaters in addition to repeaters located at the same site, if present.

XI.2 Data Base Characteristics

The data base consists of 49 sites in Western Germany. The latitudes and longitudes of the points are given in Table 11.1. Sites 3 and 49 are the furthest apart, 408 (statute) miles. The two closest sites are 19 and 25 which are 9.5 miles apart. Node 19 is the "center" of the sites and every node is within 210 miles of node 19.

In order for the K-Cover problem to be feasible for $K=1$, the repeaters must have a range of at least 50.6 miles in order for Node 3 to be able to communicate with another site (Node 8). For $K=2$, a range of 61 miles is required for 43 to be able to communicate with two sites (34 and 44). For $K=3$ an 80.7 mile range is required (for 49 to communicate with 40, 47 and 48). Finally, for $K=5$, Node 13 needs a range of 93.3 miles to communicate with 14, 15, 16, 17 and 22. These critical parameters are illustrated in Figure 11.1. For reference we give in Figure 11.2 a minimum spanning tree on the nodes. The longest link (link(3,8)) in the minimum spanning tree is 50.6 miles which implies that we need a range of at least 50.6 miles in order to have a connected network. (Note: the ranges given here while quite reasonable for tropospheric scatter systems are unrealistically long for line of sight systems especially with omni-directional antennas. In an actual system extra nodes would be required.)

XI.3 Results of Covering Analysis

Two sets of runs were performed. In the first, for $K=1, 2, 3, 5$ we set the range at the minimum for feasibility, namely: 51, 62, 81, and 94 miles, respectively. The respective minimum number of repeaters (as calculated by the heuristic H2) required were 16, 23, 24, and 34. The solutions are shown in Figures 11.3 to 11.6 respectively. In

Table 11.1

LATITUDE AND LONGITUDE FOR POINTS

	LAT	LON		LAT	LON
1.	54.00	-10.00	26.	50.50	- 9.40
2.	53.80	- 8.70	27.	50.20	- 8.40
3.	53.50	- 7.30	28.	50.40	- 9.70
4.	53.55	- 8.58	29.	50.50	-10.20
5.	53.70	- 9.20	30.	49.70	- 7.10
6.	53.10	- 9.90	31.	49.70	- 8.10
7.	53.30	-10.50	32.	49.20	- 7.20
8.	52.90	- 8.00	33.	49.50	- 7.50
9.	52.40	- 8.20	34.	48.88	- 8.90
10.	52.70	- 9.60	35.	49.40	- 9.30
11.	52.50	-10.60	36.	49.75	- 9.70
12.	52.40	-10.10	37.	49.70	-10.20
13.	51.80	- 6.10	38.	50.20	-11.00
14.	51.60	- 6.40	39.	49.80	-11.90
15.	51.70	- 6.80	40.	49.60	-11.70
16.	51.80	- 7.50	41.	49.40	-11.20
17.	51.70	- 8.20	42.	49.50	-10.40
18.	52.18	- 9.25	43.	48.40	- 8.60
19.	51.00	- 9.75	44.	48.90	- 9.70
20.	51.00	-10.40	45.	49.08	-10.57
21.	51.50	- 9.30	46.	48.73	-10.02
22.	51.10	- 7.95	47.	48.90	-11.90
23.	50.60	- 8.00	48.	49.40	-12.40
24.	50.90	- 9.50	49.	48.80	-13.00
25.	51.10	- 9.90			

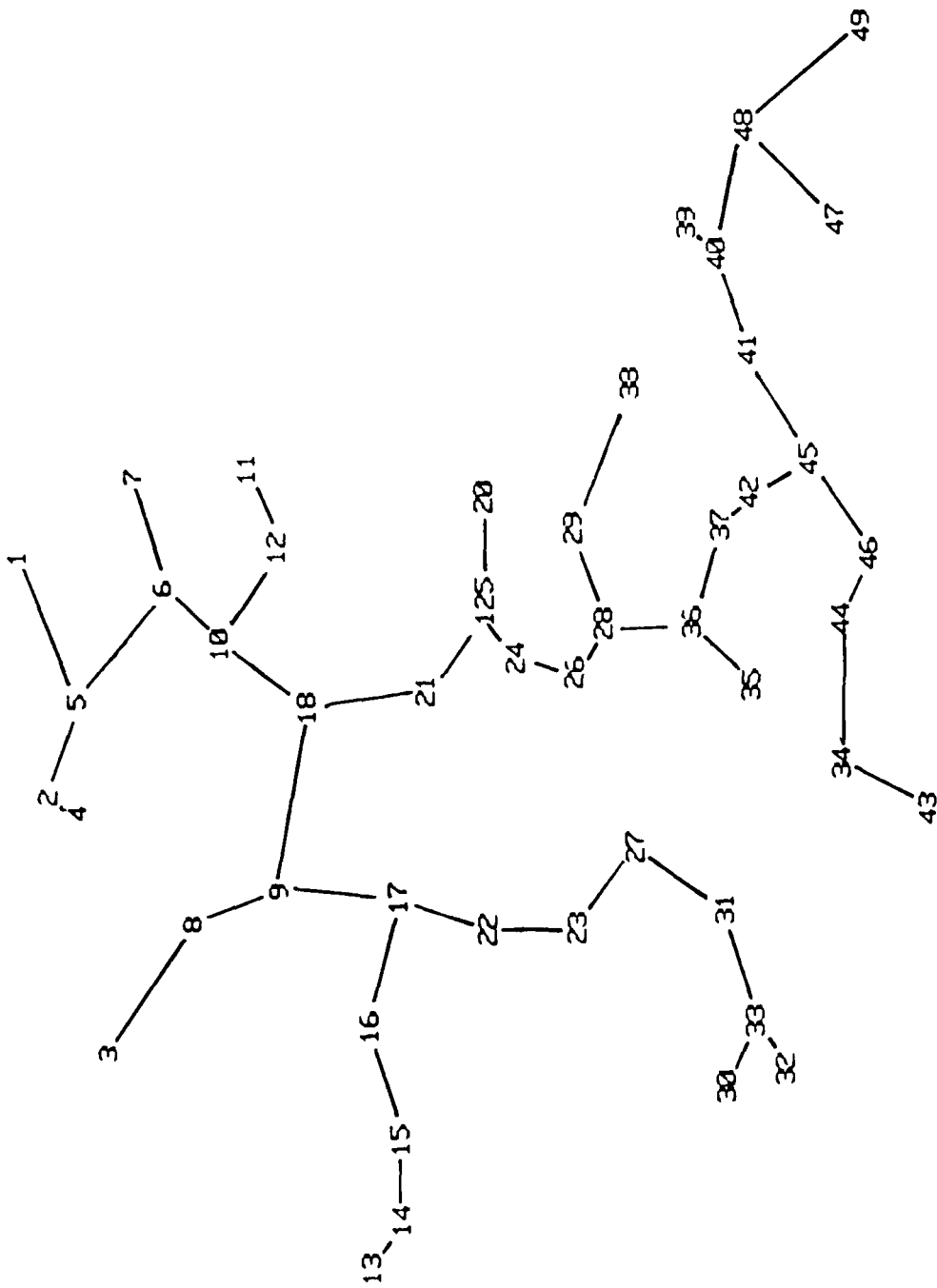


Figure 11.2: Minimum Spanning Tree

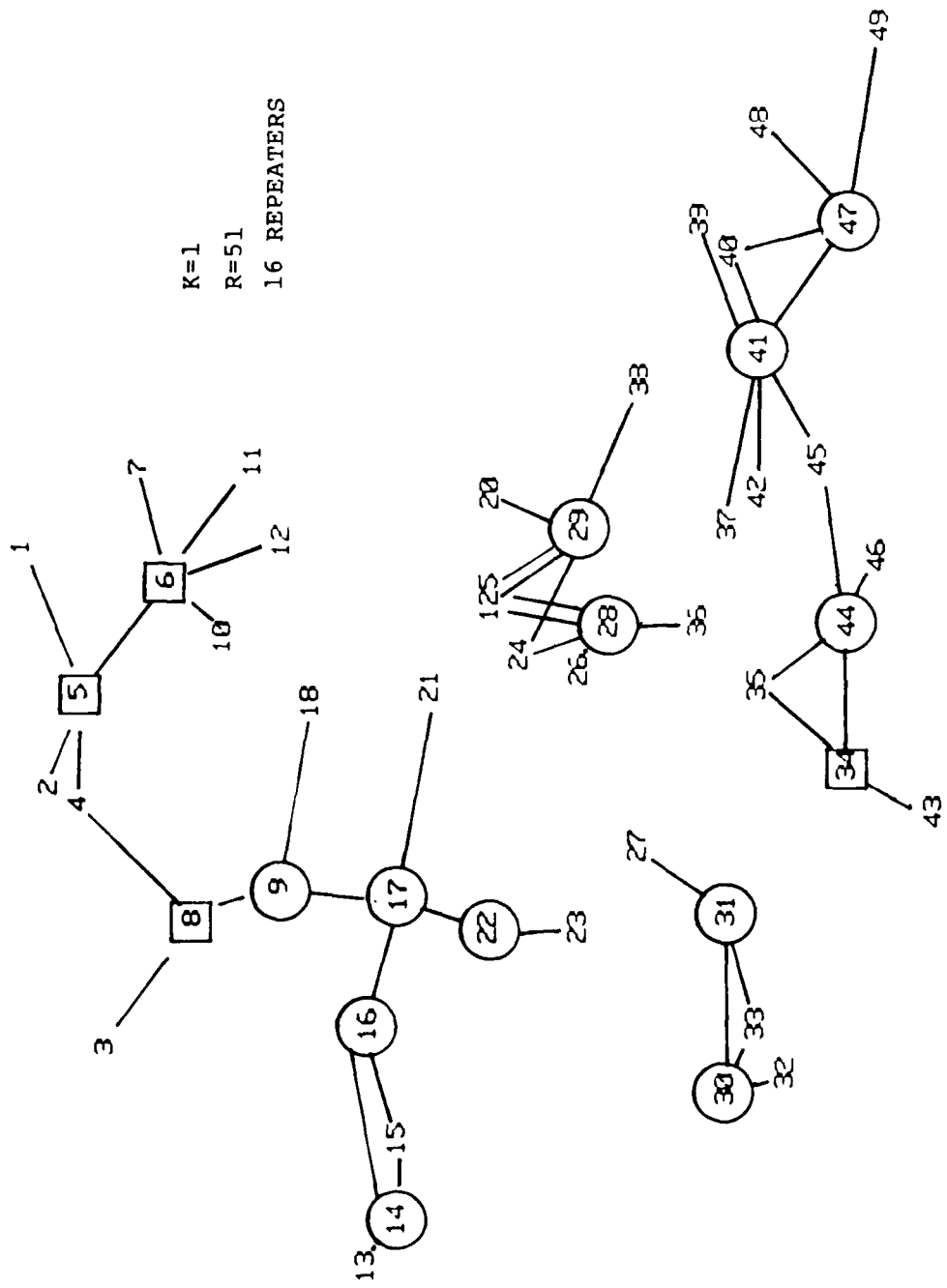


Figure 11.3

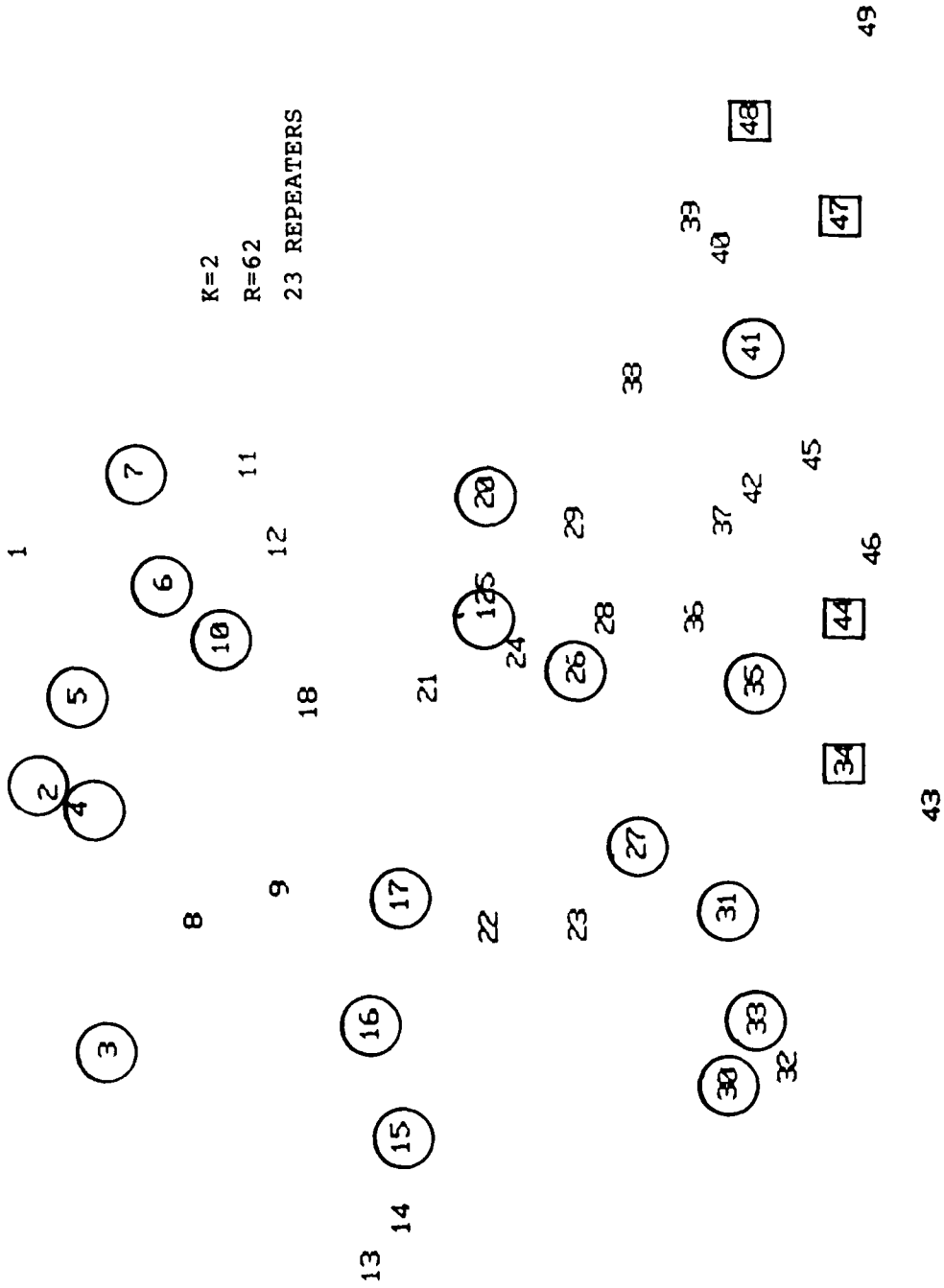


Figure 11.4

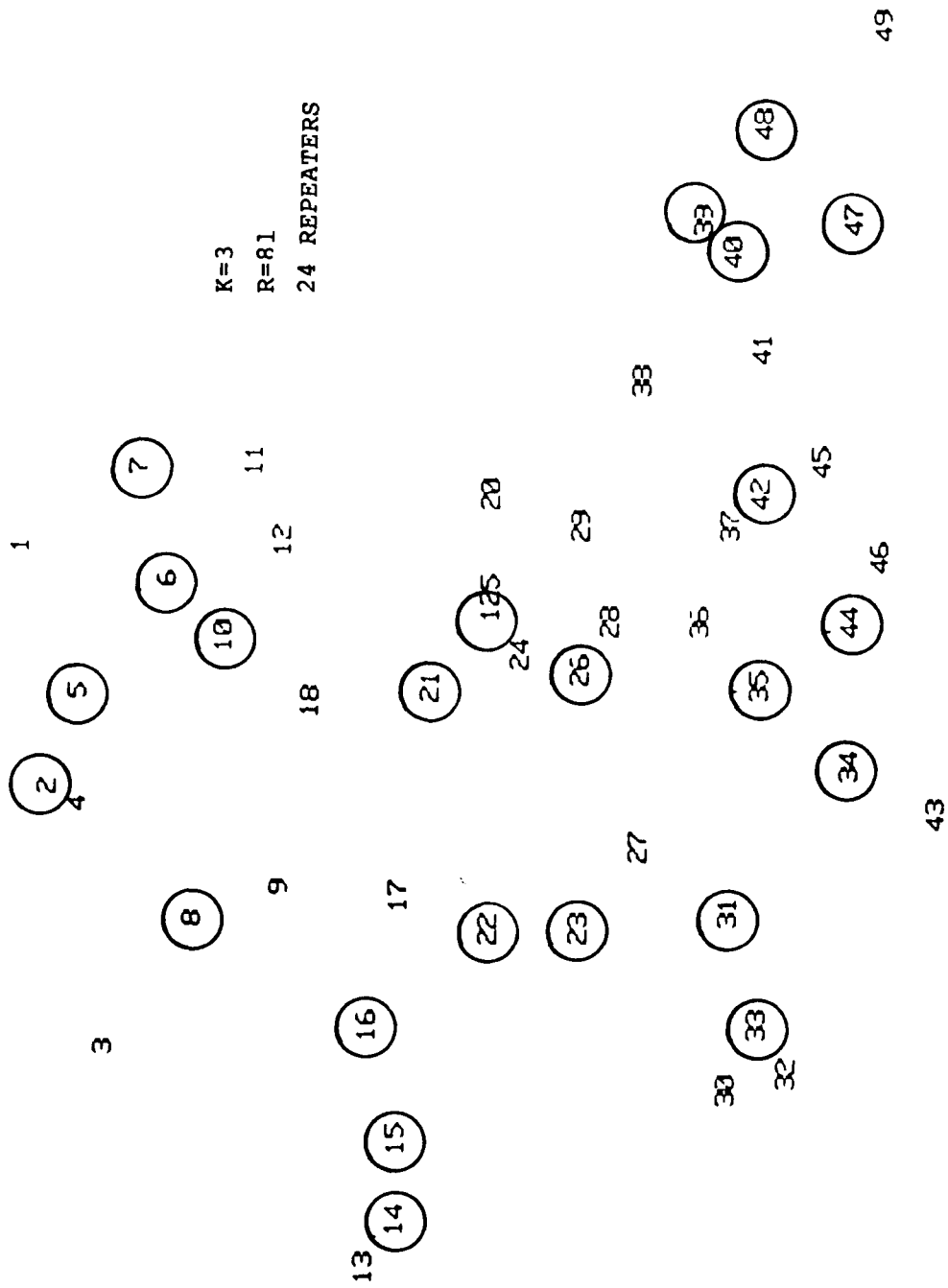


Figure 11.5

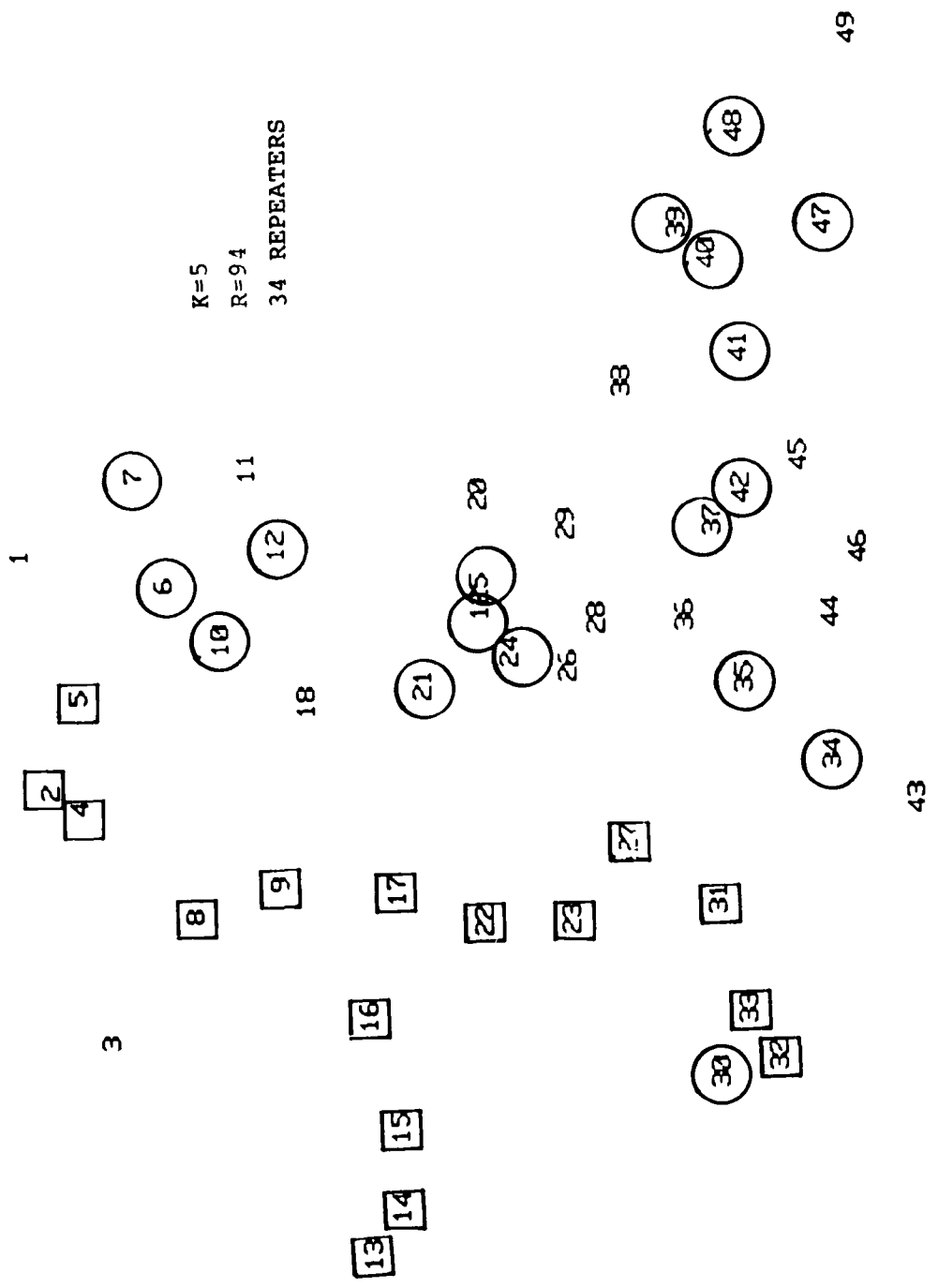


Figure 11.6

Figure 11.3 the assignment of sites to repeaters is also indicated. The square boxes indicate repeaters which must be in any feasible solution. In the second set of runs, the range was left fixed at 94 miles and (heuristic) solutions were obtained for $K=1, 2, 3,$ and 5 . The number of repeaters required were, respectively, $6, 12, 18,$ and 34 . These solutions are shown in Figures 11.7, 11.8, 11.9, and 11.6 respectively. The runs are summarized in Table 11.2.

XI.4 Random Throwdown Analysis

To determine the sensitivity of the results to the particular data base chosen, random sites were picked using the test problem generator RNDMAG (Section 9.2). The West German configuration can be enclosed in a rectangular area roughly 300 by 400 miles which is about the same area as a 350 by 350 mile square. Thus, if we scale the dimensions of the locations on the unit square produced by RNDMAG by about 350 we get to a very crude approximation an equivalent area. Table 11.3 summarizes the results of these runs. In each case 100 sample problems were considered and the results averaged.

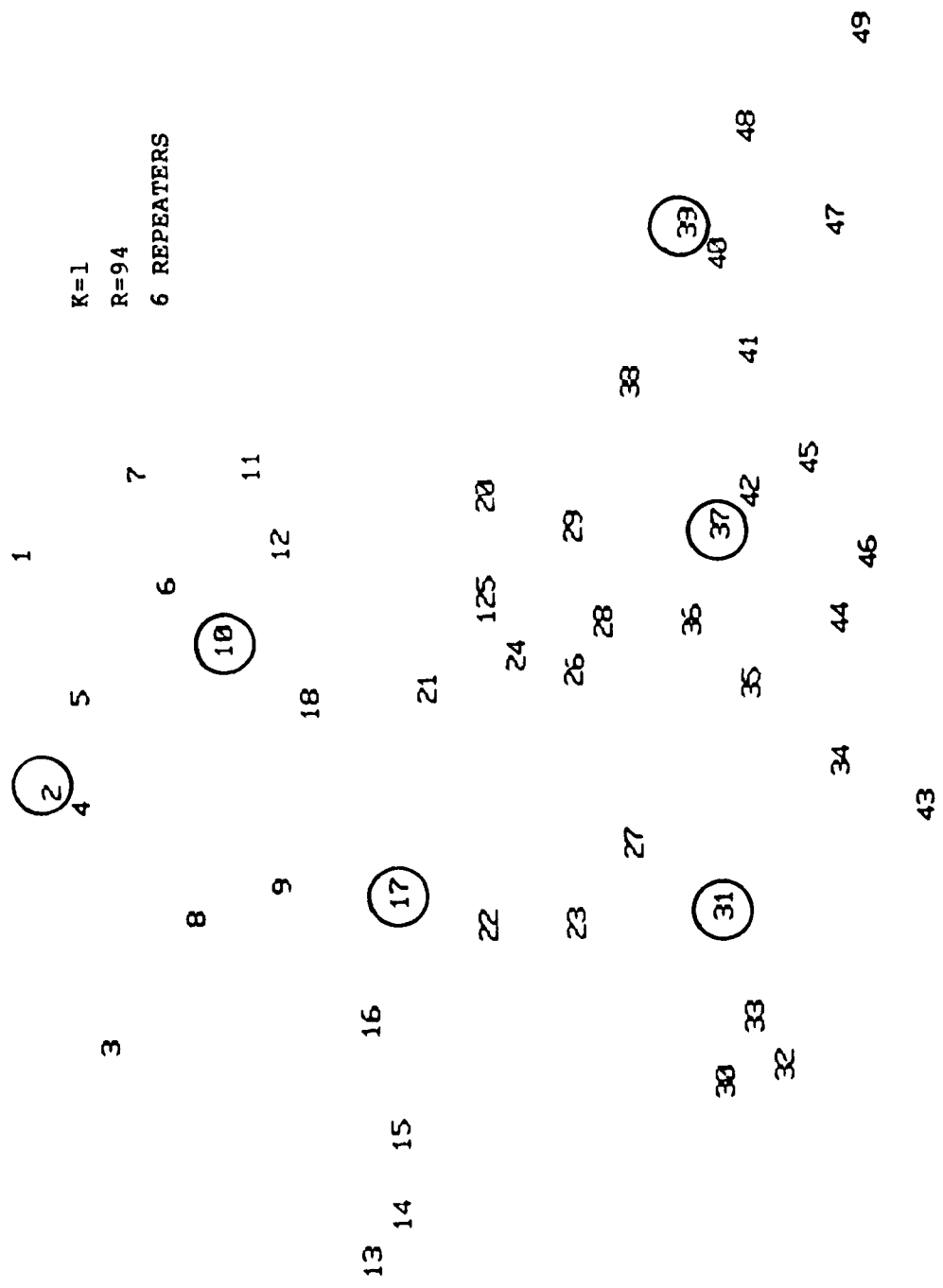


Figure 11.7

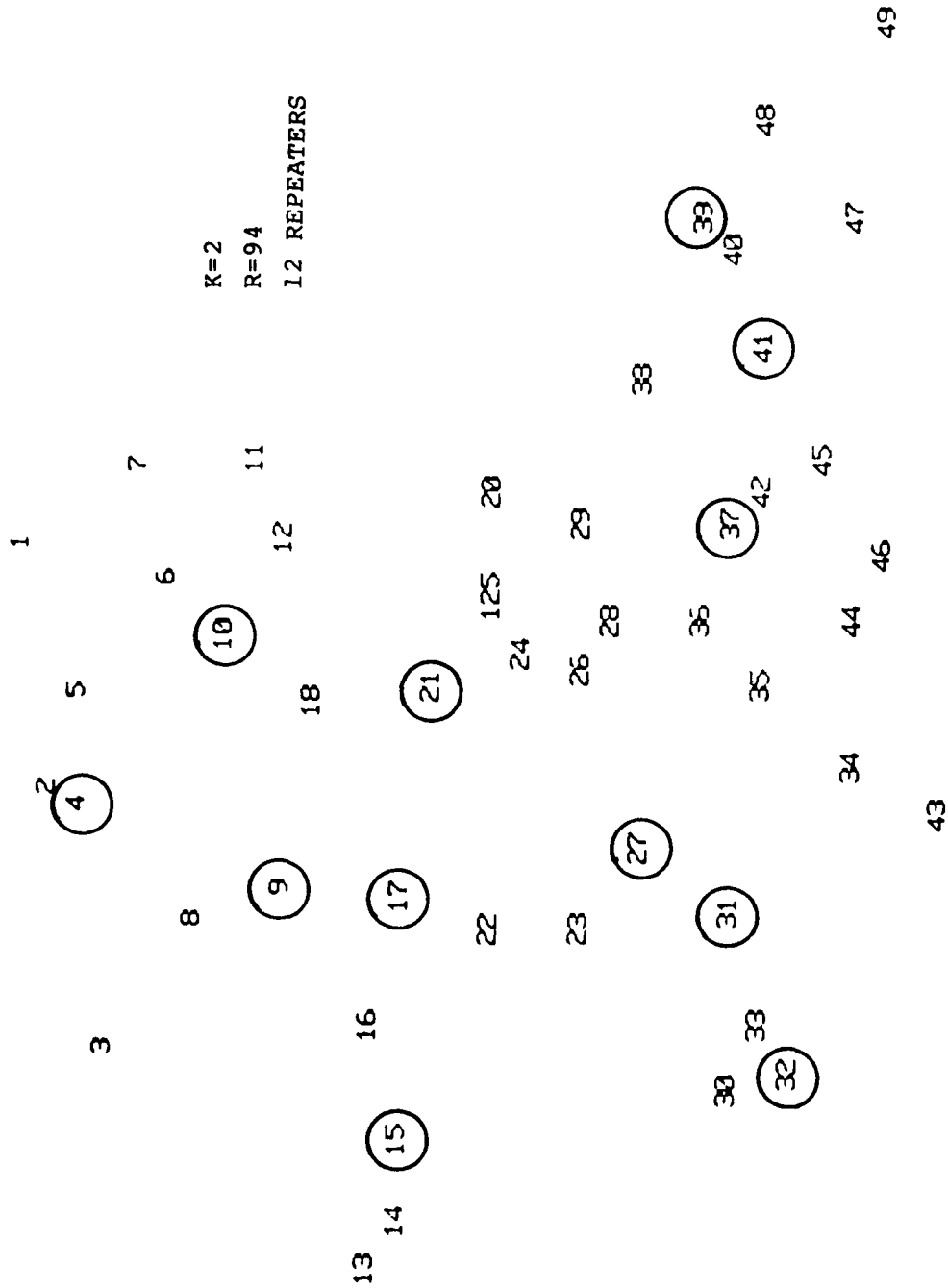


Figure 11.8

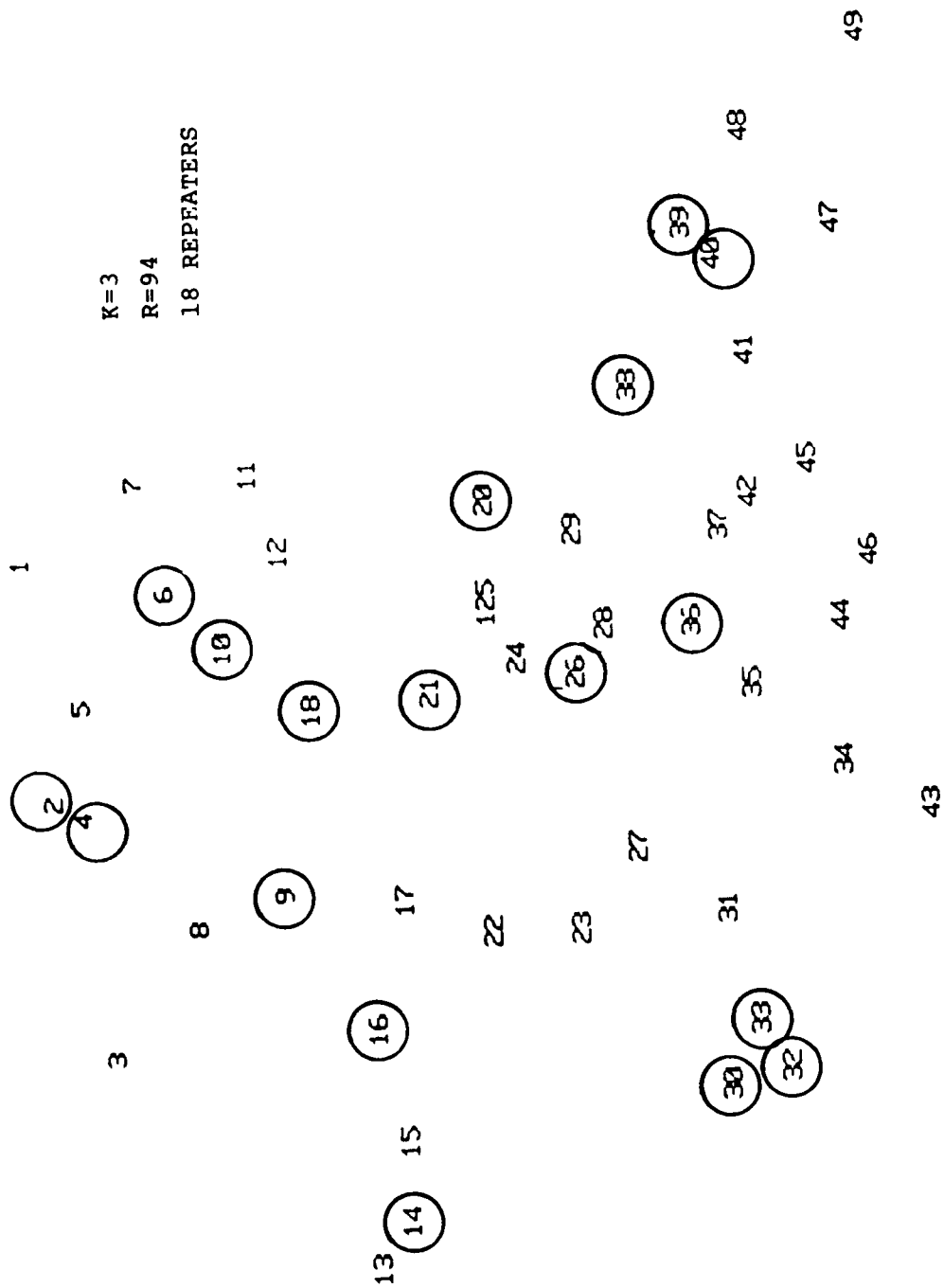


Figure 11.9

Table 11.2

WEST GERMANY COVER ANALYSIS

K	Range	Number of Repeaters
1	51	16
2	62	23
3	81	24
5	94	34
1	94	6
2	94	12
3	94	18
5	94	34

Table 11.3

COVER ANALYSIS FOR RANDOM LOCATIONS

AVERAGE CRITICAL RADII

(For 350 x 350 Square)

N	K	Average Radii
20	1	100
	2	132
	3	158
	5	198
25	1	91
	2	118
	3	141
	5	178
50	1	71
	2	89 (18.2 avg. no. of repeaters)
	3	103
	5	130 (24.3 avg. no. of repeaters)
100	1	54
	2	66
	3	77
	5	96

XII. Recommendations

During this research project we have accomplished the following.

- Identified a little studied problem of practical significance to the Air Force--The problem of optimizing the coverage of radio communication and radar surveillance/reconnaissance systems is a general problem of importance to the Air Force. In this work, we considered problems of this class with particular emphasis on features that are rarely considered but are important to the Air Force. These include the use of redundancy to provide reliability and to reduce vulnerability; the ability to solve the large problems arising in Air Force applications; and the ability to obtain reasonable approximations to solutions in a guaranteed amount of time for real time applications.
- Surveyed a wide class of solution techniques--A variety of potential techniques including heuristics, upper and lower bounds, and a variety of implicit enumeration schemes were developed and described.
- Implemented experimental solution programs--Modular experimental programs were written, debugged, and tested which allowed the empirical evaluation of the various options in a number of combinations. The resulting programs have been run on PDP 11-70 and DEC-10 computers.
- Implemented random problem generators for objective algorithm evaluation--Two different kinds of random test problem generators were developed to provide a wide variety of test problem instances in order to objectively and statistically test the algorithmic

proposals. One test problem generator was oriented towards generating geometrically random problems by placing covering points and points with covering requirements randomly in the plane. The other test problem generator generates problems in which the probability that a given coverer could cover a point requiring coverage is the same for all pairs.

- Performed empirical evaluations-- The most fruitful algorithmic options were identified on the basis of empirical studies by applying the experimental algorithms to problems produced by the test problem generators.
- Illustrated application of the method--The method was applied to a simplified design problem for radio networks in West Germany. Because of time constraints the design problem included a number of strong assumptions and simplifications. However, these deficiencies are a result of, merely, practical time constraints and not of any theoretical deficiencies of the methods.

In order to make the K(I)-covering methodology a operational part of Air Force planning, analysis, and design further work is needed.

First, some aspects of the summers work must be completed. While the method in its current state has been shown to be quite effective, because of the unavailability of linear programming codes (see Section VII.5) certain options based on linear programming have not been evaluated. Because, of the modular construction of the experimental computer codes completing this open issue is relatively simple. For example, at the Stevens Institute of Technology we have access to a linear programming code which can be

easily connected to the experimental computer code. In Section VI.2 we describe worst case bounds for heuristics to solve covering problems. We anticipate that these results can be extended to the K(I)-covering problems with relatively modest effort. Bounds would be particularly useful when using the heuristics we have proposed for real time problems because we would then have both a bound on the running time of the algorithms and on the largest possible error in the worst case. Much of the effort on this project was expended in developing an extensive and flexible set of computer algorithms to evaluate methods for solving K(I)-covering problems. The full capabilities of this software has, by no means, explored. For example, relatively few experiments were carried out in the analysis of branching rules (see Section VIII). An area that is of great practical importance although of less theoretical importance is the various kinds of simplifications which can be made to covering problems based on the particular problem considered. Two such simplifications are described in Section IV.3. There is a number of other possible simplifications which can be easily identified and can be of significant utility in individual applications.

The second step towards operational utility for the methodology is to extend it. While the weighted K(I)-covering problem was defined in Section III virtually all the work in this study and all the empirical evaluation was done for the simple K(I)-covering problem in which it is assumed that the cost of providing a coverer is always the same. In practical applications it will often be the case that some coverers are more or less expensive than others. Again the extensions should not be too complicated in most cases. The simpler case was considered merely to reduce some of the variability in the empirical evaluations. The more significant extension is to build a prototype implementation of the algorithms based on the experimental code produced in

this study. This would have two benefits. The new implementation would be based on the improved data structure described in Section X; it would also be sufficiently well written and documented so it could be released for use by others on an experimental basis.

A third step towards achieving operational capability is to apply the methodology to more realistic applications. For example, performing radio networking studies with more realistic requirements data, more sophisticated propagation models, and more accurate models of communication equipment performance and range.

Finally, the fourth step would be to disseminate the work to interested parties.

The K(I)-covering problem is only one step in filling a substantial gap in the techniques of communication network design and analysis. In recent years there has been a number of proposals for complex and large scale communication networks which are based on communication channels which operate in a broadcast mode. Examples of such channels include:

- Communication satellites used in a random access mode,
- CATV networks used for data transfer,
- Local area networks such as Ethernet which use random access,
- Microwave systems with omni-directional or steered beam antennas including proposals and implementations by Xerox (XTEN), SBS, MACOM/DCC, DARPA (Packet Radio), JTIDS, and AT and T's cellular radio system. (See also [Sussman, 1980],

Most network design techniques are oriented towards

point- to- point channels, for example, those developed for telephone networks and ARPANET. Techniques are required for broadcast networks. The work described here is an analog of the concentrator location problem in point-to-point networks. Other techniques are required for routing analysis and design, reliability analysis and design, delay analysis, etc. This is the long term objective for which the work described in this work is the first step.

Developing these broadcast network design techniques is especially important for the Air Force because future military Command, Control, Communication and Intelligence Systems will more highly dispersed than at present for survivability purposes. Likewise, they will be interconnected with highly redundant and multiply connected communication links, often in a broadcast or multiaccess mode.

REFERENCES

1. Brown, C., Fritzch, P.C., Fullerton, A.L., McDowell, R., Rabe, W.A., An/TRC-170 Vulnerability Analysis, MTR 3793, MITRE, 1979. SECRET
2. Chvatal, V., "A greedy heuristic for the set-covering problem," Mathematics of Operations Research, Vol. 4, No. 3, pp. 233 - 235, 1979.
3. Etcheberry, J., "The set-covering problem: a new implicit enumeration algorithm," Operations Research, 25, 5, pp. 760 - 772. Sept. - Oct. 1977.
4. Ford, L.R., Jr., and Fulkerson, D.R., Flows in Networks, Princeton U. Press, 1962.
5. Garey, Michael R., and Johnson, David S., Computers and Intractability, W.H. Freeman and Company, 1979.
6. Garfinkel, R.S., and Nemhauser, G.L., Integer Programming, Wiley, 1972.
7. Glover, F., "Surrogate constraint duality in mathematical programming," Operations Research 23, 6, pp. 1259-1261, Nov.-Dec. 1974.
8. Handler, G.Y., and Mirchandani, P.B., Location on Networks, MIT Press, 1979.
9. Johnson, D.S., "Approximation algorithms for combinatorial problems," Journal of Computer and System Sciences, Vol. 9, pp. 256 - 278, 1974.

10. Kahn, R., Gronemeyer, S.A., Burchfiel, J., and Kunzelman, R.C., "Advances in Radio Packet Technology," IEEE Packet Communications Networks, Vol. 66, No. 11, pp. 1468 - 1495, Nov. 1978.
11. Knuth, Donald E., The Art of Computer Programming, Volume I, Fundamental Algorithms (2ed. 1973); Volume II, Seminumerical Algorithms (2ed. 1981); Volume III, Sorting and Searching (1973); Addison-Wesley.
12. Lovasz, L., "On the ratio of optimal integral and fractional covers," Discrete Mathematics, Vol. 13, pp. 383 - 390, 1975.
13. Murty, K.G., Linear and Combinatorial Programming, Section 15.9, Wiley, 1976.
14. Network Analysis Corporation, , "The practical impact of recent computer advances on the analysis and design of large-scale networks," Semiannual Technical Report (to DARPA), Great Neck, NY, June 1974.
15. New York Times, "U.S. Says Terrain Shields Israel From Radar-Jet Peril," August 27, 1981, p.A3.
16. Ryser, H.J., Combinatorial Mathematics, Mathematical Association of America, 1963.
17. Sussman, Steven, "A survivable network of ground relays for tactical data communications," IEEE Trans. on Comm., COM-28, No. 9, Sept. 1980, pp. 1616 - 1624.
18. Toregas, C., Swain, R., Revelle, C., and Bergman, L., "Location of Emergency Service Facilities," Operations Research, 19 pp. 136 - 1373, 1971.

19. USAFE, 1978 "601 TCW TRI-TAC Equipment Requirements,"
prepared by 601 TCW/TLKC, USAFE, December 1978.

1981 USAF - SCEE SUMMER FACULTY RESEARCH PROGRAM

Sponsored by the

AIR FORCE OFFICE OF SCIENTIFIC RESEARCH

Conducted by the

SOUTHEASTERN CENTER FOR ELECTRICAL ENGINEERING EDUCATION

FINAL REPORT

EFFECTS OF ACOUSTIC DISTURBANCES ON THE BOUNDARY-
LAYER TRANSITION IN AEDC WIND TUNNELS

Prepared by:	Dr Venugopal Veerasamy
Academic Rank:	Assistant Professor
Department and University:	Mechanical Engineering Department Tennessee State University
Research Location:	Arnold Engineering Development Center Arnold Air Force Station, Tennessee
USAF Research Colleague:	Dr Keith L. Kushman and Marshall K. Kingery
Date:	August 10, 1981
Contract No:	F49620-79-C-0038

EFFECTS OF ACOUSTIC DISTURBANCES ON THE
BOUNDARY-LAYER TRANSITION IN AEDC WIND TUNNELS

by

Dr Venugopal Veerasamy

ABSTRACT

Boundary-layer transition prediction techniques are reviewed. Experimental results show that free-stream disturbances (acoustic sound, turbulence, and temperature fluctuation, etc.) contribute to the early transition process. At subsonic speeds the dominant disturbances are turbulence and/or acoustic vibrations. At transonic speeds the acoustic noise generated by the test section porous or slotted walls is predominant. At supersonic - hypersonic Mach numbers, the radiated noise from the turbulent boundary layer on the tunnel walls is the dominant source of disturbance. A mathematical model is proposed to predict the early transition due to acoustic interaction. Further theoretical and experimental programs are suggested.

ACKNOWLEDGEMENT

The author would like to thank the Air Force Systems Command, the Air Force Office of Scientific Research and the Southeastern Center for Electrical Engineering Education for providing him with the opportunity to spend a very worthwhile and interesting summer at the Arnold Engineering Development Center, Tullahoma, Tennessee. He would like to acknowledge the Center, in particular the Directorate of Technology, for its hospitality and excellent working conditions.

Finally, he would like to thank Dr Keith Kushman for suggesting this area of research and for his collaboration and guidance, and he would like to acknowledge many helpful discussions with Mr Robert H. Nichols, Mr W. T. Strike, Mr J. C. Donaldson, and Dr James Maus.

1. INTRODUCTION:

The location of boundary-layer transition over re-entry vehicles has a first order influence on skin friction drag, aerodynamic heating, flow separation etc. Although considerable progress has been made in predicting laminar and turbulent flows, the physics of the transition process is not completely understood. However, the comparison of the transition region predicted by available methods¹ with the experimental data obtained in various wind tunnels for simple geometries like flat plate and sharp cone reveals that early transition occurs due to the external disturbances which interact with the developing laminar boundary-layer to cause transition either through instability waves (turbulence, sound, entropy, etc) or in a direct manner (surface roughness, tripping mechanism, etc).

The velocity (turbulence) and entropy (temperature) fluctuations are convected along the stream lines and are easily traceable to conditions in settling chamber; but the sound sources at the settling chamber, wind tunnel walls, and test section boundaries radiate acoustic (sound) pressure disturbances that can travel across the stream lines. Therefore, a complicated mathematical analysis is required to find the effect of acoustic interaction on the boundary-layer interaction process. Further, at supersonic-hypersonic speeds, the caustic layer² creates physical and mathematical problems. The caustic layer is the region within the boundary-layer where the local fluid velocity is sonic. The radiated noise field may be partly reflected and refracted in the caustic layer. Because of the complex mathematical and fluid

mechanics process inherent in boundary-layer modeling, analytical and experimental studies are carried out at AEDC (Arnold Engineering Development Center) to evaluate flight similitude.

II. OBJECTIVE:

The main objective of this project was to investigate theoretically and experimentally the effects of acoustic disturbances on the boundary-layer transition in AEDC wind tunnels.

III. WIND TUNNEL ACOUSTIC DISTURBANCES:

Wind tunnels can be divided into subsonic, transonic, supersonic, and hypersonic wind tunnels. The acoustic disturbances are different in each wind tunnel. Figure 1 shows the acoustic disturbances in a typical wind tunnel.

In subsonic wind tunnels, the acoustic disturbances can be of standing wave type due to resonance in the test section or traveling acoustic waves caused by fan noise, etc. Intensity and spectral measurements identify the source of noise generation.

In transonic wind tunnels wall hole/slot resonance in porous and/or slotted walls is the dominant source of noise generation. Transition Reynolds number can be correlated with the tunnel noise intensity.

In supersonic and hypersonic wind tunnels, the noise is radiated from turbulent flow near the wind tunnel wall. A major effort has been underway since 1970 at NASA-Langley¹ to design and construct a $M_\infty = 5$ quiet wind tunnel free from radiated noise disturbances as illustrated in Figure 2.

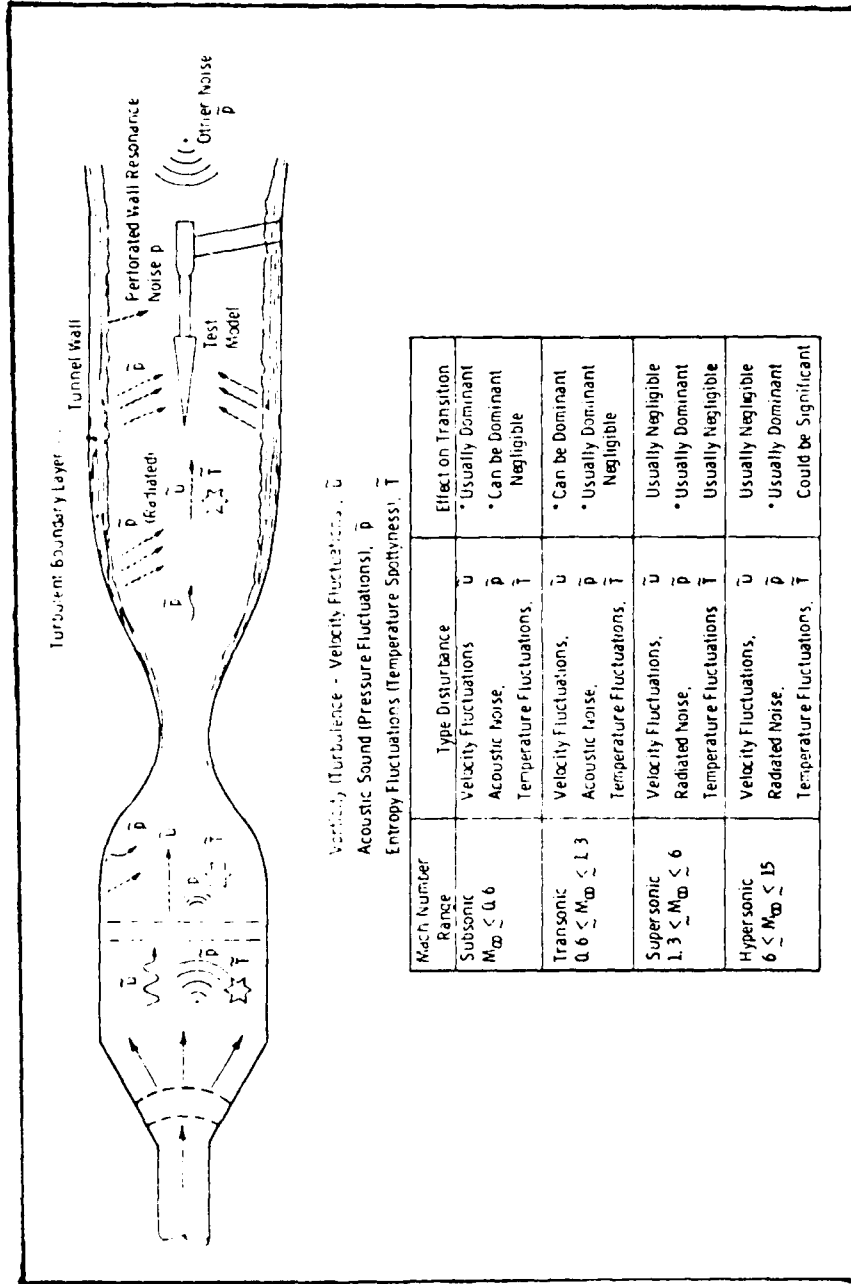


Figure 1. Acoustic Disturbances in a Wind Tunnel.

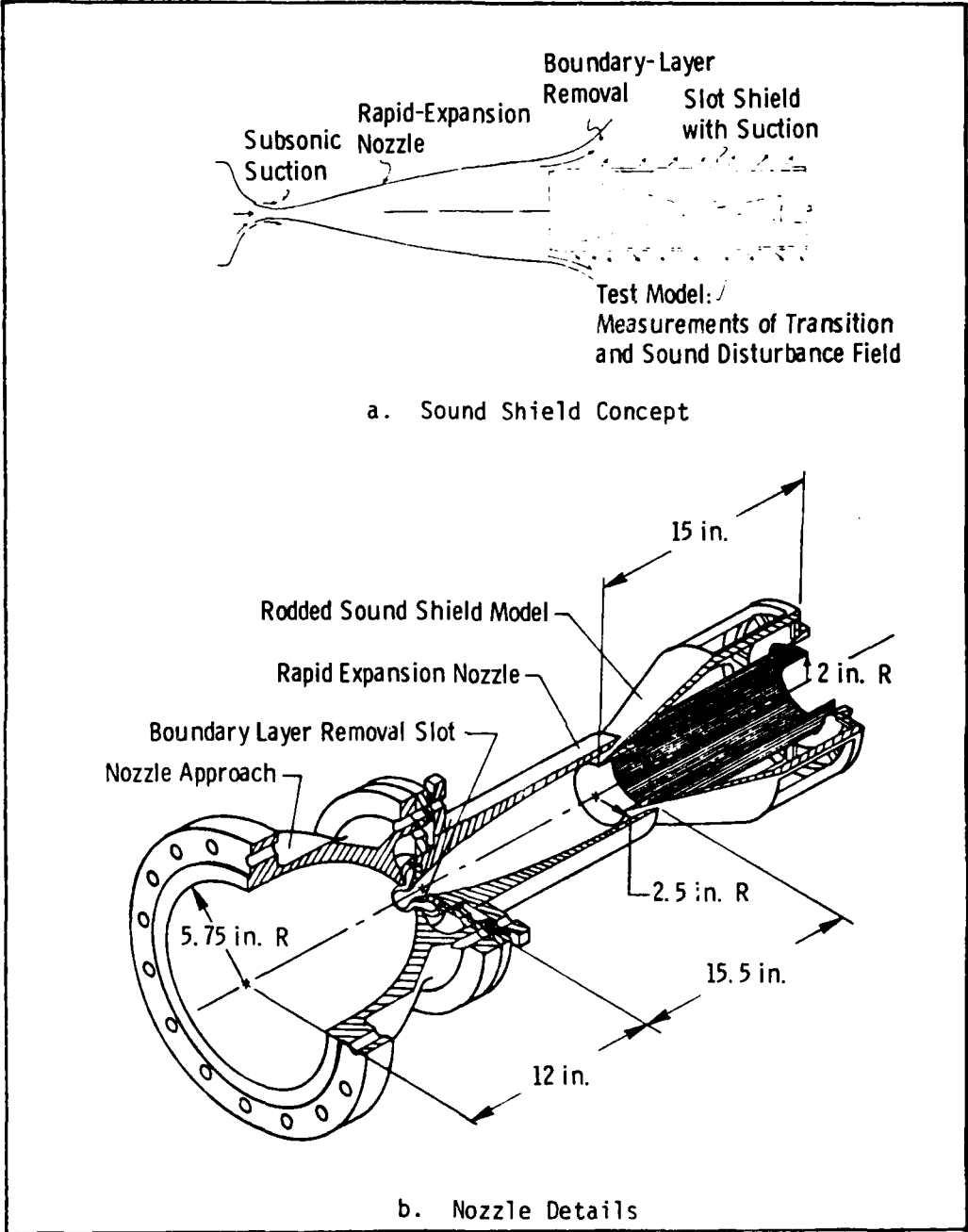


Figure 2. NASA-Langley $M_\infty = 5$ Quiet Wind Tunnel
(from Reference 1).

IV. BOUNDARY-LAYER TRANSITION STUDIES

A systematic theoretical and experimental study is necessary to predict the boundary-layer transition region. The methods that have been used for predicting transition region can be grouped into three general classifications:

1. Linear stability theory
2. Kinetic energy of turbulent approach
3. Correlations and semi-empirical methods.

The linear stability theory for incompressible and inviscid flow was developed by Raleigh.^{3,4} He predicted that the inflection point in the velocity profile contributes to the instability. Prandtl extended the linear stability theory to include viscosity. A detailed stability theory for incompressible and viscous flows was developed by Tollmien and Schlichting³. Schubauer and Skramstad⁴ confirmed the existence of Tollmien-Schlichting type waves by experiments. Mack⁶ extended linear stability theory to higher Mach numbers and Kendall⁷ provided experimental verification. One of the interesting results obtained by Mack-Kendall research at JPL (Jet Propulsion Laboratory) is that free stream radiated noise disturbance, independent of critical frequency, is amplified by the laminar boundary-layer. This amplification begins at the leading edge of a flat plate and continues downstream until transition occurs. Figure 3 shows the correlation and prediction of incompressible flow transition Reynolds numbers.⁸ Rogler^{9,10,11,12} analytically and numerically studied the interaction between an incompressible boundary-layer and a low intensity array of single wave number vortices convected at the mean free stream velocity. However, the prediction of transition region based on linear stability theory depends on the assumptions used.

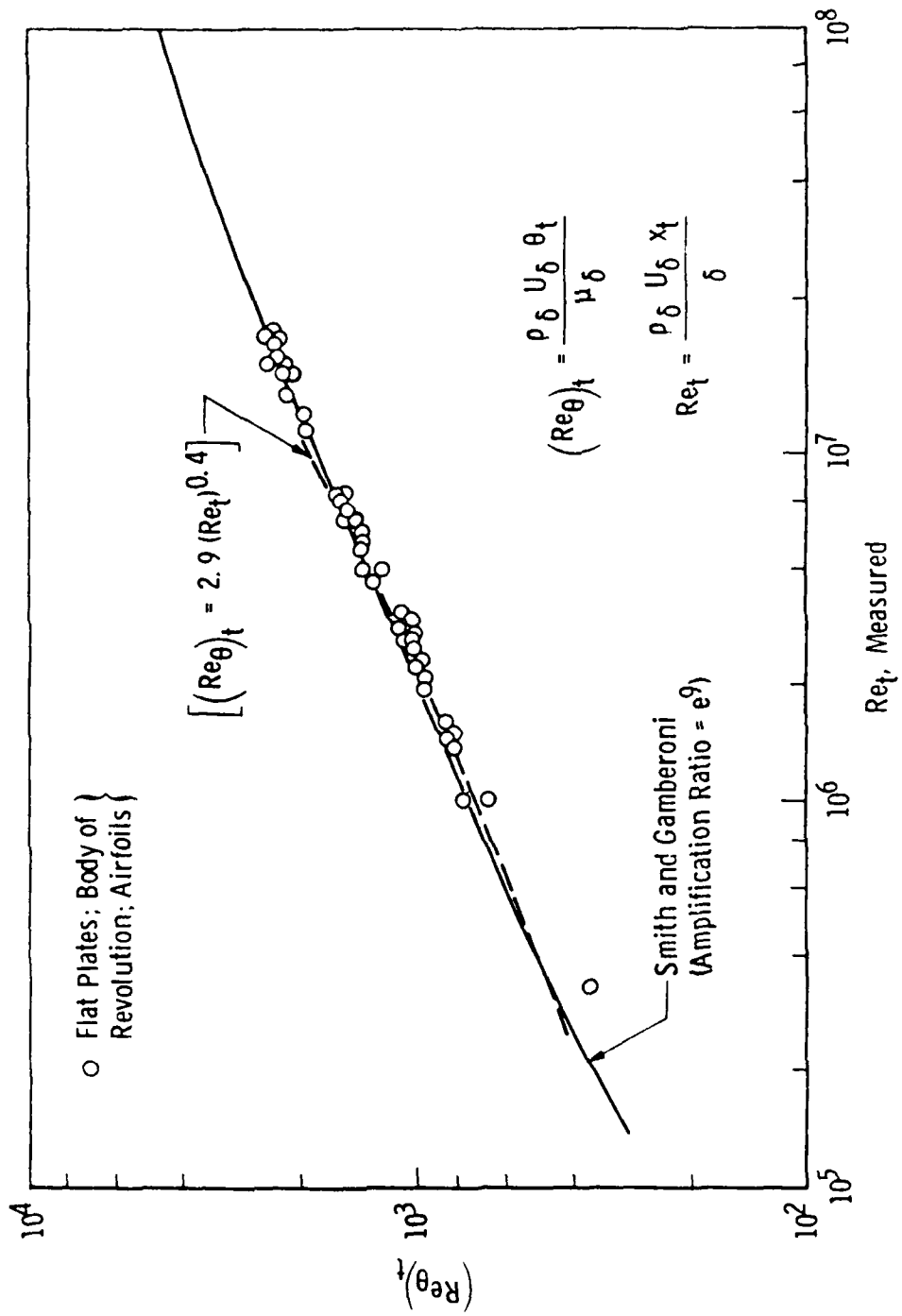


Figure 3. Correlation and Prediction of Incompressible Flow Transition Reynolds Numbers (from Reference 8).

Kinetic energy of turbulence model equations developed by Sharmroth and McDonald¹³ have been used to investigate transition. Acoustic pressure fluctuations are used as the primary source of the free stream disturbance and the calculations are done if the acoustic energy loss is specified. A small amount of (1%) acoustic energy absorption is required to trigger transition.

Correlation methods are used extensively to predict the transition location. Van Driest and Blumer¹⁴ used Liepmann's hypothesis¹⁵ that transition will occur at a critical Reynolds number $Re_{cr} = \left[\overline{u'v'} / \left(\mu \frac{\partial u}{\partial y} \right) \right]$ and developed an empirical relation for transition Reynolds number in incompressible flow. A correlation of transition Reynolds number measured in various wind tunnels and in F-15 flight test on 10° sharp cone by Dougherty¹⁶ is shown in Figure 4.

Pate¹ correlated the transition Reynolds number as a function of radiated noise parameter (C_F , δ^* and \bar{c}) for a sharp cone and flat plate and developed the following empirical equation (Figure 5):

$$Re_t = \frac{a C_F^b \bar{c}}{\sqrt{\delta^* / \bar{c}}}$$

where Re_t = transition Reynolds number

a = 0.0126 for flat plate; = 48.5 for cone.

b = -2.55 for flat plate; = -1.4 for cone.

\bar{c} = tunnel size

C_F = skin friction coefficient

δ^* = tunnel wall turbulent boundary-layer thickness.

From the above equation, it is clear that Re_t increases with the tunnel size. Since the correlation was developed for the finite-size wind tunnels, the proper boundary condition for free flight are not included. Therefore,

0.4 ≤ M_∞ ≤ 1.8 From Ref. 16

Sym	Tunnel	Sym	Tunnel
○	AEDC Tunnel 16T	○	NASA Ames 10 PT
●	AEDC Tunnel 16T (Walls Taped)	□	RAF Farnborough 8 x 8 SUT
△	AEDC Tunnel 4T	▲	USCAR 20 Inlet 16 T (From
△	AEDC Tunnel 4T (Walls with Tape or Screen)	▲	NASA Langley 16 TDT Test
○	ONERA 6 x 6 S-2 Airplane	●	NASA Langley 8 TDT Medium
○	NASA Ames 11 TWT	●	MSRDC 7 x 10T
○	NASA Ames 11 TWT (Walls Taped)	○	NASA Langley 4 SPT
△	NASA Ames 14 TWT	○	RAF Farnborough 4 VSST
▲	NASA Ames 16 TWT (Walls Taped)	○	NASA Ames 9 x 7 SUT
○	Consolidated TWT	○	NASA Langley 4 SUPWT ITS No. 11
○	ARA Ltd. F4U 9 x 8	○	Flight Data, Fig. 15

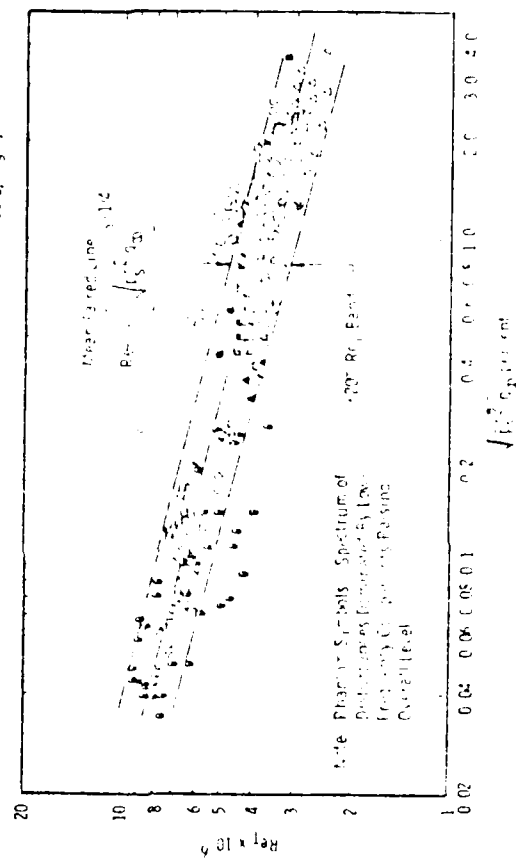


Figure 4. Correlation of Wind Tunnel and Flight Data (from Reference 16).

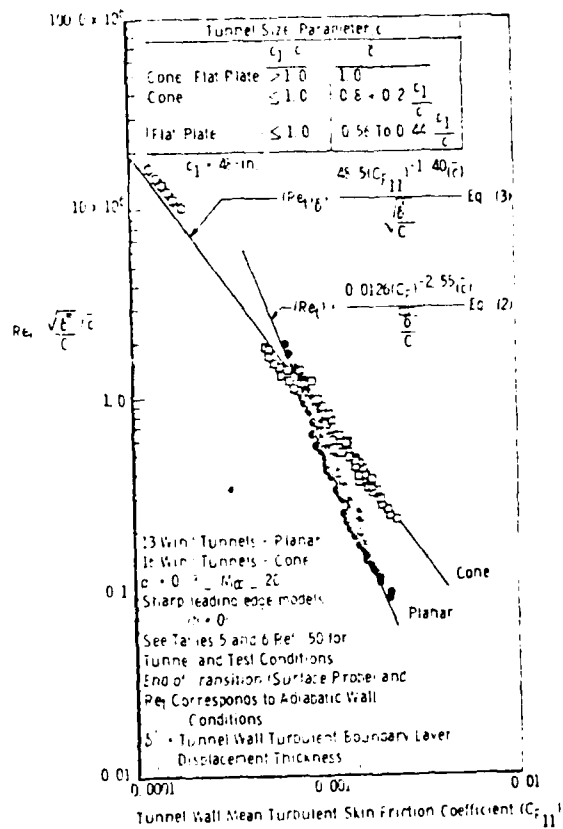


Figure 5. Correlation of Planar Model and Sharp Cone Transition Reynolds Numbers (from Reference 1).

this correlation cannot be applied to the ballistic ranges, atmospheric free flight or any test environment other than a conventional wind tunnel. Figure 5 shows the correlation of planner model and sharp cone transition Reynolds number.¹

It is quite interesting to know the transition location experimentally. Figure 6(a)¹⁷ shows that the wall temperature remains very nearly constant then raises to maximum and decays towards another constant level. The heat rate in Figure 6(b), displays the customary rise of heat flux from laminar to turbulent values. The three types of boundary layer thicknesses are shown in Figure 6(c).

Three dimensional¹⁷ view of intensity, frequency and distance from the wall is shown in Figure 7 as obtained from hot wire anemometer. (Of course, the measurement and calibration of hot wire probe are time consuming.) The spectral dispersion begins with a decrease of oscillation intensity and the appearance of turbulence.

In hypersonic wind tunnel, the effect of nose cone curvature on flow stability is the current research at AEDC. The hot wire anemometer readings are taken at maximum energy peak where the possible evidence of the existance of the caustic region. It can be expected that the acoustic noise radiated from the tunnel wall acting as a forcing function cause an interaction between the shock wave and the boundary-layer. This interaction produces the disturbance. Thus, the curvature of nose cone, free-stream Mach number and the noise radiation play an important role for boundary-layer transition.

V. MATHEMATICAL MODEL

In a fluid flow, the flow quantities can be assumed to be composed of its value for the specific basic flow and a disturbance component.

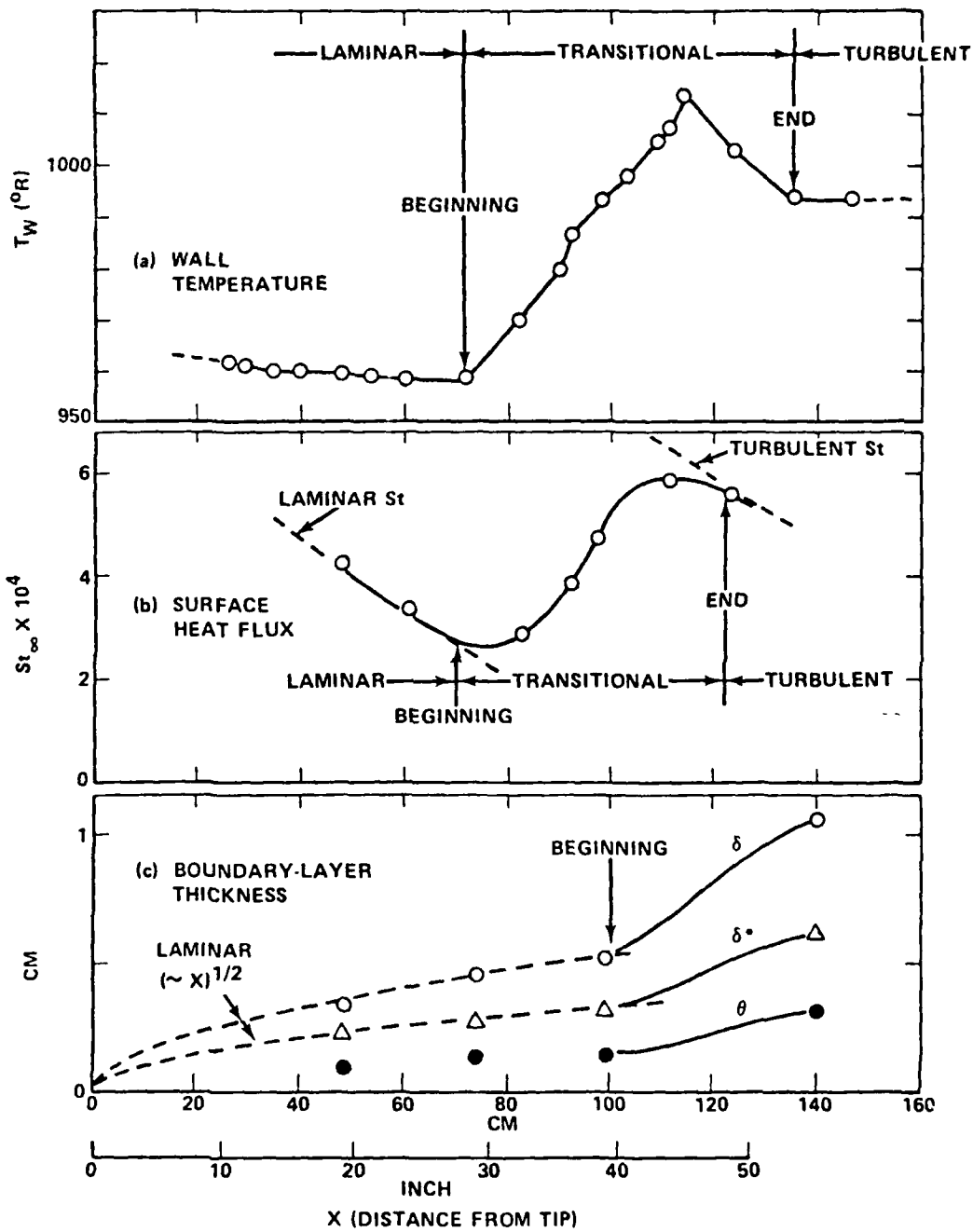


Figure 6. Transition Region by Experimental Method.

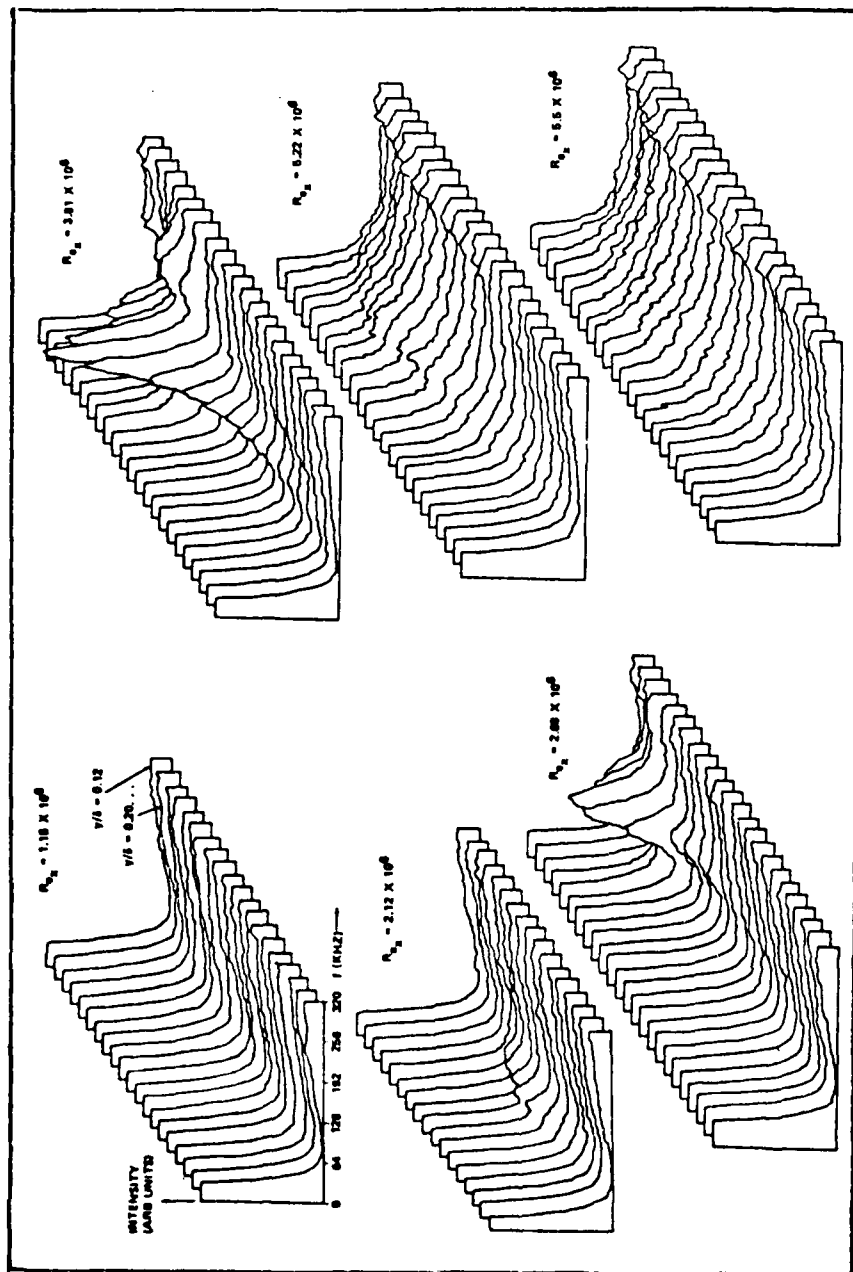


Figure 7. Three-Dimensional View of Spectrum Evaluation in the Boundary-Layer (from Reference 17).

$$Q = Q(\vec{x}) + Q'(\vec{x}, t) \quad (1)$$

The total flow satisfies the time dependent conservation laws of mass, momentum and energy, while the basic flow satisfies the steady boundary-layer equations. Subtraction of the basic flow equations from the total flow equations yields the set of conservation laws satisfied by the disturbances. The resulting partial differential equations are linearized for mathematical analysis. Further simplification of mathematical equations can be done if the fluid flow is assumed to be uniform entropy.¹⁸ In uniform entropy flow, the heat generation by viscous dissipation of mechanical turbulent energy and the production of entropy by internal conduction of heat by non-adiabatic process at the boundary conditions are negligible. Thus, the change in enthalpy can be written as

$$\delta h = \frac{\delta p}{\rho} = a^2 \frac{\delta \rho}{\rho} \quad (2)$$

where p is pressure, ρ is the density, and a is the local isentropic speed of sound.

The continuity and momentum equations can be written in terms of enthalpy, velocity and kinematic viscosity

$$\frac{1}{a^2} \frac{Dh}{Dt} + \nabla \cdot \vec{v} = 0 \quad (3)$$

$$\frac{D\vec{v}}{Dt} = -\nabla h + \nu \nabla^2 \vec{v} \quad (4)$$

where ν = Kinematic viscosity.

$$\frac{D}{Dt} = \frac{\partial}{\partial t} + \vec{v} \cdot \nabla \quad (\text{substantive derivative})$$

The density fluctuation can be considered as acoustic variable in a fluid flow. Generally, in experiment, it is easier to measure the pressure fluctuations that is

propagating with the local speed of sound. Therefore, it is reasonable to split the pressure fluctuations into two parts and identified as pseudosound (unsteady hydrodynamic pressure) and acoustic pressure (which satisfies a wave equation).

$$\partial p = \partial p_{na} + \partial p_a$$

where na and a refer non acoustic and acoustic terms respectively.

Moyal¹⁹ has demonstrated that the components of acoustic and turbulent velocities have different mathematical properties that can be used to break up the equations of motion into two groups of dynamic equations, one describing the acoustic motion and the other describing the turbulent motion. The two types of motion were shown to be coupled through non-linear terms. Therefore, the velocity fluctuations can be divided into acoustic particle velocity, \vec{v}_a , (which is potential) and turbulent velocity, \vec{u} , (which is rotational).

$$\vec{v} = \vec{u} + \vec{v}_a = \vec{u} + \nabla \phi$$

$$\nabla \times \vec{v} = \nabla \times \vec{u} = \vec{\omega}$$

$$\frac{\partial}{\partial t} (\nabla \cdot \vec{u}) = 0$$

and the acceleration term becomes

$$\frac{D\vec{v}}{Dt} = \frac{D\vec{u}}{Dt} + \nabla \left[\frac{D\phi}{Dt} + \frac{|\nabla\phi|^2}{2} \right] - \nabla\phi \times \vec{\omega} \quad (5)$$

where $\frac{D}{Dt} = \frac{\partial}{\partial t} + \vec{u} \cdot \nabla$

ϕ = Acoustic potential

$\vec{\omega}$ = vorticity.

The last term in the acceleration equation shows the coupling between the acoustic and vortical modes in free flow.

Combining Equations (4) and (5), we have

$$\frac{\overline{D}\vec{u}}{\overline{D}t} = -\nabla H + v\nabla^2\vec{u} + \nabla\phi \times \omega \quad (6)$$

where
$$H = h + \frac{\overline{D}\phi}{\overline{D}t} + \frac{|\nabla\phi|^2}{2} - v\nabla^2\phi \quad (7)$$

Combining Equations (7) and (3) a wave equation¹⁸ can be obtained for incompressible flow.

$$\frac{1}{a^2} \frac{\overline{D}^2\phi}{\overline{D}t^2} - \nabla^2\phi - \frac{v}{a^2} \frac{\overline{D}}{\overline{D}t} \nabla^2\phi = \frac{1}{a^2} \frac{\overline{D}H}{\overline{D}t} \quad (8)$$

$$\nabla \cdot \vec{u} = 0 \quad (9)$$

Figure 8 shows the acoustic interaction with a mean parallel shear flow.

$$\vec{u} = \vec{i} u_0(y) + \vec{i} \frac{\partial\psi}{\partial y} - \vec{j} \frac{\partial\psi}{\partial x} \quad (10)$$

$$\vec{\omega} = \nabla \times \vec{u} = -\vec{k} u_0'(y) - \vec{k} \nabla^2\psi \quad (11)$$

where the prime on u_0 refers ordinary differentiation with respect to y . If we take divergent and curl of Equation (6), substitute in Equations (10) and (11), and linearize with respect to small quantities of ψ , H and ϕ , the following equations can be obtained:

$$\nabla^2 H = u_0'' \frac{\partial\phi}{\partial x} + 2 u_0' \frac{\partial^2\psi}{\partial x^2} \quad (12)$$

$$-\frac{D}{Dt} \nabla^2\psi + u_0'' \frac{\partial\psi}{\partial x} + v\nabla^4\psi = u_0'' \frac{\partial\phi}{\partial y} + u_0' \nabla^2\phi \quad (13)$$

In Equations (8), (12) and (13), the acoustic and perturbation vortical modes are clearly separated.

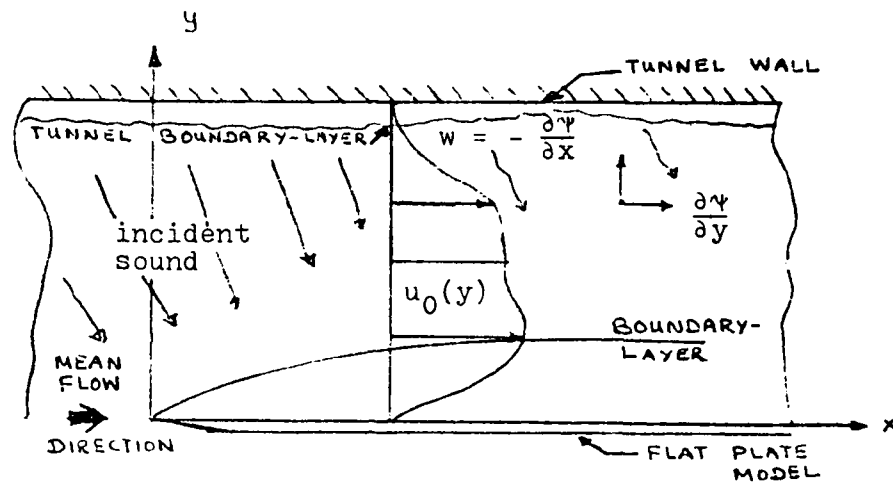


Figure 8. Acoustic Interaction with a Mean Parallel Shear Flow.

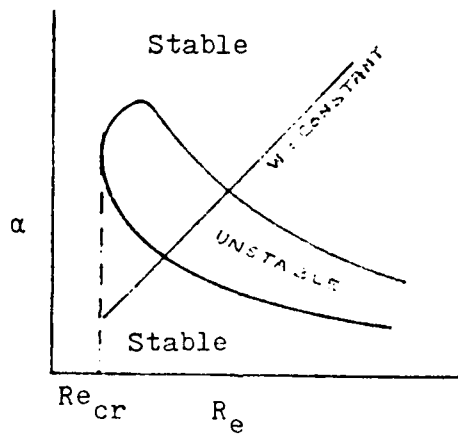


Figure 9. Stability Diagram for a Boundary-Layer Flow.

The left-hand side of Equation (13) is the Orr-Sommerfeld equation and the right-hand side is the acoustic input. Thus, the acoustic interaction can be linked with the generation of Tollmien-Schlichting waves which contribute the forcing function for boundary-layer transition.

For a noise free flow, the Orr-Sommerfeld equation can be solved²⁰ by assuming

$$Q'(\vec{x}, t) = q(y) e^{i(\alpha x + \beta z - \omega t)} \quad (14)$$

where α and β are real or complex wave numbers in x and z directions respectively; ω is real or complex frequency.

The neutral stability curve (α, Re), shown in Figure 9, encloses a region where disturbances with frequencies falling into the region are amplified by conversion of flow energy from the main flow into the boundary-layer disturbance motion, which may be called Tollmien-Schlichting waves. These waves are not acoustic disturbances because their existence is not dependent on the compressibility of the medium. The disturbances falling outside the neutral stability curve decay. The Reynolds number below which all wave numbers are damped is termed the minimum critical Reynolds number.

The right hand side of Equation (13) provides the acoustic interaction on the boundary-layer flow. The radiated noise disturbances from the wind tunnel wall should be modeled in some manner. In general, the acoustic disturbances are not harmonic waves. The generated noise due to moving sound sources^{21,22,23} may be represented as a moving, fluid dynamic type of wavy wall submerged within the shear layer. If there is any influence on the flow stability by acoustic waves, a conversion from the one wave motion into the other is possible in presence of compliant boundary.

For low speed flows, Ribner^{24,18} showed that the total enthalpy of flow field can be related to Reynolds stress as

$$\nabla^2 H = - \frac{\partial^2 u^i u^j}{\partial x^i \partial x^j} \quad (15)$$

In principle, if the Reynolds stress of a flow field is known, the total enthalpy can be calculated from Equation (15). The Acoustic potential can be determined using Equation (8). Then, the Orr-Sommerfeld Equation (13) can be solved for the prediction of transition region.

VI. RECOMMENDATIONS

Although the boundary-layer transition phenomena has received widespread attention, the mechanism involved in the transition process is not completely understood. The complex mathematical and fluid mechanics process inherent in the boundary-layer transition process offers a challenge for theoretical and experimental research. Therefore, the following research projects are recommended:

1. The theoretical model explained in Section V provides a linking mechanism between the acoustic disturbance and the flow vortices. The acoustic interaction with the boundary-layer flow should be analyzed from simple plane wave to random noise by solving Orr-Sommerfeld equation.

2. The frequency spectrum obtained in AEDC wind tunnels can be analyzed and correlated with the acoustic noise parameter (C_F , \bar{c} , δ^* etc.) for transition location and the results should be compared with the theoretical development.

3. The interaction between acoustic noise radiation, curvature of nose cone and the shock structure in supersonic-hypersonic flows should be analyzed based on the experimental data obtained at AEDC. This interaction acts as a disturbing force for the boundary-layer transition.

4. An electro-mechanical noise generator can be used to investigate the transition process by controlling the intensity and the frequency of the noise generator. To start with, a loud speaker can be used to analyze the flow instability in water tunnel. Then it can be extended for compressible flows. According to Mack's²⁵ calculations, it can be expected that the boundary-layer reacts to low frequency long wave length disturbances.

5. In addition to the acoustic interaction with the boundary-layer flow, the effect of wall temperature on the stability should be examined theoretically and experimentally since repeated stabilization and destabilization of boundary-layer occurs as the surface temperature continues dropping.

6. It is interesting to analyze the stability of flow theoretically and experimentally for a spinning nose cone at a given angle of attack.

REFERENCES

1. Pate, S.R., "Dominance of Radiated Aerodynamic Noise on Boundary-Layer Transition in Supersonic-Hypersonic Wind Tunnels," Ph.D Dissertation, The University of Tennessee, Knoxville, 1977.
2. Schopper, M.R., "A Model for the Noise Radiated by Turbulent Boundary Layers and its Interaction with Laminar Layers in Supersonic Flow," AIAA 12th Fluid and Plasma Dynamics Conference, Williamsburg, Virginia, July 1979, Paper No: 79-1523.
3. Schlichting, H. Boundary Layer Theory, 6th Ed. McGraw-Hill, New York, 1968.
4. White, F.M., Viscous Fluid Flow, McGraw-Hill, New York, 1974.
5. Schubauer, G.B., and H.K. Skranstad, "Laminar-Boundary Oscillations and Transition on a Flat Plate," NACA Report 909, 1948.
6. Mack, L.M., "Linear Stability Theory and the Problem of Supersonic Boundary-Layer Transition," AIAA Journal, Vol. 13, No: 3, March 1975, Pp. 278-289.
7. Kendall, J.M. Jr., "Supersonic Boundary-Layer Transition Studies," JPL Space Programs Summary 37-62, Vol. III, 1970.
8. Smith, A.M.O. and Gamberoni, Nathalie. "Transition, Pressure Gradient and Stability Theory," Douglas Aircraft Report No. ES 26388, August 1956.
9. Rogler, H., "Free Stream Vorticity Disturbances Adjusting to the Presence of a Plate - A Quarter - Plane Problem," Journal of Applied Mechanics, Vol. 44, No. 4, December 1977. Pp. 529-533.
10. Rogler, H., "The Interaction Between Vortex-Array Representations of Free-Stream Turbulence and Semi-Infinite Flat Plates," Journal of Fluid Mechanics, Vol. 87, Part 3, Pp. 583-606.
11. Rogler, H.L. and E. Reshotko, "Disturbances in a Boundary Layer Introduced by a Low Intensity Array of Vortices," SIAM Journal of Applied Mathematics, Vol. 28, No. 2, March 1975, Pp. 431-462.

12. Rogler, H.L. and E. Reshotko, "Spacially Decaying Array of Vortices," The Physics of Fluids Journal, Vol. 19, No. 12, 1976, Pp. 1843-1850.
13. Shamroth, S.J. and H. McDonald, "Assessment of a Transition Boundary-Layer Theory at Low Hypersonic Mach Numbers," NASA CR-2131, Langley.
14. Van Driest, E.R. and Blumer, C.B., "Boundary-Layer Transition at Supersonic Speeds: Roughness Effects with Heat Transfer," AIAA Journal, Vol. 6, No. 4, April 1968, Pp. 603-607.
15. Liepman, H.W., "Investigation of Laminar Boundary-Layer Stability and Transition on Curved Boundaries," NACA ACR3H30, August 1943.
16. Dougherty, N.S., Jr. and Fisher, D.F., "Boundary-Layer Transition on a 10-Degree Cone: Wind Tunnel/Flight Data Correlation," AIAA 17th Aerospace Science Meeting, Paper No. 80-0154, January 1980.
17. Demetriades A., "Hydrodynamic Stability and Transition to Turbulence in the Hypersonic Boundary-Layer Over a Sharp Cone," Interim Progress Report, Aeronutronic Ford Corporation, Aeronutronic Publication No. U-6139, April 1975.
18. Yates, J.E., "Application of the Bernoulli Enthalpy Concept to the Study of Vortex Noise and Jet Impingement Noise," NASA CR 2987, April 1978.
19. Moyal, J.E., "The Spectra of Turbulence in a Compressible Fluid; Eddy Turbulence and Random Noise," Cambridge Philosophical Society Proceedings, Vol. 48, 1952, Pp. 329-344.
20. Betchov, R. and W.O. Criminale, Jr., Stability of Parallel Flows, Academic Press, New York, 1967.
21. Laufer, J., "Some Statistical Properties of the Pressure Field Radiated by a Turbulent Boundary Layer," Physics of Fluids, Vol. 7, No. 8, August 1964, Pp. 1191-1197.
22. Ffowcs Williams, J.E., "The Noise From Turbulence Convected at High Speeds," Phil. Trans. Roy. Soc. (London) A255, April 1963, Pp. 469-503.

23. Phillips, O.M., "On the Generation of Sound by Supersonic Turbulent Shear Layers," Journal of Fluid Mechanics, Vol. 9, Part 1, 1960, Pp. 1-28.
24. Ribner, H.S., "The Generation of Sound by Turbulent Jets," Advances in Applied Mechanics, Edited by H.L. Dryde and Th. Von Karman, Academic Press, New York, 1964, Pp. 103-182.
25. Mach, L.M., "Progress in Compressible Boundary Layer Stability Computations," Proceedings of Boundary-Layer Transition Workshop, Vol. IV, Aerospace Corp., California, 1971 Pp. I-1 to I-36.

1981 USAF-SCEEE SUMMER FACULTY RESEARCH PROGRAM

Sponsored by the

AIR FORCE OFFICE OF SCIENTIFIC RESEARCH

Conducted by the

SOUTHEASTERN CENTER FOR ELECTRICAL ENGINEERING EDUCATION

FINAL REPORT

AN EVALUATION OF THE AIR FORCE PAVEMENT
NON-DESTRUCTIVE TESTING METHOD

Prepared by: Dr M. C. Wang
Academic Rank: Associate Professor
Department and University: Department of Civil Engineering
Pennsylvania State University
Research Location: Air Force Engineering and Services Center/RDCF
Tyndall Air Force Base, Florida 32403
USAF Research Colleague: Mr H. R. Marien
Date: August 14, 1981
Contract No: W49620-79-C-0038

AN EVALUATION OF AIR FORCE PAVEMENT
NON-DESTRUCTIVE TESTING METHOD

by
M.C. Wang

ABSTRACT

The strengths and weaknesses of the current Air Force non-destructive pavement testing (NDPT) method have been reviewed, and its effectiveness for routine applications has been evaluated.

The NDPT method is composed of two main components -- the data collection equipment and the PREDICT computer code. The data collection equipment contains an impulse loader with the necessary instrumentation and a desk-top computer for preliminary data analysis and evaluation. The entire equipment is housed in a van which is air transportable and therefore satisfies the Air Force's need of rapid worldwide deployment. The PREDICT is a finite element program which is capable of performing nonlinear analysis for both rigid and flexible pavements.

It is concluded that the current NDPT method is an effective tool for evaluating a pavement's structural capacity in terms of fatigue life. However, further improvement is needed. Recommendations for the improvement are offered.

ACKNOWLEDGMENTS

The author gratefully acknowledges the opportunity of this summer faculty research provided by the Air Force Systems Command, the Air Force Office of Scientific Research, and the Southeastern Center for Electrical Engineering Education. He would like to thank the Air Force Engineering and Services Center at Tyndall AFB for providing the necessary facilities and pleasant environment for conducting the research.

The author also likes to express his sincere appreciation to his research colleague, Mr H. R. Marien of AFESC, for his efforts of providing the needed research literature and making lodging arrangements. AFESC personnel, in particular, Messrs. L. M. Womack, P. T. Nash, J. R. Van Orman, and J. L. Greene, Capt J. D. Wilson, 1Lt R. A. McDonald, Maj J. A. Centrone, Capt T. E. Bretz, Jr., and LtCol J. K. Morrows, as well as others make this research one of the most enjoyable and productive summer research experience. For all of their support, the author wishes to convey to them the warmest thanks.

Mr H. R. Marien, Capt J. D. Wilson, and DEMP personnel reviewed the report and made valuable comments.

I. INTRODUCTION

According to Hanson [14], the U.S. Air Force owns enough airfield pavements to be able to build a 200-foot wide runway stretching from the State of Washington to the southern tip of Florida. These pavements need constant maintenance in order to satisfy their requirements of supporting the ever-increasing loads and numbers of aircraft operation. An essential element in pavement maintenance is to evaluate the structural (or load carrying) capacity of the pavement at any time. Present Air Force pavement maintenance operation requires California Bearing Ratio (CBR) tests on the base, subbase, and subgrade for flexible pavements and plate bearing tests on the subgrade for rigid pavements, both conducted in test pits [11]. This method of evaluation is very time consuming and is also destructive to the pavements.

The inherent drawbacks of the current destructive evaluation method have motivated the Air Force to develop an evaluation technique with which the necessary field data can be obtained quickly and also nondestructively. The Air Force's research for the development of nondestructive pavement evaluation technique was initiated in the late 1960's. Since then, a package of evaluation method has been developed. The nondestructive pavement testing (NDPT) method has been used to evaluate numerous pavement sections, both rigid and flexible, and the results of evaluation were compared with the conventional destructive evaluation procedure. It was found that the predicted load repetitions to failure, although in the same order of magnitude, differ significantly between the two methods for some cases [27].

II. OBJECTIVES

The primary objective of this research is to determine whether the current nondestructive pavement testing method satisfies the

Air Force's need. Specifically, the effectiveness of the NDPT program for routine applications is evaluated with regard to its degree of sophistication and the ease of use. Also, recommendations for possible improvement are offered.

III. NDPT PROGRAM

The Air Force NDPT program contains two main components -- data collection equipment and analytical method [27]. Principal features and the strengths and weaknesses of each component are reviewed below.

III.1 Data Collection Equipment

The data collection equipment is used primarily for evaluation of in-situ elastic constants (Young's modulus and Poisson's ratio) of each pavement constituent material. The elastic constant values are essential input data for the analytical method which determines the structural capacity of existing aircraft pavements.

The original test equipment was a vibrator which could be operated at a broad range of frequency of excitation with a wide range of loading intensity. The vibratory equipment was housed in the Civil Engineering Research Facility (CERF) NDPT van. The van contained the vibrator, its supporting equipment, and the instrumentation, recording and monitoring equipment. The entire system was large and not airtransportable. With this equipment, four different types of tests could be performed [31].

1. Load-deflection tests at a constant frequency.
2. Resonant frequency tests.
3. Deflection basin tests.

4. Wave propagation tests.

The wave propagation test provides dispersion curves which relate wave velocity with wave length. From these dispersion curves, the elastic modulus of each pavement constituent layer is computed. Although the computation of elastic modulus is simple, the interpretation of dispersion curves for modulus calculation is not easy and straightforward. Various approaches of data interpretation are available; however, no matter which approach is used, successful interpretation always requires correct engineering judgment [33, 41].

At the time the CERF NDPT van was fully developed, transient wave propagation behavior had become better understood and reliable instrumentation for measuring transient phenomena had become readily available. For these reasons, the development of a new test equipment using impulse loading technique to replace the steady-state vibrator was initiated in 1977 [34].

The new impulse loader has a drop weight which can be varied from 100 to 500 pounds and a drop height varying from 0 to 36 inches. The operation principle of this impulse loader is similar to the various falling weight deflectometers, described by Moore et al. [30], and Hoffman and Thompson [20]. The pavement response to the impulse loading is measured by using accelerometers which are mounted on the pavement surface. The entire test equipment is housed in a van which is easily transportable in C-130 aircraft. Detailed accounts of the equipment and operation procedures are given by Marien and Baird [27].

The measured pavement response to impulse loading is given in terms of acceleration versus time relationship. The acceleration-time data are analyzed by using Discrete Fourier Transform (DFT) technique [40] to obtain the phase angle versus frequency relationship which is then used to develop the dispersion curve. All

of these plots are done by a desk-top computer immediately after the field data are collected. From the dispersion curve, the shear wave velocity propagating through the pavement is obtained and the shear modulus of each pavement constituent material is computed by using the following equation:

$$G = \rho v_s^2 = \left(\frac{\gamma}{g}\right)v_s^2 \quad (1)$$

where

G = Shear modulus of pavement material

v_s = Shear wave velocity

ρ = Mass density of pavement material

γ = Unit weight of pavement material

g = Gravitational acceleration

Young's modulus of the pavement material is computed as follows:

$$E = 2(1 + \nu)G \quad (2)$$

where

E = Young's modulus of pavement material

ν = Poisson's ratio of pavement material

For the surface layer, the velocity of Rayleigh wave is more easily obtained from the dispersion curve. Thus, the shear wave

velocity is usually computed from the Rayleigh wave velocity by using the equation below:

$$v_s = \frac{v_R}{a} \quad (3)$$

where

v_s = Shear wave velocity

v_R = Rayleigh wave velocity

a = Constant which is a function of Poisson's ratio and varies almost linearly from 0.875 at $\nu = 0$ to 0.955 at $\nu = 0.5$ [12]

Since pavement response to impulse loading is measured from the pavement surface, the effect of surface layer on the shear wave velocity obtained from the dispersion curves for the base course material should be considered. For this consideration, the following equation is used to adjust the shear wave velocity in the base course of rigid pavements:

$$v_{s2} = \sqrt{\frac{Y_1}{G_1} \frac{G'_2}{Y_2}} v_{s2}' \quad (4)$$

where

v_{s2} = Actual in-situ shear wave velocity in the base course

v_{s2}' = Shear wave velocity of the base course as indicated by the dispersion curve

G_1 = Shear modulus of the surface layer

G_2' = Shear modulus of the base course as computed from v_{s2}'

$$\text{i.e., } G_2' = (\gamma_2/g) v_{s2}'$$

γ_1 and γ_2 = Unit weights of the surface and base course materials, respectively

From the steady-state vibratory loading tests, the Young's modulus of base course material in rigid pavements can also be corrected by using the following approximate equation [33]:

$$E_2 = (E_2')^2/E_1 \quad (5)$$

where

E_2 = Adjusted Young's modulus of the base course material

E_2' = Young's modulus determined from shear wave velocity obtained from the dispersion curve

E_1 = Young's modulus of the surface layer

The preceding methods of correction are proposed for rigid pavements only. For flexible pavements, the modulus values determined from vibratory tests are found to be about twice as high as the practical range of the modulus values. Therefore, it is suggested that the moduli of surface, base, and subgrade materials determined from the steady-state vibratory loading tests be reduced by 50 percent [31].

Poisson's ratios of the pavement constituent materials can also be computed from dispersion data using the following equation

[9]:

$$\nu = \frac{v_r^2 - 2}{2(v_r^2 - 1)} \quad (6)$$

where

ν = Poisson's ratio

v_r = Ratio of compressional wave to shear wave velocity

However, in almost all cases, the computed Poisson's ratios are larger than the values determined from triaxial tests [31]. Therefore, the values of Poisson's ratio used in pavement response analysis are usually assumed rather than computed from the dispersion data.

The entire data collection equipment including the impulse loader with the necessary instrumentation and a desk-top computer for preliminary data analysis and evaluation is housed in a van which is readily transportable in C-130 aircraft as mentioned earlier. This high degree of mobility is an important feature for the Air Force to satisfy their routine maintenance evaluation of airfield pavements. Another salient feature of the equipment is that the system is operated by a programmable controller so that the drop height can be varied very easily. The weight of falling mass can also be adjusted by putting on and taking off the weights which have two different sizes -- 32.7 and 67.2 pound a piece. Furthermore, the accompanied instrumentation can be used to monitor pavement response at different locations up to eight points.

At present, an obvious weakness of the system is the lack of an adequate procedure for determination of modulus of elasticity from the impulse loading test. Previous experience with the

steady-state vibratory loading test indicates that except for portland cement concrete the elastic modulus computed from the wave velocity data must be reduced by an arbitrary factor of 50 percent. An apparent cause for the higher than normal modulus value is the viscoelastic behavior of the pavement materials. Because of the use of impulse loading in the new testing equipment, whether or not the modulus computed from the impulse loading test results will need a similar arbitrary reduction is not yet known [1].

III.2 Analytical Method

The analytical method essentially is the computer code named PREDICT. Included in the PREDICT code are three major computer programs which will be described later. In one of the main computer programs is incorporated the constitutive equations of base and subgrade materials which are reviewed below.

III.2.1 Constitutive Equations

Because the strain inside the pavement induced by the impulse loader is relatively small compared with that of aircraft loading, the values of Young's modulus determined from the field test need be adjusted so that the modulus values will be compatible with the strain level that exists under the aircraft loading. This is particularly essential for materials such as soil, gravel, and asphalt concrete which, generally speaking, have nonlinear stress-strain behavior. For this reason, constitutive equations for soils and gravels are developed and are incorporated into the PREDICT computer code. Main features of the constitutive equations follow.

The constitutive equations of subgrade and base course materials were developed by Hardin [15, 16, 17] based on the results of one-way simple shear tests on subgrade soils and resonant

column tests on base course materials including sand and gravel. The test specimens had a range of dry density and water content that normally exists in the field. For the study on subgrade soils, hollow cylindrical specimens were prepared and loaded torsionally about the axis of the cylinder. The test specimens had outside and inside diameters of 7.32 cm and 3.58 cm, respectively, with a length of 5.13 cm. The desired states of stress were obtained by applying a torsional stress and stationary pressures inside and outside the cylindrical specimens. The rate of torsional loading varied from 0.2 to 450 kg/cm/h, and the shear strain amplitude ranged from 10^{-5} to 5×10^{-3} .

The resonant column tests were performed on two different specimen sizes -- 6-inch diameter with 12-inch length for gravel and sand, and 1.4-inch (or 2.8-inch) diameter with 3-inch length for sand. In this series of tests, the test specimens were subjected to torsional vibration about its long axis for various levels of shear strain amplitude up to a maximum of 4.5×10^{-4} . The frequency of vibration was varied to obtain a resonant condition. The resonant frequency was then used to compute the shear modulus of the test specimen. The tests were conducted under various confining pressures up to 4 bars (59 psi).

Results of the study mentioned above indicate that the hollow cylinder shear test and the resonant column test produce comparable results [17], and that the constitutive relations can be given in terms of the normalized shear modulus and normalized shear strain as shown in Figure 1 which is the graphical representation of the following equations:

$$\frac{G}{G_{\max}} = \frac{1}{1 + \gamma_h} \quad (7)$$

where

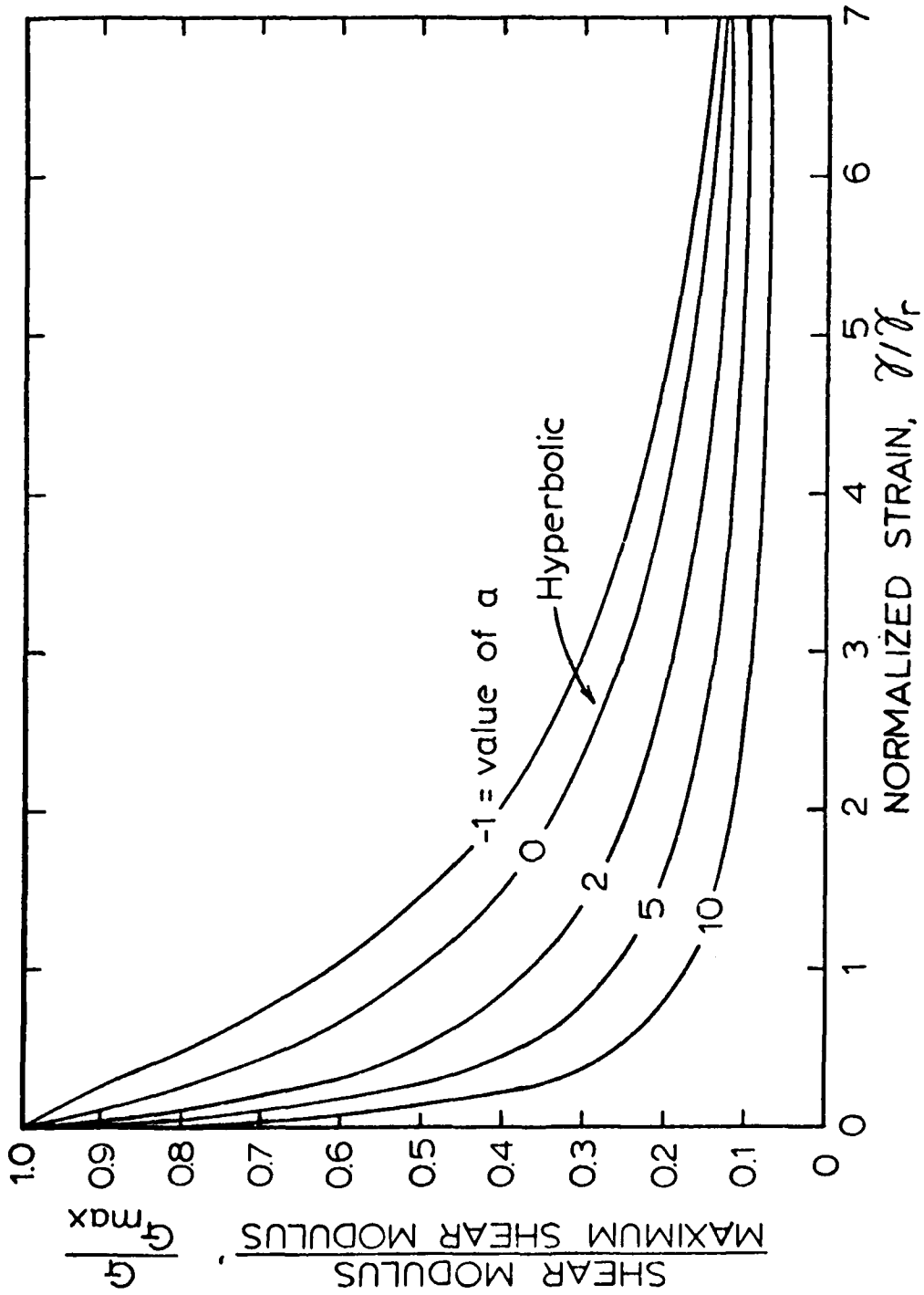


Fig. 1 Normalized Shear Modulus VS Normalized Shear Strain Relationship (after Hardin 1973b)

$$\gamma_h = \frac{\gamma}{\gamma_r} \left\{ 1 + a \text{Exp} \left[- \left(\frac{\gamma}{\gamma_r} \right)^{0.4} \right] \right\} \quad (8)$$

G = Shear modulus

G_{max} = Maximum shear modulus which is equal to the initial tangent modulus or secant modulus for strain amplitude equal to or less than 10⁻⁵

γ = Shear strain

γ_r = Reference strain defined as the ratio of shear strength in simple shear to maximum shear modulus; its value is a function of plasticity index, grain size distribution, void ratio, and degree of saturation as given in the following:

$$\gamma_r = \frac{G_{\max}}{F^2 R^2} [0.6 - 0.25 (PI)^{0.6}] \quad (9)$$

in which $F = \frac{(2.973 - e)^2}{1 + e}$ (10)

R = 1100, for sands with <15% fines

R = 1100 - 6S, for cohesive soils with >15% fines

PI = Plasticity index

e = Void ratio

S = Degree of saturation in percentage

a = Constant depending on various factors including soil type, gradation, degree of saturation, number of loading cycles, and strain time as shown in Table 1.

Meanwhile it is found that the maximum shear modulus in Equation (7) can be estimated by using the following equation:

$$G_{\max} = Y [2 + D_5^{(\sigma_o^{-0.2/3})}] \frac{(2.973 - e)^2}{1 + e} \sigma_o^{0.5} \quad (11)$$

in which

G_{\max} = Maximum shear stress in bars

σ_o = Effective mean principal stress in bars

e = Void ratio

D_5 = Grain size in mm corresponding to 5 percent passing

Y = Parameter depending on particle composition

It is suggested, however, that for practical applications of these constitutive equations in pavement evaluation the maximum shear modulus be obtained from in-situ impulse loading tests. Other data needed in the pavement evaluation are material properties including plasticity index, gradation, void ratio, and degree of saturation, number of loading cycles, and strain time. The needed material properties can be determined from undisturbed core samples or estimated from available knowledge on the pavement materials. The number of loading cycles may be estimated from

Table 1
VALUES OF CONSTANT "a"

<u>Soil Type</u>	<u>a</u>
Highly plastic soils with liquid limit >50	$0.2 (1 + 0.02S) T^{0.75}/N^{0.15}$
Low-plasticity soils and nonplastic soils with fines	$1.6 (1 + 0.02S) T^{0.2}/N^{0.6}$
Clean dry sands	$[(3.85/N) - 0.85] T^{0.025}$
Clean gravel and poorly graded sand/gravel mixtures with some fines	2.0
Well-graded sand/gravel mixtures with some fines	5.0

S = degree of saturation in percentage

N = number of loading cycles

T = time in minutes to reach a normalized strain of unity

traffic data; and the strain time must be evaluated from the aircraft speed.

According to Hardin [17], these constitutive equations are not as well defined for highly plastic soils with a liquid limit greater than 50 as for other soils, since the error involved in the determination of reference strain may be greater than 100 percent. Thus, there is a need to improve these equations so that they will be applicable to highly plastic soils equally well. Furthermore, the constitutive equations are developed primarily based on the results of simple shear tests. While simple shear condition may occur in the pavement under aircraft loading, it is generally believed that the actual state of stress inside the pavement is in a more complex form. Available data [28], indicate that the behavior of soils under triaxial compression differs from that under simple shear. Therefore, it is important that these constitutive equations be validated under triaxial state of stress condition.

Despite the need for the above mentioned improvement, there are two important features associated with the constitutive equations. These are: (1) most important variables influencing stress-strain behavior have been considered in the equation development, and (2) the equations are in a rather simple form so that they can be easily implemented for pavement evaluation. Additionally, these equations have been tested under several different loadings with mixed amplitudes and rest periods. For practical purposes, these equations can be applied to mixed traffic conditions.

III.2.2 PREDICT Computer Code

PREDICT is the finite element computer program for evaluating the load carrying capacity and for predicting the remaining ser-

vice life of an airfield pavement. In the analysis, the pavement is idealized as a layered prismatic solid and the aircraft loading is approximated by a periodic function. With this idealization, the pavement system having infinite length and depth is reduced to a structure with finite dimensions; Figure 2 illustrates this idealization with a C-5A aircraft loading. This reduced structure is then replaced by a system of prismatic elements as shown in Figure 3 [7]. The cross section area and material properties are constant throughout the entire element.

The entire computer code is composed of three main programs -- AFCAN, AFPRE, and AFPAV and a subroutine RESULT. Of these programs, AFCAN provides aircraft loading data for computation; AFPRE generates the finite element mesh, boundary conditions and load parameters for input into AFPAV which is a finite element program used to analyze pavement response; and RESULT is for performing fatigue analysis [27, 32, 33].

III.2.2.1 AFCAN Program

The AFCAN computer program has a series of subroutines for instruction of element mesh generation and for characterization of aircraft loading. In addition, the AFCAN data input cards contain pavement layer thicknesses, material properties, and nonlinear material properties.

The aircraft loading is characterized by Fourier series. Each aircraft has its own subroutine which contains the following code variables:

NUMCOS = number of cosine terms in the Fourier series

NELOAD = number of elements under the wheel (x-y plane)

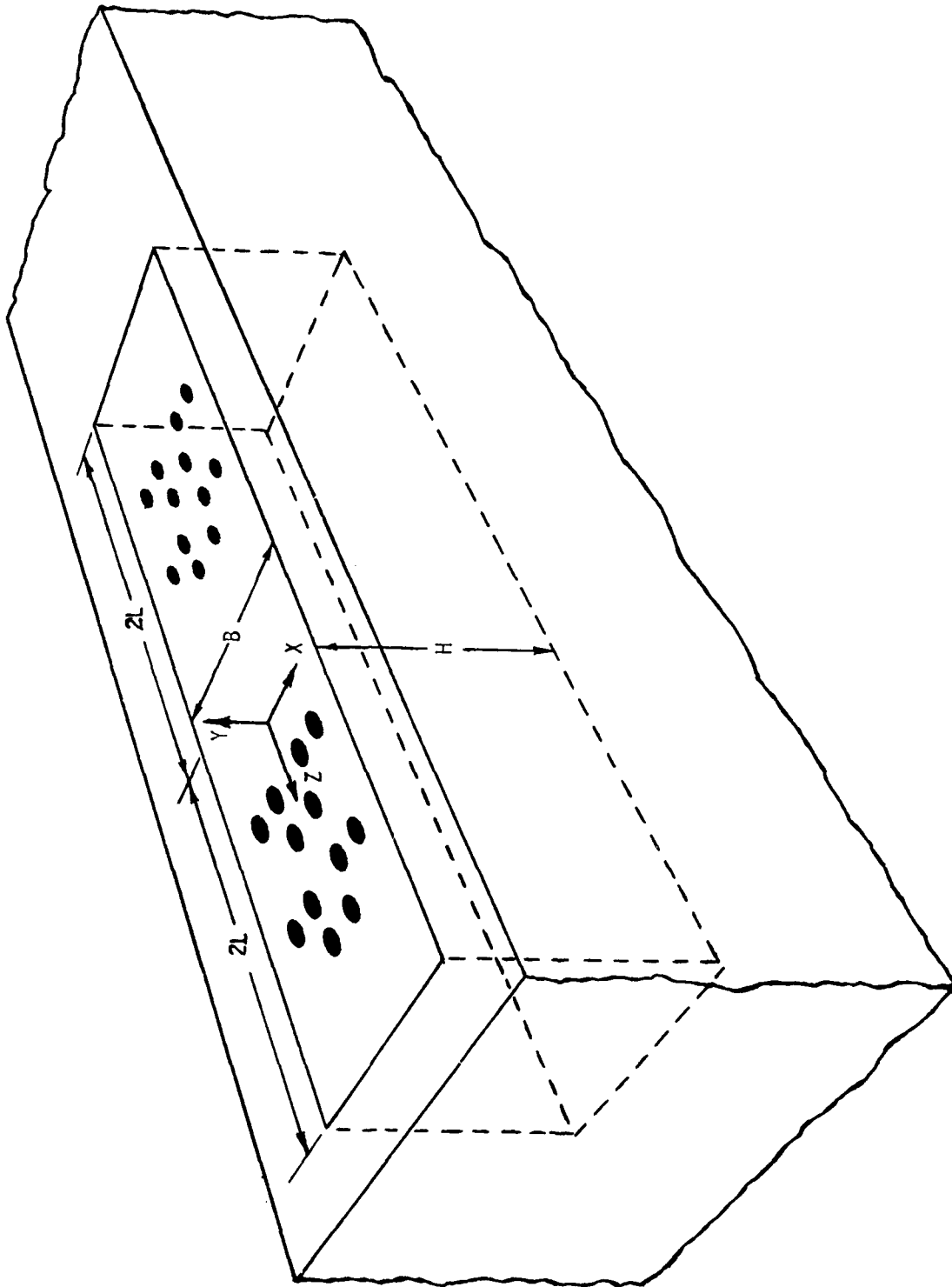


Fig. 2 Pavement Structure Idealized as Prismatic Solid (after Crawford 1975)

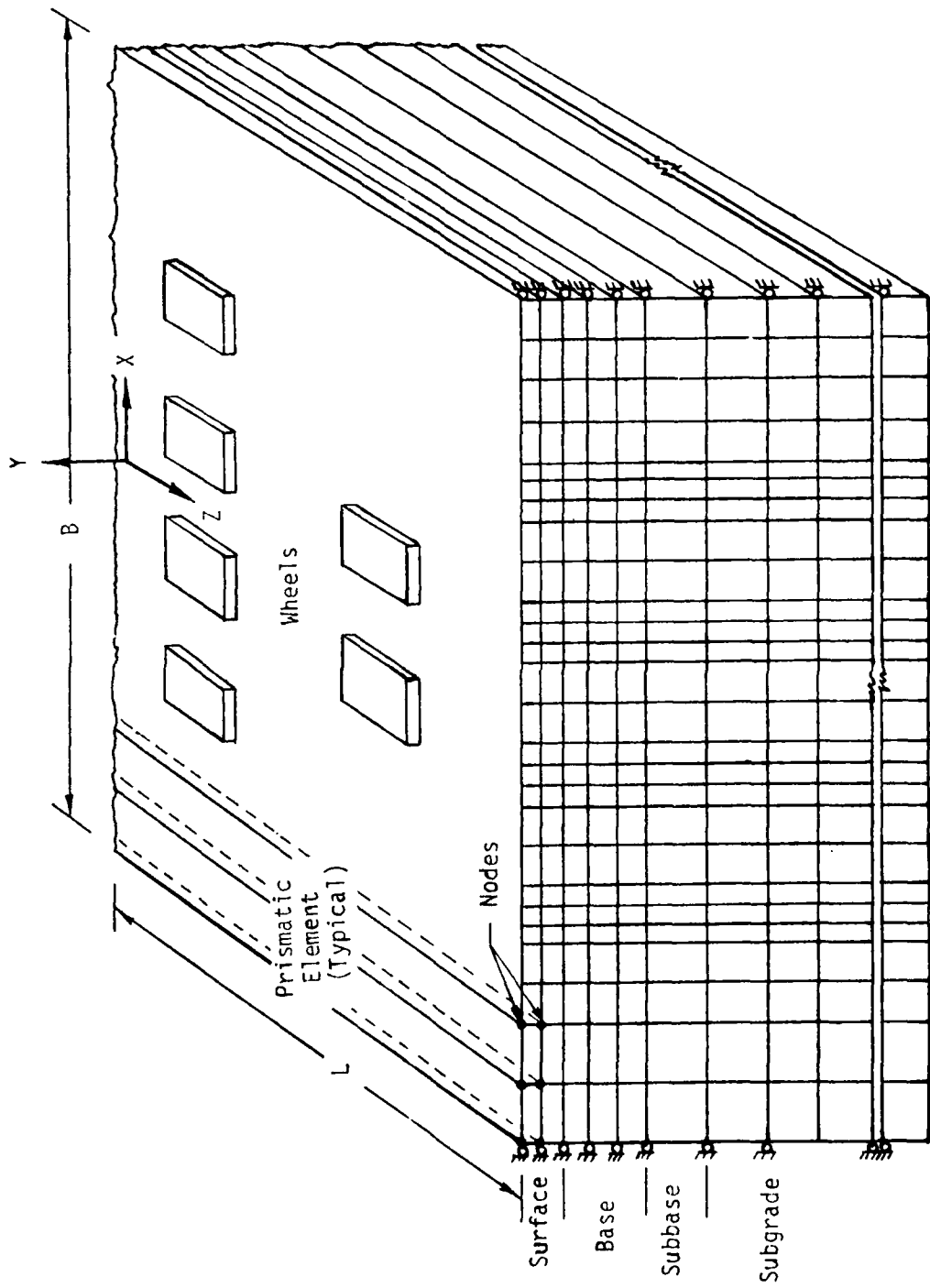


Fig. 3 Finite-Element Idealization of Pavement Structure (after Crawford 1975)

NUMELX = number of elements along the x-axis

WLOAD = wheel load

ZLEN = half period of the Fourier series

The Cartesian coordinates used in the computer program is such that the pavement cross-section is in the x-y plane and the pavement surface in the x-z plane. The depth of the mesh is arbitrarily set at 12 feet, but it can be changed, if necessary. The half-width of the mesh (XLEN) is also arbitrarily established at 25 times the half-width of the tire (XLEND) for a single wheel load. The number of column elements (NUMELX) is set in each aircraft subroutine. These values of the variables are selected on the basis of engineering judgment, the accuracy of computation results, and the cost of computation; no theoretical guidance is available for making these decisions.

The wheel loads are situated to produce symmetrical loading conditions with respect to x-y and y-z planes, and are replaced by an equivalent set of forces acting at the nodes directly under each wheel. The symmetrical loading condition requires that the Fourier series take the form of an even function in which the coefficients are given by

$$a_n = \frac{2}{p} \int_0^p f(z) \cos \left(\frac{n\pi}{p} \right) z dz \quad (12)$$

where

p = half-period of the function (ZLEN)

n = number of terms (NUMCOS)

$f(z)$ = Tire pressure (PSINOM) which is expressed in terms of Fourier series as follows

$$Fu_1 = \sum_{n=1}^n a_n \cos \left(\frac{n\pi}{p} \right) z \quad (13)$$

where Fu_1 is the force at node 1 which produces a displacement in the y -direction.

Values for tire pressure (PSINOM), wheel load (WLOAD), tire length (ZLENLD), and half-width of the tire (XLEND) are determined based on landing gear data for the particular aircraft at maximum take-off gross weight given by Hay [18] and are included in AFCAN as the standard constants. However, other values for WLOAD and PSINOM can be entered into AFCAN. When values of other than the standard constants are entered, new values of XLEND and ZLENLD will be calculated by the computer program.

For multiwheeled landing gears, the wheel loads are considered to be periodic functions, and the tire pressure diagram in the y - z plane are modeled by a Fourier series. The constants used to model the tire pressure diagram for each aircraft are shown in Table 2. These constants are selected after an overall consideration of pavement response, load modelling, boundary stress, and computation cost. According to Nielsen and Baird [33], the decisions which led to the selection of these variables are subjective. Therefore, these values may differ from those selected by other people.

III.2.2.2 AFPRE Program

The airfield preprocessor (AFPRES) program is used to generate finite element mesh and load parameters for the AFPAS program. There are two data generation schemes -- single-wheel scheme for

Table 2. Summary of Aircraft and Load Function Constants Used in AFCAN

Aircraft	WLOAD, lb	PSINOM, psi	NUMCOS	ZLEN, in	Cycles per Coverage	
					Taxiways	Runways/Aprons
F-4	27,000	265	5	43.12	7.36	13.38
F-15	23,400	260	5	40.52	7.73	14.13
F-16	15,000	275	5	31.55	9.56	17.79
F-105	23,400	220	5	44.08	7.25	13.19
F-111	47,000	150	5	75.61	4.77	8.21
FB-111A	54,000	215	5	67.68	5.16	9.00
B-1	40,500	195	9	92.00	2.45	3.50
B-52	67,100	285	9	118.00	1.12	2.85
B-57	27,700	152	5	57.66	5.85	10.37
B-747	41,600	204	10	90.00	2.57	3.63
C-5	30,100	115	15	285.00	1.35	1.66
C-9A	25,800	148	10	60.00	4.43	6.75
C-130	41,900	95	12	102.00	2.12	3.53
C-141	37,400	180	10	62.00	2.25	3.31
KC-97	44,500	180	10	70.00	4.43	6.75
KC-135	35,500	155	8	90.00	2.24	3.24
T-38	5,650	250	5	20.30	14.11	26.89

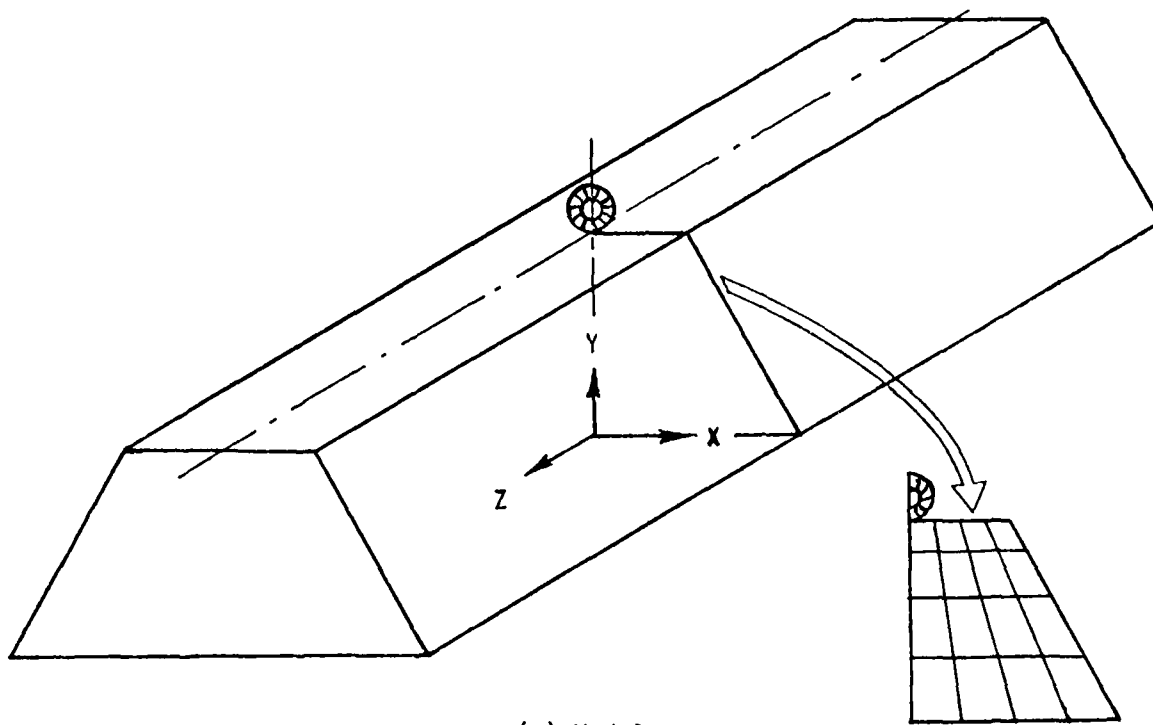
single-wheel aircraft and multiwheel scheme for multi-wheel aircraft [6]. In the single-wheel scheme, the pavement is treated as a uniform prismatic solid of trapezoidal cross-section as shown in Figure 4. In the multiwheel scheme, the pavement is divided into three regions -- surface, base, and subgrade. Within the surface region, materials, nodes, elements, and boundary conditions are arbitrary. In the base region, materials, nodes, elements, and boundary conditions are restricted to uniform horizontal layers. The subgrade region is one homogeneous material of trapezoidal cross section. Figure 5 illustrates the multiwheel scheme for C-5A aircraft loading.

AFPRES contains a series of subroutines such as SWMESH, MWMESH, and FLOAD. SWMESH reads the single-wheel data cards and generates the single-wheel mesh. MWMESH reads the multiwheel data cards and generates the multiwheel mesh. FLOAD calculates the Fourier coefficients and plots the Fourier representation of a given aircraft loading. There are also subroutines to read the material and temperature cards, to compute various quantities needed by AFPRES such as thermal strain and gravity forces, and to do various other tasks. Details of the AFPRES program are described by Nielsen [32].

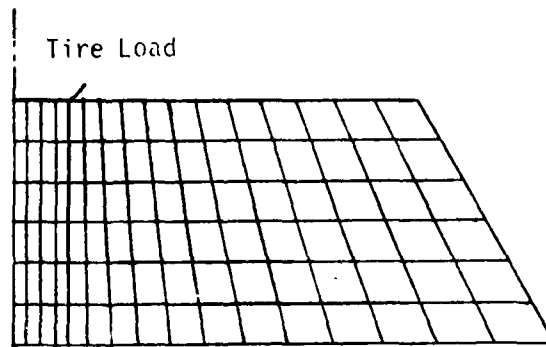
III.2.2.3 AFPRES Program

Program AFPRES is the core of the PREDICT computer code. This program is an extension of that developed by Herrmann [19]. Detailed formulation of AFPRES can be found from research reports by Pichumai [37] and Crawford [7]; the input instruction and program flow chart are given by Crawford [8] and Nielsen [32].

The constitutive equations presented in a previous section are incorporated into the AFPRES program so that the nonlinear stress-strain behavior of the pavement materials can be taken into consideration. In the analysis, the nonlinear relationship between

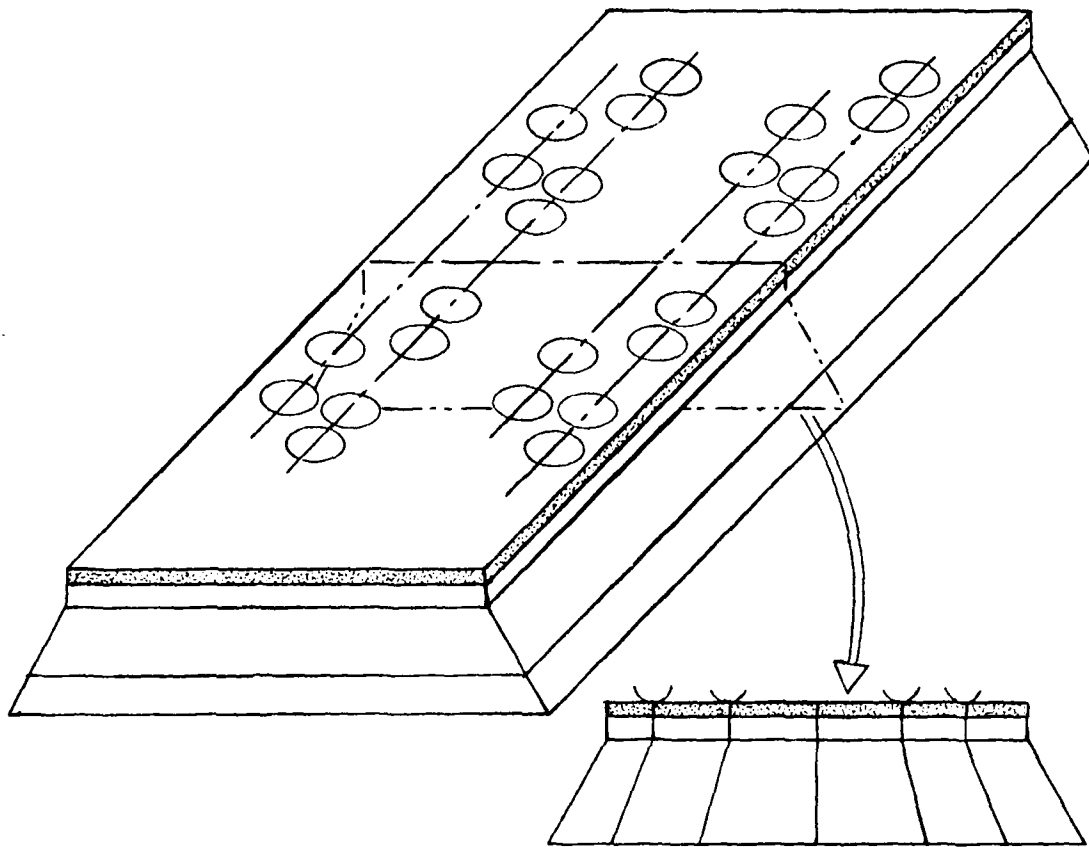


(a) Model



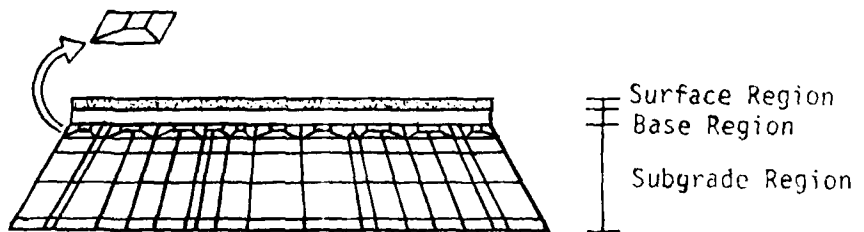
(b) Finite-Element Mesh

Fig. 4 Single-Wheel Problem (after Crawford 1972)



(a) Model

Transition Element



(b) Finite-Element Mesh

Fig 5 C-5A Aircraft Gear (after Crawford 1972)

normalized shear strain given in Figure 1 is divided into a series of segments (or steps) and each segment is approximated by a straight line. In other words, the nonlinear analysis is approximated by a series of linear-like analysis. For each step, the loading and geometric conditions are identical but the shear modulus varies. The shear modulus for a given step is obtained by entering the shear strain value computed in the preceding step into the constitutive relationship (Figure 1). For the first step of analysis, the shear modulus is taken to be the modulus value obtained from the field impulse loading tests. Under normal conditions, three to four steps of linear-like analysis are sufficient to provide satisfactory results.

It should be noted that the shear strain varies not only from element to element but also with different values of z within each element (see Figure 5). Since the shear modulus decreases with increasing shear strain as depicted by Figure 1, a conservative approach of analysis is to use the maximum shear strain in each element to find the shear modulus for the element. Therefore, it is important that the selected z values (or stations) in the calculation must encompass the locations of the largest shear strains.

AFPAV also contains provisions for consideration of no-tension materials and pavement joints effects, and for analysis of gravitational and thermal strains. For the analysis of no-tension materials, the maximum compressive strains (ϵ_x , ϵ_y , and ϵ_z) computed in each step are compared with the tension cutoff strain specified for each material. When any of the compressive strains exceeds the tension cutoff strains, the element stiffness associated with that particular compressive strain is reduced by a factor of 1000. The stiffness associated with shear strains (γ_{xy} , γ_{yz} , and γ_{zx}), however, remains unchanged regardless of tension cracking.

Joints in rigid pavements are modeled as shear connectors with certain values of shear modulus to approximate the stiffness of the joint. The assigned shear modulus of the joint should be such that the measured or known pavement performance at the joint is produced. Therefore, a trial and error procedure is usually needed to obtain an adequate shear modulus for the shear connector [7].

The gravity force is computed by multiplying the mass density of the material by the volume of the element and the acceleration constant of gravity. The force that computed is then distributed to the nodes for computation of gravitational strains. The thermal strain of each element is computed from the temperature in the element and the thermal coefficient of the material. The computed gravitational and thermal strains are added to the strains produced by the aircraft loading to obtain the total strains. The total strains are then used to determine the nonlinear shear modulus.

It should be pointed out that although the nonlinear analysis considers the variation of Young's modulus with strain level, Poisson's ratio is assumed to be constant with respect to the state of stress and strain level. Also, as mentioned earlier, the values of Poisson's ratio used in the analysis are assumed rather than computed from field test data.

III.2.2.4 RESULT Subroutine

The RESULT subroutine contains all elements of fatigue analysis. This subroutine searches for the maximum value of pavement response from the results of AFPV computation. For flexible pavements, the critical responses searched are the maximum tensile strain in the surface layer and the maximum vertical compressive strain in the subgrade. For rigid pavement, the maximum tensile stress in the concrete layer and the maximum compressive strain in the subgrade are obtained. The results of this search are

AD-A113 789

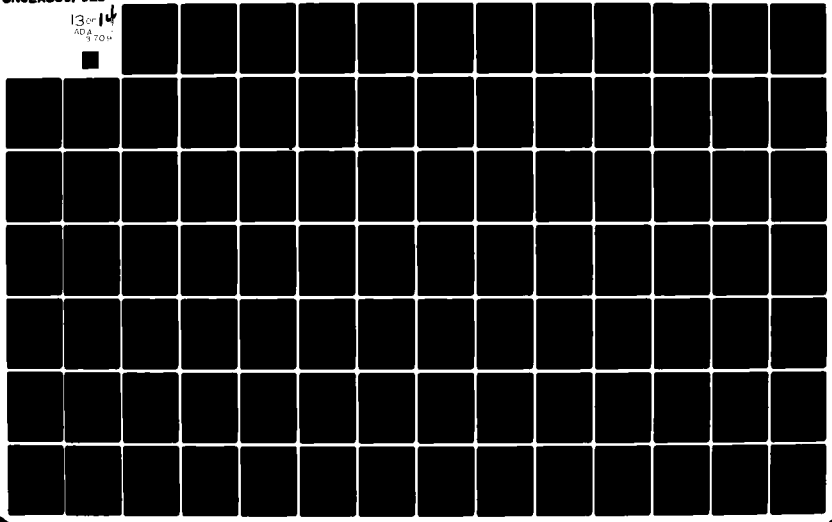
SOUTHEASTERN CENTER FOR ELECTRICAL ENGINEERING EDUCAT--ETC F/6 5/1
USAF SUMMER FACULTY RESEARCH PROGRAM. 1981 RESEARCH REPORTS. V0--ETC(U)
OCT 81 W D PEELE F49620-79-C-0038

UNCLASSIFIED

AFOSR-TR-82-0228

NL

13 of 14
204
1700



printed in a format which indicates the z-station (ZPLANE) at which the values are maximum.

The subroutine also contains the following criteria:

(1) Fatigue failure will occur in a bituminous concrete pavement when the maximum tensile strain in the surface layer reaches a critical value. According to Monismith and McLean [29], the critical strain value is a function of the modulus of elasticity of the bituminous concrete and the number of stress repetitions as shown in Figure 6.

(2) For concrete pavements, fatigue failure will develop when the maximum tensile stress in the concrete layer reaches a certain percentage of the modulus of rupture of the concrete. Packard [36] provides the relationship between the ratio of maximum tensile stress to the modulus of rupture and the number of stress repetitions required for fatigue failure (Figure 7).

(3) Fatigue failure will develop in a pavement when the maximum vertical compressive strain in the subgrade reaches a critical value. The critical compressive strain varies with the pavement stiffness and the number of stress repetitions to failure. Figure 8 summarizes the results obtained by the Waterways Experiment Station, Corps of Engineers, and the Asphalt Institute. The fatigue criterion given in Figure 8 is for the following conditions: (1) Portland cement concrete and strong bituminous concrete pavements with a surface layer modulus greater than 350,000 psi, (2) weak bituminous concrete pavements with a surface layer modulus less than 200,000 psi, and (3) heavy, multiwheeled aircraft loading, e.g., B-52 and C-5A.

The fatigue criteria and the maximum pavement response values searched above are used to determine the number of stress repeti-

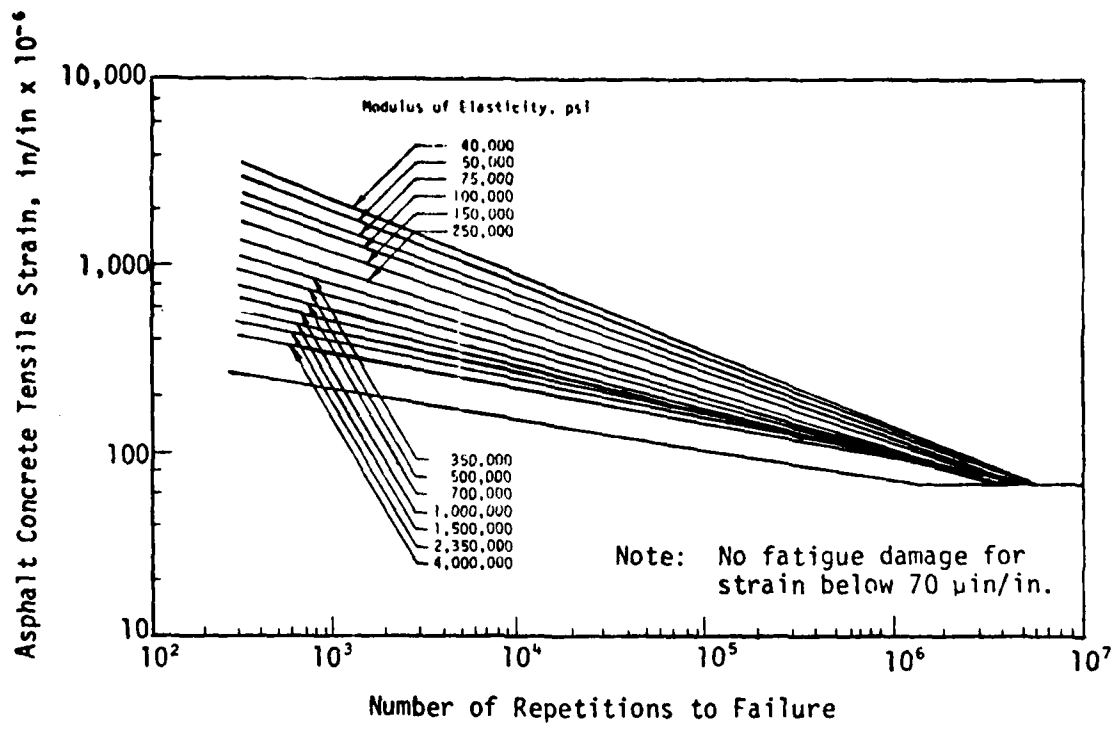


Fig. 6 Fatigue Criteria for Bituminous Concrete Pavements (after Monismith and McLean 1966)

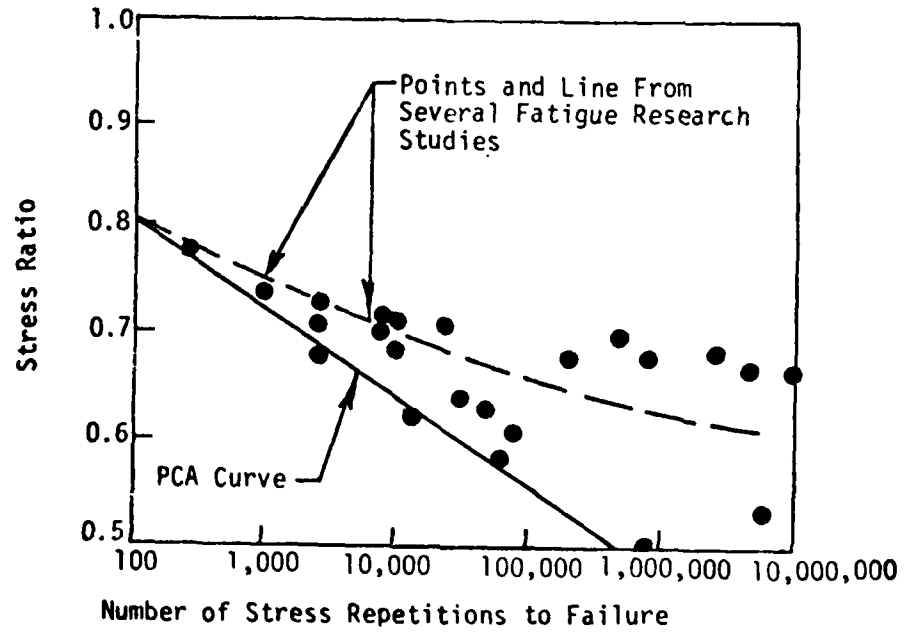


Fig. 7 Fatigue Criteria for Concrete Pavements (after Packard 1973)

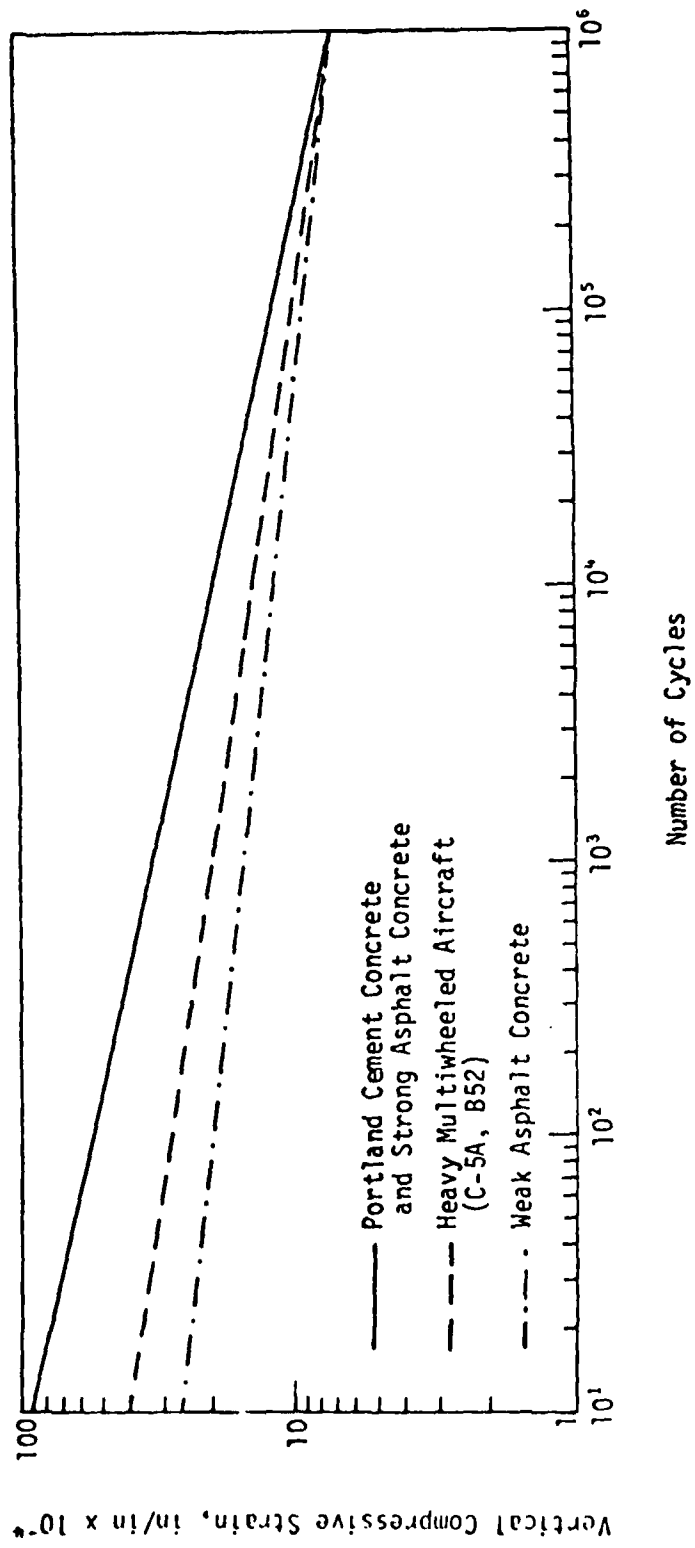


Fig. 8 Fatigue Criteria for Subgrade Materials

tions to cause fatigue failure for the particular pavement under investigation. With the concept of cycles per coverage [18], the number of operations (OPS) permitted for each material (asphalt, concrete, and/or subgrade) is printed following the stress and strain data. Also included in the output are the mixed traffic factors. Using this computer output, the effect of mixed traffic can be evaluated by multiplying the mixed traffic factor for each aircraft by the expected number of annual operations.

IV. DISCUSSIONS

The preceding review has indicated that the Air Force NDPT method employs impulse loading to determine the elastic moduli of pavement constituent layers; these modulus values are then used as input for the computer program, PREDICT, to evaluate the pavement's remaining service life. The PREDICT computer code is a finite element program capable of considering the effect of strain rate on the elastic moduli of gravel and soil. Obvious strength and weakness of the various NDPT components have been pointed out earlier; an overall evaluation regarding the soundness and effectiveness of the NDPT method follows.

The impulse loading used in the field testing produces a stress pulse in the pavement; the shape of stress pulse (described by amplitude and duration) varies with the amount of energy applied which depends greatly on the weight of falling mass, drop height, and the impact plate material, and the pavement structure which involves material types and layer thicknesses. When compared with traffic loading, impulse loading generates stress pulse of shorter duration and induces acceleration of much greater magnitude than moving wheels [4, 21]. Despite this difference, it is widely believed that impulse loading simulates actual traffic loading much better than other types of loading such as static and vibratory loadings [2, 23, 30]. Another important feature of using impulse loading for pavement testing is the size of equipment

needed. Because impulse loading can be applied without a reaction system, the equipment size usually is much smaller than that of vibratory or static loading.

As mentioned before, the Air Force impulse loader is well designed so that the weight of falling mass and drop height can be adjusted quite easily compared with other equipment of the same kind, e.g., the devices described by Moore et al. [30], and Hoffman and Thompson [20]. In addition, the sophisticated instrumentation of the impulse loader can be used to measure the velocity of wave propagation and the profile of surface deflection. However, the current NDPT method utilizes the impulse loader only for obtaining shear wave velocity which is then used to compute the elastic modulus of each pavement layer.

Various studies [3, 24, 25, 45] have shown that a strong correlation exists between the shape of surface deflection basin and the performance of flexible pavements. Other studies [5, 21, 39, 44, 46] have also demonstrated the feasibility of evaluating the elastic modulus from pavement deflection basins. All of these indicate that the surface deflection basin is a very useful datum for evaluating pavement performance and elastic modulus. Therefore, to fully utilize the well designed impulse loader, the method of modulus computation should be improved; also, a procedure should be developed so that the pavement deflection data can be incorporated into the current NDPT method.

It is common practice of pavement analysis that the flexible pavement is modeled as an elastic layer system and the rigid pavement as a rigid plate supported by the elastic half space. Therefore, different computer programs are usually needed for analysis of the two different types of pavements. For examples, some computer programs often used are BISAR [10] and Chevron n-layer program [47] for flexible pavements, and RPOD [43] for rigid

pavements. Various existing programs are reviewed by Rauhut et al. [38]. The PREDICT computer code employs the finite element method in which the pavement structure, both flexible and rigid, are approximated by a system of finite number of elements which are interconnected at nodal points. With this method, only one computer program is needed for analysis of both types of pavements. Additional advantage of the finite element program is that the flexibility of the pavement structure can be controlled by varying the element size, the nonlinear stress-strain property of the pavement material can be taken into consideration without great difficulty, and the effect of overlay, if any, can be evaluated easily. However, because of the use of prismatic elements, the PREDICT computer code is unable to consider the variation of elastic modulus with strain level and state of stress in the longitudinal direction within each element. For this reason, the current NDPT method requires a conservative approach by using the maximum shear strain in the element to determine the shear modulus. To assure that the maximum shear strain of each element is obtained, considerable attention is needed in the selection of Z values for shear strain computation. In the analysis, Z values are always expressed in terms of the element length, L (Figure 3). Further, with this approach, there is a possibility of element mesh distortion at a pavement cross section where the actual shear strain is less than the maximum shear strain of the element. Whether or not this distortion will cause undesirable effects on the results of analysis requires further study.

The preprocessor, AFPRE, in the PREDICT computer code greatly facilitates the generation of finite element mesh; it reduces considerable amount of not only human effort for data preparation but also possible errors involved in the mesh generation. Another salient feature of the PREDICT computer code is the use of AFCAN program to prepare load input. The aircraft loading is assumed to be a periodic function and can be described by Fourier series.

With this method of approximation, different aircraft gear configuration input can be prepared at a small amount of time. One difficulty involved in this input preparation, however, is the determination of adequate values for the function constants, especially NUMCOS (number of cosine terms in the Fourier series) and ZLEN (half period of the Fourier series). Considerable experience and engineering judgement are required to select appropriate values.

Other important features of the PREDICT computer code include its capability of considering the effect of joints in rigid pavement and fatigue analysis for mixed traffic conditions. The analysis of pavement fatigue life is made based on the available distress criteria which will be discussed in a later section. The pavement joint is modeled as a shear connector having a certain stiffness. A difficulty associated with the use of a shear connector is the selection of an appropriate stiffness value so that the actual joint behavior can be adequately modeled. Usually, this is accomplished by trial and error procedures until the joint behavior can be duplicated. Therefore, field data on joint behavior is needed for successful pavement evaluation using the PREDICT computer code.

Although the finite element method can take the nonlinear stress-strain material property into consideration, the PREDICT computer code is capable of performing nonlinear analysis for base and subgrade courses only because of the lack of constitutive equations of surface materials. For surface layer, either asphalt or portland cement concrete, the material property is assumed to be linearly elastic. With this assumption, the result of evaluation may be on unconservative side. This is especially true for asphaltic material since it generally possesses nonlinear property. Also, under normal condition, high shear strain exists in the asphalt layer; the high shear strain value yields a low Young's modulus. As a result, the actual pavement response such as ten-

sile strain in the asphalt layer and vertical subgrade strain may be higher than those computed from the PREDICT code. To avoid this undesirable result, nonlinear constitutive equations of surface materials should be developed and incorporated into the PREDICT computer code.

It is important to note, as pointed out before, that the test loading used in the development of constitutive equations should simulate the actual state of stress present in the pavement as much as possible. Meanwhile, appropriate yield or failure criteria should be incorporated into the constitutive equations so that possible local yielding or failure under heavy aircraft loading can be properly considered. The incorporation of appropriate yield criteria into the present constitutive equations of gravel and soil, Eqs (9) and (10), is also necessary.

With the various distress criteria (Figures 6, 7, and 8) in the subroutine RESULT, the computer code PREDICT is capable of predicting the remaining life of a pavement system in terms of fatigue failure. These criteria are critical tensile stress, tensile strain, and compressive subgrade strain values. Because they are established through laboratory testing and theoretical analysis for the particular pavement, loading, and environmental conditions involved in the development, these criteria should be expanded to accommodate the range of condition that typically exists in the Air Force airfield pavement.

Further, in the field, many factors that influence pavement performance are interrelated so that it is very difficult, if not impossible, to consider the combined effect in the laboratory investigation. As an example, the commonly existing combined effect of material variability due to inhomogeneity and nonuniform construction, irregular traffic pattern, edge loading, and environmental influences may result in a fatigue life different from

that estimated based on the results of laboratory testing and analysis. Therefore, it is imperative that these distress criteria be validated in the field. O'Brien [35] has outlined some important elements which need be observed during the field validation.

Using the preceding distress criteria, the fatigue life of a pavement can be evaluated for the critical pavement response value determined at the time of field testing. Since the asphalt and subgrade moduli vary considerably with temperature and moisture content, respectively, the fatigue life thus determined corresponds only to the pavement temperature and subgrade moisture content at testing. The evaluation of remaining service life of a pavement system is complicated by the fluctuation of pavement temperature and subgrade moisture content. Because of the variation of critical pavement response with the fluctuating temperature and moisture content, a procedure involving Miner's hypothesis usually is needed for estimating the pavement's remaining service life. For this procedure, a spectrum of seasonal variation of pavement temperature and subgrade moisture content need be established and the corresponding critical pavement responses determined. With these pavement response data, the amount of damage already occurred in the pavement is computed and the remaining service life of the pavement corresponding to this amount of damage estimated.

The pavement temperature required is the average temperature across the thickness of the asphalt concrete layer. Because it is easier to measure temperature on the pavement surface, the sum of surface temperature and five-day air temperature prior to testing has been suggested for evaluation of highway pavements [13, 42]. An approach similar to this may be used for the Air Force NDPT method. The determination of subgrade moisture content is not as simple. The precipitation data and soil type may give the trend

of water content fluctuation; however, most reliable data can only be obtained by taking soil sample through coring. Coring also provides specimens of pavement materials for laboratory testing and for determination of pavement layer thicknesses. The pavement layer thickness is an essential input for the PREDICT computer code. When the pavement construction record is not available, coring is the only effective means presently available for layer thickness determination.

Laboratory testing on cored specimens, although not required, can provide data on elastic modulus to verify the value determined from field testing. As has been pointed out before, the elastic modulus obtained from field vibratory loading test data is usually too high so that it is arbitrarily reduced by 50 percent. The laboratory testing can also provide Poisson's ratio, thus the current approach of assuming a value of Poisson's ratio for the PREDICT code can be avoided. Additionally, various soil properties such as void ratio, degree of saturation, and plasticity characteristics and others which are required by the constitutive equations can also be obtained from core samples. Therefore, laboratory testing on core sample is needed not only for verifying elastic modulus but also for providing accurate input data to the PREDICT computer code so that valid structural evaluation of existing airfield pavements can be assured.

The current NDPT method evaluates a pavement's structural capacity in terms of fatigue cracking only. There are other modes of pavement distress which also affect the pavement's performance considerably. For flexible pavements, more important distress modes are cracking caused by shrinkage or by changes in temperature and subgrade moisture, rutting, and slope variance. Both slope variance and rutting are results of permanent deformation due to traffic loading. Slope variance refers to the longitudinal roughness, whereas rutting is the channelized depression along the

wheel path. Slope variance causes discomfort to the pavement user while rutting may impound water and reduces skid resistance. Cracking due to shrinkage and change in temperature and subgrade moisture results in structural discontinuity and decreases the load carrying capacity of the pavement. Also, intrusion of water into the crack may weaken the subgrade material and accelerates pavement deterioration. For rigid pavements, cracking and spalling around joints and edges are more important than both slope variance and rutting. To consider these distress modes, appropriate constitutive equations should be incorporated into the AFPVAV program. As an example, equations involving viscoelastic and permanent strains may be needed for rutting and slope variance evaluation. With the use of finite element method in the AFPVAV, some of these distress modes can be considered without great difficulty. Others such as slope variance and edge and corner cracking may require more effort for program modification because of the prismatic element used in the AFPVAV code. Nevertheless, the AFPVAV computer program possesses sufficient flexibility for future expansion and modification.

Various weaknesses associated with the NDPT method have emerged from this discussion. The effect of these weaknesses on the results of pavement evaluation varies. Of these, the lack of an appropriate method for computation of layer modulus value obviously is the most significant shortcoming. Also significant is that the NDPT method is without constitutive equations for surface materials particularly bituminous concrete, without a system of distress criteria that encompasses a range of subgrade moisture and pavement temperature, and without provisions to take into consideration the effect of pavement temperature and subgrade moisture in the evaluation process. With these shortcomings, reasonable evaluation can hardly be acquired by using the current NDPT method. It should also be noted that the present NDPT method is incapable of evaluating a pavement's structural capacity in

terms of roughness and rutting. Other weaknesses such as the use of prismatic element in the PREDICT code, the difficulty in the selection of stiffness for shear connector, and the needed judgement in the determination of Fourier series constants for loading inputs are comparatively less important.

V. SUMMARY AND CONCLUSIONS

V.1 SUMMARY

Various features of the current Air Force NDPT method have been critically reviewed and discussed. The highlight regarding the strengths and weaknesses of the NDPT method is briefly summarized below.

V.1.1 Strengths

The data collection equipment contained in a van is air transportable and therefore satisfies the Air Force's need of rapid worldwide deployment. The impulse loader has great flexibility to vary the weight of the falling mass and the drop height very easily. It is also well instrumented so that pavement response can be measured at eight different locations. In addition, the equipment has a desk-top computer for preliminary data analysis and evaluation which screens and rejects unreasonable test data on the spot.

The PREDICT computer code is capable of performing nonlinear analysis for both flexible and rigid pavements subjected to aircraft loading of various gear configurations. The loading input can be prepared easily since each aircraft loading is contained in a subroutine. Also, the effort required for preparation of finite element mesh is greatly reduced by the preprocessor, AFPRE, in the code. Further, the code contains subroutines for

mixed traffic and fatigue analyses so that the remaining service life can be obtained directly from the computer output.

V.1.2 Weaknesses

Adequate methods for interpretation of field test data and computation of elastic constants (Young's modulus and Poisson's ratio) are not yet available. From the experience on steady state vibratory loading tests, the computed Young's modulus values are always too high except for portland cement concrete. Without methods for successful determination of elastic constants, the effort for the development of the data collection equipment cannot be fully justified.

The present PREDICT code can only perform nonlinear analysis for the base and subgrade materials because of the lack of constitutive equations for surface materials. As pointed out earlier, surface materials especially bituminous concrete behaves nonlinearly under loading. Pavement evaluation without a consideration of nonlinear stress-strain behavior of the bituminous concrete layer may yield an unconservative result.

The distress criteria now in the PREDICT code need be expanded and validated in the field so that the effect of pavement temperature and subgrade moisture can be considered. Meanwhile, provisions to take into consideration the pavement temperature and subgrade moisture at the time of testing are needed in the data collection system so that the remaining pavement service life can be properly evaluated.

Presently, the required input on pavement layer thickness for the PREDICT code cannot be obtained nondestructively if construction record of the pavement under evaluation is not available. The layer thickness must be determined through coring which causes destruction to the pavement.

V.2 CONCLUSIONS

Under the present state of knowledge, practical application of wave propagation technique to determine pavement layer thickness is still quite limited, although it has been shown [22] that the technique can be used for simple pavement conditions. Because the degree of destruction to the pavement structure resulted from coring and the effort required for field data collection are very small compared with the destructive method of pavement evaluation, the use of current NDPT method is well justified. Furthermore, the present field data collection equipment is very well designed and the computer code, PREDICT, has the capability of evaluating the fatigue life of both flexible and rigid pavements for various aircraft loadings. With these merits, the current NDPT method can become a very effective evaluation tool if the aforementioned weaknesses are corrected. Recommendations for improvement are given below.

VI. RECOMMENDATIONS

Results of the evaluation have indicated three main areas which need further research to improve the current NDPT method. Recommendations for improvement follow:

VI.1 Field Test Data Analysis and Interpretation for Determination of Elastic Constants of The Pavement Constituent Materials

A key element for successful data interpretation is a well-defined response curve. As of today, according to Baird [1], the data in the long wave length region are fairly well defined so that there seems no great difficulty to obtain reasonable Young's modulus for the subgrade material. In the short wave length region, however, there are some difficulties because the dispersion curve in this region is not clearly defined. Since the shape

of the response curve varies with many factors such as the material and size of the impact plate, type and layer thickness of the pavement, the weight of impact mass, and drop height, it might be possible to obtain adequate response data for the computation of Young's modulus of the surface and base layers by varying the influencing factors, especially the material and size of the impact plate. Therefore, during this period of equipment development, an optimization of loading elements, namely, a search of an optimum combination of impact plate material, size, falling weight, and drop height appears to be necessary.

The equipment is capable of measuring the pavement response at different locations up to eight different points. From these response data, the basin of deflection under each impulse loading may be obtained. The deflection basin data may be useful for validation of the Young's modulus values computed from the dispersion curve. Also, the shape of the deflection basin may be used to infer the structural capacity of the pavement under investigation. Therefore, a study on how the deflection data can be integrated into the current NDPT method is warranted.

VI.2 Constitutive Relationships For Surface Materials

The constitutive equations of pavement materials especially bituminous concrete should be developed and incorporated into the PREDICT code so that the effect of strain level and state of stress on the elastic modulus can be taken into consideration. The equations should be developed under a range of state of stress and strain level that exist in the field and using the loading that resembles the actual field condition. Furthermore, the developed equations should accommodate the range of temperature and mix composition that are expected in the airfield pavement.

VI.3 Distress Criteria and Evaluation of Remaining Service Life

The present distress criteria should be expanded to accommodate a broad range of loading and environmental conditions that exist in the airfield pavements. These criteria should also be validated in the field. For validation, test sites should be selected at the locations where adequate data on fatigue cracking and traffic record are available. Specimens should be taken for testing and analysis. At present, a research on the development of algorithm of fatigue criteria for bituminous concrete is underway [26]. Similar studies for portland cement concrete and subgrade soil are needed.

For estimation of a pavement's remaining fatigue life, a year-round data on seasonal variation of air temperature and subgrade moisture are required. Therefore, it is recommended that such a data bank be established and incorporated into the PREDICT computer code.

REFERENCES

1. Baird, G.T. (1981). Discussions held at the Civil Engineering Research Facility, University of New Mexico, Albuquerque, N.M. on July 13 and 14.
2. Barenberg, E.J. (1978). Comparison and Evaluation of Non-destructive Testing Methods of Airport Pavement Evaluation. Transportation Research Board Special Report 175, pp. 105-112.
3. Bissett, J.R. and Ford, M.C. (1962). A comparison of Flexible Pavement Performance with Structure. Proceedings, Association of Asphalt Paving Technologists, Volume 31, pp. 329-342.
4. Bohn, A.; Ullidtz, P.; Stubstad, R.; and Soreson, A. (1972). Danish Experiments with the French Falling Weight Deflectometer. Third International Conference on Structural Design of Asphalt Pavements, Proceedings, pp. 1119-1128.
5. Cogill, W.H. (1972). The Utilization of the Results of the Measurements of Surface Deflection Profiles as a Means of Estimating the Stiffness of Pavement Materials. Proceedings, Australian Road Research Record, Vol. 6, Part 4, pp. 142-149.
6. Crawford, J. (1972). An Analytical Model for Airfield Pavement Analysis. Technical Report No. AFWL-TR-71-70, Air Force Weapons Laboratory, Kirtland AFB, N.M., May.
7. Crawford, J. (1975). Finite Element Analysis of Pavement Structures Using AFPAV Code (Nonlinear Elastic Analysis). Technical Report No. AFWL-TR-74-71, Air Force Weapons Laboratory, Kirtland Air Force Base, N.M., April.
8. Crawford, J.E., (1976). Software for Everyday Usage of AFPAV, Technical Report Memorandum M-51-76-06, Civil Engineering Laboratory, Port Hueneme, California, March.

9. Cunny, R.W.; Cooper, S.S.; and Fry, Z.B. (1969). Comparison of Results of Dynamic in Situ and Laboratory Tests for Determination of Soil Moduli. Miscellaneous Paper S-69-48, U.S. Army Engineer Waterways Experiment Station, Vicksburg, Mississippi, October.
10. DeJong, D.L.; Peutz, M.G.F.; and Korswagen, A.R. (1973). Computer Program BISAR. External Report Koninklijke/Shell-Laboratorium, Amsterdam.
11. Department of the Air Force (1981). Airfield Pavement Evaluation Program, AF Regulation 93-5, HQ USAF, Washington, D.C., May.
12. Finn, F.; McCullough, B.F.; Nair, K.; and Hicks, R.G. (1966). Plan for Development of Nondestructive Method for Determination of Load-Carrying Capacity of Airfield Pavements. Final Report No. 1062-2(F), Materials Research and Development, Inc., Oakland, California, November.
13. Green, J.L. (1978). Literature Review - Elastic Constants for Airport Pavement Materials. Report No. FAA-RD-76-138, U.S. Department of Transportation, Federal Aviation Administration, March 1978, 137 pp.
14. Hanson, D.I. (1975). Procedure for the Nondestructive Evaluation of Flexible Airfield Pavements. Final Report, AFCEC-TR-75-1, Air Force Civil Engineering Center, Tyndall Air Force Base, Florida, January.
15. Hardin, B.O. (1971). Constitutive Relations for Airfield Subgrade and Base Course Materials, Technical Report UKY-32-71-CE5, Soil Mechanics Series No. 4, University of Kentucky.

16. Hardin, B.O. (1973). Effects of Strain Amplitude on the Shear Modulus of Soils, Technical Report No. AFWL-TR-72-201, Air Force Weapons Laboratory, Kirtland AFB, N.M., March.
17. Hardin, B.O. (1973). Shear Modulus of Gravels. Final Report, AFWL-TR-73-180, Air Force Weapons Laboratory, Kirtland AFB, N.M., November.
18. Hay, D.R. (1969). Aircraft Characteristics for Airfield Pavement Design and Evaluation. Technical Report No. AFWL-TR-69-54, Air Force Weapons Laboratory, Kirtland AFB, N.M., October.
19. Herrmann, L.R. (1968). User's Manual for PSA (Three-Dimensional Elasticity Analysis of Periodically Loaded Prismatic Solids), University of California, Davis, California, November.
20. Hoffman, M.S., and Thompson, M.R. (1981). Nondestructive Testing of Flexible Pavements Field Testing Program Summary, Report No. UILU-ENG-81-2003, Civil Engineering Studies, University of Illinois, Urbana, Illinois, June.
21. Hoffman, M.S., and Thompson, M.R. (1981). Mechanistic Interpretation of Nondestructive Pavement Testing Deflections, Report No. UILU-ENG-81-2010, Civil Engineering Studies, University of Illinois, Urbana, Illinois, June.
22. Jones, R. Surface Wave Techniques for Measuring the Elastic Properties and Thickness of Roads: Theoretical Development. British Journal of Applied Physics, Vol. 13, January 1962.
23. Koole, R.C. (1979). Overlay Design Based on Falling Weight Deflectometer Measurements. Transportation Research Record 700, TRB, pp. 55-72.

24. Kung, Y.K. (1972). A New Method in Correlation Study of Pavement Deflection and Cracking. Proceedings, Second International Conference on the Structural Design of Asphalt Pavements.
25. Leger, Ph. and Autret, P. (1972). The Use of Deflection Measurements for the Structural Design and Supervision of Pavements. Proceedings, Third International Conference on the Structural Design of Asphalt Pavements, pp. 1188-1205.
26. Marien, H.R. (1981). Personal Communication.
27. Marien, H.R., and Baird, G.T. (1981). U.S. Air Force Non-destructive Airfield Pavement Evaluation Method . Presented at the Transportation Research Board Task Force A2T56 meeting, August.
28. Mitchell, J.K. (1976). Fundamentals of Soil Behavior, New York: Wiley.
29. Monismith, C.L., and McLean, D.B. (1966). Structural Design Considerations. Proceedings, Association of Asphalt Paving Technologists, Cleveland, Ohio.
30. Moore, W.M.; Hanson, D.J.; and Hall, J.W. (1978). An Introduction to Nondestructive Structural Evaluation of Pavements. Transportation Research Circular, Transportation Research Board, Washington, D.C.
31. Nielsen, J.P., and Baird, G.T. (1975). Air Force System for Nondestructive Testing of Pavements . Symposium on Nondestructive Test and Evaluation of Airport Pavement, Vicksburg, Mississippi, November.
32. Nielsen, J.P. (1975). AFPAV Computer Code for Structural Analysis of Airfield Pavements. Final Report, AFWL-TR-75-151, Air Force Weapons Laboratory, Kirtland AFB, N.M., October.

33. Nielsen, J.P. and Baird, G.T. (1976). Pavement Evaluation System. Final Report, AFCEC-TR-76-28, Air Force Civil Engineering Center, Tyndall Air Force Base, Florida, October.
34. Nielsen, J.P. and Baird, G.T. (1977). Evaluation of an Impulse Testing Technique for Nondestructive Testing of Pavements. Final Report, CEEDO-TR-77-46, Civil and Environmental Engineering Development Office, Tyndall Air Force Base, Florida, September.
35. O'Brien, K. and Associates (1974). Distress Criteria for Pavement Systems. AFWL-TR-73-226, Air Force Weapons Laboratory, Kirtland AFB, N.M., April.
36. Packard, R.G. (1973). Design of Concrete Airport Pavement, Engineering Bulletin, Portland Cement Association.
37. Pichumani, R. (1973). Finite Element Analysis of Pavement Structures Using AFPAV Code (Linear Elastic Analysis). Technical Report No. AFWL-TR-72-186, Air Force Weapons Laboratory, Kirtland Air Force Base, N.M., May.
38. Rauhut, J.B.; Roberts, F.L.; and Kennedy, T.W. (1979). Response and Distress Models for Pavement Studies. Transportation Research Record 175, Transportation Research Board, Washington, D.C., pp. 7-14.
39. Scrivner, F.H.; Michalak, C.H.; and Moore, W.M. (1971). Calculation of the Elastic Moduli of a Two Layer Pavement System from Measured Surface Deflections. Part I and II, Texas Transportation Institute, Research Report No. 123-6.
40. Stearns, S.D. (1975). Digital Signal Analysis, Hayden Book Company.

41. Sullivan, D.L. (1979). Interpretation of Nondestructive Pavement Test Data. M.S. Thesis, University of New Mexico, Albuquerque, N.M., August.
42. The Asphalt Institute (1969). Asphalt Overlays and Pavement Rehabilitation. Manual Series No. 17, College Park, Maryland.
43. Treybig, H.J.; McCullough, B.F.; Smith, P.; and Von Quintus, H. (1978). Overlay Design and Reflection Cracking Analysis for Rigid Pavements: Volume I - Development of New Design Criteria. Federal Highway Administration, U.S. Department of Transportation, Final Report, FHWA-RD-77-66, January.
44. Vaswani, N.K. (1971). Method for Separately Evaluating Structural Performance of Subgrades and Overlaying Flexible Pavements, Highway Research Record 362, Highway Research Board, pp. 48-62.
45. Wang, M.C.; Bhajanda, A.C.; Cumberland, G.; and Larson, T.D. (1978). Pavement Evaluation by Road Rater Deflections. Transportation Research Board Record 666, Transportation Research Board.
46. Wang, M.C.; and Anani, B.A. (1981). Evaluation of In-Situ Elastic Moduli from Road Rater Deflection Basin. Paper presented at the Transportation Research Board Annual Meeting.
47. Warren, H. and Sieckmann, W.L. (1963). Numerical Computation of Stresses and Strains in a Multiple-Layer Asphalt Pavement System. International Report, Unpublished, California Research Corp., September.

1981 USAF - SCEEE SUMMER FACULTY RESEARCH PROGRAM

Sponsored by the

AIR FORCE OFFICE OF SCIENTIFIC RESEARCH

Conducted by the

SOUTHEASTERN CENTER FOR ELECTRICAL ENGINEERING EDUCATION

FINAL REPORT

THE EFFECT OF ONE HUNDRED PERCENT OXYGEN AT ONE ATA AND INCREASED

PRESSURE ON THE METABOLISM OF AN ORGANOPHOSPHATE

(PARATHION) IN THE RAT

Prepared by: Dr. Alice Ward

Academic Rank: Assistant Professor

Department and University: Department of Biological Sciences
Southern University

Research Location: United States Airforce School of Aerospace Medicine,
Hyperbaric Medicine Division

USAF Research Colleague: Col. Kenneth Hart, USAF-MC

Date: September 1, 1981

Contract No: F49620-79-C-0038

THE EFFECT OF ONE HUNDRED PERCENT OXYGEN AT ONE ATA AND INCREASED
PRESSURE ON THE METABOLISM OF AN ORGANOPHOSPHATE
(PARATHION) IN THE RAT

by

Alice Ward

ABSTRACT

In vivo studies have been carried out to determine the effect of 100% oxygen at ambient and increased pressure on the metabolism of the organophosphorous insecticide, parathion. Groups of rats administered a single intraperitoneal dose of the agent (4.5 mg/kg) were either treated immediately or after a period of ten minutes with 100% oxygen at 1 ATA or 2.4 ATA. Results indicate that oxygen at 1 ATA and 2.4 ATA does not prevent the formation of paraoxon, the toxic metabolite of parathion. Also oxygen at these pressures does not appear to influence the degradation of paraoxon. It appears that 100% oxygen at 2.4 ATA may enhance the conversion of parathion to paraoxon.

I. INTRODUCTION:

The organophosphates (OPs) are a large class of highly toxic chemicals. These substances were developed before and during World War II first as insecticides and later as chemical warfare agents (the nerve gases). The extreme toxicity of these compounds is due to their irreversible inactivation of the enzyme acetylcholinesterase.

Many of the OPs are metabolized by the mixed function oxidase (MFO) enzyme systems of mammalian liver. These enzyme systems have an essential requirement for reduced nicotinamide adenine dinucleotide phosphate (NADPH) and molecular oxygen.¹ Typically, the metabolism of OPs involve two types of reactions; activation reactions in which the parent compound is converted into a toxic metabolite and detoxification reactions in which the parent compound is degraded into nontoxic metabolites.

Parathion (diethyl 4-nitrophenyl phosphorothionate) is used extensively as an agricultural insecticide. It is metabolized by the MFO enzyme systems of mammalian liver to paraoxon (diethyl 4-nitrophenyl phosphate), a toxic metabolite and to diethyl phosphorothionate, a nontoxic metabolite.^{2,3} Paraoxon is metabolized further to diethyl phosphate (nontoxic) by a number of esterases present in animal tissues.⁴

The effect of 100 percent oxygen at 1 ATA* and increased pressure on the metabolism of OPs has not been extensively investigated. An in vitro study by Neal² revealed that 100% oxygen at 1 ATA inhibited the metabolism of parathion. He reasoned that some component of the MFO system was susceptible to an oxidation that leads to a decreased enzyme activity. Neal's investigations did not include the use of hyperbaric oxygen (HBO).

Various workers⁵ have suggested that HBO might alter the metabolism of certain types of chemicals, however experimental evidence to support this suggestion is lacking.

This study was undertaken to investigate the effect of oxygen on the metabolism of a specific organophosphate, parathion, in an in vivo system.

*ATA is the abbreviation for Atmosphere is Absolute. 1 ATA is equivalent to a barometric pressure of 760 mm Hg.

II. OBJECTIVES

The objectives of the project were to:

1. Determine if 100% oxygen at 1 ATA and increased pressure prevents the conversion of parathion to the toxic substance paraoxon.
2. Determine if 100% oxygen at 1 ATA and increased pressure influences the metabolism of paraoxon to the nontoxic substance diethyl phosphate.

III. MATERIALS AND METHODS

One hundred fifty female albino rats (Sprague-Dawley strain, 200-265 g) were divided into 5 groups of thirty. Groups I, II, IV, and V were subdivided into six groups of five. Group III was subdivided into three groups of ten.

Group I was observed in air at 1 ATA following parathion* injection and served as the positive control. Parathion, dissolved in a mixture of ethanol (20%) and propylene glycol (80%), was administered intraperitoneally (4.5 mg/kg). The total volume injected was 1 ml. No effects were observed when the solvent vehicle was injected into a group of 10 animals.

Group II was exposed to 60 minutes of 100% oxygen in the following manner. The animals in each subgroup were injected with parathion and immediately placed in sealed oxygen hoods containing 100% oxygen. The concentration of oxygen in the hoods returned to 100% in 30-45 seconds after the introduction of an animal. The treatment period was 60 minutes broken into three 20 minute periods separated by 5 minute breaks during which the animals breathed air. Following treatment the rats were returned to air. Group III was treated identically as Group II, except that injections were administered in a large pressure chamber at 2.4 ATA while the rats breathed air. The rats were then treated with oxygen at 2.4 ATA for 60 minutes in the same hoods used in Group II. At the end of the treatment period, the surviving animals were returned to air and decompressed to normal atmospheric pressure over a five minute period.

*Parathion, assessed to be more than 99% pure, was supplied by The Monsanto Company, St. Louis, Missouri.

Group IV was exposed to 60 minutes of 100% oxygen at 1 ATA. The procedure was the same as in Group II except that treatment was initiated 10 minutes after the administration of parathion.

Group V was exposed to 60 minutes of oxygen at 2.4 ATA in the following manner. Each subgroup was injected with parathion and placed in a Bethlehem Hyperbaric Animal Chamber (model # 1836-HP). The chamber was pressurized with 100% oxygen. The oxygen treatment period was 60 minutes broken into three 20 minute periods separated by five minute breaks during which the animals breathed air. The time interval between injection of the toxin and commencement of oxygen treatment was 10 minutes. At the end of the treatment period the rats were decompressed to normal atmospheric pressure over a period of five minutes.

Groups II and III were designed to achieve objective (1) and Groups IV and V were designed to accomplish objective (2). Parameters used to ascertain treatment effects were the time interval to the appearance of signs of poisoning, the time interval after injection to death, and the number of animals surviving at 24 hours.

IV. RESULTS

All the animals in Group I exposed to air at normal atmospheric pressure exhibited symptoms of poisoning within three minutes of injection. The symptoms included muscle tremors, loss of coordination, diarrhea, and excessive salivation and lacrimation. The interval to death for various animals in the sample ranged from 10-34 minutes following injection. The percent of rats surviving at 24 hours in this group was 50.00.

The animals in Group II, which were treated immediately with oxygen at 1 ATA exhibited symptoms of poisoning within three minutes of injection. The preceding interval to death ranged from 10-45 minutes following injection. The percent of rats surviving in this group at 24 hours was 46.67.

The animals in Group III, which were treated immediately with oxygen at 2.4 ATA, showed symptoms within three minutes of injection. The interval to death ranged from 10-60 minutes following injection. Twenty percent of the rats in this group survived for 24 hours following injection.

The rats in Group IV, which were treated with oxygen at 1 ATA ten minutes after injection, showed symptoms of poisoning within three minutes. The interval to death ranged from 10-50 minutes following injection. The percent of animals surviving in this group at 24 hours was 50.00.

The rats in group V, which were treated with oxygen at 2.4 ATA ten minutes following injection, exhibited symptoms of poisoning within three minutes. The preceding interval to death ranged from 16-33 minutes for various members of the sample. The percent of animals surviving at 24 hours was 46.67.

The oxygen treatments at 1 ATA and 2.4 ATA presumably did not prevent the formation of paraoxon, the toxic metabolite of parathion. The significance of the low survival rate for Group III (only 20%) is unclear at present. However, the results may substantiate the findings of Longmuir and co-workers which indicated that HBO induces the synthesis of the enzyme cytochrome P-450, the terminal enzyme of the MFO enzyme system. Our findings in this study may also indicate that HBO, working through cytochrome P-450, indirectly enhances the conversion of parathion to paraoxon.

The oxygen treatment at 1 ATA and 2.4 ATA presumably did not effect the conversion of paraoxon to diethyl phosphate.

V. RECOMMENDATIONS

HBO appears to enhance the conversion of parathion to paraoxon. It is recommended that study in this area be continued to identify the mechanism(s) responsible for this effect.

The author proposes to further investigate the finding that HBO induces the synthesis of cytochrome P-450.

REFERENCES

1. Dauterman, W. C., "Biological and Nonbiological Modifications of Organophosphorous Compounds," Bull. Wld. Hlth. Org., Vol. 44, pp. 133-150, 1971.
2. Neal, R. A., "Studies on the Metabolism of Diethyl 4-Nitrophenyl Phosphorothionate (Parathion) in vitro," Biochem. J., Vol. 103, pp. 183-191, 1967.
3. Nakatsugawa, T., and P. A. Dahm, "Microsomal Metabolism of Parathion," Biochemical Pharmacology, Vol. 17, pp. 1517-1528, 1968.
4. Norman, B. J., W. K. Vaughn and R. A. Neal, "Studies of the Mechanisms of Metabolism of Diethyl p-Nitrophenyl Phosphorothionate (Parathion) by Rabbit Liver Microsomes," Biochemical Pharmacology, Vol. 22, pp. 1091-1101, 1973.
5. Casarett, L. J., and J. Doull, Toxicology: The Basic Science of Poisons, (MacMillan Company, New York, 1975), pp. 145 and 420.
6. Longmuir, I. S., S. F. Gottlieb, L. L. Pashko, and P. Martin, "In vivo and In vitro Induction of Cytochrome P-450 Synthesis in Hyperoxia," Undersea Biomedical Research, Vol. 7, pp. 161-170, 1980.

Acknowledgement

The author would like to thank the Air Force Systems Command, the Air Force Office of Scientific Research and the Southeastern Center for Electrical Engineering Education for providing her with the opportunity to carry out an extremely interesting study at the School of Aerospace Medicine, Hyperbaric Medicine Division, Brooks A. F. B., Texas. She would like to thank the Hyperbaric Medicine Division staff for their kindness, cooperation, and their most valuable assistance.

Finally she would like to thank Col. Kenneth R. Hart for suggesting the project and for his collaboration, encouragement and assistance.

1981 USAF - SCEEE SUMMER FACULTY RESEARCH PROGRAM

Sponsored by the

AIR FORCE OFFICE OF SCIENTIFIC RESEARCH

Conducted by the

SOUTHEASTERN CENTER FOR ELECTRICAL ENGINEERING EDUCATION

FINAL REPORT

MEASUREMENTS OF TURBULENCE IN THE TROPOSPHERE AND LOWER STRATOSPHERE

USING THE MILLSTONE HILL 440 MHZ RADAR

Prepared by: Brenton J. Watkins
Academic Rank: Assistant Professor of Geophysics
Department and University: Geophysical Institute,
University of Alaska
Research Location: Air Force Geophysics Lab/LKD
Hanscom Air Force Base
Mass. 01731
USAF Research Colleague: Dr. R. E. Good
Date: Sept. 1, 1981
Contract No: F49620-79-C-0038

MEASUREMENTS OF TURBULENCE IN THE TROPOSPHERE AND LOWER STRATOSPHERE
USING THE MILLSTONE HILL 440 MHZ RADAR

by

Brenton J. Watkins

ABSTRACT

A program of experiments has been conducted to make intercomparisons of the refractivity turbulence structure constant (C_n^2) in the upper troposphere and lower stratosphere. The Millstone Hill 440 Mhz turbulence scatter radar was operated simultaneously with a number of Air Force Geophysics Lab balloon experiments. [The balloon data yield temperature fluctuation profiles that may be converted to C_n^2 profiles]. On one night a stellar scintillometer was also operated for data comparison purposes. The data indicated large (factor of 100) variations of C_n^2 with time and height. The decrease of C_n^2 with altitude ($\sim 1.4\text{db/km}$) is generally similar to that reported by other workers, however on two days the slope was considerably less. The absolute magnitude of C_n^2 from these radar data was greater (factor of 10) than found at other radar sites. However the C_n^2 data gathered in 1968 at the Millstone Hill site show similar magnitudes to those reported here.

Acknowledgement

The author would like to thank the Air Force Geophysics Lab, the Air Force Office of Scientific Research, and the Southeastern Center for Electrical Engineering Education for the opportunity to spend a very worthwhile summer, undertaking new experiments in atmospheric turbulence.

He would also like to thank MIT Neroc personnel George Lorient, Prabhat Rastogi, and Ron Wand for their help in data taking at the Millstone Hill radar site. In addition, a considerable effort in organization was undertaken by George Lorient for several months before, and during this research effort.

I. INTRODUCTION

This report summarizes a ten week research effort conducted at the Air Force Geophysics Laboratory (Hanscom AFB Mass) during the summer of 1981.

For several years an Air Force research program has been directed toward a better understanding of turbulence in the troposphere and stratosphere. This has been motivated by the need to understand the atmospheric transport mechanisms pertinent to the rate of mixing and diffusion of exhaust products in the stratosphere¹ and more recently to define the role of turbulence in affecting the transmission of optical signals through the atmosphere. Past research has mainly used two techniques, (a) balloon measurements of temperature fluctuations caused by turbulence, and (b) observation of the turbulence breakup of smoke trails released by rockets and balloons. Within recent years a new radar technique has also proven useful for this purpose^{2,3,4,5}. It is now routinely possible to monitor the level of atmospheric turbulence at various heights. In addition, optical techniques have been refined to also measure atmospheric turbulence⁶. This latter method utilizes a small optical telescope to monitor the scintillations of a bright star.

The general objective of this research program was to compare the three experimental methods because each has its own differing advantages and disadvantages, such as height resolution, cost etc.

This report summarizes the work undertaken at the radar site at Millstone Hill, Westford Massachusetts, located about 20 miles from the Air Force Geophysics Lab. The particular radar at this site was developed for turbulence scatter use beginning in 1978. Its development was funded by the National Science Foundation and operated by MIT Lincoln Lab. From January 1980 the radar has been operated by MIT North East Radio Observatory Corporation (NEROC). This work has evolved as a collaborative research effort between AFGL and NEROC, as well as this investigator (BJW). He was previously with MIT Lincoln Lab and NEROC, and was responsible for the development of that radar for turbulence scatter work⁵.

For the experiments reported here, a temporary balloon launch site was set up near the radar.

As this investigator was responsible for the radar data taking and analysis, this report will therefore focus on that particular aspect of the experiments.

II. OBJECTIVES OF THE RESEARCH EFFORT

The general research effort was to compare three different techniques for measuring turbulence in the troposphere and stratosphere. The turbulence scatter radar was to be operated during the balloon experiments and pointed in a direction to monitor the closest possible common volume. Height profiles of the refractivity turbulence structure constant C_n^2 from the radar were to be derived for subsequent comparisons. Whenever possible an optical scintillometer was also to be operated by AFGL.

Turbulence plays a critical role in the transmission of electromagnetic waves through the atmosphere. Therefore an understanding of the occurrence and morphology of atmospheric turbulence has been considered an important objective by the Air Force Geophysics Lab. The intercalibration and use of new turbulence scatter radars should aid that objective.

III. THE RADAR TURBULENCE SCATTER TECHNIQUE

The radar turbulence scatter technique uses a sensitive coherent radar to detect signal returns from weak fluctuations in the atmospheric refractive index. These fluctuations arise from temperature and humidity fluctuations which results from turbulence. The intensity of the signal returns is proportional to the volume averaged intensity of turbulence. It is also possible to determine the wind component at each height because the radar is capable of measuring the doppler shift of the turbulence scattered signals.

In Figure 1 are shown some frequency spectra. These are the basic results from the real time data taking program. A monochromatic radio frequency pulse is transmitted at 440 MHz. The received signals at each height are composed of ground clutter around the transmit frequency, doppler shifted turbulence scattered signals and background receiver noise. The spectra are actually derived by a 256 point fast fourier transform of sequential signal returns at each range. These receiver signal samples are sampled after 256 sequential transmitter pulses. Subsequent analysis programs are used to determine the signal/noise ratio (S/N) and doppler shift for the spectra at each height.

Ottersten⁷ has shown that the radar volume reflectivity η is related to the refractivity turbulence structure constant C_n^2 by,

$$C_n^2 = [\eta/0.38] \lambda^{1/3} \quad (1)$$

where λ is the radar wavelength and the scattering arises from homogeneous isotropic turbulence. The reflectivity η is related to the measured S/N ratio by⁴

$$\eta = \frac{(S/N) \alpha P_t A_e \Delta r}{9 \pi r^2 k T B} \quad (2)$$

where α = antenna efficiency
 P_t = peak pulse power
 A_e = effective antenna aperture
 Δr = range resolution
 r = range
 k = Boltzman constant
 T = receiver system temperature
 B = receiver bandwidth

The peak pulse power and system temperature are continuously monitored; the other parameters are fixed and dependent on the individual radar setup. Thus a measurement of S/N ratio can yield a C_n^2 value at each range.

AZ = 90
EL = 25

JULY 16, 1980

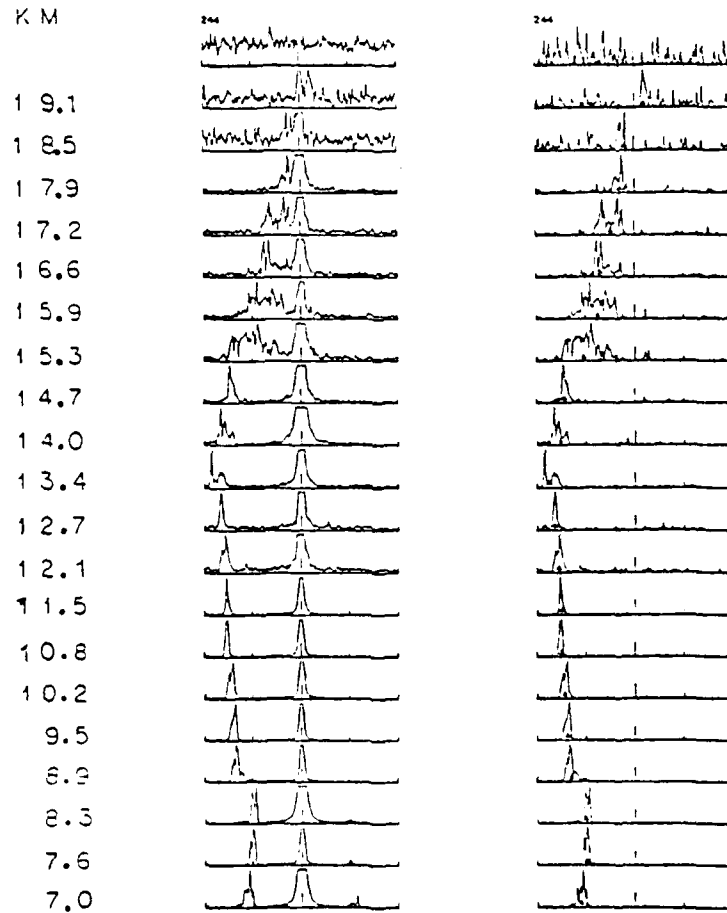


Figure 1: Examples of radar derived frequency spectra. Each spectrum has a frequency range of $440 \text{ MHz} \pm 83 \text{ Hz}$. The radar transmit frequency is 440 MHz . A doppler frequency of 93 Hz corresponds to 24 m/s . The central spike (left column) is ground clutter, the other signals are returns from turbulence scattering. The right column is the same data as the left column after processing to remove clutter and noise.

IV. THE EXPERIMENTAL PROGRAM

The joint experiments were scheduled about twice per week for the month of July, 1981. Some trial experiments were also operated during May and June. On some days, two balloons were launched about two hours apart. For convenience table 1 summarizes the launch dates and times.

The radar data were gathered with either an SDS-9300 or Harris S-125 computer, the latter being a newer more reliable machine and this is listed in the table.

Unfortunately, the optical scintillometer that was operated by AFGL, was only successfully operated on one day. This was due to both equipment failures and lack of cloudless nights.

V. RESULTS

For each experiment the radar was generally operated for at least an hour before the balloon launch. The time to gather an individual C_n^2 profile was 56 seconds on the SDS-9300, and 80 seconds on the Harris S-125 computer. Thus over the period of a few hours, a very large amount of data was accumulated. The spectral data have been processed into shorter computer disk files containing only C_n^2 and velocity component data. These data have been retained on disk files at the radar site. Copies of these files on magnetic tape can be used by AFGL for plotting data in any desired format. This report briefly summarizes only a very small portion of the total data.

(a) C_n^2 Profiles

For some initial comparisons, the C_n^2 data have been plotted for all experiments from 6/30/81 to 7/31/81. An earlier experiment on 5/21/81 has also been processed and the data are stored on a disk file. However it has not been plotted because the pen plotter failed before this final task could be done.

As a general example, Figure 2 shows data points from 30 sequential integration periods. The start times of the first and last integration

Table 1

Experiment		Computer	Data Disk File	Balloon Launch Time	Comments
Date	Time				
5/21/81		SDS Harris	DH:BAφφ	--	
6/30/81 7/1/81	2300- 0100	SDS	DS:BAφ1	--	
7/1/81	0144- 0258	SDS	DS:BAφ2	--	
7/8/81 7/9/81	1929- 0255	Harris	DH:BAφ3	0128	
7/9/81 7/10/81	2040- 0348	Harris	DH:BAφ4	0138	
7/11/81 7/12/81	1952 0315	Harris	DH:BA056	2033 0130	
7/16/81	2100	Harris	--	--	Radar Data Invalid Because of Radar Timer Failure
7/17/81	0144	SDS	DS:BAφ8	0118	
7/23/81 7/24/81	2012 0341	SDS Harris	DH:BAφ9	2057 0238	Second balloon launched at 0238 had no ΔT measurements
7/25/81	--	Harris	DH:BA10	2042	Very poor quality Radar Data
7/28/81	1956 0248	Harris	DH:BA11	2050	
7/29/81 7/30/81	1918 0236	Harris	DH:BA123	2141 0114	
7/30/81 7/31/81	1932 0252	Harris	DH:BA145	2015 0125	Optical Scintillometer also working

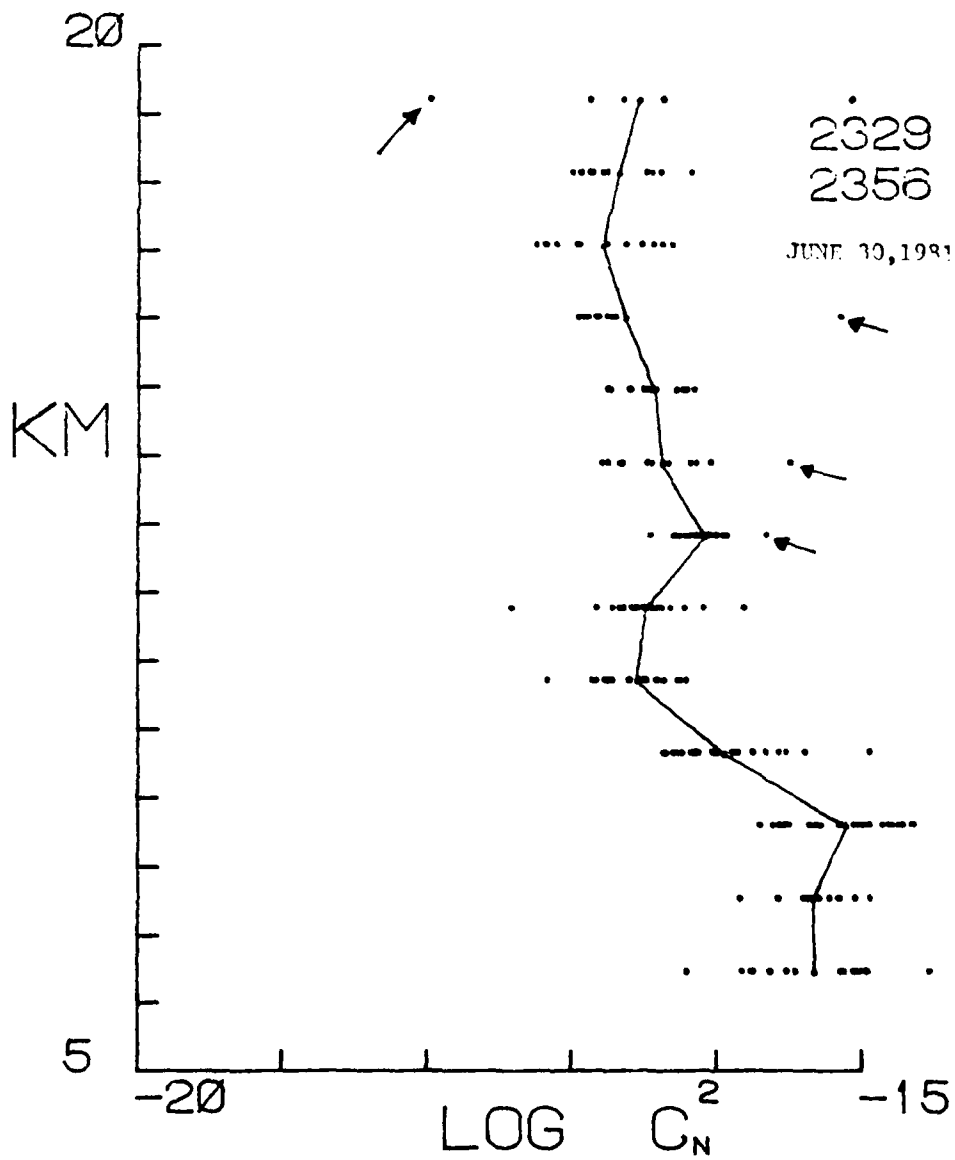


Figure 2 : Example of a height profile of the refractivity turbulence structure constant C_n^2 . The data were gathered in 30 separate integration periods from 2329 to 2356 universal time. The solid line is the averaged value.

periods are shown in the top corner of the diagram. These are universal times (four hours ahead of local time). An average profile has been drawn through the data points. The entire analysis and plotting is done by computer with no editing of data points. Within this 28 minute time there is about a factor of ten variation of C_n^2 at any particular height. There are some spurious data points marked by arrows and these can affect the average values. For example, for this Figure 2, at the 16 km height, one bad data point has moved the average value off the cluster of good data points. Any user of these data should be aware that all data points are not valid. These bad points arise from a number of reasons, eg. external RF interference.

To illustrate the short-term temporal behavior, the Figure 3 shows two profiles of C_n^2 taken during a few hours apart. It can be seen that over these six hours of time, the overall profile shape does not vary considerably, but some heights (eg. 10 km) can exhibit shorter term variations by a factor of 10-100. The Figure 4 has representative C_n^2 profiles from nine separate days radar data. The troposphere (~ 5-10 kms) in particular exhibits large day to day variations. For example the data for July 9 and July 28 have values in excess of 10^{-15} at 5 km altitude whereas the July 29 data have values about 10^{-17} at the same altitude. The stratosphere (> 10 km) data have lesser day to day variations. A remarkable feature in the July 8 data is the persistent layer at 13 km altitude with low C_n^2 values.

(b) Comparisons with Radar Data from other Locations

The decrease of C_n^2 with altitude in the stratosphere has been reported elsewhere⁸. Most profiles examined by this investigator had 1.2 - 1.5 db/km rates of C_n^2 decrease with increasing altitude. However, only a few profiles that had data with smooth height variations were measured. The majority of C_n^2 profiles [see for example the July 8 data on figure 4] had steep and varying C_n^2 gradients, and it did not seem meaningful to assign an average gradient to such data. Balsley and Peterson⁸ give a value of 1.3 db/km for their stratosphere data.

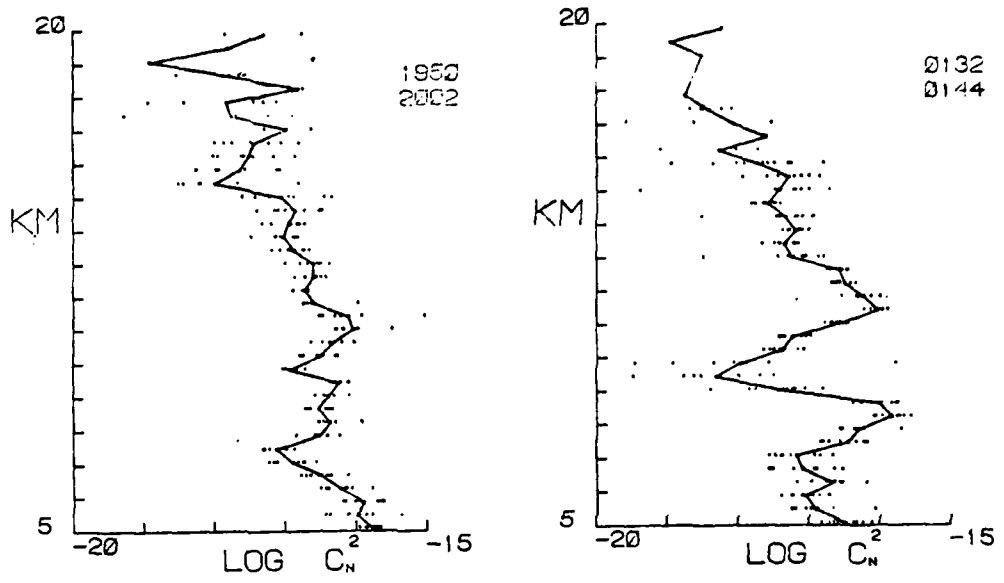


Figure 3 : Examples of two C_n^2 profiles gathered on the same day (July 30, 1981) approximately five and one half hours apart.

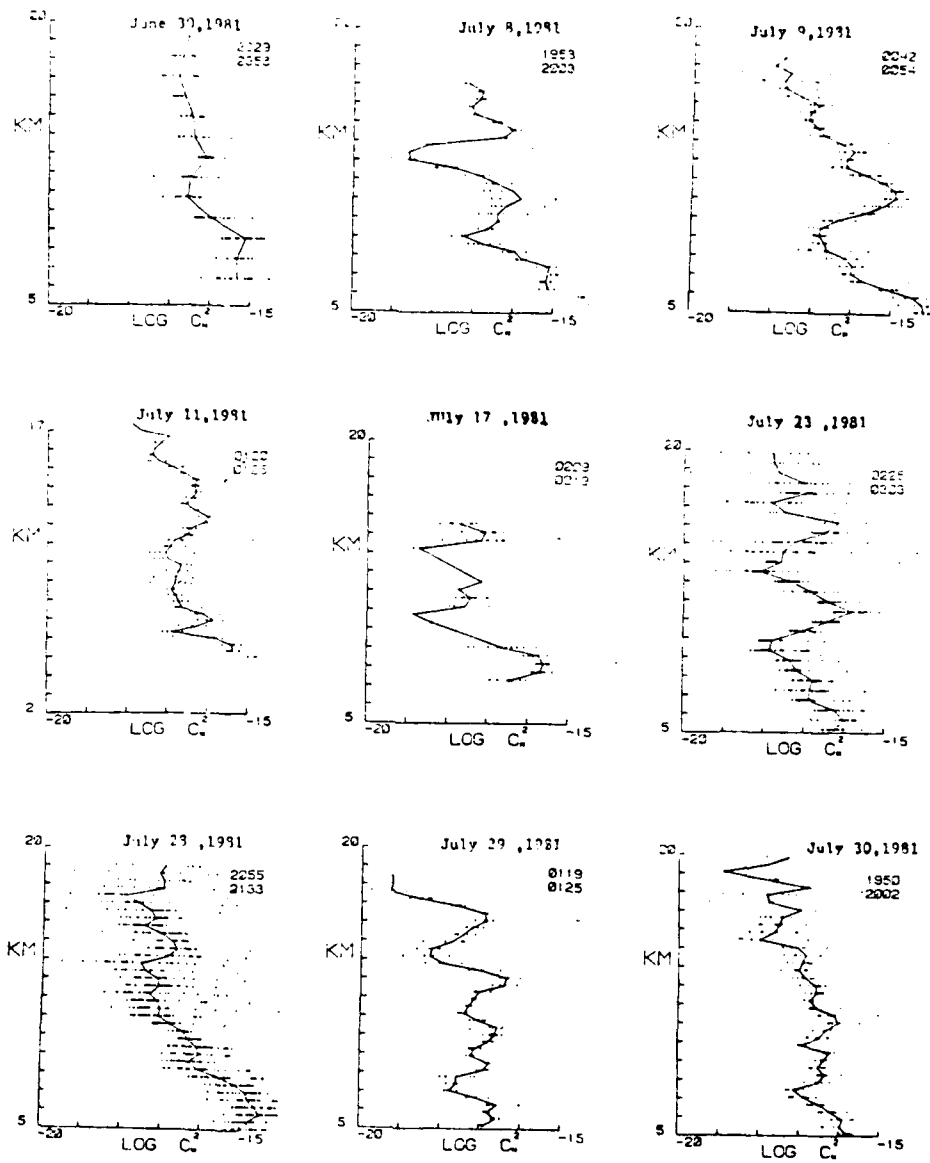


Figure 4: Representative profiles of C_n^2 for nine days during the month of July 1981.

With regard to the absolute magnitude of C_n^2 , the Millstone Hill data have been compared with data gathered at a radar located at Chatanika, Alaska⁸. The averaged data from several days of the Alaskan data are shown in Figure 5. The approximate range of C_n^2 found in the Millstone Hill data are plotted as horizontal bars. While this diagram indicates a good agreement at the upper heights (stratosphere), the Millstone data more frequently exhibited values at the higher end of range. The troposphere data (below about 10 kms altitude) from Millstone Hill were considerably greater than the Chatanika data.

Some earlier work was done at the Millstone Hill radar site by Crane⁹. Turbulence data were gathered using an entirely different radar and signal processing system. It is of interest to note that these C_n^2 data, gathered in 1968, had magnitudes similar to those found by this investigator.

(c) Comparisons with Optical Scintillometer Data

The optical scintillometer was only operated for one night in conjunction with the radar. A preliminary comparison is shown in Figure 6. The vertical resolution of the scintillometer is considerably coarser than the radar; there being only four points on the 5-20 km height interval of Figure 6. The scintillometer averages over the several kms of atmosphere between the data points. While this comparison appears favorable, a more extensive comparative analysis should be undertaken.

VI. RECOMMENDATIONS

The work outlined in this report mainly focussed on securing the basic turbulence data and considerable effort is further needed to fully define a climatology of the atmospheric refractivity turbulence structure constant. Nevertheless, the preliminary analysis conducted points to several unanswered questions, and poses several research areas that should be pursued.

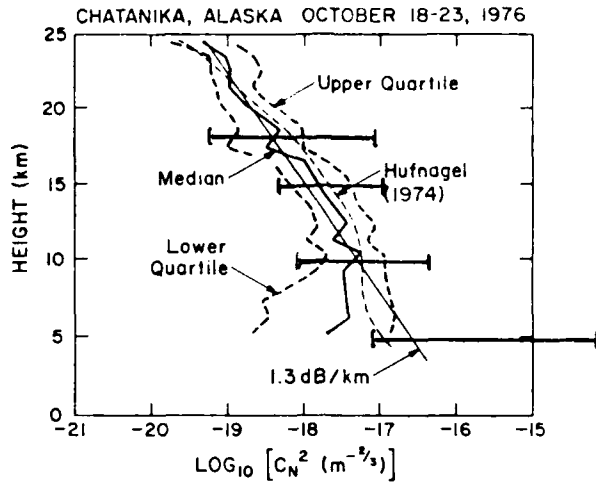


FIG. 5 Median and upper and lower quartile values of C_N^2 as a function of height based on 32 azimuth scans spaced over several days. The statistical model of Hufnagel and a line of constant rate of dropoff are shown for comparison.

(after Balsley and Peterson, 1981)

The horizontal lines are the approximate range of C_N^2 found at the Millstone Hill location. The other data were gathered at Chatanika, Alaska.

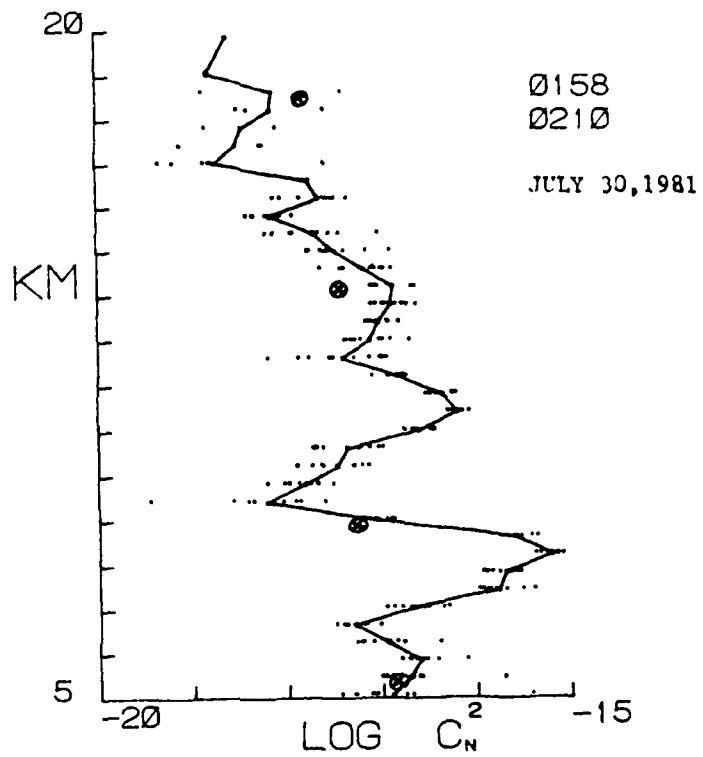


Figure 6: A comparison of radar derived C_n^2 data with optical scintillometer derived data.ⁿ The points are radar data for ten integration periods. The solid line is the average profile. The four crosses were derived from the scintillometer.

The first goal of further analysis should be to compare radar C_n^2 values with the balloon data. The AFGL balloon analysis programs are more time consuming than the radar analysis, therefore a comparison could not be made in the summer schedule. Second, a more comprehensive comparison of theoretical turbulence data should be done. In the troposphere there is substantial quantities of water vapor and the appropriate corrections to the radar measured refractivity should be made.

It should be the future goal to utilize data from turbulence scatter radars to help build a model of the atmospheric turbulence morphology. This should be of value to Air Force applications involving transmission of electromagnetic waves through the atmosphere.

More research is required to determine

- a) Is there a geographic difference in the levels of turbulence?
- b) What is the relation between weather systems and turbulence?
- c) Is there any average seasonal or diurnal variation?

It would be of great value to perform similar experiments at other radar sites. In particular the Poker Flat, Alaska radar is now operating continuously. This would afford the possibility of operating an optical scintillometer for long continuous experiments in winter when no contaminating sunlight is present.

A big advantage of the balloon and optical techniques is that they are portable. Thus the same instrument can be used at different locations which is valuable for intercomparisons of radar. This advantage should be exploited if the Air Force is to utilize the growing number of turbulence scatter radars. The future long continuous radar records could then be utilized with confidence for Air Force purposes.

REFERENCES

1. N. W. Rosenberg, R. E. Good, W. K. Vickery, and E. M. Dewan, "Experimental Investigation of Small Scale Transport Mechanisms in the Stratosphere", AIAA Journal, Vol. 12, No 8, p 1094, 1974.
2. P. K. James, "A Review of Radar Observations of the Troposphere in Clear Air Conditions", Radio Science, Vol. 15, No. 12, p. 151, 1980.
3. R. K. Crane, "A Review of Radar Observations of Turbulence in the Lower Stratosphere", Radio Science, Vol. 15, No. 12, p. 177, 1980.
4. B. B. Balsley and K. S. Gage, "The MST Radar Technique: Potential for Middle Atmosphere Studies", Pure and Applied Geophysics, Vol. 118, Nos. 1/2, p. 452, 1980.
5. B. J. Watkins and R. H. Wand, "Observations of Clear Air Turbulence and Winds with the Millstone Hill Radar", in press Journal of Geophysical Research, 1981.
6. M. Azouit and J. Vernin, "Remote Investigation of Tropospheric Turbulence by Two-Dimensional Analysis of Stellar Scintillation", Journal of Atmospheric Sciences, Vol. 37, p. 1550, 1980.
7. H. Ottersten, "Atmospheric Structure and Radar Backscattering in Clear Air", Radio Science, Vol. 4, p. 1179, 1969.
8. B. B. Balsley and V. L. Peterson, "Doppler-Radar Measurements of Clear Air Atmospheric Turbulence at 1290 MHz", J. of Applied Meteorology, Vol. 20, No. 3, 1981.
9. R. K. Crane, "Stratospheric Turbulence Analysis", Rep. AFGL-TR-77-0207 (ADO 47740), Air Force Geophysics Lab, Hanscom Air Force Base, Mass, 1977.

1981 USAF - SCEEE SUMMER FACULTY RESEARCH PROGRAM

Sponsored by the

AIR FORCE OFFICE OF SCIENTIFIC RESEARCH

Conducted by the

SOUTHEASTERN CENTER FOR ELECTRICAL ENGINEERING EDUCATION

FINAL REPORT

OPTIMAL DESIGN OF DIGITAL FLIGHT CONTROL

SYSTEMS FOLLOWING AN ANALOG MODEL

Prepared by: Hsi-Han Yeh

Academic Rank: Associate Professor

Department and University: Department of Electrical Engineering
University of Kentucky

Research Location: Flight Dynamics Laboratory, Flight Control Division,
Control Dynamics Branch, Control Analysis Group

USAF Research Colleague: David K. Bowser, Group Leader

Date: August 14, 1981

Contract No: F49620-79-C-0038

OPTIMAL DESIGN OF DIGITAL FLIGHT CONTROL

SYSTEMS FOLLOWING AN ANALOG MODEL

by

Hsi-Han Yeh

ABSTRACT

The problem of designing a digital controller to replace an analog controller in a flight control system is studied. The objective of the research is to develop a method for synthesizing the z-transfer function of the digital controller which operates at a given sampling rate and preserves the characteristics of the original continuous system as much as possible.

The mathematical tool used in this research is an extended maximum principle of the Pontryagin type, which enables one to synthesize the output signal of a zero-order hold following the digital controller. A performance index of integral squared difference between the continuous state trajectory of the digital control system and that of the continuous model is selected as a means to preserve the performance characteristics. The rationale in the choice of this performance index is that the state trajectories of a continuous control system and a digital control system can be compared over the entire time axis, whereas the comparison between their frequency responses becomes meaningless as the signal frequency approaches the folding frequency.

The z-transfer function of the digital controller is obtained in terms of the parameters of the continuous model. Recommendations for further research in this area are made.

ACKNOWLEDGMENTS

The author hereby expresses his gratitude to the Air Force Systems Command, the Air Force Office of Scientific Research and the Southeastern Center for Electrical Engineering Education for providing him with the opportunity to spend a very worthwhile and interesting summer at the Flight Dynamics Laboratory, Wright-Patterson Air Force Base, Ohio. He appreciates the hospitality and excellent working conditions that the Control Dynamics Branch offered.

The author would also like to thank Mr. David K. Bowser for his direction and guidance, Drs. Robert Schwanz and Siva Banda and Lt. Christopher Worsowicz for many helpful discussions, and Lts. Holly Emrick, Christopher Worsowicz, and Allen Ballenger for the briefing on the on-going research in the digital flight control systems area. Finally he would like to thank Miss Gail McAlister and the Department of Electrical Engineering, University of Kentucky, for typing this report.

I. INTRODUCTION

Discretization of flight control systems has been of increasing interest to the Air Force. One of the problems confronting the designer is the real-time implementation of advanced control algorithms within the computational capability of the on-board computer. Although digital computer technology continues to advance significantly, new and expanded software requirements for such functions as navigation, display and control manage to keep pace with improvements in computational capability. As a rule, only a small fraction of the CPU frame time is allocated for control law computation. Hence, from the standpoint of implementation, the sampling rate should be sufficiently low in order to allow time for computation and for the computer to be time-shared. But lower limits of the sampling rate are determined by factors such as roughness in the time response, errors due to measurement noise and sensitivity to plant parameter uncertainty and disturbances. The control system designer is then faced with the task of optimizing the performance of the digital control system at a given rate of sampling.

In converting a continuous-data (analog) controller into a digital controller, ad hoc approaches such as prewarped bilinear transform and Tustin transform techniques have typically been used. These methods have the advantage of being straightforward and easy to use, and they are intuitively appealing. But the performance of a system digitalized by these approaches resembles the performance of the baseline (continuous) system only when the sampling frequency is relatively high, because the dynamics of the plant and the feedback structure of the system are not taken into consideration.

Three years ago Rattan and the author of this report presented a method [1] using a complex-curve fitting technique to synthesize the digital controller so that the frequency response of the digitalized system matches that of the original continuous model with a least-square fit. This method was recently applied to a mathematical model of the longitudinal flight control of the YF-16 fighter aircraft at an altitude of 30,000 ft. and Mach 0.6. Results [2] better than that of Tustin transform approach have been obtained, especially for lower

sampling frequencies. However, this method does not take the time-domain performances into consideration; and only the magnitude plots of the frequency responses are matched, without regard to the phase plot. Moreover, the comparison between the frequency response of a continuous system and the frequency response of a digital control system becomes meaningless as the signal frequency approaches the folding frequency (one half of the sampling frequency). To compensate for these shortcomings, the state-variable design techniques in the time-domain should be developed,

In a previous study, the author and his associate showed that [3] by using z-transformation technique, a digital controller can always be synthesized so that the output of the digitalized system matches the output of the continuous model at all sampling instants, under the stimulation of the same input. However, if the matching between the frequency responses of two linear dynamical systems are desired, one must match the time responses over the entire time axis, not just at the sampling instants.

In this study, an attempt is made to match the continuous state trajectory of the digital control system with that of its analog (continuous-data) model. Matching the state trajectories instead of the output responses assures that the performances of the internal variables of the plant, as well as the output variable, are preserved in the discretization. It should also be emphasized that the matching is specified over the entire continuous time axis, not just at discrete sampling instants, and is quantified by a minimum integral squared error. The choice of this performance criterion is motivated by the fact that if the state trajectories of two linear dynamical systems match, then frequency responses of the two systems will also match, as seen by Laplace-transforming the state equations.

The mathematical tool used in this research is an extended maximum principle of the Pontryagin type, which enables one to synthesize a "staircase" type of optimal control signals, such as the output signal of a zero-order hold associated with a digital controller. The extended maximum principle was initiated by Chang [4] and further developed by the author and his co-workers [5-9].

II. OBJECTIVES

The main objective of this research is to derive a general mathematical expression of the digital controller which may be used to replace the continuous (analog) controller of a general system while preserving as much as possible the performance characteristics of the original continuous system. The specific objectives are

- (1) To derive an optimal control law for the digital control system.
- (2) To obtain the z-transfer function of the optimal digital controller in terms of the parameters of the continuous model.
- (3) To identify problems and to find directions for future research.

No attempt has been made, however, to obtain numerical results for flight control examples; nor was there an attempt to develop computer programs for evaluation of the z-transfer function of the digital controller, as these will be proposed for future research.

III. FORMULATION OF THE DESIGN PROBLEM

Consider a continuous control system (Fig. 1) that has satisfactory (or ideal) performances. The state and output equations of the plant are given by

$$\dot{\underline{x}}_a = A \underline{x}_a(t) + \underline{b} u_m(t) \quad (1)$$

$$y_m(t) = \bar{c} \underline{x}_a(t) + d u_m(t) \quad (2)$$

The state and output equations of the controller are given by

$$\dot{\underline{x}}_c(t) = A_c \underline{x}_c(t) + \underline{b}_c e_m(t) \quad (3)$$

$$u_m(t) = \bar{c}_c \underline{x}_c(t) + d_c e_m(t) \quad (4)$$

where $\underline{x}_a(t)$ and $\underline{x}_c(t)$ are n and n_c dimensional vectors, respectively, and $u_m(t)$, $e_m(t)$, $y_m(t)$ and $r(t)$ are scalar functions. The dimensions

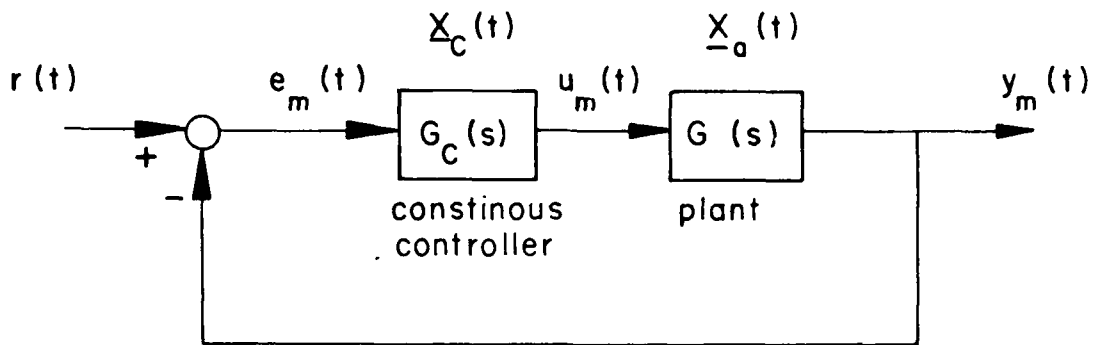


Fig. 1 Continuous System Model

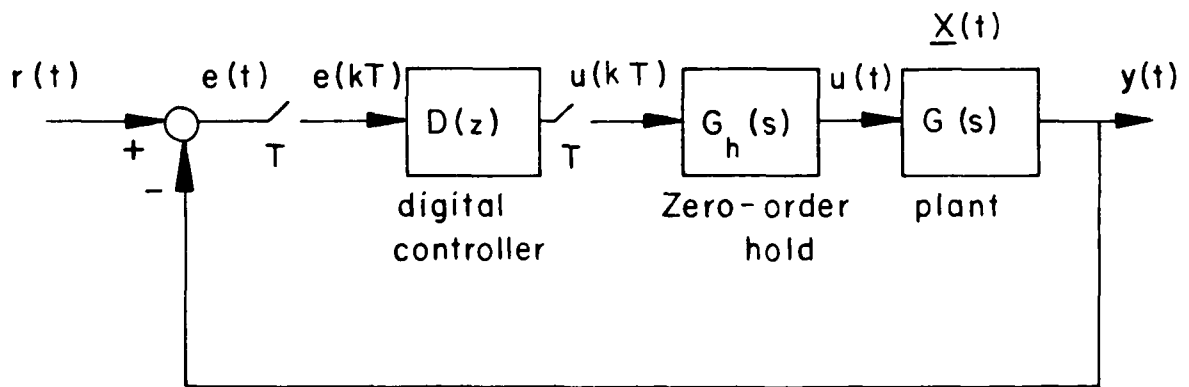


Fig. 2 The Digitalized System

of the coefficient matrices are commensurate with the vectors with which they associate. The design objective is to replace the controller $G_c(s)$ by a digital controller $D(z)$ such that the state trajectory of the digitalized system matches that of the continuous model as closely as possible. The digital control system is represented by Fig. 2, where $G(s)$ is the same plant as in the continuous model, and $D(z)$ is to be synthesized in such a way that when $r(t)$ is a unit-step function, the performance index

$$J = \int_0^{\infty} \frac{1}{2} [\underline{x}(t) - \underline{x}_a(t)]' Q [\underline{x}(t) - \underline{x}_a(t)] dt \quad (5)$$

attains its minimum, where

$$Q = \begin{bmatrix} q_1 & 0 & \dots & 0 \\ 0 & q_2 & \dots & 0 \\ \cdot & \cdot & & \cdot \\ \cdot & \cdot & & \cdot \\ \cdot & \cdot & & \cdot \\ 0 & 0 & \dots & q_n \end{bmatrix} \quad (6)$$

Note that the performance index is an integral, not a discrete sum. Therefore an attempt is made to match the trajectories over continuous time axis, not just at the sampling instants. The state and output equations of the plant in the digital control system are

$$\dot{\underline{x}}(t) = A \underline{x}(t) + \underline{b} u(kT) \quad (7)$$

$$y(t) = \bar{c} \underline{x}(t) + d u(kT) \quad (8)$$

for $kT < t \leq (k+1)T$, on account of the zero-order hold used in the digital control system (Fig. 2).

IV. THE OPTIMAL STRATEGY

(a) The Extended Maximum Principle

An extended version of the maximum principle of Pontryagin will be used to find the optimal control sequence $u(kT)$, $k = 0, 1, 2, \dots$, which minimizes the performance index (5). The error sequence $e(kT)$ can be expressed in terms of $u(kT)$, and the digital controller $D(z)$ can be determined by

$$D(z) = \frac{U(z)}{E(z)} \quad (9)$$

where $U(z)$ is the z -transform of $u(kT)$ and $E(z)$ is the z -transform of $e(kT)$.

The original Pontryagin's Maximum Principle cannot be applied to this problem in which the control function must be sampled and held, i.e.,

$$u(t) = u(kT) \quad kT < t \leq (k+1)T \quad (10)$$

The derivation of Pontryagin's maximum principle is based on the assumption that piece-by-piece patchwork of admissible control functions is again admissible. This condition is not satisfied by the output of a zero-order hold following a constant rate sampler, if the point of patching is selected at an instant other than the sampling instants. However, the extended maximum principle may be applied to the case where the control inputs are outputs of zero-order holds [5-9]. Following the derivation of [7], it can be readily shown that a necessary condition for an admissible control $u(t)$ to be optimal is that

$$\int_{kT}^{(k+1)T} \underline{b}' \underline{p}(t) dt = 0 \quad (11)$$

where $\underline{p}(t)$ is the state vector of the adjoint system satisfying

$$\dot{\underline{p}}(t) = - \frac{\partial H(\underline{x}(t), \underline{p}(t), u(t))}{\partial \underline{x}(t)} \quad (12)$$

and $H(\underline{x}(t), \underline{p}(t), u(t))$ is the Hamiltonian function given by

$$H(\underline{x}(t), \underline{p}(t), u(t)) = \underline{p}'(t) \dot{\underline{x}}(t) - \frac{1}{2} [\underline{x}(t) - \underline{x}_a(t)]' Q [\underline{x}(t) - \underline{x}_a(t)] \quad (13)$$

Now substituting (13) into (12) and invoking (6) gives the adjoint state equation

$$\dot{\underline{p}}(t) = -A' \underline{p}(t) + Q[\underline{x}(t) - \underline{x}_a(t)] \quad (14)$$

The difficulty in the application of the maximum principle is the two-point boundary value problem. In this formulation, the two-point boundary value problem is as follows: For any i , if $x_i(0)$ is given, then $p_i(0)$ is unspecified (remains to be determined from (7), (11) and (14)). If $x_i(0)$ is unspecified (remains to be determined by the maximum principle), then $p_i(0) = 0$. The same rule applies to $x_i(\infty)$ and $p_i(\infty)$.

(b) Determination of Optimal Control Sequence

In order to solve Eq. (11) for the optimal control sequence, the solution $\underline{p}(t)$ must first be obtained from Eq. (14), which calls for the solutions of $\underline{x}(t)$ in terms of $u(kT)$, and $\underline{x}_a(t)$ in terms of $r(t)$.

Let the augmented state vector of the model be

$$\underline{x}_m(t) = \begin{bmatrix} \underline{x}_a(t) \\ \underline{x}_c(t) \end{bmatrix} \quad (15)$$

It follows from Appendix A that

$$\dot{\underline{x}}_m(t) = A_m \underline{x}_m(t) + \underline{b}_m r(t) \quad (16)$$

where

$$A_m = \begin{bmatrix} A - \frac{\underline{b}d_c \bar{c}}{1+dd_c} & \frac{\underline{b}\bar{c}_c}{1+dd_c} \\ \frac{-\underline{b}_c \bar{c}}{1+dd_c} & A_c - \frac{\underline{b}_c d_c \bar{c}_c}{1+dd_c} \end{bmatrix} \quad (17)$$

$$\underline{b}_m = \begin{bmatrix} \frac{\underline{b}d_c}{1+dd_c} \\ \frac{\underline{b}_c}{1+dd_c} \end{bmatrix} \quad (18)$$

Define Q_m to be the $n \times (n + n_c)$ matrix obtained by augmenting n_c columns of zeros to Q , i.e.,

$$Q_m = [Q \ 0] \quad (19)$$

Then by definition

$$Q \underline{x}_a(t) = Q_m \underline{x}_m(t) \quad (20)$$

Assume that $r(t)$ is a step function, i.e.,

$$r(t) = \begin{cases} \alpha & t \geq 0 \\ 0 & t < 0 \end{cases} \quad (21)$$

It is shown in Appendix B that, for $kT < t \leq (k+1)T$,

$$\underline{x}(t) = \phi(t-kT) \underline{x}(kT) + \phi^S(t-kT) \underline{b} u(kT) \quad (22)$$

$$\underline{x}_m(t) = \phi_m(t-kT) \underline{x}_m(kT) + \phi_m^S(t-kT) \underline{b}_m \alpha \quad (23)$$

and

$$\begin{aligned} \underline{p}(t) = & \Psi(t-kT) \underline{p}(kT) + F(t-kT) \underline{x}(kT) + F^S(t-kT) \underline{b} u(kT) \\ & - F_m(t-kT) \underline{x}_m(kT) - F_m^S(t-kT) \underline{b}_m \alpha \end{aligned} \quad (24)$$

where

$$\phi(t) = \epsilon^{At} \quad (25)$$

$$\phi^S(t) = \int_0^t \phi(\tau) d\tau \quad (26)$$

$$\phi_m(t) = \epsilon_m^{A_m t} \quad (27)$$

$$\phi_m^S(t) = \int_0^t \phi_m(\tau) d\tau \quad (28)$$

$$\Psi(t) = \epsilon^{-A^* t} \quad (29)$$

$$F(t) = \int_0^t \Psi(t-\tau) Q \phi(\tau) d\tau = \Psi(t) * Q \phi(t) \quad (30)$$

$$F^S(t) = \int_0^t F(\tau) d\tau \quad (31)$$

$$F_m(t) = \int_0^t \Psi(t-\tau) Q_m \phi_m(\tau) d\tau = \Psi(t) * Q_m \phi_m(t) \quad (32)$$

$$F_m^S(t) = \int_0^t F_m(\tau) d\tau \quad (33)$$

Substituting Eq. (24) into Eq. (11) gives

$$\begin{aligned} \underline{b}' [\Psi^S(T) \underline{p}(kT) + F^S(T) \underline{x}(kT) + F^{SS}(T) \underline{b} u(kT) \\ - F_m^S(T) \underline{x}_m(kT) - F_m^{SS}(T) \underline{b}_m \alpha] = 0 \end{aligned} \quad (34)$$

where

$$\Psi^S(T) = \int_0^T \Psi(t) dt \quad (35)$$

$$F^{SS}(T) = \int_0^T F^S(t) dt \quad (36)$$

$$F_m^{SS}(T) = \int_0^T F_m^S(t) dt \quad (37)$$

Solving Eq. (34) for the optimal control sequence gives

$$u(kT) = \frac{b'}{b' F^{SS}(T) b} [-\Psi^S(T) p(kT) - F^S(T) \underline{x}(kT) + F_m^S(T) \underline{x}_m(kT) + F_m^{SS}(T) \underline{b}_m \alpha] \quad (38)$$

Eq. (38) may be used to compute $u(kT)$ iteratively after the two-point boundary problem is solved. In this research Eq. (9) is used to synthesize the digital controller transfer function $D(z)$. The two-point boundary problem still arises and will be treated in the next section.

V. THE DIGITAL CONTROLLER

(a) z-Transform of the Optimal Control Sequence

In order to determine $U(z)$ for use in Eq. (9), $P(z)$, $X(z)$ and $X_m(z)$ must be determined first. Setting $t = (k+1)T$ in Eqs. (22) - (24) gives

$$\underline{x}[(k+1)T] = \Phi(T) \underline{x}(kT) + \Phi^S(T) \underline{b} u(kT) \quad (39)$$

$$\underline{x}_m[(k+1)T] = \Phi_m(T) \underline{x}_m(kT) + \Phi_m^S(T) \underline{b}_m \alpha \quad (40)$$

$$\begin{aligned} p[(k+1)T] &= \Psi(T) p(kT) + F(T) \underline{x}(kT) - F_m(T) \underline{x}_m(kT) \\ &+ F^S(T) \underline{b} u(kT) - F_m^S(T) \underline{b}_m \alpha \end{aligned} \quad (41)$$

Taking z-transformation of Eqs. (39) - (41) gives, respectively,

$$\underline{X}(z) = \hat{\phi}(z) [z \underline{x}(0) + \phi^S(T) \underline{b} U(z)] \quad (42)$$

$$\underline{X}_m(z) = \hat{\phi}_m(z) \left[z \underline{x}_m(0) + \phi_m^S(T) \underline{b}_m \frac{\alpha z}{z-1} \right] \quad (43)$$

$$\begin{aligned} \underline{P}(z) = \hat{\psi}(z) \left[z \underline{p}(0) + F(T) \underline{X}(z) - F_m(T) \underline{X}_m(z) \right. \\ \left. + F^S(T) \underline{b} U(z) - F_m^S(T) \underline{b}_m \frac{\alpha z}{z-1} \right] \end{aligned} \quad (44)$$

where

$$\hat{\phi}(z) = [zI - \phi(T)]^{-1} \quad (45)$$

$$\hat{\phi}_m(z) = [zI - \phi_m(T)]^{-1} \quad (46)$$

$$\hat{\psi}(z) = [zI - \psi(T)]^{-1} \quad (47)$$

Substituting Eqs. (42) and (43) into Eq. (44) gives

$$\begin{aligned} \underline{P}(z) = \hat{\psi}(z) \{ z \underline{p}(0) + F(T) \hat{\phi}(z) z \underline{x}(0) - F_m(T) \hat{\phi}_m(z) z \underline{x}_m(0) \\ - [F_m(T) \hat{\phi}_m(z) \phi_m^S(T) + F_m^S(T)] \underline{b}_m \frac{\alpha z}{z-1} \\ + [F(T) \hat{\phi}(z) \phi^S(T) + F^S(T)] \underline{b} U(z) \} \end{aligned} \quad (48)$$

Substituting Eqs. (42), (43) and (48) into the z-transform of Eq. (38), we obtain a solution for U(z) as

$$\begin{aligned} U(z) = \frac{\underline{b}'}{\underline{b}' H(z) \underline{b}} \left[K_m(z) z \underline{x}_m(0) - K(z) z \underline{x}(0) - K_0(z) z \underline{p}(0) \right. \\ \left. + H_m(z) \underline{b}_m \frac{\alpha z}{z-1} \right] \end{aligned} \quad (49)$$

where

$$K_m(z) = [\Psi^S(T) \hat{\Psi}(z) F_m(T) + F_m^S(T)] \hat{\phi}_m(z) \quad (50)$$

$$K(z) = [\Psi^S(T) \hat{\Psi}(z) F(T) + F^S(T)] \hat{\phi}(z) \quad (51)$$

$$K_0(z) = \Psi^S(T) \hat{\Psi}(z) \quad (52)$$

$$H_m(z) = F_m^{SS}(T) + K_0(z) F_m^S(T) + K_m(z) \phi_m^S(T) \quad (53)$$

$$H(z) = F^{SS}(T) + K_0(z) F^S(T) + K(z) \phi^S(T) \quad (54)$$

(b) z-Transform of the Error Sequence

From the block diagram of Fig. 2 and Eqs. (8) and (22) we may write

$$e(t) = r(t) - y(t) = \alpha - y(t) \quad (55)$$

$$y(t) = \bar{c} \phi(t-kT) \underline{x}(kT) + [\bar{c} \phi^S(t-kT) \underline{b} + d] u(kT) \quad (56)$$

for $kT < t \leq (k+1)T$. Therefore

$$e[(k+1)T] = \alpha - \bar{c} \phi(T) \underline{x}(kT) - [\bar{c} \phi^S(T) \underline{b} + d] u(kT) \quad (57)$$

Taking z-transform of the above equation, we have

$$E(z) = e(0^+) + \frac{\alpha}{z-1} - \frac{1}{z} \bar{c} \phi(T) \underline{X}(z) - \frac{1}{z} [\bar{c} \phi^S(T) \underline{b} + d] U(z) \quad (58)$$

where $e(0^+)$ is found from Eq. (55) and Eq. (8).

$$e(0^+) = \alpha - \bar{c} \underline{x}(0^+) - d u(0^+) \quad (59)$$

Substituting Eqs. (59) and (42) into (58), we have

$$E(z) = \frac{\alpha z}{z-1} - d u(0^+) - \bar{c}[I + \phi(T) \hat{\phi}(z)] \underline{x}(0^+) - \frac{1}{z} [\bar{c}(I + \phi(T) \hat{\phi}(z)) \phi^S(T) \underline{b} + d] U(z) \quad (60)$$

where $u(0^+)$ may be obtained from Eq. (38). Setting $k = 0$ in Eq. (38) and substituting the resulting expression of $u(0^+)$ into (60) yields

$$E(z) = \left[\frac{z}{z-1} - \frac{\underline{b}' F_m^{SS}(T) \underline{b}_m}{\underline{b}' F^{SS}(T) \underline{b}} d \right] \alpha + \frac{d \underline{b}' \psi^S(T)}{\underline{b}' F^{SS}(T) \underline{b}} p(0) - \frac{d \underline{b}' F_m^S(T)}{\underline{b}' F^{SS}(T) \underline{b}} \underline{x}_m(0) + \left[\frac{d \underline{b}' F^S(T)}{\underline{b}' F^{SS}(T) \underline{b}} - \bar{c}(I + \phi(T) \hat{\phi}(z)) \right] \underline{x}(0) - \frac{1}{z} [\bar{c}(I + \phi(T) \hat{\phi}(z)) \phi^S(T) \underline{b} + d] U(z) \quad (61)$$

By virtue of the relationship given in Eq. (9), the z-transfer function of the digital controller may now be written, provided that the initial conditions $\underline{x}(0)$, $\underline{x}_m(0)$ and $p(0)$ are known.

(c) The z-Transfer Function of the Digital Controller

It is reasonable to consider the case where $\underline{x}_m(0)$ is zero. But if $\underline{x}(0)$ is given, then $p(0)$ cannot be arbitrarily specified. The maximum principle requires that $p(0)$ be such that Eqs. (7), (11) and (14) yield an optimal control sequence that drives the system from the given $\underline{x}(0)$ to a prespecified final state $\underline{x}(\infty)$, or results in $p(\infty) = 0$ if the final state is unspecified (free). Numerical determination of $p(0)$ for given $\underline{x}(\infty)$ or $p(\infty)$ is virtually impossible for systems requiring a large number of sampling periods to run, because either matrix A or $-A'$ has eigenvalues in the unstable region. On the other hand, if $\underline{x}(0)$ is

unspecified, $\underline{p}(0)$ must be set equal to zero. But then $\underline{x}(0)$ is determined by Eqs. (7), (11) and (14) and the final condition, which is either at a given value of $\underline{x}(\infty)$ or at $\underline{p}(\infty) = 0$. Again, numerical determination of $\underline{x}(0)$ is impractical for systems requiring a large number of sampling periods to run, such as flight control systems.

For the system under consideration, the state trajectory of the continuous model is assumed to start from $\underline{x}_m(0) = 0$. Let $\underline{x}(0)$, the initial state of the plant of the digital control system, be unspecified. Then $\underline{p}(0) = 0$. However, since the minimization of the performance index given in Eq. (5) means the continuous matching of $\underline{x}(t)$ with $\underline{x}_a(t)$ over an infinitely long period of time, it is reasonable to conjecture that $\underline{x}(t)$ starts at the same point as $\underline{x}_a(t)$, or very close to it, provided that the sampling frequency is considerably higher than the natural frequency of the control system. Hence the initial condition may be chosen as

$$\underline{x}_m(0) = 0 \quad (62)$$

$$\underline{x}(0) = 0 \quad (63)$$

$$\underline{p}(0) = 0 \quad (64)$$

Substituting these conditions into Eqs. (49) and (61), and using the resulting expressions in (9), we obtain

$$\begin{aligned} \frac{1}{D(z)} = & \left[\frac{z}{z-1} - \frac{\underline{b}' F_m^{SS}(T) \underline{b}_m}{\underline{b}' F^{SS}(T) \underline{b}} d \right] \cdot \frac{\underline{b}' H(z) \underline{b}}{\underline{b}' H_m(z) \underline{b}_m} \cdot \frac{z-1}{z} \\ & - \frac{1}{z} [\bar{c}(I + \phi(T) \hat{\phi}(z)) \phi^S(T) \underline{b} + d] \end{aligned} \quad (65)$$

For most control systems, and flight control systems in particular, there is no direct linkage between the control signal and the output. For these systems, the coefficient d is zero, and the z -transfer function of the digital controller is

$$D(z) = \frac{1}{\frac{\underline{b}' H(z) \underline{b}}{\underline{b}' H_m(z) \underline{b}_m} - \frac{1}{z} \bar{c}(I + \phi(T) \hat{\phi}(z)) \phi^S(T) \underline{b}} \quad (66)$$

VI. RECOMMENDATIONS

The end result presented in Eq. (66) is computationally complicated. It needs to be demonstrated through numerical examples in order to give the users an intuitive feeling of the optimality it has achieved. I propose that we first demonstrate the numerical values of $D(z)$ through a typical classroom example. Specifically we will choose as an ideal continuous model a system that has the plant

$$G(s) = \frac{1}{s+1} \quad (67)$$

and a proportional-plus-integral controller (a "washout" compensator),

$$G_c(s) = \frac{s+2}{s} \quad (68)$$

This system would be too simple to have any bearing on flight control systems, but it is amenable to hand calculation with a desk calculator and gives the designer a feeling of what will be involved in the software. We shall then develop software for computing $D(z)$ for a general single-loop control system, and use it in a design exercise in the longitudinal control of YF-16 fighter aircraft [2,10]. The control system performance of this design shall then be compared with some baseline, namely, those designed by prewarped Tustin transformation and frequency response matching, as given in Reference [2], through simulation.

In the mathematical formulation of the design problem the quadratic difference between control variables $u(t)$ and $u_m(t)$ (see Fig. 1 and Fig. 2) is not included in the performance index (5). In other words, no attempt has been made to match the control variables of the digital system and its model. It is suggested that the same mathematical design problem using

$$J = \frac{1}{2} \int_0^{\infty} \{ [\underline{x}(t) - \underline{x}_a(t)]' Q [\underline{x}(t) - \underline{x}_a(t)] + \beta [u(t) - u_m(t)]^2 \} dt \quad (69)$$

instead of (5), and the one using

$$J = \frac{1}{2} \int_0^{\infty} [\underline{x}'(t) Q \underline{x}(t) + \beta u^2(t)] dt \quad (70)$$

instead of (5) be studied. These two performance indices restrict the behavior of the control variables as well as the state trajectory of the digitalized system and hence guarantee its stability. The performance index of Eq. (70) is used when the input is set at $r(t) = 0$ and $\underline{x}(0) \neq 0$, and is a direct optimal design approach without following a model. In continuous-data or discrete-time system applications, the use of (70) as performance index is known to result in a state feedback system whose feedback gain matrix is determined by a Riccati equation. A similar result may be expected when this performance index is used in the digitally controlled continuous systems.

The present method of synthesizing an optimal control sequence may be coupled with the vector switch decomposition technique [11,12] for use in the design of multi-rate digital control systems. The practical need of multi-rate sampling in flight control systems is a natural consequence of the finite computing capabilities of the onboard computers and the need to accommodate high frequency bending moment effects. This is recommended as a follow-on research after more insight is gained from the single-rate problem.

APPENDIX A

THE OVERALL STATE EQUATIONS OF THE CONTINUOUS MODEL

The feedback structure in Fig. 1 gives

$$e_m(t) = r(t) - y_m(t) \quad (A-1)$$

Eliminating $e_m(t)$ and $y_m(t)$ among Eqs. (A-1), (2) and (4) and solving for $u_m(t)$ gives

$$u_m(t) = \frac{-d_c \bar{c}}{1+dd_c} \underline{x}_a(t) + \frac{\bar{c}}{1+dd_c} \underline{x}_c(t) + \frac{d_c}{1+dd_c} r(t) \quad (A-2)$$

Eliminating $u_m(t)$ and $y_m(t)$ among Eqs. (A-1), (2) and (4) and solving for $e_m(t)$ gives

$$e_m(t) = \frac{-\bar{c}}{1+dd_c} \underline{x}_a(t) + \frac{-d_c \bar{c}}{1+dd_c} \underline{x}_c(t) + \frac{1}{1+dd_c} r(t) \quad (A-3)$$

Substituting (A-2) into (1) and (A-3) into (3) yields, respectively,

$$\dot{\underline{x}}_a(t) = \left(A - \frac{bd_c \bar{c}}{1+dd_c} \right) \underline{x}_a(t) + \frac{b\bar{c}}{1+dd_c} \underline{x}_c(t) + \frac{bd_c}{1+dd_c} r(t) \quad (A-4)$$

$$\dot{\underline{x}}_c(t) = \frac{-b_c \bar{c}}{1+dd_c} \underline{x}_a(t) + \left(A_c - \frac{b_c d_c \bar{c}}{1+dd_c} \right) \underline{x}_c(t) + \frac{b_c}{1+dd_c} r(t) \quad (A-5)$$

APPENDIX B

SOLUTIONS OF THE STATE AND ADJOINT EQUATIONS

The solution $\underline{p}(t)$ of Eq. (14), in terms of $\underline{x}(t)$ and $\underline{x}_a(t)$, is given by

$$\underline{p}(t) = \psi(t-kT)\underline{p}(kT) + \int_{kT}^t \psi(t-\tau)Q[\underline{x}(\tau) - \underline{x}_a(\tau)] d\tau \quad (B-1)$$

for $kT < t \leq kT$, where

$$\psi(t-kT) = e^{-A'(t-kT)} \quad (B-2)$$

With the aid of Eq. (20), Eq. (B-1) can be written as

$$\begin{aligned} \underline{p}(t) &= \psi(t-kT)\underline{p}(kT) + \int_{kT}^t \psi(t-\tau)Q\underline{x}(\tau) d\tau \\ &\quad - \int_{kT}^t \psi(t-\tau)Q_{m-m}\underline{x}_m(\tau) d\tau \end{aligned} \quad (B-3)$$

The vectors $\underline{x}_m(t)$ and $\underline{x}(t)$ are solutions of Eq. (16) and Eq. (7), respectively. They are given by, for $kT < t \leq (k+1)T$,

$$\underline{x}_m(t) = \phi_m(t-kT)\underline{x}_m(kT) + \phi_m^S(t-kT)\underline{b}_m\alpha \quad (B-4)$$

$$\underline{x}(t) = \phi(t-kT)\underline{x}(kT) + \phi^S(t-kT)\underline{b}u(kT) \quad (B-5)$$

where

$$\phi_m(t-kT) = e^{A_m(t-kT)} \quad (B-6)$$

$$\phi_m^S(t-kT) = \int_{kT}^t \phi_m(t-\tau) d\tau = \int_0^{t-kT} \phi_m(\tau) d\tau \quad (B-7)$$

$$\phi(t-kT) = e^{A(t-kT)} \quad (B-8)$$

$$\phi^S(t-kT) = \int_{kT}^t \phi(t-\tau) d\tau = \int_0^{t-kT} \phi(\tau) d\tau \quad (B-9)$$

Now substituting (B-4) and (B-5) into (B-3) and invoking (B-7) and (B-9) gives, for $kT < t \leq (k+1)T$,

$$\begin{aligned} \underline{p}(t) &= \psi(t-kT)\underline{p}(kT) + \int_{kT}^t \psi(t-\tau)Q\phi(\tau-kT) d\tau \underline{x}(kT) \\ &+ \int_{kT}^t \psi(t-\tau)Q \int_{kT}^{\tau} \phi(\tau-\lambda) d\lambda d\tau \underline{b}u(kT) \\ &- \int_{kT}^t \psi(t-\tau)Q_m \phi_m(\tau-kT) d\tau \underline{x}_m(kT) \\ &- \int_{kT}^t \psi(t-\tau)Q_m \int_{kT}^{\tau} \phi_m(\tau-\lambda) d\lambda d\tau \underline{b}_m \alpha \end{aligned} \quad (B-10)$$

In view of the identities derived in Appendix C, a new set of notations may be used for the integrals which appear in the above equation, for the sake of clarity:

$$\begin{aligned} \underline{p}(t) &= \psi(t-kT)\underline{p}(kT) + F(t-kT)\underline{x}(kT) + F^S(t-kT)\underline{b}u(kT) \\ &- F_m(t-kT)\underline{x}_m(kT) - F_m^S(t-kT)\underline{b}_m \alpha \end{aligned} \quad (B-11)$$

where

$$\begin{aligned} F(t-kT) &= \int_{kT}^t \psi(t-\tau)Q\phi(\tau-kT) d\tau \\ &= \int_0^{t-kT} \psi(t-kT-\tau)Q\phi(\tau) d\tau \end{aligned} \quad (B-12)$$

$$\begin{aligned}
F^S(t-kT) &= \int_{kT}^t \psi(t-\tau) Q \int_{kT}^{\tau} \phi(\tau-\lambda) d\lambda d\tau \\
&= \int_0^{t-kT} \int_0^{\tau} \psi(\tau-\lambda) Q \phi(\lambda) d\lambda d\tau \\
&= \int_0^{t-kT} F(\tau) d\tau \tag{B-13}
\end{aligned}$$

$$\begin{aligned}
F_m^S(t-kT) &= \int_{kT}^t \psi(t-\tau) Q_m \phi_m(\tau-kT) d\tau \\
&= \int_0^{t-kT} \psi(t-kT-\tau) Q_m \phi_m(\tau) d\tau \tag{B-14}
\end{aligned}$$

$$\begin{aligned}
F_m^S(t-kT) &= \int_{kT}^t \psi(t-\tau) Q_m \int_{kT}^{\tau} \phi_m(\tau-\lambda) d\lambda d\tau \\
&= \int_0^{t-kT} \int_0^{\tau} \psi(\tau-\lambda) Q_m \phi_m(\lambda) d\lambda d\tau \\
&= \int_0^{t-kT} F_m(\tau) d\tau \tag{B-15}
\end{aligned}$$

APPENDIX C

FORMULAS OF FINITE MULTIPLE INTEGRALS

THEOREM: The convolution between $f(t)$ and the area under $g(t)$, if it exists, is equal to the area under the convolution between $f(t)$ and $g(t)$:

$$\int_0^T f(T-\tau) \int_0^\tau g(\lambda) d\lambda d\tau = \int_0^T \int_0^t f(t-\tau)g(\tau) d\tau dt \quad (C-1)$$

Proof:

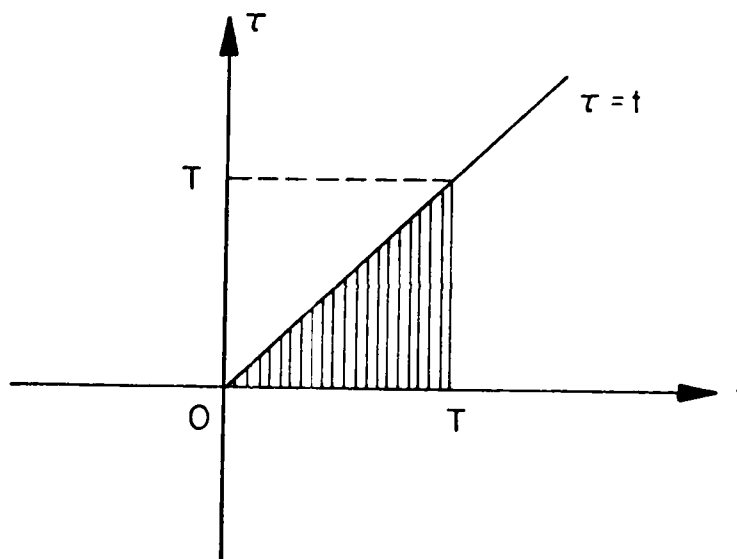


Fig. C-1. Area of integration in (t, τ) plane.

In view of Fig. C-1, interchanging the order of integration for the integral in the right-hand side of Eq. (C-1) gives

$$\int_0^T \int_0^t f(t-\tau)g(\tau) d\tau dt = \int_0^T \int_\tau^T f(t-\tau)g(\tau) dt d\tau \quad (C-2)$$

Substituting t' for $t-\tau$ and dt' for dt (regarding τ as a constant in the partial integration with respect to t) in Eq. (C-2), we obtain, after changing the integration limits accordingly,

$$\int_0^T \int_{\tau}^T f(t-\tau)g(\tau) dt d\tau = \int_0^T \int_0^{T-\tau} f(t') dt' g(\tau) d\tau \quad (C-3)$$

In a similar fashion, interchanging the order of integration in the left-hand side of Eq. (C-1) gives

$$\int_0^T f(T-\tau) \int_0^{\tau} g(\lambda) d\lambda d\tau = \int_0^T \int_{\lambda}^T f(T-\tau)g(\lambda) d\tau d\lambda \quad (C-4)$$

Substituting t for $T-\tau$ and dt for $-\tau$ and changing the integration limits accordingly in the right-hand side of Eq. (C-4) gives

$$\int_0^T \int_{\lambda}^T f(T-\tau)g(\lambda) d\tau d\lambda = \int_0^T \int_{T-\lambda}^0 (-1)f(t) dt g(\lambda) d\lambda \quad (C-5)$$

Comparison of the Eq. (C-3) with Eq. (C-5) completes the proof.

The following is a list of formulas that are used in the derivations in Appendix B. The proof involves changes of variables or changes of order of integrations, and is hence omitted.

$$\text{Formula 1.} \quad \int_{kT}^t f(t-\tau) d\tau = \int_0^{t-kT} f(\tau) d\tau$$

$$\text{Formula 2.} \quad \int_{kT}^t f(t-\tau)g(\tau-kT) d\tau = \int_0^{t-kT} f(t-kT-\tau)g(\tau) d\tau$$

$$\text{Formula 3.} \quad \int_{kT}^t f(t-\tau) \int_{kT}^{\tau} g(\tau-\lambda) d\lambda d\tau = \int_0^{t-kT} f(t-kT-\tau) \int_0^{\tau} g(\lambda) d\lambda d\tau$$

$$\text{Formula 4.} \quad \int_{kT}^t f(t-\tau) \int_{kT}^{\tau} g(\tau-\lambda) d\lambda d\tau = \int_0^{t-kT} \int_0^{\tau} f(\tau-\lambda)g(\lambda) d\lambda d\tau$$

$$\text{Formula 5. } \int_{kT}^{(k+1)T} \int_{kT}^t f(t-\tau)g(\tau-kT) d\tau dt = \int_0^T \int_0^t f(t-\tau)g(\tau) d\tau dt$$

$$\text{Formula 6. } \int_0^t f(t-\tau) \int_0^\tau g(\tau-\lambda) d\lambda d\tau = \int_0^t f(t-\tau) \int_0^\tau g(\lambda) d\lambda d\tau$$

$$\text{Formula 7. } \int_0^t f(t-\tau) \int_0^\tau g(\lambda) d\lambda d\tau = \int_0^t \int_0^\tau f(\tau-\lambda)g(\lambda) d\lambda d\tau$$

$$\text{Formula 8. } \int_0^t f(t-\tau) \int_0^\tau g(\tau-\lambda) d\lambda d\tau = \int_0^t \int_0^\tau f(\tau-\lambda)g(\lambda) d\lambda d\tau$$

$$\begin{aligned} \text{Formula 9. } & \int_{kT}^{(k+1)T} \int_{kT}^t f(t-\tau) \int_{kT}^\tau g(\tau-\lambda) d\lambda d\tau dt \\ &= \int_0^T \int_0^t f(t-\tau) \int_0^\tau g(\lambda) d\lambda d\tau dt \end{aligned}$$

$$\begin{aligned} \text{Formula 10. } & \int_{kT}^{(k+1)T} \int_{kT}^t f(t-\tau) \int_{kT}^\tau g(\tau-\lambda) d\lambda d\tau dt \\ &= \int_0^T \int_0^t \int_0^\tau f(\tau-\lambda)g(\lambda) d\lambda d\tau dt \end{aligned}$$

REFERENCES

1. K. S. Rattan and H. H. Yeh, "Discretizing Continuous Data Control Systems," Computer Aided Design, Vol. 10, No. 5, September 1978, pp. 299-306.
2. K. S. Rattan, "Digitalization of Existing Continuous Data Control Systems," AFWAL-TM-80-105-FIGC, September 1980 (Technical Memorandum), Flight Dynamics Laboratory, Wright-Patterson Air Force Base, Ohio 45433.
3. H. H. Yeh and C. S. Yeh, "On the Digital Controller Design for Point-by-point Output Matching," 10th Annual Southeastern Symposium on System Theory, Mississippi State University, March 1978.
4. S. S. L. Chang, "A General Theory of Optimal Processes," SIAM Journal of Control, Series A, Vol. 4, 1966, pp. 46-55.
5. H. H. Yeh, "An Extension of Pontryagin's Maximum Principle," Ph.D. Dissertation, Department of Electrical Engineering, Ohio State University, 1967.
6. H. H. Yeh and J. T. Tou, "On the General Theory of Optimal Processes," International Journal of Control, Vol. 9, No. 4, April 1969, pp. 433-451.
7. H. H. Yeh and Wyle Y. W. Tsan, "Optimal Synthesis of Saturating Sampled-data Systems Using Integral Performance Index," International Journal of Control, Vol. 14, No. 1, July 1971, pp. 33-42.
8. H. H. Yeh, "Optimal Control with Partially Specified Input Functions," International Journal of Control, Vol. 16, No. 1, 1972, pp. 71-80.
9. H. H. Yeh and R. J. Kuhler, "Additional Properties of an Extended Maximum Principle," International Journal of Control, Vol. 17, No. 6, 1973, pp. 1281-1286.
10. J. D. McAllister, et al., "Fighter CCV Phase II Report--Detailed Design," AFFDL-TR-76-119, October 1976, Flight Dynamics Laboratory, Wright-Patterson Air Force Base, Ohio 45433.
11. R. F. Whitbeck and L. G. Hofmann, "Analysis of Digital Flight Control System with Flying Qualities Applications," AFFDL-TR-78-115, September 1978, Flight Dynamics Laboratory, Wright-Patterson Air Force Base, Ohio 45433.
12. R. F. Whitbeck and D. J. Didaleusky, "Multi-Rate Digital Control Systems with Simulation Applications," AFWAL-TR-80-3101, September 1980, Flight Dynamics Laboratory, Wright-Patterson Air Force Base, Ohio 45433.

1981 - SCEEE SUMMER FACULTY RESEARCH PROGRAM

Sponsored by the

AIR FORCE OFFICE OF SCIENTIFIC RESEARCH

Conducted by the

SOUTHEASTERN CENTER FOR ELECTRICAL ENGINEERING EDUCATION

FINAL REPORT

AMPLITUDE VARIABILITY OF THE STEADY STATE

VISUAL EVOKED RESPONSE

Prepared by:	Robert L. Yolton, O.D., Ph.D.
Academic Rank:	Director of Research
Department and University:	Pacific University College of Optometry
Research Location:	School of Aerospace Medicine, Laser Effects Laboratory, Brooks AFB
USAF Research Colleagues:	Dr. Richard Goodson and Dr. Ralph Allen
Date:	October 1981
Contract No.:	F49620-79-C-0038

AMPLITUDE VARIABILITY OF THE STEADY STATE

VISUAL EVOKED RESPONSE

by

Robert L. Yolton

Abstract

The amplitude of the human visual evoked response (VER) has been found to be a somewhat unreliable indicator of vision and/or perception. In this study, the reliability of the steady state VER was determined for nine normal subjects using fast Fourier transform analysis procedures with 1.0 Hz and 0.25 Hz frequency bin resolutions. No correlations were found between changes in VER amplitudes and subjects' reports of shifts in attention, accommodation, fixation, or perceived organization of the stimulus.

Analysis, using analog filtering and Fourier techniques, demonstrated that there was no significant and sustained amplitude modulation of the VER by any frequency (including alpha) and that frequency drift of the VER did not contribute significantly to its amplitude variability.

A modeling approach to variability, using mixed sine waves to simulate different signal/noise ratios, established that a significant portion of the VER variability can be accounted for by noise which occurs at the same frequency as the VER and which is not ensemble averaged out of the VER data during initial processing. An empirically determined reliability versus signal/noise ratio curve is presented which shows the minimum variability which can be expected for any given signal/noise ratio.

Acknowledgement

I would like to thank the Air Force Systems Command, the Air Force Office of Scientific Research and the Southeastern Center for Electrical Engineering Education for providing support for this project.

In addition, I wish to thank the subjects who contributed data for this project, James Brakefield and Michael Thew who provided valuable technical assistance, and Roger R. Hirons and J. Randall Pitman who assisted in the latter stages of data analysis.

I. Introduction:

The visual evoked response (VER) is a well known and frequently studied gross electrical response generated primarily by neurons in the visual cortex (1). As such, the VER is a potentially valuable, non-invasive tool for use in objectively assessing many aspects of visual function and perception. VER latency data are useful in the diagnosis of optic neuritis (2), which is often associated with multiple sclerosis (3,4,5,6), and VER amplitudes are related to pattern and brightness perceptions (7). Of importance is the fact that conditions which affect these perceptions also affect VER amplitudes and it is this relationship which has led to the use of the VER for refractive error and acuity determinations (8,9,10,11,12), assessment of recovery from photic and other insults, and for other assessments requiring an objective measurement of perception/vision (7).

Usefulness of the VER as an assessment tool is somewhat compromised, however, because the amplitude of the evoked response (which is usually taken as a primary indicator of vision/perception) is often quite unreliable, i.e., the VER amplitude changes with no apparent subject, stimulus, or recording device changes (13,14,15,16).

A number of factors have been suggested to account for the variability of VER amplitude data. These factors can be divided into four classifications: 1) data analysis procedures, 2) changes in the ocular status of the subject (e.g., accommodation, fixation, etc.), 3) changes in information processing occurring at central levels in the subject's visual system (e.g., changes caused by variations in

cortical excitability (17,18,19), and/or by correlates of the alpha rhythm (20,21,22,23,24), and 4) changes in the background noise level occurring at the same frequency as the VER, and hence recorded with it.

Probably each of these four factors contribute in complex and interactive ways to the overall variability of the VER, but in order to develop the full potential of the VER as a research and clinical tool, the relative contributions of the factors must be separated so that appropriate methods can be found to reduce VER variability.

The literature is not very helpful in assessing the relative contributions of the factors. Van Brocklin, et. al. (16) have published data showing VER amplitude variability, but they made no attempt to correlate changes in VER amplitudes with changes in the subject's perceptual and/or attentional states, and they did not consider the effects of noise on the VER.

II. Objectives of the Research Effort:

Because of the lack of information in the literature, and to provide additional information on VER variability, the following study was designed, first, to replicate Van Brocklin's reliability data using an independent analysis system and procedures, second, to investigate potential correlations between VER amplitudes and subjects' reports of attention, stimulus fixation, accommodative status, and perception of stimulus organization. and, third to study the sources of VER variability using modeling techniques.

III. Procedures:

Subjects

One female and eight male subjects participated in this experiment. Mean age of the subjects was 29.1 years (range 20-39) and each was an experienced VER observer. All except BU were emmetropes or wore corrections which provided visual acuity of 20/20 or better, and none, except BU, had significant visual anomalies or pathologies. Subject BU was a unilateral 20/200 amblyope of unknown etiology.

Stimulus

Subjects were seated comfortably in a darkened, shielded room 2.6 m from a video display which subtended a 525 by 400 arc min rectangle. The display was controlled by a PDP 11/34 computer which produced a black and white checkerboard consisting of 15 arc min checks (bright checks 30 f-1, dark checks 4.5 f-1). To elicit the VER, the checks were square wave phase reversed at a single check counterphase rate of 7.5 Hz which produced a pattern reversal rate of 15.0 Hz.

There was a small black dot, clearly visible at all times, in the center of the display and subjects were instructed to fixate on this dot except during the rest periods between trials.

During data acquisition, each subject viewed the stimulus display for ten trials, each of which consisted of 60 s of blank screen (with the same mean luminance as for the checkerboard), followed by 80 s of phase reversing checkerboard; 1.5 min of rest were provided between each of the trials. VER data recorded during these ten trials were stored on magnetic tape for later analysis.

Rating Scales

To determine whether variations in VER amplitudes correlated with variations in the subjects' visual/perceptual conditions, each subject was asked to answer four questions after each of the VER trials:

1. Attention: "Rate your degree of attention during the time the checkerboard was visible on a 1 to 7 scale, with 1 being groggy, 4 being relaxed but alert, and 7 being sharp."
2. Fixation: "Rate the percentage of time when the checkerboard was visible that you were able to hold your fixation on the center dot on the display screen."
3. Accommodation: "Rate the percentage of time when the checkerboard was visible that the entire display screen stayed clear and in focus."
4. Uniformity: "Rate the percentage of time when the checkerboard was visible that the display did not appear to move about in space, rearrange itself into small segments or patterns, or form diagonal or cross hatch lines."

These questions were discussed with each subject before any data were obtained and were repeated after each of the trials. Thus, each subject responded to each of the four questions ten times.

VER Recording

Conventional procedures were used to record the VERs. Following cleaning of the skin with alcohol and the application of electrode paste, silver disc electrodes were attached to each earlobe and to the

scalp, on the midline, 1-2 cm above theinion (electrode to electrode resistances were all 5,000 ohms or less). Outputs from the electrodes were differentially amplified (amplifier frequency cutoffs 0.1 and 100 Hz), and data from the trials stored on magnetic tape.

The computer which produced the checkerboard display also produced a square wave which was synchronized with the phase reversal of the display. This square wave was recorded on tape along with the evoked potentials and served to synchronize subsequent analyses.

After all data had been recorded for a given subject, the data were digitized at a rate of 256 Hz by an analog/digital converter and stored on a magnetic disc.

Data Reduction

While specific procedures differ slightly in the experiments described below, typically the digitized VER data were ensemble averaged and then analyzed using a fast Fourier transform (FFT). Since we wanted to show how the ensemble averaging of different numbers of time epochs affected variability, data from each subject for each of the ten trials were subdivided into smaller increments. For each trial, we considered the 90th second of the trial (30 seconds after the checkerboard first became visible to the subject) as the start of our ensemble averaging period. The 90th second was selected because it was long enough after the checkerboard first became visible to allow initial transients and instabilities in the VER to pass (25). Following the 90th second, periods ranging from 1 to 40 seconds (as shown in Table 1) were ensemble averaged.

Table 1
ENSEMBLE AVERAGING INTERVALS

<u>1.0 Hz Bin Resolution</u>		<u>0.25 Hz Bin Resolution</u>	
Total Length of Ensemble Averaging Period (in seconds)	Total Number of Epochs Ensemble Averaged	Total Length of Ensemble Averaging Period (in seconds)	Total Number of Epochs Ensemble Averaged
1	1		
4	4	4	1
10	10	8	2
20	20	20	5
30	30	32	8
40	40	40	10

Because we also wanted to show how the use of different FFT frequency resolutions would effect the variability of our VERs, all of our data were analyzed twice, once using relatively wide frequency bins, and then again using relatively narrow bins. Very narrow analysis bins would seem desirable because they would exclude the maximum amount of side-band noise, however, if bins are too narrow, slight frequency drifts in the VER will cause leakage of power into more than one bin thus complicating data analysis. Having considered these factors, and others, such as computer memory space, display rates, etc., which set practical limits on bin width, we selected resolutions of 1.0 Hz (achieved by digitizing 1.0 s epochs at a rate of 256 Hz) and 0.25 Hz (achieved by using 4.0 s epochs digitized at a rate of 256 Hz). The pattern reversal of the checkerboard display produced a 15.0 Hz VER signal which was exactly centered in a bin for both the 1.0 and 0.25 Hz analyses.

As an example of how these analyses were conducted, consider the data for 10 epochs using a 1.0 Hz bin resolution. For each of the ten trials from a subject, the 90th through 99th seconds were ensemble averaged and the FFT was used to obtain the amplitude of the VER component. This resulted in ten values and the mean and standard deviation of these values were then used to calculate the Reliability Index (RI) which is the standard deviation of the values expressed as a percentage of their mean. This process was then repeated for the other epochs (as shown in Table 1) using bin resolutions of both 1.0 and 0.25 Hz.

Note that the number of epochs required for a given averaging period is different for the 1.0 versus the 0.25 Hz resolution analyses, and that the analyses are not truly independent since all were started with the 90th second of data.

These analyses provided RI data for the VERs, but since signal/noise ratios and noise variability data were considered important, analyses were also conducted on noise data (obtained while the subjects were viewing the blank screen). The same analytical procedures were used for the noise data as for the VERs, except that noise analyses began with the 15th second of each data trial. These noise analyses yielded amplitudes and RIs for the 15.0 Hz component of the noise which was present prior to the time the VER was recorded (and which may have continued during the time the VER was being recorded).

IV. Results:

Figure 1 presents a summary of the VER and noise amplitude data obtained from our nine subjects. The values are calculated for 1.0 Hz bin resolutions. Both the VER and noise curves drop rapidly at first showing the effects of ensemble averaging, but, beyond about 10 s, the slopes approach zero. The S/N curve, which is the ratio of the mean VER amplitude to the mean noise amplitude, shows a continuous increase up to 40 s where the mean S/N ratio is about 11/1. The upward trend in the curve suggests that better S/N ratios could be obtained by using longer averaging periods.

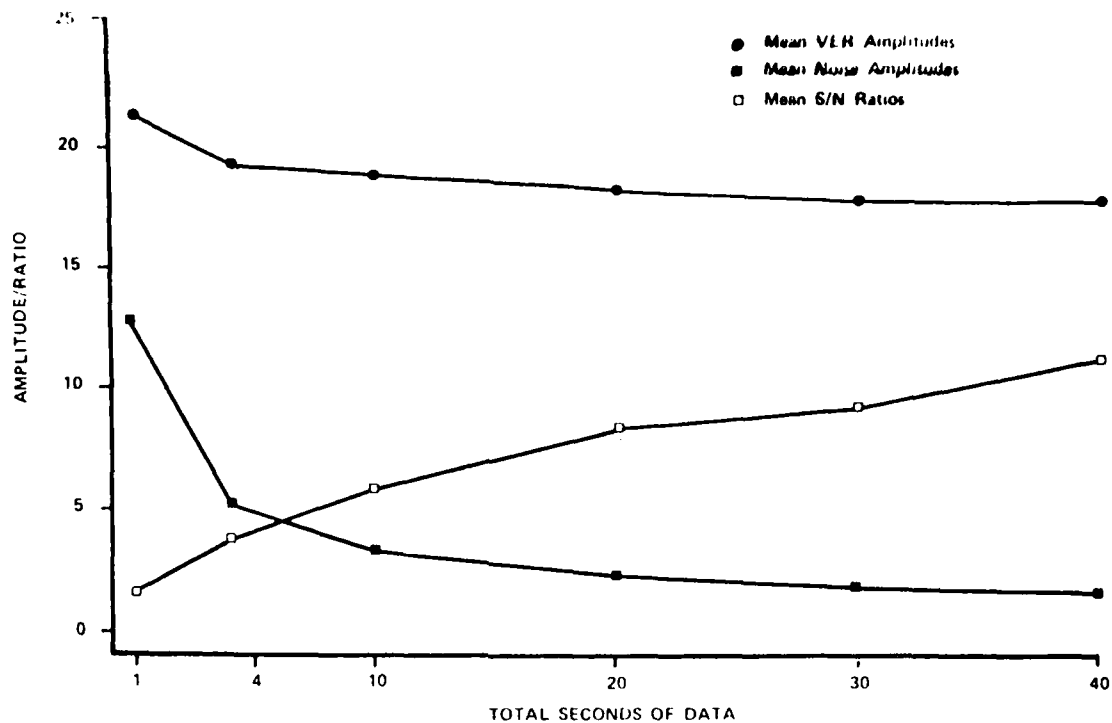


Figure 1. Mean data from nine subjects. The VEH and noise curves demonstrate how changing the length of the ensemble averaging period affects the amplitudes of these data. Beyond about 10 s, increasing the averaging period appears to have little effect on these amplitudes, but the signal to noise ratio increases steadily up to 40 s.

To compare the reliabilities of the VER amplitudes across subjects and measurement conditions, the RI was used to normalize the data. The RI is a useful measure because it is not affected by multiplying or dividing the data by a constant (as might happen if an amplifier gain setting was changed), however, the RI is affected by adding or subtracting a constant from the data, hence care was taken to assure that this did not happen during analysis.

As noted above, two bin resolution widths (1.0 and 0.25 Hz) were considered in analyzing the data from our subjects. Curves were constructed showing the relationship of the mean RI values to the length of the data sample which was ensemble averaged to produce each VER. These curves are shown in Figure 2. Also shown in this Figure are additional RI data obtained in another laboratory under somewhat similar conditions (16). These additional data are presented to demonstrate that the RIs shown in our paper are typical and are not analysis system specific.

Several points can be made from the data shown in Figure 2. First, there is little difference between the RI values found using 1.0 and 0.25 Hz resolutions. Second, the slope of the RI curve approaches zero when more than 20 s of data are used. In other words, VER data are not made considerably more reliable by analyzing more than approximately 20 s of total data per VER (or at least this is the case up to 40 s of data which was the limit used in our study). Third, the RI values show that there is significant variability in VER amplitudes.

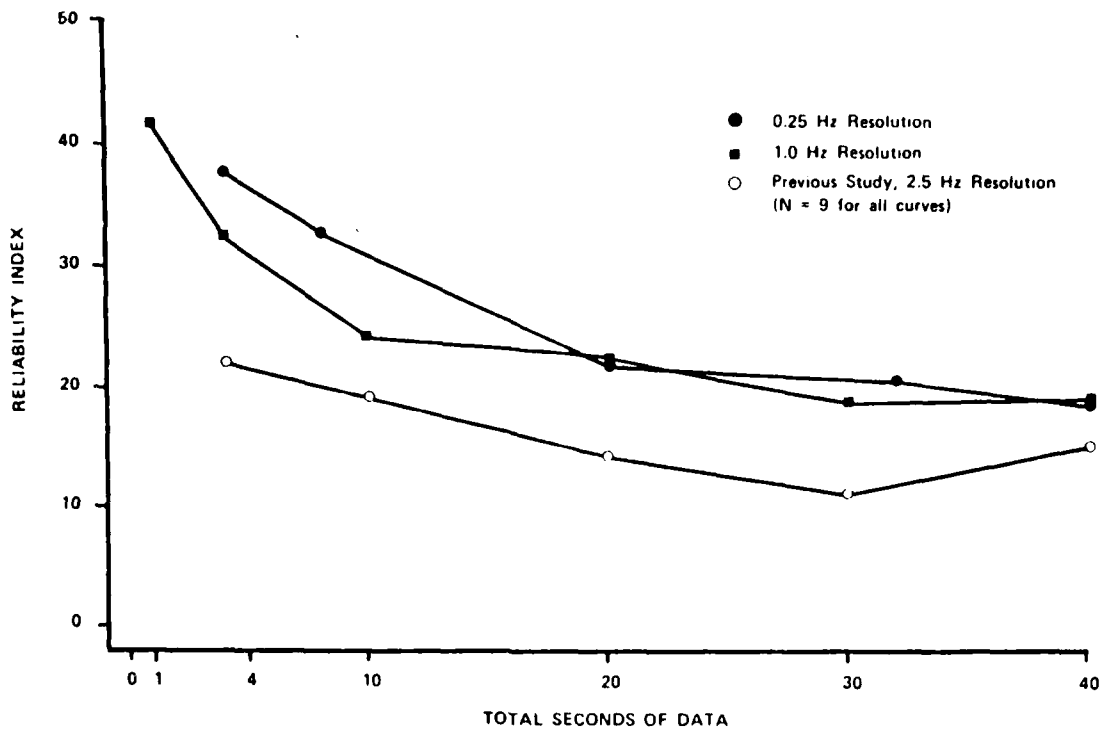


Figure 2. The upper two curves represent mean RI data from this study using 0.25 and 1.0 Hz frequency resolutions. The curves show that beyond about 20 s of data, both resolutions yield the same RI values. They also show that beyond 20 s there is only a very gradual trend toward more reliability with increasingly long averaging periods. The lower curve shows RI's from Van Brocklin et. al. (16) obtained using nine subjects and 2.50 Hz resolution Fourier bins.

To put this variability into perspective, consider subject EL whose variability data place him at the median for our nine subjects. Using 40 one-second data epochs, EL produced a mean VER amplitude of 18.44 and a standard deviation of 3.29 for his ten trials. If EL were now asked to view a different stimulus display, perhaps with the contrast changed, and ten additional VERs were recorded, the mean amplitude of the VERs from the second set of data would have to differ from the first by at least 30% before we could conclude (at the .05 level) that the two displays had produced significantly different VERs. The amplitude change of 30% can be calculated by using the Student's t-test for unrelated means in a "backwards" fashion, and assuming that the variance for the second set of data is the same as for the first. It is important to note that EL is at the median of a group of normal, trained observers and that variability from uncooperative or difficult subjects might require the means of the two sets of data to be even further apart for significance (26).

V. Factors Which May Account for VER Variability:

The data presented above demonstrate that VER amplitudes are indeed variable even when subject, stimulus, and analysis conditions are held constant. Four factors were suggested to account for this variability and they can now be assessed.

Variability Associated with Data Analysis Artifacts

Variability can enter via analysis procedures at any of several levels. Data storage devices such as tape recorders can cause artifacts, or the computer algorithms used to analyze the VER data can be faulty. For example, subtle problems such as windowing, aliasing, and frequency drifts can cause the FFT to make the VER amplitudes appear to be variable (27).

A number of quality assurance tests were conducted to insure that these problems were not occurring in our system. In one test, we used a 15.0 Hz sine wave which was repeatedly recorded on tape, digitized, and analyzed by the computer just as though it was a VER trial. When these analyses were conducted 16 separate times, the resultant RI for the data was only 0.15% which shows that very little variability is introduced by our analysis procedures.

A second test ruled out aliasing of higher frequency signals as a source of variability. In this test, an actual VER trial was repeatedly digitized with and without a Rockland 100 Hz low-pass filter placed between the tape deck and the computer. Use of this filter blocked any high frequency noise which might be aliased to 15.0 Hz. Results of this test demonstrated that aliasing did not produce the variability in our data since the RIs of the filtered and unfiltered data were less than 0.5%.

A slight drift in the frequency of the VER itself could cause the analysis procedures to make the amplitude data appear artifactually variable. The results of such a frequency drift can best be understood

by considering the VER to be a sine wave. As the frequency of such a sine wave drifts from the center of a Fourier bin, the power or amplitude representing the sine wave begins to "leak" into adjacent bins. The amount of this leakage is predictable and may be determined theoretically or empirically.

We determined amplitude leakage empirically by using a 15.0 Hz starting frequency which was then shifted sequentially in increments equal to 10% of the width of the Fourier bin. The data in Table 2 show the proportion of leakage for 1.0 Hz and 0.25 Hz resolutions that resulted from this determination.

Table 2
LEAKAGE CAUSED BY FREQUENCY DRIFT

1.0 Hz Bin Resolution Frequency (Hz)	0.25 Hz Bin Resolution Frequency (Hz)	Proportion of Amplitude Represented in Bin with 15.0 Hz Center Frequency
15.0	15.000	1.0
15.1	15.025	.98
15.2	15.050	.93
15.3	15.075	.85
15.4	15.100	.76
15.5	15.125	.64
15.6	15.150	.51
15.7	15.175	.37
15.8	15.200	.23
15.9	15.225	.11
16.0	15.250	.00

These data show that equal magnitude frequency shifts (for example, 0.5 Hz away from the 15.0 Hz center point) would have very different effects depending on whether 1.0 Hz or 0.25 Hz bins were being utilized.

If a significant amount of the variability present in the actual VERs recorded from our subjects was caused by frequency drifts, the data obtained using 0.25 Hz bins should be considerably more variable than the data obtained using the 1.0 Hz bins. As was shown in Figure 2, however, this is not the case since the variabilities using the 1.0 Hz and 0.25 Hz bins were approximately the same.

Even though it did not seem theoretically possible for frequency drifts to contribute to VER variability, the degree of drift was actually measured for one subject. Curves showing the frequency spread from two 16.0 s samples of data from subject DU are shown in Figure 3. These data show relatively little frequency drift; essentially all of the VER power is contained in a region 0.25 Hz wide which is centered on the pattern reversal rate of 15.0 Hz. The lack of frequency drift is consistent with the fact that variability using 1.0 Hz and 0.25 Hz bins is approximately the same. It is, therefore, not possible to conclude that a significant proportion of the variability seen in VER data is due to frequency drift.

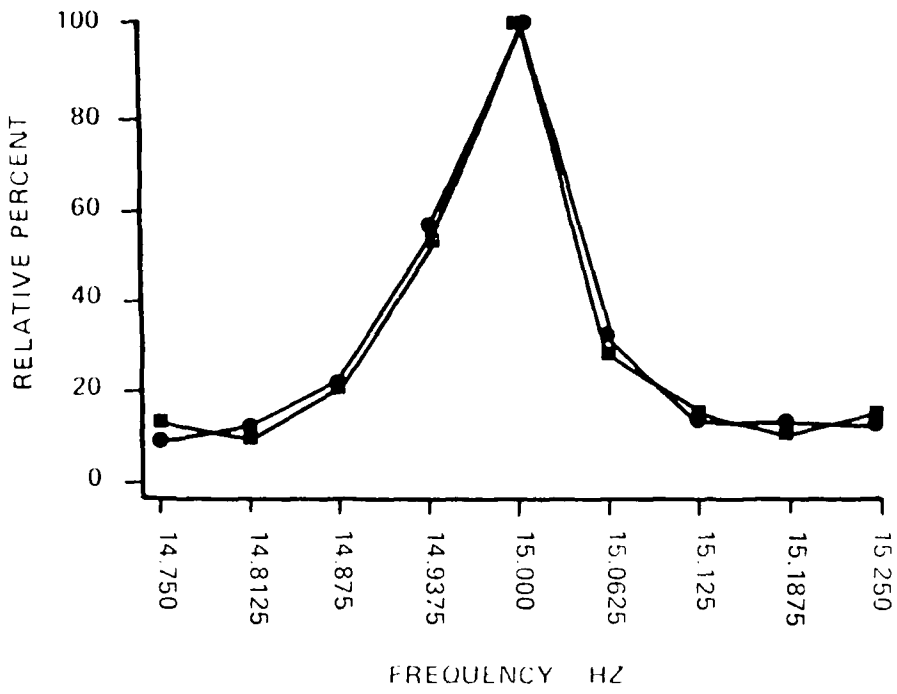


Figure 3. Frequency spread for two 16.0 s samples of VER data from subject DU.

Variability Associated with Changes in Ocular/Perceptual Status

Since the amplitude of the VER is considered to be an indicator of perception, any changes that affect stimulus clarity, brightness, contrast, or retinal location could affect VER amplitudes and be interpreted as variability. To evaluate the relationship between changes in perception and the VER, correlation coefficients were determined for our subjects' ratings of attention, fixation, accommodation and stimulus uniformity versus their VER amplitudes (which had previously been normalized by converting them to Z-scores to remove the effects of the subjects' different means and standard deviations).

Scatter plot appearances and the near zero correlations (Table 3) between the ratings and the VERs show that there is no significant relationship between changes in the subjects' visual/perceptual reports and fluctuations in the VER. This is somewhat surprising since the subjects did report changes in their ability to attend to the stimulus and in its appearance. These changes are not, however, represented as variations in amplitudes of the VERs, which suggests that factors other than those associated with perception might be responsible for amplitude variability.

Table 3
RATINGS VERSUS VER Z-SCORES

<u>Comparison</u>	<u>Correlation Coefficient</u>	
VER vs. attention	.0017	(NS)
VER vs. fixation	.001	(NS)
VER vs. accommodation	.01	(NS)
VER vs. uniformity	.0007	(NS)

There may, however, be ocular changes which could affect VER amplitudes but which may not necessarily be associated with perception. Examples are eye movements (28), blinking (29), and shifts in binocular balance (30). Armington has demonstrated blink evoked potentials (29), so it is likely that blinks occurring during the stimulus viewing period could cause VER amplitude variability. To assess the importance of this factor, blink rates were measured by gross EMG recording for three subjects who represented high, medium, and low RI scores. It was found that all three subjects blinked only two to four times per minute during the checkerboard viewing period, thus the results of these blinks would not have a differential or major effect on the subjects' RI scores.

Since all of our VER data were obtained under binocular viewing conditions, we cannot assess the proportion of variability which may have been caused by shifts in ocular dominance. We can only note that subject BU, who was a 20/200 amblyope, and who presumably had relatively stable dominance, showed about as much variability as our other subjects. Binocularity, however, must remain a possible source of variability pending further investigation.

Variability Associated with Changes in Central Processing

It has been suggested that the amplitude of the VER is modulated by (or at least correlated with) certain EEG signals. For example, a significant relationship between VER amplitude and alpha rhythm (8 to 13 Hz EEG activity) has been proposed by some (20), and denied by

AD-A113 709

SOUTHEASTERN CENTER FOR ELECTRICAL ENGINEERING EDUCAT--ETC F/G 5/1
USAF SUMMER FACULTY RESEARCH PROGRAM. 1981 RESEARCH REPORTS, VO--ETC(U)
OCT 81 W D PEELE F49620-79-C-0038

UNCLASSIFIED

AFOSR-TR-82-0228

NL

14 of 14
208 709



END
DATE
FILMED
5-82
DTIC

others (22). Theoretical predictions indicate a negative correlation between the amplitudes of the VER and alpha rhythm, but actual measurements of this relationship in normal subjects often yield a slight positive correlation (21, 24, Yolton, unpublished observations).

We investigated the relationship between VER amplitude and other EEG frequencies by selecting two subjects who had low and high VER amplitude variabilities respectively. A 1.0 s sample (the 90th s) was taken from each of the ten trials for each subject and the amplitude of each Fourier frequency component of the data from 1.0 to 13.0 Hz (in 1.0 Hz steps) was determined. These values were then correlated with the VER amplitudes obtained during the same trials. Results of these correlations are shown in Table 4. (Prior to calculating these correlations, it was determined that, because of the large number of r values that would be produced, a significance level of .01 would be used.)

Table 4
VER VERSUS EEG CORRELATIONS

EEG Center Frequency (Hz)	Low VER Variability Subject (HO)	High VER Variability Subject (WO)
1.0	.37	.40
2.0	.37	-.33
3.0	.27	.57
4.0	-.26	.53
5.0	-.35	-.15
6.0	-.15	.75
7.0	-.03	.05
8.0	-.07	.33
9.0	.10	-.06
10.0	.24	.35
11.0	.21	.05
12.0	.22	.54
13.0	.17	.47
14.0	.30	.40

There are no significant correlations shown in the table which suggest that, at least in our normal population, VER amplitudes are not modulated by, or otherwise related to, other brain rhythms including alpha.

As a second test for amplitude modulation, data from four separate 16.0 s epochs for two subjects were analyzed using an FFT which produced 0.0625 Hz resolution. The frequency components produced by this program were searched to determine if there were paired-peaks displaced equal distances from the 15.0 Hz VER frequency. Such paired-peaks would result if there had been amplitude modulation of the VER (the frequency of the modulation would be indicated by the relative displacement of the peaks from the VER peak).

In the data from these subjects, no paired-peaks were detected (Figure 4) and this indicates that there was no consistent, sustained amplitude modulation of the VER.

In a third test for amplitude modulation, we used a sample of data from subject DU. The raw VER data were analog filtered (Rockland band-pass filter, 14-16 Hz) to produce a cycle by cycle plot of these data. Gross observation of the cycle by cycle variations in the VER (Figure 5), and a Fourier analysis of these variations, revealed no evidence of amplitude modulation. Thus, while amplitude modulation of the VER might exist in short bursts (considerably less than 16.0 s), such modulation is not constant enough to be detected using a 16.0 s Fourier analysis. The short, non-repeating modulations which appear in some of the VER data might, in fact, be caused by random factors such as noise.

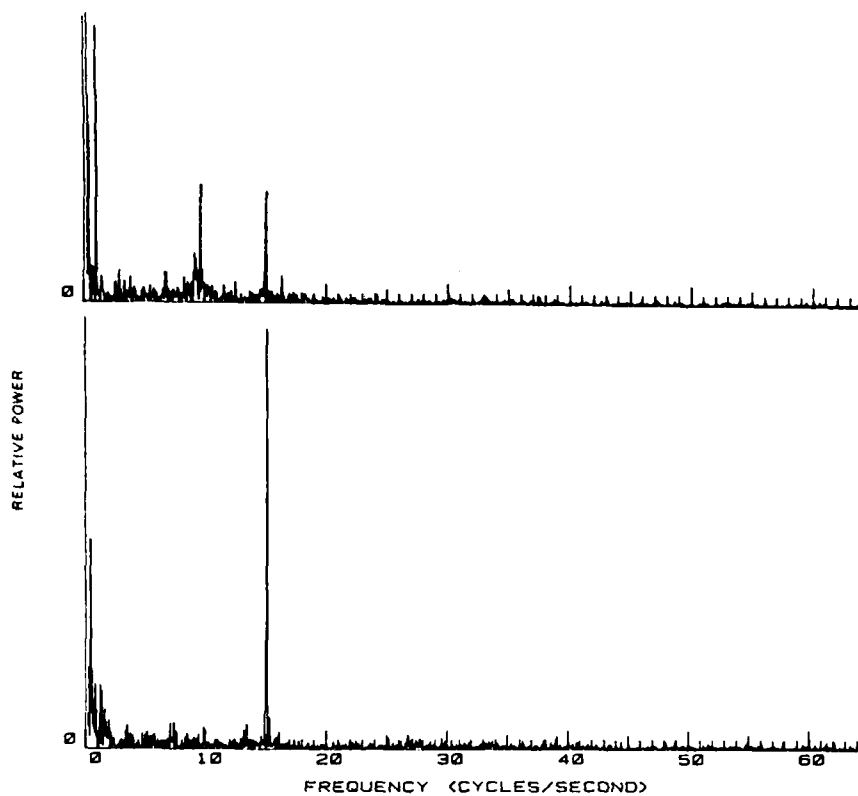


Figure 4. Power spectra from subjects EL (upper) and DU (lower).
Each trace represents 16 s of data analyzed using 0.0625 Hz bins.
EL shows alpha activity at about 9 Hz and both show VERs at 15.0 Hz.

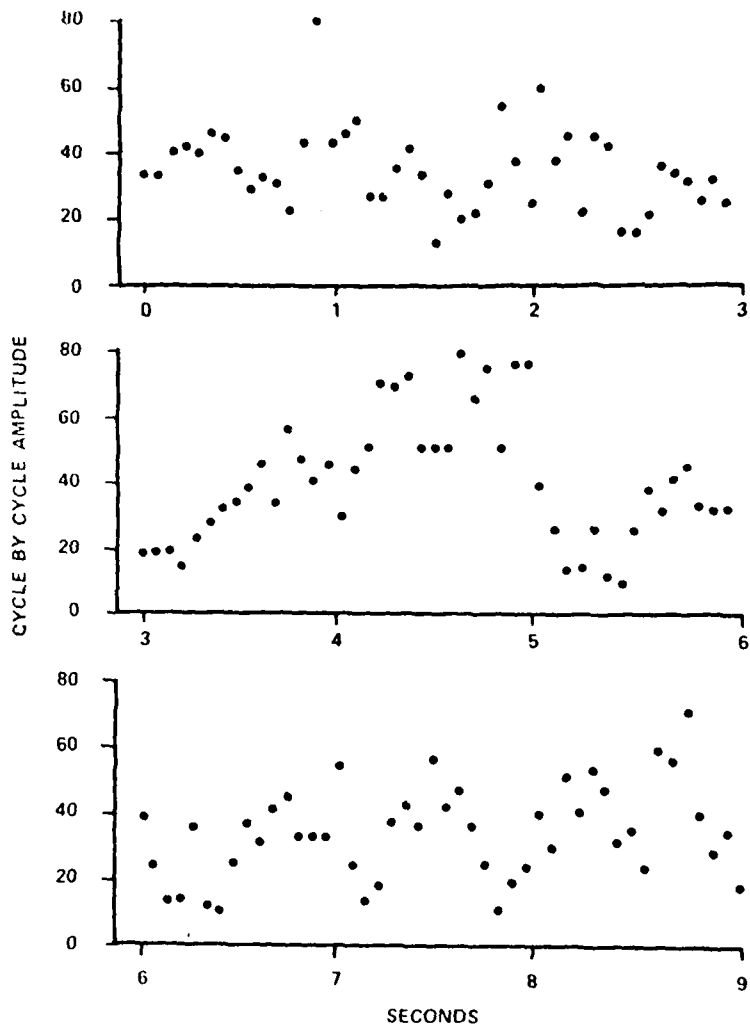


Figure 5. Cycle by cycle amplitudes for Subject DU.

It is also clear that the cycle by cycle variations of the VER are poorly related to the subject's perception since she strongly disclaimed any fluctuations in the appearance of the stimulus screen which might be related to the 600% changes in amplitude that occurred during the 16.0 s viewing period. If cycle by cycle amplitude changes are related to perception, other mechanisms in the visual system must be designed to remove their effects.

Variability Associated with Noise

The ensemble averaging process is designed to minimize the effects of non-synchronized noise which is recorded along with the VER signal, and use of the FFT can eliminate noise with frequencies outside of the Fourier bin containing the VER. These two techniques do not, however, eliminate all noise contamination. The amplitude values provided by the FFT may be considered to be the sum of two parts: one contributed by the VER itself, which has a certain mean amplitude and variability, and a second part contributed by the noise, which also has a certain mean amplitude and variability.

While it is not possible to ascertain, in any direct fashion, the fraction of the measured VER which is caused by noise, a determination of the noise amplitude and variability was made during the period just before the subject viewed the reversing checkerboard (Figure 1). An extensive discussion of the effects of this noise on VER variability will be presented below in the section on Modeling.

Other Factors

Since the VER amplitudes and the RIs for our nine subjects were individually quite different, we tried to determine whether these inter-subject differences could be correlated with body physiology or age. To make these determinations, correlations relating RIs, S/N ratios, and mean 40 s VER amplitudes to the subjects' ages and their height to weight ratios were determined as shown in Table 5.

Table 5
AGE, S/N, AND WEIGHT/HEIGHT VERSUS RI CORRELATIONS

<u>Comparison</u>	<u>r</u>	<u>value</u>
Age vs. RI	.32	(NS)
Age vs. Amplitude	-.68	($p < .05$, $df = 7$)
Age vs. S/N	-.57	(NS)
Height/weight vs. RI	.23	(NS)
Height/weight vs. Amplitude	-.23	(NS)
Height/weight vs. S/N	-.41	(NS)

The significant negative correlation between VER amplitude and age is somewhat surprising because of the limited age range represented by the subjects (20 to 39), and is not easy to explain. Decreases in skin conductance with increasing age cannot be the cause of the relationship, since all subjects had approximately equal electrode resistances, nor can relative body build, which could index thickness of muscle, fat or bone in the recording region, be the intervening variable, since the height/weight index was not correlated with amplitude.

There are many other potential sources of VER variability but few data exist to substantiate or refute their relationship to the

VER. These factors include respiration and heart rates and the resultant status of blood flow to the cortex, time since the last meal, psychological state (31), drugs the subject may have taken (32,33), etc. Although these factors seem relatively obscure, one study (34) has shown that by having the subject imagine or hallucinate objects which come between her and the display screen, the VER can be diminished or extinguished. This clearly demonstrates that the subject's psychological state can have a pronounced effect on VER amplitudes. In our study, however, with normal subjects the variations in psychological state, blood sugar, and cortical physiology that might have occurred during a single recording session would seem to be too small to have affected the VERs in any significant way, but further data are needed to allow definitive statements to be made about the effects of such subtle factors.

VI. Modeling:

Assuming that data processing and/or equipment artifacts have been eliminated, it is probable that variations in noise, ocular status and central processing all interact to produce variability in the VER. The actions of some of these factors are reduced through ensemble averaging, which tends to smooth out rapid amplitude fluctuations, but all of the factors probably contribute in an interactive fashion to the variability of the VER.

Because we found it difficult to separate the effects of these factors, a different approach was employed in which we modeled the VER using additive sine wave components. To use this approach, we

made several assumptions. First, we assumed that the VERs which were recorded from our subjects consisted of only two components: a true VER component representing the activity of the visual system, and a noise component which represented the residual noise remaining after ensemble averaging. For convenience, we named the recorded VER: "VER_R," the true VER: "VER_T" and the noise: "N." In our modeling approach, VER_R equals VER_T plus N.

Our next assumptions involved the frequency and amplitude of the VER_T and N components. Since our subjects told us that, over short periods of time, their perception of the checkerboard stimulus was relatively constant, we assumed that the amplitude and frequency of the VER_T component was also constant. To simplify the modeling process, further we assumed that the amplitude of N was constant over the modeling period that we used (1.0 s), and that the frequency of N was the same as the frequency of VER_T. These assumptions are reasonable because in the FFT processing of data from our subjects, all frequencies except those in a single narrow band are discarded, therefore, the only noise which actually adds to VER_T has approximately the same frequency as VER_T.

The final assumption that we made involved the phase relationship between VER_T and N. Clearly the sum of these two components is highly dependent on their phase relationship, and since there was no reason to believe that there should be a fixed relationship between the phases of the components, we allowed the phase relationship to vary at random between each of a series of additions of the components. Thus, in our

first modeling approach, it was this variation in phase relationship which produced the variability in the amplitudes of our VER_R simulations.

Our modeling was accomplished using a Norland 3001 computer which stored a 1.0 s epoch of a 15.0 Hz sine wave corresponding to VER_T , and then added to it a 15.0 Hz component corresponding to N . An FFT was performed on the sum of these waves and the amplitude of the 15.0 Hz sum was determined. This process was repeated ten times with the phase relationship of the two waves varied at random between each addition. From these ten simulations, we determined the mean, standard deviation, and RI of the data as described above.

Since the signal/noise ratio was important to the results of this simulation, we repeated the process with signal/noise ratios of approximately 1/1, 3/1, 5/1, 10/1, 20/1, and 25/1 (the ratios were calculated by dividing the mean of the simulated VER_R values by the mean amplitude of N). These ratios were selected because they covered the range of S/N ratios produced by our nine real subjects.

The RI values that resulted from this modeling are shown in Figure 6. Obviously, when the S/N ratio is close to 1/1, the RI is quite high (indicating high variability), but when the ratio approaches 25/1, the RI is considerably lower. Note also that the curve is relatively flat from S/N ratios of about 10/1 to 25/1.

The importance of this curve can be appreciated by considering the assumptions that we made to produce it: 1) no amplitude or frequency variability in N or VER_T , and 2) a random phase relationship

between these two components. Since there is no reason to expect a non-random relationship between the components in real VER data, the curve represents the best RIs possible for each signal noise ratio, i.e., the curve shows what happens if there is no amplitude or frequency variability in either the N or VER_T components and the only variability in VER_R arises from phase differences between these two components. Thus, for a given signal/noise ratio, no real subject should have an RI lower than the value indicated by this curve.

Also shown on Figure 6 are the RIs for our nine subjects. RIs for three of these subjects are close to the theoretical best RI curve, however, six are considerably above the curve. This suggests that some amplitude variability must be present in either the N or VER_T components of their data. Therefore, we extended our modeling experiment to consider the case where the amplitude of N was variable. We wanted to determine if we could account for the RI values from all our subjects while retaining the assumption that there was no variability in the amplitude of VER_T .

Effects of noise amplitude variability were determined by artificially varying the amplitude of N prior to its addition to VER_T . The variability was introduced by using a predetermined set of multipliers such that the RI of N was 75% for each S/N ratio. This value was chosen to be somewhat greater than the mean noise RI of 64% (SD = 10.2) for our subjects (the mean RI value for the subjects was calculated by using 40 one-second ensemble averaged epochs obtained prior to the actual viewing of the checkerboard). When this

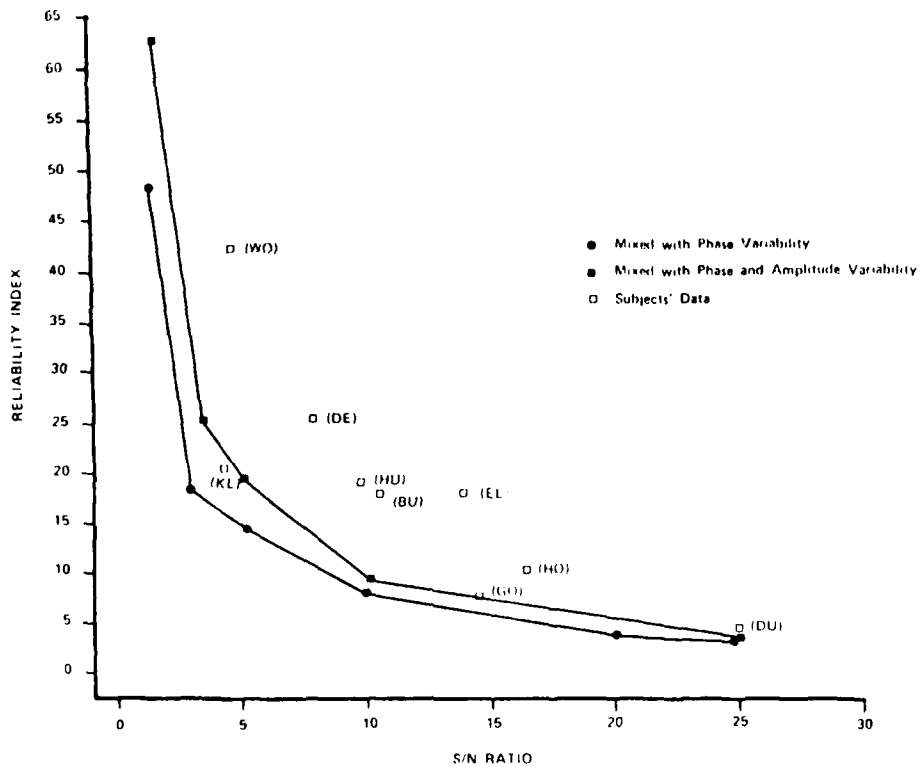


Figure 6. Results of Modeling. The filled circles represent constant amplitude N and VER_T components mixed with a random phase relationship. Filled squares have amplitude variability of the N component added. Open squares are RIs for the subjects who are identified by the letters in parentheses.

amplitude variability was introduced, in combination with the phase variability described above, the best possible RI curve moved up significantly for low S/N ratios, but, as expected, was relatively unaffected for higher ratios.

The addition of noise amplitude variability in an amount roughly equivalent to the variability of the real noise data from our subjects does not allow us to account for the RI values obtained from all of these subjects. Thus, if our modeling approach is valid, we must assume that either the variability of N increases during the time the subject is actually viewing the checkerboard (as compared to the time just before the checkerboard becomes visible), or that there is variability in VER_T itself for many of our subjects, or that there is a third, and yet unknown, component which must be added to VER_T and N to yield VER_R . While our modeling approach does not allow us to separate these three possibilities, it is important in that it does show that we cannot expect extremely reliable VERs (with RI values of less than 10%) if data have signal/noise ratios of less than about 10/1. The curves also show that pushing the S/N ratio from 10/1 to 25/1 does not make a proportional increase in reliability. It may be argued that at some point between 10/1 and 25/1, we have passed the point of diminishing returns with regard to increasing the S/N ratio. Finally the modeling approach suggests that there may indeed be variability in the VER_T component contrary to our assumption that the amplitude of this component was constant. Further work will clarify this point.

VII. Discussion:

In 1979, Van Brocklin, et. al., (16) quantified what most VER researchers already knew - the amplitude of the VER is variable. In replicating Van Brocklin's work, we found that our subjects were even more variable than theirs, and this degree of variability is sufficient to render questionable the use of steady state VER amplitudes to accurately assess perception. Certainly, the amplitude changes associated with eyes-open versus eyes-closed conditions can be discriminated in most subjects, but our rating scale data show no correlation between VER amplitude fluctuations and fairly large changes in attention, ocular status, or stimulus perception conditions. This lack of correlation suggests that the amplitude of the VER may be significantly affected by non-visual factors.

Earlier in this paper, we identified the four major factors which might contribute to VER variability - analysis procedures, ocular status, central processing, and noise. Based on our quality assurance testing, we are confident that artifacts associated with recording devices and computer programming did not contribute significantly to the variability in our data; neither did VER frequency drifts nor FFT artifacts such as aliasing. The signals that we processed and the data that we derived from these signals are valid representations of events occurring in the proximity of our recording electrodes.

While our processing equipment cannot account for a significant proportion of the VER variability, the noise which was recorded and analyzed along with the VER can. In our modeling experiment, we

showed that we could account for essentially all of the variability in the data from three of our subjects by assuming only a random phase relationship between variable amplitude noise and constant amplitude true VER components. For these three subjects, the only way to significantly increase the reliability of their data would be to increase the signal/noise ratio. This could be done by using longer ensemble averaging periods, however, long periods would make it difficult to follow rapidly changing visual phenomena. Also, with very long averaging periods, subjects tend to become restless and may produce artifacts associated with gross body movements. These large amplitude artifacts might be removed by the use of an active rejection system, but, since no such system was available for use in this study, the effects of artifact rejection cannot be estimated.

Data from six of our subjects showed more variability than we could account for by assuming a random phase relationship between the noise and true VER, and we could not account for the variability in their data by introducing noise amplitude fluctuations. For these subjects, perhaps ocular or central nervous system processing changes added variability to their data.

Undoubtedly, each of our subjects experienced changes in her/his ocular status during the stimulus viewing period, and fixation drifts, changes in pupil size, blinking, and similar factors clearly have the potential for affecting the amplitude of the VER. However, findings, such as the subjects' low blink rates and the lack of correlation between the ocular status rating scales and the VER

amplitudes, make it difficult to prove that a significant proportion of VER variability is caused by changes in these functions. Further experimentation, perhaps involving the use of pharmaceuticals, will be required to define the exact relationship of ocular status changes to VER variability.

We were also unable to demonstrate a relationship between our subjects' central nervous system processing of the VER checkerboard image and amplitude variability. No EEG rhythms, including alpha, were correlated with VER amplitudes and there was no correlation with the subjects' attention ratings. Major changes in attention, such as might be produced by a threat of electric shock, could change VER amplitudes (35), but the smaller attentional fluctuations reported by our subjects did not seem to have this effect.

The lack of correlation between VER amplitudes and perceptual reports, and our inability to find any neurological signals which covaried with the VER, raise doubts about the contribution of changes in cortical processing to VER variability. While negative evidence does not prove the lack of a relationship, the effects of changes in cortical processing, in a controlled situation, seem minimal.

VIII. Conclusions:

We conclude that a major proportion of the variability shown by our subjects is caused by noise analyzed along with the VER. For three subjects we need not consider any other factor to explain all of their variability. For the others, noise plus some interactive combination of ocular and central processing status changes may be

used to explain the variable data, but additional work will be needed to separate out the relative contributions of these factors.

IX: Recommendations:

1. Since the S/N ratio sets limits on reliability, efforts should be made to increase the S/N ratio for all data.
2. S/N ratios might be increased by implanting electrodes, or using larger skin surface electrodes.
3. S/N ratios may also be increased by taking longer samples of VER data, but this will be at the expense of temporal resolution of dynamic changes in the visual system.
4. Artifact rejection should be pursued, using intelligent systems to remove blink, eye movement, gross body movement and other signals that are confounded with the VER data.

X. Bibliography:

1. Regan D: Evoked Potential in Psychology, Sensory Physiology, and Clinical Medicine. London, Chapman and Hall, 1972.
2. Halliday AM, McDonald WI, Mushin J: Delayed visual evoked response in optic neuritis. Lancet 1:982-985, 1972.
3. Halliday AM, McDonald WI, Mushin J: Visual evoked response in diagnosis of multiple sclerosis. Brit Med J 4:661-664, Dec 15, 1973.
4. Milner BA, Regan D, Heron JR: Differential diagnosis of multiple sclerosis by visual evoked potential recording. Brain 97-:755-772, 1974.
5. Asselman P, Chadwick DW, Marsden CC: Visual evoked responses in the diagnosis and management of patients suspected of multiple sclerosis. Brain 98:261-282, 1975.
6. Van Brocklin MD, Yolton RL: Steady state VER measurement of visual system latency in normal and multiple sclerosis patients. J Am Optom Assoc 50(2):203-207, Feb 1979.
7. Sokol S: Visually evoked potentials: theory, techniques, and clinical applications. Surv Ophthal 21(1):18-44, 1976.
8. Ludlam WM, Meyers RR: The use of visual evoked responses in objective refraction. Trans NY Acad Sci 34(2):154-170, Feb 1972.
9. Regan D: Rapid objective refraction using evoked brain potentials. Invest Ophth 12(9):669-679, Sept 1973.
10. Sherman J: Visual evoked potential (VEP): Basic concepts and clinical applications. J Am Optom Assoc 50(1):19-30, Jan 1979.
11. Millodot M, Riggs LA: Refraction determined electrophysiologically. Arch Ophth 84(3):272-287, Sept 1970.
12. Duffy FH, Rengstorff RH: Ametropia measurements from the visual evoked response. Am J Optom Arch Am Acad Optom 48(9):717-728, Sept 1971.
13. Ciganek L: Variability of the human visual evoked potential: Normative data. Electroenceph Clin Neurophysiol 27:35-42, July 1969.
14. Coppola R, Tabor R, Buchsbaum MS: Signal to noise ratio and response variability measurements in single trial evoked potentials. Electroenceph Clin Neurophysiol 44(2):214-222, Feb 1978.

15. Zerlin S, Davis H: The variability of single evoked vertex potentials in man. Electroenceph Clin Neurophysiol 23:468-472, Nov 1967.
16. Van Brocklin MD, Hirons RR, Langfield WH, Yolton RL: The visual evoked response: Reliability revisited. J Am Optom Assoc 50(12):1371-1379, 1979.
17. Rudell A: The rhythm of cortical excitability. Electroenceph Clin Neurophysiol 49:125-134, 1980.
18. Skinner JE, Lindsley, DB: Enhancement of visual and auditory evoked potentials during blockade of the non specific thalamo-cortical system. Electroenceph Clin Neuro 31:1-6, 1971.
19. Lukas JH, Siegel J: Cortical mechanisms that augment or reduce evoked potentials in cats. Science 9 Oct 1979, 73-75.
20. Trimble JL, Potts AM: Ongoing occipital rhythms and the VER. I. Stimulation of the peaks of the alpha rhythm. Invest Ophthal 14(7):537-546, 1975.
21. Klem WR, Gibbons WD, Allen RG, Harrison JM: Differences among humans in steady-state evoked potentials: Evaluation of alpha activity, attentiveness and cognitive awareness of perceptual effectiveness. In preparation, 1981.
22. Kamiya J, Callaway E, Yeager CL: Visual evoked responses in subjects trained to produce alpha rhythms. Psychophysiol 5(6): 683-98, 1968.
23. Sadler RR, Eason RG: Voluntary alpha control, visually evoked potentials and peripheral physiological indicants of activation. Percept Motor Skills 44:491-96, 1972.
24. O'Malley JE, Connors CK: The effect of unilateral alpha training on visual evoked response in a dyslexic adolescent. Psychophysiol 9(4):467-479, 1973.
25. Gibbons WD, Allen RG, Richey EO: Response development time in the steady state evoked potential. Presented at Am Acad Optom, Boston, 1978.
26. Uren SM, Stewart P, Crosby PA: Subject cooperation and the visual evoked response. Invest Ophthal 18(6):648-652, 1979.
27. Ramirez RW: The FFT: Fundamentals and Concepts (070-1754-00) Tektronix, Inc, Beaverton, OR, 1975.

28. Scott DF, Moffett A, Bickford RG: Comparison of two types of visual evoked potentials: Pattern reversal and eye movement (Lambda). Electroenceph Clin Neurophysiol 52:102-104, 1981.
29. Armington JC: Visually evoked potentials accompanying blinks. Invest Ophthalmol 20(5):619-695, 1981.
30. Apkarian PA, Nakayama K, Tyler CT: Binocularity in the human visual evoked potential: Facilitation, summation and suppression. Electroenceph Clin Neurophysiol 51:32-48, 1980.
31. Shevrin H, Fritzier DE: Visual evoked response correlates of unconscious mental processes. Science 19 July 1968, 295-298.
32. Lewis EG, Dustman RE, Peters BA, Straight RC, Beck EC: The effects of varying doses of Δ^9 -Tetrahydrocannabinol on the human visual and somatosensory evoked response. Electroenceph Clin Neurophysiol 35:347-354, 1973.
33. Simpson D, Erwin CW, Linnoila M: Ethanol and menstrual cycle interactions in the visual evoked response. Electroenceph Clin Neurophysiol 52:28-35, 1981
34. Schatzman M: Ghosts in the machine. Psych Today, Jan 1981, 99.
35. Eason RG, Harter MR, White CT: Effects of attention and arousal on visually evoked cortical potentials and reaction time in man. Physiol and Behav, 4, 1969, 283-289.

1981 USAF - SCEE SUMMER FACULTY RESEARCH PROGRAM

Sponsored by the
AIR FORCE OFFICE OF SCIENTIFIC RESEARCH

Conducted by the
SOUTHEASTERN CENTER FOR ELECTRICAL ENGINEERING EDUCATION

FINAL REPORT

NEW TESTS OF THEORIES ON SHAPED CHARGE

Prepared by: Dr. Poh Shien Young
Academic Rank: Professor
Department and University: Department of Physics
Mississippi State University
Research Location: Air Force Armament Laboratory, Munitions
Division, Bombs and Warheads Branch
USAF Research Colleague: Dr. Joseph C. Foster, Jr.
Date: July 25, 1981
Contract No: F49620-79-C-0038

NEW TESTS OF THEORIES

ON

SHAPED CHARGE

by

Poh Shien Young

ABSTRACT

Two theories on the penetration of the lined shaped charge in targets have been reviewed and compared with the recent experimental data. Under this investigation is the relationship between the penetration depth and time. The discrepancies between the theoretical and experimental values exist. Explanations and suggestions for further research in this field are offered.

Acknowledgement

The author wishes to thank the Air Force Systems Command, The Air Force Office of Scientific Research and the Southeastern Center for Electrical Engineering Education for the opportunity to participate in the Faculty Summer Research Program in 1981 at the Air Force Armament Laboratory, Eglin Air Force Base, Florida. The particular acknowledgement is extended to the Bombs and Warheads Branch for the hospitality and excellent working conditions.

He wishes to express special thanks to Dr. Joseph C. Foster, Jr., Mr. Joseph A. Smith and Lt. Jorge A. Fernandez for their valuable suggestions, guidances and discussions which have made his summer months of participation very enjoyable and worthwhile.

This report represents the technical opinion of the author and not the official position of the United States Air Force Armament Laboratory.

I. INTRODUCTION

The enhancement of the penetration power of a shaped charge by a thin metal liner has been known for more than forty years.¹ A hydrodynamic² theorem in a form of the Bernoulli equation was developed to describe the relationship among the physical quantities involved. They consist of the densities of the target and the penetrating jet formed by the liner, the velocities of the jet and the penetration, and the stresses of the penetrator and the target.

According to this theorem, the deceleration of the jet upon striking the target is treated as the interactions between fluids as long as³ the penetrator velocity is higher than a critical value of $\sqrt{2(R_T - Y_p)/\rho_p}$, where ρ_p is the density of the penetrator, R_T and Y_p are the stresses of the target and penetrator respectively. When the velocity drops below this critical value, the target behaves as a rigid body. Furthermore, if R_T is greater than Y_p the penetration ceases at this velocity.

In this paper, two theories of the theorem are reviewed by use of recent experimental data.

II. OBJECTIVES OF THE RESEARCH EFFORT

There are immediate and long range objectives of this effort. During this summer, my effort has been concentrated on the analyses of the penetration by the copper jet on the steel target. The established theories on the shaped charge are employed for the analyses. The immediate objective is to obtain a better understanding on the penetration mechanics. It is anticipated that the present study will result in the improvement of the effectiveness of the shaped charge.

III. PHENOMENA

We begin with a brief description⁴ of the lined shaped charge and the penetration of a jet in a semi-infinite target. In Fig. 1, a typical shaped

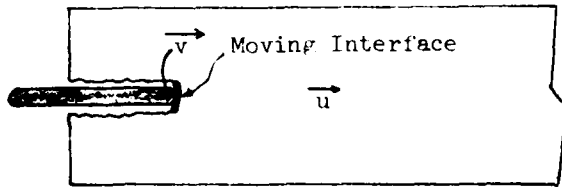


Fig. 3 (b). The penetration process as viewed from the stationary target.

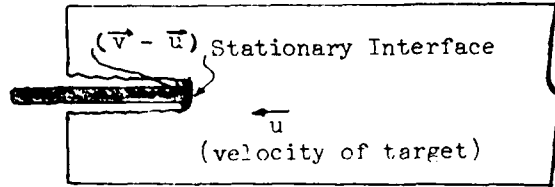


Fig. 3 (c). The penetration process as viewed from the stationary interface.

IV. THEORIES

The Pugh and Fireman Theory:⁴ In general, the penetration is a three-dimensional process. However, for a target of uniform density, it is reasonable to assume an axial symmetry of the process so that it reduces to a two-dimensional case. Further simplification is possible for analysis because of the experimental findings that the jets under investigation were thin and the impinging velocities higher³ than $\sqrt{2(R_T - Y_P)/\rho_P}$. These two conditions enable us to treat the process as a one-dimensional interaction between metallic steady flows which can be regarded as incompressible and inviscid. Here R_T is the resistance of the target while Y_P and ρ_P refer to the resistance and density of the penetrator, i. e., the jet.

Let us investigate the penetration depth as a function of time for the case where both R_T and Y_P are negligible. According to the Pugh and Fireman theory, the equation of motion reads as follows:

$$\frac{1}{2} \rho_P (v - u)^2 = \frac{1}{2} \rho_T u^2 \quad (1)$$

where ρ_T is the density of target, u and v refer to the velocities of interface and the temporary tip of the jet respectively. The quantity $(v - u)$ is equal to the relative velocity of the jet tip with respect to the interface. It is worth reviewing the Pugh coordinates system in which every part of the jet is considered having originated from a same point which may be called the virtual origin. In an ideal case, the tip and the tail of the jet trace two straight trajectories in the $x-t$ diagram during the period when the jet elongates. The intercept of the extrapolated trajectories defines the virtual origin. The two figures below illustrate its definition.

charge before explosion is shown. No sooner than the explosion takes place, the liner starts to collapse. Fig. 2 illustrates the process of collapsing.

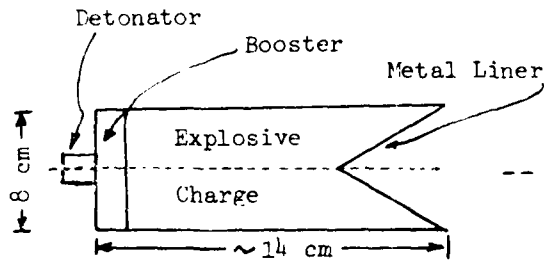


Fig. 1. Shaped charge with a metal liner.

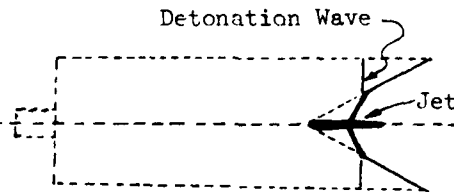


Fig. 2. Collapse of liner due to explosion.

In a period of several microseconds after explosion, the liner totally collapses into a jet which, propagates in the forward direction. According to our experimental results, which will be described in the later section, the jet consists of two portions; the front portion having a constant length, and the back one stretches in the forward and backward direction as time goes by. We may call these two portions the constant and stretching parts respectively. In the stretching part, one or more velocity gradients exist in the forward direction, i. e., each particle in this part moves faster than the one right behind it. In a matter of microseconds, the whole jet breaks up into pieces, each of which can be considered a small jet.

Now consider what happens when a jet hits a target. The jet and target materials start to melt away along the interface. This causes an elongating crater in the target. The three figures below illustrate the penetration process in a semi-infinite target.

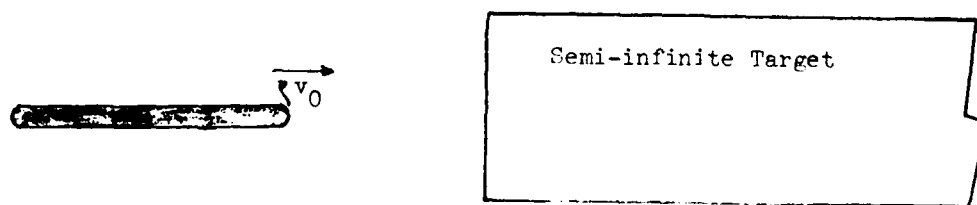


Fig. 3 (a). An unbroken jet about hitting a target.

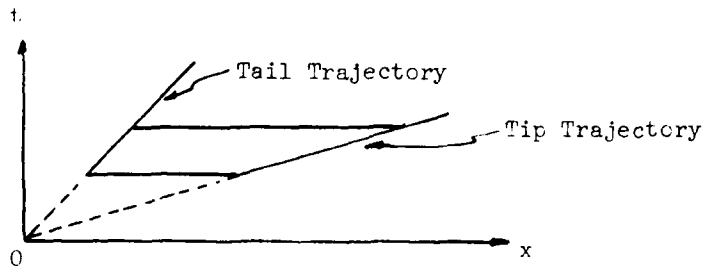


Fig. 4. A stretching jet and the virtual origin 0.

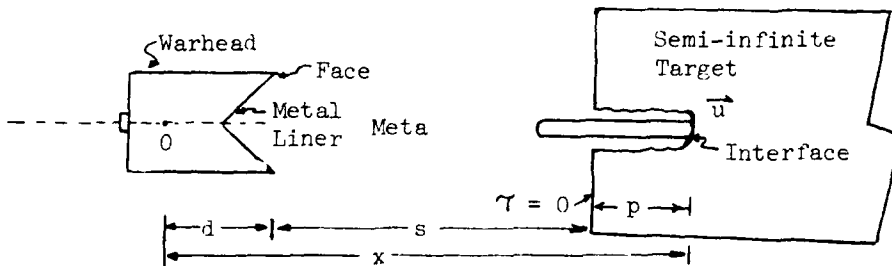


Fig. 5. The relative position between the interface and the virtual origin.

The displacement x of the interface in the Fugh coordinate is related to the penetration depth p by the equation:

$$x = d + s + p \quad (2)$$

where s (called the standoff) is fixed by the experimental setup and d is determined by the relative motion between the tip and tail of the jet. It is evident that the concept of a virtual origin does not apply to a jet of constant length because the virtual origin would have to locate at infinity in this case. However the penetration by a constant jet is simpler to analyze than a stretching jet because the former moves with a constant velocity, say v . Under the assumption⁵ that the steady state is reached almost

instantaneously at the time when the tip of the jet strikes the target, we can solve Eq. (1) for u :

$$u = \frac{v_0}{1 + \gamma} \quad (\text{constant}) \quad (3)$$

where $\gamma = \sqrt{\rho_T/\rho_P}$. (4)

In order to calculate the penetration depth p , it is more convenient to define the penetration time τ (see Fig. 5.). If we assume⁵ that penetration stops as soon as the tail of the jet has struck the target, we can express p as a function of τ for a constant u :

$$p = u \tau. \quad (5)$$

Hence for a jet of constant length l , the complete penetration depth is seen:

$$p = \frac{l}{\gamma} = \frac{l}{\sqrt{\rho_T/\rho_P}}. \quad (6)$$

The derivation of Eq. (6) is given in Appendix A.

For a stretching jet, one or more velocity gradients exists in it. Hence neither v nor u are constants. We need to use the concept of the virtual origin which leads to the following equations:

$$v = \frac{x}{t} \quad (7)$$

and

$$u = \frac{dp}{d\tau} = \frac{dx}{dt} \quad (8)$$

By substituting (7) and (8) into (1), we obtain the solution through simple integration:

$$x = x_0 \left(\frac{t}{t_0} \right)^{\frac{1}{1+\gamma}} \quad (9)$$

where x_0 and t_0 refer the initial values associated with the interface. For the case as shown in Fig. 5. we notice that the penetration is seen:

$$p = x - (d + s) \quad (10)$$

Eqs. (9) and (10) combined together indicate that the penetration ability can be increased by increasing the density of the jet material. This point will be discussed in a later section.

The Eichelberger Theory?⁵ When the strength effects of the jet and the target is taken into account, the equation of motion should be modified:

$$Y_p + \frac{1}{2} \rho_p (v - u)^2 = R_T + \frac{1}{2} \rho_T u^2 \quad (11)$$

where Y_p and R_T represent the resistance of the jet and target, with respect to the plastic deformation caused by the penetration.

This report deals with a copper liner and a steel target. Since R_T is more than ten times larger than Y_p , we can make the approximation $R_T - Y_p = R_T$. Hence Eq. (11) becomes

$$\frac{1}{2} \rho_p (v - u)^2 = \frac{1}{2} \rho_T u^2 + R_T \quad (12)$$

Generally speaking, R_T consists of the intrinsic yield strength σ_y , and the viscous effects which could depend on v , u and p :

$$R_T = \sigma_y + k_1 v + k_2 v^2 + k_3 u + k_4 (1 - e^{-k_5 p}) \quad (13)$$

For the first approximation, we assume that the target material possesses the ideal plasticity only, i.e.

$$R_T = \sigma_y \quad (\text{constant}) \quad (14)$$

By inserting (14) into (12) we obtain an equation of motion for the target of ideal plasticity.

$$u = \frac{1}{1 - \gamma^2} \left[v - \gamma \sqrt{v^2 + \frac{1}{\Lambda^2}} \right] \quad (15)$$

where

$$\Lambda = \sqrt{\frac{\rho_T}{2\sigma_y(1-\gamma^2)}} \quad (\text{constant}) \quad (16)$$

For a jet of constant length, both v (say v_0) and u are constants. Therefore Eq. (15) becomes

$$u = \frac{1}{1 - \gamma^2} \left[v_0 - \gamma \sqrt{v_0^2 + \frac{1}{A^2}} \right] \quad (17)$$

which leads the penetration p (see Fig. 5.):

$$p = \frac{1}{1 - \gamma^2} \left[v_0 - \gamma \sqrt{v_0^2 + \frac{1}{A^2}} \right] \tau \quad (18)$$

In the case of a stretching jet, neither v nor u are constants. We need to employ the concept of the virtual origin which results in Eqs. (7) and (8). Hence Eq. (15) takes the following form

$$\frac{dx}{dt} = \frac{1}{1 - \gamma^2} \left[v - \gamma \sqrt{v^2 + \frac{1}{A^2}} \right] \quad (19)$$

where $x = v t$ and $dx = v dt + t dv$.

This equation can be solved for t as a function of v (see Appendix B):

$$t = t_0 e^{(f_0 - f)} \quad (20)$$

where

$$f - f\{v\} = \ln \left[\left(\frac{1 - \gamma}{1 + \gamma} \right) e^{2 \sinh^{-1} (A v)} + 1 \right] + \left(\frac{1 - \gamma}{\gamma} \right) \sinh^{-1} (A v) \quad (21)$$

$$f_0 = f\{v_0\},$$

v_0 = tip velocity.

The penetration depth p in this case can be calculated as follows:

$$p = v t - v_0 t_0 = v t_0 e^{(f_0 - f)} - x_0 \quad (22)$$

where $x_0 = d + s$ (see Fig. 5).

It is interesting to notice that Eq. (20) reduces to Eq. (9) when R_T or σ_y is neglected. The details are provided in Appendix C.

V. EXPERIMENTS

A series of experiments has been carried out recently so as to test the theories and develop the methods of improving the penetration power of the lined shaped charge. The typical experimental setup is exemplified in Fig. 6.

Among the quantities measured in the experiments are the profiles of the jet and the penetration depth, both as functions of time. They are measured by use of the radiograph photos and the fast responding electric circuits respectively.

For the radiographs, four x-ray heads (150 keV) and 10 x-ray films (14" x 17") were placed as shown in the figure. When the jet passed through the x-ray region, two views of the jet profiles were recorded in the films.

These views provided us with the information on the length of the jet and the velocity of the various parts as functions of time.

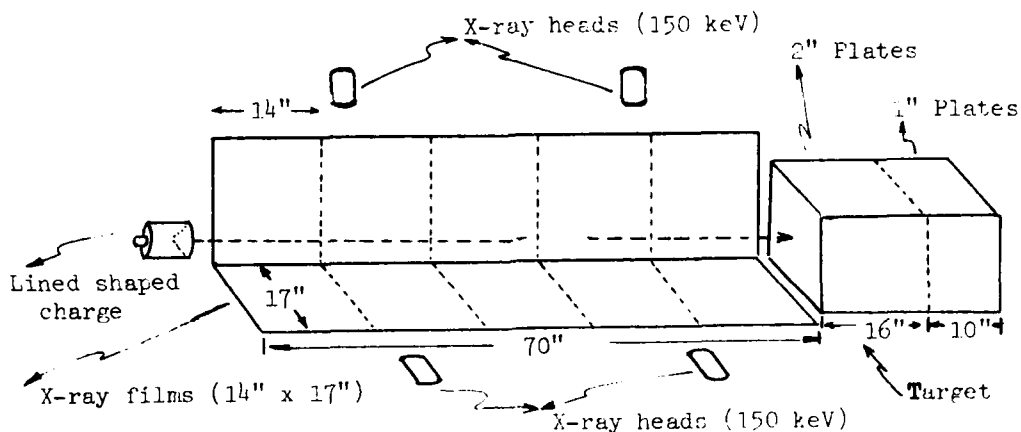


Fig. 6. Experimental setup for measuring the velocity gradients.

As shown in Fig. 6, the target consisted of a number of steel plates, say eight 2" and ten 1" plates. Each plate was sandwiched by mylar and aluminum sheets. Before the jet had pierced the aluminum sheet into the target, the sheet and the plate were insulated by the mylar sheet. When the penetration occurred, a current flowed through the aluminum sheet to the plate surface. This furnished the penetration time. After the explosion the target plates can be cut open so as to study the size and shape of the crater produced by the jet.

VI. COMPARISON OF DATA WITH THEORIES

The profile of a copper jet in one of the two experiments is expressed in the form of the velocity versus position curve in Fig. 7. The constant portion of the jet covered a distance from 95 to 150mm and moved at 8.1 km/sec (or 8.1 mm/ μ s). There were two velocity gradients in the gradient portion, one being 3.98×10^{-2} per μ s and the other 7.17×10^{-2} per μ s. As pointed out in the previous sections, no finite virtual origin can be defined

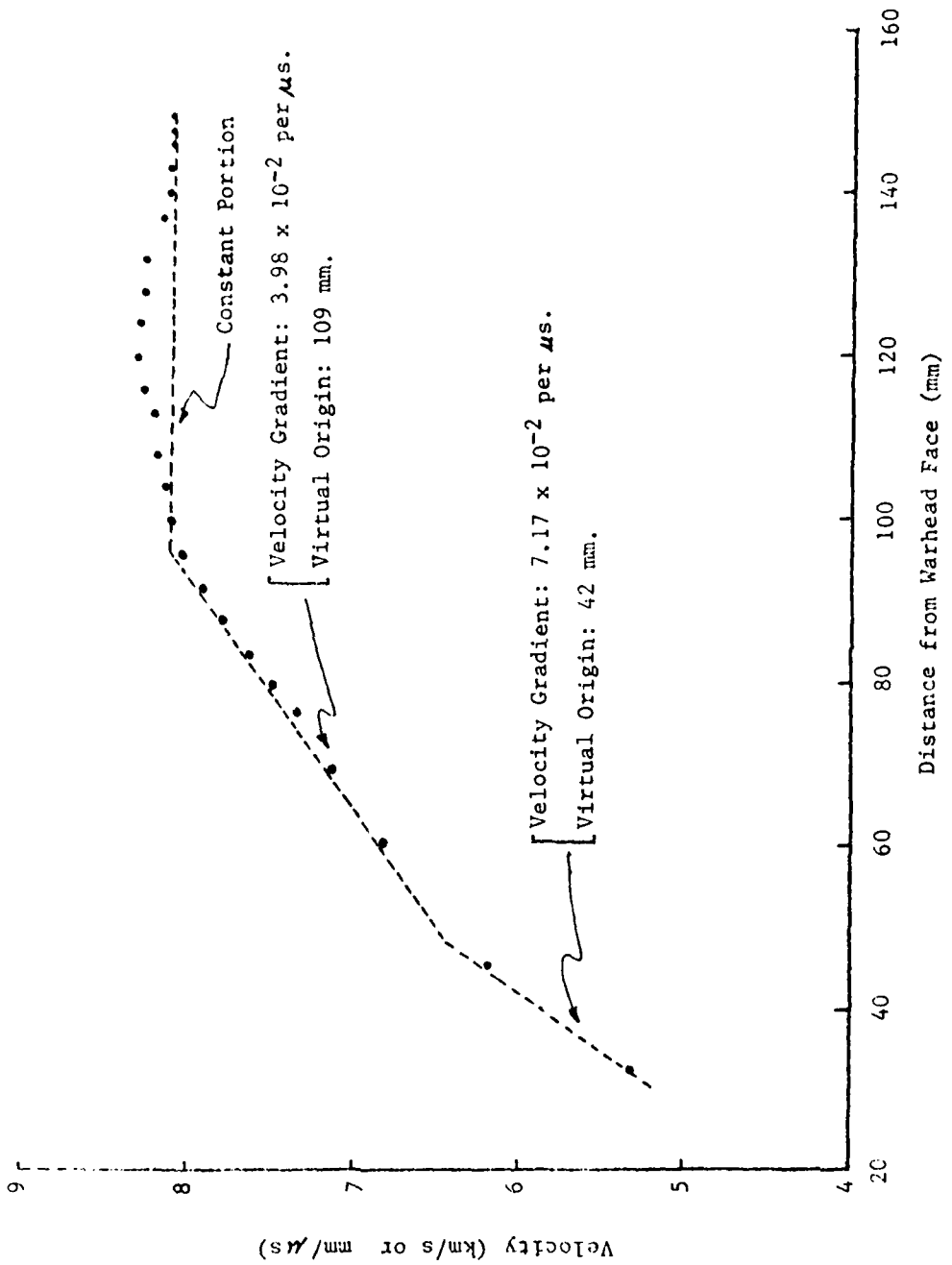


Fig. 7. Jet Position vs Velocity (42° Precision Cone, 49.7μ s Flash Time).

for the constant portion but the penetration depths are easy to calculate in both theories of Pugh-Fireman and of Eichelberger. See Appendix A for details.

There should be two different virtual origins associated with the gradient portion, each being determined by use of the same method as outlined in Fig. 4. The penetration depths are calculated through Eqs. (9) and (10) for the Pugh-Fireman theory or Eqs. (21) and (22) for the Eichelberger theory. The parameters associated with the experiments are compiled in Appendix C.

The results of the calculation are plotted as curves No. 2, 3 and 4 in Fig. 8 along with the averaged experimental data (curve 1) obtained from three experiments. The bases for these curves are listed below:

CURVES	BASES
1	Average data from three experiments.
2	The Pugh-Fireman theory modified with the concept of the multi-gradients of velocity.
3	The Eichelberger theory modified with the concept of the multi-gradients of velocity and $R_T \approx \frac{4.5y}{\sqrt{2}}$
4	Same basis as curve 3 except $R_T \approx \frac{3y}{\sqrt{2}}$.
NOTE: 1. Eichelberger modified the P-F theory by considering the strengths of the target and the jet. 2. Generally speaking, $\sigma_y = \frac{ky}{\sqrt{2}}$ where the strength factor k varies (Tate ³).	

According to our findings, the jets broke up around $\tau = 100 \mu\text{sec}$. It is therefore meaningless to compare the data points with the theoretical value at the time $\tau \geq 100 \mu\text{sec}$ because the theories only apply the continuous jet.

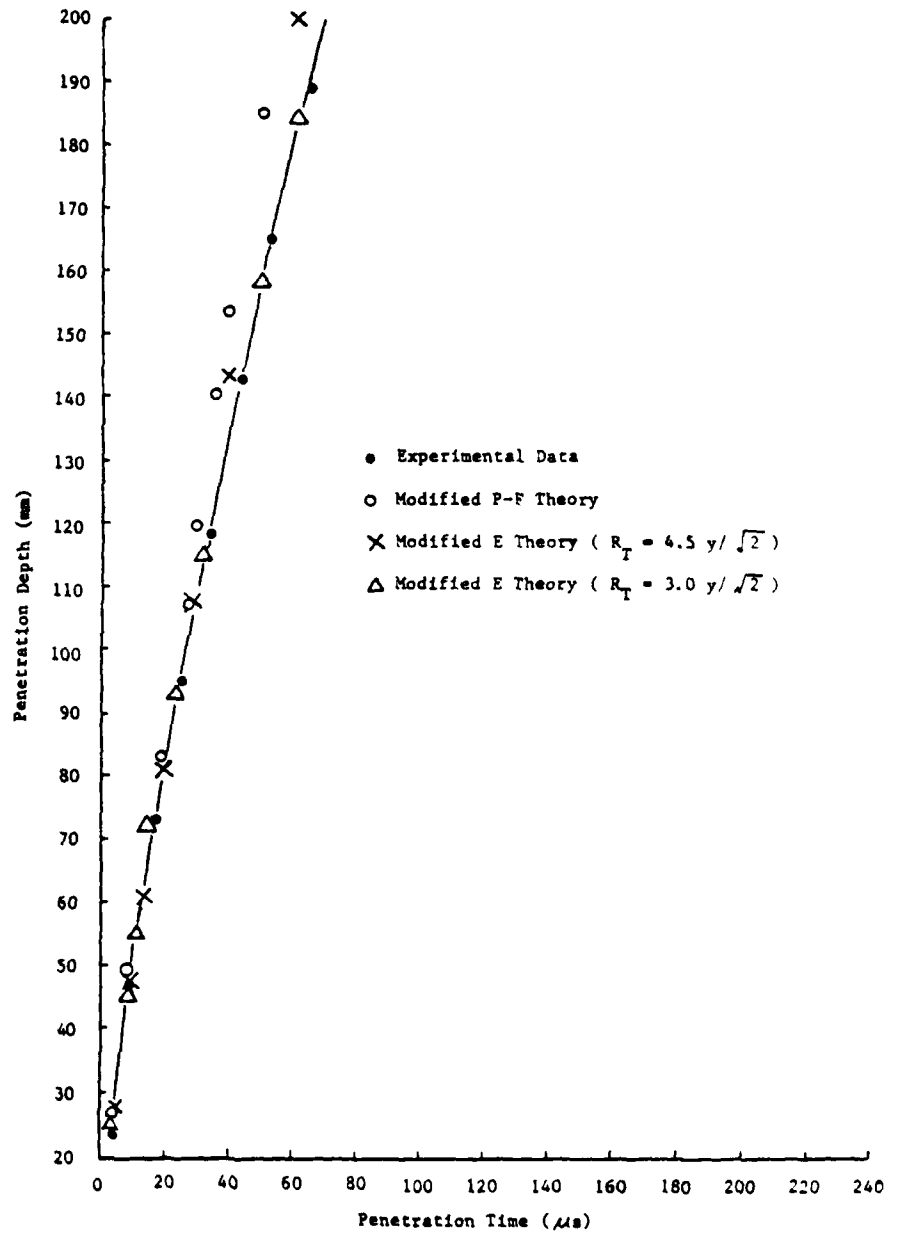


Fig. 3. Comparison of Penetration Data with Theories.

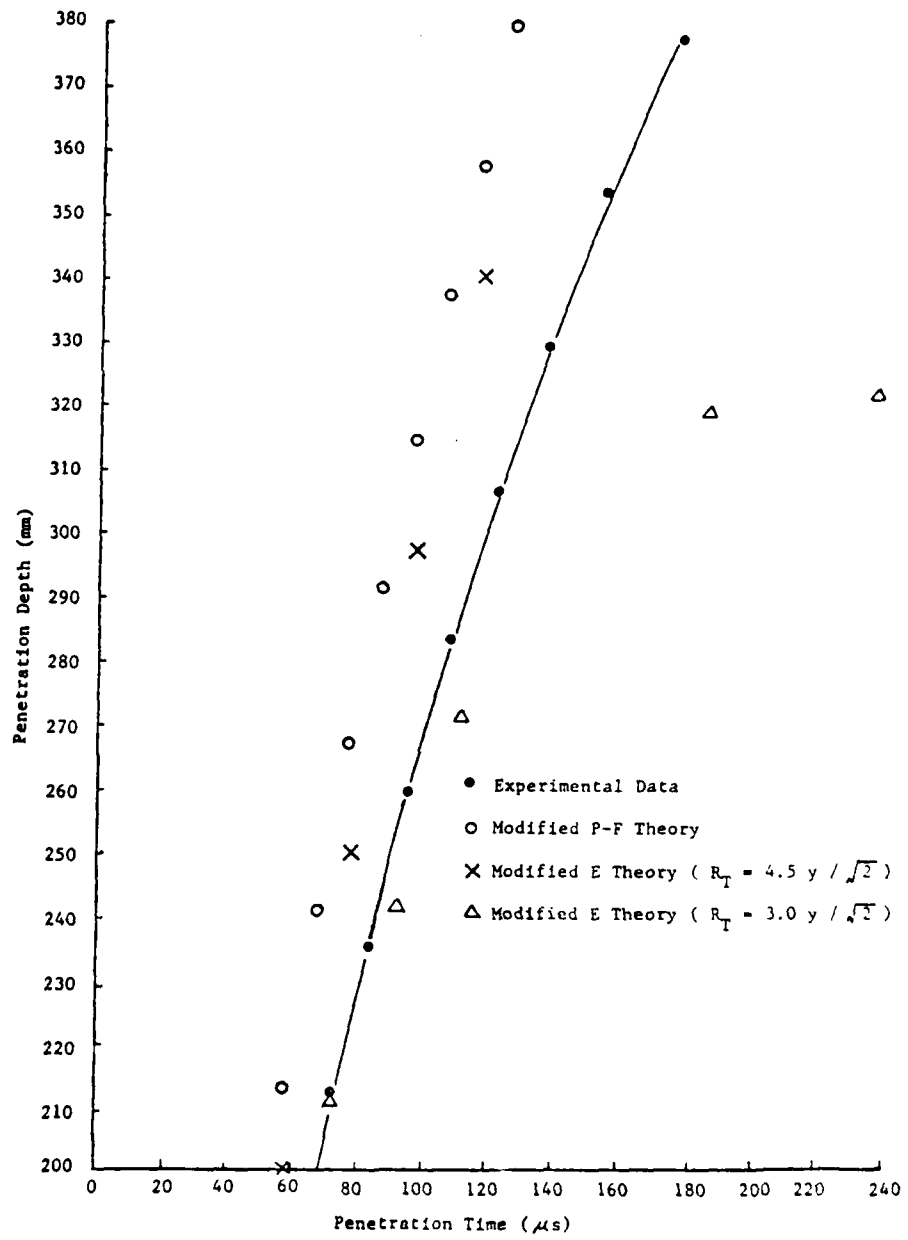


Fig. 8. Comparison of Penetration Data with Theories. (continued)

Based on the prominent discrepancy between Curves 1 and 2, the strength of the target should not be neglected even at the high velocity around 8 km/sec.

With respect to the inclusion of the target strength in the equation of motion, the strength factor k plays a sensitive role. It is possible to bring the theoretical value to a good agreement with the data by varying k .

In conclusion, the modified Eichelberger theory appears to be most successful in explaining our present data.

VII. RECOMMENDATIONS

From the preceding section, it is evident that further investigations are needed so as to obtain a better understanding on how the jets are formed and what effects does the strength factor k have on the penetration.

Our experiments have shown that the formation varies with the experiments. Is there any statistical approach which we can formulate? With respect to the target strength R_T , we would like to investigate whether other effects such as $k_1 v$, $k_2 v^2$, etc, should be included.

Furthermore, the simple Pugh-Fireman theory predicted that the penetration can be improved by increasing the density of the jet. Since we all know that there should be a limit on the improvement, it is worthwhile to find the limit.

As mentioned at the beginning of the paper, the penetration is a multi-dimensional problem while the theories thus reviewed apply the one dimensional model only. Analytic work to expand this model appears to be necessary.

With so much on the penetrator, our attention needs to be also directed to the composite target which has been known to possess more resistance than a mono-target.

REFERENCES

(Listed below are representative references)

1. V. Torrey, "Shaped Charge, Munroe Effect," *Explosives Eng.*, 23 , 160 (1945).
2. G. Birkhoff, D. P. MacDougall, E. M. Pugh and G. Taylor, "Explosives with Lined Cavities," *J. Appl. Phys.*, 19 , 563 (1948).
3. A. Tate, "Theory of Deceleration of Long Rods after Impact," *J. Mech. Phys. Solids*, 15 , 387 (1967).
4. E. M. Pugh and E. L. Fireman, "Fundamentals of Jet Penetration," NDRC Report OTB-4 (OSRD-4357), Nov., 1944.
5. R. J. Eichelberger, "Experimental Test of the Theory of Penetration by Metallic Jets," *J. Appl. Phys.*, 27 , 63 (1956).

APPENDIX A

CALCULATION OF PENETRATION DEPTH

Appendix A

Calculation of Penetration Depth

The calculation is based on the three basic assumptions:

- (i) Both jets and targets are regarded as incompressible and inviscid flows,
- (ii) The steady state is reached almost instantaneous as the tip of the jet strikes the target,
- (iii) Penetration stops as soon as the tail of the jet has struck the target

The penetration depth p is related to the penetration time τ by

$$p = \begin{cases} u\tau & \text{(for constant } u) \\ \int u \, d\tau & \text{(for varying } u) \end{cases} \quad \begin{matrix} \text{(A.1)} \\ \text{(A.2)} \end{matrix}$$

Case 1: For a jet of constant length l , moving with the tip velocity v_0 the Pugh-Fireman theory yields the equation

$$u = \frac{v_0}{1 + \gamma} \quad \text{(A.3)}$$

where $\gamma = \sqrt{\rho_T / \rho_P}$

The time τ taken for the interface to move from the face of the target to P (the total penetration depth) is equal to the time interval for the tail of the jet to travel a distance of $l + P$. Hence

$$\tau = \frac{l + P}{v_0} \quad (A.4)$$

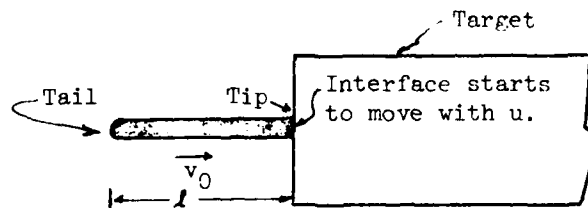


Fig. A.1(a). Beginning of Penetration by a Constant Jet.

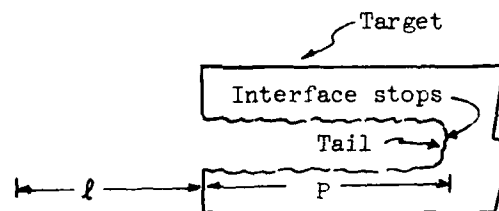


Fig. A.1(b). End of Penetration by a Constant Jet.

By substituting Eqs. (A.3) and (A.4) to (A.1), we obtain

$$P = \frac{l}{\gamma} \quad (\text{a la the P-F theory}) \quad (A.5)$$

where P is the total penetration depth of a jet of constant length l .

From the Eichelberger theory, we have

$$u = \frac{1}{1 - \gamma^2} \left[v_0 - \gamma \sqrt{v_0^2 + \frac{1}{A^2}} \right]$$

$$= \frac{v_0}{1 + \gamma^2} \quad (\text{A.6})$$

where $A = \sqrt{\frac{\rho_T}{\sigma_y(1-\gamma^2)}} \quad (\text{const}) , \quad (\text{A.7})$

and γ^* has the function similar to γ .

Hence (A.5) changes to

$$P = \frac{l}{\tau}, \quad (\text{a la the E theory}). \quad (\text{A.8})$$

Case 2: For a stretch jet, Eq. (A.2) defines the penetration depth. However, it is not easy to find u as a function of τ . The Pugh-Fireman theory provided an elegant method to circumvent this difficulty. If we assume p_i the location where the i -th particle meets the interface, then

$$p_i = v_i t_i - v_0 t_0 = x_i - x_0 \quad (\text{A-10})$$

where x_0 is the distance between 0 and the target and x_i is the final position of the i -th particle of the jet where it meets the interface.

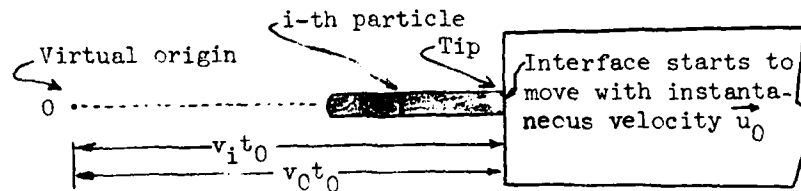


Fig. A.2 (a). The i-th Particle at Time t_0 .

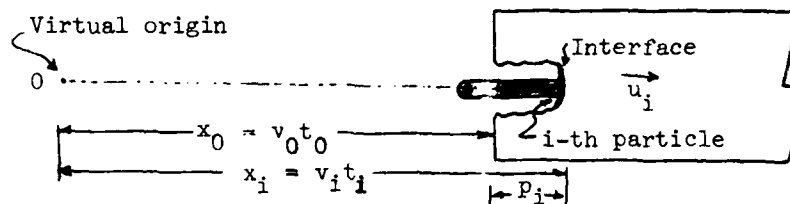


Fig. A.2 (b). The i-th Particle at Time t_i .

In the Pugh-Fireman theory, we find:

$$x_i = x_0 \left(\frac{t_i}{t_0} \right)^{\frac{1}{1+\gamma}}$$

By inserting (A.11) into (A.10), we obtain:

$$p_i = x_0 \left(\frac{t_i}{t_0} \right)^{\frac{1}{1+\gamma}} \quad (t_i \geq t_0) \quad (\text{a la the P-F theory}) \quad (\text{A.12})$$

which enables us to calculate p_i as a function of t_i since t_i is the only independent variable.

From the Eichelberger theory, we find

$$t_i = t_0 e^{(f\{v_0\} - f\{v\})} \quad (\text{A.13})$$

Therefore (A. 10) leads to

$$p_i = v_i t_0 e^{-[f\{v_0\} - f\{v_i\}]} - x_0 \quad (\text{a la the E theory}) \quad (\text{A.14})$$

where v_i is the only independent valuable. See Appendix B for the derivation of f .

APPENDIX B

SOLUTION TO EICHELBERGER THEORY

FOR

STRETCHING JET

Appendix B

Solution to Eichelberger Theory for Stretching Jet

When applying to a stretching jet and a constant target-resistance $R_T \approx \sigma_y$, the Eichelberger theory leads to the equation

$$u_i = \frac{1}{1 - \gamma^2} \left[v_i - \gamma \sqrt{v_i^2 + \frac{1}{A^2}} \right] \quad (\text{B.1})$$

where u_i = instantaneous velocity of the interface when the i -th particle moving with velocity v_i interacts with the interface.

By use of the concept of the virtual origin, the i -th particle is considered to have moved from the virtual origin to the point of interaction with the constant velocity v_i , i. e.,

$$v_i = x_i t_i \quad (\text{B.2})$$

Since $u_i = \left(\frac{dp}{d\tau} \right)_i = \left(\frac{dx}{dt} \right)_i$, (B.3)

we can convert (B.1) into:

$$\frac{dx}{dt} = \frac{1}{1 - \gamma^2} \left[v - \gamma \sqrt{v^2 + \frac{1}{A^2}} \right] \quad (\text{B.4})$$

where the common subscripts have been dropped. Note that Eq. (B.4) appears as Eq. (19). in the main text.

By use of (B.2), we can convert (B.4) into

$$v + \frac{dv}{d(\ell nt)} = Bv - c \sqrt{v^2 + \frac{1}{A^2}} \quad (\text{B.5})$$

whence

$$\frac{dv}{(B-1)v - c \sqrt{v^2 + \frac{1}{A^2}}} = d(\ell nt) \quad (\text{B.6})$$

where

$$B = \frac{1}{1 - \gamma^2} \quad , \quad c = \frac{\gamma}{1 - \gamma^2} \quad (\text{B.7})$$

By letting $v = \frac{1}{A} \sinh \theta$, we can convert $\sqrt{v^2 + \frac{1}{A^2}}$ into $\frac{1}{A} \cosh \theta$. Then by noting that $\cosh \theta = (e^\theta + e^{-\theta})/2$ and $\sinh \theta = (e^\theta - e^{-\theta})/2$ we can change the left-hand side of (B.6) into a function of $e^{2\theta}$, which is easy to integrate.

The result is

$$t = t_0 e^{\int f\{v\} - f\{v_0\}} \quad (\text{B.8})$$

where

$$f\{v\} = \ln \left[\left(\frac{1 - \gamma}{1 + \gamma} \right) e^{2 \sinh^{-1} (Av)} + 1 \right] + \left(\frac{1 - \gamma}{\gamma} \right) \sinh^{-1} (Av) \quad (\text{B.9})$$

which appears as Eq. (21) in the main text.

APPENDIX C

REDUCTION OF EICHELBERGER THEORY TO PUGH-FIREMAN THEORY

Appendix C

Reduction of Eichelberger Theory to Pugh-Fireman Theory

For comparison, both equations of motion of motion and solutions are reproduced below:

$$\frac{dx}{dt} = \begin{cases} \frac{v}{1 + \gamma} & \text{(P-F theory)} \\ BV - c \sqrt{v^2 + \frac{1}{A^2}} & \text{(E theory)} \end{cases} \quad \begin{matrix} \text{(C.1)} \\ \text{(C.2)} \end{matrix}$$

and

$$x = \begin{cases} x_0 \left(\frac{t}{t_0} \right)^{\frac{1}{1 + \gamma}} & \text{(P-F theory)} \\ vt_0 e^{(f_0 - f)} & \text{(E theory)} \end{cases} \quad \begin{matrix} \text{(C.3)} \\ \text{(C.4)} \end{matrix}$$

In this appendix, we want to show Eq. (C.4) agrees with (C.3) when R_T (or $\frac{1}{A^2}$) is neglected as compared with v , i. e. $R_T \ll v$.

Let us take a close look on $f(v)$:

$$f(v) = \ln \left[\left(\frac{1 - \gamma}{1 + \gamma} \right) e^{2 \sinh^{-1}(Av)} + 1 \right] + \left(\frac{1 - \gamma}{\gamma} \right) \sinh^{-1}(Av) \quad \text{(C.5)}$$

In our experiments, the velocity of the various portion of the jet lies between 2 and 8 km/sec. The value of A and γ are 3.247 and 0.9397 respectively. (see Appendix D for details). If we take $\bar{v} = 5$ km/sec we find that,

$$\left(\frac{1 - \gamma}{1 + \gamma} \right) e^{2 \sinh^{-1}(Av)} = 0.0310 e^{2 \sinh^{-1}(16.235)}$$

$$= 0.0310 (1056) = 32.75 \gg 1$$

Hence we can neglect 1 in (C.5) to obtain

$$\begin{aligned}
 f\{v\} &= \ln \left(\frac{1-\gamma}{1+\gamma} \right) + 2 \sinh^{-1} (Av) + \frac{1-\gamma}{\gamma} \sinh^{-1} (Av) \\
 &= \ln \left(\frac{1-\gamma}{1+\gamma} \right) + \frac{1+\gamma}{\gamma} \ln \left[Av + \sqrt{(Av)^2 + 1} \right] \\
 &\approx \ln \left(\frac{1-\gamma}{1+\gamma} \right) + \frac{1+\gamma}{\gamma} \ln [2Av] \\
 &= \ln \left(\frac{1-\gamma}{1+\gamma} \right) + \ln \left[(2Av)^{\frac{1+\gamma}{\gamma}} \right] \tag{C.6}
 \end{aligned}$$

whence

$$f_0 - f = f\{v_0\} - f\{v\} \approx \ln \left[\left(\frac{v_0}{v} \right)^{\frac{1+\gamma}{\gamma}} \right]$$

and

$$e^{(f_0 - f)} \approx \left(\frac{v_0}{v} \right)^{\frac{1+\gamma}{\gamma}} = \left(\frac{x_0/x}{t_0/t} \right)^{\frac{1+\gamma}{\gamma}}$$

Finally, we obtain

$$t = t_0 e^{(f_0 - f)} \approx t_0 \left(\frac{x_0/x}{t_0/t} \right)^{\frac{1+\gamma}{\gamma}}$$

whence (C.4) becomes

$$x \approx \left(\frac{x}{t} \right) t_0 \left(\frac{x_0/x}{t_0/t} \right)^{\frac{1+\gamma}{\gamma}}$$

or

$$t \approx t_0 \left(\frac{x_0/x}{t_0/t} \right)^{\frac{1+\gamma}{\gamma}} \tag{C.7}$$

Eq. (C.7) can be rewritten as

$$\left(\frac{t}{t_0}\right)^{-\frac{1}{\gamma}} = \left(\frac{x_0}{x}\right)^{\frac{1+\gamma}{\gamma}}$$

whence

$$x = x_0 \left(\frac{t}{t_0}\right)^{\frac{1}{1+\gamma}} \tag{C.8}$$

which agrees with (C.3)

APPENDIX D

RELATED PARAMETERS

Appendix D

Related Parameters

In our experiments, the jets and targets are made of copper and steel respectively. Their densities are 7.85 gm/cm^3 and 8.89 gm/cm^3 .

The material strength of the target R_T is thought a function of σ_y , v , u and p (penetration depth). For the first approximation, we set

$$R_T \approx \sigma_y = \frac{ky}{\sqrt{2}} \quad (\text{D.1})$$

where $y \approx 10\text{kb}$, and k varies. According to Tate, $k = 4.5$ in some cases. We found that $k = 3$ is the most desirable in this analysis.

The tip velocity v_0 and the standoff s in our experiments are 8.1 km/sec and 152.4 mm respectively.

For reference, these parameters are listed below:

$$\rho_T = 7.85 \text{ gm/cm}^3, \quad \rho_p = 8.89 \text{ gm/cm}^3,$$

$$\gamma = \rho_T/\rho_p = 0.9397, \quad s = 152.4 \text{ mm},$$

$$v_0 = 8.1 \text{ km/sec (or mm/}\mu\text{s)},$$

$$A = \sqrt{\frac{\rho_T}{2\sigma_y(1-\gamma^2)}} = \begin{cases} 3.427 \text{ }\mu\text{s/mm}, \sigma_y = \frac{4.5Y}{\sqrt{2}}. \\ 3.977 \text{ }\mu\text{s/mm}, \sigma_y = \frac{3Y}{\sqrt{2}}. \end{cases}$$

18